Transactions of the ASME®

Technical Editor, LEON M. KEER

The Technological Institute
Northwestern University
Evanston, IL 60201

APPLIED MECHANICS DIVISION

Chairman, THOMAS L. GEERS
Secretary, S. LEIBOVICH
Associate Editors,
R. M. CHRISTENSEN
C. O. HORGAN
R. L. HUSTON
D. J. INMAN
W. D. IWAN
W. G. KNAUSS
F. A. LECKIE
J. T. C. LIU
R. M. McMEEKING
A. K. NOOR
J. W. NUNZIATO
R. H. PLAUT
J. W. RUDNICKI
J. G. SIMMONDS
P. D. SPANOS
K. R. SREENIVASAN
Z. WARHAFT
L. T. WHEELER

BOARD ON COMMUNICATIONS
Chairman and Vice-President
R. NICKELL

Members-at-Large
J. LLOYD
R. REDER
F. SCHMIDT
M. FRANKE
M. KUTZ
T. MIN
F. LANDIS
R. ROCKE
W. WINER
R. GENTILE
R. MATES

President, E. L. DAMAN
Exec. Dir.
D. L. BELDEN
Treasurer, ROBERT A. BENNETT

PUBLISHING STAFF
Mng. Dir., Publ., JOS. SANSONE
Managing Editor,
CORNELIA MONAHAN
Production Editor, JUDY SIERANT
Prod. Asst., MARISOL ANDINO

Transactions of the ASME, Journal of Applied Mechanics (ISSN 0021-8936) is published quarterly (Mar., June, Sept., Dec.) for $115 per year by The American Society of Mechanical Engineers, 345 East 47th Street, New York, NY 10017. Second class postage paid at New York, NY and additional mailing offices. POSTMASTER: Send address changes to The Journal of Applied Mechanics, c/o THE AMERICAN SOCIETY OF MECHANICAL ENGINEERS, 22 Law Drive, Box 2300, Fairfield, NJ 07007-2300.

CHANGES OF ADDRESS must be received at Society headquarters seven weeks before they are to be effective. Please send old label and new address.

PRICES: To members, $27.00, annually; to nonmembers, $115.00. Add $12.00 for postage to countries outside the United States and Canada.

STATEMENT from By-Laws. The Society shall not be responsible for statements or opinions advanced in papers or . . . printed in its publications (B7.1, Par. 3).

COPYRIGHT © 1988 by the American Society of Mechanical Engineers. Reprints from this publication may be made on condition that full credit be given the TRANSACTIONS OF THE ASME, JOURNAL OF APPLIED MECHANICS, and the author, and date of publication be stated.

INDEXED by Applied Mechanics Reviews and Engineering Information, Inc.

Journal of Applied Mechanics

Published Quarterly by The American Society of Mechanical Engineers

VOLUME 55 • NUMBER 3 • SEPTEMBER 1988

507 Reviewers

TECHNICAL PAPERS

509 Deformation Bounds for Cyclically Loaded Shell Structures Operating Under Creep Conditions (88-WA/APM-32)
A. C. F. Cocks and F. A. Leckie

517 Softening Instability: Part I—Localization Into a Planar Band (88-WA/APM-34)
Z. P. Bažant

523 Softening Instability: Part II—Localization Into Ellipsoidal Regions (88-WA/APM-35)
Z. P. Bažant

530 Two-Dimensional Effects in the Necking of Elastic Bars
S. A. Silling

536 On a Modified Hellinger/Reissner Variational Theorem for the Analysis of Elastoplastic Solids
D. Karamanlidis

539 Possible Experimental X-Ray Diffractometry Evidence of Couple-Stresses
M. M. Gola and P. Coppa

545 Acoustic Microscopy at Low Frequency (88-WA/APM-51)
T. Kundu

551 The Interior Solution for Linear Problems of Elastic Plates (88-WA/APM-31)
R. D. Gregory and F. Y. M. Wan

560 Stiffness of an Elastic Circular Cylinder of Finite Length (88-WA/APM-41)
M. Robert and L. M. Keer

566 The Involution Correspondence in Plane Elastostatics for Regions Bounded by a Circle (88-WA/APM-42)
T. Honein and G. Herrmann

574 Debondings at a Semielliptic Rigid Inclusion on the Rim of a Half Plane
N. Hasebe, S. Tsutsui, and T. Nakamura

580 The Interface Crack Under Combined Loading (88-WA/APM-46)
A. K. Gautesen and J. Dundurs

587 Initiation, Propagation, and Kinking of an In-Plane Crack
C.-C. Ma

596 The Weight-Function Theory for Piecewise Homogeneous Isotropic Notches in Antiplane Strain
T.-L. Sham and H. F. Bueckner

604 Elastic Field Around a Circular Punch (88-WA/APM-53)
V. I. Fabrikant

611 A Refined Small Strain and Moderate Rotation Theory of Elastic Anisotropic Shells (88-WA/APM-37)
R. Schmidt and J. N. Reddy

618 Longitudinal Shearing of a Weakly Bonded Fiber Composite (88-WA/APM-43)
P. S. Steif and A. Dollar

624 Circular Elastic Plates on Elastic Unilateral Edge Supports
Z. Celep, D. Turhan, and R. Z. Al-Zaid

629 Large Elastic Deformation of Shear Deformable Shells of Revolution: Numerical and Experimental Results (88-WA/APM-48)
M. H. Kempski, L. A. Taber, and F.-C. Su

635 Post-Buckling Analysis of Stiffened Laminated Panel
I. Sheinman and Y. Frostig

641 Damage Coupled With Heat Conduction in Uniaxially Reinforced Composites
Y. Weitsman

648 An Analytical Model for Unanchored Fluid-Filled Tanks Under Base Excitation (88-WA/APM-49)
S. Natsiavas

654 Behavior of Unanchored Fluid-Filled Tanks Subjected to Ground Excitation (88-WA/APM-50)
S. Natsiavas and C. D. Babcock

660 Response of a Compliant Slab to Viscous Incompressible Fluid Flow (88-WA/APM-33)
C. A. Evrensel and A. Kalnins

667 Finite Element Modeling of a Punch Stretching of Square Plates
E. Nakamachi and R. Sowerby

672 Vibrations of an Inextensible, Air-Inflated, Cylindrical Membrane
R. H. Plaut and T. D. Fagan

676 The Dynamics of a Deformable Body Experiencing Large Displacements (88-WA/APM-44)
W. P. Koppens, A. A. H. J. Sauren, F. E. Veldpaus, and D. H. van Campen

681 Pseudodissipative Systems I: Stability of Generalized Equilibria
J. A. Walker

(Contents continued on Inside Book Cover)

Downloaded 04 May 2010 to 171.66.16.49. Redistribution subject to ASME license or copyright; see http://www.asme.org/terms/Terms_Use.cfm

CONTENTS (Continued)

687 **A Recursive Formulation for the Dynamic Analysis of Open Loop Deformable Multibody Systems** (88-WA/APM-47)
K. Changizi and A. A. Shabana

694 **A Statistical Study of Generalized Cell Mapping**
J.-Q. Sun and C. S. Hsu

702 **Exact Stationary Response Solution for Second Order Nonlinear Systems Under Parametric and External White Noise Excitations: Part II** (88-WA/APM-45)
Y. K. Lin and G. Cai

706 **Experimental Observation of Amplitude- and Phase-Modulated Responses of Two Internally Coupled Oscillators to a Harmonic Excitation** (88-WA/APM-52)
A. H. Nayfeh and L. D. Zavodney

711 **A Method for Testing Numerical Integrations of Equations of Motion of Mechanical Systems**
T. R. Kane and D. A. Levinson

716 **Approximate Decoupling of the Equations of Motion of Linear Underdamped Systems**
S. M. Shahruz and F. Ma

721 **Synchronized Periodic Solutions of a Class of Periodically Driven Nonlinear Oscillators**
G. M. Mahmoud and T. Bountis

729 **A Recursive Householder Transformation for Complex Dynamical Systems With Constraints**
F. M. L. Amirouche, T. Jia, and S. K. Ider

BRIEF NOTES

Thin Ellipse in Ground Effect: Lift Without Circulation — **A. Plotkin** — 735

A Semi-Infinite Crack Pentrating and Inclusion — **C. H. Wu** — 736

738 Large-Strain Behavior of Unsymmetric Laminates
L. A. Taber

740 Response of the Duffing Oscillator to a Non-Gaussian Random Excitation
I. I. Orabi and G. Ahmadi

DISCUSSION

744 **Discussion on a previously published paper by K. Kumar and J. E. Cochran, Jr.**

745 **Discussion on a previously published paper by B. Poddar, F. C. Moon, and S. Mukherjee**

746 **Discussion on a previously published paper by A. T. Dolovich, G. W. Brodland, and A. B. Thornton-Trump**

747 **Discussion on a previously published paper by A. G. Hernried and G. B. Gustafson**

BOOK REVIEWS

749 ***Cell-to-Cell Mapping, A Method of Global Analysis for Nonlinear Systems*** **by C. S. Hsu** . . . Reviewed by **B. H. Tongue**

750 ***Turbulence Management and Relaminisation*** **edited by H. W. Liepmann and R. Narasimha** . . . Reviewed by **C. R. Smith**

750 ***Contact Mechanics of Rail/Wheel Systems II*** **by G. M. L. Gladwell, H. Ghonem, and J. Kalousek** . . . Reviewed by **B. Paul**

751 ***The Mathematics of Surfaces II*** **by R. R. Martin** . . . Reviewed by **J. T. Oden**

752 Books Received by the Office of the Technical Editor

753 Worldwide Mechanics Meeting List

538 Change of Address Form

754 International Symposium on Wave Propagation in Granular Media —1989 ASME Winter Annual Meeting, San Francisco

754 Symposium on Computational Techniques for Impact, Penetration, and Performance of Solids—1989 ASME Winter Annual Meeting, San Francisco

634 Third ASCE/ASME Mechanics Conference

653 Second International Post-SMiRT Seminar

535, 579, 647, 666, 671
680, 686, 728, 743 Applied Mechanics Symposium Proceedings

Downloaded 04 May 2010 to 171.66.16.49. Redistribution subject to ASME license or copyright; see http://www.asme.org/terms/Terms_Use.cfm

Alan C. F. Cocks
Engineering Department,
The University of Leicester,
Leicester, England

F. A. Leckie
Department of Mechanical Engineering,
University of California,
Santa Barbara, CA 93106
Mem. ASME

Deformation Bounds for Cyclically Loaded Shell Structures Operating Under Creep Conditions

Constitutive relations, based on the Bailey-Orowan's creep theory, are used to develop a maximum work condition which includes the influence of an internal state. A bounding theorem on displacement is obtained for structures subjected to cyclic loading. An application of the bound is illustrated.

1 Introduction

When metals are subjected to stress at temperatures in excess of $T_m/3$, where T_m is the melting temperatures in deg K, the metal suffers time-dependent creep deformations. In addition, internal damage increases with time so that the metal ultimately ruptures. Consequently, when designing shell structures operating at such elevated temperatures, consideration must be made to insure that creep deformations do not exceed operational requirements during the life of the component. Common allowable deformations are 1 percent average and 5 percent maximum strain. In addition, the rupture conditions are that no part of the component may separate nor that local leakage can occur.

By establishing suitable constitutive equations, which give the strain rates and the rate of internal damage of the material, it is possible in principle to establish by numerical means the strain, stress and damage history at all points in the shell. Such procedures tend to be time-consuming but more important it is difficult on the basis of the calculations to draw conclusions of the type which can help reach a deeper understanding of the component behavior. The approach to be used here is to use the results of bounding theorems which make it possible to extend the limit load and shakedown concepts to conditions when time-dependent effects become important. The present paper is concerned with the prediction of deformation while the prediction of rupture is the subject of a later study. It will be demonstrated how the shakedown concept, so strongly associated with the plasticity theory, can be extended by replacing the yield stress σ_0 which causes the steady-state creep rate $\dot{\epsilon}_0$ and which, in turn, is a design parameter given by the relationship

$$\dot{\epsilon}_0 t_L = \epsilon_D$$

where t_L is the life of the component and ϵ_D is the allowable design strain.

The procedures developed shall be illustrated by studying the behavior of a cylindrical shell subjected to two different types of cyclic loading conditions. In the first example, the cylindrical shell is loaded by cyclic internal pressure and a constant ring load, Fig. 1(*a*). In the second example, a cylindrical shell, built in at its ends, is subjected to a cyclic axial end load and a constant internal pressure, Fig. 1(*b*). These examples have been selected because they are representative of the various interactions which can occur between the shell stress resultants. In applying the bounding theorems, use is made of the limit and shakedown solutions and, to this end, the procedure of Gokfeld and Cherniavsky [1] is utilized.

2 Material Behavior and Constitutive Equations

The high-temperature strain/time response of a metal subjected to constant stress has the form shown in Fig. 2. After the initial time-independent response, the strain rate decreases with time during the so-called transient period I when the hardening processes, which occur within the material, exceed the effects of thermal softening. In Region II, referred to as the steady state, the hardening and thermal rates are equal and opposite so that the strain rate remains constant. In the tertiary Region III, the effects of internal damage become evident so that the strain rate increases until rupture eventually occurs. In order to simplify the description of the material behavior, two sets of constitutive equations shall be used. When considering the deformations of the shell, equations are used which are appropriate to portions I and II of the strain/time curve when the interplay between the internal hardening and softening effects determine the strain rate. For rupture life predictions, equations are used, which describe the internal damage occurring within the metal and the increasing strain rate characteristic of the tertiary behavior. In this paper, attention will be concentrated on portions I and II of Fig. 2 where consideration must be given to the transient deformations.

Contributed by the Applied Mechanics Division for presentation at the Winter Annual Meeting, Chicago, IL, November 28 to December 2, 1988, of THE AMERICAN SOCIETY OF MECHANICAL ENGINEERS.

Discussion on this paper should be addressed to the Editorial Department, ASME, United Engineering Center, 345 East 47th Street, New York, N.Y. 10017, and will be accepted until two months after final publication of the paper itself in the JOURNAL OF APPLIED MECHANICS. Manuscript received by ASME Applied Mechanics Division, June 5, 1987; final revision, January 18, 1988.

Paper No. 88-WA/APM-32.

Copyright © 1988 by ASME
Downloaded 03 May 2010 to 171.66.16.21. Redistribution subject to ASME license or copyright; see http://www.asme.org/terms/Terms_Use.cfm

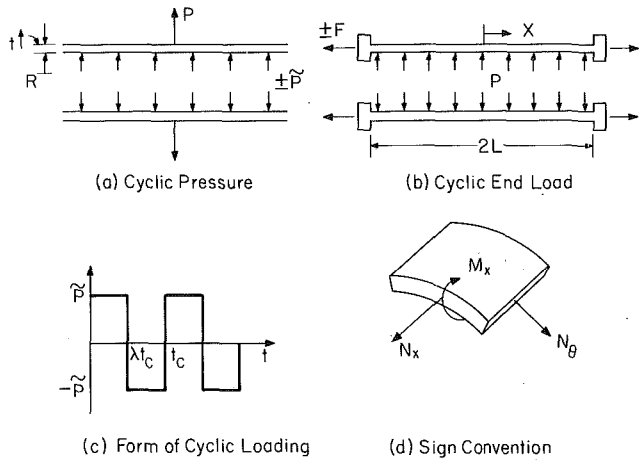


Fig. 1 Cylindrical shell subjected to cyclic loading

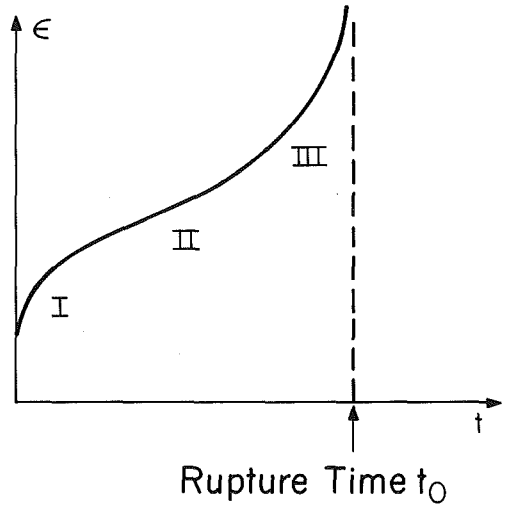


Fig. 2 Uniaxial creep curve showing the three stages of creep

Transient-Deformation Constitutive Equations. The elastic strains are defined by the equation

$$e_{ij} = Cijkl\sigma_{kl} \tag{2.1a}$$

where $C_{ijk\,l}$ is the compliance matrix.

The time-dependent response of the material can be expressed in terms of the Bailey-Orowan's theory by introducing a scalar state variable s which is a measure of the present size of the yield surface in stress space [2]. Hence

$$\dot{\epsilon}^P_{ij} = f(\phi - s)\frac{\partial \phi}{\partial \sigma_{ij}} \tag{2.1b}$$

$$\dot{s} = h(s)\, f(\phi - s) - r(s) \tag{2.1c}$$

where $\phi(\sigma_{ij})$ is a homogeneous function of degree one in σ_{ij}. In its simplest form, f is given by the step function

$$f(\phi - s) \begin{cases} > 0 \text{ when } \phi = s,\ \dot{\phi} \geq 0 \\ = 0 \text{ when } \phi < s \text{ or } \phi = s \text{ and } \dot{\phi} < 0 \end{cases} \tag{2.1d}$$

The condition $\phi > s$ cannot be achieved. The quantities $h(s)$ and $r(s)$ are the rates of strain hardening and thermal softening which depend on the value of the state variable s.

For fast loading, the term $r(s)$ in equation (2.1c) can be neglected, and $\phi = s$ so that equatioins (2.1 b, c) then give

$$\dot{\epsilon}^p_{ij} = \frac{\dot{s}}{h(s)}\frac{\partial \phi}{\partial \sigma_{ij}}$$

The function ϕ is chosen such that in a uniaxial tension test this equation reduces to

$$d\,\epsilon^p = \frac{d\sigma}{h(\sigma)}$$

The function $h(s)$ can then be determined from the uniaxial stress-strain diagram.

Under steady-state conditions, the results of uniaxial tests satisfy the relationship

$$\frac{\dot{\epsilon}^p}{\dot{\epsilon}_0} = \left[\frac{\sigma}{\sigma_0}\right]^n$$

where $\dot{\epsilon}_0$ is the strain rate corresponding to the stress σ_0, and n is the so-called creep index. At the steady-state condition $\dot{s} = 0$ in equation (2.1c) so that

$$f(\phi - s) = \frac{r(s)}{h(s)} = \frac{r(\phi)}{h(\phi)}$$

and

$$\dot{\epsilon}^p_{ij} = \frac{r(\phi)}{h(\phi)}\frac{\partial \phi}{\partial \sigma_{ij}}.$$

In uniaxial loading, this gives the result

$$\dot{\epsilon}^p = \frac{r(\phi)}{h(\phi)} = \dot{\epsilon}_0 \left[\frac{\sigma}{\sigma_0}\right]^n$$

so that the recovery function $r(\phi)$ can now be deduced since the hardening function is already known.

The energy-dissipation density rate for steady state can readily be shown to be given by

$$\dot{D}\,(\sigma_{ij}/\sigma_0) = \sigma_0\ \dot{\epsilon}_0\ \phi^n\ (\sigma_{ij}/\sigma_0) \tag{2.2}$$

It is informative to deduce the prediction of equations (2.1) to a cyclic stress loading of the form show in Fig. 3. No additional creep strain is predicted during the period of unloading while softening continues but, on reloading, the hardening is recovered with an instantaneous strain $\Delta t\ \dot{\epsilon}^p_1$, so that the final strain is equal to that of a continuously loaded specimen. Such a prediction is generally close to reality but, when in error, it overestimates the strains so that the constitutive equations form the basis of calculations which are conservative.

3 Constitutive Equations in Terms of Generalized Forces

When analyzing the behavior of cylindrical shell structures, it proves convenient to use the stress resultants $N_i = (N_\theta, N_x, M_x\}$ (Fig. 1(d)) and the corresponding generalized strains $\epsilon_i = \{\epsilon_\theta, \epsilon_x, \kappa_x\}$. The sole use of generalized forces for cyclic-loading histories perhaps requires some justification before we proceed further. Before doing this, it is pertinent to examine the applicability of the model described in the previous section to continuum problems. For fast loading (or load below the creep range), equations (2.1) predict that a material will harden isotropically. We know, however, that yield surfaces for real materials distort and translate as the material deforms plastically. This behavior is due, in part, to the development of microscopic residual stress fields which arise due to the different orientations of the slip planes within the different grains of the polycrystal. It is found, however, that the use of simple material models can give adequate descriptions of component behavior for a wide range of loading histories. When generalizing the model of the previous section, using generalized shell forces, we again obtain a material model for which the yield surface expands and contracts isotropically in generalized force space. As before, the surface for a real material will distort and translate. In addition to the reasons just discussed, this is also due to the changing nature of the stress field through the thickness of a shell element as the material deforms. For the types of problems considered here, however, this model will give an adequate description of material and component behavior for use in design. However,

Downloaded 03 May 2010 to 171.66.16.21. Redistribution subject to ASME license or copyright; see http://www.asme.org/terms/Terms_Use.cfm

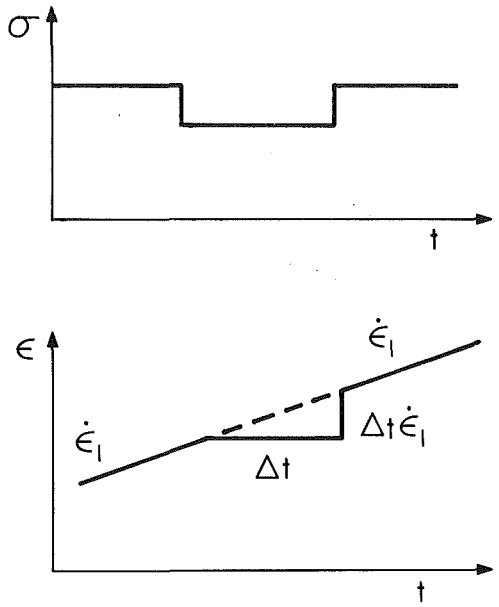


Fig. 3 Predictions of recovery model for rapid cycling

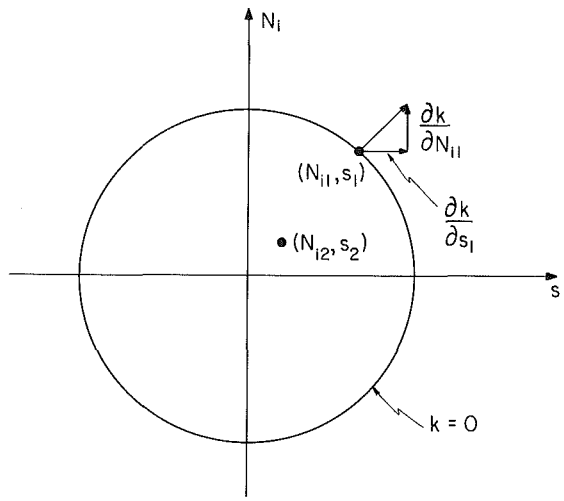


Fig. 4 Surface $k=\phi-s=0$ plotted in N_i, s space

the procedure adopted here is unsuitable for the type of shell problem considered by Karadeniz and Ponter [3] where the cyclic loading is due to a changing temperature distribution through the thickness of the shell.

The constitutive equations (2.1) can be recast in terms of a potential function Ω and the generalized forces. The potential Ω has the form

$$\Omega = F(\phi - s) + G(s) \tag{3.1a}$$

with

$$\dot{\epsilon}_i^p = \frac{\partial \Omega}{\partial N_i} = \frac{\partial F}{\partial N_i} = f(\phi - s)\frac{\partial \phi}{\partial N_i} \tag{3.1b}$$

and

$$\dot{s} = -h(s)\frac{\partial \Omega}{\partial s} = -h(s)\left[\frac{\partial F}{\partial S} + \frac{\partial G}{\partial S}\right] \tag{3.1c}$$

where $\phi(N_i)$ is a homogeneous function in N_i. Following (2.1d), strains only occur when $\phi = s$.

For the cylindrical shells considered in this paper, the potential function ϕ (N_i) is defined by the following intersecting planes

$$\begin{aligned} &n_\theta + \pm 1 \\ &n_\theta - n_x = \pm 1 \\ &n_x + m_x = \pm 1 \\ &n_x - m_x = \pm 1 \\ &n_\theta - n_x - \frac{m_x}{2} = \pm 1 \\ &n_\theta - n_x + \frac{m_x}{2} = \pm 1 \end{aligned} \tag{3.2}$$

where $n_x = N_x/N_0$, $n_\theta = N_\theta/N_0$, $m_x = M_x/M_0$.

We further assume that the normalizing quantities N_0 and M_0 are related to the reference stress σ_0 of Section 2 by the relationships and

$$N_0 = \sigma_0 t, \quad M_0 = \sigma_0 T^2/4$$

These surfaces can be recognized as those used by Hodge [3] with σ_0 replacing the yield stress σ_y when $n_x = 0$ but, for other combinations of forces, the foregoing surface in tridimensional force space is enveloped by the surface given by [4]. The aforementioned set of equations were selected because they allow a much simpler analysis than use of the full Hodge relationships permit, and the prime purpose of this paper is to demonstrate the general approach to problem-solving rather than present complex analyses of structural problems. It has been demonstrated by Ponter and Leckie [5] that using surfaces like that in equation (3.2), which is obtained from limit-load calculations, gives an upper bound on energy dissipation but that the estimates are close to the exact values.

The constant energy dissipation rate $\sigma_0\dot{\epsilon}_0$ per unit length is given by

$$\dot{D}(N_i) = N_0\dot{\epsilon}_0\phi^{n+1}(n_i) \tag{3.3}$$

4 Bounding Theorem for Deformation

Bounds will be obtained on the deformation of shells subjected to cyclic loading, following the procedures developed by Ponter [6].

Using the potential of equation (3), the generalized displacement rates are

$$\dot{\epsilon}_i^p = \frac{\partial \Omega}{\partial N_i}; \quad \dot{s} = -h(s)\frac{\partial \Omega}{\partial s} = -h(s)\left[\frac{\partial F}{\partial S} + \frac{\partial G}{\partial S}\right]$$

Plastic strain can only occur when $\phi = s$. Consider the surface plotted in N_i, s space, defined by $k = \phi - s = 0$, Fig. 4. Consider further, the two states N_{i1}, s_1 and $N_{i2}\, s_2$ where N_{i1}, s_1 lies on the surface and N_{i2}, s_2 lies on or inside the surface. Then since k is convex

$$(N_{i1} - N_{i2})\frac{\partial k}{\partial N_{i1}} + (s_1 - s_2)\frac{\partial k}{\partial s_1} \geq 0$$

Multiplying each term of this expression by f_1 $(\phi - s)$ gives

$$(N_{i1} - N_{i2})\frac{\partial F_1}{\partial N_{i1}} + (s_1 - s_2)\frac{\partial F_1}{\partial s_1} \geq 0 \tag{4.1}$$

where

$$\frac{\partial F_1}{\partial N_{i1}} = f_1(\phi - s)\frac{\partial \phi}{\partial N_{i1}} \text{ and } \frac{\partial F_1}{\partial S_1} = -f_1(\phi - s)$$

If N_{i1} and s_1 are inside the surface of Fig. 4, then $f_1(\phi - s) = 0$ and the inequality (4.1) still holds. From the convexity condition of the potential

$$G = G(s) = \frac{N_0\dot{\epsilon}_0}{(n+1)}\left(\frac{s}{N_0}\right)^{n+1}$$

the corresponding inequality is

Downloaded 03 May 2010 to 171.66.16.21. Redistribution subject to ASME license or copyright; see http://www.asme.org/terms/Terms_Use.cfm

$$(s_1 - s_2)\frac{\partial G}{\partial s_1} - G_1 + G_2 \geq 0 \tag{4.2}$$

We let $s_2 = (n/n+1)s^*$ and $s_1 = s$, the actual values of s. Since G_1 and G_2 are homogeneous function of degree $(n+1)$

$$G_1 = \frac{1}{n+1} s_1 \frac{\partial G}{\partial s_1}$$

Then (4.2) becomes

$$G\left(\frac{n}{n+1} s^*\right) \geq \frac{n}{n+1} (s^* - s) \frac{\partial G}{\partial s} \tag{4.3}$$

Identifying N_{i1}, s_1 with actual values N_i, s in the real problem and N_{i2} with N_i^* and s_2 with s^* a constant, equation (4.1) becomes

$$(N_i - N_i^*)\frac{\partial F}{\partial N_i} + (s - s^*)\frac{\partial F}{\partial s} \geq 0 \tag{4.4}$$

Combining equations (4.3) and (4.4) gives

$$\frac{n}{n+1}(N_i - N_i^*)\frac{\partial F}{\partial N_i} \geq \frac{n}{n+1}(s^* - s)\left(\frac{\partial F}{\partial s} + \frac{\partial G}{\partial s}\right) - G\left(\frac{n}{n+1} s^*\right) \tag{4.5}$$

Rearranging and noting

$$\dot{s} = -h(s)\left(\frac{\partial F}{\partial s} + \frac{\partial g}{\partial s}\right) \quad \text{and} \quad \dot{\epsilon}_i^p = \frac{\partial F}{\partial N_i}$$

finally yields the inequality

$$(N_i^* - N_i)\dot{\epsilon}_i^p \leq \frac{n+1}{n} G\left(\frac{n}{n+1} s^*\right) - (s^* - s)\frac{\dot{s}}{h(s)} \tag{4.6}$$

We now consider the situation where the load applied to the shell structure is cyclic, Fig. 5, and we examine the cyclic state. Two characteristic features of the cyclic state are that $\int_0^\tau \dot{\epsilon}^p dt$ where τ is the cycle time, is a compatible displacement field [6] and the stress N_i and state s are the same at the start and finish of the cycle. If $N_i(t)$ is in equilibrium with an applied load $P_i{}^t$, then $N_i^*(t)$ can be chosen such that it is in equilibrium with this same cyclic load history $P_i(t)$ and a constant dummy load T_i; a further constant value of s^* can be selected such that $N_i^*(t)$ always lies on or inside the surface $k = (\phi - s) = 0$. Integrating equation (4.6) over the cycle gives

$$\int_0^\tau (N_i^* - N_i)\dot{\epsilon}_i^p dt \leq \int_0^\tau \frac{n+1}{n} G\left(\frac{n}{n+1} s^*\right) dt - \int_0^\tau (s^* - s)\frac{ds}{h(s)} \tag{4.7}$$

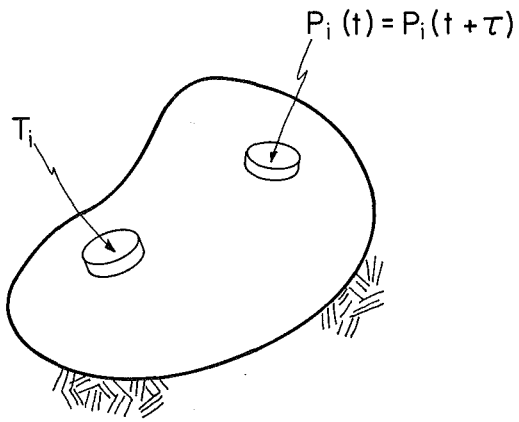


Fig. 5 Structure subjected to cyclic load and dummy load

Since the elastic strain is the same at the start and finish of the cycle, we may write

$$\int_0^\tau (N_i^* - N_i)\dot{\epsilon} dt \leq \int_0^\tau \frac{n+1}{n} G\left(\frac{n}{n+1} s^*\right) dt - \int_0^\tau (s^* - s)\frac{ds}{h(s)} \tag{4.8}$$

where $\dot{\epsilon}_i$ is the total strain rate at a given instant in time.

If we now let

$$\chi(s, s^*) = \int_s^{s^*} (s^* - s)\frac{ds}{h(s)}$$

the last term of equation (4.8) becomes

$$\int_{s_i}^{s_f} d\chi = \chi(s_f, s^*) - \chi(s_i, s^*)$$

where s_i and s_f are the values of s at the beginning and end of a cycle.

In the cyclic state $s_i = s_f$,

$$\int_0^\tau (s^* - s)\frac{ds}{h(s)} = \int_{s_i}^{s_f} d\chi = 0,$$

and equation (4.8) becomes

$$\int_0^\tau (N_i^* - N_i)\dot{\epsilon} dt \leq \int_0^\tau \frac{n+1}{n} G\left(\frac{n}{n+1} s^*\right) dt = \frac{n+1}{n} G\left(\frac{n}{n+1} s^*\right)\tau$$

Integrating over the surface of the shell gives

$$\int_s T_i \int_0^\tau \dot{u}_i dt\, ds \leq \int_s \frac{n+1}{n} G\left(\frac{n}{n+1} s^*\right)\tau ds$$

or

$$\int_s T_i u_i \leq \int_v \frac{n+1}{n} G\left(\frac{n}{n+1} s^*\right)\tau ds \tag{4.9}$$

where u_i is the displacement suffered during a cycle.

Now s^* can be chosen such that

$$\phi(N_i^*) = \phi(N_i^p(t) + N_i^t) \leq s^* \tag{4.10}$$
$$\phi(N_i^p(t_0) + N_i^t) = s^*$$

where $N^p(t)$ is in equilibrium with $P_i{}^{(t)}$ and N_i^t is in equilibrium with the dummy load T_i and to is the time in the cyclic when ϕ is a maximum. Equation (4.9) then becomes

$$\int_s T_i u_i \leq \int_s \frac{1}{n} \dot{\epsilon}_0 N_0 \left[\frac{\phi(N_i^p(t_0) + N_i^t)}{N_0}\right]^{n+1} \tau ds \tag{4.11}$$

An optimum bound can be found by making appropriate choices of the magnitude of T_i and the stress distributions N_i^p and N_i^t. However, this will not be attempted here and use will be made of solutions which arise from a shakedown analysis.

Consider the situation where a structure is subjected to a cyclic history of loading $P_i(t)$. A value of the yield stress, $\sigma_y = \sigma_0$, can be chosen such that a replica structure composed of an elastic-perfectly plastic material is on the shakedown limit. Then an equilibrium stress field exists such that

$$\phi[N_i^p(t_0)] \leq N_0 \tag{4.12}$$

When the replica structure is subjected to a dummy load, plastic collapse occurs when

$$T = T_L$$

For $T = \eta T_L$ an equilibrium stress field can be found such that

$$\phi(N_i^T) \leq \eta N \tag{4.13}$$

Downloaded 03 May 2010 to 171.66.16.21. Redistribution subject to ASME license or copyright; see http://www.asme.org/terms/Terms_Use.cfm

Substituting equations (4.10) and (4.11) into equation (4.9) and making use of the inequality

$$\phi(N_i^a + N_i^b) \le \phi(N_i^a) + \phi(N_i^b)$$

gives

$$\dot{u}_T \le \frac{N_0}{T_L}\,\dot{\epsilon}_0\,\frac{\left\{\dfrac{n}{n+1}\,(1+\eta)\right\}^n}{n\eta}\,A$$

where A is the surface area of the shell.

Optimizing w.r.t., η gives $\eta = 1/n$ and

$$\dot{u}_T \le \frac{\sigma_y}{T_L}\,\dot{\epsilon}_0 V \tag{4.14}$$

This bound requires a knowledge of the limit load T_L and the shakedown solution which determines N_0 and, hence, $\dot{\epsilon}_0$. When a bound on the mean displacement rate over an area, A_b, of the structure is required, a dummy pressure p can be applied over this area and the bound becomes

$$\dot{u}_n \le \frac{N_0}{P_L}\,\dot{\epsilon}_0\,\frac{A}{A_B} \tag{4.15}$$

where $\dot{u}_n$ is the mean displacement rate and P_L is the limit load for the dummy pressure. We use this result in Section 6 to obtain a bound on the mean displacement rate of the section of a shell.

Care should be exercised in the use of this bound. Acceptable results can be obtained in situations where, in the shakedown and limit-load solution, the entire structure deforms plastically. In the problem analyzed in this paper, however, the ratchet mechanism beyond the shakedown boundary and the collapse mechanism at the limit load are such that only a small proportion of the structure deforms plastically. We discuss the applicability of equation (4.14) to this type of problem in Section 6.

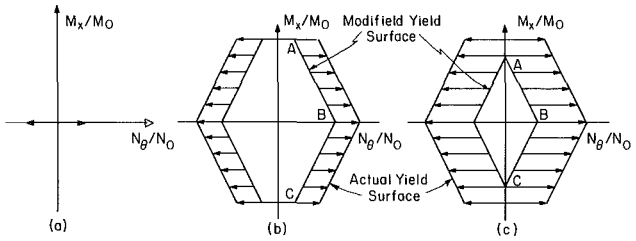


Fig. 6 Cyclic elastic stress history (*a*) is translated to construct the modified yield surface for (*b*) $p_0 < 1/2$ and (*c*) $p_0 > 1/2$

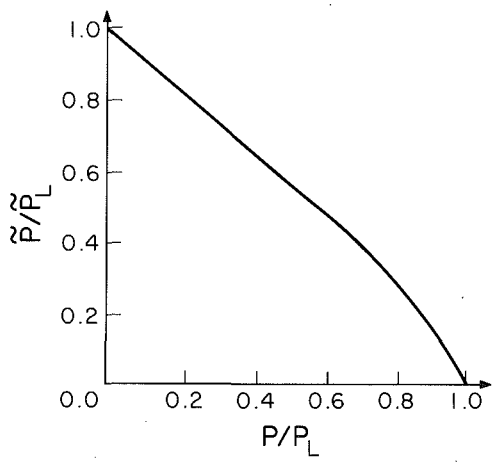


Fig 7 Shakedown boundary for the problem of Fig. 1(*a*)

5 Shakedown Solutions for Shell Problems

In order to demonstrate the application of the bounding inequality (4.14), two problems have been solved related to the cyclic loading of a cylindrical shell. The problems are illustrated in Fig. 1(*a*, *b*). In the case illustrated in Fig. 1(*a*), the stress resultants N_ϕ and M_x are involved in the yield conditions, whereas, for the case shown in Fig. 1(*b*), all three stress resultants N_ϕ, N_x, and M_x are involved in the yield conditions and, therefore, give rise to a more complex problem. The shakedown boundary corresponding to the yield force N_0 is determined using the method due to Gokhfeld and Cherniavsky [1] which involves the calculation of the limit load for yield conditions decreased by the range of the elastic stresses corresponding to the cyclic loading. This approach proves particularly useful in the second situation analyzed in this paper where only the stress resultant N_ϕ and M_x need be considered in the limit-load calculation.

The yield condition given by equation (3.2) is shown in Fig. 6 for the situation $n_x = 0$. The range of stress experienced by an element of material during the application of the cyclic pressure loading $\tilde{p}$ indicated in Fig. 1(*a*) is shown in Fig. 6(*a*). A modified yield surface is formed by tracing the locus of the center of this line, as it is translated, such that one end touches the yield surface and the other end lies on or inside the surface, Figs. 6(*b*, *c*). If a distribution of N_θ and M_x can be found that is in equilibrium with the applied constant load P and nowhere violates "modified yield," the structure will shakedown [1].

The optimum equilibrium stress field for the problem of Fig. 1(*a*) is obtained in the Appendix and the resulting shakedown boundary is given in Fig. 7. The normalization used in this plot are

$$P_L = \frac{1.73\,N_0 t}{\sqrt{Rt}}\,; \quad \tilde{P}_L = \frac{N_0}{R}$$

A similar procedure can be used to construct the shakedown boundary for the problem of Fig. 1(*b*). A plane view of the yield surface looking down the m_x-axis is shown in Fig. 8. This surface has been sectioned at a height m_x above the origin to show the range of stress experienced by a material element due to the cyclic axial force of Fig. 1(*b*) and the construction of the modified yield surface. A futher view of the resulting modified

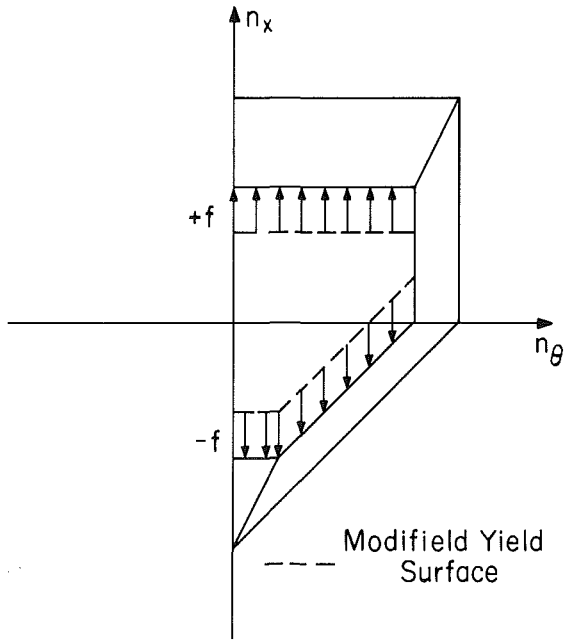


Fig. 8 Yield surface sectioned at a height $m_x = 0.4$ to reveal cyclic loading history $\pm f$ and the modified yield surface

Downloaded 03 May 2010 to 171.66.16.21. Redistribution subject to ASME license or copyright; see http://www.asme.org/terms/Terms_Use.cfm

yield surface is shown in Fig. 9 for $n_x = 0$. The optimum equilibrium stress field for this problem is obtained in the Appendix and the resulting shakedown boundary satisfies the simple linear relationship

$$\frac{P}{P_L} = 1 - \frac{F}{F_L}$$

where

$$P_L = \beta N_0 / R$$

and

$$F_L = 2\pi R N_0$$

The way in which β varies with the length $\bar{L} = L/\sqrt{Rh}$ is given in Fig. 10(*b*).

6 Displacement Bounds

In this section, we use the inequality (4.14) to obtain a bound on the mean displacement rate over an area A_b of the tube. For each of the situations examined in the previous section, we identify A_b with the area of the tube that contains the mechanism of incremental collapse in the shakedown analysis. Use of the bound also requires the determination of the relationship N_0/P_L for a uniform pressure applied over the area A_b of the shell.

The length of the tube $\bar{L}$ which deforms plastically at shakedown in the problem of Fig. 1(*a*) is shown in Fig. 11. Applying a uniform pressure over this length of the tube of magnitude P_L results in plastic collapse when

$$\frac{N_0}{P_L} = \frac{R}{\beta} \tag{6.1}$$

where β is given in Fig. 10(*a*). For the area A, we also use the area of the plastically deforming region so that the inequality (4.14) becomes

$$u_m \leq \frac{R\dot{\epsilon}_0}{\beta} \tag{6.2}$$

In this situation we note $\beta > 1$ so that a simple bound on $\dot{u}_m$ is

$$\dot{u}_m < R\dot{\epsilon}_0 \tag{6.3}$$

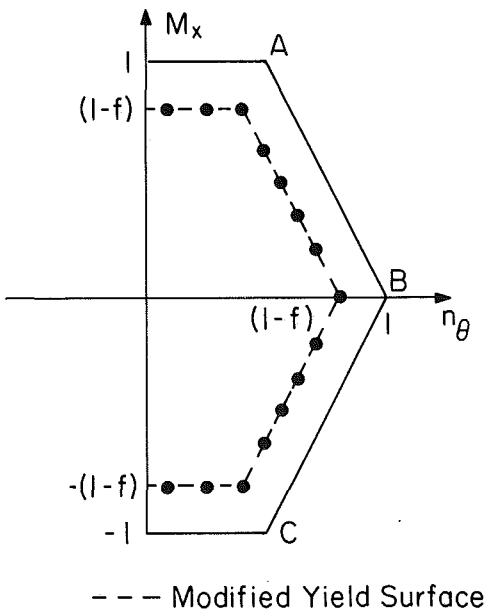


Fig. 9 Shape of modified yield surface in the plane $n_x = 0$.

provided the loading satisfies the shakedown condition for a yield stress σ_0.

The entire tube deforms plastically at shakedown in the problem of Fig. 1(*b*), so that

$$A = A_b = 2\pi RL$$

The value of N_0/PL for a uniform pressure loading is again given by equation (6.1), where β varies with L in the manner indicated in Fig. 10(*b*).

Application of the bound of equation (6.2) again results in a mean displacement rate given by equation (6.2). As before, $\beta > 0$ and the simpler bound of equation (6.3) may be used.

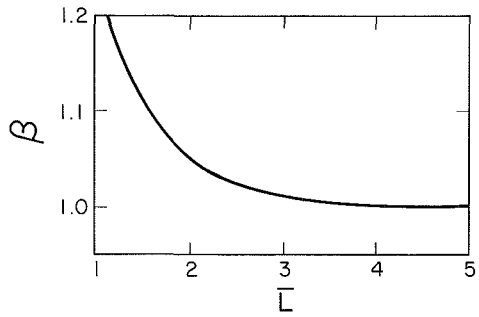
Conclusions

A method has been presented which can be used to bound the time-dependent deformations of the component made of a creeping material whose properties are described by Bailey-Orowan's recovery model.

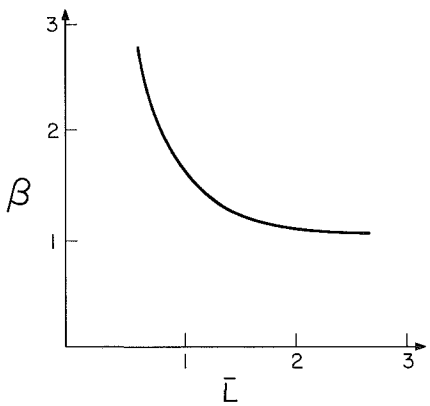
The application of the method to a shell structure demonstrates that if the structure is designed according to a shakedown condition for which the stress σ_0 plays the role of the yield stress, than the mean strain rate in the component is $\dot{\epsilon}_0$ the steady-state strain rate corresponding to the stress σ_0. This means that plasticity concepts can be readily extended to deal with creep conditions provided the deformations are governed by recovery-type behavior.

Acknowledgment

The authors acknowledge the support of the National Science Foundation under Grant MSM 82-10620.



10a



10b

Fig. 10 Limit pressure $p_L = \beta N_0/R$ for (*a*) the tube of Fig. 1(*a*) subjected to a uniform pressure over a length $\bar{L}$ and (*b*) the tube of Fig. 1(*b*) subjected to a uniform pressure over its length $\bar{L}$

Downloaded 03 May 2010 to 171.66.16.21. Redistribution subject to ASME license or copyright; see http://www.asme.org/terms/Terms_Use.cfm

References

1 Gokhfeld, D. A., and Cherniavsky, O. R., 1980, *Limit Analysis of Structures Under Thermal Loading*, Sijthoff and Noordhoff, Amsterdam.

2 Ponter, A. R. S., and Leckie, F. A., 1976, "Constitutive Relationships for the Time Dependent Deformation of Metals," *Journal of Engineering Materials and Technology*, pp. 47–51.

3 Karadeniz, S., and Ponter, A. R. S., 1984, "A Linear Programming Upper Bound Approach to the Shakedown Limit of Thin Shells Subjected to Variable Thermal Loading," *Journal of Strain Analysis*, Vol. 19, pp. 221–230.

4 Hodge, P. A., 1963, *Limit Analysis of Rotationally Symmetric Plates and Shells*, Prentice-Hall, Englewood Cliffs, NJ.

5 Ponter, A. R. S., and Leckie, F. A., 1970, "The Application of Energy Theorem for Bodies Which Creep in the Plastic Range," ASME JOURNAL OF APPLIED MECHANICS, Vol. 37, pp. 753–759.

6 Ponter, A. R. S., 1975, "Deformation Bounds for the Bailey-Orowan Theory of Creep," ASME JOURNAL OF APPLIED MECHANICS, Vol. 42, pp. 619–624.

APPENDIX

Shakedown and Limit-Load Calculations

Shakedown Analysis for Problem of Fig. 1(*a*). First, we consider the situation where $P_0 < 1/2$ and the shape of the modified yield surface is given in Fig. 6(*b*). We assume that the tube deforms plastically over a length $2\bar{L}$ such that the stress state moves along ABC of the yield surface as $\bar{x}$ increases, where the dimensionless lengths $\bar{L}$ and $\bar{x}$ are given by

$$\bar{L} = \frac{L}{\sqrt{Rh}}\ ; \quad \bar{x} = \frac{x}{\sqrt{Rh}}$$

The governing equilibrium equation for the present problem is

$$\frac{d^2 m_x}{d\bar{x}^2} + 4\, n_\theta = 0 \tag{A-1}$$

which for stress states, lying along BC of Fig. 6(*b*), becomes

$$\frac{\partial^2 m_x}{\partial \bar{x}^2} + 2m_x = -4(1 - P_0) \tag{A-2}$$

The general solution to this equation is

$$m_x = A \cos\sqrt{2}\bar{x} + b \sin\sqrt{2}\bar{x} - 2(1 - p_0) \tag{A-3}$$

Similarly for a stress state along AB of Fig. 6(*b*), equation (A – 1) becomes

$$\frac{\partial^2 m_x}{\partial \bar{x}^2} - 2m_x = -4(1 - p_0) \tag{A-4}$$

which has the general solution

$$m_\phi = C \exp(\sqrt{2}\bar{x}) + D \exp(-\sqrt{2}\bar{x}) + 2(1 - p_0) \tag{A-5}$$

We solve these equations subject to the boundary conditions

$$\begin{aligned} &m_\phi = -b \\ &\frac{\partial m_\phi}{\partial \bar{x}} = a\,\frac{P}{P_L} \qquad \text{at } \bar{x} = 0 \\ &m_\phi = b \\ &\partial m_\phi / \partial \bar{x} = 0 \qquad \text{at } \bar{x} = \bar{L} \end{aligned} \tag{A-6}$$

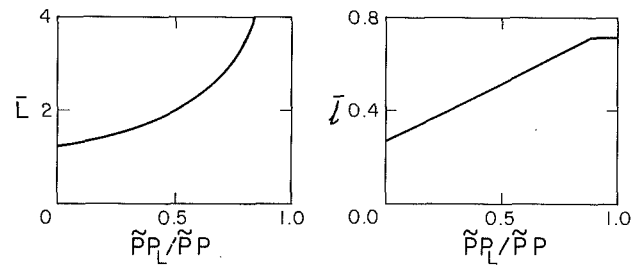


Fig. 11 Values of $\bar{L}$ and $\bar{l}$ obtained from the shakedown solution of the Appendix for the problem of Fig. 1(*a*)

with $b = 1$ and $a = 2.45$. In addition, we impose the conditions that m_ϕ and $\partial m_\phi / \partial \bar{x}$ are continuous as the solution to the governing equations changes from equation (A-3) to equation (A-5), i.e.,

$$\begin{aligned} &m_\phi = 0 \\ &\frac{\partial m_\phi}{\partial \bar{x}} \text{ is continuous} \qquad \text{at } \bar{x} = \bar{l} \end{aligned} \tag{A-7}$$

The result is

$$\frac{P}{P_L} = \frac{8(1 - P_0) - 4(1 - 2p_0)\cos\sqrt{2}\bar{l}}{\sin\sqrt{2}\bar{l}} \tag{A-8}$$

where

$$\begin{aligned} (1 - 2p_0) = {} & 2(1 - p_0)\cos\sqrt{2}\bar{l} \\ & - (1 - 2p_0)\sin\sqrt{2}\bar{l}\sinh\sqrt{2}(\bar{L} - \bar{l}) \end{aligned} \tag{A-9}$$

and

$$\cosh\sqrt{2}(\bar{L} - \bar{l}) = \frac{2(1 - p_0)}{1(-2p_0)} \tag{A-10}$$

The values of $\bar{L}$ and $\bar{l}$ given by equations (A-9) and (A-10) are shown in Fig. 11 and the shakedown boundary of equation (A-8) is plotted in Fig. 7.

An equilibrium stress field in the remainder of the tube which does not violate yield is given by

$$\begin{aligned} &m_\phi = 2\left(\frac{\bar{y}}{\bar{k}}\right)^3 - 3\left(\frac{\bar{y}}{\bar{k}}\right)^2 + 1 \\ &n_\phi = \frac{3}{2\bar{k}^2}\left[1 - 2\left(\frac{\bar{y}}{\bar{k}}\right)\right] \qquad 0 \le \bar{y} \le \bar{k} \\ &n_\theta = m_\phi = 0 \quad \bar{y} > \bar{k} \end{aligned}$$

where

$$\bar{y} = \bar{x} - \bar{L} \text{ and } k = \sqrt{\frac{3}{2(1/2 - p_0)}}$$

When $p_0 \ge 1/2$, the modified yield surface takes the form of Fig. 6(*c*). The general solutions of the governing equilibrium for Sections BC and AB of the yield surface are again given by equations (A-3) and (A-5). These must now be solved subjected to the boundary conditions of equations (A-6) and (A-7) with $b = 2(1 - p_0)$ and $a = 2.45$. The result is

$$\bar{L} = \infty;\ \bar{l} = \frac{\pi}{2\sqrt{2}}$$

and

$$\frac{P}{P_L} = 1.15\ (1 - p_0)$$

This equation completes the shakedown boundary of Fig. 7.

Limit-Load Calculation for Shell of Fig. 1(*b*). Here we obtain an expression for the limit load of the shell problem of Fig. 1(*b*), subjected to an internal pressure p. The governing equilibrium for this problem is

$$\frac{d^2 m_x}{d\bar{x}^2} + 4(n_\theta - \bar{p}) = 0 \tag{A-11}$$

where $\bar{p} = pR/N_0$.

For $\bar{n}_x = 0$, the yield condition is shown in Fig. 9. If the stress lies at a point along BC, equation (A-11) becomes

$$\frac{d^2 m_x}{d\bar{x}^2} + 2m_x = 4(\bar{p} - 1)$$

which has the general solution

$$m_x = A\cos\sqrt{2}\bar{x} + B\sin\sqrt{2}\bar{x} + 2(\bar{p} - 1) \tag{A-12}$$

Downloaded 03 May 2010 to 171.66.16.21. Redistribution subject to ASME license or copyright; see http://www.asme.org/terms/Terms_Use.cfm

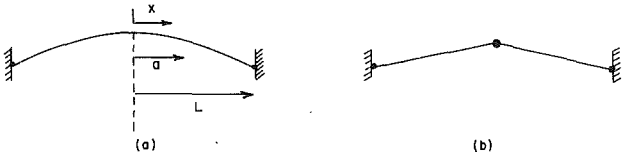


Fig. 12 Possible deflected forms

Alternatively, if the stress lies along AB of Fig. 9, equation (A-11) becomes

$$m_x = C \exp \sqrt{2}\bar{x} + D \exp(-\sqrt{2}\bar{x}) - 2(\bar{p} - 1) \tag{A-13}$$

It is expected that the deflected form of the tube is one of two types shown in Fig. 12. If the deflection has the form of Fig. 12(*a*), then equations (A-12) and (A-13) must be solved subjected to the boundary conditions

$$\begin{aligned} &\frac{\partial m_x}{\partial \bar{x}} = 0 \quad \text{at } \bar{x} = 0 \\ &m_x = 0 \quad \text{at } \bar{x} = \bar{l} \\ &\frac{\partial m}{\partial \bar{x}} \text{ is continuous} \\ &\bar{m} = 1 \quad \text{at } \bar{x} = \bar{L} \end{aligned} \tag{A-14}$$

where $\bar{l}$ is the position along the tube where the solution changes from equation (A-12) to equation (A-13).

The limiting pressure is then given by

$$\frac{P_L}{N_0 R} = \bar{p}_L = 1 + \frac{1}{\eta} \tag{A-15}$$

where

$$\eta = e^{\sqrt{2}(\bar{L}-\bar{l})}(1 + \tan \sqrt{2}\bar{l}) + e^{-\sqrt{2}(\bar{L}-\bar{l})}(1 - \tan \sqrt{2}\bar{l}) - 2 \tag{A-16}$$

The optimum bound is obtained by selecting the value of $\bar{l}$ that gives the minimum value of η. The value of $\bar{l}$ that gives the optimum bound can be obtained from

$$e^{2\sqrt{2}(\bar{L}-\bar{l})} = \frac{\tan \sqrt{2}\bar{l} + 1}{\tan \sqrt{2}\bar{l} - 1} \tag{A-17}$$

For small values of $\bar{L}$ the foregoing analysis gives a value of m_x at the center of the tube that violates the yield condition. In these situations, m_x is limited to a value of -1 at $\bar{x} = 0$, where a hinge forms, Fig. 12(*b*). This additional boundary condition requires that $\bar{l}$ is given by

$$\cos \sqrt{2}\,\bar{\sigma} = \frac{2(\bar{p}_L - 1)}{(2\bar{p}_L - 1)}$$

while the limiting pressure is still given by equations (A-15) and (A-16). The variation of limiting pressure $\bar{P}_L$ with $\bar{L}$ given by the aformentioned analysis is given in Fig. 10(*b*).

Shakedown Analysis for the Problem of Fig. 1(*b*). The modified yield surface is shown in Fig. 8 for cyclic loading of the end load F. The limit load for F acting alone is

$$F_L = 2\pi R N_0$$

If we define a dimensionless load measure as

$$f = \frac{F}{F_L}$$

then the modified yield surface is the same shape as the original surface, and reduced in size by a factor $(1 - f)$. The previous limit-load analysis applies, with N_0 replaced by $N_0(1 - f)$. The shakedown boundary is then given by

$$\frac{p}{p_L} = 1 - \frac{F}{F_L}$$

where p_L is given in Figs. (10*b*).

Downloaded 03 May 2010 to 171.66.16.21. Redistribution subject to ASME license or copyright; see http://www.asme.org/terms/Terms_Use.cfm

Softening Instability: Part I —Localization Into a Planar Band

Zdeněk P. Bažant
Professor,
Department of Civil Engineering,
Northwestern University,
Evanston, IL 60208
Mem. ASME

Distributed damage such as cracking in heterogeneous brittle materials may be approximately described by a strain-softening continuum. To make analytical solutions feasible, the continuum is assumed to be local but localization of softening strain into a region of vanishing volume is precluded by requiring that the softening region, assumed to be in a state of homogeneous strain, must have a certain minimum thickness which is a material property. Exact conditions of stability of an initially uniform strain field against strain localization are obtained for the case of an infinite layer in which the strain localizes into an infinite planar band. First, the problem is solved for small strain. Then a linearized incremental solution is obtained taking into account geometrical nonlinearity of strain. The stability condition is shown to depend on the ratio of the layer thickness to the softening band thickness. It is found that if this ratio is not too large compared to 1, the state of homogeneous strain may be stable well into the softening range. Part II of this study applies Eshelby's theorem to determine the conditions of localization into ellipsoidal regions in infinite space, and also solves localization into circular or spherical regions in finite bodies.

Introduction

Distributed damage such as cracking or void nucleation and growth may be macroscopically described by a constitutive law for a continuum that exhibits strain-softening (Bažant, 1986). In the softening range, the matrix of incremental moduli of the material is not positive-definite. After Hadamard (1903) pointed out that such a condition implies an imaginary wave speed, strain-softening has been considered an unacceptable property for a continuum and some scholars have argued that strain-softening simply does not exist (Read and Hegemier, 1984; Sandler, 1984).

The various mathematical arguments for the nonexistence of strain-softening, however, overlooked one crucial experimental fact pointed out in 1974 by Bažant (1986): A material in the strain-softening state also has available to it another matrix of incremental moduli which applies for unloading and is positive-definite. This fact makes an essential difference. It causes that the material in a strain softening-state can propagate unloading waves, and that solutions to various dynamic and static problems with strain-softening exist, even for the classical, local continuum. Some solutions are unique, representing limits of finite-element discretizations, which converge quite rapidly (Bažant and Belytschko, 1985, 1987; Belytschko et al., 1986). In some cases, strain-softening apparently leads to chaos (Belytschko et al., 1986). Generally, the dynamic strain-softening problems (for a local continuum) belong to the class of "ill-posed" initial boundary-value problems, which are well known and accepted as realistic in other branches of physics (e.g., Joseph et al., 1985; Joseph, 1986, Yoo, 1985). Therefore, there is nothing fundamentally wrong with the concept of strain-softening from the mathematical viewpoint.

From the physical viewpoint, however, strain-softening in a classical local continuum is an unacceptable concept because structures are predicted to fail with zero energy dissipation. The reason is that the zone of softening damage often localizes into a line or surface while the energy dissipation per unit volume is finite. This difficulty, however, may be overcome by introducing some form of localization limiters (Bažant and Belytschko, 1987)—mathematical formulations that prevent the strain-softening damage to localize into a region of zero volume. Among numerous possibilities, the limitation to localization may be best introduced by treating the softening damage as nonlocal while the elastic behavior, including unloading, is treated as local (Pijaudier-Cabot and Bažant, 1986; Bažant, Lin, and Pijaudier-Cabot, 1987; Bažant and Pijaudier-Cabot, 1987). Physical justification of this nonlocal formulation has been given on the basis of homogenization of a quasi-periodic microcrack array (Bažant, 1987). Other possibilities are, e.g., the use of strain gradient or higher-order derivatives (or gradients) of the yield function in the constitutive equation (e.g., Floegl and Mang, 1981; Mang and Eberhardsteiner, 1985; Schreyer and Chen, 1986; Triantafyllidis and Aifantis, 1986).

In this paper we will seek analytical solutions to

Contributed by the Applied Mechanics Division for presentation at the Winter Annual Meeting, Chicago, IL, November 28 to December 2, 1988, of THE AMERICAN SOCIETY OF MECHANICAL ENGINEERS.
Discussion on this paper should be addressed to the Editorial Department, ASME, United Engineering Center, 345 East 47th Street, New York, N.Y. 10017, and will be accepted until two months after final publication of the paper itself in the JOURNAL OF APPLIED MECHANICS. Manuscript received by ASME Applied Mechanics Division, March 13, 1987; final revision, February 1, 1988.
Paper No. 88-WA/APM-34.

Copyright © 1988 by ASME
Downloaded 03 May 2010 to 171.66.16.21. Redistribution subject to ASME license or copyright; see http://www.asme.org/terms/Terms_Use.cfm

multidimensional localization. They appear to be possible with the well-known approach which uses the simplest and earliest type of localization limiter proposed in 1974 by Bažant (1976) and later implemented in the finite-element crack band model (Bažant and Cedolin, 1979, 1980; Bažant, 1982; Bažant and Oh, 1983, 1984). Despite the presence of strain-softening, the constitutive equation is in this approach treated as local, but the softening damage is not allowed to localize into a region whose size is less than a certain characteristic length l of the material. This length is determined empirically by fitting test data and roughly corresponds to the size of the representative volume used in statistical theory of heterogeneous materials (Kröner, 1967). For concrete, l is of the order of the maximum aggregate size. Although this approach is, admittedly, crude and does not permit resolving the distribution of damage density throughout the softening region, it has given some surprisingly good results for the overall structural response. This was confirmed by comparisons with extensive fracture test data (Bažant and Oh, 1983; Bažant 1982, 1984) and later also by comparisons with accurate nonlocal finite-element solutions (Bažant and Pijaudier-Cabot, 1987; Bažant, Pijaudier-Cabot, and Pan, 1986; Bažant and Zubelewicz, 1986; see the Appendix).

The method of analysis of strain-localization instability due to softening and its thermodynamic basis were formulated in 1974 (Bažant, 1976) and the stability conditions for one-dimensional localization in a bar and flexural localization in a beam were derived. The equivalence to failure analysis on the basis of fracture energy was also demonstrated (Bažant, 1982). Several other studies reanalyzed the one-dimensional localization from other viewpoints yielding equivalent results (e.g., Ottosen, 1986).

Rudnicki and Rice (1975) and Rice (1976) made important pioneering studies of localization into a planar band in an infinite space. They focused their studies primarily on localization caused by the geometrically nonlinear effects of finite strain before the peak of the stress-strain diagram (i.e., in the plastic hardening range), but they also obtained some critical states for negative values of the plastic hardening modulus. Rudnicki (1977) further analyzed, on the basis of Eshelby's theorem, an infinite space that contains a weakened zone of ellipsoidal shape, determined for localization into such a zone the critical neutral equilibrium states of homogeneous stress and strain, and demonstrated various cases of localization instabilities in the hardening as well as softening regime. Although the studies of Rudnicki and Rice represented an important advance, they did not actually address the stability conditions but were confined to neutral equilibrium conditions for the critical state. They did not consider a general incremental stress-strain relation but were limited to von Mises plasticity (Rudnicki and Rice 1975) or Drucker-Prager plasticity (Rudnicki, 1977), in some cases enhanced with a vertex hardening term. They also did not consider bodies of finite dimensions, for which the size of the localization region usually has a major influence on the critical state and, in the case of planar localization bands, did not consider unloading to occur outside the localization band, which is important for finite bodies. The present study attempts to take all these conditions and effects into account.

The purpose of the present study is to obtain exact analytical solutions for some multidimensional localization problems with softening, using the method introduced in 1974 by Bažant (1976, 1979), which is based on a local continuum with an imposed lower bound on the size h of the softening region. In this paper, we will analyze localization of strain into a planar band, both without and with geometrical nonlinearity of strain and, in a subsequent companion paper, we will analyze in a similar manner the localization of strain into ellipsoidal regions, including the special case of spherical and circular regions. The solution for ellipsoidal regions will be based on the celebrated Eshelby's theorem for eigenstrain in an ellipsoidal inclusion in an infinite elastic solid.

The present study (including Part II) will deal only with stability of equilibrium states, and not with bifurcations of the equilibrium path. As is known from Shanley's column theory, such bifurcations can occur at increasing load and do not necessarily coincide with the limit of stable equilibrium.

Before embarking on our analysis, comments on several related aspects are in order. It has been widely believed that softening is properly treated by fracture mechanics, in particular, by line-crack fracture models with a cohesive zone characterized by a softening stress-displacement relation. One problem with this approach may be that the stress-displacement relation might not be unique and might depend on the fracture specimen geometry. This is suggested by nonlocal finite-element results as well as the difficulties in fitting test data for various specimen geometries on the basis of the same material properties. Another problem is that this approach is limited to single fractures or noninteracting multiple fractures, and becomes unobjective (with regard to the choice of mesh) when multiple interacting cracks are present (Bažant, 1986). The formulation could be made objective by imposing a certain minimum admissible spacing of cracks as a material property, but this runs into difficulty when the interacting cracks are not parallel. (Line cracks with a fixed minimum spacing h are, of course, macroscopically equivalent to distributed cracking if the cumulative cracking strain over distance h is made to be equal to the crack opening displacement.)

Softening Band Within a Finite Layer or Infinite Solid

Let us analyze the stability of softening that is localized in an infinite layer which is called the softening band (or localization band) and forms inside an infinite layer of thickness L ($L \geq h$); see Fig. 1. The minimum possible thickness h of the band is assumed to be a material property, proportional to the characteristic length l. The layer is initially in equilibrium under a uniform (homogeneous) state of strain ϵ_{ij}^0 and stress σ_{ij}^0 assumed to be in the strain-softening range (Fig. 2). Latin lower case subscripts refer to Cartesian coordinates x_i ($i = 1, 2, 3$) of material points in the initial state. The initial

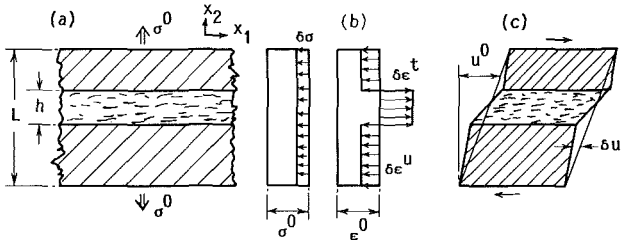


Fig. 1 Planar localization band in a layer

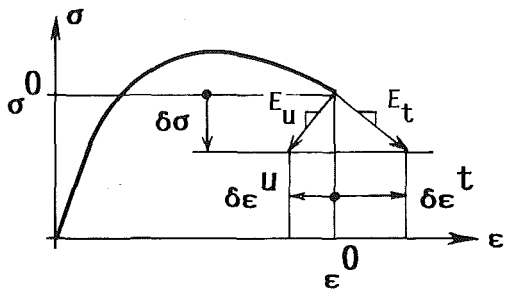


Fig. 2 Stress-strain diagram with softening and unloading

Downloaded 03 May 2010 to 171.66.16.21. Redistribution subject to ASME license or copyright; see http://www.asme.org/terms/Terms_Use.cfm

equilibrium is disturbed by small incremental displacements δu_i whose gradients $\delta u_{i,j}$ are uniform both inside and outside the band (subscripts preceded by a comma denote derivatives). The values of $\delta u_{i,j}$ inside and outside the band are denoted as $\delta u^t_{i,j}$ and $\delta u^u_{i,j}$ and are assumed to represent further loading and unloading, respectively, and so the increments $\delta u_{i,j}$ represent strain localization. We choose axis x_2 to be normal to the layer (Fig. 1). As the boundary conditions, we assume that the surface points of the layer are fixed during the incremental deformation, i.e., $\delta u_i = 0$ at the surfaces $x_2 = 0$ and $x_2 = L$ of the layer. Assuming homogeneous strains inside and outside of the band, compatibility of displacements at the band surface requires that

$$\delta u^u_{i,1} = \delta u^t_{i,1} = 0, \quad \delta u^u_{i,3} = \delta u^t_{i,3} = 0 \tag{1}$$

$$h\delta u^t_{i,2} + (L-h)\delta u^u_{i,2} = 0 \quad (i = 1,2,3). \tag{2}$$

We assume that the incremental material properties are characterized by incremental moduli tensors D^t_{ijpq} and D^u_{ijpq} for loading and unloading (Fig. 2). These two tensors may be either prescribed by the given constitutive law directly as functions of ϵ^0_{ij} and possibly other state variables, or they may be implied indirectly. The latter case occurs, e.g., for continuum damage mechanics. The crucial fact is that D^u_{ijpq} differs from D^t_{ijpq} and is always positive-definite, even if there is strain-softening. Noting that $\epsilon_{ij} = (u_{i,j} + u_{j,i})/2$ and $D_{ijkm} = D_{jimk}$, we may write the incremental stress-strain relations as follows (repetition of subscripts implies Einstein's summation rule)

$$\delta\sigma^t_{ji} = D^t_{jikm}\delta\epsilon^t_{km} = D^t_{jikm}\delta u^u_{k,m} \quad \text{for loading} \tag{3}$$

$$\delta\sigma^u_{ji} = D^u_{jikm}\delta\epsilon^u_{km} = D^u_{jikm}\delta u^u_{k,m} \quad \text{for unloading.} \tag{4}$$

Stability of the initial equilibrium state may be decided on the basis of the work ΔW that must be done on the layer per unit area in the (x_1, x_3)-plane in order to produce the increments δu_i. This work, which represents the Helmholtz free energy under isothermal conditions and the total energy under adiabatic conditions, may be expanded as $\Delta W = \delta W + \delta^2 W + \ldots$ where δW = first variation (first-order work done by σ^0_{ij} on $\delta u_{i,j}$) and $\delta^2 W$ = second variation (the second-order work). If the initial state is an equilibrium state, δW must vanish. We, therefore, need to calculate only $\delta^2 W$. Using equations (3), (4), and (1), as well as the relation $\delta u^t_{i,2} = -\delta u^u_{i,2}(L-h)/h$ which follows from equation (2), we get

$$\delta^2 W = \frac{h}{2}\,\delta\sigma^t_{2i}\delta u^t_{i,2} + \frac{L-h}{2}\,\delta\sigma^u_{2i}\delta u^u_{i,2}$$

$$= \frac{h}{2}(\delta\sigma^t_{2i} - \delta\sigma^u_{2i})\delta u^t_{i,2} = \frac{h}{2}(D^t_{2ij2}\delta u^t_{j,2} - D^u_{2ij2}\delta u^u_{j,2})\delta u^t_{i,2} \tag{5}$$

$$\delta^2 W = \frac{h}{2}\left(D^t_{2ij2} + \frac{h}{L-h}\,D^u_{2ij2}\right)\delta u^t_{j,2}\delta u^t_{i,2}. \tag{6}$$

We may denote

$$Z_{ij} = D^t_{2ij2} + \frac{h}{L-h}\,D^u_{2ij2} \tag{7}$$

or

$$\mathbf{Z} = [Z_{ij}] = \begin{bmatrix} D^t_{2112}, & D^t_{2122}, & D^t_{2132} \\ D^t_{2212}, & D^t_{2222}, & D^t_{2232} \\ D^t_{2312}, & D^t_{2322}, & D^t_{2332} \end{bmatrix} + \frac{h}{L-h}\begin{bmatrix} D^u_{2112}, & D^u_{2122}, & D^u_{2132} \\ D^u_{2212}, & D^u_{2222}, & D^u_{2232} \\ D^u_{2312}, & D^u_{2322}, & D^u_{2332} \end{bmatrix} \tag{8}$$

Matrix $\mathbf{Z}$ is symmetric ($Z_{ij} = Z_{ji}$) if and only if $D^t_{2ij2} = D^t_{2ji2}$ and $D^u_{2ij2} = D^u_{2ji2}$. This is assured if D^t_{kijm} as well as D^u_{kijm} has a symmetric matrix. Our derivation, however, is valid in general for nonsymmetric Z_{ij} or D^t_{kijm}. The necessary stability condition may be stated according to equation (6) as follows

$$\delta^2 W = \frac{h}{2}\,\delta u^t_{i,2}Z_{ij}\delta u^t_{j,2} > 0 \text{ for any } \delta u^t_{i,2}. \tag{9}$$

The expression in equation (9) is a quadratic form. If $\delta^2 W$ is positive for all possible variations $\delta u^t_{i,2}$, no change of the initial state can occur if no work is done on the body, and so the initial state of uniform strain is stable. On the other hand, if $\delta^2 W$ is negative for some variation $\delta u^t_{i,2}$, the change of the initial state releases energy, which is ultimately dissipated as heat, thus increasing the entropy S of the system by $\Delta S = -\delta^2 W/T$ where T = absolute temperature. Hence, due to the second law of thermodynamics, such a change of initial state must happen spontaneously. Therefore, we must conclude that the intial state of homogeneous strain is unstable if $\delta^2 W$ (or Z_{ij}) ceases to be positive-definite. Positive-definiteness of the 3×3 matrix Z_{ij} is a necessary condition of stability. (We cannot claim equation (9) to be sufficient for stability since we have not analyzed all possible localization modes. However, changing $>$ to $<$ yields a sufficient condition for instability.)

Positive-definiteness of the 6×6 matrix $\mathbf{Z}^* = \mathbf{D}_t + \mathbf{D}_u h/(L-h)$ (where $\mathbf{D}_t$ and $\mathbf{D}_u$ are the 6×6 matrices of incremental moduli for loading and unloading) implies stability. However, the body can be stable even if $\mathbf{Z}^*$ is not positive-definite.

If the softening band is infinitely thin ($h/L \to 0$), or the layer is infinitely thick ($L/h \to \infty$), we have $Z_{ij} = D^t_{2ij2}$, and so matrix $\mathbf{Z}$ loses positive-definiteness when the (3×3) matrix of D^t_{2i2} ceases to be positive-definite. This condition, whose special case for von Mises plasticity was obtained by Rudnicki and Rice (1975) and Rice (1976), indicates that instability may occur right at the peak of the stress-strain diagram. However, for a continuum approximation of a heterogeneous material, for which h must be finite, the loss of stability can occur only after the strain undergoes a finite increment beyond the peak of the stress-strain diagram. For $L \to h$, the softening band is always stable.

Strain-localization instability in a uniaxially stressed bar represents a one-dimensional problem. It also may be obtained from the present three-dimensional solution as the special case for which the softening material is incrementally orthotropic, with $D^t_{2222} = \mathrm{E}_t$ (< 0) and $D^u_{2222} = \mathrm{E}_u$ (> 0) as the only nonzero incremental moduli. Equations (7) and (9) then yield the stability condition presented in 1974 (Bažant, 1976)

$$-\frac{\mathrm{E}_t}{\mathrm{E}_u} < \frac{h}{L-h} \quad \text{or} \quad \frac{\mathrm{E}_t}{h} + \frac{\mathrm{E}_u}{L-h} > 0. \tag{10}$$

This simple condition clearly illustrates that for finite L/h the localization instability can occur only at a finite slope $|\mathrm{E}_t|$, i.e., some finite distance beyond the peak of the stress-strain diagram.

If the end of the bar at $x = L$ is not fixed but has an elastic support with spring constant C_s, one may obtain the solution by imagining the bar length to be augmented to length L', the additional length L' having the same stiffness as the spring; i.e., $L' - L = C_s/\mathrm{E}_u$. Therefore, the stability condition is $-\mathrm{E}_t/\mathrm{E}_u < h/(L'-h)$, which yields the condition given before (Bažant, 1976).

The stability condition for a layer whose surface points are supported by an elastic foundation (Fig. 3) may be treated similarly, i.e., by adding to the layer of thickness L another layer of thickness $L' - L$ such that its stiffness is equivalent to the given foundation modulus.

The case when the outer surfaces of the layer are kept at

Downloaded 03 May 2010 to 171.66.16.21. Redistribution subject to ASME license or copyright; see http://www.asme.org/terms/Terms_Use.cfm

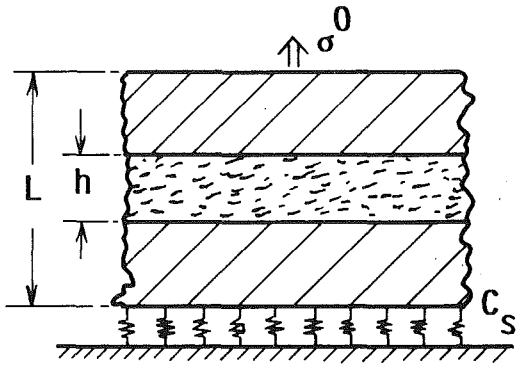


Fig. 3 Layer with localization band and an elastic foundation

constant load $p_i^0 = \sigma_{ij}^0 n_j$ during localization is equivalent to adding a layer of inifinite thickness $L' - L$. Therefore, the necessary stability condition is that the 3×3 matrix of D_{2ij2}^t be positive-definite, i.e., no softening can occur.

Another simple type of localization may be caused by softening in pure shear, Fig. 2(*c*). In this case, $\delta u_{1,2} \neq 0$, $\delta u_{2,2} = \delta u_{3,2} = 0$, and $D_{2112}^t = G_t$, $D_{2112}^u = G_u$ are the shear moduli. According to equations (7) and (9), the necessary stability condition is

$$-\frac{G_t}{G_u} < \frac{h}{L-h}. \tag{11}$$

Consider now the limiting case of an infinite space. While in a layer an infinitely long softening band must be parallel to the layer surface, for an infinite space, the softening band can have any orientation. Since $L \to \infty$, we have $Z_{ij} = D_{2ij2}^t$, and if the band is normal to axis x_2, stability requires that $\delta^2 W = \delta u_{i,2}^t D_{2ij2}^t \delta u_{j,2}^t h/2 =$ positive-definite. To generalize this condition to a band of arbitrary orientation, we may carry out an arbitrary rotation transformation of coordinates from x_i to x_i'. The transformation relations are $x_i = c_{ij} x_j'$ where c_{ij} are the direction cosines of the old coordinate base vectors in the new coordinates. According to the rules of transformation of tensors, we now have $2\delta^2 W = h(c_{ik} c_{2m} \delta u_{k,m}')\ (c_{2p} c_{iq} c_{jr} c_{2s} D_{pqrs}')\ (c_{ju} c_{2v} \delta u_{u,v}')$ where the primes refer to the new coordinates x_j'. Noting that $c_{ik} c_{iq} = \delta_{kq}$, $c_{jr} c_{ju} = \delta_{ru}$, we obtain

$$2\delta^2 W = h \delta a_{pq} D_{pqsr}'' \delta a_{sr} \quad \text{with} \quad \delta a_{pq} = c_{2p} \delta u_{q,m} c_{2m}. \tag{12}$$

For arbitrary rotations, δa_{pq} can have any values. Thus the 6×6 matrix of moduli D_{pqsr}'', and also D_{ijkm}^t, must be positive-definite in order to insure that the strain cannot localize into an infinite planar band of any orientation. The same requirement was stated by Hadamard (1903), who derived it from the condition that the wave speed would not become imaginary. Hadamard's analysis, however, implied that $\mathbf{D}^u = \mathbf{D}^t$.

Finally, consider another case of boundary conditions: The case when the plane surfaces of an infinite layer slide freely over rigid bodies during the localization. The boundary conditions at $x_2 = 0$ and $x_2 = L$ now are $\delta\sigma_{21} = \delta\sigma_{23} = 0$. Similar to equation (6), we now have

$$\delta^2 W = \frac{h}{2}\left(D_{2222}^t + \frac{h}{L-h} D_{2222}^u\right)\delta u_{2,2}^t \delta u_{2,2}^t + \tfrac{1}{2}(\delta N_{11}\delta u_{1,1} + \delta N_{33}\delta u_{3,3} + 2\delta N_{13}\delta u_{1,3}) \tag{13}$$

in which δN_{11}, δN_{33}, δN_{13} are homogeneously distributed in-plane incremental normal and shear force resultants over the whole thickness of the layer. Overall equilibrium now requires that $\delta N_{11} = \delta N_{33} = \delta N_{13} = 0$. Hence, the necessary condition of stability against localization is

$$D_{2222}^t + \frac{h}{L-h} D_{2222}^u > 0. \tag{14}$$

Extension to Geometrically Nonlinear Effects in Finite Strain

Strain localization in an infinite planar band can be also easily solved even when the geometrically nonlinear effects are taken into account. The geometrical nonlinearity we consider is due to finite strains or finite rotations, not to changes in the geometrical configuration of the structure. The deviations δu_i and $\delta\epsilon_{ij}$ from the initial state, characterized by homogeneous stresses σ_{ij}^0, are again considered to be infinitely small, and the energy expression ΔW that governs stability is second-order small. However, the contribution to $\delta^2 W$, which arises from the geometrically nonlinear finite-strain expression, is also second-order small, and so it must be included. This may be done if the material stress increment $\delta\sigma_{ij}$ in the work expression is replaced by the mixed (first) Piola-Kirchhoff stress increment $\delta\tau_{ij}$, which is referred to the initial state and is nonsymmetric (Malvern, 1969). As is well known, $\delta\tau_{ij} = \delta T_{ij} - \sigma_{ik}^0 \delta u_{j,k} + \sigma_{ij}^0 \delta u_{k,k}$ where δT_{ij} = material increment of the true (Cauchy) stress. Since neither $\delta\sigma_{ij}$ nor $\delta\tau_{ij}$ is invariant at coordinate rotations, one must use in the incremental stress-strain relation the objective stress increment $\delta\sigma_{ij}$ (representing the objective stress rate times the increment of time); $\delta\sigma_{ij}$ is symmetric.

The relationship between $\delta\sigma_{ij}$ and $\delta\tau_{ij}$ may be written (Bažant, 1971) in the general form

$$\delta\tau_{ij} = \delta\sigma_{ij} + R_{ij\,km\,rs}\sigma_{rs}^0 \delta u_{k,m} = H_{ijkm}\delta u_{k,m} \tag{15}$$

$$H_{ijkm} = D_{ijkm} + R_{ij\,km\,rs}\sigma_{rs}^0 \tag{16}$$

where we substituted $\delta\sigma_{ij} = D_{ijkm}\delta u_{k,m}$. Coefficients $R_{ij\,pq\,rs}$ are certain constants which take into account the geometrical nonlinearity of finite strain. The values of $R_{ij\,km\,pq}$ are different for various possible choices of the objective stress rate and the associated type of the finite-strain tensor. The expressions which are admissible according to the requirements of tensorial invariance and objectivity are (Bažant 1971)

$$R_{ij\,pq\,rs}\sigma_{rs}^0 = \delta_{ip}\sigma_{qj}^0 - \alpha(\delta_{ip}\sigma_{qj}^0 + \delta_{iq}\sigma_{pj}^0 + \delta_{jp}\sigma_{qi}^0 + \delta_{jq}\sigma_{pi}^0) \tag{17}$$

where α can be an arbitrary constant. The case $\alpha = 0$ corresponds to Truesdell's objective stress rate and Green's (Lagrangian) finite-strain tensor; the case $\alpha = 1/4$ to the finite-strain theory of Biot; the case $\alpha = 1/2$ to the Jaumann's objective stress rate and the finite strain theory of Southwell, Biezeno-Hencky, and Neuber (and to the logarithmic strain); and the case $\alpha = 3/4$ to Cotter-Rivlin's convected stress rate (see, equations (14*a*), (15), (17*a*), and (22) in Bažant, 1971). In general, α can be any real number. For each different α-value, however, different values of incremental moduli D_{ijpq} must be used so as to obtain physically equivalent results; generally [cf. Bažant, 1971, equation (19)]

$$D_{ijpq} = [D_{ijpq}]_{\alpha=0} + \alpha(\delta_{ip}\sigma_{qj}^0 + \delta_{iq}\sigma_{pj}^0 + \delta_{jp}\sigma_{qi}^0 + \delta_{jq}\sigma_{pi}^0). \tag{18}$$

From equation (5), in which $\delta\sigma_{ij}$ must now be replaced by $\delta\tau_{ij}$, the necessary stability condition is

$$\begin{aligned} 2\delta^2 W &= h\delta\tau_{2i}^t \delta u_{i,2}^t + (L-h)\delta\tau_{2i}^u \delta u_{i,2}^u \\ &= h(\delta\tau_{2i}^t - \delta\tau_{2i}^u)u_{i,2}^t = h(H_{2ij2}^t \delta u_{j,2}^t - H_{2ij2}^u \delta u_{j,2}^u)\delta u_{i,2}^t \\ &= h\delta u_{i,2}^t Z_{ij}\delta u_{j,2}^t > 0 \quad \text{for any } \delta u_{i,2}^t \end{aligned} \tag{19}$$

in which

$$\begin{aligned} Z_{ij} &= H_{2ij2}^t + \frac{h}{L-h} H_{2ij2}^u \\ &= D_{2ij2}^t + \frac{h}{L-h} D_{2ij2}^u + \frac{L}{L-h} R_{2ij2rs}\sigma_{rs}^0. \end{aligned} \tag{20}$$

In particular, if we use the Lagrangian (Green's) finite strain

Downloaded 03 May 2010 to 171.66.16.21. Redistribution subject to ASME license or copyright; see http://www.asme.org/terms/Terms_Use.cfm

which is associated with Truesdell's objective stress rate (α = 0), we have

$$Z_{ij} = \left[D^t_{2ij2} + \frac{h}{L-h} D^u_{2ij2}\right]_{\alpha=0} + \frac{L}{L-h} \sigma^0_{i2}\delta_{2j}. \quad (21)$$

If we use Jaumann's objective stress rate (α = 1/2), we have

$$Z_{ij} = \left[D^t_{2ij2} + \frac{h}{L-h} D^u_{2ij2}\right]_{\alpha=1/2} + \frac{L}{2(L-h)}(\sigma^0_{i2}\delta_{2j} - \sigma^0_{j2}\delta_{2i} - \sigma^0_{22}\delta_{ij} - \sigma^0_{ij}). \quad (22)$$

It must be emphasized that the conditions of positive-definiteness of matrix $[Z_{ij}]$ for various possible values of α are all physically equivalent [even though for each different α-value the incremental moduli D^t_{2ij2} and D^u_{2ij2} are different, as dictated by equation (18)]. This fact often has been forgotten. The use of various types of objective stress rates often has been discussed in the literature on the basis of some imagined numerical convenience, and the fact that the incremental moduli cannot be the same for different objective stress rates has been overlooked (despite the analysis in Bažant, 1971). These practices, widespread in the finite-element literature, are of course incorrect.

As for the identification of the incremental moduli from test data, it can be done only in reference to a certain chosen objective stress rate. Different values of the moduli must result for different choices although the results are equivalent physically (see, Bažant, 1971).

The condition det $[Z_{ij}] = 0$ obviously represents the critical state. The special case of this condition for which the constitutive law consists of von Mises plasticity enhanced by vertex hardening, $L/h \to \infty$ (infinite space), $\alpha = 1/2$ (Jaumann's rate), and the initial stress σ^0_{ij} is pure shear σ^0_{12}, was derived by Rudnicki and Rice (1975). Their analysis was concerned only with the critical state of neutral equilibrium, rather than with stability. The values of the unloading moduli D^u_{ijkm} and the fact that they are different from D^t_{ijkm} and positive-definite were irrelevant for their analysis.

Rudnicki and Rice (1975) showed that, due to geometrical nonlinearity, the critical state of strain localization can develop in plastic materials while the matrix of D^t_{ijkm} is still positive-definite, i.e., before the final yield plateau of the stress-strain diagram is reached. This may explain the formation of shear bands in plastic (nonsoftening) materials. The destabilizing effect is then due exclusively to geometrical nonlinearity. According to a geometrically linear analysis (small strain theory), strain localization could develop in plastic (nonsoftening) materials only upon reaching the yield plateau but not earlier.

From equation (20), it appears that the geometrical nonlinearity can have a significant effect on strain localization only if the incremental moduli for loading are of the same order of magnitude as the initial stresses σ^0_{ij}; precisely, if max $|D^t_{ijkm}|$ and max $|\sigma^0_{ij}|$ are of the same order of magnitude. (The unloading moduli D^u_{ijkm} of structural materials are always several orders of magnitude larger.) Thus the importance of geometrical nonlinearity depends on D^t_{ijkm}. For strain-softening type of localization, the geometrical nonlinearity can be important only if the instability develops at a very small negative slope of the stress-strain diagram, which occurs very close to the peak stress point. This can occur only if the layer thickness L is much larger than l. If $L - h \ll l$, instability occurs when the downward slope of the stress-strain diagram (Fig. 2) is of the same order of magnitude as the initial elastic modulus E, and this is inevitably orders of magnitude larger than the initial stresses σ^0_{ij}.

Therefore, we must conclude that the role of geometrical nonlinearity in localization due to strain-softening cannot be significant except if the localization occurs immediately after the peak point of the stress-strain diagram (Fig. 2). Then the values of the strains at localization instability obtained by geometrically nonlinear and linear analyses cannot differ significantly since they must both be close to the peak point of the stress-strain diagram. For the postcritical large deformations, however, geometrical nonlinearity is no doubt always important.

Conclusions

The condition of stability of a layer against localization of strain into a band reduces to the condition of positive-definiteness of a certain matrix which represents a weighted average of the matrices of loading and unloading moduli of the material. The weight of the loading (softening) moduli increases with the ratio of the band thickness to the layer thickness. If this ratio tends to zero (infinite space), the instability is determined solely by the loading moduli and occurs as soon as this matrix ceases to be positive-definite. When the band thickness is finite, instability does not occur until the initial strain exceeds the strain at peak stress by a finite amount. Geometrical nonlinearity of strain has a significant effect only for a very small band-to-layer thickness ratio, and unstable localization then occurs near the peak stress state.

Extension to localization that is not unidirectional and numerical examples are relegated to a subsequent companion paper.

Acknowledgment

Partial financial support under AFOSR Contract F49620-87-C-0030DEF with Northwestern University, monitored by Dr. Spencer T. Wu, is gratefully acknowledged.

References

Bažant, Z. P., 1971, "A Correlation Study of Formulations of Incremental Deformation and Stability of Continuous Bodies," ASME JOURNAL OF APPLIED MECHANICS, Vol. 38, No. 4, pp. 919–928.

Bažant, Z. P., 1976, "Instability, Ductility and Size Effect in Strain-Softening Concrete," *Journal of Engineering Mechanics*, ASCE, Vol. 102, pp. 331–344; Discussions, Vol. 103, pp. 357–358, 775–777, Vol. 104, pp. 501–502; based on Structural Engineering Report No. 74-8/640, Northwestern University, Aug. 1974, and private communication to K. Gerstle, S. Sture, and A. Ingraffea, in Boulder, CO, June 1974.

Bažant, Z. P., 1982, "Crack Band Model for Fracture of Geomaterials," *Proceedings of the 4th International Conference on Numerical Methods in Geomechanics*, Edmonton, AB, Canada, June, Z. Eisenstein, ed., Vol. 3, (invited lectures), pp. 1137–1152.

Bažant, Z. P., 1984, "Mechanics of Fracture and Progressive Cracking in Concrete Structures," in *Fracture Mechanics Applied to Concrete Structures*, Sih, G. C., and DiTomasso, A., eds., Martinus Nijhoff, The Hague, pp. 1–94.

Bažant, Z. P., 1986, "Mechanics of Distributed Cracking," *Applied Mechanics Reviews*, Vol. 39, pp. 675–705.

Bažant, Z. P., 1987, "Why Continuum Damage is Nonlocal: Justification by Quasi-Periodic Microcrack Array," *Mechanics Research Communications*, Vol. 14, (5/6), pp. 407–420.

Bažant, Z. P., Belytschko, T. B., and Chang, T.-P., 1984, "Continuum Theory for Strain Softening," *Journal of Engineering Mechanics*, Vol. 110, pp. 1666–1692.

Bažant, Z. P., and Belytschko, T. B., 1985, "Wave Propagation in a Strain-Softening Bar: Exact Solution," *Journal of Engineering Mechanics*, ASCE, Vol. 111 (3).

Bažant, Z. P., and Belytschko, T. B., 1987, "Strain-Softening Continuum Damage: Localization and Size Effect," Preprints, International Conference on Constitutive Laws for Engineering Materials, Vol. 1, held in Tucson, AZ, Jan. 1987, ed. by C. S. Desai et al., University of Arizona, Elsevier, New York, pp. 11–33.

Bažant, Z. P., and Cedolin, L., 1979, "Blunt Crack Band Propagation in Finite Element Analysis," *Journal of Engineering Mechanics*, ASCE, Vol. 105, (2), pp. 297–315.

Bažant, Z. P., and Cedolin, L., 1980, "Fracture Mechanics of Reinforced Concrete," *Journal of Engineering Mechanics*, ASCE, Vol. 106, (6), pp. 1287–1306; Discussion, Vol. 108, 1982, pp. 464–471.

Bažant, Z. P., Lin, F.-B., and Pijaudier-Cabot, G., 1987, "Yield Limit Degradation: Nonlocal Continuum Model With Local Strain," Preprints, International Conference on Computational Plasticity, held in Barcelona, Apr. 1987,

Downloaded 03 May 2010 to 171.66.16.21. Redistribution subject to ASME license or copyright; see http://www.asme.org/terms/Terms_Use.cfm

R. Owen, and E. Hinton, (U. of Wales, Swansea) and E. Oñate, (Techn. U. Barcelona), eds.

Bažant, Z. P., and Oh, B. H., 1983, "Crack Band Theory for Fracture of Concrete," *Materiaux et Constructions* (Rilem, Paris), Vol. 16, (93), pp. 155–177.

Bažant, Z. P., and Oh, B. H., 1984, "Rock Fracture via Softening Finite Elements," *Journal of Engineering Mechanics*, ASCE, Vol. 110, (7), pp. 1015–1035.

Bažant, Z. P., and Panula, L., 1978, "Statistical Stability Effects in Concrete Failure," *Journal of Engineering Mechanics*, ASCE, Vol. 104, (5), pp. 1195–1212.

Bažant, Z. P., Pijaudier-Cabot, G., and Pan, J., 1986, "Strain Softening Beams and Frames," Report, Center for Concrete and Geomaterials, Northwestern University.

Bažant, Z. P., and Pijaudier-Cabot, G., 1987, "Nonlocal Damage: Continuum Model and Localization Instability," Report No. 87-2/498n, Center for Concrete and Geomaterials, Northwestern University.

Bažant, Z. P., and Zubelewicz, A., 1986, "Strain-Softening Bar and Beam: Exact Nonlocal Solution," *International Journal of Solids and Structures*, in press.

Belytschko, T., Bažant, Z. P., Hyun, Y.-W., and Chang, T.-P., 1986, "Strain-Softening Materials and Finite Element Solutions," *Computers and Structures*, Vol. 23, (2), pp. 163–180.

Floegl, H., and Mang, H. A., 1981, "On Tension Stiffening in Cracked Reinforced Concrete Slabs and Shells Considering Geometric and Physical Nonlinearity," *Ingenieur-Archiv*, Vol. 51, pp. 215–242.

Hadamard, J., 1903, *Lecons sur la propagation des ondes*, Hermann, Paris. Chapter VI.

Joseph, D. D., Renardy, M., and Saut, J.-C., 1985, "Hyperbolicity and Change of Type in the Flow of Viscoelastic Fluids," *Archive for Rational Mechanics and Analysis*, Vol. 87, (3), pp. 213–251.

Joseph, D. D., 1986, "Change of Type and Loss of Evolution in the Flow of Viscoelastic Fluids," *Journal of Non-Newtonian Fluid Mechanics*, Vol. 20, pp. 117–141.

Kröner, E., 1967, "Elasticity Theory of Materials with Long-range Cohesive Forces," *International Journal of Solids and Structures*, Vol. 3, pp. 731–742.

Malvern, L. E., 1969, *Introduction to the Mechanics of a Continuous Medium*, Prentice-Hall, Englewood Cliffs, NJ.

Mang, H., and Eberhardsteiner, J., 1985, "Collapse Analysis of Thin R.C. Shells on the Basis of a New Fracture Criterion," U.S.-Japan Seminar on the Finite Element Analysis of Reinforced Concrete Structures, Preprints, pp. 217–238 (and *Proceedings, ASCE*, New York 1986, C. Meyer, and H. Okamura, eds.

Ottosen, N. S., 1986, "Thermodynamic Consequences of Strain Softening in Tension," *Journal of Engineering Mechanics*, ASCE, Vol. 112 (11), pp. 1152–1164.

Pijaudier-Cabot, G., and Bažant, Z., 1986, "Nonlocal Damage Theory," Report No. 86-8/428n, Center for Concrete and Geomaterials, Northwestern University, Evanston, IL; also ASCE *Journal of Engineering Mechanics*, Vol. 111 (1987) in press.

Read, H. E., and Hegemier, G. P., 1984, "Strain-Softening of Rock, Soil and Concrete," A Review Article, *Mechanics of Materials*, Vol. 3, (4), pp. 271–294.

Rice, J. R., 1976, "The Localization of Plastic Deformation," Preprints, 14th International Congress of International Union of Theoretical and Applied Mechanics held in Delft, Netherlands, W. Koiter, ed., North Holland, Amsterdam.

Rudnicki, J. W., and Rice, J. R., 1975, "Conditions for the Localization of Deformation in Pressure Sensitive Dilatant Materials," *Journal of the Mechanics and Physics of Solids*, Vol. 23, pp. 371–394.

Rudnicki, J. W., 1977, "The Inception of Faulting in a Rock Mass With a Weakened Zone," *Journal of Geophysical Research*, Vol. 82, No. 5, pp. 844–854.

Sandler, I. S., 1984, "Strain-Softening for Static and Dynamic Problems," *Proceedings, Symposium on Constitutive Equations: Micro, Macro and Computational Aspects*, ASME Winter Annual Meeting held in New Orleans, Dec., K. William, ed., ASME, New York, pp. 217–231.

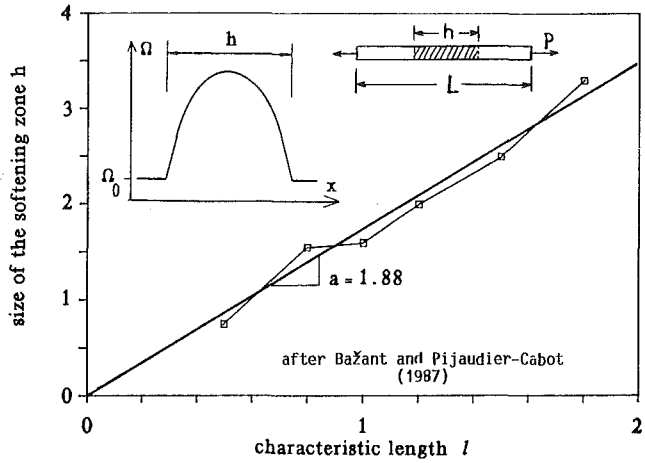


Fig. 4 Comparison of approximate local solution based on prescribed softening segment length h (dashed lines) with the exact nonlocal solution (solid lines), obtained for a bar of length L by Bažant and Pijaudier-Cabot (1987)

Schreyer, H. L., and Chen, Z., 1986, "One-Dimensional Softening With Localization," ASME JOURNAL OF APPLIED MECHANICS, Vol. 53, No. 4, pp. 791–797.

Triantafyllidis, N., and Aifantis, E. C., 1986, "A Gradient Approach to Localization of Deformation, I: Hyperelastic Materials," *Journal of Elasticity*, Vol. 16, pp. 225–237.

Yoo, J. Y., Ahrens, M., and Joseph, D. D., 1985, "Hyperbolicity and Change of Type in Sink Flow," *Journal of Fluid Mechanics*, Vol. 171, pp. 203–214.

APPENDIX

In the crack band model, the minimum possible size h of the softening zone in a local continuum is considered to be a material constant. The degree to which this approach can capture nonlocal behavior is illustrated by the comparison in Fig. 4, taken from Bažant and Pijaudier-Cabot (1987). The data points show the length h of the strain-softening segment in a bar of length $L > h$, made of a nonlocal strain-softening material with characteristic length l. Nonlocal is only the fracturing (or damage) strain while the elastic strain, including unloading, is local. The results represent accurate solutions of an integral equation for the static uniaxial localization instability in a bar that is initially strained uniformly, with a strain in the strain-softening range. In contrast to the present analysis, the length h of the localization segment is unknown and is solved as a function of the assumed characteristic length l. The results show that approximately $h = a$ where $a \approx$ constant ($a \approx 1.88$). Since l is a material constant, h may also be approximately considered to be a constant, as assumed in the crack band model.

Downloaded 03 May 2010 to 171.66.16.21. Redistribution subject to ASME license or copyright; see http://www.asme.org/terms/Terms_Use.cfm

Softening Instability: Part II—Localization Into Ellipsoidal Regions

Zdeněk P. Bažant
Professor,
Department of Civil Engineering,
Northwestern University,
Evanston, IL 60208
Mem. ASME

Extending the preceding study of exact solutions for finite-size strain-softening regions in layers and infinite space, exact solution of localization instability is obtained for the localization of strain into an ellipsoidal region in an infinite solid. The solution exploits Eshelby's theorem for eigenstrains in elliptical inclusions in an infinite elastic solid. The special cases of localization of strain into a spherical region in three dimensions and into a circular region in two dimensions are further solved for finite solids—spheres in 3D and circles in 2D. The solutions show that even if the body is infinite the localization into finite regions of such shapes cannot take place at the start of strain-softening (a state corresponding to the peak of the stress-strain diagram) but at a finite strain-softening slope. If the size of the body relative to the size of the softening region is decreased and the boundary is restrained, homogeneous strain-softening remains stable into a larger strain. The results also can be used as checks for finite element programs for strain-softening. The present solutions determine only stability of equilibration states but not bifurcations of the equilibrium path.

Introduction

The strain-localization solutions in the preceding paper (Bažant, 1987) deal with unidirectional localization of strain into an infinite planar band. If the body is finite, localization into such a band does not represent an exact solution because the boundary conditions cannot be satisfied. In this paper, we will seek exact solutions for multidirectional localization due to strain-softening in finite regions. In particular, we will study localization into ellipsoidal regions, including the special cases of a spherical region in three dimensions and a circular region in two dimensions. All definitions and notations from the preceding paper (Bažant, 1987, Part I) are retained.

Softening Ellipsoidal Region in Infinite Solid

This type of strain-localization instability can be solved by application of Eshelby's (1957) theorem for ellipsoidal inclusions with uniform eigenstrain. Consider an ellipsoidal hole, Fig. 1(*a*), in a homogeneous infinite medium that is elastic and is characterized by elastic moduli matrix $\mathbf{D}_u$. We imagine fitting and glueing into this hole an ellipsoidal plug of the same material, Fig. 1(*a*), which must first be deformed by uniform strain ϵ^0 (the eigenstrain) in order to fit into the hole perfectly (note that a uniform strain changes an ellipsoid into another ellipsoid). Then the strain in the plug is unfrozen, which causes the plug to deform with the surrounding medium to attain a new equilibrium state. The famous discovery of Eshelby (1957) was that if the plug is ellipsoidal and the elastic medium is homogeneous and infinite, the strain increment ϵ^e in the plug which occurs during this deformation is *uniform* and is expressed as

$$\epsilon^e_{ij} = S_{ijkm}\epsilon^0_{km}. \tag{1}$$

S_{ijkm} are components of a fourth-rank tensor which depend only on the ratios a_1/a_3 and a_2/a_3 of the principal axes of the ellipsoid and, and for the special case of isotropic materials, on Poisson ratio ν_u; see, e.g., Mura (1982) and Christensen (1979). Due to symmetry of ϵ^0_{ij} and ϵ^e_{ij}, $S_{ijkm} = S_{jikm} = S_{ijmk}$, but in general $S_{ijkm} \neq S_{kmij}$. Coefficients S_{ijkm} are, in general, expressed by elliptic integrals; see also Mura (1982). Extension of Eshelby's theorem to generally anisotropic materials was later accomplished at Northwestern University by Kinoshita and Mura (1971) and Lin and Mura (1973).

It will be convenient to rewrite equation (1) in a matrix form

$$\boldsymbol{\epsilon}^e = \mathbf{Q}_u\boldsymbol{\epsilon}^0 \tag{2}$$

or

Contributed by the Applied Mechanics Division for presentation at the Winter Annual Meeting, Chicago, IL, November 28 to December 2, 1988, of The American Society of Mechanical Engineers.
Discussion on this paper should be addressed to the Editorial Department, ASME, United Engineering Center, 345 East 47th Street, New York, N.Y. 10017, and will be accepted until two months after final publication of the paper itself in the Journal of Applied Mechanics. Manuscript received by ASME Applied Mechanics Division, March 13, 1987; revision, February 1, 1988.
Paper No. 88-WA/APM-35.

Copyright © 1988 by ASME
Downloaded 03 May 2010 to 171.66.16.21. Redistribution subject to ASME license or copyright; see http://www.asme.org/terms/Terms_Use.cfm

$$\begin{Bmatrix} \epsilon^e_{11} \\ \epsilon^e_{22} \\ \epsilon^e_{33} \\ 2\epsilon^e_{12} \\ 2\epsilon^e_{23} \\ 2\epsilon^e_{31} \end{Bmatrix} = \left[\begin{array}{ccc:ccc} S_{1111} & S_{1122} & S_{1133} & S_{1112} & S_{1123} & S_{1131} \\ S_{2211} & S_{2222} & S_{2233} & S_{2212} & S_{2223} & S_{2231} \\ S_{3311} & S_{3322} & S_{3333} & S_{3312} & S_{3323} & S_{3331} \\ \hdashline 2S_{1211} & 2S_{1222} & 2S_{1233} & 2S_{1212} & 2S_{1223} & 2S_{1231} \\ 2S_{2311} & 2S_{2322} & 2S_{2333} & 2S_{2312} & 2S_{2323} & 2S_{2331} \\ 2S_{3111} & 2S_{3122} & 2S_{3133} & 2S_{3112} & 2S_{3123} & 2S_{3131} \end{array}\right] \begin{Bmatrix} \epsilon^0_{11} \\ \epsilon^0_{22} \\ \epsilon^0_{33} \\ 2\epsilon^0_{12} \\ 2\epsilon^0_{23} \\ 2\epsilon^0_{31} \end{Bmatrix} \tag{3}$$

in which $\epsilon = (\epsilon_{11}, \epsilon_{22}, \epsilon_{33}, 2\epsilon_{12}, 2\epsilon_{23}, 2\epsilon_{31})^T$ and superscript T denotes the transpose of a matrix.

For isotropic materials, the only nonzero elements of matrix $\mathbf{Q}$ are those between the dashed lines marked in equation (3), which is the same as for the stiffness matrix. The factors 2 in matrix $\mathbf{Q}_u$ in equation (3) are due to the fact that the column matrix of strains is (6×1) rather than (9×1) and, therefore, must involve shear angles $2\epsilon_{12}$, $2\epsilon_{23}$ and $2\epsilon_{31}$ rather than tensorial shear strain components ϵ_{12},ϵ_{23} and ϵ_{31}, or else $\boldsymbol{\sigma}^T\delta\boldsymbol{\epsilon}$ where $\boldsymbol{\sigma}^T = (\sigma_{11}, \sigma_{22}, \sigma_{33}, \sigma_{12}, \sigma_{23}, \sigma_{31})$ would not be a correct work expression. (The work expression $\sigma_{ij}\delta\epsilon_{ij}$, as well as the sum implied in equation (1) for each fixed i,j, has 9 terms in the sum, not 6.) For example, writing out the terms of equation (1) we have

$$\epsilon^e_{11} = \ldots + (S_{1112}\epsilon^0_{12} + S_{1121}\epsilon^0_{21}) + \ldots = \ldots + S_{1112}(2\epsilon^0_{12}) + \ldots \tag{4}$$

while the factors 2 arise as follows

$$\begin{aligned} 2\epsilon^e_{12} &= 2[\ldots + S_{1233}\epsilon^0_{33} + (S_{1112}\epsilon^0_{12} + S_{1121}\epsilon^0_{21}) \\ &\quad + (S_{1223}\epsilon^0_{23} + S_{1232}\epsilon^0_{32}) + \ldots] \\ &= \ldots (2S_{1233})\epsilon^0_{33} + (2S_{1212})2\epsilon^0_{12} \\ &\quad + (2S_{1223})2\epsilon^0_{23} + \ldots \end{aligned} \tag{5}$$

The stress in the ellipsoidal plug, $\boldsymbol{\sigma}^e$ (which is uniform), may be expressed according to Hooke's law as

$$\boldsymbol{\sigma}^e = \mathbf{D}_u(\boldsymbol{\epsilon}^e - \boldsymbol{\epsilon}^0). \tag{6}$$

After substituting $\boldsymbol{\epsilon}^0 = \mathbf{Q}_u^{-1}\boldsymbol{\epsilon}^e$, according to equation (2), we get $\boldsymbol{\sigma}^e = \mathbf{D}_u(\boldsymbol{\epsilon}^e - \mathbf{Q}_u^{-1}\boldsymbol{\epsilon}^e)$ or

$$\boldsymbol{\sigma}^e = \mathbf{D}_u(\mathbf{1} - \mathbf{Q}_u^{-1})\boldsymbol{\epsilon}^e \tag{7}$$

where $\mathbf{1}$ is a unit 6×6 matrix. The surface tractions that the ellipsoidal plug exerts upon the surrounding infinite medium, Fig. 1(*a*), are $p^e_i = \sigma^e_{ij}\, n_j$, in which n_j denotes the components of a unit normal $\mathbf{n}$ of the ellipsoidal surface (pointed from the ellipsoid outward).

Consider now infinitesimal variations $\delta\mathbf{u}$, $\delta\boldsymbol{\epsilon}$, $\delta\boldsymbol{\sigma}$ from the initial equilibrium state of uniform strain $\boldsymbol{\epsilon}^0$ in an infinite homogeneous anisotropic solid (without any hole). The matrices of incremental elastic moduli corresponding to $\boldsymbol{\epsilon}^0$ are $\mathbf{D}_l$ for further loading and $\mathbf{D}_u$ for unloading, $\mathbf{D}_u$ being positive-definite. We imagine that the initial equilibrium state is disturbed by applying surface tractions δp_i over the surface of the ellipsoid with axes a_1, a_2, a_3, Fig. 1(*b*). We expect δp_i to produce loading inside the ellipsoid and unloading outside. We try to calculate the displacements δu_i produced by tractions δp_i at all loading points on the ellipsoid surface.

Let $\delta\epsilon^e_{ij}$, δu^e_i be the strain and displacement variations produced (by tractions δp_i) in the ellipsoid, and denote the net tractions acting on the softening ellipsoid as δp^l_i, and those on the rest of the infinite body, i.e., on the exterior of the ellipsoid, as δp^e_i. As for the distributions of δp^l_i and δp^e_i over the ellipsoid surface, we assume them to be such that $\delta p^l_i = \delta\sigma^l_{ij} n_j$ and $\delta p^e_i = \delta\sigma^e_{ij} n_j$ where $\delta\sigma^l_{ij}$ and $\delta\sigma^e_{ij}$ are arbitrary constants; $\delta\sigma^l_{ij}$ is the stress within the softening ellipsoidal region, which is uniform (and represents an equilibrium field), and $\delta\sigma^e_{ij}$ is a fictitious uniform stress in this region which would equilibrate δp^e_i. Stresses $\delta\sigma^e_{ij}$ in reality exist only on the outside of the ellipsoid surface.

Equilibrium requires that $\delta p_i = \delta p^l_i - \delta p^e_i$. The first-order work δW done by σ^0_{ij} must vanish if the initial state is an equilibrium state. The second-order work done by δp_i may be calculated as

$$\begin{aligned} \delta^2 W &= \int_S \frac{1}{2}\delta p_i \delta u^e_i dS \\ &= \frac{1}{2}\int_S \delta p^l_i \delta u^e_i dS - \frac{1}{2}\int_S \delta p^e_i \delta u^e_i dS \\ &= \frac{1}{2}\delta\sigma^l_{ij}\int_S n_j \delta u^e_i dS - \frac{1}{2}\delta\sigma^e_{ij}\int_S n_j \delta u^e_i dS \end{aligned} \tag{8}$$

where S = surface of the softening ellipsoidal region. Note that $\delta\sigma^e_{ij}$ are not the actual stresses in the solid but merely serve the purpose of characterizing the surface tractions δp^e_i. Applying Gauss' integral theorem and exploiting the symmetry of tensors $\delta\sigma^l_{ij}$ and $\delta\sigma^e_{ij}$, we further obtain

$$\begin{aligned} \delta^2 W &= \frac{1}{2}(\delta\sigma^l_{ij} - \delta\sigma^e_{ij})\int_V \delta u^e_{i,j} dV \\ &= \int_V \frac{1}{2}(\delta\sigma^l_{ij} - \delta\sigma^e_{ij})\frac{1}{2}(\delta u^e_{i,j} + \delta u^e_{j,i}) dV \\ &= \int_V \frac{1}{2}(\delta\sigma^l - \delta\sigma^e)^T \delta\epsilon^e dV \end{aligned} \tag{9}$$

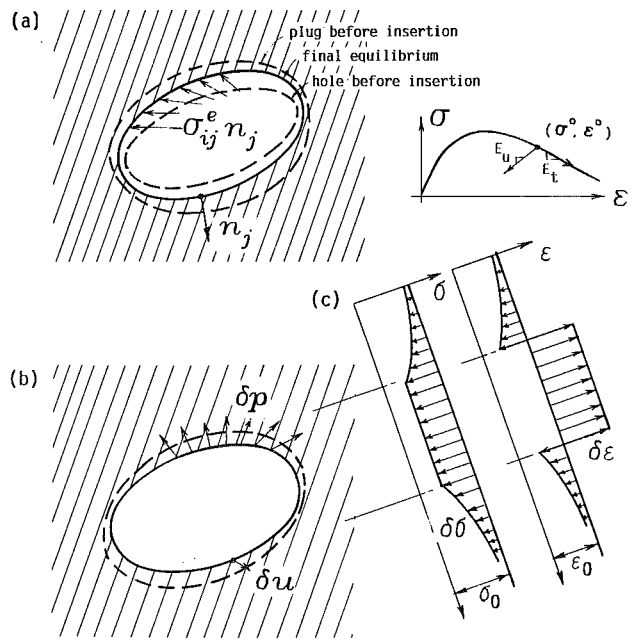


Fig. 1(*a*) Ellipsoidal plug (inclusion) inserted into infinite elastic solid, and (*b*) localization of strain into an elliptic region

Downloaded 03 May 2010 to 171.66.16.21. Redistribution subject to ASME license or copyright; see http://www.asme.org/terms/Terms_Use.cfm

where V = volume of the softening ellipsoidal region, and subscripts preceded by a comma denote partial derivatives. We changed here to matrix notation and also recognized that $\frac{1}{2}(\delta u^e_{i,j} + \delta u^e_{j,i}) = \delta\epsilon^e_{ij}$. Now we may substitute

$$\delta\sigma^t = \mathbf{D}_t \delta\epsilon^e \tag{10}$$

or $\delta\sigma^{t^T} = \delta\epsilon^{e^T}\mathbf{D}_t$ (assuming $\mathbf{D}_t^T = \mathbf{D}_t$). According to equation (7), we also have, as a key step

$$\delta\sigma^e = \mathbf{D}_u(\mathbf{1} - \mathbf{Q}_u^{-1})\delta\epsilon^e. \tag{11}$$

In contrast to our previous consideration of the elastic ellipsoidal plug made of the same elastic material, equations (2)–(7), the sole meaning of $\delta\sigma^e$ now is to characterize the tractions δp_i^e acting on the ellipsoidal surface of the infinite medium lying outside the ellipsoid. Noting that the integrand in equation (9) is constant, we thus obtain

$$\delta^2 W = \frac{1}{2}\delta\epsilon^{e^T}\mathbf{Z}\delta\epsilon^e V = \frac{1}{2}Z_{ijkm}\delta\epsilon^e_{ij}\delta\epsilon^e_{km}V \tag{12}$$

in which $\mathbf{Z}$ denotes the following 6×6 matrix

$$\mathbf{Z} = \mathbf{D}_t + \mathbf{D}_u(\mathbf{Q}_u^{-1} - \mathbf{1}). \tag{13}$$

Equation (12) defines a quadratic form. If the initial uniform strain ϵ^0 is such that the associated $\mathbf{D}_t$ and $\mathbf{D}_u$ give $\delta^2 W > 0$ for all possible $\delta\epsilon^e_{ij}$, then no localization in an ellipsoidal region can begin from the initial state of uniform strain ϵ^0 spontaneously, i.e., without applying loads δp. If, however, $\delta^2 W$ is negative for some $\delta\epsilon^e_{ij}$, the localization leads to a release of energy which is first manifested as a kinetic energy and is ultimately dissipated as heat. Such a localization obviously increases entropy of the system, and so it will occur, as required by the second law of thermodynamics. Therefore, the necessary condition of stability of a uniform strain field in an infinite solid is that matrix $\mathbf{Z}$ given by equation (13) must be *positive-definite*.

The expressions for Eshelby's coefficients S_{ijkm} from which matrix $\mathbf{Q}_u$ is formed (see, e.g., Mura, 1982) depend on the ratios a_1/a_3, a_2/a_3 of the axes of the ellipsoidal localization region. They also depend on the ratios of the unloading moduli D^u_{ijkm}. If, e.g., the unloading behavior is assumed to be isotropic, they depend on the unloading Poisson ratio ν_u. Matrix $\mathbf{D}_u$ is determined by ν_u and unloading Young's modulus E_u. If, just for the sake of illustration, the loading behavior is assumed to be also isotropic, matrix $\mathbf{D}_t$ is determined by ν_t and E_t (Poisson's ratio and Young's modulus for loading). E_t, ν_t, E_u, ν_u, in turn, depend on the strain ϵ^0_{ij} at the start of localization. Since a division of $\mathbf{Z}$ by E_u does not affect positive-definiteness, only the ratio $\mathrm{E}_t/\mathrm{E}_u$ matters. Thus, $\mathbf{Z}$ is a function of the form

$$\mathbf{Z} = \mathrm{E}_u\hat{\mathbf{Z}}\left(\frac{a_1}{a_3}, \frac{a_2}{a_3}, \nu_u, \nu_t, \frac{\mathrm{E}_t}{\mathrm{E}_u}\right)$$

$$= \mathrm{E}_u\bar{\mathbf{Z}}\left(\frac{a_1}{a_3}, \frac{a_2}{a_3}, \epsilon^0_{ij}\right) \tag{14}$$

where $\hat{\mathbf{Z}}$ and $\bar{\mathbf{Z}}$ are nondimensional matrix functions.

Note that matrix $\mathbf{Z}$, which decides the localization instability, is independent of the size of the ellipsoidal localization region. This is the same conclusion as already made for a planar localization band in an infinite solid. No doubt, the size of the localization ellipsoid would matter for finite-size solids, same as it does for localization bands in layers.

The previously obtained solution for a planar localization band in an infinite solid must be a special case of the present solution for an ellipsoid. Localization in line cracks also must be obtained as a special case for $a_3 \to \infty$; however, the present solution is not realistic for this case since energy dissipation due to strain-softening is finite per unit volume and, therefore, vanishes for a crack (the volume of which is zero). For this case, it would be necessary to include the fracture energy (surface energy) in the energy criterion of stability, same as in fracture mechanics. In this study, though, we take the view that, due to material heterogeneity, it makes no sense to apply a continuum analysis to localization regions whose width is less than a certain length h proportional to the maximum size of material inhomogeneities.

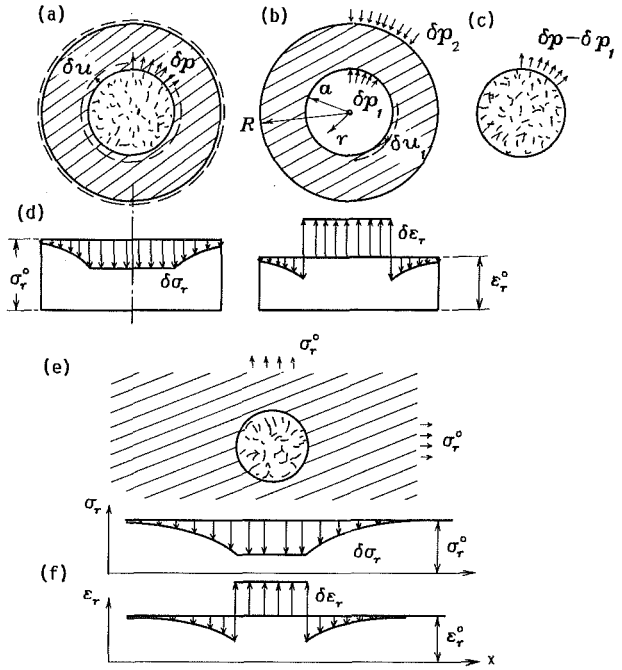


Fig. 2 Localization of strain into spherical and circular regions

Spherical Softening Region in a Sphere or Infinite Solid

Localization in a spherical region is a special case of the preceding solution for ellipsoidal regions. However, the solution may now be easily obtained even when the solid is finite. Consider a spherical hole of radius a inside a sphere of radius R, (Fig. 2(*a*)). We assume polar symmetry of the deformation field and restrict our attention to materials that are isotropic for unloading. As shown by Lamé (1852) (see, e.g., Timoshenko and Goodier, 1970, p. 395), the elastic solution for the radial displacements and the radial normal stresses at a point of radial coordinate r is

$$u = Ar + Dr^{-2}, \quad \sigma_r = \mathrm{E}_u(\bar{A} - 2\bar{D}r^{-3}) \tag{15}$$

where $\bar{A} = A/(1-2\nu_u)$, $\bar{D} = D/(1+\nu_u)$; E_u, ν_u = Young's modulus and Poisson's ratio of the sphere, and A, D = arbitrary constants to be found from the boundary conditions.

We now consider a solid sphere of radius R which is initially under uniform hydrostatic stress σ^0 and strain ϵ^0 ($\sigma^0 = \sigma^0_{kk}/3$, $\epsilon^0 = \epsilon^0_{kk}/3$), and seek the conditions for which the initial strain may localize in an unstable manner into a spherical region of radius a. Such localization may be produced by applying on the solid sphere at $r=a$ radial outward tractions δp (i.e. pressure) uniformly distributed over the spherical surface of radius a, Fig. 2(*a*). To determine the work of δp, we need to calculate the radial outward displacement δu_i at $r=a$. We will distinguish several types of boundary conditions on the outer surface $r=R$.

***(a)* Outer Surface Kept Under Constant Load.** As the boundary condition during localization, we assume that the initial radial pressure p_2^0 applied at outer surface $r = R$ is held constant, i.e., $\delta p_2 = 0$. For $\delta\sigma_r = -\delta p_1$ at $r=a$ and $\delta\sigma_r = -\delta p_2 = 0$ at $r = R$, equation (11) may be solved to yield $\bar{A} = a^3\delta p_1/\mathrm{E}(R^3 - a^3)$, $\bar{D} = \bar{A}R^3/2$, and from equation (15)

Downloaded 03 May 2010 to 171.66.16.21. Redistribution subject to ASME license or copyright; see http://www.asme.org/terms/Terms_Use.cfm

$$\delta u_1 = \frac{\delta p_1}{C_u},\quad \frac{1}{C_u} = \frac{a}{E_u(R^3-a^3)}\left[(1-2\nu_u)a^3 + \frac{1+\nu_u}{2}R^3\right]. \quad (16)$$

The inner spherical softening region of radius a, Fig. 2(*c*), is assumed to remain in a state of uniform hydrostatic stress and strain, and its strain-softening properties to be isotropic, characterized by E_t and ν_t. Thus the strains for $r<a$ are $\delta\epsilon = \delta u_1/a$, the stresses are $\delta\sigma = 3K_t\,\delta u_1/a = C_t\delta u_1$ with $C_t = 3K_t/a$; K_t = bulk modulus for further loading (softening); $3K_t = E_t/(1-2\nu_t)$, with $E_t<0$, $K_t<0$, for softening. The surface tractions acting on the softening region, Fig. 2(*c*), are equal to $C_t\delta u_1$ where $C_t = 3K_t/a$. Hence, by equilibrium, the total distributed traction at surface $r=a$ must be $\delta_p = C_u\delta u_1 + C_t\delta u_1$ and the work done by δp is $\Delta W = 4\pi a^2(\frac{1}{2}\delta p\delta u_1) = 2\pi a^2(C_u + C_t)\delta u_1^2$. Thus the necessary condition of stability of the initial uniform strain ϵ^0 in the solid sphere is $C_u + C_t > 0$, which yields the necessary condition for stability

$$-\frac{E_t}{E_u} < \frac{2(1-2\nu_t)(R^3-a^3)}{2(1-2\nu_u)a^3 + (1+\nu_u)R^3}. \quad (17)$$

Changing $<$ to $>$, we obtain the sufficient condition for strain-localization instability.

***(b)* Outer Surface Kept Fixed.** In this case we assume that during localization $\delta u = 0$ at $r=R$, and $\delta\sigma_r = -\delta p_1$ at $r=a$. From equation (15), we may then solve $D = -AR^3$ and

$$A = -\frac{\delta p_1}{E_u}\left(\frac{1}{1-2\nu_u} + \frac{2R^3}{(1+\nu_u)a^3}\right)^{-1} \quad (18)$$

which yields

$$\delta p_1 = C_u\delta u_1,\quad C_u = \frac{E_u a^2}{R^3-a^3}\left(\frac{1}{1-2\nu_u} + \frac{2R^3}{(1+\nu_u)a^3}\right). \quad (19)$$

The work done on the solid sphere by tractions $\delta p = C_u\delta u_1 + C_t\delta u_1$ applied at surface $r=a$ is $\Delta W = 2\pi a^2\,(C_u + C_t)\,\delta u_1^2$ where $C_t = E_t/(1-2\nu_t)a$ as before. Thus the necessary stability condition is $C_u + C_t > 0$, which can now be reduced to the condition

$$-\frac{E_t}{E_u} < \frac{1-2\nu_t}{R^3-a^3}\left(\frac{a^3}{1-2\nu_u} + \frac{2R^3}{1+\nu_u}\right). \quad (20)$$

Assuming that $|E_t|$ increases continuously after the peak of the stress-strain diagram as ϵ_0 is increased, instability develops at the value $a=a_{cr}$ which minimizes $|E_t|$ under the restriction $h/2 \le a \le R$ where h is the given minimum admissible size of the strain-softening region, representing a material property. For the case of prescribed pressure at the boundary $r=R$, we find from equation (17) that $a_{cr} = R$, which corresponds to $E_t = 0$. So the sphere becomes unstable right at the start of strain-softening, i.e., no strain-softening can be observed when the boundary is not fixed. For the case of a fixed (restrained) boundary at $r=R$, equation (20), one can verify that Min $|E_t|$ is finite and occurs at a_{cr} = Min $a=h/2$ (provided that $\nu_u \ge 0$).

For $R/a \to \infty$, equation (20) yields the stability condition for the case of infinite solid fixed at infinity, Fig. 2(*e*, *f*)

$$-\frac{E_t}{E_u} < \frac{2(1-2\nu_t)}{1+\nu_u} \quad (21)$$

It is interesting that for $R/a \to \infty$ equation (17) yields the same condition, but this limit case is of questionable significance since we found that $a_{cr} = R$ when the boundary is not fixed. Note that the stability condition in equation (21) does not depend on the radius a of the softening region; yet, unlike the softening in a layer in infinite solid, solved before, instability does not begin at the peak of stress-strain diagram (where $E_t = 0$) but begins only at a certain finite negative slope of the stress-strain diagram. This slope can in fact be rather steep ($-E_t = 2E_u$ for $\nu_t = \nu_u = 0$).

Circular Softening Region in a Planar Disk or Infinite Plate

Working in two dimensions, consider a circular hole of radius a inside a homogeneous isotropic circular disk of radius R Fig. 2(*a*,*b*). We assume a plane-stress state and, then, according to Lamé's solution, the radial displacement u and the radial normal stresses are (see, e.g., Flügge, 1962, p. 37–13; or Timoshenko-Goodier, 1970, p. 70)

$$u = \frac{1-\nu_u}{E_u}\,\frac{a^2p_1 - R^2p_2}{R^2-a^2}r + \frac{1+\nu_u}{E_u}\,\frac{R^2a^2(p_1-p_2)}{(R^2-a^2)r} \quad (22)$$

$$\sigma_r = \frac{R^2a^2(p_2-p_1)}{(R^2-a^2)r^2} + \frac{a^2p_1 - R^2p_2}{R^2-a^2},$$

$$\epsilon_2 = \frac{2\nu_u(p_2R^2 - p_1a^2)}{E_u(R^2-a^2)} \quad (23)$$

where p_1 and p_2 are the pressures applied along the hole perimeter and along the outer perimeter of the disk, respectively, and ϵ_2 is the transverse strain in the plate, which is independent of r. Depending on the boundary conditions, we distinguish three cases:

***(a)* Outer Boundary Kept Under Constant Load.** As the boundary condition during the strain localization instability, we now assume that the initial radial pressure p_2 applied at the outer boundary $r=R$ of the disk is held constant, i.e., $\delta p_2 = 0$. Equation (22) then yields for $\delta u_1 = \delta u$ at $r = a$, Fig. 2(*b*), the relation

$$\delta u_1 = \frac{\delta p_1}{C_u},\quad \frac{1}{C_u} = \frac{a}{E_u}\left(\nu_u + \frac{R^2+a^2}{R^2-a^2}\right). \quad (24)$$

The inner circular softening region of radius a, Fig. 2(*c*), is assumed to remain in a uniform state of stress and strain. Thus the strains for $r<a$ are $\delta\epsilon_r = \delta u_1/a$. Assuming the plate to be thin compared to radius a, we may assume the strain-softening region to be also in a plane-stress state, and then $\delta\epsilon_r = \delta\sigma_r(1-\nu_t)/E_t$. Hence,

$$\delta\sigma_r = C_t\delta u_1,\quad C_t = \frac{1}{a}\,\frac{E_t}{1-\nu_t}. \quad (25)$$

Now, we consider uniformly distributed outward tractions δp to be applied along the circle $r=a$ on the solid disk (without the hole). By equilibrium, $\delta p = C_u\delta u_1 + C_t\delta u_1$ and the work done by δp is $\Delta W = 2\pi a(\frac{1}{2}\,\delta p\delta u_1) = \pi a(C_u + C_t)\delta u_1^2$. Thus the necessary condition of stability of the initial state of uniform strain is $C_u + C_t > 0$. According to equations (24) and (25), the stability condition for plane stress becomes

$$-\frac{E_t}{E_u} < \frac{1-\nu_t}{\nu_u + \dfrac{R^2+a^2}{R^2-a^2}} \quad \text{(thin plate)}. \quad (26)$$

As another limiting case, we may consider a long cylinder of radius R (and length $>> R$), in which case the softening region is forced to have along the cylinder axis the same strain ϵ_z as the unloading region. However, the softening region is not in a plane-strain state either. Assuming that the planes normal to the cylinder axis remain plane, consider now that, unlike before, the axial stresses σ_z are nonzero. We must impose the equilibrium condition that the resultants of σ_z^t in the softening region and of σ_z^u in the unloading region cancel each other, i.e., $\pi(R^2 - a^2)\sigma_z^u = -\pi a^2\sigma_z^t$. We leave it to a possible user to work out the solution in detail and we now restrict our attention to the case $a << R$, for which, according to equation (20) ($\delta p_2 = 0$), we have $\delta\epsilon_z = 2\nu_u\delta p_1 a^2/(a^2 - R^2)E_u \simeq 0$ (for $r \ge a$), while also $\delta\sigma_z = 0$. Therefore, we may assume for the incremental deformation in the strain-softening region a state of plane strain. The solution may then be obtained simply by

Downloaded 03 May 2010 to 171.66.16.21. Redistribution subject to ASME license or copyright; see http://www.asme.org/terms/Terms_Use.cfm

replacing E_t with $E_t' = E_t/(1-\nu_t^2)$, and ν_t with $\nu_t' = \nu_t/(1-\nu_t)$ (the unloading region remains in plane stress in this case). Equation (26) thus transforms to

$$-\frac{E_t}{E_u} < \frac{(1+\nu_t)(1-2\nu_t)}{\nu_u + \dfrac{R^2+a^2}{R^2-a^2}} \quad \text{(long cylinder, } a<<R\text{)}. \tag{27}$$

When a/R is not very small, the solution may be expected to lie between equations (26) and (27).

(*b*) **Outer Boundary Kept Fixed.** In this case, we have during localization $\delta u = 0$ at $r = R$ and $\delta\sigma_r = -\delta p_1$ at $r = a$. Taking the variations of equations (22) at $r = R$ and $r = a$, we get

$$\frac{1-\nu_u}{E_u}\frac{a^2\delta p_1 - R^2\delta p_2}{R^2-a^2}R + \frac{1+\nu_u}{E_u}\frac{R^2a^2(\delta p_1-\delta p_2)}{(R^2-a^2)R} = 0 \tag{28}$$

$$\delta u_1 = \frac{1-\nu_u}{E_u}\frac{a^2\delta p_1 - R^2\delta p_2}{R^2-a^2}a + \frac{1+\nu_u}{E_u}\frac{R^2a^2(\delta p_1-\delta p_2)}{(R^2-a^2)a}. \tag{29}$$

Eliminating δp_2 from these two equations, we get the relation $\delta p_1 = C_u \delta u_1$ with

$$\frac{1}{C_u} = \frac{1}{E_u(R^2-a^2)}\left\{a[(1-\nu_u)a^2 + (1+\nu_u)R^2] - \frac{4R^2a^3}{(1-\nu_u)R^2 + (1+\nu_u)a^2}\right\}. \tag{30}$$

By the same reasoning as before, the necessary condition for the stability of the initial uniform strain ϵ^0 is $C_u + C_t > 0$ where C_t is again given by equation (25). This condition yields

$$-\frac{E_t}{E_u} < \frac{(1-\nu_t)(R^2-a^2)}{R^2+a^2+\nu_u(R^2-a^2) - \dfrac{4R^2a^2}{(1-\nu_u)R^2+(1+\nu_u)a^2}} \quad \text{(thin plate)}. \tag{31}$$

For the case of a long cylinder of length $>> R$ and with $a << R$, we may obtain the solution again by replacing E_t, ν_t with E_t', ν_t'. This yields

$$-\frac{E_t}{E_u} < \frac{(1+\nu_t)(1-2\nu_t)(R^2-a^2)}{R^2+a^2+\nu_u(R^2-a^2) - \dfrac{4R^2a^2}{(1-\nu_u)R^2+(1+\nu_u)a^2}} \quad \text{(long cylinder, } a<<R\text{)}. \tag{32}$$

Instability develops at the value $a = a_{cr}$ which minimizes $|E_t|$ under the restriction that $h/2 \le a \le R$. For the case of prescribed load at outer boundary, we find from equation (26) or (27) that $a_{cr} = R$, which corresponds to $E_t = 0$. Thus the disk becomes unstable right at the start of strain-softening, i.e., no strain-softening can be observed. For the case of a fixed (restrained) boundary at $r = R$, we find that, for $a \to R$, $\lim(-E_t/E_n) = \infty$ (to verify it one needs to substitute $a = R - \delta$ and consider $\delta \to 0$); consequently Min $|E_t|$ is finite, and it is found to occur at $a_{cr} = \text{Min } a = h/2$.

For $R/a \to \infty$, equation (31) or (32) yields the stability condition for the case of infinite plate fixed at infinity, Fig. 2(*e*, *f*)

$$-\frac{E_t}{E_u} < \frac{1-\nu_t}{1+\nu_u} \quad \text{for thin plate} \tag{33}$$

$$-\frac{E_t}{E_u} < \frac{(1+\nu_t)(1-2\nu_t)}{1+\nu_u} \quad \text{for massive solid}. \tag{34}$$

It is interesting that for $R/a \to \infty$ equations (26) and (27) yield the same conditions, but these limits are of questionable significance since we found that $a_{cr} = R$ when the boundary is not fixed. Note that the stability conditions in equations (33) and (34) are independent of the size of the localization region,

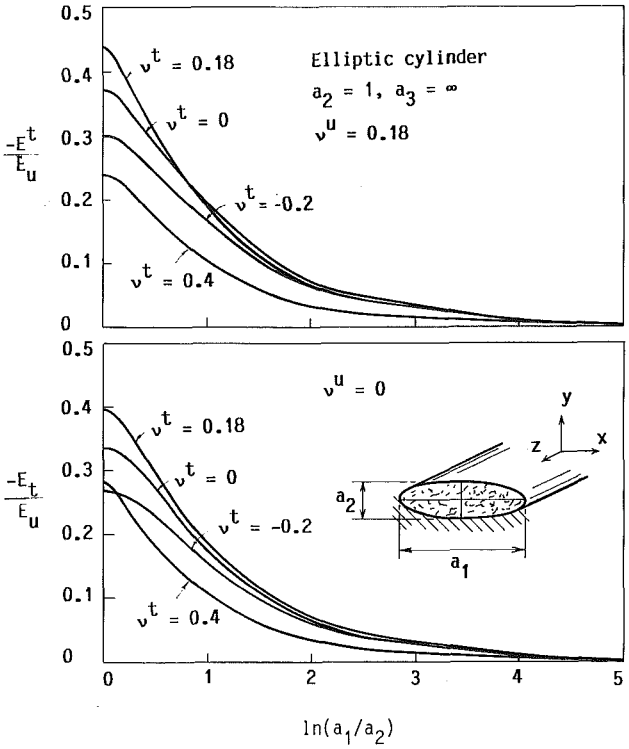


Fig. 3(*a*, *b*)

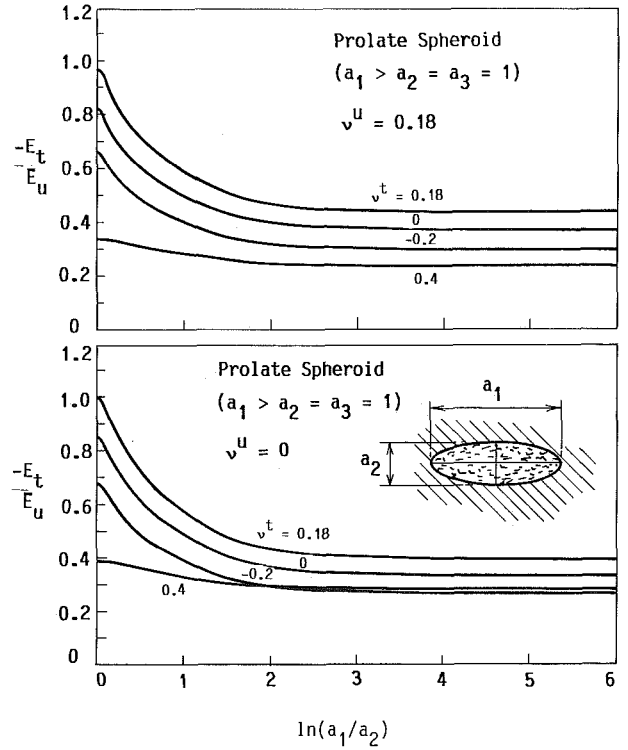


Fig. 3(*c*, *d*)

Fig. 3 Tangential modulus E_t at the limit of stability against localization into ellipsoidal region as a function of ratio a_1/a_2 of principal axes of ellipsoid

Downloaded 03 May 2010 to 171.66.16.21. Redistribution subject to ASME license or copyright; see http://www.asme.org/terms/Terms_Use.cfm

same as we found it for spherical localization regions and layers.

Softening Annulus or Shell

Solution on the basis of equations (22) and (23) or (25) is also possible for curved softening bands limited by two circles (an annulus) or by two spherical surfaces (a shell). In this case, the softening layer is not in a homogeneous state of strain and stress. The resulting formulas are more complicated. They represent a transition between the solution for a softening circle (or cylinder, sphere) and a softening band.

Numerical Examples and Discussion of Results

Figure 3 shows some numerical results for localization of strain into ellipsoidal domains in infinite space. The results were calculated for domains in the shape of infinitely long elliptic cylinder ($a_3 \to \infty$ and various a_1/a_2) as well as prolate spheroid ($a_1 > a_2 = a_3$, various ratios a_1/a_2). The material was assumed to be incrementally isotropic, with matrices $\mathbf{D}_t$ and $\mathbf{D}_u$ characterized by Young's moduli E_t and E_u, and Poisson ratios $\nu_u = 0.18$ with various values of ν_t. The assumption of incremental isotropy is here made for the sake of simplicity. In reality, the incremental moduli at strain-softening must be expected to be anisotropic, except when the initial state is a purely volumetric strain. A subsequent paper (Bažant and Lin, 1987) gives numerical results for incrementally anisotropic moduli corresponding to von Mises plasticity and nonassociated Drucker-Prager plasticity with a negative plastic modulus.

Matrix $\mathbf{Z}$, equation (13), was evaluated by computer on the basis of S_{ijkm} taken from Mura (1982, equations (11.22) and (11.29)). The smallest eigenvalue of matrix $\mathbf{Z}$ was calculated by a computer library subroutine. Iterative search by Newton method was made to find the value of E_t/E_u for which the smallest eigenvalue is zero and is about to become negative, which indicates loss of positive-definiteness.

The results are plotted in Figs. 3(*a–d*). For the infinite cylinder, Fig. 3(*a,b*), as a_1/a_2 increases, the localization instability occurs at smaller $|E_t/E_u|$. The case $a_1/a_2 \to \infty$ corresponds to an infinite planar band, and the results are identical to those obtained before for this case. In particular, $|E_t|$ tends to 0 as $a_1/a_2 \to \infty$; i.e., instability occurs right at the peak of the stress-strain diagram.

For the prolate spheroid, Fig. 3(*c, d*), the instability also occurs at decreasing $|E_t/E_u|$ as a_1/a_2 increases, but for $|E_t| \to \infty$, which corresponds to an infinite circular tube, a finite value of $|E_t|$, depending on Poisson's ratio, is still required for instability. This limiting case is equivalent to two-dimensional localization in a circular region, equation (34). On the other hand, the case $a_1/a_2 = 1$, Fig. 3(*c,d*), is equivalent to localization into a spherical region, equation (21).

Figures 4(*a–d*) shows the plots for various incremental Poisson's ratios of $|E_t/E_u|$ at incipient localization instability as a function of R/a for the following cases: (1) sphere, displacement fixed, equation (20); (2) localization in planar band in uniaxial extension (Equation (12) of Bažant, 1987, $R/a = L/h$); (3) localization in planar shear band (Bažant, 1987, equation (13), $R/a = L/h$).

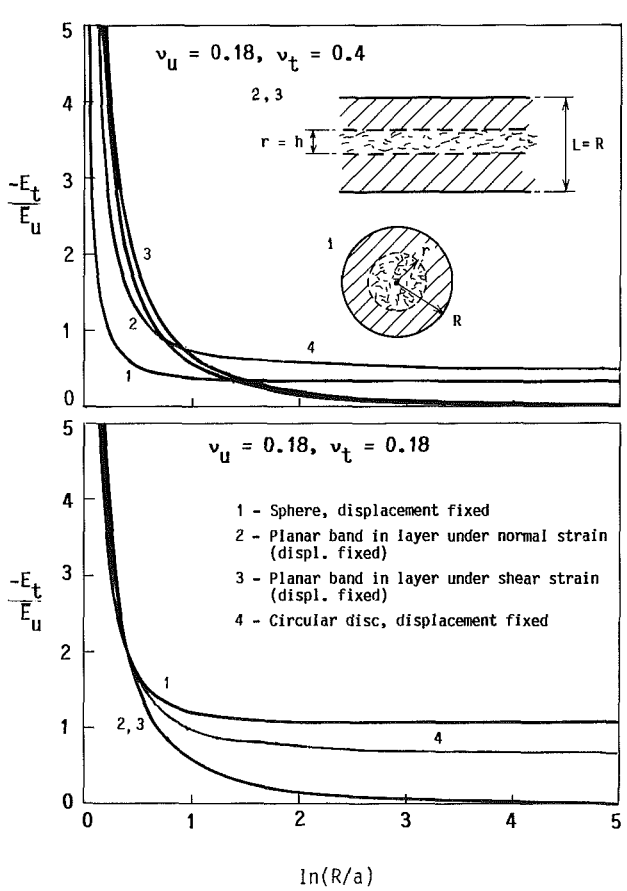


Fig. 4(*a, b*)

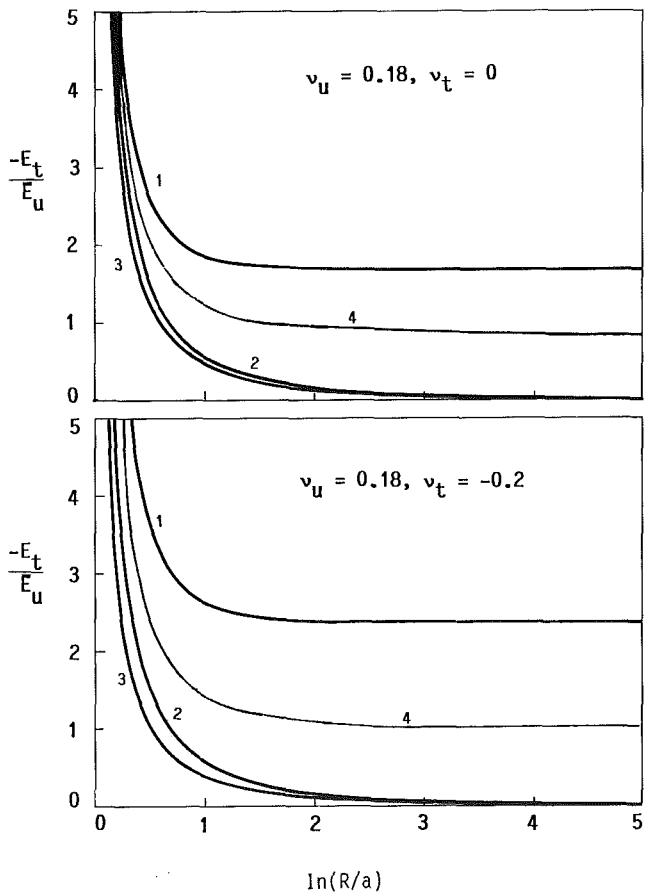


Fig. 4(*c, d*)

Fig. 4 Tangential modulus E_t at the limit of stability against localization into spherical and circular regions of radius r within a sphere or disk of radius R

Downloaded 03 May 2010 to 171.66.16.21. Redistribution subject to ASME license or copyright; see http://www.asme.org/terms/Terms_Use.cfm

We see from Fig. 4 that the value of E_t at instability depends strongly on the relative size $R(a)$ of the body as well as the Poisson's ratios. For infinite body size ($R/a \to \infty$), instability of planar bands occurs at $E_t = 0$, i.e., at the peak of stress-strain diagram. The same happens under load-controlled conditions for the cases of spherical or circular regions with $R/a \to 1$ (i.e., the smallest possible body size for which the body remains at homogeneous strain). For $R/a > 1$, the spherical or circular regions generally require a finite slope $|E_t|$ to produce localization instability, provided the boundary is under prescribed displacement during the localization.

The results show that a localization instability in the form of a planar band always develops at a smaller $|E_t|$, and thus at a smaller initial strain, than the localization instability in the form of an ellipsoidal softening region. That does not mean, however, that the planar band would always occur in practice. A planar localization band cannot accommodate the boundary conditions of a finite solid restrained on its boundary, and a localization region similar to an ellipsoid may then be expected to form. It is remarkable how slowly the slope $|E_t|$ at instability decreases as a function of a_1/a_2. The value of the aspect ratio that is required to reduce $|E_t|$ at instability from about 0.4 to about 0.04 of E_u is $a_1/a_2 = e^3 = 20$. This means that if a very long planar softening band cannot be accommodated within a given solid, the deformation at softening instability is considerably increased.

The present solutions represent upper bounds on $|E_t|$ at actual localization. When the stability condition for some of the previously considered softening regions is violated, instability with such a region is possible and must occur since it leads to an increase of entropy. However, it is possible that localization into some form of region that we could not solve would occur earlier, at a smaller initial strain. For this reason, the present stability conditions are only necessary rather than sufficient. However, their opposites (i.e., $<$ changed to $>$) represent sufficient conditions for instability.

In the preceding analysis of ellipsoidal softening regions, we solved only the case of infinite solids and were unable to examine the effect of the boundary conditions at infinity. Now, from the fact that spherical and circular softening regions are special cases of ellipsoidal ones, we must conclude that our solution for ellipsoidal region is applicable only if the ellipsoidal region is of finite size, which is guaranteed only if the infinite body is fixed at infinity rather than having prescribed loads at infinity. Otherwise the limit cases $a_{cr} = R$ for spherical or circular softening regions discussed after (equations (20) and (32)) would not be satisfied.

Conclusion

The solutions to multidirectional localization problems with ellipsoidal, spherical and circular localization regions indicate that, in general, a loss of positive-definiteness of matrix $\mathbf{D}_t$ of tangential moduli for loading does not necessarily produce instability. Rather, the stability criterion requires positive-definiteness of a certain weighted average of the incremental moduli matrices $\mathbf{D}_t$ and $\mathbf{D}_u$ for loading and unloading. The weights depend on the relative size of the body. Not only for finite but also for infinite bodies restrained at the boundary, unstable strain localization into finite-size ellipsoidal regions cannot take place for a certain range of nonpositive-definite tangential moduli matrices. By contrast, unstable strain localization into an infinitely long planar band of finite thickness occurs in an infinite space as soon as $\mathbf{D}_t$ loses positive-definiteness.

The present results can be used to check the correctness of finite-element programs for strain-softening.

Acknowledgment

Partial financial support under AFOSR Contract F49620-87-C-0030DEF with Northwestern University, monitored by Dr. Spencer T. Wu, is gratefully acknowledged. Graduate research assistant F.-B. Lin deserves thanks for his valuable assistance in numerical calculations.

References

Bažant, Z. P., 1987, "Softening Instability: Part I: Localization Into a Planar Band," Report No. 87-2/498s, Center for Concrete and Geomaterials, Northwestern University, Evanston, IL.

Bažant, Z. P., and Lin, F.-B., 1987, "Localization of Softening in Ellipsoids and Bands: Parameter Study," Report No. 87-7/4981s, Center for Concrete and Geomaterials, Northwestern University, July, ASCE *Journal of Engineering Mechanics*, in press.

Christensen, R. M., 1979, *Mechanics of Composite Materials*, John Wiley, New York.

Eshelby, J. D., 1957, "The Determination of the Elastic Field of an Ellipsoidal Inclusion and Related Problems," *Proceedings of the Royal Society of London*, Vol. A241, pp. 376.

Flügge, W., Ed., 1962, *Handbook of Engineering Mechanics*, McGraw-Hill, New York.

Kinoshita, N., and Mura, T., 1971, "Elastic Fields of Inclusions in Anisotropic Media," *Phys. Stat. Sol.* (*a*), Vol. 5, pp. 759–768.

Lamé, G., 1852, *Leçons sur la théorie de l'élasticité*, Gauthier-Villars, Paris.

Lin, S. C., and Mura, T., 1973, "Elastic Fields of Inclusions in Anisotropic Media (II)," *Phys. Stat. Sol.* (*a*), Vol. 15, pp. 281–285.

Mura, T., 1982, *Micromechanics of Defects in Solids*, Martinus Nijhoff Publishers, The Hague.

Timoshenko, S. P., and Goodier, J. N., 1970, *Theory of Elasticity*, 3rd Ed., McGraw-Hill, New York.

Downloaded 03 May 2010 to 171.66.16.21. Redistribution subject to ASME license or copyright; see http://www.asme.org/terms/Terms_Use.cfm

Two-Dimensional Effects in the Necking of Elastic Bars

S. A. Silling
Brown University,
Division of Engineering,
Providence, RI 02912
Assoc. Mem. ASME

Numerical solutions for incompressible hyperelastic bars undergoing smooth necking in plane strain show complex phenomena in which two-dimensional effects are inherently important. In long bars, the two-dimensional effects are confined to a transition zone between the necked and non-necked phases. In spite of the two-dimensional effects, the nominal stress in necked long bars is close to the Maxwell stress under certain conditions. For very long bars there are necked equilibrium deformations in which the overall stretch is less than that of the maximum in the constitutive relation.

1 Introduction

Elastic bars with nonmonotone nominal stress-stretch relations in uniaxial stress are among the prototypes for the study of mechanically induced phase transformations in elasticity. By regarding this class of problems as completely one-dimensional, Ericksen (1975) deduced many interesting properties of strong minimizers of potential energy. Such a purely one-dimensional treatment predicts, for hard-device problems in which the overall stretch is between the maximum and minimum of the stress-stretch curve, that a strong minimizer may consist of an arbitrarily fine mixture of the two stable phases. The nominal stress, which must be constant in such a one-dimensional model in equilibrium, is equal to the Maxwell stress when both phases are present. There is thus an infinite number of solutions to the one-dimensional hard-device problem under these conditions.

The purpose of the present work is to assess how multidimensional effects, particularly necking, may influence the validity of the phase equilibrium approach described above. It is demonstrated that in the hard device plane-strain bar problem, the situation regarding uniqueness is strongly influenced by the two-dimensional effects in necking. In fact, for the problems considered below, there are at most *two* stable solutions rather than an infinite number. The amount of potential energy attributable to purely two-dimensional effects in the transition zone between necked and non-necked phases is computed here numerically, and it is shown to be significant. In many cases this energy is comparable to the difference between the energy of the unstable homogeneous solution and that of the one-dimensional strong minimizer. Thus the assumption that an elastic bar necessarily seeks out the Maxwell stress is called into question, although it is shown below that this assumption is a good approximation for sufficiently long bars when the transition zone is far from the ends of the bar.

Contributed by the Applied Mechanics Division for publication in the JOURNAL OF APPLIED MECHANICS.

Discussion on this paper should be addressed to the Editorial Department, ASME, United Engineering Center, 345 East 47th Street, New York, N.Y. 10017, and will be accepted until 2 months after publication of the paper itself in the JOURNAL OF APPLIED MECHANICS. Manuscript received by ASME Applied Mechanics Division, April 15, 1987; final revision, December 4, 1987.

Most of the following discussion is concerned with hyperelastic incompressible materials which develop *smooth* necks, i.e., those materials in which true discontinuities such as Lüders bands or shear bands do not appear. However, it is to be expected that two-dimensional effects are important even in the presence of such discontinuities.

The development of smooth necks during the stretching of an elastic bar has been studied extensively from the point of view of bifurcation during a quasi-static process. Bifurcations in elastic rectangular bodies were studied in the theory of finite elasticity by Wesolowski (1962) and in a more general way by Sawyers and Rivlin (1974). Both of these studies employed the method of adjacent equilibrium. Wesolowski concluded that bifurcation in tension can occur in the hard-device problem only at stretches greater than that of the first maximum in the stress-stretch curve. This result was confirmed in a quite general way by Hill and Hutchinson (1975), and it was demonstrated numerically by Tvergaard, Needleman, and Lo (1981). Antman (1973) investigated smooth bifurcations in the loading of bars in a one-dimensional formulation and also concluded that necking can occur only after a maximum in load. Most numerical work in the area of necking has focused on elastic-plastic materials, as in Needleman (1972) and Burke and Nix (1979).

The previous work summarized above mainly concerns the following question: During the quasi-static stretching of a bar, what is the lowest stretch at which further extension results in nonuniqueness? In contrast, the present work concerns the following related question: For an elastic bar with a prescribed amount of stretch, what is the deformation with the lowest possible potential energy? Previous work along these lines has included the phase equilibrium approach of Ericksen (1975) and James (1980). Spector (1984), who has studied the implications of various constitutive inequalities of finite elasticity for the bifurcations in compressible materials, provides a more extensive summary of previous work.

In this paper the term *neck* means an interval along the axis of the bar where the bar has narrowed. The term *phase* means an interval of either narrowed or non-narrowed material. A *transition zone* is the region where one phase connects to another. In order to emphasize that the stretching process con-

Copyright © 1988 by ASME
Downloaded 03 May 2010 to 171.66.16.21. Redistribution subject to ASME license or copyright; see http://www.asme.org/terms/Terms_Use.cfm

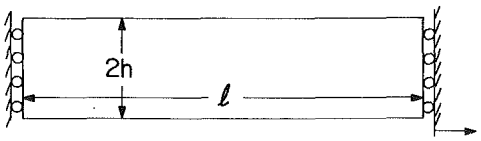


Fig. 1 Hard-device bar problem

sidered in this discussion is not quasi-static, the term *bifurcation* will be avoided. Instead, the lowest stretch at which a nonunique solution is possible will be called the *critical stretch for nonuniqueness*.

2 Problem Description

A rectangular bar of thickness $2h$ and length l is composed of a homogeneous, incompressible, isotropic, hyperelastic solid (see Fig. 1). Plane strain is assumed. The upper and lower surfaces are traction-free. The left and right faces are free of shear tractions, and they are displaced so that the overall stretch of the bar is a given positive constant λ_0.

It is easily shown that for such a solid in plane strain, the constitutive law is completely describable by the stress-stretch curve under conditions of uniaxial stress. Assume that such a curve is specified by $\sigma_{11}=f(\lambda)$, where σ_{11} is the nominal (first Piola-Kirchhoff) uniaxial stress component, f is a smooth function, and λ is the uniaxial stretch. The family of materials considered here is characterized by the four parameters σ_1, σ_2, q_1, and q_2, and the uniaxial response is given as follows:

$$f(\lambda)=\begin{cases}\sigma_1\left[1-\left(\dfrac{\lambda-q_1}{q_1-1}\right)^2\right], & 0<\lambda\le q_1\\ \dfrac{\sigma_1+\sigma_2}{2}+\dfrac{\sigma_1-\sigma_2}{2}\cos\pi\dfrac{\lambda-q_1}{q_2-q_1}, & q_1\le\lambda\le q_2\\ \sigma_2+\sigma_1\left(\dfrac{\lambda-q_2}{q_1-1}\right)^2, & q_2\le\lambda\end{cases} \tag{1}$$

The stress-stretch relation for uniaxal stress is shown in Fig. 2. A strain energy density function for the material may be found from $W(\lambda)=\int_1^\lambda f(t)dt$. The Maxwell stress associated with phase transitions under conditions of uniaxial stress is found to occur at

$$\lambda_M^- = q_1-(q_1-1)\sqrt{\frac{\sigma_1-\sigma_2}{2\sigma_1}} \tag{2}$$

and

$$\lambda_M^+ = q_2+(q_1-1)\sqrt{\frac{\sigma_1-\sigma_2}{2\sigma_1}}, \tag{3}$$

and the value of the Maxwell stress is

$$\sigma_M=f(\lambda_M^-)=f(\lambda_M^+)=\frac{\sigma_1+\sigma_2}{2}. \tag{4}$$

For general plane-strain deformations, let λ denote the local stretch, i.e., the larger of the two principal stretches. Any isotropic, incompressible, elastic material in plane strain has a constitutive relation for the in-plane Cauchy stress tensor τ expressible as $\tau=\phi(\lambda)\mathbf{G}-p\mathbf{1}$, where λ is the local stretch, ϕ is some scalar-valued function, and p is an arbitrary scalar. $\mathbf{G}$ is the left Cauchy-Green stretch tensor $\mathbf{G}=\mathbf{F}\mathbf{F}^T$, where $\mathbf{F}$ is the deformation gradient tensor. In the present case ϕ may be determined from f, and the result is

$$\tau=\begin{cases}\dfrac{f(\lambda)}{\lambda-1/\lambda^3}\mathbf{G}-p\mathbf{1}, & \lambda\neq 1\\ -p\mathbf{1}, & \lambda=1\end{cases} \tag{5}$$

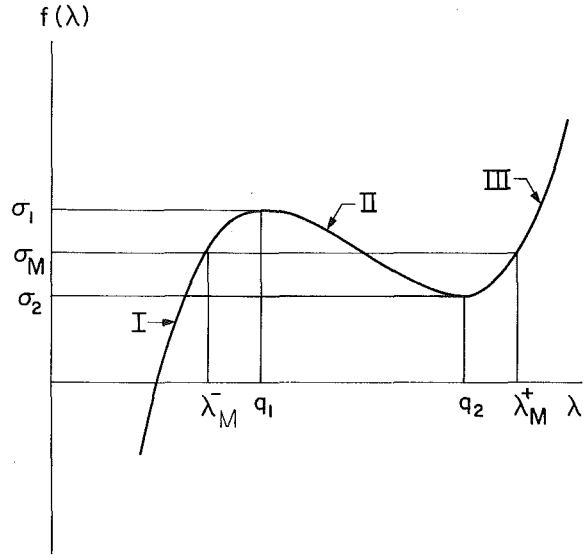


Fig. 2 Nominal stress-stretch curve in uniaxial stress

It is crucial to known whether or not the equilibrium equation can undergo a loss of ellipticity for a material. This issue is straightforward in the case of hyperelastic incompressible materials in plane strain. Abeyaratne (1980) has shown that in such cases ellipticity is determined by the local slope of $\tau(k)$, the shear stress as a function of shear under conditions of simple shear. Ellipticity can be lost if and only if $\tau'(k)\le 0$ for some $k\ge 0$, where the prime denotes differentiation. Since all incompressible plane strain deformations are locally expressible as a simple shear followed by a rigid deformation, the above criterion for loss of ellipticity can be expressed in terms of λ. The relation between local stretch and local shear is

$$k=|\lambda-1/\lambda|, \tag{6}$$

which comes from computation of the eigenvalues λ^2 and $1/\lambda^2$ of $\mathbf{G}$ in a simple shear deformation with shear k of the form

$$[\mathbf{F}]=\begin{pmatrix}1 & k\\ 0 & 1\end{pmatrix}. \tag{7}$$

(5), (6), and (7) may be combined to yield

$$\tau(k)=\tau_{12}=\frac{f(\lambda)}{1+1/\lambda^2} \tag{8}$$

Differentiating (8) and using the fact that k varies monotonically with λ, it follows that ellipticity can be lost if and only if

$$f'(\lambda)\le -\frac{2f(\lambda)}{\lambda^3+\lambda} \tag{9}$$

for some $\lambda>0$.

The interesting fact about (9), and the reason that smooth necking is possible for incompressible elastic bars in plane strain, is that $f'(\lambda)$ may be nonmonotic provided that any downward sloping segments are not too steep. For the family of materials under consideration here, it has been found that ellipticity is assured for the choice $q_1=1.2$ whenever both $1.4\le q_2\le 3$ and $\sigma_2/\sigma_1\ge 0.95$.

3 Numerical Method

The numerical method used was CHIMP (Silling, 1985), a finite-difference program for nonlinear elastostatics. The program uses dynamic relaxation, the computation of an equilibrium deformation by integration over time of the dynamic equation of motion with viscous damping terms in-

Downloaded 03 May 2010 to 171.66.16.21. Redistribution subject to ASME license or copyright; see http://www.asme.org/terms/Terms_Use.cfm

cluded. The formulation of CHIMP is fully consistent with the nonlinear theory of elasticity, and no linearization is used at any stage of the calculation. This method is especially suitable for the study of elastic stability issues in continuous bodies because the equilibrium solution is a large-time limit of a dynamic problem, and is therefore at least metastable dynamically. The method does not use a variational or virtual work formulation, but directly computes the total force on each node due to stresses in adjacent zones in each time step. The accelerations derived from these forces are integrated using explicit central differencing in time. The new node positions in each time step are used to compute new strains and stresses.

In all cases discussed below, the initial condition for the bar was its unstressed state. Only the upper half of the bar was modeled. The left and right sides were subject to zero shear traction. The left side had zero displacement in the x_1-direction. The right side was displaced using a ramp function of time. Following completion of the ramp, the calculation was continued until the kinetic energy in the mesh was negligible and all oscillations died out. A square mesh with 16 equally spaced rows of nodes across the width of bar was used. The calculations were carried out on a Cyber 205 computer and typically required 2–4 minutes of CPU time.

4 Strain Energy in a Transition Zone

This section presents results for the computation of the excess strain energy due to two-dimensional effects in a transition zone. Equilibrium solutions were computed for bar lengths ranging from h to $6h$ for the following two materials:

(*i*) $q_1 = 1.2$, $q_2 = 1.5$, $\sigma_1 = 1$, $\sigma_2 = 0.95$ (the *hard* material),
(*ii*) $q_1 = 1.2$, $q_2 = 3$, $\sigma_1 = 1$, $\sigma_2 = 0.95$ (The *soft* material).

For the hard material, the overall stretch was $\lambda_0 = 1.35$, while for the soft material $\lambda_0 = 2.1$. Figure 3 shows the distribution of phases in the meshes for a bar length of $3h$ for the two materials at these stretches. The shading in the figures corresponds to one of the three branches of the nominal stress-stretch curve as shown in Fig. 2.

Let Φ_M be the total strain energy of a strong minimizer of potential energy in the one-dimensional model by Ericksen (1975), i.e., one of the infinite number of piecewise smooth deformations whose stress equals the Maxwell stress when multiple phases are present. Φ_M for the entire bar may be found from

$$\Phi_M = 2hl[(1-\alpha)W(\lambda_M^-) + \alpha W(\lambda_M^+)], \tag{10}$$

$$\alpha = \frac{\lambda_0 - \lambda_M^-}{\lambda_M^+ - \lambda_M^-} \tag{11}$$

in which α is the fraction of the orginal bar length which changes phase. Let Φ be the total strain energy of the numerical solution, and let Φ_H be the total strain energy of the homogeneous ("trivial") solution. Figures 4*a*, *b* show curves of the *excess energies* $\Phi - \Phi_M$ and $\Phi_H - \Phi_M$ for the equilibrium solutions as a function of length for each of the two materials with $h = 1$. Since Φ_M is the energy of a strong minimizer, all of the excess energies are nonnegative. Note that the curve of $\Phi_H - \Phi_M$ is a straight line, since this quantity is proportional to length.

The central idea in this discussion is that the excess energy $\Phi - \Phi_M$ must be entirely the result of two-dimensional effects, since it would be zero if no narrowing of the bar occurred.

For small lengths, the curves of $\Phi - \Phi_M$ coincide with the lines for the homogeneous solutions, since no necking occurs. For larger lengths ($l \geq 1.5h$ for the hard material, $l \geq 1.31h$ for the soft material) a transition zone does appear. As shown in Fig. 4*a*, *b*, $\Phi - \Phi_M$ is constant for bars longer than a certain length. This is consistent with the observation that transition zones have the same shape and size for bars beyond this certain length, implying that the two-dimensional effects have the same influence. The constant excess energy of a transition zone for a given material and a given bar thickness h will be called E_T. Because of scaling considerations, E_T must be proportional to h^2 for given values of l/h, λ_0, and the material parameters. The following values were computed for $h = 1$: for

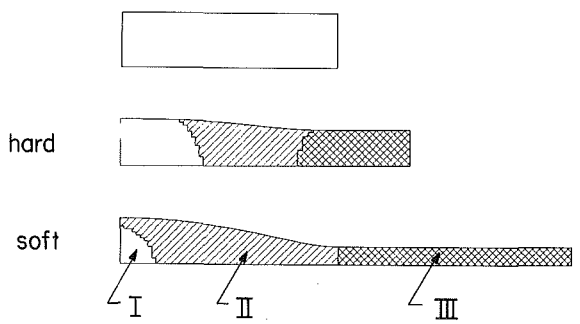


Fig. 3 Initial and necked states in hard and soft materials, $l = 3h$

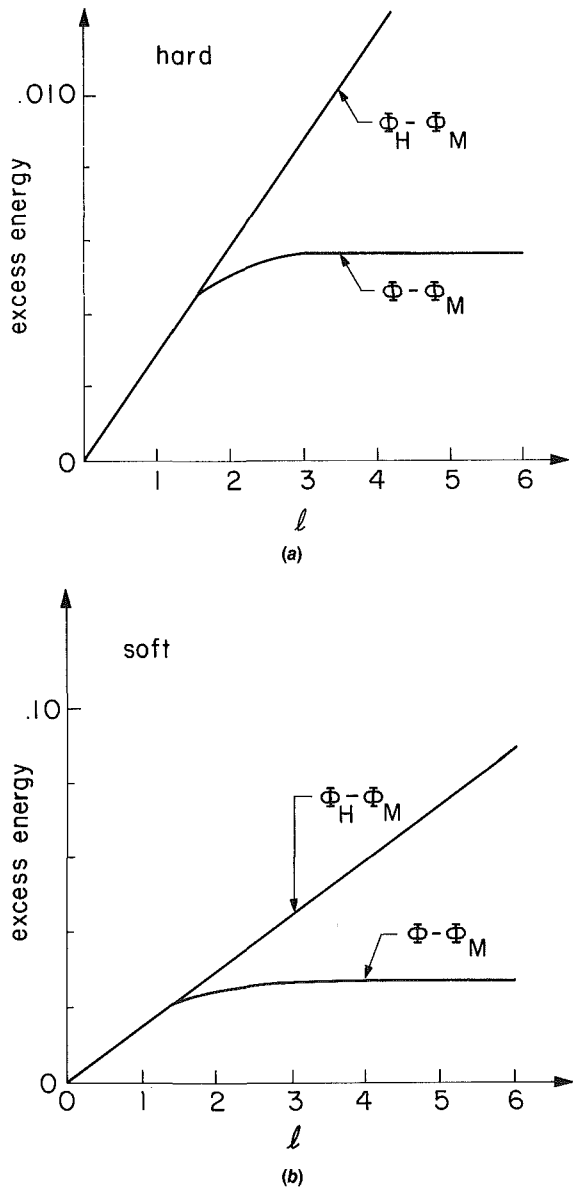


Fig. 4 Excess energies as a function of initial bar length

Downloaded 03 May 2010 to 171.66.16.21. Redistribution subject to ASME license or copyright; see http://www.asme.org/terms/Terms_Use.cfm

the hard material, $E_T = 0.00566$; for the soft material $E_T = 0.0273$.

Note the similarity in shapes of the curves in Fig. 4*a*, *b* for the two materials, although the stretches in the high-strain phases are quite different. This shows that the geometric effects being considered here are of importance in both the hard and soft materials.

5 Stretching of a Bar of Fixed Length

In this section results are presented for the computation of equilibrium deformations in stretched bars composed of the soft material. Two lengths of bars are considered: $l = 3h$ and $l = 6h$. The initial condition is the unstretched state, and the boundary conditions are as described previously.

The following results were found by computing many separate equilibrium deformations at various stretches rather than by doing a single calculation with gradually increasing stretch. The use of many equilibrium deformations was necessary because the path followed by the solution is extremely sensitive to dynamic effects. Since the results are for many separate equilibrium computations, the sequence of these deformations does not represent a quasi-static process. Nonuniqueness is detected at lower stretches using the present method than with quasi-static simulations because the dynamic effects in the mesh tend to overcome any energy barrier which separates a deformation just prior to bifurcation from its post-bifurcated condition in a quasi-static process. It was found in the computed results that a necked bar contains at most one transition zone when equilibrium is reached, although depending on which side of the mesh is displaced, either of two mirror images may be obtained. The smallest and largest values of λ_0 for which a necked equilibrium deformation is possible in a given bar will be called the *lower* and *upper critical stretches for nonuniqueness*.

Figure 5 shows the neck size δ as a function of stretch for $h = 1$. δ is defined as the maximum current width of the half-bar along its length minus the minimum width. Note that the neck size is discontinuous at the lower critical stretch, but it is continuous at the upper one. For the long bar, the neck size is constant over a considerable range of stretches, and in this range one-dimensional effects dominate. This is the range over which the transition zone is sufficiently far from the ends of the bar that it does not interact significantly with them. For the short bar, two-dimensional effects are important over the entire range of stretches, since the neck size begins diminishing almost immediately after the neck first appears.

Figure 6 shows the excess energies $\Phi - \Phi_M$ and $\Phi_H - \Phi_M$ as a function of stretch for the two bar lengths. For overall stretches λ_0 such that $\lambda_0 \leq \lambda_M^-$ or $\lambda_0 \geq \lambda_M^+$, these excess energies are zero, since the strong minimizer is simply the homogeneous deformation at these stretches. As λ_0 is increased from λ_M^-, the $\Phi - \Phi_M$ curves initially continue to follow the $\Phi_H - \Phi_M$ curves, because nonuniqueness has not yet occurred. After it occurs in the long bar, $\Phi - \Phi_M$ remains constant over a considerable range of stretches, and it is equal in magnitude to E_T as discussed in the previous section. After nonuniqueness occurs in the short bar, two-dimensional effects are felt immediately as the deformation begins approaching a homogeneous fully-necked condition.

A useful approximation is supported by the data in Fig. 6. Nonuniqueness first occurs when the excess energy in the homogeneous deformation is sufficient to sustain the two-dimensional distortions needed to form a transition zone, i.e., when $\Phi_H - \Phi_M = E_T$. This approximation will be called the *excess energy criterion*. The approximation is only valid for bars of sufficient length for a "fully developed" transition zone with energy E_T to fit between the ends. (Shorter bars may still neck, but their excess energy may be less than E_T, as shown in the previous section.)

Figure 7 shows the mean nominal stress component σ_{11} across the width of the bar as a function of stretch. This is essentially the total tensile force transmitted by the bar. In addition to the computed paths for the two bar lengths, the figure shows the path for the one-dimensional strong minimizer, which follows a straight horizontal path at the Maxwell line. The figure also shows the path that the homogeneous solution would follow, which is merely the original stress-stretch relation for the material.

At the lower critical stretch, the computed mean stress drops suddenly from that of the homogeneous deformation to the Maxwell stress. Increasing the stretch beyond this value causes the transition zone to progress gradually to the other end of the bar from the one where it formed. During this progression the mean stress remains nearly constant at σ_M. In this

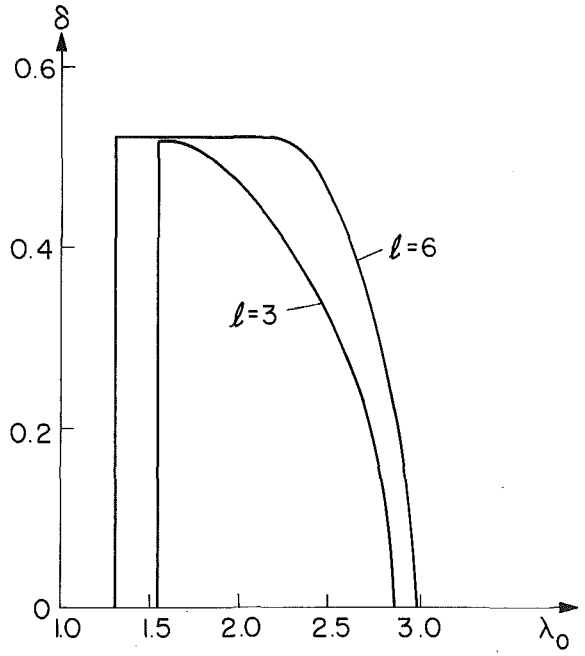


Fig. 5 Neck size as a function of stretch

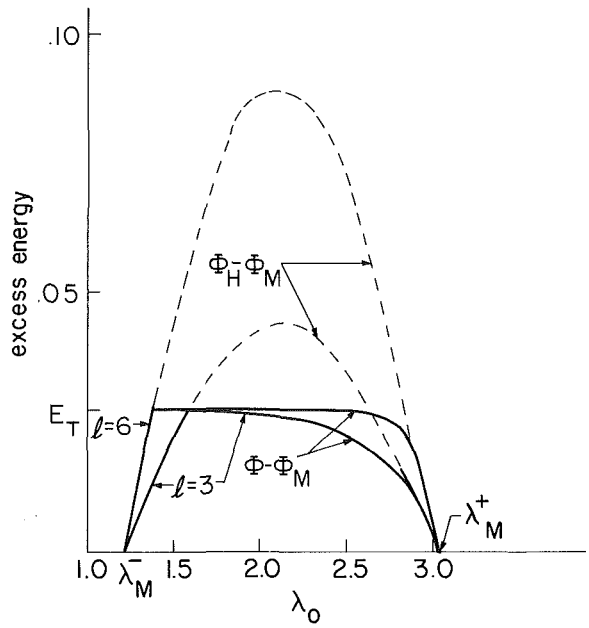


Fig. 6 Excess energies as a function of stretch

Downloaded 03 May 2010 to 171.66.16.21. Redistribution subject to ASME license or copyright; see http://www.asme.org/terms/Terms_Use.cfm

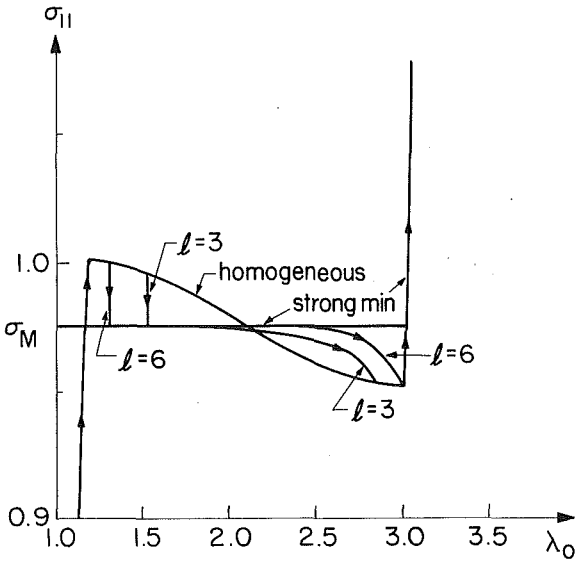


Fig. 7 Mean tensile stress across bar width as a function of stretch

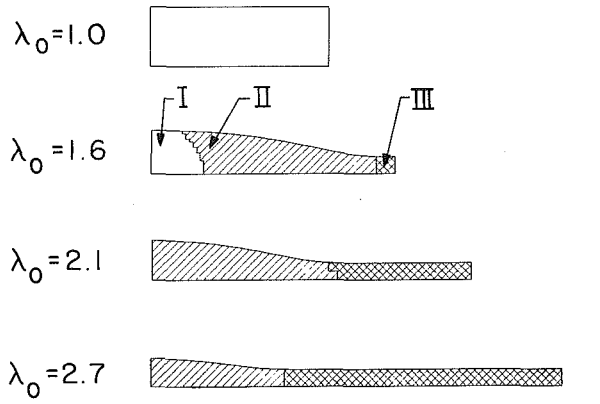


Fig. 8 Necked states in soft material bar, $l = 3h$, for various stretches

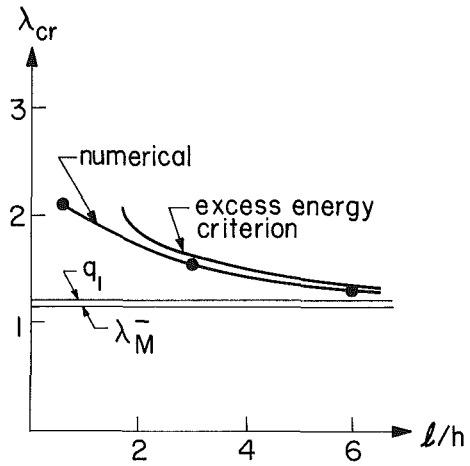


Fig. 9 Lower critical stretch for nonuniqueness as a function of bar length

range the one-dimensional strong minimizer model is a good approximation, as previously discussed. As the transition zone approaches the end of the bar, two-dimensional effects are once again felt, and the mean stress approaches that of the homogeneous deformation.

Figure 8 shows the shape of the deformed bar and the distribution of phases for various stretches in the case $l = 6$. Note the sudden appearance of the transition zone at the lower critical stretch, in contrast with its gradual disappearance near the upper one.

Finally, Fig. 9 shows the lower critical stretch λ_{cr} at which a necked equilibrium deformation initially occurs as a function of l/h for bars composed of the soft material. For sufficiently long bars, this stretch is nearly equal to the stretch at which the homogeneous deformation has an excess energy of E_T, agreeing with the excess energy criterion. Nonuniqueness occurs at lower stretches in long bars than in shorter bars, since a shorter bar must be stretched farther in order to accumulate excess energy E_T. The critical stretch predicted by the excess energy criterion is also shown in the figure. The divergence of the two curves for very short bars is the result of the fact that a neck in a very short bar has less excess energy than E_T (see Fig. 4). Thus a very short bar, if it necks at all, necks sooner than the excess energy criterion predicts.

As previously mentioned, the excess energy $\Phi - \Phi_M$ for a bar of fixed length first becomes positive at the overall stretch $\lambda_0 = \lambda_{\bar{M}}$. This stretch is less than q_1, the stretch at the maximum of the constitutive relation for uniaxial stress. Therefore the excess energy criterion predicts that necked deformations can exist at stretches below q_1 for sufficiently long bars. To test the prediction, a bar with $l/h = 30$ composed of the hard material was simulated with overall stretch $\lambda_0 = 1.19$. Recall that for this material $\lambda_{\bar{M}} = 1.1684$ and $q_1 = 1.2$. These parameters were chosen because at these values of length and stretch $\Phi_H - \Phi_M > E_T$. The numerical solution showed that a neck does indeed form. From the point of view of bifurcation of a quasi-static process, the necked deformation in this case could be regarded as having snapped back following bifurcation (Tvergaard, Needlemen, and Lo, 1981).

6 Conclusions

It has been shown here that for an incompressible hyperelastic material that undergoes smooth necking in uniaxial stress, each transition zone between necked and nonnecked phases contains a fixed amount of strain energy over and above that of a one-dimensional model based on strong minimization of potential energy. This excess energy is caused by the distortions inside the transition zone and is multidimensional in nature. The amount of excess energy stored in a transition zone, E_T, is of the same order as the difference between the energy of a strong minimizer in one dimension and that of the unstable homogeneous deformation at the same overall stretch. For long bars, the mean stress across the bar width is close to the Maxwell stress, as long as the transition zone is not too close to either of the ends of the bar. This indicates that the one-dimensional strong minimizer model by Ericksen (1975) is applicable under these conditions to the extent that it predicts the correct stress.

The computer solutions show that no more than one transition zone appears, consistent with the observation that each transition zone requires extra energy. In contrast, the one-dimensional strong minimizer model allows for fine mixtures of the phases. The conclusion is that a fine mixture of phases is not a stable deformation when multidimensional effects are considered, since *each* transition zone would consume an additional E_T. This conclusion is consistent with the results found from gradient theory models and similar approaches such as those discussed by Coleman (1983), Triantafyllidis and Aifantis (1986), and Carr, Gurtin and Slemrod (1985). It is hoped that the numerical results presented here will aid in the development of specific constitutive relations in the gradient theory. A difficult test of a gradient theory model would be to predict the behavior at stretches close to the critical stretches for nonuniqueness, where the two-dimensional nature of the deformation is quite complex.

Downloaded 03 May 2010 to 171.66.16.21. Redistribution subject to ASME license or copyright; see http://www.asme.org/terms/Terms_Use.cfm

These results are consistent with the recent work of Owen (1987), who explored the stability of bars within the framework of Antman (1973).

Acknowledgment

The author gratefully acknowledges the support of the National Science Foundation through a grant of computer resources at the John von Neumann Center, and through 1987 Presidential Young Investigator Award MSM-8658107. Helpful discussions with Professor Alan Needleman are also acknowledged.

References

Abeyaratne, R., 1980, "Discontinuous Deformation Gradients in Plane Finite Elastostatics of Incompressible Materials," *Journal of Elasticity*, Vol. 10, pp. 255–293.

Antman, S. S., 1973, "Nonuniqueness of Equilibrium States for Bars in Tension," *Journal of Mathematical Analysis and Applications*, Vol. 44, pp. 333–349.

Burke, M. A., and Nix, W. D., 1979, "A Numerical Study of Necking in the Plane Tension Test," *International Journal of Solids and Structures*, Vol. 15, pp. 379–393.

Carr, J., Gurtin, M. E., and Slemrod, M., 1985, "One-Dimensional Structured Phase Transformations Under Prescribed Loads," *Journal of Elasticity*, Vol. 15, pp. 133–142.

Coleman, B. D., 1983, "Necking and Drawing in Polymeric Fibers Under Tension," *Archive for Rational Mechanics and Analysis*, Vol. 83, pp. 115–137.

Ericksen, J. L., 1975, "Equilibrium of Bars," *Journal of Elasticity*, Vol. 5, pp. 191–201.

Hill, R., and Hutchinson, J. W., 1975, "Bifurcation Phenomena in the Plane Tension Test," *Journal of the Mechanics and Physics of Solids*, Vol. 23, pp. 239–264.

James, R. D., 1980, "The Propagation of Phase Boundaries in Elastic Bars," *Archive for Rational Mechanics and Analysis*, Vol. 73, pp. 125–158.

Needleman, A., 1972, "A Numerical Study of Necking in Circular Cylindrical Bars," *Journal of the Mechanics and Physics of Solids*, Vol. 20, pp. 111–127.

Owen, N., 1987, "Existence and Stability of Necking Deformations for Nonlinearly Elastic Rods," *Archive for Rational Mechanics and Analyis*, Vol. 98, pp. 357–383.

Sawyers, K. N., and Rivlin, R. S., 1974, "Bifurcation Conditions for a Thick Elastic Plate Under Thrust," *International Journal of Solids and Structures*, Vol. 10, pp. 483–501.

Silling, S. A., 1985, "CHIMP–A Computer Program for Finite Elastostatics," California Institute of Technology Division of Engineering and Applied Science, Report 54.

Spector, S. J., 1984, "On the Absence of Bifurcation for Elastic Bars in Uniaxial Tension," *Archive for Rational Mechanics and Analysis*, Vol. 85, pp. 171–199.

Triantafyllidis, N., and Aifantis, E. C., 1986, "A Gradient Approach to Localization of Deformation. I. Hyperelastic Materials," *Journal of Elasticity*, Vol. 16, pp. 225–237.

Tvergaard, V., Needleman, A., and Lo, K. K., 1981, "Flow Localization in the Plane Strain Tensile Test," *Journal of Mechanics and Physics of Solids*, Vol. 29, pp. 115–142.

Wesolowski, Z., 1962, "Stability in Some Cases of Tension in the Light of the Theory of Finite Strain," *Archiwum Mechaniki Stosowanej*, Vol. 14, pp. 875–899.

Downloaded 03 May 2010 to 171.66.16.21. Redistribution subject to ASME license or copyright; see http://www.asme.org/terms/Terms_Use.cfm

On a Modified Hellinger/Reissner Variational Theorem for the Analysis of Elastoplastic Solids

Dimitrios Karamanlidis
Assistant Professor,
Department of Civil Engineering,
University of Rhode Island,
Kingston, RI 02881
Mem. ASME

A new general variational theorem is proposed for the analysis of elastoplastic solids. By utilizing the method of Lagrangian multipliers, a Hellinger/Reissner-type theorem is derived wherein the yield criterion along with the flow rule are satisfied a posteriori *as Euler/Lagrange equations. The proposed formulation represents a rational generalization of the classical Hellinger/Reissner variational theorem for it treats all relevant field equations for an elastoplastic boundary-value problem as natural constraints.*

Introduction

The development of finite element models for the numerical analysis of materially nonlinear continua has been the preoccupation of many researchers over the past two decades. This could be attributed to an increased need in realistically modeling a wide range of practically important problems such as concrete creep, solids and rocks, metal-forming processes, ductile fracture initiation, and stable crack growth in cracked bodies, to name just a few.

Variational theorems (and their generalizations to account for discontinuities at interelement boundaries in a finite-element assembly) have played a central role ever since; however, the vast majority of the work reported thus far utilizes the principle of virtual work or alternatives thereof (cf. references [1, 4, 6, 9, 11–13] which also include extensive lists of references). Notable exceptions are the works by Backlund [2], Barnard and Sharman [3], Pian [7], and Spilker [8] who used "mixed" finite element formulations with stresses and displacements being approximated independently from each other.

As revealed by the pertinent literature (cf., for example, [7, 8]), mixed models based on Hellinger/Reissner-type variational theorems or modifications thereof have been found in many cases to possess certain advantages over conventional assumed displacement models from both a theoretical as well as computational standpoint. More specifically: (*i*) Sufficiently accurate results are obtained for both displacements and stresses by using relatively simple trial functions; (*ii*) C^0-continuous elements for the analysis of bending problems do not "lock" when applied to very thin structures; (*iii*) Exact representation of the elemental rigid body and constant strain modes is easily achieved even in the case of arbitrarily curved elements. Furthermore, the fact that, in a mixed model, stresses are approximated directly is of particular attractiveness in the case of problems involving plasticity effects.

The standard approach for solving a nonlinear structural mechanics problem consists in adopting an incremental/iterative procedure. The obtained approximate solution satisfies all the field equations of the boundary-value problem, i.e., equilibrium equations, constitutive equations and strain-displacement relations along with the pertinent boundary conditions. In the case of an elastoplastic problem, the yield criterion, along with a pertinent flow rule (cf. [10]), also have to be satisfied at the end of each solution step.

In all of the foregoing cited work, pointwise checks have been adopted; i.e., in order to determine the regions which underwent plastic deformations, the stress state at certain characteristic element points (e.g., Gaussian stations, centroid, etc.) was evaluated. Reportedly, this approach might in some cases lead to numerical difficulties in the form of "oscillations" like those described in [3]. Second and to the opinion of this author more importantly, it seems inconsistent from a theoretical standpoint to impose a pointwise satisfaction of the yield criterion whereas the equilibrium equations (and in the case of a mixed model also the compatibility equations) are fulfilled in an integral average sense only.

The primary purpose of this paper is to present a consistent variational formulation as a rational basis for the approximate solution of structural mechanics boundary-value problems including plasticity effects. More precisely, a modified version of the Hellinger/Reissner variational theorem [10] is presented wherein (unlike [7]) not only the incremental displacement and stress fields but also the equivalent stress and equivalent plastic strain increments, $\Delta\sigma_u$ and $\Delta\epsilon_\eta^p$, respectively, represent independent variables. Thus, no pointwise checks for the yield criterion and the flow rule are needed within this formulation.

Conventional Mixed Formulation

For a three-dimensional continuum made from elastoplastic

Contributed by the Applied Mechanics Division for publication in the JOURNAL OF APPLIED MECHANICS.
Discussion on this paper should be addressed to the Editorial Department, ASME, United Engineering Center, 345 East 47th Street, New York, NY 10017, and will be accepted until two months after final publication of the paper itself in the JOURNAL OF APPLIED MECHANICS. Manuscript received by ASME Applied Mechanics Division, June 18, 1986; final revision, January 21, 1988.

Copyright © 1988 by ASME
Downloaded 03 May 2010 to 171.66.16.21. Redistribution subject to ASME license or copyright; see http://www.asme.org/terms/Terms_Use.cfm

material, the incremental form of the Hellinger/Reissner principle (cf. [7]) states that

$$\pi_R(\Delta u_i,\Delta\sigma_{ij}) = \int_V U_{\Delta c}(\Delta\sigma_{ij})dV - \int_V \Delta\sigma_{ij}\Delta u_{i,j}dV$$

$$+\int_V \Delta\bar{p}_i\Delta u_i dV + \int_{S_\sigma}\Delta\bar{T}_i\Delta u_i dS + (\text{correction terms})$$

$$= \text{stationary} \tag{1}$$

where the independent functions subject to variations are the incremental displacement vector Δu_i and the incremental stress tensor $\Delta\sigma_{ij}$. In the foregoing, V denotes the volume of the continuum under consideration, whereas S_σ and S_u are the parts of the boundary $\partial V(=S_\sigma+S_u)$ on which tractions and displacements are specified, respectively. Furthermore

$$U_{\Delta c}(\Delta\sigma_{ij}) = \frac{1}{2}\Delta\boldsymbol{\sigma}^T\mathbf{D}^{ep}\Delta\boldsymbol{\sigma} \tag{2}$$

represents the complementary strain energy density while $\mathbf{D}^{ep}$ denotes the elastoplastic constitutive matrix (cf. [10, 11, 13]). In accordance with [7] the "correction terms" in equation (1) which consist of two parts; namely, "equilibrium imbalance" and "compatibility mismatch" terms must be included so as to prevent that due to inherent linearization errors the obtained approximate solution drifts away from the true solution. The development of a mixed finite-element model on the basis of equation (1) requires Δu_i and $\Delta\sigma_{ij}$ to be approximated independently by means of elementwise defined interpolants, viz.

$$\Delta\mathbf{u} = \mathbf{N}\Delta\hat{\mathbf{u}} \quad \text{and} \quad \Delta\boldsymbol{\sigma} = \mathbf{P}\boldsymbol{\beta} \tag{3a,b}$$

where $\mathbf{N}$ and $\mathbf{P}$ contain the displacement and stress field interpolants, respectively, $\boldsymbol{\beta}$ is the vector of generalized stress coefficients, whereas $\Delta\hat{\mathbf{u}}$ is the elemental nodal displacement vector. The stationarity of the functional in equation (1) is subject to the condition that interelement displacement continuity is imposed *a priori* while the interelement surface traction reciprocity is satisfied *a posteriori* ("natural" constraint). Because of this, the coefficients $\boldsymbol{\beta}$ can be eliminated elementwise from the variational equation (cf. [7, 8] for more details). Then, the elemental tangent stiffness matrix is obtained, viz.

$$\mathbf{K}_T = \mathbf{G}^T\mathbf{H}^{-1}\mathbf{G} \tag{4}$$

where

$$\mathbf{H} = \int_V \mathbf{P}^T\mathbf{D}^{ep}\mathbf{P}dV \tag{5a}$$

and

$$\int_V \Delta\sigma_{ij}\Delta u_{i,j}dV = \boldsymbol{\beta}^T\mathbf{G}\delta\hat{\mathbf{u}} \tag{5b}$$

Clearly, in order to form the elastoplastic flexibility matrix, $\mathbf{H}$, the stress state in the element interior has to be evaluated upon considering the yield criterion along with a pertinent flow rule. If one uses, for example, the Prandtl/Reuss equations along with the Huber/von Mises/Hencky criterion, the following relations hold true (cf. [10])

$$\Delta\epsilon^p_{ij} = \alpha^*\frac{3s_{ij}}{2H'\sigma_u}\Delta\sigma_u \tag{6a}$$

$$\Delta\epsilon^p_u = \alpha^*\frac{3s_{ij}}{2H'\sigma_u}\Delta\sigma_{ij} \tag{6b}$$

$$H'\Delta\epsilon^p_u = \alpha^*\Delta\sigma_u \tag{6c}$$

As mentioned previously, $\Delta\sigma_u$ and $\Delta\epsilon^p_u$ are the incremental uniaxial stress and plastic strain, respectively, s_{ij} denotes the deviatoric part of σ_{ij}, H' is a work hardening parameter (i.e., $H'=0$ for an elastic, ideally plastic material), whereas

$$\alpha^* = \begin{cases} 0 & \text{for elastic deformations} \\ 1 & \text{for plastic deformations} \end{cases}$$

When equation (1) is used as the variational basis for the finite-element analysis of elastoplastic continua, it is common practice to require that equations (6*a–c*) are fufilled exactly at certain characteristic locations in the interior of the element, e.g., Gaussian stations, centroid, etc. As pointed out earlier, from a theoretical standpoint, it does not seem obvious at all why it is necessary (or even advantageous) to satisfy equations (6*a–c*) exactly whereas the equilibrium and compatibility conditions are fulfilled in an average sense only ("natural constraints"). With this as the motivation, a novel mixed variational formulation shall be presented next wherein not only the equilibrium and compatibility conditions but also equations (6) are satisfied as natural constraints. We note for the record that a somewhat related approach has been proposed previously by Nagtegaal et al. [5], in the context of nearly incompressible problems.

Modified Mixed Formulation

In deriving a modified version of equation (1), we relax the subsidiary constraint represented by equation (6*b*) by means of a Lagrangian multiplier λ (cf. [10]). This leads to the variational theorem

$$\pi_{mR}(\Delta u_i,\Delta\sigma_{ij},\lambda,\Delta\epsilon^p_u) = \int_V U_{\Delta c}(\Delta\sigma_{ij},\Delta\epsilon^p_u)dV$$
$$-\int_V\Delta\sigma_{ij}\Delta u_{i,j}dV$$
$$+\int_V\Delta\bar{p}_i\Delta u_i dV + \int_{S_\sigma}\Delta\bar{T}_i\Delta u_i dS$$
$$-\int_V\lambda\left(\Delta\epsilon^p_u - \alpha^*\frac{3s_{ij}}{2h'\sigma_u}\Delta\sigma_{ij}\right)dV$$
$$+(\text{correction terms}) = \text{stationary} \tag{7a}$$

where

$$U_{\Delta c}(\Delta\sigma_{ij},\Delta\epsilon^p_u) = \frac{1}{2}\Delta\boldsymbol{\sigma}^T\mathbf{D}^e\Delta\boldsymbol{\sigma} + \frac{H'}{2}(\Delta\epsilon^p_u)^2 \tag{8}$$

In the foregoing equation (7), the independent functions subject to variations are Δu_i, $\Delta\sigma_{ij}$, λ, and $\Delta\epsilon^p_u$. Taking these variations, one arrives at the Euler/Lagrange equations of the variational theorem (7), i.e.,

$$\delta\Delta u_i:\ \Delta\sigma_{ij,j} + \Delta\bar{p}_i = 0 \qquad \text{in } V \tag{9a}$$

$$\delta\Delta\sigma_{ij}:\ D^e_{ijkl}\Delta\sigma_{kl} + \alpha^*\frac{3s_{ij}}{2H'\sigma_u}\Delta\sigma_u$$
$$= \frac{1}{2}(\Delta u_{i,j} + \Delta u_{j,i}) \qquad \text{in } V \tag{9b}$$

$$\delta\lambda:\ \Delta\epsilon^p_u - \alpha^*\frac{3s_{ij}}{2H'\sigma_u}\Delta\sigma_{ij} = 0 \qquad \text{in } V \tag{9c}$$

$$\delta\Delta\epsilon^p_u:\ H'\Delta\epsilon^p_u - \lambda = 0 \qquad \text{in } V \tag{9d}$$

It is seen that equations (9*a*, *b*) represent the incremental linear momentum balance and strain-displacement relations, respectively. Further, by comparing equation (9*d*) with equation (6*c*), the physical meaning of the Lagrangian multiplier λ can be determined, viz.

$$\lambda = \alpha^*\Delta\sigma_u \tag{10}$$

Substituting equation (10) into equation (7*a*) gives the following

Downloaded 03 May 2010 to 171.66.16.21. Redistribution subject to ASME license or copyright; see http://www.asme.org/terms/Terms_Use.cfm

$$\pi_{mR}(\Delta u_i, \Delta\sigma_{ij}, \Delta\sigma_u, \Delta\epsilon_u^p) = \int_V U_{\Delta c}(\Delta\sigma_{ij}, \Delta\epsilon_u^p)\,dV$$
$$-\int_V \Delta\sigma_{ij}\Delta u_{i,j}\,dV$$
$$+\int_V \Delta\bar{p}_i \Delta u_i\,dV + \int_{S_\sigma} \Delta\bar{T}_i \Delta u_i\,dS$$
$$-\int_V \alpha^* \Delta\sigma_u \left(\Delta\epsilon_u^p - \alpha^* \frac{3s_{ij}}{2H'\sigma_u}\Delta\sigma_{ij}\right)dV$$
$$+ (\text{corrections terms}) = \text{stationary} \qquad (7b)$$

On the basis of equation (7*b*), a mixed finite element model can be developed such that, in the interior of each element, stresses and displacements along with the uniaxial stress and plastic strain increments are approximated independently from each other. Strictly speaking, the only condition to be met *a priori* by the trial functions is the interelement displacement continuity. It is, however, advantageous to choose the stress field interpolants so as to fulfill certain subsidiary conditions (e.g., linear momentum balance). On the other hand, interelement traction reciprocity as well as the flow rule and the yield criterion are fulfilled *a posteriori* as the Euler/Lagrange equations of the variational theorem.

References

1 Argyris, J. H., 1965, "Elasto-plastic Matrix Displacement Analysis of Three-Dimensional Continua," *J. Roy. Aero. Soc.*, Vol. 69, pp. 633–635.

2 Backlund, J., 1973, "Finite Element Analysis of Nonlinear Structures," PhD. thesis, Chalmers University of Technology.

3 Barnard, A. J., and Sharman, P. W., 1973, "The Elasto-plastic and Large-Displacement Response of Plates to Blast Loading," Technical Report, Loughborough University of Technology.

4 Marcal, P. V., and King, I. P., 1967, "Elastic-plastic Analysis, of Two-dimensional Stress Systems by the Finite Element Method," *International Journal of Mechanical Sciences*, Vol. 9, pp. 143–155.

5 Nagtegaal, J. C., Parks, D. M., and Rice, J. R., 1974, "On Numerically Accurate Finite Element Solutions in the Fully Plastic Range," *Comp. Meth. Appl. Mech. Eng.*, Vol. 4, pp. 153–178.

6 Nayak, G. C., and Zienkiewicz, O. C., 1972, "Elasto-plastic Stress Analysis. Generalization for Various Constitutive Relations Including Strain Softening," *Int. J. Num. Meth. Eng.*, Vol. 5, pp. 113–135.

7 Pian, T. H. H., 1976, "Variational Principles for Incremental Finite Element Methods," *Journal of the Franklin Institute*, Vol. 302, pp. 473–488.

8 Spilker, R. L., 1974, "A Study of Elasto-Plastic Analysis by the Assumed-Stress Hybrid Finite-Element Model, with Application of Thick Shells of Revolution," PhD thesis, Massachusetts Institute of Technology.

9 Stricklin, J. A., Heisler, W. A., and Reiseman, W., 1973, "Evaluation of Solution Procedures for Material and/or Geometrically Non-Linear Structural Analysis," *Journal of AIAA*, Vol. 11, pp. 292–299.

10 Washizu, K., 1982, *Variational Methods in Elasticity and Plasticity*, 3rd ed., Pergamon Press, Oxford.

11 Yamada, Y., Yoshimura, N., and Sakurai, T., 1968, "Plastic Stress-strain Matrix and its Application for the Solution of Elastic-plastic Problems by the Finite Element Method," *International Journal of Mechanical Sciences*, Vol. 10, pp. 343–354.

12 Zienkiewicz, O. C., Valliappan, S., and King, I. P., 1969, "Elasto-plastic Solutions of Engineering Problems. Initial-Stress Finite Element Approach," *Int. J. Num. Meth. Eng.*, Vol. 1, pp. 75–100.

13 Zienkiewicz, O. C., 1977, *The Finite Element Method*, 3rd ed., McGraw-Hill, Maidenhead.

Downloaded 03 May 2010 to 171.66.16.21. Redistribution subject to ASME license or copyright; see http://www.asme.org/terms/Terms_Use.cfm

Possible Experimental X-Ray Diffractometry Evidence of Couple-Stresses

M. M. Gola
Dip. di Meccanica,
Politecnico di Torino,
Torino, Italy 10129
Mem. ASME

P. Coppa
Dip. Ing. Meccanica,
Universitá "Tor Vergata,"
Roma, Italy

The technique of measuring residual strain using X-ray diffractometry is examined with respect to prior attempts to experimentally validate couple-stress or micropolar theories. When subjected to grinding, polycrystalline materials (such as steel or others of technical interest) exhibit residual strains with very peculiar features whose explanation is still controversial. This paper suggests how a formally correct explanation can be formulated in terms of the theories based on couple-stresses. This new hypothesis is critically compared with competing theories found in the recent literature. It is proposed that, for the case of thin layers subjected to extremely high stress gradients, X-ray diffractometry is the most appropriate technique for investigating couple-stress or micropolar phenomena.

Introduction

The literature of the past 30 years reveals a renewed interest in extended elasticity theories, which are characterized by a nonzero couple tensor in the elementary volume. In classical theory, the load transmission through the surface of every volume element can be completely described by a stress vector applied to the center of gravity of the surface; however, as pointed out by Koiter (1964), "this is an assumption which can neither be proved directly, nor disproved. It can only be tested by a confrontation of its predictions for measurable quantities with experiment."

The first formulations of theories making use of nonzero couple-stresses date to about 100 years ago (Voigt, 1887; Cosserat, E., and F., 1909). More recently there has been a significant interest in attempting to explain phenomena emerging from the fatigue behavior of machine parts subjected to high stress concentrations; see (Koiter, 1964) and references therein.

More than one extension of the classical theory of elasticity exists: the "couple-stress theory" attributed to Mindlin and Tiersten (1962); the "micropolar theory" of Eringen and Suhubi (1964); the "micropolar gradient coherent theory" of Brulin and Hjalmars (1979).

The basic hypotheses of the couple-stress theory are that the ratio between the moment acting on a surface and the surface area will not tend to zero as the area approaches zero in the limit and that the rotation field is completely determined from displacement gradients. In the other theories, a higher generality is introduced by adding a rotation field independent of displacement gradients. For the purpose of the present work, it is important to note that the equilibrium equations for couple-stress and micropolar theories coincide but that the constitutive equations and the strain-displacement (and microrotation) relations do not.

In the couple-stress theory, the antisymmetric part of the stress tensor as well as the first invariant of the couple-stress tensor are indeterminate, and there are four elastic constants for isotropic materials. In micropolar theories, all tensors are completely determinate, and isotropic materials have six elastic constants.

The essential part of the present work depends only upon the equilibrium equations. Therefore, without loss of validity, only the more simple couple-stress theory is invoked.

The attempts to experimentally validate extended theories of elasticity can be summarized as follows.

Koiter (1964) showed that if couple-stresses are to explain fatigue results near stress concentrations, unacceptable discrepancies arise with experimentally proven classical predictions relative to the stiffness of plates in bending.

Gauthier and Jahsman (1975) tested a granular material whose microstructure should exhibit micropolar effects. Their torsion and bending results were compared with the theoretical predictions, from which they concluded that any possible micropolar behavior was masked by material property variations.

Schijve (1966) and Ellis with Smith (1967) performed bending tests on thin steel and aluminum laminates, but they did not find effects which confirmed the existence of phenomena related to the nonclassical theories. They concluded that couple-stress effects would be observed only if the plate thickness approached the grain size. In this circumstance, however, continuum theories approach the limit of their validity.

Yang and Lakes (1981, 1982) performed torsion and bending experiments on bone and came to the conclusion that micropolar theory effects were demonstrated. However, in this case, the results, depending on measurements of twist and

Contributed by the Applied Mechanics Division for publication in the JOURNAL OF APPLIED MECHANICS.

Discussion on this paper should be addressed to the Editorial Department, ASME, United Engineering Center, 345 East 47th Street, New York, N.Y. 10017, and will be accepted until two months after final publication of the paper itself in the JOURNAL OF APPLIED MECHANICS. Manuscript received by ASME Applied Mechanics Division, May 8, 1987; final revision, October 26, 1987.

Copyright © 1988 by ASME
Downloaded 03 May 2010 to 171.66.16.21. Redistribution subject to ASME license or copyright; see http://www.asme.org/terms/Terms_Use.cfm

displacement, are expected to be critically influenced by material parameters whose determination is difficult.

Askar (1972) followed a completely different philosophy by inducing a shear wave in a crystal and finding that some of the translational energy was transformed into rotational energy, possibly through a micropolar mechanism. The present authors do not feel competent to judge this particular line of research.

In summary, the search for very small displacement effects is a common feature of static test methodologies. These require a very accurate knowledge of the material behavior; moreover test specimens have to be very small, since couple-stress or micropolar effects are expected to become relevant only as extremely short-range phenomena, in the presence of high strain gradients. In this respect, strain detection with X-ray diffractometry on ground specimens should, in principle, be the elective technique. In fact

(*a*) The subsurface layer penetrated by X-rays is in the range of 5–20 microns (Barrett and Massalski, 1966; Cullity, 1978)

(*b*) The layer which undergoes residual stresses in grinding ranges from about 20–100 microns (Faninger and Walburger, 1976; Wolfstieg and Macherauch, 1976; Macherauch and Wolfstieg, 1977; Mittal and Rowe, 1982; Tönshoff et al., 1982; Coppa et al., 1983; Hauk and Krug, 1984).

To the authors' knowledge, theoretical and experimental couple-stress theories on one side and X-ray stress analysis on the other have evolved, up to the present day, without ever having come into contact with each other. In the next section, it will be shown that X-ray stress analysis has raised a problem whose features are of a kind which has formal links with couple-stress effects.

Shear Stress and X-Ray Analysis

As to the technique itself, X-ray diffraction is an effective and reliable method of evaluating residual stresses in subsurface layers of metallic polycrystalline materials and, in the past 20 years, has acquired the status of a routine laboratory test. It is based on the indirect measurement of the distance variations of crystal lattice planes due to straining of the material (Barrett and Massalski, 1966; Cullity, 1978; SAE, 1971).

The method is well known. Briefly, from the measurement of a shift in diffraction angle ϑ, Fig. 1, and from Bragg's law, it is possible to deduce variations of interplanar distance, and therefore of the strain $e_{\varphi\psi}$ along the direction L_3 of Fig. 2. This is compared with the same strain calculated from isotropic elasticity

$$\epsilon_{\varphi\psi} = \frac{1+\nu}{E}(\sigma_{11}\cdot\cos^2\varphi + \sigma_{22}\sin^2\varphi + \sigma_{12}\sin 2\varphi - \sigma_{33})\cdot\sin^2\psi - \frac{\nu}{E}(\sigma_{11}+\sigma_{22}+\sigma_{33}) + \frac{1+\nu}{E}(\sigma_{13}\cos\varphi + \sigma_{23}\sin\varphi)\cdot\sin 2\psi \quad (1)$$

and thus allows the determination of stresses defined in the reference system, shown in Fig. 2. In a relevant number of practical cases, the relationship between the stress or strain and the $\sin^2\psi$ parameter is linear, since stresses σ_{13}, σ_{23} are absent.

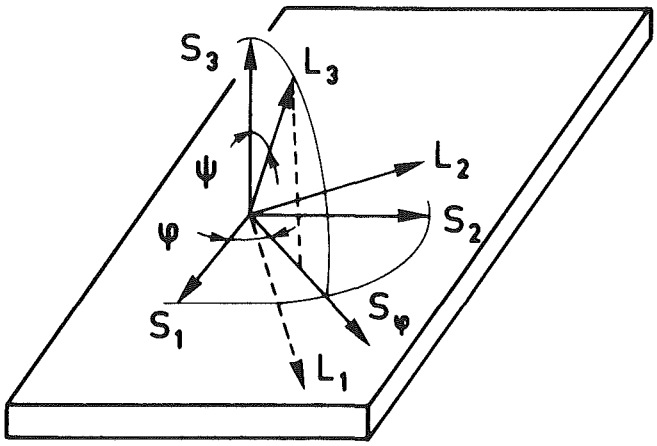


Fig. 2(*a*) Reference system on the specimen surface; S_1 is the grinding direction, L_3 is the normal to the diffracting crystal planes

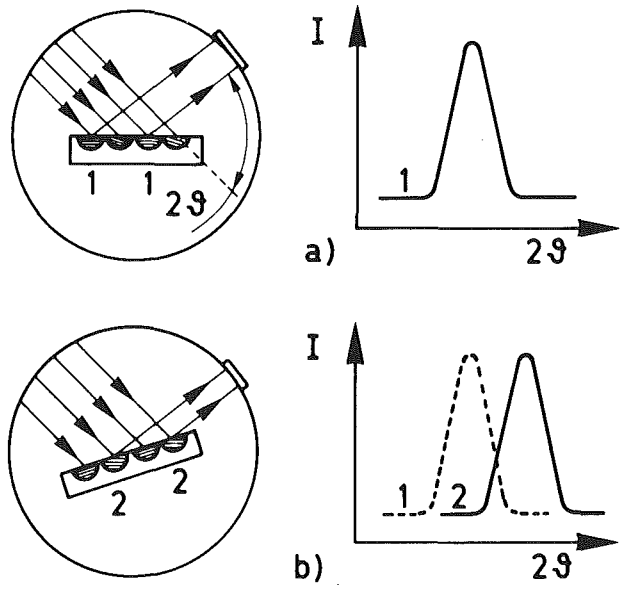


Fig. 1 Diffracted intensity *I* on crystals with different orientations: a change of interplanar distance is related to a shift in the intensity curve; from (Noyan, 1983) adapted

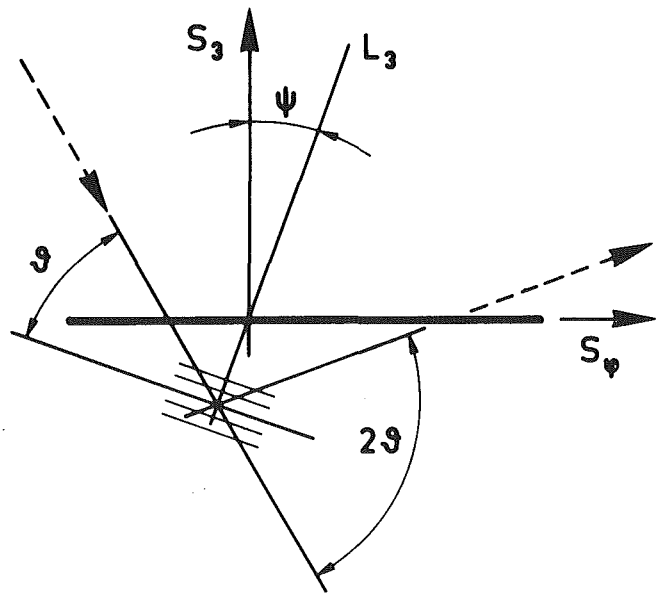


Fig. 2(*b*) Geometry in the plane of the X-ray beam

Downloaded 03 May 2010 to 171.66.16.21. Redistribution subject to ASME license or copyright; see http://www.asme.org/terms/Terms_Use.cfm

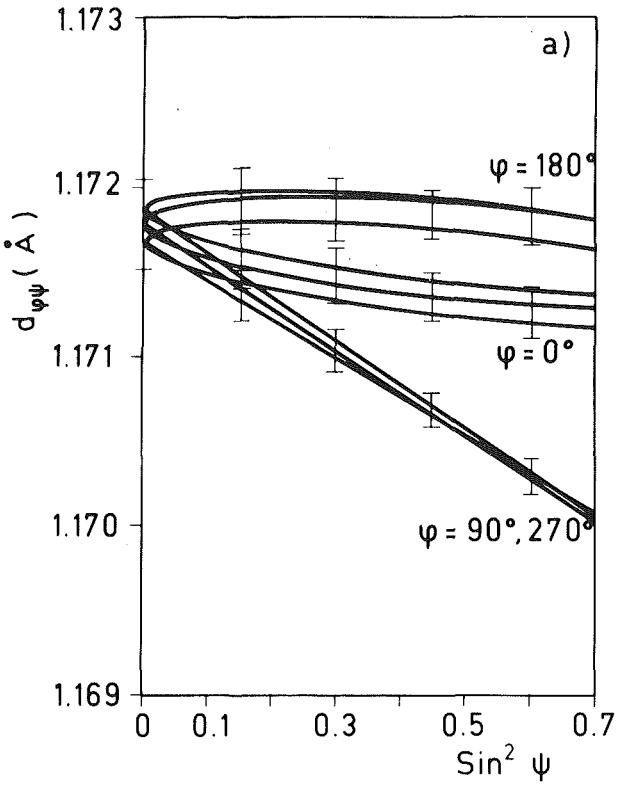


Fig. 3(a) Feed depth = 12.5 m

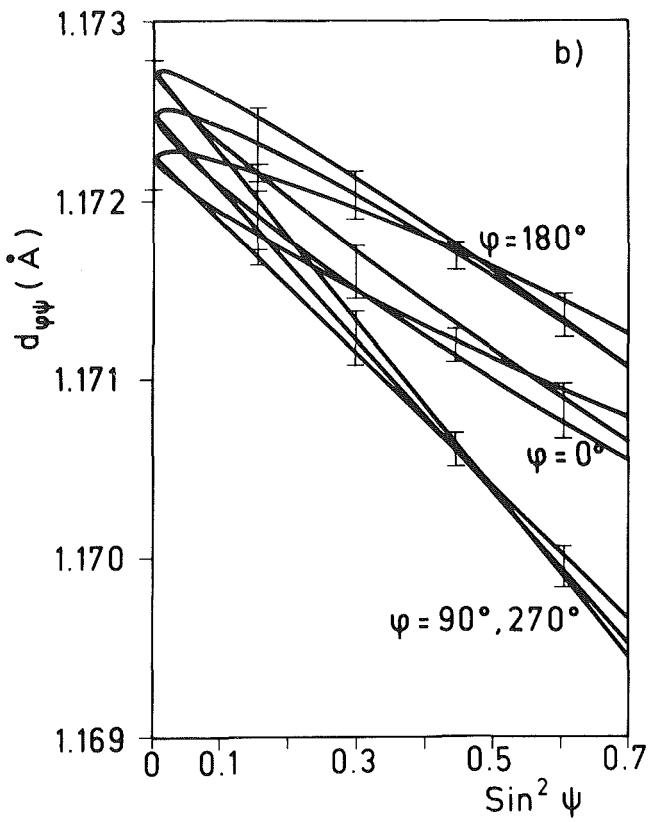


Fig. 3(b) Feed depth = 25.0 m

Fig. 3 ψ-splitting in one-phase martensitic steel for two groups of three specimens each: wheel speed = 30 m/s; feed speed = 17.5 m/min

Mechanical parts, subjected to grinding, abrasive wear or any kind of machining involving tangential forces, have X-ray diffraction results similar to the ones, shown in Fig. 3, where angles $\varphi = 0^\circ$ and $\varphi = 180^\circ$ indicate the grinding direction. This phenomenon, traditionally referred to as ψ-splitting," is explained by the presence of term $\sin 2\psi$ in equation (1). However, the very presence of this term is not obvious, since both equilibrium equations and boundary conditions have to be satisfied in the subsurface layer.

Around ten years ago, researchers began concentrating their efforts on ψ-splitting. The literature shows that, for some years, it was believed that shear strains were produced by shear stresses, in the Cauchy sense, in the presence of very high subsurface stress gradients. Later, it became evident that, in this way, only boundary conditions for stresses were satisfied, whereas differential equilibrium equations yield the result that stress components σ_{13}, σ_{23}, σ_{33} must equal zero everywhere in the subsurface depth (Hauk et al., 1981; Coppa et al. 1983; Brakman, 1983; Coppa and Gola, 1985).

Recently, two hypotheses have been put forward to justify ψ-splitting. They are as follows:

Anisotropy Hypothesis. (Brakman, 1983) Stresses are "macrostresses" in the Cauchy sense and ψ-splitting can be justified by elastic anisotropy induced near the surface by cutting forces; thus no shear stress would exist.

Phase Compensation Hypothesis. (Hauk et al., 1981; Hauk et al., 1982a; Noyan and Cohen, 1983; Hauk, 1983) Shear stresses take place in different phases of the material and have opposite signs, so that they compensate internally. Within this frame, stresses are no longer macrostresses in the Cauchy sense, but are "pseudomacrostresses," since they shift the diffraction intensity curves but would not be revealed by mechanical "stress-relaxation" tests. This is the hypothesis which has gained more favor with the majority of people in the field.

Both hypotheses do not strictly require the presence of a subsurface stress gradient, even if it is necessary to propose that a gradient exists. The second hypothesis does not require that shear stress (here, a pseudomacrostress) in one of the phases should be zero at the surface. On the grain scale, something of this kind will happen at the surface but, in such a case, the concept of stress simply breaks down. It may be worthwhile to remark incidentally that ideas of this kind are still evolving. Noyan and Cohen (1983 p. 137), state that σ_{33} and σ_{13} can exist "only as gradients in the near-surface layers, being by definition zero at the surface." However, in work that followed shortly thereafter (Noyan, 1983), these gradients are not invoked. Hauk et al. (1982a) take stresses as pseudomacrostresses but, then, in Hauk and Krug (1984), when elaborating further on the same data, set σ_{13} arbitrarily equal to zero at the surface when obtaining interpolation curves for the experimental points.

The anisotropy hypothesis was developed in the context of the Reuss model of the polycrystal (Reuss, 1929; Bollenrath et al., 1967), but it could, in principle, be valid for any of the available models (Bollenrath et al., 1967; Kröner, 1963) since in substance it simply implies that, when the material is anisotropic, principal stresses generate shear strains in their same reference system. The idea of work-induced anisotropy (texture) is totally acceptable in principle but

(*a*) The work of Brakman (1983) does not quantitatively compare the measured ψ-splitting with the degree of anisotropy necessary to product it.

(*b*) Hauk et al. (1982a) report cases of ground specimens showing ψ-splitting but not anisotropy using an experimental method, known as the "pole figures," which

Downloaded 03 May 2010 to 171.66.16.21. Redistribution subject to ASME license or copyright; see http://www.asme.org/terms/Terms_Use.cfm

measures diffracted intensity; see also, Hauk (1983) and references therein.

(*c*) Results of Dölle and Cohen (1980) show that a ground sample subjected to bending exhibits the corresponding changes in normal stresses but no change in shear stresses. (These results represent overwhelming evidence against the anisotropy hypothesis.)

A discussion of the second hypothesis is much more complicated. Indeed, measurements of two-phase materials show strain differences between phases. Moreover, there are cases where inner compensation of shear stresses on the basis of the volume was found for two-phase materials, such as ferrite-cementite steel (Hauk, 1983; Hanabusa and Fujiwara, 1982) and brass (Hauk, 1983; Hauk et al., 1982b).

The fact that ψ-splitting is also found in strictly one-phase materials, such as pure iron (Hanabusa and Fujiwara, 1982) or martensitic steel (Coppa, et al. 1983; Coppa and Gola, 1985), as shown in Fig. 3(*a*,*b*) is explained as follows. In one-phase materials, compensation takes place between two different regions of the crystal which, after plastic working, have different concentrations of dislocations (Greenough, 1949, p. 557). In this case, two phases are created in the "mechanical" sense, but one of them would be too incoherent to give a contribution to diffraction. This established idea has experimental support in plastic stretching (Kolb and Macherauch, 1965; Cullity, 1977), and can be applied as such to grinding residual shear stresses (Dölle and Cohen, 1980, p. 163; Hanabusa and Fujiwara, 1982; Noyan, 1983). The X-ray diffraction measurements themselves, of course, cannot be used to verify if shear stress compensation occurs.

A number of experiments especially designed to test the hypothesis of inner compensation were unsuccessful; Table 1 gives a representative account of the state of research, and also lists whether the results are in favor (F) or against (A) the stress compensation hypothesis, or undecided (?).

Table 1 Shear stresses are compensated between phases on volume basis: results against (A) or in favor (F) or undecided (?)

Class	Material	Remarks	Reference	Comment
One phase materials	Fe-ARMCO	$\sigma_{13} \approx$ zero	Dölle and Cohen, 1980	?
	Fe	σ_{13} non zero	Hanabusa and Fujiwara, 1982	?
	Cu	σ_{13} non zero	Hauk, Oudelhoven and Vaessen, 1982a	?
	Mart. Steel	σ_{13} non zero	Coppa and Gola, 1985	?
Two phase materials	Fe-Fe_3C	--------	Hanabusa and Fujiwara, 1982	F
	50% Feα 50% Feγ	σ_{13} of same signs	Hauk, 1983	A
	Brass α,β	--------	Hauk, Stujtie and Vaessen, 1982b	F
Highly heterogen. two-phase synter.	60% Cu 40% Fe	σ_{13} of same signs	Hauk, Oudelhoven and Vaessen, 1982a	A
	30% Cu 70% Fe	σ_{13} of same signs	Hauk, Oudelhoven and Vaessen, 1982a	A

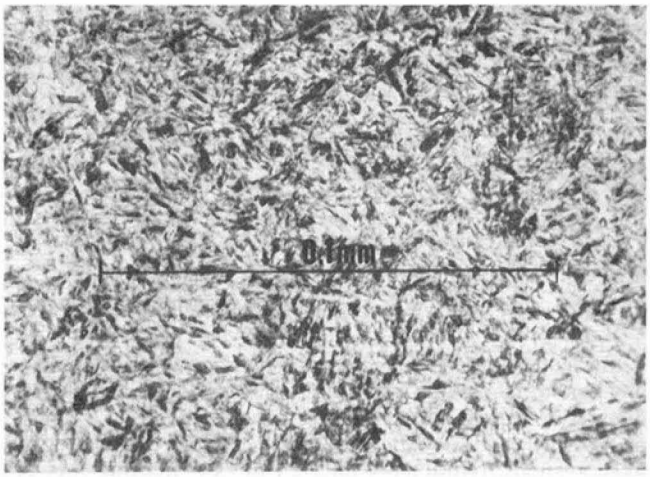


Fig. 4 Micrograph of the martensitic steel: steel: 48 Cr Mo 4 UNI 7845; treatment: oil quench from 860°C; 24 hr at −196°C (liquid nitrogen); hardness = 55 HRC; structure: martensitic, residual austenite less than 2 percent

Couple-Stresses and Residual Stresses

Within the frame of the couple-stress theory, and following the formulation of Koiter (1964), the nonsymmetric stress is split into a symmetrical part s_{ij} and an antisymmetrical part r_{ij}

$$s_{ij}=\frac{1}{2}(\sigma_{ij}+\sigma_{ji}), \quad r_{ij}=\frac{1}{2}(\sigma_{ij}-\sigma_{ji}) \tag{2a,b}$$

while for couples

$$\mu_{ij}=\mu\delta_{ij}+m_{ij} \tag{3}$$

where μ_{ij} is the spherical part of the tensor and m_{ij} is the deviatoric part.

Translational equilibrium equations are the same as those of the classical theory

$$\sigma_{ik,i}=0 \tag{4a}$$

while those for rotations assume the form

$$\epsilon_{ijk}\sigma_{jk}+\mu_{ji,j}=0 \tag{4b}$$

(δ_{ij} and ϵ_{ijk} are Kronecker and Ricci tensors; $_{,j}$ stands for derivative with respect to the jth variable.)

In the present case, having taken direction 1 as the grinding direction, (Fig. 2(*a*)) the nonsymmetric tensor σ_{ij} must satisfy the following conditions.

Mirror Symmetry About Grinding Direction (Any S_3)

$$\sigma_{12}=\sigma_{21}=\sigma_{23}=\sigma_{32}=0 \tag{5}$$

Boundary ($S_3=0$)

$$\sigma_{33}=\sigma_{31}=0 \tag{6}$$

Invariance Along Directions 1 and 2

$$\sigma_{ik,1}=0; \quad \sigma_{ik,2}=0 \tag{7}$$

As a consequence of (6) and (7), equation (4*a*) brings

$$\sigma_{33}=\sigma_{31}=0 \quad (\text{any } S_3) \tag{8}$$

while σ_{11}, σ_{22}, σ_{13} are different from zero.

Moreover, for the couples:

Invariance

$$\mu_{ik,1}=0; \quad \mu_{ik,2}=0 \tag{10}$$

Mirror Symmetry (Any S_3)

$$\mu_{33}=0 \tag{11}$$

and the conditions (5) and (8) lead to

$$\sigma_{13}-\mu_{32,3}=0 \tag{12}$$

Figure 5 illustrates pictorially the effect of equation (12) $\bar{\sigma}_{13}$ is the average stress over the surface of application.

A solution of the residual-stress problem requires knowledge of how the thermoelastic phenomena evolve during grinding. Moreover, in terms of couple-stresses, it requires knowledge of the nonclassical material parameters that appear in the constitutive equations (Koiter, 1964). Finally, it is necessary to ascertain whether the couple-stress or the micropolar theory is applicable.

Downloaded 03 May 2010 to 171.66.16.21. Redistribution subject to ASME license or copyright; see http://www.asme.org/terms/Terms_Use.cfm

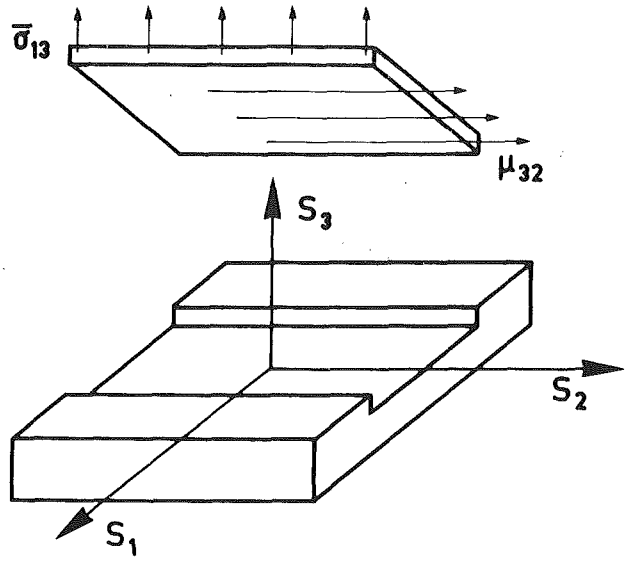


Fig. 5 Equilibrium of a layer of thickness S_3: $\bar{\sigma}_{13}$ is the average value on the thickness; μ_{32} is the value at depth S_3

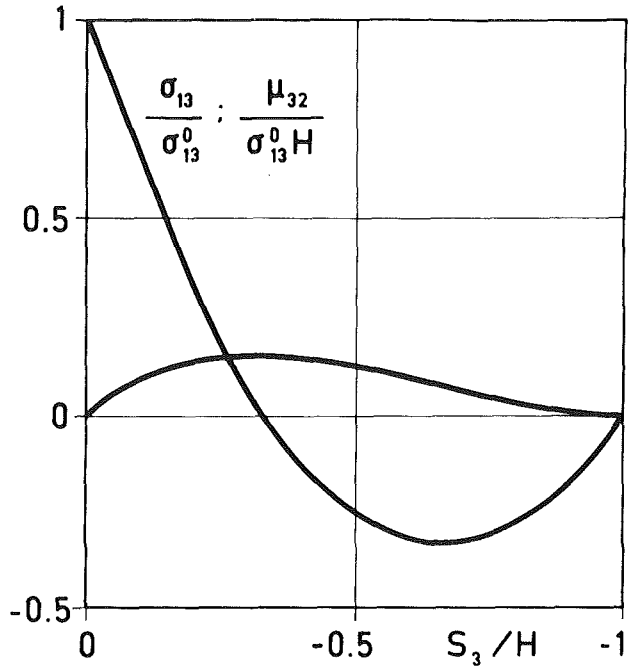


Fig. 6 Illustrative cubic interpolation of shear stress over thickness H: shear stress and couple-stress represented nondimensionally

It is, therefore, clear that any attempt at a solution would be based on a number of tentative hypotheses. In our case, we know that the state of residual strain can be found by experiment. In the simple terms of the equilibrium equations alone, the residual shear stress σ_{13} must have a sign inversion in depth S_3, whatever the residual stress distribution. Figure 6 shows the simplest possible case, in which residual shear stress σ_{13} is imagined to have a cubic law within the subsurface depth H, and the following boundary conditions are satisfied

$$\sigma_{13} = \sigma_{13}^{\circ}; \quad \mu_{32} = 0 \quad (\text{at } S_3 = 0) \tag{13}$$

$$\sigma_{13} = \mu_{32} = 0 \quad (\text{at } S_3 = -H) \tag{14}$$

This sign inversion is necessary in the couple-stress hypothesis and unnecessary in the hypothesis of inner compensation. It can, therefore, be used to discriminate between the two.

A case of inversion in the sign of ψ-splitting, or of shear stress, is found earlier in the literature (Faninger and Walburger, 1976) for a ground steel; later, in (Tönshoff et al., 1982), the same situation is described with the comment that the sign inversion in the ψ-curves and the resulting direction inversion of the shear stresses remain to be clarified.

The reader should note that, within the inner compensation hypothesis, residual shear stresses may, in principle, be unaffected by electrolytic removal which is used to explore the material in depth, but that, within the couple stress hypothesis, this removal alters the boundary conditions, so that a correction is required to adjust the quantitative values.

In Hauk and Krug (1984), stresses found at different depths with different wavelengths are shown together with "real" stresses calculated with a reconstruction procedure, taking into account the attenuation of radiation in the penetrated layer. In this case, a sign inversion also occurs.

ψ-Splitting and Material Parameters

A description of the displacement field takes the following into account: If direction S_1, defined in Fig. 2, is the direction of grinding, i.e., the direction along which tangential cutting forces are applied, and also, considering that the thickness of plastic deformation is orders-of-magnitude lower than the width of the grinding wheel, it is clear that all displacements u in the subsurface layer will be contained in the 1-3 plane (displacements u_1 and u_3). According to Koiter (1964), the strain tensor is defined as usual

$$\epsilon_{ij} = \frac{1}{2}(u_{i,j} + u_{j,i}) \tag{15}$$

and the rotation tensor

$$\omega_i = \frac{1}{2}\epsilon_{ijk}u_{k,j} \tag{16}$$

from which the tensor of torsio-flection

$$\chi_{ij} = \omega_{i,j} \tag{17}$$

The only torsio-flexural term that will exist in the case of grinding is χ_{23}.

As to material properties, in the couple-stress theory, the stress-strain relationships become

$$s_{ij} = 2G\left(\epsilon_{ij} + \frac{\nu}{1-2\nu}\epsilon_{hh}\delta_{ij}\right) \tag{18}$$

$$m_{ji} = 4G\ell^2(\chi_{ij} + \eta\chi_{ji}) \tag{19}$$

where G and ν are the same parameters as in the classical theory and ℓ and η are two new additional parameters; in particular, ℓ is referred to as the "characteristic length."

Since the stress-strain equation (18) has the same structure as that in the classical theory, equation (1) holds if s_{ij} is put in place of σ_{ij}; taking into account (2a), (5), and (8), it follows that

$$\epsilon_{\varphi\psi} = \frac{1+\nu}{E}(\sigma_{11}\cos^2\vartheta + \sigma_{22}\sin^2\vartheta)\cdot\sin^2\psi - \frac{\nu}{E}(\sigma_{11}+\sigma_{22}) + \frac{1+\nu}{2E}\sigma_{13}\cos\varphi\cdot\sin 2\psi \tag{20}$$

which differs from the classical formula only for the numerical coefficient of the last term and for the somewhat different meaning of the shear stress σ_{13}. It is interesting to note that, in order to be able to analyze X-ray results, there is no need to make assumptions on the additional material parameters ℓ and η.

The aim of this work is not to speculate about the physical nature of these parameters but it is very interesting to observe that the constitutive equations of the couple-stress theory coincide with those put forward by Kröner (1963), where it is

Downloaded 03 May 2010 to 171.66.16.21. Redistribution subject to ASME license or copyright; see http://www.asme.org/terms/Terms_Use.cfm

shown that an arrangement of dislocations, due to plastic deformation, is described in continuum language, in terms of a couple-stress field. The material constant he derived, which plays the same role of the "characteristic length," is proportional to the distance between evenly distributed edge dislocations and, therefore, in practice, between the mean dislocation distance.

Conclusions

The presence of subsurface residual shear strains in ground metal specimens is evidenced very clearly by the standard technique of X-ray diffractometry. This evidence takes the form of a splitting of the curves which relate strain and $\sin^2\psi$, where ψ is the angle between the normal to the specimen surface and the normal to the crystal plane being explored.

These strains are explained today by the presence of shear stresses which cannot exist as macrostresses in the Cauchy sense due to equilibrium and boundary conditions, and which, therefore, must exist as pseudomacrostresses mutually compensating between phases of the material.

It has been shown in the present work that a formally correct explanation of the experimental results also can be given in terms of couple-stress or micropolar theories. It also has been shown that the proposed hypothesis is founded on a physically sound kinematical description of elastoplastic displacements which occur during grinding, obeys equilibrium equations, and produces a formula linking strain to stress in X-ray diffraction measurements. This formula has the same structure as the classical one.

The current and the proposed explanations are both physically based on conjectures regarding distributions of dislocations after plastic working, and this makes it evident that they may complement rather than contradict each other. The discussion considered that

(1) The hypothesis of inner compensation is confirmed in a number of cases, but is contradicted in an equivalent number of other cases:

(2) A hypothesis based on the presence of couple-stresses predicts that such a tensor will be revealed only in the presence of extremely high strain gradients; residual strains after grinding are characterized by very high gradients; results in the literature show sign inversions of shear stress which are explained by equilibrium and boundary conditions in terms of couple-stresses.

The X-ray diffraction explores layers of material whose depth is of the same order of magnitude as the depth of any possible couple-stress phenomena produced by grinding. Therefore, it is evident that this method of direct and local detection of strains is the technique of choice for the experimental validation of extended theories of elasticity.

References

Askar, A., 1972, "Molecular crystals and the polar theories of the continua . . . " *Int. J. Engng. Sci.*, Vol. 10, pp. 293–300.

Barrett, C. S., and Massalski, T. B., 1966, "Structure of Metals," McGraw-Hill, pp. 466–485.

Bollenrath, F., Hauk, V., and Müller E. H., 1967, "Zur Berechnung der vielkristallinen Elastizitätskonstanten aus den Werten der Einkristalle," *Z. Metallkd.*, Vol. 58, pp. 76–82.

Brakman, C. M., 1983, "Residual stress in cubic materials with orthorombic or monoclinic specimen symmetry: Influence of texture on ψ-splitting and nonlinear behaviour," *J. Appl. Cryst.*, Vol. 16, pp. 325–340.

Brulin, O., and Hjalmars, S., 1979, "Grade consistent micropolar theory and equivalent media," TRITA-MEK-79-15, Royal Inst. Technol., Dept. Mechs., Stockolm.

Coppa, P., Gola, M. M., and Marinsek, G., 1983, "Misura delle tensioni residue ai raggi X: tensioni da rettifica," *Proc. XI Conv. Naz. AIAS*, Torino-Ivrea, pp. 497–512.

Coppa, P., Gola, M. M., 1985, "Tensioni residue di rettifica e teorie estese dell'elasticitá," *Proc. XIII Conv. Naz. AIAS*, Bergamo, pp. 384–399.

Cosserat, E., and F., 1909, "Theorie des corps deformables," A. Hermann et fils, Paris.

Cullity, B. O., 1978, *Elements of X-Ray Diffraction*, Addison-Wesley, pp. 447–478.

Cullity, B. O., 1977, "Some problems in X-Ray stress measurements," *Adv. X-Ray Anal.*, Vol. 20, pp. 259–270.

Dölle, H., and Cohen, J. B., 1980, "Residual stresses in ground steels," *Met. Trans. A*, Vol. 11A, pp. 159–164.

Ellis, R. W., and Smith, C. W., 1967, "A thin plate analysis and experimental evaluation of couple stress effects," *Experimental Mechanics*, Vol. 7, pp. 372–380.

Eringen, A. C., and Suhubi, E. S., 1964, "Nonlinear theory of simple microelastic solids-I," *International Journal of Engineering Science*, Vol. 2, pp. 189–203.

Faninger, G., and Walburger, H., 1976, "Anomalien bei der röntgenographischen Ermittlung von Schleifeneigenspannungen," Härt. Techn. Mitt., Vol. 31, pp. 79–82.

Gauthier, R. D., and Jahsman, W. E., 1975, "A Quest for Micropolar Elastic Constants," ASME JOURNAL OF APPLIED MECHANICS, Vol. 42, pp. 369–374.

Greenough, G. B., 1949, "Residual lattice strains in plastically deformed polícrystalline metal aggregates," *Proceedings of the Royal Society, Series A*, Vol. 1987, pp. 556–567.

Hanabusa, T., and Fujiwara, H., 1982, "On the relation between ψ-splitting and microscopic residual shear stresses in unidirectionally deformed surfaces," Härt. Techn. Mitt., Beiheft, Carl Hanser Verlag, pp. 209–214.

Hauk, V. M., Oudelhoven, R., and Vaessen, G., 1981, "Ueber die Art der Eigenspannungen nach Schleifen," Härt. Techn. Mitt., Vol. 36, pp. 258–261.

Hauk, V. M., Oudelhoven, R., and Vaessen, G., 1982a, "The state of residual stress in the near surface region of homogeneous and heterogeneous materials after grinding," *Met. Trans. A*, Vol. 13A, pp. 1239–1244.

Hauk, V., Stuitje, P. T. J., and Vaessen, G., 1982b, "Darstellung und Kompensation von Eigenspannungzüstanden in bearbeiteten Oberflächenschichten heterogener Werkstoffe," Härt. Techn. Mitt., Beiheft, Carl Hanser Verlag, pp. 129–133.

Hauk, V. M., 1983, "Stress evaluation on materials having non-linear lattice strain distributions," *Adv. X-Ray Anal.*, Vol. 27, pp. 101–120.

Hauk, V. M., and Krug, W. K., 1984, "Der theoretische Einfluss tiefenabhängiger Eigenspannungzustände auf die röntgenographische Spannungsermittlung, II," Härt. Techn. Mitt., Vol. 39, pp. 273–279.

Koiter, W. T., 1964, "Couple stresses in the theory of elasticity," Koninkl. Ned. Akad. Wet. LXVII, B, pp. 14–44.

Kolb, K., and Macherauch, E., 1965, "Die Eigenspannungsausbildung in verformten Stählen," *Arch Eisenhüttenwesen*, Vol. 36, H. 1, pp. 9–27.

Kröner, E., 1963, "On the physical reality of torque stresses in continuum mechanics," *International Journal of Engineering Science*, Vol. 1, pp. 261–278.

Macherauch, E., and Wolfstieg, U., 1977, "Recent german activities in the field of X-Ray stress analysis," *Materials Science and Engineering*, Vol. 30, pp. 1–13.

Mindlin, R. D., and Tiersten, H. F., 1962, "Effects of couple stresses in linear elasticity," *Archive for Rational Mechanics and Analaysis*, Vol. 11, pp. 415–448.

Mittal, R. N., and Rowe, G. W., 1982, "Residual stresses and their removal from ground En 31 steel components," *Metals Techn.*, Vol. 9, pp. 191–197.

Noyan, I. C., 1983, "Equilibrium conditions for the average stresses measured by X-Rays," *Met. Trans. A*, Vol. 14A, pp. 1907–1914.

Noyan, I. C. and Cohen, J. B., 1983, "Determining stresses in the presence of nonlinearities in interplanar spacing vs. $\sin^2\psi$," *Adv. X-Ray Anal.*, Vol. 27, pp. 129–147.

Reuss, A., 1929, "Berechnung der Fliessgrenze von Mischkristallen auf grund der Plastizitätsbedingungen für Einkristalle," *Zeitschrift fur Angew Angewandte Mathematik und Mechanik*, H.1, Bd. 9, pp. 49–58.

SAE, 1971, "Residual stress measurement by X-Ray diffraction," Soc. Autom. Engrs., N.Y.

Schijve, J., 1966, "Note on Couple Stresses," *Journal of Mechanics and Physics of Solids*, Vol. 14, pp. 113–120.

Tönshoff, H. K., Brinksmeier, E., and Nölke, H. H., 1982, "Vergleich von röntgenographischen und mechanischen Messungen an geschliffenen 100 Cr 6 Proben," Härt. Techn. Mitt., Beiheft, Carl Hanser Verlag, pp. 121–128.

Voigt, W., 1887, Gött. Abh., in "Lehrbuch der Kristallphysik," Johnson Reprint Corp. – Teubner Verlag, rep. 1966 of 1928 ed., pp. 596–616.

Wolfstieg, U., and Macherauch, E., 1976, "Zur azimut-und-tiefen Verteilung von röntgenographisch ermittelten Schleifeigenspannungen," Härt. Techn. Mitt., Vol. 31, pp. 83–85.

Yang, J. F. C., and Lakes, R. S., 1981, "Transient Study of Couple Stress Effects in Compact Bone: Torsion," ASME *Journal of Biomechanical Engineering*, Vol. 103, pp. 275–279.

Yang, J. F. C., and Lakes, R. S., 1982, "Experimental studies of micropolar and couple stress elasticity in compact bone in bending," *Journal of Biomechanics*, Vol. 15, pp. 91–98.

Downloaded 03 May 2010 to 171.66.16.21. Redistribution subject to ASME license or copyright; see http://www.asme.org/terms/Terms_Use.cfm

Acoustic Microscopy at Low Frequency

Tribikram Kundu
Assistant Professor.
Department of Civil Engineering and Engineering Mechanics,
University of Arizona,
Tucson, Arizona 85721
Assoc. Mem. ASME

A new design of the acoustic microscopy experimental set up is proposed and analyzed in this paper. The proposed microscope can operate at low frequency (0.1 to 3 MHz) and can be efficiently used in fracture mechanics, structural, and geomechanics applications. In the new design there is no buffer rod and the transducer is proposed to have a shape of a cylindrical shell to produce a line focus beam which is necessary to measure material anisotropy. A line receiver is introduced instead of standard transducer-cum-receiver arrangements. A line receiver can receive only one specularly reflected ray and a few critically reflected rays and thus produces less complicated interference pattern or acoustic material signature (AMS) which is easier to analyze. The shape of the generated AMS depends on the exact location of the receiver strip. Finally, theoretically synthesized AMS of an aluminum plate for different receiver locations are presented.

1 Introduction

Since the mechanically scanning acoustic microscope was first introduced by Lemons and Quate in 1973, its applications have been widely studied to detect microscopically the variation of acoustic properties of various materials in the fields of biological science, solid material science, and nondestructive evaluation. In the last fifteen years, the resolution of acoustic microscopes has been improved to micron and angstrom levels exceeding the power of an optical microscope. The resolution in mid-1984 was less than 0.2 microns in heated water when the frequency was 5 GHz. In liquid helium it was below 200 angstrom for an operating frequency of 8 GHz (Quate (1985)). Today, for certain applications, acoustic microscopes have been found to be more useful than other microscopes.

When so much research effort is going on in improving the resolution and high frequency performance of acoustic microscopes, it should not be forgotten that for some other applications one needs acoustic microscopes of comparatively low operating frequency, say, a few MHz. At low frequency the acoustic waves can penetrate deeper into a specimen and thus detect a deep crack or impurity in a material. Of course it reduces the resolution of the microscope but for many applications, such as detection of internal cracks and damaged surfaces in rocks and structural elements, one doesn't need very high resolution. Because, at high resolutions, the microscope sees all materials as polycristaline nonhomogeneous materials and it detects grain boundaries near the surface instead of internal cracks at a depth. So researchers in the area of solid mechanics and fracture mechanics use acoustic waves in the frequency range 0.1 to 3 MHz for nondestructive testing techniques (Dowding and Mueller (1987); Mal (1987)). For this reason it is important to study the performance of an acoustic microscope in this frequency range. Commercially available acoustic microscopes operate at frequencies greater than 8 MHz. In this paper it is investigated how, with some modifications in design, an acoustic microscope can be effectively used at a lower frequency.

The acoustic microscope was first introduced as an acoustic scanner instrument in the early 1970s. Afterward, in the late 1970s it was discovered that if the microscope lens is moved vertically over a specimen, then microscope output voltage gives alternately maxima and minima which are produced by successive constructive and destructive interference between specularly and nonspecularly reflected acoustic beams (Atalar et al. (1977); Weglein (1979); Wilson and Weglein (1984); Kundu et al. (1985)). This voltage pattern is known as the acoustic material signature (AMS) or, simply, the $V(z)$ curve. Several elastic properties of the specimen such as its Rayleigh or Lamb wave velocities, compressional wave velocity and wave attenuation factor can be obtained from the specimen's AMS (Weglein (1985)). Kushibiki and Chubachi (1985) could experimentally measure the surface leaking acoustic wave velocities (SLAW) with less than 0.2 percent error and attenuation with about 20 percent error.

A common problem of the presently available acoustic microscopes is that all of them have a buffer rod which introduces aberration and systematic noise due to reverberations at the end of the buffer rod that tend to overlap in time with the reflected signal from the object. To get rid of this aberration and noise, Liang et al. (1985) proposed to use an acoustic transducer having spherical shell shape. However, as pointed out by Kushibiki et al. (1981), a spherical lens has a serious drawback in measuring material properties of an anisotropic material. This drawback comes from the fact that a spherical

Contributed by the Applied Mechanics Division for presentation at the Winter Annual Meeting, Chicago, IL, November 28 to December 2, 1988, of THE AMERICAN SOCIETY OF MECHANICAL ENGINEERS.
Discussion on this paper should be addressed to the Editorial Department, ASME, United Engineering Center, 345 East 47th Street, New York, N.Y. 10017, and will be accepted until two months after final publication of the paper itself in the JOURNAL OF APPLIED MECHANICS. Manuscript received by ASME Applied Mechanics Division, July 31, 1987; final revision, March 31, 1988.
Paper No. 88-WA/APM-51.

Copyright © 1988 by ASME
Downloaded 03 May 2010 to 171.66.16.21. Redistribution subject to ASME license or copyright; see http://www.asme.org/terms/Terms_Use.cfm

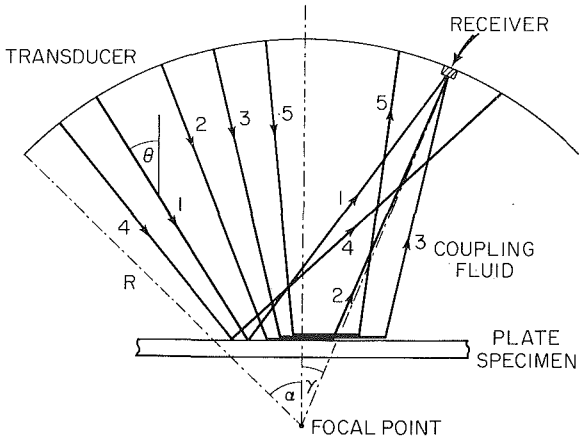


Fig. 1 Schematic of the transducer, receiver, and specimen orientations. Rays 1, 2, and 3 can reach the receiver after reflection but 4 and 5 fail to do so.

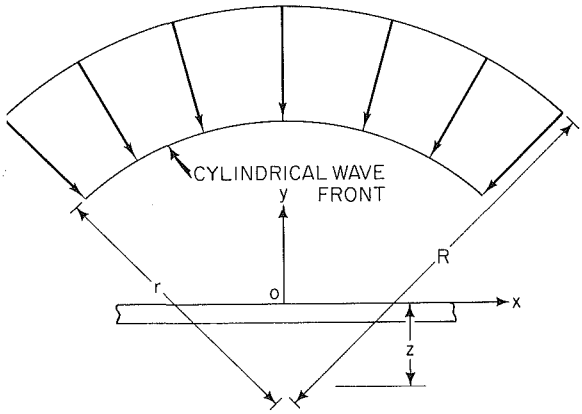


Fig. 2 Schematic of the converging acoustic waves of cylindrical wave front generated by the transducer

lens excites the surface skimming leaky waves propagating in all directions, so that the acoustic properties are measured as a mean value around the beam axis. Thus, a point focus beam can only be used for an isotropic specimen. When the specimen is anisotropic, a cylindrical lens, to produce a line focus beam, is used to measure direction-dependent material properties.

To obtain an aberration and noise-free line focus beam, it is proposed here that a cylindrical shell-shaped acoustic transducer should be used instead of conventional concave circular lens with a buffer rod. The cylindrical shell transducer can directly produce a line focus beam. AMS generated by this beam of 3 MHz frequency for an aluminium plate of 1 mm thickness is theoretically studied in this paper. As described in the next section, a new geometry of the receiver is also proposed here to limit the number of surface skimming acoustic waves that can take part in the interference phenomenon of AMS.

2 Problem Geometry

The schematic of the transducer, receiver, and specimen orientation with the coupling fluid in between the specimen and the transducer is shown in Fig. 1. The transducer, (the piezoelectric element) has the shape of a cylindrical shell which generates acoustic waves converging to a line focus beam at a distance R, the radius of curvature of the shell. If a specimen is placed between the transducer and the line of focus at a distance z from the latter as shown in the figure, some part of the incident energy will be specularly reflected and some other part will be nonspecularly reflected with some horizontal shift. Specular or nonspecular reflection of a ray is decided by its angle of incidence. It is now well known that if an acoustic beam of finite width strikes a fluid-solid interface, it undergoes nonspecular reflection if the angle of incidence coincides wtih some critical angle related to the elastic properties of the reflector (Bertoni and Tamir (1973); Pitts et al. (1977); Bogy and Gracewski (1983)).

If the receiver has the same shape as the transducer, then all specularly and nonspecularly reflected rays will strike the receiver and a complex interference pattern will be produced by all these rays. Such an interference pattern is almost impossible to analyze. It should be mentioned here that in a conventional acoustic microscope the buffer rod in between the lens and the receiver guarantees that only one specularly reflected beam and one, or at the most a few, nonspecularly reflected beams can reach the receiver (Weglein (1979); Kundu (1987)). To obtain the same result in absence of a buffer rod the receiver is modified to a line receiver, whose cross-section is a point shown in Fig. 1. With a line receiver the ray #1 (Fig. 1), whose incident angle is θ, reaches the receiver after specular reflection. Two more rays, 2 and 3, whose incident angles are equal to some critical angles which are smaller than θ, also reach the receiver after a horizontal shift under nonspecular reflection. From simple geometry it can be shown that for a ray whose incident angle is greater than θ, the reflected beam cannot reach the receiver after either specular or nonspecular reflection (ray 4). A beam which is incident at a critical angle that is much smaller than θ also cannot reach the receiver if the horizontal shift at the fluid-solid interface is not very large (ray 5). So, for any receiver position γ (γ is the angle that the receiver makes with the transducer central axis at its focal point in Fig. 1), a specularly reflected ray (ray 1) and only a few nonspecularly reflected rays (rays 2 and 3) whose incident angles are slightly smaller than θ can reach the receiver. Thus, with this transducer-receiver arrangement AMS are generated by only a few rays and they are much easier to analyze.

3 Problem Formulation

The first step for solving the problem described in the previous section is to obtain the angle of incidence θ for the specularly reflected ray (ray 1 of Fig. 1) for a given transducer geometry, receiver orientation, and reflecting surface position. After some geometric and trigonometric manipulation, it can be shown that

$$\theta = \arctan\left(\frac{\sin\gamma}{\sin\gamma - 2z/R}\right) \tag{1}$$

γ, z, and R are shown in Fig. 1.

In addition to the ray which is incident at angle θ, all other rays which are incident at critical angles less than θ should also be analyzed to obtain the total motion of the receiver which is proportional to the voltage produced by it.

3.1 Acoustic Field Produced by the Transducer. Acoustic wave field produced by the transducer will have a converging cylindrical wave front. From energy consideration, one can arrive at the potential expression of this propagating wave at a distance r from the focal point (see Fig. 2),

$$\phi = P(x)A\left(\frac{R}{r}\right)^{1/2} e^{ik_f(R-r)} \tag{2a}$$

where A is the amplitude of the wave generated by the transducer, $k_f = \omega/\alpha_f$, ω is the circular frequency of the generated acoustic wave and α_f is the acoustic wave velocity in the coupling fluid. $P(x)$ is the pupil function of the lens, which, in the most general case, takes into account the nonuniform excitation of the transducer and any aberration

Downloaded 03 May 2010 to 171.66.16.21. Redistribution subject to ASME license or copyright; see http://www.asme.org/terms/Terms_Use.cfm

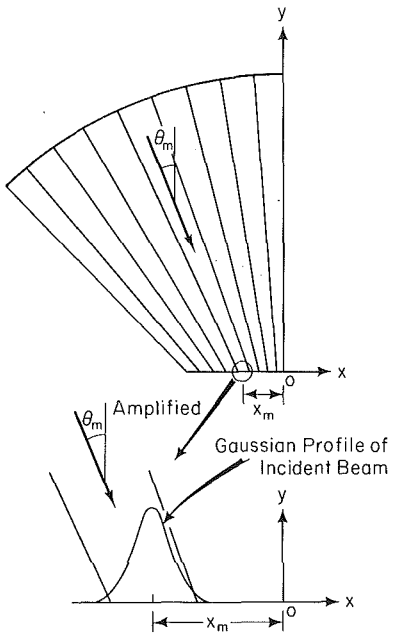


Fig. 3 Discretization of the incident field into a number of acoustic beams of finite width with a Gaussian variation of field strength

and edge diffraction effects. In the simplest case for an ideal situation (Liang et al. (1985)),

$$P(x)=\begin{cases}1, & \text{if } 0\le |x|\le z\tan\alpha;\\ 0, & \text{if } |x|>z\tan\alpha.\end{cases} \tag{2b}$$

This simplifying assumption is justified on the following ground. It is true that the edge diffraction is not modeled properly by the above equation and, hence, the true acoustic field near the edge of the illuminated region ($x\simeq z\tan\alpha$) is different from its mathematical representation. However, for that region the angle of incidence of the acoustic beam is large, and it will be seen later that those large angles do not contribute to the AMS significantly. Thus, any error in modeling the edge of the illuminated region will not introduce significant error in the final results.

Since r varies along the reflecting surface the incident wave potential will be a function of x, the position of the point of interest on the reflecting surface.

$$\phi_i(x,0)=\frac{\sqrt{R}}{(x^2+z^2)^{1/4}}\exp\{ik_f[R-(x^2+z^2)^{1/2}]\} \tag{3}$$

In the above equation, A is set equal to 1.

3.2 Discretization of the Incident Field. The incident field $\phi_i(x, 0)$ is now assumed to be composed of several acoustic beams of finite width striking the reflector at different incident angles as shown in Fig. 3. It has already been shown that out of all these incident beams, only the beams incident at angle θ and at critical angles less than θ are important for AMS computation. So only those beams will be considered in the analysis.

For algebraic simplicity, it is assumed that each bounded beam has a Gaussian variation of field strength (Fig. 3), whose expression is given by

$$\phi_i^{(m)}(x,0)=\exp\left\{-\left(\frac{x_m+x}{a}\right)^2+ik_m(x_m+x)\right.$$
$$\left.+ik_f[R-(x_m^2+z^2)^{1/2}]\right\}\frac{\sqrt{R}}{(x_m^2+z^2)^{1/4}} \tag{4}$$

where

$$x_m=z\tan\theta_m$$
$$k_m=k_f\sin\theta_m$$

and a is a measure of the width of the incident beam.

Equation (4) is obtained based on our engineering judgement: by equating the peak value of the Gaussian beam strength to the field strength at the point of incidence, calculated from equation (3), with the beam width parameter "a." It will be shown later (in Fig. 7) that although "a" has a strong influence on the detail of an AMS shape it doesn't significantly affect the period of oscillations of the AMS, which is an important parameter for characterizing the material.

Alternatively, this discretization can be obtained by Gaussian beam summation method as advocated by Popov (1982), White et al. (1987), or by complex source point technique as proposed by Pott and Haris (1984); Haris and Pott (1985); and Lu et al. (1987).

3.3 The Reflected Field. To obtain the reflected field of equation (4), its Fourier inversion with respect to x is carried out (Bertoni and Tamir (1973)) to get

$$\Phi_i^{(m)}(k,0)=\int_{-\infty}^{\infty}\phi_i^{(m)}(x,0)e^{-ikx}dx=\frac{a\sqrt{\pi R}}{(x_m^2+z^2)^{1/4}}$$
$$\exp\left\{-(k-k_m)^2\left(\frac{a}{2}\right)^2+ik_f[R-(x_m^2+z^2)^{1/2}]\right\} \tag{5}$$

In the above expression, $\Phi_i^{(m)}(k, 0)$ becomes negligibly small for $|k-k_m| > \pi/a$.

The reflected field at any point (x, y) can now be obtained by simply multiplying $\Phi_i^{(m)}(k, 0)$ by the plane wave reflection coefficient $R(k)$ of the reflector and a propagation term and, then inverting it,

$$\phi_r^{(m)}(x,y)=\frac{1}{2\pi}\int_{-\infty}^{\infty}R(k)\Phi_i^{(m)}(k,0)e^{i(kx+\eta y)}dk \tag{6}$$

where

$$\eta=\begin{cases}(k_f^2-k^2)^{1/2} & \text{for } |k|<k_f\\ i(k^2-k_f^2)^{1/2} & \text{for } |k|>k_f\end{cases} \tag{7}$$

The reflection coefficient $R(k)$, for uniform as well as multilayered plates and half spaces, can be obtained by Thomson-Haskell matrix method as described in Kundu et al. (1985) and Kundu and Mal (1986).

The infinite integral of equation (6) is carried out numerically between the limits ($k_m - \pi/a$) and ($k_m + \pi/a$), beyond which the integrand is negligibly small.

Since we are interested in the receiver motion, point (x, y) is considered at the receiver position. Reflected fields at (x, y), due to all rays of interest, are computed from equation (6). Then they are superimposed to compute the total reflected field and, hence, the voltage generated by the receiver is obtained. Repeating this operation for different values of z, the total AMS or $V(z)$ curve is constructed.

4 Simplified Ray Analysis

As an alternative to the cumbersome wave-number integral approach which was discussed in the previous section, the following simplified ray analysis approach may give us a first approximation of the expected shape of the AMS.

Figure 4 shows the schematic of specularly and nonspecularly reflected rays. The specularly reflected ray is incident at angle θ whereas the nonspecularly reflected ray is incident at a critical angle $\delta < \theta$. δ corresponds to a wave velocity c of the reflector, which may be Rayleigh, Lamb, P, or S wave velocity. c and δ are related in the following manner

Downloaded 03 May 2010 to 171.66.16.21. Redistribution subject to ASME license or copyright; see http://www.asme.org/terms/Terms_Use.cfm

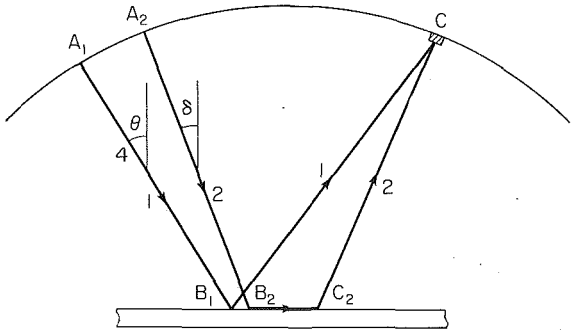


Fig. 4 Ray diagrams of two different paths 1 and 2 travelled by specularly and nonspecularly reflected beams

$$\delta = \arcsin\left(\frac{\alpha_f}{c}\right) \tag{8}$$

As mentioned previously, α_f is the acoustic wave velocity in the fluid.

At the transducer surface (points A_1 and A_2) rays 1 and 2 have the same phase, but they travel different paths before they reach the receiver. Ray 1 travels A_1B_1C path with a velocity α_f where as ray 2 travels A_2B_2 and C_2C segments with a velocity α_f and B_2C_2 length with a velocity c. After some geometric manipulation and trigonometric simplification, the phases of two rays at the receiver can be obtained as

$$k_f\left(R - \frac{z}{\cos\theta} + R\,\frac{\sin(\theta+\gamma)}{\sin 2\theta}\right) \tag{9}$$

$$k_f\Bigg(R - \frac{2z}{\cos\delta} + R\,\frac{\cos\gamma}{\cos\delta} z\sin\delta(\tan\delta + \tan\gamma) + \tan\delta\sin(\gamma-\delta)\left[R - \frac{z}{\cos\gamma}\right]\Bigg) \tag{10}$$

From the above expressions one can calculate the phases of the two rays at the receiver position, but is is impossible to obtain their amplitudes without carrying out the computations described in Section 3. However, for calculating the spacings between two successive dips of an AMS, the phases of returning waves are more important than their amplitudes. To obtain this spacing, amplitude of all returning waves is arbitrarily assigned to one. Then expressions (9) and (10) are simply added to obtain the receiver motion for different z. If contributions of critically reflected rays other than the one shown in Fig. 4 are to be considered, then their phases at the receiver position would have to be computed by an expression similar to that of (10) with δ replaced by the incident angles of those rays. Then all these phases should be added to get the total receiver motion.

5 Results

Numerical results are given in this section for an aluminium plate of one mm thickness, immersed in water. The transducer has a cylindrical shape as shown in Fig. 1 with $\alpha = 45$ deg and radius of curvature $R = 170$ mm. The frequency of the transducer generated acoustic waves is 3 MHz. At this frequency the dispersion equation of the Al-plate has five roots which in km/s are 30.01, 7.82, 6.12, 3.36 and 2.84. The acoustic wave velocity (α_f) in water is 1.5 km/s. Then five critical angles corresponding to the five Lamb Roots of the Al-plate can be obtained from equation (8); these are 2.865, 11.06, 14.20, 26.55, and 31.93 deg. The receiver is positioned at an angle $\gamma = 20$ deg (see Fig. 1). The top reflecting surface of the plate is moved from the focal point upwards to a distance of 21 mm and the receiver motion is computed as a function of this movement. We will call this generated curve as AMS.

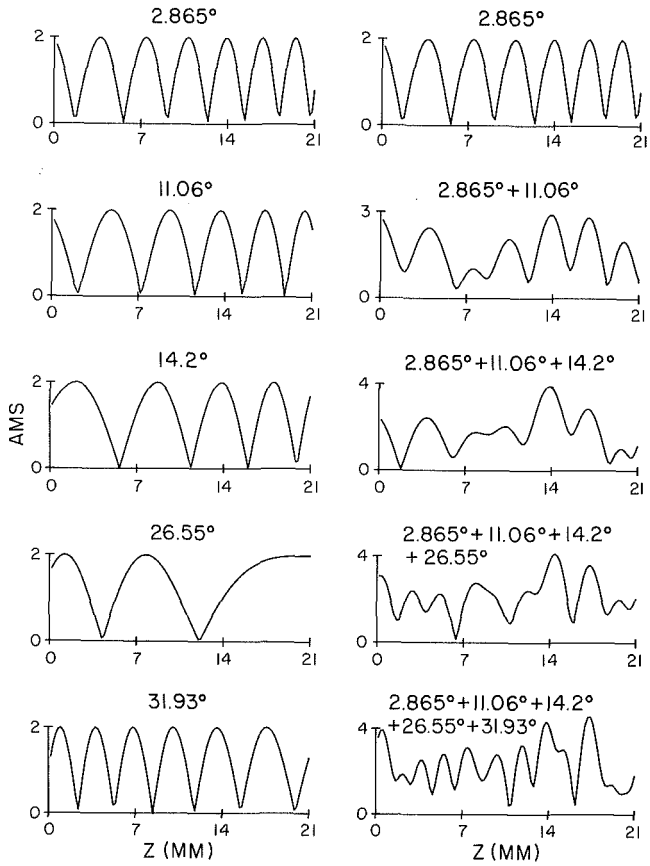


Fig. 5 AMS of the 1 mm thick Al-plate generated by simplified ray theory (Section 4). Left column considers five critical angles separately, right column shows the cumulative effect. $\gamma = 20$ deg, $\alpha = 45$ deg, $R = 17$ cm, and frequency = 3 MHz.

As a first approximation, expressions (9) and (10) are used to compute the interference pattern generated by the specularly and nonspecularly reflected rays. Results are shown in Fig. 5. The left column shows the interference pattern produced by only two rays, one is directly reflected and the other is critically reflected. The incident angle of the critical ray varies from 2.865 deg (top figure) to 31.93 deg (bottom figure). The incident angle of the specularly reflected ray is a function of z as given in equation (1). The right column shows the cumulative effect, when one (top figure) through all five (bottom figure) critical angles are considered in computing the AMS. It can be seen from these plots that when only one critical angle is considered in the interference pattern then more or less uniform spacings between the dips are obtained in the AMS. But as the number of critical angles is increased, the AMS pattern becomes much more complex and then its shape is almost impossible to analyse to obtain information about the reflector material. However, actual AMS pattern produced by the experimental setup of Fig. 1 will be much simpler than the AMS pattern shown in the bottom right corner of Fig. 5. This is because with the proposed experimental setup only a few (one or two) critically reflected rays will have significant amplitude at the receiver location.

Finally, AMS of the 1 mm thick Al-plate is computed following the formulation outlined in Section 3. One difficulty in this computation is associated with the choice of the beam width factor "a" of equation (4). Ideally a should vary with z and the angle of incidence of the beam. In Fig. 6 it is shown how strongly the variation of a affects the reflected beam pro-

Downloaded 03 May 2010 to 171.66.16.21. Redistribution subject to ASME license or copyright; see http://www.asme.org/terms/Terms_Use.cfm

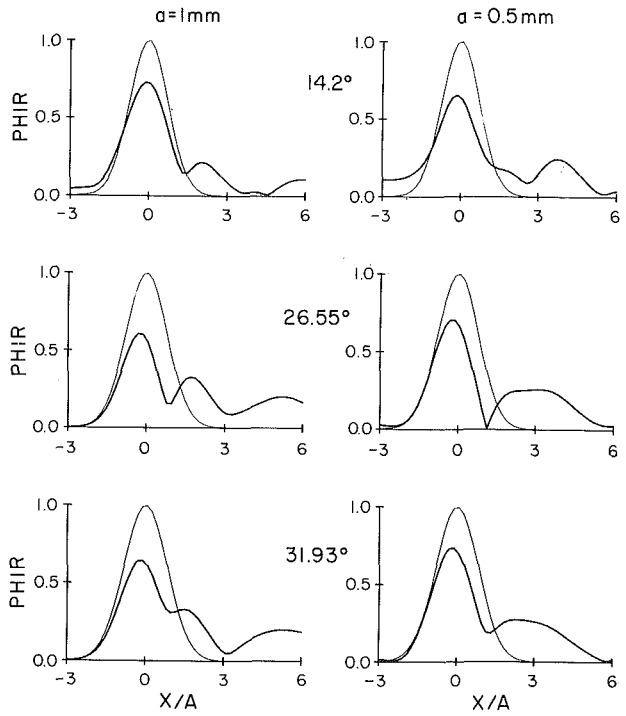


Fig. 6 Incident (thin curves) and reflected beam profiles (thick curves) when an acoustic beam of 3 MHz frequency and with the width factor a (see equation (4)) equal to 1 mm (left column) or 0.5 mm (right column) is reflected by an aluminium plate of 1 mm thickness, immersed in water. Three critical angles of incidence shown here are 14.2 deg (top row), 26.55 deg (middle row), and 31.93 deg (bottom row).

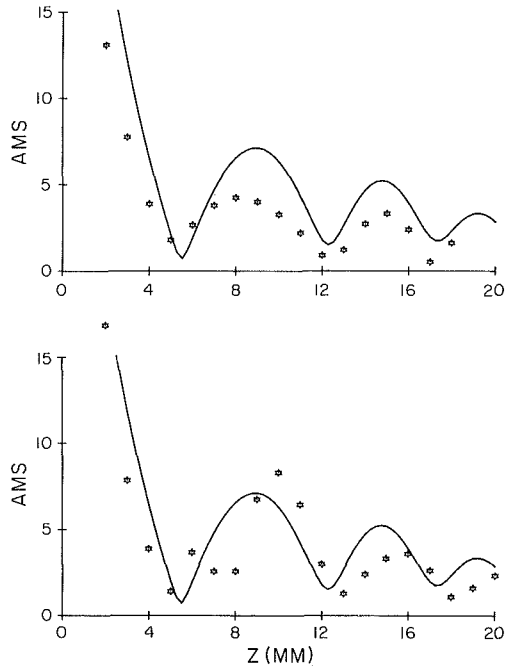


Fig. 7 AMS of the 1 mm thick Al-plate synthesized by wave number integral approach (Section 3). γ, α, R and frequency are the same as Fig. 5. The solid curve is obtained when $a = 1$ mm and contributions of only those critical angles which are less than θ (see Fig. 1) are considered. Stars in the top figure are obtained when a is reduced to 0.5 mm. Stars in the bottom figure are obtained when contributions of all critical angles are considered with $a = 1$ mm.

file. Incident acoustic beams have a Gaussian variation of the strength profile (Fig. 3) with two different values of a, 1 mm (left column) and 0.5 mm (right column). Incident and reflected beam profiles for three critical angles of incidence are shown in this figure, which are 14.2 (top row), 26.55 (middle row), and 31.93 (bottom row) degrees. Similar plots were obtained for other critical angles also. In each plot the thin curve represents the incident beam and the thick curve is the reflected beam profile. It can be seen that the intensity of leaky waves varies with the beam width factor. How strongly does it affect the AMS shape? The answer to this question can be found in the top graph of Fig. 7. In this plot AMS of the Al-plate is shown for two different values of a. The solid line corresponds to $a = 1$ mm and the stars correspond to $a = 0.5$ mm. It should be noted here that although the curve and the stars do not coincide exactly, the spacing length between two dips does not change with a. This is an important observation because it proves that a small error in the choice of a does not significantly affect the spacing length which is in our interest for obtaining the material properties of the reflector. It should also be noted here that the spacing of the AMS in Fig. 7 is close to that of the middle plot of the left column of Fig. 5. That plot of Fig. 5 was generated by the interference between specularly reflected beam and the critical beam, incident at an angle of 14.2 deg. It clearly indicates that out of all critically reflected rays, only the ray incident at 14.2 deg has significant effect at the receiver position when $\gamma = 20$ deg.

The bottom graph of Fig. 7 studies the change in AMS shape when all critical angles are considered in computing the AMS, instead of considering only the critical angles less than the incident angle θ of the specularly reflected ray. According to Fig. 4, a critically incident ray after some horizontal shift and then reflection can reach the receiver only if the critical angle is less than θ. However, since it is assumed that every beam has some width, they may overlap one another because

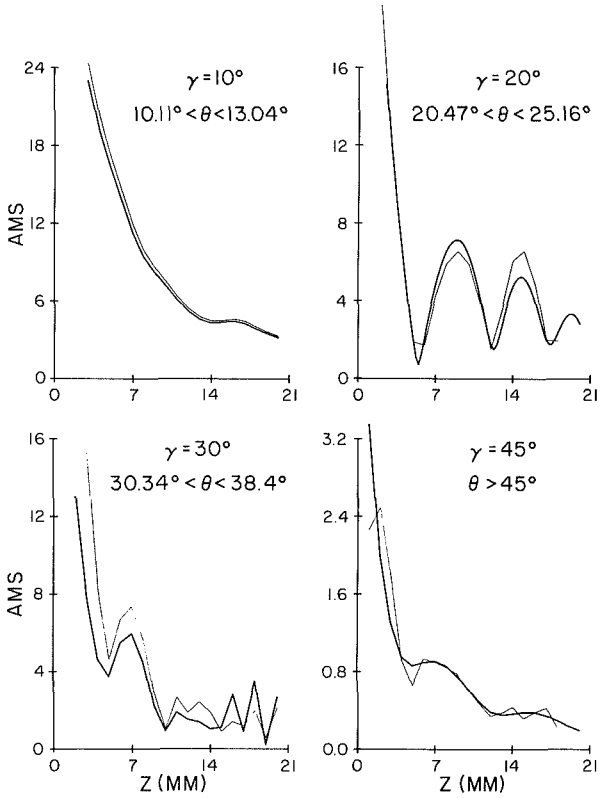


Fig. 8 AMS of the Al-plate for four different receiver positions $\gamma = 10$, 20, 30, and 45 deg. Range of θ (see Fig. 1 and equation (1)) for every γ is listed in the plots. Thick curves are the AMS of the Al-plate when it has water on its both sides and thin curves are obtained when lower water half-space is removed.

of some error in the width factor a. Then beams with incident angles greater than θ can also contribute to the interference pattern. For $\gamma = 20$ deg, θ varies from 20.47 (for $z = 1$ mm) to

Downloaded 03 May 2010 to 171.66.16.21. Redistribution subject to ASME license or copyright; see http://www.asme.org/terms/Terms_Use.cfm

25.16 deg (for z = 21 mm). So, ideally, critical angles 26.55 and 31.93 deg should never contribute to the AMS. However, if the computer program is instructed to compute the motion at the receiver position coming from these two critical angles, we get some nonzero value because of the overlapping and the finite width of the beams. If these values are included in constructing the AMS, its shape is changed from the solid curve to the stars shown in the figure. Here also the error in the spacing distance coming from considering all critical angles is not very significant, although the details of the AMS shape change quite a bit.

Finally, in Fig. 8 it is shown how the AMS shape varies as the receiver orientation changes from γ = 10 to 45 deg. The range of θ for every γ is mentioned in each plot. It should be noted here that θ increases with γ and, hence, for bigger γ more critically reflected rays contribute to the AMS pattern and make it more complex. When γ is too big, say 45 deg, θ is greater than 45 deg. But the transducer with its present geometry cannot generate any wave with incident angle greater than 45 deg and, hence, no specularly reflected ray can reach the transducer for that receiver orientation. However, some nonspecularly reflected rays may strike the receiver after a horizontal shift at the fluid-reflector interface. In each plot the thick curve represents the AMS of Al-plate when it has water on both sides and the thin curve represents the AMS of the same plate when the top surface of the plate is still under water but the bottom surface is stress free. It can be concluded from this figure that the presence or absence of the water half-space beneath the Al-plate doesn't have significant effect on the AMS patterns.

6 Concluding Remarks

The analysis of a new design of the acoustic microscopy set-up shows some promising aspects regarding the use of acoustic microscopes at low frequency. It gives a way of getting rid of the buffer rod but still producing AMS from the interference among only a few rays. Numerical results show that simplified ray analysis can predict the spacing between two successive dips of the AMS with reasonable accuracy if one knows a priori which incident rays have significant contributions to the AMS.

The scope of this paper is limited to the synthesis of AMS with the new microscope geometry. It needs further investigation to analyze these material signatures for obtaining material properties and geometries of the reflector specimen.

Acknowledgment

This research was partially supported by the National Science Foundation under Grant Number MSM-8502120.

References

Atalar, A., Quate, C. F., and Wickramasinghe, H. K., 1977, "Phase Imaging in Reflection with the Acoustic Microscope," *Applied Physics Letters*, Vol. 31, pp. 791–793.

Bertoni, H. L., and Tamir, T., 1973, "Unified Theory of Rayleigh-Angle Phenomena for Acoustic Beams at Liquid-Solid Interface," *Applied Physics*, Vol. 2, pp. 157–172.

Bogy, D. B., and Gracewski, S. M., 1983, "On the Plane Wave Reflection Coefficient and Nonspecular Reflection of Bounded Beams for Layered Half Spaces Under Water," *Journal of the Acoustical Society of America*, Vol. 74, pp. 591–599.

Dowding, C. H., and Mueller, C. G., 1987, "Factors Affecting the Relative Magnitude of Acoustic Emissions Generated During the Fracture of Granite," *Proceedings of the 28th U.S. Symposium on Rock Mechanics*, Tucson, Arizona, pp. 359–366.

Harris, J. G., and Pott, J., 1985, "Further Studies of the Scattering of a Gaussian Beam from a Fluid-Solid Interface," *Journal of the Acoustical Society of America*, Vol. 78, pp. 1072–1080.

Kundu, T., 1987, "On Some Aspects of Acoustic Material Signature," *Multiple Scattering of Elastic Waves in Random Media and Random Rough Surfaces*, V. K. Varadan and V. V. Varadan, eds., Kurtz Brothers, Pennsylvania, pp. 832–844.

Kundu, T., and Mal, A. K., 1986, "Acoustic Material Signature of a Layered Plate," *International Journal of Engineering Science*, Vol. 24, No. 12, pp. 1819–1829.

Kundu, T., Mal, A. K., and Weglein, R. D., 1985, "Calculation of the Acoustic Material Signature of a Layered Solid," *Journal of the Acoustical Society of America*, Vol. 77, No. 2, pp. 353–361.

Kushibiki, J., and Chubachi, N., 1985, "Material Characterization by Line-Focus-Beam Acoustic Microscope," *IEEE Transactions on Sonics and Ultrasonics*, Vol. SU-32, pp. 189–212.

Kushibiki, J., Ohkubo, A., and Chubachi, N., 1981, "Linearly Focused Acoustic Beams for Acoustic Microscopy," *Electron Letters*, Vol. 17, pp. 520–522.

Lemons, R. A., and Quate, C. F., 1973, "A Scanning Acoustic Microscope," *Proceedings of IEEE Ultrasonic Symposium*, pp. 18–20.

Liang, K. K., Kino, G. S., and Khuri-Yakub, B. T., 1985, "Material Characterization by the Inversion of $V(z)$," *IEEE Transactions on Sonics and Ultrasonics*, Vol. SU-32, pp. 213–224.

Lu, I. T., Felsen, L. B., and Ruan, Y. Z., 1987, "Spectral Aspects of the Gaussian Beam Method: Reflection from a Homogeneous Half-Space," *Geophys. Journal of the Royal Astronomical Society*, Vol. 89, pp. 915–932.

Mal, A. K., 1987, Private Communication.

Pitts, L. E., Plona, T. J., and Mayer, W. G., 1977, "Theory of Nonspecular Reflection Effects for an Ultrasonic Beam Incident on a Solid Plate in Liquid," *IEEE Transactions on Sonics and Ultrasonics*, Vol. SU-24, pp. 101–108.

Popov, M. M., 1982, "A New Method of Computation of Wave Fields Using Gaussian Beams," *Wave Motion*, Vol. 4, pp. 85–92.

Pott, J., and Harris, J. G., 1984, "Scattering of an Acoustic Gaussian Beam from a Fluid-Solid Interface," *Journal of the Acoustical Society of America*, Vol. 76, pp. 1829–1838.

Quate, C. F., 1985, "Acoustic Microscopy: Recollections," *IEEE Transactions on Sonics and Ultrasonics*, Vol. SU-32, pp. 132–135.

Weglein, R. D., 1979, "A Model for Predicting Acoustic Material Signatures," *Applied Physics Letters*, Vol. 34, pp. 179–181.

Weglein, R. D., 1985, "Acoustic Micrometrology," *IEEE Transactions on Sonics and Ultrasonics*, Vol. SU-32, pp. 225–234.

White, B. S., Norris, A., Bayliss, A., and Burridge, R., 1987, "Some Remarks on the Gaussian Beam Summation Method," *Geophys. Journal of the Royal Astronomical Society*, Vol. 89, pp. 579–636.

Wilson, R. G., and Weglein, R. D., 1984, "Acoustic Microscopy of Materials and Surface Layers," *Journal of Applied Physics*, Vol. 55, pp. 3261–3275.

Downloaded 03 May 2010 to 171.66.16.21. Redistribution subject to ASME license or copyright; see http://www.asme.org/terms/Terms_Use.cfm

The Interior Solution for Linear Problems of Elastic Plates

R. D. Gregory
Department of Mathematics,
University of Manchester,
Manchester M13 9PL,
England

F. Y. M. Wan[1]
Department of Applied Mathematics,
University of Washington, FS-20,
Seattle, WA 98195
Mem. ASME

Necessary conditions have been established recently for the prescribed data along the cylindrical edge(s) of an elastic flat plate to induce only an exponentially decaying elastostatic state. The present paper describes how these conditions may be used to determine the interior solution (or its various thin and thick plate theory approximations) of plate problems. The results in turn show that the necessary conditions for a decaying state are also sufficient conditions. Boundary conditions for the interior solution of circular plate problems with edgewise nonuniform boundary data are discussed in detail and then applied to two specific problems. One of them is concerned with a circular plate compressed by two equal and opposite point forces at the plate rim. The solution process for this problem illustrates for the first time how the stretching action in the plate interior induced by transverse loads can be properly analyzed.

1 Introduction

The exact solution of *linear* elastostatic problems for thin plates is known to consist of an *interior* component and *layer* components. The interior solution is significant throughout the plate, whereas a layer solution has only a localized effect in a region near an edge of the plate with a typical layer width of the order of the plate thickness. Boundary conditions at an edge of the plate are generally satisfied by a combination of the two types of solution components. The interior solution has been known since the work of M. Lévy (1877) and confirmed more recently by Friedrichs and Dressler (1961), Gol'denveizer (1962), Gol'denveizer and Kolos (1965), Reiss (1962), Reiss and Locks (1961) and Reissner (1963). On the other hand, the exact layer solutions or their accurate approximations are difficult to obtain (see Friedrichs and Dressler (1961), for example). To the extent that the layer solution behavior may not be needed for some design purposes, there has been a continual effort over the years to determine the interior solution of Lévy or its approximation (in the form of the Kirchhoff thin plate theory or some moderately thick plate solution) without any reference to the layer solutions (Reissner, 1985). For stress edge data, Saint-Venant's principle has been invoked to derive an appropriate set of stress boundary conditions for plate theory solutions (Love, 1944; Timoshenko and Goodier, 1951). Strictly speaking, this principle does not apply to plate problems, as one linear dimension of the loaded area (namely, the circumference of the plate's midplane) or the characteristic length of the edge load there, is *not* small compared to a representative plate span. Another interesting approach which also makes use of Saint-Venant's principle has been proposed by Kolos (1965) but is not entirely satisfactory for reasons given previously (Gregory and Wan, 1984, 1985a, 1985b).

A new and completely different method was developed recently by Gregory and Wan (1984) for the determination of the "exact" or approximate interior solution without any knowledge of the layer solution components for the same problem. In contrast to previous attempts, all of which were based on some form of Saint-Venant's principle, the key to our method lies in a novel application of the Betti-Rayleigh reciprocal theorem. Necessary conditions have been deduced from this theorem for any admissible set of edge data to induce only an elastostatic state which decays exponentially at a distance away from the plate edge of the order of the plate thickness. These necessary conditions are to be translated into an appropriate set of boundary conditions for the Lévy solution or some (approximating) plate theory solution. They effectively allow us to split the prescribed edge data correctly into two parts, one for the interior solution components and the other for the layer solution components. The special case of plates with straight edges in a state of plane strain induced by edgewise uniform data was first treated by this method (Gregory and Wan, 1984). The resulting edge conditions, for the interior solution component, made it possible for us to solve some specific displacement boundary-value problems in thin and thick plate theories which had not admitted a rational solution previously (Gregory and Wan, 1984).

Next, Gregory and Wan (1985a) treated the axisymmetric bending of circular plates. For stress edge data, our results show that indiscriminate applications of Saint-Venant's principle for this class of problems may lead to qualitatively and quantitatively incorrect solutions in the plate interior; they in

[1]The research of this author is supported by the NSF through Grant No. DMS-8606198.

Contributed by the Applied Mechanics Division for presentation at the Winter Annual Meeting, Chicago, IL, November 28 to December 2, 1988, of THE AMERICAN SOCIETY OF MECHANICAL ENGINEERS.

Discussion on this paper should be addressed to the Editorial Department, ASME, United Engineering Center, 345 East 47th Street, New York, N.Y. 10017, and will be accepted until two months after final publication of the paper itself in the JOURNAL OF APPLIED MECHANICS. Manuscript received by ASME Applied Mechanics Division, October 5, 1987; final revision, January 13, 1988.

Paper No 88-WA/APM-31.

Copyright © 1988 by ASME
Downloaded 03 May 2010 to 171.66.16.21. Redistribution subject to ASME license or copyright; see http://www.asme.org/terms/Terms_Use.cfm

effect delimit the range of applicability of the principle for axisymmetric bending problems. Correct boundary conditions for the Lévy solution, or its approximations, were also deduced for edgewise nonuniform data along the straight edge of a semi-infinite plate in bending (Gregory and Wan, 1985a).

The development, for axisymmetric bending of a circular plate, is complemented by an analogous treatment for axisymmetric stretching (and torsion) in Gregory and Wan (1985b). The boundary conditions obtained there for the interior solution also delimit the applicability of Saint-Venant's principle in the case of stress edge data. Together, the two sets of results for axisymmetric stress distributions enabled us to rationally deduce the correct interior solution for a simply supported plate, subject to a point force at the center of its upper face (Gregory and Wan, 1985b).

For the plane-strain case, the necessary conditions for the edge data to induce only a decaying state were also shown to be sufficient conditions in Gregory and Wan (1984) because we have the explicit solutions for all Papkovich-Fadle eigenfunctions which are known to form a complete set (Gregory, 1980). For all other cases, the boundary conditions obtained for the interior solution component do not guarantee that the interior solution determined by these conditions is the correct solution in the plate interior up to exponentially small terms. In other words, we must still prove that the necessary conditions derived and used in Gregory and Wan (1985a and 1985b) are also sufficient conditions. In the present paper, we prove this sufficiency and thereby substantiate the claim made earlier in this introduction on the various "correct interior solutions." The sufficiency proof also offers a general method for determining the correct interior solution for general edge geometry and edgewise nonuniform loads. This general method, to be described in Section 3 of this paper, will be applied to a number of problems for a circular plate involving edgewise nonuniform data.

2 Decaying States in Elastic Plates

We consider in this paper flat plates bounded by two flat faces $z=\pm h$, and a cylindrical edge E_c, consisting of a midplane edge curve Γ and the generators $|z|\le h$ normal to Γ (Fig. 1). The plate material is homogeneous, isotropic and linearly elastic; some results for anisotropic plates in plane-strain or axisymmetric deformations have been obtained recently in Lin and Wan (1988). With no loss of generality, we take the plates to be free of body loads and the faces $z=\pm h$ to be free of surface tractions as these types of load terms can always be removed by substracting away a suitable equilibrium state of an infinite plate of the same material. The only loading is prescribed along the curved edge of the plate E_c and any set of edge data, consistent with the virtual work principle, is admissible. For the sake of definiteness, we will consider here only the case of *stress* data so that three appropriate combinations of the stress components σ_{ij} are prescribed on E_c in the form

$$\sigma_{nn}=\bar{\sigma}_{nn}(t,z),\quad \sigma_{nt}=\bar{\sigma}_{nt}(t,z),\quad \sigma_{nz}=\bar{\sigma}_{nz}(t,z) \tag{2.1}$$

where n, t, and z indicate directions normal, tangent, and transverse to the edge curve Γ, respectively, as shown in Fig. 1, and $\sigma_{n\alpha}=\sigma_{kj}n_k\alpha_j$ (summing in j and k from 1 to 3) with n_k (α_k) being the directional cosine of the direction $n(\alpha)$ and the direction x_k. Several other types of edge data were also considered in Gregory and Wan (1984, 1985a). The necessary modifications to the argument which follows are obvious for these and other sets of admissible edge data. So are the modifications required for a plate with more than one cylindrical edge.

The (fully three-dimensional) problem of determining the elastostatic state $\{\sigma, \mathbf{u}\}$ in the plate arising from the prescribed edge data (2.1) is generally intractable analytically. In this

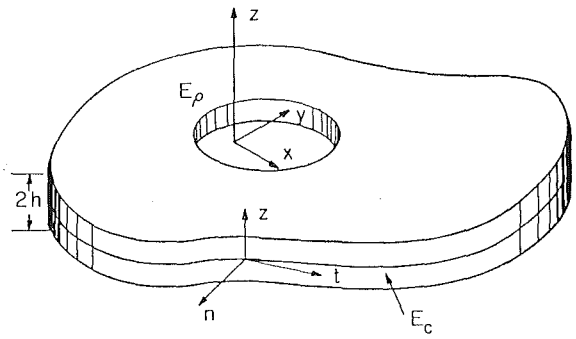


Fig. 1

paper, we shall be concerned with approximate solutions of this problem in the spirit of thin and thick plate theories; see also Gregory and Wan (1984). We will make this precise with the following definitions.

An *elastostatic state* of the plate consists of stress and displacement components $\{\sigma, \mathbf{u}\}$ which satisfy the conditions of equilibrium and compatibility with no body forces in the plate and no surface tractions on the two faces.

An elastostatic state in the plate is said to be a *decaying state* if as $h\to 0$

$$\{\sigma,\mathbf{u}\}=0(Me^{-\gamma d/h}) \tag{2.2}$$

where d is the minimum distance of the observation point from the edge of the plate, M is the maximum modulus of the prescribed edge tractions and γ is a positive constant independent of the half-plate thickness h.

An elastostatic state is said to be a *symmetric* (or *stretching*) *interior state* of a flat plate (with traction-free faces) and denoted by a superscript E (for Extension) if it has the (quasi-two-dimensional) form given in Appendix I. The corresponding formulas for an *antisymmetric* (or *bending*) *interior state* are given in Appendix I of Gregory and Wan (1985a).

The fundamental thesis of plate theory is that the exact three-dimensional solution $\{\sigma, \mathbf{u}\}$ of the plate problem as described at the beginning of this section has a resolution of the form

$$\{\sigma,\mathbf{u}\}=\{\sigma^I,\mathbf{u}^I\}+\{\sigma^d,\mathbf{u}^d\} \tag{2.3}$$

where $(\ )^I$ denotes an interior state (consisting of either symmetric or antisymmetric states, or both) and $(\ )^d$ denotes a decaying state (with one or more components). Such a resolution has been proved rigorously for the special case of an infinite strip plate in plane-strain deformation (see Theorem (1) of Gregory and Wan (1984)). A similar argument would apply to a circular plate in axisymmetric deformation. To our knowledge, there is no fully rigorous proof for plates of general shape; however, the asymptotic results of the sixties leave little doubt that such a resolution does exist. Thus $\{\sigma^I, \mathbf{u}^I\}$ is an approximation to the exact solution $\{\sigma,\mathbf{u}\}$ of the problem with an error which is exponentially small as $h\to 0$ except near the edge E_c of the plate. Near E_c, there is a boundary layer (with a layer width of the order of the plate thickness) where the contribution from $\{\sigma^d, \mathbf{u}^d\}$ is not negligible.

The decaying state or edge zone solution $\{\sigma^d, \mathbf{u}^d\}$ is known to have a rather complex analytical structure (see Friedrichs and Dressler (1961) for example). It is therefore desirable to find the interior solution $\{\sigma^I, \mathbf{u}^I\}$ (or its plate theory approximations) without considering the edge zone solution $\{\sigma^d, \mathbf{u}^d\}$. The difficulty in doing this is now clear: The conditions (2.1) which determine $\{\sigma, \mathbf{u}\}$ are to be applied at the edge E_c where $\{\sigma^d, \mathbf{u}^d\}$ is generally not negligible compared to $\{\sigma^I, \mathbf{u}^I\}$; thus the conditions (2.1) cannot be applied to $\{\sigma^I, \mathbf{u}^I\}$ alone. In fact, $\{\sigma^I, \mathbf{u}^I\}$ is usually too restricted in its z-dependence and generally cannot satisfy (2.1) even if we try to do so (Love,

Downloaded 03 May 2010 to 171.66.16.21. Redistribution subject to ASME license or copyright; see http://www.asme.org/terms/Terms_Use.cfm

1944; Timoshenko and Goodier, 1951). These observations bring us to the central question in plate theory: What are the correct conditions to be applied to the interior solution at the edge of the plate E_c?

A procedure has been developed recently (Gregory and Wan, 1984, 1985a and 1985b), to answer this question of a proper splitting of the edge data for the two kinds of elastostatic state components. The central step in seeking the appropriate boundary conditions for the exact (Lévy) or approximate (thin or thick plate) interior solution is to decide *what (necessary) conditions must the data in (2.1) (or any admissible set of data) satisfy in order that the resulting solution for the plate problem should be solely a decaying state.* It was shown (Gregory and Wan, 1984) that for the data (2.1) to induce only a decaying state, it is necessary to have

$$\int\int_{E_c} \{\bar{\sigma}_{nn} u_n^{(2)} + \bar{\sigma}_{nt} u_t^{(2)} + \bar{\sigma}_{nz} u_z^{(2)}\} dS = 0 \tag{2.4}$$

up to exponentially small terms where $\{\boldsymbol{\sigma}^{(2)}, \mathbf{u}^{(2)}\}$ is any elastostatic state of the same plate satisfying the following conditions (in addition to the conditions of equilibrium and compatibility in the plate interior and traction-free conditions on the plate faces required by the definition of an elastostatic state of the plate):

(*i*) It has no singularity in some neighborhood of E_c well beyond the boundary layer adjacent to E_c.

(*ii*) It is traction-free also on E_c.

(*iii*) It has at worst an algebraic growth as $h \to 0$.

Note that in view of (*ii*), a nontrivial state (2) must have singularities somewhere in the plate unless it is a rigid-body displacement field. Different choices for the stipulated state (2) will lead to infinitely many independent necessary conditions in general.

For instance, a countably infinite number of suitable $\{\boldsymbol{\sigma}^{(2)}, \mathbf{u}^{(2)}\}$ states may be generated as follows: Suppose $\{\boldsymbol{\sigma}^*, \mathbf{u}^*\}$ is any of the states given in Appendix II. These states are singular at $r=0$ (with the origin of the cylindrical coordinates chosen to be in the interior of plate) and are traction-free on $z = \pm h$, $r > 0$. They are not, however, traction-free on E_c. We can now add to $\{\boldsymbol{\sigma}^*, \mathbf{u}^*\}$ an elastostatic state which is regular throughout the plate and is chosen (uniquely to within a rigid motion) to annihilate any nonzero tractions on E_c due to state $\{\boldsymbol{\sigma}^*, \mathbf{u}^*\}$. The resulting state is a possible $\{\boldsymbol{\sigma}^{(2)}, \mathbf{u}^{(2)}\}$ and will be denoted by $\{\boldsymbol{\Sigma}^s, \mathbf{U}^s\}$. It can be characterized by the singularity at $r=0$ of, say, the radial stress component Σ^s_{rr}. For a fixed integer $n \geq 2$, there are four such singular states with an angular variation of $\cos(n\theta)$ or $\sin(n\theta)$. There are two such states for $n=1$ and only one for $n=0$ if we do not allow multivalued displacement fields. The set of all states $\{\boldsymbol{\Sigma}^s, \mathbf{U}^s\}$ obtained by this construction will be denoted by **S**. Thus we can say that for the traction data (2.1) on E_c to induce a decaying state in the plate, it is necessary that

$$\int\int_{E_c} \{\bar{\sigma}_{nn} U_n^s + \bar{\sigma}_{nt} U_t^s + \bar{\sigma}_{nz} U_z^s\} dS = 0 \tag{2.5}$$

for all states $\{\boldsymbol{\Sigma}^s, \mathbf{U}^s\}$ in **S**, giving a countable infinity of necessary conditions. For special classes of the problems, symmetry requirements reduce this countably infinite set of necessary conditions to a finite number of conditions; they can be translated into an appropriate set of boundary conditions for thin plate theory, thick plate theories or the complete interior solution. This was in fact done for the axisymmetric stretching (and torsion) problems for circular plates (Gregory and Wan, 1985b).

The elastostatic states in **S** constructed from the singular states in Appendix II are associated with the stretching and shearing action of the plate with single-valued displacement fields. Evidently, there is another countable infinity of states having similar singularities and angular variations associated with the bending action of the plate. For the special case of axisymmetric bending of circular plates, the countably infinite necessary conditions also reduce to a finite number of conditions; they were then translated into an appropriate set of boundary conditions for the interior (or plate theory) solution of the problem (Gregory and Wan, 1983a). As bending and stretching are uncoupled in a linear theory, we will focus the subsequent development in this paper on the stretching problem for conciseness.

3 Sufficient Conditions for a Decaying State

The necessary conditions implied by (2.4) have been shown to be also sufficient for the edge data to induce only a decaying state for infinite strip plates under plane-strain deformation (Gregory and Wan, 1984). The proof, for that special class of problems, makes use of the completeness of the Papkovich-Fadle eigenfunctions (Gregory, 1980) and, therefore, does not extend to more general geometry and edge data. In this section, we will show how the reciprocal theorem may also be used to determine the interior stress state for general edge geometry and edge tractions. When we apply the result to edge tractions, which satisfy the necessary conditions (2.4), the interior solution will be found to be the trivial state, $\sigma_{ij}^I \equiv u_j^I \equiv 0$. The necessary conditions (2.4) are therefore also sufficient for the edge data to induce only a decaying state.

Suppose the prescribed edge tractions induce only a symmetric (stretching) interior state. With Σ^s vanishing identically on E_c and with Σ^s and σ (the elastostatic state induced by $\bar{\sigma}_{nn}$, $\bar{\sigma}_{nt}$ and $\bar{\sigma}_{nz}$) both vanishing on $z = \pm h$, we have

$$\begin{aligned}
&\int\int_{E_c} \{\bar{\sigma}_{nn} U_n^s + \bar{\sigma}_{nt} U_t^s + \bar{\sigma}_{nz} U_z^s\} dS \\
&= \int\int_{E_c} \{[\bar{\sigma}_{nn} U_n^s + \bar{\sigma}_{nt} U_t^s + \bar{\sigma}_{nz} U_z^s] - [u_n \Sigma^s_{nn} + u_t \Sigma^s_{nt} + u_z \Sigma^s_{nz}]\} dS \\
&+ \int\int_{z=h} \{[\sigma_{zn} U_n^s + \sigma_{zt} U_t^s + \sigma_{zz} U_z^s] - [u_n \Sigma^s_{zn} + u_t \Sigma^s_{zt} + u_z \Sigma^s_{zz}]\} dS \\
&- \int\int_{z=-h} \{[\sigma_{zn} U_n^s + \ldots.] - [u_n \Sigma^s_{zn} + \ldots.]\} dS.
\end{aligned} \tag{3.1}$$

We now apply the reciprocal theorem over the plate with the cylinder $r < \rho$ removed, as there are no singularities of $\{\boldsymbol{\Sigma}^s, \mathbf{U}^s\}$ in the interior of this volume. The result requires the right-hand side of (3.1) to be equal to a similar integral over only the cylindrical edge surface $E_\rho \equiv \{r=\rho, \ |z| \leq h, \ 0 \leq \theta \leq 2\pi\}$ so that

$$\begin{aligned}
&\int\int_{E} \{\bar{\sigma}_{nn} U_n^s + \bar{\sigma}_{nt} U_t^s + \bar{\sigma}_{nz} U_z^s\} dS \\
&= \int_{-h}^{h} \int_0^{2\pi} \{[\sigma_{rr} U_r^s + \sigma_{r\theta} U_\theta^s + \sigma_{rz} U_z^s] \\
&\qquad - [u_r \Sigma^s_{rr} + u_\theta \Sigma^s_{r\theta} + u_z \Sigma^s_{rz}]\}|_{r=\rho} \rho d\theta dz.
\end{aligned} \tag{3.2}$$

For any fixed ρ, sufficiently small and independent of h, we may replace $\{\boldsymbol{\Sigma}^s, \mathbf{U}^s\}$ by the dominating singular state $\{\boldsymbol{\sigma}^*, \mathbf{u}^*\}$ on E_ρ. As $h \to 0$, we have $\{\boldsymbol{\sigma}, \mathbf{u}\} \sim \{\boldsymbol{\sigma}^I, \mathbf{u}^I\}$ on E_ρ except for Exponentially Small Terms (E.S.T.) giving

$$\begin{aligned}
&\int\int_{E_c} \{\bar{\sigma}_{nn} U_n^s + \bar{\sigma}_{nt} U_t^s + \bar{\sigma}_{nz} U_z^s\} dS \\
&= \int_{-h}^{h} \int_0^{2\pi} \{[\sigma^I_{rr} U_r^* + \sigma^I_{r\theta} U_\theta^* + \sigma^I_{rz} U_z^*] \\
&\qquad - [u_r^I \sigma_{rr}^* + u_\theta^I \sigma_{r\theta}^* + u_z^I \sigma_{rz}^*]\}|_{r=\rho} \rho d\theta dz
\end{aligned} \tag{3.3}$$

except for E.S.T.

Now $(\boldsymbol{\sigma}^I, \mathbf{u}^I)$ is a stretching interior state $\{\boldsymbol{\sigma}^E, u^E\}$ (by our choice of edge data) and is derived from a biharmonic (stress)

Downloaded 03 May 2010 to 171.66.16.21. Redistribution subject to ASME license or copyright; see http://www.asme.org/terms/Terms_Use.cfm

function F (see Appendix I). Any $F(r,\theta)$ which satisfies $\nabla^2\nabla^2 F=0$ and gives rise to a single-valued interior state regular in a neighborhood of $r=0$ has a local expansion of the form

$$F(r,\theta)=\sum_{m=2}^{\infty}[(a_m r^m+b_m r^{m+2})\cos(m\theta)+ \\ +(c_m r^m+d_m r^{m+2})\sin(m\theta)]+b_1 r^3\cos\theta+d_1 r^3\sin\theta+b_0 r^2. \tag{3.4}$$

with the stress-free parts of F omitted from the expansion. The corresponding stress and displacement fields can be found in Appendix I. Let us substitute these expressions into (3.3) and also take $\{\Sigma^s, \mathbf{U}^s\}$ to be that member of $\mathbf{S}$ associated with the singular field derived from $F^*=r^{-k}\cos(k\theta)$ for some fixed integer k (see (II-1a) and (II-2a) of Appendix II). We denote this particular singular field $\{\Sigma^s, \mathbf{U}^s\}$ by $\{\Sigma^k, \mathbf{U}^k\}$. Upon integrating term-by-term with respect to θ, all terms associated with a_m and b_m for $m\neq k$ give no contribution to the integral because of the orthogonality property of the trigonometric functions involved. For the same reason, neither do terms associated with c_m and d_m for all m. After some cancellations among the remaining terms, we are left with the rather remarkable result

$$\int\int_{E_c}[\bar\sigma_{nn}U_n^k+\bar\sigma_{nt}U_t^k+\bar\sigma_{nz}U_z^k]dS=\frac{16\pi h}{E}\,k(k+1)b_k \\ (k\geq 2) \tag{3.5}$$

except for E.S.T. (left out when we approximate $\{\sigma, \mathbf{u}\}$ by $\{\sigma^I, \mathbf{u}^I\}$ on E_ρ) as the right-hand side of (3.5) is independent of ρ. (The parameter E which appears in the denominator there is the Young's modulus of the material.)

By taking the singular field corresponding to $F^*=r^{-k+2}\cos(k\theta)$ instead, we obtain, except for E.S.T.,

$$\int\int_{E_c}[\bar\sigma_{nn}U_n^k+\bar\sigma_{nt}U_t^k+\bar\sigma_{nz}U_z^k]dS=-\frac{16\pi h}{E}\,k(k-1)a_k \\ (k\geq 2) \tag{3.6}$$

The right-hand side is again independent of the radius parameter ρ. Similar relations for c_k and d_k ($k\geq 2$), b_1, d_1 and b_0 can also be obtained by using other singular fields given in Appendix II. In all cases, U_n^s, U_t^s and U_z^s are the displacement components corresponding to the relevant state (2) in $\mathbf{S}$ for the particular singular field chosen.

Formulas (3.5) and (3.6), together with the corresponding formulas for b_1, d_1 and b_0, completely determine F (see (3.4)) and, hence, the interior stress state in terms of the stress edge data. In effect, they constitute a procedure for assigning an appropriate portion of the edge data to the interior solution to ensure its correct determination. Applications of this procedure to specific problems will be given in later sections of this paper. Here, we will use these results to show that *the necessary conditions (2.5) (which form a subset (2.4)) are in fact sufficient conditions for the elastostatic state induced by the edge data to be a decaying state except possibly for a rigid body displacement field.*

The proof of sufficiency is now straightforward. If (2.5) is satisfied with $\{\Sigma^s, \mathbf{U}^s\}$ corresponding to the $F^*=r^{-k}\cos(k\theta)$ (and with $\bar\sigma$ generating only a stretching state), it follows from (3.5) that

$$b_k=0 \quad (k\geq 2) \tag{3.7}$$

Similarly, we have from (3.6) and the corresponding formulas for b_1, d_1 and b_0

$$a_k=0 \quad (k\geq 2), \quad b_1=d_1=b_0=0 \tag{3.8}$$

Consequently, the stress function F which generates the stretching interior state is necessarily zero (except for exponentially small terms). We have thus proved the following:

Theorem. The elastostatic state generated by the stress edge data is necessarily a decaying state (except possibly for a rigid-body displacement field) if the data satisfies the conditions (2.5).

Combining this theorem (and its counterpart for plate bending) with results previously obtained by Gregory and Wan (1984, 1985a, 1985b), we now have that the requirement (2.4) or (2.5) are necessary *and* sufficient conditions for the stress edge data to induce only a decaying state, possibly up to a rigid-body displacement field. With straightforward modifications, the analysis of this section applies also to other admissible edge data and the aforementioned theorem can thereby be extended to include these edge data as well.

4 Boundary Conditions for Some Interior Solutions

The deviation of the interior solution from the exact solution, $\{\sigma-\sigma^I, \mathbf{u}-\mathbf{u}^I\}$, must be a decaying state. It follows that this difference must satisfy the necessary and sufficient conditions (2.5) in the case of prescribed stress edge data (2.1). As an immediate consequence, $\{\sigma^I, \mathbf{u}^I\}$ must satisfy the condition

$$\int\int_{E_c}\{\sigma_{nn}^I U_n^s+\sigma_{nt}^I U_t^s+\sigma_{nz}^I U_z^s\}dS \\ =\int\int_{E_c}\{\bar\sigma_{nn}U_n^s+\bar\sigma_{nt}U_t^s+\bar\sigma_{nz}U_z^s\}dS \tag{4.1}$$

for all $\{\Sigma^s, \mathbf{U}^s\}$ in $\mathbf{S}$. It is effectively these (countably infinite) conditions which completely determine the interior state up to a rigid motion in the last section. (Analogous conditions can also be formulated for the determination of the interior state induced by displacement or mixed edge data.) In the form (4.1), these conditions also conveniently provide the appropriate boundary conditions for thin and thick plate theories. Different symmetry restrictions often reduce the infinite number of necessary and sufficient conditions (4.1) to a finite number of conditions in particular cases as seen from our previous results. The actual boundary conditions for the interior solution of some special cases for circular plates will be worked out below for applications in later sections.

(*a*) Axially Symmetric Stretching of a Circular Plate. This case has already been worked out (Gregory and Wan 1985b) and the results are summarized here for the sake of completeness. When the stress data and the resulting deformation are axisymmetric, the conditions (4.1) for the circular plate $\{r\leq a, |z|\leq h\}$, are satisfied identically for all $\{\Sigma^s, \mathbf{U}^s\}$ having an angular variation of the form $\cos(k\theta)$ or $\sin(k\theta)$, $k\geq 1$. The one axially symmetric $\{\Sigma^s, \mathbf{U}^s\}\equiv\{\Sigma^0, \mathbf{U}^0\}$ in S is found to be

$$\Sigma_{rr}^0=E\left(1-\frac{a^2}{r^2}\right), \quad \Sigma_{\theta\theta}^0=E\left(1+\frac{a^2}{r^2}\right), \\ \Sigma_{r\theta}^0=\Sigma_{rz}^0=\Sigma_{\theta z}^0=\Sigma_{zz}^0=0, \quad U_\theta^0=0 \tag{4.2}$$

$$U_r^0=(1-\nu)r+(1+\nu)\frac{a^2}{r}, \quad U_z^0=-2\nu z.$$

It follows that at $r=a$, the axisymmetric interior solution must satisfy the condition

$$\int_{-h}^{h}\left[\sigma_{rr}^I-\frac{\nu}{a}\,z\sigma_{rz}^I\right]_{r=a}dz=\int_{-h}^{h}\left\{\bar\sigma_{rr}-\frac{\nu}{a}\,z\bar\sigma_{rz}\right\}dz \tag{4.3}$$

or, in terms of the Airy stress function F (see Appendix I) in cylindrical coordinates

Downloaded 03 May 2010 to 171.66.16.21. Redistribution subject to ASME license or copyright; see http://www.asme.org/terms/Terms_Use.cfm

$$\left[\frac{1}{r}\frac{\partial F}{\partial r}\right]_{r=a}=\frac{1}{2h}\int_{-h}^{h}\left\{\bar{\sigma}_{rr}-\frac{\nu}{a}z\bar{\sigma}_{rz}\right\}dz \tag{4.4}$$

In either form, the stress boundary condition for the axisymmetric stretching of the circular plate is *not* identical to the condition obtained by the application of the (unproved) Saint-Venant principle

$$\left[\frac{1}{r}\frac{\partial F}{\partial r}\right]_{r=a}=\frac{1}{2h}\int_{-h}^{h}\bar{\sigma}_{rr}dz \tag{4.5}$$

Some consequences of this difference have already been discussed (Gregory and Wan, 1985a and 1985b). Given that the edge data are applied over the entire circular edge of the plate, $\{r=a,\ |z|\le h\}$, Saint-Venant's principle is in fact inappropriate for this problem as the surface tractions are not localized. The incorrect condition (4.5) is nevertheless appropriate for the leading term (thin plate) approximation in powers of h/a for plate stretching (or the theory of generalized plane stress) as long as $\bar{\sigma}_{rr}$ is not $0(h\bar{\sigma}_{rz}/a)$ or smaller.

(*b*) Lateral Deformation of a Circular Plate. Suppose that the circular plate with traction-free faces, $z=\pm h$, is in equilibrium under traction along its edge $r=a$ with an angular variation of the form $\sin\theta$ or $\cos\theta$

$$\bar{\sigma}_{rr}(\theta,z)=\hat{\sigma}_{rr}(z)\{\cos\theta,\sin\theta\},\ \bar{\sigma}_{r\theta}(\theta,z)=\hat{\sigma}_{r\theta}(z)\{\sin\theta,-\cos\theta\},$$
$$\bar{\sigma}_{rz}(\theta,z)=\hat{\sigma}_{rz}(z)\{\cos\theta,\sin\theta\} \tag{4.6}$$

where $\hat{\sigma}_{rr}$ and $\hat{\sigma}_{r\theta}$ are even functions of z while $\hat{\sigma}_{rz}$ is an odd function of z. Overall force equilibrium in the x and y-direction requires

$$\int_{-h}^{h}[\hat{\sigma}_{rr}(z)-\hat{\sigma}_{r\theta}(z)]dz=0 \tag{4.7}$$

For the edge data (4.6), all those states, $\{\boldsymbol{\Sigma}^s,\mathbf{U}^s\}$, having an angular variation of the form $\cos(n\theta)$ or $\sin(n\theta)$ with $n\neq 1$, do not contribute to the right-hand side of the condition (4.1). It follows from the analysis at the end of Section 3 that the stress and displacement components of the plate depend on θ in the form $\cos\theta$ or $\sin\theta$. The corresponding singular field $\{\boldsymbol{\Sigma}^s,\mathbf{U}^s\}\equiv\{\boldsymbol{\Sigma}^1,\mathbf{U}^1\}$ can be constructed according to the procedure outlined in Section 3 to be

$$\Sigma^1_{rr}=2E\left[\frac{r}{a}-\frac{a^3}{r^3}\right]\{\cos\theta,\sin\theta\},$$

$$\Sigma^1_{r\theta}=2E\left[\frac{r}{a}-\frac{a^3}{r^3}\right]\{\sin\theta,-\cos\theta\}$$

$$\Sigma^1_{\theta\theta}=2E\left[3\frac{r}{a}+\frac{a^3}{r^3}\right]\{\cos\theta,\sin\theta\},$$

$$\Sigma^1_{rz}=\Sigma^1_{\theta z}=\Sigma^1_{zz}=0,$$

$$U^1_r=\left[(1-3\nu)\frac{r^2}{a}+(1+\nu)\frac{a^3}{r^2}-\frac{4\nu}{3a}(h^2-3z^2)\right]\{\cos\theta,\sin\theta\} \tag{4.8}$$

$$U^1_\theta=\left[(5+\nu)\frac{r^2}{a}+(1+\nu)\frac{a^3}{r^2}+\frac{4\nu}{3a}(h^2-3z^2)\right]\times\{\sin\theta,-\cos\theta\}$$

$$U^1_z=-\frac{8\nu r}{a}z\{\cos\theta,\sin\theta\}.$$

If we now insert U^1_r, U^1_θ and U^1_z from (4.8) into (4.1), we get, with $\sigma^I_{rr}=\sigma^E_{rr}\equiv s_{rr}(r,z)\{\cos\theta,\sin\theta\}$, $\sigma^I_{r\theta}=\sigma^E_{r\theta}\equiv s_{r\theta}(r,z)\{\sin\theta,-\cos\theta\}$ and $\sigma^I_{rz}=\sigma^E_{rz}\equiv 0$

$$\int_{-h}^{h}\left\{s_{rr}(a,z)\left[2(1-\nu)-\frac{4\nu}{3a^2}(h^2-3z^2)\right]+s_{r\theta}(a,z)\left[2(3+\nu)+\frac{4\nu}{3a^2}(h^2-3z^2)\right]\right\}dz$$
$$=\int_{-h}^{h}\left\{\hat{\sigma}_{rr}(z)\left[2(1-\nu)-\frac{4\nu}{3a^2}(h^2-3z^2)\right]+\hat{\sigma}_{rz}\left[-8\nu\frac{z}{a}\right]+\hat{\sigma}_{r\theta}(z)\left[2(3+\nu)+\frac{4\nu}{3a^2}(h^2-3z^2)\right]\right\}dz \tag{4.9}$$

As we have $F(r,\theta)=\hat{F}(r)\{\cos\theta,\sin\theta\}$ and therefore $s_{rr}(r,z)=s_{r\theta}(r,z)=d(r^{-1}\hat{F})/dr$ (see (I-21*a*, *b*)), the relation (4.9) may be written as

$$\frac{d}{dr}\left(\frac{\hat{F}}{r}\right)\Big|_{r=a}=\frac{1}{2h}\int_{-h}^{h}\hat{\sigma}_{rr}dz-\frac{\nu}{2ha}\int_{-h}^{h}\hat{\sigma}_{rz}zdz+\frac{\nu}{4a^2h}\int_{-h}^{h}(\hat{\sigma}_{rr}-\hat{\sigma}_{r\theta})z^2dz \tag{4.10}$$

where we have made use of (4.7) to simplify the right-hand side. Given that $F(r,\theta)=r^3\{b_1\cos\theta,d_1\sin\theta\}$, the condition (4.10) completely determines the stress function F and, hence, the interior stress state of the plate.

It is of some interest to note that for the present class of problems, possible candidates for state (2) for (2.4) include the rigid-body displacement fields $\{u_x=1,\ u_y=u_z=0\}$ and $\{u_y=1,\ u_x=u_z=0\}$. Upon inserting these into (2.4), applied to the residual edge data $\{\boldsymbol{\sigma}-\boldsymbol{\sigma}^I,\mathbf{u}-\mathbf{u}^I\}$, we get for both cases

$$\int_{-h}^{h}\{\hat{\sigma}_{rr}-\hat{\sigma}_{r\theta}\}dz=\int_{-h}^{h}\{s_{rr}-s_{r\theta}\}dz \tag{4.11}$$

With $s_{rr}-s_{r\theta}=0$ (and independent of z), we have again the overall force equilibrium requirement (4.7), now as a consequence of the reciprocal theorem.

(*c*) Higher Harmonics for a Circular Plate. For stress data with angular variation of the form $\cos(n\theta)$ or $\sin(n\theta)$, $n\ge 2$, it does not seem possible to obtain the needed singular fields $\{\boldsymbol{\Sigma}^s,\mathbf{U}^s\}$ in simple explicit form. In the case $n=2$, for example, we would need to seek a regular elastostatic field which satisfies the stress boundary conditions

$$\sigma_{rr}(a,\theta,z)=\{\cos(2\theta),\sin(2\theta)\},$$
$$\sigma_{r\theta}(a,\theta,z)=\{\sin(2\theta),-\cos(2\theta)\},\quad \sigma_{rz}(a,\theta,z)=0 \tag{4.12}$$

to cancel the contribution to the edge tractions by the singular field associated with $F^*=-(a^4/6r^2)\{\cos(2\theta),\sin(2\theta)\}$ and another regular elastostatic field which satisfies the stress boundary conditions

$$\sigma_{rr}(a,\theta,z)=\left\{1-\frac{\nu(h^2-3z^2)}{(1+\nu)a^2}\right\}\{\cos(2\theta),\sin(2\theta)\}$$

$$\sigma_{r\theta}(a,\theta,z)=\left\{\frac{1}{2}-\frac{\nu(h^2-3z^2)}{(1+\nu)a^2}\right\}\{\sin(2\theta),-\cos(2\theta)\}$$

$$\sigma_{rz}(a,\theta,z)=0 \tag{4.13}$$

to cancel the effect of $F^*=(a^2/4)\{\cos(2\theta),\sin(2\theta)\}$. (Actually, we need only the displacement fields $\mathbf{U}^s$ associated with the foregoing two singular fields to be used in the boundary conditions (4.1) for the interior solution.)

The two boundary-value problems for two three-dimensional regular elastostatic fields with the stress boundary conditions (4.12) and (4.13), respectively, [and the corresponding problems for $n>2$] are *canonical* problems in that they do not depend on the actual stress data and can be solved once and for all, numerically or otherwise. The solutions for

Downloaded 03 May 2010 to 171.66.16.21. Redistribution subject to ASME license or copyright; see http://www.asme.org/terms/Terms_Use.cfm

these problems may be used in (3.5) and (3.6) for the same circular plate with any admissible set of stress data. The situation is similar to that of displacement boundary-value problems for a semi-infinite plate in plane-strain deformation (Gregory and Wan, 1984). Three canonical displacement boundary-value problems were solved numerically there, and the results were then used to get the correct displacement boundary conditions of the same semi-infinite strip plate for a number of different problems.

5 Lateral Deformation of a Vertical Circular Plate Under Its Own Weight

Let the circular plate $\{r \le a,\ |z| \le h\}$ of uniform density ρ be so-positioned that the direction of gravity is in the positive x-direction. The plate is supported vertically at its center $r=0$ by means of a force $P=2\pi h a^2 \rho g$ in the negative x-direction. The plate is thus traction-free at the two faces and at its only edge $r=a$. The gravity load in the plate interior is in equilibrium with only one nonvanishing stress component in a Cartesian coordinate system; namely, $\sigma^g_{xx} = -\rho g x$. In terms of cylindrical coordinates (r,θ,z), we have correspondingly

$$\sigma^g_{rr} = -\frac{1}{4}\rho g r[3\cos(\theta)+\cos(3\theta)],$$

$$\sigma^g_{r\theta} = \frac{1}{4}\rho g r[\sin(\theta)+\sin(3\theta)]$$

$$\sigma^g_{\theta\theta} = -\frac{1}{4}\rho g r[\cos(\theta)-\cos(3\theta)],$$

$$\sigma^g_{rz} = \sigma^g_{\theta z} = \sigma^g_{zz} = 0. \tag{5.1}$$

On the other hand, the side force at the plate center is known to be associated with a multivalued stress function

$$F_P = -\frac{1}{4}\rho g a^2[(1-\nu) r \ln(r)\cos(\theta) - 2r\theta\sin(\theta)] \tag{5.2}$$

giving rise to a stress field with components

$$\sigma^P_{rr} = \frac{\rho g a^2}{4r}\left[(3+\nu) - \frac{2\nu}{3r^2}(h^2-3z^2)\right]\cos(\theta),$$

$$\sigma^P_{r\theta} = -\frac{\rho g a^2}{4r}\left[(1-\nu) + \frac{2\nu}{3r^2}(h^2-3z^2)\right]\sin(\theta),$$

$$\sigma^P_{\theta\theta} = -\frac{\rho g a^2}{4r}\left[(1-\nu) - \frac{2\nu}{3r^2}(h^2-3z^2)\right]\cos(\theta),$$

$$\sigma^P_{rz} = \sigma^P_{\theta z} = \sigma^P_{zz} = 0. \tag{5.3}$$

For the solution of the original problem, a third stress field must be added to the two fields $\boldsymbol{\sigma}^g$ and $\boldsymbol{\sigma}^P$ so that the total stress state is in equilibrium with the external loads, vanishes at the two faces $z=\pm h$ and vanishes at the edge $r=a$. The third stress field $\boldsymbol{\sigma}^c$ is therefore in equilibrium with no external load in the plate interior and vanishes at the two faces $z=\pm h$. At the edge $r=a$, it must be the negative of the sum of $\boldsymbol{\sigma}^g$ and $\boldsymbol{\sigma}^P$ so that

$$\sigma^c_{rr}|_{r=a} = -\frac{1}{4}\rho g a\left\{\left[\nu - \frac{2\nu}{3a^2}(h^2-3z^2)\right]\cos(\theta) - \cos(3\theta)\right\} \equiv \bar{\sigma}_{rr}$$

$$\sigma^c_{r\theta}|_{r=a} = -\frac{1}{4}\rho g a\left\{\left[\nu - \frac{2\nu}{3a^2}(h^2-3z^2)\right]\sin(\theta) + \sin(3\theta)\right\} \equiv \bar{\sigma}_{r\theta}$$

$$\sigma^c_{rz}|_{r=a} = 0. \tag{5.4}$$

Note that the edge data (5.4) satisfies the overall equilibrium requirement (4.7).

It would appear from the form of (5.4) that we could not apply the results of Sections 3 and 4 to obtain the interior solution (given by a stress function F_c) induced by the data $\bar{\sigma}_{rr}$ and $\bar{\sigma}_{r\theta}$, without first obtaining a numerical solution for the singular field $\{\boldsymbol{\Sigma}^s, \mathbf{U}^s\}$ associated with the $\cos(3\theta)$ and $\sin(3\theta)$ term in the data. However, we may set

$$F_c(r,\theta) = F_1(r,\theta) - \frac{1}{24}\rho g r^3\cos(3\theta) \tag{5.5}$$

with $\nabla^4 F_1 = 0$ implying $\nabla^4 F_c = 0$. In terms of the stress components corresponding to F_1, the boundary conditions (5.4) become

$$\sigma^c_{rr}|_{r=a} = -\frac{1}{4}\rho g a\left[\nu - \frac{2\nu}{3a^2}(h^2-3z^2)\right]\cos(\theta) \equiv \hat{\sigma}^c_{rr}\cos(\theta)$$

$$\sigma^c_{r\theta}|_{r=a} = -\frac{1}{4}\rho g a\left[\nu - \frac{2\nu}{3a^2}(h^2-3z^2)\right]\sin(\theta) \equiv \hat{\sigma}^c_{r\theta}\sin(\theta)$$

$$\sigma^c_{rz}|_{r=a} = 0. \tag{5.6}$$

Evidently, the interior solution induced by the stress data (5.6) is necessarily the stretching state corresponding to $F_1 = b_1 r^3\cos\theta$ by the results of Section 3. In that case, the condition (4.10) with $\hat{\sigma}^c_{r\theta} = \hat{\sigma}^c_{rr}$ gives

$$2ab_1 = \frac{1}{2h}\int_{-h}^{h}\hat{\sigma}^c_{rr}dz = -\frac{\nu}{4}\rho g a \quad \text{or} \quad b_1 = -\frac{\nu}{8}\rho g \tag{5.7}$$

Combining the various stress fields, we have for the actual interior (stretching) state

$$\sigma^I_{rr} = -\frac{1}{4}\rho g a\left[(1+\nu)\frac{r}{a} - (3+\nu)\frac{a}{r} + \frac{2\nu a}{3r^3}(h^2-3z^2)\right]\cos(\theta)$$

$$\sigma^I_{r\theta} = -\frac{1}{4}\rho g a\left[(1-\nu)\frac{r}{a} - (1-\nu)\frac{a}{r} - \frac{2\nu a}{3r^3}(h^2-3z^2)\right]\sin(\theta)$$

$$\sigma^I_{\theta\theta} = -\frac{1}{4}\rho g a\left[(1+3\nu)\frac{r}{a} + (1-\nu)\frac{a}{r} - \frac{2\nu a}{3r^3}(h^2-3z^2)\right]\cos(\theta)$$

$$\sigma^I_{rz} = \sigma^I_{\theta z} = \sigma^I_{zz} = 0. \tag{5.8}$$

Given that $\hat{\sigma}^c_{rr} \equiv \hat{\sigma}^c_{r\theta}$ for our problem so that there is no contribution from the second integral in (4.10) to the interior solution, the same results can be obtained by applying Saint-Venant's principle to the solution corresponding to F_1. This will not always be the case for other stress data.

We have been deliberately vague about how the vertical force P is applied at the plate center except that the resulting stress fields in the plate should behave as given by (5.3) near $r=0$. In general, there may be another layer phenomenon centered at $r=0$ similar to that for the axisymmetric case worked out in Gregory and Wan (1985b). While we could do so, we will not enter into a discussion of this layer phenomenon; it would obscure the development pertaining to the main thrust of this paper.

Downloaded 03 May 2010 to 171.66.16.21. Redistribution subject to ASME license or copyright; see http://www.asme.org/terms/Terms_Use.cfm

6 Circular Disk Compressed by Equal and Opposite Point Forces at the Rim

Consider a circular plate $\{r \le a,\ |z| \le h\}$ under equal and opposite point loads of magnitude P at the points $r=a$, $\theta=0$ and $z=\pm h$. The stress boundary conditions at $r=a$ may be compactly expressed in terms of the Dirac delta functions $\delta(\theta)$ and $\delta(z \pm h)$

$$\sigma_{rr}|_{r=a} = \bar{\sigma}_{rr} \equiv 0,\ \sigma_{r\theta}|_{r=a} = \bar{\sigma}_{r\theta} \equiv 0,$$
$$\sigma_{rz}|_{r=a} = \bar{\sigma}_{rz} \equiv -\frac{P}{a}\,\delta(\theta)[\delta(z-h) - \delta(z+h)]. \tag{6.1}$$

For our solution process, however, it is more convenient to resolve $\bar{\sigma}_{rz}$ into its Fourier components with respect to θ to get

$$\bar{\sigma}_{rz} = -\frac{P}{a}\,[\delta(z-h) - \delta(z+h)]\left[\frac{1}{2\pi} + \frac{1}{\pi}\sum_{n=1}^{\infty}\cos(n\theta)\right] \tag{6.2}$$

In the spirit of the development in the previous sections, we will examine the individual Fourier components of this loading separately.

(a) The $n=0$ Component. This corresponds to an axisymmetric loading of the form

$$\bar{\sigma}_{rr}^{(0)} = \bar{\sigma}_{r\theta}^{(0)} = 0, \quad \bar{\sigma}_{rz}^{(0)} = -\frac{P}{2\pi a}\,[\delta(z-h) - \delta(z+h)] \tag{6.3}$$

The interior solution induced by the set of stress data may be determined by the condition (4.4) which, with (6.3) for edge data, becomes

$$\frac{1}{r}\frac{\partial F_0}{\partial r}\bigg|_{r=a} = \frac{1}{2h}\int_{-h}^{h}\left[\bar{\sigma}_{rr}^{(0)} - \nu\frac{z}{a}\bar{\sigma}_{rz}^{(0)}\right]dz = \frac{\nu P}{2\pi a^2} \tag{6.4}$$

Given $F_0 = b_0 r^2$ for axisymmetric problems, we have from (6.4) $b_0 = \nu P/4\pi a^2$ so that $F_0 = \nu P r^2/4\pi a^2$. The corresponding nonvanishing stress and displacement components, denoted by a superscript (0), are

$$\sigma_{rr}^{(0)} = \sigma_{\theta\theta}^{(0)} = \frac{\nu P}{2\pi a^2},$$

$$Eu_r^{(0)} = \nu(1-\nu)\,\frac{Pr}{2\pi a^2}, \quad Eu_z^{(0)} = -\frac{\nu^2 Pz}{\pi a^2} \tag{6.5}$$

(b) The $n=1$ Component. This corresponds to a lateral loading of the form

$$\bar{\sigma}_{rr}^{(1)} = \bar{\sigma}_{r\theta}^{(1)} = 0,$$

$$\bar{\sigma}_{rz}^{(1)} = -\frac{P}{\pi a}\,[\delta(z-h) - \delta(z+h)]\cos(\theta) \equiv \hat{\sigma}_{rz}^{(1)}\cos(\theta) \tag{6.6}$$

which satisfies the overall equilibrium requirement (4.7). The interior solution induced by this set of edge data corresponds to the stress function $F_1 = b_1 r^3\cos(\theta)$. The unknown constant b_1 is determined by the boundary condition (4.10) which, with (6.6) for edge data, becomes

$$2ab_1 = -\frac{\nu}{2ah}\int_{-h}^{h}\hat{\sigma}_{rz}^{(1)} z\,dz = \frac{\nu P}{\pi a^2} \quad \text{or} \quad b_1 = \frac{\nu P}{2\pi a^3} \tag{6.7}$$

so that $F_1 = \nu P r^3\cos(\theta)/2\pi a^3$. The corresponding nonvanishing stress and displacements components, denoted by superscript (1), are

$$\sigma_{rr}^{(1)} = \frac{\nu P}{\pi a^3}\,r\cos(\theta), \quad \sigma_{\theta\theta}^{(1)} = 3\sigma_{rr}^{(1)}, \quad \sigma_{r\theta}^{(1)} = \frac{\nu P}{\pi a^3}\,r\sin(\theta)$$

$$Eu_z^{(1)} = -\frac{4\nu^2 P}{\pi a^3}\,zr\cos(\theta)$$

$$Eu_r^{(1)} = \frac{\nu P}{2\pi a^3}\left\{(1-3\nu)r^2 - \frac{4\nu}{3}(h^2 - 3z^2)\right\}\cos(\theta) \tag{6.8}$$

$$Eu_\theta^{(1)} = \frac{\nu P}{2\pi a^3}\left\{(5+\nu)r^2 + \frac{4\nu}{3}(h^2 - 3z^2)\right\}\sin(\theta)$$

In principle, we can continue the process to determine the contribution of the higher harmonics in the edge load (6.2) to the interior solution. To do so, we would need the solution for $\{\Sigma^s, \mathbf{U}^s\}$ for each of the higher harmonics as described in Section 3. In general, these solutions will have to be obtained numerically as noted in Section 4 and will not be pursued in this paper. If we should determine the collection of $\{\Sigma^s, \mathbf{U}^s\}$ for the higher harmonic components of stress function, these canonical solutions are independent of the actual loading; hence, they can be used for other stress boundary-value problems for the same plate.

It is often asserted in the literature for linearly elastic plates that, when the external load is entirely normal to the midplane of the plate, then the interior of the plate is in transverse bending action. Even without calculating the contributions from the higher harmonics of the load term to the interior solution, we see from the results of (6.5) and (6.8) for the present problem that this is not so in general. The example of this section shows for the first time how the stretching interior state induced by transvere loads can be properly analyzed.

7 Concluding Remarks

The results in Sections 2 and 3 of this paper effectively complete the development initiated in Gregory and Wan (1984) and continued in Gregory and Wan (1985a, 1985b). Together, they form the theoretical foundation for a correct formulation of the appropriate boundary conditions for the interior solution (or its various approximations) for plate problems. The method outlined herein for stress data in plate extension problems also applies to plate bending problems as well as other types of admissible edge data. In the spirit of plate theories, our results allow the determination of the correct solution for plate problems accurate in the plate interior to any prescribed order of $(h/d)^n$ without the solution of the related boundary-layer problems.

The separate consideration of the interior and boundary-layer solution components for plate problems made possible by the results of this paper also has another interpretation when viewed in the context of the present day computing power. To attempt a numerical solution (by a finite-element method or otherwise) for a three-dimensional elasticity problem, it would seem attractive to be able to compute separately solution components with different scale lengths and thereby avoid the need for the use of meshes or elements, which differ in size by orders of magnitude. Moreover, with the interior solution being computed separately, the numerical solution for the boundary-layer solution components may now be restricted to a narrow region near the plate edge(s) in which these solution components are expected to be important.

References

Friedrichs, K. O., and Dressler, R. F., 1961, "A Boundary Layer Theory for Elastic Plates," *Comm. Pure Appl. Math.*, Vol. 14, pp. 1–33.

Gol'denveizer, A. L., 1962, "Derivation of an Approximate Theory of Bending of a Plate by the Method of Asymptotic Integration of the Equations of the Theory of Elasticity," *P.M.M.*, Vol. 26, pp. 668–686.

Gol'denveizer, A. L., and Kolos, A. V., 1965, "On the Derivation of Two-Dimensional Equation in the Theory of Thin Elastic Plates," *P.M.M.*, Vol. 29 (1), pp. 141–155.

Gregory, R. D., 1980, "The Traction Boundary Value Problem for the Elastostatic Semi-Infinite Strip, Existence of Solutions, and Completeness of the Papkovich-Fadle Eigenfunctions," *Journal of Elasticity*, Vol. 10, pp. 295–327.

Gregory, R. D., and Wan, F. Y. M., 1984, "Decaying States of Plane Strain in a Semi-Infinite Strip and Boundary Conditions for Plate Theory," *Journal of Elasticity*, Vol. 14, pp. 27–64.

Gregory, R. D., and Wan, F. Y. M., 1985*a*, "On Plate Theories and Saint-Venant's Principle," *International Journal of Solids and Structures*, Vol. 21, pp. 1005–1024.

Downloaded 03 May 2010 to 171.66.16.21. Redistribution subject to ASME license or copyright; see http://www.asme.org/terms/Terms_Use.cfm

Gregory, R. D., and Wan, F. Y. M., 1985*b*, "Edge Effects in the Stretching of Plates," *Local Effects in the Analysis of Structures*, Ladeveze, P., Ed., Elsevier Science Publishers B.V., Amsterdam, pp. 35–54.

Kolos, A. V., 1965, "Methods of Refining the Classical Theory of Bending and Extension of Plates," *P.M.M.*, Vol. 29 (4), pp. 777–781.

Lévy, M., 1877, "Mémoire sur la theorie des plaques élastique planes," *J. Math Pure Appl.*, Vol. 30, pp. 219–306.

Lin, Y., and Wan, F. Y. M., "First Integrals and the Interior Solution for Orthotropic Plates in Plane Strain or Axisymmetric Deformations," *Studies in Applied Math.*, Vol. 78, to appear.

Love, A. E. H., 1944, *The Mathematical Theory of Elasticity*, 4th Ed., Dover Publications, New York.

Reiss, E. L., 1962, "Symmetric Bending of Thick Circular Plates," *Journal of S.I.A.M.*, Vol. 10, pp. 596–609.

Reiss, E. L., and Locke, S., 1961, "On the Theory of Plane Stress," *Quarterly of Applied Mathematics*, Vol. 19, pp. 195–203.

Reissner, E., 1963, "On the Derivation of Boundary Conditions for Plate Theory," *Proceedings of the Royal Society*, Vol. A 276, pp. 178–186.

Reissner, E., 1985, "Reflections on the Theory of Elastic Plates," *Applied Mechanics Reviews*, Vol. 38, pp. 1453–1464.

Timoshenko, S., and Goodier, J. N., 1951, *Theory of Elasticity*, 2nd Ed., McGraw-Hill, New York.

APPENDIX I

Interior Solution for Extension and Torsion of Plates With Traction-Free Faces

For an isotropic and homogeneous plate with traction-free faces at $z=\pm h$, the in-plane shear and extension portion of the interior solution may be expressed in terms of a biharmonic (Airy stress) function F by

$$\sigma_{xx}^E=\frac{\partial^2}{\partial y^2}\left[1+\frac{\nu(h^2-3z^2)}{6(1+\nu)}\nabla^2\right]F,\qquad \sigma_{yy}^E=\ldots \tag{I-1,2}$$

$$\sigma_{xy}^E=-\frac{\partial^2}{\partial x\partial y}\left[1+\frac{\nu(h^2-3z^2)}{6(1+\nu)}\nabla^2\right]F,$$

$$\sigma_{xz}^E=\sigma_{yz}^E=\sigma_{zz}^E=0 \tag{I-3,4}$$

$$Eu_x^E=E\tilde{u}_x-\frac{\nu}{6}(h^2-3z^2)\frac{\partial}{\partial x}(\nabla^2F),$$

$$Eu_y^E=\ldots\ldots\ldots,\qquad Eu_z^E=-\nu z\nabla^2F \tag{I-5,6,7}$$

where $\nabla^2(\nabla^2F)=0$ and

$$E\frac{\partial\tilde{u}_x}{\partial x}=\nabla^2F-(1+\nu)\frac{\partial^2F}{\partial x^2},\quad E\frac{\partial\tilde{u}_y}{\partial y}=\ldots\ldots \tag{I-8,9}$$

$$E\left(\frac{\partial\tilde{u}_y}{\partial x}+\frac{\partial\tilde{u}_x}{\partial y}\right)=-2(1+\nu)\frac{\partial^2F}{\partial x\partial y}, \tag{I-10}$$

∇^2 being the two-dimensional Laplacian in x and y. The formulas for σ_{yy}^E, u_y^E and $\tilde{u}_y$ are obtained from σ_{xx}^E, u_x^E and $\tilde{u}_x$ by interchanging x and y. It should be noted that these formulas are *not* identical to the formulas of generalized plane stress. The additional terms in our formulas ensure that the interior state is a genuine three-dimensional elastostatic state.

In cylindrical coordinates, the corresponding formula for the interior solution of plate extension and torsion are

$$\{\sigma_{\theta\theta}^E,\sigma_{rr}^E\}=\left\{\frac{\partial^2}{\partial r^2},\ \nabla^2-\frac{\partial^2}{\partial r^2}\right\}\left[1+\frac{\nu(h^2-3z^2)}{6(1+\nu)}\nabla^2\right]F \tag{I-11}$$

$$\sigma_{r\theta}^E=-\frac{\partial^2}{\partial r\partial\theta}\left\{\frac{1}{r}\left[1+\frac{\nu(h^2-3z^2)}{6(1+\nu)}\nabla^2\right]F\right\},$$

$$\sigma_{rz}^E=\sigma_{\theta z}^E=\sigma_{zz}^E=0 \tag{I-12,13}$$

$$Eu_r^E=E\tilde{u}_r-\frac{\nu}{6}(h^2-3z^2)\frac{\partial}{\partial r}\nabla^2F \tag{I-14}$$

$$Eu_\theta^E=E\tilde{u}_\theta-\frac{\nu}{6}(h^2-3z^2)\frac{1}{r}\frac{\partial}{\partial\theta}\nabla^2F,$$

$$Eu_z^E=-\nu z\nabla^2F \tag{I-15,16}$$

where $\nabla^2\nabla^2F=0$ with ∇^2 being the two-dimensional Laplacian in polar coordinates and where

$$E\frac{\partial\tilde{u}_r}{\partial r}=\nabla^2F-(1+\nu)\frac{\partial^2F}{\partial r^2} \tag{I-17}$$

$$E\left(\frac{1}{r}\frac{\partial\tilde{u}_\theta}{\partial\theta}+\frac{1}{r}\tilde{u}_r\right)=(1+\nu)\frac{\partial^2F}{\partial r^2}-\nu\nabla^2F \tag{I-18}$$

$$E\left(\frac{\partial\tilde{u}_\theta}{\partial r}-\frac{1}{r}\tilde{u}_\theta+\frac{1}{r}\frac{\partial\tilde{u}_r}{\partial\theta}\right)=-2(1+\nu)\frac{\partial^2}{\partial r\partial\theta}\left(\frac{1}{r}F\right) \tag{I-19}$$

The following stress function fields and the associated regular symmetric elastostatic states are useful in the development of Section 3 of this paper.

(*1*) $F=r^{m+2}\{\cos(m\theta),\sin(m\theta)\},\ (m\geq 1)$ (I-20*a*,*b*)

$$\sigma_{\theta\theta}^E=(m+1)\left[(m+2)r^m+\frac{2\nu(h^2-3z^2)}{3(1+\nu)}m(m^2-1)r^{m-2}\right]\{\cos(m\theta),\sin(m\theta)\}$$

$$\sigma_{rr}^E=-(m+1)\left[(m-2)r^m+\frac{2\nu(h^2-3z^2)}{3(1+\nu)}m(m^2-1)r^{m-2}\right]\{\cos(m\theta),\sin(m\theta)\}$$

$$\sigma_{r\theta}^E=m(m+1)\left[r^m+\frac{2\nu(h^2-3z^2)}{3(1+\nu)}(m^2-1)r^{m-2}\right]\{\sin(m\theta),-\cos(m\theta)\}$$

$$\sigma_{rz}^E=\sigma_{\theta z}^E=\sigma_{zz}^E=0 \tag{I-21*a*,*b*}$$

$$Eu_r^E=\left\{[2(1-\nu)-m(1+\nu)]r^{m+1}-\frac{2\nu}{3}(h^2-3z^2)m(m+1)r^{m-1}\right\}\{\cos(m\theta),\sin(m\theta)\}$$

$$Eu_\theta^E=\left\{[2(1-\nu)+(m+2)(1+\nu)]r^{m+1}+\frac{2\nu}{3}(h^2-3z^2)m(m+1)r^{m-1}\right\}\{\sin(m\theta),-\cos(m\theta)\}$$

$$Eu_z^E=-4\nu z(m+1)r^m\{\cos(m\theta),\sin(m\theta)\}.$$

(*2*) $F=r^m\{\cos(m\theta),\sin(m\theta)\},\ (m\geq 2)$ (I-22*a*,*b*)

$$\sigma_{\theta\theta}^E=m(m-1)r^{m-2}\{\cos(m\theta),\sin(m\theta)\}=-\sigma_{rr}^E$$

$$\sigma_{r\theta}^E=m(m-1)r^{m-1}\{\sin(m\theta),-\cos(m\theta)\}$$

$$\sigma_{rz}^E=\sigma_{\theta z}^E=\sigma_{zz}^E=0,\quad Eu_z^E=0 \tag{I-23*a*,*b*}$$

$$Eu_r^E=-(1+\nu)mr^{m-1}\{\cos(m\theta),\sin(m\theta)\}$$

$$Eu_\theta^E=(1+\nu)mr^{m-1}\{\sin(m\theta),-\cos(m\theta)\}.$$

(*3*) $F=r^2$ (I-24)

Downloaded 03 May 2010 to 171.66.16.21. Redistribution subject to ASME license or copyright; see http://www.asme.org/terms/Terms_Use.cfm

$$\sigma^E_{\theta\theta}=\sigma^E_{rr}=2,\ \sigma^E_{r\theta}=\sigma^E_{rz}=\sigma^E_{\theta z}=\sigma^E_{zz}=0$$

$$Eu^E_r=2(1-\nu)r,\ Eu^E_z=-4\nu z,\ Eu^E_\theta=0. \tag{I-25}$$

APPENDIX II

Singular States for Plates With Traction-Free Faces

For an isotropic, homogeneous and linearly elastic plate with traction-free faces at $x=\pm h$, we have the following singular elastostatic states derived from different biharmonic functions F (with a singularity at $r=0$) by way of the formulas in Appendix I. Evidently these singular states are associated with (single-valued) in-plane extension and shear of the plate.

(1) $F^*=r^{-n}[\cos(n\theta),\sin(n\theta)\},\ (n\geq 2)$ (II-1a,b)

$$\sigma^*_{rr}=-n(n+1)r^{-n-2}\{\cos(n\theta),\sin(n\theta)\}=-\sigma^*_{\theta\theta}$$

$$\sigma^*_{r\theta}=-n(n+1)r^{-n-2}\{\sin(n\theta),-\cos(n\theta)\} \tag{II-2a,b}$$

$$\sigma^*_{rz}=\sigma^*_{\theta z}=\sigma^*_{zz}=0,\ Eu^*_z=0$$

$$Eu^*_r=(1+\nu)nr^{-n-1}\{\cos(n\theta),\sin(n\theta)\}$$

$$Eu^*_r=(1+\nu)nr^{-n-1}\{\sin(n\theta),-\cos(n\theta)\}.$$

(2) $F^*=r^{-n+2}\{\cos(n\theta),\sin(n\theta)\},\ (n\geq 2)$ (II-3a,b)

$$\sigma^*_{rr}=-(n-1)\left\{(n+2)r^{-n}-\frac{2\nu(h^2-3z^2)}{3(1+\nu)}\right.$$
$$\left.n(n+1)r^{-n-2}\right\}\{\cos(n\theta),\sin(n\theta)\}$$

$$\sigma^*_{\theta\theta}=(n-1)\left\{(n-2)r^{-n}-\frac{2\nu(h^2-3z^2)}{3(1+\nu)}\right.$$
$$\left.n(n+1)r^{-n-2}\right\}\{\cos(n\theta),\sin(n\theta)\}$$

$$\sigma^*_{r\theta}=-n(n-1)\left\{r^{-n}-\frac{2\nu(h^2-3z^2)}{3(1+\nu)}\right.$$
$$\left.(n+1)r^{-n-2}\right\}\{\sin(n\theta),-\cos(n\theta)\} \tag{II-4a,b}$$

$$\sigma^*_{rz}=\sigma^*_{\theta z}=\sigma^*_{zz}=0$$

$$Eu^*_r=\left\{[2(1-\nu)+n(1+\nu)]r^{-n+1}\right.$$
$$\left.-\frac{2\nu}{3}(h^2-3z^2)n(n-1)r^{-n-1}\right\}\{\cos(n\theta),\sin(n\theta)\}$$

$$Eu^*_\theta=\left\{[(1+\nu)(n-2)-2(1-\nu)]r^{-n+1}\right.$$
$$\left.-\frac{2\nu}{3}(h^2-3z^2)n(n-1)r^{-n-1}\right\}\{\sin(n\theta),-\cos(n\theta)\}$$

$$Eu^*_u=4\nu(n-1)zr^{-n}\{\cos(n\theta),\sin(n\theta)\}.$$

(3) $F^*=r^{-1}\{\cos\theta,\sin\theta\}$ (II-5a,b)

$$\sigma^*_{\theta\theta}=\frac{2}{r^3}\{\cos\theta,\sin\theta\}=-\sigma^*_{rr},\ \sigma^*_{r\theta}=-\frac{2}{r^3}\{\sin\theta,-\cos\theta\},$$
$$\sigma^*_{rz}=\sigma^*_{\theta z}=\sigma^*_{zz}=0,\quad Eu^*_z=0 \tag{II-6a,b}$$

$$Eu^*_r=(1+\nu)r^{-2}\{\cos\theta,\sin\theta\},$$

$$Eu^*_\theta=-(1+\nu)r^{-2}\{\sin\theta,-\cos\theta\}$$

(4) $F^*=\ln(r)$ (II-7)

$$\sigma^*_{\theta\theta}=-\frac{1}{r^2}=-\sigma^*_{rr},\qquad \sigma^*_{r\theta}=\sigma^*_{rz}=\sigma^*_{\theta z}=\sigma^*_{zz}=0,$$

$$Eu^*_r=-(1+\nu)r^{-2},\qquad Eu^*_\theta=Eu^*_z=0.$$

It should be noted that the singular fields $r\ln(r)\{\cos\theta,\sin\theta\}$ and $r^2\ln(r)$ all give rise to a multivalued displacement field and will not be considered herein. Also, singular states, for the transverse midplane displacement $w(r,\theta)$, similar to those given by (II-1), (II-3), (II-5) and (II-7) are available for transverse bending problems.

Downloaded 03 May 2010 to 171.66.16.21. Redistribution subject to ASME license or copyright; see http://www.asme.org/terms/Terms_Use.cfm

Michel Robert
IBM T. J. Watson Research Center,
Printer Mechanics,
Yorktown Heights, NY 10598

L. M. Keer
Departments of Civil and
Mechanical Engineering,
The Technological Institute,
Northwestern University,
Evanston, IL 60201
Fellow ASME

Stiffness of an Elastic Circular Cylinder of Finite Length

An analytical solution is proposed to determine the stiffness of an elastic circular cylinder clamped at one end, while the other end undergoes any rigid-body displacement; the lateral surface is stress-free. The validity of Saint-Venant's principle has been assessed by computing the solution of this problem for cylinders having different aspect ratios. On the other hand, the solution agrees with the thin layer theory when the aspect ratio becomes infinitely small. Therefore, the solution proposed here fills up the gap between beam theory and thin layer theory.

1 Formulation of the Problem

Consider a circular cylinder of radius R and length H, the material properties of which are assumed to be linear elastic and isotropic. The following loading conditions are applied: The curved lateral surface is stress-free, one of the ends ($\bar{z} = 0$) remains fixed (zero displacement), while the other end ($\bar{z} = H$) undergoes any rigid-body displacement; see Fig. 1. In the aforementioned configuration, flat ends of the cylinder remain circular throughout the deformation.

In order to be able to deal with more general results, the following dimensionless variables will be used

$$L = H/R \tag{1-1}$$

$$r = \bar{r}/R; \quad \theta = \theta; \quad z = \bar{z}/R \tag{1-2}$$

$$u = \bar{u}/R; \quad v = \bar{v}/R; \quad w = \bar{w}/R \tag{1-3}$$

$$\sigma_{rz} = \bar{\sigma}_{rz}/2\mu; \quad \sigma_{\theta z} = \bar{\sigma}_{\theta z}/2\mu; \quad \sigma_{zz} = \bar{\sigma}_{zz}/2\mu \tag{1-4}$$

where $(\bar{r}, \theta, \bar{z})$ are the usual cylindrical coordinates; $\bar{u}$, $\bar{v}$, and $\bar{w}$ are the radial, tangential, and axial displacement, respectively; and μ is the shear modulus of the material.

The most general rigid-body motion of the right end ($z = L$) can be decomposed into the following basic components:

(a) Translation parallel to the z-axis,
(b) Rotation about the z-axis,
(c) Translation perpendicular to the z-axis,
(d) Rotation perpendicular to the z-axis.

The deformations corresponding to the aforementioned displacements can be interpreted, respectively, as (see Fig. 2):

(a) Uniaxial traction,
(b) Uniform torsion,
(c) and (d) Shearing and bending.

Let us choose the x-axis to be in the direction of the shear and assume that the bending moment is parallel to the y-axis. Using this frame orientation, displacements and stresses can be written as follows

$$\begin{cases} u = u_1 \cos\theta \\ v = v_0 + v_1 \sin\theta \\ w = w_0 + w_1 \cos\theta \end{cases} \tag{1-5a}$$

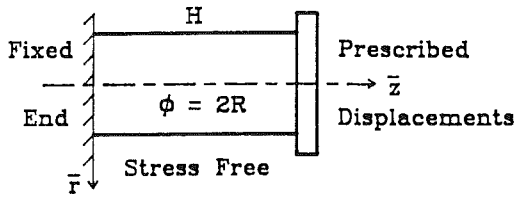


Fig. 1 Schematic configuration of the cylinder loading under study: zero displacements at $\bar{z} = 0$, stress-free lateral surface at $\bar{r} = R$, any prescribed rigid-body displacements at $\bar{z} = H$

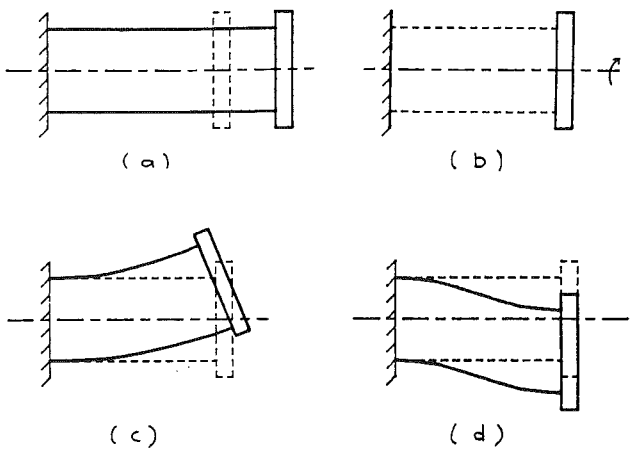


Fig. 2 Displacements prescribed at $\bar{z} = H$ schematically decomposed into: (a) traction; (b) torsion; (c) bending and (d) shearing.

Contributed by the Applied Mechanics Division for presentation at the Winter Annual Meeting, Chicago, IL, November 28 to December 2, 1988, of THE AMERICAN SOCIETY OF MECHANICAL ENGINEERS.

Discussion on this paper should be addressed to the Editorial Department, ASME, United Engineering Center, 345 East 47th Street, New York, N.Y. 10017, and will be accepted until two months after final publication of the paper itself in the JOURNAL OF APPLIED MECHANICS. Manuscript received by ASME Applied Mechanics Division, July 9, 1987; final revision, January 26, 1988.

Paper No. 88-WA/APM-41.

Copyright © 1988 by ASME
Downloaded 03 May 2010 to 171.66.16.21. Redistribution subject to ASME license or copyright; see http://www.asme.org/terms/Terms_Use.cfm

$$\begin{cases} \sigma_{rz} = (\sigma_{rz})_1 \cos\theta \\ \sigma_{\theta z} = (\sigma_{\theta z})_0 + (\sigma_{\theta z})_1 \sin\theta \\ \sigma_{zz} = (\sigma_{zz})_0 + (\sigma_{zz})_1 \cos\theta \end{cases} \tag{1-5b}$$

where subscripts 0 is associated with traction and torsion, while subscript 1 is associated with shear bending. The net forces and moments to be applied to the right end of the cylinder are therefore given by

$$\tfrac{1}{2}\frac{T}{\mu} = \int_0^{2\pi}\int_0^R (\sigma_{zz})(\bar{r})\bar{r}d\bar{r}d\theta = 2\pi R^2 \int_0^1 (\sigma_{zz})_0(r) r dr,$$

$$\tfrac{1}{2}\frac{C}{\mu} = \int_0^{2\pi}\int_0^R (\sigma_{\theta z})(\bar{r})\bar{r}^2 d\bar{r}d\theta = 2\pi R^3 \int_0^1 (\sigma_{\theta z})_0(r) r^2 dr,$$

$$\tfrac{1}{2}\frac{P}{\mu} = \int_0^{2\pi}\int_0^R (\sigma_{rz}\cos\theta - \sigma_{\theta z}\sin\theta)\bar{r}d\bar{r}d\theta$$

$$= \pi R^2 \int_0^1 [(\sigma_{rz})_1 - (\sigma_{\theta z})_1] r dr d\theta,$$

$$\tfrac{1}{2}\frac{M}{\mu} = \int_0^{2\pi}\int_0^R (\sigma_{zz})(\bar{r})\bar{r}^2 \cos\theta\, d\bar{r}d\theta = \pi R^3 \int_0^1 (\sigma_{zz})_1(r) r^2 dr.$$

where T, C, P, M represents the traction force, torque, shear force and bending moment, respectively. At the right end of the cylinder, the prescribed displacements can be written as

$$\begin{bmatrix} u_0 \\ v_0 \\ w_0 \end{bmatrix} = \delta_T \begin{bmatrix} 0 \\ 0 \\ L \end{bmatrix} + \delta_C \begin{bmatrix} 0 \\ 2Lr \\ 0 \end{bmatrix} \quad \text{and}$$

$$\begin{bmatrix} u_1 \\ v_1 \\ w_1 \end{bmatrix} = \delta_B \begin{bmatrix} -\tfrac{1}{2}L^2 \\ \tfrac{1}{2}L^2 \\ Lr \end{bmatrix} + \delta_S \begin{bmatrix} L \\ -L \\ 0 \end{bmatrix}$$

where subscripts T, C, B and S correspond to traction, torque, bending and shearing, respectively; see Fig. 2. Note that for large strains, the displacements associated with the bending deformation δ_B do not conserve the circular shape of the flat end. We therefore assume here that the bending rotation of the flat end is small enough to neglect the second-order displacements in the x-direction, which is consistent with the small strain theory of elasticity used herein.

The net forces and moments to apply at the right end can, therefore, be expressed in the following form

$$\tfrac{1}{2}\frac{1}{\mu}\begin{bmatrix} T \\ C \\ M \\ P \end{bmatrix} = \mathbf{E} \times \begin{bmatrix} \delta_T \\ \delta_C \\ \delta_B \\ \delta_S \end{bmatrix} \tag{1-6}$$

where $\mathbf{E}$ is the stiffness matrix of the cylinder. Due to the uncoupled effects of the displacements, the stiffness relations can be written as

$$\tfrac{1}{2}\frac{1}{\mu}\begin{bmatrix} T \\ C \\ M \\ P \end{bmatrix} = \begin{bmatrix} E_{TT} & 0 & 0 & 0 \\ 0 & E_{CC} & 0 & 0 \\ 0 & 0 & E_{MB} & E_{MS} \\ 0 & 0 & 0 & E_{PS} \end{bmatrix} \times \begin{bmatrix} \delta_T \\ \delta_C \\ \delta_B \\ \delta_S \end{bmatrix} \tag{1-7}$$

Thus the problem is now reduced to finding the foregoing five unknowns and to study their evolution with respect to the aspect ratio $L = H/R$ of the cylinder. It is already known that for a large aspect ratio, Saint-Venant's principle can be used so that the cylinder problem can be treated within the framework of the beam theory. On the other hand, for a small aspect ratio, the cylinder can be considered as a thin layer for which analytical solutions can also be easily derived. the analytical results given here are applicable for any aspect ratio and, thereby, make the bridge between beam and thin layer theories.

2 Analytical Resolution

The resolution method used for this problem was first described in Power and Childs (1971) and Duncan-Fama (1972), then improved in Gerhardt and Cheng (1981) and extended in Robert and Keer (1987) for the asymmetric case. This method is based on an eigenfunction expansion technique for which the stress-free condition on the lateral surface is automatically satisfied. The determination of the coefficients in this expansion, also called participating factors, is made through the displacements prescribed on the right and left interfaces.

With the formulation used in the previously mentioned references, a new set of unknowns $\eta_m(r, z)$ and $\xi_m(r, z)$ are introduced in such a way that the equilibrium equations in absence of body forces can be written as

$$\mathbf{L}_m(\eta_m) + \frac{\partial^2}{\partial z^2}(\eta_m) = 0 \tag{2-1a}$$

$$\mathbf{L}_m^*(\xi_m) + \frac{\partial^2}{\partial z^2}(\xi_m) = 0 \tag{2-1b}$$

$\mathbf{L}_m$ and $\mathbf{L}_m^*$ are two formally adjoints linear operators in the radial variable r

$$\mathbf{L}_m(\eta) = \begin{bmatrix} \dfrac{\partial^2\eta^1}{\partial r^2} + \left(\dfrac{1-4m^2}{4r^2}\right)\eta^1 \\ \dfrac{\partial^2\eta^2}{\partial r^2} - \left(\dfrac{3+4m^2}{4r^2}\right)\eta^2 + \dfrac{\partial\eta^1}{\partial r} - \dfrac{\eta^1}{2r} - \dfrac{2m}{r^2}\eta^3 \\ \dfrac{\partial^2\eta^3}{\partial r^2} - \left(\dfrac{3+4m^2}{4r^2}\right)\eta^3 - \dfrac{2m}{r}\eta^1 - \dfrac{2m}{r^2}\eta^2 \end{bmatrix} \tag{2-2a}$$

$$\mathbf{L}_m(\xi) = \begin{bmatrix} \dfrac{\partial^2\xi^1}{\partial r^2} + \left(\dfrac{1-4m^2}{4r^2}\right)\xi^1 - \dfrac{\partial\xi^2}{2r} - \dfrac{\xi^2}{2r} - \dfrac{m}{r}\xi^3 \\ \dfrac{\partial^2\xi^2}{\partial r^2} - \left(\dfrac{3+4m^2}{4r^2}\right)\xi^2 - \dfrac{2m}{r^2}\xi^3 \\ \dfrac{\partial^2\xi^3}{\partial r^2} - \left(\dfrac{3+4m^2}{4r^2}\right)\xi^3 - \dfrac{2m}{r^2}\xi^2 \end{bmatrix} \tag{2-2b}$$

and η_m and ξ_m are given by

$$\eta_m(r,z) = r^{1/2}\begin{bmatrix} \dfrac{1}{1-\nu}\left\{\dfrac{1}{r}\dfrac{\partial}{\partial r}(ru_m) + (\sigma_{zz})_m + \dfrac{m}{r}v_m\right\} \\ u_m \\ v_m \end{bmatrix} \tag{2-3a}$$

Downloaded 03 May 2010 to 171.66.16.21. Redistribution subject to ASME license or copyright; see http://www.asme.org/terms/Terms_Use.cfm

$$\xi_m(r,z) = r^{1/2} \begin{bmatrix} (1-\nu) w_m \\ \dfrac{\partial w_m}{\partial r} - (\sigma_{rz})_m \\ -(\sigma_{\theta z})_m - \dfrac{m}{r} w_m \end{bmatrix} \tag{2-3b}$$

Equations (2.1) are now solved by separation of variables and η_m and ξ_m are sought in the form

$$\eta_m(r,z) = \eta_m^*(r,z) + \sum_{\lambda_{mk} \neq 0} a_{mk} e^{-\lambda_{mk} z} \eta_{mk}(r) \tag{2-4a}$$

$$\xi_m(r,z) = \xi_m^*(r,z) + \sum_{\lambda_{mk} \neq 0} a_{mk} e^{-\lambda_{mk} z} \xi_{mk}(r) \tag{2-4b}$$

where $\eta_{mk}(r)$ and $\xi_{mk}(r)$ are the nonzero radial eigenvalue solution vectors and $\eta_m^*(r, z)$ and $\xi_m^*(r, z)$ represent the solution vectors corresponding to the case $\lambda_m = 0$.

For each case ($m = 0$ and $m = 1$), the corresponding sets of eigenvalues $\{\lambda_{mk}\}$ are determined such that the stress-free conditions

$$(\sigma_{rr})_m = (\sigma_{rz})_m = (\sigma_{r\theta})_m = 0 \tag{2-5}$$

expressed in terms of $\eta_{mk}(r)$ or $\xi_{mk}(r)$ are satisfied on the lateral surface ($r = 1$). The eigenvalue equations, as well as the radial eigenfunctions, have been derived in Robert and Keer (1987) and are given next.

(*a*) Axially Symmetric Part of the Deformation ($m = 0$). The eigenvalues λ_k must satisfy the following transcendental equation

$$\lambda^2 J_2(\lambda) \left(\lambda^2 \left[J_0^2(\lambda) + J_1^2(\lambda) \right] - 2(1-\nu) J_1^2(\lambda) \right) = 0 \tag{2-6}$$

The first set of radial eigenfunctions is associated with the zeros of J_2 and can be expressed as

$$\Phi'_{0_k}(r) = \begin{bmatrix} u'_{0_k} \\ w'_{0_k} \\ (\sigma_{zz})'_{0_k} \\ (\sigma_{rz})'_{0_k} \end{bmatrix} = \mathbf{0} \quad \text{and} \quad \Psi'_{0_k} = \begin{bmatrix} v'_{0_k} \\ (\sigma_{\theta z})'_{0_k} \end{bmatrix} = \begin{bmatrix} J_1(\delta_k r) \\ -\delta_k J_1(\delta_k r) \end{bmatrix}$$

where $J_2(\delta_k) = 0$ for $k = 1, 2, 3, \ldots$.

The second set of solutions are associated with the roots of

$$\lambda^2 \left[J_0^2(\lambda) + J_1^2(\lambda) \right] - 2(1-\nu) J_1^2(\lambda) = 0 \tag{2-7}$$

and are given

$$\begin{cases} u_{0_k}(r) = [\lambda_k^2 J_{0_k} + 2(1-\nu)\lambda_k J_{1_k}] J_1(\lambda_k r) - \lambda_k^2 J_{1_k} r J_0(\lambda_k r) \\ w_{0_k}(r) = [\lambda_k^2 J_{0_k} - 2(1-\nu)\lambda_k J_{1_k}] J_0(\lambda_k r) + \lambda_k^2 J_{1_k} r J_1(\lambda_k r) \end{cases} \tag{2-8a}$$

$$\begin{cases} (\sigma_{zz})_{0_k}(r) = [-\lambda_k^3 J_{0_k} + 2\lambda_k^2 J_{1_k}] J_0(\lambda_k r) - \lambda_k^3 J_{1_k} r J_1(\lambda_k r) \\ (\sigma_{rz})_{0_k}(r) = -\lambda_k^3 J_{0_k} J_1(\lambda_k r) + \lambda_k^3 J_{1_k} r J_0(\lambda_k r) \end{cases} \tag{2-8b}$$

with

$$v_{0_k}(r) = (\sigma_{\theta z})_{0_k}(r) = \mathbf{0}$$

where

$$J_{0_k} = J_0(\lambda_k) \quad \text{and} \quad J_{1_k} = J_1(\lambda_k)$$

Finally, the homogeneous solution corresponding to the zero eigenvalue $\lambda_0 = 0$ is given by

$$\Phi_0^*(r,z) = \begin{bmatrix} u_0^* \\ w_0^* \\ (\sigma_{zz})_0^* \\ (\sigma_{rz})_0^* \end{bmatrix} = \alpha_{01}^* \begin{bmatrix} -\nu r \\ z \\ 1+\nu \\ 0 \end{bmatrix} + \alpha_{03}^* \begin{bmatrix} 0 \\ 1 \\ 0 \\ 0 \end{bmatrix} \tag{2-9a}$$

and

$$\Psi_0^*(r,z) = \begin{bmatrix} v_0^* \\ (\sigma_{\theta z})_0^* \end{bmatrix} = \alpha_{02}^* \begin{bmatrix} 2rz \\ r \end{bmatrix} + \alpha_{04}^* \begin{bmatrix} r \\ 0 \end{bmatrix} \tag{2-9b}$$

where the constants α_{01}^*, α_{02}^*, α_{03}^* and α_{04}^* correspond, respectively, to a uniform traction in the z-direction, a uniform torsion, a rigid-body translation parallel to the z-axis and a rigid-body rotation about the z-axis.

(*b*) Asymmetric Part of the Deformation ($m = 1$). Let γ be an eigenvalue for the asymmetric case ($m = 1$); γ has to verify the following equation

$$\gamma^2 \Big(\gamma^2 J_1^3(\gamma) - 4\gamma J_1^2(\gamma) J_2(\gamma) + (\gamma^2 + 2\nu + 2) J_1(\gamma) J_2^2(\gamma) - 2\gamma J_2^3(\gamma) \Big) = 0 \tag{2-10}$$

It is of interest to note that in the asymmetric case ($m = 1$), it is not possible to uncouple the real roots from the complex roots, which was easily done in the axisymmetric case by taking into account first the torsion problem (corresponding to the real roots), and then the problem without torsion (corresponding to the complex roots).

The following radial eigenfunctions are obtained for $\gamma_k \neq 0$

$$\begin{cases} (u+v)_{1_k}(r) = -\gamma_k J_{1_k} J_{2_k} r J_1(\gamma_k r) + [3\gamma_k J_{1_k}^2 - 2(1+\nu) J_{1_k} J_{2_k} + 2\gamma_k J_{2_k}^2] J_2(\gamma_k r) \\ (u-v)_{1_k}(r) = -\gamma_k J_{1_k} J_{2_k} r J_1(\gamma_k r) + [\gamma_k J_{1_k}^2 - 2(2-\nu) J_{1_k} J_{2_k} + 2\gamma_k J_{2_k}^2] J_0(\gamma_k r) \\ w_{1_k}(r) = \gamma_k J_{1_k} J_{2_k} r J_2(\gamma_k r) + J_{1_k} [\gamma_k J_{1_k} - 2(2-\nu) J_{2_k}] J_1(\gamma_k r) \end{cases} \tag{2-11a}$$

$$\begin{cases} (\sigma_{rz} + \sigma_{\theta z})_{1_k}(r) = \gamma_k^2 J_{1_k} J_{2_k} r J_1(\gamma_k r) - \gamma_k [2\gamma_k J_{1_k}^2 - 2 J_{1_k} J_{2_k} + \gamma_k J_{2_k}^2] J_2(\gamma_k r) \\ (\sigma_{rz} - \sigma_{\theta z})_{1_k}(r) = \gamma_k^2 J_{1_k} J_{2_k} r J_1(\gamma_k r) - \gamma_k^2 J_{2_k}^2 J_0(\gamma_k r) \\ (\sigma_{zz})_{1_k}(r) = -\gamma_k^2 J_{1_k} J_{2_k} r J_2(\gamma_k r) + \gamma_k J_{1_k} [-\gamma_k J_{1_k} + 4 J_{2_k}] J_1(\gamma_k r) \end{cases} \tag{2-11b}$$

where

$$J_{1_k} = J_1(\gamma_k) \quad \text{and} \quad J_{2_k} = J_2(\gamma_k).$$

The zero-eigenvalue solutions obtained when $\gamma_0 = 0$ are given by

$$\begin{cases} (u+v)_1^*(r) = \alpha_{11}^*(-\nu z r^2) + \alpha_{12}^*(-\nu r^2) \\ (u-v)_1^*(r) = \alpha_{11}^* \left(-\dfrac{1}{3} z^3 + \dfrac{3+2\nu}{2} z \right) + \alpha_{12}^*(-2z^2) + \alpha_{13}^*(-2z) + \alpha_{14}^* \\ w_1^*(r) = \alpha_{11}^* \left(\dfrac{1}{2} z^2 r - \dfrac{1}{4} r^3 \right) + \alpha_{12}^* z r + \alpha_{13}^* r \end{cases} \tag{2-12a}$$

Downloaded 03 May 2010 to 171.66.16.21. Redistribution subject to ASME license or copyright; see http://www.asme.org/terms/Terms_Use.cfm

$$\begin{cases} (\sigma_{zz})_1^*(r) & = \alpha_{11}^*(1+\nu)zr + \alpha_{12}^*(1+\nu)r \\ (\sigma_{rz}+\sigma_{\theta z})_1^*(r) & = \alpha_{11}^*\left(-\dfrac{1+2\nu}{4}\, r^2\right) \\ (\sigma_{rz}-\sigma_{\theta z})_1^*(r) & = \alpha_{11}^*\left(\dfrac{3+2\nu}{4} - \dfrac{1}{2}\, r^2\right) \end{cases} \tag{2-12b}$$

where the constants α_{11}^*, α_{12}^*, α_{13}^* and α_{14}^* correspond, respectively, to a "mixed shearing" (see Love (1944), page 329), a pure bending, a rigid-body rotation about the y-axis, and a rigid-body translation parallel to the x-axis.

(c) Net Forces and Moments. As shown in Robert and Keer (1987) using a biorthogonal product between radial eigenfunctions the following relations hold

$$\int_0^1 (\sigma_{zz})_{0_k} r dr = 0 \qquad \text{for all } \lambda_k \neq 0 \tag{2-13a}$$

$$\int_0^1 (\sigma_{\theta z})'_{0_k} r^2 dr = 0 \qquad \text{for all } \delta_k \neq 0 \tag{2-13b}$$

$$\int_0^1 (\sigma_{zz})_{1_k} r^2 dr = 0 \qquad \text{for all } \gamma_k \neq 0 \tag{2-13c}$$

$$\int_0^1 (\sigma_{rz}-\sigma_{\theta z})_{1_k} r dr = 0 \qquad \text{for all } \gamma_k \neq 0 \tag{2-13d}$$

The foregoing equations, respectively, mean that the nonzero eigenvalue solution does not produce any net force in the z-direction, any torque, any bending moment nor any net force in the x-direction. Therefore, the stiffness matrix **E** will depend only upon the homogeneous solution associated with the given prescribed displacements

$$\tfrac{1}{2}\frac{T}{\mu} = 2\pi R^2 \int_0^1 (\sigma_{zz})_0^*(r) r dr = \pi R^2 (1+\nu)\alpha_{01}^*; \tag{2-14a}$$

$$\tfrac{1}{2}\frac{C}{\mu} = 2\pi R^3 \int_0^1 (\sigma_{\theta z})_0^*(r) r^2 dr = \tfrac{1}{2}\pi R^3 \alpha_{02}^* \tag{2-14b}$$

$$\tfrac{1}{2}\frac{P}{\mu} = \pi R^2 \int_0^1 [(\sigma_{rz})_1^* - (\sigma_{\theta z})_1^*] r dr d\theta = \tfrac{1}{4}\pi R^2 (1+\nu)\alpha_{11}^* \tag{2-14c}$$

$$\tfrac{1}{2}\frac{M}{\mu} = \pi R^3 \int_0^1 (\sigma_{zz})_1^*(r) r^2 dr = \tfrac{1}{4}\pi R^3 (1+\nu)(L\,\alpha_{11}^* + \alpha_{12}^*) \tag{2-14d}$$

where the constants α_{11}^*, α_{12}^*, α_{13}^* and α_{14}^* have to be solved for different aspect ratios in terms of the rigid-body displacements coefficients δ_T, δ_C, δ_B and δ_S.

3 Closed-Form Solution for Two Limit Cases

The two limit cases are obtained when the aspect ratio $L = H/R$ goes either to zero or to infinity. In the first case, thin layer theory can be applied while, in the second case, the stiffness of the cylinder can be determined within the framework of the beam theory.

(a) Infinitely Small Aspect Ratio. In this case, the cylinder can be thought as an infinite circular layer ($R = \infty$) of thickness unity ($H = 1$) for which the contribution of the stress near the edge can be neglected. Therefore, the following solutions are valid only for r less than one, since they do not satisfy the stress-free condition on the curved surface of this infinite layer.

Traction and Torsion Problems

$$\Phi_0(r,z) = \begin{bmatrix} u_0 \\ w_0 \\ (\sigma_{zz})_0 \\ (\sigma_{rz})_0 \end{bmatrix} = \delta_T \begin{bmatrix} 0 \\ z \\ \left(\dfrac{1-\nu}{1-2\nu}\right) \\ 0 \end{bmatrix};$$

$$\Psi_0(r,z) = \begin{bmatrix} v_0 \\ (\sigma_{\theta z})_0 \end{bmatrix} = \delta_C \begin{bmatrix} 2rz \\ r \end{bmatrix} \tag{3-1}$$

Bending and Shearing Problems

$$\Phi_1(r,z) = \delta_B \begin{bmatrix} -\tfrac{1}{2} z^2 \\ zr \\ \left(\dfrac{1-\nu}{1-2\nu}\right) r \\ 0 \end{bmatrix} + \delta_S \begin{bmatrix} z \\ 0 \\ 0 \\ \tfrac{1}{2} \end{bmatrix};$$

$$\Psi_1(r,z) = \delta_B \begin{bmatrix} \tfrac{1}{2} z^2 \\ 0 \end{bmatrix} + \delta_s \begin{bmatrix} -z \\ -\tfrac{1}{2} \end{bmatrix} \tag{3-2}$$

Therefore, the net forces and moments are given by

$$\tfrac{1}{2}\frac{T}{\mu} = \pi R^2 \left(\frac{1-\nu}{1-2\nu}\right)\delta_T \qquad \text{or} \qquad \frac{T}{S} = (\lambda + 2\mu)\delta_T \tag{3-3a}$$

$$\tfrac{1}{2}\frac{C}{\mu} = \tfrac{1}{2}\pi R^3 \delta_C \qquad \text{or} \qquad \frac{R\,C}{I} = 4\mu\delta_C \tag{3-3b}$$

$$\tfrac{1}{2}\frac{P}{\mu} = \tfrac{1}{2}\pi R^2 \delta_S \qquad \text{or} \qquad \frac{P}{S} = \mu\delta_S \tag{3-3c}$$

$$\tfrac{1}{2}\frac{M}{\mu} = \tfrac{1}{4}\pi R^3 \left(\frac{1-\nu}{1-2\nu}\right)\delta_B \qquad \text{or} \qquad \frac{R\,M}{I} = (\lambda + 2\mu)\delta_B \tag{3-3d}$$

where λ and μ are the Lamé coefficients of the material

$$2\mu = E/(1+\nu), \quad \lambda = 2\mu\nu/(1-2\nu)$$

and S and I are the area and the moment of inertia of the cross section

$$S = \int\int d\bar{x}\, d\bar{y}$$

$$I = \int\int \bar{x}^2 d\bar{x}\, d\bar{y} = \tfrac{1}{4} R^2 S \quad \text{for a circular cylinder.}$$

(b) Infinitely Large Aspect Ratio. In this limit configuration, the classical beam theory can be applied through Saint-Venant's principle and the following resultant forces and moments are obtained

$$\frac{T}{S} = E\,\delta_T \tag{3-4a}$$

$$\frac{R\,C}{I} = 4\mu\,\delta_C \tag{3-4b}$$

$$\frac{R\,M}{I} = E\left(\delta_B + \frac{6}{L}\,\delta_S\right) \tag{3-4c}$$

$$\frac{P}{S} = \frac{E}{4}\,\delta_S\,\frac{12}{L^2} \tag{3-4d}$$

Downloaded 03 May 2010 to 171.66.16.21. Redistribution subject to ASME license or copyright; see http://www.asme.org/terms/Terms_Use.cfm

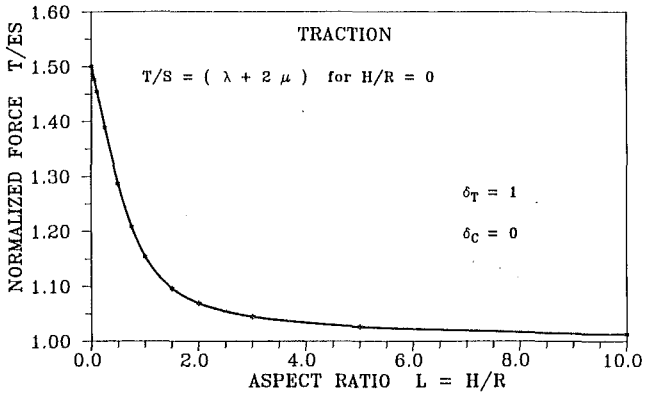


Fig. 3 Normalized traction force *T/ES* obtained for different aspects ratios $L = H/R$; Poisson's ratio is taken to be 1/3 and the axial displacement coefficient δ_T equals one

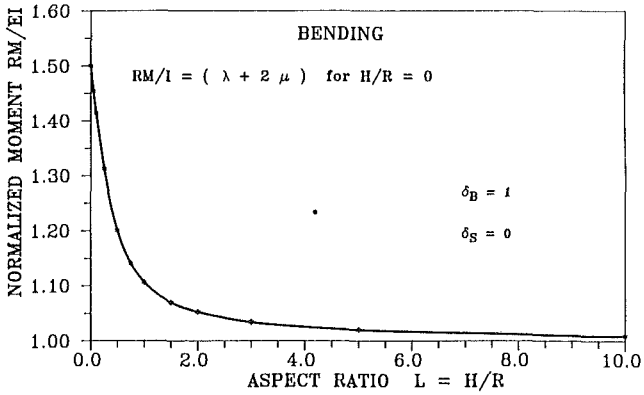


Fig. 4 Normalized bending moment *RM/EI* obtained for different aspect ratios $L = H/R$; Poisson's ratio is taken to be 1/3 and the bending displacement coefficient δ_B equals one

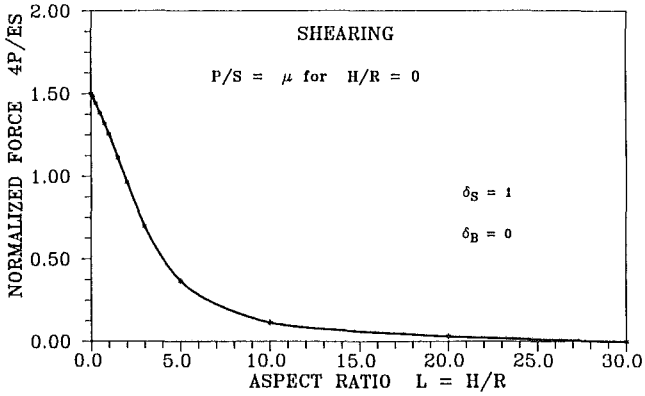


Fig. 5 Normalized shear force 4*P/ES* obtained for different aspect ratios $L = H/R$; Poisson's ratio is taken to be 1/3 and the shearing displacement coefficient δ_S equals one

The equations associated with δ_S were derived by considering the superposition of the beam solutions for a concentrated load P and moment M such that the rotation of the end is zero.

4 Analytical Solution for Any Aspect Ratio

For a nonzero and finite aspect ratio $L = H/R$, the determination of the homogeneous solution requires in fact the determination of all the participating factors a_{mk}. This is done as in Gerhardt and Cheng (1981) and Robert and Keer (1987)

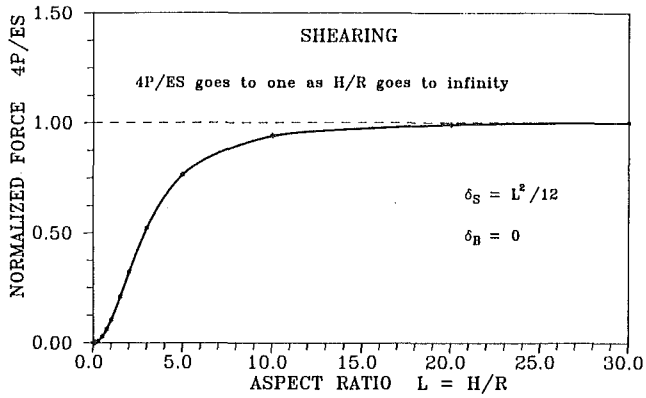


Fig. 6 Normalized shear force 4*P/ES* obtained for different aspect ratios $L = H/R$; Poisson's ratio is taken to be 1/3 and the shearing displacement coefficient δ_S equals $L^2/12$

with a Galerkin-type method: Those equations are obtained with the prescribed displacements on the right and left interfaces ($z = 0$ and $z = L$) and can be written in the most general case as

$$\int_0^1 [(u_m - u_m^*)\chi_{mj}^1 + (v_m - v_m^*)\chi_{mj}^2 + (w_m - w_m^*)\chi_{mj}^3]rdr$$

$$= \sum_{k=1}^{N} a_{mk} e^{-\lambda_{mk} z} \int_0^1 [u_{mk}\chi_{mj}^1 + v_{mk}\chi_{mj}^2 + w_{mk}\chi_{mj}^3]rdr \qquad (4.1)$$

at $z = 0$ and $z = L$, for $m = 0$ or 1 and $j = 0, 1, 2 \cdots, N$; where u_m, v_m and w_m are the mth harmonics of the prescribed displacements at the flat ends. The optimum weighting functions χ_{mj}^1, χ_{mj}^2 and χ_{mj}^3 are found in Gerhardt and Cheng (1981) and Robert and Keer (1987) and are given next.

(*a*) Torsion Problem. The exact solution for the uniform torsion problem is by definition the homogeneous solution and, therefore, the participating factors a_{0_k} are all equal to zero. The simplicity of the solution can be explained by the fact that no Poisson's effect is involved during a uniform torsion. Thus, in this case, the stiffness does not depend upon the aspect ratio of the cylinder.

(*b*) Traction Problem. For $j = 0$

$$\chi_{00}^1 = \chi_{00}^2 = 0 \quad \text{and} \quad \chi_{00}^3 = 1$$

For $j \neq 0$

$$\begin{cases} \chi_{0j}^1 = [\lambda_j^3 J_{0_j} + (1-2\nu)\lambda_j^2 J_{1_j}]J_1(\lambda_j r) - \lambda_j^3 J_{1_j} r J_0(\lambda_j r) \\ \chi_{0j}^2 = 0 \\ \chi_{0j}^3 = [-\lambda_j^3 J_{0_j} + (3-2\nu)\lambda_j^2 J_{1_j}]J_0(\lambda_j r) - \lambda_j^3 J_{1_j} r J_1(\lambda_j r) \end{cases} \qquad (4\text{-}2)$$

where $J_{0_j} = J_0(\lambda_j)$; $J_{1_j} = J_1(\lambda_j)$ and λ_j is a nonzero eigenvalue for axially symmetric case $m = 0$.

(*c*) Bending and Shearing Problem. For $j = 0$, we have two different sets of weighting functions

$$\begin{cases} \chi_{10}^{1\prime} = 0 \\ \chi_{10}^{2\prime} = 0 \\ \chi_{10}^{3\prime} = r \end{cases} \qquad (4\text{-}3a)$$

and

$$\begin{cases} \chi_{10}^2 = -(3+2\nu)(1-r^2) \\ \chi_{10}^2 = (3+2\nu) + (-1+2\nu)r^2 \\ \chi_{10}^3 = 0 \end{cases} \qquad (4\text{-}3b)$$

Downloaded 03 May 2010 to 171.66.16.21. Redistribution subject to ASME license or copyright; see http://www.asme.org/terms/Terms_Use.cfm

For $j \neq 0$, the weighting functions are given by

$$\begin{cases} \chi^1_{1_j} + \chi^2_{1_j} = A^1 \gamma_j J_{1_j} J_{2_j} r J(\gamma_j r) \\ \qquad + [B^1_j \gamma J^2_{1_j} + 2C^1 J_{1_j} J_{2_j} + D^1 \gamma_j J^2_{2_j}] J_2(\gamma_j r) \\ \chi^2_{1_j} - \chi^2_{1_j} = A^2 \gamma_j J_{1_j} J_{2_j} r J_1(\gamma_j r) \\ \qquad + [B^2 \gamma_j J^2_{1_j} + 2C^2 J_{1_j} J_{2_j} + D^2 \gamma_j J^2_{2_j}] J_0(\gamma_j r) \\ \chi^3_{1_j} = A^3 \gamma_j J_{1_j} J_{2_j} r J_2(\gamma_j r) \\ \qquad + [B^3 \gamma_j J^2_{1_j} + 2C^3 J_{1_j} J_{2j} + D^3 \gamma_j J^2_{2_j}] J_1(\gamma_j r) \end{cases} \tag{4.4}$$

where $J_{1_j} = J_1(\gamma_j)$; $J_{2_j} = J_2(\gamma_j)$; γ_j is a nonzero eigenvalue for the asymmetric case $m = 1$ and

$$A^1 = 2(1-\nu) \qquad A^2 = 2(1-\nu) \qquad A^3 = 2(1-\nu)$$

$$B^1 = -5+6\nu \qquad B^2 = -1+2\nu \qquad B^3 = 2(1-\nu)$$

$$C^1 = -2\nu^2 - \nu + 2 \qquad C^2 = 2\nu^2 - 5\nu + 2 \qquad C^3 = (1-\nu)(-5+2\nu)$$

$$D^1 = -3+4\nu \qquad D^2 = -3+4\nu \qquad D^3 = 0$$

The aforementioned weighting functions have been found in such a way that the truncated system of linear equations (4.1) is the more diagonally dominant possible.

A closed form for the integral $\int_0^1 [u_{mk}\, \chi^1_{mj} + v_{mk}\, \chi^2_{mj} + w_{mk}\, \chi^3_{mj}]\, rdr$ can be found in Robert and Keer (1987) for both $m = 0$ and $m = 1$. The Galerkin system (4.1) has been solved for each of the following cases

$\delta_T = 1$; $\delta_C = \delta_B = \delta_S = 0$ (Traction only; see Fig. 3)

$\delta_B = 1$; $\delta_T = \delta_C = \delta_S = 0$ (Bending only; see Fig. 4)

$\delta_S = 1$; $\delta_T = \delta_C = \delta_B = 0$ (Shear only; see Fig. 5)

$\delta_S = \dfrac{L^2}{12}$; $\delta_T = \delta_C = \delta_B = 0$ (Shear only; see Fig. 6)

with a number of terms in the eigenfunction expansion corresponding to 40 pairs and 40 triplets for $m = 0$ and $m = 1$, respectively. Only the case, when Poisson's ratio ν equals 1/3, has been studied, and the aspect ratio $L = H/R$ was taken between 0.05 and 30. Figures 3–6 illustrate the results and the convergence to the two limit cases studied previously is clear.

Acknowledgments

This work was supported in part through a Royal E. Cabell fellowship from Northwestern University. The authors gratefully acknowledge support from the International Business Machines Corporation.

References

Duncan, M. E., and Fama, Q. J., 1972, "Radial Eigen Functions for the Elastic Circular Cylinder," *Mechanics Applied Mathematics*, Vol. 25, pp. 479–495.

Gerhardt, T. D., and Cheng, S., 1981, "A Diagonally Dominant Solution for the Cylinder End Problem," ASME JOURNAL OF APPLIED MECHANICS, Vol. 48, pp. 876–880.

Love, A. E. H., 1944, *A Treatise on the Mathematical Theory of Elasticity*, Dover, New York.

Power, L. D., and Childs, S. B., 1971, "Axisymmetric Stresses and Displacements in a Finite Circular Bar," *International Journal of Engineering Science*, Vol. 9, pp. 241–255.

Robert, M., and Keer, L. M., 1987, "An Elastic Circular Cylinder with Displacement Prescribed at the Ends," *Quarterly Journal of Mechanics and Applied Mathematics*, Vol. 40, pp. 339–381.

Downloaded 03 May 2010 to 171.66.16.21. Redistribution subject to ASME license or copyright; see http://www.asme.org/terms/Terms_Use.cfm

The Involution Correspondence in Plane Elastostatics for Regions Bounded by a Circle

T. Honein
Graduate Student.

G. Herrmann
Professor of Applied Mechanics.
Fellow ASME.

Division of Applied Mechanics,
Stanford University,
Durand Building,
Stanford, CA 94305

It is shown that the elastic field induced by prescribed displacements or surface tractions acting on a circular disk (inner region) can be expressed in terms of the elastic field induced by the same quantities acting on the circular boundary (hole) of an infinite plane (outer region), and vice versa. It is shown further that this correspondence is an involution. This novel representation permits one to express the elastic field in a disk with either vanishing displacements or tractions along the boundary in terms of the elastic field of an infinite domain, provided all singularities are in the inner region. Similarly, the elastic field in the outer region can be expressed in terms of the elastic field of the infinite domain, provided all singularities reside in the outer region. The expressions so-derived possess simple algebraic character and are universal in the sense of being independent of the applied loads (singularities) in the two problems.

Introduction

We are concerned here with homogeneous isotropic bodies within the framework of linear, plane elastostatics (plane stress or plane strain). We propose to show that the solutions of the first and the second boundary-value problem for a circular disk (inner region) may be expressed in terms of the corresponding problem for an infinite plane containing a circular hole of same radius (outer region) and vice versa. This correspondence is universal in the sense that it is independent of the specifics of the boundary data prescribed. A further important feature is that the relations established here between the potentials, the components of stress and the components of displacement of the corresponding problems are algebraic and do not involve integration or solution of some other equations. An immediate consequence of the correspondence mentioned is that, by simple and obvious superposition, any boundary-value problem for the inner or the outer region may be solved more easily in terms of the corresponding solutions (meaning applications of like singularities) for the infinite, homogeneous plane (complete region). Again, the relations between the solutions for the two (inner and outer) bounded problems on one hand, and those for the unbounded problem on the other, are universal and algebraic.

It appears to be a remarkable and peculiar fact that the correspondence existing between the inner and outer regions, as well as between these regions and the complete region, have not been exploited earlier. Indeed, the corresponding problems of the inner and outer regions have been treated in the literature as separate and independent, as will be documented later.

By contrast, in other field theories such as electrostatics, the procedure to be advanced here has been in existence since the middle of the last century and is based on inversion and the Kelvin transformation; see (Maxwell, 1954 and Kellogg, 1953). It is widely used as the "methods of images"; see (Jackson, 1975).

An important difference between the usual method of images and the method proposed here is the fact that, in the former, the sources are being transformed, while here we intend to transform the solutions. In harmonic problems this difference is irrelevant while for biharmonic it is not. In our procedure, as will be seen, the sources (singularities) are left in place.

In examining the literature available, it becomes clear that the inner and outer regions are treated as separate problems; see Muskhelishvili (1953a). The two parts forming the entire plane are merely connected to effect the analytic continuation of relevant complex potentials.

Numerous different problems for the inner region (disk) and outer region (plane with a circular hole) are treated by Muskhelishvili (1953b) in different sections as separate problems. The problem of a disk under concentrated forces and couples acting at internal points is not reduced there (p. 328) to the problem of the infinite plane subjected to the same forces, but involves a tedious evaluation of Cauchy's integral with branch cuts, which obviously depends on the loading, rather than a substitution into a universal algebraic formula, as proposed here. Similarly, Green and Zerna (1968), as well as Sokolnikoff (1983), follow in the footsteps of

Contributed by the Applied Mechanics Division for presentation at the Winter Annual Meeting, Chicago, IL, November 28 to December 2, 1988, of THE AMERICAN SOCIETY OF MECHANICAL ENGINEERS.

Discussion on this paper should be addressed to the Editorial Department, ASME, United Engineering Center, 345 East 47th Street, New York, NY 10017, and will be accepted until two months after final publication of the paper itself in the JOURNAL OF APPLIED MECHANICS. Manuscript received by ASME Applied Mechanics Division, July 20, 1987; final revision, February 5, 1988.

Paper No. 88-WA/APM-42.

Copyright © 1988 by ASME
Downloaded 03 May 2010 to 171.66.16.21. Redistribution subject to ASME license or copyright; see http://www.asme.org/terms/Terms_Use.cfm

Muskhelishvili and treat the inner and outer problems separately; Milne-Thomson (1968) also doesn't recognize the interdependence between the outer and inner problem. For example, the first boundary-value problem for the outer region and for the disk are treated separately in different sections (pp. 116, 117). To make the analytic continuation possible, Milne-Thomson is, as others, obliged to apply the Plemelj theorem. On p. 74, Milne-Thomson (1968) advances what he calls the "first circle theorem" and the "second circle theorem" which in the outer problem yield vanishing surface tractions in terms of the potentials of the complete problem. It is noted, however, that the expressions given would alter the singularities of the original problem and thus are valid only under very special circumstances. The term "circle theorem" was established originally by Milne-Thomson in fluid dynamics of potential flow in 1940, see (Milne-Thomson, 1960), but he did not succeed in carrying it over into elastostatics. He apparently was not aware of the work by Kelvin and Maxwell. More recently, Kienzler and Zhuping (1987) derived a formula to calculate the distribution of hoop stresses at the boundary of a circular hole in an infinite plane subjected to arbitary (in plane) loads. It is this formula, which also appears somewhat disguised on p. 281 in Green and Zerna (1968) which prompted the present authors to reexamine this whole problem area in a more general setting. An extension of the circle theorem to thermoelasticity was carried out by the present authors (1987).

In presenting the developments which follow here, it was decided to employ the formalism of functions of a complex variable of plane elastostatics, as initiated by Filon (1903) and evolved by Kolosov and Muskhelishvili and presented by Muskhelishvili (1953b) and Sokolnikoff (1983). This formalism allows for compactness and lucidity and is preferred here over Fourier series representation employed by Kienzler and Zhuping (1987).

It is to be emphasized that the technique of analytic continuation is not employed here. Indeed our developments stay within the realm of elementary operations on functions of a complex variable.

In the first section, the transformations of inversion and of Kelvin in the plane are introduced and discussed. This is followed in the next section by a summary of fundamental relations of plane elastostatics according to Kolosov-Muskhelishvili formalism. In the third section, these transformations are applied to elastostatics, leading, in Section IV, to the establishment of a correspondence between the "dual" problems for the inner and outer regions. This correspondence is shown to be an involution. In Section V simple superposition leads to the establishment of an algebraic relationship between the elastic fields for the inner or the outer problem on one hand and the much simpler corresponding problem for the complete region, on the other. Both, first and second boundary-value problems are considered. Several specific examples to illustrate the two correspondence principles are presented in Section VI and some conclusions are drawn in Section VII.

I Inversion and Kelvin's Transformation in the Plane

In a plane of infinite extent consider a circle C of radius a centered at O. Let M be a point of a plane located at a distance $r \neq 0$ from O, see Fig. 1. The inverse of M with respect to C is the point M^* which is a distance r^* from O such that

$$rr^* = a^2,$$

and lies on the semi-infinite straight line OM. Obviously, if $r \lessgtr a$ then $r^* \gtrless a$ and vice versa. This means that the inner region is mapped on the outer region and vice versa. The inversion transformation is an involution, i.e., a transformation which is its own inverse.

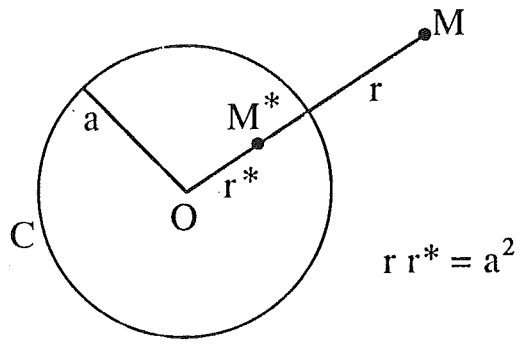


Fig. 1 Inversion with respect to circle C

If we consider the complex plane $z = x + iy$, then $M = M(z)$ and $M^* = M^*(z^*)$, with

$$i^2 = -1; \quad z = re^{i\theta}; \quad z^* = r^* e^{i\theta} = \frac{a^2}{r} e^{i\theta} = \frac{a^2}{\bar{z}},$$

where $\bar{z} = x - iy$ is the complex conjugate of z. We now proceed to introduce the Kelvin transformation, first established in 1847; see (Maxwell, 1954, and Kellogg, 1953). Let $u(r, \theta)$ be some harmonic function of polar coordinates r, θ, i.e.,

$$\nabla^2 u = \frac{\partial^2 u}{\partial r^2} + \frac{1}{r}\frac{\partial u}{\partial r} + \frac{1}{r^2}\frac{\partial^2 u}{\partial \theta^2} = 0.$$

Suppose one wishes to evaluate u not at r, θ, but rather at the inverse point a^2/r, θ. We define

$$\tilde{u}(r, \theta) = u\left(\frac{a^2}{r}, \theta\right)$$

and consider $\tilde{u}$ to be a function of r, θ. It is readily shown that

$$\nabla^2 \tilde{u}(r, \theta) = \frac{a^4}{r^4} \nabla^2 u\left(\frac{a^2}{r}, \theta\right) = 0$$

Thus inversion carries one harmonic function into another and this is known as the Kelvin transformation.

Next, we wish to establish a connection between the Kelvin transformation and functions of a complex variable. Let $\xi(r, \theta)$ be a harmonic function of polar coordinates. Thus, as is well known, ξ may be considered as the real part of a holomorphic function $\zeta(z)$,

$$\zeta(z) = \xi(r, \theta) + i\eta(r, \theta)$$

and hence

$$\zeta'(z) = e^{-i\theta}\frac{\partial \zeta}{\partial r} = -ie^{-i\theta}\frac{1}{r}\frac{\partial \zeta}{\partial \theta}$$

where a prime indicates differentiation with respect to the argument. The associated Cauchy-Riemann conditions are

$$\frac{\partial \xi}{\partial r}(r, \theta) = \frac{1}{r}\frac{\partial \eta}{\partial \theta}(r, \theta)$$

$$\frac{1}{r}\frac{\partial \xi}{\partial \theta}(r, \theta) = -\frac{\partial \eta}{\partial r}(r, \theta)$$

Let us now subject the functions ξ and η to the Kelvin transformation

$$\tilde{\xi}(r, \theta) = \xi\left(\frac{a^2}{r}, \theta\right)$$

$$\tilde{\eta}(r, \theta) = \eta\left(\frac{a^2}{r}, \theta\right)$$

leading to

$$\frac{\partial \tilde{\xi}}{\partial r}(r, \theta) = -\frac{a^2}{r^2}\frac{\partial \xi}{\partial r}\left(\frac{a^2}{r}, \theta\right)$$

Downloaded 03 May 2010 to 171.66.16.21. Redistribution subject to ASME license or copyright; see http://www.asme.org/terms/Terms_Use.cfm

$$= -\frac{a^2}{r^2}\left(\frac{r}{a^2}\right)\frac{\partial \eta}{\partial \theta}\left(\frac{a^2}{r}, \theta\right) = -\frac{1}{r}\frac{\partial \tilde{\eta}}{\partial \theta}(r, \theta),$$

and

$$\frac{1}{r}\frac{\partial \tilde{\xi}}{\partial \theta}(r, \theta)$$

$$= \frac{1}{r}\frac{\partial \xi}{\partial \theta}\left(\frac{a^2}{r}, \theta\right) = \frac{1}{r}\left(-\frac{a^2}{r}\right)\frac{\partial \eta}{\partial r}\left(\frac{a^2}{r}, \theta\right)$$

$$= -\frac{a^2}{r^2}\frac{\partial \eta}{\partial r}\left(\frac{a^2}{r}, \theta\right) = \frac{\partial \tilde{\eta}}{\partial r}(r, \theta).$$

Hence $-\tilde{\eta}$ is the harmonic conjugate of $\tilde{\xi}$. This means that if

$$\zeta(z) = \xi(r, \theta) + i\eta(r, \theta)$$

then

$$\zeta\left(\frac{a^2}{\bar{z}}\right) = \xi\left(\frac{a^2}{r}, \theta\right) + i\eta\left(\frac{a^2}{r}, \theta\right) = \tilde{\xi}(r, \theta) + i\tilde{\eta}(r, \theta)$$

is not a holomorphic function, since the Cauchy-Riemann conditions are violated and thus $d/d\,\zeta(a^2/\bar{z})$ does not exist. However

$$\overline{\zeta\left(\frac{a^2}{\bar{z}}\right)} = \tilde{\xi}(r, \theta) - i\tilde{\eta}(r, \theta)$$

is holomorphic. Since this transformation, which carries a holomorphic function $\zeta(z)$ into another holomorphic function $\overline{\zeta(a^2/\bar{z})}$ will be employed frequently in the sequel, we shall introduce the abbreviated notation

$$\hat{\zeta}(z) = \overline{\zeta\left(\frac{a^2}{\bar{z}}\right)}$$

for convenience. We note that the "$\hat{\ }$" or the "hat" transformation, which is an involution, is natural or canonical since it maps holomorphic (or analytical) functions from the interior domain Ω_i with $r<a$ (including the center O) to the exterior domain Ω_o with $r>a$ (including the point at infinity). In the place of the "hat" symbol, Milne-Thomson (1960) uses a "bar" symbol, which appears, however, to be somewhat confusing.

II Fundamental Relations of Plane Elastostatics

We consider an elastic body (homogeneous and isotropic) occupying an open region Ω of $\mathbf{R}^2$ with piecewise smooth boundary $\partial\Omega$ consisting of a finite number of contours $\Gamma_j, j=1, 2, \ldots, n$. A point on one of these contours shall be specified by prescribing the arc length s measured from a reference point on that contour.

Let $t_\alpha(s)\,(\alpha=1, 2)$ denote the components of traction at a point of the boundary with respect to a Cartesian system of coordinates Ox_1, x_2. If one defines (see Sokolnikoff, 1983)

$$f_1 + if_2 = i\int_0^s [t_1(\lambda) + it_2(\lambda)]d\lambda$$

where the sense of integration is always such that the material is on the left as λ increases, then the first boundary-value problem of plane elastostatics is reduced to the determination of the complex Kolosov-Muskhelishvili potentials $\phi(z), \psi(z)$. These are subjected to the boundary condition

$$\phi(z) + z\overline{\phi'(z)} + \overline{\psi(z)} = f_1 + if_2 + \text{constant} \quad \text{on } \partial\Omega$$

where the constants have different values on each of the contours forming the boundary $\partial\Omega$. The components of stress in polar coordinates are related to ϕ and ψ by

$$\sigma_{rr} + \sigma_{\theta\theta} = 2[\phi'(z) + \overline{\phi'(z)}] = 4\ \text{Re}\ [\phi'(z)] \qquad \text{(II-1}a\text{)}$$

$$\sigma_{\theta\theta} - \sigma_{rr} + 2i\sigma_{r\theta} = 2[\bar{z}\phi''(z) + \psi'(z)]e^{2i\theta} \qquad \text{(II-1}b\text{)}$$

where Re designates the real part of the argument.

The components of displacement u_α in Cartesian coordinates are given by

$$2\mu(u_1 + iu_2) = \kappa\phi(z) - z\phi'(z) - \overline{\psi(z)}$$

and in polar coordinates by

$$2\mu(u_r + iu_\theta) = e^{-i\theta}(\kappa\phi(z) - z\overline{\phi'(z)} - \overline{\psi(z)}) \qquad \text{(II-2)}$$

where μ is the shear modulus and

$$\kappa = 3 - 4\nu, \qquad \text{for plane strain,}$$

and

$$\kappa = \frac{(3-\nu)}{(1+\nu)} \qquad \text{for plane stress,}$$

ν being Poisson's ratio.

III Application of the Transformations in Elastostatics

In what follows, we shall be concerned with the interior Ω_i and the exterior (or outer) region Ω_o bounded by a circle. It is relevant to set down some consequences of analyticity of the potentials ϕ and ψ as applied to elastostatics.

In the interior region, ϕ_i and ψ_i may be expanded in a power series of z (no dependence on $\bar{z}$)

$$\phi_i(z) = \sum_{n=0}^{\infty} a_n z^n$$

$$\psi_i(z) = \sum_{n=0}^{\infty} b_n z^n$$

In the outer region, ϕ_o and ψ_o may be expanded into (see, Sokolnikoff, 1983)

$$\phi_0(z) = -\frac{F_1 + iF_2}{2\pi(\kappa+1)}\log(z) + (B + iC)z + \sum_{n=0}^{\infty}\frac{A_n}{z^n}$$

$$\psi_o(z) = \frac{\kappa(F_1 - iF_2)}{2\pi(1+\kappa)}\log(z) + (B' + iC')z + \sum_{n=0}^{\infty}\frac{B_n}{z^n}$$

where F_1 and F_2 are the resultants of the tractions t_1 and t_2, respectively, along the circle. These expansions presuppose single-valued displacements.

The last terms, respectively, are analytic including the point at infinity. It is well known that the real constants B, B' and C' are related to tractions at infinity. The constant C has no effect on the state of stress and is related to the rotation

$$\omega = \frac{1}{2}\left(\frac{\partial u_2}{\partial x_1} - \frac{\partial u_1}{\partial x_2}\right),$$

at infinity $\omega(\infty)$. We stipulate now that $\omega(\infty) = 0$ and furthermore that the stress field $\sigma_{ij} \to 0$ as $z \to \infty$. Thus $B = B' = C = C' = 0$. The first terms, respectively, are nonvanishing only if the tractions are not self-equilibrating on the circular boundary. This implies that a resultant force on the circular boundary will always be accompanied by a singularity of the complex potentials at infinity. For self-equilibrating loads on the circular boundary and the previous stipulation, the expansions for ϕ_o, ψ_o take the form

$$\phi_o = \sum_{n=0}^{\infty}\frac{A_n}{z^n}$$

$$\psi_o = \sum_{n=0}^{\infty}\frac{B_n}{z^n}$$

which is analytic in the whole outer region, including the point at infinity. It is now obvious, that, if a function $f(z)$ is

Downloaded 03 May 2010 to 171.66.16.21. Redistribution subject to ASME license or copyright; see http://www.asme.org/terms/Terms_Use.cfm

analytic in the interior, then $\hat{f}(z)(\equiv\overline{f(a^2/\bar{z})})$ will be analytic in the exterior, including the point at infinity, and vice versa; that is, if

$$f_i(z)=\sum_{n=0}^{\infty}a_n z^n$$

in the interior, then

$$\hat{f}_i(z)=\sum_{n=0}^{\infty}\bar{a}_n\frac{a^{2n}}{z^n}$$

is analytic in the exterior, including the point at infinity. Conversely, if

$$f_o(z)=\sum_{n=0}^{\infty}\frac{A_n}{z^n}$$

is analytic in the exterior, including the point at infinity, then

$$\hat{f}_o(z)=\sum_{n=0}^{\infty}\frac{\bar{A}_n}{a^{2n}}z^n$$

will be analytic in the interior.

IV Involution Correspondence Between Inner and Outer Regions

In this section, we shall establish the relations between the potentials for the inner and the outer regions for the case when the common boundary is subjected to the same set of self-equilbrating surface tractions (first boundary-value problem) or same displacements (second boundary-value problem). To this end, we suppose first that the solution for the inner region is specified in terms of ϕ_i, ψ_i. As pointed out in the previous section, ϕ_o, ψ_o can be set analytic in the outer region, including the point at infinity. Therefore, we set

$$\phi_0 = \hat{f}_i$$

$$\psi_o = \hat{h}_i$$

where f_i, h_i are both analytic *inside* the circle, *including the origin*, and are to be determined.

Since the inner and outer regions are subjected to the same set of surface tractions or displacements, the quantity $\alpha\phi(z)+z\overline{\phi'(z)}+\overline{\psi(z)}$ must be the same (up to an additive constant which is discarded) for both regions along the boundary $|z|=a$, or $z\bar{z}=r^2=a^2$, where $\alpha=1$ for the first boundary-value problem and $\alpha=-\kappa$ for the second. This means that along the boundary

$$\alpha\phi_i(z)+z\overline{\phi_i'(z)}+\overline{\psi_i(z)}=\alpha\phi_o(z)+z\overline{\phi_o'(z)}+\overline{\psi_o(z)}$$

$$=\alpha\hat{f}_i(z)+z\left[-\frac{a^2}{z^2}f_i'\left(\frac{a^2}{\bar{z}}\right)\right]+h_i\left(\frac{a^2}{\bar{z}}\right)$$

$$=\alpha\overline{f_i(z)}-\frac{z^3}{a^2}f_i'(z)+h_i(z)$$

In addition along the boundary $z\overline{\phi_i'(z)}=\overline{(a^2/z)\phi_i'(z)}$ and hence

$$\overline{\alpha\phi_i(z)+\frac{a^2}{z}\phi_i'(z)+\psi_i(z)}=-\frac{z^3}{a^2}f_i'(z)+h_i(z)+\alpha\overline{f_i(z)} \tag{IV-1}$$

One may be tempted to define the relations

$$f_i(z) = \frac{1}{\alpha}\left[\frac{a^2}{z}\phi_i'(z)+\psi_i(z)\right]$$

$$h_i(z) = \frac{z^3}{a^2}f_i'(z)+\alpha\phi_i(z)$$

but $(a^2/z)\phi_i'(z)$ is not analytic at the center of the circle. This singularity, however, can be removed by subtracting and adding the term

$$\overline{\frac{a^2}{z}\phi_i'(0)}=\frac{a^2}{\bar{z}}\overline{\phi_i'(0)},$$

to the left-hand side of (IV-1).

The boundary condition now reads

$$\overline{\alpha\phi_i(z)+\frac{a^2}{z}[\phi_i'(z)-\phi_i'(0)]+\psi_i(z)}$$

$$+z\overline{\phi_i'(0)}=-\frac{z^3}{a^2}f_i'(z)+h_i(z)+\alpha\overline{f_i(z)}$$

Thus the sought functions $f_i(z)$, $h_i(z)$ are now obtained as

$$f_i(z) = \frac{1}{\alpha}\left[\frac{a^2}{z}[\phi_i'(z)-\phi_i'(0)]+\psi_i(z)\right]$$

$$h_i(z) = \frac{z^3}{a^2}f_i'(z)+\alpha\phi_i(z)+z\overline{\phi_i'(0)} \tag{IV-2}$$

in terms of the given inner potentials.

Finally, the solution for the outside region is given by

$$\phi_o(z) = \hat{f}_i(z) \tag{IV-3a}$$

$$\psi_o(z) = \alpha\hat{\phi}_i(z)+\frac{a^2}{z}\phi_i'(0)+\frac{a^4}{z^3}\hat{f}_i'(z) \tag{IV-3b}$$

in terms of $\phi_i(z)$, $\psi_i(z)$ for the inner region.

Conversely, suppose that the solution for the outer region is given by ϕ_o, ψ_o which are assumed to be analytic outside the circle including the point at infinity. This time we set

$$\phi_i = \hat{f}_o$$

$$\psi_i = \hat{h}_o$$

where f_o, h_o are both analytic *outside* the circle, *including the point at infinity*, and are to be found.

An argument similar to that mentioned previously, leads to

$$\alpha\phi_o(z)+z\overline{\phi_o'(z)}+\overline{\psi_o(z)}=\alpha\phi_i(z)+z\overline{\phi_i'(z)}+\overline{\psi_i(z)}$$

$$=\alpha\hat{f}_o(z)+z\left[-\frac{a^2}{\bar{z}^2}f_o'\left(\frac{a^2}{\bar{z}}\right)\right]+h_o\left(\frac{a^2}{\bar{z}}\right)$$

$$=\alpha\overline{f_o(z)}-\frac{z^3}{a^2}f_o'(z)+h_o(z)$$

Again, one is tempted to define

$$f_o(z) = \frac{1}{\alpha}\left[\frac{a^2}{z}\phi_o'(z)+\psi_o(z)\right]$$

$$h_o(z) = \frac{z^3}{a^2}f_o'(z)+\alpha\phi_o(z)$$

but $(z^3/a^2)f_o'(z)$ is not analytic at the point at infinity. This singularity, however, can be removed this time by subtracting and adding the term

$$\overline{\frac{a^2}{z}\left(\frac{(\hat{\psi}_o)'(0)-\alpha(\hat{\psi}_o)'(0)}{1-\alpha^2}\right)}=\frac{a^2}{\bar{z}}\left(\frac{(\hat{\psi}_o)'(0)-\alpha\overline{(\hat{\psi}_o)'(0)}}{1-\alpha^2}\right).$$

It will be shown later that the term

$$\frac{\overline{(\hat{\psi}_o)'(0)}-\alpha(\hat{\psi}_o)'(0)}{1-\alpha^2}$$

reduces to $(\hat{\psi}_o)'(0)/2$ for the first boundary-value problem ($\alpha=1$) and thus is well defined.

Downloaded 03 May 2010 to 171.66.16.21. Redistribution subject to ASME license or copyright; see http://www.asme.org/terms/Terms_Use.cfm

The boundary condition becomes

$$\alpha\phi_o(z)+z\frac{(\hat{\psi}_o)'(0)-\alpha\overline{(\hat{\psi}_o)'(0)}}{1-\alpha^2}$$

$$+\overline{\frac{a^2}{z}\left(\phi_o'(z)-\frac{\overline{(\hat{\psi}_o)'(0)}-\alpha(\hat{\psi}_o)'(0)}{1-\alpha^2}\right)+\psi_o(z)}$$

$$=-\frac{z^3}{a^2}f_o'(z)+h_o(z)+\alpha\overline{f_o(z)}$$

Thus the sought functions $f_o(z)$, $h_o(z)$ are now obtained as

$$f_o(z) = \frac{1}{\alpha}\left[\frac{a^2}{z}\left(\phi_o'(z)-\frac{\overline{(\hat{\psi}_o)'(0)}-\alpha(\hat{\psi}_o)'(0)}{1-\alpha^2}\right)+\psi_o(z)\right]$$

$$h_o(z) = \frac{z^3}{a^2}f_o'(z)+\alpha\phi_o(z)+z\frac{(\hat{\psi}_o)'(0)-\alpha\overline{(\hat{\psi}_o)'(0)}}{1-\alpha^2}$$

Then the solution for the inner region is given by

$$\phi_i(z) = \hat{f}_o(z)$$

$$\psi_i(z) = \alpha\hat{\phi}_o(z)+\frac{a^2}{z}\frac{\overline{(\hat{\psi}_o)'(0)}-\alpha(\hat{\psi}_o)'(0)}{1-\alpha^2}+\frac{a^4}{z^3}\hat{f}_o'(z)$$

in terms of $\phi_o(z)$, $\psi_o(z)$ for the outer region.

It may appear that the transformation, giving the solution for the outer problem in terms of that of the inner, and its inverse are different in form. However, we presently show that they are, in fact, identical, i.e., the transformation is an involution. In the process, useful expressions relating the averaged stresses and displacements along arbitrary circles are obtained. They are applicable to the situation where the singularities are contained completely either in the interior or in the exterior.

Consider the inner region first and recall that

$$\phi_i'(z)=\frac{1}{4}(\sigma^i_{rr}+\sigma^i_{\theta\theta})+\frac{2\mu}{1+\kappa}i\omega^i,$$

This shows that $(\sigma^i_{rr}+\sigma^i_{\theta\theta})$ and ω^i are harmonic conjugates. An application of the mean-value theorem for harmonic functions yields

$$\phi_i'(0) = \frac{1}{4}(\sigma^i_{rr}+\sigma^i_{\theta\theta})(0)+\frac{2\mu}{1+\kappa}i\omega^i(0)$$

$$= \frac{1}{4}\langle\sigma^i_{rr}+\sigma^i_{\theta\theta}\rangle+\frac{2\mu}{1+\kappa}i\langle\omega^i\rangle \qquad \text{(IV-4)}$$

where $\langle g\rangle$ designates the mean value of g along the circle, i.e.,

$$\langle g\rangle\equiv\frac{1}{2\pi}\int_0^{2\pi}g\,d\theta$$

An integration of the stress equation (II-1*b*)

$$\sigma^i_{\theta\theta}-\sigma^i_{rr}+2i\sigma^i_{r\theta}=2[\bar{z}\phi_i''(z)+\psi_i'(z)]e^{2i\theta},$$

along the circle and an application of the residue theorem lead to

$$\langle\sigma^i_{\theta\theta}-\sigma^i_{rr}\rangle+2i\langle\sigma^i_{r\theta}\rangle=0,$$

proving that

$$\langle\sigma^i_{\theta\theta}\rangle=\langle\sigma^i_{rr}\rangle, \qquad \text{(IV-5)}$$

and

$$\langle\sigma^i_{r\theta}\rangle=0.$$

Note that the last equation is simply a consequence of moment equilibrium.

A similar consideration applied to the displacement equation (II-2)

$$2\mu(u^i_r-iu^i_\theta)=e^{i\theta}[\kappa\overline{\phi_i(z)}-\bar{z}\phi_i'(z)-\psi_i(z)],$$

gives

$$2\mu(\langle u^i_r\rangle-i\langle u^i_\theta\rangle)=a[\kappa\overline{\phi_i'(0)}-\phi_i'(0)] \qquad \text{(IV-6)}$$

Equations (IV-4)–(IV-6) can be combined to obtain relations between averaged stresses and displacements

$$\langle u^i_r\rangle=\frac{a(\kappa-1)}{8\mu}\langle\sigma^i_{rr}+\sigma^i_{\theta\theta}\rangle=\frac{a(\kappa-1)}{4\mu}\langle\sigma^i_{rr}\rangle=\frac{a(\kappa-1)}{4\mu}\langle\sigma^i_{\theta\theta}\rangle$$

$$\langle u^i_\theta\rangle=a\langle\omega^i\rangle=a\omega^i(0)$$

We note that these are valid for arbitrary circles in a two-dimensional homogeneous and isotropic elastic medium in static equilibrium provided no singularities lie inside the circles.

In an analogous fashion, but now considering quantities on the circle pertaining to the outer region, we obtain

$$\langle\sigma^o_{\theta\theta}+\sigma^o_{rr}\rangle = 0 \qquad \text{(IV-7)}$$

$$\langle\omega^o\rangle = 0 \qquad \text{(IV-8)}$$

$$\langle\sigma^o_{\theta\theta}-\sigma^o_{rr}\rangle+2i\langle\sigma^o_{r\theta}\rangle = -2\overline{(\hat{\psi}_o)'(0)} \qquad \text{(IV-9)}$$

$$2\mu(\langle u^o_r\rangle-i\langle u^o_\theta\rangle) = -a\overline{(\hat{\psi}_o)'(0)} \qquad \text{(IV-10)}$$

Again, combining the last two equations, the following relations hold provided the exterior is free of singularities:

$$\langle u^o_r\rangle = \frac{a}{4\mu}\langle\sigma^o_{\theta\theta}-\sigma^o_{rr}\rangle=\frac{a}{2\mu}\langle\sigma^o_{\theta\theta}\rangle=-\frac{a}{2\mu}\langle\sigma^o_{rr}\rangle$$

$$\langle u^o_\theta\rangle = -\frac{a}{2\mu}\langle\sigma^o_{r\theta}\rangle$$

Note that equation (IV-8) is simply a consequence of our assumption that the rotation at infinity is zero.

We are now in a position to apply these results to establish that the correspondence between the inner and outer regions is an involution.

To begin with consider the first boundary-value problem. It is necessary in what follows to remove the indeterminacy in the complex potentials (ϕ_i, ψ_i) by setting

$$\langle\omega^i\rangle=\omega^i(0)=0.$$

With this choice and noting that $\langle\sigma^o_{r\theta}\rangle=0$, equations (IV-4), (IV-5), (IV-7), and (IV-9) give

$$\phi_i'(0) = \frac{1}{2}\langle\sigma^i_{rr}\rangle$$

$$\langle\sigma^o_{rr}\rangle = \overline{(\hat{\psi}_o)'(0)}.$$

This shows that $(\hat{\psi}_o)'(0)$ is real in this case and that

$$\frac{\overline{(\hat{\psi}_o)'(0)}-\alpha(\hat{\psi}_o)'(0)}{1-\alpha^2}$$

reduces to $(\hat{\psi}_o)'(0)/2$ as claimed earlier.

Now, if one defines

$$K_I=\frac{1}{4\pi}\int_0^{2\pi}(\mathbf{t}\cdot\mathbf{n})d\theta=\frac{1}{2}\langle\sigma^i_{rr}\rangle=\frac{1}{2}\langle\sigma^o_{rr}\rangle,$$

where $\mathbf{t}$ is the traction and $\mathbf{n}$ is the outward unit normal of the region under consideration, then the correspondence between the inner and outer region takes the form

$$\phi_o(z) = \hat{f}_i(z)$$

Downloaded 03 May 2010 to 171.66.16.21. Redistribution subject to ASME license or copyright; see http://www.asme.org/terms/Terms_Use.cfm

$$\psi_o(z) = \hat{\phi}_i(z) + \frac{a^2}{z}K_{\mathrm{I}} + \frac{a^4}{z^3}\hat{f}_i'(z)$$

where

$$f_i(z) = \psi_i(z) + \frac{a^2}{z}(\phi_i'(z) - K_{\mathrm{I}}).$$

For the correspondence between the outer and inner region the modifiers i and o need merely be interchanged reflecting the fact that the correspondence is an involution.

We emphasize that K_{I} has been defined in such a manner as to relate the correspondence to values prescribed on the common boundary but no explicit integration need to be performed in any practical calculations, since $K_{\mathrm{I}} = \phi_i'(0) = \frac{1}{4}(\sigma_{rr}^i + \sigma_{\theta\theta}^i)(0) = (\hat{\psi}_o)'(0)/2$.

Next, consider the second boundary-value problem. In this case, we define

$$K_{\mathrm{II}} = \frac{L - \alpha\bar{L}}{1-\alpha^2} \qquad (\alpha = -\kappa)$$

where

$$L = -\frac{2\mu}{a}(\langle u_r^i\rangle - i\langle u_\theta^i\rangle) = -\frac{2\mu}{a}(\langle u_r^o\rangle - i\langle u_\theta^o\rangle),$$

then equations (IV-6) and (IV-10) give

$$K_{\mathrm{II}} = \phi_i'(0) = \frac{\overline{(\hat{\psi}_o)'(0)} - \alpha(\hat{\psi}_o)'(0)}{1-\alpha^2},$$

so that the correspondence between the inner and outer region takes the form

$$\phi_o(z) = \hat{f}_i(z)$$

$$\psi_o(z) = \alpha\hat{\phi}_i(z) + \frac{a^2}{z}K_{\mathrm{II}} + \frac{a^4}{z^3}\hat{f}_i'(z)$$

where

$$f_i(z) = \frac{1}{\alpha}\left[\psi_i(z) + \frac{a^2}{z}(\phi_i'(z) - K_{\mathrm{II}})\right].$$

To invert the foregoing relation, one needs merely to interchange i and o showing again that the correspondence is an involution.

We note that K_{I} is the real part of K_{II}. Therefore K_{I} may be replaced by K_{II} in the foregoing expressions without affecting the state of stress. In the sequel, the symbol K will replace K_{II}, thus allowing for unified expressions for both boundary-value problems. Conversely K can be substituted for K_{I} if one is interested only in the state of stress.

We record here the relations between interfacial stresses of the inner and outer region for both boundary-value problems.

$$\sigma_{rr}^i = \frac{1}{\alpha}\sigma_{rr}^o + \frac{\alpha^2-1}{4\alpha}I^o + \left(\frac{\alpha-1}{\alpha}\right)\mathrm{Re}\ (K),$$

$$\sigma_{\theta\theta}^i = -\frac{3}{\alpha}\sigma_{\theta\theta}^o + \left(\frac{9-\alpha^2}{4\alpha}\right)I^o - \left(\frac{3+\alpha}{\alpha}\right)\mathrm{Re}\ (K),$$

$$\sigma_{r\theta}^i = \frac{1}{\alpha}\sigma_{r\theta}^o + \frac{\alpha-1}{\alpha}\left[(1+\alpha)\left(\frac{2\mu}{1+\kappa}\right)\omega^o - \mathrm{Im}\ (K)\right]$$

where I is the first stress invariant, i.e., $I = (\sigma_{rr} + \sigma_{\theta\theta})$, and Im designates the imaginary part of the argument. The inversion of the aforementioned equations amounts to merely interchanging i and o.

The relations between the two elastic fields throughout in terms of stresses and displacements are given in the Appendix.

V Correspondence Between Inner, Outer Regions and the Entire Plane

Having established complete correspondence between the potentials ϕ_o, ψ_o for the outer region and the potentials for the inner region ϕ_i, ψ_i, we are ready to consider the potentials ϕ_o^*, ψ_o^*, and ϕ_i^*, ψ_i^* for the outer and inner regions, respectively, each in terms of the potentials ϕ, ψ for the entire plane.

Thus we begin by assumming that $\phi(z)$, $\psi(z)$ have been determined for the entire plane acted upon by some singularities and we wish to determine in the first problem the potentials for the outer region bounded by a circle C of radius a subjected either to zero tractions or zero displacements, under the assumption that the inner region is free of singularities. To obtain the modified potentials, we merely have to add to $\phi(z)$, $\psi(z)$ the field produced by the opposite tractions or displacements applied along C. Thus we readily obtain

$$\phi_o^*(z) = \phi(z) - \hat{f}(z)$$

$$\psi_o^*(z) = \psi(z) - \alpha\hat{\phi}(z) - \frac{a^2}{z}K - \frac{a^4}{z^3}f'(z),$$

where

$$f(z) = \frac{1}{\alpha}\left[\psi(z) + \frac{a^2}{z}(\phi'(z) - K)\right].$$

Similarily, if we wish to determine in a second problem the modified potentials $\phi_i^*(z)$, $\psi_i^*(z)$ for the inner regions bounded by a traction- or displacement-free circle C, then we have to apply an analogous reasoning to obtain the identical expression

$$\phi_i^*(z) = \phi(z) - \hat{f}(z)$$

$$\psi_i^*(z) = \psi(z) - \alpha\hat{\phi}(z) - \frac{a^2}{z}K - \frac{a^4}{z^3}\hat{f}'(z)$$

except that in this case no singularities are allowed to be applied in the outer region and the singularities in the inner region are self-equilibrating.[1]

Thus complete duality for the two problems is achieved.

To obtain the elastic field for the modified problem one need simply subtract the elastic field given in the Appendix from that of the entire plane.

Let us note that the case of a half-plane can be obtained either by considering an appropriate limiting procedure of the foregoing transformations or developing an argument along similar lines. The transformations, that lead from a whole plane solution (ϕ, ψ) to a half-plane solution (ϕ^*, ψ^*) where the boundary assumed to be along, say, the x-axis is traction or displacement-free, are

$$\phi^*(z) = \phi(z) - \overline{f(\bar{z})}$$

$$\psi^*(z) = \psi(z) - \alpha\overline{\phi(\bar{z})} + z\overline{f'(\bar{z})}$$

where

$$f(z) = \frac{1}{\alpha}[\psi(z) + z\phi'(z)],$$

provided the singularities produce a decaying elastic field at infinity.

It is worth mentioning here that our approach, based on the correspondence between inner and outer regions, is different from that presented by, e.g., Green and Zerna (1968) or England (1971) for the outer region and for the half-plane. These authors, using analytic continuation, established relations between the outer region and the entire plane, without recognizing any correspondence between the inner and outer region.

[1] It is to be noted that some self-equilibrating singularities in the inner region are necessarily accompanied by singularities located at the point at infinity, such as dislocations. These cases have to be treated separately.

Downloaded 03 May 2010 to 171.66.16.21. Redistribution subject to ASME license or copyright; see http://www.asme.org/terms/Terms_Use.cfm

VI Examples

Example (*a*). As a first simple example, we consider the problem of a circular disk subjected to uniform pressure p along its boundary. The (trivial) solution to this problem is given by the potentials

$$\phi_i(z) = -pz/2;\ \psi_i(z) = 0,$$

and corresponds to the homogeneous stress field

$$\sigma_{\theta\theta} = \sigma_{rr} = -p$$

We immediately can obtain the solution of the corresponding problem for the outer region. We apply the general formulas of Section IV, noting that $f(z) = 0$ in this case and obtain

$$\phi_o(z) = 0;\ \psi_o = -pa^2/z$$

which corresponds to the nonhomogeneous stress field

$$\sigma_{\theta\theta} = -\sigma_{rr} = pa^2/r^2$$

It is to be noted that in the literature the foregoing two problems have been treated as being completely separate and independent from each other; see Sokolnikoff (1983).

Example (*b*). To illustrate the general expression of Section V, we consider an infinite plane subjected to uniform remote traction T along, say, the x-axis. This state of stress corresponds to potentials

$$\phi(z) = Tz/4;\quad \psi(z) = -Tz/2$$

The solution for the problem for the outer region, i.e., infinite plane bounded by a circular traction-free cavity of radius a or a rigid inclusion, is obtained immediately after putting $f(z) = -Tz/2$, as

$$\phi^*(z) = \frac{T}{2}\left(\frac{z}{2} + \frac{a^2}{\alpha z}\right);$$

$$\psi^*(z) = -\frac{T}{2}\left(z + \frac{1+\alpha}{2}\frac{a^2}{z} - \frac{1}{\alpha}\frac{a^4}{z^3}\right),$$

leading to well-known stress fields recorded, e.g., in Sokolnikoff (1983), England (1971), and Muskhelishvili (1953b).

Example (*c*). As a third example, we consider a point force of magnitude F enclosing an angle γ with the x-axis and acting at a point z_0 of the complex plane with $|z_0| > a$, where a is the radius of a prospective circular hole or rigid inclusion centered at the origin.

The solution with the traction-free hole or rigid inclusion actually present can be obtained as follows:

If the force acted at the origin, then the solution is terms of complex potentials would be (for the complete plane, see (England, 1971)

$$\phi_1(z) = -\frac{1}{2\pi(1+\kappa)} Fe^{i\gamma} \log(z)$$

$$\psi_1(z) = \frac{\kappa}{2\pi(1+\kappa)} Fe^{-i\gamma} \log(z)$$

However, since the force acts at z_0, the solution is given by

$$\phi(z) = \phi_1(z - z_0)$$

$$\psi(z) = \psi_1(z - z_0) - \bar{z}_0 \phi_1'(z - z_0)$$

leading to

$$\phi(z) = -\frac{Fe^{i\gamma}}{2\pi(1+\kappa)} \log(z - z_0)$$

$$\psi(z) = \frac{\kappa F e^{-i\gamma}}{2\pi(1+\kappa)} \log(z - z_0) + \bar{z}_0 \frac{Fe^{i\gamma}}{2\pi(1+\kappa)} \frac{1}{z - z_0}$$

A direct substitution into the formulas of Section V leads to the solution of a point force acting in an infinite plane with a circular hole ($\alpha = 1$) or rigid inclusion ($\alpha = -\kappa$)

$$\phi_o^*(z) = \frac{-F}{2\pi(1+\kappa)}\left[e^{i\gamma} \log(z - z_0) + \frac{\kappa e^{i\gamma}}{\alpha} \log\left(\frac{a^2}{z} - \bar{z}_0\right) - \frac{(z - z_0)e^{-i\gamma}}{\alpha(a^2/z - \bar{z}_0)} - \frac{ze^{i\gamma}}{\alpha \bar{z}_0}\right]$$

$$\psi_o^*(z) = \frac{F}{2\pi(1+\kappa)}\left\{\kappa e^{-i\gamma} \log(z - z_0) + \frac{\bar{z}_0 e^{i\gamma}}{z - z_0} + \alpha e^{-i\gamma} \log\left(\frac{a^2}{z} - \bar{z}_0\right) - \frac{a^4}{\alpha z^3}\left[\frac{\kappa e^{i\gamma}}{a^2/z - \bar{z}_0} + \frac{(z - z_0)e^{-i\gamma}}{(a^2/z - \bar{z}_0)^2} + \frac{z^2 e^{-i\gamma}}{a^2}\left(\frac{1}{a^2/z - \bar{z}_0} + \frac{1}{\bar{z}_0}\right)\right] - \frac{a^2 e^{i\gamma}}{z z_0}\right\}$$

VII Conclusions

In this paper, a correspondence was established between the inner and outer regions bounded by a circle for the first and second boundary-value problems. This correspondence was shown to be an involution. Furthermore, the elastic fields of the inner, the outer region and the half-plane, respectively, as generated by singularities within these regions, were related to the corresponding problems for the entire plane. These relations are simple, algebraic and universal, in the sense of being independent of any particular loading.

In the course of these developments, a number of seemingly novel expressions of plane, isotropic elastostatics have been revealed as a by-product. They involve relations between quantities, such as components of stress and displacement, averaged over a circle and may be referred to as mean-value theorems. It seems that a detailed discussion of these new theorems and their implications deserves special consideration, which will be the subject of a separate paper.

Numerous extensions of the proposed methodology are possible. Currently, the authors are completing a study of the analogous problems for plane elastic inclusions and for the case of antiplane strain. Other ramifications, which are under study, include those to three-dimensional problems, anisotropic bodies, elliptic cavities, plate theories, Cosserat continua, elastic fields coupled to electric and magnetic fields, viscoelastic bodies, as well as applications to crack mechanics. Further it is contemplated to treat several circular or straight boundaries (i.e., more than one), and thus arrive at efficient universal procedures for finite bodies, based, for example, on the Schwarz alternating method; see (Sokolnikoff, 1983).

Acknowledgment

This work was performed under the auspices of the U.S. Department of Energy through a contract with Stanford University. This support is gratefully acknowledged.

References

England, A. H., 1971, *Complex Variable Methods in Elasticity*, Wiley-Interscience, London.

Filon, L. N. G., 1903, "On the approximate solution of the bending of a beam of rectangular cross-section," *Phil. Transactions* (*A*), Vol. 201, pp. 63–155.

Honein, T., and Herrmann, G., 1987, "The Two-Dimensional Problem of Thermoelasticity for an Infinite Region Bounded by a Circular Cavity," *Thermomechanical Couplings in Solids*, H. D. Bui and Q. S. Nguyen, eds., Elsevier Science Publishers B. V. (North-Holland).

Jackson, J. D., 1975, *Classical Electrodynamics*, John Wiley, New York.

Kellogg, O. D., 1953, *Foundations of Potential Theory*, Dover Publications, New York.

Kienzler, R., and Zhuping, D., 1987, "On the Distribution of Hoop Stresses

Downloaded 03 May 2010 to 171.66.16.21. Redistribution subject to ASME license or copyright; see http://www.asme.org/terms/Terms_Use.cfm

Around Circular Holes in Elastic Sheets," ASME JOURNAL OF APPLIED MECHANICS, Vol. 54, pp. 110–114.

Maxwell, J. C., 1954, *A Treatise on Electricity & Magnetism*, Vol. 1, Dover Publications, New York.

Milne-Thomson, L. M., 1960, *Theoretical Hydrodynamics*, Macmillan, London.

Milne-Thomson, L. M., 1968, *Plane Elastic Systems*, Springer-Verlag.

Muskhelishvili, N. I., 1953a, *Singular Integral Equations*, Noordhoff, Groningen-Holland.

Muskhelishvili, N. I., 1953b, *Some Basic Problems of the Mathematical Theory of Elasticity*, Noordhoff, Groningen-Holland.

Sokolnikoff, I. S., 1983, *Mathematical Theory of Elasticity*, Krieger Publishing Company, Florida.

APPENDIX

Having the correspondence between the inner and outer region in terms of complex potentials, one is able to obtain the relations between the elastic fields of the two regions. In the derivation of the following equations, use has been made of the equations of Sections II and III. An important role has been played by the inversion and Kelvin's transformation.

Using the notations of the previous sections, we have for the two boundary-value problems

$$\sigma^o_{rr} = \left(1-\frac{a^2}{2r^2}\right)\left(\frac{a^2}{\alpha r^2}\right)(\widetilde{\sigma^i_{rr}}-\widetilde{\sigma^i_{\theta\theta}}) + \frac{1}{4\alpha}\left(1-\frac{a^2}{r^2}\right)\left(r-\frac{a^2}{r}\right)\frac{\partial \tilde{I}^i}{\partial r} + \frac{1}{2\alpha}\left(1-\frac{1-\alpha^2}{2}\frac{a^2}{r^2}\right)\tilde{I}^i + \frac{1}{\alpha}\left(-2+(1+\alpha)\frac{a^2}{r^2}\right)\mathrm{Re}\,(K) - \frac{1}{\alpha r^2}\left(r-\frac{a^2}{r}\right)\left(\frac{a^2}{r}\frac{\partial \widetilde{\sigma^i_{r\theta}}}{\partial\theta}-\frac{1}{4}\left(r-\frac{a^2}{r}\right)\frac{\partial^2 \tilde{I}^i}{\partial\theta^2}\right)$$

$$\sigma^o_{\theta\theta} = \left(1+\frac{a^2}{2r^2}\right)\left(\frac{a^2}{\alpha r^2}\right)\left(\widetilde{\sigma^i_{rr}}-\widetilde{\sigma^i_{\theta\theta}}\right) + \frac{1}{4\alpha}\left(3+\frac{a^2}{r^2}\right)\left(r-\frac{a^2}{r}\right)\frac{\partial \tilde{I}^i}{\partial r} + \frac{1}{2\alpha}\left(1+\frac{1-\alpha^2}{2}\frac{a^2}{r^2}\right)\tilde{I}^i - \frac{1}{\alpha}\left(2+(1+\alpha)\frac{a^2}{r^2}\right)\mathrm{Re}\,(K) + \frac{1}{\alpha r^2}\left(r-\frac{a^2}{r}\right)\left(\frac{a^2}{r}\frac{\partial \widetilde{\sigma^i_{r\theta}}}{\partial\theta}-\frac{1}{4}\left(r-\frac{a^2}{r}\right)\frac{\partial^2 \tilde{I}^i}{\partial\theta^2}\right)$$

$$\sigma^o_{r\theta} = \frac{a^4}{\alpha r^4}\widetilde{\sigma^i_{r\theta}} + \frac{1}{4\alpha r}\left(r-\frac{a^2}{r}\right)\left[-\left(1+\frac{a^2}{r^2}\right)\frac{\partial \tilde{I}^i}{\partial\theta} + \frac{2a^2}{r^2}\left(\frac{\partial \widetilde{\sigma^i_{\theta\theta}}}{\partial\theta}-\frac{\partial \widetilde{\sigma^i_{rr}}}{\partial\theta}\right)-\left(r-\frac{a^2}{r}\right)\frac{\partial^2 \tilde{I}^i}{\partial r\partial\theta}\right], + \frac{a^2}{r^2}\frac{(\alpha-1)}{\alpha}\left[(\alpha+1)\frac{2\mu}{1+\kappa}\omega^i-\mathrm{Im}\,(K)\right]$$

and, for the second boundary-value problem

$$u^o_r = \widetilde{u^i_r}-\frac{1}{2\mu\kappa}\left(r-\frac{a^2}{r}\right)\left\{\frac{a^2}{2r^2}(\widetilde{\sigma^i_{\theta\theta}}-\widetilde{\sigma^i_{rr}})-\frac{1}{4}\left(r-\frac{a^2}{r}\right)\frac{\partial \tilde{I}^i}{\partial r} + (\kappa-1)\left(\frac{\tilde{I}^i}{4}-\mathrm{Re}\,(K)\right)\right\}$$

$$u^o_\theta = \widetilde{u^i_\theta}+\frac{1}{2\mu\kappa}\left(r-\frac{a^2}{r}\right)\left\{-\frac{a^2}{r^2}\widetilde{\sigma^i_{r\theta}}+\frac{1}{4r}\left(r-\frac{a^2}{r}\right)\frac{\partial \tilde{I}^i}{\partial\theta} + (1+\kappa)\left[\frac{2\mu}{1+\kappa}\widetilde{\omega^i}-\mathrm{Im}\,(K)\right]\right\}$$

The inversion of these relations amounts to merely interchanging i and o.

Downloaded 03 May 2010 to 171.66.16.21. Redistribution subject to ASME license or copyright; see http://www.asme.org/terms/Terms_Use.cfm

Debondings at a Semielliptic Rigid Inclusion on the Rim of a Half Plane

N. Hasebe

S. Tsutsui

T. Nakamura

Department of Civil Engineering,
Nagoya Institute of Technology,
Gokisocho, Showaku,
Nagoya, 466, Japan

An elastic half plane with a semielliptic rigid inclusion is analyzed as a mixed boundary value problem with a clamped edge. A rational mapping function of a sum of fractional expressions and the complex stress functions are used for the analysis. The debondings emanated from both ends of the semielliptic inclusion under uniform tension is examined and singular values of the stress at the debonded tips are obtained. By using these values, it is examined for some elliptical shapes how the debonding propagates. The stress values at the base of the semielliptic inclusion are also examined. Even if the loading is uniform compression, the debonding may occur at the base.

Introduction

The plane elastic analyses of a half plane with a notch of various shapes have been carried out by many researchers. Even with respect to semicircular and semielliptic notches, the studies were reported by Maunsell (1936), Ishibashi (1940), Weinel (1941), Ling (1948, 1978), Higuchi and Suzuki (1949), Mitchell (1965), Hasebe (1972), Bowie and Freese (1978), and Nishitani (1978). However, only a few (e.g., Hasebe and Takeuchi, 1985) are reported for the problem of a half plane with a rigid inclusion of notch shape on the rim as far as we know. In this paper, a half plane with a semielliptic rigid inclusion is analyzed as a mixed boundary value problem. A complex variable method is used for the analysis. A rigid inclusion is an extreme state where Young's modulus is infinite. On the contrary, a notch is another extreme state where Young's modulus is zero. Thus, general states for an elastic inclusion must exist between these two extreme states. Therefore, the study of a rigid inclusion is important. The analysis of the inclusion problem is necessary as a model of various materials; metals, composite materials, concrete, etc. When the inclusion is considered as an elliptic rigid column or beam, the elastic plane is a model of a floor or wall in buildings. The debondings emanated from both ends of the semielliptic inclusion under uniform tension are analyzed and the singular values of the stress at the debonded tips are obtained. The stress values at the base of the semielliptic inclusion are also examined.

Mapping and Stress Function

A conformal mapping function which maps a physical region in the z-plane into a unit circle in the ζ-plane is given as follows (Hasebe, 1972), (see Fig. 1):

$$z = -ia\frac{(1+\zeta^2)^{1/2}}{1-\zeta} - ib\frac{1+\zeta}{1-\zeta} \tag{1}$$

If $a=0$, the region is a half plane and if $b=0$, it is a half plane with an edge crack. A rational mapping function is formulated from equation (1) as follows:

$$z = \frac{E_0}{1-\zeta} + \sum_{k=1}^{24}\frac{E_k}{\zeta_k-\zeta} + E_{-1} \equiv \omega(\zeta) \tag{2}$$

where E_0, E_k, E_{-1}, and ζ_k are constants. The formulation of equation (2) was described in references (Hasebe, 1979, 1980, 1972). The complex variable method using the regular complex stress functions, $\varphi(\zeta)$ and $\psi(\zeta)$, in the unit circle are used for the analysis (Muskhelishvili, 1963). The general solutions of $\varphi(\zeta)$ and $\psi(\zeta)$ were obtained for arbitrary boundary condition (Hasebe, 1979). However, if a part of traction free exists on the boundary, then $\varphi(\zeta)$ and $\psi(\zeta)$ can be obtained from the following procedure. The procedure is the same as that of the mixed boundary value problem for the thin plate bending (Hasebe, 1984). The function $\psi(\zeta)$ is obtained by the principle of analytic continuation from the boundary condition of the traction free as follows (Muskhelishvili, 1963):

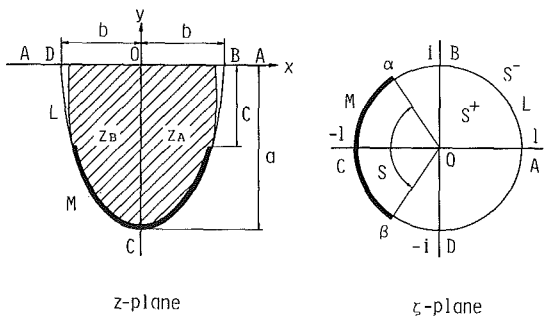


Fig. 1 Physical plane and the unit circle

Contributed by the Applied Mechanics Division for publication in the JOURNAL OF APPLIED MECHANICS.

Discussion on this paper should be addressed to the Editorial Department, ASME, United Engineering Center, 345 East 47th Street, New York, NY 10017, and will be accepted until two months after final publication of the paper itself in the JOURNAL OF APPLIED MECHANICS. Manuscript received by ASME Applied Mechanics Division, August 25, 1987; final revision, December 11, 1987.

Copyright © 1988 by ASME
Downloaded 03 May 2010 to 171.66.16.21. Redistribution subject to ASME license or copyright; see http://www.asme.org/terms/Terms_Use.cfm

$$\psi(\zeta) = -\overline{\varphi(1/\zeta)} - \frac{\overline{\omega(1/\zeta)}}{\omega'(\zeta)}\varphi'(\zeta) \tag{3}$$

The bar indicates a complex conjugate term and the prime does the differentiation with respect to its argument. The boundaries for the external force and the displacement are denoted by L and M, respectively. In this paper, L is $\overset{\frown}{z_B DAB z_A}$ and M is $\overset{\frown}{z_A C z_B}$ in Fig. 1. Then by using equation (3), the boundary condition on L is

$$\varphi(\sigma) + \frac{\omega(\sigma)}{\overline{\omega'(\sigma)}}\overline{\varphi'(\sigma)} + \overline{\psi(\sigma)} = \varphi^+(\sigma) - \varphi^-(\sigma)$$

$$= i\int [P_x(s) + iP_y(s)]ds \tag{4}$$

in which $P_x(s)$ and $P_y(s)$ are external forces in the x- and y-directions, respectively. The shoulder sign + and − denote the regions inside and outside the unit circle, respectively (see Fig. 1). The integral of s denotes that along the boundary. σ denotes ζ on the unit circle.

The boundary condition on M is

$$\kappa\varphi(\sigma) - \frac{\omega(\sigma)}{\overline{\omega'(\sigma)}}\overline{\varphi'(\sigma)} - \overline{\psi(\sigma)} = \kappa\varphi^+(\sigma) + \varphi^-(\sigma)$$

$$= 2G(u+iv) \tag{5}$$

in which u and v are components of the displacement in the x- and y-directions, respectively; G is the shear modulus; and κ is $3-4\nu$ for the plane strain, $(3-\nu)/(1+\nu)$ for the generalized plane stress; and ν is the Poisson ratio. It is thus sufficient to solve a Rieman-Hilbert problem which satisfies equations (4) and (5). Its solution can be obtained as follows (Muskhelishvili, 1963):

$$\varphi(\zeta) = \frac{\chi(\zeta)}{2\pi i}\int_{L+M}\frac{H(\sigma)}{\chi(\sigma)(\sigma-\zeta)}d\sigma + \chi(\zeta)G(\zeta) \tag{6}$$

$$H(\sigma) = \begin{cases} i\int [P_x(s) + iP_y(s)]ds & \text{on } L \\ \dfrac{2G}{\kappa}(u+iv) & \text{on } M \end{cases}$$

in which the Plemelj function $\chi(\zeta) = (\zeta-\alpha)^m(\zeta-\beta)^{1-m}$ and $m = \frac{1}{2} - i[1n\kappa/(2\pi)]$ are chosen, because of the continuity of the displacement at α and β which are the junctures L and M (see Fig. 1). The branch is chosen so that $\lim_{\zeta\to\infty}[\chi(\zeta)/\zeta] = 1$. The function $G(\zeta)$ is a rational one with poles outside the unit circle and is determined from equation (3) so that $\psi(\zeta)$ is regular in the unit circle. In the second term on the right-hand side of equation (3), the function $\omega'(\zeta)$ has no zero, and $\varphi'(\zeta)$ is regular in the unit circle. Then the function $\overline{\omega(1/\zeta)} = \bar{\omega}(1/\zeta)$ has poles of first order at $\zeta = 1/\bar{\zeta}_k$ ($\equiv \zeta_k'$) in the unit circle (see equation (2)). Consequently, it is possible to write the following equation in the unit circle:

$$\frac{\overline{\omega(1/\zeta)}}{\omega'(\zeta)}\varphi'(\zeta) = \sum_{k=1}^{24}\frac{A_k\overline{B_k}}{\bar{\zeta}_k - \dfrac{1}{\zeta}} + \text{regular part} \tag{7}$$

in which $A_k = \varphi'(\zeta_k')$; and $B_k = E_k/\overline{\omega'(\zeta_k')}$. Thus, in order that $\psi(\zeta)$ is regular in the unit circle, the first term on the right-hand side of equation (3) has to cancel the irregular term of equation (7). In other words, the function $G(\zeta)$ is determined in the following way. The function $\overline{\varphi(1/\zeta)}$ using equation (6) can be divided into regular and irregular parts as follows:

$$\overline{\varphi\left(\frac{1}{\bar{\zeta}}\right)} = \frac{\overline{\chi(\zeta_k)}\ \overline{G(\zeta_k)}}{\bar{\zeta}_k - \dfrac{1}{\zeta}} + \text{regular part} \tag{8}$$

Consequently, $G(\zeta_k)$ is determined;

$$-\overline{\chi(\zeta_k)}\ \overline{G(\zeta_k)} - A_k\overline{B_k} = 0 \tag{9}$$

Based on the aforementioned, finally $\varphi(\zeta)$ is

$$\varphi(\zeta) = \frac{\chi(\zeta)}{2\pi i}\int_{L+M}\frac{H(\sigma)}{\chi(\sigma)(\sigma-\zeta)}d\sigma - \chi(\zeta)\sum_{k=1}^{24}\frac{\overline{A_k}B_k}{\chi(\zeta_k)(\zeta_k-\zeta)} \tag{10}$$

Since $\varphi'(\zeta_k') = A_k$ ($k = 1, 2, \ldots, 24$), the simultaneous equations with respect to A_k and $\bar{A}_k$ can be obtained, and so the real and imaginary parts of A_k can be determined. The method mentioned above is mathematically the same as that of Muskhelishvili (1963). He, however, derived the first derivative of $\varphi(\zeta)$ and thus the integral of $\varphi'(\zeta)$ has to be carried out to calculate the components of displacement and it is not easy generally. Further, the solution of equation (10) is simpler than this solution to determine the unknown constant A_k. As the loading condition, uniform tension P in the x-direction at infinity is considered. Then the boundary conditions are

$$u = v = 0 \quad \text{on } M$$

$$p_x = p_y = 0 \quad \text{on } L$$

$$\begin{cases} \sigma_x = p & \text{when } \zeta \to 1 \\ \sigma_y = \tau_{xy} = 0 \end{cases}$$

Finally, the function $\varphi(\zeta)$ is obtained as follows:

$$\varphi(\zeta) = \chi(\zeta)\left\{\frac{PE_0}{4\chi(1)(1-\zeta)} - \sum_{k=1}^{24}\frac{(\bar{A}_kB_k + PE_k/4)}{\chi(\zeta_k)(\zeta_k-\zeta)}\right\} \tag{11}$$

in which $A_k = \varphi'(\zeta_k') - P\omega'(\zeta_k')/4$ ($k = 1, 2, \ldots, 24$) in this case. Equation (11) is the same solution as that of Hasebe (1979).

Stress Intensity of Debonding

A Stress Intensity of Debonding at Point z_A. The debonded tips z_A and z_B in the z-plane correspond to points α and β in the ζ plane (see Fig. 1). The complex stress function in the z-plane is generally expressed as follows:

$$\phi(z) = (z-z_A)^m(z-z_B)^{1-m}f(z) + f_0(z) \tag{12}$$

in which functions $f(z)$ and $f_0(z)$ are regular in the region. First, we examine the stress singularity at the debonded tip z_A. The first derivative of $\phi(z)$ is expanded in the Taylor series except for the singular term at z_A as follows:

$$\phi'(z) = (z-z_A)^{m-1}\sum_{j=0}^{\infty}\alpha_j(z-z_A)^j + \sum_{j=0}^{\infty}\epsilon_j(z-z_A)^j \tag{13}$$

in which α_j and ϵ_j are constants.

If $(z-z_A)$ is infinitesimal, equation (13) is approximated by the first term,

$$\phi'(z) = \alpha_0(z-z_A)^{m-1} \tag{14}$$

If we express the stress function in the ζ plane as $\varphi'(\zeta) = (\zeta-\alpha)^{m-1}(\zeta-\beta)^{-m}g(\zeta)$ (see equation (11)) and since $\phi'(z) = \varphi'(\zeta)/\omega'(\zeta)$, the value α_0 in equation (14) is obtained by

Downloaded 03 May 2010 to 171.66.16.21. Redistribution subject to ASME license or copyright; see http://www.asme.org/terms/Terms_Use.cfm

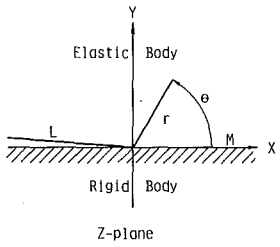


Fig. 2(a) Z coordinate system with the origin at Z_A

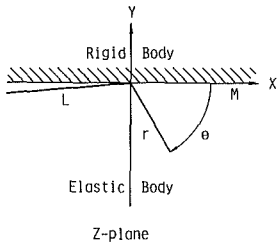


Fig. 2(b) Z coordinate system with the origin at Z_B

$$\alpha_0 = \lim_{z \to z_A} (z - z_A)^{1-m} \phi'(z)$$

$$= \frac{|\omega'(\alpha)(\alpha-\beta)|^{1-m} g(\alpha)}{\omega'(\alpha)(\alpha-\beta)} \exp\{i(1-m)(\theta_A + \theta_\beta - \theta_\alpha)\} \tag{15}$$

When ζ_R denotes a point on the rigid boundary, $\theta_A = \lim_{\zeta_R \to \alpha} \{\arg[\omega(\zeta_R) - \omega(\alpha)]\}$; $\theta_\alpha = \lim_{\zeta_R \to \alpha} [\arg(\zeta_R - \alpha)]$; and $\theta_\beta = \arg(\alpha - \beta)$. According to the Plemelj function $\chi(\zeta)$, $(\theta_\beta - \theta_\alpha)$ denotes the angle between the chord $\widehat{\alpha\beta}$ and a tangent of the unit circle at α. In this paper, $\theta_\beta - \theta_\alpha = \pi + s/2$ for $\angle \alpha 0 \beta = s$ $(0 \leq s < 2\pi)$ (see Fig. 1). If $z - z_A$ is expressed as $z - z_A = \widehat{r \exp}[i(\theta_A + \theta)]$ for $0 < \theta < \pi$ (Fig. 2), then equation (14) is also expressed as follows:

$$\phi'(z) = \tilde{\alpha}_0 \{r \cdot \exp(i\theta)\}^{m-1} \tag{16}$$

in which

$$\tilde{\alpha}_0 = \frac{|\omega'(\alpha)(\alpha-\beta)|^{1-m} g(\alpha)}{\omega'(\alpha)(\alpha-\beta)} \exp\{i(1-m)(\theta_\beta - \theta_\alpha)\} \tag{17}$$

We perform a transformation of the coordinate system from z to Z in which the rigid boundary is on the X-axis and the debonded tip z_A is the origin (see Fig. 2(*a*)). Paying attention to $\phi'(z) = \Phi'(Z)$, and to $r \cdot \widehat{\exp}(i\theta) = Z$, the following expression is obtained from equation (16):

$$\Phi'(Z) = \tilde{\alpha}_0 Z^{m-1} \tag{18}$$

Using equation (18), the stress components on the rigid boundary $\theta = 0$ are obtained as follows (Hasebe et al., 1987b):

$$\sigma_Y = \frac{1+\kappa}{r^{0.5}} |\tilde{\alpha}_0| \cos\{\theta_0 - \gamma \cdot 1n(r)\}$$

$$\tau_{XY} = -\frac{1+\kappa}{r^{0.5}} |\tilde{\alpha}_0| \sin\{\theta_0 - \gamma \cdot 1n(r)\} \tag{19}$$

$$\sigma_X = \frac{3-\kappa}{r^{0.5}} |\tilde{\alpha}_0| \cos\{\theta_0 - \gamma \cdot 1n(r)\}$$

in which $\theta_0 = \arg \tilde{\alpha}_0$, $\gamma = 1n(\kappa)/(2\pi)$. Since σ_y is the stress component normal to the rigid surface, σ_y is responsible for debonding. Similarly, τ_{xy} and σ_x are responsible for slipping and cracking into the matrix, respectively. Therefore, $|\tilde{\alpha}_0|$ indicates the intensity for the debonding and the crack initiation at the debonding tip. Thus, we call $\tilde{\alpha}_0$ as "the stress intensity of debonding (SID)" at z_A in this paper. Hasebe et al. (1987b) gave the same α_0 and $\tilde{\alpha}_0$ as follows:

$$\alpha_0 = \frac{h(\alpha)}{\{\omega'(\alpha)\}^m} \tag{20}$$

$$\tilde{\alpha}_0 = \frac{h(\alpha)}{\{\omega'(\alpha)\}^m} \exp\{i(m-1)\lambda\} \tag{21}$$

$h(\alpha)$ denotes the value of function $h(\zeta)$ at $\zeta = \alpha$, where $h(\zeta)$ is defined by $\varphi'(\zeta) = (\zeta - \alpha)^{m-1} h(\zeta) + h_0(\zeta)$ (see equation (11)); λ is the rotation angle of the coordinate transformation, $Z = z \cdot \exp(-i\lambda)$. Equations (20) and (21) contain the function $[\omega'(\alpha)]^m$, which is multivalued since m is the complex constant, $m = \frac{1}{2} - i[1n\ \kappa/(2\pi)]$. Therefore, attention must be paid to the calculation of $\tilde{\alpha}_0$. However, since equation (17) does not contain the multivalued term, it is convenient to use equation (17) instead of equation (21) to calculate $\tilde{\alpha}_0$.

B SID at Point z_B. We examine singularity at the debonded tip z_B in the same way as in the preceding section.

A transformation of the coordinate system from z to Z is carried out, and Fig. 2(*b*) shows the Z coordinate system in which the rigid boundary is on the X-axis and the debonded tip z_B is the origin. Then $\Phi'(Z)$ is expressed as follows:

$$\Phi'(Z) = \tilde{\beta}_0 Z^{-m} = \tilde{\beta}_0 \{r \cdot \exp(i\theta)\}^{-m} \tag{22}$$

in which $Z = r \cdot \exp(i\theta)$ for $-\pi < \theta < 0$,

$$\tilde{\beta}_0 = \frac{|\omega'(\beta)(\beta-\alpha)|^m g(\beta)}{\omega'(\beta)(\beta-\alpha)} \exp\{-im(\theta_\beta' - \theta_\alpha')\} \tag{23}$$

in which $\theta_\alpha' = \arg(\beta - \alpha)$; and $\theta_\beta' = \lim_{\zeta_R \to \beta} [\arg(\zeta_R - \beta)]$; and $\theta_\beta' - \theta_\alpha' = \pi + s/2$; and s denotes the angle $\angle \alpha 0 \beta$ in Fig. 1. The components of the stress and the displacement in the vicinity of the origin z_B are given by using equation (22);

$$\begin{aligned}
\sigma_Y = {} & \frac{B_I}{r^{0.5}} [\exp(-\gamma\theta)\cos(\Theta) + \kappa \cdot \exp(\gamma\theta)\cos(\Theta+\theta) \\
& + \exp(-\gamma\theta)\{2\gamma \cdot \cos(\Theta-\theta) - \sin(\Theta-\theta)\}\sin(\theta)] \\
& - \frac{B_{II}}{r^{0.5}} [\exp(-\gamma\theta)\sin(\Theta) + \kappa \cdot \exp(\gamma\theta)\sin(\Theta+\theta) \\
& + \exp(-\gamma\theta)\{2\gamma \cdot \sin(\Theta-\theta) + \cos(\Theta-\theta)\}\sin(\theta)] \\
\tau_{XY} = {} & \frac{B_I}{r^{0.5}} [-\exp(-\gamma\theta)\sin(\Theta) - \kappa \cdot \exp(\gamma\theta)\sin(\Theta+\theta) \\
& + \exp(-\gamma\theta)\{2\gamma \cdot \sin(\Theta-\theta) + \cos(\Theta-\theta)\}\sin(\theta)] \\
& + \frac{B_{II}}{r^{0.5}} [-\exp(-\gamma\theta)\cos(\Theta) - \kappa \cdot \exp(\gamma\theta)\cos(\Theta+\theta) \\
& + \exp(-\gamma\theta)\{2\gamma \cdot \sin(\Theta-\theta) - \cos(\Theta-\theta)\}\sin(\theta)] \\
\sigma_X = {} & \frac{B_I}{r^{0.5}} [3\exp(-\gamma\theta)\cos(\Theta) - \kappa \cdot \exp(\gamma\theta)\cos(\Theta+\theta) \\
& - \exp(-\gamma\theta)\{2\gamma \cdot \cos(\Theta-\theta) - \sin(\Theta-\theta)\}\sin(\theta)] \\
& - \frac{B_{II}}{r^{0.5}} [3\exp(-\gamma\theta)\sin(\Theta) - \kappa \cdot \exp(\gamma\theta)\sin(\Theta+\theta) \\
& - \exp(-\gamma\theta)\{2\gamma \cdot \sin(\Theta-\theta) + \cos(\Theta-\theta)\}\sin(\theta)] \\
u = {} & \frac{B_I r^{0.5}}{G(1+4\gamma^2)} [\kappa \cdot \exp(-\gamma\theta)\{2\gamma \cdot \sin(\Theta+\theta) + \cos(\Theta+\theta)\} \\
& - \kappa \cdot \exp(\gamma\theta)\{2\gamma \cdot \sin(\Theta) + \cos(\Theta)\} \\
& - (1+4\gamma^2)\exp(-\gamma\theta)\sin(\theta)\sin(\Theta)] \\
& + \frac{B_{II} r^{0.5}}{G(1+4\gamma^2)} [\kappa \cdot \exp(-\gamma\theta)\{2\gamma \cdot \cos(\Theta+\theta) - \sin(\Theta+\theta)\} \\
& - \kappa \cdot \exp(\gamma\theta)\{2\gamma \cdot \cos(\Theta) - \sin(\Theta)\} \\
& - (1+4\gamma^2)\exp(-\gamma\theta)\sin(\theta)\cos(\Theta)] \\
v = {} & \frac{B_I r^{0.5}}{G(1+4\gamma^2)} [\kappa \cdot \exp(-\gamma\theta)\{-2\gamma \cdot \cos(\Theta+\theta) + \sin(\Theta+\theta)\}
\end{aligned} \tag{24}$$

Downloaded 03 May 2010 to 171.66.16.21. Redistribution subject to ASME license or copyright; see http://www.asme.org/terms/Terms_Use.cfm

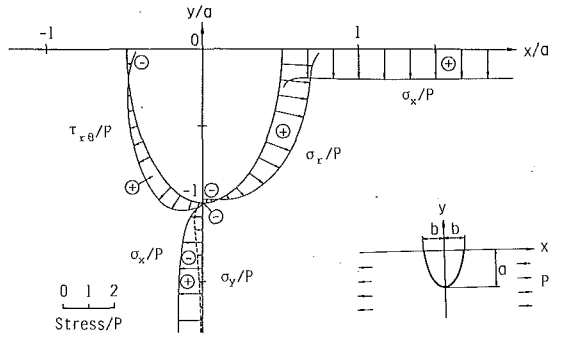


Fig. 3 Stress distribution: $\kappa = 2$, $b/a = 0.5$, and $c/a = 0$

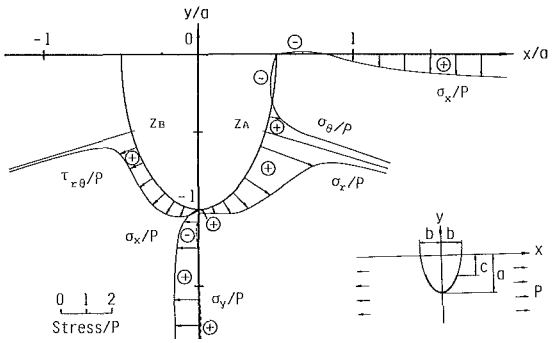


Fig. 4 Stress distribution: $\kappa = 2$, $b/a = 0.5$, and $c/a = 0.5$

$$
\begin{aligned}
&-\kappa\cdot\exp(\gamma\theta)\{-2\gamma\cdot\cos(\Theta)+\sin(\Theta)\}\\
&-(1+4\gamma^2)\exp(-\gamma\theta)\sin(\theta)\cos(\Theta)]\\
+\frac{B_{II}r^{0.5}}{G(1+4\gamma^2)}&[\kappa\cdot\exp(-\gamma\theta)\{2\gamma\cdot\sin(\Theta+\theta)+\cos(\Theta+\theta)\}\\
&-\kappa\cdot\exp(\gamma\theta)\{2\gamma\cdot\sin(\Theta)+\cos(\Theta)\}\\
&+(1+4\gamma^2)\exp(-\gamma\theta)\sin(\theta)\sin(\Theta)]
\end{aligned}
$$

where $\tilde{\beta}_0 = B_I + iB_{II}$ and $\Theta = \gamma\cdot 1n(r) - \theta/2$.

Using equation (24), the stress components on the rigid boundary ($\theta = 0$) are expressed as follows:

$$
\begin{aligned}
\sigma_Y &= \frac{1+\kappa}{r^{0.5}}\,|\tilde{\beta}_0|\cos\{\theta_0' + \gamma\cdot 1n(r)\}\\
\tau_{XY} &= -\frac{1+\kappa}{r^{0.5}}\,|\tilde{\beta}_0|\sin\{\theta_0' + \gamma\cdot 1n(r)\} \qquad (25)\\
\sigma_X &= \frac{3-\kappa}{r^{0.5}}\,|\tilde{\beta}_0|\cos\{\theta_0' + \gamma\cdot 1n(r)\}
\end{aligned}
$$

in which $\theta_0' = \arg\tilde{\beta}_0$. Therefore, $|\tilde{\beta}_0|$ also gives the intensity for the debonding and the crack initiation at the debonded tip. Thus, we call $\tilde{\beta}_0$ as "the stress intensity of debonding" at z_B. This value of $\tilde{\beta}_0$ corresponds to $-\tilde{\beta}_0/\kappa$ in reference Hasebe et al. (1987a). By comparing equation (25) with equation (19), we note that $\tilde{\alpha}_0$ and $\tilde{\beta}_0$ are complex conjugate each other in the case of the symmetric stress state as in this paper. When two debonding tips exist, the magnitude of $\tilde{\alpha}_0$ and $\tilde{\beta}_0$ tells which debonding is likely to propagate faster.

Results of Analysis

A Stress Distribution. Figure 3 shows the stress distribution without the debonding for $\kappa = 2$ ($\nu = 1/4$ for plane strain and $\nu = 1/3$ for generalized plane stress). Figure 4 shows one for $c/a = 0.5$, where c indicates the debonding length and a does the length of the semiaxis of the elliptical inclusion (see Fig. 1). The suffixes r and θ represent the normal and tangential directions on the elliptical boundary. And the stresses σ_r and σ_θ on the rigid boundary have the following relation (Hasebe, 1979): $\sigma_\theta/\sigma_r = (3-\kappa)/(1+\kappa)$. As shown in Fig. 3, σ_r takes positive or negative values at point C (see Fig. 1) depending on the value κ, b/a, and c/a. Thus, if σ_r is negative at C under uniform tension, then σ_r takes positive value at point C under uniform compression, and thus the debonding may occur. The stresses at points B and D before the emanation of the debonding ($c/a = 0$) become infinite for $\kappa \neq 3$ and become finite value only for $\kappa = 3$ (Williams, 1952). As shown in Fig. 4, σ_r and σ_θ at the debonded tip on M have positive infinite values and, thus, the growth of debonding or a crack into the matrix is likely to occur.

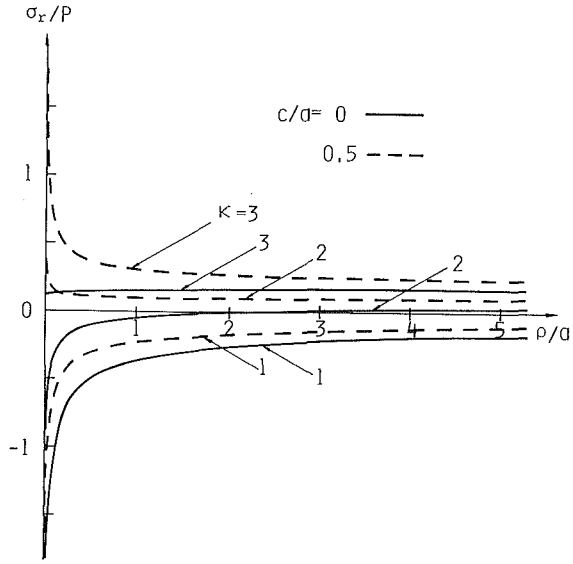


Fig. 5 σ_r at the base of the semielliptical rigid inclusion

B σ_r at Point C. In Fig. 3, σ_r at point C takes a negative value for $P > 0$, and then a positive value for $P < 0$, and, thus, the debonding is likely to occur for $P < 0$. Therefore, the investigation of σ_r at point C is important. We study the relations among σ_r, the radius of curvature ρ, and κ. Figure 5 shows the relations for $c/a = 0$ and 0.5. For $c/a = 0$ and $\kappa = 3$, in all cases, σ_r has the positive values, and for $\kappa = 2$, σ_r changes from negative to positive as ρ/a increases, and for $\kappa = 1$, σ_r has the negative values in all cases. For $c/a = 0.5$, in all cases, σ_r has the positive values for $\kappa = 3$ and 2, and has the negative values for $\kappa = 1$. When ρ/a becomes small, σ_r increases infinitely except the case of $c/a = 0$ and $\kappa = 3$.

In general, the stress σ at the tip of the clamped edge is expressed by the radius of curvature ρ as follows (Hasebe et al., 1986):

$$\sigma = \sum_{j=1}^{\infty} k_j \rho^{m_j} \qquad (26)$$

in which $m_j s$ are roots of the characteristic equations which are determined by the corner angle and the boundary condition, and by the stress state symmetric or antisymmetric with respect to the bisector of the corner. $\mathrm{Re}[m_j + 1] > 0$ is used for $\rho < 1$, and $\mathrm{Re}[m_j + 1] < 0$ for $\rho > 1$ ($\mathrm{Re}[\cdot]$ indicates the real part of $[\cdot]$). $k_j s$ are constants determined by the shape of the elastic body, the boundary condition, and m_j. For $\rho < 1$, $m_j s$ are named $m_1, m_2, \ldots$ in order of increasing value of the real part. Then, for the symmetric stress state and the corner angle 360°, $m_1 = -0.5$, $m_2 = 0$, $m_3 = 0.5$, $m_4 = 1, \ldots$. The semielliptic shape in this paper corresponds to the corner angle 360°. For $\rho < 1$, the stress σ_r is expressed with considerable accuracy by the first few terms of equation (26) (Hasebe et al., 1986). Now we consider the following approximate expression with the first four terms:

Downloaded 03 May 2010 to 171.66.16.21. Redistribution subject to ASME license or copyright; see http://www.asme.org/terms/Terms_Use.cfm

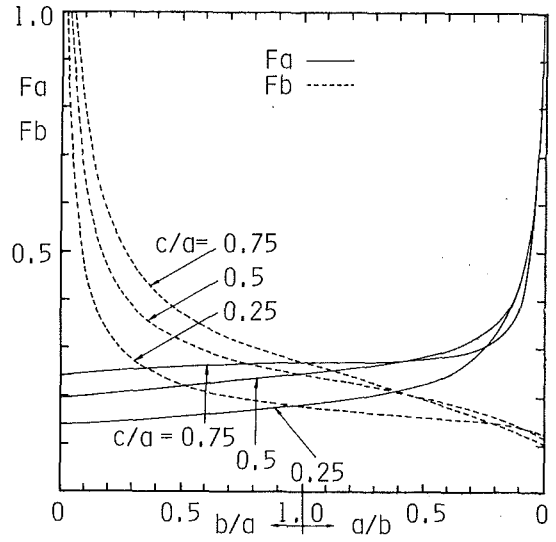


Fig. 6 Nondimensional stress intensity of debonding for some c/a ($\kappa = 2$)

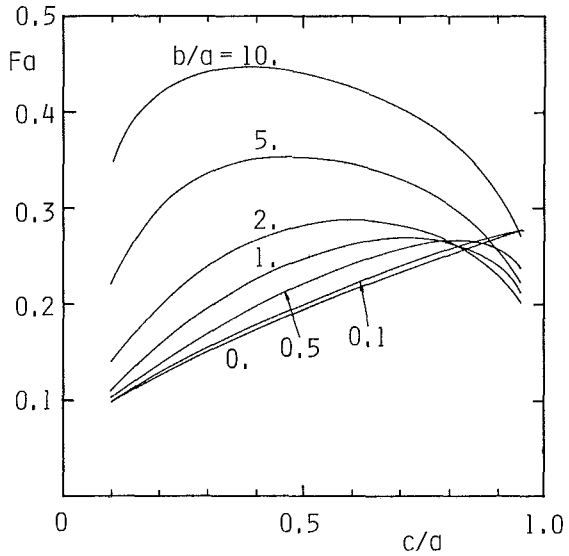


Fig. 7 Nondimensional stress intensity of debonding F_a for some b/a ($\kappa = 2$)

$$\frac{\sigma_r}{P} = k_1\sqrt{\frac{a}{\rho}} + k_2 + k_3\sqrt{\frac{\rho}{a}} + k_4\frac{\rho}{a} \tag{27}$$

The values of k_1, k_2, k_3, and k_4 were obtained by the least squares method using 19 values of σ_r/P for ρ/a, ranging from 0.01 to 0.1 at every increment 0.01, and ranging 0.1 to 1 at every increment 0.1. Table 1 shows the values of k_1, k_2, k_3, and k_4. Table 2 shows the exact values of σ_r/P and their errors to the values given by equation (27) for $c/a = 0$ and 0.5, and $\kappa = 2$. All of the errors are less than 0.2 percent and, thus, the stress σ_r at point C is represented accurately by equation (27) and can be calculated for any ρ/a less than 1.

C The Stress Intensity of Debonding. In this paper, we use the following two nondimensional values for SID:

$$F_a = \frac{|\tilde{\alpha}_0|}{P\sqrt{a}} \qquad F_b = \frac{|\tilde{\alpha}_0|}{P\sqrt{b}} \tag{28}$$

Figure 6 shows the variation of SID with respect to the length of the semiaxis of the elliptic inclusion, a and b. F_a (solid line) show SID versus b for constant a. Since F_a increases for larger b, the debonding is apt to occur. F_b (dashed line) shows SID versus a for constant b. Since F_b increases for larger a, the debonding is also apt to occur. Figure 7 shows the variation of F_a for the debonding length. The curves are convex and have the maximum values. Therefore, when the toughness value against debonding is larger than that maximum value, the debonding does not propagate. The values of c/a where F_a takes the maximum value decrease for larger b/a.

Table 1 Coefficients of equation (27)

c/a	κ	k_1	k_2	k_3	k_4
0	3	-0.0001	0.1222	0.0398	-0.0115
	2	-0.1152	0.0447	0.0329	-0.0089
	1	-0.3077	-0.0700	0.0300	-0.0082
0.5	3	0.1670	0.0850	0.0813	-0.0275
	2	0.0363	0.0158	0.0701	-0.0240
	1	-0.1744	-0.0854	0.0557	-0.0184

Table 2 σ_r at the base of the semielliptic rigid inclusion and errors of equation (27) ($\kappa = 2$)

ρ/a	c/a=0		c/a=0.5	
	σ_r/P	Error (%)	σ_r/P	Error (%)
0.01	-1.10367	0.006	0.38575	-0.106
0.02	-0.76522	-0.007	0.28160	0.059
0.04	-0.52496	-0.010	0.21008	0.091
0.08	-0.35388	0.003	0.16205	-0.030
0.1	-0.30995	0.012	0.15045	-0.083
0.2	-0.19984	0.033	0.12374	-0.182
0.4	-0.12015	0.016	0.10796	-0.009
0.8	-0.06180	-0.040	0.09984	0.084
1	-0.04645	0.077	0.09843	-0.186
2	-0.00695		0.09668	
4	0.02295		0.09764	
8	0.04582		0.10000	
10	0.05199		0.10091	

Conclusion

An elastic half plane with a semielliptic rigid inclusion was analyzed as the mixed boundary value problem. The plane was clamped at the elliptic part and subjected to uniform tension in the x-direction at infinity. By using the mapping function with the form of equation (2), we can analyze the half plane with a notch or a rigid inclusion of any shape (for example, Hasebe and Iida, 1978). The debonding propagation can be examined by the magnitude of $|\tilde{\alpha}_0|$ and $|\tilde{\beta}_0|$ in equations (17) and (23). The debonding on the boundary was studied for some elliptic shapes. When a = constant and b increases, the debonding is apt to occur. When b = constant and a increases, the debonding is also apt to occur. The values of F_a have the maximum value. Equations (17) and (23) hold for any conformal mapping function $\omega(\zeta)$. The stress σ_r at point C is represented accurately by equation (27). σ_r takes positive or negative values depending on κ, b/a and c/a. If σ_r takes a negative value under uniform tension, then σ_r takes positive value under uniform compression. Therefore, uniform compression is important for the debonding. When $\kappa = 3$ and c/a

Downloaded 03 May 2010 to 171.66.16.21. Redistribution subject to ASME license or copyright; see http://www.asme.org/terms/Terms_Use.cfm

$= 0$, the stress concentration of σ_r at point C does not arise for small ρ/a.

When the debonding length at z_A and z_B are not equal, the analysis can be carried out by changing the values of α and β. However, since then the inclusion is subjected to the rotation, it must be considered (Hasebe and Takeuchi, 1985).

References

Bowie, O. L., and Freese, C. E., 1978, "Analysis of Notches Using Conformal Mapping," *Mechanics of Fracture V*, G. C. Sih, ed., Noordhoff International Publishing, Chapter 3.

Hasebe, N., 1972, "Stress Analysis of a Semi-Infinite Plate with a Semi-Elliptic Notch," *Bulletin of the Nagoya Institute of Technology*, Vol. 24, pp. 295–301.

Hasebe, N., and Iida, J., 1978, "A Crack Originating From a Triangular Notch on a Rim of a Semi-Infinite Plate," *Engineering Fracture Mechanics*, Vol. 10, pp. 773–782.

Hasebe, N., 1979, "Uniform Tension of a Semi-Infinite Plate With a Crack at an End of a Stiffened Edge," *Ingenieur-Archiv*, Band 48, pp. 129–141.

Hasebe, N., and Inohara, S., 1980, "Stress Analysis of a Semi-Infinite Plate with an Oblique Edge Crack," *Ingenieur-Archiv*, Band 49, pp. 51–62.

Hasebe, N., 1983, "Mixed Boundary Value Problem of Plate With Crack," ASCE *Journal of Engineering Mechanics*, Vol. 110, pp. 37–48.

Hasebe, N., and Takeuchi, T., 1985, "Stress Analysis of a Semi-Infinite Plate with a Thin Rigid Body," *International Journal of Engineering Science*, Vol. 23, pp. 531–539.

Hasebe, N., Sugimoto, T., and Nakamura, T., 1986, "Stress Analysis of a Blunted Notch in a Clamped Edge," ASCE *Journal of Engineering Mechanics*, Vol. 112, pp. 142–153.

Hasebe, N., Okumura, M., and Nakamura, T., 1987a, "Stress Analysis of a Debonding and a Crack around a Circular Rigid Inclusion," *International Journal of Fracture*, Vol. 32, pp. 169–183.

Hasebe, N., Okumura, M., and Nakamura, T., 1987b, "A Debonding and a Crack on a Circular Rigid Inclusion Subjected to Rotation," *International Journal of Fracture*, Vol. 33, pp. 195–208.

Higuchi, S., and Suzuki, M., 1949, "Distribution of Stresses in the Semi-infinite Plate Having an Elliptic Notch Under Uniform Tension," Technical Report on Tohoku University, Vol. 14, pp. 95–107.

Isibashi, T., 1940, "Stresses in a Semi-infinite Plate with a Circular Notch Under Uniform Tension," Memoirs of the Faculty of Engineering Kyushu Imperial University, Japan, Vol. 9, pp. 131–143.

Ling, C. B., 1948, "On the Stresses in a Notched Plate Under Tension," *Journal of Mathematics and Physics*, Vol. 26, pp. 181–186.

Ling, C. B., 1978, "Stress Analysis of Edge Notches," *Mechanics of Fracture V*, G. C. Sih, ed., Noordhoff International Publishing, Chap. 3.

Maunsell, F. G., 1936, "Stresses in a Notched Plate Under Tension," *Philosophical Magazine*, Vol. 21, pp. 765–773.

Mitchell, L. H., 1965, "Stress Concentration at Semicircular Notch," ASME JOURNAL OF APPLIED MECHANICS, Vol. 32, 87, Series E, pp. 938–939.

Muskhelishvili, N. I., 1963, "Some Basic Problems of Mathematical Theory of Elasticity," 4th ed., Noordhoff, The Netherlands.

Nisitani, H., 1978, "Solutions of Notch Problems by Body Force Method," *Mechanics of Fracture V*, G. C. Sih, ed., Noordhoff International Publishing, Chapter 1.

Weinel, E., 1941, "Die Spannung serhoehung durch Keisbogenkerben," *Zeitschrift fur Angewandte Mathematik und Mechanik*, Band 21, pp. 228–230.

Downloaded 03 May 2010 to 171.66.16.21. Redistribution subject to ASME license or copyright; see http://www.asme.org/terms/Terms_Use.cfm

A. K. Gautesen
Department of Mathematics
and Ames Laboratory,
Iowa State University,
Ames, IA 50011

John Dundurs
Departments of Civil Engineering
and Mechanical Engineering,
Northwestern University,
Evanston, IL 60201
Fellow, ASME

The Interface Crack Under Combined Loading

The interface crack subjected to a combined tension-compression and shear loading is considered in the Comninou formulation, which by properly incorporating contact zones at the crack tips avoids contradictions, such as overlapping of material. It is shown that the resulting integral equation can be solved exactly. Moreover, simple asymptotic—yet very accurate—formulae are derived for the quantities of major physical interest and a comparison made with the previous results given by Comninou.

1 Introduction

The basic ideas about the interface crack, as modeled in this paper, are due to Comninou (1977, 1978): The conventional formulation, which assumes that there is a direct transition from the perfect bond between the two materials to crack faces that are free of tractions leads to contradictions, in that solutions constructed on this basis exhibit overlapping of material (England, 1965; Malyshev and Salganik, 1965). The only other possibility is, then, that the crack faces are always in contact at the very tips of the crack. The Comninou formulation of the interface crack is free of contradictions, and it is possible to satisfy the conditions of a positive gap between the crack faces on the open part of the crack and compressive normal tractions in the contact zones. It is also known that solutions in the Comninou formulation are unique (Shield, 1982).

The first problem considered by Comninou (1977) was that of the interface crack in a tension field. She reduced the formulation to a single integral equation and succeeded in extracting the results of physical interest for an extreme mismatch between the two materials by a numerical method. The present authors (Gautesen and Dundurs, 1987a; Gautesen and Dundurs, 1987b) have recently shown that the Comninou integral equation can be solved exactly, and that it is possible to give simple asymptotic—yet very accurate—formulae for the size of the contact zones, the mode II stress intensity factor, and the stress concentration factor for the finite but possibly very large tension transmitted by the bond at the tips of the crack.

In the present article we turn to the other problems considered by Comninou (Comninou, 1978; Comninou and Schmueser, 1979) involving shear, and combined shear and tension-compression loading of the interface crack. We show that the governing integral equation for this more general case also can be solved exactly, and we derive accurate results covering the whole range of mismatch in the elastic constants of the two materials. It should be noted that no effects of friction in the contact zones are considered. For some estimates of what friction would do upon a monotonic application of shear loading, the reader may wish to consult the article by Comninou and Dundurs (1980).

2 Formulation and Solution of the Problem

The geometry of the interface crack with some of the symbols used is shown in Fig. 1.

The governing integral equations for this problem, as given by Comninou and Schmueser (1979) are

$$\beta B_x(x)+\frac{1}{\pi}\int_{-a}^{b}\frac{B_y(\xi)d\xi}{\xi-x}=\frac{T}{C}, \quad -a<x<b \tag{2.1}$$

$$\beta[H(x-b)-H(x+a)]B_y(x)+\frac{1}{\pi}\int_{-L}^{L}\frac{B_x(\xi)d\xi}{\xi-x}=\frac{S}{C}, \quad |x|<L \tag{2.2}$$

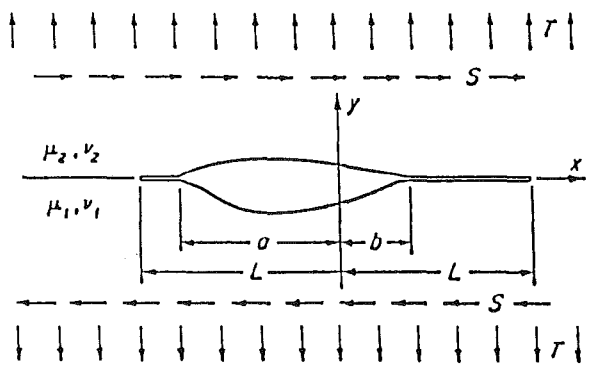


Fig. 1 Geometry of the interface crack

Contributed by the Applied Mechanics Division for presentation at the Winter Annual Meeting, Chicago, IL, November 28 to December 2, 1988, of THE AMERICAN SOCIETY OF MECHANICAL ENGINEERS.

Discussion on this paper should be addressed to the Editorial Department, ASME, United Engineering Center, 345 East 47th Street, New York, N.Y. 10017, and will be accepted until two months after final publication of the paper itself in the JOURNAL OF APPLIED MECHANICS. Manuscript received by ASME Applied Mechanics Division, April 3, 1987; final revision, February 1, 1988.

Paper No. 88-WA/APM-46.

Copyright © 1988 by ASME
Downloaded 03 May 2010 to 171.66.16.21. Redistribution subject to ASME license or copyright; see http://www.asme.org/terms/Terms_Use.cfm

where $B_x(x)$ and $B_y(x)$ are the dislocation densities of the glide and climb arrays, H denotes the Heaviside step function and

$$C=\frac{2\mu_1(1+\alpha)}{(1-\beta^2)(\kappa_1+1)}=\frac{2\mu_2(1-\alpha)}{(1-\beta^2)(\kappa_2+1)} \tag{2.3}$$

$$\alpha=\frac{\mu_2(\kappa_1+1)-\mu_1(\kappa_2+1)}{\mu_2(\kappa_1+1)+\mu_1(\kappa_2+1)} \tag{2.4}$$

$$\beta=\frac{\mu_2(\kappa_1-1)-\mu_1(\kappa_2-1)}{\mu_2(\kappa_1+1)+\mu_1(\kappa_2+1)} \tag{2.5}$$

Moreover, μ denotes the shear modulus, and $\kappa = 3-4\nu$ for plane strain, where ν is Poisson's ratio. Without loss of generality, we can take $S \geq 0$ and $0 < \beta \leq \frac{1}{2}$.

The dislocation densities also must satisfy the auxiliary conditions

$$\int_{-L}^{L} B_x(x)dx=0, \quad \int_{-a}^{b} B_y(x)dx=0 \tag{2.6a,b}$$

It is important to note that $B_y(-a) = B_y(b) = 0$.

The equations (2.1) and (2.2) are first transformed so that the intervals of integration are symmetric by setting

$$x=L\frac{s-\gamma}{1-\gamma s}, \quad \xi=L\frac{r-\gamma}{1-\gamma r} \tag{2.7a,b}$$

$$CB_x(x)=(1-\gamma s)^2A_x(s), \quad CB_y(x)=(1-\gamma s)^2A_y(s) \tag{2.8a,b}$$

where

$$\gamma=\frac{L(a-b)}{L^2-ab+(L^2-a^2)^{1/2}(L^2-b^2)^{1/2}} \tag{2.9}$$

Then the integral equations (2.1) and (2.2) become

$$\beta A_x(s)+\frac{1}{\pi}\int_{-c}^{c}\frac{(1-\gamma r)A_y(r)dr}{(1-\gamma s)(r-s)}=\frac{T}{(1-\gamma s)^2}, \quad |s|<c \tag{2.10}$$

$$-\beta H(c^2-s^2)A_y(s)+\frac{1}{\pi}\int_{-1}^{1}\frac{(1-\gamma r)A_x(r)dr}{(1-\gamma s)(r-s)}=\frac{S}{(1-\gamma s)^2}, \quad |s|<1 \tag{2.11}$$

where

$$c=\frac{a(L^2-b^2)^{1/2}+b(L^2-a^2)^{1/2}}{L[(L^2-b^2)^{1/2}+(L^2-a^2)^{1/2}]} \tag{2.12}$$

The auxiliary conditions (2.6a,b) expressing the requirement that the total amounts of dislocations vanish over the respective intervals are now

$$\int_{-1}^{1}A_x(s)ds=0, \quad \int_{-c}^{c}A_y(s)ds=0 \tag{2.13a,b}$$

Note that for $b<a$, $0<\gamma<1$ and $0<c<1$. The integral equations can be simplified further by using the auxiliary conditions (2.13a,b) and the identity

$$\int_{-\alpha}^{\alpha}\frac{(1-\gamma r)A(r)dr}{(1-\gamma s)(r-s)}=\int_{-\alpha}^{\alpha}\frac{A(r)dr}{r-s}-\frac{\gamma}{1-\gamma s}\int_{-\alpha}^{\alpha}A(r)dr \tag{2.14}$$

The result is

$$\beta A_x(s)+\frac{1}{\pi}\int_{-c}^{c}\frac{A_y(r)dr}{r-s}=\frac{T}{(1-\gamma s)^2}, \quad |s|<c \tag{2.15}$$

$$-\beta H(c^2-s^2)A_y(s)+\frac{1}{\pi}\int_{-1}^{1}\frac{A_x(r)dr}{r-s}=\frac{S}{(1-\gamma s)^2}, \quad |s|<1 \tag{2.16}$$

Next, we solve the integral equation (2.16) for A_x and impose the corresponding auxiliary condition (2.13a). This yields

$$A_x(s)=-\frac{\beta}{\pi}\int_{-c}^{c}\frac{(1-r^2)^{1/2}A_y(r)dr}{(1-s^2)^{1/2}(r-s)}+\frac{S}{(1-s^2)^{1/2}}\frac{d}{d\gamma}\left[\frac{(1-\gamma^2)^{1/2}}{1-\gamma s}\right], \quad |s|<1 \tag{2.17}$$

Upon substitution of (2.17) into (2.15), we find that

$$\frac{1}{\pi}\int_{-c}^{c}\frac{A_y(r)}{r-s}[(1-s^2)^{1/2}-\beta^2(1-r^2)^{1/2}]dr=\frac{d}{d\gamma}\left[\frac{\gamma T(1-s^2)^{1/2}-\beta S(1-\gamma^2)^{1/2}}{1-\gamma s}\right], \quad |s|<c \tag{2.18}$$

Furthermore, the condition $B_y(b) = B_y(-a) = 0$ becomes

$$A_y(\pm c)=0 \tag{2.19}$$

We now manipulate (2.18) so that the resulting equations are in a form such that the results of Gautesen and Dundurs (1987a) apply. We first note that the left side of the integral equation (2.18) transforms even (odd) functions of r into odd (even) functions of s, and consequently write

$$A_y(r)=A_o(r)+A_1(r) \tag{2.20}$$

where

$$A_j(r)=\frac{1}{2}[A_y(r)-(-1)^jA_y(-r)], \quad j=0, 1 \tag{2.21}$$

Clearly, $A_o(r)$ and $A_1(r)$ are, respectively, odd and even functions of r. Therefore, $A_o(r)$ and $A_1(r)$ satisfy the integral equations

$$\frac{1}{\pi}\int_{-c}^{c}\frac{A_o(r)}{r-s}[(1-s^2)^{1/2}-\beta^2(1-r^2)^{1/2}]dr=\frac{d}{d\gamma}\left[\frac{\gamma T(1-s^2)^{1/2}-\beta S(1-\gamma^2)^{1/2}}{1-\gamma^2s^2}\right], \quad |s|<c \tag{2.22}$$

$$\frac{1}{\pi}\int_{-c}^{c}\frac{A_1(r)}{r-s}[(1-s^2)^{1/2}-\beta^2(1-r^2)^{1/2}]dr=\frac{d}{d\gamma}\left[\frac{\gamma s[\gamma T(1-s^2)^{1/2}-\beta S(1-\gamma^2)^{1/2}}{1-\gamma^2s^2}\right], \quad |s|<c \tag{2.23}$$

Adding (2.22) and (2.23) gives, of course, (2.18). Moreover, substitution of (2.20) into the remaining auxiliary condition (2.13b) yields

$$\int_{o}^{c}A_1(s)ds=0 \tag{2.24}$$

Finally, multiplication of (2.23) by s and substitution of the identity

$$\int_{-c}^{c}\frac{sA_1(r)}{r-s}[(1-s^2)^{1/2}-\beta^2(1-r^2)^{1/2}]dr=\int_{-c}^{c}\frac{rA_1(r)}{r-s}[(1-s^2)^{1/2}-\beta^2(1-r^2)^{1/2}]dr-\int_{-c}^{c}A_1(r)[(1-s^2)^{1/2}-\beta^2(1-r^2)^{1/2}]dr \tag{2.25}$$

yields upon using the auxiliary condition (2.24) the appropriate form of the integral equation for $A_1(s)$:

$$\frac{1}{\pi}\int_{-c}^{c}\frac{rA_1(r)}{r-s}[(1-s^2)^{1/2}-\beta^2(1-r^2)^{1/2}]dr=\frac{d}{d\gamma}\left[\frac{\gamma T(1-s^2)^{1/2}-\beta S(1-\gamma^2)^{1/2}}{\gamma(1-\gamma^2s^2)}\right]+I_1 \tag{2.26}$$

where

Downloaded 03 May 2010 to 171.66.16.21. Redistribution subject to ASME license or copyright; see http://www.asme.org/terms/Terms_Use.cfm

$$I_1 = -\frac{\beta^2}{\pi}\int_{-c}^{c}(1-r^2)^{1/2}A_1(r)\,dr + \frac{d}{d\gamma}\left[\frac{\beta S(1-\gamma^2)^{1/2}}{\gamma}\right] \quad (2.27)$$

Also, the condition (2.19) becomes then

$$A_j(\pm c) = 0, \quad j = 0,1 \quad (2.28)$$

We now construct the solutions of the integral equations (2.22) and (2.26) satisfying the side conditions (2.24) and (2.28). Since the unknowns $r^j A_j(r)$, $j = 0, 1$, in (2.22) and (2.24) are odd functions of r satisfying (2.28), the corresponding integral operators in (2.22) and (2.26) are identical to the integral operator associated with the interface crack in a tension field for which the exact solution has been given by the present authors (Gautesen and Dundurs, 1987a,b). From these results it follows that the solution to the present integral equations (2.22) and (2.26) satisfying (2.28) can be obtained from the solution of the integral equation

$$\frac{1}{\pi}\int_E \frac{u_j(y)}{x-y}\,[1-\beta^2\mathrm{sgn}(xy)]\,dy = f_j(x), \quad x\epsilon E, \quad j = 0, 1 \quad (2.29)$$

which satisfies

$$u_j(\pm 1) = u_j(\pm k) = 0, \quad j = 0, 1 \quad (2.30)$$

Herein

$$x = (1-s^2)^{1/2}, \quad 0<s<c \quad (2.31)$$

$$y = (1-r^2)^{1/2}, \quad 0<r<c \quad (2.32)$$

$$u_j(y) = r^j(1-r^2)^{1/2}A_j(r); \quad j = 0,1; \quad 0<r<c \quad (2.33)$$

$$u_j(-y) = u_j(y) \quad (2.34)$$

$$E = \{x: k<|x|<1\} \quad (2.35)$$

$$k = (1-c^2)^{1/2} \quad (2.36)$$

$$f_j(x) = -\frac{(\tau^2+1)^{3/2}}{\tau}\,\frac{d}{d\tau}\left[\frac{(\tau^2+1)^{(j+1)/2}[Tx-\beta S\tau\,\mathrm{sgn}(x)]}{\tau^2+x^2}\right] + jI_1\,\mathrm{sgn}(x), \quad j = 0, 1 \quad (2.37)$$

$$\tau = (\gamma^{-2}-1)^{1/2} \quad (2.38)$$

with the constant I_1 defined by (2.27).

From equations (A.6)–(A.13) derived in the Appendix it follows that

$$\mathrm{sgn}(x)f_j(x) = \frac{(1+\tau^2)^{3/2}}{\tau}\,\frac{d}{d\tau}\left\{(1+\tau^2)^{(j+1)/2}\left[\frac{1}{2}\,(\beta Sa_o - Tb_o) + \sum_{n=1}^{\infty}(\beta Sa_n - Tb_n)\cos[n\pi\psi(x)]\right]\right\} + jI_1, \quad j = 0,1 \quad (2.39)$$

where $\psi(x)$ is defined by (A.3). Upon substitution of (2.39) into (2.29) we find from the relations (A.14)–(A.18) that the solution to the integral equation (2.29) is

$$u_j(x) = -\frac{(1+\tau^2)^{3/2}}{\tau}\,\frac{d}{d\tau}\left\{(1+\tau^2)^{(j+1)/2}\sum_{n=1}^{\infty}\frac{\beta Sa_n - Tb_n}{\Delta(n)} \cdot \sinh(n\lambda_o)\cosh(n\lambda_o)\sin[n\pi\psi(x)]\right\}, \quad j = 0,1 \quad (2.40)$$

provided that

$$\frac{(1+\tau^2)^{3/2}}{\tau}\,\frac{d}{d\tau}\left\{(1+\tau^2)^{(j+1)/2}\left[\beta Sa_o - Tb_o - 2\beta^2\sum_{n=1}^{\infty}\frac{(-1)^n(\beta Sa_n - Tb_n)\cosh(n\lambda_o)}{\Delta(n)}\right]\right\} + 2jI_1 = 0, \quad j = 0,1 \quad (2.41)$$

Moreover, substitutions from (2.32) and (2.33) reduce the auxiliary condition (2.24) to

$$\int_k^1 \frac{u_1(y)\,dy}{1-y^2} = 0 \quad (2.42)$$

Then, from (2.40) and (A.19), we find that (2.42) becomes

$$\frac{d}{d\tau}\left\{(1+\tau^2)\sum_{n=1}^{\infty}\frac{(-1)^n(\beta Sa_n - Tb_n)\sinh^2(n\lambda_o)}{\Delta(n)}\right\} = 0 \quad (2.43)$$

We now discuss the solution. With u_j given explicitly by (2.40), $A_j(r)$ for $0<r<c$ with $j = 1,2$ is defined by (2.33). For $-c<r<0$, we use $A_j(r) = -(-1)^j A_j(-r)$. Then A_y is given by (2.20) and A_x by (2.17). Finally, the densities of the glide and climb arrays of dislocations B_x and B_y are found from (2.7) and (2.8). Equation (2.41) for $j = 1$ becomes an identity, but with $j = 0$ together with equation (2.43) provides the two conditions that determine the unknown parameters τ and k. The relationship of these parameters to a and b is found from (2.7a) by the substitutions $(x, s) = (b, c)$ and $(x, s) = (-a, -c)$ and use of (2.36) and (2.38). The result is

$$\frac{a}{L} = 1 - \frac{k^2\tau^2}{[1+(1-k^2)^{1/2}][1+(1+\tau^2)^{1/2}][(1-k^2)^{1/2}+(1+\tau^2)^{1/2}]} \quad (2.44)$$

$$\frac{b}{L} = \frac{L}{a}\left[1-k^2-\frac{k^2(2-k^2)}{k^2+\tau^2}\right] \quad (2.45)$$

It may be remarked that in the present problem k is always small in comparison to 1. Thus, $1-a/L$ is always small, and $1-b/L$ is small except when $\tau = 0(k)$.

We shall now express (2.41) for $j = 0$ and (2.43) in alternate forms. For this purpose we define the series (the quantities λ, λ_o and q are defined in the Appendix):

$$Q_1(w) = \sum_{n=-\infty}^{\infty}\frac{(-1)^n\sin(nw)}{\sinh(n\lambda_o)} = \frac{w}{\lambda_o} + 2\sum_{n=1}^{\infty}\frac{(-1)^n\sin(nw)}{\sinh(n\lambda_o)} \quad (2.46)$$

$$Q_2(w) = \sum_{n=-\infty}^{\infty}\frac{(-1)^n\cosh(n\lambda_o)\sin(nw)}{\sinh(n\lambda_o)\Delta(n)} \quad (2.47)$$

$$Q_3(w) = \sum_{n=-\infty}^{\infty}\frac{(-1)^n\cos(nw)}{\Delta(n)} \quad (2.48)$$

$$Q_4(w) = \sum_{n=-\infty}^{\infty}\frac{(-1)^n\sinh(n\lambda_o)\sin(nw)}{\Delta(n)} \quad (2.49)$$

$$Q_5(w) = \sum_{n=-\infty}^{\infty}\frac{(-1)^n\cosh(n\lambda_o)\cos(nw)}{\Delta(n)} \quad (2.50)$$

We begin by obtaining an alternate expression for a_o. In (A.6), set $x = 1$, note that $\psi(1) = 1$, and substitute for a_n from (A.9). The result is

$$a_o = 2\tau/(1+\tau^2) + \lambda q'(\tau)[(\lambda q/\lambda_o) - Q_1(\lambda q)] \quad (2.51)$$

We observe that

$$2\sum_{n=1}^{\infty}[(-1)^n a_n\cosh(n\lambda_o)/\Delta(n)] - \beta^{-2}a_0 = \lambda q'(\tau)[Q_2(\lambda q) - \lambda q/(\lambda_o\beta^2)] - \beta^{-2}\{2\tau/(1+\tau^2) + \lambda q'(\tau)[(\lambda q/\lambda_o) - Q_1(\lambda q)]\} = \lambda q'(\tau)[Q_1(\lambda q)/\beta^2 + Q_2(\lambda q)] - 2\beta^{-2}\tau/(1+\tau^2) \quad (2.52)$$

With b_n defined by (A.10), we note that

Downloaded 03 May 2010 to 171.66.16.21. Redistribution subject to ASME license or copyright; see http://www.asme.org/terms/Terms_Use.cfm

$$2\sum_{n=1}^{\infty}[(-1)^n b_n \cosh(n\lambda_o)/\Delta(n)] - \beta^{-2}b_0 = \lambda q'(\tau)Q_3(\lambda q) \tag{2.53}$$

Upon substitution from (2.52) and (2.53) into (2.41) with $j=0$ it follows that

$$\frac{d}{d\tau}\{\lambda(1+\tau^2)^{1/2}q'(\tau)[\beta S[Q_1(\lambda q)/\beta^2 + Q_2(\lambda q)] - TQ_3(\lambda q)] - 2\beta^{-2}(\beta S)\tau/(1+\tau^2)^{1/2}\} = 0 \tag{2.54}$$

Next, we observe that

$$2\sum_{n=1}^{\infty}[(-1)^n a_n \sinh^2(n\lambda_o)/\Delta(n)] = \lambda q'(\tau)Q_4(\lambda q) \tag{2.55}$$

and that

$$2\sum_{n=1}^{\infty}[(-1)^n b_n \sinh^2(n\lambda_o)/\Delta(n)] = 2\sum_{n=1}^{\infty}\{(-1)b_n[\Delta(n)+\beta^2\cosh^2(n\lambda_o)]/\Delta(n)\} = \beta^2\lambda q'(\tau)Q_5(\lambda q) + 2/(1+\tau^2) \tag{2.56}$$

where we have used (A.7) with $x=1$ to evaluate the series $2\sum_{n=1}^{\infty}(-1)^n b_n$. Upon substitution of (2.55) and (2.56) into (2.43), it follows also that

$$\frac{d}{d\tau}\{(1+\tau^2)q'(\tau)[\beta S Q_4(\lambda q) - \beta^2 T Q_5(\lambda q)]\} = 0 \tag{2.57}$$

The small k approximations for Q_1, Q_2, Q_3, Q_4 and Q_5 are given in the Appendix.

3 Physical Quantities

In this section we give expressions for a and b which determine the extent of the contact zones, the mode II stress intensity factors, and the large normal stresses outside the crack tips.

The equations (2.54) and (2.57) resulting from the auxiliary conditions are solved for k and τ by converting the slowly converging series in these equations to rapidly converging series. Since the method used is similar to that used in a previous paper (Gautesen and Dundurs, 1987b), we omit the details. We find that

$$k = 4\exp\left\{-[\pi/(2\beta_o)]\left[\frac{1}{2}\pi + \tan^{-1}(2\beta_o/\pi)\right]\right\} \tag{3.1}$$

where

$$\beta_o = \frac{1}{2}\log[(1+\beta)/(1-\beta)] \tag{3.2}$$

Thus, k is very small for $0 < \beta \leq \frac{1}{2}$, and (2.44) and (2.45) simplify to

$$a/L = 1 - \frac{1}{2}\{k\tau/[1+(1+\tau^2)^{1/2}]\}^2 \tag{3.3}$$

$$b/L = (L/a)[1 - k^2 - 2k^2/(k^2+\tau^2)] \tag{3.4}$$

Hence, we conclude that, for $\beta > 0$, the extent $L-a$ of the left contact zone is small for all τ, while the extent $L-b$ of the right contact zone is large only when $\tau = 0(k)$. It is found that τ satisfies the nonlinear equation

$$\frac{\tau}{k} = \sinh\left\{\frac{\pi}{2\beta_o}\left[\frac{\pi}{2} - \chi + \tan^{-1}\frac{2\beta_o(1+k^2/\tau^2)^{1/2}}{\pi}\right]\right\} + \frac{\exp(-\pi\chi/\beta_o)}{k\sinh[\pi\chi/(2\beta_o)]} \tag{3.5}$$

where χ is related to the applied shear and tension by

$$(\cos\chi, \sin\chi) = (T,S)/(T^2+S^2)^{1/2} \tag{3.6}$$

Equation (3.5) can be solved for τ/k by a Newton-Raphson iteration scheme. We note that for $(\tau/k) >> 1$, (3.5) becomes

$$\tau = \frac{1}{\sinh[\pi\chi/(2\beta_o)]} \tag{3.7}$$

while for $(\tau/k) = 0(1)$, (3.5) becomes

$$\frac{\tau}{k} = \sinh\left\{\frac{\pi}{2\beta_o}\left[\frac{\pi}{2} - \chi + \tan^{-1}\frac{2\beta_o(1+k^2/\tau^2)^{1/2}}{\pi}\right]\right\} \tag{3.8}$$

When (3.7) applies, $L-b$ is small, and when (3.8) applies $L-b$ is large. The transition from $L-b$ small to large occurs roughly when

$$\beta = \tanh\left[0.65\left(\frac{1}{2}\pi - \chi\right)\right] \tag{3.9}$$

The mode II stress intensity factors $K_2(\pm L)$ can be shown to be given by

$$L^{-1/2}K_2(\pm L) = S + \{2\beta\tau/[\pi(1+\tau^2)]\}[(1+\tau^2)^{1/2} \mp 1](I_{11} \pm I_{10} + J) \tag{3.10}$$

where

$$I_{jl} = \int_k^1 y^{-j}u_l(y)\,dy \tag{3.11}$$

$$J = \int_k^1 y(1-y^2)^{-1}u_1(y)\,dy \tag{3.12}$$

(see the paper by Comninou (1977) for the definition of K_2 for an interface crack with contact zones, and the asymptotic analysis which shows that the shear stresses are of the order $r^{-1/2}$ near the tips). The normal stress just beyond the crack tips is (it is finite, but for tension may be a very large multiple of T)

$$\sigma_{yy}(\pm L^{\pm}, 0) = T + \{2[(1+\tau^2)^{1/2} \mp 1]^2/[\pi(1+\tau^2)]\}(I_{20} \pm I_{21}) \tag{3.13}$$

After substitution from (2.40) for u_l in (3.11) and (3.12), the integrations are performed by using the identities found before (Gautesen and Dundurs, 1987a). The results are

$$I_{1j} = -\lambda L_j\left\{\sum_{n=1}^{\infty}[1-(-1)^n]f_n\right\} \tag{3.14}$$

$$I_{2j} = -\frac{2\lambda^2}{\pi k}L_j\left\{\sum_{n=1}^{\infty} n\tanh(n\lambda_o)f_n\right\} \tag{3.15}$$

$$J = -\lambda L_1\left\{\sum_{n=1}^{\infty}(-1)^n[1-\cosh(n\lambda_o)]f_n\right\} \tag{3.16}$$

where

$$\Delta(n)f_n = \beta S\coth(n\lambda_o)\sin[n\lambda q(\tau)] - T\cos[n\lambda q(\tau)] \tag{3.17}$$

$$L_j f = \frac{(1+\tau^2)^{3/2}}{\tau}\frac{d}{d\tau}\left\{\frac{(1+\tau^2)^{j/2}}{(k^2+\tau^2)^{1/2}}f\right\} \tag{3.18}$$

Accurate approximations for small k to the series in (3.14)-(3.16) can be obtained by the methods used before (Gautesen and Dundurs, 1987b). We omit the details.

4 Results and Conclusion

The results based on the derived expressions are shown graphically emphasizing the dependence on the composite parameter β. The curves are given for the five ratios $T/S = -0.4, -0.2, 0, 0.2$, and 0.4.

Downloaded 03 May 2010 to 171.66.16.21. Redistribution subject to ASME license or copyright; see http://www.asme.org/terms/Terms_Use.cfm

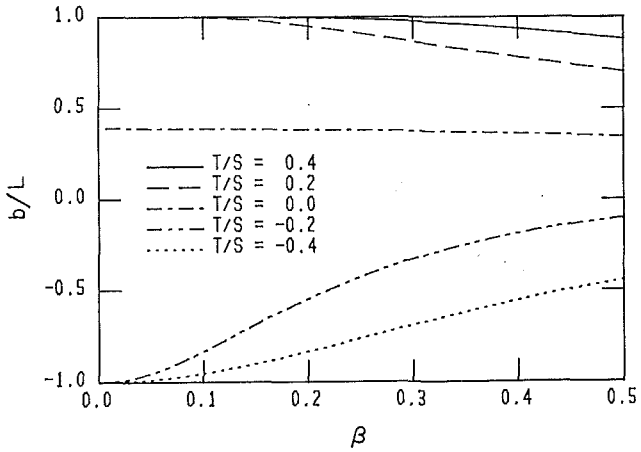


Fig. 2 Extent of the large contact zone

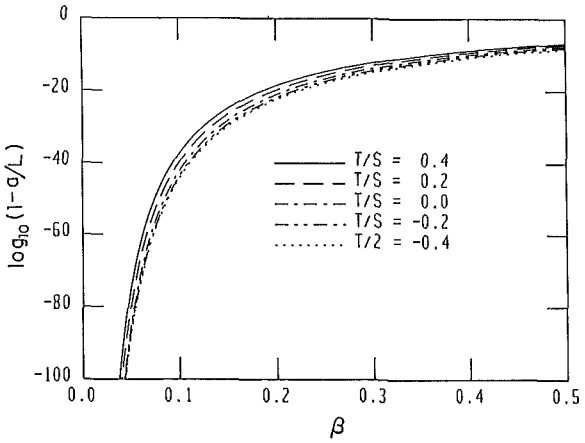


Fig. 3 Extent of the small contact zone

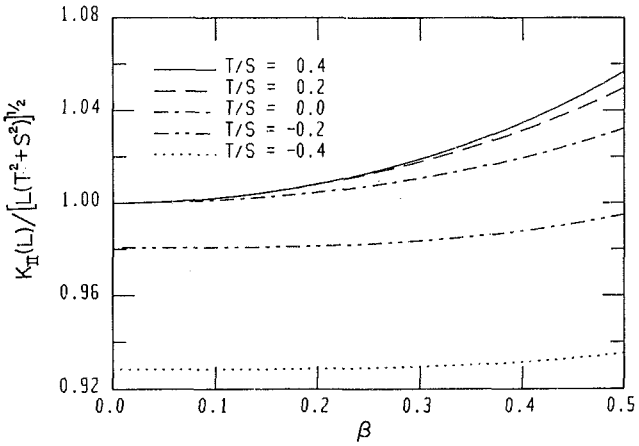


Fig. 4 Mode II stress intensity factor at the end with the large contact zone

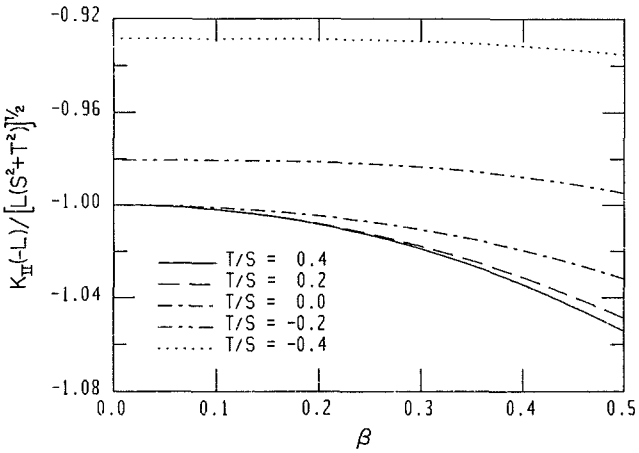


Fig. 5 Mode II stress intensity factor at the end with the small contact zone

The variation of b/L, which determines the extent of the large contact zone, is shown in Fig. 2 for $\beta > 0$. It is interesting to note that, depending on the sign of T/S, the extent of the large contact zone may increase or decrease with β, but that there is little variation for $T/S = 0$. For $\beta = 0.5$ and $T/S = 0$, Comninou (1978) found $b/L = 0.34$, whereas our value is 0.342 rounded to three digits. For $\beta = 0.41$, the corresponding values are 0.36 versus 0.345. Moreover, the results reported by Comninou and Schmueser (1979) in their Fig. 2 for $\beta = 0.5$ and nonzero values of T/S are in good agreement within plotting accuracy with the values in Fig. 2 of this paper.

The variation of the small contact zone with β is shown in Fig. 3. The only previously reported values are by Comninou (1978): $1 - a/L$ of order 10^{-7} for $\beta = 0.5$, and of order 10^{-9} for $\beta = 0.41$. We find 2.2×10^{-8} and 2.0×10^{-10}, respectively.

The variation with β of the mode II stress intensity factor $K_2(+L)$ at the tip with the large contact zone is shown in Fig. 4. It should be noted that the normalizing factor in the graph involves the quantity $(T^2 + S^2)^{1/2}$, and that within the range of the ratios T/S used, the values of the normalized stress intensity factor hover around 1. Comparison with the previously reported results by Comninou and Schmueser (1979) for $\beta = 0.5$ requires a rescaling because of the different normalizing factors used. When this is done, the comparison is just as favorable as for the extent of the large contact zone. Thus, the values of $K_2(+L)/L^{1/2}S$, as scaled from Fig. 3 in the Comninou-Schmueser paper are 1.01, 1.015, 1.03, 1.07 and 1.135 for $T/S = -0.4, -0.2, 0, 0.2, 0.4$, respectively, whereas we find 1.008, 1.015, 1.032, 1.071, 1.138.

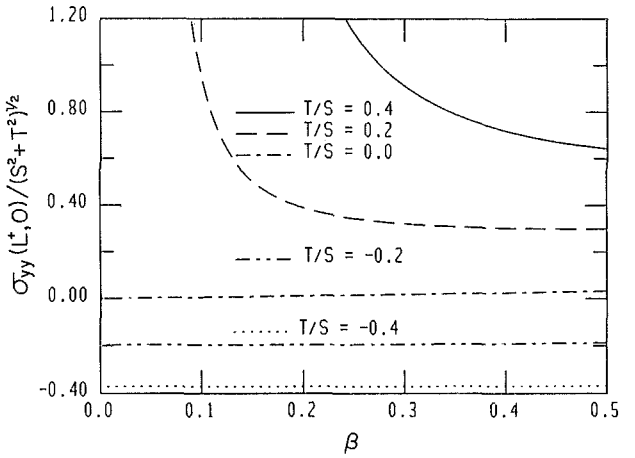


Fig. 6 Normal stress at the end with the large contact zone

Figure 5 shows the variation with β of the mode II stress intensity factor $K_2(-L)$ at the tip with the small contact zone. Comparison with the results given by Comninou and Schmueser (1979) for $\beta = 0.5$ using numerical integration now

Downloaded 03 May 2010 to 171.66.16.21. Redistribution subject to ASME license or copyright; see http://www.asme.org/terms/Terms_Use.cfm

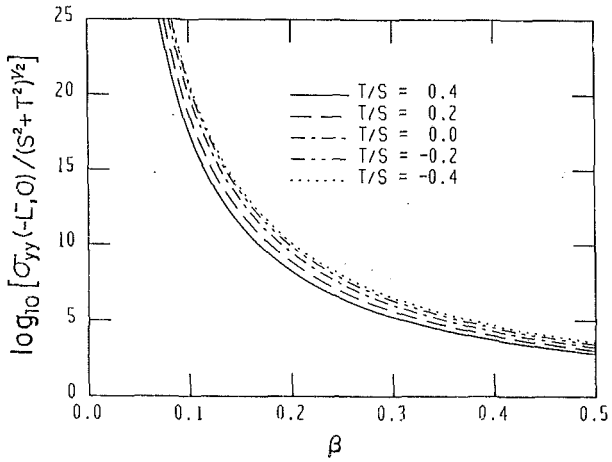


Fig. 7 Normal stress at the end with the small contact zone

is not at all favorable. The values of $K_2(-L)/SL^{1/2}$ scaled from Fig. 4 in the Comninou-Schmueser paper are -0.295, -0.355, -0.445, -0.60, and -0.785 for $T/S = -0.4$, -0.2, 0, 0.2, and 0.4, respectively. Adjusting for the different normalizing factor used, our corresponding values are -1.007, -1.015, -1.032, -1.070, and -1.136, indicating an entirely different trend.

Figures 6 and 7 show the finite normal stress just outside the crack tips. Except for the case $S=0$, which was discussed before (Gautesen and Dundurs, 1987b), no values with which our results could be compared have been reported in the literature.

Acknowledgement

This work of one of the authors (AKG) was supported in part by the Applied Mathematical Sciences subprogram of the Office of Energy Research, US Department of Energy, under Contract No. W-7405-ENG-82.

References

Comninou, M., 1977, "The Interface Crack," ASME JOURNAL OF APPLIED MECHANICS, Vol. 44, pp. 631–636.

Comninou, M., 1978, "The Interface Crack in a Shear Field," ASME JOURNAL OF APPLIED MECHANICS, Vol. 45, pp. 287–290.

Comninou, M., and Dundurs, J., 1980, "On the Behavior of Interface Cracks," *Res Mechanica*, Vol. 1, pp. 249–264.

Comninou, M., and Schmueser, D., 1979, "The Interface Crack in a Combined Tension-Compression and Shear Field," ASME JOURNAL OF APPLIED MECHANICS, Vol. 46, pp. 345–358.

England, A. H., 1965, "A Crack Between Dissimilar Media," ASME JOURNAL OF APPLIED MECHANICS, Vol. 32, pp. 400–402.

Gautesen, A. K., and Dundurs, J., 1987a, "On the Solution to a Cauchy Principal Value Integral Equation Which Arises in Fracture Mechanics," *SIAM Journal on Applied Mathematics*, Vol. 47, pp. 109–116.

Gautesen, A. K., and Dundurs, J., 1987b, "The Interface Crack in a Tension Field," ASME JOURNAL OF APPLIED MECHANICS, Vol. 54, pp. 93–98.

Malyshev, B. M., and Salganik, R. L., 1965, "The Strength of Adhesive Joints Using the Theory of Fracture," *International Journal of Fracture Mechanics*, Vol. 1, pp. 114–128.

Shield, R. T., 1982, "Uniqueness for Elastic Crack and Punch Problems," ASME JOURNAL OF APPLIED MECHANICS, Vol. 49, pp. 516–518.

APPENDIX

The Appendix presents (1) some generalized cosine series, (2) the solution to a certain integral equation, and (3) alternate expressions for certain series. All results follow from the previous work of Gautesen and Dundurs (1987a, 1987b).

Cosine Series

With $f(x) = -f(-x)$, we can write

$$f(x)=\left\{\frac{1}{2}\,c_o+\sum_{n=1}^{\infty}c_n\cos[n\pi\psi(x)]\right\}\operatorname{sgn}x,\quad x\epsilon E \tag{A.1}$$

where

$$c_n=2\int_k^1 f(x)\cos[n\pi\psi(x)](d\psi/dx)dx \tag{A.2}$$

$$\psi(x)=\frac{2\lambda}{\pi^2}F(x)=\frac{F(x)}{F(1)} \tag{A.3}$$

$$F(x)=\int_k^{|x|}[(1-s^2)(s^2-k^2)]^{-1/2}ds \tag{A.4}$$

$$\lambda=\pi^2/[2F(1)] \tag{A.5}$$

In particular, we have

$$\frac{\tau\operatorname{sgn}x}{\tau^2+x^2}=\left\{\frac{1}{2}\,a_o+\sum_{n=1}^{\infty}a_n\cos[n\pi\psi(x)]\right\}\operatorname{sgn}x,\quad x\epsilon E \tag{A.6}$$

$$\frac{x}{\tau^2+x^2}=\left\{\frac{1}{2}\,b_o+\sum_{n=1}^{\infty}b_n\cos[n\pi\psi(x)]\right\}\operatorname{sgn}x,\quad x\epsilon E \tag{A.7}$$

where

$$a_o=2\tau\int_k^1(\tau^2+x^2)^{-1}\psi'(x)dx \tag{A.8}$$

$$a_n=\lambda q'(\tau)\sin[n\lambda q(\tau)]/\sinh(n\lambda_o),\quad n=1,2,\ldots \tag{A.9}$$

$$b_n=\lambda q'(\tau)\cos[n\lambda q(\tau)]/\cosh(n\lambda_o),\quad n=0,1,\ldots \tag{A.10}$$

$$q(\tau)=\frac{2}{\pi}\int_o^{\tau}[(1+s^2)(k^2+s^2)]^{-1/2}ds \tag{A.11}$$

$$\lambda_o=\lambda\phi(k) \tag{A.12}$$

$$\phi(\tau)=\frac{2}{\pi}\int_o^{\tau}[(1-s^2)(k^2-s^2)]^{-1/2}ds \tag{A.13}$$

and a prime denotes differentiation of a function with respect to its argument.

Solution of an Integral Equation

The solution to the integral equation

$$\frac{1}{\pi}\int_E\frac{u(x)}{x-y}[1-\beta^2\operatorname{sgn}(xy)]dy$$

$$=\left\{\frac{1}{2}\,c_o+\sum_{n=1}^{\infty}c_n\cos[n\pi\psi(x)]\right\}\operatorname{sgn}x,\quad x\epsilon E \tag{A.14}$$

satisfying

$$u(\pm1)=u(\pm k)=0 \tag{A.15}$$

is

$$u(x)=-\sum_{n=1}^{\infty}\{c_n\sinh(n\lambda_o)\cosh(n\lambda_o)\sin[n\pi\psi(x)]/\Delta(n)\} \tag{A.16}$$

provided that

$$c_o-2\beta^2\sum_{n=1}^{\infty}[(-1)^n c_n\cosh(n\lambda_o)/\Delta(n)]=0 \tag{A.17}$$

where

$$\Delta(n)=\sinh^2(n\lambda_o)-\beta^2\cosh^2(n\lambda_o) \tag{A.18}$$

Also, we have

$$\int_k^1\frac{u(x)dx}{1-x^2}=\frac{\pi}{2}\sum_{n=1}^{\infty}[(-1)^n c_n\sinh^2(n\lambda_o)/\Delta(n)] \tag{A.19}$$

Downloaded 03 May 2010 to 171.66.16.21. Redistribution subject to ASME license or copyright; see http://www.asme.org/terms/Terms_Use.cfm

Series Approximations

We now give small k approximations to the series $Q_j(w)$ defined by (2.46)–(2.50). For $|w| < \pi$, all approximations are accurate to $0(k^4)$. These approximations are

$$Q_1(w) = \frac{\pi}{\lambda_o}\{R^+(w) - R^+(-w)\} \tag{A.20}$$

$$Q_2(w) = -\frac{\pi}{\beta^2\lambda_o}\{\csc(\alpha\pi)\sin(\alpha w) - \{1-\cos[\alpha(\pi-w)]\}R^-(w) + \{1-\cos[\alpha(\pi+w)]\}R^-(-w)\} \tag{A.21}$$

$$Q_3(w) = -\frac{\pi}{\beta\lambda_o}\{\csc(\alpha\pi)\cos(\alpha w) + \sin[\alpha(\pi-w)]R^-(w) + \sin[\alpha(\pi+w)]R^-(-w)\} \tag{A.22}$$

$$Q_4(w) = -\frac{\pi}{\lambda_o(1-\beta^2)^{1/2}}\{\csc(\alpha\pi)\sin(\alpha w) - \cos[\alpha(\pi-w)]R^+(w) + \cos[\alpha(\pi+w)]R^+(-w)\} \tag{A.23}$$

$$Q_5(w) = -\frac{\pi}{\beta\lambda_o(1-\beta^2)^{1/2}}\{\csc(\alpha\pi)\cos(\alpha w) - \sin[\alpha(\pi-w)]R^+(w) - \sin[\alpha(\pi+w)]R^+(-w)\} \tag{A.24}$$

with

$$R^{\pm}(w) = \frac{2\exp[-\pi(\pi-w)/\lambda_o]}{1\pm\exp[-\pi(\pi-w)/\lambda_o]} \tag{A.25}$$

where β_o is given by (3.2) and $\alpha = \beta_o/\lambda$.

Downloaded 03 May 2010 to 171.66.16.21. Redistribution subject to ASME license or copyright; see http://www.asme.org/terms/Terms_Use.cfm

Initiation, Propagation, and Kinking of an In-Plane Crack

Chien-Ching Ma
Associate Professor.
Department of Mechanical Engineering,
National Taiwan University,
Taipei, Taiwan 10764, Republic of China

Consider an infinite linear elastic body containing a semi-infinite crack loaded by a longitudinal stress pulse parallel to the crack face. After the stress wave strikes the crack at time $t = 0$, *the stress gradually intensifies at the crack tip. At some finite delay time* t_f, *the crack begins to extend straight ahead with constant speed* v_o. *At some later time* t_b, *the crack suddenly stops, then kinks and propagates with constant speed* v_c, *making an angle* δ *with the original crack. The exact full field solution of the propagating crack is constructed by using a superposition of fundamental solutions for a particular class of problems. When the crack suddenly stops, the stress field for a stationary crack with the new crack length is radiated out from the stopped crack tip. The dynamic stress intensity factor at the kinked crack tip can then be obtained by using a perturbation method.*

Introduction

In this section, the main developments in the theory of elastodynamic crack growth analysis are reviewed and the work herein is motivated. Since Yoffe (1951) mathematically determined the stress field around the tip of a steadily moving crack of constant length, considerable progress has been made in the areas of theoretical and numerical stress analysis for dynamic brittle fracture. A first step in removing the restriction to constant crack tip speed in dynamic crack growth analysis was made by Kostrov (1966) who studied the growth of a mode III crack at arbitrary speed by using a special analytical technique. Some of the objectives to steady-state crack propagation analysis were overcome by Broberg (1960) and Baker (1962) who were among the first to present detailed analyses of crack propagation as a transient process. The paper by Baker, although limited in its application, has results which turn out to have far more applicability than originally realized. In a series of papers, Freund (1972a, 1972b, 1973, 1974) developed important analytical methods for evaluation of the transient stress field and dynamic stress intensity factor of a crack in a two-dimensional geometric configuration under quite general dynamic loading. For a semi-infinite crack growth in an otherwise unbounded body, it was found that the stress intensity factor has the form of a universal function of instantaneous crack tip speed times the stress intensity factor for a stationary crack of fixed length, equal to the instantaneous length of the actual crack subjected to the same loading, whether the loading is time-independent or time-dependent. In deriving this result, Freund also showed that if the crack stops instantaneously, a normal stress distribution is radiated out along the fracture plane ahead of the stopped crack at the shear wave speed and is exactly the stress distribution that would have resulted had the crack tip been at the new crack tip position for all time. In other words, it is the stress distribution appropriate for the given incident wave and the new crack length, and it is completely independent of the fact that the crack tip had been in motion. From the linear elastic point of view, very little has followed which is of fundamental importance except for work that has expanded on Freund's work. That is, many of the details of what occurs around the crack tip were not fully explored by Freund and only now are these being understood.

When dynamic loading is applied to a body with an internal crack, the resulting stress waves may cause the initiation of crack growth and continued crack propagation. A frequently observed fracture event is the kinking or bifurcation of an initially straight crack. The direction of propagation, as well as the velocity of crack propagation, will depend on the local stress field around the crack tip. To understand the observed bifurcation events in brittle materials, the dynamic solution for cracks which suddenly branch or kink is required. It is only recently that correct solutions for the problem in which a crack kinks (or bifurcates) have been given. Burgers and Dempsey (1982) gave some closed form results in antiplane strain and Burgers (1982) extended the range of these antiplane results to all angles of kinking (and bifurcation) using a numerical scheme. Dempsey et al. (1982) have used a comformal mapping technique to obtain the analytical solution for a kinking crack in mode III under stress wave loading. The solutions of Burgers and Dempsey (1982) and Dempsey et al. (1982) verified the numerical method being applied by Burgers (1982). This method has been used by Burgers (1983) and Burgers and Dempsey (1984) to provide numerical solutions to the plane strain crack kinking and bifurcation problems. The approximate method for both mode III and mixed mode I–II crack kinking under stress-wave loading was used by Achenbach et al. (1984). All the results mentioned above have been

Contributed by the Applied Mechanics Division for publication in the JOURNAL OF APPLIED MECHANICS.
Discussion on this paper should be addressed to the Editorial Department, ASME, United Engineering Center, 345 East 47th Street, New York, N.Y. 10017, and will be accepted until two months after final publication of the paper itself in the JOURNAL OF APPLIED MECHANICS. Manuscript received by ASME Applied Mechanics Division, November 16, 1987; final revision, February 11, 1988.

Copyright © 1988 by ASME
Downloaded 03 May 2010 to 171.66.16.21. Redistribution subject to ASME license or copyright; see http://www.asme.org/terms/Terms_Use.cfm

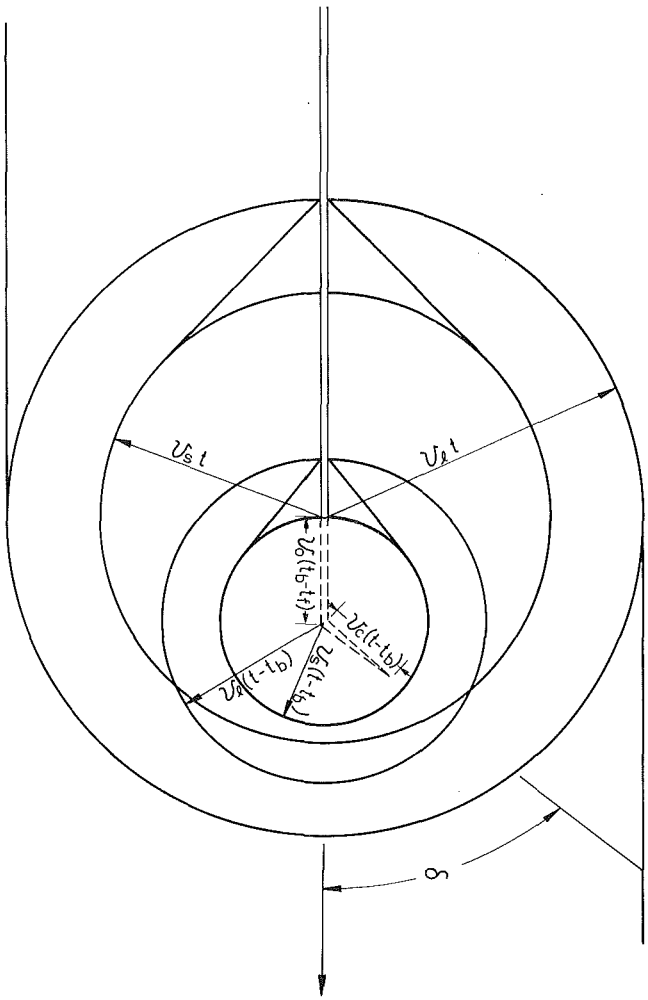


Fig. 1 Stress wave pattern for mode I stress wave loading of a crack which propagates straight at time t_f and kinks at time t_b

restricted to being self-similar in the radial coordinate and time. It is assumed that the new crack initiates out of the original crack tip at an angle at the instant the loading was applied. This gave the problem the property of self-similarity and greatly simplified it. To make the model more physically realistic, a finite delay time in the initiation of the non-planar crack was considered by Ma and Burgers (1986, 1987) in mode III and mixed mode I–II crack kinking.

The experimental observation by Ravi-Chandar and Knauss (1984) for crack face loading and Ravi-Chandran (1986) for stress wave loading in mode I, all indicate that the crack will most likely grow straight ahead from the original crack for some time before it kinks or bifurcates. To simulate the real physical response theoretically, the kinking event can be thought of as the rapidly propagating crack suddenly stopping and then kinking. The full stress field due to the sudden stopping must first be worked out and this is an important analytical step in developing a criterion for kinking of a rapidly propagating crack. Ma and Burgers (1988) analyzed the mode III case and found that when the crack suddenly stops, the full stress field which is radiated out with the shear wave speed from the stopped crack tip corresponds to the stationary crack stress field of a crack whose crack tip has been at the stopped crack position for all time. The same conclusion was arrived at by Eshelby (1969) much earlier, but the method Eshelby used could not be generalized to plane strain problems. We consider a stationary semi-infinite crack in an infinite body which is subjected to stress wave loading. The stress wave front is parallel to the crack faces and reaches the crack line at time $t=0$. To model the actual problem reasonably accurately, we assume the crack start to propagate straight after some time t_f with a constant speed. At some later time t_b, the crack stops instantaneously and kinks. The pattern of wavefronts is shown in Fig. 1. The analytical solution method used in the antiplane strain (Ma and Burgers, 1988) is briefly applied here to the plane strain problem, which permits some features of the stopping crack that were not explored by Freund to be investigated.

Required Fundamental Solutions

It is necessary to account for material inertia effects in the analysis of dynamic loading and rapid crack growth in solids. In a stationary $x-z$ coordinate system, a homogeneous, isotropic linearly elastic medium is governed by the two-dimensional wave equations

$$\frac{\partial^2\Phi}{\partial x^2}+\frac{\partial^2\Phi}{\partial z^2}=a^2\frac{\partial^2\Phi}{\partial t^2}, \tag{1.1}$$

$$\frac{\partial^2\psi}{\partial x^2}+\frac{\partial^2\psi}{\partial z^2}=b^2\frac{\partial^2\psi}{\partial t^2}, \tag{1.2}$$

where

$$a=\sqrt{\frac{\rho}{\lambda+2\mu}}=\frac{1}{v_l}, \qquad b=\sqrt{\frac{\rho}{\mu}}=\frac{1}{v_s}.$$

Equations (1.1) and (1.2) are the uncoupled wave equations, Φ and ψ are referred to as the longitudinal and shear wave potentials, a and b are the slownesses of longitudinal and shear waves respectively, μ and ρ are the shear modulus and the mass density of the material, and λ is the Lame elastic constant. The displacements are derived from the potentials according to

$$u=\Phi_{,x}-\psi_{,z} \qquad w=\Phi_{,z}+\psi_{,x} \tag{1.3}$$

where u and w are the displacements in the x and z directions. The stresses can be written in terms of the potentials by means of Hooke's law.

We first consider a normal pressure of magnitude σ_0 applied uniformly on the crack faces of the stationary crack. The deformation will occur in mode I. Since there is symmetry with respect to the plane $z=0$, the problem can be viewed as a half-plane problem with the material occupying the region $z \geq 0$, subject to the mixed boundary conditions on $z=0$.

$$\begin{aligned}
&\sigma_{zz}(x,0,t)=-\sigma_0 H(t) && \text{for } -\infty<x<0,\\
&\sigma_{xz}(x,0,t)=0 && \text{for } -\infty<x<\infty,\\
&w(x,0,t)=0 && \text{for } 0<x<\infty,
\end{aligned} \tag{1.4}$$

where H represents the unit step function. The formulation is completed by specifying zero initial data. The details of the plane strain problem of diffraction of a pulse by a stationary crack have been presented by de Hoop (1958), and only the pertinent results of the full field solutions for stresses for $\theta < \pi/2$ are presented:

$$\frac{\sigma^s_{zz}}{A}(r,\theta,t)=\int_{ar}^{t} Im\left[\frac{(2\lambda^2-b^2)^2\Phi(s)}{\lambda(a+\lambda)^{1/2}}\right]_{\lambda=\lambda_L} ds$$

$$+\int_{br}^{t} Im\,[4\lambda(a-\lambda)^{1/2}(b^2-\lambda^2)^{1/2}\Phi(s)]_{\lambda=\lambda_T} ds,$$

$$\frac{\sigma^s_{xz}}{A}(r,\theta,t)=\int_{ar}^{t} Im\,[2(2\lambda^2-b^2)\,(a-\lambda)^{1/2}\Phi(s)]_{\lambda=\lambda_L} ds$$

$$-\int_{br}^{t} Im\,[2(2\lambda^2-b^2)\,(a-\lambda)^{1/2}\Phi(s)]_{\lambda=\lambda_T} ds, \tag{1.5}$$

Downloaded 03 May 2010 to 171.66.16.21. Redistribution subject to ASME license or copyright; see http://www.asme.org/terms/Terms_Use.cfm

$$\frac{\sigma^s_{xx}}{A}(r,\theta,t)=$$

$$-\int_{ar}^{t} Im\left[\frac{(2\lambda^2-b^2)\,(2\lambda^2+b^2-2a^2)\,\Phi(s)}{\lambda(a+\lambda)^{1/2}}\right]_{\lambda=\lambda_L} ds$$

$$-\int_{br}^{t} Im\,[4\lambda(a-\lambda)^{1/2}(b^2-\lambda^2)^{1/2}\;\;\Phi(s)]_{\lambda=\lambda_T} ds,$$

where

$$A=\frac{\sigma_0\sqrt{a}}{\pi\, ckS^0_+(0)},\quad k=2(b^2-a^2),$$

$$\lambda_L(s)=-\frac{s}{r}\cos\theta+i\left(\frac{s^2}{r^2}-a^2\right)^{1/2}\sin\theta,$$

$$\lambda_T(s)=-\frac{s}{r}\cos\theta+i\left(\frac{s^2}{r^2}-b^2\right)^{1/2}\sin\theta,$$

$$S^0_{\pm}(\lambda)=\exp\left\{-\frac{1}{\pi}\int_a^b \tan^{-1}\left(\frac{4y^2(y^2-a^2)^{1/2}\,(b^2-y^2)^{1/2}}{(b^2-2y^2)^2}\right)\frac{dy}{y\pm\lambda}\right\},\qquad(1.6)$$

$$\Phi(s)=\frac{\partial\lambda/\partial s}{(\lambda-c)S^o(\lambda)}.$$

$c=1/v_R$ is the slowness of Rayleigh wave of the material and satisfies the equation

$$(2c^2-b^2)^2+4c^2(a^2-c^2)^{1/2}(b^2-c^2)^{1/2}=0.$$

The stress field near the crack tip is obtained by taking the limit $r\to 0$ on equation (1.5). The first two terms for the stresses are (Ma and Burgers, 1987)

$$\sigma^s_{zz}\approx\frac{2}{\pi}\sigma_0\omega_0\left(\frac{t}{r}\right)^{1/2}\cos\frac{\theta}{2}\left(1+\sin\frac{\theta}{2}\sin\frac{3\theta}{2}\right)-\sigma_0+o(1),$$

$$\sigma^s_{xz}\approx\frac{2}{\pi}\sigma_0\omega_0\left(\frac{t}{r}\right)^{1/2}\cos\frac{\theta}{2}\sin\frac{\theta}{2}\cos\frac{3\theta}{2}+o(1),\qquad(1.7)$$

$$\sigma^s_{xx}\approx\frac{2}{\pi}\sigma_0\omega_0\left(\frac{t}{r}\right)^{1/2}\cos\frac{\theta}{2}\left(1-\sin\frac{\theta}{2}\sin\frac{3\theta}{2}\right)-\sigma_0C_{xx}+o(1),$$

where

$$\omega_0=\frac{\sqrt{a}}{c\,S^0_+(0)}=\frac{\sqrt{2a(b^2-a^2)}}{b^2},$$

$$C_{xx}=\frac{b^2-2a^2}{b^2}+\frac{\sqrt{a}(2c^2-b^2)}{c^2S^0_+(0)S^0_-(c)(a+c)}.$$

The first term shows the square root singularity in stress and is called the stress intensity factor controlled field.

In the study of dynamic crack growth phenomena, it is very important to have available as complete a description of the prevailing mechanical fields as possible. Interest in the stress intensity factor in considering dynamic crack growth stems from its potential as a driving force for the fracture process. From the experimental point of view, measurements of the field quantities near the crack tip are used to obtain the stress intensity factor, such as in the paper of Ravi-Chandar and Knauss (1984) where the shadow spot method is used. The shadow spot technique gives very accurate measurements of the stress intensity factor as a function of time but is subject to some limitations. Interpretation of the stress field near the edge of a crack in a loaded body in terms of a stress intensity factor magnitude is usually based on the assumption that a stress intensity factor controlled field does indeed exist and that the size of the region over which the material response is inelastic, which is sufficiently small compared to the size of the region over which the stress intensity controlled field exists, is negligible. On the other hand, the shadow spot method measures the influence of the crack tip deformation field on a parallel light field and that the crack tip deformation is measured a finite distance from the crack tip. The location of the measurements for the shadow spot method are normally on the order of millimeters away from the crack tip. Furthermore, the experimental data and field observations are interpreted as though the crack tip stress intensity factor field is fully established over this entire region. Whether or not the data obtained from the experimental observations are within the stress intensity controlled field is important in the determination of the correct stress intensity factor.

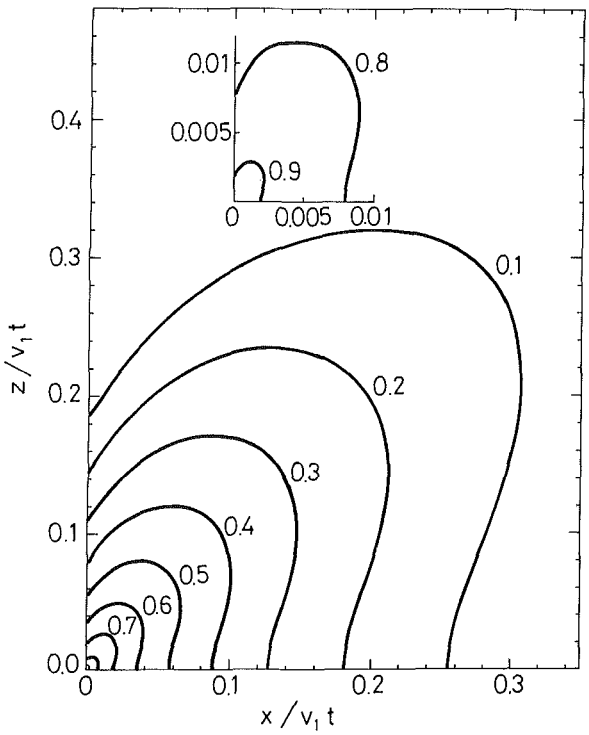


Fig. 2 The ratio of σ^s_{zz} for the exact solution and the stress intensity factor controlled field due to uniform loading on the crack faces

In order to investigate the region where the stress intensity factor controlled field is valid for the stationary crack, a comparison is made between the singular part of the stress field and the complete stress field near the crack tip. The ratio of the stress σ^s_{zz} evaluated from the actual stress (1.5) to the corresponding stress calculated from the stress intensity controlled field (1.7) has been computed numerically for Poisson's ratio $\nu = .25$ (i.e., $b=\sqrt{3}a$ and $c=1.8839\,a$) and is plotted in Fig. 2. If we accept that for a ratio up of 0.9, the actual stress is accurately described by the stress intensity factor controlled field. Then, the region of the stress intensity factor controlled field will be valid only for points close to the crack tip, within a distance from the crack of 0.2 percent of the distance to the cylindrical longitudinal wave front. If we plot the ratio in the x-z plane, the ratio curve will move out as time increases. Hence, if we fix a material point, the ratio of actual stress and stress calculated from the stress intensity factor field

Downloaded 03 May 2010 to 171.66.16.21. Redistribution subject to ASME license or copyright; see http://www.asme.org/terms/Terms_Use.cfm

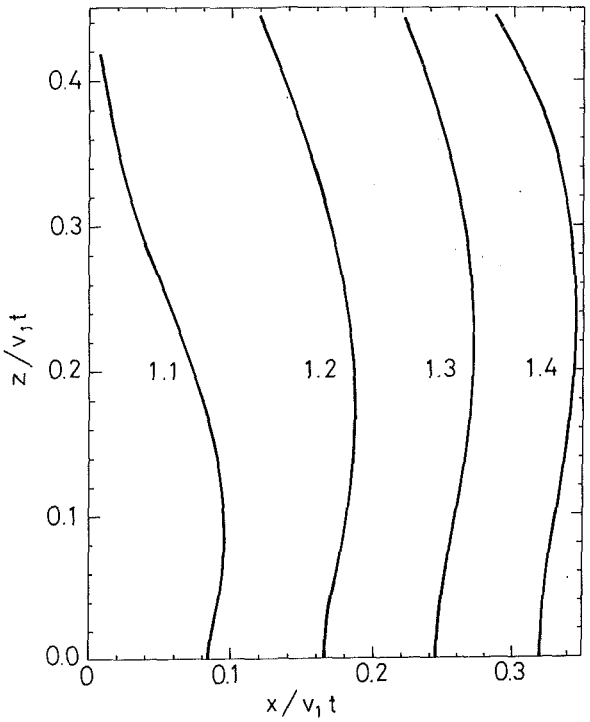


Fig. 3 The ratio of σ_{zz}^s for the exact solution and the stress intensity factor controlled field due to stress wave loading

will increase as time increases. After some finite time, this ratio will reach 0.9 and this material point will be inside the stress intensity factor field. Hence, the stress intensity factor field needs time to build up over a region of given size near the tip in the highly transient process. For an incident stress wave loading, we assume that a ratio of 1.1 defines the region where the stress intensity factor controlled field is suitably accurate. It is found that this region will be up to 8 percent of the distance to longitudinal wave front in the x-direction as shown in Fig. 3. It appears from the result that the time required for the singular stress field to become a good estimate of the actual stress is quite large. Hence, the use of a singular term to represent the actual stress field should be carefully considered, especially in the early stage of the dynamic transient field.

In the case of dynamic loading of a stationary crack, the ability to find K-controlled field over a region near the crack tip may hinge only on waiting for the wavefronts to pass and the transients to die away. In the case of dynamic crack growth, however, the transients are being continuously refreshed. The internal stress in the body at a point on the prospective fracture plane gradually builds up as crack tip approaches. This gradually accumulated stress is then suddenly released with the passage of the crack tip, and the resulting transient fields must radiate out continuously through the region surrounding the crack tip. The limitations on the assumption that the stress intensity factor field is fully established over a region of given size near the tip of a growing crack has been studied by Ma and Freund (1986). They have shown that the difference between the asymptotic field and the actual field along the crack line can be substantial for a significant time after crack initiation.

In order for the crack to extend at constant speed v_0 for $t > t_f$ in the direction of the fracture plane, the crack must negate the traction distribution of the stress σ_{zz}^s on $\theta = 0$

$$(\sigma_{zz}^s)_0 = \sigma_{zz}^s(\theta=0) = -\frac{\sigma_0\omega_0}{\pi}\int_a^{t/x} Im\left(\frac{1}{\eta\,\omega_+^0(-\eta)}\right)d\eta, \qquad (1.8)$$

where

$$\omega_+^0(\lambda) = \frac{(a+\lambda)^{1/2}}{(\lambda+c)\,S_+^0(\lambda)},$$

$$\omega_0 = \omega_+^0(0) = \frac{\sqrt{a}}{c\,S_+^0(0)}.$$

The stress distribution (1.8) varies with position and time only through the ratio t/x. This implies that any fixed stress level radiates out along the x-axis at the constant speed $u = x/t$. The solutions of stresses for constant speed crack propagation can be obtained by determining the elastic field for a concentrated force appearing through the moving crack tip, and then building up the general stress distribution (1.8) by superposition. It was shown by Freund (1973) that the concentrated force element needed to construct the solution can be expressed by the following boundary conditions,

$$\begin{aligned}
&\sigma_{zz}^F(x,0,t) = (mt+n)\delta(x-ut)H(t), \quad \text{for} -\infty < x < v_0 t,\\
&\sigma_{xz}^F(x,0,t) = 0, \quad \text{for} -\infty < x < \infty,\\
&w^F(x,0,t) = 0, \quad \text{for } v_0 t < x < \infty,
\end{aligned} \qquad (1.9)$$

where δ is the Dirac delta function, and m and n are arbitrary constants. The crack tip is at rest at $x=0$ and there are no loads acting on the body for $t<0$. At time $t=0$, the crack tip begins to move in the x-direction with speed v_0 and simultaneously a symmetric pair of concentrated normal forces appears at the crack tip with magnitude n and moves in the x-direction with speed $u < v_0$. The amplitude of the forces increases linearly in time. The x-coordinate is eliminated in favor of the coordinate $\xi = x - v_0 t$, so that the ξ, z-coordinate system moves with the origin at the crack tip. The complete transformed solution of (1.9) is found by means of Laplace transforms and the Wiener-Hopf technique. The exact transient solution can then be found by inverting the Laplace transforms by de Hoop's method. The full field solution can be expressed as follows (Freund, 1973):

$$\sigma_{zz}^F = \sigma_{zz}^{F_1} + \sigma_{zz}^{F_2} \qquad (1.10)$$

where for F_1, $m=0$, $n=1$, and for F_2, $m=1$, $n=0$.

$$\sigma_{zz}^{F_1} = -\frac{h\,\omega_+(h)}{\pi\,k_d}$$

$$\left\{ Im\left(\frac{(\lambda^2-\beta^2)^2\,\dfrac{\partial\lambda}{\partial t}}{\alpha_+(\lambda-c_1)(\lambda-d)^2 S_-(\lambda)(h-\lambda)} \right)_{\lambda=\lambda_{L+}} \right.$$

$$\left. + Im\left(\frac{4\lambda^2\alpha\,\beta\,\dfrac{\partial\lambda}{\partial t}}{\alpha_+(\lambda-c_1)(\lambda-d)^2 S_-(\lambda)(h-\lambda)} \right)_{\lambda=\lambda_{S+}} \right\}, \qquad (1.11)$$

$$\sigma_{zz}^{F_2} = -\frac{h^2}{\pi k_d}$$

$$\left\{ \int_{t_l}^{t} Im\left(\frac{(\lambda^2-\beta^2)^2\,\dfrac{\partial\lambda}{\partial\eta}}{\alpha_+(\lambda-c_1)(\lambda-d)^2 S_-(\lambda)} \left(\frac{\omega_+(h)}{\lambda-h}\right)_h \right)_{\lambda=\lambda_{L+}} d\eta \right.$$

$$\left. + \int_{t_s}^{t} Im\left(\frac{4\lambda^2\alpha\,\beta\,\dfrac{\partial\lambda}{\partial\eta}}{\alpha_+(\lambda-c_1)(\lambda-d)^2 S_-(\lambda)} \left(\frac{\omega_+(h)}{\lambda-h}\right)_h \right)_{\lambda=\lambda_{S+}} d\eta \right\}, \qquad (1.12)$$

where

Downloaded 03 May 2010 to 171.66.16.21. Redistribution subject to ASME license or copyright; see http://www.asme.org/terms/Terms_Use.cfm

$$\lambda_L+=\frac{-(\xi t+\frac{a^2}{d}z^2)+iz\{t^2-a^2[\left(\xi+\frac{t}{d}\right)^2+z^2]\}^{1/2}}{\xi^2+\left(1-\frac{a^2}{d^2}\right)z^2},$$

$$\lambda_S+=\frac{-(\xi t+\frac{b^2}{d}z^2)+iz\{t^2-b^2[\left(\xi+\frac{t}{d}\right)^2+z^2]\}^{1/2}}{\xi^2+\left(1-\frac{b^2}{d^2}\right)z^2},$$

$$k_d=4\left(1-\frac{a^2}{d^2}\right)^{1/2}\left(1-\frac{b^2}{d^2}\right)^{1/2}-\left(2-\frac{b^2}{d^2}\right)^2$$

$$t_l=\frac{a\left\{\frac{a}{d}\xi+[\xi^2+\left(1-\frac{a^2}{d^2}\right)z^2]^{1/2}\right\}}{\left(1-\frac{a^2}{d^2}\right)},$$

$$t_S=\frac{b\left\{\frac{b}{d}\xi+[\xi^2+\left(1-\frac{b^2}{d^2}\right)z^2]^{1/2}\right\}}{\left(1-\frac{b^2}{d^2}\right)},$$

$$S_\pm(\lambda)=\exp\left\{-\frac{1}{\pi}\int_{a_{2,1}}^{b_{2,1}}\tan^{-1}\left(\frac{4\eta^2|\alpha||\beta|}{(2\eta^2-b^2-b^2\eta^2/d^2\mp 2b^2\eta/d)^2}\right)\frac{d\eta}{\eta\pm\lambda}\right\},$$

$$\alpha(\lambda)=(a^2-\lambda^2+a^2\lambda^2/d^2-2a^2\lambda/d)^{1/2},$$

$$\beta(\lambda)=(b^2-\lambda^2+b^2\lambda^2/d^2-2b^2\lambda/d)^{1/2},$$

$$\alpha_\pm=[a\pm\lambda\,(1\mp a/d)]^{1/2},$$

$$\omega_+(\lambda)=\frac{\alpha_+(\lambda)}{(\lambda+c_2)\,S_+(\lambda)},$$

$$a_2=\frac{a}{1-a/d},\quad b_2=\frac{b}{1-b/d},\quad c_2=\frac{c}{1-c/d}.$$

The parameter $d=1/v_0$ is the slowness of the crack velocity. The parameter $h=1/(v_0-u)$ is the inverse of the relative speed between the moving load and the crack tip, the subscript h denotes differentiation with respect to h. The above solution will be referred to as the fundamental solution.

The Stress Field Solution for the Propagating Crack

Using the superposition scheme described by Freund (1973) the full field solution for the stress around the propagating crack tip due to the loading from the diffraction of the stationary crack field [i.e., $-(\sigma_{zz}^s)_0$] on the new crack faces, can be constructed by choosing $m=-1$, $n=-t^*=-ht_f/d$, replacing t by $t-t^*$ and $\xi=x-v_0t$ by $\xi=x-v_0(t-t_f)$ in (1.10) and integrating over the appropriate range of $u=x/t$. The range of u for which the stresses due to the longitudinal wave of the force element in (1.10) will reach the point (ξ, z) after the crack tip begins to move at $t=t_f$ with speed v_0, is the range of x/t between $x=0$, $t=t_f$ and $x=x^*$, $t=t_f+x^*d$, where x^* is the distance the crack has propagated along the crack line from which a longitudinal wave, emitted at the instant the crack tip reaches x^*, will just reach the point at (ξ,z). This means that $x^*=v_0(t-t_f)-v_0t_l$ and

$$\sigma_{zz}^c=\int_0^{u_l^*}(\sigma_{zz}^{F1}+\sigma_{zz}^{F2})_l\,(m=-1,\ n=-t^*,\ t-t^*)(\sigma_{zz}^s)_0\left(\frac{1}{u}\right)du \tag{1.13}$$

$$+\int_0^{u_S^*}(\sigma_{zz}^{F1}+\sigma_{zz}^{F2})_s\,(m=-1,\ n=-t^*,\ t-t^*)\,(\sigma_{zz}^s)_0\left(\frac{1}{u}\right)du,$$

where

$$u_l^*=\frac{v_0(t-t_f)-v_0t_l}{t-t_l},\quad u_s^*=\frac{v_0(t-t_f)-v_0t_s}{t-t_s}$$

$(\sigma_{zz}^{F1}+\sigma_{zz}^{F2})_l$ denotes the stress of the longitudinal wave part and is the sum of the first term of σ_{zz}^{F1} and σ_{zz}^{F2} in (1.11) and (1.12), while $(\sigma_{zz}^{F1}+\sigma_{zz}^{F2})_s$ is the shear wave part.

Since the complicated functions are written as functions of h, it is advantageous to replace the variable of integration by h. The range of integration on h is $d<h<h_l^*$ and $d<h<h_s^*$. Then

$$\sigma_{zz}^c=\int_d^{h_l^*}\frac{1}{\pi k_d}\left\{\int_{t_l}^{t-t^*}Im\left(\frac{(\lambda^2-\beta^2)^2\frac{\partial\lambda}{\partial\eta}\omega_+(h)}{\alpha_+(\lambda-c_1)\,(\lambda-d)^2\,S_-(\lambda)\,(\lambda-h)}\right)_{\lambda=\lambda_L+}d\eta\right\}_h(\sigma_{zz}^s)_0(h)dh$$

$$+\int_d^{h_S^*}\frac{1}{\pi k_d}\left\{\int_{t_s}^{t-t^*}Im\left(\frac{4\lambda^2\alpha\beta\,\omega_+(h)\frac{\partial\lambda}{\partial\eta}}{\alpha_+(\lambda-c_1)\,(\lambda-d)^2\,S_-(\lambda)\,(\lambda-h)}\right)_{\lambda=\lambda_S+}d\eta\right\}_h$$

$$(\sigma_{zz}^s)_0(h)dh \tag{1.14}$$

where

$$h_l^*=\frac{(t-t_l)d}{t_f},\quad h_s^*=\frac{(t-t_s)d}{t_f}.$$

The integral in (1.14) is ideally suited for integration by parts, which will allow us to rewrite it into more simple expressions. However, we find that the function $(\sigma_{zz}^s)_0$ has a square root singularity at $h=d$. If the integration by parts is applied, neither the integrated term nor the remaining integral will exist, even though the sum exists. To get around this difficulty, the method given by Freund (1973) is used. The lower limit of integration d in (1.14) is replaced by $d+\epsilon$, $\epsilon<<d$. It can be shown that those terms which are singular at $\epsilon=0$ exactly cancel each other and the desired result can be obtained by taking the limit as $\epsilon\to 0$.

For simplicity, only the first part of (1.14) is derived in detail; the second part can then be obtained in similar manner. Integration by parts of the first equation in (1.14) and making use of the explicit expression for $(\sigma_{zz}^s)_0$ yields

$$\frac{1}{\pi k_d}\left\{\int_{t_l}^{t-t^*}Im\left(\frac{(\lambda^2-\beta^2)^2\frac{\partial\lambda}{\partial\eta}\omega_+(h)}{\alpha_+(\lambda-c_1)\,(\lambda-d)^2\,S_-(\lambda)\,(\lambda-h)}\right)_{\lambda=\lambda_L+}d\eta\right\}$$

$$(\sigma_{zz}^s)_0\,(h)\Big|_{d+\epsilon}^{h_l^*}$$

$$-\int_{d+\epsilon}^{h_l^*}\frac{1}{\pi k_d}\left\{\int_{t_l}^{t-t^*}Im\right.$$

Downloaded 03 May 2010 to 171.66.16.21. Redistribution subject to ASME license or copyright; see http://www.asme.org/terms/Terms_Use.cfm

$$\left(\frac{(\lambda^2-\beta^2)^2\,\frac{\partial\lambda}{\partial\eta}\,\omega_+(h)}{\alpha_+(\lambda-c_1)\,(\lambda-d)^2\,S_-(\lambda)\,(\lambda-h)}\right)_{\lambda=\lambda_{L+}} d\eta\Big\}\,\left((\sigma^s_{zz})_0\right)_h\,dh$$

$$=-\frac{\sigma_0}{\pi k_d}\left(\frac{2\omega_0\,d}{\pi\epsilon^{1/2}}-1\right)$$

$$\left\{\int_{t_l}^{t-t_f} Im\left(\frac{(\lambda^2-\beta^2)^2\,\frac{\partial\lambda}{\partial\eta}\,\omega_+(d)}{\alpha_+(\lambda-c_1)\,(\lambda-d)^3\,S_-(\lambda)}\right)_{\lambda=\lambda_{L+}} d\eta\right\}$$

$$-\int_{d+\epsilon}^{h_l^*}\frac{\sigma_0 d d^{1/2}\omega_0\left(1-\frac{c}{d}\right)S_+^0\left(\frac{-h}{v_0h-1}\right)}{\pi^2 k_d h(h-d)^{3/2}}\left\{\int_{t_l}^{t-t^*} Im\right.$$

$$\left.\left(\frac{(\lambda^2-\beta^2)^2\,\frac{\partial\lambda}{\partial\eta}}{S_+(h)\alpha_+(\lambda-c_1)\,(\lambda-d)^2\,S_-(\lambda)\,(\lambda-h)}\right)_{\lambda=\lambda_{L+}} d\eta\right\}\,dh$$

Applying Cauchy's integral theorem and working out the details, it is found that

$$\sigma^C_{zz}=\sigma^B_{zz}-\sigma^D_{zz}-\sigma^S_{zz}, \tag{1.15}$$

$$\sigma^B_{zz}=-\frac{a^{1/2}}{\pi\,c_2\,k_d S_+(0)}$$

$$\left\{\int_{t_l}^{t} Im\left(\frac{(\lambda^2-\beta^2)^2\,\frac{\partial\lambda}{\partial\eta}}{\alpha_+(\lambda-c_1)\,(\lambda-d)^2\,S_-(\lambda)\,\lambda}\right)_{\lambda=\lambda_{L+}} d\eta\right.$$

$$\left.+\int_{t_s}^{t} Im\left(\frac{4\lambda\,\alpha\,\beta\,\frac{\partial\lambda}{\partial\eta}}{\alpha_+(\lambda-c_1)\,(\lambda-d)^2\,S_-(\lambda)}\right)_{\lambda=\lambda_{S+}} d\eta\right\}, \tag{1.16}$$

$$\sigma^D_{zz}=-\frac{\omega_+(d)}{\pi\,k_d}$$

$$\left\{\int_{t_l}^{t-t_f} Im\left(\frac{(\lambda^2-\beta^2)^2\,\frac{\partial\lambda}{\partial\eta}}{\alpha_+(\lambda-c_1)(\lambda-d)^3\,S_-(\lambda)}\right)_{\lambda=\lambda_{L+}} d\eta\right.$$

$$\left.+\int_{t_s}^{t-t_f} Im\left(\frac{4\lambda^2\alpha\,\beta\,\frac{\partial\lambda}{\partial\eta}}{\alpha_+(\lambda-c_1)\,(\lambda-d)^3\,S_-(\lambda)}\right)_{\lambda=\lambda_{S+}} d\eta\right\}. \tag{1.17}$$

Equation (1.15) indicates that the full field solution (i.e., σ^C_{zz}) of a crack propagating with constant speed subjected to loading [i.e., σ^s_{zz} $(\theta=0)$] on the new crack faces can be expressed by three terms, each term having its own physical meaning. The first term represents the solution due to the uniform loading on the original and new crack faces for a crack which begins to grow at constant speed at a time t_f after the loading is applied. The functional form of this first term is the same as the solution of the problem with uniform loading on the original and new crack faces with no delay time and corresponds to Baker's problem (Baker, 1962). The only dependence on delay time is through the definition of ξ. The second term represents the solution for a crack which starts to propagate at time t_f with constant speed and with loading applied uniformly on the new crack faces only. The third term represents the solution for a stationary crack subject to uniform loading on original crack faces with crack tip located at $x=0$, $z=0$.

Hence, the full field solution of a crack propagating at constant speed with uniform loading on the original crack faces only can be represented by the first two terms of the solution shown in (1.15). If the loading condition is an incident stress wave parallel to the original crack faces, the full field solution of a propagating crack has only the first term in (1.15) plus the stress wave loading, so that

$$\sigma^w_{zz}=\sigma^B_{zz}+\sigma_0.$$

The solution shown above represents a very interesting result that the stress field of the propagating crack due to stress wave loading is independent of delay time t_f and has exactly the same functional form as the stress field of the Baker's problem plus the stress wave loading part. This result was also observed by Achenbach and Nuismer (1971) with no delay time effect.

The displacement field on the crack faces behind the propagating crack tip due to stress wave loading is also obtained by a similar method as discussed for stress. We start with the fundamental solution for the boundary condition in (1.9), the displacement on the crack faces behind the moving crack tip is

$$w^F(\zeta,0,t)=-\frac{n\,b^2\,h\,\alpha_+(h)}{\pi\mu d^2 k_d(h+c_2)S_+(h)}$$

$$\int_{a_1}^{t/\zeta} Im\left(\frac{\alpha_-(\eta)}{(\eta-c_1)\,(\eta-h)\,S_-(\eta)}\right)d\eta$$

$$+\frac{m\,b^2\,h^2}{\pi\,\mu\,d^2\,k_d}\int_{a_1}^{t/\zeta}(t-\eta\zeta)\,Im$$

$$\left\{\frac{\alpha_-(\eta)}{S_-(\eta)(\eta-c_1)}\left(\frac{\alpha_+(h)}{S_+(h)(h+c_2)(\eta-h)}\right)_h\right\}d\eta, \tag{1.18}$$

where ζ is the negative of ξ. The displacement $w^C(\zeta,0,t)$ of the crack faces behind the propagating crack tip due to the stress distribution $-(\sigma^S_{zz})_0$ applied on the new crack faces yields

$$w^c(\zeta,0,t)=\int_0^{u_0^*} w^F\,(m=-1,\,n=-t^*,$$

$$\zeta,\,0,\,t-t^*)(\sigma^s_{zz})_0\left(\frac{1}{u}\right)du$$

$$=-\frac{b^2}{\pi\,\mu\,d^2\,k_d}\int_d^{h_0^*}\left\{\int_{a_1}^{(t-t^*)/\zeta}(t-t^*-\eta\zeta)Im\right.$$

$$\left.\left(\frac{\alpha_-(\eta)\,\alpha_+(h)}{S_-(\eta)(\eta-c_1)S_+(h)(h+c_2)(\eta-h)}\right)d\eta\right\}_h(\sigma^S_{zz})_0\,dh$$

$$=\frac{\sigma_0\,b^2\,a^{1/2}}{\pi\mu d^2\,k_d c_2 S_+(0)}\int_{a_1}^{t/\zeta}(t-\eta\zeta)\,Im\left(\frac{\alpha_-(\eta)}{(\eta-c_1)\,\eta\,S_-(\eta)}\right)d\eta$$

$$-\frac{\sigma_0 b^2}{\pi\mu k_d d d^{1/2}\,(d+c_2)S_+(d)}\int_{a_1}^{(t-t_f)/\zeta}(t-t_f-\eta\zeta)\,Im$$

$$\left(\frac{\alpha_-(\eta)}{S_-(\eta)(\eta-c_1)(d-\eta)}\right)d\eta, \tag{1.19}$$

where

Downloaded 03 May 2010 to 171.66.16.21. Redistribution subject to ASME license or copyright; see http://www.asme.org/terms/Terms_Use.cfm

$$u_0^* = \frac{t - t_f - \zeta a_1}{d\,(t - \zeta a_1)}, \quad h_0^* = \frac{(t - \zeta a_1)d}{t_f}, \quad a_1 = \frac{a}{1 + a/d}.$$

The second term in (1.19) is the solution due to uniform loading σ_0 on the new crack faces. Hence, for the incident stress wave loading condition, the second term will be canceled out and one term will remain,

$$w^W(\zeta, 0, t) = \frac{\sigma_0\, b^2\, a^{1/2}}{\pi \mu d^2 k_d c_2 S_+(0)} \int_{a_1}^{t/\zeta} (t - \eta\zeta)\, Im \left(\frac{\alpha_-(\eta)}{(\eta - c_1)\,\eta\, S_-(\eta)}\right) d\eta. \tag{1.20}$$

Again, the displacement on the crack faces due to stress wave loading is independent of the delay time and has exactly the same functional form as for the solution of displacement for Baker's problem. This result can be easily interpreted. Consider two identical bodies, each containing a half-plane crack, subjected to the same stress wave loading which strikes both cracks at the same time. Assume the delay time before the cracks start to propagate of the two cases are different. This result implies that, after the two cracks propagate, and for any distance behind the moving crack tip, the normal displacements of the crack faces in the two cases are identical, no matter what values of the delay time. This result will be used to construct the field solutions for the stopped crack in next section.

The Stress Field Solution for the Stopped Crack

In the previous section, several special properties of the elastic field of a crack subjected to stress wave loading and extending at a constant speed were determined. It is found that the complete elastic field for the sudden stopping of a constant velocity crack can then be obtained. In order to stop the crack at the position $x = l_s$, we must close the displacement of the crack faces for $l_s < x < v_0\,(t - t_f)$. Now, consider a modified problem of a semi-infinite crack with the crack tip at $x = l_s = v_0\,(t_b - t_f)$. At time $t = t_f + l_s/v_0$, the traction distribution $(\sigma_{zz}^s)_0\ \{t/[\xi + v_0(t - t_f - l_s/v_0)]\} + \sigma_0$ acts on the new crack faces. If we follow the same method used in the last section to construct the displacement field on the new crack faces $l_s < x < v_0\,(t - t_f)$ for this modified problem, we will get the same result as the solution for the stress wave loading, because the only difference between these two cases is the value of the delay time. Subtracting the displacement solution for the modified problem from the original stress wave solution will make the crack suddenly stop at $x = l_s$. The new problem will then be an incident stress wave striking the crack at time $t = 0$, the crack tip beginning to move at constant speed v_0 at time $t = t_f$, and after some time later $t = t_f + l_s/v_0$, the crack tip suddenly stopping at $x = l_s$.

The main conclusion is that, upon the sudden stopping of crack, the stress distribution of the full field radiated out from the stopped crack tip, traveling behind the shear wave front, is exactly the stress distribution that would have resulted had the crack tip been at $x = l_s$ for all time. In other words, it is the stress distribution appropriate for the given incident stress wave and the new crack length, and is completely independent of the fact that the crack-tip had been in motion. Freund (1973) has come to a similar conclusion, but only for the σ_{zz} stress component along the crack line. The generalization to the complete stress field allows the problem of crack kinking to be considered next.

The History of Dynamic Stress Intensity Factor

Experimentally, it is very rare to see a crack kink without first growing straight ahead for some distance (Ravi-Chandar and Knauss, 1984, Ravi-Chandran, 1986). In mode I, Freund (1973) includes the delay time effect but does not consider crack kinking. Achenbach et al. (1984) and Ma and Burgers (1987) deal with the crack kinking out from the original crack tip. There are no results that can describe the stress intensity factor of the whole fracture process. If we want to model more realistically the crack kinking process, a possible model is to consider that the originally stationary crack starts to propagate straight ahead after some delay time, and at some later time the crack stops and instantaneously kinks. Knowing the stress field of the stopped crack, we are able to complete the history of the stress intensity factor of the whole fracture process.

Consider a semi-infinite crack which is initially at rest, the incident stress wave loading strikes the crack tip at time $t = 0$. At time $t = t_f$, the crack starts in motion straight ahead of the fracture plane with constant velocity v_0 and stops at the position $x = l_s$. Instantaneously, the crack kinks from the stopped crack tip and propagates with constant velocity v_c, making an angle δ with respect to the crack plane. A perturbation method is applied to calculate the stress intensity factor for the kinked crack. The first order approximation can be expressed by the stress intensity factor for a straight crack propagating in its own plane subjected to the negative of the tractions on the kinked crack faces. The stress field for the stopped crack considered in this paper is very similar to that used by Ma and Burgers (1987), in which the crack kinks out from the stationary crack. The only difference is the magnitude of the delay time. For the crack which stops at $x = l_s$ and kinks instantaneously, we can consider the crack to be at $x = l_s$ for all the time and to kink after the delay time $t_b = t_f + l_s/v_0$. Hence, the stress intensity factor of the kinked crack after stopping can be obtained by replacing t_f by t_b in the solution given in Ma and Burgers (1987);

$$K_I = 2\sigma_0 \left(\frac{2\,t_b}{\pi\, d_c(1 - a/d_c)}\right)^{1/2} \left\{ -\omega_+(d_c)(d^* - d_c)^{1/2} \left(\cos^2\delta + C_{xx}\sin^2\delta + 2\left(\frac{a}{b}\right)^2 \sin^2\delta - 1\right) + \omega_0 d_c \omega_+(d_c)\cos^3\frac{\delta}{2} + \frac{\omega_0 d_c}{\pi} \int_{d_c}^{d^*} \frac{(d^* - h)^{1/2}}{(h - d_c)^{1/2}} \left(\frac{\omega_+(d_c)}{h - d_c}\cos^3\frac{\delta}{2} - \frac{\omega_+(h) d_c^{5/2}}{k(h - d_c)^3} (\sigma_{\theta\theta}^L)_h^*\right) dh \right\}, \tag{2.1}$$

$$K_{II} = 2\sigma_0 \left(\frac{2\,t_b}{\pi\, d_c(1 - b/d_c)}\right)^{1/2} \left\{ -u_+(d_c)(d^* - d_c)^{1/2} \frac{1 - C_{xx} - 2\left(\frac{a}{b}\right)^2}{2} \sin 2\delta + \frac{\omega_0 d c u_+(d_c)}{4} \left(\sin\frac{\delta}{2} + \sin\frac{3\delta}{2}\right) + \frac{\omega_0 d_c}{\pi} \int_{d_c}^{d^*} \frac{(d^* - h)^{1/2}}{(h - d_c)^{1/2}} \left(\frac{u_+(d_c)}{4(h - d_c)} \left(\sin\frac{\delta}{2} + \sin\frac{3\delta}{2}\right) - \frac{u_+(h) d_c^{5/2}}{k(h - d_c)^3} (\sigma_{\theta r}^L)_h^*\right) dh \right\}, \tag{2.2}$$

where

$$d^* = \frac{t}{v_c t_b}, \quad d_c = \frac{1}{v_c},$$

$$u_+(h) = \frac{\beta_+(h)}{(h + c_2) S_+(h)}.$$

Downloaded 03 May 2010 to 171.66.16.21. Redistribution subject to ASME license or copyright; see http://www.asme.org/terms/Terms_Use.cfm

The components $(\sigma^L_{\theta\theta})^*_n$ and $(\sigma^L_{\theta r})^*_n$ can be found in Appendix A (Ma and Burgers, 1987). Kinking of a primary crack under pure mode I loading generally results in both mode I and mode II conditions on the kinked crack, giving both mode I and mode II stress intensity factors. For kinking angles less than 45°, the error introduced by using this approximate method will within 2 percent for the mode I stress intensity factor and 5 percent for the mode II when compared with the numerical results (Burgers, 1983) for delay time equal to zero.

The stress intensity factor of the whole time history is given by

$$K = \begin{cases} K_I^s & 0 \le t \le t_f \\ K_I^s\, k(d) & t_f < t < t_b, \\ K_I,\ K_{II} & t > t_b \end{cases} \tag{2.3}$$

where

$$K_I^S = 2\sqrt{\frac{2t}{\pi}}\,\sigma_0\,\omega_0,$$

$$k(d) = \frac{d}{S_+(d)(d+c_2)\left(1-\frac{a}{d}\right)^{1/2}}$$

and K_I^S is the stress intensity factor for the stationary crack, and K_I and K_{II} are shown in (2.1) (2.2). If one wants to study the criterion for a crack kinking event, it is clear that the most significant time period involved is when crack kinking has just occured, in other words, $t - t_b << 1$. It might be argued that this will have a major role on the determination of the direction and crack speed of continued crack propagation. The stress intensity factor just after the kinking occurs has the form

$$K_I = K_I^S\, k(d_c)\cos^3\left(\frac{\delta}{2}\right), \quad \text{as } t \to t_b,$$

$$K_{II} = \frac{\sqrt{2}\sigma_0\,\omega_0\,u_+(d_c)(d_c t)^{1/2}}{2\sqrt{\pi}\left(1-\frac{b}{d_c}\right)^{1/2}}\left(\sin\frac{\delta}{2}+\sin\frac{3\delta}{2}\right),$$

$$\text{as } t \to t_b.$$

The Criteria of Kinking

For mixed mode I-II fracture, the energy flux into the propagating crack tip can be written in terms of the corresponding dynamic stress intensity factors,

$$E = -\frac{b^2}{2\mu d^3 R(d)}\left(1-\frac{a^2}{d^2}\right)^{1/2}(K_I)^2 + \left(1-\frac{b^2}{d^2}\right)^{1/2}(K_{II})^2\Big) \tag{3.1}$$

where

$$R(d) = \left(\frac{b^2}{d^2}-2\right)^2 - 4\left(1-\frac{a^2}{d^2}\right)^{1/2}\left(1-\frac{b^2}{d^2}\right)^{1/2}.$$

We consider a maximum energy release rate criterion for the kinked crack. This criterion suggests that the kinked crack will choose to propagate in the direction and at a velocity for which the energy flux into the crack tip is a maximum. For a crack subjected to an inplane longitudinal stress wave loading parallel to the crack line, the crack will tend to propagate straight ahead and no kink will occur if the maximum energy release rate criterion is used.

An alternative fracture criterion was proposed by Freund (1975). Since the time for bifurcation to occur is very short, the local stress and strain fields can not readjust by any significant amount. At each instant, including the instant just prior to bifurcation, the rate of energy supplied to the crack tip by the loads is equal to the rate of energy required to drive the crack at its current speed. Therefore, it seems reasonable to assume that the energy release rate just after kinking has the same value as immediately before kinking. The stress intensity factor just before and just after kinking are given in (2.3). The energy balance criterion is given by the following equation

$$\frac{\left(1+\frac{a}{d}\right)^{1/2}}{d\,R(d)\,S_+^2(d)\,(d+c_2)^2\left(1-\frac{a}{d}\right)^{1/2}} \tag{3.2}$$

$$= \frac{1}{d_c R(d_c) S_+^2(d_c)\left(d_c+\frac{c}{1-c/d_c}\right)^2}\left\{\left(\frac{1+a/d_c}{1-a/d_c}\right)^{1/2}\cos^6\left(\frac{\delta}{2}\right)+\frac{1}{16}\left(\frac{1+b/d_c}{1-b/d_c}\right)^{1/2}\left(\sin\frac{\delta}{2}+\sin\frac{3\delta}{2}\right)^2\right\}$$

The kinked crack speed a/d_c and the kinked angle δ is calculated for crack speed $a/d = 0.1, 0.2$ and is plotted in Fig. 4.

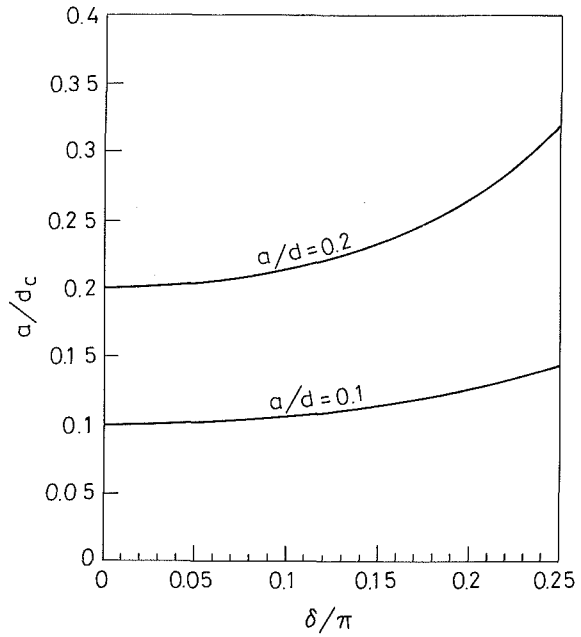


Fig. 4 The kinked crack angle and kinked crack speed by using the criterion in equation (4.2) for the propagating straight crack speed $a/d = 0.1, 0.2$

Discussion

The earliest analytical work on crack propagation and arrest for a general anti-plane strain loading was considered by Eshelby (1969). The crack moves with some arbitrary time-dependent velocity and at some instant of time comes to an abrupt stop. The important result is that behind a circular wavefront travelling with the shear wave speed and centered at the arrested crack tip, a time-independent stress field is established. This static field is exactly the stress field for the applied loading and the new length of the crack. The stress field of the suddenly stopping crack due to the anti-plane stress wave loading including the delay time effect was investigated by Ma and Burgers (1988) using a more direct method of superposition and obtained the same conclusion.

Downloaded 03 May 2010 to 171.66.16.21. Redistribution subject to ASME license or copyright; see http://www.asme.org/terms/Terms_Use.cfm

For in-plane problems, the solution is more complicated due to the presence of two types of stress wave. Freund (1972a) considered the problem of a semi-infinite crack in an infinite body subjected to a general arbitrary static mode I loading. He found that if the crack is arrested suddenly, a static field is established along the fracture plane behind the shear wavefront centered at the stopped crack tip. This time-independent field is the appropriate stress field for the applied loading and the new crack length. For the points not lying on the fracture plane, the stresses are time dependent and attain their appropriate static value for an infinitely long time. Freund (1973) extended the problem of a suddenly arrest crack to stress wave loading but focused his attention to the stress field along the crack plane ahead of the stopped crack tip. The above analysis of this paper has extended this work to the full field solution around the suddenly arrested crack. The theoretical analysis of the stress field for the mode I stopping crack is similar to that has been used in the mode III case. The main procedure for constructing the solution follows Freund with some modification and it shows a clear and direct way of constructing the solution. First, the diffraction field of the stationary crack due to the crack face pressure is worked out and the stress distribution that is radiated out on the prospective fracture plane ahead of the crack is determined. Some fundamental solutions are obtained in order to use the superposition scheme to construct the full field solutions for the propagating crack. The stress field of the propagating crack due to the application of the pressure only on the original crack face can be obtained by superimposing the stress distribution that results from sudden application of the crack face normal pressure for the stationary crack and the stress distribution that results from growth of the crack under the action of crack face tractions which exactly negate the stresses on the crack line. This complicated solution is found to be the sum of the solutions for some simpler problems. The full field solution of a propagating crack with constant velocity due to stress wave loading can then be represented by the Baker's solution plus the stress pulse. When the crack suddenly stops, the stationary solution is radiated out for the full field and is exactly the same stress distribution that a stationary crack tip would have if it had been at the stopped point for all time. This remarkable result immediately allows us to make a statement about the stress intensity factor for the kinked crack case, the case of a kinked crack initiates out from the original crack tip with delay time was solved by Ma and Burgers (1987). The delay time is now t_b but nothing else changes, so the results can be obtained directly from the solutions obtained by Ma and Burgers (1987).

Vu and Kinra (1981) have looked at the stopping crack problem experimentally. They used large plates of PMMA containing a long edge crack and subjected to a tensile fracture. The crack is initially at rest and then propagates rapidly under load and after a finite amount of crack extension, is abruptly arrested at a predetermined point. The strain field emitted during the run-arrest event was measured in detail using strain gage techniques, it was shown that the field becomes static behind the shear wave front emitted by the arrested tip, to the accuracy of the experiments.

Acknowledgments

The author is grateful to Dr. P. Burgers for encouragement in doing this problem and helpful discussions. The research support of the author by the National Science Foundation (U.S.A.), Solid Mechanics Program through Grant MEA-83006644 and by the National Science Council (Republic of China) through Grant NSC 75-0401-E042-08 are gratefully acknowledged.

References

Achenbach, J. D., and Nuismer, R., 1971, "Fracture Generated by a Dilatational Wave," *International Journal of Fracture*, Vol. 7, pp. 77–88.

Achenbach, J. D., Kuo, M. K., and Dempsey, J. P., 1984, "Mode III and Mixed Mode I-II Crack Kinking under Stress Wave Loading," *International Journal of Solids and Structures*, Vol. 20, pp. 395–410.

Baker, B. R., 1962, "Dynamic Stresses Created by a Moving Crack," ASME JOURNAL OF APPLIED MECHANICS, Vol. 29, pp. 449–458.

Broberg, K. B., 1960, "The Propagation of a Brittle Crack," *Arkiv for Pysik*, Vol. 18, pp. 159–192.

Burgers, P., 1982, "Dynamic Propagation of a Kinked or Bifurcated Crack in Anti-plane Strain," ASME JOURNAL OF APPLIED MECHANICS, Vol. 49, pp. 371–376.

Burgers, P., and Dempsey, J. P., 1982, "Two Analytical Solutions for Dynamic Crack Bifurcation in Anti-Plane Strain," ASME JOURNAL OF APPLIED MECHANICS, Vol. 49, pp. 366–370.

Burgers, P., 1983, "Dynamic Kinking of a Crack in Plane Strain," *International Journal of Solids and Structures*, Vol. 19, pp. 735–752.

Burgers, P., and Dempsey, J. P., 1984, "Plane Strain Dynamic Crack Bifurcation," *International Journal of Solids and Structures*, Vol. 20, pp. 609–618.

de Hoop, A. T., 1958, "Representation Theorems for the Displacement in an Elastic Solid and Their Application to Elastodynamic Diffracture Theory," Doctoral Dissertation, Technische Hogeschool, Delft.

Dempsey, J. P., Kuo, M. K., and Achenbach, J. D., 1982, "Mode III Crack Kinking Under Stress Wave Loading," *Wave Motion*, Vol. 4, pp. 181–190.

Eshelby, J. D., 1969, "The Field of a Crack Extending Non-uniformly Under Anti-Plane Loading," *Journal of the Mechanics and Physics of Solids*, Vol. 17, pp. 177–199.

Freund, L. B., 1972a, "Crack Propagation in an Elastic Solid Subjected to General Loading – I. Constant Rate of Extension," *Journal of the Mechanics and Physics of Solids*, Vol. 20, pp. 129–140.

Freund, L. B., 1972b, "Crack Propagation in an Elastic Solid Subjected to General Loading – II. Nonuniform Rate of Extension," *Journal of the Mechanics and Physics of Solids*, Vol. 20, pp. 141–152.

Freund, L. B., 1973, "Crack Propagation in an Elastic Solid Subjected to General Loading – III. Stress Wave Loading," *Journal of the Mechanics and Physics of Solids*, Vol. 21, pp. 47–61.

Freund, L. B., 1974, "Crack Propagation in an Elastic Solid Subjected to General Loading – IV. Obliquely Incident Stress Pulse," *Journal of the Mechanics and Physics of Solids*, Vol. 22, pp. 137–146.

Freund, L. B., 1975, "Bifurcation of a Propagating Crack in a Brittle Solid," 12th Annual Meeting, Society of Engineering Science, U. of Texas Press, Austin, pp. 1015–1022.

Kostrov, B. V., 1966, "Unsteady Propagation of Longitudinal Shear Cracks," *Applied Mathematics and Mechanics*, Vol. 30, pp. 1241–1248.

Ma, C. C., and Freund, L. B., 1986, "The Extent of the Stress Intensity Factor Field During Crack Growth Under Dynamic Loading Condition," ASME JOURNAL OF APPLIED MECHANICS, Vol. 53, pp. 303–310.

Ma, C. C., and Burgers, P., 1986, "Mode III Crack Kinking with Delay Time: An Analytical Approximation," *International Journal of Solids and Structures*, Vol. 22, pp. 883–899.

Ma, C. C., and Burgers, P., 1987, "Dynamic Mode I and Mode II Crack Kinking Including Delay Time Effects," *International Journal of Solids and Structures*, Vol. 23, pp. 897–918.

Ma, C. C., and Burgers, P., 1988, "Initiation, Propagation and Kinking of an Antiplane Crack," ASME JOURNAL OF APPLIED MECHANICS, Vol. 55, pp. 111–119.

Ravi-Chandar, K., and Knauss, W. G., 1984, "An Experimental Investigation into Dynamic Fracture: I. Crack Initiation and Arrest," *International Journal of Fracture*, Vol. 25, pp. 247–262.

Ravi-Chandran, G., 1986, "Dynamic Fracture under Plane Wave Loading," Ph.D. Thesis, Brown University.

Vu, B. Q., and Kinra, V. K., 1981, "Brittle Fracture of Plates in Tension Static Field Radiated by a Suddenly Stopping Crack," *Engineering Fracture Mechanics*, Vol. 15, pp. 107–114.

Yoffe, E., 1951, "The Moving Griffith Crack," *Philosophical Magazine*, Vol. 42, pp. 739–750.

Downloaded 03 May 2010 to 171.66.16.21. Redistribution subject to ASME license or copyright; see http://www.asme.org/terms/Terms_Use.cfm

T.-L. Sham
Department of Mechanical Engineering, Aeronautical Engineering and Mechanics, Rensselaer Polytechnic Institute, Troy, NY 12180-3590

H. F. Bueckner
Schenectady, NY

The Weight-Function Theory for Piecewise Homogeneous Isotropic Notches in Antiplane Strain

An extension of the two-dimensional weight-function theory in linear elastic crack mechanics is introduced for piecewise homogeneous isotropic notched structures under antiplane strain conditions. Using the concepts of fundamental fields and elastic reciprocity, we show that the notch-interface stress-intensity factor for a notch with the tip situated at the material interface can be computed for any antiplane strain loading through the notch-interface weight function by quadrature. Closed-form notch-interface weight functions are given for some simple geometries.

1 Introduction

The weight functions were introduced by Bueckner (1970) for the determination of stress-intensity factors in cracked bodies. By employing the reciprocity theorem in linear elasticity, Bueckner (1970) has shown that the stress-intensity factors induced at the crack tip by any surface tractions can be calculated through the weight functions by quadratures. The weight functions are universal functions for the given crack configuration and body geometry and, interpreted as displacements, they lead to stresses which are in equilibrium with zero body forces and zero tractions on the crack faces. The field of weight functions and their corresponding strains and stresss are referred to as a fundamental field (Bueckner, 1970). The fundamental field is distinguished from some other elastic fields by the unboundedness of its strain energy in the neighborhood of the crack tip.

Considering the energetic forces associated with crack tip motions, Rice (1972) has made an alternative derivation of Bueckner's results and has given a different method for determining the weight function for a Mode I crack. Rice (1972) noted that when the dependence of the stress-intensity factor and the displacements on the crack tip position is known under one symmetrical loading, the Mode I weight function can be computed by differentiating the displacements with respect to the crack tip position. Generalization of the weight-function theory to three dimensions in cracked solids has been given by Bueckner (1977a, 1977b, 1987) and Rice (1972, 1985a, 1985b).

In this paper, we develop a weight-function theory for a piecewise homogeneous notched structure under antiplane strain deformation. We employ the concepts of fundamental fields and Betti's elastic reciprocity to show that the notch-interface stress-intensity factor induced at the notch tip by any antiplane strain loading can be determined by quadrature through the notch-interface weight function as in the case of a cracked structure.

In a similar fashion, Stern (1973) has also employed Betti's reciprocity theorem for computing stress-intensity factors. Applications of the Stern procedure can be found in Stern and Soni (1976); Stern, Becker, and Dunham (1976); Hong and Stern (1978); Stern (1979) and Carpenter (1984a, 1984b). A comparison of the Stern procedure and the weight-function method for computing stress-intensity factors is given in Section 3.3.

2 Preliminaries

The two-dimensional notched body that we consider is linear elastic and isotropic. The notched body is of *finite* extent in the x_1-x_2 plane (Fig. 1) and the body is formed by bonding together perfectly two homogeneous materials, each with different elastic properties. The notch tip is located at the interface of this bimaterial and we employ both Cartesian and polar coordinate systems, centered at the notch tip as shown in Fig. 1. The polar angle θ for the upper notch face is θ_1 and that for the lower notch face is θ_2. We refer to the material in the angular range, $0 \le \theta \le \theta_1$, as Material I and that in the angular range, $\theta_2 \le \theta \le 0$, as Material II. The notched body is subjected to an external loading system which consists of prescribed surface tractions on the boundary S_T and the notch faces S_N, imposed boundary displacements on the surface S_u, and body force loading in the interior. This external loading system is also assumed to produce antiplane strain deformations.

2.1 Governing Equations. Under antiplane strain deformation conditions in either Material I or Material II, the only nonzero displacement is the out-of-plane component w which depends on the in-plane coordinates x_1 and x_2. This leads to two nontrivial stresses

$$\sigma_{31} = \mu \frac{\partial w}{\partial x_1}, \quad \sigma_{32} = \mu \frac{\partial w}{\partial x_2}$$

Contributed by the Applied Mechanics Division for publication in the JOURNAL OF APPLIED MECHANICS.
Discussion on this paper should be addressed to the Editorial Department, ASME, United Engineering Center, 345 East 47th Street, New York, NY 10017, and will be accepted until two months after final publication of the paper itself in the JOURNAL OF APPLIED MECHANICS. Manuscript received by ASME Applied Mechanics Division, November 1986; final revision, March 21, 1988.

Copyright © 1988 by ASME
Downloaded 03 May 2010 to 171.66.16.21. Redistribution subject to ASME license or copyright; see http://www.asme.org/terms/Terms_Use.cfm

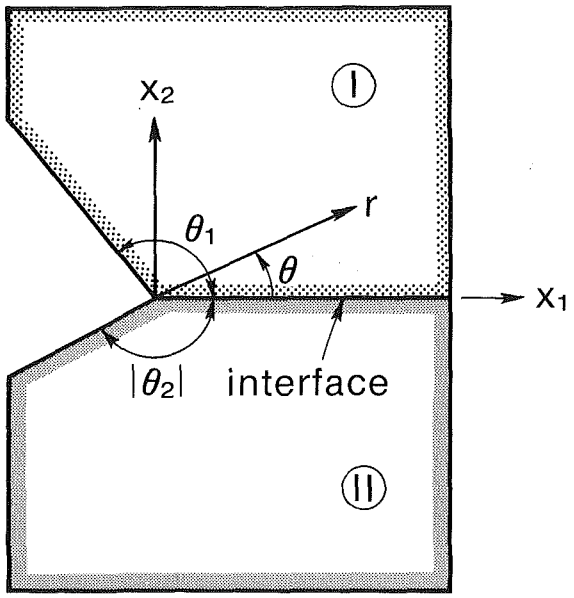


Fig. 1 Notched body consisting of two homogeneous isotropic components. The notch tip is located at the interface of the bimaterial (I and II) and $0 < \theta_1 \leq \pi$, $0 > \theta_2 \geq -\pi$. Perfect bonding along the interface is assumed.

where μ is the appropriate shear modulus. In terms of the displacement w the equilibrium equation is

$$\mu \nabla^2 w + f = 0 \tag{1}$$

where $f = f(x_1, x_2)$ is the body force per unit volume acting in the direction of the x_3-axis and ∇^2 is the Laplacian.

For sharp cracks in homogeneous bodies under plane-strain or plane-stress conditions it is commonly accepted that the stresses exhibit the order $r^{-1/2}$ near the crack tip $r = 0$. This feature has been rigorously established by Bueckner (1973) under the assumptions that

(*i*) No body forces are present;
(*ii*) Tractions on the crack faces are of the induced type (opposing one another at opposite face points) and admit Taylor expansions in r in some neighborhood of $r = 0$.

The assumption on the body forces can be weakened. It suffices to exempt a neighborhood of $r = 0$, however small, from such forces. Even this condition is not necessary. Certain bounded and even unbounded body force fields near the crack tip will not invalidate the order $r^{-1/2}$ of the stresses. So far the exact domain of validity of this feature with respect to body force loading has not been established.

One can expect similar phenomena for the situation of Fig. 1. The order of $r^{-1/2}$ will be replaced by $r^{\gamma - 1}$ with some $\gamma > 0$ for stress fields without body forces in a neighborhood of $r = 0$. As in the case of sharp cracks less stringent conditions on the body forces are possible. It is not the aim of this paper to pursue this particular matter in all detail. Nevertheless we have shown that there are limits to such generalizations. Certain fields of body forces seem to be acceptable at first sight but turn out to be inadmissible after a closer look. The Appendix describes a class of such fields.

Briefly speaking, we assume that the asymptotic behavior of the elastic field in the neighborhood of the notch tip is governed by the equation

$$\mu \nabla^2 w = 0 \tag{2}$$

with zero tractions on the notch faces as boundary conditions. Thus the asymptotic elastic field can be represented by one analytic function, $\omega(z)$ of z $(= x_1 + ix_2)$ as

$$\mu w = \text{Im}\ \omega(z) \tag{3}$$

$$\sigma_{32} + i\sigma_{31} = \omega'(z) \tag{4}$$

in the neighborhood of the notch tip, and the total force acting on an oriented differential arc length dl and attacking the material to the left of the path traversed is given by

$$T dl = -\text{Re}[d\omega]. \tag{5}$$

Here i is the imaginary unit and we shall use a bar over a complex quantity to denote its complex conjugate.

3 Antiplane Strain Notch-Interface Weight Functions

3.1 General Elastic Field Near the Notch Tip. We shall first investigate the asymptotic deformation behavior near the notch tip under antiplane strain conditions. The shear moduli for Material I and II are μ_1 and μ_2, respectively.

Let the analytic functions $\omega_p(z)$ which characterize the asymptotic behavior of the antiplane strain elastic field be of the following power form in the respective parts of the notched body

$$\omega_p(z) = A_p z^\gamma + B_p z^{\bar\gamma} \tag{6}$$

where A_p, B_p and γ are complex constants and where

$$z^\gamma \equiv e^{\gamma(\log r + i\theta)}, \quad z^{\bar\gamma} \equiv e^{\bar\gamma(\log r + i\theta)}, \quad z = re^{i\theta}, \quad -\pi \leq \theta \leq \pi.$$

We use the subscript p, with $p = 1$ and 2, to denote quantities in Material I and Material II, respectively. Earlier investigations (e.g., England, 1965; and Erdogan, 1965) of the problem of an in-plane interfacial crack suggest that the stress and deformation field in the neighborhood of the crack tip has the complex representation of the form z raised to a complex power. Thus one cannot assume *a priori* that the constant γ in (6) is real. Henceforth, we shall assume $\gamma \neq \bar\gamma$ unless otherwise stated.

In order to satisfy the zero traction conditions on the notch faces, we must have, from (5), Re $[\omega_p]$ = constant or

$$e^{\gamma \log r}[A_p e^{\gamma i\theta_p} + \bar B_p e^{-\gamma i\theta_p}] + e^{\bar\gamma \log r}[\bar A_p e^{-\bar\gamma i\theta_p} + B_p e^{\bar\gamma i\theta_p}] = \text{constant}.$$

Since this equation has to hold for all r the brackets must vanish; hence

$$\omega_p(z) = a_p e^{-\gamma i\theta_p} z^\gamma - \bar a_p e^{-\bar\gamma i\theta_p} z^{\bar\gamma} \tag{7}$$

where a_p are complex constants.

On the interface, the assumption of perfect bonding implies that both traction and displacement are continuous across the interface. Hence for $x_2 = 0$ and $x_1 > 0$, the respective continuity conditions for the traction and displacement are

$$\text{Re}\,[\omega_1' - \omega_2'] = 0, \tag{8a}$$

$$\text{Im}\left[\frac{\omega_1}{\mu_1} - \frac{\omega_2}{\mu_2}\right] = 0. \tag{8b}$$

Using the expression for ω_p from (7), we write the equations of continuity for the traction and displacement on the interface as follows

$$e^{(\gamma-1)\log r}[\gamma a_1(e^{-\gamma i\theta_1} - e^{\gamma i\theta_1}) - \gamma a_2(e^{-\gamma i\theta_2} - e^{\gamma i\theta_2})] + e^{(\bar\gamma - 1)\log r}[\bar\gamma \bar a_1(e^{\bar\gamma i\theta_1} - e^{-\bar\gamma i\theta_1}) - \bar\gamma \bar a_2(e^{\bar\gamma i\theta_2} - e^{-\bar\gamma i\theta_2})] = 0,$$

$$e^{\gamma \log r}\left[\frac{a_1}{\mu_1}(e^{-\gamma i\theta_1} + e^{\gamma i\theta_1}) - \frac{a_2}{\mu_2}(e^{-\gamma i\theta_2} + e^{\gamma i\theta_2})\right] - e^{\bar\gamma \log r}\left[\frac{\bar a_1}{\mu_1}(e^{\bar\gamma i\theta_1} + e^{-\bar\gamma i\theta_1}) - \frac{\bar a_2}{\mu_2}(e^{\bar\gamma i\theta_2} + e^{-\bar\gamma i\theta_2})\right] = 0.$$

It is noted that these continuity equations have to be satisfied on the entire interface (all r), thus all brackets must vanish.

Downloaded 03 May 2010 to 171.66.16.21. Redistribution subject to ASME license or copyright; see http://www.asme.org/terms/Terms_Use.cfm

Since each bracket appears together with its complex conjugate it suffices to write

$$[\gamma \sin(\gamma\theta_1)]a_1 - [\gamma \sin(\gamma\theta_2)]a_2 = 0$$

$$\left[\frac{1}{\mu_1}\cos(\gamma\theta_1)\right]a_1 - \left[\frac{1}{\mu_2}\cos(\gamma\theta_2)\right]a_2 = 0$$

as interface continuity conditions. Writing them in matrix form, we obtain

$$\mathbf{M}(\gamma)\begin{Bmatrix} a_1 \\ a_2 \end{Bmatrix} = \begin{Bmatrix} 0 \\ 0 \end{Bmatrix} \tag{9}$$

with

$$\mathbf{M}(\gamma) = \begin{bmatrix} \gamma \sin(\gamma\theta_1) & -\gamma \sin(\gamma\theta_2) \\ \dfrac{1}{\mu_1}\cos(\gamma\theta_1) & -\dfrac{1}{\mu_2}\cos(\gamma\theta_2) \end{bmatrix}.$$

These are two homogeneous algebraic equations with unknowns a_1 and a_2. For nontrivial solutions, the determinant D of $\mathbf{M}$ has to vanish

$$D \equiv \det \mathbf{M}(\gamma) = 0 \tag{10}$$

where

$$D = \frac{\gamma}{\mu_1}\sin(\gamma\theta_2)\cos(\gamma\theta_1) - \frac{\gamma}{\mu_2}\sin(\gamma\theta_1)\cos(\gamma\theta_2).$$

This provides a characteristic equation for the complex exponent γ. So far $\gamma \neq \bar{\gamma}$ has been assumed. At this juncture, we consider the possibility of a real $\gamma \neq 0$. In this case, (7), (9), (10) stay valid if a_1, a_2 are confined to imaginary values. This entails no loss of generality. From here on, we drop the assumption $\gamma \neq \bar{\gamma}$ and consider all possible solutions of (10), real or complex-valued. It is clear that any such solution γ will yield functions ω_p which satisfy all conditions on the notch faces $\theta = \theta_p$ and on the interface $\theta = 0$. We observe that $\gamma = 0$ solves (10) and yields a mere translation of the elastic body. We exclude $\gamma = 0$ from here on. It is also observed that the determinant D is an even function of γ. Thus, if γ_0 is a solution to (10), so is $-\gamma_0$. The coefficient matrix $\mathbf{M}$ is of rank one for any value of γ which satisfies (10).

We next introduce the following abbreviations:

$$\Theta = \frac{\theta_1 - \theta_2}{2}, \quad 0 < \Theta \leq \pi$$

$$\Delta\Theta = \frac{\theta_1 + \theta_2}{2}, \quad 0 \leq |\Delta\Theta| < \frac{\pi}{2}, \quad 0 \leq \left|\frac{\Delta\Theta}{\Theta}\right| < 1$$

$$\mu = \frac{\mu_1 + \mu_2}{2}, \quad \Delta\mu = \frac{\mu_1 - \mu_2}{2}, \quad 0 \leq \left|\frac{\Delta\mu}{\mu}\right| < 1.$$

Since $\gamma \neq 0$, the characteristic equation (10) can be rewritten as

$$\sin(2\gamma\Theta) + \frac{\Delta\mu}{\mu}\sin(2\gamma\Delta\Theta) = 0. \tag{11}$$

This equation is further simplified as we set

$$\left|\frac{\Delta\Theta}{\Theta}\right| = \Psi; \quad \operatorname{sgn}(\Delta\Theta)\,\frac{\Delta\mu}{\mu} = m; \quad 2\gamma\Theta = t.$$

Now (11) takes the form

$$f(t) \equiv \sin t + m \sin(\Psi t) = 0 \tag{12}$$

The function $f(t)$ is holomorphic; it is also holomorphic in the parameters m and Ψ. We now consider (12) under the restrictions $|m| < 1$ and $0 \leq \Psi \leq 1$. Let t be a real or complex zero of f; writing $t = u + iv$ with real u, v, we obtain from (12)

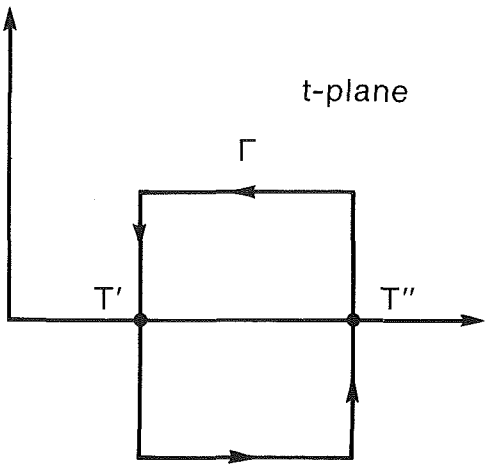


Fig. 2 Path Γ in the complex *t*-plane used for determining the number of zeros of *f(t)* inside Γ

$$\sin u \cosh v + m \sin(\Psi u)\cosh(\Psi v) = 0$$

$$\cos u \sinh v + m \cos(\Psi u)\sinh(\Psi v) = 0.$$

If $\Psi v \neq 0$ then

$$m^2 = \sin^2 u \frac{\cosh^2 v}{\cosh^2(\Psi v)} + \cos^2 u \frac{\sinh^2 v}{\sinh^2(\Psi v)}.$$

Now $\cosh v \geq \cosh(\Psi v)$ and $|\sinh v| \geq |\sinh(\Psi v)|$. Therefore

$$m^2 \geq \cos^2 u + \sin^2 u = 1$$

which contradicts $|m| < 1$. Consequently $\Psi v = 0$. If $\Psi \neq 0$, then $v = 0$ and $t = u =$ real. If $\Psi = 0$ then $f(t) = \sin t = 0$ and $t = n\pi$ with some integer n. In any case, t is real and (11) has nothing but real zeros in t.

Returning to (12) we assert:

Let n be an integer and $T' = (2n-1)\pi/2$, $T'' = (2n+1)\pi/2$. Then $f(t)$ has precisely one zero in the closed interval $[T', T'']$.

In this context, we observe that $\sin T'' = (-1)^n$, $\sin T' = -(-1)^n$. Since $|m| < 1$, we have $\operatorname{sgn}[f(T')] = \operatorname{sgn}(\sin T')$ and $\operatorname{sgn}[f(T'')] = \operatorname{sgn}(\sin T'')$. This makes it obvious that $f(t)$ has at least one zero in the open interval (T', T''). We further observe that $t = n\pi$ is the only zero in the special case $\Psi = 0$.

In order to complete the proof of our assertion, we consider the path Γ in the complex t-plane as shown in Fig. 2. We use the well-known formula

$$N = \frac{1}{2\pi i}\int_\Gamma \frac{f'(t)}{f(t)}\,dt$$

for the number of zeros of $f(t)$ inside Γ. Now $f(t)$ cannot vanish on Γ. For fixed m and all Ψ of $0 \leq \Psi \leq 1$, the function $f(t)$ is also uniformly bounded away from zero on the path. This implies that the integrand in the preceding formula is continuous in t and Ψ so that N is continuous in Ψ. But $N = 1$ for $\Psi = 0$, which completes the proof. The special case $n = 0$ refers to the interval $-\pi/2 \leq t \leq \pi/2$. Here $t = 0$ is the one and only zero. It leads to the excluded trivial case $\gamma = 0$.

Of greatest importance is the case $n = 1$. Here we deal with the interval $\pi/2 \leq t \leq 3\pi/2$. If $\Psi = 0$ or $m = 0$ then $t = \pi$ so that

$$\gamma = \frac{\pi}{2\Theta} \geq \frac{1}{2}.$$

In general **any** t of the open interval $(\pi/2, 3\pi/2)$ can be a zero of $f(t)$. In order to prove this point, we select a positive number $p < 1$ and introduce

$$q = t - \pi/2$$

and

Downloaded 03 May 2010 to 171.66.16.21. Redistribution subject to ASME license or copyright; see http://www.asme.org/terms/Terms_Use.cfm

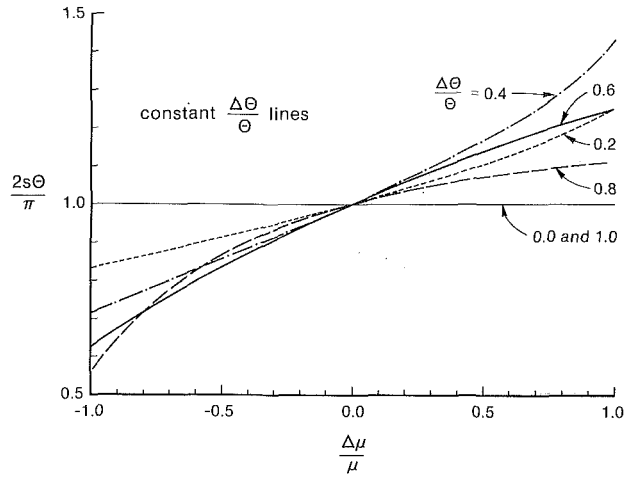


Fig. 3 Plots of $2s\Theta/\pi$, with s being the roots of the characteristic equation (12) in the interval (13), as a function of the mismatch in the elastic moduli, $\Delta\mu/\mu$, for selected notch face polar angles

$$q' = pq \quad \text{if} \quad q \le \pi/2;$$
$$q' = p(\pi - q) \quad \text{if} \quad q > \pi/2.$$

Finally, we choose

$$m = -\frac{\cos q}{\cos q'} \quad \text{and} \quad \Psi = \frac{(\pi/2) - q'}{(\pi/2) + q}.$$

Evidently Ψ is positive and below unity. Furthermore $\cos q' > \cos q$ for $q \le \pi/2$ and $-\cos q = \cos(\pi - q) < \cos[p(\pi - q)] = \cos q'$ for $q > \pi/2$. The latter implies $|m| < 1$. Clearly $f(t) = 0$. With respect to γ any value of the interval

$$\frac{\pi}{4\Theta} < \gamma < \frac{3\pi}{4\Theta} \tag{13}$$

can be a zero of the characteristic equation for suitable m and Ψ. In particular a positive $\gamma < 1/2$ is possible.

We conclude this discussion of γ with the remark that $\sin(\gamma\theta_1)$ and $\sin(\gamma\theta_2)$ vanish together if only one of them vanishes. This follows from (10). In this case, $\gamma\theta_1 = n_1\pi$, $\gamma\theta_2 = -n_2\pi$, $2\gamma\Theta = (n_1 + n_2)\pi$ with certain integers n_1, n_2. If $\gamma > 0$, then n_1, n_2 are positive so that $2\gamma\theta \ge 2\pi$; clearly γ cannot be in the important interval (13).

Turning now to a_1, a_2 and the functions $\omega_p(z)$, we observe that the reality of γ leads to

$$\omega_p = (a_p - \bar{a}_p) e^{-\gamma i\theta_p} z^\gamma.$$

As already mentioned (and without loss of generality), we may set $a_p = ib_p$ where b_1, b_2 are real and take the place of a_1, a_2 in (9). If (b_1, b_2) is a nontrivial solution of (9) then both $b_1 \ne 0$ and $b_2 \ne 0$. Thus one of these, say b_1, can be arbitrarily prescribed; the other follows suit. If $\sin(\gamma\theta_1) \ne 0$, then it is useful to introduce coefficients b, c defined by

$$b = b_1 \sin(\gamma\theta_1) \quad \text{and} \quad \mu_1 c = b_1 \cos(\gamma\theta_1).$$

This entails

$$b = b_2 \sin(\gamma\theta_2) \quad \text{and} \quad \mu_2 c = b_2 \cos(\gamma\theta_2).$$

With the aid of b, c, we may write

$$\omega_p = 2(b + i\mu_p c) z^\gamma, \quad p = 1,2.$$

If we confine γ to the interval (13), we may choose

$$a_p = \frac{ia}{2\sin(\gamma\theta_p)}, \quad a = \text{arbitrary real}$$

so that

$$\omega_p = \frac{ia}{\sin(\gamma\theta_p)} e^{-\gamma i\theta_p} z^\gamma = a[1 + i \operatorname{ctg}(\gamma\theta_p)] z^\gamma. \tag{14}$$

3.2 Notch Tip Regular Fields. The case $\theta_1 = \pi$, $\theta_2 = -\pi$, $\mu_1 = \mu_2$ is well known from the literature of antiplane strain (Mode III) deformation. The characteristic equation (12) yields the set of all integers as possible values for 2γ. Of these, the smallest positive one yields $\gamma = 1/2$ and determines the asymptotic behavior at the crack tip of those fields which are usually encountered in mechanical engineering.

In the general case of our consideration, the smallest positive γ is found in the interval (13). We refer to it in the form $\gamma = s$. Figure 3 displays the values of s obtained by solving the characteristic equation (12), which is transcendental in nature, numerically in the interval (13). Since the zeros to equation (12) must be the same when $\Delta\Theta$ and $\Delta\mu$ both change signs the values of s in the negative range of $\Delta\Theta/\Theta$ can be obtained by a mirror reflection of the values of s in the positive $\Delta\Theta/\Theta$ range with respect to the axis $\Delta\mu/\mu = 0$. Thus only the results in the range $0 \le \Delta\Theta/\Theta \le 1$ are shown in Fig. 3. We can expect s to determine the asymptotic behavior of a large family of fields at the notch tip. Following the concepts of regular field and fundamental field introduced by Bueckner (1970) for a cracked body, we shall call the elastic field, which has the asymptotic behavior given by this choice of γ, a regular field for the notched body.

Extending the convention in elastic crack mechanics, we define a notch-interface stress-intensity factor, K^N, for the notched body under antiplane strain deformation as

$$K^N \equiv \lim_{r \to 0} (2\pi r)^{1-s} \sigma_{32}(r, \theta = 0). \tag{15}$$

With this definition, the analytic functions $\omega_p(z)$ which characterize the asymptotic behavior of the regular field become

$$\omega_p(z) = \frac{K^N}{s(2\pi)^{1-s}} \left[1 + i \frac{\cos(s\theta_p)}{\sin(s\theta_p)}\right] z^s. \tag{16}$$

The corresponding displacement and stresses in the respective parts of the body near the notch tip are

$$w_p = \frac{K^N r^s}{\mu_p s(2\pi)^{1-s}} \frac{\cos[s(\theta_p - \theta)]}{\sin(s\theta_p)},$$

$$(\sigma_{32})_p = \frac{K^N}{(2\pi r)^{1-s}} \frac{\sin[(1-s)\theta + s\theta_p]}{\sin(s\theta_p)},$$

$$(\sigma_{31})_p = \frac{K^N}{(2\pi r)^{1-s}} \frac{\cos[(1-s)\theta + s\theta_p]}{\sin(s\theta_p)}.$$

In these formulas, the notch tip geometry shows up through θ_1, θ_2, and s. The relative mismatch of the elastic properties of Materials I, II is represented by s in the stress asymptotics and also by μ_1, μ_2 in those of displacement. The effects of external loading and body shape in the large enter through the notch-interface stress-intensity factor. If $\Delta\Theta = 0$, i.e., $\theta_2 = -\theta_1$, then $s = \pi/(2\Theta)$ regardless of any disparity in the materials. The relative spatial variation of the stresses near the notch tip is universal for all notched structures with the same material notch angle 2Θ. The same happens if $\Delta\mu = 0$. In this case, $\Delta\Theta = 0$ can be assumed without loss of generality since the x_1-axis can be chosen to bisect the material notch angle. Under these circumstances, the preceding asymptotics specialize into those of Ohr et al. (1985).

3.3 Fundamental Field and Weight Function. It was observed in Section 3.1 that both γ and $-\gamma$ satisfy the characteristic equation (12) simultaneously. If now $\gamma = -s$ is chosen the functions ω_p become

$$\Omega_p^* = c_p^f z^{-s} \tag{17}$$

with

$$c_p^f = -isc \left[\frac{\sin(s\theta_1)\sin(s\theta_2)}{\sin(s\theta_p)}\right] e^{is\theta_p}, \quad c = \text{real constant}.$$

Downloaded 03 May 2010 to 171.66.16.21. Redistribution subject to ASME license or copyright; see http://www.asme.org/terms/Terms_Use.cfm

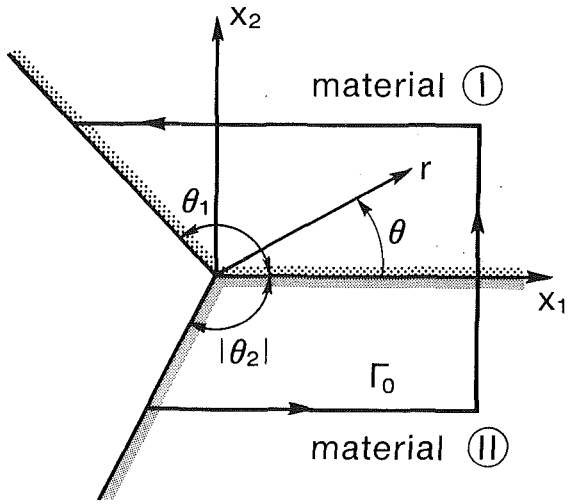


Fig. 4 Infinite notched structure with the notch tip located at the bimaterial interface

In the sequel, we set $c=1$. The field so-defined has unbounded energy of deformation in any neighborhood of the notch tip. The field is defined in the infinite notched structure of Fig. 4. It has no body forces and it exhibits no tractions on the notch faces $\theta=\theta_1$, θ_2. The stresses are of the order $O(r^{-s-1})$. The resultant of tractions along the path Γ_0 of Fig. 4 or any other path of the same type vanishes. Following Bueckner's weight-function theory (1970, 1973) for cracked bodies, we shall refer to the field by Ω_1^*, Ω_2^* as fundamental field of the notched body of Fig. 4.

In order to define fundamental fields for other structures, e.g., the configuration of Fig. 5 with the same notch angles as Fig. 4, we construct

$$\Omega_p=\Omega_p^*+\omega_p^* \tag{18}$$

where ω_1^*, ω_2^* define a regular field without body forces and without tractions on the notch faces. Moreover, the regular field must annihilate on S_T the tractions and on S_u the displacements induced by the Ω_p^*. At the notch tip, the behavior of this fundamental field follows the asymptotic relations

$$\Omega_p\sim\Omega_p^*. \tag{19}$$

We now apply the reciprocity theorem of linear elasticity to a fundamental field Ω_p and a regular field ω_p^r for the notched body. Due to the bonding conditions (8*a*), (8*b*) the reciprocity theorem for a homogeneous body can be applied, without change in form, to a piecewise homogeneous body. Since the reciprocity theorem holds only for fields of bounded strain energy, we shall exclude the interior of a small cylinder $r=R_0$ from the domain to which the reciprocity theorem is applied. Ultimately, we shall consider the result in the limit $R_0\to 0$.

Let A be the cross section of the configuration of Fig. 5 and let $A'\subset A$ be a subdomain, bounded by the contour Σ which consists of two circular arcs centered at the notch tip, L_1 and L_2, both of radius R_0, the boundaries S_T and S_u, and the remaining part of the notch faces, $S_{N'}$ (Fig. 5). We distinguish quantities of the regular and fundamental field by the superscripts r and f, respectively. The reciprocity theorem can now be written in the form

$$\int_\Sigma (w^r T^f-w^f T^r)\,\mathrm{d}l + \int_{A'}(w^r f^f-w^f f^r)\,\mathrm{d}A=0. \tag{20}$$

Using the properties

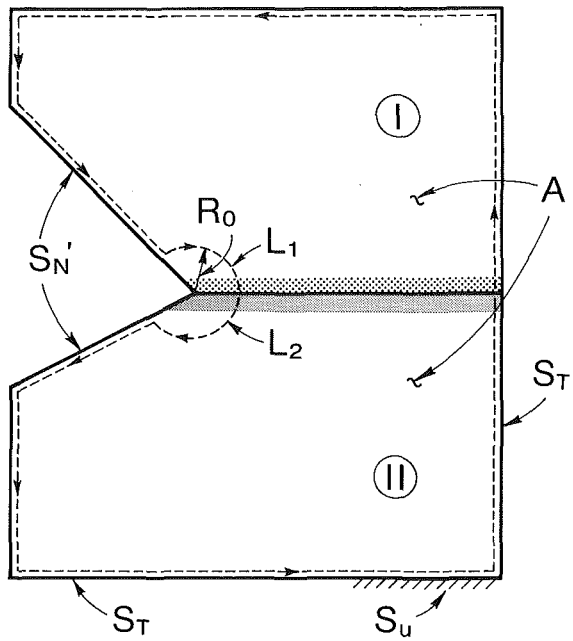


Fig. 5 Dashed lines represent the contour Σ which bounds the subdomain on which reciprocity between the fundamental field and the regular field is invoked

$$T^f=0 \quad \text{on the notch faces } S_{N'}$$
$$T^f=0 \quad \text{on } S_T$$
$$w^f=0 \quad \text{on } S_u$$
$$f^f=0 \quad \text{in } A'$$

we obtain

$$\int_{L_1+L_2}(w^r T^f-w^f T^r)\,\mathrm{d}l = \int_{S_T+S_{N'}} w^f T^r\,\mathrm{d}l-\int_{S_u} w^r T^f\,\mathrm{d}l+\int_{A'} w^f f^r\,\mathrm{d}A. \tag{21}$$

Let H be the integral on the left of (21). Using the asymptotic equations for the regular field (16) and the fundamental field (17 and 19), we find

$$H\sim\sum_{p=1}^{2}\int_{L_p}\frac{1}{\mu_p}\left[\mathrm{Im}\,[\Omega_p^*]\mathrm{d}(\mathrm{Re}\,[\omega_p])-\mathrm{Im}\,[\omega_p]\mathrm{d}(\mathrm{Re}\,[\Omega_p^*])\right].$$

Performing integration by parts on the second term, and noting from (16) and (17) that $\mathrm{Re}\,[\Omega_p^*]=0$ at $\theta=\theta_p$ and $\mathrm{Im}\,[(\omega_1)/\mu_1]\,\mathrm{Re}\,[\Omega_1^*]=\mathrm{Im}\,[(\omega_2)/\mu_2]\,\mathrm{Re}\,[\Omega_2^*]$ on $\theta=0$, we obtain

$$H\sim\sum_{p=1}^{2}\frac{1}{\mu_p}\,\mathrm{Im}\int_{L_p}\Omega_p^*\,\mathrm{d}\omega_p.$$

Writing (16) as

$$\omega_p=c_p^r\,z^s$$

and using (17), we get

$$H\sim\sum_{p=1}^{2}\frac{s}{\mu_p}\,\mathrm{Im}\left[c_p^f\,c_p^f\int_{L_p}\frac{dz}{z}\right].$$

But

$$\int_{L_1}\frac{dz}{z}=-\mathrm{i}\theta_1 \qquad \int_{L_2}\frac{dz}{z}=\mathrm{i}\theta_2;$$

therefore, as R_0 shrinks to zero, we have

$$H\to gK^N \quad \text{with} \quad gK^N=s\,\mathrm{Re}\,[-\theta_1 c_1^r c_1^f+\theta_2 c_2^r c_2^f].$$

In detail

Downloaded 03 May 2010 to 171.66.16.21. Redistribution subject to ASME license or copyright; see http://www.asme.org/terms/Terms_Use.cfm

$$g=\frac{1}{(2\pi)^{1-s}}\left[-\frac{\sin(s\theta_2)}{\mu_1\sin(s\theta_1)}s\theta_1+\frac{\sin(s\theta_1)}{\mu_2\sin(s\theta_2)}s\theta_2\right]. \quad (22)$$

Equations (21) and (22) yield the notch-interface stress-intensity factor K^N in the form

$$K^N=\int_{S_T+S_N}hT^r\mathrm{d}l-\int_{S_u}w^rT^f\mathrm{d}l+\int_A hf^r\mathrm{d}A \quad (23)$$

where h is the displacement field derived from the normalized analytic functions Ω_p^f

$$\Omega_p^f=\Omega_p(z)/g. \quad (24)$$

We call $h = h(x_1, x_2)$ the *antiplane strain weight function* for the notched body; note that $T^f = T^f(x_1, x_2)$ is now the traction generated by h. The weight function h as defined is an universal function for the given notched body with prescribed boundary portions S_T, S_u. The antiplane strain notch-interface stress-intensity factor K^N induced by **any** antiplane strain loading system f^r in A, T^r on $S_T + S_N$, w^r on S_u can be computed by the formula (23). The weight-function theory developed here for the notched body under antiplane strain conditions extends that given by Bueckner (1970, 1973) for a cracked body.

In the application of the reciprocity theorem in (20), one may replace the fundamental field Ω_p by the singular field Ω_p^* of (17). Using superscripts r and s to denote, respectively, quantities of the regular and singular field, one may write an analog of (23) as

$$gK^N=\int_{S_T+S_N+S_u}(w^sT^r-w^rT^s)\mathrm{d}l+\int_A w^sf^r\mathrm{d}A. \quad (25)$$

This provides an alternative integration formula for K^N. However, in order to use (25), one must procure supplementary information on the regular field; namely, the traction T^r on S_u and the displacement w^r on S_T.

By the same procedure, Stern (1973) obtained an analog of (25). In his paper, a notch in a homogeneous elastic structure under general plane deformation is considered. Body forces are absent; so are tractions on the notch faces. Adapted to antiplane strain, Stern's formula becomes a special case of (25), namely

$$gK^N=\int_{S_T+S_u}[w^sT^r-w^rT^s]\mathrm{d}l. \quad (26)$$

Under the same load restrictions, the weight-function formula (23) simplifies into

$$K^N=\int_{S_T}hT^r\mathrm{d}l-\int_{S_u}w^rT^f\mathrm{d}l. \quad (27)$$

Stern observed that the regular field of his formula, (26) in our notation, can be obtained by any convenient numerical procedure and will yield supplementary boundary data on S_T, S_u which are relatively insensitive to the accuracy of the field quantities near the notch tip. Thus (26) would represent an accuracy enhancing procedure for post-processing the numerically calculated regular field in order to determine K^N.

If one wishes to determine K^N for only one particular case of prescribed traction and displacement then (26) and (27) are equivalent with respect to numerical effort and accuracy. Both procedures demand the calculation of a regular field, namely of ω_p^r for (26) and ω_p^* for (27). In both cases, the field data are used on boundary portions which are remote from the crack tip. However, if the elastic structure is to be analyzed for more than one system of loading for fixed S_T and S_u, then the determination of K^N by means of (27) has a distinct advantage over (26) because of the universality of both Ω_p^* and ω_p^*.

In the case of an infinite domain, such as shown in Fig. 4, it seems plausible to replace (23) by

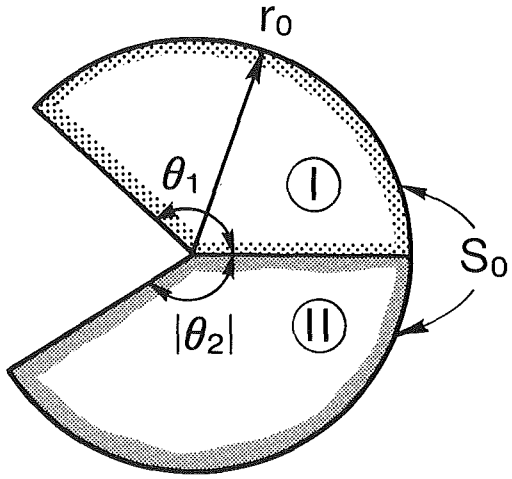


Fig. 6(a) Configuration of a finite notched cylindrical body for which a fundamental field is given in closed form

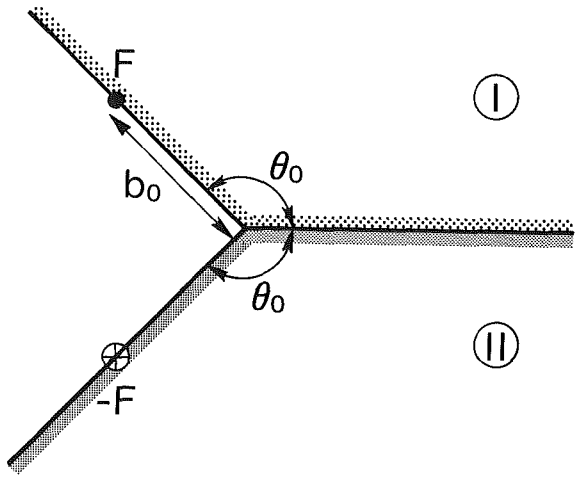


Fig. 6(b) Configuration of a piecewise homogeneous infinite notched body loaded by two point forces on the notch faces. The notch stress-intensity factor is determined for this configuration in closed form using the weight function.

$$K^N=\int_{S_N}hT^r\mathrm{d}l+\int_A hf^r\mathrm{d}A. \quad (28)$$

But this need not be so. To stay within the framework of weight-function theory, one should first apply the reciprocity theorem to a finite domain, e.g., Fig. 6(*a*), and let $r_0\to\infty$ thereafter. To fix ideas let us assume that body forces and notch face tractions of the regular field vanish for sufficiently large r; e.g., for $r>r'$. In this case, we obtain for $r_0 > r'$

$$K^N=\int_{S_N}hT^r\mathrm{d}l+\int_A hf^r\mathrm{d}A+K' \quad (29)$$

with

$$K'=\int_{S_0}[hT^r-w^rT^f]\mathrm{d}l.$$

Here K' is necessarily independent of r_0. In particular, $K' = 0$ if the products rhT^r and rw^rT^f go to zero as r goes to ∞. Under these circumstances, (28) is applicable. An example is given in Section 4.2.

4 Determination of Notch-Interface Weight Functions in Antiplane Strain

4.1 Closed-Form Examples of Fundamental Fields. There are two special cases in which the fundamental fields can be given in closed form. For the configuration of Fig. 4

Downloaded 03 May 2010 to 171.66.16.21. Redistribution subject to ASME license or copyright; see http://www.asme.org/terms/Terms_Use.cfm

the fundamental field is given by the analytic functions in Ω_p^* of (17).

We next consider a notched cylindrical body with a cross section bounded by the notch faces and a circular arc of radius r_0 as depicted in Fig. 6(*a*). A fundamental field for this notched body is given by the analytic functions

$$\Omega_p(z) = -is\left[\frac{\sin(s\theta_1)\sin(s\theta_2)}{\sin(s\theta_p)}\right]\left[e^{is\theta_p} z^{-s} + e^{-is\theta_p}\left(\frac{z}{r_0^2}\right)^s\right]. \quad (30)$$

These represent a linear combination with real combination coefficients of two fields of type (14) for $\gamma = s$ and $\gamma = -s$. Obviously the real parts of the analytic functions $\Omega_p(z)$ on the circular arc $z = r_0 e^{i\theta}$ are zero. Therefore the tractions of (30) generate zero traction on the circular arc and the notch faces. Also, the displacement and traction given by the Ω_p are continuous across the interface.

4.2 Evaluation of the Notch-Interface Stress-Intensity Factor. As an application of the formula (28) for calculating the notch-interface stress-intensity factor, we shall consider the infinite notched body of Fig. 6(*b*). Let the two notch face angles be the same, in particular, $\theta_1 = |\theta_2| = \theta_0$. The notched body is loaded by two concentrated forces F, $-F$ on the notch faces at the boundary points $z = b_0 e^{i\theta_0}$ and $z = b_0 e^{-i\theta_0}$, respectively. Here $F > 0$ denotes a force in the direction of the positive x_3-axis. Since the two notch face angles are the same, from Section 3.2, we find that $s = \pi/(2\Theta) = \pi/(2\theta_0)$ solves the characteristic equation (12). The analytic functions for the fundamental field given in (17) simplify to

$$\Omega_p(z) = -sz^{-s} \quad (31)$$

and the weight function in the respective parts of the body is

$$h_p = -\frac{(2\pi)^{1-s}s}{\mu_p \frac{\pi}{2}\left(\frac{1}{\mu_1}+\frac{1}{\mu_2}\right)} \operatorname{Im}[z^{-s}]. \quad (32)$$

By formula (28), the notch-interface stress-intensity factor for this infinite notched body loaded by two opposing point forces is

$$K^N = (2\pi)^{1-s}\frac{2Fs}{\pi b_0^s} \quad (33)$$

where we have assumed that the regular field decays sufficiently fast at infinity.

This can be confirmed by a direct analysis of the regular field. This field can be represented in closed form by

$$\omega_p(z) = \frac{iF}{\pi}\log\left[\frac{(z/b_0)^s + i}{(z/b_0)^s - i}\right]; \quad \text{main branch of log} \quad (34)$$

where $s = \pi/(2\theta_0)$. Indeed

$$\omega_p = O(z^{-s}) \quad \text{as} \quad z \to \infty$$

which permits us to apply (28). The notch-interface stress-intensity factor can be obtained directly by using its definition in (15). We note that $\sigma_{32} = \operatorname{Re}[\omega'(z)]$ and on the x_1-axis, we have

$$\sigma_{32} = \frac{2Fs}{\pi b_0^s} r^{s-1}\frac{1}{(r/b_0)^{2s}+1}.$$

As r approaches zero, this leads to a notch-interface stress-intensity factor which agrees with the one obtained by the weight-function formula (33).

4.3 Computational Method for Determining Notch-Interface Weight Functions in Complex Structures. Closed-form results for the weight functions of notched structures are limited to simple geometries and numerical procedures have to be employed in general to compute the notch-interface weight functions for more complicated geometries. It has been noted that the fundamental field given by the normalized analytic function Ω_p^f gives rise to unbounded strain energy in the neighborhood of the notch tip. This poses numerical difficulties in the computation of the notch-interface weight functions using conventional finite-element methods since they are based on the minimization of the elastic energy of the body. Sham (1987a) has introduced a variational principle for determining singular fields in finite bodies which overcomes such difficulties. A specialized form of this variational principle has been given for weight functions in cracked bodies and this leads to a simple and accurate finite-element method for computing weight functions associated with cracks (Sham, 1987a). The same finite-element procedure can also be used to determine the weight functions in notched structures (Sham, 1987b).

Acknowledgments

TLS is grateful to the support of the National Science Foundation Solid Mechanics Program through a research initiation Grant MEA83-07402.

References

Bueckner, H. F., 1970, "A Novel Principle for the Computation of Stress Intensity Factors," *Zeitschrift fur angewandte Mathematik und Mechanik*, Vol. 50, pp. 529–546.

Bueckner, H. F., 1973, "Field Singularities and Related Integral Representations," *Mechanics of Fracture I: Methods of Analysis and Solution of Crack Problems*, Sih, G. C., Ed., Noordhoff, Leyden, pp. 239–314.

Bueckner, H. F., 1977a, "The Weight Functions of Mode I of the Penny-Shaped and of the Elliptic Crack," *Fracture Mechanics and Technology, Volume II*, G. C. Sih and C. L. Chow, eds., Sijthoff and Noordhoff, pp. 1069–1090.

Bueckner, H. F., 1977b, "The Edge Crack in a Half Space," *Fracture Mechanics and Technology, Volume II*, G. C. Sih and C. L. Chow, eds., Sijthoff and Noordhoff, pp. 1091–1107.

Bueckner, H. F., 1987, "Weight Functions and Fundamental Fields for the Penny-Shaped and the Half-Plane Crack in Three-Space," *International Journal of Solids and Structures*, Vol. 23, pp. 57–93.

Carpenter, W. C., 1984a, "Calculation of Fracture Mechanics Parameters for a General Corner," *International Journal of Fracture*, Vol. 24, pp. 45–58.

Carpenter, W. C., 1984b, "Mode I and Mode II Stress Intensities for Plates with Cracks of Finite Opening" *International Journal of Fracture*, Vol. 24, pp. 201–214.

England, A. H., 1965, "A Crack Between Dissimilar Media," ASME Journal of Applied Mechanics, Vol. 32, pp. 400–402.

Erdogan, F., 1965, "Stress Distribution in Bonded Dissimilar Media," ASME Journal of Applied Mechanics, Vol. 32, pp. 403–410.

Hong, C.-C., and Stern, M., 1978, "The Computation of Stress Intensity Factors in Dissimilar Materials," *Journal of Elasticity*, Vol. 8, pp. 21–34.

Ohr, S. M., Chang, S.-J., and Thomson, R., 1985, "Elastic Interaction of a Wedge Crack with a Screw Dislocation," *Journal of Applied Physics*, Vol. 57, pp. 1839–1843.

Rice, J. R., 1972, "Some Remarks on Elastic Crack Tip Stress Fields," *International Journal of Solids and Structures*, Vol. 8, pp. 751–758.

Rice, J. R., 1985a, "First Order Variation in Elastic Fields Due to Variation in Location of a Planar Crack Front," ASME Journal of Applied Mechanics, Vol. 52, pp. 571–579.

Rice, J. R., 1985b, "Three-Dimensional Elastic Crack Tip Interactions with Transformation Strains and Dislocations," *International Journal of Solids and Structures*, Vol. 21, pp. 781–791.

Sham, T.-L., 1987a, "A Unified Finite Element Method for Determining Weight Functions in Two and Three Dimensions," *International Journal of Solids and Structures*, Vol. 23, pp. 1357–1372.

Sham, T.-L., 1987b, "Weight Functions for Piecewise Homogeneous Isotropic Notches in Antiplane Strain by Finite Element Method," to appear in *Journal of Engineering Fracture Mechanics*.

Stern, M., 1973, "A Boundary Integral Representation for Stress Intensity Factors," *Proceedings of the 10th Anniversary Meeting of the Society of Engineering Science*, Raleigh, N.C., November 5–7, 1973.

Stern, M., 1979, "The Numerical Calculation of Thermally Induced Stress Intensity Factors," *Journal of Elasticity*, Vol. 9, pp. 91–95.

Stern, M., Becker, E. B., and Dunham, R. S., 1976, "A Contour Integral Computation of Mixed-Mode Stress Intensity Factors," *International Journal of Fracture*, Vol. 12, pp. 359–368.

Stern, M. and Soni, M. L., 1976, "On the Computation of Stress Intensities

Downloaded 03 May 2010 to 171.66.16.21. Redistribution subject to ASME license or copyright; see http://www.asme.org/terms/Terms_Use.cfm

at Fixed-Free Corners," *International Journal of Solids and Structures*, Vol. 12, pp. 331–337.

Wu, K. C., and Hui, C. Y., 1987a, "A Complex-Variable Method for Two-Dimensional Internal Stress Problems and Its Applications to Crack Growth in Nonelastic Materials, Part I: Theory," ASME JOURNAL OF APPLIED MECHANICS, Vol. 54, pp. 59–64.

Wu, K. C., and Hui, C. Y., 1987b, "A Complex-Variable Method for Two-Dimensional Internal Stress Problems and Its Applications to Crack Growth in Nonelastic Materials, Part II: Applications," ASME JOURNAL OF APPLIED MECHANICS, Vol. 54, pp. 65–71.

APPENDIX

Extraordinary Elastic Fields With Bounded Strain Energy

We consider a homogeneous notched cylindrical body with a cross section bounded by the notch faces and a circular arc of radius r_0 as depicted in Fig. *A*-1. The polar angles for the upper and lower notch faces are Θ and $-\Theta$, respectively. This notched body is free of traction on the perimeter of its cross section but is loaded by a distributed body force $f = (r/r_0)^\lambda F \sin(\rho\theta)$, where $\rho = \pi/(2\Theta)$ and $0 < \Theta \leq \pi$.

The displacement w induced by this body force field is

$$\frac{\mu w}{Fr_0^2} = \frac{\sin(\rho\theta)}{\rho^2 - (\lambda+2)^2}\left[-\frac{\lambda+2}{\rho}\left(\frac{r}{r_0}\right)^\rho + \left(\frac{r}{r_0}\right)^{\lambda+2}\right], \quad \lambda+2 \neq \rho \tag{A-1}$$

This field has *finite* strain energy in the notched structure when $\lambda > -2$.

For the special case of a sharp crack, $\rho = 1/2$, the displacement in the cracked body is

$$\frac{\mu w}{Fr_0^2} = \frac{4\sin(\theta/2)}{1-4(\lambda+2)^2}\left[-2(\lambda+2)\sqrt{\frac{r}{r_0}} + \left(\frac{r}{r_0}\right)^{\lambda+2}\right], \quad \lambda+2 \neq 1/2 \tag{A-2}$$

The first term inside the brackets exhibits the well-known characteristic $\sqrt{r}$-dependence and its corresponding stress field is singular as $1/\sqrt{r}$. However, by prescribing a value for λ greater than -2 but less than $-3/2$, the second term inside the brackets of (*A*-2) would give a stress field which is more singular than $1/\sqrt{r}$ and yet the total strain energy in the body remains finite. Thus the usual argument of using finite strain energy as a criterion to rule out singular stresses other than those corresponding to the $1/\sqrt{r}$ singularity for a sharp crack is no longer valid when a strong enough singular body force field is present. In engineering applications, the gravity and the centrifugal forces are the typical body force loadings encountered and they would not alter the dominant $1/\sqrt{r}$ stress singularity associated with a sharp crack in a linear elastic body. But when fictitious body forces are employed as a mathematical tool in solving boundary-value problems for cracked bodies, for example, thermal stress analysis or interaction between transformation strains and crack tips (Rice, 1985; Wu and Hui 1987a, 1987b), the $1/\sqrt{r}$ stress singularity may not necessarily be the dominant singularity and care should be exercised.

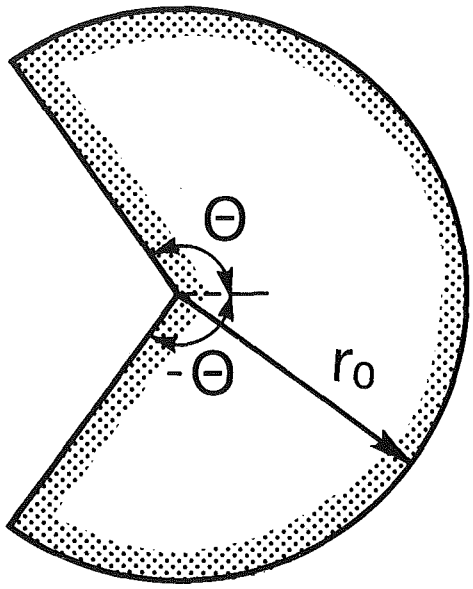


Fig. A-1 Configuration of a homogeneous notched cylindrical body loaded by a distributed body force field

Returning to the solution given in equation (*A*-2) for the cracked body, one finds

$$\frac{\mu w}{Fr_0^2} = 2\sin(\theta/2)\sqrt{\frac{r}{r_0}}\left[1 - \frac{1}{2}\log\frac{r}{r_0}\right] \tag{A-3}$$

when $\lambda + 2 \to 1/2$, and the observation concerning the possible existence of a stress field that is more singular than $1/\sqrt{r}$, but with bounded strain energy in the neighborhood of the tip, remains unchanged in this special case.

Downloaded 03 May 2010 to 171.66.16.21. Redistribution subject to ASME license or copyright; see http://www.asme.org/terms/Terms_Use.cfm

Elastic Field Around A Circular Punch

V. I. Fabrikant
Department of Mechanical Engineering,
Concordia University,
Montreal, H3G 1M8, Canada

A solution is called complete when the explicit expressions are derived for the field of displacements as well as stresses in an elastic body. A new method is proposed here which allows us to obtain exact and complete solutions to various contact problems in elementary functions; no integral transforms or special function expansions are involved. The method is based on the new results in potential theory obtained earlier by the author. The main potential function and the relevant Green's functions are derived explicitly. The interaction between an arbitrarily located concentrated load and a circular flat punch is considered. The use of the method is illustrated by examples.

Introduction

The great majority of the punch problems solved deals with the stresses and displacements in the plane $z=0$ only. There are just a few complete solutions published (Sneddon, 1951; Elliott, 1949), where explicit expressions are given for the field of displacements and stresses for the most simple axisymmetric problems for a circular punch. We are unaware of any non-axisymmetric punch problem solved compeltely in elementary functions. Knowledge of complete solutions is indispensable for consideration of more complicated problems of punch interactions, influence of external loads on punches, etc.

A new method is introduced which gives an exact closed form complete solution to the elastic contact problem for a circular punch of arbitrary profile. The solution, valid for a general mixed boundary value problem, is presented in the next section. The general solution is applied to the elastic contact problem, with all the relevant Green's functions derived, and expressed in elementary functions. It is shown that the complete solution can also be expressed in elementary functions for any polynomial profile. The elastic field behavior in the vicinity of the punch edge is found to be the same as in elastic crack problems.

The following notation is used throughout the paper.

$$l_1(t)=\frac{1}{2}\{[(\rho+t)^2+z^2]^{1/2}-[(\rho-t)^2+z^2]^{1/2}\} \tag{1}$$

$$l_2(t)=\frac{1}{2}\{[(\rho+t)^2+z^2]^{1/2}+[(\rho-t)^2+z^2]^{1/2}\}. \tag{2}$$

The integral L-operator is defined by

$$L(k)f(\phi)=\frac{1}{2\pi}\int_0^{2\pi}\lambda(k,\ \phi-\phi_0)f(\phi_0)d\phi_0, \tag{3}$$

where

$$\lambda(k,\psi)=\frac{1-k^2}{1+k^2-2k\cos\psi}.$$

The following three points are specified M, N, and N_0. Their polar cylindrical coordinates are $(\rho,\ \phi,\ z)$, $(r,\ \psi,\ 0)$, and $(\rho_0,\ \phi_0,\ 0)$, respectively.

$$R_0=R(M,N_0)=[\rho^2+\rho_0^2-2\rho\rho_0\cos(\phi-\phi_0)+z^2]^{1/2}. \tag{4}$$

$$R=[\rho^2+\rho_0^2-2\rho\rho_0\cos(\phi-\phi_0)]^{1/2}, \tag{5}$$

$$\eta=(a^2-\rho^2)^{1/2}(a^2-\rho_0^2)^{1/2}/a. \tag{6}$$

$$h=(a^2-l_1^2)^{1/2}(a^2-\rho_0^2)^{1/2}/a, \tag{7}$$

The contractions l_1 and l_2 everywhere in the paper stand for $l_1(a)$ and $l_2(a)$ respectively, as they are defined by equations (1) and (2). Note that h tends to η, as defined by (6), for $z\to 0$ and $\rho<a$.

$$q=\rho e^{i\phi}-\rho_0 e^{i\phi_0},\ s=(a^2-\rho\rho_0 e^{i(\phi-\phi_0)})^{1/2}. \tag{8}$$

Theory

General Solution. Consider a transversely isotropic elastic body which is characterized by five elastic constants A_{ik} defining the following stress-strain relationships:

$$\begin{aligned}
\sigma_x &= A_{11}\frac{\partial u_x}{\partial x}+(A_{11}-2A_{66})\frac{\partial u_y}{\partial y}+A_{13}\frac{\partial w}{\partial z},\\
\sigma_y &= (A_{11}-2A_{66})\frac{\partial u_x}{\partial x}+A_{11}\frac{\partial u_y}{\partial y}+A_{13}\frac{\partial w}{\partial z},\\
\sigma_z &= A_{13}\frac{\partial u_x}{\partial x}+A_{13}\frac{\partial u_y}{\partial y}+A_{33}\frac{\partial w}{\partial z},
\end{aligned} \tag{9}$$

$$\tau_{xy}=A_{66}\left(\frac{\partial u_x}{\partial y}+\frac{\partial u_y}{\partial x}\right),\tau_{yz}=A_{44}\left(\frac{\partial u_y}{\partial z}+\frac{\partial w}{\partial y}\right),$$

$$\tau_{zx}=A_{44}\left(\frac{\partial w}{\partial x}+\frac{\partial u_x}{\partial z}\right).$$

Contributed by the Applied Mechanics Division for presentation at the Winter Annual Meeting, Chicago, IL, November 28 to December 2, 1988, of THE AMERICAN SOCIETY OF MECHANICAL ENGINEERS.

Discussion on this paper should be addressed to the Editorial Department, ASME, United Engineering Center, 345 East 47th Street, New York, N.Y. 10017, and will be accepted until two months after final publication of the paper itself in the JOURNAL OF APPLIED MECHANICS. Manuscript received by ASME Applied Mechanics Division, October 29, 1987; final revision, March 10, 1988.
Paper No. 88-WA/APM-53.

Copyright © 1988 by ASME
Downloaded 03 May 2010 to 171.66.16.21. Redistribution subject to ASME license or copyright; see http://www.asme.org/terms/Terms_Use.cfm

The equilibrium equations are:

$$\frac{\partial\sigma_x}{\partial x}+\frac{\partial\tau_{xy}}{\partial y}+\frac{\partial\tau_{zx}}{\partial z}=0,\quad \frac{\partial\tau_{xy}}{\partial x}+\frac{\partial\sigma_y}{\partial y}+\frac{\partial\tau_{yz}}{\partial z}=0,$$

$$\frac{\partial\tau_{zx}}{\partial x}+\frac{\partial\tau_{yz}}{\partial y}+\frac{\partial\sigma_z}{\partial z}=0. \tag{10}$$

Introduce complex tangential displacements $u=u_x+iu_y$, and $\bar{u}=u_x-iu_y$. This will allow us to reduce the number of equations in (10) by one, and to rewrite these equations in a more compact manner, after substitution of (9) in (10), namely,

$$\frac{1}{2}(A_{11}+A_{66})\Delta u+A_{44}\frac{\partial^2 u}{\partial z^2}$$

$$+\frac{1}{2}(A_{11}-A_{66})\Lambda^2\bar{u}+(A_{13}+A_{44})\Lambda\frac{\partial w}{\partial z}=0, \tag{11}$$

$$A_{44}\Delta w+A_{33}\frac{\partial^2 w}{\partial z^2}+\frac{1}{2}(A_{13}+A_{44})\frac{\partial}{\partial z}(\bar{\Lambda}u+\Lambda\bar{u})=0. \tag{12}$$

Here the following differential operators were used:

$$\Delta=\frac{\partial^2}{\partial x^2}+\frac{\partial^2}{\partial y^2},\quad \Lambda=\frac{\partial}{\partial x}+i\frac{\partial}{\partial y}, \tag{13}$$

and the overbar everywhere indicates the complex conjugate value. Note also that $\Delta=\Lambda\bar{\Lambda}$. One can verify that equations (11) and (12) can be satisfied by

$$u=\Lambda(F_1+F_2+iF_3),\quad w=m_1\frac{\partial F_1}{\partial z}+m_2\frac{\partial F_2}{\partial z} \tag{14}$$

where all three functions F_k satisfy the equation (Elliott, 1948):

$$\Delta F_k+\gamma_k^2\frac{\partial^2 F_k}{\partial z^2}=0,\quad \text{for } k=1,2,3, \tag{15}$$

and the values of m_k and γ_k are related by the following expression (Elliott, 1948):

$$\frac{A_{44}+m_k(A_{13}+A_{44})}{A_{11}}$$

$$=\frac{m_k A_{33}}{m_k A_{44}+A_{13}+A_{44}}=\gamma_k^2,\quad \text{for } k=1,2;$$

$$\gamma_3=(A_{44}/A_{66})^{1/2}. \tag{16}$$

Introducing the notation $z_k=z/\gamma_k$, for $k=1,2,3$, we may call function $F_k=F(x,y,z_k)$ harmonic. Note the property $m_1m_2=1$, which seems to have escaped the attention of previous researchers, and which will help us to simplify various expressions to follow. The other elastic constants which will be used throughout the paper are:

$$G_1=\beta+\gamma_1\gamma_2 H,\qquad G_2=\beta-\gamma_1\gamma_2 H,$$

$$H=\frac{(\gamma_1+\gamma_2)A_{11}}{2\pi(A_{11}A_{33}-A_{13}^2)},\quad \alpha=\frac{(A_{11}A_{33})^{1/2}-A_{13}}{A_{11}(\gamma_1+\gamma_2)},\quad \beta=\frac{\gamma_3}{2\pi A_{44}}. \tag{17}$$

Introduce the following parameters:

$$\sigma_1=\sigma_x+\sigma_y,\ \sigma_2=\sigma_x-\sigma_y+2i\tau_{xy},\ \tau_z=\tau_{zx}+i\tau_{yz}. \tag{18}$$

This will simplify expressions (9), namely

$$\sigma_1=(A_{11}-A_{66})(\bar{\Lambda}u+\Lambda\bar{u})+2A_{13}\frac{\partial w}{\partial z},\ \sigma_2=2A_{66}\Lambda u,$$

$$\sigma_z=\frac{1}{2}A_{13}(\bar{\Lambda}u+\Lambda\bar{u})+A_{33}\frac{\partial w}{\partial z},\ \tau_z=A_{44}\left[\frac{\partial u}{\partial z}+\Lambda w\right]. \tag{19}$$

We have now only four components of stress, instead of six, as it was in (9). The substitution of (14) in (19) yields:

$$\sigma_1=2A_{66}\frac{\partial^2}{\partial z^2}\{[\gamma_1^2-(1+m_1)\gamma_3^2]F_1+[\gamma_2^2-(1+m_2)\gamma_3^2]F_2\},$$

$$\sigma_2=2A_{66}\Lambda^2(F_1+F_2+iF_3),$$

$$\sigma_z=A_{44}\frac{\partial^2}{\partial z^2}[(1+m_1)\gamma_1^2F_1+(1+m_2)\gamma_2^2F_2]$$

$$=-A_{44}\Delta[(1+m_1)F_1+(1+m_2)F_2],$$

$$\tau_z=A_{44}\Lambda\frac{\partial}{\partial z}[(1+m_1)F_1+(1+m_2)F_2+iF_3]. \tag{20}$$

Here we used the fact that each F_k satisfies equation (15), and the relation (for $k=1,2$): $A_{11}\gamma_k^2-A_{13}m_k=A_{44}(1+m_k)$ which is an immediate consequence of (16). Expressions (14) and (20) give a general solution, expressed in terms of three functions F_k. It is very attractive to express each function F_k through just *one* harmonic function as follows:

$$F_k(x,y,z)=c_kF(x,y,z_k), \tag{21}$$

where $z_k=z/\gamma_k$, and c_k is an as yet unknown complex constant. As we shall see further, this is possible indeed.

Contact Problem for a Smooth Punch. A smooth punch is pressed against a transversely isotropic elastic half-space $z\geq 0$ by a normal force P. Let S denote the domain of contact. The mixed boundary conditions on the plane $z=0$ are:

$$\sigma_z=0,\ \text{for } (\rho,\phi)\notin S;\ w=\omega(\rho,\phi),$$

$$\text{for } (\rho,\phi)\in S,\ \tau_z=0,\ \text{for } -\infty>(x,y)>\infty. \tag{22}$$

We may assume according to (21) that

$$F_1(z)=c_1F(z_1),\quad F_2(z)=c_2F(z_2),\quad F_3(z)=0. \tag{23}$$

Substitution of (23) and (20) in the third condition (22) yields:

$$c_1=-c_2\gamma_1/m_1\gamma_2 \tag{24}$$

Recall from (20) that σ_z is defined by the second z-derivative of the potential function F. In order to satisfy the first condition (22), we need to define the main potential function F so that its second z-derivative vanishes at $z=0$ outside the domain of contact. We known that the first z-derivative of the potential of a simple layer is zero outside the domain of integration. So, if we integrate the kernel of the simple layer $R(M,N)^{-1}$ with respect to z, the required representation takes the form

$$F(\rho,\phi,z)=F(M)=\iint_S \ln[R(M,N)+z]\sigma(N)\,dS_N. \tag{25}$$

Here σ is the normal stress exerted by the punch, and is equal and opposite to σ_z for $z=0$. The simple layer potential property yields inside the domain of contact:

$$\frac{\partial^2 F}{\partial z^2}\Big|_{z=0}=-2\pi\sigma, \tag{26}$$

which, combined with (20), gives the second equation for the constants c_1 and c_2

$$2\pi A_{44}[(1+m_1)c_1+(1+m_2)c_2]=1. \tag{27}$$

Equations (24) and (27) define the constants

$$c_1=H\gamma_1/(m_1-1),\ c_2=H\gamma_2/(m_2-1). \tag{28}$$

The simplifications made in (28) are due to the properties

$$m_1m_2=1,\ (m_1-1)/(m_1+1)=2\pi A_{44}H(\gamma_1-\gamma_2)$$

Downloaded 03 May 2010 to 171.66.16.21. Redistribution subject to ASME license or copyright; see http://www.asme.org/terms/Terms_Use.cfm

Finally, substitution of (23), (25) and (28) in the second equation (14) yields for $z=0$ the well known governing integral equation of elastic contact problem for a smooth punch:

$$\omega(N_0)=H\iint_S \frac{\sigma(N)}{R(N,N_0)}dS_N \tag{29}$$

An approximate analytical solution of (29) for a flat punch of arbitrary shape can be found in (Fabrikant, 1986b, 1986c). The case of a curved punch was considered in (Fabrikant, 1987). An exact solution in closed form is available for a circular punch of arbitrary profile (Fabrikant, 1986a). The method is based on the integral representation for reciprocal of distance between two point (Fabrikant, 1971a). The integral equation (29) can be rewritten for a circular domain of contact of radius a as follows (see Fabrikant, 1986a for details)

$$4H\int_0^\rho \frac{dx}{(\rho^2-x^2)^{1/2}} \int_x^a \frac{\rho_0 d\rho_0}{(\rho_0^2-x^2)^{1/2}} L\left(\frac{x^2}{\rho\rho_0}\right)\sigma(\rho_0,\phi)=\omega(\rho,\phi)$$

Its exact closed form solution is (Fabrikant, 1986a):

$$\sigma(\rho,\phi)=-\frac{1}{\pi^2 H\rho}L(\rho)\frac{d}{d\rho} \int_\rho^a \frac{xdx}{(x^2-\rho^2)^{1/2}} L\left(\frac{1}{x^2}\right)\frac{d}{dx}\int_0^x \frac{\rho_0 d\rho_0}{(x^2-\rho_0^2)^{1/2}}L(\rho_0)\omega(\rho_0,\phi).$$

Differentiation under the integral sign leads to another form of solution (Fabrikant, 1986a)

$$\sigma(\rho,\phi)=\frac{1}{\pi^2 H}\left[\frac{\Phi(a,\rho,\phi)}{(a^2-\rho^2)^{1/2}} -\int_\rho^a \frac{dx}{(x^2-\rho^2)^{1/2}}\frac{\partial}{\partial x}\Phi(x,\rho,\phi)\right], \tag{30}$$

where

$$\Phi(x,\rho,\phi)=\frac{1}{x}\int_0^x \frac{ydy}{(x^2-y^2)^{1/2}}\frac{d}{dy}\left[yL\left(\frac{y\rho}{x^2}\right)w(y,\phi)\right].$$

Note that expression (30) consists of two terms, the first one being singular at $\rho=a$, and the second one vanishing at the punch boundary. In the case of unknown radius of the domain of contact, it can be easily found from the condition $\sigma(a, \phi)=0$ which translates into $\Phi(a, a, \phi)=0$.

The potential function F can be found in two stages. First of all, one has from (25):

$$\frac{\partial F}{\partial z}=\int_0^{2\pi}\int_0^a \frac{\sigma(r,\psi)rdrd\psi}{[\rho^2+r^2-2r\rho\cos(\phi-\psi)+z^2]^{1/2}} \tag{31}$$

Substitution of (30) in (31) yields, after integration,

$$\frac{\partial F}{\partial z}=\frac{1}{\pi^2 H}\int_0^{2\pi}\int_0^a\left[\frac{R_0}{h} +\tan^{-1}\left(\frac{h}{R_0}\right)\right]\frac{z}{R_0^3}\omega(\rho_0,\phi_0)\rho_0 d\rho_0 d\phi_0. \tag{32}$$

Here $R_0=[\rho^2+\rho_0^2-2\rho\rho_0\cos(\phi-\phi_0)+z^2]^{1/2}$, and h is defined by (7). Expression (32) is convenient to use for numerical computation. In the case of exact evaluation of the integrals, an equivalent expression

$$\frac{\partial F}{\partial z}=\frac{1}{\pi^2 H}\int_0^{2\pi} d\psi\int_0^a \frac{[l_2^2(x)-x^2]^{1/2}}{l_2^2(x)-l_1^2(x)}\lambda\left(\frac{\rho}{l_2^2(x)},\ \phi-\psi\right) \times dx\frac{d}{dx}\int_0^x \frac{\rho_0 d\rho_0}{(x^2-\rho_0^2)^{1/2}}L(\rho_0)\omega(\rho_0,\psi) \tag{32a}$$

is recommended. One can deduce from (32a) that an arbitrary polynomial ω allows evaluation of $\partial F/\partial z$ in elementary functions. It can also be shown that the complete solution for any polynomial ω can be presented in elementary functions.

The next integration of (32) with respect to z gives the expression for the potential function directly through the prescribed displacement under the punch, namely,

$$F(\rho,\phi,z)=\frac{1}{\pi^2 H} \int_0^{2\pi}\int_0^a \kappa(\rho,\phi,z;\ \rho_0,\phi_0)\ \omega(\rho_0,\phi_0)\ \rho_0 d\rho_0 d\phi_0, \tag{33}$$

where

$$\kappa(\rho,\phi,\ z;\ \rho_0,\phi_0)=-\frac{1}{R_0}\tan^{-1}\left(\frac{h}{R_0}\right) +\frac{1}{(a^2-\rho_0^2)^{1/2}}\left[\ln\frac{a+(a^2-l_1^2)^{1/2}}{l_1} +\frac{1}{(\zeta-1)^{1/2}}\tan^{-1}\left[\frac{(a^2-l_1^2)^{1/2}}{a(\zeta-1)^{1/2}}\right] +\frac{1}{(\bar\zeta-1)^{1/2}}\tan^{-1}\left[\frac{(a^2-l_1^2)^{1/2}}{a(\bar\zeta-1)^{1/2}}\right]\right\},\ \zeta=\frac{\rho}{\rho_0}e^{i(\phi-\phi_0)}. \tag{34}$$

Now all the Green's functions, related to the field of displacements and stresses can be obtained from (34) by differentiation, in elementary functions:

$$\frac{\partial\kappa}{\partial z}=\frac{z}{R_0^3}\left[\frac{R_0}{h}+\tan^{-1}\left(\frac{h}{R_0}\right)\right], \tag{35}$$

$$\Lambda\kappa=\frac{q}{R_0^3}\tan^{-1}\left(\frac{h}{R_0}\right)-\frac{z^2}{h\bar q R_0^2} -\frac{1}{(a^2-\rho_0^2)^{1/2}\bar q(\bar\zeta-1)^{1/2}}\tan^{-1}\frac{(a^2-l_1^2)^{1/2}}{a(\bar\zeta-1)^{1/2}}, \tag{36}$$

$$\frac{\partial^2\kappa}{\partial z^2}=\frac{1}{R_0^3}\left(1-\frac{3z^2}{R_0^2}\right)\left[\frac{R_0}{h}+\tan^{-1}\left(\frac{h}{R_0}\right)\right] +\frac{1}{h(R_0^2+h^2)}\left[\frac{z^2}{R_0^2}-\frac{\rho^2-l_1^2}{l_2^2-l_1^2}\right], \tag{37}$$

$$\Lambda\frac{\partial\kappa}{\partial z}=-\frac{3zq}{R_0^5}\left[\frac{R_0}{h}+\tan^{-1}\left(\frac{h}{R_0}\right)\right] +\frac{z}{h(R_0^2+h^2)}\left[\frac{\rho e^{i\phi}}{l_2^2-l_1^2}+\frac{q}{R_0^2}\right], \tag{38}$$

$$\Lambda^2\kappa=-\frac{3q^2}{R_0^5}\tan^{-1}\left(\frac{h}{R_0}\right) -\frac{q^2 h}{R_0^4(R_0^2+h^2)}+\frac{2z^2}{h\bar q^2 R_0^2}\left(2-\frac{z^2}{R_0^2}\right) +\frac{1}{(a^2-\rho_0^2)^{1/2}}\left[\frac{3}{\bar q^2(\bar\zeta-1)^{1/2}}\tan^{-1}\frac{(a^2-l_1^2)^{1/2}}{a(\bar\zeta-1)^{1/2}} +\frac{a(a^2-l_1^2)^{1/2}}{\bar q^2(a^2\bar\zeta-l_1^2)}-\frac{a(a^2-l_1^2)^{1/2}\rho^2 e^{2i\phi}}{l_1^2(R_0^2+h^2)(l_2^2-l_1^2)}\right]. \tag{39}$$

Formulae (34–39) are the main new results of this paragraph. They give a complete solution for the considered contact problem when combined with formulae (14), (20), (23), and (28). When the prescribed displacement can be expressed as a sum of powers in x and y, the complete solution is elementary. Some particular examples will be considered in the next section.

Downloaded 03 May 2010 to 171.66.16.21. Redistribution subject to ASME license or copyright; see http://www.asme.org/terms/Terms_Use.cfm

Illustrative Examples

Here we present the complete solutions to some simple punch problems. The axisymmetric solutions were reported in the literature, so that we shall be able to compare the results. The non-axisymmetric one seems to be new.

Example 1: Flat Centrally Loaded Circular Punch. Consider a transversely isotropic elastic half-space $z \geq 0$, penetrated by a rigid circular punch of radius a. The punch loading is statically equivalent to a centrally applied normal force P. Denote the punch settlement by $\omega = \text{const}$. Solution of the integral equation (29) is given by (30), and in this particular case takes the form

$$\sigma(\rho,\phi) = \frac{\omega}{\pi^2 H (a^2-\rho^2)^{1/2}}. \tag{40}$$

Integration of the last expression over the circle $\rho \geq a$ relates the punch settlement ω with the total force P as

$$P = \frac{2\omega a}{\pi H}.$$

The substitution of (40) in (25) leads to an integral which can be identified by a partial derivative with respect to a of the main potential function Ψ (Appendix ($AA0$)). Differentiation with respect to a of ($A1$) yields

$$F = \frac{2\omega}{\pi H}\left[z\sin^{-1}\left(\frac{a}{l_2}\right) - (a^2-l_1^2)^{1/2} + a\ln[l_2 + (l_2^2-\rho^2)^{1/2}]\right]. \tag{41}$$

The appropriate differentiation (see Appendix) of the potential function (41) gives the complete solution:

$$u = \frac{2\omega a e^{i\phi}}{\pi\rho}\sum_{k=1}^{2}\frac{\gamma_k}{m_k-1}\left[1-\frac{(a^2-l_{1k}^2)^{1/2}}{a}\right], \tag{42}$$

$$w = \frac{2\omega}{\pi}\sum_{k=1}^{2}\frac{m_k}{m_k-1}\sin^{-1}\left(\frac{a}{l_{2k}}\right), \tag{43}$$

$$\sigma_1 = -\frac{4\omega A_{66}}{\pi}\sum_{k=1}^{2}\frac{\gamma_k^2-(m_k+1)\gamma_3^2}{\gamma_k(m_k-1)}\frac{(a^2-l_{1k}^2)^{1/2}}{l_{2k}^2-l_{1k}^2}, \tag{44}$$

$$\sigma_2 = \frac{4\omega A_{66}e^{2i\phi}}{\pi}\sum_{k=1}^{2}\frac{\gamma_k}{(m_k-1)}, \times\left\{\frac{(a^2-l_{1k}^2)^{1/2}}{l_{2k}^2-l_{1k}^2} - \frac{2a}{\rho^2}\left[1-\frac{(a^2-l_{1k}^2)^{1/2}}{a}\right]\right\}, \tag{45}$$

$$\sigma_z = \frac{\omega}{\pi^2 H(\gamma_1-\gamma_2)}\sum_{k=1}^{2}(-1)^k\gamma_k\frac{(a^2-l_{1k}^2)^{1/2}}{l_{2k}^2-l_{1k}^2}, \tag{46}$$

$$\tau_z = \frac{\omega e^{i\phi}}{\pi^2 H(\gamma_1-\gamma_2)}\sum_{k=1}^{2}(-1)^k\frac{l_{1k}(l_{2k}^2-a^2)^{1/2}}{l_{2k}(l_{2k}^2-l_{1k}^2)}. \tag{47}$$

Here l_{1k} and l_{2k} correspond to the notations (1) and (2), with parameter z formally replaced by z_k.

This problem was first solved by Elliott (1949). His solution is essentially in agreement with ours. The fact that he uses the notation ρ as an elastic parameter and as a polar radius simultaneously, somewhat complicates the comparison.

Introduce the stress intensity factor as

$$k_1 = \lim_{\rho\to a}\{(a-\rho)^{1/2}\sigma_z\}, \text{ for } z=0. \tag{48}$$

Substitution of (46) in (48) yields

$$k_1 = -\frac{\omega}{\pi^2 H\sqrt{2a}} = -\frac{P}{2\pi}\left(\frac{a}{2}\right)^{1/2}. \tag{49}$$

Introduce the local system of spherical coordinates (r, θ, ϕ), with the coordinate origin located at the punch edge. The following asymptotics are valid for the main parameters used in (42–47):

$$\rho = a + r\cos\theta,\ z = r\sin\theta,\ l_{1k} \approx a - \frac{1}{2}rS_k^2,\ l_{2k} \approx a + \frac{1}{2}rT_k^2,$$

$$l_{2k}^2 - l_{1k}^2 \approx 2arQ_k,\quad (a^2-l_{1k}^2)^{1/2} \approx (ar)^{1/2}S_k,$$

$$(l_{2k}^2-a^2)^{1/2} \approx (ar)^{1/2}T_k,\ \sin^{-1}\left(\frac{a}{l_{2k}}\right) \approx -\left(\frac{r}{a}\right)^{1/2}T_k. \tag{50}$$

Here the notation was introduced:

$$Q_k = [\cos^2\theta + (1/\gamma_k^2)\sin^2\theta]^{1/2},$$

$$S_k = [Q_k - \cos\theta]^{1/2},\ T_k = [Q_k + \cos\theta]^{1/2},$$

$$\text{for } k = 1,2,3. \tag{51}$$

The asympototical behavior of the field of stresses and displacements near the punch edge can be derived by substitution of (50)–(51) and (49) in (42)–(47). The result is:

$$u = u_n = 2\pi H k_1\sqrt{2r}\left[\frac{\gamma_1 S_1}{m_1-1} + \frac{\gamma_2 S_2}{m_2-1}\right] + 0(1), \tag{52}$$

$$w = -2\pi H k_1\sqrt{2r}\left[\frac{m_1 T_1}{m_1-1} + \frac{m_2 T_2}{m_2-1}\right] + 0(1), \tag{53}$$

$$\sigma_1 = 2\pi A_{66} H k_1\left(\frac{2}{r}\right)^{1/2}\sum_{k=1}^{2}\frac{\gamma_k^2-(m_k+1)\gamma_3^2}{\gamma_k(m_k-1)}\frac{S_k}{Q_k} + 0(1), \tag{54}$$

$$\sigma_2 = -2\pi A_{66} H k_1\left(\frac{2}{r}\right)^{1/2}\sum_{k=1}^{2}\frac{\gamma_k S_k}{(m_k-1)Q_k} + 0(\sqrt{r}), \tag{55}$$

$$\sigma_z = \frac{k_1}{\sqrt{2r}(\gamma_1-\gamma_2)}\left[\frac{\gamma_1 S_1}{Q_1} - \frac{\gamma_2 S_2}{Q_2}\right] + 0(1) \tag{56}$$

$$\tau_z = \tau_{zn} = -\frac{k_1}{\sqrt{2r}(\gamma_1-\gamma_2)}\left[\frac{T_1}{Q_1} - \frac{T_2}{Q_2}\right] + 0(\sqrt{r}), \tag{57}$$

Comparison of (52)–(57) with the corresponding results for cracks (Kassir and Sih, 1975) indicates that they become identical if one substitutes formally θ by $\pi-\theta$. This is easy to explain. The punch problem is mathematically equivalent to an external crack problem. There exist a notion that the asymptotic behavior of stresses and displacements near the edge of an arbitrary flat crack with a smooth boundary is completely defined by three stress intensity factors. This means that the asymptotics of an internal crack and an external one should be the same. The system of local axes was introduced in previous paragraph so that the angle θ was measured from the direction outside the crack. In the case of the punch problem the axis On should be inverted inside the circle, this will make the expressions (52)–(57) identical to the relevant expressions for a crack.

Example 2: Inclined Punch on an Elastic Half-Space. The case of a flat circular punch pressed against a transversely isotropic elastic half-space by a noncentrally applied force P can be considered as a superposition of two: that of a centrally loaded punch, which was considered earlier, and a punch subjected to a tilting moment $\mathfrak{M}$ which will be considered here. Let the displacements under the punch be

Downloaded 03 May 2010 to 171.66.16.21. Redistribution subject to ASME license or copyright; see http://www.asme.org/terms/Terms_Use.cfm

$$\omega = b_x y - b_y x. \tag{58}$$

Here b_x and b_y are the tilting angles about the axes Ox and Oy, respectively. Introduce the complex tilting angle

$$b = b_x + ib_y.$$

Expression (58) can be rewritten now as

$$\omega(\rho,\phi) = \Im\{\bar{b}\rho e^{i\phi}\}. \tag{59}$$

Here $\Im$ indicates the imaginary part. The substitution of (59) in (30) yields

$$\sigma(\rho,\phi) = \frac{2\,\Im\{\bar{b}\rho e^{i\phi}\}}{\pi^2 H(a^2-\rho^2)^{1/2}}. \tag{60}$$

Integration of (60) gives the following relationships between the tilting moments M_x, M_y and the angles b_x and b_y, namely,

$$M_x = \frac{4a^3}{3\pi H} b_x,\ M_y = \frac{4a^3}{3\pi H} b_y \tag{61}$$

It might be of interest to compare (61) with similar results obtained for a flat punch with a complete adhesion (Fabrikant, 1971b). This relationship has the form

$$M_x = \frac{4a^3\theta(\theta^2+1)}{3H\tanh\pi\theta} b_x,$$

$$M_y = \frac{4a^3\theta(\theta^2+1)}{3H\tanh\pi\theta} b_y,\ \tanh\pi\theta = \alpha/(\gamma_1\gamma_2)^{1/2},$$

and the remaining elastic constants are defined by (16) and (17). Since $\pi\theta(\theta^2+1) \geq \tanh\pi\theta$, we may conclude that the tilting moment, needed to produce the same angle of inclination, is greater for a bonded punch. They become equal in the limiting case of $\theta \to 0$, which in the case of an isotropic body corresponds to the Poisson ratio equal 1/2. Evaluation of the potential function (25) leads to the integral

$$\int_0^{2\pi}\int_0^a \frac{\rho_0 e^{i\phi_0}}{(a^2-\rho_0^2)^{1/2}} \ln(R_0+z)\rho_0 d\rho_0 d\phi_0. \tag{62}$$

Taking into consideration that

$$\frac{\rho e^{i\phi}}{(a^2-\rho^2)^{1/2}} = -\Lambda(a^2-\rho^2)^{1/2},$$

the integral in (62) can be computed by parts, with the result given by $-\Lambda\Psi$ [see Appendix (A5)]. The potential function takes the form:

$$F = \frac{2\,\Im\{\bar{b}\rho e^{i\phi}\}}{\pi H}\left[z\sin^{-1}\frac{a}{l_2} - (a^2-l_1^2)^{1/2}\left(1-\frac{l_1^2+2a^2}{3\rho^2}\right) - \frac{2a^3}{3\rho^2}\right]. \tag{63}$$

All the necessary derivatives are readily available from Appendix, and we can write the complete solution:

$$u = \frac{2i}{\pi}\sum_{k=1}^{2}\frac{\gamma_k}{m_k-1}\left\{b\left[z_k\sin^{-1}\left(\frac{a}{l_{2k}}\right) - (a^2-l_{1k}^2)^{1/2}\right] - \bar{b}e^{2i\phi}\frac{2a^3-(l_{1k}^2+2a^2)(a^2-l_{1k}^2)^{1/2}}{3\rho^2}\right\}, \tag{64}$$

$$w = \frac{2}{\pi}(b_y x - b_y x)\sum_{k=1}^{2}\frac{m_k}{m_k-1}\left[\sin^{-1}\left(\frac{a}{l_{2k}}\right) - \frac{a(l_{2k}^2-a^2)^{1/2}}{l_{2k}^2}\right], \tag{65}$$

$$\sigma_1 = -\frac{8A_{66}}{\pi}(b_x y - b_y x)a^2 \sum_{k=1}^{2}\frac{\gamma_k^2-(m_k+1)\gamma_3^2}{\gamma_k(m_k-1)}\frac{(a^2-l_{1k}^2)^{1/2}}{l_{2k}^2(l_{2k}^2-l_{1k}^2)}, \tag{66}$$

$$\sigma_2 = \frac{2A_{66}ie^{i\phi}}{\pi}\sum_{k=1}^{2}\frac{\gamma_k}{m_k-1}\left\{b\frac{al_{1k}(a^2-l_{1k}^2)^{1/2}}{l_{2k}(l_{2k}^2-l_{1k}^2)} - \bar{b}e^{2i\phi}\left[\frac{4[(l_{1k}^2+2a^2)(a^2-l_{1k}^2)^{1/2}-2a^3]}{3\rho^3} + \frac{al_{1k}(a^2-l_{1k}^2)^{1/2}}{l_{2k}(l_{2k}^2-l_{1k}^2)}\right]\right\}, \tag{67}$$

$$\sigma_z = \frac{2(b_x y - b_y x)}{\pi^2 H(\gamma_1-\gamma_2)}\sum_{k=1}^{2}(-1)^k\gamma_k\frac{a^2(a^2-l_{1k}^2)^{1/2}}{l_{2k}^2(l_{2k}^2-l_{1k}^2)}, \tag{68}$$

$$\tau_z = \frac{i}{\pi^2 H(\gamma_1-\gamma_2)}\sum_{k=1}^{2}\left\{b\left[\sin^{-1}\left(\frac{a}{l_{2k}}\right) - \frac{a(l_{2k}^2-a^2)^{1/2}}{l_{2k}^2-l_{1k}^2}\right] + \bar{b}e^{2i\phi}\frac{al_{1k}^2(l_{2k}^2-a^2)^{1/2}}{l_{2k}^2(l_{2k}^2-l_{1k}^2)}\right\}. \tag{69}$$

To the best of our knowledge, this problem has not been solved before.

Discussion

Here we discuss some immediate and future applications of the method presented in this paper. Comparison is made also with some results reported in the literature.

Investigation of various interactions (loads with cracks and punches, between cracks, etc.) becomes readily available due to the new theory. For example, consider the interaction of a concentrated load P_0, applied at an arbitrary point (ρ, ϕ, z) in the z-direction, with a flat circular punch of radius a. One can deduce from (43) that the normal displacement w at the point (ρ, ϕ, z), due to a unit force applied to the punch, is

$$w = \frac{H}{a}\sum_{k-1}^{2}\frac{m_k}{m_k-1}\sin^{-1}\left(\frac{a}{l_{2k}}\right),$$

Application of the reciprocal theorem immediately gives the punch settlement ω due to the load P_0

$$\omega = \frac{H}{a}P_0\sum_{k=1}^{2}\frac{m_k}{m_k-1}\sin^{-1}\left(\frac{a}{l_{2k}}\right).$$

The tilting angle b of the punch can be obtained in a similar manner from (65). The result is

$$b = \frac{3H}{2a^3}P_0\sum_{k=1}^{2}\frac{m_k}{m_k-1}\left[\rho\sin^{-1}\left(\frac{a}{l_{2k}}\right) - \frac{l_{1k}(l_{2k}^2-a^2)^{1/2}}{l_{2k}}\right].$$

It is of interest to indicate several solutions to the governing integral equation (29) in the case of a circular punch which are equivalent to (30). One such solution was obtained in (Fabrikant, 1986a):

$$\sigma(\rho,\phi) = \frac{1}{\pi^2 H}\times\left\{\frac{1}{(a^2-\rho^2)^{1/2}}\frac{\partial}{\partial a}\int_0^a\frac{\rho_0 d\rho_0}{(a^2-\rho_0^2)^{1/2}}L\left(\frac{\rho\rho_0}{a^2}\right)\omega(\rho_0\phi) - \frac{1}{2\pi}\int_0^{2\pi}\int_0^a\frac{1}{R}\tan^{-1}\left(\frac{\eta}{R}\right)\Delta\omega(\rho_0,\phi_0)\rho_0 d\rho_0 d\phi_0\right\}.$$

Here R and η are defined by (5) and (6) respectively, and Δ is a

Downloaded 03 May 2010 to 171.66.16.21. Redistribution subject to ASME license or copyright; see http://www.asme.org/terms/Terms_Use.cfm

two-dimensional Laplace operator. Taking into consideration that σ can be expressed through the limiting case of (37) for $z \to 0$, the following expression can be obtained

$$\sigma(\rho,\phi) = -\frac{1}{4\pi^2 H}\left\{\Delta\int_0^{2\pi}\int_0^a \frac{\omega(\rho_0,\phi_0)}{R}\rho_0 d\rho_0 d\phi_0 + \frac{2}{\pi}\int_0^{2\pi}\int_0^a\left[\frac{R}{\eta} - \tan^{-1}\left(\frac{R}{\eta}\right)\right]\frac{\omega(\rho_0,\phi_0)}{R^3}\rho_0 d\rho_0 d\phi_0\right\}.$$

This result was first derived by Leonov (1953). Another type of solution can be expressed through the second z-derivative of (33) for $z=0$. Taking into consideration that for a harmonic function the second z-derivative is equivalent to $-\Delta$, the following result is valid:

$$\sigma(\rho,\phi) = -\frac{1}{2\pi^3}H\left\{-\Delta\int_0^{2\pi}\int_0^a \frac{1}{R}\tan^{-1}\left(\frac{\eta}{R}\right)\omega(\rho_0,\phi_0)\rho_0 d\rho_0 d\phi_0 + \frac{a}{(a^2-\rho^2)^{3/2}}\int_0^{2\pi}\int_0^a \frac{1-\bar{t}}{(1-t)(1-\bar{t})}\frac{\omega(\rho_0,\phi_0)}{(a^2-\rho_0^2)^{1/2}}\rho_0 d\rho_0 d\phi_0\right\}$$

$$= -\frac{1}{\pi^2 H}\left\{-\Delta\int_\rho^a \frac{dx}{(x^2-\rho^2)^{1/2}}\int_0^x \frac{\rho_0 d_0}{(x^2-\rho_0^2)^{1/2}}L\left(\frac{\rho\rho_0}{x^2}\right)\omega(\rho_0,\phi) + \frac{a}{(a^2-\rho^2)^{3/2}}\int_0^a \frac{\rho_0 d\rho_0}{(a^2-\rho_0^2)^{1/2}}L\left(\frac{\rho\rho_0}{a^2}\right)\omega(\rho_0,\phi_0)\right\}.$$

The last formula corresponds to the solution by Mossakovskii et al. (1985).

Conclusion

The new method is proven capable of solving various nonaxisymmetric problems as easy as axisymmetric ones. Some of the problems solved are still beyond the reach of the existing methods, and many more new solutions are to come. The fact, that the new method does not use any integral transforms or special function expansions, makes it available for use by an average engineer.

Acknowledgment

The reported research was supported by a grant from the Natural Sciences and Engineering Research Council of Canada.

References

Elliot, H. A., 1948, "Three-Dimensional Stress Distributions in Hexagonal Aeolotropic Crystals," *Proc. Cambridge Phil. Soc.*, Vol. 44, pp. 522–533.

Elliott, H. A., 1949, "Axial Symmetric Stress Distributions in Aeolotropic Hexogonal Crystals. The Problem of the Plane and Related Problems," *Proc. Cambridge Phil. Soc.*, Vol. 45, pp. 621–630.

Fabrikant, V. I., 1971a, "Closed Form Solution of a Two-Dimensional Integral Equation," *Izvestiya Vyssikh Uchebnykh Zavedenii, Matematika*, No. 2, pp. 102–104, (in Russian).

Fabrikant, V. I., 1971b, "Effect of Shearing Force and Tilting Moment on a Cylindrical Punch Attached to a Transversely Isotropic Half-Space," *Journal of Applied Mathematics and Mechanics (PMM)*, No. 1, pp. 147–151.

Fabrikant, V. I., 1986a, "A New Approach to Some Problems in Potential Theory," *Zeitschrift für Angewandte Mathematik und Mechanik*, Vol. 66, pp. 363–368.

Fabrikant, V. I., 1986b, "Flat Punch of Arbitrary Shape on an Elastic Half-Space," *International Journal of Engineering Science*, Vol. 24, pp. 1731–1740.

Fabrikant, V. I., 1986c, "Inclinded Flat Punch of Arbitrary Shape on an Elastic Half-Space," ASME Journal of Applied Mechanics, Vol. 53, pp. 798–806.

Fabrikant, V. I., 1987, "Frictionless Elastic Contact Problem for a Curved Rigid Punch of Arbitrary Shape," *Acta Mechanica*, Vol. 67, pp. 1–25.

Kassir, M. K., and Sih, G., 1975, *Three-Dimensional Crack Problems*, Noordhoff International Publishing, Leyden.

Leonov, M. Ya., 1953, "General Problem of a Circular Punch Pressed Against an Elastic Half-Space," *Prikladnaya Matematika i Mekhanika*, Vol. 17, pp. 87–98, (in Russian).

Mossakovskii, V. I., Kachalovskaya, N. E., and Golidova, S. S., 1985, *Contact Problems of the Mathematical Theory of Elasticity*, Naukova Dumka, Kiev, (in Russian).

Sneddon, I. N., 1951, *Fourier Transforms*, McGraw-Hill, New York.

APPENDIX

Here the main potential function is given, together with selected partial derivatives. Define the potential function by

$$\Psi = \int_0^{2\pi}\int_0^a (a^2-\rho_0^2)^{1/2}\ln(R_0+z)\rho_0 d\rho_0 d\phi_0, \qquad (AA0)$$

where $R_0 = [\rho^2+\rho_0^2-2\rho\rho_0\cos(\phi-\phi_0)+z^2]^{1/2}$. The function is called main because the potential functions for various punch and crack problem can be expressed through it or its derivatives.

First of all, let us compute

$$\frac{\partial\Psi}{\partial z} = \int_0^{2\pi}\int_0^a \frac{(a^2-\rho_0^2)^{1/2}}{R_0}\rho_0 d\rho_0 d\phi_0. \qquad (AA1)$$

Make use of the integral representation for the reciprocal of the distance between two points, namely,

$$\frac{1}{R_0} = \frac{2}{\pi}\int_0^{l_1}\frac{dx}{\{[\rho^2-x^2][\rho_0^2-g^2(x)]\}^{1/2}}\lambda\left(\frac{x^2}{\rho\rho_0}, \phi-\phi_0\right), \qquad (AA2)$$

which is a modification of the result established in (Fabrikant, 1986a). Here

$$g^2(x) = x^2[1+z^2/(\rho^2-x^2)]. \qquad (AA3)$$

We substitute $(AA2)$ in $(AA1)$ and change the order of integration. We obtain, after integration with respect to ϕ_0

$$\frac{\partial\Psi}{\partial z} = 4\int_0^{l_1}\frac{dx}{(\rho^2-x^2)^{1/2}}\int_{g(x)}^a \frac{(a^2-\rho_0^2)^{1/2}\rho_0 d\rho_0}{[\rho_0^2-g^2(x)]^{1/2}} = \pi\int_0^{l_1}\frac{a^2-g^2(x)}{(\rho^2-x^2)^{1/2}}dx$$

$$= \pi\int_0^{l_1}\left[\frac{a^2-x^2}{(\rho^2-x^2)^{1/2}} - \frac{z^2x^2}{(\rho^2-x^2)^{3/2}}\right]dx$$

$$= \frac{\pi}{2}\left[(2a^2+2z^2-\rho^2)\sin^{-1}\left(\frac{l_1}{\rho}\right) - \frac{2a^2-3l_1^2}{a}(l_2^2-a^2)^{1/2}\right]. \qquad (AA4)$$

Now we need to integrate $(AA4)$ with respect to z in order to obtain Ψ. This can be done in elementary manner by using the integration by parts with subsequent substitution $z = (a^2-l_1^2)^{1/2}(\rho^2-l_1^2)^{1/2}/l_1$ or $z = (l_2^2-a^2)^{1/2}(l_2^2-\rho^2)^{1/2}/l_2$. Here we present, as an example, computation of the integral

$$\int\sin^{-1}\left(\frac{l_1}{\rho}\right)dz = z\sin^{-1}\left(\frac{l_1}{\rho}\right) - \int\frac{zdl_1}{(\rho^2-l_1^2)^{1/2}} = z\sin^{-1}\left(\frac{l_1}{\rho}\right) - \int\frac{(a^2-l_1^2)^{1/2}}{l_1}dl_1$$

$$= z\sin^{-1}\left(\frac{l_1}{\rho}\right) - (a^2-l_1^2)^{1/2} + a\ln\frac{a+(a^2-l_1^2)^{1/2}}{l_1} \qquad (AA5)$$

One has to remember that an arbitrary function of ρ might be lost during integration with respect to z. This function can usually be found from the conditions at 0 or ∞. For example,

Downloaded 03 May 2010 to 171.66.16.21. Redistribution subject to ASME license or copyright; see http://www.asme.org/terms/Terms_Use.cfm

if the result should be finite at $\rho=0$ in (A45), we should add $a\ln\rho$ which changes the logarithm into $\ln[l_2+(l_2^2-\rho^2)^{1/2}]$. The final result is

$$\Psi=\frac{\pi}{2}\left[z(2a^2-\rho^2+\frac{2}{3}z^2)\sin^{-1}\frac{a}{l_2}+\frac{1}{3}(a^2-l_1^2)^{1/2}\left(5\rho^2-\frac{10}{3}a^2-2l_2^2-\frac{11}{3}l_1^2\right)+\frac{4}{3}a^3\ln[l_2+(l_2^2-\rho^2)^{1/2}]\right] \quad (A)$$

The following derivatives may be computed:

$$\frac{\partial\Psi}{\partial x}=\pi x\left[-z\sin^{-1}\frac{a}{l_2}+(a^2-l_1^2)^{1/2}\left(1-\frac{l_1^2+2a^2}{3\rho^2}\right)+\frac{2a^3}{3\rho^2}\right] \quad (A2)$$

$$\frac{\partial\Psi}{\partial y}=\pi y\left[-z\sin^{-1}\frac{a}{l_2}+(a^2-l_1^2)^{1/2}\left(1-\frac{l_1^2+2a^2}{3\rho^2}\right)+\frac{2a^3}{3\rho^2}\right] \quad (A3)$$

$$\frac{\partial\Psi}{\partial z}=\frac{\pi}{2}\left[(2a^2+2z^2-\rho^2)\sin^{-1}\frac{a}{l_2}-\frac{2a^2-3l_1^2}{a}(l_2^2-a^2)^{1/2}\right] \quad (A4)$$

$$\Lambda\Psi=\pi\rho e^{i\phi}\left[-z\sin^{-1}\frac{a}{l_2}+(a^2-l_1^2)^{1/2}\left(1-\frac{l_1^2+2a^2}{3\rho^2}\right)+\frac{2a^3}{3\rho^2}\right] \quad (A5)$$

$$\frac{\partial^2\Psi}{\partial x^2}=\pi\left[-z\sin^{-1}\frac{a}{l_2}+(a^2-l_1^2)^{1/2}+\left(1-\frac{2x^2}{\rho^2}\right)\frac{2a^3-(l_1^2+2a^2)(a^2-l_1^2)^{1/2}}{3\rho^2}\right] \quad (A6)$$

$$\frac{\partial^2\Psi}{\partial y^2}=\pi\left[-z\sin^{-1}\frac{a}{l_2}+(a^2-l_1^2)^{1/2}+\left(1-\frac{2y^2}{\rho^2}\right)\frac{2a^3-(l_1^2+2a^2)(a^2-l_1^2)^{1/2}}{3\rho^2}\right] \quad (A7)$$

$$\frac{\partial^2\Psi}{\partial x\partial y}=-2\pi xy\frac{2a^3-(l_1^2+2a^2)(a^2-l_1^2)^{1/2}}{3\rho^4} \quad (A8)$$

$$\Lambda^2\Psi=-2\pi e^{2i\phi}\frac{2a^3-(l_1^2+2a^2)(a^2-l_1^2)^{1/2}}{3\rho^2} \quad (A9)$$

$$\Delta\Psi=2\pi\left[-z\sin^{-1}\frac{a}{l_2}+(a^2-l_1^2)^{1/2}\right] \quad (A10)$$

$$\frac{\partial^2\Psi}{\partial z^2}=2\pi\left[z\sin^{-1}\frac{a}{l_2}-(a^2-l_1^2)^{1/2}\right] \quad (A11)$$

$$\frac{\partial}{\partial z}\Lambda\Psi=\pi\rho e^{i\phi}\left[-\sin^{-1}\frac{a}{l_2}+\frac{a(l_2^2-a^2)^{1/2}}{l_2^2}\right] \quad (A12)$$

$$\frac{\partial^3\Psi}{\partial x^2\partial z}=\pi\left\{-\sin^{-1}\frac{a}{l_2}+\frac{a(l_2^2-a^2)^{1/2}}{l_2^2}\left[1+\frac{2a^2x^2}{l_2^2(l_2^2-l_1^2)}\right]\right\} \quad (A13)$$

$$\frac{\partial^3\Psi}{\partial y^2\partial z}=\pi\left\{-\sin\frac{a}{l_2}+\frac{a(l_2^2-a^2)^{1/2}}{l_2^2}\left[1+\frac{2a^2y^2}{l_2^2(l_2^2-l_1^2)}\right]\right\} \quad (A14)$$

$$\frac{\partial^3\Psi}{\partial z^3}=2\pi\left\{\sin^{-1}\frac{a}{l_2}-\frac{a(l_2^2-a^2)^{1/2}}{l_2^2-l_1^2}\right\} \quad (A15)$$

$$\frac{\partial^3\Psi}{\partial x\partial y\partial z}=2\pi\frac{a^3xy(l_2^2-a^2)^{1/2}}{l_2^4(l_2^2-l_1^2)} \quad (A16)$$

$$\frac{\partial^3\Psi}{\partial x\partial z^2}=2\pi\frac{a^2x(a^2-l_1^2)^{1/2}}{l_2^2(l_2^2-l_1^2)} \quad (A17)$$

$$\frac{\partial^3\Psi}{\partial y\partial z^2}=2\pi\frac{a^2y(a^2-l_1^2)^{1/2}}{l_2^2(l_2-l_1^2)} \quad (A18)$$

$$\frac{\partial}{\partial z}\Lambda^2\Psi=2\pi\rho^2e^{2i\phi}\frac{a^3(l_2^2-a^2)^{1/2}}{l_2^4(l_2^2-l_1^2)} \quad (A19)$$

$$\frac{\partial}{\partial z}\Delta\Psi=2\pi\left[-\sin^{-1}\frac{a}{l_2}+\frac{a(l_2^2-a^2)^{1/2}}{l_2^2-l_1^2}\right] \quad (A20)$$

$$\frac{\partial^2}{\partial z^2}\Lambda\Psi=2\pi a^2\rho e^{i\phi}\frac{(a^2-l_1^2)^{1/2}}{l_2^2(l_2^2-l_1^2)} \quad (A21)$$

$$\Lambda\Delta\Psi=-2\pi a^2\rho e^{i\phi}\frac{(a^2-l_1^2)^{1/2}}{l_2^2(l_2^2-l_1^2)} \quad (A22)$$

$$\Lambda^3\Psi=-2\pi e^{3i\phi}\times\left\{\frac{4[(l_1^2+2a)(a^2-l_1^2)^{1/2}-2a^3]}{3\rho^3}+\frac{al_1(a^2-l_1^2)^{1/2}}{l_2(l_2^2-l_1^2)}\right\} \quad (A23)$$

$$\frac{\partial^4\Psi}{\partial z^4}=-2\pi\frac{za[l_1^4+a^2(2a^2+2z^2-3\rho^2)]}{(l_2^2-l_1^2)^3(l_2^2-a^2)^{1/2}} \quad (A24)$$

$$\frac{\partial^4\Psi}{\partial\rho\partial z^3}=-2\pi\frac{l_1(l_2^2-a^2)^{1/2}}{l_2(l_2^2-l_1^2)^3}[a^2(4l_2^4-5\rho^2)+l_1^4] \quad (A25)$$

$$\frac{\partial^2}{\partial z^2}\Lambda^2\Psi=2\pi\rho^2e^{2i\phi}a^3z\frac{a^2(6l_2^2-2l_1^2+\rho^2)-5l_2^4}{l_2^4(l_2^2-l_1^2)^3(l_2^2-a^2)^{1/2}} \quad (A26)$$

The following identities were used during the derivation of (A1-A26):

$$l_1l_2=a\rho,\quad l_1^2+l_2^2=a^2+\rho^2+z^2, \quad (A27)$$

$$(l_2^2-\rho^2)^{1/2}(l_2^2-a^2)^{1/2}=zl_2,\quad (a^2-l_1^2)^{1/2}(\rho^2-l_1^2)^{1/2}=zl_1,$$

$$(a^2-l_1^2)^{1/2}(l_2^2-a^2)^{1/2}=za,\quad (l_2^2-\rho^2)^{1/2}(\rho^2-l_1^2)^{1/2}=z\rho. \quad (A28)$$

$$\frac{\partial l_1}{\partial z}=-\frac{zl_1}{l_2^2-l_1^2},\quad \frac{\partial l_2}{\partial z}=\frac{zl_2}{l_2^2-l_1^2},$$

$$\frac{\partial l_1}{\partial\rho}=\frac{al_2-\rho l_1}{l_2^2-l_1^2}=\frac{\rho(a^2-l_1^2)}{l_1(l_2^2-l_1^2)},\quad \frac{\partial l_2}{\partial\rho}=\frac{\rho l_2-al_1}{l_2^2-l_1^2}=\frac{\rho(l_2^2-a^2)}{l_2(l_2^2-l_1^2)}. \quad (A29)$$

Downloaded 03 May 2010 to 171.66.16.21. Redistribution subject to ASME license or copyright; see http://www.asme.org/terms/Terms_Use.cfm

A Refined Small Strain and Moderate Rotation Theory of Elastic Anisotropic Shells

R. Schmidt
Institute of Civil Engineering Mechanics,
University of Wuppertal,
D-5600 Wuppertal, West Germany

J. N. Reddy
Clifton C. Garvin Professor,
Department of Engineering Science
and Mechanics,
Virginia Polytechnic Institute
and State University,
Blacksburg, VA 24061
Mem. ASME

A general refined shell theory that accounts for the transverse deformation, small strains, and moderate rotations is presented. The theory can be reduced to various existing shell theories including: the classical (i.e., linear Kirchhoff-Love) shell theory, the Donnell-Mushtari-Vlasov shell theory, the Leonard-Koiter-Sanders moderate rotations shell theory, the von Kármán type shear-deformation shell theory and the moderate-rotation shear-deformation plate theory developed by Reddy. The present theory is developed from an assumed displacement field, nonlinear strain-displacement equations that contain small strain and moderate rotation terms, and the principle of virtual displacements. The governing equations exhibit strong coupling between the membrane and bending deformations, which should alter the bending, stability, and post-buckling behavior of certain shell structures predicted using the presently available theories.

1 Introduction

The advent of fiber-reinforced composite materials and their use in aerospace, automobile and civilian (e.g., medical and sports equipment) structures has generated interest in an accurate modeling of the kinematic behavior of composite plates and shells. The classical (e.g., Kirchhoff-Love) shell theory is based on an assumption of infinite rigidity in transverse direction (i.e., neglect of the transverse strains). The theory is found to yield adequate results for thin isotropic shells. However, composite-material shells exhibit finite transverse rigidity (i.e., the transverse shear modulus is quite smaller compared to the inplane shear modulus) and, therefore, the classical shell theory is inadequate for an accurate description of the state of deformation in composite shells. Use of the nonlinear strain-displacement equations in the development of shell theories is motivated by the need for an accurate prediction of load-deflection curves, analysis of stability and post-buckling behavior and natural vibration data for the design of shell structures.

The transverse deformation is accounted either through an assumed displacement field or through an assumed stress field. In both cases, the displacements or stresses are expanded in terms of the thickness coordinate to a desired degree. Basset (1890) presented a shell theory based on an assumed displacement field, and Reissner (1966) developed a shear-deformation shell theory based on an assumed stress field. Following these works, many linear theories have been proposed in the literature (see, for example, Koiter, 1967; Naghdi, 1956, 1963; Dong and Tso, 1972; Whitney and Sun, 1974; and Reddy, 1984a). These differ from each other in accounting for only transverse shear strains, transverse normal strains, the number of terms retained in the expansions, or inclusion of higher-order effects (i.e., shallow shells, deep shells, etc.).

Consideration of geometric nonlinearity in shells is originally due to Donnell (1933), von Kármán (1910, 1965), Marguerre (1939) and Mushtari (1938), among others. Following these pioneering works several generalizations and/or modifications of the theories appeared in the literature. The geometric nonlinearity in shells should be accounted in three different levels: (*i*) The von Kármán type nonlinearity that accounts only for the products and squares of the derivatives of the transverse deflection in the strain-displacement equations; (*ii*) The moderate rotation theories that account for moderate rotation terms; (*iii*) The large rotation theories that account for large rotations.

Full nonlinear theories are those which do not neglect any nonlinear terms in the strain-displacement equations. The von Kármán type nonlinearity in the Kirchhoff-Love shell theories is considered by Marguerre (1939), Donnell (1933), Mushtari (1938) and Vlasov (1949). The von Kármán type nonlinearity in the first-order (i.e., Sanders, 1959) shell theory is discussed by Reddy (1982). Moderate rotation theories, with the Kirchhoff-Love assumptions, are presented by Reissner (1950), Mushtari and Galimov (1961), Leonard (1961), Sanders (1963), Koiter (1966) and Pietraszkiewicz (1977). Moderate rotation theories with shear-deformation effects are considered by Wempner (1973), Galimov (1977), Librescu and

Contributed by the Applied Mechanics Division for presentation at the Winter Annual Meeting, Chicago, IL, November 28 to December 2, 1988, of THE AMERICAN SOCIETY OF MECHANICAL ENGINEERS.

Discussion on this paper should be addressed to the Editorial Department, ASME, United Engineering Center, 345 East 47th Street, New York, N.Y. 10017, and will be accepted until two months after final publication of the paper itself in the JOURNAL OF APPLIED MECHANICS. Manuscript received by ASME Applied Mechanics Division, April 27, 1987; final revision, December 1, 1987.
Paper No. 88-WA/APM-37.

Copyright © 1988 by ASME
Downloaded 03 May 2010 to 171.66.16.21. Redistribution subject to ASME license or copyright; see http://www.asme.org/terms/Terms_Use.cfm

Schmidt (1986). Large rotation theories, limited to the Kirchhoff-Love assumption, are discussed by Pietraszkiewicz (1984), Schmidt (1984a,b) and others (see Schmidt, 1985a for additional references). Full nonlinear theories of shells are presented by Koiter (1966), Budiansky (1968), Schroeder (1972), Koiter and Simmonds (1973), Pietraszkiewicz (1981, 1984) and Schmidt (1985b) in the context of the Kirchhoff-Love assumption, and by Reissner (1963), Naghdi (1956, 1972), Habip and Ebcioglu (1965), Librescu (1973, 1987), Yokoo and Matsunaga (1974) and Krätzig (1971) in the context of shear-deformation theories.

Full nonlinear theories of shells are not only complex but not warranted in the analysis of most shell structures. On the other hand, the von Kármán type nonlinear shell theories may not accurately represent certain phenomena; for example, the buckling and post-buckling of shells. A compromise between simplicity and accuracy is provided by a consistent moderate rotation theory. Moderate rotation theories with shear-deformation effects, which are limited in number, are either developed in an *ad-hoc* way (i.e., keeping nonlinear terms that are *believed* to be essential) or cast in an abstract form that is not directly useful for analysis. The objective of the present study is to present a consistent shear-deformation shell theory with moderate rotations. The derivation is based on an order-of-magnitude assumption of various strain and rotation measures, the nonlinear strain-displacement equations and the principle of virtual work. The present work differs from that of Librescu and Schmidt (1986) in two basic respects. First, in the framework of the first-order shear-deformation theory, the strain-displacement relations are further reduced to a simple form by invoking the order-of-magnitude assumptions. The simplified form is more effective for analysis purposes, and contains terms of the lower-order theories more explicitly. Second, the governing equations are derived in terms of the displacements, for the first-order expansion in thickness coordinate, for ready use in the analysis.

Preliminaries

Let V be the volume of the undeformed body, and A_s and A_u be the two parts of the lateral boundary surface A of V on which the stresses and displacements are prescribed, respectively. Let S^+ and S^- denote the top and bottom surfaces of the volume V, and Ω be the undeformed midsurface of the shell such that

$$V=\Omega\times\left(-\frac{h}{2}\,,\ \frac{h}{2}\right)$$

where h is the total thickness of the shell. Let Γ_s and Γ_u denote the intersections of A_s and A_u, respectively, with Ω.

Points of V are defined by a general convected coordinate system $(\theta^1, \theta^2, \theta^3)$, with (θ^1, θ^2) denoting the curvilinear surface coordinates of a point in Ω and θ^3 denoting the normal coordinate. Covariant and contravariant base vectors at points of Ω are denoted by $\mathbf{a}_\alpha$, $\mathbf{a}^\alpha$ with corresponding metrics $a_{\alpha\beta}$, $a^{\alpha\beta}$, Greek indices having values 1 and 2

$$a_{\alpha\beta}=\mathbf{a}_\alpha\cdot\mathbf{a}_\beta,\quad a^{\alpha\beta}=\mathbf{a}^\alpha\cdot\mathbf{a}^\beta,\quad \mathbf{a}^\alpha\cdot\mathbf{a}_\beta=\delta^\alpha_\beta$$
$$\mathbf{a}_\alpha=\frac{\partial\mathbf{r}}{\partial\theta^\alpha}=\mathbf{r}_{,\alpha},\quad \mathbf{r}=\mathbf{r}(\theta^2,\theta^2) \tag{1}$$

where $\mathbf{r}$ is the position vector of a typical point (θ^1, θ^2) in Ω, δ^α_β is the Kronecker delta, and the notation $(\cdot)_{,\alpha}$ denotes differentiation with respect to θ^α. Similarly, covariant and contravariant base vectors at points of V are denoted by $\mathbf{g}_i$, $\mathbf{g}^i$ with corresponding metrics g_{ij}, g^{ij}, Latin indices having values 1, 2, and 3. Thus (see Reddy and Rasmussen, 1982 for additional details on tensor algebra and calculus),

$$g_{ij}=\mathbf{g}_i\cdot\mathbf{g}_j,\quad g^{ij}=\mathbf{g}^i\cdot\mathbf{g}^j,\quad \mathbf{g}^i\cdot\mathbf{g}_j=\delta^i_j$$

$$\mathbf{g}_i=\frac{\partial\mathbf{R}}{\partial\theta^i}=\mathbf{R}_{,i},\quad \mathbf{R}=\mathbf{R}(\theta^1,\theta^2,\theta^3) \tag{2}$$

where $\mathbf{R}$ is the position vector of a typical point $(\theta^1, \theta^2, \theta^3)$ in V.

The position vector $\mathbf{R}$ at point $(\theta^1, \theta^2, \theta^3)$ can be expressed in terms of $\mathbf{r}$ and the unit vector $\mathbf{n}$ normal to the midsurface Ω at point (θ^1, θ^2). The unit normal $\mathbf{n}$ is defined by

$$\mathbf{n}=\frac{\partial\mathbf{R}}{\partial\theta^3}\bigg|_{\theta^3=0}=\mathbf{g}_3=\mathbf{g}^3. \tag{3}$$

Then it follows that

$$\mathbf{R}=\mathbf{r}+\theta^3\mathbf{n},\quad \mathbf{a}_\alpha\cdot\mathbf{n}=0$$
$$g_{\alpha3}=g^{\alpha3}=0,\quad g_{33}=g^{33}=1. \tag{4}$$

The covariant components of the curvature tensor are defined by

$$b_{\alpha\beta}=\mathbf{r}_{,\alpha\beta}\cdot\mathbf{n}$$
$$=\mathbf{a}_{\alpha,\beta}\cdot\mathbf{n}=-\mathbf{a}_\alpha\cdot\mathbf{n}_{,\beta}. \tag{5}$$

The mixed components of the curvature tensor are given by

$$b^\alpha_\beta=a^{\alpha\mu}b_{\mu\beta} \tag{6}$$

where summation on repeated indices is implied. In view of definitions (1)–(5), the covariant base vectors $\mathbf{g}_\alpha$ and $\mathbf{a}_\beta$ are related according to the equation

$$\mathbf{g}_\alpha=c^\beta_\alpha\mathbf{a}_\beta,\quad c^\beta_\alpha=\delta^\beta_\alpha-\theta^3b^\beta_\alpha \tag{7}$$

where c^β_α are known as the mixed components of the shifter tensor. Thus

$$g_{\alpha\beta}=c^\lambda_\alpha c^\mu_\beta a_{\lambda\mu}. \tag{8}$$

The following additional definitions and relationships are needed in the sequel

$$a=\det\ (a_{\alpha\beta}),\quad g=\det\ (g_{ij}),\quad c=\sqrt{g/a}\,.$$

Order-of-Magnitude Assumptions

Let $\mathbf{u}$ denote the displacement vector associated with a point $(\theta^1, \theta^2, \theta^3)$ in V. The displacement vector can be expressed either in terms of the base vectors $\mathbf{g}_i$ (or $\mathbf{g}^i$) in V or $\mathbf{a}_\alpha$ and $\mathbf{n}$ in Ω

$$\mathbf{u}=U^i\mathbf{g}_i=U_i\mathbf{g}^i$$
$$=u^\alpha\mathbf{a}_\alpha+u^3\mathbf{n}=u_\alpha\mathbf{a}^\alpha+u_3\mathbf{n} \tag{9}$$

where (U^i, U_i) and (u^α, u_α) denote the contravariant and covariant components of vector $\mathbf{u}$ in V and Ω, respectively.

The nonlinear strain-displacement equations of elasticity referred to the base vectors $\mathbf{g}_i$ in V are given by

$$E_{ij}=\frac{1}{2}(U_{i;j}+U_{j;i}+U_{m;i}U^m_{;j}) \tag{10}$$

where E_{ij} denote the components of the Green strain tensor and $(\cdot)_{;j}$ denotes covariant derivative with respect to θ^j:

$$\frac{\partial\mathbf{u}}{\partial\theta^j}=U^i_{;j}\mathbf{g}_i=U_{i;j}\mathbf{g}^i \tag{11a}$$

The covariant derivative of a vector with respect to θ^α in Ω is denoted by $(\cdot)|_\alpha$

$$\frac{\partial\mathbf{u}}{\partial\theta^\alpha}=u^\beta|_\alpha\mathbf{a}_\beta=u_\beta|_\alpha\mathbf{a}^\beta \tag{11b}$$

The covariant derivatives of a vector $\mathbf{u}$ in V are related to its covariant derivatives in Ω according to the expressions

$$U_{\alpha;\beta}=c^\lambda_\alpha(u_{\lambda|\beta}-b_{\lambda\beta}u_3)$$
$$U_{\alpha;3}=c^\lambda_\alpha u_{\lambda,3}$$

Downloaded 03 May 2010 to 171.66.16.21. Redistribution subject to ASME license or copyright; see http://www.asme.org/terms/Terms_Use.cfm

$$U_{3;\alpha} = u_{3,\alpha} + b_\alpha^\lambda u_\lambda$$
$$U_{3;3} = u_{3,3} \tag{12}$$

To derive a consistent moderate rotation theory it is necessary to impose restrictions on the orders of magnitudes of the total strains, and then retain terms which are considered to be relatively important in the strain-displacement equations. To include moderate rotation terms within the assumed order of magnitude of the total strains, it is useful to write the nonlinear strain-displacement equations in terms of the linear components of strains and rotations

$$e_{ij} = \frac{1}{2}(U_{i;j} + U_{j;i}), \quad \omega_{ij} = \frac{1}{2}(U_{i;j} - U_{j;i}).$$

It should be noted that ω_{ij} denotes the linear, hence the leading, part of the total rotation (see Wempner, 1973).

Rewriting the nonlinear strain-displacement equations in terms of e_{ij} and ω_{ij}, one obtains the expression

$$E_{ij} = e_{ij} + \frac{1}{2}\omega_{ki}\omega^k{}_j + \frac{1}{2}(e_{kj}\omega^k{}_i + e_{ki}\omega^k{}_j) + \frac{1}{2}e_{ki}e^k{}_j. \tag{13}$$

In the foregoing expression, various terms are of different magnitude for different problems. The assumption of small strains means that

$$E_{ij} = 0(\theta^2), \quad \theta^2 \ll 1. \tag{14a}$$

Furthermore, we assume that the shell material line elements undergo moderate rotations of the normal, while the rotations about the normal remain small. This yields the following orders of magnitude

$$\omega_{\alpha 3} \approx 0(\theta), \quad \omega_{\alpha\beta} \approx 0(\theta^2). \tag{14b}$$

Equations (13), (14*a*) and (14*b*) imply that

$$e_{ij} = 0(\theta^2). \tag{14c}$$

Such an order-of-magnitude assumption on strains was adopted by several authors (see, for example, Sanders, 1963; Koiter, 1966; Galimov, 1977; Wempner, 1973; Librescu and Schmidt, 1986; Reddy, 1987 and Pietraszkiewicz, 1979), and the same will be used in the present development. The strains are assumed to be small [of $0(\theta^2)$], terms of one-order higher than the strains are retained, and terms of relative order θ^2 compared to strains are neglected in the present theory.

The use of order-of-magnitude of assumption (14) in equation (13) and neglecting terms of order θ^4 and higher, results in the following strain-displacement equations

$$E_{\alpha\beta} = e_{\alpha\beta} + \frac{1}{2}\omega_{3\beta}\omega_{3\alpha} + \frac{1}{2}(e_{3\beta}\omega_{3\alpha} + e_{3\alpha}\omega_{3\beta})$$

$$E_{\alpha 3} = e_{\alpha 3} + \frac{1}{2}\omega_{\beta 3}\omega^\beta{}_\alpha + \frac{1}{2}(e_{\beta\alpha}\omega^\beta{}_3 + e_{33}\omega^3{}_\alpha)$$

$$E_{33} = e_{33} + \frac{1}{2}\omega_{\alpha 3}\omega^\alpha{}_3 + e_{\alpha 3}\omega^\alpha{}_3 \tag{15}$$

where the underlined terms are of magnitude θ^3.

Kinematics of Deformation

Consider a shell of uniform thickness h. In the interest of accounting for the transverse strains, it is assumed that the straight lines normal to the midsurface before deformation remain straight but not normal after deformation, and may undergo extensions. The classical Kirchhoff-Love theory is based on the kinematical assumption of infinite rigidity in the transverse direction (straight normals remain straight and normal, and are inextensible). This is the assumption of *plane strain*. This assumption leads to wrong constitutive equations for the transverse shear forces and the transverse normal stresses. In order to remedy this, two tricks are often used (which are also part of the classical Kirchhoff-Love theory): (*a*) It is forbidden to calculate the transverse shear forces from constitutive equations; (*b*) It is assumed in the constitutive equations that $S^{33} \equiv 0$, instead of $E^{33} \equiv 0$. The assumption that $S^{33} = 0$ is of course inconsistent with the plane-strain assumption, but this is the discrepancy of the classical Kirchhoff-Love theory. In order to improve the theoretical foundation of this theory, Koiter (1966), presented what he calls a theory "on the basis of a modified version of the Kirchhoff-Love hypotheses" and what today usually is referred to as the first-approximation theory of thin, elastic, isotropic shells. He describes this as follows (see Koiter, 1966): "The modification of the classical, mutually contradictory Kirchhoff-Love hypotheses consisted of their replacement by a single assumption of an approximately plane state of stress parallel to the middle surface." Koiter (1960) showed that for the case of an approximately plane state of stress [$S^{\alpha 3} = 0(\theta S^{\alpha\beta})$, $S^{33} = 0(\theta^2 \cdot S^{\alpha\beta})$] the contradictory assumptions of the classical Kirchhoff-Love theory are compatible with each other in the error margin of this elastic isotropic shell theory (which cannot be improved by any means, i.e., even by taking transverse shear or normal effects into account). The last two of the following three assumptions of the Kirchhoff-Love kinematic hypothesis are not used in the development of the present theory:

1 The straight lines normal to the shell midsurface before deformation remain straight after deformation.

2 The straight lines normal to the midsurface are inextensible.

3 The straight lines normal to the shell midsurface before deformation remain normal after the deformation.

Assumption 3 leads to the neglect of the transverse shear strains, while assumption 2 results in the neglect of the transverse normal strain. Assumption 1 leads to a linear variation of the displacements through the thickness. It should be noted that no assumption concerning the variation of stresses through the thickness of the shell is made.

The displacement components (u_α, u_3) are assumed to vary through the shell thickness according to the expressions

$$u_i = u_i^{(0)} + \theta^3 u_i^{(1)} \tag{16}$$

where $u_i^{(0)}$ denote the displacement along the θ^i-direction at a point (θ^1, θ^2) in Ω, and $(u_1^{(1)}, u_2^{(1)})$ denote rotations of a normal. Substituting equation (16) into equation (15), the following relations are obtained

$$E_{\alpha\beta} = E_{\alpha\beta}^{(0)} + \theta^3 E_{\alpha\beta}^{(1)} + (\theta^3)^2 E_{\alpha\beta}^{(2)} = \sum_{n=0}^{2} (\theta^3)^n E_{\alpha\beta}^{(n)}$$

$$E_{\alpha 3} = \sum_{n=0}^{\infty} (\theta^3)^n E_{\alpha 3}^{(n)}$$

$$E_{33} = \sum_{n=0}^{\infty} (\theta^3)^n E_{33}^{(n)} \tag{17}$$

where

$$E_{\alpha\beta}^{(n)} = e_{\alpha\beta}^{(n)} + \frac{1}{2}\sum_{m=0}^{n} [\omega_{3\alpha}^{\{m\}}\omega_{3\beta}^{\{n-m\}} + (\omega_{3\beta}^{\{n-m\}}e_{3\alpha}^{\{m\}} + \omega_{3\alpha}^{\{n-m\}}e_{3\beta}^{\{m\}})]$$

Downloaded 03 May 2010 to 171.66.16.21. Redistribution subject to ASME license or copyright; see http://www.asme.org/terms/Terms_Use.cfm

$$E_{\alpha 3}^{(n)} = e_{\alpha 3}^{(n)} + \frac{1}{2}\sum_{m=0}^{n}[\omega_{\lambda 3}^{(m)}\omega_{\cdot\alpha}^{(n-m)\lambda} + e_{\lambda\alpha}^{(m)}\omega_{\cdot 3}^{(n-m)\lambda} + e_{33}^{(m)}\omega_{\cdot\alpha}^{(n-m)3}]$$

$$E_{33}^{(n)} = e_{33}^{(n)} + \frac{1}{2}\sum_{m=0}^{n}[\omega_{\lambda 3}^{(m)}\omega_{\cdot 3}^{(n-m)\lambda} + 2e_{\lambda 3}^{(m)}\omega_{\cdot 3}^{(n-m)\lambda}] \tag{18}$$

and

$$e_{\alpha\beta}^{(n)} = \frac{1}{2}[\phi_{\alpha\beta}^{(n)} + \phi_{\beta\alpha}^{(n)} - b_\alpha^\lambda\phi_{\lambda\beta}^{(n-1)} - b_\beta^\lambda\phi_{\lambda\alpha}^{(n-1)}]$$

$$e_{\alpha 3}^{(n)} = \frac{1}{2}[\phi_{\alpha 3}^{(n)} + (n+1)u_\alpha^{(n+1)} - nb_\alpha^\lambda u_\lambda^{(n)}]$$

$$e_{33}^{(n)} = (n+1)u_3^{(n+1)}$$

$$\omega_{\alpha\beta}^{(n)} = \frac{1}{2}[\phi_{\alpha\beta}^{(n)} - \phi_{\beta\alpha}^{(n)} - b_\alpha^\lambda\phi_{\lambda\beta}^{(n-1)} + b_\beta^\lambda\phi_{\lambda\alpha}^{(n-1)}]$$

$$\omega_{\cdot\beta}^{(n)\alpha} = \frac{1}{2}\sum_{m=0}^{n}(B^m)^{\alpha\lambda}[\phi_{\lambda\beta}^{(n-m)} - \phi_{\beta\lambda}^{(n-m)} - m\phi_{\beta\lambda}^{(n-m)} + (m+1)b_\beta^\gamma\phi_{\gamma\lambda}^{(n-m-1)}]$$

$$\omega_{3\alpha}^{(n)} = \frac{1}{2}[\phi_{\alpha 3}^{(n)} - (n+1)u_\alpha^{(n+1)} + nb_\alpha^\lambda u_\lambda^{(n)}]$$

$$\omega_{\cdot 3}^{(n)\alpha} = \frac{1}{2}\sum_{m=0}^{n}(B^m)^{\alpha\lambda}[(n-m+1)u_\lambda^{(n-m+1)} - (m+1)\phi_{\lambda 3}^{(n-m)}] \tag{19}$$

In the interest of brevity, the following notation was introduced in writing equations (17) and (18)

$$\phi_{\alpha 3}^{(n)} = u_{3,\alpha}^{(n)} + b_\alpha^\lambda u_\lambda^{(n)}$$
$$\phi_{\alpha\beta}^{(n)} = u_{\alpha|\beta}^{(n)} - b_{\alpha\beta}u_3^{(n)}$$
$$(B^n)_\beta^\alpha = b_\lambda^\alpha(B^{n-1})_\beta^\lambda = b_\beta^\lambda(B^{n-1})_\lambda^\alpha$$
$$(B^n)^{\alpha\beta} = (B^n)_\lambda^\alpha a^{\lambda\beta}, \quad \phi_{\cdot\beta}^{(n)\alpha} = a^{\alpha\lambda}\phi_{\lambda\beta}^{(n)} \tag{20}$$
$$(B^0)_\beta^\alpha = \delta_\beta^\alpha \quad \text{and} \quad (B^n)_\beta^\alpha = \phi_{\alpha\beta}^{(n)} = 0 \quad \text{for} \quad n<0.$$

Equations (18)–(19) can be further simplified by invoking the assumptions (14) and neglecting terms of order θ^4. The simplified equations are given by (terms of order θ^4 are shown with an underline to indicate the simplification achieved)

$$E_{\alpha\beta}^{(0)} = \theta_{\alpha\beta}^{(0)} + \frac{1}{2}\phi_{\alpha 3}^{(0)}\phi_{\beta 3}^{(0)} - \underline{\frac{1}{2}e_{3\alpha}^{(0)}e_{3\beta}^{(0)}} + 0(\theta^4)$$

$$E_{\alpha\beta}^{(1)} = \theta_{\alpha\beta}^{(1)} - \frac{1}{2}(b_\alpha^\mu\phi_{\mu\beta}^{(0)} + b_\beta^\mu\phi_{\mu\alpha}^{(0)}) + \frac{1}{2}(\phi_{\alpha 3}^{(0)}\phi_{\beta 3}^{(1)} + \phi_{\beta 3}^{(0)}\phi_{\alpha 3}^{(1)}) - \underline{\frac{1}{2}(e_{3\alpha}^{(0)}e_{3\beta}^{(1)} + e_{3\beta}^{(0)}e_{3\alpha}^{(1)})} + 0\left(\frac{\theta^4}{h}\right)$$

$$E_{\alpha\beta}^{(2)} = -\frac{1}{2}(b_\alpha^\lambda\phi_{\lambda\beta}^{(1)} + b_\beta^\lambda\phi_{\lambda\alpha}^{(1)}) + \frac{1}{2}\phi_{\alpha 3}^{(1)}\phi_{\beta 3}^{(1)} - \underline{\frac{1}{2}e_{3\alpha}^{(1)}e_{3\beta}^{(1)}} + 0\left(\frac{\theta^4}{h^2}\right)$$

$$E_{\alpha 3}^{(0)} = \frac{1}{2}(\phi_{\alpha 3}^{(0)} + u_\alpha^{(1)}) + \frac{1}{2}u^{\lambda(1)}\phi_{\lambda\alpha}^{(0)} + \frac{1}{4}u_3^{(1)}(\phi_{\alpha 3}^{(0)} - u_\alpha^{(1)}) - \underline{\frac{1}{2}e_{\cdot 3}^{(0)\lambda}(e_{\lambda\alpha}^{(0)} + \omega_{\lambda\alpha}^{(0)})} + 0(\theta^4)$$

$$E_{\alpha 3}^{(1)} = \frac{1}{2}u_{3,\alpha}^{(1)} + \frac{1}{2}u^{(1)\lambda}u_{\lambda|\alpha}^{(1)} - \frac{1}{4}u_{3,\lambda}^{(1)}\phi_{\cdot\alpha}^{(0)\lambda} - \underline{\frac{1}{2}e_{\lambda 3}^{(0)}(e_{\cdot\alpha}^{(1)\lambda} + \omega_{\cdot\alpha}^{(1)\lambda}) + \frac{1}{2}e_{33}^{(0)}e_{\alpha 3}^{(1)}} + 0\left(\frac{\theta^4}{h}\right)$$

$$E_{\alpha 3}^{(2)} = \underline{-\frac{1}{2}e_{\lambda 3}^{(0)}(e_{\cdot\alpha}^{(2)\lambda} + \omega_{\cdot\alpha}^{(2)\lambda})} - \underline{\frac{1}{2}e_{\lambda 3}^{(1)}(e_{\cdot\alpha}^{(1)\lambda} + \omega_{\cdot\alpha}^{(1)\lambda})} + 0\left(\frac{\theta^4}{h^2}\right)$$

$$E_{33}^{(0)} = u_3^{(1)} + \frac{1}{2}u_\lambda^{(1)}u^{(1)\lambda} - \underline{\frac{1}{2}e_{\lambda 3}^{(0)}e_{\cdot 3}^{(0)\lambda}} + 0(\theta^4)$$

$$E_{33}^{(1)} = \underline{-\frac{1}{2}e_{\lambda 3}^{(0)}e_{\cdot 3}^{(1)\lambda} - \frac{1}{2}e_{\lambda 3}^{(1)}e_{\cdot 3}^{(0)\lambda}} + 0\left(\frac{\theta^4}{h}\right)$$

$$E_{33}^{(2)} = \underline{-\frac{1}{2}e_{\lambda 3}^{(0)}e_{\cdot 3}^{(2)\lambda} - \frac{1}{2}e_{\lambda 3}^{(1)}e_{\cdot 3}^{(1)\lambda}} + 0\left(\frac{\theta^4}{h^2}\right)$$

where

$$\theta_{\alpha\beta}^{(n)} = \frac{1}{2}(u_{\alpha|\beta}^{(n)} + u_{\beta|\alpha}^{(n)} - 2b_{\alpha\beta}u_3^{(n)}) \tag{21}$$

All other strain components are of order (θ^4/h^m) $(m \geq 3)$ and hence are zero in the present theory.

Derivation of Governing Equations

Equations of Motion. Let S^{ij} denote the components of the second Piola-Kirchhoff stress tensor measured per unit area of the undeformed body but referred to base vectors in the deformed body, f^i be the body force component measured per unit volume of the undeformed body, and ρ be the density of the undeformed body. Let $\hat{S}^i$ be the specified components of the stress vector per unit area of the undeformed lateral surface of the body, P^i be the specified components of the stress vector per unit area of the undeformed surface $S = S^+ + S^-$ of the body, and δ be the variational operator. Then the principle of virtual displacements for the dynamic case can be expressed in the form

$$0 = \int_0^T\left\{-\int_V[\rho\ddot{u}^i\delta u_i]dV + \int_V S^{ij}\delta E_{ij}dV - \int_V f^i\delta u_i dV - \int_{A_s}\hat{S}^i\delta u_i dA - \int_S P^i\delta u_i dS\right\}dt$$

$$= \int_0^T\int_V\left\{-\rho(\ddot{u}^{i(0)} + \theta^3\ddot{u}^{i(1)})(\delta u_i^{(0)} + \theta^3\delta u_i^{(1)}) + S^{\alpha\beta}[\delta E_{\alpha\beta}^{(0)} + \theta^3\delta E_{\alpha\beta}^{(1)} + (\theta^3)^2\delta E_{\alpha\beta}^{(2)}] + 2S^{\alpha 3}[\delta E_{\alpha 3}^{(0)} + \theta^3\delta E_{\alpha 3}^{(1)}] + S^{33}[\delta E_{33}^{(0)}] - f^i(\delta u_i^{(0)} + \theta^3\delta u_i^{(1)})\right\}dVdt - \int_0^T\int_{A_s}\hat{S}^i(\delta u_i^{(0)} + \theta^3\delta u_i^{(1)})dAdt - \int_0^T\int_S P^i(\delta u_i^{(0)} + \theta^3\delta u_i^{(1)})dSdt \tag{22}$$

Downloaded 03 May 2010 to 171.66.16.21. Redistribution subject to ASME license or copyright; see http://www.asme.org/terms/Terms_Use.cfm

where t denotes time; $\dot{u}_i = \partial u_i/\partial t$; dV denotes the volume element; dA the lateral surface element in the undeformed body; dS is the elemental area of the upper and lower surfaces. The virtual displacements are subject to the kinematic constraint

$$\delta u_i = 0 \quad \text{on} \quad A_u.$$

To reduce the three-dimensional problem to a two-dimensional one, the displacements and strains are expanded in terms of the thickness coordinate, θ^3. The volume element dV is related to the area element $d\Omega$ by

$$dV = cd\theta^3 d\Omega.$$

Similarly

$$dS = cd\Omega, \quad n_\alpha dA = \nu_\alpha cd\theta^3 d\Gamma$$

$d\Omega$ is the area element of the midsurface; $d\Gamma$ is the line element of the boundary Γ of Ω; n_α are the components of the unit normal vector on the lateral surface A; ν_α are the components of the unit normal vector on the boundary curve Γ. It follows that

$$n_\alpha(\theta^1,\theta^2,0) = \nu_\alpha(\theta^1,\theta^2).$$

In view of these relations, equation (22) can be expressed as

$$\begin{aligned}
0 = &\int_0^T \int_\Omega \Big\{ (I_1\ddot{u}^{i(0)} + I_2\ddot{u}^{i(1)})\delta u_i^{(0)} + (I_2\ddot{u}^{i(0)} + I_3\ddot{u}^{i(1)})\delta u_i^{(1)} \\
&+ R^{\alpha\beta}_{(0)}\delta E^{(0)}_{\alpha\beta} + R^{\alpha\beta}_{(1)}\delta E^{(1)}_{\alpha\beta} + R^{\alpha\beta}_{(2)}\delta E^{(2)}_{\alpha\beta} \\
&+ 2R^{\alpha 3}_{(0)}\delta E^{(0)}_{\alpha 3} + 2R^{\alpha 3}_{(1)}\delta E^{(1)}_{\alpha 3} + R^{33}_{(0)}\delta E^{(0)}_{33} \\
&- F^i_{(0)}\delta u_i^{(0)} - F^i_{(1)}\delta u_i^{(1)} \Big\} d\Omega dt \\
&- \int_0^T \int_{\Gamma_S} [\hat{S}^i_{(0)}\delta u_i^{(0)} + \hat{S}^i_{(1)}\delta u_i^{(1)}] d\Gamma dt \\
&- \int_0^T \int_\Omega [P^i_{(0)}\delta u_i^{(0)} + P^i_{(1)}\delta u_i^{(1)}] d\Omega dt \\
= &\int_0^T \int_\Omega \Big\{ (I_1\ddot{u}^{i(0)} + I_2\ddot{u}^{i(1)})\delta u_i^{(0)} + (I_2\ddot{u}^{i(0)} + I_3\ddot{u}^{i(1)})\delta u_i^{(1)} \\
&- R^{\alpha\beta}_{(0)}|_\beta[\delta u^{(0)}_\alpha] - R^{\alpha\beta}_{(0)}b_{\alpha\beta}\delta u_3^{(0)} - [R^{\alpha\beta}_{(0)}\phi^{(0)}_{\alpha 3}]|_\beta \delta u_3^{(0)} \\
&+ R^{\alpha\beta}_{(0)}\phi^{(0)}_{\alpha 3}b^\lambda_\beta \delta u^{(0)}_\lambda \\
&+ \ldots + R^{33}_{(0)}[\delta u_3^{(1)} + \delta u^{(1)}_\lambda u^{(1)\lambda}] \\
&- F^i_{(0)}\delta u_i^{(0)} - F^i_{(1)}\delta u_i^{(1)} \Big\} d\Omega dt \\
&- \int_0^T \int_\Omega [P^i_{(0)}\delta u_i^{(0)} + P^i_{(1)}\delta u_i^{(1)}] d\Omega dt \\
&- \int_0^T \int_{\Gamma_S} [\hat{S}^i_{(0)}\delta u_i^{(0)} + \hat{S}^i_{(1)}\delta u_i^{(1)}] d\Gamma dt + \int_0^T \int_{\Gamma_S} \Big[R^{\alpha\beta}_{(0)}\nu_\beta (\delta u^{(0)}_\alpha \\
&+ \phi^{(0)}_{\alpha 3}\delta u_3^{(0)}) \Big] + \ldots \Big] dS dt
\end{aligned} \tag{23}$$

where

$$R^{ij}_{(n)} = \int_{-h/2}^{h/2} cS^{ij}(\theta^3)^n d\theta^3, \quad I_i = \int_{-h/2}^{h/2} c\rho(\theta^3)^{i-1} d\theta^3$$

$$F^\alpha_{(n)} = \int_{-h/2}^{h/2} cf^\alpha(\theta^3)^n d\theta^3, \quad F^3_{(n)} = \int_{-h/2}^{h/2} cf^3(\theta^3)^n d\theta^3$$

$$\int_{A_s} \hat{S}^i \delta u_i dA = \int_{\Gamma_s} \{\hat{S}^\alpha_{(n)}\delta u_\alpha + \hat{S}^3_{(n)}\delta u_3^{(n)}\} ds$$

$$\hat{S}^\alpha_{(n)} = \int_{-h/2}^{h/2} c^\alpha_\lambda \hat{t}^{\beta\lambda}_{\nu\beta}(\theta^3)^n d\theta^3, \quad P^i_{(n)} = [(\theta^3)^n cP^i]_{-h/2}^{h/2}, \tag{24}$$

where $\hat{t}^{\beta i}$ are the first Piola-Kirchoff stress tensor components. Collecting the coefficients of the variation of each independent variable and setting the collections to zero, one obtains the equations of motion

$$\begin{aligned}
\delta u^{(0)}_\alpha: &\quad T^{\alpha\beta}_{(0)}|_\beta - b^\alpha_\beta T^{3\beta}_{(0)} = I_1\ddot{u}^{\alpha(0)} + I_2\ddot{u}^{\alpha(1)} - P^\alpha_{(0)} - F^\alpha_{(0)} \\
\delta u_3^{(0)}: &\quad T^{3\beta}_{(0)}|_\beta + b_{\alpha\beta}T^{\alpha\beta}_{(0)} = I_1\ddot{u}^{3(0)} + I_2\ddot{u}^{3(1)} - P^3_{(0)} - F^3_{(0)} \\
\delta u^{(1)}_\alpha: &\quad T^{\alpha\beta}_{(1)}|_\beta - b^\alpha_\beta \tilde{T}^{3\beta}_{(1)} + Q^{\alpha 3}_{(1)} = I_2\ddot{u}^{\alpha(0)} + I_3\ddot{u}^{\alpha(1)} - P^\alpha_{(1)} - F^\alpha_{(1)} \\
\delta u_3^{(1)}: &\quad T^{3\beta}_{(1)}|_\beta + b_{\alpha\beta}\tilde{T}^{\alpha\beta}_{(1)} + Q^{33}_{(1)} = I_2\ddot{u}^{3(0)} + I_3\ddot{u}^{3(1)} - P^3_{(1)} - F^3_{(1)}
\end{aligned} \tag{25}$$

where

$$T^{\alpha\beta}_{(0)} = R^{\alpha\beta}_{(0)} - b^\alpha_\lambda R^{\lambda\beta}_{(1)} + u^{(1)\alpha}R^{\beta 3}_{(0)} - \frac{1}{2}u_3^{(1)}|^\alpha R^{\beta 3}_{(1)}$$

$$T^{3\beta}_{(0)} = \left(1 + \frac{1}{2}u_3^{(1)}\right)R^{\beta 3}_{(0)} + \phi^{(0)}_{\lambda 3}R^{\lambda\beta}_{(0)} + \phi^{(1)}_{\lambda 3}R^{\lambda\beta}_{(1)}$$

$$T^{\alpha\beta}_{(1)} = R^{\alpha\beta}_{(1)} - b^\alpha_\lambda R^{\lambda\beta}_{(2)} + u^{(1)\alpha}R^{\beta 3}_{(1)}$$

$$\tilde{T}^{\alpha\beta}_{(1)} = R^{\alpha\beta}_{(1)} - b^\alpha_\lambda R^{\lambda\beta}_{(2)}$$

$$T^{3\beta}_{(1)} = R^{\beta 3}_{(1)} - \frac{1}{2}\phi^{(0)\beta}_{\cdot\lambda}R^{\lambda 3}_{(1)} + \phi^{(0)}_{\lambda 3}R^{\lambda\beta}_{(1)} + \phi^{(1)}_{\lambda 3}R^{\lambda\beta}_{(2)}$$

$$\tilde{T}^{3\beta}_{(1)} = \phi^{(0)}_{\lambda 3}R^{\lambda\beta}_{(1)} + \phi^{(1)}_{\lambda 3}R^{\lambda\beta}_{(2)}$$

$$\begin{aligned}
Q^{\alpha 3}_{(1)} = &-\Big[\Big(1 - \frac{1}{2}u_3^{(1)}\Big)R^{\alpha 3}_{(0)} + \phi^{(0)\alpha}_{\cdot\lambda}R^{\lambda 3}_{(0)} + u^{(1)\alpha}|_\lambda R^{\lambda 3}_{(1)} \\
&+ u^{(1)\alpha}R^{33}_{(0)}\Big] \\
Q^{33}_{(1)} = &-\Big[R^{33}_{(0)} + \frac{1}{2}\Big(\phi^{(0)}_{\alpha 3} - u^{(1)}_\alpha\Big)R^{\alpha 3}_{(0)}\Big]
\end{aligned} \tag{26}$$

The natural boundary conditions of the theory are given by

$$\begin{aligned}
\delta u^{(0)}_\alpha: &\quad T^{\alpha\beta}_{(0)}\nu_\beta - \hat{S}^\alpha_{(0)} = 0 \\
\delta u_3^{(0)}: &\quad T^{3\alpha}_{(0)}\nu_\alpha - \hat{S}^3_{(0)} = 0 \\
\delta u^{(1)}_\alpha: &\quad T^{\alpha\beta}_{(1)}\nu_\beta - \hat{S}^\alpha_{(1)} = 0 \\
\delta u_3^{(1)}: &\quad T^{3\alpha}_{(1)}\nu_\alpha - \hat{S}^3_{(1)} = 0
\end{aligned} \tag{27a}$$

The essential (or geometric) boundary conditions involve specifying the displacements,

$$u_i^{(0)} = \hat{u}_i^{(0)}, \quad u_i^{(1)} = \hat{u}_i^{(1)} \tag{27b}$$

where $\hat{u}_i^{(0)}$ and $\hat{u}_i^{(1)}$ are specified quantities.

This completes the developments of the equations of motion of the moderate rotation theory. It should be noted that equations (26) are considerably simpler than those presented by Librescu and Schmidt (1986), which includes terms underlined in equation (21) and, hence, results in many additional terms that should be negligible by the original assumption concerning the order of magnitude of linear strains and rotations.

Let us compare briefly equations (25)–(27) with those derived by Wempner (1973) and Pietraszkiewicz (1979) for the moderate rotation first-order shear-deformation shell theory. Both, in contrast to the present paper, also account for moderate rotations about the normal. Wempner's (1973) equilibrium equations (12.359)–(12.361), when specialized for the case of small rotations about the normal, contain only one nonlinear term, namely, the third term of $T^{3\beta}_{(0)}$ in equation (26). This is due to the fact that his strain-displacement relations (if specialized for the case of small rotations about the normal) also take into account only one nonlinear term, namely, the second term of $E^{(0)}_{\alpha\beta}$ in equation (21). In addition, the strains $E^{(2)}_{\alpha\beta}$, $E^{(1)}_{\alpha 3}$, and $E^{(0)}_{33}$ are omitted in Wempner (1973). The equilibrium equations given by Pietraszkiewicz (1979), equation

Downloaded 03 May 2010 to 171.66.16.21. Redistribution subject to ASME license or copyright; see http://www.asme.org/terms/Terms_Use.cfm

(7.2.5), have not been derived variationally, but obtained by simplifying the equilibrium equations of the fully nonlinear theory directly (i.e., introducing the moderate rotation order estimates for linearized strains and rotations and omitting those terms which are small when compared to the leading terms). It is known, however, that this method can lead to inadequate and inconsistent equations, because it can result in omission of such terms in the equilibrium equations which would correspond to important terms in associated variationally consistent moderate rotation strain-displacement relations [see Librescu and Schmidt, 1986, equations (4.15)-(16)]. Indeed, Pietraszkiewicz's equilibrium equations, when specialized for small rotations about the normal, do not contain many nonlinear terms present in our equations (25)-(26), which are obtained by a variational procedure based on appropriately simplified kinematic measures. Also, due to the definition of some stress measures, the equilibrium equations in Pietraszkiewicz (1979) are valid only for isotropic materials. Furthermore, no static boundary conditions are given and no moderate rotation strain-displacement relations are presented there, but the use of the fully nonlinear kinematical relations is proposed. As a result, in contrast to the theory presented in this paper, no variational principle can be formulated.

Laminate Constitutive Equations. The resultants $R^{ij}_{(n)}$ defined in equation (24) can be related to the strains $E^{(n)}_{ij}$ in equation (21) (hence, the displacements and their gradients) through the laminate stiffnesses. These relations are derived from the constitutive equations of an individual lamina (see Reddy, 1984*b*)

$$S^{ij} = C^{ijkl}E_{kl} \text{ (sum on repeated indices)} \tag{28}$$

where C^{ijkl} are the components of the elasticity tensor and E_{kl} are the total strain components of equation (17). For an orthotropic lamina, equation (28) can be written in the alternative form (commonly used in composite laminates literature)

$$\begin{aligned} S^{\alpha\beta} &= Q^{\alpha\lambda}E_{\lambda\beta} + Q^{33}E_{33} \\ S^{\alpha 3} &= Q^{\alpha\lambda}E_{\lambda 3} + Q^{\alpha 3}E_{33} \\ S^{33} &= Q^{3\lambda}E_{\lambda 3} + Q^{33}E_{33} \end{aligned} \tag{29}$$

where $(Q^{\alpha\beta}, Q^{\alpha 3}, Q^{33})$ are the equivalent elasticity components. Substitution of equation (29) into the definition of $R^{ij}_{(n)}$ gives the constitutive equations of a laminate made of orthotropic layers. For example, $R^{\alpha\beta}_{(n)}$ are related to the strains $E^{(m)}_{ij}$ by

$$\begin{aligned} R^{\alpha\beta}_{(n)} &= \int_{-h/2}^{h/2} cS^{\alpha\beta}(\theta^3)^n d\theta^3 \\ &= \int_{-h/2}^{h/2} c[Q^{\alpha\lambda}E_{\lambda\beta} + Q^{33}E_{33}](\theta^3)^n d\theta^3 \\ &= \int_{-h/2}^{h/2} c\{Q^{\alpha\lambda}[E^{(0)}_{\lambda\beta} + \theta^3 E^{(1)}_{\lambda\beta} + (\theta^3)^2 E^{(2)}_{\lambda\beta}] \\ &\quad + Q^{33}E^{(0)}_{33}\}(\theta^3)^n d\theta^3 \\ &= \sum_{m=0}^{2} A^{\alpha\lambda}_{(m+n)}E^{(m)}_{\lambda\beta} + A^{33}_{(n)}E^{(0)}_{33} \end{aligned} \tag{30}$$

where

$$\begin{aligned} A^{\alpha\lambda}_{(m)} &= \int_{-h/2}^{h/2} cQ^{\alpha\lambda}(\theta^3)^m d\theta^3 \\ A^{33}_{(m)} &= \int_{-h/2}^{h/2} cQ^{33}(\theta^3)^m d\theta^3 \end{aligned} \tag{31}$$

Similar, relations between $(R^{\alpha 3}_{(n)}, R^{33}_{(n)})$ and $E^{(m)}_{ij}$ can be obtained.

Special Cases

In this setion, equations (26) are simplified to obtain the equations associated with a couple of known plate and shell theories. First, simplification is made to obtain the equations of plates.

Moderate Rotation Theory of Plates (of Reddy, 1987). Set the components of the curvature tensor b^{α}_{β} to zero [hence $c = 1$, $\phi^{(n)}_{\alpha\beta} = u^{(n)}_{\alpha|\beta}$, $\phi^{(n)}_{\alpha 3} = u^{(n)}_{3|\alpha}$] and obtain the moderate rotation theory of plates in curvilinear coordinates:

$$\left[R^{\alpha\beta}_{(0)} + u^{(1)\alpha}R^{\beta 3}_{(0)} - \frac{1}{2}u^{(1)}_{3}|^{\alpha}R^{\beta 3}_{(1)}\right]|_{\beta} = I_1\ddot{u}^{\alpha(0)} + I_2\ddot{u}^{\alpha(1)} - P^{\alpha}_{(0)} - F^{\alpha}_{(0)}$$

$$\left[\left(1 + \frac{1}{2}u^{(1)}_{3}\right)R^{\beta 3}_{(0)} + u^{(0)}_{3|\lambda}R^{\lambda\beta}_{(0)} + u^{(1)}_{3|\lambda}R^{\lambda\beta}_{(1)}\right]|_{\beta} = I_1\ddot{u}^{3(0)} + I_2\ddot{u}^{3(1)} - P^{3}_{(0)} - F^{3}_{(0)}$$

$$\left[R^{\alpha\beta}_{(1)} + u^{(1)\alpha}R^{\beta 3}_{(1)}\right]|_{\beta} - \left[\left(1 - \frac{1}{2}u^{(1)}_{3}\right)R^{\alpha 3}_{(0)} + u^{(0)\alpha}|_{\lambda}R^{\lambda 3}_{(0)} + u^{(1)\alpha}|_{\lambda}R^{\lambda 3}_{(1)} + u^{(1)\alpha}R_{(0)}\right] = I_2\ddot{u}^{\alpha(0)} + I_3\ddot{u}^{\alpha(1)} - P^{\alpha}_{(1)} - F^{\alpha}_{(1)}$$

$$\left[R^{\beta 3}_{(1)} - \frac{1}{2}u^{(0)\beta}|_{\lambda}R^{\lambda 3}_{(1)} + u^{(0)}_{3|\lambda}R^{\lambda\beta}_{(1)} + u^{(1)}_{3|\lambda}R^{\lambda\beta}_{(2)}\right]|_{\beta} - \left[R^{33}_{(0)} + \frac{1}{2}(u^{(0)}_{3\alpha} - u^{(1)}_{\alpha}R^{\alpha 3}_{(0)}\right] = I_2\ddot{u}^{3(0)} + I_3\ddot{u}^{3(1)} - P^{3}_{(1)} - F^{3}_{(1)} \tag{32}$$

Of course, many other special plate theories including the first-order shear-deformation theory of Reissner-Hencky-Mindlin can be obtained from equation (32). The von Kármán plate theory with shear deformation can be obtained from the first three equations in equation (32) by setting the underlined terms to zero.

The von Kármán Type Shear-Deformation Shell Theory. The von Kármán type shell theory with shear deformation can be obtained from the present theory, not from equation (26) directly but by using the linear parts of all strains except $E^{(0)}_{\alpha\beta}$ in the virtual work expression (22). This gives

$$\begin{aligned} &[R^{\alpha\beta}_{(0)} - b^{\alpha}_{\lambda}R^{\lambda\beta}_{(1)}]|_{\beta} - b^{\alpha}_{\beta}[R^{\beta 3}_{(0)} + \phi^{(0)}_{\lambda 3}R^{\lambda\beta}_{(0)}] = I_1\ddot{u}^{\alpha(0)} + I_2\ddot{u}^{\alpha(1)} - P^{\alpha}_{(0)} - F^{\alpha}_{(0)} \\ &[R^{\beta 3}_{(0)} + \phi^{(0)}_{\lambda 3}R^{\lambda\beta}_{(0)}]|_{\beta} + b_{\alpha\beta}[R^{\alpha\beta}_{(0)} - b^{\alpha}_{\lambda}R^{\lambda\beta}_{(1)}] = I_1\ddot{u}^{3(0)} + I_2\ddot{u}^{3(1)} - P^{3}_{(0)} - F^{3}_{(0)} \\ &[R^{\alpha\beta}_{(1)} - b^{\alpha}_{\lambda}R^{\lambda\beta}_{(2)}]|_{\beta} - R^{\alpha 3}_{(0)} = I_2\ddot{u}^{\alpha(0)} + I_3\ddot{u}^{\alpha(1)} - P^{\alpha}_{(1)} - F^{\alpha}_{(1)} \\ &[R^{\beta 3}_{(1)}]|_{\beta} + b_{\alpha\beta}[R^{\alpha\beta}_{(1)} - b^{\alpha}_{\lambda}R^{\lambda\beta}_{(2)}] - R^{33}_{(0)} = I_2\ddot{u}^{3(0)} + I_3\ddot{u}^{3(1)} - P^{3}_{(1)} - F^{3}_{(1)} \end{aligned} \tag{33}$$

The classical Kirchhoff-Love shell theory with the von Kármán type nonlinearity (i.e., the Donnell-Mushtari-Vlasov shell theory) can be obtained from equation (33).

Summary

A consistent first-order shear-deformation shell theory with small strains and moderate rotations is developed using the

Downloaded 03 May 2010 to 171.66.16.21. Redistribution subject to ASME license or copyright; see http://www.asme.org/terms/Terms_Use.cfm

order-of-magnitude assumptions and the principle of virtual displacements. The displacements of a typical point in the shell are assumed to vary linearly through the shell thickness. The resulting shell equations exhibit strong coupling between membrane and bending deformations. Specialization of the equations to moderate rotation plate theory and the von Kármán type shell theory with shear deformation is illustrated. Solution of the equations for certain shell or plate structures should yield new results concerning the load-deflection as well as stability and buckling behavior due to the inclusion of moderate rotation terms.

Acknowledgments

The authors are grateful to the NATO Science Program for partial support of the research reported here. The second author also gratefully acknowledges the support of the research by Alexander von Humboldt Foundation Research Fellowship.

References

Basset, A. B., 1890, "On the Extension and Flexure of Cylindrical and Spherical Thin Elastic Shells," *Phil. Trans. Royal Soc.*, (London), Series A. Vol. 181, No. 6, pp. 433–480.

Budiansky, B., 1968, "Notes on Nonlinear Shell Theory," ASME JOURNAL OF APPLIED MECHANICS, Vol. 35, pp. 393–401.

Dong, S. B., and Tso, K. W., 1972, "On a Laminated Orthotropic Shell Theory Including Transverse Shear Deformation," ASME JOURNAL OF APPLIED MECHANICS, Vol. 39, pp. 1091–1096.

Donnell, L. H., 1933, "Stability of Thin-Walled Tubes Under Torsion," NACA TR 479.

Galimov, K. Z., 1977, *Theory of Shells with Transverse Shear Deformation Effect* (in Russian), Kazan' University Press, Kazan'.

Habip, L. M., and Ebcioglu, I. K., 1965, "On the Equations of Motion of Shells in the Reference State," *Ingenieur-Archiv*, Vol. 34, pp. 28–32.

Koiter, W. T., 1960, "A Consistent First Approximation in the General Theory of Thin Elastic Shells," *Proc. IUTAM Symp. on the Theory of Thin Shells*, Delft, 1959, North-Holland Publ. Co., Amsterdam, pp. 12–33.

Koiter, W. T., 1966, "On the Nonlinear Theory of Thin Elastic Shells," *Proc. Kon. Ned. Al. Wet.*, Series B, Vol. 69, pp. 1–54.

Koiter, W. T., 1966, "On the Nonlinear Theory of Thin Elastic Shells," *Proc. Kon. Ned. Ak. Wet.*, Series B, Vol. 69, pp. 1–54.

Koiter, W. T., 1967, "Foundations and Basic Equations of Shell Theory. A Survey of Recent Progress," *Theory of Shells*, Niordson, F. I., Ed., IUTAM Symposium, Copenhagen, pp. 93–105.

Koiter, W. T., and Simmonds, J. C., 1973, "Foundations of Shell Theory," in *Theoretical and Applied Mechanics*, (*Proc. of the 13th Int. Congress of Theoretical and Applied Mechanics*, Moscow 1972) Springer-Verlag, New York, pp. 150–176.

Krätzig, W. B., 1971, "Allgemeine Schalentheorie beliebiger Werkstoffe und Verformungen," *Ingenieur-Archiv*, Vol. 40, pp. 311–326.

Leonard, R. W., 1961, "Nonlinear First Approximation Thin Shell and Membrane Theory," Thesis, Virginia Polytechnic Institute, Blacksburg, VA.

Librescu, L., 1973, *Elastostatics and Kinetics of Anisotropic and Heterogeneous Shell-Type Structures*, Noordhoff Int. Publ., Leyden.

Librescu, L., 1987, "Refined Geometrically Nonlinear Theories of Anisotropic Laminated Shells," *Quarterly of Applied Mathematics*, Vol. 44, pp. 1–22.

Librescu, L., and Schmidt, R., 1986, "Refined Theories of Elastic Anisotropic Shells Accounting for Small Strains and Moderate Rotations," paper presented at the 10th US National Congress of Applied Mechanics, Austin, TX.

Marguerre, K., 1939, "Zur Theorie der gekrümmten Platte grosser Formänderung," *Proc. 5th Int. Congress of Applied Mechanics*, Cambridge, MA, 1938, pp. 93–101.

Mushtari, K. M., 1938, "Some Generalizations of the Theory of Thin Shells With Applications to the Stability Problem of Elastic Equilibrium (in Russian)," *Izviestiia fiz.-mat. ob-va pri kazan unte*, Vol. 11, pp. 71–150.

Mushtari, K. M., and Galimov, K. Z., 1961, *Nonlinear Theory of Thin Elastic Shells*, The Israel Program for Sci. Transl., Jerusalem 1961 (translation of Nelineinaya teoriya uprugikh obolochek, Tatknigoizdat, Kazan', 1957).

Naghdi, P. M., 1956, "A Survey of Recent Progress in the Theory of Elastic Shells," *Applied Mechanics Reviews*, Vol. 9, No. 9, pp. 365–368.

Naghdi, P. M., 1963, "Foundations of Elastic Shell Theory," *Progress in Solid Mechanics*, Vol. 4, Sneddon, I. N., and Hill, R., Eds., North-Holland, Amsterdam.

Naghdi, P. M., 1972, "The Theory of Shells and Plates," in *Handbuch der Physik*, Vol. VIa/2, Flügge, S., Ed., Springer-Verlag, Berlin, pp. 425–640.

Pietraszkiewicz, W., 1977, *Introduction to the Nonlinear Theory of Shells*, Mitteilungen aus dem Institut für Mechanik, Nr. 10, Ruhr-Universität, Bochum.

Pietraszkiewicz, W., 1979, "Finite Rotations and Lagrangian Description in the Nonlinear Theory of Shells," Polish Academy of Sciences, Institute of Fluid-Flow Machinery, Warszawa, Poland.

Pietraszkiewicz, W., 1984, "Lagrangian Description and Incremental Formulation in the Nonlinear Theory of Thin Shells," *Int. J. Non-Linear Mechanics*, Vol. 19, pp. 115–140.

Pietraszkiewicz, W., and Szwabowicz, M. L., 1981, "Entirely Lagrangian Nonlinear Theory of Thin Shells," *Arch. Mech.*, Vol. 33, pp. 273–288.

Reddy, J. N., 1982, "Bending of Laminated Anisotropic Shells by a Shear Deformable Finite Element," *Fibre Science & Technology*, Vol. 17, pp. 9–24.

Reddy, J. N., 1984*a*, "Exact Solutions of Moderately Thick Laminated Shells," *Journal of Engineering Mechanics*, ASCE, Vol. 110, No. 5, pp. 794–809.

Reddy, J. N., 1984*b*, *Energy and Variational Methods in Applied Mechanics*, John Wiley, New York.

Reddy, J. N., 1987, "A Small Strain and Moderate Rotation Theory of Laminated Anisotropic Plates," ASME JOURNAL OF APPLIED MECHANICS, Vol. 54, pp. 623–626.

Reddy, J. N., and Rasmussen, M. L., 1982, *Advanced Engineering Analysis*, Wiley & Sons, New York.

Reissner, E., 1950, "On Axisymmetric Deformation of Thin Shells of Revolution," *Proc. Symp. Appl. Math.*, Vol. 3, McGraw-Hill, New York, pp. 27–52.

Reissner, E., 1963, "On the Equations for Finite Symmetrical Deflections of Thin Shells of Revolution," in *Progress in Applied Mechanics, The Prager Anniversary Volume*, New York, pp. 171–178.

Reissner, E., 1966, "On the Foundations of the Theory of Elastic Shells," *Proc. 11th Int. Congress on Applied Mechanics*, Munich 1964, Gortler, H., (Ed.), pp. 20–30, Springer-Verlag, Berlin, W. Germany.

Sanders, J. L., 1959, "An Improved First Approximation Theory of Thin Shells," NASA TR-24.

Sanders, J. L., 1963, "Nonlinear Theories for Thin Shells," *Quarterly of Applied Mathematics*, Vol. 21, pp. 21–36.

Schmidt, R., 1984*a*, "On Geometrically Nonlinear Theories for Thin Elastic Shells," in *Flexible Shells, Theory and Applications,"* (*Proc. of the Euromech-Colloquium 165, München 1983*) Axelrad, E. L., and Emmerling, F. A., Eds., Springer-Verlag, Berlin, pp. 76–90.

Schmidt, R., 1984*b*, "Thin Elastic Shells Undergoing Small Strains and Large Rotations—A Simple Consistent Theory and Variational Principles," in *Numerical Methods for Nonlinear Problems*, Vol. 2, Taylor, C., Hinton, E., and Owen, D. R. J., Eds., Pineridge Press, Swansea, pp. 170–181.

Schmidt, R., 1985*a*, "A Current Trend in Shell Theory: Constrained Geometrically Nonlinear Kirchhoff-Love Type Theories Based on Polar Decomposition of Strains and Rotations," *Computers and Structures*, Vol. 20, pp. 265–275.

Schmidt, R., 1985*b*, "On the Entirely Lagrangian First Approximation Theory of Thin Elastic Shells Undergoing Small Strains and Arbitrary Rotations," *ZAMM*, Vol. 65, pp. 119–121.

Schroeder, F. H., 1972, "Die Stabilitätsgleichungen der technischen Schalentheorie," *Zeitschrift für Flugwissenschaften*, Vol. 20, pp. 430–448.

von Kármán, T., 1910, "Festigkeitslehre im Maschinenbau," *Encykl. der Math. Wiss.*, Vol. IV/4, Teubner, Leipzig, pp. 311–385.

von Kármán, T., and Kerr, A. D., 1965, "Instability of Spherical Shells Subjected to External Pressure," in *Topics in Applied Mechanics*, Memorial Volume to the late Professor E. Schwerin, pp. 1–22.

Vlasov, V. Z., 1949, "General Theory of Shells and Its Applications in Engineering," NASA TT F-99, 1964, translation of *Obscaja teorija obolocek i ee prilozenija w technike*, Moscow-Leningrad.

Wempner, G. A., 1973, *Mechanics of Solids With Applications to Thin Bodies*, McGraw-Hill, New York.

Whitney, J. M., and Sun, C. T., 1974, "A Refined Theory for Laminated Anisotropic Cylindrical Shells," ASME JOURNAL OF APPLIED MECHANICS, Vol. 41, pp. 471–476.

Yokoo, Y., and Matsunaga, H., 1974, "A General Nonlinear Theory of Elastic Shells," *International Journal of Solids and Structures*, Vol. 10, pp. 261–274.

Downloaded 03 May 2010 to 171.66.16.21. Redistribution subject to ASME license or copyright; see http://www.asme.org/terms/Terms_Use.cfm

Paul S. Steif

Anna Dollar

Department of Mechanical Engineering,
Carnegie-Mellon University,
Pittsburgh, PA 15213

Longitudinal Shearing of a Weakly Bonded Fiber Composite

The longitudinal shearing of a unidirectional fiber composite which sustains slippage at the fiber-matrix interface is studied theoretically. An expression for the effective shear modulus of the composite, assuming a dilute concentration of fibers, is derived. The necessary quantities are found from the solution to the problem of a single slipping fiber in an infinite matrix. A singular integral equation governing this problem is derived and solved numerically. Results for the progression of slip and for the effective shear modulus are presented.

Introduction

It is increasingly recognized that the fiber-matrix interface plays an important role in the deformation of composite materials. In fact, for composites that have relatively brittle constituents, such as ceramic-matrix composites, slippage at the interface may constitute the principal source of inelastic deformation. The energy absorption during deformation and the fracture resistance in these materials may, therefore, hinge on the extent to which the loading produces interfacial slippage. Previous work in this area consists primarily of highly approximate treatments of fiber-matrix slippage (Kelly, 1970; Aveston and Kelly, 1973; Budiansky, Hutchinson, and Evans, 1986) that are a part of existing models of composite tensile strength and toughness.

In order to focus on the inelasticity associated with deforming a weakly bonded, brittle-constituent composite, we study a fiber composite subjected to a realistic loading which is simple enough to permit an accurate calculation of the internal slippage. Specifically, we consider a unidirectional composite subjected to a remote longitudinal shear stress (see Fig. 1(*a*)). We assume the fiber and the matrix each deform elastically. A generic point on the fiber-matrix interface is presumed to sustain shear stresses up to some maximum value at which point slip can occur with the shear stress maintained at the maximum value. For simplicity, and for the purpose of isolating the consequences of slippage, the composite is taken to possess a dilute concentration of fibers. Consistent with the assumption of a dilute concentration, we treat the problem of a single fiber in an infinite matrix subjected to longitudinal shear. A singular integral equation, which governs the slippage induced at the interface, is derived and solved numerically. Finally, an expression for the longitudinal shear modulus of the composite is derived, and it is shown to depend on the average stress in the fiber and the slippage at the interface, quantities which emerge readily from the numerical solution.

Analysis of a Single Fiber in an Infinite Matrix

The problem of a single fiber in an infinite matrix subjected to remote shearing is shown schematically in Fig. 1(*b*). Without loss of generality, we take the fiber to be of unit

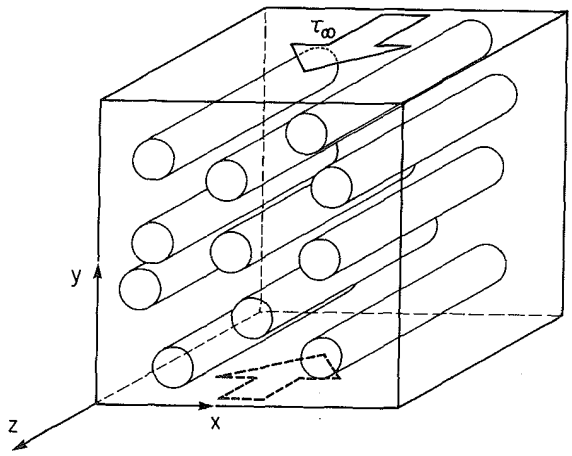


Fig. 1(*a*) Schematic of the longitudinal shearing of a fiber composite.

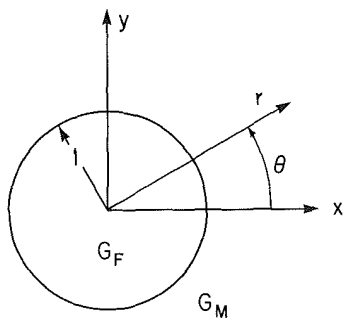


Fig. 1(*b*) Definition of coordinate system for analysis of a single fiber in an infinite matrix.

Contributed by the Applied Mechanics Division for presentation at the Winter Annual Meeting, Chicago, IL November 28 to December 2, 1988, of THE AMERICAN SOCIETY OF MECHANICAL ENGINEERS.

Discussion on this paper should be addressed to the Editorial Department, ASME, United Engineering Center, 345 East 47th Street, New York, N.Y. 10017, and will be accepted until two months after final publication of the paper itself in the JOURNAL OF APPLIED MECHANICS. Manuscript received by ASME Applied Mechanics Division, September 4, 1987; final revision, January 28, 1988.

Paper No. 88-WA/APM-43.

Copyright © 1988 by ASME
Downloaded 03 May 2010 to 171.66.16.21. Redistribution subject to ASME license or copyright; see http://www.asme.org/terms/Terms_Use.cfm

radius and situated at the origin of the x-y plane. The matrix lies in the region exterior to the fiber, and the only nonzero stress component as $|x^2 + y^2| \to \infty$ is σyx which has a value τ_∞. The fiber is isotropic with shear modulus G_F, and the matrix is isotropic with shear modulus G_M. Under this loading the deformation is one of anti-plane strain: The only nonzero displacement is the out-of-plane component $w(x, y)$, and the nonzero stresses are σ_{xz} and σ_{yz}. At the fiber-matrix interface, the traction σ_{rz} and the displacement w are continuous, provided σ_{rz} is less than the critical shear stress for slip τ_s. (A r-θ polar coordinate system centered at the origin has also been introduced). If $\sigma_{rz} = \tau_s$, then the displacement w can be discontinuous.

Under sufficiently small remote loadings, the shear stress at the interface nowhere exceeds τ_s. Then, the problem reduces to that of a fiber (cylindrical inclusion) perfectly bonded to an unbounded matrix. The solution to this problem is well known: The displacement is harmonic, and it varies as r in the fiber and as r and $1/r$ in the matrix. For conciseness, we represent the solution in complex variable form:

$$\omega = \tau_\infty \begin{cases} \dfrac{2\lambda}{\lambda+1} z & |z|<1 \\ z + \dfrac{\lambda-1}{\lambda+1}\dfrac{1}{z} & |z|>1 \end{cases} \tag{1}$$

where $\omega(z)$, the complex stress potential, is a sectionally holomorphic function of $z = x + iy$, and $\lambda = G_F/G_M$. The stress components are related to $\omega(z)$ according to

$$\omega'(z) = \sigma_{yz} + i\sigma_{xz}$$

where $(\,)'$ denotes the complex derivative with respect to z. The displacement w is given by

$$w = \frac{1}{G}\, Im\,[\omega]$$

where Im [ ] denotes the imaginary part of the enclosed complex-valued quantity.

The radial shear stress is maximum at the "top" and "bottom" of the fiber (at $z = \pm i$), where it is equal to

$$(\sigma_{rz})_{\max} = \pm\frac{2\lambda}{\lambda+1}\tau_\infty$$

Thus, there is no slip if

$$\frac{2\lambda}{\lambda+1}\tau_\infty < \tau_s$$

Once the applied stress exceeds this critical value, slip occurs over some portion of the interface. By the symmetries of the problem, it is clear that there are two slip zones, one on the top of the fiber, $\alpha < \theta < \pi - \alpha$, and a symmetric one on the bottom, $\pi + \alpha < \theta < 2\pi - \alpha$, where $0 < \alpha < \pi/2$. On these slip zones the condition $\sigma_{rz} = \tau_s$ must be enforced. The extent of slip, characterized by the parameter α, is also a part of the solution.

We will express the solution to this problem for values of τ_∞ greater than $(\lambda+1)\,\tau_s/2\lambda$ as a superposition of the perfectly bonded solution (1) and a suitable distribution of screw dislocations along the slip zones. Hence, the problem can be equivalently stated as finding the stress field which vanishes as $|z| \to \infty$, satisfies continuity of traction and displacement along portions of the interface that have undergone no slip, and has tractions

$$\sigma_{rz} = \tau_s - \frac{2\lambda}{\lambda+1}\tau_\infty \sin\theta \tag{2}$$

along the slipped portions of the interface.

The extent of slip, as measured by α, is determined by insisting that σ_{rz} nowhere exceed the value given in (2). This is tantamount to the condition that the stress intensity factor is zero at the ends of the slip zone. (Note the stress is square-root singular at the "interface" crack when the loading is Mode III.) Hence, slip occurs to the extent that the positive stress intensity due to the remote loading is precisely canceled by the negative stress intensity associated with the prevailing friction stress.

The kernel solution is clearly that of a screw dislocation located at the fiber–matrix interface. A concise method of deriving this dislocation solution is given in the Appendix; the result is

$$\omega'(z) = d_m \begin{cases} \dfrac{1+B}{z-z_0} & |z|<1 \\ \dfrac{1+B\,z_0/z}{z-z_0} & |z|>1 \end{cases} \tag{3}$$

where the dislocation, located at z_0, has Burger's vector b, and

$$d_m = \frac{G_M\, b}{2\pi} \qquad B = \frac{G_F - G_M}{G_F + G_M}$$

Dislocations of intensity $b(\theta)$ are distributed along the slipped portions of interface, $\alpha < \theta < \pi - \alpha$ and $\pi + \alpha < \theta < 2\pi - \alpha$. This distribution of dislocations preserves continuity of traction and displacement along the unslipped portions of interface since the kernel dislocation solution (3) itself does. Noting that $\sigma_{\theta z} + i\sigma_{rz} = z\omega'$ on $|z| = 1$, one finds the stresses in the fiber to be given by

$$\sigma_{\theta z} + i\sigma_{rz} = -\frac{G_M}{2\pi}\int_\Gamma \frac{z(1+B)b(t)dt}{i\,t\,(t-z)}$$

and the stresses in the matrix to be given by

$$\sigma_{\theta z} + i\sigma_{rz} = -\frac{G_M}{2\pi}\int_\Gamma \frac{(z+Bt)b(t)dt}{i\,t\,(t-z)}$$

where $t = e^{i\theta}$ and Γ denotes the two contours on which slip occurs.

The stresses as one approaches Γ may be calculated using the Plemelj formulae (Muskhelishvili, 1963):

$$\left(G\frac{\partial w}{\partial\theta} + i\sigma_{rz}\right)_F = -\frac{G_M}{2\pi i}\left\{\oint_\Gamma \frac{z(1+B)b(t)dt}{t(t-z)} + \pi i(1+B)b(z)\right\} \tag{4a}$$

$$\left(G\frac{\partial w}{\partial\theta} + i\sigma_{rz}\right)_M = -\frac{G_M}{2\pi i}\left\{\oint_\Gamma \frac{(z+Bt)b(t)dt}{t(t-z)} - \pi i(1+B)b(z)\right\} \tag{4b}$$

where the subscripts F and M denote limits as one approaches the interface from the fiber and from the matrix, and the integrals are interpreted in the Cauchy Principal Value sense. (We have properly equated $\sigma_{\theta z}$ at the interface with $G\partial w/\partial\theta$.)

Now, it is possible to identify the component σ_{rz} with the integral and $G\partial w/\partial\theta$ with the term which is proportional to $b(z)$. This is done by first noting the equivalence of the Cauchy integrals in (4a) and (4b), which follows from

Downloaded 03 May 2010 to 171.66.16.21. Redistribution subject to ASME license or copyright; see http://www.asme.org/terms/Terms_Use.cfm

$$\oint_\Gamma \frac{zb(t)dt}{t(t-z)} - \oint_\Gamma \frac{tb(t)dt}{t(t-z)} = \oint_\Gamma \frac{-b(t)dt}{t} = \int -ib(\theta)d\theta = 0$$

where the condition of zero net Burgers has been enforced.

Then, since

$$I = \oint_\Gamma \frac{b(t)\,dt}{t-z} = \oint \frac{ib(\theta)e^{i\theta}d\theta}{e^{i\theta}-e^{i\phi}}$$

is real, as shown by

$$I - \bar{I} = \oint \left[\frac{i\,e^{i\theta}}{e^{i\theta}-e^{i\phi}} - \frac{(-i)\,e^{-i\theta}}{e^{-i\theta}-e^{-i\phi}}\right] b(\theta)\,d\theta = \int i\,b(\theta)\,d\theta = 0$$

(we have set $z = e^{i\phi}$), one merely equates real and imaginary parts to obtain

$$\sigma_{rz} = i\,C\,e^{i\phi} \oint \frac{b(\theta)\,d\theta}{e^{i\theta}-e^{i\phi}} \tag{5a}$$

$$G_M\left(\frac{\partial w}{\partial \theta}\right)_M = -G_F\left(\frac{\partial w}{\partial \theta}\right)_F = \pi\,C\,b(\theta) \tag{5b}$$

where

$$C = \frac{G_M G_F}{\pi(G_M + G_F)}$$

Of course, (5*b*) reduces to the usual relation between $b(\theta)$ and $\partial w/\partial\theta$ when $G_M = G_F$.

The interval of integration can be simplified by noting these relations which follow from symmetry about the x and y axes

$$b(\theta) = b(-\theta) \qquad b(\theta) = -b(\pi - \theta)$$

Therefore, using (5*a*), one can express the shear stress as

$$\sigma_{rz} = 2C\sin\phi \int_\alpha^{\pi/2} \frac{b(\theta)\cos\theta d\theta}{\cos^2\phi - \cos^2\theta} \tag{6}$$

Recall that part of the solution will be the extent of slip α for a given level loading.

An integral equation is readily arrived at by combining (2) with (6). The equation is simplified by setting

$$b(\theta) = \frac{\tau_\infty}{G_M}\,\beta(\theta)$$

whence

$$\int_\alpha^{\pi/2} \frac{\cos\theta\,\beta(\theta)\,d\theta}{\cos^2\phi - \cos^2\theta} = \pi\left[\frac{1}{T\sin\phi} - 1\right] \tag{7}$$

where

$$T = \frac{2\lambda}{1+\lambda}\,\frac{\tau_\infty}{\tau_s}$$

Equation (7) is only applicable once slipping has occurred; this corresponds to values of T greater than 1.

In practice, the domain was converted to $0 < x < 1$, using the change of variable

$$\theta = \frac{\pi}{2} - \xi x \tag{8}$$

where $\xi = \pi/2 - \alpha$. A discretized version of equation (7), now on a fixed domain, was solved numerically. The condition mentioned earlier of zero net stress intensity factor at the ends of the slip zone implies that $\beta(\theta)$ must vanish at the ends of the slip zone (Dundurs and Comninou, 1979). When the dislocation density vanishes at both ends of an interval, then a consistency condition must also be satisfied (Muskhelishvili, 1977). The extent of slip is thus determined by adjusting ξ so as to satisfy the consistency condition.

Calculation of the Effective Modulus

An expression for the effective longitudinal modulus of a fiber composite with internal slippage is now derived. The derivation is similar in spirit to that given by Horii and Nemat-Nasser (1983) for a homogeneous solid with cracks. Consider a large solid V_∞ containing fibers and matrix which deforms in such a way that the displacements are continuous except possibly at the fiber-matrix interface. Define the volume averaged stress and strain as usual; i.e.,

$$\bar{\sigma}_{ij} = \frac{1}{V_\infty}\int_{V_\infty} \sigma_{ij}dV \qquad \bar{\epsilon}_{ij} = \frac{1}{V_\infty}\int_{V_\infty} \epsilon_{ij}dV$$

Now, view the solid as composed of three constituents: fiber, matrix, and interface. By integrating over the volume of each constituent separately, one can write the average stress and strain as

$$\bar{\sigma}_{ij} = c_M\,\bar{\sigma}_{ij}^M + c_F\,\bar{\sigma}_{ij}^F + c_I\,\bar{\sigma}_{ij}^I \tag{9a}$$

$$\bar{\epsilon}_{ij} = c_M\,\bar{\epsilon}_{ij}^M + c_F\,\bar{\epsilon}_{ij}^F + c_I\,\bar{\epsilon}_{ij}^I \tag{9b}$$

where c_M, c_F and c_I are the respective volume fractions of matrix, fiber and interface. Note that, for a frictional interface, $c_I\,\bar{\sigma}_{ij}^I \to 0$ since $c_I \to 0$ and the stresses remain finite. On the other hand, the jump in displacement renders the term $c_I\,\bar{\epsilon}_{ij}^I$ finite and nonzero.

Specializing to the relevant shear component, and using the fiber and matrix shear moduli G_F and G_M, one finds that

$$2\bar{\epsilon}_{yz} = c_M\frac{\bar{\sigma}_{yz}^M}{G_M} + c_F\frac{\bar{\sigma}_{yz}^F}{G_F} + \frac{1}{V_\infty}\int_{\Gamma_I} wn_y\,ds$$

where Γ_I denotes all surfaces with displacement discontinuities.

We define the effective modulus G_e, to be

$$G_e = \frac{\bar{\sigma}_{yz}}{2\,\bar{\epsilon}_{yz}}$$

and, hence,

$$\frac{G_M}{G_e} = 1 + c_F\left[\left(\frac{G_M}{G_F} - 1\right)\frac{\bar{\sigma}_{yz}^F}{\bar{\sigma}_{yz}}\right] + \frac{G_M}{V_\infty \bar{\sigma}_{yz}}\int_{\Gamma_I} w\,n_y ds \tag{10}$$

The specialization to a *dilute* solution (low concentration) of fibers subjected to a remote stress $\sigma_{yz} = \tau_\infty$ is readily carried out; the result is

$$\frac{G_e}{G_M} = 1 + c_F A \tag{11}$$

where the reinforcement coefficient A is given by

$$A = \left(1 - \frac{G_M}{G_F}\right)\frac{\bar{\sigma}_{yz}^F}{\tau_\infty} - \frac{G_M}{\pi\,\tau_\infty}\int_{\Gamma_I} wn_y ds \tag{12}$$

Field quantities are now calculated from the solution to the problem of a single fiber in an infinite matrix. Deriving (11) and (12) from (10) requires one to assume that the product $c_F A << 1$. Since $|A| \leq 2$, this is, in effect, only a restriction on the concentration of fibers c_F.

Evaluation of the average fiber stress was done by calculating the average fiber stress for a single dislocation, integrating over the dislocation density and, finally, adding the average fiber stress associated with the solution for the perfectly bonded fiber. The result is

$$\frac{\bar{\sigma}_{yz}^F}{\tau_\infty} = \frac{2\lambda}{\lambda+1}\left[1 - \frac{2}{\pi}H_1\right]$$

where

Downloaded 03 May 2010 to 171.66.16.21. Redistribution subject to ASME license or copyright; see http://www.asme.org/terms/Terms_Use.cfm

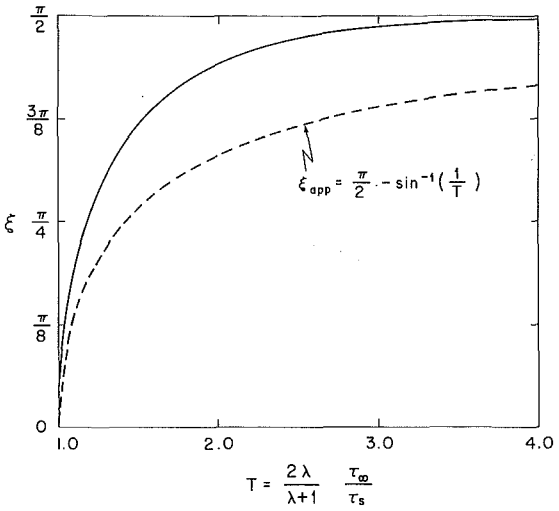


Fig. 2 Extent of slip zone as a function of normalized loading parameter T. (--- ~ approximate slip extent based on stress prior to slip.)

$$H_1 = \int_\alpha^{\pi/2} \beta(\theta) \cos\theta \, d\theta$$

The integral of the displacement around the slip surface yields

$$\frac{G_M}{\tau_\infty} \int_{\Gamma_I} w n_y ds = 4 H_2$$

where

$$H_2 = \int_\alpha^{\pi/2} \left[\int_\alpha^{\theta} \beta(\theta') \, d\theta' \right] \sin\theta \, d\theta$$

Using the change of variable (8), one can rewrite H_1 and H_2 in the form

$$H_1 = \xi \int_0^1 \beta(x) \sin \xi x \, dx$$

$$H_2 = \xi^2 \int_0^1 \left[\int_x^1 \beta(x') \, dx' \right] \cos \xi x \, dx$$

Recognizing H_1 and H_2 as proportional to finite Fourier transforms (or simply integrating by parts), allows one to show that H_1 and H_2 are equal. In practice, H_1 was evaluated numerically from the discretized solution to the singular integral equation. One can finally express A as

$$A = 2 \left[\frac{\lambda - 1 - 4\lambda H_1/\pi}{\lambda + 1} \right] \tag{13}$$

It can be shown that the appropriate limits are recovered. Trivially, when there is no slip, $H_1 = 0$ (since $\beta(x) = 0$), and $A = 2(\lambda-1)/(\lambda+1)$, which is the perfectly bonded result. On the other hand, when $\tau_\infty/\tau_s \to \infty$, H_1 was found to approach $\pi/2$, yielding $A = -2$, independent of λ. In this limit, complete slippage has occurred, so that the matrix no longer senses the fiber but only a resisting shear stress of fixed magnitude τ_s. Indeed, $A = -2$ is the result for a composite with holes instead of fibers.

Limiting Solution for Complete Slippage

In this section, we explicitly derive the solution for the limiting case of $\tau_\infty/\tau_s >> 1$. In this limit, the slip zone encompasses the entire fiber-matrix interface; i.e., $\alpha \to 0$. The regions $0 < r < 1$ and $1 < r < \infty$ are now decoupled in the following sense. The boundary conditions for the matrix problem are

$$\sigma_{rz} = \tau_s \text{sgn}(y) \qquad \text{on } r = 1$$
$$\sigma_{yz} + i\,\sigma_{xz} \to \tau_\infty \qquad r \to \infty$$

and the boundary condition for the fiber problem is

$$\sigma_{rz} = \tau_s \text{ sgn}(y) \text{ on } r = 1$$

The solution for the matrix is written in the form $w = w_\infty + w_1$, where

$$w_\infty = \frac{\tau_\infty}{G_M} r \sin\theta$$

The function w_1 is harmonic in the region $1 < r < \infty$ (as is w). Using separation of variables, a series solution is found:

$$w_1 = \sum_{k=1}^{\infty} b_k r^{-k} \sin k\theta$$

where

$$b_k = \begin{cases} \dfrac{-4\,\tau_s}{\pi G_M} + \dfrac{\tau_\infty}{G_M} & k = 1 \\ \dfrac{2\,\tau_s}{\pi G_M k^2} [(-1)^k - 1] & k > 1 \end{cases}$$

A solution for $0 < r < 1$ is found to be

$$w = \sum_{k=1}^{\infty} a_k r^k \sin k\theta$$

$$a_k = \frac{2\,\tau_s}{\pi G_F k^2} [1 - (-1)^k]$$

The average fiber stress is readily found via integration to be

$$\bar{\sigma}_{yz}^F = \frac{4}{\pi} \tau_s$$

The term involving the slippage at the interface is now

$$\frac{G_M}{\pi \tau_\infty} \int_{\Gamma_I} w n_y ds = 2 - \frac{4}{\pi} \left(1 + \frac{G_M}{G_F} \right) \frac{\tau_s}{\tau_\infty}$$

Combining these expressions, one obtains the asymptotic result

$$\frac{G_e}{G_M} = 1 + c_F \left[-2 + \frac{8}{\pi} \frac{\tau_s}{\tau_\infty} \right] \tag{14}$$

Results

The progression of slip, measured by $\xi = \pi/2 - \alpha$, is depicted as a function of the loading parameter T in Fig. 2. Some sense of the rate at which the slip zone propagates may be gained by comparison with a highly approximate calculation. The slip zone spreads to the angle α when the traction σ_{rz} at that angle just reaches the value τ_s. An approximate solution to this problem is to calculate α on the basis of the traction distribution *prior* to slippage. That is, let α_{app} be given by

$$\frac{2\lambda}{\lambda+1} \tau_\infty \sin \alpha_{app} = \tau_s$$

The dashed curve in Fig. 2 is $\xi_{app} = \pi/2 - \alpha_{app}$. Note the actual propagation of slip is faster than the prediction based on the stress distribution before slip. This suggests that there is an intensification of the stress which accompanies slippage, even though the traction cannot exceed τ_s.

Downloaded 03 May 2010 to 171.66.16.21. Redistribution subject to ASME license or copyright; see http://www.asme.org/terms/Terms_Use.cfm

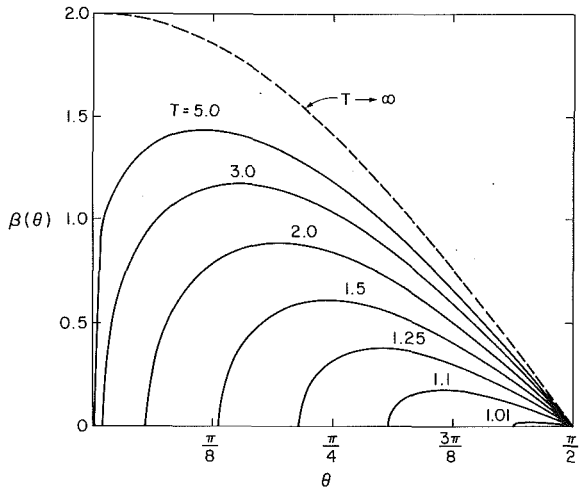


Fig. 3 Angular variation of the normalized dislocation distribution. (--- ~ dislocation distribution for complete slip, $T \to \infty$.)

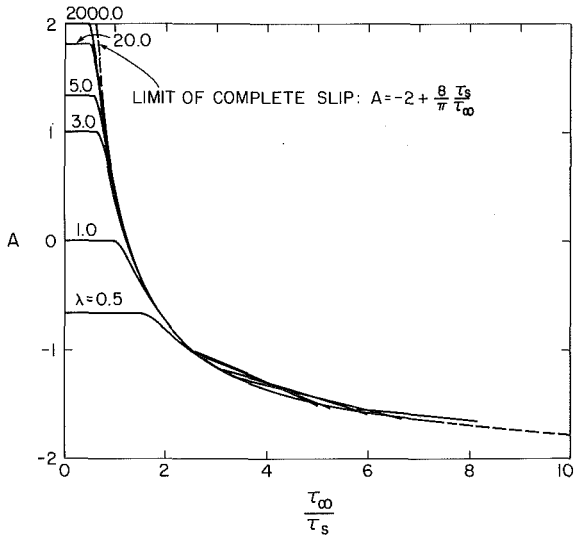


Fig. 4 Reinforcement coefficient as a function of normalized applied stress. (--- ~ reinforcement coefficient for complete slip, $T \to \infty$.)

In Fig. 3, the normalized dislocation density $\beta(\theta) = b(\theta) G_M/\tau_\infty$ is plotted for several values of the loading parameter T. Because of the normalization, the increase in the dislocation intensity is not to be associated with the increased remote straining, but rather with the degree to which the loading exceeds the critical stress for slippage. Also shown in Fig. 3 is the dislocation density for $T \to \infty$ (dashed curve). This distribution, given by $\beta(\theta) = 2\cos\theta$, may be obtained from the asymptotic solution derived above.

The reinforcement coefficient A, which appears in the dilute solution approximation to the effective modulus, is plotted in Fig. 4 as a function of the parameter τ_∞/τ_s. As expected, the stiffness of the composite makes the transition from that of a perfectly bonded composite at low stresses to that of a composite with *holes* for fibers at large stresses. For comparison, the asymptotic solution for large τ_∞/τ_s, which is independent of λ, is plotted as the dashed curve. We emphasize that these results are valid for low fiber concentrations.

For the purpose of exhibiting the inelasticity associated with the interface, we consider loading in shear followed by complete unloading. Unloading initially occurs in a completely elastic fashion, meaning that the incremental stresses and strains upon unloading are, initially, connected by the effective modulus of the perfectly bonded composite. During this unloading, no additional slippage occurs. Reverse slip occurs when the critical shear stress, now of the opposite sign, is reached somewhere along the interface. Again, this condition is satisfied first at the top and bottom of the fiber. Since the shear stress here was τ_s at the maximum load, reverse slip begins only when the unloading has proceeded twice as far as was required to initiate slip upon loading.

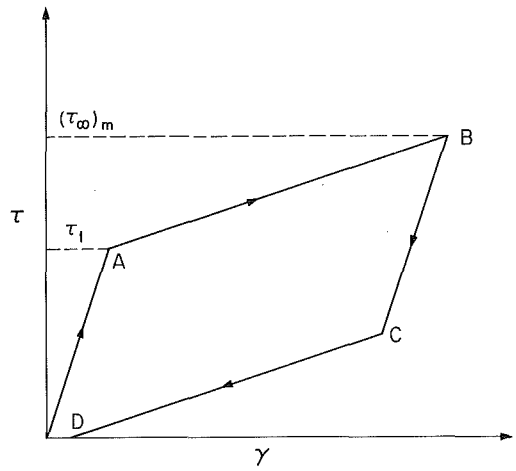


Fig. 5 Variation of stress and strain during a cycle of loading and unloading

Let $(\tau_\infty)_m$ be the maximum applied shear stress. Then, reverse slip occurs when

$$\tau_\infty = (\tau_\infty)_m - 2\left(\frac{2\lambda}{\lambda+1}\right)\tau_s \tag{15}$$

Note that this condition holds only if the right hand side of (15) is positive. If it is negative, then there is no reverse slip upon complete unloading. In general, the relation between the additional stresses and strains induced by unloading is identical to the stress-strain relation prevailing during loading, except with τ_s replaced by $2\tau_s$.

We now calculate the amount of energy dissipated by a loading-unloading cycle and the attendant permanent strain. This is done approximately by replacing the actual stress-strain curve by a piecewise linear curve. Let the stress-strain curve be given by the perfectly bonded result for $\tau_\infty < \tau_1$, and by the asymptotic result (14) for $\tau_\infty \geq \tau_1$. If the stress-strain curve is to be continuous at τ_1, then

$$\tau_1 = \frac{2(\lambda+1)}{\pi\lambda}\tau_s$$

The stress cycle is shown schematically in Fig. 5. Because we have replaced the actual stress-strain curve by an approximate one, the transition points A and C only correspond approximately to slip initiation and reverse – slip initiation. Stresses and strains at the labelled points are:

A: $\tau = \tau_1$, $\gamma = \frac{\tau_1}{G_M}\left[1 + 2c_F\frac{1-\lambda}{1+\lambda}\right]$

B: $\tau = (\tau_\infty)_m$, $\gamma = \frac{(\tau_\infty)_m}{G_M}[1+2c_F] - \frac{4\lambda}{1+\lambda}\frac{\tau_1}{G_M}c_F$

C: $\tau = (\tau_\infty)_m - 2\tau_1$, $\gamma = \frac{(\tau_\infty)_m}{G_M}[1+2c_F] - \frac{2\tau_1}{G_M}\left[1+\frac{2}{1+\lambda}c_F\right]$

D: $\tau = 0$, $\gamma = \frac{2\lambda}{1+\lambda}\frac{\tau_1}{G_M}c_F$

One immediately sees that the permanent strain is

Downloaded 03 May 2010 to 171.66.16.21. Redistribution subject to ASME license or copyright; see http://www.asme.org/terms/Terms_Use.cfm

$$\gamma = \frac{2\lambda}{1+\lambda}\frac{\tau_1}{G_M}c_F$$

Integrating under the stress-strain curves, one finds the energy absorbed in a single cycle, E_{abs}, to be

$$E_{abs} = \frac{2\lambda}{1+\lambda}\frac{\tau_1}{G_M}[4(\tau_\infty)_m - 5\tau_1]c_F$$

The relative accuracy of these expressions increases with $(\tau_\infty)_m/\tau_s$, since the approximate stress-strain curve is then valid over a larger fraction of the cycle.

Acknowledgments

This work has been supported by the National Science Foundation under grant MSM-8451080, by the General Electric Engine Business Group, by the Alcoa Technical Center, and by the Department of Mechanical Engineering, Carnegie-Mellon University.

References

Aveston, J., and Kelly, A., 1973, "Theory of Multiple Fracture of Fibrous Composites," *J. Mat. Sci.*, Vol. 8, pp. 352–362.

Budiansky, B., Hutchinson, J. W., and Evans, A. G., 1986, "Matrix Fracture in Fiber-Reinforced Ceramics," *J. Mech. Phys. Solids*, Vol. 34, pp. 167–189.

Dundurs, J., and Comninou, M., 1979, "Some Consequences of the Inequality Conditions in Contact and Crack Problems," *J. Elasticity*, Vol. 9, pp. 71–82.

Dundurs, J., and Mura, T., 1964, "Interaction Between an Edge Dislocation and a Circular Inclusion," *J. Mech. Phys. Solids*, Vol. 12, pp. 177–189.

Dundurs, J., and Sendeckyj, G. P., 1965, "Edge Dislocation Inside a Circular Inclusion," *J. Mech. Phys. Solids*, Vol. 13, pp. 141–147.

Horii, H., and Nemat-Nasser, S., 1983, "Overall Moduli of Solids With Microcracks: Load-Induced Anisotropy," *J. Mech. Phys. Solids*, Vol. 31, pp. 155–171.

Kelly, A., 1970, "Interface Effects and the Work of Fracture of a Fibrous Composite," *Proc. of Roy. Soc. Lond.*, Vol. A319, pp. 95–116.

Muskhelishvili, N. I., 1977, *Singular Integral Equations*, Noordhoff International Publishing, The Netherlands.

APPENDIX

In this Appendix we briefly derive the stress fields associated with a screw dislocation located at the fiber–matrix interface. Solutions to the corresponding edge dislocation problems have been given by Dundurs and Mura (1964) and Dundurs and Sendeckyj (1965). Consider first the dislocation to be located at the point z_0 in the matrix, where $|z_0| > 1$. Let ω_0 be the solution for a single screw dislocation with Burger's vector b located at z_0 in a *homogeneous* body having moduli equal to those of the matrix. Hence, ω_0 is given by

$$\omega_0 = d_M \ln(z - z_0) \qquad (A\text{-}1)$$

where $d_M = G_M b/2\pi$.

We write the solution to the inhomogeneous problem in the form

$$\omega = \begin{cases} \omega_0 + \omega_F & |z|<1 \\ \omega_0 + \omega_M & |z|>1 \end{cases} \qquad (A\text{-}2)$$

where ω_F is analytic in $|z|<1$, and ω_M is analytical in $|z|>1$.

Define the functions $\Omega_F = z\omega_F'$ and $\Omega_M = z\omega_M'$ where the prime denotes differentiation with respect to z. Then, continuity of shear traction implies

$$(\Omega_F - \bar{\Omega}_F)_- = (\Omega_M - \bar{\Omega}_M)_+ \text{ on } |z|=1 \qquad (A\text{-}3)$$

while continuity of displacement requires

$$\frac{1}{G_F}(\Omega_F + \bar{\Omega}_F)_- = \frac{1}{G_M}(\Omega_M + \bar{\Omega}_M)_- + \left(\frac{1}{G_M} - \frac{1}{G_F}\right)\left(\frac{d_M z}{z - z_0} + \frac{d_M \bar{z}}{\bar{z} - \bar{z}_0}\right) \text{ on } |z|=1 \qquad (A\text{-}4)$$

where $(\ )_+$ denotes the limit as one approaches the interface from the matrix and $(\ )_-$ denotes an approach from the fiber. Note that the displacement condition actually enforces continuity of $\partial w/\partial\theta = \mathrm{Re}[\Omega]/G$.

Now, define the functions

$$\Omega_F^*(z) = \overline{\Omega_F\left(\frac{1}{\bar{z}}\right)} \qquad \Omega_M^*(z) = \overline{\Omega_M\left(\frac{1}{\bar{z}}\right)}$$

such that Ω_F^* is analytic in $|z|>1$ and Ω_M^* is analytic in $|z|<1$.

Since equation (A-3) implies

$$(\Omega_F + \Omega_M^*)_- = (\Omega_F^* + \Omega_M)_+$$

one can define a function Φ, given by

$$\phi = \begin{cases} \Omega_F + \Omega_M^* & |z|<1 \\ \Omega_M + \Omega_F^* & |z|>1 \end{cases}$$

which is entire. Let Φ be equal to the constant c, which, from the relations

$$\Omega_M^* = c - \Omega_F$$
$$\Omega_F^* = c - \Omega_M$$

must be real.

Now, use

$$\bar{z} = \frac{1}{z} \text{ on } |z|=1$$

to rearrange equation (A-4) into the form

$$(\Omega_F)_- - d_M B\frac{z}{z - z_0} = (\Omega_M)_+ + d_M B\frac{1}{1 - \bar{z}_0 z} + Bc \qquad (A\text{-}5)$$

where

$$B = \frac{G_F - G_M}{G_F + G_M}$$

An analytic continuation argument applied to (A-5) implies that both sides are equal to a constant which must be zero if there is to be no singularity at $z=0$. The solution is completed by insisting that the net dislocation in the infinite plane be equal to b, and that the net force be zero; i.e.,

$$\oint (\omega_0' + \omega_M')dz = i\,G_M b$$

from which $c=0$.

The stress function thereby derived is given by

$$\omega' = \begin{cases} \dfrac{d_M(1+B)}{z - z_0} & |z|<1 \\ \dfrac{d_M}{z - z_0} - \dfrac{d_M B}{z(1 - \bar{z}_0 z)} & |z|>1 \end{cases}$$

A similar procedure is used to find the solution to the problem of a dislocation located at a point inside the fiber; the result is

$$\omega' = \begin{cases} \dfrac{d_F}{z - z_0} + \dfrac{d_F B\bar{z}_0}{1 - \bar{z}_0 z} & |z|<1 \\ \dfrac{d_F}{z - z_0} + d_F\left(\dfrac{G_M}{G_F} - 1\right)\dfrac{1}{z} - \dfrac{d_F B z_0}{z(z - z_0)} & |z|>1 \end{cases}$$

where $d_F = G_F b/2\pi$. When one lets $|z_0| \to 1$, the solutions coincide, and the result is given by equation (3).

Downloaded 03 May 2010 to 171.66.16.21. Redistribution subject to ASME license or copyright; see http://www.asme.org/terms/Terms_Use.cfm

Zekai Celep
Professor.
Faculty of Civil Engineering,
Istanbul Technical University,
80626 Ayazaga,
Istanbul, Turkey

Doğan Turhan
Professor.
Department of Mechanical Engineering,
Faculty of Engineering
and Architecture,
Karadeniz Technical University,
Trabzon, Turkey

Rajeh Zaid Al-Zaid
Assistant Professor.
Department of Civil Engineering,
College of Engineering,
King Saud University,
Riyadh 11421, Saudi Arabia

Circular Elastic Plates on Elastic Unilateral Edge Supports

The response of an elastic circular plate supported unilaterally by elastic springs along its edge is studied. A load which is uniformly distributed along a circular arc of the plate is considered. The loss of the contact along the edge of the plate, the variations of deflections and those of reactions are presented. The influences of the position of loading, the spring constant, and Poisson's ratio are shown in various figures.

Introduction

The behavior of plates supported elastically is usually determined by assuming continuous contact along the boundary of the plate. Although this assumption is often justifiable, there are many practical problems where unilateral support is of interest. The treatment of this type of problem requires the determination of the contact region which usually depends on the configuration of the loading as well as the stiffnesses of the elastic support and the plate. It is well known that when a simply supported rectangular plate is loaded laterally, the corners of the plate in general have a tendency to rise and if this is prevented by anchoring them, the corner reactions have to be transferred from the plate to the support. The lift-off of the corner was investigated by considering an infinitely extended plate subjected to a concentrated load near the corner by Keer and Mak (1981). Dempsey et al. (1984) studied a uniformly loaded square plate and determined the extent of the contact. In two recent papers, Dempsey and Li (1986) gave a method of solution for determining the contact region and presented its numerical implementation for concentrated and uniform loadings. In the foregoing studies, the support was assumed to be unilateral but rigid. Salamon et al. (1986) investigated the same rectangular plate supported elastically. They used the finite element method and found out that the plate lifts off the foundation, except for low support stiffnesses.

This paper investigates the extent of the contact for a circular plate under a uniformly distributed load along a circular arc. The plate is assumed to be unilaterally supported around its periphery by elastic springs. Numerical results are presented showing the extent of the contact, and the distributions of displacements and support reactions for various loading configurations, spring constants, and Poisson's ratios.

Statement of the Problem

Consider a thin elastic circular plate of stiffness D and radius a as shown in Fig. 1. The plate is subjected to a total load of P which is applied as a uniformly distributed load along a circular arc of radius b and angle $2\theta_1$. It is assumed that the plate is elastically supported by linear springs having a translational constant of k along its periphery. Since the springs are assumed to be acting unilaterally, a possible lift-off region is expected. Because of the symmetry of the lateral

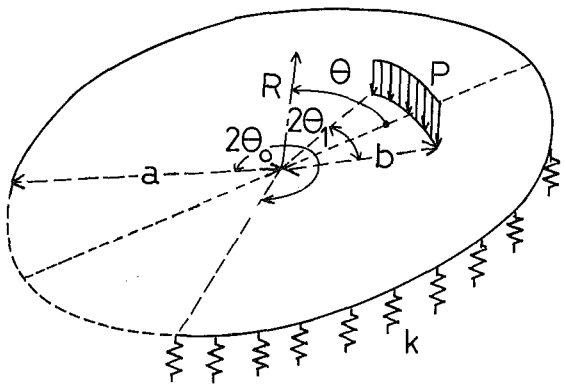


Fig. 1 Circular plate on unilateral edge supports

Contributed by the Applied Mechanics Division for publication in the JOURNAL OF APPLIED MECHANICS.

Discussion on this paper should be addressed to the Editorial Department, ASME, United Engineering Center, 345 East 47th Street, New York, N.Y. 10017, and will be accepted until two months after final publication of the paper itself in the JOURNAL OF APPLIED MECHANICS. Manuscript received by ASME Applied Mechanics Division, February 12, 1987; final revision, December 11, 1987.

Copyright © 1988 by ASME
Downloaded 03 May 2010 to 171.66.16.21. Redistribution subject to ASME license or copyright; see http://www.asme.org/terms/Terms_Use.cfm

load, only one half of the plate is considered where the boundary $\theta_0 < \theta \le \pi$ corresponds to the loss of the contact. Dividing the plate into two parts by a cylindrical section of radius b, two separate solutions can be written as done by Timoshenko and Woinowsky-Krieger (1959).These solutions are

$$w(r,\theta) = a\sum_{m=0}^{\infty} w_m(r)\cos m\theta;$$

$$\bar{w}(r,\theta) = a\sum_{m=0}^{\infty} \bar{w}_m(r)\cos m\theta \tag{1}$$

for the inner and outer parts of the plate, respectively, where

$$\begin{aligned} w_m(r) &= A_m r^m + B_m r^{m+2} && \text{for } m \ge 0,\\ \bar{w}_0(r) &= C_o + D_o r^2 + E_o \ln r + F_o r^2 \ln r,\\ \bar{w}_1(r) &= C_1 r + D_1 r^3 + E_1 r^{-1} + F_1 r \ln r,\\ \bar{w}_m(r) &= C_n r^m + D_m r^{-m} + E_m r^{m+2} + F_m r^{-m+2} && \text{for } m \ge 2,\\ r &= R/a. \end{aligned} \tag{2}$$

The plate is assumed to be supported free from bending moment at the outer edge. For unilateral support with translational springs, it is required that the shearing force at the edge be proportional to the corresponding deflection, provided that the spring carries a compressive force; otherwise the shearing force vanishes:

$$\sum_{m=0}^{\infty}\left\{\frac{d}{dr}\left[\frac{d^2}{dr^2}+\frac{1}{r}\frac{d}{dr}-\frac{m^2}{r^2}\right] -(1-\upsilon)\frac{m^2}{r^2}\left[\frac{d}{dr}-\frac{1}{r}\right]\right\}\bar{w}_m\cos m\theta = H(\theta)k^*\sum_{m=0}^{\infty}\bar{w}_m\cos m\theta \qquad \text{for } r=1, \tag{3}$$

where $k^* = ka^3/D$ is the non-dimensional spring constant and

$$H(\theta) = 1 \quad \text{for} \quad 0 \le \theta \le \theta_o,$$
$$H(\theta) = 0 \quad \text{for} \quad \theta_o < \theta \le \pi,$$

and θ_o denotes the contact angle (Fig. 1). For elimination of the polar angle θ in equation (3), the orthogonality of the trigonometric functions case be used. It follows then

$$\left\{\frac{d}{dr}\left[\frac{d^2}{dr^2}+\frac{1}{r}\frac{d}{dr}-\frac{m^2}{r^2}\right] -(1-\upsilon)\frac{m^2}{r^2}\left[\frac{d}{dr}-\frac{1}{r}\right]\right\}\bar{w}_m = k^*\sum_{n=0}^{\infty}E_{mn}\bar{w}_n \text{ for } r=1, \tag{4}$$

where

$$E_{oo} = \theta_o/\pi,\ E_{mo} = 2E_{om} = \frac{2\sin m\theta_o}{m\pi},$$

$$E_{mm} = \left[\theta_o + \frac{\sin 2m\theta_o}{2m}\right]/\pi \qquad \text{for } m \ge 1,$$

$$E_{mn} = \left[\frac{\sin(m-n)\theta_o}{m-n} + \frac{\sin(m+n)\theta_o}{m+n}\right]/\pi$$
$$\text{for } m \ne n \text{ and } m \ge 1,\ n \ge 1.$$

The boundary conditions at the interface of the two parts of the plate require the displacement function, and its first and second derivatives with respect to r, to be continuous. However, the shearing force displays a discontinuity due to the loading along the dividing circle. For the application of harmonic balance, the load is represented in form of the series as

$$\frac{P}{a}\sum_{n=0}^{\infty}p_n\cos n\theta = \frac{P}{2\pi b} + \frac{P}{\pi\theta_1 b}\sum_{n=1}^{\infty}\frac{1}{n}\cos n\theta\sin\theta_1. \tag{5}$$

Thus, the balance in shearing force of the two parts of the plate can be written as follows

$$\frac{d}{dr}\left[\frac{d^2}{dr^2}+\frac{1}{r}\frac{d}{dr}-\frac{m^2}{r^2}\right](\bar{w}_m - w_m) = P^* p_m \text{ for } r = r_b, \tag{6}$$

where $P^* = Pa/D$ denotes the nondimensional load. The boundary conditions at the outer edge and the interface yield a set of linear algebraic equations for the unknown constants A_m, B_m, C_m, D_m, E_m and F_m (Appendix). Finally, the condition for the contact angle θ_o is as follows

$$\bar{w}(r=1, \theta=\theta_o) = a\sum_{m=0}^{\infty}\bar{w}_m(r=1)\cos n\theta_o = 0 \tag{7}$$

Note that equation (7) can be used as long as $0 < \theta_o \le \pi$; and the case of $\theta_o = \pi$ for $\bar{w}(r=1,\ \theta=\pi) \ge 0$ corresponds to the complete contact between springs and plate. Thus, the equations required for determining all the unknowns are obtained.

Numerical Analysis and Discussion

Since E_{mn} contains the unknown contact angle θ_o, the system of linear algebraic equations will be a nonlinear one when equation (7) is included. This indicates that the numerical treatment has to be an iterative one. In this context, one should remember also that a finite number of unknowns can be considered. Numerical calculations are carried out at the Computer Center of the King Saud University, Riyadh. To investigate the convergence of the numerical scheme, several test cases are carried out by considering different number of terms in the series expansions. For the results presented in the figures, it is found that the accuracy of the curves can be assured by considering nine terms and the contact angle θ_o

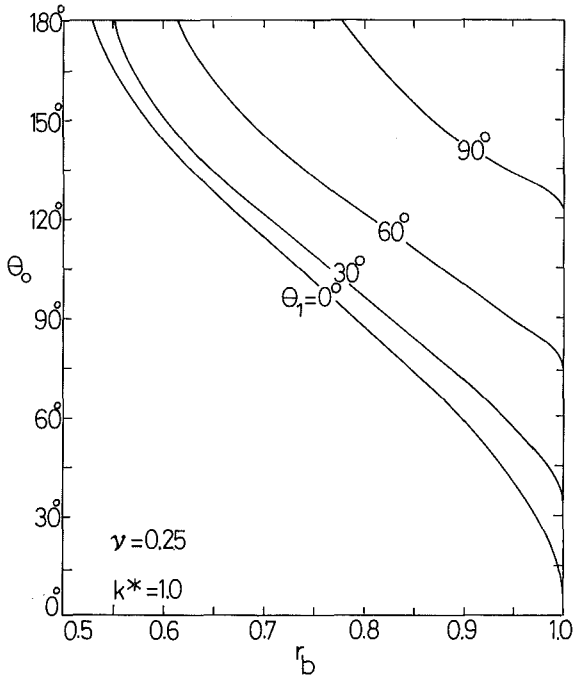


Fig. 2 The contact angle θ_o versus the configuration of the loading r_b and θ_1

Downloaded 03 May 2010 to 171.66.16.21. Redistribution subject to ASME license or copyright; see http://www.asme.org/terms/Terms_Use.cfm

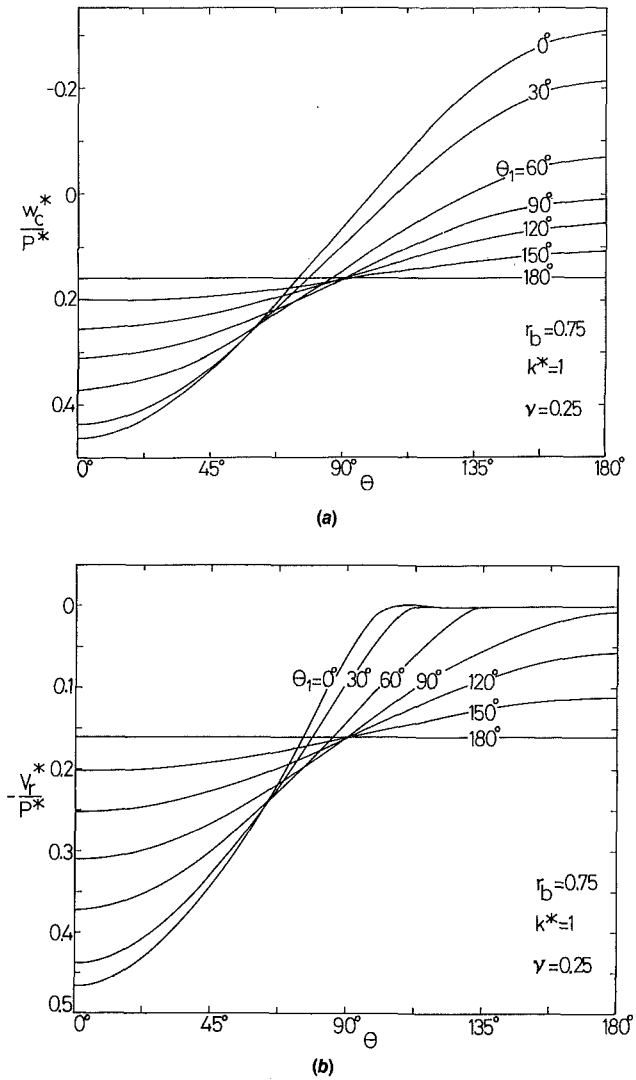


Fig. 3 (a) The nondimensional displacement w_c^* and, (b) the nondimensional shearing force V_r^* along the edge of the plate subjected to a line load

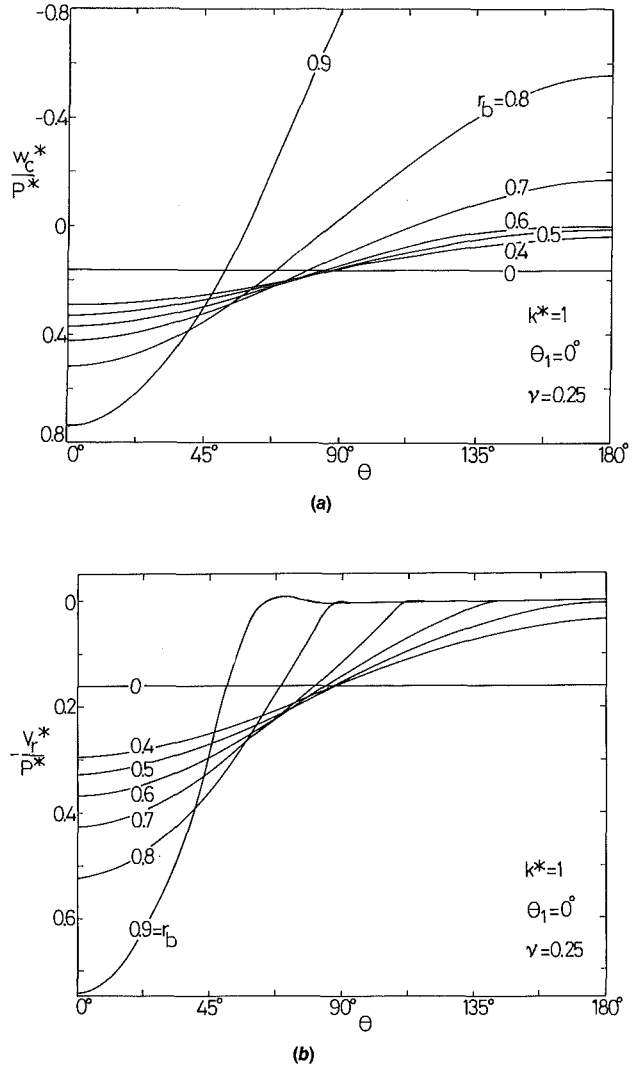


Fig. 4 (a) The nondimensional displacement w_c^* and, (b) the nondimensional shearing force V_r^* along the edge of the plate subjected to a concentrated load

could be obtained in five or six iterations. In the numerical solution, the overall equilibrium of the plate is checked by considering the vertical external load and support reactions of the plate and their moments as follows

$$P^* = 2k^* \int_0^{\theta_o} \bar{w}(r=1,\ \theta)d\theta,$$

$$P^* r_b \sin\theta_1/\theta_1 = 2k^* \int_0^{\theta_o} \bar{w}(r=1,\ \theta)\ \cos\theta\ d\theta. \qquad (8)$$

The numerical results are also assessed by solving the same problem for a rigid plate and comparing the results with those of the elastic plate supported by very soft springs.

The numerical solutions are carried out for various values of the parameters of the problem. The results yield that the contact angle does not depend on the loading level whether the load is a line load or a concentrated one. Figure 2 shows the contact angle θ_o of the plate subjected to a total load P^* which is uniformly distributed along a circular arc having a radius of r_b and angle of $2\theta_1$. The case $\theta_1 = 0$ corresponds to the concentrated load. As it is seen, the plate experiences a growth of contact for a given loading position as θ_1 increases and for $\theta_o = \pi$ the complete contact develops. As the loading approaches the outer edge of the plate, the contact angle θ_o decreases and seems to approach to θ_1. Figure 3 illustrates the variations of the nondimensional displacement $w_c^* = \bar{w}\ (r=1,\ \theta)/a$ and the nondimensional shearing force $V_r^* = a^2 V_r/D$ at the edge of the plate. The shearing force is obtained by including the twisting couples along the edge of the plate. Similar variations are represented in Fig. 4 for a concentrated load ($\theta_1 = 0$) with different loading radii. As expected, the shearing force vanishes when the plate lifts off. However, as seen in Fig. 4*b*, V_r^* seems to assume small values of tensile forces for $r_b = 0.9$ in a limited range of θ which is purely due to numerical error. The numerical error sharply decreases as r_b assumes smaller values than 0.9. This corresponds to the fact as the loading approaches the outer edge of the plate the numerical error increases, whereas the numerical error sharply decreases when the loading approaches the center of the plate. A sharp increase in both positive and negative displacements occurs as the load comes nearer to edge of the plate. Figure 5 shows the effect of the Poisson's ratio on the contact angle. It shows that the extent of contact gets larger as Poisson's ratio increases and this effect is more pronounced for smaller values of the loading radius. The effect of the relative stiffness of the supporting springs is displayed in Fig. 6. It should be noted that as the springs get stiffer, the contact region increases, and this increase is especially pronounced again for smaller values of r_b. The curve for $\log k^* = -3$ is assessed by solving the rigid plate equations.

Finally, Figs. 7(*a*) and 7(*b*) show the effect of the spring constant on the contact angle for various loading angles and

Downloaded 03 May 2010 to 171.66.16.21. Redistribution subject to ASME license or copyright; see http://www.asme.org/terms/Terms_Use.cfm

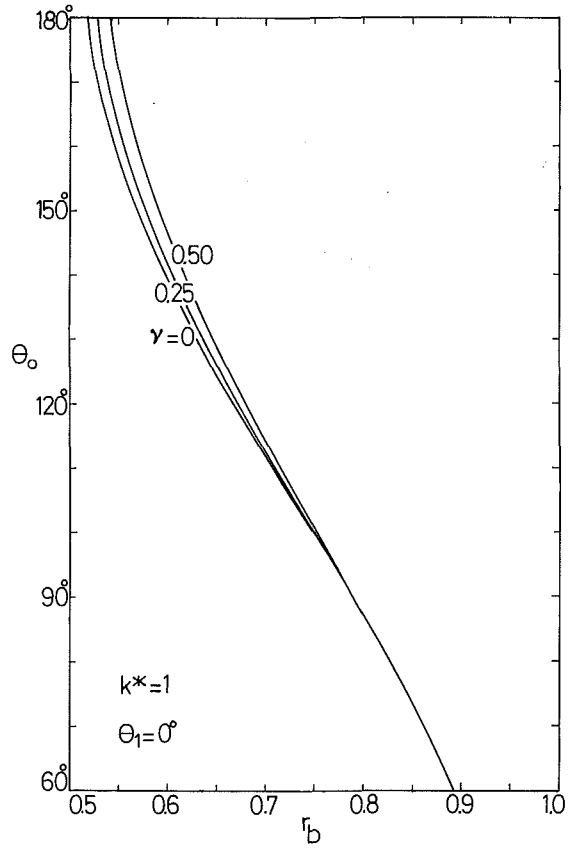


Fig. 5 The contact angle θ_o versus the loading radius r_b for various Poisson's ratios ν

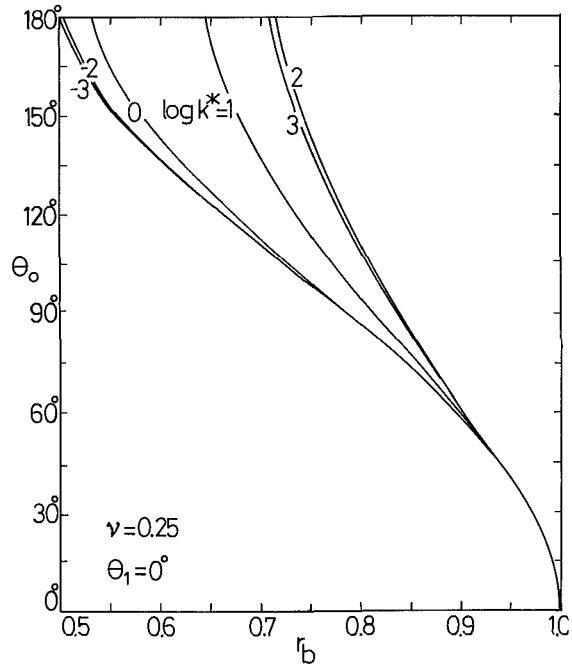
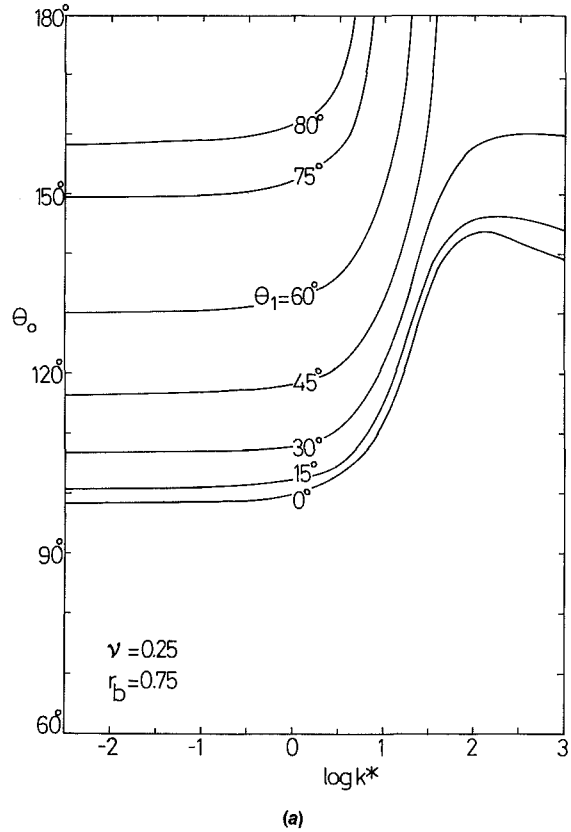
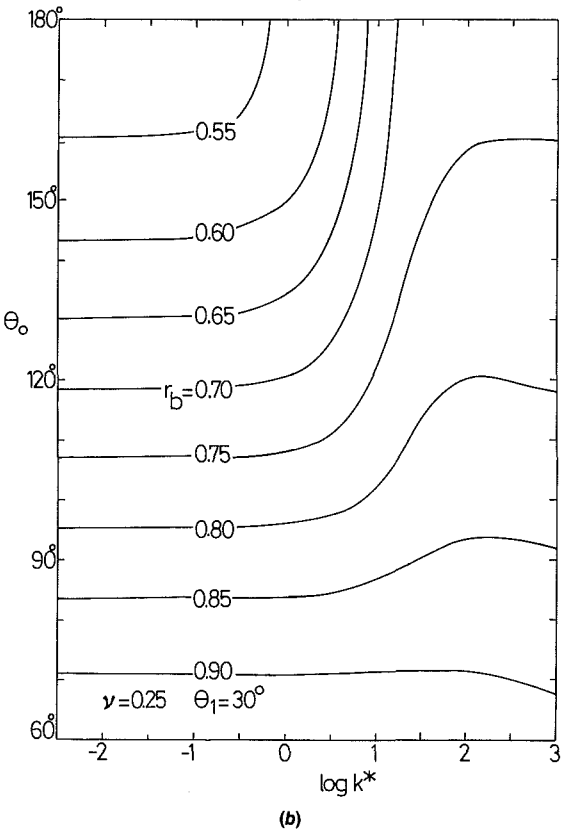


Fig. 6 The contact angle θ_o versus the loading radius r_b for various spring constants k^*



(a)



(b)

Fig. 7 The contact angle θ_o versus the spring constants k^* for various (a) loading angles θ_1, and (b) loading radii r_b

radii. As expected, the contact region gets larger as the length of the arc where the total load is uniformly distributed increases, and as the load approaches the center of the plate. The curves show that the effect of the spring constant is less pronounced for the smaller values of k^*.

Conclusion

In the present study a straightforward method is presented to solve the lift-off problem for a circular plate. The solution is obtained by employing Fourier series which is quite suitable

Downloaded 03 May 2010 to 171.66.16.21. Redistribution subject to ASME license or copyright; see http://www.asme.org/terms/Terms_Use.cfm

for computer applications. The plate is assumed to be supported by elastic springs in order to cover a large range of supporting conditions including the rigid support as a limiting case. The numerical results yield that, whereas the contact region does not depend on the loading level whether the load is a line load or a concentrated one, it is highly sensitive to the distribution angle θ_1 and the loading radius r_b.

References

Dempsey, J. P., Keer, L. M., Patel, N. B., and Glasser, M. L., 1984, "Contact Between Plates and Unilateral Supports," ASME JOURNAL OF APPLIED MECHANICS, Vol. 51, pp. 324-328.

Dempsey, J. P., and Li, H., 1986, "Rectangular Plates on Unilateral Supports: Part 1—Theory and Numerical Analysis," ASME JOURNAL OF APPLIED MECHANICS, Vol. 53, pp. 146-150.

Dempsey, J. P., and Li, H., 1986, "Rectangular Plates on Unilateral Supports: Part 2—Implementation; Concentrated and Uniform Loading," ASME JOURNAL OF APPLIED MECHANICS, Vol. 53, pp. 151-156.

Keer, L. M., and Mak, A. F., 1981, "Loss of Contact in the Vicinity of a Right Angle Corner for a Simply Supported, Laterally Loaded Plate," ASME JOURNAL OF APPLIED MECHANICS, Vol. 48, pp. 597-600.

Salamon, N. J., Pawlak, T. P., and Mahmoud, F. F., 1986, "Plates in Unilateral Contact with Simple Supports: Pressure Loading," ASME JOURNAL OF APPLIED MECHANICS, Vol. 53, pp. 141-145.

Timoshenko, S. P., and Woinowsky-Krieger, S., *Theory of Plates and Shells*, McGraw-Hill, New York, 1959.

APPENDIX

The system of the algebraic linear equations for the constants A_m, B_m, C_m, D_m, E_m and F_m are:

$$2(1+\upsilon)D_o-(1-\upsilon)E_o+(3+\upsilon)F_o=0,$$

$$2(3+\upsilon)D_1+2(1-\upsilon)E_1+(1+\upsilon)F_1=0,$$

$$m(m-1)(1-\upsilon)C_m+m(m+1)(1-\upsilon)+[(m+2)(m+1+\upsilon)-\upsilon m^2]E_m+[(m-2)(m-1-\upsilon)-\upsilon m^2]F_m=0 \quad \text{for } m\geq 2,$$

$$4F_o-E_{oo}k^*(C_o+D_o)-E_{o1}k^*(C_1+D_1+E_1)-\sum_{n=2}^{\infty}E_{on}k^*(C_n+D_n+E_n+F_n)=0,$$

$$(6+2\upsilon)D_1+2(1-\upsilon)E_1-(3-\upsilon)F_1-E_{1o}k^*(C_o+D_o)-E_{11}k^*(C_1+D_1+E_1)-\sum_{n=2}^{\infty}E_{1n}k^*(C_n+D_n+E_n+F_n)=0,$$

$$m^2(1-m)(1-\upsilon)C_m+m^2(1+m)(1-\upsilon)D_m+m(m+1)(4-m(1-\upsilon))E_m+m(m-1)(4-m(1-\upsilon))F_m-E_{mo}k^*(C_o+D_o)-E_{m1}k^*(C_1+D_1+E_1)-\sum_{n=2}^{\infty}E_{mn}k^*(C_n+D_n+E_n+F_n)=0 \text{ for } m\geq 2,$$

$$A_o+B_or_b^2-C_o-D_or_b^2-E_o\ln r_b-F_or_b^2\ln r_b=0,$$

$$A_1r_b^2+B_1r_b^4-C_1r_b^2-D_1r_b^4-E_1-F_1r_b^2\ln r_b=0,$$

$$A_mr_b^{2m}+B_mr_b^{2m+2}-C_mr_b^{2m}-D_m-E_mr_b^{2m+2}-F_mr_b^2=0 \quad \text{for } m\geq 2,$$

$$2B_or_b^2-2D_or_b^2-E_o-F_or_b^2(2\ln r_b+1)=0,$$

$$A_1r_b^2+3B_1r_b^4-C_1r_b^2-3D_1r_b^4+E_1-F_1r_b^2(\ln r_b+1)=0,$$

$$mA_mr_b^{2m}+(m+2)B_mr_b^{2m+2}-mC_mr_b^{2m}+mD_m-(m+2)E_mr_b^{2m+2}+(m-2)F_mr_b^2=0 \text{ for } m\geq 2,$$

$$2B_or_b^2-2D_or_b^2+E_o-F_or_b^2(2\ln r_b+3)=0,$$

$$6B_1r_b^4-6D_1r_b^4-2E_1-F_1r_b^2=0,$$

$$m(m-1)A_mr_b^{2m}+(m+2)(m+1)r_b^{2m+2}-m(m-1)C_mr_b^{2m}-m(m+1)D_m-(m+2)(m+1)E_mr_b^{2m+2}-(m-2)(m-1)F_mr_b^2=0 \quad \text{for } m\geq 2,$$

$$8F_o=P^*/\pi,$$

$$8r_b^2B_1+2F_1-8D_1r_b^2=-P^*r_b\sin\theta_1/(\theta_1\pi),$$

$$4m(m+1)B_mr_b^{2m}-4m(m+1)E_mr_b^{2m}-4m(m-1)F_m=-P^*r_b^m\sin m\theta_1/(m\theta_1\pi) \text{ for } m\geq 2.$$

Finally, the contact condition is

$$C_o+D_o+(C_1+D_1)\cos\theta_o+\sum_{n=2}^{\infty}(C_n+D_n+E_n+F_n)\cos\theta_o=0.$$

Downloaded 03 May 2010 to 171.66.16.21. Redistribution subject to ASME license or copyright; see http://www.asme.org/terms/Terms_Use.cfm

M. H. Kempski
Department of Mechanical Engineering,
Rochester Institute of Technology,
Rochester, NY 14623
Assoc. Mem. ASME

L. A. Taber
Mem. ASME

Fong-Chin Su

Department of Mechanical Engineering,
University of Rochester,
Rochester, NY 14627

Large Elastic Deformation of Shear Deformable Shells of Revolution: Numerical and Experimental Results

Through an integrating matrix approach, a numerical solution is obtained to the equations governing large elastic deformation of a clamped circular cylinder due to internal pressure. The shell equations include the effects of large strains, thickness changes, and transverse shear deformation. The numerical solution is compared to results from an asymptotic analysis and from experiments on rubber cylinders. A specialized Rivlin-Saunders strain-energy density function is assumed for the rubber, with material constants determined from tensile tests and deformed cylinder profiles at a high inflation pressure.

Introduction

This work continues the investigation of Taber (1987b), where asymptotic expansions were presented to the equations governing large axisymmetric deformation of incompressible, elastic shells of revolution. The shell theory used here, which combines the field equations of Reissner (1969, 1972) and an extension of the constitutive formulations proposed by Simmonds (1986) for rubberlike shells, includes the effects of large strains, thickness changes, and transverse shear deformation. Results for clamped pressure vessels indicate that nonlinear membrane action dominates everywhere except near the edge, where a primary, membrane-type boundary layer and a secondary boundary layer, composed of separate stretching and bending components, develop (Taber, 1987a,b).

The objectives of the current effort are twofold. First a numerical solution of the fundamental equations is used to validate the asymptotic analyses of Taber (1987a,b). The equations are solved through an integrating matrix approach, which is modified to accommodate a mixed system of nonlinear differential and algebraic equations in a systematic fashion. Secondly, an attempt is made to validate the shell theory itself through experiments on clamped, rubberlike, circular cylinders that are subjected to internal pressure. Material constants for the rubber are deduced from tensile and cylindrical membrane test data under the assumption of a Rivlin-Saunders (1951) type of strain-energy density function.

Contributed by the Applied Mechanics Division for presentation at the Winter Annual Meeting, Chicago, IL, November 28 to December 2, 1988, of THE AMERICAN SOCIETY OF MECHANICAL ENGINEERS.

Discussion on this paper should be addressed to the Editorial Department, ASME, United Engineering Center, 345 East 47th Street, New York, N.Y. 10017, and will be accepted until two months after final publication of the paper itself in the JOURNAL OF APPLIED MECHANICS. Manuscript received by ASME Applied Mechanics Division, February 15, 1988; final revision, April 4, 1988.
Paper No. 88-WA/APM-48.

Theoretical Study

Governing Equations. A set of governing equations for axisymmetric deformation of a general shell of revolution is given in Taber (1987b). These relations, which are valid for large membrane and moderately large bending and transverse shear strains, are based on the geometry depicted in Fig. 1(*a*). For numerical convenience, the equations are combined to form the following system of four first-order ordinary differential equations and three algebraic equations:

$$\begin{aligned} r' &= \lambda_\Phi c + \gamma s \\ \Phi' &= \kappa_\Phi + \Phi_0' \\ \bar{H}' &= \partial w/\partial \lambda_\theta - pr_0(\lambda_\Phi s - \gamma c) \\ \bar{M}_\Phi' &= c\partial w/\partial \kappa_\theta + \bar{H}(\lambda_\Phi s - \gamma c) - pr^2(\lambda_\Phi c + \gamma s)/2 \\ 0 &= r_0 \partial w/\partial \lambda_\Phi - \bar{H}c - pr^2 s/2 \\ 0 &= r_0 \partial w/\partial \kappa_\Phi - \bar{M}_\Phi \\ 0 &= r_0 \partial w/\partial \gamma - \bar{H}s + pr^2 c/2. \end{aligned} \tag{1}$$

In these equations, prime denotes differentiation with respect to the *undeformed* meridional arc length x, subscript "0" indicates undeformed geometry, p is the internal pressure, and

$$s \equiv \sin\Phi, \qquad c \equiv \cos\Phi$$
$$\bar{H} \equiv r_0 H, \qquad \bar{M}_\Phi \equiv r_0 M_\Phi. \tag{2}$$

Part of the motivation for writing the governing equations in the form of equations (1) is to facilitate the incorporation of different strain-energy functions. Given the two-dimensional strain-energy density function $w(\lambda_\Phi, \kappa_\Phi, \gamma, r, \Phi)$ and the boundary conditions, equations (1) can be solved for the deformed radial coordinate r and the meridional *face* angle Φ, the reference surface stretch ratio λ_Φ, shear strain γ, and curvature-change measure κ_Φ; and the horizontal force and moment resultant quantities $\bar{H}$ and $\bar{M}_\Phi$.[1] Note that all quan-

[1] Here, the bars over the strain measures $\bar{\lambda}_\Phi$ and $\bar{\gamma}$ in Taber (1987b) are removed.

Copyright © 1988 by ASME
Downloaded 03 May 2010 to 171.66.16.21. Redistribution subject to ASME license or copyright; see http://www.asme.org/terms/Terms_Use.cfm

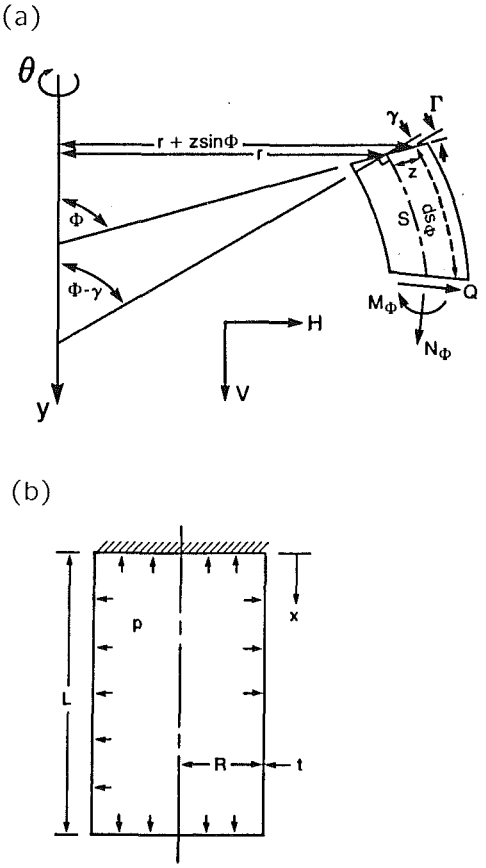


Fig. 1(*a*) Geometry and forces on a deformed shell element, and (*b*) Clamped cylinder geometry (*x*: undeformed meridional coordinate; *y*: deformed vertical coordinate)

tities are defined relative to the *undeformed* geometry of the reference surface. With the solution to equations (1), the *deformed* vertical coordinate y can be computed from the relation

$$y' = \lambda_\Phi s - \gamma c. \tag{3}$$

Numerical Solution Technique. Since the constitutive equations for large strain are often highly nonlinear, numerical convergence can be a problem. Recent studies by Parnell (1984) and Cagan and Taber (1986) have found the integrating matrix technique, which was developed mainly by Vakhitov (1966) and Hunter (1970), to be quite reliable in solving geometrically nonlinear shell problems, and so we decided to try the method on the current materially nonlinear problem. Here, we essentially follow Parnell's (1984) work, performing a spatial discretization of the governing differential equations with a modification to incorporate the nonlinear algebraic equations. This paper outlines the mechanics of applying the method; for discussion of the theoretical background, the reader is referred to Vakhitov (1966), Hunter (1970), and Parnell (1984).

Consider a system composed of N_D differential and N_A algebraic equations. The state vector of $N = N_D + N_A$ dependent variables is defined by

$$\mathbf{y}(x) = \begin{Bmatrix} \mathbf{y}_D \\ \mathbf{y}_A \end{Bmatrix} \tag{4}$$

where $\mathbf{y}_D$ contains the N_D variables that enter the formulation in differential form and $\mathbf{y}$ contains the N_A residue state variables. For the current problem,

$$\mathbf{y}_D = [r, \Phi, \bar{H}, \bar{M}_\Phi]^T, \quad \mathbf{y}_A = [\lambda_\Phi, \gamma, \kappa_\Phi]^T. \tag{5}$$

In general, the governing equations can be written in the form

$$\frac{d\mathbf{y}_D}{dx} = \mathbf{b}_D(\mathbf{y})$$

$$\mathbf{0} = \mathbf{b}_A(\mathbf{y}) \tag{6}$$

with the vectors $\mathbf{b}_D$ and $\mathbf{b}_A$ containing the nonlinear terms.

The integrating matrix is used to integrate the differential equations $(6)_1$, which will be considered first. The inherent accuracy of the integrating matrix approach lies in the degree n of the Newton's forward difference interpolating polynomial that is used to construct a local weighting matrix $\mathbf{u}_n$ [see Parnell (1984) for explicit forms of $\mathbf{u}_n$ up to third order]. If the shell is discretized into M subintervals, then $\mathbf{u}_n$ is an $(M+1) \times (M+1)$ matrix with the first row being all zeros.

Following Parnell (1984), we pursue a local ordering of the global state vector, i.e., the local state vectors for all shell segments are combined serially to form the discrete global state vector $\mathbf{y}_D$, where the hat indicates a discretized global quantity. Similarly, expanding each element u_{ij} of $\mathbf{u}_n$ into a diagonal block $\mathbf{u}_{ij}$ of size $N_D \times N_D$, i.e., each diagonal entry of $\mathbf{u}_{ij}$ is equal to u_{ij}, leads to the global weighting matrix

$$\mathbf{U}_n = \begin{bmatrix} \mathbf{u}_{11} & \mathbf{u}_{12} & \cdots & \cdots & \mathbf{u}_{1,M+1} \\ \mathbf{u}_{21} & \mathbf{u}_{22} & \cdots & \cdots & \mathbf{u}_{2,M+1} \\ \mathbf{u}_{31} & \mathbf{u}_{32} & \ddots & & \vdots \\ \vdots & \ddots & \ddots & \ddots & \vdots \\ \vdots & & \ddots & \ddots & \mathbf{u}_{M,M+1} \\ \mathbf{u}_{M+1,1} & \cdots & \cdots & \mathbf{u}_{M+1,M} & \mathbf{u}_{M+1,M+1} \end{bmatrix} \tag{7}$$

which is a banded matrix with $\mathbf{u}_{1j} = 0$. $\bar{\mathbf{U}}_n$ acts effectively as an integral operator, giving (Parnell, 1984)

$$\bar{\mathbf{U}}_n \cdot \frac{d\hat{\mathbf{y}}_D}{dx} = \bar{\mathbf{J}} \cdot \hat{\mathbf{y}}_D \tag{8}$$

where

$$\bar{\mathbf{J}} = \begin{bmatrix} \mathbf{0} & \mathbf{0} & \mathbf{0} & \cdots & \cdots & \mathbf{0} \\ -\mathbf{I} & +\mathbf{I} & \mathbf{0} & \cdots & \cdots & \mathbf{0} \\ \mathbf{0} & -\mathbf{I} & +\mathbf{I} & \mathbf{0} & & \vdots \\ \vdots & \ddots & \ddots & \ddots & \vdots & \\ \vdots & & \mathbf{0} & -\mathbf{I} & +\mathbf{I} & \mathbf{0} \\ \mathbf{0} & \cdots & \cdots & \mathbf{0} & -\mathbf{I} & +\mathbf{I} \end{bmatrix} \tag{9}$$

in which $\mathbf{I}$ is the identity matrix. Both $\bar{\mathbf{J}}$ and $\bar{\mathbf{U}}_n$ contain $(M+1) \times (M+1)$ blocks, each of size $(N_D \times N_D)$. Thus, through the application of the operator $\bar{\mathbf{U}}_n$, the discrete form of the differential equations $(6)_1$ is reduced to a system of nonlinear *algebraic* equations, which can be solved along with those given by equations $(6)_2$.

For computational purposes, we next cast these equations into a more convenient form. First, in the manner of equation (4), the global nonlinear vector is defined by

$$\mathbf{b}(\mathbf{y}) = \begin{Bmatrix} \mathbf{b}_D \\ \mathbf{b}_A \end{Bmatrix}. \tag{10}$$

Next, the matrices $\bar{\mathbf{U}}_n$ and $\bar{\mathbf{J}}$ are modified by redefining the component subblocks to be

Downloaded 03 May 2010 to 171.66.16.21. Redistribution subject to ASME license or copyright; see http://www.asme.org/terms/Terms_Use.cfm

$$\mathbf{I} \equiv \begin{bmatrix} 1 & & & & & \\ & 1 & & & & \\ & & \ddots & & & \\ & & & 1 & & \\ & & & & 0 & \\ & & & & & \ddots \\ & & & & & & 0 \end{bmatrix} \tag{11}$$

$$\mathbf{u}_{ij} \equiv \begin{bmatrix} u_{ij} & & & & & \\ & u_{ij} & & & & \\ & & \ddots & & & \\ & & & u_{ij} & & \\ & & & & -\delta_{ij} & \\ & & & & & \ddots \\ & & & & & & -\delta_{ij} \end{bmatrix} \tag{12}$$

where δ_{ij} is the Kronecker delta and the changes occur after the first N_D rows of these $N \times N$ matrices. As noted previously, the first row of subblocks in $\bar{\mathbf{U}}_n$ and $\bar{\mathbf{J}}$ is zero. If these rows are deleted to give the modified matrices $\mathbf{U}_n$ and $\mathbf{J}$, then the appropriate generalization of equation (8) is

$$\mathbf{U}_n \bullet \frac{d\hat{\mathbf{y}}}{dx} = \mathbf{J} \bullet \hat{\mathbf{y}}. \tag{13}$$

Finally, with the boundary conditions expressed in the form

$$\mathbf{B}_1 \bullet \mathbf{y}_1 = \mathbf{a}_1, \quad \mathbf{B}_2 \bullet \mathbf{y}_{M+1} = \mathbf{a}_{M+1}, \tag{14}$$

adding the discretized version of equations (6) yields

$$\mathbf{f}(\mathbf{y}) = \begin{bmatrix} \mathbf{B}_1 \bullet \mathbf{y}_1 - \mathbf{a}_1 \\ \mathbf{J} \bullet \hat{\mathbf{y}} - \mathbf{U}_n \bullet \mathbf{b}(\hat{\mathbf{y}}) \\ \mathbf{B}_2 \bullet \mathbf{y}_{M+1} - \mathbf{a}_{M+1} \end{bmatrix} = \mathbf{0}, \tag{15}$$

which represents a system of $(M+1) \times N$ nonlinear algebraic equations for the $(M+1) \times N$ unknown state variables. The system $\mathbf{f} = \mathbf{0}$ was solved through an implicit Newton-Raphson scheme (Parnell, 1984), which generally converged with little difficulty.

Comparison of Analytical and Numerical Results. One purpose of this research is to assess the accuracy of the asymptotic analyses of Taber (1987a,b). Here, we consider a relatively long ($L/R = 10$) and moderately thick ($R/t = 40$) circular cylinder (Fig. (1*b*)) of undeformed length L, radius R, and thickness t that is composed of a neo-Hookean material, with a strain-energy density W per unit undeformed volume given by equation (16) with $\alpha = 0$. The two-dimensional energy density function w is obtained by integrating W over the undeformed shell thickness (see Simmonds (1986) and Taber (1987b)). With the cylinder clamped to rigid end plates, which are free to move axially, the boundary conditions are taken to be $\Phi = 0$ and $r = R$ at the edges.

For a nondimensional internal pressure $pR/Ct = 1.5$, numerical and analytical results are compared in Fig. 2, which shows distributions of meridional bending moment M_Φ, membrane stress resultant N_Φ, reference surface stretch ratio λ_Φ, and transverse shear strain γ near the edge of the cylinder ($x = 0$). Curves are shown for cases neglecting ($g = 0$) and including ($g = 1.2$) transverse shear deformation.[2] The results demonstrate generally good agreement between the two solutions, with the greatest discrepancy occurring in λ_Φ. For thinner shells (not shown), the asymptotic solution grows more accurate, and so these curves appear to validate the boundary-layer behavior described in Taber (1987a,b). Also, note the large transverse shear strain near the shell edge (Fig. (2*d*)). As shown later in the experimental results (Fig. 4), this shear

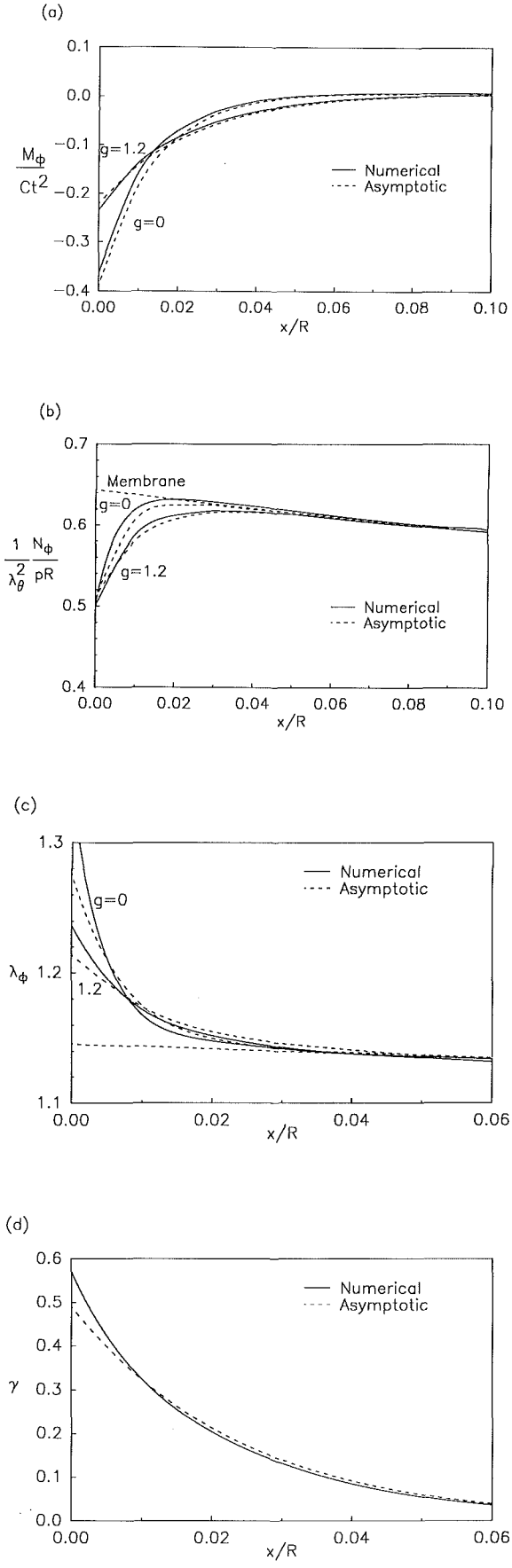


Fig. 2 Calculated bending moment (*a*), membrane stress resultant (*b*), stretch ratio (*c*), and transverse shear strain (*d*) distributions near clamped edge of pressurized cylinder ($R/t = 40$, $L/R = 10$, $pR/Ct = 1.5$)

[2]The parameter g is a shear correction factor (Taber, 1987b).

Downloaded 03 May 2010 to 171.66.16.21. Redistribution subject to ASME license or copyright; see http://www.asme.org/terms/Terms_Use.cfm

deformation allows the shell profile to approach that of a membrane.

Experimental Study

Strain-Energy Density Function. The three-dimensional strain-energy density formulation of particular interest in this report is

$$W = C[(I_1 - 3) + \alpha(I_2 - 3)^b] \tag{16}$$

which, being a specialization of the form deduced experimentally by Rivlin and Saunders (1951), was used by Fulton and Simmonds (1986) in studies of annular membranes subjected to vertical edge loads. Equation (16), in which C, α, and b are material constants, contains the neo-Hookean ($\alpha = 0$) and Mooney-Rivlin ($b = 1$) forms as special cases. The first two strain invariants are

$$I_1 = \Lambda_\Phi^2 + \Lambda_\theta^2 + 1/\Lambda_\Phi^2\Lambda_\theta^2 + \Gamma^2/\Lambda_\Phi^2$$
$$I_2 = \Lambda_\Phi^2\Lambda_\theta^2 + 1/\Lambda_\Phi^2 + 1/\Lambda_\theta^2 + \Gamma^2/\Lambda_\theta^2/\Lambda_\Phi^2, \tag{17}$$

with Λ_Φ and Λ_θ being stretch ratios and Γ the transverse shear strain in the shell.

We note, however, that the Rivlin-Saunders (1951) type of strain-energy function, involving a linear dependence on I_1 and a general nonlinear dependence on I_2, was originally postulated for strain invariant values greater than about five. Experimental inaccuracies associated with the evaluation of gradients in strain energy with respect to the invariants (i.e., $\partial W/\partial I_i$) may preclude the application of this form to the realm of small to moderate strain ($\Lambda < 1.5$), which is the range of interest in the current study. To circumvent these errors, Wineman et al. (1979), and Haines and Wilson (1979) have suggested alternative schemes for determining the functional form of W for rubberlike materials. These researchers employed design optimization techniques to determine the appropriate strain-energy function for rubber and soft biological tissues.

Wineman et al. (1979) suggested fitting the deflection contours of inflated circular membranes to those predicted from piecewise continuous strain-energy formulations. The functions for W would be applicable only over specified strain invariant intervals, with the forms determined from the functional variation of the strain energy with respect to a given strain invariant. With $\partial W/\partial I_1$ and $\partial W/\partial I_2$ regarded as "surfaces" over the admissible domain of I_1 and I_2, global optimization of all piecewise constitutive forms is achieved by minimizing the sum of the squares of the disparity between experimental and calculated deflection contours.

Haines and Wilson (1979) investigated a direct optimization of various polynomial expressions of the Rivlin type to a strain-energy "surface" formed by directly plotting experimentally obtained values of W versus I_1 and I_2. The surface was bounded by I_1-I_2 paths determined by simple extension and equibiaxial extension tests, with pure shear experiments falling on a path between these extremes. Material constants were determined through a least-squares fit to the "W-surface" such that the pointwise disparity between analytical and experimental strain energy values was minimized. The technique matched six-term power series in the strain invariants to experimental data (Treloar, 1944; Jones and Treloar, 1975), and subsequent prediction of stresses from the constitutive relations gave excellent correlation with experiment.

In spite of the potential pitfalls of using equation (16) for the realm of moderately large strain considered in our cylinder-inflation experiments, we chose W in this form for mathematical simplicity. Simple extension tests were conducted on silicone rubber samples to determine the appropriate material constants over the range of interest. The proposed strain-energy formulation (16) was fit to the experimental strain-energy data according to the methodology of Haines and Wilson (1979), with further refinement based on predicted cylindrical membrane behavior at high pressurization levels, similar to the procedure of Wineman et al. (1979).

Equation (16) was fit to the experimental strain-energy data by minimizing the objective function

$$F = \sum_{i=1}^{m} \{ W_i - C[(I_1 - 3)_i + \alpha(I_2 - 3)_i^b]^2 \} \tag{18}$$

with respect to the material parameters (C, α, b), where m is the total number of experimental data points (I_1, I_2, W) used. The sole use of tensile test data, however, does not give unique values for the unknown constants. Thus, cylinder profile data at a high level of inflation ($pR/Ct = 1.4$) was used to obtain unique values of the material parameters. Such an approach was plausible, based on the work of Wineman et al. (1979) and verification tests performed by Haines and Wilson (1979).

Experimental Methodology. Test specimens were formed of silicone rubber (General Electric RTV 615) based on considerations of handling ease and cost effectiveness of this material. Bulk quantities of the material were mixed according to the recommendations of the manufacturer, vacuum degassed for 20 minutes under 725 mm mercury, and injected by hand into molds to form flat sheets or cylindrical shells of uniform thickness. The injection process utilized 50 cc plastic syringes fitted to #8 French urethral catheters. The molds were fashioned from machined pieces of stock aluminum to produce sheet or cylindrical specimens of 3 mm uniform thickness. Subsequent to the injection process, degassing was repeated to insure that air-bubble inclusions would be minimized in the cured samples. Curing was performed in a standard laboratory oven at 100 deg C for one hour, followed by ambient air cooling to room temperature. Specimen removal from the mold was aided by coating all interior mold surfaces with a thin film of petroleum jelly prior to mold assembly and rubber injection. In addition, specimen removal was aided by subsequent refrigeration, which took advantage of the difference in thermal expansion coefficients between the mold and specimen material.

Tensile test specimens, cut from the molded sheet with a cutting tool fashioned to ASTM D 412 specifications, possessed nominal gage length and width measurements of 50 mm and 6 mm, respectively. Loading of the tensile test specimens was performed on an Instron Model 1125 Universal Testing Instrument, with each specimen preconditioned to a nominal peak extension ratio of 2.5 at an extension rate of 20 mm/minute. Each sample was allowed to recover for at least ten minutes between successive preconditioning cycles, and any gage length adjustments required to accommodate grip seating were performed prior to the succeeding cycle.

Cylinder-inflation experiments (Fig. (1*b*)) employed rigid aluminum end caps to invoke clamped end conditions while providing an axial degree of freedom for cylinder deformation at all inflation pressures. The caps were precision machined to fit inside the rubber cylinders, and positive sealing was insured through the use of standard automotive hose clamps. Clamping distortion, which may influence deflection near the edge of the shell, was circumvented by placing the hose clamps above the protruding portion of the end cap and by the addition of precision-machined aluminum retaining rings which slipped over the rubber shell and aligned with the projecting edge of the end cap. Each end cap was drilled and tapped to allow inflation from a regulated dry-nitrogen pressure bottle through 3 mm copper tubing. Inflation pressure was measured by a transducer (Omega Engineering PX303-050GSV) mounted in-line. Nominal cylinder radius-to-thickness (R/t) and length-to-

Downloaded 03 May 2010 to 171.66.16.21. Redistribution subject to ASME license or copyright; see http://www.asme.org/terms/Terms_Use.cfm

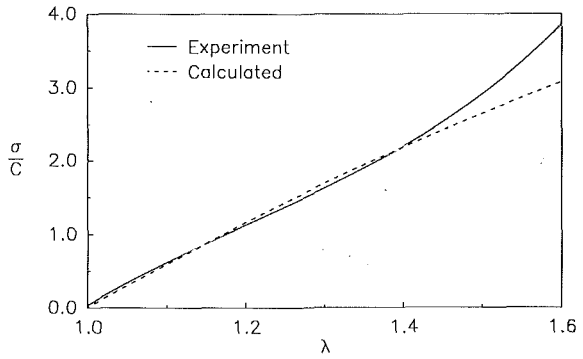


Fig. 3 Tensile test stress versus stretch ratio curves

radius (L/R) ratios of 8.5 and 5.7, respectively, were employed, and preconditioning was performed to a peak inflation pressure of 93 kPa.

Deformation characteristics of the loaded tensile and cylinder specimens were recorded on video tape. Specific geometric points on each specimen were identified through the use of an inked stamp prior to loading, while output of the respective load cell or pressure transducer was displayed on a digital voltmeter located within the field of vision of the video camera. Deformed geometry and load data were digitized during playback through use of a Video Caliper (Vista Electronics, La Mesa, California), which allowed for distortion-free geometric measurement within a frozen video image.

Comparison of Numerical and Experimental Results. Based on the tensile test data from the silicone rubber samples, the least-squares minimization scheme outlined above suggested the following range for the strain-energy coefficients: C = 300–370 kPa, α = 0.2–0.4, and b = 1.5–4.5. Subsequently, considerations of the deformed cylinder geometry at a high inflation pressure (pR/Ct = 1.4) produced the unique parameter values C = 340 kPa, α = 0.4, and b = 1.5 under the assumption that membrane behavior dominates sufficiently far from the edge. Calculation of the tensile test stress-strain curve from equation (16) using these numbers (Fig. 3) indicates good agreement with experiment up to $\lambda \cong 1.4$, which is a value larger than the maximum stretch ratio in the cylinder-inflation tests examined here.

Computed and measured deformed cylinder profile data are depicted in Fig. 4, where u is the radial displacement and y is the deformed axial location from the clamped boundary. For pR/Ct = 1, the data show that, near the edge, the solution for the shell with shear deformation (g = 1.2) is significantly more accurate than either the membrane solution or the solution based on shell theory without shear deformation (g = 0). The enhanced accuracy of shear deformable shell calculations is also seen at the higher pressurization level (pR/Ct = 1.4). However, at this load, it is the membrane solution that shows the closest agreement to the experimental profile data, especially near the shell edge. This observation supports the assumption used to determine the material constants but appears contrary to the fact that we are dealing with a rather thick 'shell'.

That the inclusion of bending stiffness actually produces worse agreement in the edge boundary layer for pR/Ct = 1.4 suggests at least two possibilities: (1) inside surface slippage of the silicone rubber cylinder from the clamping mechanism; and (2) at large strain, the shear correction factor g is larger than the small-strain value of 1.2. With regard to the first possibility, while the hose clamps maintained positive cylinder sealing throughout the inflation tests, the possibility of slippage at the retaining rings could not be ruled out. With regard to the second possibility, a larger value for g would lead to the

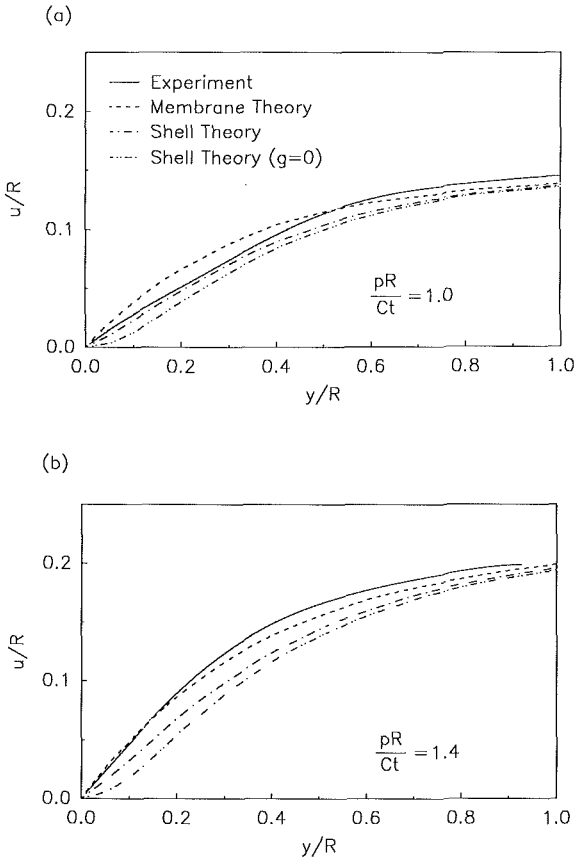


Fig. 4 Comparison of numerical and experimental deflection profiles near clamped edge of cylinder at two pressure levels (R/t = 8.5, L/R = 5.7; u: radial displacement, y: deformed axial coordinate)

transition from shell-like to membranelike behavior, as described in Taber (1987b), at a lower pressure. Further investigation of this discrepancy is left to future study.

Acknowledgment

This work was supported by the National Science Foundation under grant No. MSM-8611490. The authors would like to thank David Murphy, an undergraduate student at the University of Rochester, and David Hathaway and Robert Aman of the RIT Engineering Model Shop for their assistance in machining the various molds and fixtures used to conduct the experiments.

References

Cagan, J., and Taber, L. A., 1986, "Large Deflection Stability of Spherical Shells with Ring Loads," ASME JOURNAL OF APPLIED MECHANICS, Vol. 53, pp. 897–901.

Fulton, J. P., and Simmonds, J. G., 1986, "Large Deformations Under Vertical Edge Loads of Annular Membranes with Various Strain Energy Densities," *International Journal of Non-Linear Mechanics*, Vol. 21, pp. 257–267.

Haines, D. W., and Wilson, W. D., 1979, "Strain-Energy Density Function for Rubber-Like Materials," *Journal of Mechanics and Physics of Solids*, Vol. 27, pp. 345–360.

Hunter, W. F., 1970, "Integrating Matrix Method for Determining the Natural Vibration Characteristics of Propeller Blades," NASA TN D-6604.

Jones, D. F., and Treloar, L. R. G., 1975, 'The Properties of Rubber in Pure Homogeneous Strain," *Journal of Physics and Applied Physics*, Vol. 8, pp. 1285–1304.

Parnell, T. K., 1984, "Numerical Improvement of Asymptotic Solutions and Nonlinear Shell Analysis," Ph.D. Thesis, Stanford University.

Reissner, E., 1969, "On Finite Symmetrical Deflections of Thin Shells of Revolution," ASME JOURNAL OF APPLIED MECHANICS, Vol. 36, pp. 267–270.

Downloaded 03 May 2010 to 171.66.16.21. Redistribution subject to ASME license or copyright; see http://www.asme.org/terms/Terms_Use.cfm

Reissner, E., 1972, "On Finite Symmetrical Strain in Thin Shells of Revolution," ASME JOURNAL OF APPLIED MECHANICS, Vol. 39, pp. 1137–1138.

Rivlin, R. S., and Saunders, D. W., 1951, "Large Elastic Deformations of Isotropic Materials VII. Experiments on the Deformation of Rubber," *Philosophical Transactions of the Royal Society of London, Series A*, Vol. 243, pp. 251–288.

Simmonds, J. G., 1986, "The Strain-Energy Density of Rubber-Like Shells of Revolution Undergoing Torsionless, Axisymmetric Deformation (Axishells)," ASME JOURNAL OF APPLIED MECHANICS, Vol. 53, pp. 593–596.

Taber, L. A., 1987a, "On Boundary Layers in a Pressurized Mooney Cylinder," ASME JOURNAL OF APPLIED MECHANICS, Vol. 54, pp. 280–286.

Taber, L. A., 1987b, "Large Elastic Deformation of Shear Deformable Shells of Revolution: Theory and Analysis," ASME JOURNAL OF APPLIED MECHANICS, Vol. 54, pp. 578–584.

Treloar, L. R. G., 1944, "Stress-Strain Data for Vulcanized Rubber Under Various Types of Deformation," *Transactions of the Faraday Society*, Vol. 40, pp. 59–70.

Vakhitov, M. B., 1966, "Integrating Matrices As a Means of Numerical Solution of Differential Equations in Structural Mechanics," *Izvestiya VUZ Aviatsionnaya Tekhnika*, Vol. 9, pp. 50–61, (English: *Soviet Aeronautics*, Vol. 9, pp. 27–33.

Wineman, A., Wilson, D., and Melvin, J. W., 1979, "Material Identification of Soft Tissue Using Membrane Inflation," *Journal of Biomechanics*, Vol. 12, pp. 841–850.

Downloaded 03 May 2010 to 171.66.16.21. Redistribution subject to ASME license or copyright; see http://www.asme.org/terms/Terms_Use.cfm

Izhak Sheinman
Associate Professor,
Faculty of Civil Engineering,
Technion–Israel Institute of Technology,
Haifa, Israel 32000

Yeoshua Frostig
Research Engineer,
Israel Aircraft Industries,
Engineering Division

Post-Buckling Analysis of Stiffened Laminated Panel

An analytical-numerical procedure is applied to investigate the post-buckling behavior of a composite laminated stiffened panel. The panel is modeled by plate elements for which the nonlinear equations are derived (via a variational principle) in terms of the lateral displacement and Airy stress function, and treated by resolving the variables into eigenfunctions in conjunction with a finite-difference scheme.

I Introduction

Stiffened laminated composite panels are acquiring widespread use in aerospace and other technical applications. Knowledge of the bifurcation buckling load and insight into the post-buckling behavior are essential for reliable lightweight structural design.

Generally, structures under buckling can be characterized either by the bifurcation point or by the limit point, in which case the entire nonlinear behavior must be known. Straight stiffened panels fall under the first category, but even the nonlinear buckling curves are essential, as the overall load carrying capacity exceeds the buckling load of the skin and the post-buckling behavior should be considered in determining the interaction between the skin and the stiffeners.

Extensive research on buckling and post-buckling behavior of many kinds of structures is reported in the open literature. A fairly extensive review on laminated plates and shells given by Leissa (1985) indicates that most of this research was confined to unstiffened panels (see, for example, Chan, 1978; Zhang and Matthews, 1983 and 1985). The few works devoted to stiffened systems concern either isotropic panels (e.g., Hui et al., 1981; Tvergaard, 1973), or laminated panels with the stiffeners treated as beam elements (Venkatesh, 1983), or in the linear classical buckling load of laminated panels (Williams and Stein, 1976), or, finally, a symmetric stacking sequence with a specific type of stiffener (Dickson et al., 1980).

Williams and Stein (1976) report some experimental studies of the bifurcation buckling load, and the post-buckling behavior of stiffened laminated panels is likewise experimentally treated by Argarwal (1982), Bauld and Khot (1987) and Starness et al. (1985). Comparison with analytical results has been made with the aid of general purpose finite element codes such as STAGS (Almroth and Brogan, 1980), which seems inappropriate when parametric studies, or preliminary design, is of concern.

The present study is an attempt to provide a suitable tool for the analysis of arbitrary stiffened laminated panels, modeled by plate elements. By extending these elements to the stiffeners in addition to the skin, the local buckling response as well as the overall response can be obtained. The nonlinear equilibrium equations, the boundary conditions, and the continuity conditions for the stiffener attachment points are derived via a variational principle in terms of the displacement function $w(x,y)$ and the Airy stress function $F(x,y)$. The resulting nonlinear partial differential equations are replaced by resolving the two functions into eigenfunctions in the longitudinal direction and applying a finite-difference scheme in the transverse direction. Galerkin analysis is used with a view to minimum error in the truncation process. Then, by means of Newton's method, the nonlinear set is converted into a linear sequence. The outlined procedure is illustrated for the cases of an unstiffened and a stiffened panel.

II Analytical Formulation

Kinematics. Consider a composite plate consisting of homogeneous orthotropic layers of arbitrary orientations with total thickness t. Let (x,y) be the plate coordinates of the reference surface and z the normal coordinate (Fig. 1). For span-to-thickness ratios exceeding 12, the Kirchhoff-Love hypothesis can be used as the basic assumption (see Sheinman and Adan, 1987), thus, leaving three dependent variables, namely the displacements in the x, y, and normal directions–u, v and w, respectively. The kinematic relations for a plate element are:

$$\begin{aligned} U(x,y,z) &= u(x,y) - zw'(x,y) \\ V(x,y,z) &= v(x,y) - z\dot{w}(x,y) \\ W(x,y,z) &= w(x,y) \end{aligned} \tag{1}$$

where $(\,)'$ and $(\dot{})$ denote derivatives with respect to the x- and y-coordinates, respectively.

Resorting to the von Karman nonlinear kinematic equations for a geometrically imperfect $(w^\circ(x,y))$ plate, the strain-displacement relation can be written as:

$$\{\epsilon\} = \{\bar{\epsilon}\} + z\{\chi\} \tag{2}$$

where

Contributed by the Applied Mechanics Division for publication in the JOURNAL OF APPLIED MECHANICS.
Discussion on this paper should be addressed to the Editorial Department, ASME, United Engineering Center, 345 East 47th Street, New York, NY 10017, and will be accepted until two months after final publication of the paper itself in the JOURNAL OF APPLIED MECHANICS. Manuscript received by ASME Applied Mechanics Division, July 20, 1987; final revision, November 30, 1987.

Copyright © 1988 by ASME
Downloaded 03 May 2010 to 171.66.16.21. Redistribution subject to ASME license or copyright; see http://www.asme.org/terms/Terms_Use.cfm

$$\{\bar{\epsilon}\} = \begin{Bmatrix} \bar{\epsilon}_{xx} \\ \bar{\epsilon}_{yy} \\ \bar{\gamma}_{xy} \end{Bmatrix} = \begin{Bmatrix} u' + \tfrac{1}{2}w'(w' + 2w^{\circ\prime}) \\ \dot{v} + \tfrac{1}{2}\dot{w}(\dot{w} + 2\dot{w}^{\circ}) \\ \dot{u} + v' + \tfrac{1}{2}w'(\dot{w} + 2\dot{w}^{\circ}) + \tfrac{1}{2}\dot{w}(w' + 2w^{\circ\prime}) \end{Bmatrix} \tag{3}$$

and

$$\{\chi\}^T = \{\chi_{xx}, \chi_{yy}, 2\chi_{xy}\} = \{-w'', -\ddot{w}, -2\dot{w}'\} \tag{4}$$

Constitutive Relations. Under the classical laminate theory, the stress-strain relation for the plate element is

$$\begin{Bmatrix} N \\ M \end{Bmatrix} = \begin{bmatrix} A & B \\ B & D \end{bmatrix} \begin{Bmatrix} \bar{\epsilon} \\ \chi \end{Bmatrix} \tag{5}$$

where $\{N\}^T = \{N_{xx}, N_{yy}, N_{xy}\}^T$ is the membrane force vector, $\{M\}^T = \{M_{xx}, M_{yy}, M_{xy}\}^T$ is the bending moment vector, and the coefficients of the elastic matrix are given by

$$(A_{ij}, B_{ij}, D_{ij}) = \int_z Q_{ij}(1, z, z^2)dz \tag{6}$$

A_{ij}, B_{ij}, and D_{ij}, being respectively the membrane, coupling and flexural rigidities which are generally functions of x and y, and Q_{ij} are the laminae transformed reduced stiffnesses.

Equilibrium and Boundary Conditions. The variational principle of the plate element can be formulated as

$$\delta\pi_p = \delta\pi_A + \delta\pi_x + \delta\pi_y = 0 \tag{7}$$

where

$$\delta\pi_A = -\int_A \{(N'_{xx} + \dot{N}_{xy})\delta u + (\dot{N}_{yy} + N'_{xy})\delta v + (M''_{xx} + 2\dot{M}'_{xy} + \ddot{M}_{yy} + N_{xx}(w'' + w^{\circ\prime\prime}) + N_{yy}(\ddot{w} + \ddot{w}^{\circ}) + 2N_{xy}(\dot{w}' + \dot{w}^{\circ\prime}))\delta w\}dA$$

$$\delta\pi_x = -\int_x \{(N_{xy}\delta u + N_{yy}\delta v + (N_{yy}(\dot{w} + \dot{w}^{\circ}) + N_{xy}(w' + w^{\circ\prime}) + \dot{M}_{yy} + M'_{xy})\delta w - M_{yy}\delta\dot{w} - M_{xy}\delta w'\}dx \tag{8}$$

$$\delta\pi_y = \int_y \{(N_{xx}\delta u + N_{xy}\delta v + (N_{xx}(w' + w^{\circ\prime}) + N_{xy}(\dot{w} + \dot{w}^{\circ}) \perp M'_{xx} + \dot{M}'_{xy})\delta w - M_{xx}\delta w' - M_{xy}\delta\dot{w}\}dy$$

The equilibrium equations are derived by setting $\delta\pi_A = 0$, the boundary conditions at the y-edges by setting $\delta\pi_x = 0$ and at the x-edges by $\delta\pi_y = 0$.

Continuity Requirements. The continuity requirements, assuming rigid connections, are derived for four stiffener versions, IND = 1,2,3, and 4, as illustrated in Fig 2.

The requirements regarding the displacements are:

For IND = 1

$$u^{(1)} = u^{(2)};\ u^{(1)} = u^{(3)};\ v^{(1)} = v^{(2)};\ v^{(1)} = w^{(3)};$$
$$w^{(1)} = w^{(2)};\ w^{(1)} = -v^{(3)};\ \dot{w}^{(1)} = \dot{w}^{(2)};\ \dot{w}^{(1)} = \dot{w}^{(3)}$$

For IND = 2

$$u^{(1)} = u^{(3)};\ v^{(1)} = w^{(3)};\ w^{(1)} = -v^{(3)};\ \dot{w}^{(1)} = \dot{w}^{(3)} \tag{9}$$

For IND = 3

$$u^{(2)} = u^{(3)};\ v^{(2)} = w^{(3)};\ w^{(2)} = -v^{(3)};\ \dot{w}^{(2)} = \dot{w}^{(3)}$$

and for IND = 4

$$u^{(1)} = u^{(2)};\ v^{(1)} = v^{(2)};\ w^{(1)} = w^{(2)};\ \dot{w}^{(1)} = \dot{w}^{(2)},$$

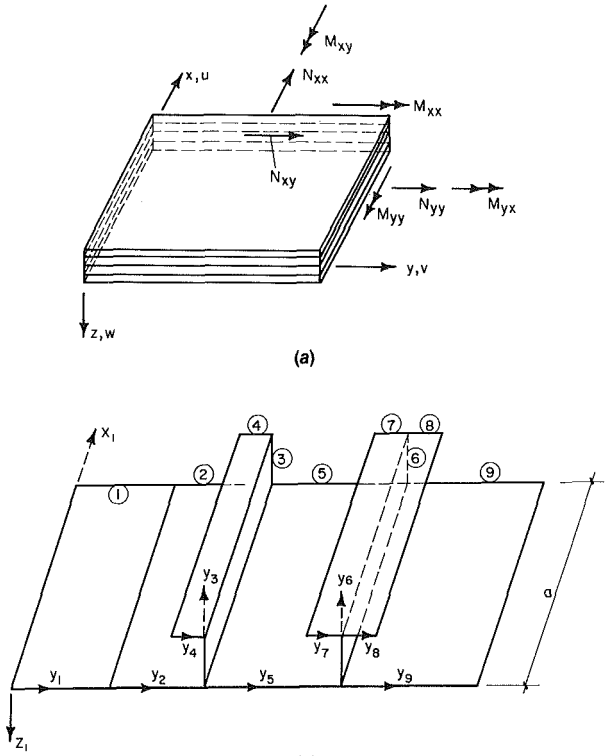


Fig. 1 Sign convention; (*a*) Single plate element; (*b*) Typical stiffened panel

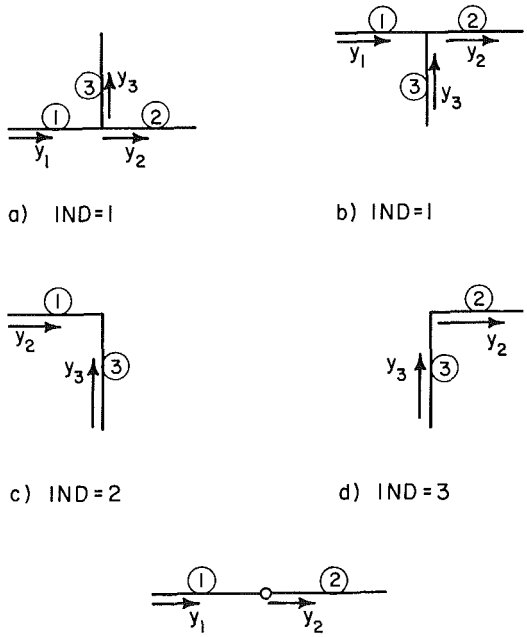


Fig. 2 Stiffener coordinate system

the superscript indicating the plate number refers to the stiffener attachment point.

The requirements regarding the forces are formulated below only for IND = 1; those for the other variates follow from the former by suitable application of the superscripts. The relevant variational principle reads (see Sheinman, 1987b).

Downloaded 03 May 2010 to 171.66.16.21. Redistribution subject to ASME license or copyright; see http://www.asme.org/terms/Terms_Use.cfm

$$\delta\pi_x^{(1)} + \delta\pi_x^{(2)} + \delta\pi_x^{(3)} = 0 \tag{10}$$

where $\delta\pi_x$ is as for equation (8) and the superscript is as above. Accordingly, the requirements read explicitly as:

$$N_{xy}^{(1)} - N_{xy}^{(2)} - \delta N_{xy}^{(3)} = 0 \tag{11}$$

$$N_{yy}^{(1)} - N_{yy}^{(2)} - \delta\{\dot{M}_{yy}^{(3)} + 2M'^{(3)}_{xy} + N_{yy}^{(3)}(\dot{w}^{(3)} + \dot{w}^{\circ(3)}) + N_{xy}^{(3)}(w'^{(3)} + w^{\circ\prime(3)})\} = 0$$

$$\dot{M}_{yy}^{(1)} - \dot{M}_{yy}^{(2)} + 2M'^{(1)}_{xy} - 2M'^{(2)}_{xy} + \delta N_{yy}^{(3)} + N_{yy}^{(1)}(\dot{w}^{(1)} + \dot{w}^{\circ(1)}) + N_{xy}^{(1)}(w'^{(1)} + w^{\circ\prime(1)}) - N_{yy}^{(2)}(\dot{w}^{(2)} + \dot{w}^{\circ(2)}) - N_{xy}^{(2)}(w'^{(2)} + w^{\circ\prime(2)}) = 0$$

$$M_{yy}^{(2)} - M_{yy}^{(1)} + \delta M_{yy}^{(3)} = 0$$

where $\delta = 1$ for the case in Fig. 2(*a*) and $\delta = -1$ for that in Fig. 2(*b*).

Airy Stress Function. The Airy stress function $F(x,y)$ is introduced as $N_{xx} = \ddot{F}$; $N_{yy} = F''$ and $N_{xy} = -\dot{F}'$, thus, the in-plane two equilibrium equations are identically satisfied. At this juncture the usual procedure is to obtain the compatibility equation and express it, as well as the out of plane equilibrium equation, the boundary conditions, and the continuity equations (equations (9), (11)), in terms of $w(x,y)$ and $F(x,y)$. For this purpose, the strain $\{\bar{\epsilon}\}$ and moment $\{\mathbf{M}\}$ vectors should first be expressed in these terms.

Equation (5) yields the following expressions:

$$\{\bar{\epsilon}\} = [a]\{F\} - [b]\{\chi\}; \quad \{\mathbf{M}\} = [b]^T\{F\} + [d]\{\chi\} \tag{12}$$

where

$$\{F\}^T = \{\ddot{F},\ F'',\ -\dot{F}'\}$$

$$[a] = [A]^{-1} \text{ (symmetric)}$$

$$[b] = [a][B] \text{ (not necessarily symmetric)} \tag{13}$$

$$[d] = [D] - [B][b] \text{ (symmetric)}$$

The inplane compatibility equation reads

$$\ddot{\bar{\epsilon}}_{xx} + \bar{\epsilon}''_{yy} - \dot{\bar{\gamma}}'_{xy} = \dot{w}'(\dot{w}' + 2\dot{w}^{\circ\prime}) - 1/2w''(\ddot{w} + 2\ddot{w}^{\circ}) - 1/2\ddot{w}(w'' + 2w^{\circ\prime\prime}). \tag{14}$$

Substitution of equation (12) in the equilibrium equation and the compatibility equation yields:

Equilibrium

$$L_h(w) + L_q(F) + L(F, w + w^{\circ}) = 0 \tag{15}$$

Compatibility

$$L_q(w) + L_g(F) + 1/2L(w, w + 2w^{\circ}) = 0$$

where L and L_p are differential operators defined as:

$$L(S,T) = S''\ddot{T} - 2\dot{S}'\dot{T}' \perp \ddot{S}T'' \tag{16}$$

$$L_p(S) = p_{40}S'''' + p_{31}\dot{S}''' + p_{22}\ddot{S}'' + p_{13}\dddot{S}' + p_{04}\ddddot{S}$$

with $p = h,g,q$;

$h_{40} = -d_{11}$	$g_{40} = a_{22}$	$q_{40} = b_{21}$
$h_{31} = -4d_{13}$	$g_{31} = -2a_{23}$	$q_{31} = -b_{31} + 2b_{23}$
$h_{22} = -2d_{12} - 4d_{33}$	$g_{22} = 2a_{12} + a_{33}$	$q_{22} = b_{11} + b_{22} - 2b_{33}$
$h_{13} = -4d_{32}$	$g_{13} = -2a_{13}$	$q_{13} = 2b_{13} - b_{32}$
$h_{04} = -d_{22}$	$g_{04} = a_{11}$	$q_{04} = b_{12}$

The displacements, u and v, in the boundary conditions as well as in the continuity requirements (equations (9), (11)), were eliminated by a procedure following Sheinman and Simitses (1977).

The advantage of the Airy stress function lies mainly in reducing the unknown functions from three (u, v, and w) to two (w and F). On the other hand, the conditions on u and v (equations (9)) are replaced by conditions on their derivatives, so that a condition like $u = 0$ or $v = 0$, as in the case where the stiffener is clamped, cannot be satisfied.

III Solution Procedure

The set of partial differential equations is first reduced to one of ordinary differential equations by separation of variables using:

$$w(x,y) = \sum_m^{NW} w_m(y)g_m(x)$$

$$F(x,y) = \sum_n^{NF} f_n(y)X_n(x) - \iint \bar{N}_{xx}(y)dydy + \bar{N}_{xy}xy \tag{17}$$

$$w^{\circ}(x,y) = \sum_m^{NW} w_m^{\circ}(y)g_m(x)$$

NW and NF being the number of retained terms in the truncated series of w and F functions, respectively.

The functions $g_m(x)$ are chosen as the natural modes of an isotropic beam which satisfy the boundary conditions imposed upon the transverse deflection w. Inplane equilibrium is satisfied only if $X_n(x)$ is chosen to be a natural mode of an isotropic clamped beam. For the clamped case with $g_n(x) = X_n(x)$ the mode functions are:

$$\phi_i(x) = \cosh\beta_i x - \cos\beta_i x - \gamma_i(\sinh\beta_i x - \sin\beta_i x) \tag{18}$$

where

$$\gamma_i = (\cosh\beta_i a - \cosh\beta_i a)/(\sinh\beta_i a - \sin\beta_i a) \tag{19}$$

β_i are the eigenvalues calculated from

$$1 - \cosh\beta_i a \cdot \cos\beta_i a = 0 \tag{20}$$

a being the length of the stiffened panel $w_m(y)$ and $f_n(y)$ are unknown functions of y to be replaced in a finite-difference scheme whereby the boundary conditions at the y-edges will be specified. $\bar{N}_{xx}(y)$ and $\bar{N}_{xy}$ are the applied external axial and shear loads; the former applied at the longitudinal edges may be a function of y while the latter should be constant.

Although they are applied at the boundaries, it is assumed that the initial internal forces are the same throughout the x, y-intervals, and subsequently corrected in the course of the iteration procedure by introducing w_m and f_n functions. The error is minimized by a Galerkin-type weighted residual method, the weighted functions being $g_p(x)$ and $X_p(x)$ dependent on the required boundary conditions at the x-edges. According to the procedure, the following Galerkin integrals must vanish:

For the equilibrium equations:

$$\int_o^a (\text{equilibrium equation})\, g_p(x)dx = 0 \tag{21}$$

$$p = 1,2, \ldots NW$$

For the compatibility equations:

$$\int_o^a (\text{compatibility equation})\, X_p(x)dx = 0 \tag{22}$$

$$p = 1,2, \ldots NF$$

For the continuity requirements, as well as for the boundary conditions at the y-edges, the integral should similarly vanish with $X_p(x)$ for the conditions on u and v, and with $g_p(x)$ for

Downloaded 03 May 2010 to 171.66.16.21. Redistribution subject to ASME license or copyright; see http://www.asme.org/terms/Terms_Use.cfm

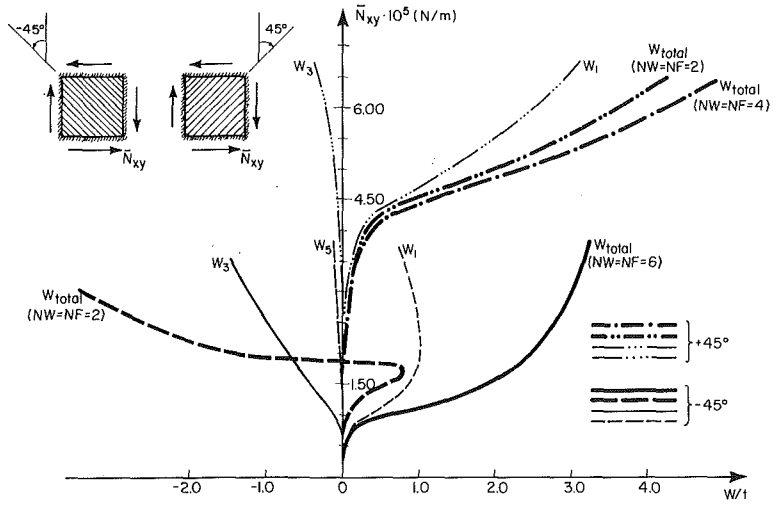


Fig. 3 Load-deflection curves for laminated plate under shear loading (at $x/a = 1/2$)

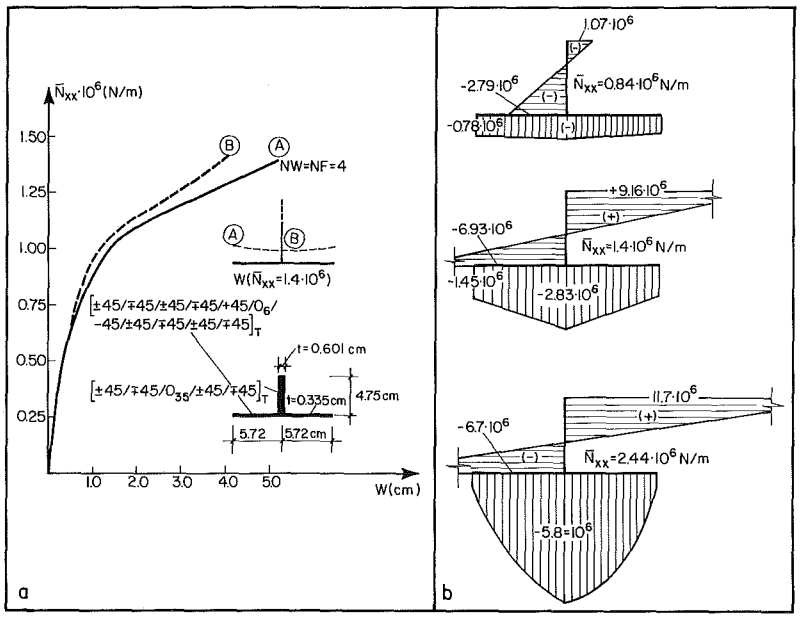


Fig. 4 Stiffened panel results at $x/a = 0.5$ with length $a = 0.75$m. (*a*) Load-deflection curves; (*b*) variation of internal axial force (N_{xx}) for some load levels ($\bar{N}_{xx}$)

the condition on w. For mixed requirements like $v^{(1)} = w^{(3)}$, either X_p or g_p may be taken.

The use of the above procedure ensures satisfaction of the continuity requirements in the global sense only. That numerical phenomenon usually occurs whenever integral methods are used. However, results achieved using that procedure compare well with those published in the open literature.

Next, the generalized Newton method (Thurston, 1965) is used to reduce the nonlinear field equations, continuity requirements and boundary conditions at the y-edges to a linear sequence. Finally, a central finite-difference scheme in the y-direction for the w_m and f_n functions with fictitious points is used to convert the ordinary differential equations into algebraic ones. The finite-difference interval may differ for each region (plate element).

IV Numerical Examples and Discussion

For the procedure outlined above, a general computer program PANEL was written, covering the nonlinear behavior of any stiffened laminated panel under external shear and axial loading. The boundary conditions for the x-edges are satisfied by using the appropriate eigenfunctions. For this stage, a special symbolic program using the REDUCE compiler (Hearn, 1985) was written for implementation of the Galerkin integral coefficients.

The boundary conditions at the y-edges may be arbitrary, determined by a special finite-difference algorithm. The solution methodology is demonstrated through two examples: (*a*) an unstiffened single plate under shear, using data from Zhang and Matthews (1983), and (*b*) a stiffened panel under axial load, using data from Williams and Stein (1976). While in the original references only the bifurcation point was considered, here the entire behavior is covered.

a) **Unstiffened Single Plate.** This example, which demonstrates the convergence procedure, concerns a clamped-clamped Boron/epoxy single laminated plate under external shear with data as follows: length $a = 0.25$m, width $b = 0.25$m, total thickness $t = 0.0025$m, ply thickness $t_{ply} = 0.000625$m,

Downloaded 03 May 2010 to 171.66.16.21. Redistribution subject to ASME license or copyright; see http://www.asme.org/terms/Terms_Use.cfm

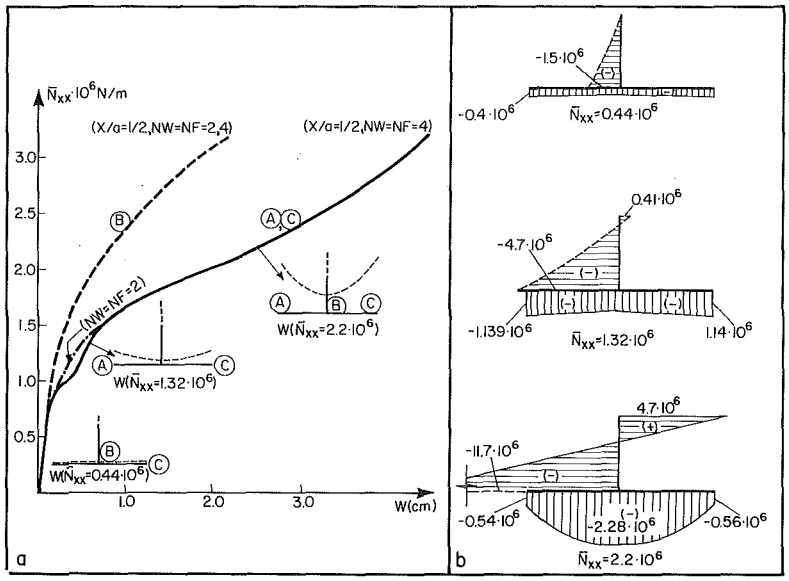


Fig. 5 Stiffened panel results at x/a = 0.5 with length a = 0.375m; (a) Load-deflection curves; (b) variation of internal axial force (N_{xx}) for some load levels ($\bar{N}_{xx}$)

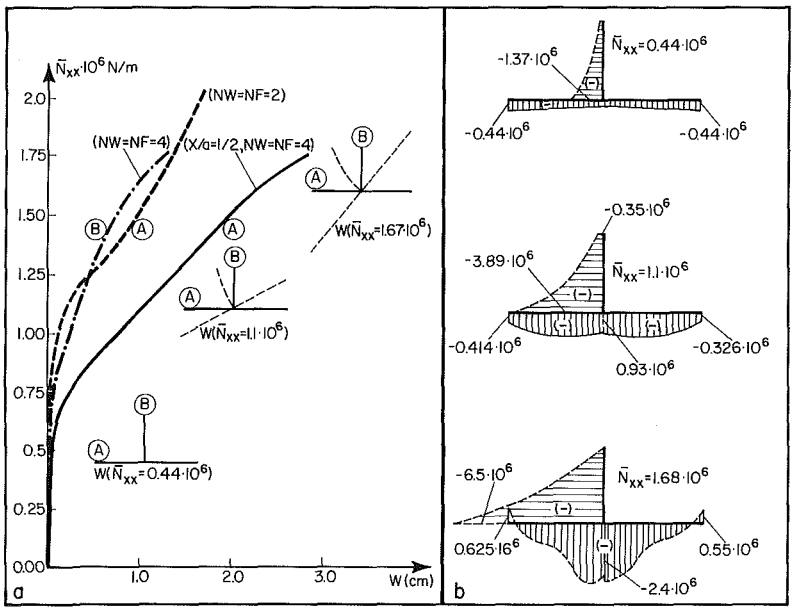


Fig. 6 Stiffened panel results at x/a = 0.5 with length a = 0.1875m; (a) Load-deflection curves; (b) variation of internal axial force (N_{xx}) for some load levels ($\bar{N}_{xx}$)

laminate with $E_{11}=2.069\cdot10^{11}N/m^2$, $E_{22}=0.207\cdot10^{11}N/m^2$, $G_{12}=0.052\cdot10^{11}N/m^2$, ($E_{11}/E_{22}=9.9951$, $G_{12}/E_{22}=0.2512$), $\nu_{12}=0.38$. The initial imperfection was taken as $w^\circ(y)=\delta\sin(\pi y/b)$ with $\delta=0.00025$m amplitude.

Two stacking combinations and orientations are examined: $[+45]_4$ and $[-45]_4$. In both cases there is no stretching-bending coupling ($B_{ij}=0$), but the shear coupling (A_{16}, A_{26}) and torsion coupling (D_{16}, D_{26}) are pronounced.

The load-deflection curves for the two stacking combinations are plotted in Fig. 3, which shows that for $+45^\circ$ orientation the solution converges with $NW=NF=2$, while for -45° there is convergence with $NW=NF=6$. This can be explained through the w_m function: for $+45^\circ$ w_1 is the dominant value, w_3 is relatively small, while for -45° w_1 and w_3 are of the same order. Although in the latter case convergence with $NW=NF=2$ is very poor, there is an indication of the appropriate bifurcation point, which is obtainable by finding the load level at which the determinant is minimum—namely $\bar{N}_{xy}=4.6.10^5N/m$ for $[+45]_4$ and at $\bar{N}_{xy}=0.88.10^5N/m$ for $[-45]_4$. The low bifurcation load with the $[-45^\circ]_4$ panel is due to the compression exerted on the epoxy matrix. These bifurcation points yield exactly the same buckling load reported by Zhang and Matthews (1983) (see Fig. 5 with $R=\infty$ there).

***b*) Stiffened Panel.** This example concerns a Graphite/epoxy open-section stiffened by a blade type, clamped at the x-edges and free at the y-edges, loaded in longitudinal compression. The data used: width of skin 2•5.72 cm (see Fig. 4), height of stiffener 4.75 cm, thickness of skin 0.335 cm, thickness of stiffener 0.60 cm, laminate with $E_{11}=1.31.10^{11}N/m^2$, $E_{22}=0.13\cdot10^{11}N/m^2$, $G_{12}=0.064\cdot10^{11}N/m^2$, ($E_{11}/E_{22}=10.0769$, $G_{12}/E_{22}=0.4923$), $\nu_{12}=0.38$, and ply thickness $t_{ply}=0.014$ cm.

Downloaded 03 May 2010 to 171.66.16.21. Redistribution subject to ASME license or copyright; see http://www.asme.org/terms/Terms_Use.cfm

The stacking combination and orientation are shown in Fig. 4. This stacking combination entails shear (A_{i6}), torsion (D_{i6}) and stretching-bending (B_{ij}) coupling for the skin, and only low torsion coupling for the stiffener. The initial imperfection (for the skin area) was taken as $w^*(y) = \delta = 0.0335$ cm (in the x-direction the imperfection coincides with the mode function). The example was run for a wide range of lengths a ($0.1875\text{m} \le a \le 1.5\text{m}$) in order to examine all possible buckling modes, and only part of the results are presented.

The load-deflection curves for $a = 0.75$, 0.375, and 0.1875 are plotted in Figs. 4, 5, and 6, respectively. The buckling modes are: for $a = 1.5$m as an Euler column; for $a = 0.75$m onset of crippling reflected in the difference of the load-deflection curves for points A and B in Fig. 4; for $a = 0.375$ crippling mode of the skin; for $a = 0.1875$ the twisting mode.

The variation of the internal axial force N_{xx} for different levels of the external applied load $\bar{N}_{xx}$ is also shown in Figs. 4, 5, and 6 for $a = 0.75$, 0.375, and 0.1875m, respectively.

V Conclusions

A nonlinear theory and a solution procedure are presented for stiffened laminated panels of arbitrary stacking combination and orientation. The nonlinear equations are written in terms of the displacements and the Airy stress function. The partial differential equations are reduced to algebraic ones by using Galerkin's method in the x-direction and the finite difference method in the y-direction. The chosen functions in the x-direction for the Galerkin procedure are taken as the eigenfunctions of an isotropic beam.

The theory and solution procedure are general and suitable for the post-buckling behavior of stiffened laminated panels. The procedure was applied for many stiffened and unstiffened panels under axial and shear loading. Of the principal findings, the following should be emphasized:

1 Use of Galerkin approach instead of the discretization method provides an extremely convenient procedure for analysis of stiffened panels.

2 Post-buckling curves covering local, twisting and overall buckling are obtainable by the procedure.

3 Reduction of the number of unknown functions from three (u,v,w) to two (w and F) saves considerable CPU computer time. On the other hand, the procedure is limited to external loads applied through the boundaries.

4 Only a finite number of terms in the w and F functions need to be used in the numerical solution.

5 Although the continuity requirements are satisfied globally rather than locally, because of the Galerkin procedure, it seems that the results are not affected by this.

Acknowledgments

This work is sponsored by Israel Aircraft Industries, Engineering Division. Special thanks are due to Dr. A. Segal. The financial support provided by I.A.I. is gratefully acknowledged. The authors are also indebted to Ing. E. Goldberg for editorial assistance.

References

Agarwal, B. L., 1982, "Post-Buckling Behavior of Composite Stiffened-Curved Panels Loaded in Compression," *Experimental Mechanics*, pp. 231–236.

Almroth, B. O., and Brogan, F. A., 1980, "The STAGS Computer Code," NASA CR-2950.

Bauld, Jr., N. R., and Khot, N. S., 1982, "A Numerical and Experimental Investigation of the Buckling Behavior of Composite Panels," *Computers & Structures*, Vol. 15, No. 4, pp. 393–403.

Chan, D. P., 1978, "An Analytical Study of the Post-Buckling of Laminated Anisotropic Plates," *Fibre Science and Technology*, Vol. 11, pp. 165–187.

Dickson, J. N., Cole, R. T., and Wang, J. T. S., 1980, "Design of Stiffened Composite Panels," *Fibre Composite in Structural Design*, pp. 313–327.

Giri, J., and Simitses, G. J., 1980, "Deflection Response of General Laminated Composite Plates to Inplane and Transverse Loads," *Fibre Science and Technology*, Vol. 13, pp. 225–242.

Hearn, A. C., 1985, "REDUCE-User's Manual," Version 3.2. The Rand Corporation, CP78, Santa Monica, Calif.

Hui, D., Tennyson, R. C., and Hansen, J. S., 1981, "Mode Interaction of Axially Stiffened Cylindrical Shells: Effect of Stringer Axial Stiffness, Torsional Rigidity and Eccentricity," ASME JOURNAL OF APPLIED MECHANICS, Vol. 48, pp. 915–922.

Leissa, A. W., 1985, "Buckling of Laminated Composite Plates and Shell Panels," AFWAL-TR-853069, AF Wright Aeronautical Lab.

Sheinman, I., and Simitses, G. J., 1977, "Buckling of Geometrically Imperfect Stiffened Cylinders Under Axial Compression," *AIAA Journal*, Vol. 15, pp. 374–382.

Sheinman, I., and Adan, M., 1987a, "The Effect of Shear Deformation on Post-Buckling Behavior of Laminated Beams," ASME JOURNAL OF APPLIED MECHANICS, Vol. 54, pp. 558–562.

Sheinman, I., 1987b, "Nonlinear Equations of Laminated Panels With Laminated Stiffeners," *Composite Structures*, Vol. 8, pp. 287–292.

Starnes, Jr., J. H., Knight, Jr., N. F., and Rouse, M., 1985, "Post-Buckling Behavior of Selected Flat Stiffened Graphite-Epoxy Panels Loaded in Compression," *AIAA Journal*, Vol. 23, No. 8, pp. 1236–1246.

Thurston, G. A., 1965, "Newton's Method Applied to Problems in Nonlinear Mechanics," ASME JOURNAL OF APPLIED MECHANICS, Vol. 87, pp. 383–388.

Tvergaard, V., 1973, "Imperfection-Sensitivity of a Wide Integrally Stiffened Panel Under Compression," *Int. J. Solids Structures*, Vol. 9, pp. 177–192.

Venkatesh, A., and Rao, K. P., 1983, "Analysis of Laminated Shells With Laminated Stiffeners Using Rectangular Shell Finite Elements," *Computer Methods in Applied Mechanics and Engineering*, Vol. 88, pp. 255–272.

Williams, J. G., and Stein, M., 1976, "Buckling Behavior and Structural Efficiency of Open-Section Stiffened Composite Compression Panels," *AIAA Journal*, Vol. 14, No. 11, pp. 1618–1626.

Zhang, Y., and Mattews, F. L., 1983, "Initial Buckling of Curved Panels of Generally Layered Composite Materials," *Composite Structures*, Vol. 1, pp. 3–30.

Zhang, Y., and Matthews, F. L., 1985, "Large Deflection Behaviour of Simply Supported Laminated Panels Under Inplane Loading," ASME JOURNAL OF APPLIED MECHANICS, Vol. 52, pp. 553–558.

Downloaded 03 May 2010 to 171.66.16.21. Redistribution subject to ASME license or copyright; see http://www.asme.org/terms/Terms_Use.cfm

Damage Coupled With Heat Conduction in Uniaxially Reinforced Composites

Y. Weitsman
Professor.
Mechanics and Materials Center,
Civil Engineering Department,
Texas A&M University
College Station, Texas 77843
Mem. ASME

This paper presents a continuum damage model for a unidirectionally reinforced composite based upon fundamental concepts of continuum mechanics and irreversible thermodynamics. Damage is incorporated by two symmetric, second-rank, tensor-valued, internal state variables which represent the total areas of "active" and "passive" cracks contained within a representative material volume element. Constitutive relations are derived for both the mechanical response and heat flux in the presence of damage. It is shown that damage growth contributes to dissipation in the coupled heat conduction process. A specific fracture mechanics solution is employed to relate "microlevel" crack growth processes to "macrolevel" damage growth expressions. This approach lends itself to a probabilistic formulation of the continuum damage model.

1 Introduction

Continuum damage modelling, initiated by Kachanov (1958), has become a very active research area in the last decade. A comprehensive review of the subject was given recently by Krajcinovic (1986). Another extensive review was provided by Bazant (1986), where emphasis was placed on applications to concrete. Therefore, a detailed listing of the important contributions to the subject, made by many distinguished investigators, will be omitted herein.

Applications of continuum damage concepts to composites were provided by Talreja (1985 a,b), Allen et al. (1985 a,b, and 1987) and Weitsman (1987 a,b). In those works, "damage" was introduced as an internal state variable which was vector valued (Talreja), second-rank asymmetric tensor (Allen), or a skew-symmetric tensor (Weitsman). All the above works emphasized damage effects on compliances, with the latter (Weitsman) including also interactions between damage and diffusion.

The present paper differs from most existing damage models in the choice of damage parameters. Specifically, damage is described by two symmetric second-rank tensors, which represent the total areas of "active" (open) and "passive" (closed) microcracks within a statistically representative volume of damaged material. The selection of symmetric second-rank tensors resembles the approach of Vakulenko and Kachanov (1971) and is akin to the choice made by Murakami and Ohno (1981), although the decisions of the latter authors were motivated by different physical and mathematical arguments. The incorporation of closed microcracks into the damage model is deemed important since significant dissipation can occur by friction at the surfaces of these "passive" flaws, an effect which should be included in the coupled heat conduction equation.

In addition, it is argued in this paper that damage growth relations are derivable from micromechanical considerations of crack growth. This argument is demonstrated by a specific, "microlevel", sample solution, although several important ingredients are still missing therein. The essential point here is that when damage is associated with flaw areas—as done in this paper—then damage growth relations can be correlated with concepts of fracture mechanics, and derived accordingly.

The effects of damage on material moduli can be investigated by methods other than those of continuum damage mechanics. Prominent among those other methods is the self consistent scheme as developed by Laws (1977, 1980), and Laws et al. (1983). In addition, these effects can be studied by variational approaches (Hashin, (1985) and Fang et al. (1986)). However, these methods do not address damage growth and, in the absence of a thermodynamic basis, cannot account for coupling with heat and diffusion.

2 The Representation of Damage

Consider a fiber-reinforced composite material containing a profusion of microcracks. By hypothesis, a continuum damage model applies when all geometric features of the material—which include fibers and microcracks—are distributed in a statistically homogeneous manner. Consequently, it is possible to select a representative volume element (RVE) of finite size, as shown in Fig. 1, whose response characterizes the behavior of the damaged composite.

A complete accounting for the response of the RVE requires recognition of all N microcracks contained therein, with due

Contributed by the Applied Mechanics Division for publication in the JOURNAL OF APPLIED MECHANICS.
Discussion on this paper should be addressed to the Editorial Department, ASME, United Engineering Center, 345 East 47th Street, New York, N.Y. 10017, and will be accepted until two months after final publication of the paper itself in the JOURNAL OF APPLIED MECHANICS. Manuscript received by ASME Applied Mechanics Division, June 12, 1987; final revision, January 29, 1988.

Copyright © 1988 by ASME
Downloaded 03 May 2010 to 171.66.16.21. Redistribution subject to ASME license or copyright; see http://www.asme.org/terms/Terms_Use.cfm

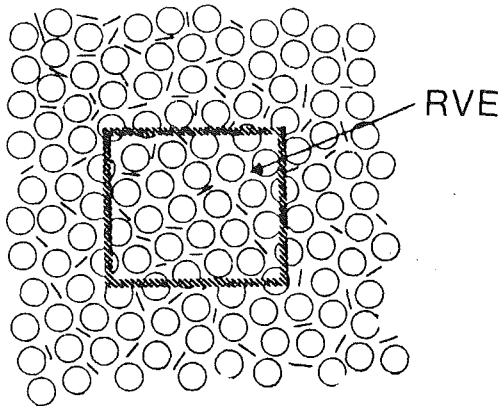


Fig. 1 A representative volume element for a fiber-reinforced composite with both active and passive microcracks

consideration for their interactions. This forbidding and intractable task is superfluous in many respects, because the locations of fibers, as well as the positions, sizes and shapes of the microflaws are at best known only in a statistical sense. Furthermore, the response of the material is sought only at the macrolevel. Consequently, several approximations will be undertaken in order to reduce the problem to a manageable size, yet retaining its essential features.

Inasmuch as the shapes of the cracks are unknown, they will be represented by equivalent *flat* flaws. Since each such flat flaw possesses both size and orientation, it appears plausible to represent damage by a set of N vector-valued variables $\underline{D}^{(k)} = D^{(k)}\underline{n}^{(k)}$ ($k=1, \ldots N$. No sum on k). However since each microcrack possesses two equal and opposite surfaces, the description should not discriminate between $+\underline{n}^{(k)}$ and $(-\underline{n}^{(k)})$, which is accomplished by choosing the dyadic product $\mathbf{A}^{(k)} = D^{(k)}\underline{D}^{(k)}$ to represent the kth flaw. This choice follows an analogous approach by Spencer (1972).

In view of the paucity of information regarding the positions and sizes of the individual microflaws it is proposed to represent damage by the dyadic sum of all $\mathbf{A}^{(k)}$ ($k=1, \ldots N$) contained in the RVE, namely by

$$\mathbf{A} = \sum_{k=1}^{N} \mathbf{A}^{(k)} = \sum_{k=1}^{N} \underline{D}^{(k)}\underline{D}^{(k)} \tag{1}$$

Obviously, $\mathbf{A}$ is a symmetric, second-rank tensor.

The presence of damage affects distinct aspects of material response in different ways. For instance, stiffness reductions are due mainly to the displacement discontinuities that occur at opposite faces of open (active) cracks, while heat due to friction occurs mostly at the interfaces of closed (passive) cracks. On the other hand, the moisture diffusion phenomenon is likely to couple with both active and passive flaws.

Consequently, damage will be described by two symmetric second-rank tensors $\mathbf{A}$ and $\mathbf{C}$, representing both active and passive cracks within the RVE.

In the sequel it will be advantageous to employ nondimensional quantities. Accordingly, both $\mathbf{A}$ and $\mathbf{C}$ will be divided by a characteristic area Δ, say, any one of the walls of the RVE, to give the internal state variables

$$\mathbf{a} = \mathbf{A}/\Delta^2 \text{ and } \mathbf{c} = \mathbf{C}/\Delta^2 \tag{2}$$

Unlike the infinitesimal strain tensor ϵ_{ij}, the symmetric tensors a_{ij} and c_{ij} are not necessary small. Consequently, in the development of constitutive relations, Taylor series expansions are useful in ϵ_{ij} but not in a_{ij} and c_{ij}.

It is worth noting that for randomly oriented microflaws of identical areas, namely $a_{ij}^{(k)} = an_i^{(k)}n_j^{(k)}$, $c_{ij}^{(k)} = cn_i^{(k)}n_j^{(k)}$, one obtains, upon integration over the unit sphere or the unit circle, $a_{ij} = a\delta_{ij}$ and $c_{ij} = c\delta_{ij}$ in both two and three dimensions. This result appeals to the notion that randomly distributed microflaws should not affect the macro symmetry of the damaged material. A vectorial representation of damage ($\underline{D}^{(k)} = D^{(k)}\underline{n}^{(k)}$) will not satisfy this expectation.

3 Basic Equations

Fundamental considerations of continuum mechanics and irreversible thermodynamics (e.g., Truesdell (1966), Jaunzemis (1967)) yield the following expressions for the balance of energy and the "reduced entropy inequality":

$$\rho_o\dot{\phi} = -q_{i,i} - \rho_o s\dot{T} - \rho_o T\dot{s} - \dot{\sigma}_{ij}\epsilon_{ij} \tag{3}$$

and

$$-\rho_o\dot{\phi} - \rho_o s\dot{T} - \dot{\sigma}_{ij}\epsilon_{ij} - (q_i/T)g_i \geq 0 \tag{4}$$

In equations (3) and (4), where infinitesimal deformation is assumed ($\epsilon_{ij} << 1$), ρ_o denotes the constant mass density, s is entropy density, T is temperature, q_i and σ_{ij} are components of the heat-flux vector and the Cauchy stress-tensor, respectively, and ϕ is the Gibbs free energy, given by

$$\rho_o\phi = \rho_o u - \rho_o Ts - \sigma_{ij}\epsilon_{ij} \tag{5}$$

where u is the internal energy density.

Also, in equations (3) and (4), dot denotes derivative with respect to time and $g_i = \partial T/\partial x_i$ where x_i are Cartesian coordinates.

Assume a constitutive response given by

$$\phi = \phi(\sigma_{ij}, a_{ij}, c_{ij}, T)^1 \tag{6}$$

Since the inequality (4) cannot be violated for any process it follows that

$$\epsilon_{ij} = -\rho_o\frac{\partial\phi}{\partial\sigma_{ij}} \tag{7}$$

$$s = -\frac{\partial\phi}{\partial T} \tag{8}$$

and

$$-\Gamma_{ij}\dot{a}_{ij} - \Pi_{ij}\dot{c}_{ij} - (q_i/T)g_i \geq 0 \tag{9}$$

In equation (9) Γ_{ij} and Π_{ij} are the "affinities" given by

$$\Gamma_{ij} = \rho_o\frac{\partial\phi}{\partial a_{ij}}, \quad \Pi_{ij} = \rho_o\frac{\partial\phi}{\partial c_{ij}}$$

The above affinities can be interpreted as macrolevel energy release rates and energy dissipation rates associated with the growth of the total area of the active microcracks, and size changes of the passive flaws, contained within the RVE.

Substitution of equations (7) and (8) into equation (3) leads to the coupled heat conduction equation

$$-q_{k,k} = \left(\Gamma_{ij} - T\frac{\partial\Gamma_{ij}}{\partial T}\right)\dot{a}_{ij} + \left(\Pi_{ij} - T\frac{\partial\Pi_{ij}}{\partial T}\right)\dot{c}_{ij}$$

$$+ T\frac{\partial\epsilon_{ij}}{\partial T}\dot{\sigma}_{ij} + \rho_o C\dot{T} \tag{10}$$

In equation (10) $C = -T\,\partial^2\phi/\partial T^2$ denotes specific heat at constant stress and damage.

4 Unidirectionally Reinforced Composites

Consider an extended material region, reinforced by unidirectional straight fibers parallel to the x_3 axis. This

[1] Familiar arguments rule out dependence of ϕ on g_i.

Downloaded 03 May 2010 to 171.66.16.21. Redistribution subject to ASME license or copyright; see http://www.asme.org/terms/Terms_Use.cfm

material can be represented by an equivalent, homogeneous, transversely isotropic medium. Let the medium contain a statistically homogeneous array of active and passive microcracks, as sketched in Fig. 1, and let these cracks be represented by the two tensors a_{ij} and c_{ij} introduced in section 2.

Assuming that the damaged material possesses no "handedness" (chirality), then its response possesses reflective symmetries in the x_1-x_2 and x_2-x_3 planes. This circumstance corresponds to symmetry T_4, as defined by Smith (1982).

Accordingly, the free energy ϕ in equation (6) should be expressed in terms of the transversely isotropic (T_4 symmetry) invariants of σ_{ij}, a_{ij} and c_{ij}. According to Smith (1982) there are 45 such invariants. Substantial simplifications occur upon assuming that, while both a_{ij} and c_{ij} cause softening of the material stiffnesses, symmetry is affected by a_{ij} alone. In addition, the assumption of small strains ($\epsilon_{ij} << 1$) permits ϕ to be expanded in powers of σ_{ij} terminating at the second power. These assumptions reduce the number of relevant invariants to 28 as listed below.

(*a*) Linear in σ_{ij}:

$$I_1=\sigma_{33},\ I_2=\sigma_{11}+\sigma_{22},\ I_3=(\sigma_{11}-\sigma_{22})(a_{11}-a_{22})+4\sigma_{12}a_{12},$$

$$I_4=\sigma_{13}a_{13}+\sigma_{23}a_{23},\ I_5=(\sigma_{11}-\sigma_{22})(a_{13}^2-a_{23}^2)+4\sigma_{12}a_{13}a_{23},$$

$$I_6=(a_{11}-a_{22})(\sigma_{13}a_{13}-\sigma_{23}a_{23})+2a_{12}(\sigma_{13}a_{23}+\sigma_{23}a_{13}).$$

(*b*) Quadratic in σ_{ij}:

$$J_1=(\sigma_{11}-\sigma_{22})^2+4\sigma_{12}^2,\ J_2=\sigma_{13}^2+\sigma_{23}^2,$$

$$J_3=(\sigma_{11}-\sigma_{22})(\sigma_{13}a_{13}-\sigma_{23}a_{23})+2\sigma_{12}(\sigma_{13}a_{23}+\sigma_{23}a_{13}),$$

$$J_4=(a_{11}-a_{22})(\sigma_{13}^2-\sigma_{23}^2)+4a_{12}\sigma_{13}\sigma_{23},$$

$$J_5=[(\sigma_{11}-\sigma_{22})a_{12}-(a_{11}-a_{22})\sigma_{12}](\sigma_{13}a_{23}-\sigma_{23}a_{13}).$$

In additions, it is necessary to include the invariants of a_{ij} and c_{ij} as follows:

$$H_1=a_{33},\ H_2=a_{11}+a_{22},\ H_3=(a_{11}-a_{22})^2+4a_{12}^2,$$

$$H_4=a_{13}^2+a_{23}^2,\ H_5=(a_{11}-a_{22})(a_{13}^2-a_{23}^2)+4a_{12}a_{13}a_{23},$$

five invariants H_6-H_{10} formed by replacing c_{ij} *for* a_{ij} in

H_1-H_5, and

$$H_{11}=a_{13}c_{13}+a_{23}c_{23},\ H_{12}=(a_{11}-a_{22})(c_{11}-c_{22})+4a_{12}c_{12},$$

$$H_{13}=(a_{11}-a_{22})(a_{13}c_{13}-a_{23}2_{23})+2_{12}(a_{13}c_{23}+a_{23}c_{13}),$$

$$H_{14}=(a_{11}-a_{22})(c_{13}^2-c_{23}^2)+4a_{12}c_{13}c_{23},$$

$$H_{15}=(c_{11}-c_{22})(a_{13}^2-a_{23}^2)+4c_{12}a_{13}a_{23},$$

$$H_{16}=(c_{11}-c_{22})(a_{13}c_{13}-a_{23}c_{23})+2c_{12}(a_{13}c_{23}+a_{23}c_{13}),$$

$$H_{17}=[(a_{11}-a_{22})c_{12}-(c_{11}-c_{22})a_{12}](a_{13}c_{23}-a_{23}c_{13}).$$

Employment of the above invariants in equation (6) gives

$$-\rho_o\phi=-\rho_o\phi_o+K_1I_1+K_2I_2+K_3I_3+K_4I_4+K_5I_5+K_6I_6$$
$$+L_1I_1^2+L_2I_2^2+L_3I_3^2+L_4I_4^2+L_5I_5^2+L_6I_6^2+L_7I_1I_2$$
$$+L_8I_1I_3+L_9I_1I_4+L_{10}I_1I_5+L_{11}I_1I_6+L_{12}I_2I_3$$
$$+L_{13}I_2I_4+L_{14}I_2I_5+L_{15}I_2I_6+L_{16}I_3I_4+L_{17}I_3I_5$$
$$+L_{18}I_3I_6+L_{19}I_4I_5+L_{20}I_4I_6+L_{21}I_5I_6+L_{22}J_1$$
$$+L_{23}J_2+L_{24}J_3+L_{25}J_5+L_{26}J_5 \tag{11}$$

In equation (11), ϕ_o, $K_i(i=1,\ldots 6)$, and $L_j(j=1,\ldots 26)$ are functions of the seventeen invariants H_1-H_{17} and of T.

In view of equation (7), expression (11) yields the following strain-stress relation:

$$\epsilon_p=S_{po}+S_{pq}\sigma_q \tag{12}$$

where

$$S_{10}=K_2+K_3(a_{11}-a_{22})+K_5\gamma_{12}^{(2)}$$
$$S_{20}=K_2+K_3(a_{22}-a_{11})+K_5\gamma_{12}^{(2)}$$
$$S_{30}=K_1 \tag{13}$$
$$S_{40}=K_4a_{23}+K_6\gamma_{23}^{(2)}$$
$$S_{50}=K_4a_{13}+K_6\gamma_{13}^{(2)}$$
$$S_{60}=4K_3a_{12}+4K_5a_{13}a_{23}$$

and

$$S_{11}=2L_2+2L_3(a_{11}-a_{22})^2+2L_5(\gamma_{12}^{(2)})^2$$
$$+2L_{12}(a_{11}-a_{22})+2L_{14}\gamma_{12}^{(2)}+2L_{17}(a_{11}-a_{22})\gamma_{12}^{(2)}+2L_{22}$$

$$S_{12}=2L_2-2L_3(a_{11}-a_{22})^2-2L_5(\gamma_{12}^{(2)})^2$$
$$-2L_{17}(a_{11}-a_{22})\gamma_{12}^{(2)}-2L_{22}$$

$$S_{13}=L_7+L_8(a_{11}-a_{22})+L_{10}\gamma_{12}^{(2)}$$

$$S_{14}=L_{13}a_{23}+L_{15}\gamma_{23}^{(2)}+L_{16}(a_{11}-a_{22})a_{23}$$
$$+L_{18}(a_{11}-a_{22})\gamma_{23}^{(2)}+L_{19}\gamma_{12}^{(2)}a_{23}+L_{21}\gamma_{12}^{(2)}\gamma_{23}^{(2)}$$
$$-L_{24}a_{23}-L_{26}a_{12}a_{13}$$

$$S_{15}=L_{13}a_{13}+L_{15}\gamma_{13}^{(2)}+L_{16}(a_{11}-a_{22})a_{13}$$
$$+L_{18}(a_{11}-a_{22})\gamma_{13}^{(2)}+L_{19}\gamma_{12}^{(2)}a_{13}+L_{21}\gamma_{12}^{(2)}\gamma_{13}^{(2)}$$
$$+L_{24}a_{13}+L_{26}a_{12}a_{23}$$

$$S_{16}=8L_3(a_{11}-a_{22})a_{12}+8L_5\gamma_{12}^{(2)}a_{13}a_{23}$$
$$+4L_{12}a_{12}+4L_{14}a_{13}a_{23}+4L_{17}\gamma_{12}^{(3)}$$

$$S_{22}=2L_2+2L_3(a_{11}-a_{22})^2+2L_5(\gamma_{12}^{(2)})^2+2L_{12}(a_{22}$$
$$-a_{11})-2L_{14}\gamma_{12}^{(2)}+2L_{17}(a_{11}-a_{22})\gamma_{12}^{(2)}+2L_{22}$$

$$S_{23}=L_7+L_8(a_{22}-a_{11})\text{-}L_{10}\gamma_{12}^{(2)}$$

Downloaded 03 May 2010 to 171.66.16.21. Redistribution subject to ASME license or copyright; see http://www.asme.org/terms/Terms_Use.cfm

$$S_{24} = L_{13}a_{23} + L_{15}\gamma_{23}^{(2)} + L_{16}(a_{22} - a_{11})a_{23}$$
$$+ L_{18}(a_{22} - a_{11})\gamma_{23}^{(2)} - L_{19}\gamma_{12}^{(2)}a_{23} - L_{21}\gamma_{12}^{(2)}\gamma_{23}^{(2)}$$
$$+ L_{24}a_{23} + L_{26}a_{12}a_{13}$$

$$S_{25} = L_{13}a_{13} + L_{15}\gamma_{13}^{(2)} + L_{16}(a_{22} - a_{11})a_{13}$$
$$+ L_{18}(a_{22} - a_{11})\gamma_{13}^{(2)} - L_{19}\gamma_{12}^{(2)}a_{13} - L_{21}\gamma_{12}^{(2)}\gamma_{13}^{(2)}$$
$$- L_{24}a_{23} - L_{26}a_{12}a_{23}$$

$$S_{26} = 8L_3(a_{22} - a_{11})a_{12} - 8L_5\gamma_{12}^{(2)}a_{13}a_{23} + 4L_{12}a_{12}$$
$$+ 4L_{14}a_{13}a_{23} - 4L_{17}\gamma_{12}^{(3)}$$

$$S_{33} = 2L_1$$

$$S_{34} = L_9a_{23} + L_{11}\gamma_{23}^{(2)}$$

$$S_{35} = L_9a_{13} + L_{11}\gamma_{13}^{(2)}$$

$$S_{36} = 4L_8a_{12} + 4L_{10}a_{13}a_{23}$$

$$S_{44} = 2L_4a_{13}a_{23} + 2L_6(\gamma_{23}^{(2)})^2$$
$$+ 2L_{20}a_{23}\gamma_{23}^{(2)} + 2L_{23} + 2L_{25}(a_{22} - a_{11})$$

$$S_{45} = 2L_4a_{13}^2 + 2L_6\gamma_{23}^{(2)}\gamma_{13}^{(2)}$$
$$+ 2L_{20}a_{12}(a_{13}^2 + a_{23}^2) + 4L_{25}a_{12}$$

$$S_{46} = 4L_{16}a_{23}a_{12} + 4L_{18}a_{12}\gamma_{23}^{(2)} + 4L_{19}a_{13}a_{23}^2$$
$$+ 4L_{21}a_{13}a_{23}\gamma_{23}^{(2)} + 2L_{24}a_{13} + L_{26}a_{13}(a_{11} - a_{22})$$

$$S_{55} = 2L_4a_{13}a_{23} + 2L_6(\gamma_{13}^{(2)})^2$$
$$+ 2L_{20}a_{13}\gamma_{13}^{(2)} + 2L_{23} + 2L_{25}(a_{11} - a_{22})$$

$$S_{56} = 4L_{16}a_{13}a_{12} + 4L_{18}a_{12}\gamma_{13}^{(2)} + 4L_{19}a_{13}^2a_{23}$$
$$+ 4L_{21}a_{13}a_{23}\gamma_{13}^{(2)} + 4L_{24}a_{23} + L_{26}a_{23}(a_{22} - a_{11})$$

$$S_{66} = 32L_3a_{12}^2 + 32L_5a_{13}^2a_{23}^2 + 16L_{17}a_{13}a_{23}a_{12} + 2L_{22}. \quad (14)$$

In equations (13) and (14)

$$\gamma_{12}^{(2)} = a_{13}^2 - a_{23}^2$$

$$\gamma_{23}^{(2)} = (a_{22} - a_{11})a_{23} + 2a_{12}a_{13}$$

$$\gamma_{13}^{(2)} = (a_{11} - a_{22})a_{13} + 2a_{12}a_{23}$$

$$\gamma_{12}^{(3)} = (a_{11} - a_{22})a_{13}a_{23} + (a_{13}^2 - a_{23}^2)a_{12}$$

In those equations the familiar truncated notation was employed for strains and stresses, namely $\sigma_1 = \sigma_{11}$, $\sigma_2 = \sigma_{22}$, $\sigma_3 = \sigma_{33}$, $\sigma_4 = \sigma_{23}$, $\sigma_5 = \sigma_{31}$, $\sigma_6 = \sigma_{12}$, and $\epsilon_1 = \epsilon_{11}$, $\epsilon_2 = \epsilon_{22}$, $\epsilon_3 = \epsilon_{33}$, $\epsilon_4 = 2\epsilon_{23}$, $\epsilon_5 = 2\epsilon_{31}$, $\epsilon_6 = 2\epsilon_{12}$.

Note that equations (13) and (14) contain the five classical compliances L_1, L_2, L_7, L_{22} and L_{23} and the two expansional terms, K_1 and K_2, of transverse isotropy. In the presence of damage the above seven quantities may depend on the 17 invariants $H_1 - H_{17}$. Perhaps more significantly, the active state variable a_{ij} may cause the symmetry of the material to depart from transverse isotropy. It can be shown by straightforward substitution that if all microcracks are normal to the x_1 direction, namely $a_{11} \neq 0$ and all remaining $a_{ij} = 0$, the material possesses—as expected—orthotropic symmetry. Orthotropy is retained also if $a_{11} \neq 0$ and $a_{22} \neq 0 (a_{22} \neq a_{11})$ and all other a_{ij} vanish. On the other hand, if all microcracks are normal to the x_3 direction, the original transverse isotropy is retained, except that the five compliances and the two expansional terms depend on a_{33} (and the invariants of c_{ij}).

If all expansional strains S_{po} are assumed linear in the temperature-difference ΔT then $K_i (i = 1, \ldots 6)$ in equations (13) can be replaced by $\alpha_i \Delta T$, where $\alpha_i (i = 1, \ldots 6)$ are damage-dependent coefficients of thermal expansion.

5 Coupling of Damage with Heat Conduction

The general form of the coupled heat conduction equation was given in equation (10). Assuming that heat flow is not impeded across the contacting surfaces of the passive cracks, consider the following constitutive expression for q_i

$$q_i = q_i(a_{ij}, T, g_i) \quad (15)$$

In equation (15) $g_i = \partial T / \partial x_i$ as before.

Specific expressions for transverse isotropy (T_4 symmetry) are obtained by forming all invariants among the two distinct vectors q_i and g_i, and the symmetric second-rank tensor a_{ij}. These invariants were listed by Smith (1982).

Upon collecting the factors of the individual components of q_i, we obtain the following flux-gradient expressions:

$$q_i = k_{ij}g_j \quad (16)$$

where

$$k_{11} = k_1 + k_3(a_{11} - a_{22}) + k_4\gamma_{12}^{(2)}$$

$$k_{12} = 2k_3a_{12} + 2k_4a_{13}a_{23}$$

$$k_{13} = k_5a_{13} + k_6\gamma_{13}^{(2)}$$

$$k_{22} = k_1 + k_3(a_{22} - a_{11}) - k_4\gamma_{12}^{(2)} \quad (17)$$

$$k_{23} = k_5a_{23} + k_6\gamma_{23}^{(2)}$$

$$k_{33} = k_2$$

Note that, in general, $k_i (i = 1, \ldots 6)$ depend on the five invariants $H_1 - H_5$ of a_{ij} listed in section 4. Also, terms which violated Onsager's principle were eliminated from equations (17) to ascertain the $k_{ij} = k_{ij}$.

Insertion of equations (12) and (16) into equation (10) yields

$$-k_{ij}T_{,ij} = \rho_o C\dot{T} + D \quad (18)$$

where the dissipation D is given by

$$D = k_{ij,i}T_{,j} + T\left(\frac{\partial S_{po}}{\partial T} + \frac{\partial S_{pq}}{\partial T}\sigma_q\right)\dot{\sigma}_p + \left(1 - T\frac{\partial}{\partial T}\right)$$
$$\times \left[\left(\rho_o\frac{\partial \phi_o}{\partial a_{ij}} - \frac{\partial S_{po}}{\partial a_{ij}}\sigma_p - \frac{1}{2}\frac{\partial S_{pq}}{\partial a_{ij}}\sigma_p\sigma_q\right)\dot{a}_{ij}\right.$$
$$\left. + \left(\rho_o\frac{\partial \phi_o}{\partial c_{ij}} - \frac{\partial S_{po}}{\partial c_{ij}}\sigma_p - \frac{1}{2}\frac{\partial S_{pq}}{\partial c_{ij}}\sigma_p\sigma_q\right)\dot{c}_{ij}\right] \quad (19)$$

Consider, for instance the one dimensional case $\sigma_1 = \sigma$,

Downloaded 03 May 2010 to 171.66.16.21. Redistribution subject to ASME license or copyright; see http://www.asme.org/terms/Terms_Use.cfm

$a_{11}=a$, $c_{11}=c$, with all remaining σ_p, a_{ij} and c_{ij} vanishing. Also, assume all expansional strains to vary linearly with ΔT, neglect the dependence of the compliances S_{pq} on T, and let all spatial variations depend only on the coordinate $x_1=x$.

In this case, equations (18) and (19) reduce to

$$-(k_1+k_3a)T_{,xx}=\rho_o C\dot{T}+\tilde{D} \tag{20}$$

where

$$\tilde{D}=(k_1+k_3a)_{,x}T_{,x}+T(\alpha_2+\alpha_3a)\dot{\sigma}+\rho_o\left(1-T\frac{\partial}{\partial T}\right)$$

$$\times\left(\frac{\partial\phi_o}{\partial a}+\frac{\partial\phi_o}{\partial c}\right)-\frac{1}{2}\sigma^2\left(\frac{\partial S_{11}}{\partial a}\dot{a}+\frac{\partial S_{11}}{\partial c}\dot{c}\right) \tag{21}$$

In equation (21) $S_{11}=2(L_2+L_{22}+L_3a^2+L_{12}a)$ and k_1, k_3, α_2, α_3, L_2, L_{22}, L_3, L_{13} depend on a and c.

6 Damage Growth Relations: Micromechanical Considerations

Damage growth relations are an essential component of a continuum damage model, since they endow the theory with a predictive capability. In several previous works such relations were expressed empirically, derived by analogy with the plastic yield surface, or established formally from thermodynamic considerations.

It is suggested herein to relate damage growth to information derived from suitable microlevel fracture mechanics solutions. This approach will be demonstrated by a specific example, as discussed below.

Suppose that crack interactions can be neglected and that all microcracking is confined to the fiber/matrix interfaces. This circumstance corresponds to an arc crack at the interface between a cylindrical inclusion and an extended exterior region, which was studied by England (1966), Perlman and Sih (1967), Toya (1974), and Piva (1982).[2]

Among those analyses, Toya's solution is the most suitable for the present purpose because it provides expressions for crack growth based upon considerations of energy release rates and furnishes information on crack surfaces' interpenetration.[3] The latter information provides evidence for the presence or absence of passive cracks.

In the absence of a solution that incorporates both active and passive cracks at the interface between the inclusion and the exterior, only an outline of the method will be provided.

Consider an elastic, isotropic, inclusion of radius R embedded in an extended elastic exterior region. Let the region be subjected to a remote load $\sigma_x=p$ and let an interfacial crack exist at $r=R$, $\omega-\beta\le\theta\le\omega+\beta$, where r and θ are polar coordinates (see Fig. 2).

Assume that all microcracks are confined to the inclusion/exterior (fiber/matrix) interface then, following Toya (equation (4.7)), the criterion for crack growth is given by an explicit expression of the form

$$p^2RF(\nu_1,\ \nu_2,\ \mu_1/\mu_2,\ \omega,\ \beta)=G_c \tag{22}$$

where ν_2 and μ_2 are the Poisson's ratio and shear modulus of the fiber and, in the present case, ν_1 and μ_1 are to be interpreted as the analogous properties of the equivalent, homogeneous, fiber-reinforced composite. G_c is the critical energy release rate for debonding between the fiber and the matrix.

According to Toya, equation (22) may have two solutions for β (and ω) in the range $0<\beta\le\pi$ and $0\le\omega<2\pi$. If two such solutions exist, say, β_1 and $\beta_2>\beta_1$, then β_1 corresponds to the initial crack and β_2 to the final crack size. The result obtained from equation (22) may be superseded by the requirement that crack closure occurs at some intermediate angle $\beta_3(\beta_1<\beta_3<\beta_2)$ if the discontinuity in the radial displacement Δu_r across the crack interface becomes negative in the range $\omega_2-\beta_2<\theta<\omega_2+\beta_2$. Although such a test is provided by Toya (equation (3.57)), in the form

$$\Delta u_r=U(\nu_1,\ \nu_2,\ \mu_1/\mu_2,\ \beta_3,\ \omega_2)=0 \tag{23}$$

the modification necessitated in the solution is not yet available.

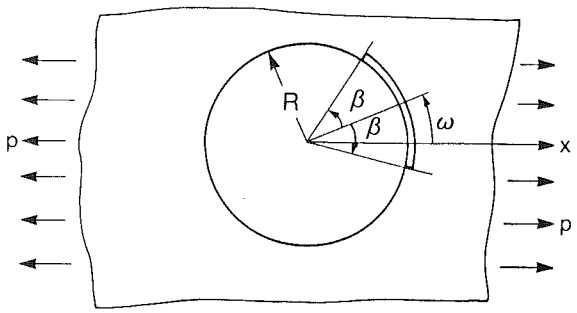


Fig. 2 A crack at the interface of a cylindrical inclusion and an exterior region ($r=R$, $\omega-\beta<\theta<\omega+\beta$) which is subjected to remote uniaxial tension $\sigma_x=p$

However, in principle one should obtain for $p>p_{\text{threshold}}$ that an initial crack, characterized by size β_{in} and location ω_{in}, reaches a final configuration prescribed by β_f and ω_f. The final configuration may correspond to an entirely open, partially closed or an entirely closed crack.

In view of equation (1), the corresponding expressions for the damage variables for this single crack are

$$\mathbf{a}=\rho^2\cdot 2\beta_a(\cos\omega_a\ \mathbf{e}_x+\sin\omega_a\ \mathbf{e}_y)(\cos\omega_a\ \mathbf{e}_x+\sin\omega_a\ \mathbf{e}_y)$$

$$=2\beta_a\rho^2[\cos^2\omega_a\ \mathbf{e}_x\ \mathbf{e}_x+\sin\omega_a\ \cos\omega_a(\mathbf{e}_x\ \mathbf{a}_y$$

$$+\mathbf{e}_y\ \mathbf{e}_x)+\sin^2\omega_a\ \mathbf{e}_y\ \mathbf{e}_y] \tag{24a}$$

and, by analogy

$$\mathbf{c}=2\beta_c\rho^2[\cos^2\omega_c\ \mathbf{e}_x\ \mathbf{e}_x+\sin\omega_c\ \cos\omega_c(\mathbf{e}_x\ \mathbf{e}_y+\mathbf{e}_y\ \mathbf{e}_x)$$

$$+\sin^2\omega_c\ \mathbf{e}_y\ \mathbf{e}_y] \tag{24b}$$

In equations (24) and (25), β_a and ω_a characterize the geometry of the active crack, while β_c and ω_c correspond to the closed (passive) crack. Also, ρ^2 is a nondimensional quantity that relates the inclusion's radius to a dimension of the RVE.

Damage growth is given by

$$\Delta\mathbf{a}=\mathbf{a}(\beta_a,\ \omega_a)_{\text{final}}-\mathbf{a}(\beta_a,\ \omega_a)_{\text{initial}}$$

$$\Delta\mathbf{c}=\mathbf{c}(\beta_c,\ \omega_c)_{\text{final}}-\mathbf{c}(\beta_c,\ \omega_c)_{\text{initial}}{}^4 \tag{25}$$

In the context of a rate-independent constitutive response, as in the present work, the increments Δa_{ij} and Δc_{ij} replace the time rates $\dot{a}_{ij}$ and $\dot{c}_{ij}$.

Relations (22) and (23) show that damage growth, as given in equations (25), is highly nonlinear in the crack parameters β and ω—which determine the damage variables a_{ij} and c_{ij} through equations (24).

[2] All these papers exclude the case of partially closed cracks. An extension to account for this circumstance is now under study.

[3] Away from the immediate vinicity of the crack tips. Interpenetration always exists along a miniscule arc near the crack tips due to the oscillatory nature of the singularity.

[4] Conceivably in many circumstances $(\beta_c)_{\text{initial}}=0$, whereby also $\mathbf{c}_{\text{initial}}=0$.

Downloaded 03 May 2010 to 171.66.16.21. Redistribution subject to ASME license or copyright; see http://www.asme.org/terms/Terms_Use.cfm

Turning to the case of N inclusions with N microcracks within the RVE, the sizes and orientations for the initial cracks β_i, $\omega_i (i=1, \ldots N)$ may be described by random variables B and Ω, where β_i and ω_i are their realizations. Obviously $0<B<\pi$ and $0\leq\Omega\leq 2\pi$. These random variables may be described by probability density functions $f_B(\beta)$ and $f_\Omega(\omega)$, respectively, and if B and Ω are independent, then $f_{B\Omega}(\beta, \omega) f_B(\beta) f_\Omega(\omega)$. In this case, if $f_B(\beta)$ and $f_\Omega(\omega)$ are known, the realization of β and ω, and thereby of the initial damage, can be obtained by sampling.

Given expressions (22)–(25), once the complete solution which includes the case of crack closure becomes known, the incrementals of damage $\Delta\mathbf{a}$ and $\Delta\mathbf{c}$ can be determined. Upon repeating the sampling and predicting process N times, statistical information such as the first two moments of the corresponding distributions of $\Delta\mathbf{a}$ and $\Delta\mathbf{c}$, $f_{\Delta\mathbf{A}}$ $(\Delta\mathbf{a})$ and $f_{\Delta\mathbf{C}}$ $(\Delta\mathbf{c})$ are given by

$$E[\Delta\mathbf{a}] = \sum_{i=1}^{N} \Delta\mathbf{a}_i / N$$

$$\text{Var } [\Delta\mathbf{a}] = \sum_{i=1}^{N} \{\Delta\mathbf{a}_i - E[\Delta\mathbf{a}]\}^2 \tag{26}$$

and similar expressions with $\Delta\mathbf{c}$.

It is, of course, likely that even if the initial distribution of damage is normal, the distributions of $\Delta\mathbf{a}$ and $\Delta\mathbf{c}$ may be other than normal. In such a case the statistical characterization of damage growth may require quantities other than expectation and variance.

7 Relationships With Other Results

The effects of cracks on material compliances were related by other approaches, most prominently by the self consistent scheme as employed by Laws et al. (1977, 1980, 1983). Specifically, the effects of a system of parallel cracks of equal size on the compliances of a unidirectionally reinforced composite were obtained by Laws, Dvorak and Hejazi (1983). It can be readily shown that the above results remain essentially valid in the case when the parallel cracks are of unequal sizes.[5] In this case the self consistent scheme predicts that the above crack system will modify all the compliances according to a complicated but well defined nonlinear relationship in the crack density β. These results may be compared with the constitutive relations (14) of the present work when $a_{11} = a \neq 0$ and all other a_{ij} vanish. Since both approaches result in orthotropic symmetry which involves nine compliances, it should presumably be possible to establish the dependence of the nine terms $L_1, L_2, L_3, L_7, L_8, L_{12}, L_{22}, L_{23}, L_{25}$ in equation (14) by comparison with the dependence of the compliances $S_{11}, S_{12}, S_{13}, S_{22}, S_{23}, S_{33}, S_{44}, S_{55}$ and S_{66} on β according to the self consistent scheme. Note, however, that since the self consistent scheme provides an inflexible accounting for crack interactions, while the present theory is more versatile, it may be preferable to compare the expressions (14) against experimental data, whenever such become available.

It is also worth noting that in equation (14) orthotropy was derived as a mathematical consequence of the damage model employed herein, while orthotropy must be introduced as an independent hypothesis in the self consistent scheme.

Regarding the interaction between temperature, heat flux and damage, consider the model problems addressed by Florence and Goodier (1963), Barber (1976), and Martin-Moran et al. (1983). Although these cases involved a single penny-shaped crack in an extended, isotropic, homogeneous elastic medium they clearly demonstrate that both heat fluxes and thermal stresses are influenced most substantially by the presence of the crack. In fact, both quantities become singular at the crack tips. It was further shown that the temperature field, and therefore the heat fluxes, was affected by the thermal boundary conditions at the crack surfaces. Additional solutions to appropriate thermoelastic model problems in the presence of cracks are necessary for better insight into the coupling phenomena. Such solutions may then provide the necessary details for equations (18) and (20).

8 Concluding Remarks

In this paper, a continuum damage model which included thermomechanical phenomena was developed for unidirectionally reinforced, elastic media.

Damage was incorporated by means of two second-rank, symmetric tensors that represented the total areas of open (active) and closed (passive) microcracks contained within a representative volume element. Constitutive relations, including a coupled heat conduction equation, were established from fundamental aspects of irreversible thermodynamics and continuum mechanics. It was assumed that material symmetry is affected by the active cracks only, while moduli softening is influenced by the passive cracks as well.

It was demonstrated that damage growth relations can, in principle, be derived from fracture mechanics solutions on the micro scale, in which case statistical aspects of the crack configurations may play an important role. Some comparisons were provided between the present model and the self consistent scheme.

It appears that further progress in damage modeling requires the establishment of solutions to well selected model problems in fracture mechanics and the development of proper accounting for crack interactions. Similarly, fundamental thermoelastic solutions are necessary in the presence of cracks and inclusions in order to gain further insight into the coupling of damage and temperature.

Acknowledgments

The author wishes to thank Professors N. Stubbs of Texas A&M University and N. Laws of the University of Pittsburgh for helpful discussions.

This work was performed under Grant AFOSR-87-0218 from the Directorate of Aerospace Sciences, Air Force Office of Scientific Research. This support is gratefully acknowledged.

References

Allen, D. H., Groves, S. E., and Harris, C. E., 1985, "A Thermomechanical Constitutive Theory for Elastic Composites with Distributed Damage, Part I: Theoretical Development," Report MM-5023-85-14, Texas A&M University.

Allen, D. H., Groves, S. E., and Harris, C. E., 1985, "A Thermomechanical Constitutive Theory for Elastic Composites with Distributed Damage, Part II: Application to Matrix Cracking in Laminated Composites," Report MM-5023-85-15, Texas A&M University.

Allen, D. H., Harris, C. E., Groves, S. E., and Norvell, R. G., 1987, "Characterization of Stiffness Loss in Crossply Laminates with Curved Matrix Cracks," *Composites '86: Recent Advances in Japan and the United States*. K. Kawata, S. Umekawa & A. Kobayashi, eds., *Proc. Japan-U.S. CCM-III*, Tokyo, 1986, pp. 223–229.

Barber, J. R., 1976, "A Disturbance of a Uniform Steady-State Heat Flux by

[5] For an elliptical inclusion with semi-axes (ka, kb) instead of (a, b) the tensor $\mathbf{P}_{ijkl}$ in equation (3) of Laws et al. (1983) remains unchanged. It is only necessary to replace the volume fraction c_3 by $k^2 c_3$ in equations (17), (18) and (26), (27) of that work. For a system of parallel ellipses of size distribution determined by some probability density $f_K(k)$, it is necessary to replace c_3 by $c_3 \int k^2 f_K(k)\, dk$ in the above equations. The reduction to the case of cracks continues unhindered. It is only required to modify the definition of the quantity β in equation (30) of that work.

Downloaded 03 May 2010 to 171.66.16.21. Redistribution subject to ASME license or copyright; see http://www.asme.org/terms/Terms_Use.cfm

a Partially Conducting Plane Crack," *International Journal of Heat and Mass Transfer*, Vol. 19, pp. 956–958.

Bazant, Z., 1986, "Mechanics of Distributed Cracking," *Applied Mechanics Reviews*, Vol. 39, No. 5, pp. 675–705.

England, A. H., 1966, "An Arc Crack around a Circular Elastic Inclusion," ASME JOURNAL OF APPLIED MECHANICS, Vol. 33, pp. 637–640.

Fang, G.-P., Schapery, R. A., and Weitsman, Y., 1988, "Thermally-Induced Fracture in Composites," *Proc. ASME Symposium on Composite Materials*, Anaheim, CA, Dec. 1986, S. S. Wang, ed., forthcoming.

Florence, A. L., and Goodier, J. N., 1963, "The Linear Thermoelastic Problem of Uniform Heat Flow Disturbed by a Penny-Shaped Crack," *International Journal of Engineering Science*, Vol. 1, pp. 533–540.

Hashin, Z., 1985, "Analysis of Cracked Laminates: A Variational Approach," *Mechanics of Materials*, Vol. 4, pp. 121–136.

Jaunzemis, W., 1967, *Continuum Mechanics*, McMillan, New York.

Kachanov, L. M., 1958, "On Creep Rupture Time," *Izv. Acad. Nauk SSSR, Otd. Techn. Nauk*, No. 8, pp. 26–31.

Krajcinovic, D., 1986, "Continuum Damage Mechanics," *Applied Mechanics Update*, C. R. Steele and G. S. Springer, eds. ASME, pp. 397–406.

Laws, H., 1977, "A Note on Interaction Energies Associated with Cracks in Anisotropic Solids," *Philosophical Magazine*, Vol. 36, No. 2, pp. 367–372.

Laws, N., 1980, "The Elastic Response of Composite Materials," *Physics of Modern Materials*, Vol. I, International Atomic Energy Agency, pp. 465–520.

Laws, N., Dvorak, G. J., and Hejazi, M., 1983, "Stiffness Changes in Unidirectional Composites Caused by Crack Systems," *Mechanics of Materials*, Vol. 2, pp. 123–137.

Martin-Moran, C. J., Barber, J. R., and Comninou, M., 1983, "The Penny-Shaped Interface Crack with Heat Flow. Part I: Perfect Contact," ASME JOURNAL OF APPLIED MECHANICS, Vol. 50, pp. 29–36.

Murakami, S. and Ohno, N., 1981, "A Continuum Theory of Creep and Creep Damage," *Creep in Structures*, International Union of Theoretical and Applied Mechanics, 3rd Symposium, Leicester, UK, September 8–12, 1980. A. R. S. Ponter and D. R. Hayhurst, eds., Springer-Verlag, pp. 422–444.

Perlman, A. B. and Sih, G. C., 1967, "Elastostatic Problems of Curvilinear Cracks in Bonded Dissimilar Materials," *International Journal of Engineering Science*, Vol. 5, pp. 845–867.

Piva, A., 1982, "Crack Along a Circular Interface Between Dissimilar Media," *Meccanica*, Vol. 17, pp. 85–90.

Smith, G. F., 1982, "On Transversely Isotropic Functions of Vectors, Symmetric Second-Order Tensors and Skew-Symmetric Second-Order Tensors," *Quarterly of Applied Mathematics*, Vol. 39, pp. 509–516.

Spencer, A. J. M., 1972, *Deformation of Fibre-Reinforced Materials*, Oxford, (Especially pages 79–81).

Talreja, R., 1985, "A Continuum Mechanics Characterization of Damage in Composite Materials," *Proceedings of the Royal Society, London, Series A*, Vol. 399, pp. 195–216.

Talreja, R., 1985, "Transverse Cracking and Stiffness Reduction in Composite Laminates," *Journal of Composite Materials*, Vol. 19, pp. 355–375.

Toya, M., 1974, "A Crack Along the Interface of a Circular Inclusion Embedded in an Infinite Solid," *Journal of the Mechanics and Physics of Solids*, Vol. 22, pp. 325–348.

Truesdell, C., 1966, *Six Lectures on Modern Natural Philosophy*, Springer-Verlag, New York (Especially page 39).

Vakulenko, A. A., and Kachanov, M. L., 1971, "Continuum Model of Medium with Cracks," *Mekhanika Tverdogo Tela*, No. 4, pp. 159–166.

Weitsman, Y., 1987, "Environmentally Induced Damage in Composites," *Proceedings of the Fifth International Symposium on Continuum Models of Discrete Systems*, Nottingham, July 12–14, 1985. A. J. M. Spencer, ed., pp. 187–192.

Weitsman, Y., 1987, "Damage Coupled with Heat Conduction in Uniaxially Reinforced Composites," *Constitutive Modeling for Nonconventional Materials*, ASME, V. Stokes and D. Krajcinovic, eds., pp. 161–174.

Downloaded 03 May 2010 to 171.66.16.21. Redistribution subject to ASME license or copyright; see http://www.asme.org/terms/Terms_Use.cfm

An Analytical Model for Unanchored Fluid-Filled Tanks Under Base Excitation

S. Natsiavas
Assistant Professor,
Mechanical and Aerospace Engineering Department,
Arizona State University,
Tempe, AZ 85287
Assoc. Mem. ASME

A set of equations is derived describing the dynamic response of cylindrical liquid storage tanks under horizontal ground excitation. The structure consists of a flexible cylindrical tank with a roof and a bottom plate and rests on a flexible ground through a rigid foundation. Portion of the base of the tank may separate from and lift off the foundation during ground motion. The solution of the hydrodynamic problem is first found in closed form. Then, Hamilton's principle is applied and the equations governing the behavior of the coupled fluid/structure/ground system are derived. During this procedure, the base uplifting is modeled by an appropriate rotational nonlinear spring placed between the base of the tank and the foundation.

Introduction

Cylindrical tanks are easy and economical to fabricate and structurally efficient in sustaining the hydrostatic pressure caused by their contents. However, if compressive stresses are generated due to operational or environmental loads, a buckling failure may occur which can result in loss of contents and other undesirable consequences (Rinne, 1967; Hanson, 1973). Due to the high cost required by proper anchoring, the majority of the tanks in the field are essentially unanchored and their bases separate from and lift off their foundations during sufficiently strong ground motion. This uplifting causes severe loading on the sidewall/bottom joint as well as high stresses in the bottom plate.

Most of the previous investigations on the subject have studied the response of anchored tanks (e.g., Housner, 1957; Edwards, 1969; Veletsos and Yang, 1976; Nash et al., 1978; Haroun, 1980, 1983; Liu and Lam, 1983). The analytical formulation of the dynamic response of unanchored tanks during the ground motion is more complicated and inherently nonlinear. During 1977–1982, some experiments with unanchored tanks were conducted by Clough et al. (1979, 1982) at Berkeley and by Shih and Babcock (1981, 1987) at Caltech, which provided a good source of information for the behavior of unanchored tanks. Some analytical work has also been reported recently, dealing with various aspects of the base uplift. In 1985, Auli et al. presented an approximate approach for obtaining the stress distribution at the bottom of an unanchored tank. At the same time, Ishida and Kobayashi presented a four degree-of-the-freedom simplified mechanical model in an attempt to analyze approximately the rocking response of tanks. Finally, Peek (1986) presented analytical methods for computing the loads and stresses in the shell and the bottom plate of unanchored tanks, under the action of static lateral loads.

The objective of the present work is the creation of an analytical model that will lead to a better understanding of the response and failure mechanisms of unanchored tanks, subjected to base excitation. The response of anchored tanks can also be easily obtained by this approach, as a special case. Numerical results obtained by employing this analysis are compared and found in good agreement with experimental data. These results are presented in a companion paper.

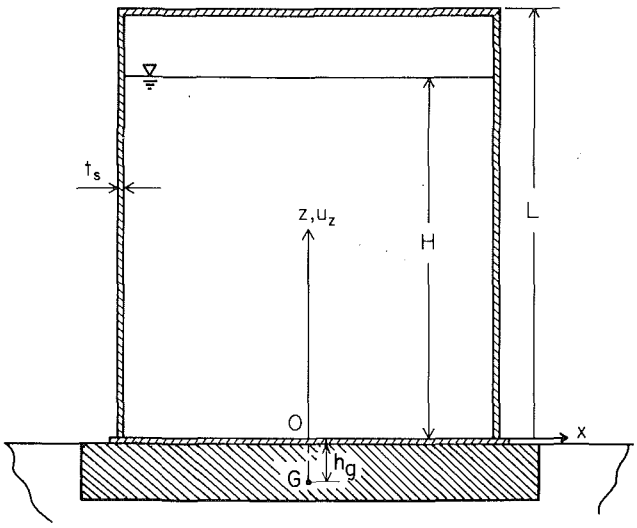
Definition of System Geometry

The system considered is shown in Fig. 1. The tank has radius R, length L, thickness t_s, it is partly filled with a liquid of density ρ_l up to a level H and it is covered above by a roof. Ground motion is assumed to be aligned with the horizontal x-axis and to have a known displacement history $x_g(t)$. This motion is transferred to the tank through its foundation, which is assumed to be rigid but to rest on flexible ground. Apart from the point G, which is located along the vertical z-axis and purely translates by $x_g(t)$ with the ground, all the other points in the foundation rotate around G through the angle ϕ_f, due to the ground flexibility. If the tank is unanchored, part of the bottom plate may lift off and lose contact with the foundation. Then, the bottom periphery of the cylindrical part rotates an additional angle ϕ_u about the y-axis. Therefore, the bottom section of the cylindrical part rotates through a total angle $\phi = \phi_f + \phi_u$, about the y-axis illustrated in Fig. 2. Finally, polar coordinates r,θ,z and time t are used for the description of the system variables and u_r,u_θ,u_z are the structural displacements in the radial, circumferential, and axial direction, respectively.

Contributed by the Applied Mechanics Divison for presentation at the Winter Annual Meeting, Chicago, IL, November 28 to December 2, 1988, of THE AMERICAN SOCIETY OF MECHANICAL ENGINEERS.

Discussion on this paper should be addressed to the Editorial Department, ASME, United Engineering Center, 345 East 47th Street, New York, N.Y. 10017, and will be accepted until two months after final publication of the paper itself in the JOURNAL OF APPLIED MECHANICS. Manuscript received by ASME Applied Mechanics Division, July 20, 1987; final revision, February 20, 1988.
Paper No. 88-WA/APM-49.

Copyright © 1988 by ASME
Downloaded 03 May 2010 to 171.66.16.21. Redistribution subject to ASME license or copyright; see http://www.asme.org/terms/Terms_Use.cfm



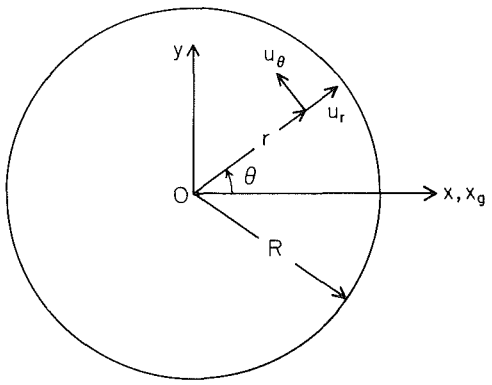


Fig. 1 Coordinate system for a cylindrical tank

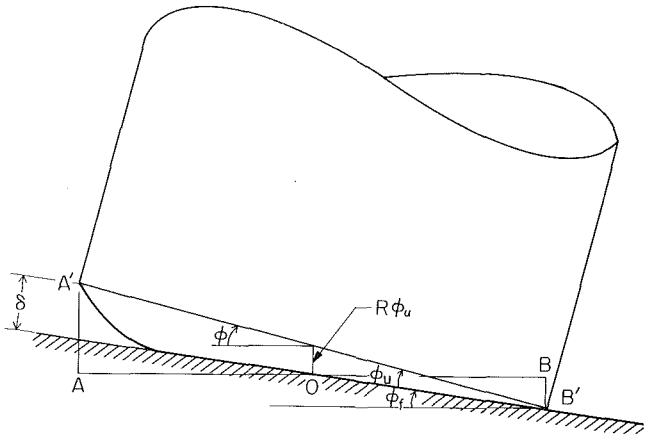


Fig. 2 Definition of base uplifting and foundation rocking angles

Choice of Method of Approach

The behavior of the system under consideration is governed by a nonlinear system of coupled partial differential equations. A structural vibration may drive and affect the liquid response, which in turn affects the structural response by developing and exerting hydrodynamic pressures on the structure. When the structure is allowed to lift off its foundation, the formulation becomes unavoidably nonlinear (contact problem). Furthermore, the deformation of the bottom plate during uplift can become so large that linear bending theory is no longer adequate in modeling its behavior. An immediate consequence is that if a theoretical approach is sought, one must employ approximate methods in developing and solving the governing equations. The most popular approximate techniques used for obtaining finite-dimensional field equations for the system are those employing finite element or other energy methods. For the problem at hand, previous analytical and experimental investigations (Veletsos and Yang, 1976; Clough and Niwa, 1979; Shih, 1981; Haroun, 1983) have provided reasonable descriptions of the expected modes. Therefore, an energy method is chosen here as most appropriate for the geometrical discretization of the structure. The basic steps of this method are explained in the following four sections.

Displacement Form of the Structural Components

The cylindrical part of the structure is modeled as a thin shell whose middle surface displacements are of the following form:

$$u_r(\theta,z,t) = [x_g(t) + h_g\phi_f(t) + z\phi(t) + u_r^e(z,t)]\cos\theta \quad (1)$$

$$u_\theta(\theta,z,t) = -[x_g(t) + h_g\phi_f(t) + z\phi(t) + u_\theta^e(z,t)]\sin\theta \quad (2)$$

$$u_z(\theta,z,t) = R\,|\phi_u(t)| + [-R\phi(t) + u_z^e(z,t)]\cos\theta \quad (3)$$

The flexible part of the cylindrical shell displacements can generally be decomposed into selected modes, characterized by two integers n and m, which represent the number of the full circumferential and half axial waves of the mode, respectively. The axisymmetric $n=0$ shell modes are not included in this formulation. These modes are excited during vertical ground motion, which is not of concern in this work. The effects of the $n>1$ shell modes are also neglected here. For unanchored and/or imperfect tanks, some of the $n>1$ modes may be excited but the resultant shear force and overturning moment are zero. In addition, there exist experimental data suggesting that the tank response and failure is predominated by loads which result from the $n=1$-beam-type-modes (Shih and Babcock, 1981, 1987). However, the importance of some of the $n>1$ modes needs to be investigated further for relatively broad tanks, for which the coupling of these modes with the beam-type modes is expected to be stronger.

The flexible parts of the displacements are expanded in the following forms:

$$u_r^e(z,t) = \sum_{m=1}^{N1} [w_m(z)\psi_m(t)],$$

$$u_\theta^e(z,t) = \sum_{m=1}^{N2} [v_m(z)\xi_m(t)] \text{ and } u_z^e(z,t) = \sum_{m=1}^{N3} [u_m(z)\zeta_m(t)],$$

where $N1$, $N2$, and $N3$ are appropriately chosen integers, depending on the accuracy needed for each case. The functions w_m, v_m, and u_m are also chosen based upon both experimental and theoretical observations and results provided by previous investigations. Using equation (1), the displacement form for a rigid roof at the top of the tank is readily obtained. The trial functions for the cylindrical shell are chosen so that:

$$w_m(0) = v_m(0) = u_m(0) = 0, \quad m = 1,2, \ldots$$

Then, if the extra subscript u denotes the part of the displacements due to uplift, the total bottom plate displacements can be expressed by:

$$\hat{u}_r(r,\theta t) = [x_g(t) + h_b\phi_f(t)]\cos\theta + u_{ru}(r,\theta,t) \quad (4)$$

$$\hat{u}_\theta(r,\theta,t) = -[x_g(t) + h_b\phi_f(t)]\sin\theta + u_{\theta u}(r,\theta,t) \quad (5)$$

Downloaded 03 May 2010 to 171.66.16.21. Redistribution subject to ASME license or copyright; see http://www.asme.org/terms/Terms_Use.cfm

$$\hat{u}_z(r,\theta,t) = -r\phi_f(t)\cos\theta + u_{zu}(r,\theta,t) \tag{6}$$

Ground/Structure Interaction

The dynamic response of a structure supported on flexible ground can be significantly different from the response of the same structure supported rigidly. However, the exact formulation of the general sound/structure interaction problem is still associated with considerable difficulties and uncertainties. Analytical solutions are available for some simple cases, in most of which a rigid circular or rectangular footing is considered to rest on a homogeneous, isotropic, linearly elastic, semi-infinite body which undergoes small strains. Based on results of such solutions, the ground/structure interaction modes can often be represented by equivalent springs (Richart et al., 1970; Tsai et al., 1974).

In the present study, the ground/structure interaction is modeled by placing two springs at the point G of the foundation. One of them is infinitely rigid and avoids any sliding of the foundation with respect to the ground. The other one is a rotational spring, allowing for rocking of the foundation and the whole structure by an angle ϕ_f about the y-axis. It is believed that in this way the important aspects of the ground/structure interaction are adequately modeled.

Fluid Response in a Cylindrical Tank

For the purposes of the present investigation, the fluid is assumed to be ideal and the flow irrotational. The fluid velocity field can then be expressed in terms of a scalar potential function Φ, which by applying the continuity equation is found to satisfy the Laplacian, throughout the fluid domain. Considering small amplitude surface waves, conservative body forces, neglecting the free surface tension effects and matching the fluid and structural velocities normal to the wetted shell and bottom plate surfaces, the boundary value problem for Φ is set up as follows:

$$\nabla^2\Phi(r,\theta,z,t) = 0 \quad \text{in the fluid domain} \tag{7}$$

$$\frac{\partial^2\Phi}{\partial t^2} + g\frac{\partial\Phi}{\partial z} = 0 \quad \text{on } z = H \tag{8}$$

$$\frac{\partial\Phi}{\partial z} = \frac{\partial\hat{u}_z}{\partial t}(r,\theta,t) \quad \text{at } z = 0 \tag{9}$$

$$\frac{\partial\Phi}{\partial r} = \frac{\partial u_r}{\partial t}(\theta,z,t) \quad \text{at } r = R \tag{10}$$

Then, if P_o is the external pressure on the liquid free surface, the pressure distribution in the fluid domain is given by:

$$P(r,\theta,z,t) = P_o + \rho_l g(H-z) - \rho_l\frac{\partial\Phi}{\partial t}(r,\theta,z,t) \tag{11}$$

The last term in the above expression gives the hydrodynamic pressure, P_d, resulting from the fluid motion.

First, the velocity potential Φ and the structural velocities are expanded in Fourier series in the θ-direction. Utilizing the linearity of the system and the orthogonality properties of the sine and cosine functions in $0<\theta\le 2\pi$, it is then clear that instead of the initial system in equations (7)-(10), only the problem for each Fourier component of Φ, $\partial\hat{u}_z/\partial t$ and $\partial u_r/\partial t$ say, Φ_n, f_n, and h_n, respectively, has to be solved. Using standard separation of variables techniques, it is found (Natsiavas, 1986) that the general solution of this problem has the following form:

$$\Phi_n(r,z,t) = \left(\frac{r}{R}\right)^n\left[a_n(t)\frac{z}{H} + b_n(t)\right]$$

$$+\sum_{s=1}^{\infty}\left\{J_n\left(k_{ns}\frac{r}{R}\right)\left[A_{ns}(t)\cosh\left(k_{ns}\frac{r}{R}\right)\right.\right.$$

$$\left.\left.+B_{ns}(t)\sinh\left(k_{ns}\frac{z-H}{R}\right)\right] + I_n\left(\lambda_s\frac{r}{H}\right)C_{ns}(t)\cos\left(\lambda_s\frac{z}{H}\right)\right\},$$

where J_n is the Bessel function and I_n is the modified Bessel function of the first kind of order n and

$$J_n'(k_{ns}) = 0$$

$$s = 1,2,\ldots, \quad n = 0,1,\ldots$$

$$\lambda_s = s\pi$$

The prime indicates derivative of a Bessel function with respect to its argument. For analytical convenience, h_n is decomposed into a rocking and a flexible component, as follows:

$$h_n(z,t) \equiv \alpha_n(t)z + \bar{h}_n(z,t).$$

Applying the boundary conditions of the system, together with some properties of the Bessel functions, the time functions a_n, b_n, A_{ns}, B_{ns} and C_{ns} are determined to be as follows, for zero initial conditions:

$$a_n(t) = \frac{1}{n}RH\alpha_n(t)$$

$$(a_o(t) = 0 = b_o(t))$$

$$b_n(t) = \frac{R}{nH}\int_0^H \bar{h}_n(z,t)dz$$

$$C_{ns}(t) = \frac{2}{\lambda_s I_n'(\lambda_s R/H)}\int_o^H \bar{h}_n(z,t)\cos\left(\lambda_s\frac{z}{H}\right)dz$$

$$B_{ns}(t) = 2R^2\frac{b_{ns}(t) - \alpha_n(t)J_n(k_{ns})}{k_{ns}(k_{ns}^2 - n^2)J_n^2(k_{ns})\cosh(\mu_{ns})}$$

$$A_{ns}(t) = D_{ns}(t) - \omega_{ns}\int_o^t [E_{ns}(\tau) + D_{ns}(\tau)]\sin\omega_{ns}(t-\tau)d\tau$$

with

$$b_{ns}(t) = \left(\frac{k_{ns}^2}{R^3}\right)\int_o^R rJ_n\left(k_{ns}\frac{r}{R}\right)f_n(r,t)dr$$

$$E_{ns}(t) = \frac{2n\ a_n(t)}{\not<_{ns}(k_{ns}^2 - n^2)J_n(k_{ns})\sinh(\mu_{us})} + \frac{B_{ns}(t)}{\sinh(\mu_{ns})}$$

$$D_{ns}(t) = -2\frac{n[a_n(t) + b_n(t)] + d_{ns}(t)}{(k_{ns}^2 - n^2)J_n(k_{ns})\cosh(\mu_{ns})}$$

$$d_{ns}(t) = \sum_{p=1}^{\infty}\left[(-1)^p\frac{(\lambda_p R/H)I_n'(\lambda_p R/H)}{1 + (\lambda_p/\mu_{ns})^2}C_{np}(t)\right]$$

$$\mu_{ns} = k_{ns}\frac{H}{R} \text{ and } \omega_{ns}^2 = g\frac{k_{ns}}{R}\tanh(\mu_{ns}).$$

For the scope of this study, the solution of the fluid response problem is only needed for the cases of rigid body translation and rotation as well as for the beam-type modes of the shell. In all these cases $n=1$ and the solution is much simpler than the general solution. For example, for a tank rotation about the y-axis with:

$$f(r,\theta,t) = -cr\dot{\phi}(t)\cos\theta \text{ and } h(\theta,z,t) = z\dot{\phi}(t)\cos\theta,$$

it easily follows from the general solution that the corresponding hydrodynamic pressure is:

Downloaded 03 May 2010 to 171.66.16.21. Redistribution subject to ASME license or copyright; see http://www.asme.org/terms/Terms_Use.cfm

$$P_\phi(r,\theta,z,t) = -p_l R\cos\theta\{f_\phi(r,z)R\ddot{\phi}(t) + \sum_{s=1}^{\infty}[f_{\phi s}(r,z)R\bar{A}_{\phi s}(t)]\} \tag{12}$$

with

$$f_\phi(r,z) = \frac{rz}{R^2} - 2\sum_{s=1}^{\infty} J_1\left(k_s\frac{r}{R}\right) \times \frac{\mu_s\cosh(\mu_s z/H) - (c+1)\sinh(\mu_s - \mu_s z/H)}{J_1(k_s)k_s(k_s^2-1)\cosh(\mu_s)} \tag{13}$$

$$f_{\phi s}(r,z) = 2J_1\left(k_s\frac{r}{R}\right) \times \frac{c+1-\cosh(\mu_s)+\mu_s\sinh(\mu_s)}{J_1(k_s)k_s(k_s^2-1)\sinh(\mu_s)}\cosh\left(\mu_s\frac{z}{H}\right) \tag{14}$$

$$\bar{A}_{\phi s}(t) = \int_o^t \omega_s\ddot{\phi}(\tau)\sin\omega_s(t-\tau)d\tau.$$

In all the above equations the subscript $n=1$ is dropped–except for J_1–for simplicity. The expressions for the other cases considered are found similarly. In all the cases, the so-called impulsive and convective terms are readily identified.

Equations of Motion for Unanchored Tanks

The equations describing the dynamic behavior for the overall system are derived by using Hamilton's principle in the form:

$$\delta T + \delta W = \delta U \tag{15}$$

where T is the kinetic energy, W is the work done by the "external" forces, and U is the strain energy of the system. The kinetic energy of the system is obtained directly by using the expressions for the structural displacements. The total strain energy U of the system consists of the strain energy U_c of the shell, the strain energy U_u of the bottom plate and the energy U_f developed from the interaction between the foundation and the ground. Lack of knowledge of the total bottom plate displacements prevents the explicit calculation of δU_u at this point.

For the case considered, the hydrodynamic pressure can be decomposed as

$$P_d = P_x + P_f + P_u + \sum_{m=1}^{N1} P_m.$$

The component P_x represents the hydrodynamic pressure due to rigid body translation of the tank along the x-axis. P_f is the pressure resulting from the rigid body rotation ϕ_f about the y-axis, due to the ground flexibility. It is given by equation (12) but with ϕ replaced by ϕ_f and by setting $c=1$ in the expressions for f_ϕ and $f_{\phi s}$. Finally, P_u results from the uplifting motion of the structure, while the components P_m express the hydrodynamic pressure developed by the flexible radial modes of the shell.

Applying the liquid pressure as an external normal load on the wetted surfaces of the tank, the components of the traction vector are readily identified. Then, using the variations of the assumed displacements and neglecting the virtual work due to body forces, one can write:

$$\delta W = \delta W_c + \delta W_b \tag{16}$$

where

$$\delta W_c = \int_o^H\int_o^{2\pi} P(R,\theta,z,t)\delta u_r(\theta,z,t)Rd\theta dz,$$

$$\delta W_b = -\int_o^R\int_o^{2\pi} P(r,\theta,0,t)\delta u_z(r,\theta,t)rd\theta dr.$$

Since the uplifting part u_{zu} of the bottom plate vertical displacement is unknown, the virtual displacement δu_{zu}—which is part of the virtual displacement resulting in δW_b—and the pressure component P_u associated with the uplifting motion of the tank cannot be determined. To overcome this, it is first observed that in the above calculation for δW_c, only the $\cos\theta$ component of the total pressure P will survive the required θ-integration and will eventually contribute to δW_c. This is so because the virtual displacement appearing in the corresponding integrand is proportional to $\cos\theta$, implying that only the $\cos\theta$ component of P_u, and therefore of u_{zu}, is of importance in determining δW_c. A reasonable and convenient choice for this component of u_{zu} is $-cr\phi_u\cos\theta$, where c is a constant. Clearly, $c=1$ means that the bottom plate participates completely in the rocking motion of the structure due to uplift, while $c=0$ means that the bottom plate remains flat and only the shell undergoes the rocking motion due to uplift. What happens in reality is something in between these two extreme cases. Using the above assumption for the displacement u_{zu}, the hydrodynamic pressure due to uplift is decomposed as

$$P_u = \bar{P}_u + \Delta P_u,$$

where $\bar{P}_u$ represents the $\cos\theta$ component and ΔP_u contains the rest of P_u. The $\bar{P}_u$ component is found from equation (12), replacing ϕ by ϕ_u. These then allow the computation of δW_c, without requiring knowledge of ΔP_u. Next, using equation (6), the virtual work δW_b done at the bottom plate area S_b is further decomposed in two parts, as

$$\delta W_b = \delta W_f + \delta W_u \tag{17}$$

$$\delta W_f = \int_{S_b} P(r,\theta,0,t)[-r\delta\phi_f(t)\cos\theta]dS,$$

$$\delta W_u = \int_{S_u} P(r,\theta,0,t)\delta u_{zu}(r,\theta,t)dS,$$

where S_u is the uplifted area of the bottom plate. For the calculation of δW_f, only the $\cos\theta$ component of P—and, therefore, of P_u—is needed. Using the previously assumed form for the $\cos\theta$ component of u_{zu} one can then determine δW_f, but the virtual work δW_u done on the bottom plate due to uplift can not be determined directly here, since u_{zu} is unknown.

Uplift Formulation and Static Tilt Tests. As a consequence of the fact that the uplifting part of the bottom plate displacements is unknown, some terms appearing during the application of Hamilton's principle are not amenable to direct formulation. These terms include δW_u, δU_u and the kinetic energy of the uplifted part of the bottom plate. Although the contribution of the latter term seems to be negligible and can be ignored, the other two terms are thought to be important and are included in the present analysis, as explained below.

Using the relations (15)-(17), Hamilton's principle can be expressed in the following form:

$$\delta T + (\delta W_c + \delta W_f + \delta W_u) = (\delta U_c + \delta U_f + \delta U_u).$$

Collecting the two unknown terms δW_u and δU_u together and defining the virtual quantity δV_u, by

$$\delta V_u \equiv \delta U_u - \delta W_u \tag{18}$$

the extended form of Hamilton's principle can be rewritten as

Downloaded 03 May 2010 to 171.66.16.21. Redistribution subject to ASME license or copyright; see http://www.asme.org/terms/Terms_Use.cfm

$$\delta V_u = \delta T + (\delta W_c - \delta U_c) + (\delta W_f - \delta U_f) \tag{19}$$

Direct analytical evaluation for the δV_u term in the above equation requires the solution of the contact problem at the base of the tank for any instant in time. In those calculations, nonlinear strain-displacement relations should be used for the behavior of the bottom plate. However, these difficulties can be overcome following approximate approaches. Namely, critical examination of Shih's (1981) experimental data revealed that the behavior of the tank may be described adequately by placing an appropriate rotational spring between the bottom plate and the foundation. The characteristics of this nonlinear spring can be obtained from static considerations alone. Next, a procedure is explained for obtaining this spring's characteristics from static tilt tests. For such tests, the δT term is absent. By assuming a rigid foundation the δW_f and δU_f terms also disappear. Then, carrying the bar symbol as a distinction between the quantities corresponding to the static tilt tests and the similar quantities for the dynamic case, equation (19) takes the form:

$$\delta \bar{V}_u = \delta \bar{W}_c - \delta \bar{U}_c.$$

From the experimental data of Clough and Niwa (1979), it can be deduced that the flexible components of the shell displacements are negligible compared to the rocking component due to base uplift. This being the case, then

$$\delta \bar{W}_c = \int_{S_c} \bar{P}_{st}(R,\theta,z)(z\delta\phi_u \cos\theta) dS,$$

where $\bar{P}_{st}$ is the hydrostatic pressure exerted on the wetted cylindrical shell, of surface S_c, of the tilted tank. If one defines the resulting moment with respect to the origin 0 by

$$\bar{M}_c \equiv \int_{S_c} \bar{P}_{st}(R,\theta,z) z \cos\theta dS$$

and if $\delta \bar{U}_c$ is left out, then it follows that

$$\delta \bar{V}_u = \bar{M}_c \delta\phi_u. \tag{20}$$

Finally, by assuming that

$$\delta \bar{V}_u = \delta V_u \tag{21}$$

and using (21), equation (19) can be rewritten as

$$\bar{M}_c \delta\phi_u = \delta T + (\delta W_c - \delta U_c) + (\delta W_f - \delta U_f) \tag{22}$$

The equations (20) and (21) imply that during the static tilt tests the shell flexibility effects are negligible. Also, both the pressure distribution and the deformation at the bottom plate should be close enough to those developed during the dynamic base excitation. The available information suggests that these assumptions are sufficiently accurate, at least for tall tanks. For completeness, the validity of these assumptions should also be investigated for the case of broad tanks and proper modifications must be imposed, if needed.

Governing Equations for the Coupled System. Knowledge of the relation between the moment $\bar{M}_c$ and the system parameters allows one to proceed from equation (22) to generate the system equations in matrix form, as follows:

$$\mathbf{M}\ddot{\underline{x}} + \mathbf{K}\underline{x} = -\ddot{x}_g(t)\underline{\mathbf{f}} \tag{23}$$

The vector $\underline{x}$ contains the unknowns of the problem in the following order:

$$\underline{x}(t) = [\psi_1, \ldots \psi_{N1}, \xi_1, \ldots \xi_{N2}, \zeta_1, \ldots \zeta_{N3}, R\phi_f, R\phi_u, \underline{x}_{sl}]^T.$$

The terms of the mass matrix $\mathbf{M}$, the nonlinear stiffness matrix $\mathbf{K}$ and the vector $\underline{\mathbf{f}}$ have been found in closed form by the author (1986). The vector $\underline{x}_{sl}$ accounts for the sloshing degrees-of-freedom. The sloshing terms appear only in the expressions of the hydrodynamic pressures, while the variations in Hamilton's principle apply only to the displacements. For this reason, the sloshing effects are included in the analysis by making use of the definition of the sloshing spectral accelerations.

Summary

An analytical model is developed for the response of unanchored fluid-filled tanks, subjected to base excitation. First, the hydrodynamic problem is solved in closed form for the most general motion of the tank. This eliminates the unknowns describing the fluid response—except for those associated with sloshing—and only parameters associated with the structural response remain to be determined. Then, application of Hamilton's principle in the structural domain completes the geometrical discretization and results in a system of ordinary differential equations governing the behavior of the coupled fluid/structure/ground system. During this procedure, the complex nonlinear behavior of base uplift is modeled by placing an appropriate nonlinear spring between the bottom of the tank and its foundation. Equivalent springs are also used for the formulation of the ground flexibility. Effects due to shell flexibility and liquid sloshing are also included in the analysis. Beam-type deformation, with additional provisions for circumferential straining and inplane shear of the cylindrical shell and horizontal base excitation are assumed. The applicability and effectiveness of this analysis is verified by comparison with experimental work, reported in a companion paper.

Acknowledgments

The author wishes to thank his advisor, Professor C. D. Babcock, for suggesting this problem and for his indispensable help throughout the period of this research study. The help of Professor P. C. Jennings in reviewing and correcting the final manuscripts is also gratefully acknowledged. This work was supported by the California Institute of Technology, through the President's Venture Fund.

References

Auli, W., Fischer, D. F., and Rammerstorfer, F. G., 1985, "Uplifting of Earthquake-Loaded Liquid-Filled Tanks," ASME *1985 PVP Conf.*, New Orleans, LA.

Anonym, 1984, "AWWA Standard for Welded Steel Tanks for Water Storage," *ANSI/AWWA Standard D100-84*, American Water Works Association, Denver, CO.

Clough, R. W., Niwa, A., and Clough, D. P., 1979, "Experimental Study of Cylindrical Tanks," *J. Struct. Div.*, ASCE, Vol. 105, No. ST12, pp. 2565–2590.

Clough, R. W., and Niwa, A., 1979, "Static Tilt Tests of a Tall Cylindrical Liquid Storage Tank," Univ. of California, Berkeley, Report No. UCB/EERC-79/06.

Edwards, N. W., 1969, "A Procedure for the Dynamic Analysis of Thin Walled Cylindrical Liquid Storage Tanks Subjected to Lateral Ground Motion," Ph.D. Dissertation, Univ. of Michigan, Ann Arbor.

Hanson, R. D., 1973, "Behavior of Liquid-Storage Tanks," *The Great Alaska Earthquake of 1964* (Engr. Section), National Academy of Sciences, Washington, DC, pp. 331–339.

Haroun, M. A., 1980, "Dynamic Analyses of Liquid Storage Tanks," Ph.D. Thesis, Report No. EERL 80-04, Caltech, Pasadena, CA.

Haroun, M. A., 1983, "Vibration Studies and Tests of Liquid Storage Tanks," *Earthq. Engr. Struct. Dyn.*, Vol. 11, pp. 179–206.

Housner, G. W., 1957, "Dynamic Pressures on Accelerated Fluid Containers," *Bull. Seism. Soc. America*, Vol. 47, No. 1, pp. 15–35.

Liu, W. K., and Lam, D., 1983, "Nonlinear Analysis of Liquid-Filled Tanks," *J. Engr. Mech.*, ASCE, Vol. 109, No. 6, pp. 1344–1357.

Ishida, K., and Kobayashi, N., 1985, "An Effective Method of Analyzing Rocking Motion for Unanchored Cylindrical Tanks Including Uplift," ASME *1985 PVP Conf.*, New Orleans, LA.

Manos, G. C., and Clough, R. W., 1982, "Further Study of the Earthquake Response of a Broad Cylindrical Liquid Storage Tank Model," Univ. of California, Berkeley, Report No. UCB/EERC-82/07.

Nash, W. A., Balendra, T., Shaaban, S. H., and Mouzakis, T., 1978, "Finite Element Analysis of Seismic Response of Cylindrical Tanks," ASCE *Conv. Expos.*, Preprint 3315), Chicago, IL.

Downloaded 03 May 2010 to 171.66.16.21. Redistribution subject to ASME license or copyright; see http://www.asme.org/terms/Terms_Use.cfm

Natsiavas, S., 1986, "On the Seimic Response of Liquid Storage Tanks," *GALCIT SM Report 86-2*, Caltech, Pasadena, CA.

Peek, R., 1986, "Analysis of Unanchored Liquid Storage Tanks Under Seismic Loads," Ph.D. Thesis, Report No. EERL 86-01, Caltech, Pasadena, CA.

Richart, Jr., F. E., Hall, J. R., and Woods, R. D., 1970, *Vibrations of Soils and Foundations*, Prentice-Hall, Inc., Englewood Cliffs, NJ.

Rinne, J. E., 1967, "Oil Storage Tanks," *The Prince William Sound, Alaska Earthquake of 1964 and Aftershocks*, U.S. Dept. of Commerce, E.S.S.A., Coast and Geodetic Survey, Washington, DC, Vol. II, Part A, pp. 245–252.

Shih, C. F., 1981, "Failure of Liquid Storage Tanks Due to Earthquake Excitation," Ph.D. Thesis, Report No. EERL 81-04, Caltech, Pasadena, CA.

Shih, C. F., and Babcock, C. D., 1987, "Buckling of Oil Storage Tanks in SPPL Tank Farm During the 1979 Imperial Valley Earthquake," ASME *Journal of Pressure Vessels and Technology*, Vol. 109, pp. 249–255.

Tsai, N. C., Niehoff, D., Swatta, M., and Hadjian, A. H., 1974, "The Use of Frequency-Independent Soil-Structure Interaction Parameters," *Nucl. Engr. Des.*, Vol. 31, No. 2, pp. 168–185.

Veletsos, A. S., and Yang, J. Y., 1976, "Dynamics of Fixed-Base Liquid Storage Tanks," *Proceedings of the U.S.-Japan Seminar for Earthq. Engr. Res.*, Tokyo, Japan.

Wozniak, R. S., and Mitchell, W. W., 1978, "Basis of Seismic Response Provisions for Welded Oil Storage Tanks," *Proceedings of the API Convention*, Toronto, Canada.

Downloaded 03 May 2010 to 171.66.16.21. Redistribution subject to ASME license or copyright; see http://www.asme.org/terms/Terms_Use.cfm

Behavior of Unanchored Fluid-Filled Tanks Subjected to Ground Excitation

S. Natsiavas
Assistant Professor.
Mechanical and Aerospace Engineering,
Arizona State University,
Tempe, AZ 85287
Assoc. Mem. ASME

C. D. Babcock
Professor of Aeronautics and Applied Mechanics.
California Institute of Technology,
Pasadena, CA 91125

An analysis developed for the response of liquid storage tanks under horizontal base excitation is employed and numerical results are obtained for unanchored tanks. These results are compared and found to be in good agreement with experimental data. Base uplift is shown to cause a dramatic reduction in the effective beam-type stiffness of a tank, which in turn reduces the tank response frequency and changes the developed hydrodynamic loads significantly. Based on these results, an explanation is provided for some great qualitative and quantitative differences in the behavior of a tank, resulting from its base fixity condition alone.

Introduction

Most of the analytical studies performed on the behavior of fluid-filled tanks during base excitation have focused on the response of anchored tanks (e.g., Housner, 1957; Veletsos, 1974; Haroun, 1980; Daysal and Nash, 1982). On the other hand, most of the storage tanks encountered in the field are essentially unanchored. Even when some type of anchoring is provided, the connection between the base of the tank and its foundation is usually insufficient to prevent tank lift off during strong earthquakes. This fact has repeatedly been made clear in reports of earthquake response (Rinne, 1967; Jennings, 1971; Hanson, 1973). In these cases, the connections or the tank foundation itself cannot resist earthquake loads with magnitude close to the loads which cause buckling at the bottom of an anchored tank and they usually fail under much lower loads than those causing buckling. As a result, the bottom of the tank lifts off the foundation before buckling occurs.

The analytical modeling of the behavior of an unanchored tank during base excitation is inherently nonlinear and, as a consequence, not much analytical work has been reported on the dynamic response so far. However, experimental studies have shown that an unanchored tank develops much greater axial membrane stresses at the bottom than an anchored one under the same loading conditions (Shih, 1981). Also, in some cases the buckling at the bottom of an unanchored tank can appear for amplitudes of the ground acceleration an order of magnitude less than those for an anchored tank. This is due to the different mechanisms by which the earthquake loads are developed and resisted by anchored and unanchored tanks. Similar results were provided by other experimental studies too (Clough et al., 1979a, and 1979b; Manos and Clough, 1982). These studies demonstrated the need for better models in designing liquid storage tanks against earthquake loads. The recent work reported by Auli, Fischer, and Rammerstorfer (1985), Ishida and Kobayashi (1985), and Peek (1986) represents efforts towards improving the analysis of the behavior of unanchored tanks.

In this paper, the analysis developed by the first author (1987) is applied to cases of unanchored tanks, for which there are available experimental results. First, data from static tilt tests are obtained in order to derive the characteristics of the nonlinear rotational spring modeling the base uplift of the unanchored tanks considered. The effect of this spring on the dynamics of the system is then examined parametrically. Finally, numerical results are obtained and compared with experimental data, for unanchored tanks under harmonic and transient base excitation.

Some Observations on the Dynamics of Unanchored Tanks

In developing the analysis for the dynamic response of unanchored tanks, some of the experimental results presented by Shih (1981) were first examined critically. Those experiments were run with model tanks made of plastic with material properties and dimensions as shown in Table 1. In applying these results to a steel tank, the geometry of the prototype has to be scaled by 41, the frequencies by 6.4, while the amplitude of the base acceleration should be the same in both the model and the prototype. Examination of the experimental results revealed a substantial reduction in the frequency of the predominant response mode. This reduction was solely induced by the base uplift. For example, for the IIb2 model tank (see Table 1) the lowest $n=1$ frequency was reduced from about 32 Hz in the anchored case to about 8 Hz for the unan-

Contributed by the Applied Mechanics Division for presentation at the Winter Annual Meeting, Chicago, IL, November 28 to December 2, 1988 of THE AMERICAN SOCIETY OF MECHANICAL ENGINEERS.

Discussion on this paper should be addressed to the Editorial Department, ASME, United Engineering Center, 345 East 47th Street, New York, N.Y. 10017, and will be accepted until two months after final publication of the paper itself in the JOURNAL OF APPLIED MECHANICS. Manuscript received by ASME Applied Mechanics Division, July 20, 1987; final revision, February 23, 1988.

Paper No. 88-WA/APM-50.

Copyright © 1988 by ASME
Downloaded 03 May 2010 to 171.66.16.21. Redistribution subject to ASME license or copyright; see http://www.asme.org/terms/Terms_Use.cfm

Table 1 Dimensions and properties of model tanks

Young's Modulus, E	5.07×10^{9} N/m^2
Poisson's Ratio, υ	0.3
Density, ρ_s	1390 Kg/m^3
Shell Radius, R	0.0635 m
Shell Length, L	0.2667 m
Shell Thickness, t_s	0.762×10^{-4}m
Roof Mass, m_r	0.0085 kg
Roof Moment of Inertia, I_r	8.6×10^{-6}kg/m^2
Foundation Moment of Inertia, I_f	0.037 kg m^2

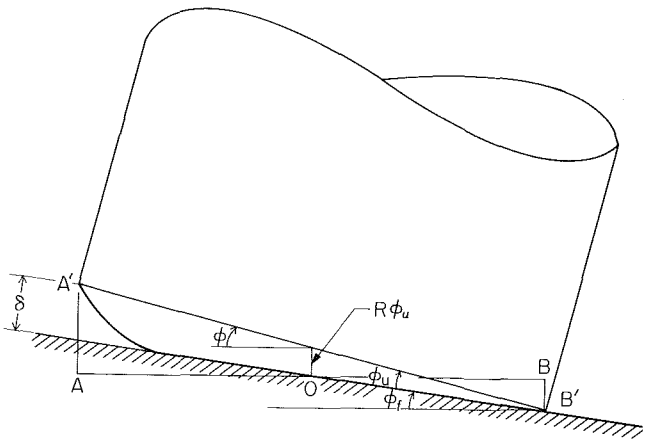


Fig. 1 Definition of base uplifting and foundation rocking angles

chored case. Such a drastic change in the fundamental frequency, resulting from changes in the fixity conditions, is typical in structures.

For the purposes of the present work, and in order to obtain analytical results for the IIb2 tank, static tilt tests were first performed for this specific tank. During these experiments the tank was filled with water up to specified levels and the uplifting displacement δ – see Fig. 1 – was measured for various tilting angles. In each case, the overturning moment $\bar{M}_c$ with respect to the center of the bottom plate, caused by the hydrostatic pressure exerted on the shell surface, is computed. It is pointed out here that studies like those of Peek (1986) or Auli et al. (1985) can provide the relation between $\bar{M}_c$ and ϕ_u analytically. This implies that the complete response behavior of unanchored tanks can be determined analytically.

The results of the present static tilt tests are shown in Fig. 2. Similar results can also be obtained from the data of Clough and Niwa (1979) and Manos and Clough (1982). These results reflect directly the fact that the base uplifting phenomenon is nonlinear. They also show that sufficiently large base uplift results in a substantial decrease of the stiffness at the base of the tank. These data, are in qualitative agreement with the results of the dynamic experiments of Shih (1981). These observations triggered the development of the present analytical model.

Base Uplift and Tank Dynamics

To examine the effect of the uplift on the tank dynamics, a parametric study is first carried out. The analysis developed by Natsiavas (1987) is applied, with:

$$w_m(z)=v_m(z)=u_m(z)=\sin\left[(2m-1)\frac{\pi z}{2L}\right]$$

and the IIb2 tank is chosen as model with water height $H=3R$. For this preliminary study, an equivalent linear relation between the base moment and the uplift angle was assumed, of the form:

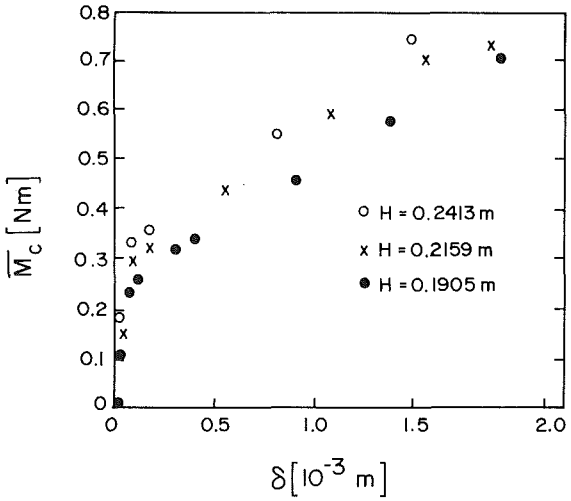


Fig. 2 Base moment versus uplift deflection for model tank IIb2

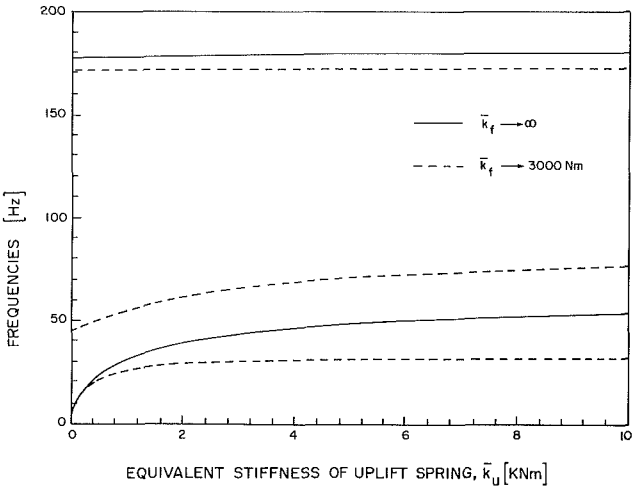


Fig. 3 Response frequencies versus uplift spring stiffness

$$\bar{M}_u=\bar{k}_u\phi_u.$$

Varying the value $\bar{k}_u$ of the effective stiffness of the spring modeling the base uplift, the first frequencies of the structure are obtained and plotted in Fig. 3. To predict the first two frequencies sufficiently accurately nine degrees-of-freedom ($N1=N1=N3=3$), representing the shell flexibility, had to be included in the calculations. The continuous lines in Fig. 3 represent frequencies for the case of rigid ground, while the broken lines give the frequencies for the case of a flexible ground with effective constant rotational stiffness $\bar{k}_f=3000$ Nm. For the case where the tank is anchored to its foundation ($\bar{k}_u \to \infty$), it is found that the first two frequencies of the system approach the values of 60 and 179 Hz for the case of rigid ground and the values of 32 and 83 Hz for the case of a flexible ground with $\bar{k}_f = 3000$ Nm, respectively.

For the system examined, the values of the uplift spring stiffness (30-500 Nm) lie in the range where the fundamental structural frequency is drastically affected by changes in the stiffness $\bar{k}_u$. Thus, one may expect this to have an important effect on the dynamics of the system, for excitations with a typical frequency content (5-30 Hz). Finally, comparing the continuous with the broken lines of Fig. 3, it is obvious that the ground flexibility results in an additional reduction of the structural frequencies, as expected. Also, for a ground excitation with a typical frequency content, the second mode may

Downloaded 03 May 2010 to 171.66.16.21. Redistribution subject to ASME license or copyright; see http://www.asme.org/terms/Terms_Use.cfm

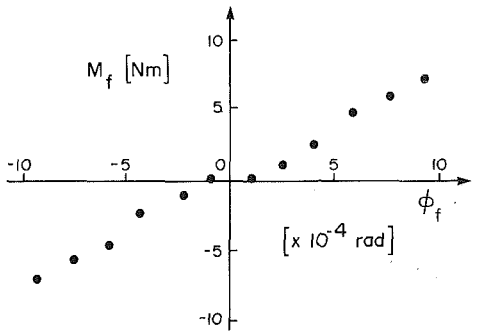


Fig. 4 Moment versus rotation relation of the shaking table

have an effect on the dynamics of the structure only for the case of a flexible ground.

Harmonic Buckling Tests

An explanation is provided here for the behavior of unanchored tanks during experiments reported by Shih (1981). For the harmonic tests, the base acceleration was of the form:

$$\ddot{x}_g(t) = a_0 \sin\omega t.$$

For any forcing frequency, the amplitude a_0 was increased gradually up until buckling – in the form of the diamond-shaped mode – occurred at the base of the tank. Here, results are obtained for the case of the IIb2 tank with $H = 3R$. The characteristics of the springs modeling the uplift are chosen from Fig. 2. Measuring the rotational stiffness of the shaking table used in the experiments resulted in a nonlinear moment versus rotation relationship, as shown in Fig. 4. This behavior is probably due to lack of good contact between the bearings of the table and the shafts they translate on. Since the resulting equations of motion are nonlinear, a direct time integration scheme (backward differentiation of order 1 to 5) is employed in obtaining the response history of the system. A damping matrix, $\mathbf{D}$, is chosen according to

$$\mathbf{D} = M\mathbf{X}\bar{D}\mathbf{X}^{-1},$$

where $\mathbf{X}$ is the matrix whose columns are the eigenvectors of $M^{-1}K$ and $\bar{\mathbf{D}}$ is a diagonal matrix. This choice of $\mathbf{D}$ preserves the normal modes for linear cases. In the present calculations, $\mathbf{D}$ is chosen so that 5 percent critical damping exists in all modes after proper linearization of the equations of motion of the system.

As a first step, the analysis is applied by using the values of the critical ground acceleration amplitude a_0, measured by Shih (1981). The corresponding moments, with respect to the center of the bottom plate of the tank, are then computed for any forcing frequency ω. Next, it is assumed that the buckling at the tank bottom starts for the same value in both the static and the dynamic cases. This critical value of the base moment was measured during the static tilt tests to be 0.71 Nm for the tank considered. Then, iterations are performed by changing the amplitude a_0 until the computed moment at the tank bottom has an amplitude of 0.71 Nm.

The results of the above procedure are shown in Fig. 5. In that figure, the x's indicate the experimental data of Shih (1981), while the continuous line represents the computed results, using the present analysis. The broken line, which is apparent at the low frequency range only, represents the results obtained by the same analysis after excluding the sloshing modes from the formulation. Obviously, the sloshing effects are important only when the forcing frequency is very close to the lowest sloshing frequency, which is about 2.7 Hz here. Also, it becomes clear that the behavior of the system for $\omega > 4$ Hz is governed by the uplift and not the sloshing modes.

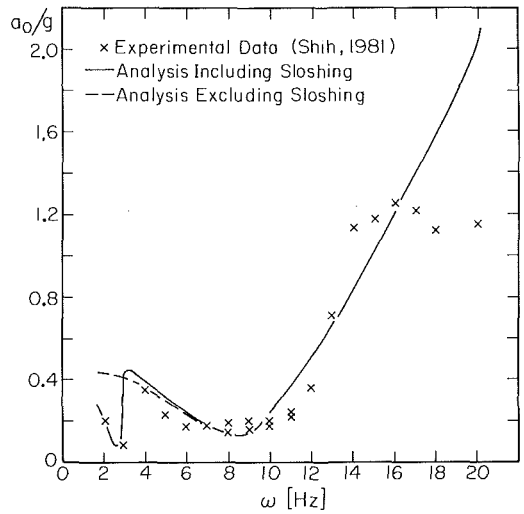


Fig. 5 Critical base acceleration versus excitation frequency

Finally, although near the fundamental frequency the sloshing response cannot be captured by linear analysis, the bottom moment is computed accurately. Only the fundamental sloshing mode was included in the computations, except for $\omega = 4$ Hz, which is close to the frequency of the second sloshing mode, where this sloshing mode was also included for better accuracy.

In all the above calculations, the shell flexibility effects were found to be negligible. Including the degrees-of-freedom associated with the shell flexibility caused virtually no change in the results which were obtained by using only the degrees-of-freedom modeling the base uplift and the ground flexibility effects. This important feature of the behavior was also captured by the preliminary linearized analysis and is in agreement with experimental observations, according to which the predominant response mode was rocking of the tank (Clough and Niwa, 1979; Shih, 1981). Examining in more detail the response histories of the system degrees-of-freedom, the sloshing effects are found to be important for $\omega = 2.5$ to 5 Hz. In the range $\omega = 7$ to 12 Hz, the uplift component is dominant, while for the rest of the frequencies the acceleration $R\ddot{\phi}_u$ was also important and comparable to a_o. As can be concluded from this information and Fig. 5, the first structural resonant frequency is about 8 Hz for the levels of excitation considered. The similar frequency for the same but anchored tank was found to be about 32 Hz (Shih, 1981). This dramatic change in the frequency of the predominant response mode of the structure is caused by the base uplift alone and has an important consequence. Namely, in the frequency range 4 to 8 Hz, the critical base acceleration for the anchored tank was measured by Shih (1981) to be about an order of magnitude larger than that for the unanchored one.

Comparing the analytical with the experimental values, good agreement is observed over all the frequency range examined, indicating the applicability and the effectiveness of the present analytical model, at least for the case of tall tanks. The largest discrepancy is observed for $\omega > 17$ Hz. However, even in those cases the base moment calculated using the experimental value for the critical base acceleration is close to 0.71 Nm. .For example, the moment calculated with the experimental critical a_0 for $\omega = 20$ Hz is 0.60 Nm.

During the numerical iterations, for values of ω between 6 and 9 Hz, some jump phenomena were observed. Namely, small changes in a_0 resulted in large differences in the moment amplitudes. This is expected for a softening nonlinear mode, such as the base uplift mode. Another feature of the behavior, encountered during the computations and associated with the

Downloaded 03 May 2010 to 171.66.16.21. Redistribution subject to ASME license or copyright; see http://www.asme.org/terms/Terms_Use.cfm

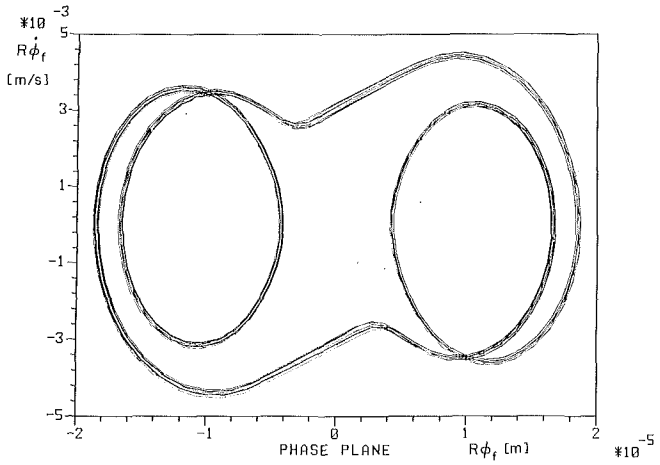


Fig. 6 Phase-plane for the foundation rocking dof ($t = 2.5$–3 sec)

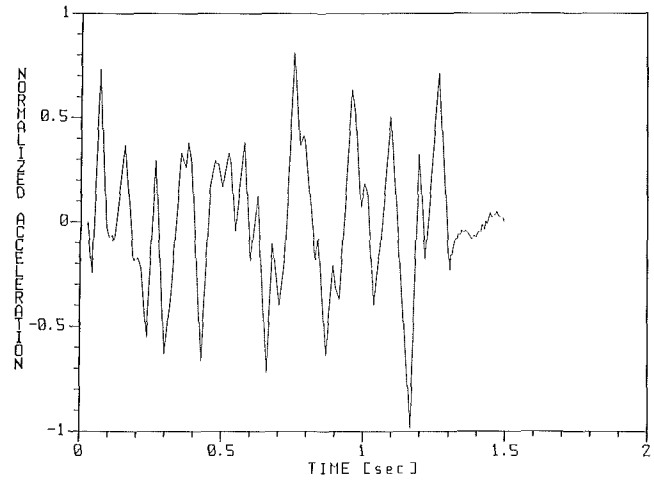


Fig. 7 Base acceleration history for the transient model tests (Shih, 1981), with simulated earthquake excitation

strongly nonlinear nature of the system, is discussed next. Namely, since the excitation is harmonic in time, one might expect the system to reach a periodic steady-state response in a few tens of cycles for the chosen level of damping. However, in some cases no periodic response was detected in the time ranges examined, while in some other cases a periodic steady-state solution was reached after relatively long periods of time. For example, Fig. 6 shows the phase-plane for the foundation rocking mode for $\omega = 20$ Hz, $a_0 = 2.06$ g and for the time period between 2.5 and 3 sec. In this case, a periodic steady-state was obtained, after about 100 forcing cycles. For 2 percent critical damping, a periodic steady-state was obtained after about 200 forcing periods. Trying to simulate better the experimental procedure, the analysis was run for the same case but with a ground acceleration amplitude of the form $a_0(1 - e^{-3t})$. In this case, a periodic steady-state solution was obtained after about the first 15 forcing cycles.

In order to investigate if this behavior was something characteristic of the system or due to a possible failure of the employed numerical scheme, the nonlinearity of the system was isolated and studied more carefully (Natsiavas, 1987). The highlights of this study are presented in the appendix. This study provided sufficient evidence that the strange behavior of the system was inherent to its dynamics and allowed the analysis for the structural system to be taken further. It must be pointed out that the long-time response of the system, when not periodic, was not far from being periodic and as a consequence there was no problem in determining the amplitude of the base moment.

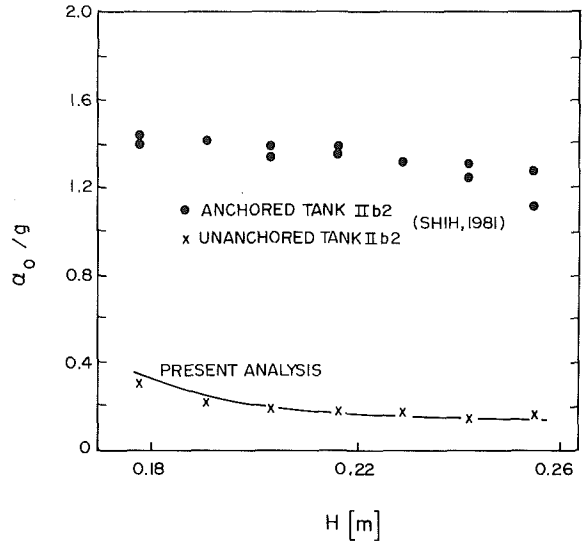


Fig. 8 Critical base acceleration versus water depth for the transient model tests with simulated earthquake excitation

Transient Buckling Tests

Results on the behavior of unanchored tanks subjected to transient base excitation are presented here and compared with experimental data reported by Shih (1981). These results are similar in nature to those presented for the harmonic base excitation cases and show once again that the behavior of the same tank can be quite different depending on the base fixity condition alone.

Using the same model tank (IIb2), results are obtained for a base excitation with acceleration history as shown in Fig. 7. This history was chosen to simulate an earthquake excitation. The results are presented in Fig. 8, where the x's indicate the experimental values obtained by Shih (1981) for an unanchored tank. The nearby continuous line represents the results by application of the present analysis, following the same methodology as for the harmonic base excitation cases. The dots indicate Shih's experimental results again but refering to the anchored case. Comparing the results for the anchored and unanchored case a large difference – factor of 4 to 7 – is again observed in the critical base acceleration. Two important factors are believed to cause this difference. First, the base loads result from a different response mechanism which produces different pressure distribution on the tank walls. The other reason is the large stress concentration which is expected for unanchored tanks, due to partial contact of the tank bottom with the ground.

The results obtained by the present analysis for the transient base excitation are again in good agreement with the experimental data. The amplitude of the critical ground acceleration was found to be virtually unaffected by inclusion of the sloshing modes in the formulation. Examining the computed history of the moment at the bottom of the tank, in most of the cases, the maximum moment occurred at a time when the amplitude of the base acceleration was also close to its maximum. However, in some cases the peak in the moment occurred well before the acceleration peak. It was also observed that although the excitation is transient – with most of its energy content concentrated between 0 and 20 Hz – the tank tends to respond in a frequency which is close to its resonant frequency, deduced from Fig. 5. Finally, the effects of shell flexibility, which were neglected for these calculations, seem once more to play no significant role.

Downloaded 03 May 2010 to 171.66.16.21. Redistribution subject to ASME license or copyright; see http://www.asme.org/terms/Terms_Use.cfm

Summary and Conclusions

Both the experimental and the analytical results presented show that there is a drastic change in the dynamic characteristics of an unanchored fluid-filled tank compared to the same tank, fully anchored. The effective stiffness of the beam-type deflection of the tank is substantially reduced when the base of the tank is allowed to lift off its foundation. This reduces the frequency of the predominant response mode of the structure, which in turn affects significantly the developed hydrodynmamic pressures through the fluid/structure coupling mechanism. When the tank is anchored, with base excitation of a typical frequency content, the hydrodynamic pressures are mostly due to the rigid body translation of the tank and partly due to the shell flexibility. For an unanchored tank, however, there is a pressure component resulting from the rocking of the tank induced by the base uplift. For the cases considered, this component was found to be comparable to that caused by the rigid body translation, or even bigger. Also, the pressure due to shell flexibility was practically negligible. These, together with the fact that a large stress concentration is expected for the axial membrane stresses at the base of an unanchored tank, explains why there can be a tremendous difference in the value of the amplitude of the ground acceleration causing buckling in an anchored or in an unanchored tank. Finally, the present results show that it can be significantly unconservative to calculate loads for an unanchored tank by assuming the tank to be anchored, as suggested by the current seismic codes as well as some previous studies on the subject.

Acknowledgments

The first author wishes to thank Prof. T. K. Caughey for valuable discussions on the nonlinear dynamics of the system presented in the appendix. The help of Prof. P. C. Jennings in reviewing and correcting the final manuscript is also gratefully acknowledged. This work was supported by the California Institute of Technology, through the President's Venture Fund and partly by the Los Alamos National Laboratories (Order Number 9-X15-Z3031-1).

References

Auli, W., Fischer, D. F., and Rammerstorfer, F. G., 1985, "Uplifting of Earthquake-Loaded Liquid-Filled Tanks," ASME *Proceedings of the 1985 PVP Conference*, New Orleans, LA.

Clough, R. W., Niwa, A., and Clough, D. P., 1979, "Experimental Study of Cylindrical Tanks," *J. Struct. Div.*, ASCE, Vol. 105, No. ST12, pp. 2565–2590.

Clough, R. W., and Niwa, A., 1979, "Static Tilt Tests of a Tall Cylindrical Liquid Storage Tank," Univ. of California, Berkeley, Report No. UCB/EERC-79/06.

Daysal, H., and Nash, W. A., 1984, "Soil Structure Interaction Effects on the Seismic Behavior of Cylindrical Liquid Storage Tanks," *Proc. 8th World Conf. Earthq. Engr.*, San Francisco, CA, Vol. 7, pp. 445–452.

Guckenheimer, J., and Holmes, P., 1983, *Nonlinear Oscillations, Dynamical Systems, and Bifurcations of Vector Fields*, Springer-Verlag, New York.

Hanson, R. D., 1973, "Behavior of Liquid-Storage Tanks," *The Great Alaska Earthquake of 1964*, Engr. Section, National Academy of Sciences, Washington, DC, pp. 331–339.

Housner, W. A., 1963, "The Dynamic Behavior of Water Tanks," *Bull. Seism. Soc. America*, Vol. 53, No. 1, pp. 381–387.

Haroun, M. A., 1980, "Dynamic Analyses of Liquid Storage Tanks," Ph.D. Thesis, Report No. EERL 80-04, Caltech, Pasadena, CA.

Ishida, K., and Kobayashi, N., 1985, "An Effective Method of Analyzing Rocking Motion for Unanchored Cylindrical Tanks Including Uplift," ASME *Proceedings of the 1985 PVP Conference*, New Orleans, LA.

Jennings, P. C., ed., 1971, "Engineering Features of the San Fernando Earthquake," Report No. EERL 71-02, Caltech, Pasadena, CA, pp. 434–470.

Manos, G. C., and Clough, R. W., 1982, "Further Study of the Earthquake Response of a Broad Cylindrical Liquid Storage Tank Model," Univ. of California, Berkeley, Report No. UCB/EERC-82/07.

Natsiavas, S., 1987, "Response and Failure of Fluid-Filled Tanks Under Base Excitation," Ph.D. Thesis, GALCIT SM Report 86-26, Caltech, CA.

Peek, R., 1986, "Analysis of Unanchored Liquid Storage Tanks Under Seismic Loads," Ph.D. Thesis, Report No. EERL 86-01, Caltech, Pasadena, CA.

Rinne, J. E. 1967, "Oil Storage Tanks," *The Prince William Sound, Alaska Earthquake of 1964 and Aftershocks*, U.S. Dept. of Commerce, E.S.S.A., Coast and Geodetic Survey, Washington, DC, Vol. II, Part A, pp. 245–252.

Shih, C. F., 1981, "Failure of Liquid Storage Tanks Due to Earthquake Excitation," Ph.D. Thesis, Report No. EERL 81-04, Caltech, Pasadena, CA.

Veletsos, A. S., 1974, "Seismic Effects in Flexible Liquid Storage Tanks," *Proc. 5th World Conf. Earthquake Engr.*, Rome, Italy, Vol. 1, pp. 630–639.

APPENDIX

Complicated Dynamics of a Simple Oscillator

Some unusual results are presented, obtained from the study of a single degree-of-freedom oscillator whose behavior is described by the following equation:

$$\ddot{x}+2\zeta\bar{\omega}\dot{x}+k(x)=f\sin\omega t.$$

The restoring force of this oscillator has the general form:

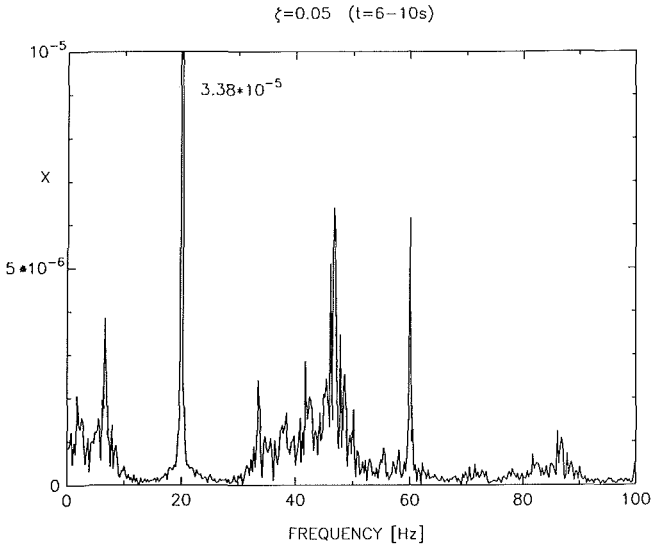


Fig. 9 Fourier spectrum of the displacement history

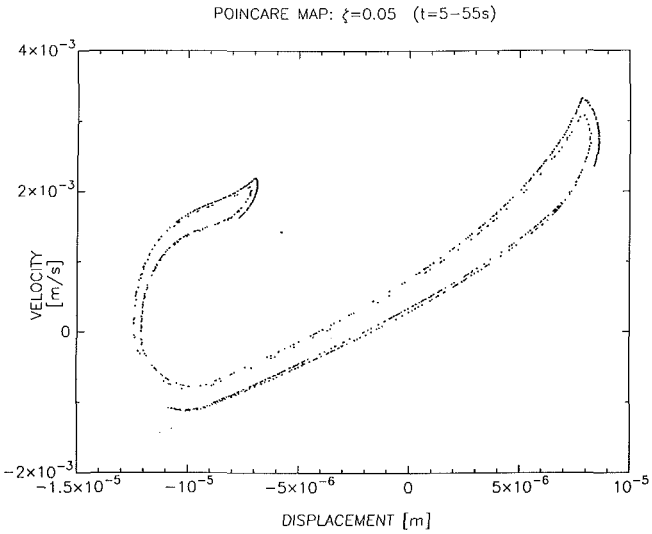


Fig. 10 Poincare map

Downloaded 03 May 2010 to 171.66.16.21. Redistribution subject to ASME license or copyright; see http://www.asme.org/terms/Terms_Use.cfm

$$k(x) = \begin{cases} \omega_1^2 x, & |x| \leq x_c \\ \omega_2^2 x + (\omega_1^2 - \omega_2^2) x_c \, sgn(x), & |x| > x_c, \end{cases}$$

as suggested by the experimental data shown in Figs. 2 and 4. This system satisfies all the theoretical requirements for the existence of a unique solution. However, its complete response history cannot be obtained in closed form since the determination of the instances of time at which the displacement x takes the value x_c or $-x_c$ requires the solution of a transcendental equation. Therefore, the response of the system is determined according to the following procedure. Any time the solution x crosses the x_c or $-x_c$ line in the x-t plane, the appropriate form of the oscillator equation is first chosen, depending on which x-interval the solution enters. Then, the corresponding values of x and $\dot{x}$ at the cross-point are used as initial conditions and the complete time history (homogeneous plus particular solution) is utilized in closed form, just up until the next crossing of x and x_c or $-x_c$ happens. The value of t_c – and therefore of $\dot{x}_c$ – at each cross-point is iteratively obtained to a specific numerical accuracy.

Following the above procedure, it was observed that for cases with sufficiently small changes in the stiffness ($\omega_1 \sim \omega_2$), relatively small or large forcing amplitudes f and large ζ, a periodic steady-state was obtained. However, the response could be very complicated for cases in which the above were not satisfied. Typical results are presented here for the case with $\zeta = 0.05$, $\bar{\omega} = 60$ Hz, $x_c = 9 \times 10^{-6}$ m, $f = 1$ m/s^2, $\omega = 20$ Hz, $\omega_1 = 4$ Hz, $\omega_2 = 65$ Hz and zero initial conditions. Figure 9 shows the Fourier spectrum for the response between 6 and 10 sec. The nonperiodicity of the solution in that time interval is indicated by the fact that the spectrum is distributed broadly over wide frequency bands. Drawing the phase-plane over such long periods of time, the trajectories densely fill a large area. If, instead of drawing the whole trajectory, a single point of it is plotted on the phase-plane every forcing period, a Poincare map is obtained. Figure 10 shows the Poincare map for the system, for the time between 5 and 55 sec (100-1100 forcing cycles). This map provides an additional indication for the nonperiodicity of the solution. The shape of the obtained strange attractor was found to be independent on the initial conditions and the accuracy of the numerical calculations, which is not the case for the solution itself. Also, this map indicates a boundedness in the solution. Note that the same system exhibited a periodic steady-state for $\zeta = 0.15$.

The above results are not yet extensive but, since they were derived from the exact solution, they indicate that the system examined can exhibit a strange behavior for some combinations of its parameters. The characteristics of the solution in these cases, such as the non periodic long-time response and the large sensitivity to the initial conditions and the numerical accuracy in computing the crossing times, suggest that the system under consideration may experience *chaotic* behavior for some combinations of its parameters. So far, such behavior has been observed experimentally and numerically for other systems (e.g., Guckenheimer and Holmes, 1983).

Downloaded 03 May 2010 to 171.66.16.21. Redistribution subject to ASME license or copyright; see http://www.asme.org/terms/Terms_Use.cfm

Response of a Compliant Slab to Viscous Incompressible Fluid Flow

C. A. Evrensel
Department of Mechanical Engineering,
University of Nevada-Reno,
Reno, NV 89557-0030
Mem. ASME

A. Kalnins
Department of Mechanical Engineering
and Mechanics,
Lehigh University,
Bethlehem, PA 18015
Mem. ASME

The interaction of a compliant slab and the flow of a viscous fluid is explored theoretically. Both laminar and turbulent boundary-layer flow cases are considered. The slab is treated as an infinite, elastic or viscoelastic solid of finite thickness, bonded to a rigid half-space. The two media are coupled through stresses and velocities, in both tangential and normal directions, on the deformed surface of the slab. The proposed mathematical model is used to predict the appearance of unstable surface waves of the coating. According to the model, instabilities of a highly viscoelastic slab originate in the form of waves with phase speeds at about 2.3 percent of the flow velocity while the wave speed for a slab with zero to moderate viscosity is in the range of 50–60 percent of the flow velocity, which confirms previous experimental results. The predicted onset velocities of slow propagating waves for turbulent flow over plastisol gel are within 10 percent of those observed experimentally.

Introduction

The interaction of compliant surfaces with boundary-layer flows has been extensively studied in the past two decades. The increase in the interest in this problem can be attributed to the possibilities of new applications, such as skin-friction drag reduction of moving vehicles, sound absorption, vibration reduction, noise shielding, etc. The design of a compliant coating to achieve a particular objective requires the understanding of the interaction mechanism between the fluid and solid media; that is, the goal of this paper.

The response of a viscoelastic compliant coating to turbulent boundary-layer flow has been experimentally studied by Boggs et al. (1962), Hansen et al. (1980), and Gad-el-Hak et al. (1984). They all reported that a motion of the surface of the coating appeared in the form of very slowly moving waves when the flow speed exceeded a well-defined threshold. The wave speed at the onset was about 2–3 percent of the free-stream flow velocity. Boggs et al., were the first to point to the existence of these large-amplitude, spanwise standing waves, called "static divergence" waves. Gad-el-Hak (1986a) repeated the experiments for a coating with low viscosity gelatin and reported the appearance of waves with smaller amplitudes, propagating with much higher velocities, with about 50 percent of the flow velocity. In another paper, Gad-el-Hak (1986b) gave an overview of the state-of-the-art of the interaction between fluid flow and a compliant coating.

There are two well-known mechanisms that can set a compliant coating in motion: direct excitation and instability (also called self-excited vibration or flutter). These mechanisms are covered by standard texts on aeroelasticity, such as, for example, Dowell (1970). The difference between the mechanisms is that, in the case of instability, a perfectly flat surface is a possible state, while in the case of direct excitation it is not. In the case of instability, a wave on the surface, once initiated, changes the flow in such a way that the changed flow tends to increase the amplitude of the wave. It is important to note that the wave motion in the slab is sustained by what the surface wave does to the fluid and not by any action in the fluid that can take place in the absence of the wave. If there is no wave on the surface, there is no excitation coming from the flow.

Since all the experimental results, cited in the foregoing, report a definite onset flow velocity, below which no waves are observed, then it is concluded that it is the instability mechanism that was observed in these experiments. Additional arguments in support of this claim can be found in a number of other papers, such as, for example, in the paper by Evrensel and Kalnins (1985). Since the goal of this paper is to produce a mathematical model that can explain the cited experimental results, it will be the instability mechanism that will be pursued in this paper.

The instability problem has been studied theoretically by using models for the fluid and solid of various degrees of sophistication. Benjamin (1959), Landahl (1962), Kaplan (1964), and Metcalfe (1985) used either the boundary-layer flow over moving wavy, rigid walls or replaced the slab with a membrane. Duncan et al. (1985), considered an inviscid, incompressible fluid and a two-dimensional viscoelastic slab and, after introducing two experimentally determinable parameters, succeeded in making close predictions of the onset velocities of the slow-propagating waves.

Evrensel and Kalnins (1985) reconsidered the inviscid, incompressible fluid model and noted discrepancies between the results of this model and the experiments. One major

Contributed by the Applied Mechanics Division for presentation at the Winter Annual Meeting, Chicago, IL, November 28 to December 2, 1988, of THE AMERICAN SOCIETY OF MECHANICAL ENGINEERS.

Discussion on this paper should be addressed to the Editorial Department, ASME, United Engineering Center, 345 East 47th Street, New York, N.Y. 10017, and will be accepted until two months after final publication of the paper itself in the JOURNAL OF APPLIED MECHANICS. Manuscript received by ASME Applied Mechanics Division, February 24, 1987; final revision, December 2, 1987.

Paper No. 88-WA/APM-33.

Copyright © 1988 by ASME
Downloaded 03 May 2010 to 171.66.16.21. Redistribution subject to ASME license or copyright; see http://www.asme.org/terms/Terms_Use.cfm

discrepancy was that the onset flow velocity of the slow-propagating wave forms was reported in the experiments to increase sharply when the thickness of the coating was decreased, while the theoretical predictions of the inviscid fluid model showed little effect of the coating thickness on the onset velocity. Also, the predicted wavelengths were much smaller than those observed in the experiments.

The inviscid, incompressible fluid model predicts the surface pressure of the coating to be in phase and have a certain amplitude relationship with the elevation of the surface wave form. If these phase and amplitude relationships are artificially changed, as they were by Duncan et al. (1985), then a better agreement with experimental results is obtained. This led Evrensel and Kalnins (1985) to suggest that the inclusion of viscosity of the fluid might provide a more realistic phase and amplitude relationship, which could also lead to a better agreement with the experimental results. This is what provided the motivation of the present paper in which the fluid is assumed to have viscosity and establish a boundary-layer profile.

For a laminar boundary layer, the velocity profile is taken as that of the Blasius solution. If the boundary layer is turbulent, it is argued here that it is the mean velocity of the flow, and not its fluctuating part, that sustains the unstable waves in the slab. The argument is based on the very essence of the instability mechanism; namely, that the crest of a surface wave is subjected to a negative pressure, pulling it further up, and the trough of the wave is subjected to a positive pressure, pushing it further down. It seems reasonable to assert that the fluctuating part of the velocity would be unable to produce that effect and that it must be the mean flow that produces the instability. Therefore, for the purposes of this paper, it is assumed that the only information needed of a turbulent boundary layer is its mean velocity profile and that the 1/7th power law gives a reasonable representation of it. The slope of the mean profile near the wall, where 1/7th power law fails, is approximated by using Blasius' semiempirical formula for the skin-friction coefficient (White (1974)).

Thus the problem considered in this paper is a viscoelastic slab bonded to a rigid half-space, with a boundary-layer flow on top. The two media are fully coupled through stresses and velocities in both tangential and normal directions at the interface, and the boundary conditions are satisfied at the deformed surface of the slab. The key feature of this model is that the amplitude and phase relationships at the interface are given by the solution, and no additional external parameters are needed. The complete solution is given for the two-dimensional equations of the perturbed viscous boundary layer. A numerical method that reduces a boundary-value problem to a set of initial-value problems, which has been advocated and used by Kalnins (1964) for many years, is used. The results show better qualitative and quantitative agreements with experimental observations than those that assume inviscid flow.

Statement of the Problem. Consider the flow of a viscous fluid, with a known boundary-layer profile $U(y)$, over the flat surface of an infinite elastic (or viscoelastic) slab of thickness d, bonded to a rigid half-space (see Fig. 1). The flow can be laminar or turbulent. The objective is to examine the behavior of the slab with an increasing uniform flow velocity and to determine the onset flow velocity for the initiation of the unstable surface waves.

Formulation of the Problem. The problem can be divided into three regions, as shown in Fig. 1:

1 Region I: Slab
2 Region II: Viscous flow with a known primary velocity profile $U(y)$
3 Region III: Viscous fluid flow with constant primary velocity U_0

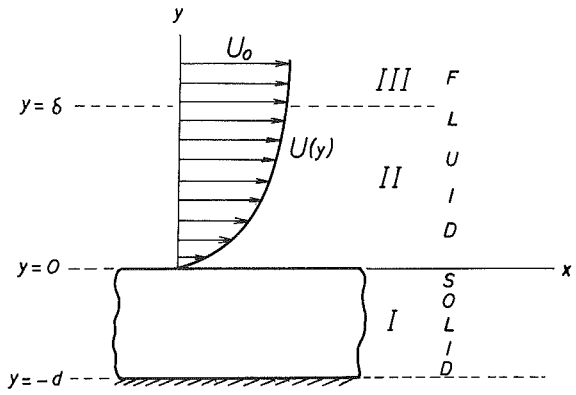


Fig. 1 Geometry of the problem

Region II

Two-dimensional momentum, continuity equations and stress-velocity relations for an incompressible fluid are given as

$$\frac{\partial u}{\partial t}+u\frac{\partial u}{\partial x}+v\frac{\partial u}{\partial y}=\frac{1}{\rho_f}\left(\frac{\partial \sigma_{xx}}{\partial x}+\frac{\partial \tau_{xy}}{\partial y}\right)$$

$$\frac{\partial v}{\partial t}+u\frac{\partial v}{\partial x}+v\frac{\partial v}{\partial y}=\frac{1}{\rho_f}\left(\frac{\partial \tau_{xy}}{\partial x}+\frac{\partial \sigma_{yy}}{\partial y}\right)$$

$$\frac{\partial u}{\partial x}+\frac{\partial v}{\partial y}=0 \qquad (1)$$

$$\sigma_{xx}=-p+2\mu\frac{\partial u}{\partial x}$$

$$\sigma_{yy}=-p+\mu\frac{\partial v}{\partial y}$$

$$\tau_{xy}=\mu\left(\frac{\partial u}{\partial y}+\frac{\partial v}{\partial x}\right)$$

where u, v are the velocities in the x and y-directions, t is time, ρ_f is fluid density, σ_{xx}, σ_{yy} are normal stresses, τ_{xy} is shear stress, p is pressure, μ is viscosity. Writing each variable as composed of a primary part and a perturbed part and assuming the usual wave form

$$u(x,y,t)=U(y)+u_1(y)e^{i\alpha(x-ct)}$$
$$v(x,y,t)=v_1(y)e^{i\alpha(x-ct)}$$
$$\sigma_{xx}(x,y,t)=-P(x)+\sigma_{xx_1}(y)e^{i\alpha(x-ct)}$$
$$\sigma_{yy}(x,y,t)=-P(x)+\sigma_{yy_1}(y)e^{i\alpha(x-ct)}$$
$$\tau_{xy}(x,y,t)=\mu\frac{dU(y)}{dy}+\tau_{xy_1}(y)e^{i\alpha(x-ct)}$$
$$p(x,y,t)=P(x)+p_1(y)e^{i\alpha(x-ct)}$$

In this formulation, the variables with a subscript 1 are the disturbed parts of these variables due to the wave motion in the surface of the slab and are assumed to be infinitesimals. Velocity $U(y)$ and pressure $P(x)$ belong to the primary flow. Substituting these into equation (1), ignoring second-order infinitesimals, knowing that $P(x)$ and $U(y)$ also satisfy these equations, and nondimensionalizing velocities by the real part of the complex shear wave speed of the slab, C_{T_r}, stresses by $\rho_f C_{T_r}{}^2$, distances by boundary-layer thickness δ, and letting

$$\bar{v}_1=v_1/C_{T_r},\quad \bar{u}_1=u_1/C_{T_r},\quad \bar{U}=U/C_{T_r},$$
$$\bar{\sigma}_{yy_1}=\sigma_{yy_1}/\rho_f C_{T_r}{}^2,\quad \bar{\sigma}_{xx_1}=\sigma_{xx_1}/\rho_f C_{T_r}{}^2,\quad \bar{\tau}_{xy_1}=\tau_{xy_1}/\rho_f C_{T_r}{}^2,$$
$$\bar{\alpha}=\alpha\delta,\quad \bar{c}=c/C_{T_r},\quad \bar{y}=y/\delta \qquad (2)$$

and then dropping the bars, the governing differential equations can be obtained as

Downloaded 03 May 2010 to 171.66.16.21. Redistribution subject to ASME license or copyright; see http://www.asme.org/terms/Terms_Use.cfm

$$\frac{dv_1}{dy} = -i\alpha u_1$$

$$\frac{du_1}{dy} = \mathrm{Re}_c \tau_{xy_1} - i\alpha v_1$$

$$\frac{d\sigma_{yy_1}}{dy} = -i\alpha\tau_{xy_1} + i\alpha(U-c)v_1 \tag{3}$$

$$\frac{d\tau_{xy_1}}{dy} = -i\alpha\sigma_{yy_1} + \frac{dU}{dy}v_1 + \left[i\alpha(U-c) + \frac{4\alpha^2}{\mathrm{Re}_c}\right]u_1$$

where $\mathrm{Re}_c = \rho_f \delta C_{T_r}/\mu$

Region III

Although the effect of viscosity is negligible in Region III, it is included to have a smoother interface. Also, the primary velocity $U(y)$ is constant in this region. Substituting $U(y) = U_0$, into (3) and letting

$$v_1 = A_1 e^{\beta y}, \quad u_1 = A_2 e^{\beta y}, \quad \sigma_{yy_1} = A_3 e^{\beta y}, \quad \tau_{xy_1} = A_4 e^{\beta y} \tag{4}$$

results in 4 homogeneous equations in A's. Equating the determinant of the coefficient matrix to zero and solving for β gives

$$\beta_{1,2} = \pm\alpha$$

$$\beta_{3,4} = \pm\alpha\sqrt{1 + i\mathrm{Re}_c(U_0 - c)/\alpha}$$

Since velocities and stresses must die out as $y \to \infty$, taking only the $(-)$ sign, substituting them into (3), then into (2), eliminating all unknown coefficients gives the stress-velocity relation for $y \geq \delta$ as

$$\begin{bmatrix} i\frac{q}{1-q}(U_0-c) & \frac{1}{1-q}(U_0-c) - 2i\frac{\alpha}{\mathrm{Re}_c} \\ 2i\frac{\alpha}{\mathrm{Re}_c} - \frac{1}{1-q}(U_0-c) & i\frac{1}{1-q}(U_0-c) \end{bmatrix} \begin{bmatrix} v_1 \\ u_1 \end{bmatrix}$$

$$+ \begin{bmatrix} -1 & 0 \\ 0 & -1 \end{bmatrix} \begin{bmatrix} \sigma_{yy_1} \\ \tau_{xy_1} \end{bmatrix} = \begin{bmatrix} 0 \\ 0 \end{bmatrix} \tag{5}$$

where

$$q = \sqrt{1 + i\frac{\mathrm{Re}_c}{\alpha}(U_0 - c)}.$$

When this equation is evaluated at $y = \delta$, the boundary condition between Region II and Region III is obtained.

Region I

The solution for a two-dimensional viscoelastic (or elastic) slab in a form needed in the present paper, is well known, and is included in a paper by Evrensel and Kalnins (1985). Knowing that the displacements at $y = -d$, u_y and u_z, are zero, and the time-dependence is harmonic, $e^{-i\alpha ct}$, the stress-velocity relation at $y = 0$ can be written as

$$\begin{bmatrix} \sigma^s_{yy} \\ \tau^s_{xy} \end{bmatrix}_{y=0} = \frac{i}{\alpha} \begin{bmatrix} K_{11} & K_{12} \\ K_{21} & K_{22} \end{bmatrix} \begin{bmatrix} v^s \\ u^s \end{bmatrix}_{y=0} \tag{6}$$

where the superscipt s stands for solid, i.e., it distinguishes the solid variables from fluid variables which do not have any superscripts. The K_{ij}'s are given by Evrensel and Kalnins (1985).

Boundary Conditions on Surface of Slab

For the slab, there are no undisturbed velocity components. This is not true for the fluid, where there is the undisturbed velocity profile $U(y)$ which is zero at $y = 0$. Figure 2 demonstrates the positions of the solid and fluid particles at an arbitrary location x and time t.

The horizontal velocity of the fluid particle at $y = \eta$ can be written as

$$u(x,\eta,t) = U(\eta) + u_1(\eta)e^{i\alpha(x-ct)}$$

Noting that η and u_1 are assumed to be small, expanding U and u_1 about $\eta = 0$, ignoring the second and higher-order infinitesimals and knowing that $U(0) = 0$, the horizontal velocity of the fluid particle at $y = \eta$ is obtained as

$$U(\eta) = \eta\frac{dU(0)}{dy} + u_1(0)e^{i\alpha(x-ct)}$$

In the same way, the shear stress at $y = \eta$

$$\tau_{xy}(\eta) = \mu\frac{dU(0)}{dy} + \mu\eta\frac{d^2U(0)}{dy^2} + \tau_{xy_1}(0)e^{i\alpha(x-ct)}$$

Then, the solid and fluid variables at $y = \eta$ can be written as

Solid	*Fluid*
$v^s(x,\eta,t) = v^s_1(0)e^{i\alpha(x-ct)}$	$v(x,\eta,t) = v_1(0)e^{i\alpha(x-ct)}$
$u^s(x,\eta,t) = u^s_1(0)e^{i\alpha(x-ct)}$	$u(x,\eta,t) = \eta\frac{dU(0)}{dy} + u_1(0)e^{i\alpha(x-ct)}$
$\sigma^s_{yy}(x,\eta,t) = \Sigma^s_{yy}(0) + \sigma^s_{yy_1}(0)e^{i\alpha(x-ct)}$	$\sigma(x,\eta,t) = -P(x) + \sigma_{yy_1}(0)e^{i\alpha(x-ct)}$
$\tau^s_{xy}(x,\eta,t) = T^s_{xy}(0) + \tau^s_{xy_1}(0)e^{i\alpha(x-ct)}$	$\tau(x,\eta,t) = \mu\frac{dU(0)}{dy} + \mu\eta\frac{d^2U(0)}{dy^2} + \tau_{xy_1}(0)e^{i\alpha(x-ct)}$

Knowing that $\Sigma^s_{yy}(0)$, $T^s_{xy}(0)$ for the slab, and $-P(x)$, μ $(dU(0)/dy)$ for the fluid belong to the undisturbed problem, they will cancel each other.

Using $\eta = \hat{\eta}e^{i\alpha(x-ct)}$ and $v^s_1 e^{i\alpha(x-ct)} = \partial\eta/\partial t = -i\alpha c\hat{\eta}e^{i\alpha(x-ct)}$ and substituting these into (6), using the same nondimensionalization given in equations (2), the boundary condition at $y = 0$ for Region II can be obtained as

$$\begin{bmatrix} K_{11} + \frac{i}{\alpha c}\frac{dU(0)}{dy}K_{12} & K_{12} \\ K_{21} + \frac{iK_{22}}{\alpha c}\frac{dU(0)}{dy} + \frac{1}{\alpha c\mathrm{Re}_c}\frac{d^2U(0)}{dy^2} & K_{22} \end{bmatrix} \begin{bmatrix} v_1(0) \\ u_1(0) \end{bmatrix}$$

$$+ \begin{bmatrix} -1 & 0 \\ 0 & -1 \end{bmatrix} \begin{bmatrix} \sigma_{yy_1}(0) \\ \tau_{xy_1}(0) \end{bmatrix} = \begin{bmatrix} 0 \\ 0 \end{bmatrix} \tag{7}$$

Downloaded 03 May 2010 to 171.66.16.21. Redistribution subject to ASME license or copyright; see http://www.asme.org/terms/Terms_Use.cfm

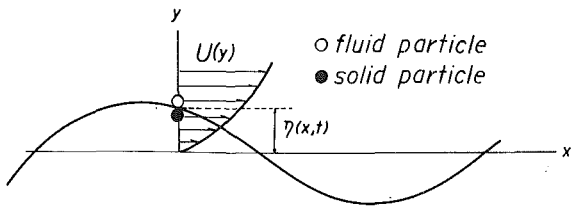


Fig. 2 Boundary conditions for fluid flow on deformed surface of slab

where $\bar{K}_{ij} = iK_{ij}/(\rho_f \alpha \bar{c} C_{T_r}{}^2)$ is used and then bar on $\bar{K}_{ij}$ is dropped.

Solution

The problem is to solve equations (3), subject to boundary conditions (7) at $y = 0$ and (5) at $y = \delta$. This is a boundary-value-eiengvalue problem for a given profile $U(y)$, with eigenvalues α and c and eigenvector $\{v_1\ u_1\ \sigma_{yy_1}\ \tau_{xy_1}\}$.

Although the governing differential equations are linear in both eigenvalues and y, the boundary conditions are not linear in neither α nor c.

Because of the nonlinearities, the traditional methods developed for linear eigenvalue problems cannot be used. A method for the numerical solutions of boundary-value problems, developed by Kalnins (1964) has been used. This method reduces a boundary-value problem to a set of initial-value problems.

If the flow is turbulent, the horizontal velocity profile has a fluctuating part as well as a mean profile $U(y)$. In calculations for the turbulent flow, only the mean profile $U(y)$ is used as the undisturbed flow velocity. The reasons for this is that the goal of this paper is to explore the stability analysis, not noise analysis. Dowell (1970) has given an excellent discussion on the distinction between externally excited response (due to turbulent boundary-layer pressure fluctuations, noise) and self-excited response (due to aeroelastic instability, flutter) for the vibration of a flexible structure immersed in fluid flow; see also, Evrensel and Kalnins (1985).

Results

All results given in this paper, if not indicated otherwise, are for slab thickness $d/\delta = 1$, wave number $\alpha\delta = 1.5$. The slab material is plastisol gel that is the compliant coating used by Gad-el-Hak (1984) in his experiment. This material has the real part of the shear modulus $G_r = 77$ dyn/cm^2, Poisson's ratio $\nu = 0.5$. The properties of the fluid are those of water.

For the laminar boundary-layer profile, Blasius' solution is used. A mean turbulent profile is approximated by the 1/7th power law. Although, the chosen form approximates the mean profile reasonably well for most of the portion of the boundary layer, it fails near the wall. Also, the derivative at $y = 0$ is infinite. To overcome this difficulty, the slope of $U(y)$ at the wall is estimated by using Blasius' semiempirical formula for the skin-friction coefficient; see, White (1974).

As mentioned earlier, this is an eigenvalue-boundary-value problem with infinitely many eigenvalues and eigenvectors. Since the higher eigenvalues have higher frequencies and damp out faster, they are not observed unless externally excited. For this reason, the results are presented only for the lower ones.

Laminar Flow Over Rigid Wall

Figure 3 shows eigenvectors v_1 and u_1 for a laminar flow over a flat rigid wall. On the same plot, the theoretical solution for u_1 by Kaplan and experimental results by Schubauer and Skramstad are also given (see, White (1974), page 408). As can be seen from Fig. 3, the results are almost exactly the same. This was a first check for the mathematical model

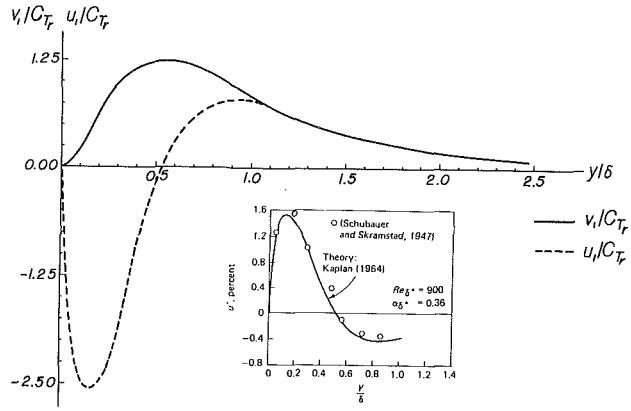


Fig. 3 Perturbed velocities, v_1, u_1, in the y and x-directions for laminar flow over rigid wall, $U_0/C_{T_r} = 1.14$, $c/C_{T_r} = 0.5087 - 0.03688i$. Figure showing the theoretical solution by Kaplan and experimental results by Schubauer and Skramstad is taken from White (1974, p. 408).

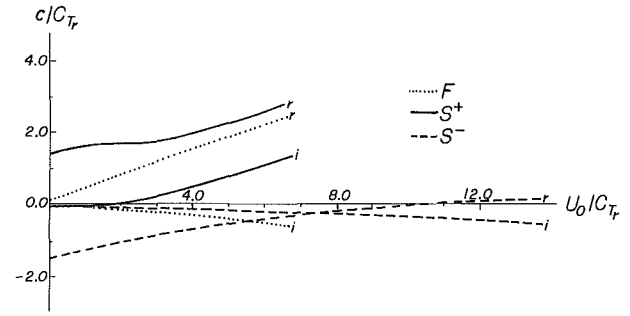


Fig. 4 Phase speed versus free-stream flow velocity for laminar flow over elastic slab; r and i stands for the real and imaginary parts of the phase speed c, respectively

Table 1 Dimensionless phase speed, c/U_0, for laminar flow over rigid wall

Re_{δ^*}	$\alpha\delta^*$	c/U_o From Fig. 5.6 in White (1974)	c/U_o Predictions of the model developed in this study
520	0.3	0.4 + 0i	0.395 - 0.00018i
550	0.3	0.39 + 0.001i	0.392 + 0.00106i
1900	0.17	0.3 + 0.015i	0.293 + 0.0156i

developed and the numerical solution scheme used. The eigenvalues α and c for a changing Reynolds number are given in a number of references, usually in the form of α versus Re plot for different c's (see, for example White (1974), page 403). To check the model and methods used, different points on these plots are calculated and they are given, together with the values taken from White (1974), in Table 1. Note that the values given in the third column are read from a figure in White (1974) and may not be very accurate. Agreement is acceptable.

Laminar Flow Over Elastic Slab

The change in phase speed, c/C_{Tr}, for a given wave number is given in Fig. 4. Three modes are plotted, two of which are designated solid modes and the third a fluid mode. This is an expected result for a coupled problem. The fluid mode is named as F on this plot because this mode has almost the same characteristics as that for flow over a rigid wall. The two additional modes are caused by the elasticity of the slab and they are called solid modes, S^+ and S^-. For this specific set of parameters, the F mode has a positive phase speed, i.e., the real part of c is positive. But the imaginary part of c is

Downloaded 03 May 2010 to 171.66.16.21. Redistribution subject to ASME license or copyright; see http://www.asme.org/terms/Terms_Use.cfm

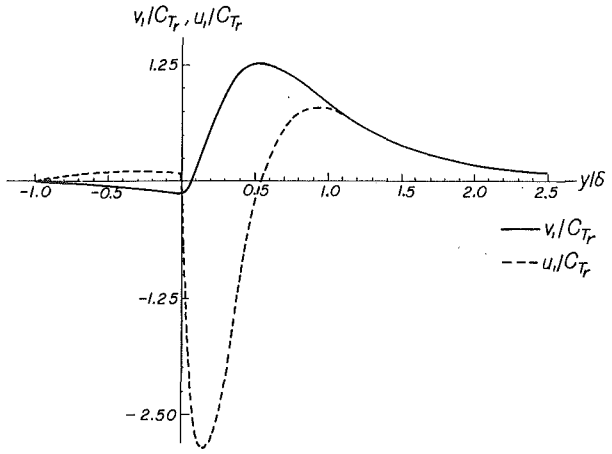


Fig. 5 Perturbed velocities for laminar flow over elastic slab, U_0/C_{T_r} = 1.14, c/C_{T_r} = 0.5234 − 0.03776i; fluid, F, mode

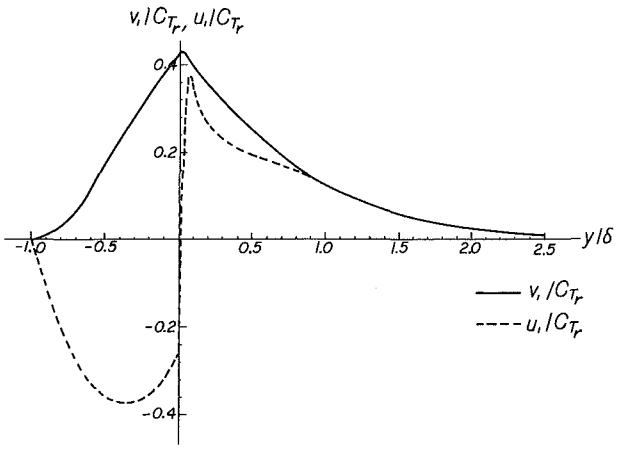


Fig. 6 Perturbed velocities for laminar flow over elastic slab, U_0/C_{T_r} = 1.14, c/C_{T_r} = 1.1805 − 0.02141i; solid, S^-, mode

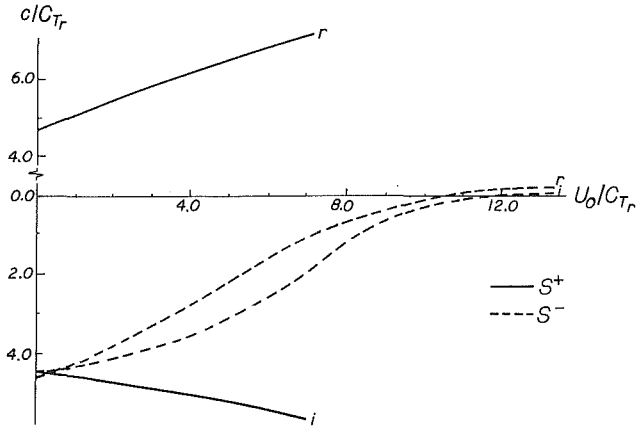


Fig. 7 Phase speed versus free-stream flow velocity for laminar flow over highly viscoelastic slab

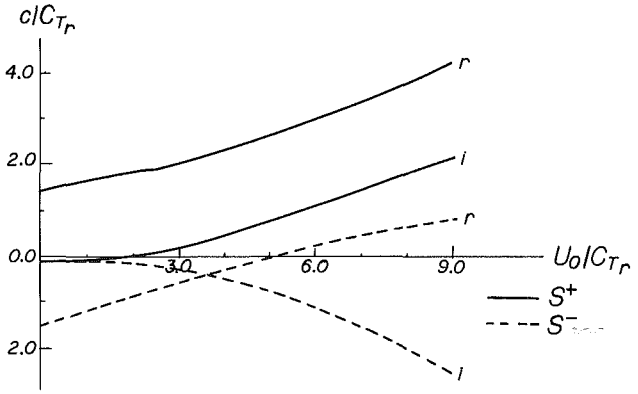


Fig. 8 Phase speed versus free-stream flow speed for turbulent flow over elastic slab

negative, indicating stability, i.e., they are downstream running stable waves. For the S^- mode, the real part of c is negative, indicating an upstream running wave, up to a certain flow velocity, and then it becomes positive, indicating a downstream running wave, if this flow velocity is exceeded. The imaginary part of the phase speed is negative for all values of c, which means that this mode is always stable. On the other hand, the S^+ mode is stable up to a critical flow velocity, U_0/C_{T_r} = 2, and becomes unstable if the flow velocity exceeds this critical value. The real part of c is always positive, and its magnitude is about 50–60 percent of U_0. For different parameter values, the general behavior of S^+ and S^- modes does not change, but only the critical flow velocity, where S^+ mode becomes unstable, changes. In other words, for laminar flow over an elastic slab, it is possible to see downstream propagating waves on the surface of the slab with a velocity of 50–60 percent U_0 and the static divergence waves cannot be observed. This also is true for a slightly viscoelastic slab, but it may not hold if the viscosity of the slab is high enough, which will be discussed in the next section.

Figure 5 gives the eigenvectors v_1 and u_1 for the fluid mode. As mentioned earlier, this mode is very similar to the case of flow over rigid wall. If Fig. 5 is compared with Fig. 3, this can easily be verified. For this mode, the velocities in the slab are relatively small, i.e., the slab is not participating. Almost all the wave motion is in the fluid.

The solution for the solid mode, S^- is given in Fig. 6. For this mode, the velocities in the slab are about of the same order as in the fluid, i.e., the solid also takes part in the action. Both velocities decrease exponentially outside the boundary layer as required by the inviscid solution.

Laminar Flow Over Viscoelastic Slab

The inclusion of viscosity for the slab produces qualitatively similar results to those of the inviscid model (Evrensel and Kalnins (1985)). A plot of the dispersion relation for the laminar flow over a highly viscous slab is given in Fig. 7. Material properties correspond to the plastisol gel used by Gad-el-Hak et al. (1984), in their experiment. As expected, the S^+ mode is stabilized by the slab viscosity. The portion of the S^- mode, where the real part of the phase speed is negative, is also stabilized, i.e., the imaginary part of c is increased in negative values, but the part of this mode with a positive propagation velocity is destabilized and the imaginary part of c becomes positive at $U_0/C_{T_r} \simeq 12$, where the real part is positive and very small. In other words, for a highly viscous slab it is possible to see slow propagating waves in the downstream direction, and they are usually called static divergence waves. For this case, the fast propagating waves cannot be observed.

Turbulent Flow Over Elastic Slab

Figure 8 gives the dispersion relation for a turbulent flow over an elastic slab. As can be seen, for the upper mode, S^+, the real part of c is always positive and the imaginary part is negative for small flow velocities but it becomes positive if the flow velocity exceeds a critical value, indicating instability. This critical flow velocity is about 2, which is almost the same as that for laminar flow. In other words, if the dimensionless

Downloaded 03 May 2010 to 171.66.16.21. Redistribution subject to ASME license or copyright; see http://www.asme.org/terms/Terms_Use.cfm

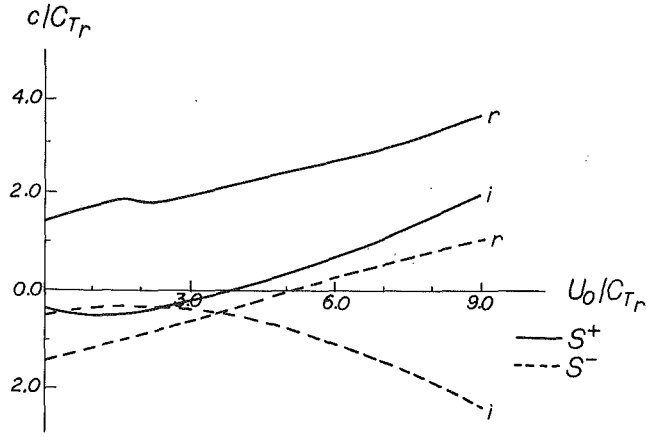


Fig. 9 Phase speed versus free-stream velocity for turbulent flow over a slightly viscoelastic slab

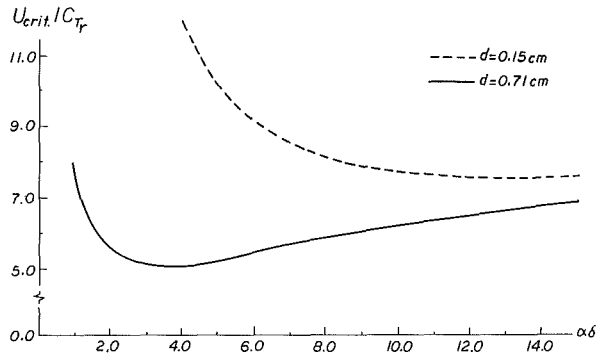


Fig. 10 Critical flow velocity, where the real part of c is zero, versus wave number for turbulent flow over elastic slab

flow velocity is above 2, it is possible to see unstable surface waves downstream propagating with a phase speed 50–60 percent of the flow velocity.

For the lower mode, S^-, the real part of c is negative for low flow speeds but it is positive for higher speeds, but the imaginary part of c remains negative for all values of the flow velocity; i.e., this mode is always stable for the elastic slab. In other words, as in the laminar flow case, static divergence waves cannot be observed for an elastic slab. Only the fast downstream propagating waves are predicted.

Turbulent Flow Over a Viscoelastic Slab With a Small Loss Tangent

In Fig. 9, the case of turbulent flow over a slightly viscoelastic slab is presented. For this example, the loss tangent is assumed to be small, about 1/3rd of the value for the plastisol gel, to demonstrate the effect of the slab viscosity. As in the case of laminar flow, the introduction of viscosity in the solid has stablilized the S^+ mode, i.e., pushed the critical flow velocity where the instability originates to a higher value. For an elastic slab, this dimensionless critical flow velocity was about 2, but for a slightly viscoelastic slab it is almost twice of that, about 4.

The S^- mode is still stable. If the imaginary parts of the phase speeds for elastic and slightly viscoelastic cases are compared, it can be concluded that the slab viscosity stabilizes the upstream, but destabilizes the downstream running waves. If the slab viscosity is high enough, these downstream running waves might become unstable, as in the laminar flow case, and it is possible to observe static divergence waves.

Table 2 Comparison of predicted dimensionless onset flow velocities, U_0/C_{T_r}, and wavelengths, λ, for water flow over plastisol gel with experimental observations of Gad-el-Hak (1984)

	Theory		Experiment	
	U_0/C_{T_r}	λ(cm)=$2\pi/\alpha$	U_0/C_{T_r}	λ(cm)
d = 0.15cm	7.5	0.5	8	1.13
d = 0.71cm	5	1.7	4.75	3.72

For a slightly viscoelastic slab, such as gelatin, which was recently tested by Gad-el-Hak (1986a), the S^- mode is always stable, but the S^+ mode might become unstable if the flow velocity is high enough. This means that, for an elastic or slightly viscoelastic slab, static divergence waves cannot be observed, but the fast, downstream running waves, with phase speeds 50–60 percent of the flow velocity, can be seen, as experimentally verified by Gad-el-Hak (1986a).

Turbulent Flow Over a Viscoelastic Slab With a Large Loss Tangent

The laminar flow case suggests that the S^- mode might become unstable at a critical flow velocity if the slab viscosity is high enough. The flow speed where the real part of c changes sign gives a close estimate of the onset speed of the static divergence waves for a highly viscoelastic slab (see Fig. 7). Figure 10 gives the change of this critical speed with the wave number α for a given slab thickness d. Critical flow velocity has a minimum, which can be called the onset flow velocity for a given slab thickness and the value of α at this minimum is the wave number of the unstable waves at the onset. These predictions and the experimentally observed values of the onset flow velocities and wavelengths are given in Table 2. In calculation of wavelength, $\delta = 1$ cm is used. As can be seen, the theory is in good agreement with the experiment for the onset flow velocities, but the agreement is not as good for the onset wavelengths.

Also, if the turbulent and laminar flow cases are compared, it can be concluded that the onset speed of static divergence waves is much higher for the laminar case. This case is also experimentally verified.

Conclusion

The model developed in this paper is self-sufficient; i.e., it does not need any empirical factors such as pressure-elevation amplitudes and phase shifts that were used by Duncan et al. (1985). The results presented also suggest that the present model is capable of explaining most of those experimental results that were not explained by the inviscid flow model, even when adjusted by amplitude and phase factors.

This is a linear model which can predict the onset flow velocity and wavelength for the initiation of the instability, as well as the response of the coupled fluid-solid system to an infinitesimal disturbance for flow velocities lower than the onset. However, due to its basic assumption, infinitesimal disturbance, it cannot predict the amplitudes of the unstable surface waves.

The results which are in good agreement with the experimental findings can be summarized as follows:

1 Instabilities of a slightly viscoelastic slab originate in the form of waves with phase speeds of about 50 percent of the flow velocity.

2 The onset velocities of the appearance of the slow-propagating wave forms are much higher for laminar than for turbulent boundary layers.

Downloaded 03 May 2010 to 171.66.16.21. Redistribution subject to ASME license or copyright; see http://www.asme.org/terms/Terms_Use.cfm

3 The onset velocities are sensitive to slab thickness. They increase sharply as the slab thickness decreases.

4 The predicted onset velocities for turbulent flow over plastisol gel are within 10 percent of those observed experimentally.

The agreement of the predicted onset wavelengths of the slow-propagating waves reported with those reported in experiments is not as good. The experimentally observed wavelengths are about twice as long as those predicted theoretically by the viscous fluid model. This disagreement might be caused by the sensitivity of the wavelength to the flow velocity. For example, if the flow velocity is increased 10 percent, the wavelength doubles.

Acknowledgments

This work was sponsored by the Office of Naval Research through the Compliant Coating Drag Reduction Program, under Contract No. N00014-81-K-0398. The authors thank the monitor of the program, Dr. M. M. Reischman, for the support of this project. This paper is a part of C. A. Evrensel's PhD dissertation, which was accepted by Lehigh University in June 1985.

References

Benjamin, T. B., 1959, "Shearing Flow Over a Wavy Boundary," *Journal of Fluid Mechanics*, Vol. 9, pp. 513.

Boggs, F. W., and Hahn, E. R., 1962, "Performance of Compliant Skins in Contact with High Velocity Flow in Water," in *Proceedings of the 7th Joint-Navy-Air Force Conference on Elastomer Research and Development*, U.S. Office of Naval Research, pp. 443.

Dowell, E. H., 1970, "Noise or Flutter or Both," *Journal of Sound and Vibrations*, Vol. 11, pp. 159.

Duncan, J. H., Waxman, A. M., and Tulin, M. P., 1985, "The Dynamics of Waves at the Interface Between a Viscoelastic Coating and a Fluid Flow," *Journal of Fluid Mechanics*, Vol. 158, pp. 177.

Evrensel, C. A., and Kalnins, A., 1985, "Response of a Compliant Slab to Inviscid Incompressible Fluid Flow," *Journal of the Acoustical Society of America*, Vol. 78, pp. 2034.

Gad-el-Hak, M., Blackwelder, R. F., and Riley, J. J., 1984, "On the Interaction of Compliant Coatings With Boundary Layer Flows," *Journal of Fluid Mechanics*, Vol. 140, pp. 257.

Gad-el-Hak, M., 1986a, "The Response of Elastic and Viscoelastic Surfaces to a Turbulent Boundary Layer," ASME JOURNAL OF APPLIED MECHANICS, Vol. 53, pp. 206.

Gad-el-Hak, M., 1986b, "Boundary Layer Interactions With Compliant Coating: An Overview," *Applied Mechanics Reviews*, Vol. 39, No. 4, April.

Hansen, R. J., Hunston, D. L., Ni, C. C., and Reischman, N. M., 1980, "An Experimental Study of Flow-Generated Waves on a Flexible Surface," *Journal of Sound and Vibration*, Vol. 68, pp. 317.

Kalnins, A., 1964, "Free Vibration of Rotationally Symmetric Shells," *Journal of the Acoustical Society of America*, Vol. 36, pp. 1355.

Kaplan, R. E., 1964, PhD dissertation, Massachusetts Institute of Technology, Cambridge, MA.

Landahl, M. T., 1962, "On the Stability of a Laminar Incompressible Boundary Layer Over a Flexible Surface," *Journal of Fluid Mechanics*, Vol. 13, pp. 609.

Metcalfe, R. W., and Domaradzki, J. A., 1985, "Direct Numerical Simulations of Flow Over Active and Compliant Boundaries," Drag Reduction and Boundary Layer Control Symposium, Washington, D.C.

White, F. M., 1974, *Viscous Fluid Flow*, McGraw-Hill, New York.

Downloaded 03 May 2010 to 171.66.16.21. Redistribution subject to ASME license or copyright; see http://www.asme.org/terms/Terms_Use.cfm

Finite Element Modeling of the Punch Stretching of Square Plates

E. Nakamachi
Yatsushiro National College of Technology, Yatsushiro, Kumamoto, Japan

R. Sowerby
Department of Mechanical Engineering, McMaster University, Hamilton, Ontario, Canada

The paper presents an updated Lagrangian-type finite element procedure, formulated with reference to a surface embedded coordinated system. Membrane shell theory is employed, and an attempt is made to calculate the strain distribution incurred by a peripherally clamped square plate, when impressed by a rigid punch. Three different punch geometries were considered. The material is treated as a rate insentive, elastic work-hardening solid, which obeys the J_2 flow theory; both finite deformation and normal anisotropy can be considered. A linear relationship between the Jaumann rate of Cauchy stress and the Eulerian rate of Green's strain tensor is derived. A slip-stick model was adopted for the interfacial frictional conditions. This was achieved by considering the equilibrium of a constant strain-element node in contact with the tools, and deciding whether such a node would stick or slip under Coulomb friction conditions. It is demonstrated that the punch geometry and frictional conditions exert a strong influence on the deformation mode, and hence, upon the overall strain distribution. The predictions were checked against experimental observations when stretch-forming square plates of pure aluminum, 0.5-mm thick. Contours of equal height on the deforming blanks were determined using a Moiré fringe technique. The agreement between theory and experiment was favorable.

Finite Element Formulation

Figure 1(*a*) shows triangular membrane, constant strain, elements in a known state C after finite deformation from the undeformed configuration C_0. There follows an incremental deformation and C is mapped into $\bar{C}$. A surface embedded coordinate system, see (Nakamachi et al., 1982; Nakamachi and Sowerby, 1982; Green and Zerna, 1968), is adopted, where θ^1 and θ^2 are attached to the middle surface of the element, and θ^3 is perpendicular to the θ^1 and θ^2 plane, the base vectors are $\mathbf{G}_j$. In the incremental deformation from C to $\bar{C}$, a generic point P in the plate is displaced by Δu and

$$\Delta u = \Delta u^j \mathbf{G}_j;\ \Delta u^j = \Psi^N \Delta u^j_N;\ |\mathbf{G}_3| = \lambda \quad (N = 1,3). \tag{1}$$

In (1), $\lambda = h/h_0$ is the ratio of the thickness of the plate in C and C_0, Δu^i_N are the nodal incremental displacements and $\Psi^N (= \Phi^N + \beta^N_\alpha \theta^\alpha)$ is the Lagrangian interpolation function. The convention that Greek indices range over values 1,2 and Latin indices over 1,2, and 3 is adopted herein.

The increments of Green's strain tensor are expressed by

$$\Delta\gamma_{\alpha\beta} = (\Delta u_\alpha|_\beta + \Delta u_\beta|_\alpha)/2 = (\beta_{N\beta}\Delta u^N_\alpha + \beta_{N\alpha}\Delta u^N_\beta)/2$$
$$\Delta\gamma_{33} = \lambda\Delta\lambda = A^{\alpha\beta}_{33}\Delta\gamma_{\alpha\beta} \tag{2}$$

It is assumed the process is one of plane stress and the coefficients $A^{\alpha\beta}_{33}$ can be derived on this basis. Covariant differentiations of the displacements leads to (Nakamachi et al., 1982),

$$\Delta u_j|_i = {}_N\Psi^r_{ji}\Delta u^N_r, \quad \Delta u^j|_i = {}^N\Phi^j_{ri}\Delta u^r_N \tag{3}$$

When the material contacts the punch the incremental surface force $\Delta\mathbf{T}$ per unit area, acting at the interface, is expressed as the sum of pressure load $\Delta\mathbf{s}$ and frictional force $\Delta\tau$, which is derived from Coulomb's law. In what follows p and Δp are the pressure and its increment, respectively, and μ is the coefficient of friction. Hence

$$\Delta\mathbf{T}dA = \Delta T^i\mathbf{G}_i dA = \Delta\mathbf{s}dA + \Delta\tau dA$$
$$\Delta\mathbf{s}dA = (p+\Delta p)\bar{\mathbf{n}}\overline{dA} - p\mathbf{n}dA \tag{4}$$
$$\Delta\tau dA = \mu(p+\Delta p)\bar{\mathbf{v}}\overline{dA} - \mu p\mathbf{v}dA$$

In the foregoing $\bar{\mathbf{n}}$ and $\mathbf{n}$ are the unit normal vectors at the infinitesimal surface dA in $\bar{C}$ and C. While $\bar{\mathbf{v}}$ and $\mathbf{v}$ are the unit tangential vectors in $\bar{C}$ and C, defined in the sliding direction of the contacting point. It is assumed that the frictional force acts to oppose sliding.

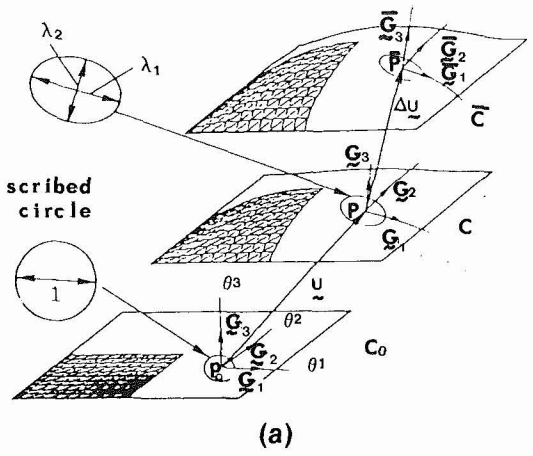
The pressure increment Δp is determined by satisfying equilibrium in a direction normal to the membrane surface as follows

$$-\Delta p = h\Delta\tau^{\alpha\beta}b_{\alpha\beta} + \Delta\lambda h_0\tau^{\alpha\beta}b_{\alpha\beta} + h\tau^{\alpha\beta}\Delta b_{\alpha\beta} \tag{5}$$

The terms $\tau^{\alpha\beta}$ and $\Delta\tau^{\alpha\beta}$ are the Cauchy stress and its Oldroyd increment, while $b_{\alpha\beta}$ and $\Delta b_{\alpha\beta}$ define the curvature tensor and its increment. These latter quantities can be derived from the

Contributed by the Applied Mechanics Division for publication in the JOURNAL OF APPLIED MECHANICS.
Discussion on this paper should be addressed to the Editorial Department, ASME, United Engineering Center, 345 East 47th Street, New York, NY 10017, and will be accepted until two months after final publication of the paper itself in the JOURNAL OF APPLIED MECHANICS. Manuscript received by ASME Applied Mechanics Division, March 21, 1988.

Copyright © 1988 by ASME
Downloaded 03 May 2010 to 171.66.16.21. Redistribution subject to ASME license or copyright; see http://www.asme.org/terms/Terms_Use.cfm



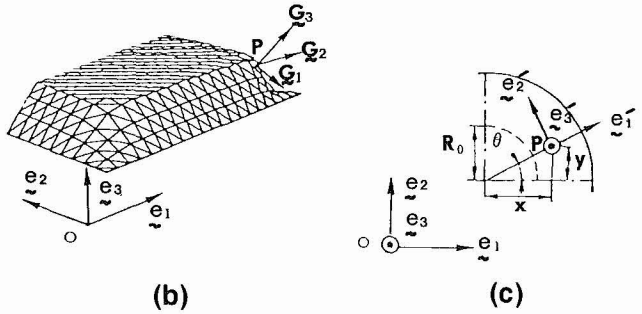


Fig. 1 (*a*) Displacements and embedded coordinate system for a triangular element; (*b*) reference Cartesian coordinates e_j; (*c*) coordinate system at the punch corner

known principal curvatures B_{ij} (referred to $\mathbf{e}_i$) and B'_{ij} (referred to $\mathbf{e}'_i$), as shown in Fig. 1(*b*). B_{ij} and B'_{ij} are evaluated from the punch geometry and

$$\mathbf{b} = b_{\alpha\beta}\mathbf{G}^\alpha \otimes \mathbf{G}^\beta = B_{\delta\nu}\mathbf{e}_\delta \otimes \mathbf{e}_\nu = B'_{\xi\zeta}\mathbf{e}'_\zeta \otimes \mathbf{e}'_\xi,$$
$$\mathbf{G}_i = \theta^j_i \mathbf{e}_j \quad \text{and} \quad \mathbf{e}_i = \theta'^j_i \mathbf{e}'_j \tag{6}$$

The incremental pressure Δp is expressed as follows

$$\Delta_p = Q^M_i \Delta u^i_M \qquad (M = 1, 3)$$
$$Q^M_\eta = (-hE^{\alpha\beta\delta\nu} b_{\alpha\beta} - pG^{\delta\nu})(\beta^M_\delta G_{\eta\nu} + \beta^M_\nu G_{\eta\delta})/2 - h\tau^{\alpha\beta} S^M_{\alpha\beta\eta} \tag{7}$$
$$Q^M_3 = -h\tau^{\alpha\beta} S^M_{\alpha\beta 3}$$

In the above

$$S^M_{\alpha\beta i} = B_{\delta\nu}(\theta^\delta_a \theta^\nu_i \beta^M_\beta + \theta^\nu_\beta \theta^\delta_i \beta^M_a) + [B'_{\delta\nu}(\theta'^{\,\delta}_a \Pi^\nu_{\beta i} + \theta'^{\,\nu}_\beta \Pi^\delta_{ai}) + C_{22i}\theta'^{\,2}_a \theta'^{\,2}_\beta]\Psi^M.$$

The nonvanishing coefficients of Π^β_{ai} and C_{22i} are given only at the corner of the punch shoulder, see Fig. 1(*b*), as

$$\Pi^1_{1i} = \Pi^2_{2i} = x/r[(1/x - x/r^2)\theta^1_i - y/r^2\theta^2_i]$$
$$\Pi^1_{2i} = -\Pi^2_{1i} = y/r[(1/y - y/r^2)\theta^2_i - x/r^2\theta^1_i] \tag{8}$$
$$C_{22i} = -R_0(x\theta^1_i + y\theta^2_i)/(r^3\rho'_1),$$

where ρ'_1 is the radius of curvature in the direction e'_1. The values x, y, r, R_0 are shown in Fig. 1(*c*). For simplicity, it is assumed that the sliding direction $\tilde{\mathbf{v}}$ is equal to $\mathbf{v}$, which is determined in the previous incremental step.

Finally, the incremental forces are expressed as

$$\Delta T^\alpha = -\lambda p G^{\beta\alpha}\beta^M_\beta \Delta u^3_M + \mu Q^M_i \Delta u^i_M v^\alpha + \mu p v^\alpha \beta^M_\beta \Delta u^\beta_M$$
$$\Delta T^3 = Q^M_i \Delta u^i_M/\lambda + p\beta^M_\alpha \Delta u^\alpha_M/\lambda + \mu p v^\alpha \beta^M_\alpha \Delta u^3_M \tag{9}$$

The material is treated as an elastic, work-hardened solid

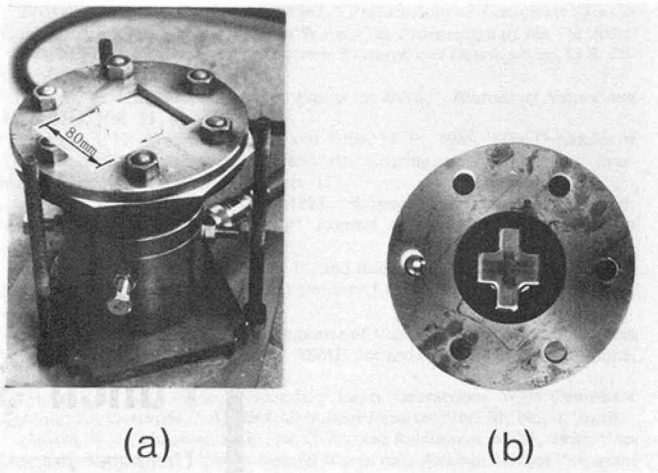


Fig. 2 (*a*) Punch stretching apparatus; (*b*) as (*a*) but with die and testpiece removed

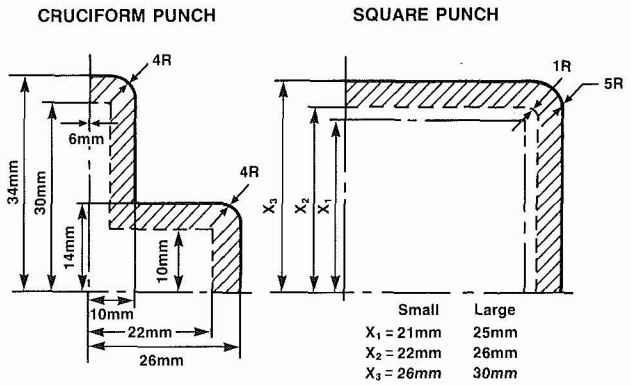


Fig. 3 Dimension of the punches

which satisfies the J_2 flow theory, taking into account finite deformation. The linear relationship between Jaumann increment of Cauchy stress and Eulerian increment of strain is, see Nakamachi et al. (1982),

$${}_J\Delta\tau^{\alpha\beta} = D^{\alpha\beta\delta\nu}\Delta\gamma_{\delta\nu}, \quad \Delta\tau^{\alpha\beta} = E^{\alpha\beta\delta\nu}\Delta\gamma_{\delta\nu}$$

$$E^{\alpha\beta\delta\nu} = D^{\alpha\beta\delta\nu} - (G^{\beta\nu}\tau^{\delta\alpha} + G^{\delta\beta}\tau^{\nu\alpha} + G^{\alpha\delta}\tau^{\beta\nu} + G^{\alpha\nu}\tau^{\beta\delta})/2 \tag{10}$$

The virtual work equation leads to the equation of motion of the finite element in the following incremental form

$$\mathbf{K}\Delta\mathbf{u} = (K^{iM}_{jN} + {}_{(\sigma)}K^{iM}_{jN} + {}_{(G)}K^{iM}_{jN} + {}_{(s)}R^{iM}_{jN})\Delta u^j_M = 0 \tag{11}$$

where

$$K^{\alpha M}_{\beta N} = E^{\delta\alpha\nu\lambda}\beta^M_\nu G_{\lambda\beta}\beta_{N\delta}\lambda h_0 A_e$$
$${}_{(\sigma)}K^{iM}_{jN} = (n^{\delta\nu}\beta^M_\nu \beta_{N\delta})\delta^i_j A_e$$
$${}_{(G)}K^{\alpha M}_{\beta N} = (n^{\alpha\nu}\beta^M_\beta \beta_{N\nu} + A^{\delta\eta}_{33}\beta^M_\eta G_{\delta\beta}\beta_{N\nu} n^{\alpha\nu}/\lambda^2)A_e$$
$${}_{(s)}R^{\alpha M}_{\beta N} = -\mu(Q^M_\beta v^\alpha + pv^\alpha\beta^M_\beta)A_N$$
$${}_{(s)}R^{3M}_{3N} = -(Q^M_3/\lambda + \mu p v^\alpha \beta^M_\delta)A_N$$
$${}_{(s)}R^{\alpha M}_{3N} = (\lambda p G^{\beta\alpha}\beta^M_\beta - \mu Q^M_3 v^\alpha)A_N$$
$${}_{(s)}R^{3M}_{\alpha N} = -(Q^M_\alpha/\lambda + p\beta^M_\alpha/\lambda)A_N$$

Previously shown

$$n^{\alpha\beta} = \tau^{\alpha\beta}\lambda h_0, \; A_N = \sqrt{a}\int_{A_0} \Psi_N dA \text{ and } A_e = \sqrt{a}\int_{A_0} dA.$$

Note that A_0 is the area of the finite element in the initial state C_0 and δ^i_j is the Kronecker delta.

Downloaded 03 May 2010 to 171.66.16.21. Redistribution subject to ASME license or copyright; see http://www.asme.org/terms/Terms_Use.cfm

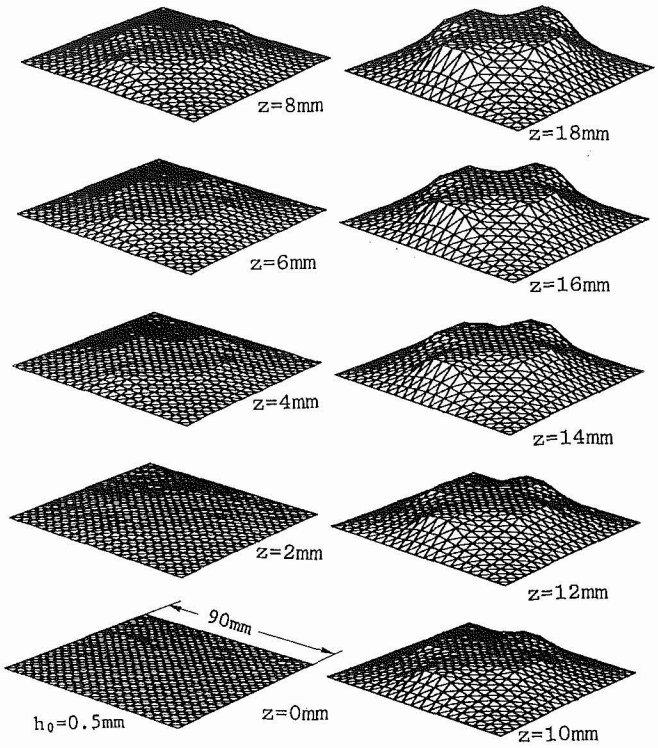


Fig. 4 Predicted shape of the deforming specimen when impressed with the cruciform punch, $\mu = 0.20$

The stiffness matrices $\mathbf{K}$ are assembled to be the total stiffness matrix $\bar{\mathbf{K}}$, referred to the fixed Cartesian axes in the usual manner. The incremental displacement $\Delta\mathbf{u}$ is given by the sum of the increment of the punch travel $\Delta\mathbf{U}$ and the unknown incremental displacement Δu^*. Therefore the stiffness equation can be rewritten as

$$\bar{\mathbf{K}}\Delta\mathbf{u}^* = -\bar{\mathbf{K}}\Delta\mathbf{U} \tag{12}$$

When the workpiece contacts the punch, the subsequent motion of the material element is along the punch surface. In this incremental calculation procedure, a friction model, named *slip-stick*, is employed (Nakamachi and Sowerby, 1982), where the equilibrium at a contacting node is checked, viz.,

$$|n^{\alpha\beta}|_{\alpha}\mathbf{G}_{\beta}| - |\mu p\mathbf{v}| \tag{13}$$

≥ 0 slip under Coulomb's law and < 0 sticking.

Results and Conclusion

Pure aluminum (1100-0) sheets, 0.50-mm thick, were clamped around their periphery and impressed by rigid punches, the apparatus is shown in Fig 2. The bottom faces of the punches were spherical with a radius of curvature of 1000 mm. Three different punches were employed, two were square in cross section; while the cross section of the third was like a *cruciform*. The geometries are shown in Fig. 3. In all cases, the blend radii (ρ_1 and ρ_1') joining the base of the punch to its stem (or flank), were 4 mm; see Fig. 3.

Uniaxial tensile tests performed on the aluminum revealed the following mechanical property data: Young's modulus (E) = 65 GPa, Yield stress (σ_y) = 25 MPa and Poisson's ratio (ν) = 0.325. The representative stress-strain curve was assumed to be

$$\bar{\sigma} = 180(9.7886 \times 10^{-4} + \bar{\epsilon}^p)^{0.285} \text{ MPa} \tag{14}$$

The aforementioned material properties were employed in finite element analysis.

The die plate was bolted in position, as is evident from Fig. 2. The die opening was a square of 80-mm side and the die radius was about 2 mm. There was not observable drawing in of the flange in any of the experiments. In the finite element model, it was assumed the blank was rigidly clamped (no drawing-in). The die radius was ignored in the analysis, that is, the radius was taken as zero rather than 2 mm. Due to symmetry only one quarter of the blank was considered, and this was divided into 200 triangular elements. Two coefficients of friction were used in the analysis, a value of 0.2 was assumed to characterize an unlubricated (or dry) condition, while $\mu = 0.02$ represented a lubricated test. In the actual tests, Molyslip was used as a lubricant.

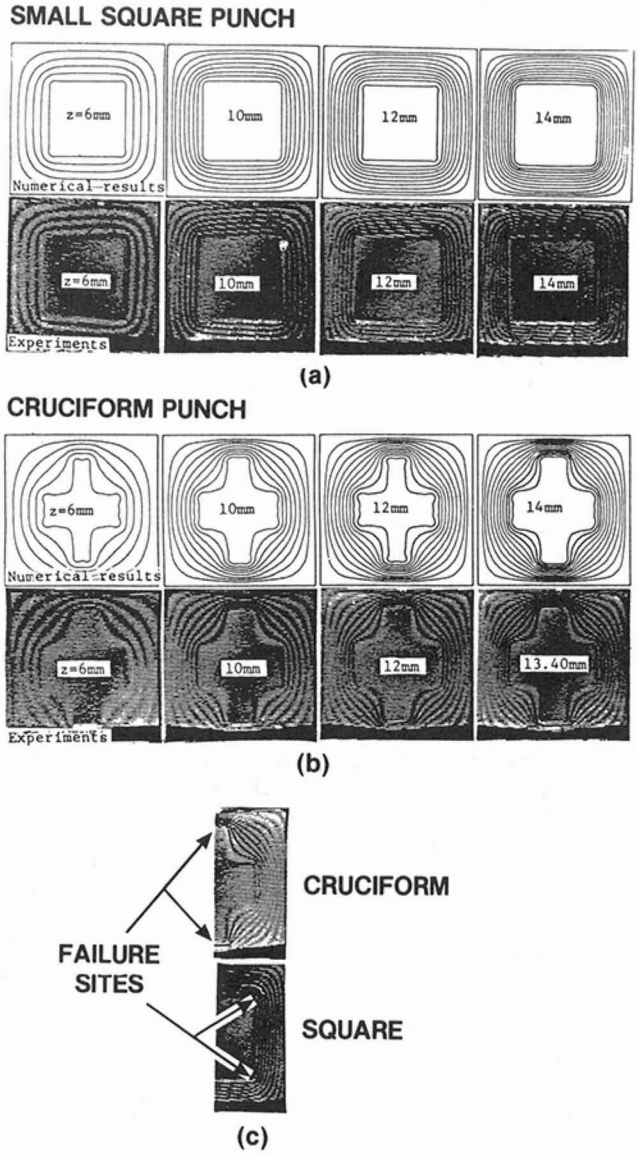


Fig. 5 Comparison of the predicted (with $\mu = 0.02$) and experimental (Moiré topography), equal height contours; (*a*) small square punch, (*b*) cruciform punch, and (*c*) experimentally determined failure sites of the two punches

Figure 4 shows the predicted blank shape at different stages in the deformation process when using the *cruciform* punch under dry conditions. When performing the experiments a Moiré fringe technique, see Takasaki (1970), was employed to determine contours of equal height on the deforming blank. In the present work, the difference in height between succesive fringes was 1.19 mm. Variations in the fringe patterns with punch penetration are shown in Figs. 5(*a*, *b*), for the *cruciform* and smaller *square* punch, respectively; the punches

Downloaded 03 May 2010 to 171.66.16.21. Redistribution subject to ASME license or copyright; see http://www.asme.org/terms/Terms_Use.cfm

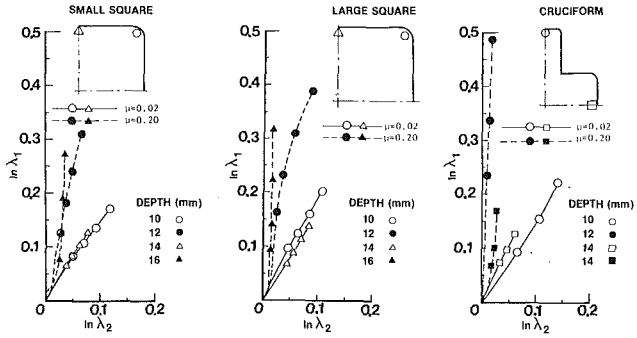


Fig. 6 Predicted path of the principal natural strains, ln λ_1 and ln λ_2, at specific locations on the base of each punch

were lubricated. The predicted equal height contours are shown in these figures for comparison. The experimentally determined failure sites (due to thinning of the material) for each punch are shown in Fig. 5(*c*).

The strain predictions confirm the observed failure zones, as demonstrated in Fig. 6. Two possible failure sites were considered for each of the three punches, and principal surface strains were then calculated within elements which coincided with the selected locations as the punch descended. The calculated largest principal surface strain coincided with the failure site. The absence of lurication moves the strain path towards plane strain at the points considered.

Figures 7(*a–c*) show the calculated contours of principal surface strains, as a function of punch travel, under dry and lubricated conditions. It is predicted that very little stretching of the material occurs over the base of each punch under dry conditions. Furthermore at each stage in the deformation process, the absence of a lubricant resulted in higher strain levels and larger strain gradients in the specimen.

A comparison of the predicted and measured variation of punch load with penetration is provided in Fig. 8 for each punch. The corresponding trends are favorable but the predicted loads show more fluctuations. There are only a few publications in the open literature on the stretch forming of nonaxisymmetric shapes. Stoughton (1986) has considered the stretching of peripherally clamped, rectangular, low carbon steel sheets with a rectangular punch. Of concern was the thinning of material in the vicinity of the punch nose radius. Stoughton (1986) provided results from a finite element, membrane code and from the same code modified to allow (in an approximate manner) for bending. The hybrid bending model predicted localized thinning, consistent with the experimental findings; a coefficient of friction was selected to provide the most consistent correlation with experimental data. The present investigation presents a more realistic friction model, but does not allow for thinning due to bending. This may be one of the reasons for the discrepancy between the predicted and measured loads in Fig. 8. Odell and Clausen (1977) have performed calculations, based on both a membrane and bending numerical model, for the axisymmetric cup drawing process; the bending analysis predicted the lowest drawing load. A disturbing feature of the results of Fig. 8 is that the variation is not consistent for each test, and consequently, it is difficult to isolate the cause of the error. As already mentioned, there was no observable drawing-in of the clamped flange in any of the tests; consequently, frictional sliding at the clamps is not a factor. The fluctuations in the predicted drawing loads in the present work is attributed to the method employed for assessing the punch force. A value was computed only when every node of the individual element contacted the punch; those elements in partial contact were ignored.

The present work emphasises the strong influence of punch geometry and frictional conditions on the level and distribution of strain in stretch formed blanks. The same finite element code can also be used to simulate drawing operations (Nakamachi, 1987), although the computational time is invariably increased. This is due to the fact that elements can unload when material is drawn-in. It is necessary to check all elements for this possibility, and to ascertain the stage where they may again begin to deform plastically. There is also the danger of buckling the component in drawing operations, and a reliable and easily implemented criterion for predicting the onset of wrinkling has yet to be established. The deep drawing of square cups has been investigated by Toh and Kobayashi (1985) and Iseki and Murota (1984 and 1986). A finite element, membrane analysis was employed in each of these drawing studies. The correlation between the predicted and experimental punch load-punch travel behavior tended to be poor.

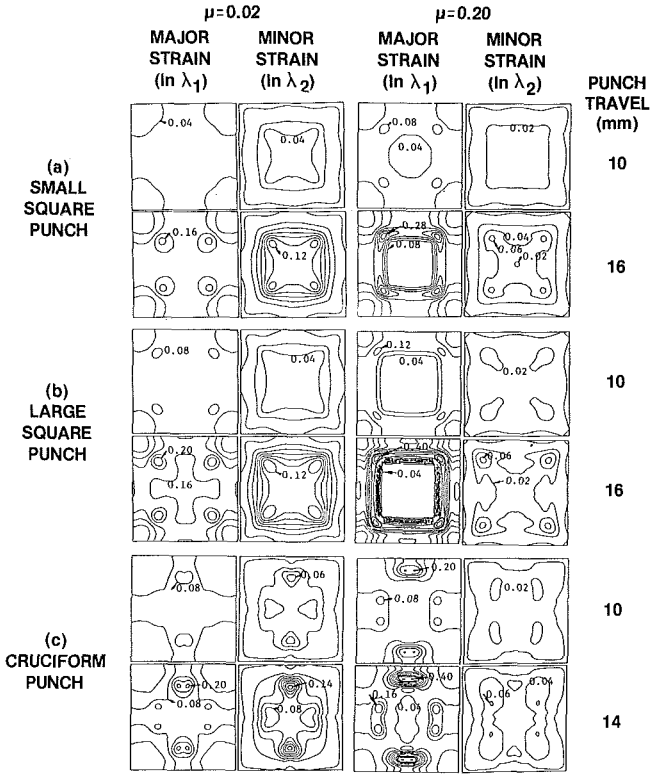


Fig. 7 Predicted contours of the principal strains for the three punches for two different friction conditions

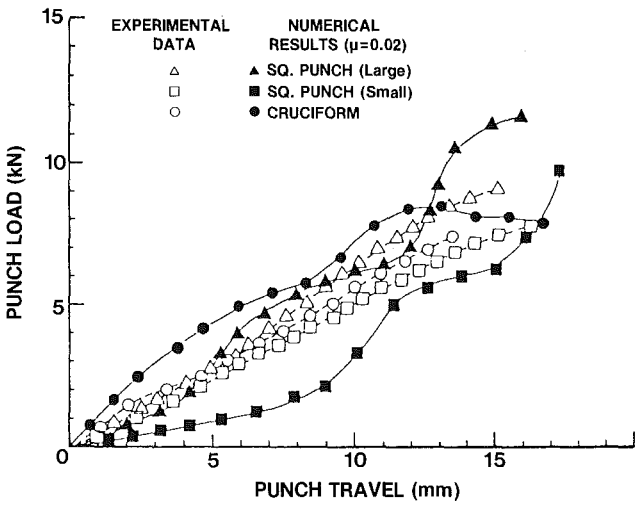


Fig. 8 Comparison of the predicted (with $\mu = 0.02$) and experimental punch load versus punch travel for the three punches

Downloaded 03 May 2010 to 171.66.16.21. Redistribution subject to ASME license or copyright; see http://www.asme.org/terms/Terms_Use.cfm

things as interfacial frictional conditions and boundary conditions (e.g., how the flange of the blank is constrained), and how these may change during forming. Without these input data, the results of any analysis are likely to be severely limited.

The application of large strain finite element codes to analyze complex stamping operations is usually expensive. The costs can become prohibitive (even to large corporations) if the programs are run indiscriminately, making only minor adjustments to boundary conditions and the like. Ideally such codes should receive input from an experienced die designer, and the execution will serve to complement the designer's intuition. The modeling must be close to the actual operating conditions, otherwise, the real effect of making minor changes to the operating conditions (including modifications to the blank shape) cannot be estimated.

References

Green, A. E., and Zerna, W., 1968, *Theoretical Elasticity*, Oxford University Press.

Iseki, H., and Murota, T., 1984, "Analysis of Deep Drawing of Non-Axisymmetric Cups by the Finite Element Method," *Proceedings 1st International Conference on Technology of Plasticity*, Japan Society Tech. Plasticity, pp. 678–684.

Iseki, H., and Murota, T., 1986, "On the Determination of the Optimum Blank Shape of Non-Axisymmetric Drawn Cups by the Finite Element Method," *Bulletin JSME*, Vol. 29, pp. 1033–1040.

Nakamachi, E., Takezono, S., and Sowerby, R., 1982, "A Numerical Analysis of the Hydraulic Bulging of Circular Disks Into Axisymmetric Dies," ASME JOURNAL OF APPLIED MECHANICS, Vol. 99, pp. 501–506.

Nakamachi, E., and Sowerby, R., 1982, "A Numerical Analysis of the Punch Stretching of Peripherally Clamped Circular Disks," *Numerical Methods in Industrial Forming Processes*, J. F. T. Pittman, et al., eds., Pinderidge Press, pp. 641–651.

Nakamachi, E., 1987, "Finite Element Modeling of the Punch Press Forming of Sheet Metal," *Proceedings 2nd International Conference on Technology of Plasticity*, Springer-Verlag, pp. 625–632.

Odell, E. I., and Clausen, W. E., 1977, "Numerical Solution of a Deep Drawing Problem," ASME *Journal of Engineering for Industry*, Vol. 99, pp. 206–209.

Stoughton, T. B., 1986, "Finite Element Modeling of 1008 AK Sheet Steel Stretched Over a Rectangular Punch with Bending Effects," in *Computer Modeling of Sheet Metal Forming Processes*, N. M. Wang and S. C. Tang, eds., The Metallurgical Society Inc., Warrendale, PA, pp. 143–160.

Takasaki, H., 1970, "Moire Topography," *Applied Optics*, Vol. 9, pp. 1467–1472.

Toh, C. H., and Kobayashi, S., 1985, "Deformation and Blank Analysis in Square Cup Drawing," *Int. J. Mach. Tool Des. Res.*, Vol. 25, pp. 15–32.

Downloaded 03 May 2010 to 171.66.16.21. Redistribution subject to ASME license or copyright; see http://www.asme.org/terms/Terms_Use.cfm

R. H. Plaut
Professor.
Mem. ASME
T. D. Fagan
Graduate Student
Department of Civil Engineering,
Virginia Polytechnic Institute
and State University,
Blacksburg, VA 24061

Vibrations of an Inextensible, Air-Inflated, Cylindrical Membrane

Two-dimensional vibrations of a long cylindrical membrane are considered. The membrane is attached to a horizontal base along two generators and is inflated with air. It is assumed that the membrane material is inextensible. The weight of the membrane is included in the analysis. First, the equilibrium shape of the cross-section is determined, and then small vibrations about this configuration are studied. It is found that the vibration frequencies decrease as the membrane weight is increased.

Introduction

A cylindrical membrane, anchored along two generators and inflated by a uniform pressure, is considered. The material is assumed to be inextensible, and its weight is included in the analysis. The membrane is assumed to be sufficiently long so that a two-dimensional analysis of a cross-section is appropriate.

If the membrane weight is neglected, the static shape of the cross-section is circular. Small, two-dimensional vibrations about this circular static shape were analyzed by Firt (1983). When the membrane weight is included, the analysis becomes considerably more difficult. The effect of the weight on the vibration frequencies is determined here, and the corresponding vibration modes are found.

This work is an initial part of a study on the dynamic behavior of inflatable dams. The effect of membrane weight on the equilibrium configurations of such dams was analyzed previously by Parbery (1978).

Static Analysis

Consider a portion of the membrane with unit width along the generators. The cross-sectional shape is shown in Fig. 1. The horizontal coordinate is x, the vertical coordinate is y, the arc length from the origin is s, the perimeter is s_0, and the angle between the horizontal and the membrane tangent is $\psi_0(s)$. The membrane is anchored to a horizontal base at $(x, y) = (0, 0)$ and $(b, 0)$. For this unit width, the forces acting on the membrane are the internal gauge air pressure q (force/length) and the membrane weight p (force/length).

A free-body diagram of an element of the cross-section from s to $s + ds$ is depicted in Fig. 2. The tension is denoted T_1. If forces are summed in the normal direction and the resulting equation is divided by ds, one obtains the equilibrium equation (Parbery, 1976)

$$T_1 \frac{d\psi_0}{ds} = p \cos \psi_0 - q \tag{1}$$

after letting $ds \to 0$. Similarly, equilibrium in the tangential direction yields

$$\frac{dT_1}{ds} = p \sin \psi_0. \tag{2}$$

From Fig. 2, one can also write

$$\frac{dy}{ds} = \sin \psi_0, \tag{3}$$

$$\frac{dx}{ds} = \cos \psi_0. \tag{4}$$

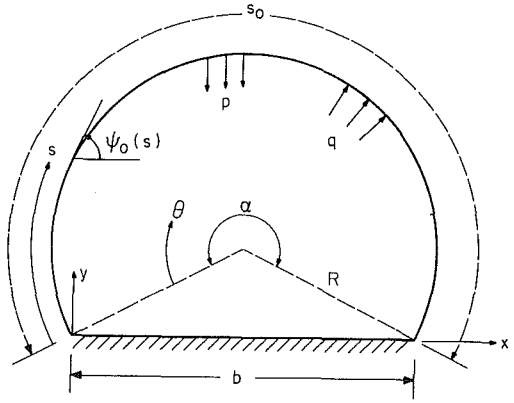


Fig. 1 Equilibrium configuration of cross section

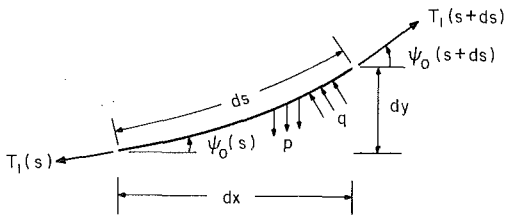


Fig. 2 Element of cross section in equilibrium

Contributed by the Applied Mechanics Division for publication in the JOURNAL OF APPLIED MECHANICS.

Discussion on this paper should be addressed to the Editorial Department, ASME, United Engineering Center, 345 East 47th Street, New York, N.Y. 10017, and will be accepted until two months after final publication of the paper itself in the JOURNAL OF APPLIED MECHANICS. Manuscript received by ASME Applied Mechanics Division, October, 13, 1987; final revision, February 1, 1988.

Copyright © 1988 by ASME
Downloaded 03 May 2010 to 171.66.16.21. Redistribution subject to ASME license or copyright; see http://www.asme.org/terms/Terms_Use.cfm

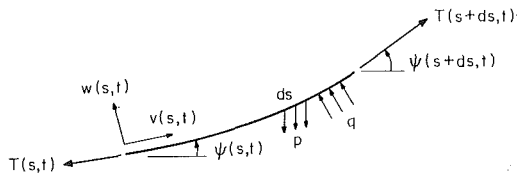


Fig. 3 Element of cross-section during motion

Equations (1)-(4) govern the equilibrium of the membrane. By combining (2) and (3), one can show that

$$T_1 = py + T_0 \tag{5}$$

where T_0 is the tension at the supports. If the membrane weight is neglected ($p=0$), then (1)-(5) lead to a circular cross-section of radius R, with

$$T_1 = T_0, \quad \frac{d\psi_0}{ds} = -\frac{q}{T_0} = -\frac{1}{R}. \tag{6}$$

Dynamic Analysis

In order to analyze the vibrations of the membrane about its equilibrium configuration, consider the element shown in Fig. 3. The tension T depends on position s and time t, as do the angle ψ of the membrane tangent, the tangential displacement v, and the normal displacement w. For this portion of the membrane with unit width, the constant mass per unit length along the cross-section is denoted μ.

With the use of Fig. 3, the equations of motion in the tangential and normal directions are found to be

$$\mu \frac{\partial^2 v}{\partial t^2} = \frac{\partial T}{\partial s} - p \sin \psi \tag{7}$$

and

$$\mu \frac{\partial^2 w}{\partial t^2} = T \frac{\partial \psi}{\partial s} + q - p \cos \psi, \tag{8}$$

respectively. It is convenient to solve (8) for T, differentiate the result with respect to s, substitute into (7), and multiply by $(\partial\psi/\partial s)^2$. This yields

$$\mu\left(\frac{\partial \psi}{\partial s}\right)^2 \frac{\partial^2 v}{\partial t^2} = -\mu \frac{\partial^2 \psi}{\partial s^2} \frac{\partial^2 w}{\partial t^2} + \mu \frac{\partial \psi}{\partial s} \frac{\partial^3 w}{\partial s \partial t^2} + q \frac{\partial^2 \psi}{\partial s^2} - \frac{dq}{ds} \frac{\partial \psi}{\partial s} - p \frac{\partial^2 \psi}{\partial s^2} \cos \psi - 2p\left(\frac{\partial \psi}{\partial s}\right)^2 \sin \psi \tag{9}$$

where we allow q to be a function of s for now.

The dynamic curvature, $\partial\psi/\partial s$, can be related to the static curvature, $d\psi_0/ds$. From results in Henrych (1981), the change in curvature, ΔK, is given by the geometrical relation

$$\Delta K = \left[\frac{\partial^2 w}{\partial s^2} + \left(\frac{d\psi_0}{ds}\right)^2 w + \frac{d^2\psi_0}{ds^2} v\right] \Big/ \left(1 + \frac{\partial v}{\partial s} - \frac{d\psi_0}{ds} w\right). \tag{10}$$

For the linear analysis to be carried out here, (10) can be reduced to give

$$\frac{\partial \psi}{\partial s} = \frac{d\psi_0}{ds} + \frac{\partial^2 w}{\partial s^2} + \left(\frac{d\psi_0}{ds}\right)^2 w + \frac{d^2\psi_0}{ds^2} v. \tag{11}$$

The assumption of inextensibility implies that the tangential strain is zero, i.e., (Firt, 1983),

$$\frac{1}{R}\left(\frac{\partial v}{\partial \psi} - w\right) = 0, \tag{12}$$

where R is the radius of curvature. With the use of (11), one can then write

$$w = \left(\frac{d\psi_0}{ds}\right)^{-1} \frac{\partial v}{\partial s} \tag{13}$$

for the linear analysis. Using (13) in (11) and then integrating, one obtains

$$\psi = \psi_0 + \frac{\partial w}{\partial s} + \frac{d\psi_0}{ds} v. \tag{14}$$

Equations (11), (13), and (14) are now substituted into (9). The resulting equation in $v(s, t)$ is linearized. With the notation

$$A = \frac{d\psi_0}{ds}, \quad B = \frac{d^2\psi_0}{ds^2}, \quad C = \frac{d^3\psi_0}{ds^3}, \quad D = \frac{d^4\psi_0}{ds^4}, \tag{15}$$

and with subscripts s and t denoting partial derivatives, this yields the equation of motion

$$\mu v_{sstt} - 2\mu A^{-1} B v_{stt} - \mu A^2 v_{tt} - T_1 v_{ssss} + k_1 v_{sss} + k_2 v_{ss} + k_3 v_s + k_4 v = 0 \tag{16}$$

where

$$k_1 = -2p \sin \psi_0 + 4A^{-1} B T_1, \tag{17}$$

$$k_2 = 5pA^{-1} B \sin \psi_0 - 2pA \cos \psi_0 - 8A^{-2} B^2 T_1 + 3A^{-1} C T_1 - A^2 T_1, \tag{18}$$

$$k_3 = (-5pA^{-2} B^2 + 2pA^{-1} C - 2pA^2) \sin \psi_0 + 2pB \cos \psi_0 + 8A^{-3} B^3 T_1 - 7A^{-2} BCT_1 + A^{-1} DT_1 - ABT_1, \tag{19}$$

$$k_4 = -pAB \sin \psi_0 - 2pA^3 \cos \psi_0 + B^2 T_1 - ACT_1. \tag{20}$$

Constant terms have been eliminated from (16) with the use of (1) and its derivative, which can be written as

$$q_s = -2pA \sin \psi_0 - T_1 B \tag{21}$$

after applying (2).

With q constant here, one can set q_s, q_{ss}, and q_{sss} equal to zero, and the resulting equations can be utilized to simplify the k_j. One can then write

$$k_1 = -10p \sin \psi_0, \tag{22}$$

$$k_2 = -8pA \cos \psi_0 + 12pA^{-1} B \sin \psi_0 - A^2 T_1, \tag{23}$$

$$k_3 = 2pA^2 \sin \psi_0 + 9pB \cos \psi_0 - 2pA^{-1} C \sin \psi_0, \tag{24}$$

$$k_4 = 0. \tag{25}$$

Let the vibration frequencies and modes be denoted ω and $V(s)$, respectively, with

$$v(s, t) = V(s) \cos \omega t. \tag{26}$$

Equation (26) is substituted into (16), leading to the equation

$$-T_1 V'''' + k_1 V''' + k_2 V'' + k_3 V' + k_4 V - \omega^2(\mu V'' - 2\mu A^{-1} B V' - \mu A^2 V) = 0 \tag{27}$$

with boundary conditions

$$V = V' = 0 \text{ at } s = 0 \text{ and } s = s_0, \tag{28}$$

due, in part, to (13).

Case of Negligible Weight

Consider the case $p=0$. With the use of (6) and (15), (28) can be put in the form

$$R^4 V'''' (s) + (1+\lambda) R^2 V'' (s) - \lambda V(s) = 0 \tag{29}$$

where

$$\lambda = \mu R \omega^2 / q. \tag{30}$$

If the internal angle θ is used as the coordinate, with central angle α, as shown in Fig. 1, one has

$$s = R\theta, \; s_0 = R\alpha. \tag{31}$$

Equation (29) then becomes

Downloaded 03 May 2010 to 171.66.16.21. Redistribution subject to ASME license or copyright; see http://www.asme.org/terms/Terms_Use.cfm

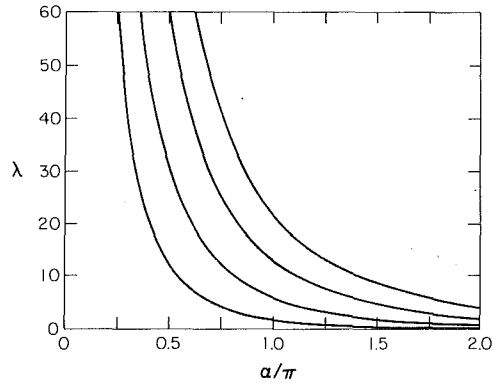


Fig. 4 Lowest four eigenvalues as function of central angle for $p=0$ (Hsieh, 1988)

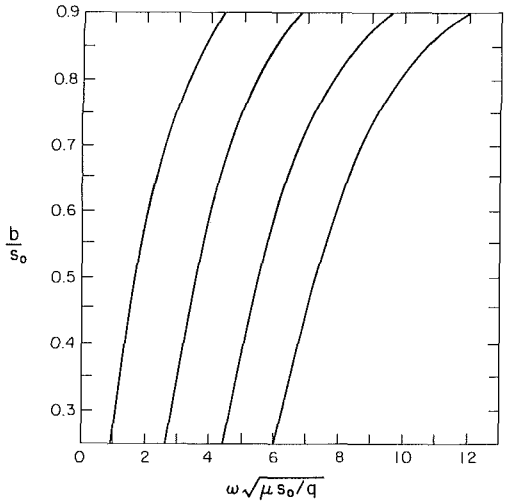


Fig. 5 Lowest four frequencies as function of base/perimeter ratio for $p=0$

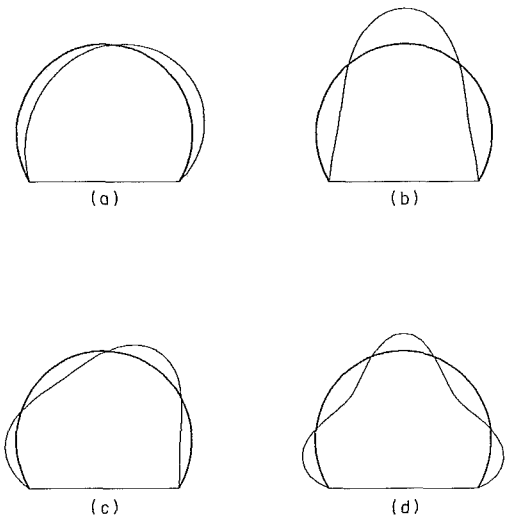


Fig. 6 Mode shapes for $b/s_0=2/5$ and $p=0$

$$V''''(\theta)+(1+\lambda)V''(\theta)-\lambda V(\theta)=0, \tag{32}$$

with boundary conditions

$$V(0)=V(\alpha)=V'(0)=V'(\alpha)=0 \tag{33}$$

from (28).

Equation (32) is the same as (1.10) in Chapter IV of Firt (1983), except that the dependent variable there is the normal displacement rather than the tangential displacement. The general solution is

Table 1 Eigenvalues $\lambda=\mu R\omega^2/q$

$10\alpha/\pi$	λ_1	λ_2	λ_3	λ_4
1	396.03	815.64	1596.02	2416.06
2	96.11	201.93	396.08	602.02
3	40.69	88.30	173.94	266.10
4	21.42	48.56	96.27	148.54
5	12.62	30.19	60.40	94.14
6	7.95	20.24	40.98	64.61
7	5.22	14.27	29.32	46.81
8	3.53	10.42	21.80	35.27
9	2.44	7.81	16.68	27.37
10	1.70	5.96	13.05	21.74
11	1.20	4.62	10.39	17.58
12	0.85	3.62	8.39	14.42
13	0.60	2.85	6.85	11.98
14	0.42	2.26	5.64	10.05
15	0.29	1.80	4.69	8.50
16	0.19	1.44	3.91	7.24
17	0.12	1.15	3.28	6.21
18	0.07	0.92	2.77	5.35
19	0.03	0.73	2.34	4.63
20	0.00	0.57	1.98	4.01

Table 2 Static tension parameter $\bar{T}_0=T_0/(qs_0)$

p/q	$b/s_0=1/4$	$b/s_0=1/3$	$b/s_0=2/5$
0	0.2021	0.2194	0.2353
0.001	0.2017	0.2190	0.2348
0.005	0.2001	0.2173	0.2331
0.010	0.1981	0.2153	0.2310
0.020	0.1943	0.2112	0.2267
0.030	0.1904	0.2071	0.2224
0.040	0.1866	0.2030	0.2181

$$V(\theta)=K_1\cos\frac{\beta\theta}{\alpha}+K_2\sin\frac{\beta\theta}{\alpha}+K_3\cosh\frac{\gamma\theta}{\alpha}+K_4\sinh\frac{\gamma\theta}{\alpha} \tag{34}$$

where

$$\beta=\frac{\alpha}{\sqrt{2}}(1+\lambda+\sqrt{1+6\lambda+\lambda^2})^{1/2}, \tag{35}$$

$$\gamma=\frac{\alpha}{\sqrt{2}}(-1-\lambda+\sqrt{1+6\lambda+\lambda^2})^{1/2}. \tag{36}$$

Applyling (33) leads to the characteristic equation

$$2\beta\gamma(1-\cos\beta\cosh\gamma)+(\gamma^2-\beta^2)\sin\beta\sinh\gamma=0. \tag{37}$$

The mode shapes in the tangential and normal directions, respectively, are given by

$$V(\theta)=c\left(-\cos\frac{\beta\theta}{\alpha}+M\sin\frac{\beta\theta}{\alpha}+\cosh\frac{\gamma\theta}{\alpha}-\frac{M\beta}{\gamma}\sinh\frac{\gamma\theta}{\alpha}\right), \tag{38}$$

$$W(\theta)=-\frac{c\beta}{\alpha}\left(M\cos\frac{\beta\theta}{\alpha}+\sin\frac{\beta\theta}{\alpha}-M\cosh\frac{\gamma\theta}{\alpha}+\frac{\gamma}{\beta}\sinh\frac{\gamma\theta}{\alpha}\right), \tag{39}$$

where c is an arbitrary constant and

$$M=\left(\sin\beta+\frac{\gamma}{\beta}\sinh\gamma\right)/(\cosh\gamma-\cos\beta). \tag{40}$$

Numerical solutions for the lowest four roots λ_i of (37) have been obtained by Firt (1983) for $\alpha=\pi$, Fagan (1987), and Hsieh (1988). Hsieh's results are listed in Table 1 and plotted in Fig. 4. The eigenvalues λ_i, defined by (30), increase rapidly as α decreases below π. An alternative plot is presented in Fig. 5, where the abscissa is the nondimensional frequency

Downloaded 03 May 2010 to 171.66.16.21. Redistribution subject to ASME license or copyright; see http://www.asme.org/terms/Terms_Use.cfm

$\omega\sqrt{\mu s_0/q}$ and the ordinate is the ratio b/s_0 of the base length to the perimeter of the membrane. Mode shapes corresponding to the first four frequencies are shown in Fig. 6 for the case $b/s_0 = 2/5$. The mode associated with λ_1 is antisymmetric.[1] Note that

$$\int_0^{\alpha} W(\theta)\,d\theta = V(0) - V(\alpha) = 0. \tag{41}$$

The mode shapes do not vary significantly with changes in α(or b/s_0).

Effect of Membrane Weight

It is convenient to put the equations in terms of the following nondimensional quantities:

$$\begin{aligned} \bar{s} &= s/s_0,\ \bar{x} = x/s_0,\ \bar{y} = y/s_0,\ \bar{w} = w/s_0,\ \bar{v} = v/s_0, \\ \bar{W} &= W/s_0,\ \bar{V} = V/s_0,\ \bar{T}_0 = T_0/(qs_0),\ \bar{T}_1 = T_1/(qs_0), \\ \bar{T} &= T/(qs_0),\ \bar{p} = p/q,\ \bar{t} = t\sqrt{q/(\mu s_0)}, \\ \bar{\omega} &= \omega\sqrt{\mu s_0/q}. \end{aligned} \tag{42}$$

In order to determine the equilibrium configuration, (5) is substituted into (1), and the resulting equation is solved together with (3) and (4) by a shooting method (Fagan, 1987). The unknowns, in nondimensional form, are the parameter $\bar{T}_0$ and the functions $\psi_0(\bar{s})$, $\bar{x}(\bar{s})$, and $\bar{y}(\bar{s})$. The boundary conditions are $\bar{x} = \bar{y} = 0$ at $\bar{s} = 0$ and $\bar{x} = b/s_0$, $\bar{y} = 0$ at $\bar{s} = 1$. Some results for $\bar{T}_0$ are listed in Table 2. It is seen that the tension parameter $\bar{T}_0$ decreases as p/q increases and as b/s_0 decreases.

Once the equilibrium shape is known, (27), with boundary conditions (28), is solved (in nondimensional form) using the finite difference method (Fagan, 1987). Numerical results are presented in Fig. 7 for the lowest four frequencies. The abscissa is the nondimensional frequency $\omega\sqrt{\mu s_0/q}$, with different ranges in parts (*a*), (*b*), (*c*), and (*d*) of the figure. The ordinate is the ratio p/q of the membrane weight to the internal pressure. Three values of the base-to-perimeter ratio b/s_0 are considered: 1/4, 1/3, and 2/5.

It is seen from Fig. 7 that the vibration frequencies decrease as p/q is increased. The curves are almost linear, and their slopes are approximately -0.47 for the first frequency, -0.34 for the second, -0.27 for the third, and -0.23 for the fourth. The corresponding mode shapes do not vary significantly with p/q and are similar to those shown in Fig. 6. One can conclude that the weight of the membrane does not have a large effect on the vibration frequencies and modes.

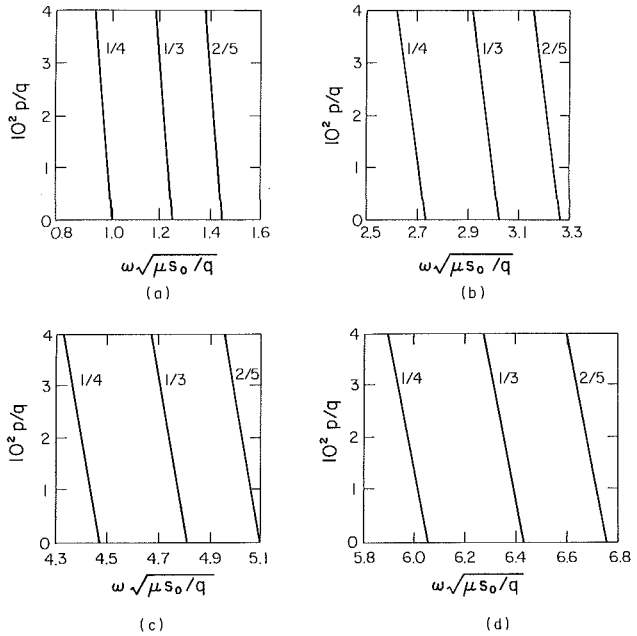


Fig. 7 Lowest four frequencies as function of p/q for $b/s_0 = 1/4$, 1/3, and 2/5

Acknowledgment

This research was sponsored by the U.S. National Science Foundation under Grant No. MSM-8505853.

References

Fagan, T. D., 1987, "Effect of Membrane Weight on Vibrations of Air-Inflated Dams," M.S. Thesis, Virginia Polytechnic Institute and State University, Blacksburg, VA.

Firt, V., 1983, *Statics, Formfinding and Dynamics of Air-Supported Membrane Structures*, Martinus Nijhoff, The Hague.

Henrych, J., 1981, *The Dynamics of Arches and Frames*, Elsevier, Amsterdam, pp. 21–27.

Hsieh, J. -C., 1988, "Free Vibrations of Inflatable Dams," Ph.D. Dissertation, Virginia Polytechnic Institute and State University, Blacksburg, VA.

Irvine, H. M., 1981, *Cable Structures*, The MIT Press, Cambridge, MA, p. 89.

Parbery, R. D., 1976, "A Continuous Method of Analysis for the Inflatable Dam," *Proceedings of the Institution of Civil Engineers*, Part 2, Vol. 61, pp. 725–736.

Parbery, R. D., 1978, "Factors Affecting the Membrane Dam Inflated by Air Pressure," *Proceedings of the Institution of Civil Engineers*, Part 2, Vol. 65, pp. 645–654.

[1] An actual membrane, with some extensibility, may have a symmetric mode which has no nodes and has a frequency lower than those found here (e.g., see Irvine, 1981). For a discussion of the effect of extensibility on the static analysis, see Parbery (1978).

Downloaded 03 May 2010 to 171.66.16.21. Redistribution subject to ASME license or copyright; see http://www.asme.org/terms/Terms_Use.cfm

W. P. Koppens
Research Associate.
A. A. H. J. Sauren
Senior Research Associate.
F. E. Veldpaus
Senior Research Associate.
D. H. van Campen
Professor.

Department of Mechanical Engineering,
Eindhoven University of Technology,
5600 MB Eindhoven, The Netherlands

The Dynamics of a Deformable Body Experiencing Large Displacements

A general description of the dynamics of a deformable body experiencing large displacements is presented. These displacements are resolved into displacements due to deformation and displacements due to rigid body motion. The former are approximated with a linear combination of assumed displacement fields. D'Alembert's principle is used to derive the equations of motion. For this purpose, the rigid body displacements and the displacements due to deformation have to be independent. Commonly employed conditions for achieving this are reviewed. It is shown that some conditions lead to considerably simpler equations of motion and a sparser mass matrix, resulting in CPU time savings when used in a multibody program. This is illustrated with a uniform beam and a crank-slider mechanism.

Introduction

The dynamics of an individual deformable body constitute a building block for the dynamics of systems of deformable bodies. The dynamics of systems of deformable bodies have been studied by, among others, Sunada and Dubowsky (1981), Singh et al. (1984), Van der Werff and Jonker (1984), Agrawal and Shabana (1985), and Haug et al. (1986). In order to get tractable expressions for the elastic forces, they resolve the displacements into displacements due to deformation and displacements due to rigid body motion. They approximate the displacements due to deformation with a linear combination of assumed displacement fields.

In order to obtain a unique resolution of displacements, the displacements due to deformation are not allowed to represent a rigid body motion. This can be accomplished in various ways. Consequently, different options are available in the literature about the dynamics of systems of deformable bodies.

McDonough (1976) considered a resolution of displacements that has not found acceptance in literature, despite its potential merits such as the partial decoupling of rigid body motion from displacements due to deformation. This decoupling results in a simplification of the equations of motion and a more sparse mass matrix. Only Agrawal and Shabana (1985) have described this subdivision but they did not show its potential merits. It is the purpose of this paper to point out the merits of the resolution considered by McDonough (1976) and to apply it to analyzing the dynamics of systems of deformable bodies.

This paper considers the dynamics of an individual deformable continuous body. Using an optional resolution of displacements into displacements due to deformation and displacements due to rigid body motion, the equations of motion for the body are derived. Next, the two options that can be found in literature for bringing about a unique resolution of displacements are reviewed, namely, the option usually used in literature (Sunada and Dubowsky, 1981; Singh et al., 1984; Agrawal and Shabana, 1985; and Haug et al., 1986) and the option considered by McDonough (1976) and Agrawal and Shabana (1985). The displacements due to deformation are approximated with a linear combination of assumed displacement fields. It is shown that, using the resolution described by McDonough (1976), the equations of motion become more simple and the mass matrix becomes more sparse. This is illustrated with a description of the two-dimensional motion for a uniform beam. The method has been implemented in the multibody program DADS (CADSI, 1986) and is applied to a crank-slider mechanism.

The Kinematics of a Deformable Body

Consider a body $\mathcal{B}$ in its configuration G_t at time t (see Fig. 1). Let $\vec{x}$ be the position vector of an arbitrary material point P of the body, measured from an inertial point O.

Let G be a time-independent reference configuration of which all relevant quantities are known. Let $\vec{X}$ be the position vector of the point of G corresponding to P, measured from O. An invertible continuous transformation will exist mapping $\vec{X}$ on to $\vec{x}$, i.e., $\vec{x}=\vec{x}(\vec{X}, t)$.

The body in G_t can be considered as the result of a deformation of the body in G with displacement field $\vec{u}(\vec{X}, t)$, followed by a rigid body displacement defined by a translation vector $\vec{c}(t)$ and a rotation tensor $\mathbf{Q}(t)$

$$\vec{x}(\vec{X}, t)=\vec{c}(t)+\mathbf{Q}(t)\cdot\{\vec{X}+\vec{u}(\vec{X}, t)\}. \quad (1)$$

Contributed by the Applied Mechanics Division for presentation at the Winter Annual Meeting, Chicago, IL, November 28 to December 2, 1988, of THE AMERICAN SOCIETY OF MECHANICAL ENGINEERS.

Discussion on this paper should be addressed to the Editorial Department, ASME, United Engineering Center, 345 East 47th Street, New York, N.Y. 10017, and will be accepted until two months after final publication of the paper itself in the JOURNAL OF APPLIED MECHANICS. Manuscript received by ASME Applied Mechanics Division, September 22, 1987.

Copyright © 1988 by ASME
Downloaded 03 May 2010 to 171.66.16.21. Redistribution subject to ASME license or copyright; see http://www.asme.org/terms/Terms_Use.cfm

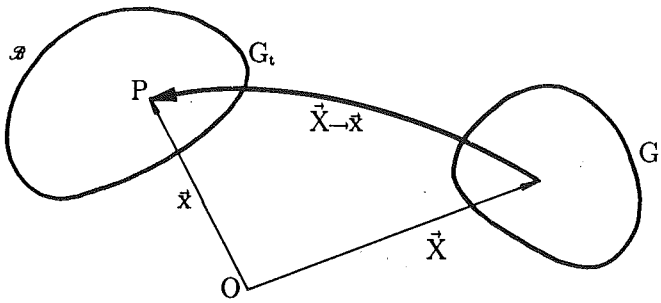


Fig. 1 Configurations G and G_t of body $\mathcal{B}$

The vector $d\vec{x}$ between two neighboring points in G_t and the vector $d\vec{X}$ between the corresponding points in G are related by

$$d\vec{x}=\mathbf{Q}(t)\cdot\{d\vec{X}+\vec{u}(\vec{X}+d\vec{X},\,t)-\vec{u}(\vec{X},\,t)\}. \tag{2}$$

This equation can be rewritten as

$$d\vec{x}=\mathbf{F}\cdot d\vec{X}, \tag{3}$$

where the deformation tensor $\mathbf{F}$ is given by

$$\mathbf{F}=\mathbf{Q}\cdot\{\mathbf{I}+(\vec{\nabla}\,\vec{u})^c\}. \tag{4}$$

Here, $\vec{\nabla}$ is the gradient operator with reference to G, and $\mathbf{I}$ is the identity tensor. The superscript c denotes conjugation: the conjugate to a tensor $\mathbf{A}$ is the tensor $\mathbf{A}^c$ such that $\vec{v}\cdot\mathbf{A}\cdot\vec{w}=\vec{w}\cdot\mathbf{A}^c\cdot\vec{v}$, $\forall\ \vec{v},\ \vec{w}$.

The acceleration and the virtual displacement of a material point are obtained by differentiating (1) twice with respect to time and by taking the variation of (1), respectively. This yields

$$\ddot{\vec{x}}=\ddot{\vec{c}}+\mathbf{Q}\cdot\{\vec{\omega}\times[\vec{\omega}\times(\vec{X}+\vec{u})]+\dot{\vec{\omega}}\times(\vec{X}+\vec{u})+2\vec{\omega}\times\dot{\vec{u}}+\ddot{\vec{u}}\}, \tag{5}$$

$$\delta\vec{x}=\delta\vec{c}+\mathbf{Q}\cdot\{\delta\vec{\pi}\times(\vec{X}+\vec{u})+\delta\vec{u}\}, \tag{6}$$

where $\vec{\omega}$ and $\delta\vec{\pi}$ are the axial vectors of the skew-symmetric tensors $\mathbf{Q}^c\cdot\dot{\mathbf{Q}}$ and $\mathbf{Q}^c\cdot\delta\mathbf{Q}$, respectively. The axial vector of a skew-symmetric tensor $\mathbf{S}$ is the vector $\vec{p}$, such that $\mathbf{S}\cdot\vec{v}=\vec{p}\times\vec{v}$, $\forall\vec{v}$.

The Equations of Motion

The equations of motion are given by (cf. Malvern, 1969)

$$\vec{\nabla}\cdot(\mathbf{T}\cdot\mathbf{F}^c)+\rho\vec{b}=\rho\ddot{\vec{x}}, \tag{7}$$

where $\mathbf{T}$ is the second Piola-Kirchhoff stress tensor, ρ is the mass density of G and $\vec{b}$ is a specific body force vector. Without losing the general validity of the conclusions of this paper, we may let $\vec{b}\equiv\vec{0}$.

Assume the body is stress-free in the reference configuration. Then, for isotropic linear elastic material behavior, $\mathbf{T}$ is related to the strain by (cf. Gurtin, 1981)

$$\mathbf{T}=2\mu\mathbf{E}+\lambda\ \mathrm{tr}(\mathbf{E})\mathbf{I}, \tag{8}$$

where μ and λ are the Lamé elastic constants, and $\mathbf{E}$ is the Green-Lagrange strain tensor, defined by

$$\mathbf{E}=\tfrac{1}{2}\{\mathbf{F}^c\cdot\mathbf{F}-\mathbf{I}\}. \tag{9}$$

An equivalent form of the equations of motion can be obtained with d'Alembert's principle. Multiplying (7) with a virtual displacement $\delta\vec{x}$ and integration over the reference volume Ω yields

$$\int_\Omega\{\vec{\nabla}\cdot(\mathbf{T}\cdot\mathbf{F}^c)-\rho\ddot{\vec{x}}\}\cdot\delta\vec{x}\,d\Omega=0. \tag{10}$$

Applying the divergence theorem, we arrive at

$$\int_\Omega\mathbf{T}:\delta\mathbf{E}\,d\Omega+\int_\Omega\rho\ddot{\vec{x}}\cdot\delta\vec{x}\,d\Omega=\int_\Gamma(\mathbf{F}\cdot\mathbf{T}\cdot\vec{n})\cdot\delta\vec{x}\,d\Gamma, \tag{11}$$

where Γ is the surface of G and $\vec{n}$ is the unit outward normal vector to Γ. The surface integral vanishes for that part of the surface where the displacements have been prescribed since there $\delta\vec{x}\equiv\vec{0}$. On the remaining part of the surface, a surface loading of $\vec{q}$ per unit of undeformed area is prescribed and $\mathbf{T}$ has to satisfy

$$\vec{q}=\mathbf{F}\cdot\mathbf{T}\cdot\vec{n}. \tag{12}$$

Without losing the general validity of the conclusions of this paper, we may let $\vec{q}\equiv\vec{0}$.

Substituting (8) into (11) yields

$$\int_\Omega\{2\mu\mathbf{E}+\lambda tr(\mathbf{E})\mathbf{I}\}:\delta\mathbf{E}\,d\Omega+\int_\Omega\rho\ddot{\vec{x}}\cdot\delta\vec{x}\,d\Omega=0. \tag{13}$$

The first term represents the variation in strain energy δU of the body due to a virtual displacement $\delta\vec{x}$. In general, this expression is too complicated to evaluate; consequently approximations are used instead.

Discretization of the Body

Approximating the displacement field $\vec{u}(\vec{X},\,t)$ with a linear combination of assumed displacement fields gives

$$\vec{u}(\vec{X},\,t)=\sum_{i=1}^{N}\alpha_i(t)\vec{\Phi}_i(\vec{X})=\underset{\sim}{\alpha}^T(t)\underset{\sim}{\vec{\Phi}}(\vec{X}), \tag{14}$$

where $\alpha(t)$ is a column matrix of generalized coordinates and $\underset{\sim}{\vec{\Phi}}(\vec{X})$ is a column matrix of the assumed displacement fields. The wavy underscore denotes a column matrix and the superscript T denotes transposition of a matrix. This approach leads to a finite element approximation when the displacement fields are nonzero in just a part of the body; otherwise, it leads to an assumed-modes approximation. A finite element approximation usually results in a model of the body with many degrees of freedom, which is undesirable as for CPU time. For this reason usually an assumed-modes approximation is preferred. Different types of displacement fields are dealt with by Yoo and Haug (1986).

Substituting (5), (6) and (14) into (13) yields

$$\begin{aligned}&\delta U\\&+\delta\vec{c}\cdot\{m\ddot{\vec{c}}+\mathbf{Q}\cdot[\vec{\omega}\times(\vec{\omega}\times\vec{d}_1)+\dot{\vec{\omega}}\times\vec{d}_1+2\vec{\omega}\times(\dot{\underset{\sim}{\alpha}}^T\underset{\sim}{\vec{c}}_2)+\ddot{\underset{\sim}{\alpha}}^T\underset{\sim}{\vec{c}}_2]\}\\&+\delta\vec{\pi}\cdot\{\vec{d}_1\times(\mathbf{Q}^c\cdot\ddot{\vec{c}})+\vec{\omega}\times(\mathbf{J}\cdot\vec{\omega})+\mathbf{J}\cdot\dot{\vec{\omega}}+2(\dot{\underset{\sim}{\alpha}}^T\underset{\sim}{\mathbf{D}}_2)\cdot\vec{\omega}+\ddot{\underset{\sim}{\alpha}}^T\underset{\sim}{\vec{d}}_3\}\\&+\delta\underset{\sim}{\alpha}^T\{\ddot{\vec{c}}\cdot(\mathbf{Q}\cdot\underset{\sim}{\vec{c}}_2)-\vec{\omega}\cdot(\underset{\sim}{\mathbf{D}}_2\cdot\vec{\omega})+\dot{\vec{\omega}}\cdot\underset{\sim}{\vec{d}}_3-2\vec{\omega}\cdot(\underset{\sim}{\vec{c}}_7\dot{\underset{\sim}{\alpha}})+\underset{\sim}{c}_8\ddot{\underset{\sim}{\alpha}}\}=0,\end{aligned} \tag{15}$$

where m is the mass of the body; the quantities $\vec{c}_2$, $\underset{\sim}{\vec{c}}_7$, $\underset{\sim}{c}_8$, $\vec{d}_1$, $\underset{\sim}{\mathbf{D}}_2$, $\underset{\sim}{\vec{d}}_3$ and $\mathbf{J}$ are defined in the appendix. An underscore denotes a matrix.

Preventing Rigid Body Motion in the Displacement Field $\vec{u}$

We want to describe the motion of the body in terms of displacements due to deformation defined by $\underset{\sim}{\alpha}$ and in terms of a rigid body motion defined by $\vec{c}$ and $\mathbf{Q}$. Then virtual variations of $\delta\vec{c}$, $\delta\vec{\pi}$, and $\delta\underset{\sim}{\alpha}$ must be independent. Consequently, the displacement fields $\vec{\Phi}_i$ must be mutually independent and such that a rigid body motion can not be represented by the linear combination (14).

Two kinds of conditions for preventing rigid body motion can be found in literature, namely, conditions for displacements of selected material points of the body and conditions for mean displacements of the body. The first kind of conditions is used by, among others, Sunada and Dubowsky (1981), Singh et al. (1984), Van der Werff and Jonker (1984), Agrawal and Shabana (1985), and Haug et al. (1986). The second kind of conditions is used by Agrawal and Shabana (1985), McDonough (1976), and others.

Downloaded 03 May 2010 to 171.66.16.21. Redistribution subject to ASME license or copyright; see http://www.asme.org/terms/Terms_Use.cfm

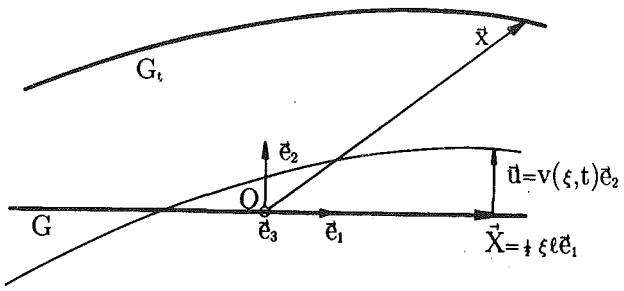


Fig. 2 Free beam

Conditions for Displacements of Selected Material Points. This kind of condition is also used in finite element analysis of structures. It comes to prescribing a minimum number of displacements of selected material points to prevent rigid body motion. For example, the displacements due to deformation of one material point P_c are required to be zero. This condition can be imposed on all displacement fields:

$$\vec{\Phi}_i(P_c)=\vec{0},\ i=1,2,\ \ldots,\ N. \tag{16}$$

Now, the body can still perform rigid body rotations around P_c. Hence, in addition, rigid body rotations have to be prevented. This may be achieved by constraining the rotation of a body-fixed frame (cf. Singh et al., 1984).

Conditions for Mean Displacement of the Body. A rigid body translation involves a displacement of the center of mass. Consequently, a linear combination of the assumed displacement fields $\vec{\Phi}_i$ can not represent a rigid body translation when the assumed displacement fields $\vec{\Phi}_i$ do not cause a displacement of the center of mass. This can be expressed mathematically as

$$\frac{1}{m}\int_\Omega \rho\vec{\Phi}_i d\Omega=\vec{0},\ i=1,2,3,\ \ldots,\ N. \tag{17}$$

The translation vector $\vec{c}$ will represent the translation of the center of mass of the body when this condition is used.

An infinitesimal small rigid body rotation around O can be represented by the vector field

$$\vec{u}_{\text{rotation}}=\chi\vec{e}\times\vec{X}, \tag{18}$$

where χ is the rotation angle and $\vec{e}$ is a unit vector parallel to the rotation axis. It can be seen that the displacements due to the rigid body rotation are perpendicular to $\vec{X}$. Consequently, a linear combination of the assumed displacement fields $\vec{\Phi}_i$ can not represent a rigid body rotation when the assumed displacement fields $\vec{\Phi}_i$ are on a mean parallel to $\vec{X}$. This can be expressed mathematically as

$$\int_\Omega \rho\vec{X}\times\vec{\Phi}_i\, d\Omega=\vec{0},\ i=1,2,3,\ \ldots,\ N. \tag{19}$$

(ρ has been used as a weighting factor in order to cancel the term $\tilde{\vec{c}}_6$ (see appendix) and $\tilde{d}_3$ becomes proportional with $\underset{\sim}{\alpha}$.) Examples of displacement fields satisfying (17) and (19) are modes of free vibration (Ashley, 1967).

When in addition to conditions (17), the center of mass in the reference configuration is chosen to coincide with O, all terms involving $\tilde{d}_1$ and $\tilde{\vec{c}}_2$ in the equations of motion (15) cancel. When this is taken into account, (15) reduces to

$$\begin{aligned}&\delta U\\&+\delta\vec{c}\cdot\{m\ddot{\vec{c}}\}\\&+\delta\vec{\pi}\cdot\{\vec{\omega}\times(\mathbf{J}\cdot\vec{\omega})+\mathbf{J}\cdot\dot{\vec{\omega}}+2(\dot{\underset{\sim}{\alpha}}^T\underset{\sim}{\mathbf{D}}_2)\cdot\vec{\omega}+\ddot{\underset{\sim}{\alpha}}^T\tilde{\vec{d}}_3\}\\&+\delta\underset{\sim}{\alpha}^T\{-\vec{\omega}\cdot(\underset{\sim}{\mathbf{D}}_2\cdot\vec{\omega})-\dot{\vec{\omega}}\cdot(\tilde{\vec{c}}_7\underset{\sim}{\alpha})-2\vec{\omega}\cdot(\tilde{\vec{c}}_7\dot{\underset{\sim}{\alpha}})+\underset{\sim}{c}_8\ddot{\underset{\sim}{\alpha}}\}=0.\end{aligned} \tag{20}$$

There is just a weak coupling between displacements due to deformation and displacements due to rigid body motion. Cancellation of all terms involving $\tilde{d}_1$ and $\tilde{\vec{c}}_2$ makes the mass matrix more sparse, which may be advantageous when sparse matrix techniques are used for solving the equations of motion. This will be illustrated now for a uniform beam.

Example: Free Uniform Beam

Consider the uniform slender beam of length l and mass m shown in Fig. 2. We choose a reference configuration G with straight centroidal axis and with its center of mass coinciding with O. Introduce an orthonormal right-handed vector base $\tilde{\vec{e}}$, such that $\vec{e}_1$ is parallel to the centroidal axis of the beam.

The motion of the beam is restricted to the plane spanned by $\vec{e}_1$ and $\vec{e}_2$. Using the Bernoulli-Euler beam theory, only the displacements of the centroidal axis need to be considered. The centroidal axis is assumed to be inextensible. The lateral displacements due to deformation are approximated by

$$v(\xi,\ t)=a_0(t)+a_1(t)\xi+a_2(t)\xi^2+a_3(t)\xi^3, \tag{21}$$

where ξ is the dimensionless distance in the reference configuration for a material point of the centroidal axis measured from the center of mass and made dimensionless with $l/2$. The rotary inertia of the cross-section of the beam will be neglected and the expression for the strain energy of the beam which will be used is

$$U=(4EI/l^3)\int_{-1}^{1}(\partial^2 v/\partial\xi^2)^2 d\xi. \tag{22}$$

The vectors and tensor used to describe the kinematics of the beam are resolved into their components in the base $\tilde{\vec{e}}$. This yields

$$\vec{c}=c_1\vec{e}_1+c_2\vec{e}_2, \tag{23}$$

$$\vec{X}=\tfrac{1}{2}\xi\, l\vec{e}_1, \tag{24}$$

$$\vec{u}=v(\xi,\ t)\vec{e}_2, \tag{25}$$

$$\mathbf{Q}=(\vec{e}_1\vec{e}_1+\vec{e}_2\vec{e}_2)\cos\varphi+(\vec{e}_2\vec{e}_1-\vec{e}_1\vec{e}_2)\sin\varphi+\vec{e}_3\vec{e}_3, \tag{26}$$

where φ is the rigid body rotation of the body,

$$\vec{\omega}=\dot{\varphi}\vec{e}_3,\qquad \delta\vec{\pi}=\delta\varphi\vec{e}_3. \tag{27}$$

The displacement field (21) contains rigid body displacements. These are eliminated by using the two kinds of conditions discussed earlier.

1 Conditions on displacements of selected material points. We choose for the material point the middle of the beam ($\xi=0$), and require that:

a the lateral displacement is zero,

b the rotation is zero.

The first condition yields $v(0,\ t)\equiv 0$. Hence

$$a_0\equiv 0. \tag{28}$$

The second condition yields $dv/d\xi\,|_{0,t}\equiv 0$. Hence

$$a_1\equiv 0. \tag{29}$$

Eliminating rigid body motions from the displacement field (21) using the conditions (28) and (29) yields

$$v(\xi,\ t)=\alpha_1(t)\phi_1(\xi)+\alpha_2(t)\phi_2(\xi), \tag{30}$$

where the assumed displacement fields $\phi_1(\xi)$ and $\phi_2(\xi)$ are

$$\phi_1(\xi)=\xi^2, \tag{31}$$

$$\phi_2(\xi)=\xi^3. \tag{32}$$

Elaboration of (15) for the strain energy expression (22) and the assumed displacement fields (31) and (32) yields for the coefficients of δc_1, δc_2, $\delta\varphi$, $\delta\alpha_1$ and $\delta\alpha_2$, respectively

$$\delta c_1\colon m\{\ddot{c}_1-[\alpha_1(\ddot{\varphi}\cos\varphi-\dot{\varphi}^2\sin\varphi)+2\dot{\varphi}\,\dot{\alpha}_1\cos\varphi+\ddot{\alpha}_1\sin\varphi]/3\},$$

$$\delta c_2\colon m\{\ddot{c}_2-[\alpha_1(\ddot{\varphi}\sin\varphi+\dot{\varphi}^2\cos\varphi)+2\dot{\varphi}\,\dot{\alpha}_1\sin\varphi-\ddot{\alpha}_1\cos\varphi]/3\},$$

$$\begin{aligned}\delta\varphi\colon m\{&-\alpha_1(\ddot{c}_1\cos\varphi+\ddot{c}_2\sin\varphi)/3+\ddot{\varphi}(l^2/12+\alpha_1^2/5+\alpha_2^2/7)\\&+2\dot{\varphi}(\alpha_1\dot{\alpha}_1/5+\alpha_2\dot{\alpha}_2/7)+l\ddot{\alpha}_2/10\},\end{aligned}$$

Downloaded 03 May 2010 to 171.66.16.21. Redistribution subject to ASME license or copyright; see http://www.asme.org/terms/Terms_Use.cfm

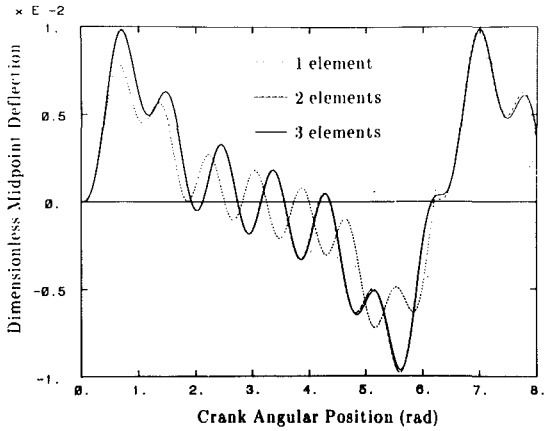


Fig. 3 Dimensionless deflection of the midpoint of the connecting rod

$$\delta\alpha_1: m\{(-\ddot{c}_1\sin\varphi+\ddot{c}_2\cos\varphi)/3-\dot{\varphi}^2\alpha_1/5+\ddot{\alpha}_1/5\}+64\alpha_1 EI/l^3,$$

$$\delta\alpha_2: m\{l\ddot{\varphi}/10-\dot{\varphi}^2\alpha_2/7+\ddot{\alpha}_2/7\}+192\alpha_2 EI/l^3. \quad (33)$$

2 *Conditions on mean displacements of the body.* The conditions discussed above are:

a the displacement of the center of mass due to the displacements (21) equals zero,

b the displacements $\vec{u}=v(\xi,\ t)\vec{e}_2$ and the position vector $\vec{X}$ are on a mean parallel.

The first condition is equivalent to (cf. (17))

$$\int_{-1}^{1} v(\xi,\ t)d\xi\equiv 0. \quad (34)$$

Substituting (21) into this equation yields

$$3a_0+a_2\equiv 0. \quad (35)$$

The second condition is equivalent to (cf. (19))

$$\int_{-1}^{1}\xi\ v(\xi,\ t)d\xi\equiv 0. \quad (36)$$

substituting (21) into this equation yields

$$5a_1+3a_3\equiv 0. \quad (37)$$

Eliminating rigid body motions from the displacement field (21) using conditions (35) and (37) yields

$$v(\xi,\ t)=\alpha_1(t)\phi_1(\xi)+\alpha_2(t)\phi_2(\xi), \quad (38)$$

where the assumed displacement fields $\phi_1(\xi)$ and $\phi_2(\xi)$ are

$$\phi_1(\xi)=\tfrac{1}{2}(-1+3\xi^2), \quad (39)$$

$$\phi_2(\xi)=\tfrac{1}{2}(-3\xi+5\xi^3). \quad (40)$$

Elaborating (20) for the strain energy expression (22) and the assumed displacement fields (39) and (40) yields for the coefficients of δc_1, δc_2, $\delta\varphi$, $\delta\alpha_1$ and $\delta\alpha_2$, respectively

$$\delta c_1: m\ddot{c}_1,$$

$$\delta c_2: m\ddot{c}_2,$$

$$\delta\varphi: m\{\ddot{\varphi}(l^2/12+\alpha_1^2/5+\alpha_2^2/7)+2\dot{\varphi}(\alpha_1\dot{\alpha}_1/5+\alpha_2\dot{\alpha}_2/7)\},$$

$$\delta\alpha_1: (m/5)(\ddot{\alpha}_1-\dot{\varphi}^2\alpha_1)+144\alpha_1 EI/l^3,$$

$$\delta\alpha_2: (m/7)(\ddot{\alpha}_2-\dot{\varphi}^2\alpha_2)+1200\alpha_2 EI/l^3. \quad (41)$$

Comparison of (33) and (41) reveals that the equations of motion become more simple when the given conditions on mean displacements are used: there is no coupling between the rigid body translational motion and the displacements due to deformation; the coupling between the rigid body rotation and the displacements due to deformation is nonlinear in terms of the displacements due to deformation.

Numerical Results

In order to demonstrate the merits of using the description based on mean displacement conditions for describing the dynamics of multibody systems with deformable bodies, the consequences of this description have been implemented in the two-dimensional version of the multibody program DADS (CADSI, 1986), i.e., multiplications involving $\vec{d}_1$, $\vec{c}_2$ and $\vec{c}_6$ are skipped and the increased sparseness of the mass matrix is taken into account. This version is used to analyze the crank-slider mechanism considerd by Song and Haug (1980).

The model consists of three rigid bodies (the crank, the slider block, and a supporting body) and a deformable connecting rod. In order to demonstrate the influence of the number of deformable bodies in the system, the system was analyzed with the connecting rod divided into one, two, and three deformable beams. The deformation fields used for approximating the deflection of these beams are given by (38) and (39).

Figure 3 shows the deflection at the midpoint of the connecting rod, made dimensionless with its length. The ratios of the required CPU time for the revised version and the standard version for the system with one, two, and three deformable beams are .97, .93, and .92, respectively. Hence, the revised version of DADS requires less CPU time; the reduction in CPU time increases when the number of deformable bodies increases.

Concluding Remarks

The kinematics of a deformable body experiencing large displacements is described. The displacements are resolved into displacements due to deformation and displacements due to rigid body motion. This resolution is not unique. A review of conditions leading to a unique resolution is given. It is shown that the infrequently used conditions for mean displacements lead to simpler equations of motion and a more sparse mass matrix. This is implemented in the multibody program DADS, which uses sparse matrix techniques for solving the equations of motion. The results show that a reduction of the required CPU time is achieved when the conditions for mean displacements are used. The proposed description is in particular advantageous for multibody programs that use finite elements for approximating deformable bodies.

One of the reviewers, Professor Haug of the University of Iowa, is suspicious that there is an additional advantage. Absolute coordinate formulations of equations of motion, particularly including flexibility effects, can lead to challenges in stable symbolic factorization of sparse matrices in the equations of motion. He expects that the sparse matrix symbolic factorization will be substantially more stable when there is a larger number of precisely zero terms in the system mass matrix.

References

Agrawal, O. P., and Shabana, A. A., 1985, "Dynamic Analysis of Multibody Systems Using Component Modes," *Computers & Structures*, Vol. 21, pp. 1303–1312.

Ashley, H., 1967, "Observations on the Dynamic Behavior of Large Flexible Bodies in Orbit," *A.I.A.A. J.*, Vol. 5, pp. 460–469.

CADSI, 1986, *DADS User's Manual, Rev. 4.0*, Computer Aided Design Software, Oakdale, Iowa.

Gurtin, M. E., 1981, *An Introduction to Continuum Mechanics*, Academic Press, New York.

Haug, E. J., Wu, S. C., and Kim, S. S., 1986, "Dynamics of Flexible Machines, A Variational Approach," *Dynamics of Multibody Systems*, Bianchi, G., and Schiehlen, W., eds., Springer-Verlag, Berlin, pp. 55–67.

Malvern, L. E., 1969, *Introduction to the Mechanics of a Continuous Medium*, Prentice-Hall, Englewood Cliffs, N.J.

McDonough, T. B., 1976, "Formulation of the Global Equations of Motion of a Deformable Body," *A.I.A.A. J.*, Vol. 14, pp. 656–660.

Downloaded 03 May 2010 to 171.66.16.21. Redistribution subject to ASME license or copyright; see http://www.asme.org/terms/Terms_Use.cfm

Singh, R. P., VanderVoort, R. J., and Likins, P. W., 1984, "Dynamics of Flexible Bodies in Tree Topology-A Computer Oriented Approach," *AIAA Dynamics Specialists Conference*, Palm Springs, CA, pp. 327-337.

Song, J. O., and Haug, E. J., 1980, "Dynamic Analysis of Planar Flexible Mechanisms," *Computer Methods in Applied Mechanics and Engineering*, Vol. 24, pp. 359-381.

Sunada, W., and Dubowsky, S., 1981, "The Application of Finite Element Methods to the Dynamic Analysis of Flexible Spatial and Co-Planar Linkage Systems," *J. of Mechanical Design*, Vol. 103, pp. 643-651.

Werff, K. van der, and Jonker, J. B., 1984, "Dynamics of Flexible Mechanisms," *Computer Aided Analysis and Optimization of Mechanical System Dynamics*, Haug, E. J., ed., Springer-Verlag, Berlin, pp. 381-400.

Yoo, W. S., and Haug, E. J., 1986, "Dynamics of Articulated Structures, Part I: Theory," *J. of Structural Mechanics*, Vol. 14, pp. 105-126.

APPENDIX

$$\vec{c}_1 = \int_\Omega \rho \vec{X}\, d\Omega$$

$$\underset{\sim}{\vec{c}_2} = \int_\Omega \rho \underset{\sim}{\vec{\Phi}}\, d\Omega$$

$$\mathbf{C}_3 = \int_\Omega \rho \{ (\vec{X}\cdot\vec{X})\mathbf{I} - \vec{X}\vec{X} \} d\Omega$$

$$\underset{\sim}{\mathbf{C}}_4 = \int_\Omega \rho \{ (\underset{\sim}{\vec{\Phi}}\cdot\vec{X})\mathbf{I} - \underset{\sim}{\vec{\Phi}}\vec{X} \} d\Omega$$

$$\underset{\sim}{\mathbf{C}}_5 = \int_\Omega \rho \{ (\underset{\sim}{\vec{\Phi}}\cdot\underset{\sim}{\vec{\Phi}}^T)\mathbf{I} - \underset{\sim}{\vec{\Phi}}\underset{\sim}{\vec{\Phi}}^T \} d\Omega$$

$$\underset{\sim}{\vec{c}_6} = \int_\Omega \rho \{ \vec{X}\times\underset{\sim}{\vec{\Phi}} \} d\Omega$$

$$\underset{\sim}{\vec{c}_7} = \int_\Omega \rho \{ \underset{\sim}{\vec{\Phi}}\times\underset{\sim}{\vec{\Phi}}^T \} d\Omega$$

$$\underset{\sim}{c_8} = \int_\Omega \rho \{ \underset{\sim}{\vec{\Phi}}\cdot\underset{\sim}{\vec{\Phi}}^T \} d\Omega$$

$$\mathbf{J} = \mathbf{C}_3 + \underset{\sim}{\alpha}^T(\underset{\sim}{\mathbf{C}}_4 + \underset{\sim}{\mathbf{C}}_4^s) + \underset{\sim}{\alpha}^T\underset{\sim}{\mathbf{C}}_5\underset{\sim}{\alpha}$$

$$\vec{d}_1 = \vec{c}_1 + \underset{\sim}{\alpha}^T\underset{\sim}{\vec{c}_2}$$

$$\underset{\sim}{\mathbf{D}}_2 = \underset{\sim}{\mathbf{C}}_4 + \underset{\sim}{\mathbf{C}}_5\underset{\sim}{\alpha}$$

$$\underset{\sim}{\vec{d}_3} = \underset{\sim}{\vec{c}_6} - \underset{\sim}{\vec{c}_7}\underset{\sim}{\alpha}$$

Downloaded 03 May 2010 to 171.66.16.21. Redistribution subject to ASME license or copyright; see http://www.asme.org/terms/Terms_Use.cfm

J. A. Walker
Department of Mechanical Engineering,
Northwestern University,
Evanston, IL 60208

Pseudodissipative Systems I: Stability of Generalized Equilibria

A class of mechanical systems called "pseudodissipative" is defined in terms of the Lagrange formulation of dynamics. Generalized equilibria of such systems are studied with regard to their stability properties. Both broad results and simple results are obtained.

1 Introduction

The study of stability of generalized equilibria of Lagrange's motion equations began with J. L. Lagrange (Lagrange, 1788) and has a history so extensive that any attempt to fully describe and accredit existing results (Routh, 1860; Liapunov, 1892; Malkin, 1952) might be as controversial as it would be long. On the other hand, it seems worthwhile to consolidate, extend, and simplify the most useful stability results for generalized equilibria, and this is our objective here.

In the following Section 2 we define a large class of "pseudodissipative systems" that appears to embrace all systems classically studied for stability, and we state a simple result (Corollary 2.1) for existence of generalized equilibria. In Section 3 we obtain quite general results (Theorems 3.1–3.2) on stability, asymptotic stability, and instability of generalized equilibria of pseudodissipative systems. These results are based on modifications (9)–(10) of two classical Liapunov functions (Malkin, 1952; LaSalle and Lefschetz, 1961), and allow for both friction and kinematic constraints. Theorems 3.1–3.2 lead to much simpler Corollaries 3.1–3.2 which are applied to an example in Section 4. We find no reason to linearize or even write the motion equations.

2 Notation and Terminology

Consider a collection of particles observed by some inertial observer, and choose n "generalized coordinates" $(q_1,q_2,\ldots,q_n)\equiv q\in O\subset R^n$, where O is some open subset of R^n; the dimension n of the *generalized position* $q\in R^n$ need not be minimal. We denote by $u\in R^n$ the corresponding *generalized speed*; i.e., $u(t)=\dot{q}(t)$ along motions $q(\cdot):R\to R^n$. The resulting *generalized kinetic energy* $T:R\times O\times R^n\to R$ and *generalized force* $Q:R\times O\times R^n\to R^n$ depend upon the *generalized state* $(q,u)\in O\times R^n$ and possibly the current time $t\in R$. Any and all kinematic constraints on (q,u) may be accounted for by defining a *kinematically possible set* $C(t)\subset O\times R^n$, consisting of all generalized states (q,u) kinematically possible at time $t\in R$. A C^1-smooth function $q(\cdot):R\to R^n$ is kinematically possible on $[t_1,t_2)$ if $(q(t),\dot{q}(t))\in C(t)$ for all $t\in[t_1,t_2)$.

Aside from some of the foregoing notation, we depart from the classical Lagrange formulation only by assuming that Q is explicitly known, continuous, and "pseudodissipative" in the following sense:

Definition 2.1. The generalized force will be called *pseudodissipative* if there exists a C^1-smooth function $U:R\times O\times R^n\to R$, affine with respect to its third argument $u\in R^n$, and another function $D:R\times O\times R^n\to R^n$ such that

$$\sum_{\ell=1}^{n}(u_\ell-v_\ell)[D_\ell(t,q,u)-D_\ell(t,q,v)]\le 0 \tag{1}$$

for all $(t,q,u,v)\in R\times O\times R^n\times R^n$, and along every kinematically possible $q(\cdot)$,

$$\sum_{\ell=1}^{n}\delta_\ell(t)Q_\ell(t,q(t),\dot{q}(t))=\sum_{\ell=1}^{n}\delta_\ell(t)D_\ell(t,q(t),\dot{q}(t))$$

$$+\sum_{\ell=1}^{n}\delta_\ell(t)\left[d/dt\frac{\partial}{\partial u_\ell}U(t,q(t),\dot{q}(t))-\frac{\partial}{\partial q_\ell}U(t,q(t),\dot{q}(t))\right] \tag{2}$$

for all C^1-smooth $\delta(\cdot):R\to R^n$ such that $(q(t),\dot{q}(t)+\delta(t))\in C(t)$ for all $t\in R$.

U will be called a *pseudopotential* and the function $L\equiv T-U$ will be called the *Lagrangian*. Due to property (1), D will be called the *dissipative part* of Q.

The generalized force Q will be called *strongly* pseudodissipative if equality occurs in condition (1) *only* when $u=v$. Q will be called *pseudoconservative* if $D\equiv 0$.

It can be shown that the generalized force is pseudodissipative if and only if at least one possible selection[1] Q meets the monotonicity condition (1) required of D; we *could* choose $U\equiv 0$ and $D\equiv Q$, since the pair (U,D) of Definition 2.1 is far from unique. Definition 2.1 is stated as it is because the idea of pseudodissipative Q is most useful if D depends little or not at all on its second argument $q\in O$, and this often requires nontrivial U to be chosen. The idea of pseudoconservative $Q(D\equiv 0)$ is classical but does not permit frictional forces to be active. The more general idea of Defini-

[1] $Q:R\times O\times R^n\to R^n$ is not necessarily unique unless $C(t)\equiv O\times R^n$.

Contributed by the Applied Mechanics Division for publication in the JOURNAL OF APPLIED MECHANICS.
Discussion on this paper should be addressed to the Editorial Department, ASME, United Engineering Center, 345 East 47th Street, New York, N.Y. 10017, and will be accepted until two months after final publication of the paper itself in the JOURNAL OF APPLIED MECHANICS. Manuscript received by ASME Applied Mechanics Division, August 31, 1987; final revision, January 7, 1988.

Copyright © 1988 by ASME
Downloaded 03 May 2010 to 171.66.16.21. Redistribution subject to ASME license or copyright; see http://www.asme.org/terms/Terms_Use.cfm

tion 2.1 does allow for frictional influences, both internal and external, on our collection of particles; it also allows for the presence of motors with declining torque/speed relations, both within and without the collection.

For continuous pseudodissipative $Q:R\times O\times R^n\to R^n$, Lagrange's formulation produces the following consequence of Newton's section law:

Theorem 2.1. If a C^1-smooth function $q(\cdot):R\to R^n$ is dynamically possible on $[t_o,t_f)$, then for all $t\in[t_o,t_f)$

$$(q(t),\dot{q}(t))\in C(t) \tag{3}$$

and

$$0=\sum_{\ell=1}^{n}\delta_\ell(t)\left[d^+/dt\frac{\partial}{\partial u_\ell}L(t,q(t),\dot{q}(t))\right.$$

$$\left.-\frac{\partial}{\partial q_\ell}L(t,q(t),\dot{q}(t))-D_\ell(t,q(t),\dot{q}(t))\right] \tag{4}$$

for all C^1-smooth $\delta(\cdot):R\to R^n$ such that $(q(t),\ \dot{q}(t)+\delta(t))\in C(t), t_o\le t\le t_f$.

Henceforth we shall assume that

(*a*) A particular initial instant t_o has been chosen and the time-interval of interest is $[t_o,\infty)$,

(*b*) Q is known, continuous, and pseudodissipative on $[t_o,\infty)$,

(*c*) For each $(q^o,u^o)\in C(t_o)$, there exists a unique C^1-smooth solution $q(\cdot):[t_o,\infty)\to R^n$ of (3) and (4) such that $q(t_o)=q^o$ and $\dot{q}(t_o)=u^o$. Moreover, at each $t>t_o$, $(q(t),\dot{q}(t))$ depends continuously on (q^o,u^o).

Obviously, the simplest type of solution of (3)–(4) would be a constant solution, $q(t)\equiv q^e$ for some fixed $q^e\in R^n$; the corresponding initial generalized state $(q^e,0)\in C(t_o)$ is called a *generalized equilibrium*.

Corollary 2.1. If L is time-invariant, then $(q^e,0)$ is a generalized equilibrium if and only if, for all $t\ge t_o$,

$$(q^e,0)\in C(t) \tag{5}$$

and

$$0=\sum_{\ell=1}^{n}\delta_\ell(t)\left[\frac{\partial}{\partial q_\ell}L(t_o,q^e,0)+D_\ell(t,q^e,0)\right] \tag{6}$$

for every C^1-smooth $\delta(\cdot):R\to R^n$ such that $(q^e,\delta(t))\in C(t)$ for $t\ge t_o$.

If a generalized equilibrium $(q^e,0)$ does exist, then often one is interested in its stability properties. In the following definition we utilize both the open set

$$n_h\equiv\{(q,u)\in R^n\times R^n\,|\,0<\|q-q^e\|+\|u\|<h\} \tag{7}$$

and its closure

$$\bar{n}_h\equiv\{(q,n)\in R^n\times R^n\,|\,\|q-q^e\|+\|u\|\le h\}, \tag{8}$$

which are related to $(q^e,0)$ and parameterized by $h>0$.

Definition 2.2. Let $q(\cdot):[t_o,\infty)\to R^n$ denote the unique solution of (3) and (4) that corresponds to a given but arbitrary initial state $(q^o,u^o)\in C(t_o)$, and let a particular generalized equilibrium $(q^e,0)$ be considered. The generalized equilibrium $(q^e,0)$ is said to be *stable* if to each $\epsilon>0$ there corresponds some $h>0$ such that the statement $(q^o,u^o)\in C(t_o)\cap n_h$ implies that $(q(t),\dot{q}(t))\in\bar{n}_\epsilon$ for all $t\ge t_o(h>0$ varies with $\epsilon>0$, in general). The generalized equilibrium $(q^e,0)$ is *unstable* if it is not stable.

If $(q^e,0)$ *is* stable and there exists some $h>0$ such that the statement $(q^o,u^o)\in C(t_o)\cap n_h$ implies that $\|q(t)-q^e\|+\|\dot{q}(t)\|\to 0$ as $t\to\infty$, then $(q^e,0)$ is said to be *asymptotically* stable.

Some authors say that Definition 2.2 defines "Liapunov stability", as opposed to something else which they call "infinitesimal stability". No definition of the latter term is available, but it appears to mean only that the stability properties of $(q^e,0)$ cannot be ascertained by linearizing about $(q^e,0)$. We shall do no linearization here.

In all of the subsequent stability results we shall assume that L is time-invariant. At each generalized equilibrium $(q^e,0)\in R^n\times R^n$, we shall employ three q^e-related functions defined on $O\times R^n$:

$$G(q,u)\equiv -L(t_o,q,u)+\sum_{\ell=1}^{n}u_\ell\frac{\partial}{\partial u_\ell}L(t_o,q,u)$$

$$+\sum_{\ell=1}^{n}(q_\ell-q_\ell^e)\frac{\partial}{\partial q_\ell}L(t_o,q^e0), \tag{9}$$

$$J(q,u;\Gamma)\equiv\sum_{i=1}^{n}\sum_{j=1}^{n}\gamma_{ij}(q_i^e-q_i)$$

$$\times\left[\frac{\partial}{\partial u_j}L(t_o,q,u)-\frac{\partial}{\partial u_j}L(t_o,q^e,0)\right], \tag{10}$$

$$R(q,u;\Gamma)\equiv\sum_{i=1}^{n}\sum_{j=1}^{n}\gamma_{ij}u_i\left[\frac{\partial}{\partial u_j}L(t_o,q,u)-\frac{\partial}{\partial u_j}L(t_o,q^e,0)\right]$$

$$+\sum_{i=1}^{n}\sum_{j=1}^{n}\gamma_{ij}(q_i-q_i^e)\left[\frac{\partial}{\partial q_j}L(t_o,q,u)+D_j(t_o,q,u)\right], \tag{11}$$

where $\Gamma\equiv[\gamma_{ij}]$ is some real $n\times n$ matrix. We shall also employ the $(q^e,0)$-related set η_h of (7) and a subset

$$\Omega_h\equiv\{(q,u)\in n_h\,|\,G(q,u)<G(q^e,0)\}, \tag{12}$$

both of which are parameterized by $h>0$.

Definitions (7)–(12) are made here in order to simplify the statements and proofs of the following Theorems 3.1–3.2 and their Corollaries 3.1–3.2.

3 Stability Results for Generalized Equilibria

The following Theorems 3.1–3.2 are based upon Definition 2.1 and assumptions (*a*)–(*c*) of the foregoing Section 2. Although quite complicated, Theorems 3.1–3.2 lead to the much simpler (and more restricted) Corollaries 3.1–3.2.

Theorem 3.1. Suppose that $(q^e,0)\in R^n\times R^n$ is a generalized equilibrium and the following conditions hold for some $h>0$:

(*a*) $n_h\cap C(t)$ is time-invariant and the statement $(q,u)\in n_h\cap C(t_o)$ implies that both $(q,0)\in C(t_o)$ and equation (6) holds with $\delta(t)\equiv -u$.

(*b*) The Lagrangian $L:R\times O\times R^n\to R$ is time-invariant and $D(t,q,0)=D(t,q^e,0)$ for all (t,q) with $\|q-q^e\|<h, t\ge t_o$.

(*c*) $G(q,u)>G(q^e,0)$ (strictly) for all $(q,u)\in n_h\cap\bar{C}(t_o)$, where $\bar{C}(t_o)$ denotes the closure of $C(t_o)$.

Then $(q^e,0)$ is *stable*. If Q is pseudoconservative ($D\equiv 0$), then $(q^e,0)$ is *not* asymptotically stable.

Suppose that the following condition also holds:

(*d*) The dissipative part $D:R\times O\times R^n\to R^n$ is time-invariant and there does *not* exist a solution $q(\cdot):[t_o,\infty)\to R^n$ of equation's (3)–(4) along which $(q(t),\dot{q}(t))\in n_h$, $G(q(t),\dot{q}(t))$ is constant, and

$$\sum_{\ell=1}^{n}\dot{q}(t)[D_\ell(t_o,q(t),\dot{q}(t))-D_\ell(t_o,q^e,0)]=0 \text{ for all } t\ge t_o.$$

Then $(q^e,0)$ is *asymptotically* stable.

If the foregoing conditions (*a*) and (*b*) holds, (*d*) holds with

Downloaded 03 May 2010 to 171.66.16.21. Redistribution subject to ASME license or copyright; see http://www.asme.org/terms/Terms_Use.cfm

η_h replaced by Ω_h, but in place of (*c*) we have its strong contradiction

(*e*) The set $\Omega_\epsilon \cap C(t_o)$ is non-empty for every $\epsilon > 0$,

then $(q^e,0)$ is *unstable*.

Sketch of proof. Under assumptions (*a*)–(*b*), we consider some dynamically possible $q(\cdot):[t_o,\infty)\to R^n$ such that $(a(t),\dot{q}(t))\in n_h$ for all $t\hookrightarrow[t_o,t_1)$, some $t_1 > t_o$. Supposing for simplicity that $q(\cdot)$ is C^2-smooth, and choosing $\delta(t) \equiv -\dot{q}(t)$ in equations (4) and (6) for $t\in[t_o,t_1)$, we compute that

$$(d^+/dt)G(q(t),\dot{q}(t)) = \sum_{\ell=1}^{n} \dot{q}_\ell(t)[D_\ell(t,q(t),\dot{q}(t)) - D_\ell(t,q(t),0)] \le 0$$

for all $t\in[t_o,t_1)$. Hence, G is a Liapunov function (Walker, 1980) on $n_h \cap C(t_o)$.

Condition (*c*) and a basic Liapunov stability argument now imply that $(q^e, 0)$ is stable but, if Q is pseudoconservative, $(q^e,0)$ is not asymptotically stable. If Q is not pseudoconservative, then LaSalle's invariance principle (Walker, 1980) leads to the remaining asymptotic stability and instability conclusions. This concludes our sketch of the proof.

We note that condition (*c*) of Theorem 3.1 requires that $(q^e,0)$ provide a strict local minimum of G over $\bar{C}(t_o)$, while condition (*e*) requires that $(q^e,0)$ *not* provide even a weak local minimum of G over $C(t_o)$. The stability part of Theorem 3.1 generalizes the Lagrange/Dirichlet "principle of minimum potential energy" (Malkin, 1952; LaSalle and Lefschetz, 1961) which is valid under more restricted conditions.

Condition (*a*) of Theorem 3.1 requires that no known function of time has been chosen to be one of the generalized coordinates q_ℓ, a trick which might otherwise have been employed to ensure time-invariance of L, as required by condition (*b*).

Condition (*d*) appears to be quite complicated, but often it is not difficult to check. For instance, if Q is strongly pseudodissipative and D is time-invariant, then condition (*d*) is satisfied provided that $(q^e,0)$ is isolated (i.e., some η_h contains no other generalized equilibrium).

Theorem 3.1 provides conditions sufficient to ensure that $(q^e,0)$ is stable, asymptotically stable, or unstable when Q is pseudodissipative. Another instability result is provided by the following Theorem 3.2, which is most likely to be useful when Q has a dissipative part D that is too weak for us to easily check condition (*d*) of Theorem 3.1. Both q and u are treated as $n\times 1$ matrices in condition (*a*) of Theorem 3.2.

Theorem 3.2. Suppose that $(q^e,0)\in R^n \times R^n$ is a generalized equilibrium and the following conditions hold for some $h > 0$ and some real $n\times n$ matrix Γ:

(*a*) $\Omega_h \cap C(t)$ is time-invariant and the statement $(q,u)\in\Omega_h \cap C(t_o)$ implies that $(q,0)\in C(t_o)$, $(q,\mathbf{u}+\Gamma^T(q-q^e))\in C(t_o)$, and equation (6) holds with $\delta(t) \equiv -u$.

(*b*) Both the dissipative part $D:R\times O\times R^n \to R^n$ and the Lagrangian $L:R\times O\times R^n \to R$ are time-invariant, and $D(t_o,q,0) = D(t_o,q^e,0)$ for all q with $\|q-q^e\| < h$.

(*c*) The set $\Omega_\epsilon \cap C(t_o)$ is nonempty for every $\epsilon > 0$.

(*d*) There exists a real number $\mu \ge 0$ such that

$$R(q,u;\Gamma) - \mu \sum_{\ell=1}^{n} u_\ell[D_\ell(t_o,q,u) - D_\ell(t_o,q,0)] \ge 0 \text{ for all } (q,u)\in\Omega_h \cap C(t_o).$$

(*e*) There does *not* exist a solution $q(\cdot):[t_o,\infty)\to R^n$ of equations (3)–(4) along which $(q(t),\dot{q}(t))\in\Omega_h$, $G(q(t),\dot{q}(t))$ and $J(q(t),\dot{q}(t);\Gamma)$ are constant, and $R(q(t),\dot{q}(t);\Gamma) = 0 = \sum_{\ell=1}^{n} \dot{q}_\ell(t)[D_\ell(t_o,q(t),\dot{q}(t)) - D_\ell(t_o,q^e,0)]$.

Then $(q^e,0)$ is *unstable*.

Sketch of proof. Consider some dynamically possible $q(\cdot):[t_o,\infty)\to R^n$ such that $(q(t_o),\dot{q}(t_o))\in\Omega_h$, and let $t_1 > t_o$ be such that $(q(t),\dot{q}(t))\in\Omega_h$ for all $t\in[t_o,t_1)$. For the sake of simplicity, suppose that $q(\cdot)$ is C^2-smooth. Due to condition (*a*) we may choose $\delta(t) \equiv -\dot{q}(t)$ in equations (4) and (6) for $t\in[t_o,t_1)$; we may also choose $\delta(t) \equiv \Gamma^T(q(t)-q^e)$ in equation (4). From (*b*) it follows that

$$(d^+/dt)G(q(t),\dot{q}(t)) = \sum_{\ell=1}^{n} \dot{q}_\ell(t)[D_\ell(t_o,q(t),\dot{q}(t)) - D_\ell(t_o,q(t),0)] < 0,$$

$$(d^+/dt)J(q(t),\dot{q}(t);\Gamma) = -R(q(t),\dot{q}(t);\Gamma),$$

for all $t\in[t_o,t_1)$. Thus G is a Liapunov function (Walker, 1980) on $\Omega_h \cap C(t_o)$ and, due to condition (*d*), so is $J+\mu G$. Under conditions (*c*) and (*e*), LaSalle's invariance principle (Walker, 1980) implies that $(q^e,0)$ is unstable, and this concludes our sketch of the proof.

Often condition (*e*) of Theorem 3.2 is not difficult to check. If condition (*d*) is strongly satisfied (>0 replaces ≥ 0), then condition (*e*) is met. Condition (*e*) also is met if Q is strongly pseudodissipative (see Definition 2.1) and $(q^e,0)$ is isolated, but then the conditions of Theorem 3.2 are more restrictive (less likely to be met) than are those of Theorem 3.1. That is, for strongly pseudodissipative Q Theorem 4.3 provides a less restricted instability result.

Condition (*d*) of Theorem 3.2 may be weakened somewhat. The nonuniqueness of U and D leads to nonuniqueness of R in equation (11), and R may be replaced in conditions (*d*)–(*e*) by many other functions $\hat{R}$ of the form

$$\hat{R}(q,u;\Gamma) \equiv R(q,u;\Gamma) - \sum_{i=1}^{n}\sum_{j=1}^{n} \gamma_{ij}u_i\left[\frac{\partial}{\partial q_j}F(q) - \frac{\partial}{\partial q_j}F(q^e) + \sum_{\ell=1}^{n}(q_\ell - q_\ell^e)\frac{\partial^2}{\partial q_\ell \partial q_j}F(q)\right] \tag{13}$$

where $F:O\to R$ is any C^2-smooth function[2]. Moreover, the open set Ω_h may consist of two or more disjoint open components, and Theorem 3.2 remains valid if Ω_h is replaced by any such component which meets conditions (*a*) and (*c*).

It is not difficult to investigate definiteness of real symmetric $n\times n$ matrices, so the following two corollaries to Theorems 3.1–3.2 may be much easier to apply. In Corollaries 3.1–3.2 we assume that $(q^e,0)$ is some generalized equilibrium and utilize related $n\times n$ matrices $\mathbf{M} = [\mathbf{m}_{ij}]$, $\mathbf{K} = [\mathbf{k}_{ij}]$, $\mathbf{B} = [\mathbf{b}_{ij}]$, $\mathbf{C} = [\mathbf{c}_{ij}]$, and $\bar{\mathbf{C}}$ defined as follows:

$$\mathbf{m}_{ij} \equiv \partial^2 L(t_o,q^e,0)/\partial u_i \partial u_j,\ \mathbf{k}_{ij} \equiv -\partial^2 L(t_o,q^e,0)/\partial q_i \partial q_j, \tag{14}$$

$$\mathbf{b}_{ij} \equiv \partial^2 L(t_o,q^e,0)/\partial q_i \partial u_j,\ \mathbf{c}_{ij} \equiv -\partial D_i(t_o,q^e,0)/\partial u_j, \tag{15}$$

$$\bar{\mathbf{C}} \equiv (\mathbf{C}+\mathbf{C}^T)/2. \tag{16}$$

We note that $\mathbf{M}$, $\mathbf{K}$, and $\bar{\mathbf{C}}$ are symmetric, while both $\mathbf{M}$ and $\bar{\mathbf{C}}$ are at least positive semidefinite.

The proofs of Corollaries 3.1–3.2 are based on estimates of the functions appearing in Theorems 3.1–3.2, and have been relegated to an appendix.

Corollary 3.1. Suppose that $(q^e,0)\in R^n \times R^n$ is a generalized equilibrium and the following conditions hold:

(*a*) There exists $h > 0$ such that $C(t) \subset n_h$ for all $t \ge t_o$.

(*b*) The Lagrangian $L:R\times O\times R^n \to R$ is time-invariant and C^2-smooth, and $D(t,q,0) = D(t,q^e,0)$ for all $(t,q)\in R\times 0$.

(*c*) Both $\mathbf{M}$ and $\mathbf{K}$ are positive definite.

[2] In Definition 2.1, notice that the pair (U,D) can be replaced by $(\hat{U},D)$ with $\hat{U} \equiv U + \sum_{\ell=1}^{n} u_\ell\, \partial/\partial q_\ell\, F(q)$.

Downloaded 03 May 2010 to 171.66.16.21. Redistribution subject to ASME license or copyright; see http://www.asme.org/terms/Terms_Use.cfm

Then $(q^e,0)$ is *stable*. If Q is pseudoconservative ($D\equiv 0$), then $(q^e,0)$ is *not* asymptotically stable.

If, in addition to (*a*)-(*c*),

(*d*) The dissipative part D: $R\times O\times R^n\to R^n$ is time-invariant and C^1-smooth, and $\bar{\mathbf{C}}$ is positive definite,

then $(q^e,0)$ is *asymptotically* stable.

If the foregoing conditions (*a*), (*b*), and (*d*) hold, but in place of (*c*) we have its strong contradiction

(*e*) $\det(\mathbf{K})\neq 0$ but $\mathbf{K}$ is *not* positive definite,

then $(q^e,0)$ is *unstable*.

Corollary 3.2. Suppose that $(q^e,0)\in R^n\times R^n$ is a generalized equilibrium and the following conditions hold:

(*a*) There exists $h>0$ such that $C(t)\supset n_h$ for all $t\geq t_o$.

(*b*) The Lagrangian $L:R\times O\times R^n\to R$ is time-invariant and C^2-smooth, the dissipative part $D:R\times O\times R^n\to R^n$ is time-invariant and C^1-smooth, and $D(t_o,q,0)=D(t_o,q^e,0)$ for all $q\in O$.

(*c*) $\det(\mathbf{K})\neq 0$ but $\mathbf{K}$ is not positive definite.

(*d*) There exist real numbers $\mu\geq 0$, $\nu\geq 0$, and real $n\times n$ matrices $\boldsymbol{\Gamma}$, $\mathbf{S}=\mathbf{S}^{\mathrm{T}}$, such that the symmetric $2n\times 2n$ matrix $\mathbf{P}(\mu,\nu,\boldsymbol{\Gamma},\mathbf{S})\equiv$

$$\begin{bmatrix} \nu\mathbf{K}-\boldsymbol{\Gamma}\mathbf{K}-\mathbf{K}\boldsymbol{\Gamma}^T & \vdots & \boldsymbol{\Gamma}(\mathbf{B}-\mathbf{S}-\mathbf{C})+(\mathbf{B}-\mathbf{S})\boldsymbol{\Gamma}^T \\ \cdots & \cdots & \cdots \\ (\mathbf{B}\text{-}\mathbf{S}\text{-}\mathbf{C})^T\boldsymbol{\Gamma}^T+\boldsymbol{\Gamma}(\mathbf{B}\text{-}\mathbf{S})^T & \vdots & \nu\mathbf{M}+\boldsymbol{\Gamma}\mathbf{M}+\mathbf{M}\boldsymbol{\Gamma}^T+2\mu\bar{\mathbf{C}} \end{bmatrix} \tag{17}$$

is positive definite.

Then $(q^e,0)$ is *unstable*.

Condition (*d*) of Corollary 3.2 is made complicated by its own generality. In a given application, we may demonstrate the existence of suitable parameters μ, ν, $\boldsymbol{\Gamma}$ and $\mathbf{S}$ by making a parameter selection which "works"; i.e., it yields $\mathbf{P}(\mu,\nu,\boldsymbol{\Gamma},\mathbf{S})>0$. The following comments pertain to the selection of μ, ν, $\boldsymbol{\Gamma}$, and $\mathbf{S}$ in condition (*d*):

Comment 3.1. Since $\bar{\mathbf{C}}\geq 0$, it is often best to choose very large $\mu>0$ when attempting to satisfy condition (*d*) of Corollary 3.2. If $\bar{\mathbf{C}}>0$, Corollary 3.2 should not be employed, since it is then no more informative than the simpler Corollary 3.1.

Comment 3.2. The $n\times n$ matrix $\mathbf{S}=\mathbf{S}^T$ affects condition (*d*) of Corollary 3.2 only through the "off-diagonal" submatrices in $\mathbf{P}$, and the choice $\mathbf{S}=(\mathbf{B}+\mathbf{B}^T-\bar{\mathbf{C}})/2$ usually seems best.

Comment 3.3. For $n=1$, condition (*c*) of Corollary 3.2 requires that $\mathbf{K}=\mathbf{k}_{11}<0$. If $\mathbf{M}+\mathbf{C}=\mathbf{m}_{11}+\mathbf{c}_{11}>0$, condition (*d*) is then satisfied by the choices $\mu=1$, $\nu=0$, $\boldsymbol{\Gamma}=\boldsymbol{\gamma}_{11}=1$, and $\mathbf{S}=\mathbf{s}_{11}=\mathbf{b}_{11}-\mathbf{C}_{11}/2\mathbf{c}_{11}$.

Comment 3.4. If $n>1$ and $\mathbf{K}<0$, it seems best to choose $\nu=0$ and $\boldsymbol{\Gamma}=I$.

Comment 3.5. Suppose that $n>1$ and $\mathbf{K}$ is indefinite. It seems best to choose $\boldsymbol{\Gamma}$ such that $\nu\mathbf{K}-\boldsymbol{\Gamma}\mathbf{K}-\mathbf{K}\boldsymbol{\Gamma}^T>0$ and $\nu\mathbf{M}+\boldsymbol{\Gamma}\mathbf{M}+\mathbf{M}\boldsymbol{\Gamma}^T>0$ for some $\nu\geq 0$. This can always be done[3] if $\mathbf{M}>0$ and $\det(\mathbf{K})\neq 0$.

When applicable, Corollaries 3.1-3.2 usually are much easier to employ than are our best results, Theorems 3.1-3.2. In the following section we demonstrate the simplicity of these corollaries by applying them to an example.

[3] Suitable $\boldsymbol{\Gamma}$ can be explicitly constructed in terms of the solutions (λ,g) of the eigenvalue problem $(\lambda\mathbf{M}+\mathbf{K})g=0$. It is necessary to choose $\boldsymbol{\Gamma}\neq I$ at two of the four physically distinct generalized equilibria of the undamped double pendulum.

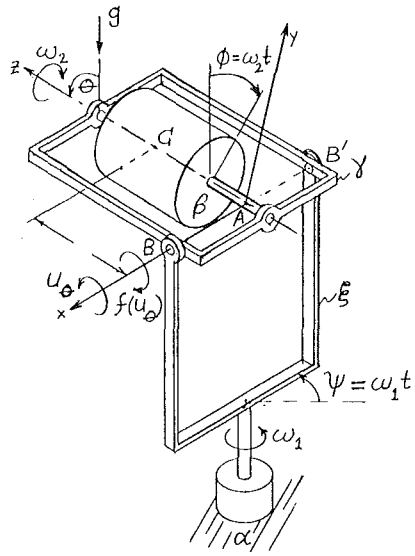


Fig. 1 Mechanism of example

4 Example

The housing γ of a constant-speed motor (speed ω_2) with armature β is hinged to a clevis ξ which is driven at a constant rate ω_1 about a vertical axis by another constant-speed motor attached to the floor α, assumed to be inertial (see Fig. 1). Along motions, friction at the bearings B and B' creates an opposing torque $f(\dot{\theta}(t))$ about the horizontal bearing axis Ax, where $f:R\to R$ is C^1-smooth, $f(0)=0$, and $f'(u_\theta)\geq 0$ for all $u_\theta\in R$. $Axyz$ is a principal coordinate system for both the armature β and the housing γ of the upper motor, and C is the mass center of this motor (mass m).

Choosing the upper motor $(\gamma+\beta)$ to be our collection and defining $q\equiv\theta\in O\equiv R^1$, we see that $u=u_\theta\in R^1$, $C(t)=R^1\times R^1$ for all $t\in R$,

$$Q(t,\theta,u_\theta)=mg\ell\sin\theta-f(u_\theta)\in R^1, \tag{18}$$

and

$$T(t,\theta,u_\theta)=(1/2)[\bar{J}_1u_\theta^2+\bar{J}_2\omega_1^2\sin^2\theta + J_3(\omega_2^2+2\omega_1\omega_2\cos\theta)+\bar{J}_3\omega_1^2\cos^2\theta] \tag{19}$$

where $\bar{J}_1=J_1+I_1$, $\bar{J}_2=J_1+I_2$, $\bar{J}_3=J_3+I_3$,

$$J^{(\beta)}_{Axyz}=\begin{bmatrix} J_1 & 0 & 0 \\ 0 & J_1 & 0 \\ 0 & 0 & J_3 \end{bmatrix},$$

$$J^{(\gamma)}_{Axyz}=\begin{bmatrix} I_1 & 0 & 0 \\ 0 & I_2 & 0 \\ 0 & 0 & I_3 \end{bmatrix}. \tag{20}$$

Hence Q is pseudodissipative with

$$U(t,\theta,u_\theta)=mg\ell\cos\theta, \tag{21}$$

$$D(t,\theta,u_\theta)=-f(u_\theta)\in R^1, \tag{22}$$

and $L\equiv T-U$. For convenience we define two new parameters

$$\sigma\equiv\omega_1^2(\bar{J}_3-\bar{J}_2),\quad \zeta\equiv J_3\omega_1\omega_2-mg\ell, \tag{23}$$

and note that

Downloaded 03 May 2010 to 171.66.16.21. Redistribution subject to ASME license or copyright; see http://www.asme.org/terms/Terms_Use.cfm

	$\sigma < -\lvert\zeta\rvert$	$\sigma > \lvert\zeta\rvert$	$\zeta < -\lvert\sigma\rvert$	$\zeta > \lvert\sigma\rvert$
$(\theta^e,0)_1$	UNSTABLE	STABLE	UNSTABLE	STABLE
$(\theta^e,0)_2$	UNSTABLE	STABLE	STABLE	UNSTABLE
$(\theta^e,0)_{3,4}$	STABLE	UNSTABLE	IMPOSSIBLE	

Fig. 2 Stability table for example

$$\frac{\partial}{\partial\theta}L(t,\theta,u_\theta) = -[\sigma\cos\theta + \zeta]\sin\theta. \tag{24}$$

Since $f(0)=0$, Corollary 2.1 shows that there exist at least two physically distinct generalized equilibria

$$(\theta^e,0)_1 = (0,0), \quad (\theta^e,0)_2 = (\pi,0),$$

and for $|\sigma| > |\zeta|$ there exist two more:

$$(\theta^e,0)_3 \text{ with } \sin\theta^e > 0 \text{ and } \zeta + \sigma\cos\theta^e = 0,$$

$$(\theta^e,0)_4 \text{ with } \sin\theta^e < 0 \text{ and } \zeta + \sigma\cos\theta^e = 0.$$

At every $(\theta^e,0)$ we find the matrices of (14)–(17) to be

$$\mathbf{M} = \mathbf{m}_{11} = \tilde{J}_1 > 0, \quad \mathbf{B} = \mathbf{b}_{11} = 0,$$

$$\tilde{\mathbf{C}} = \mathbf{C} = \mathbf{c}_{11} = f'(0) \geq 0,$$

$$\mathbf{K} = \mathbf{k}_{11} = (\eta + \sigma\cos\theta^e)\cos\theta^e - \sigma\sin^2\theta^e,$$

$$P(\mu,\nu,\gamma_{11},s_{11}) = \begin{bmatrix} -2\mathbf{k}_{11} & 0 \\ 0 & 2\tilde{J}_1 + 2f'(0) \end{bmatrix},$$

upon choosing the parameters in $\mathbf{P}$ as suggested by Comment 3.3.

At $(\theta^e,0)_1$ we have $\theta^e = 0$ and $\mathbf{k}_{11} = \sigma + \zeta$, so Corollary 3.1 implies stability for $\sigma + \zeta > 0$. If $\sigma + \zeta < 0$, then $\mathbf{P}_1 > 0$ and Corollary 3.2 implies instability.

At $(\theta^e,0)_2$ we have $\theta^e = 0$ and $\mathbf{k}_{11} = \sigma - \zeta$, so Corollary 3.1 implies stability for $\sigma > \zeta$. If $\sigma < \zeta$, then $\mathbf{P}_2 > 0$ and Corollary 3.2 implies instability.

At both $(\theta^e,0)_3$ and $(\theta^e,0)_4$ we have $\sin\theta^e \neq 0$, $\zeta + \sigma\cos\theta^e = 0$, and $\mathbf{k}_{11} = -\sigma\sin^2\theta^e$, so Corollary 3.1 implies stability for $\sigma < 0$. If $\sigma > 0$, then $\mathbf{P}_{3,4} > 0$ and Corollary 3.2 implies instability.

The foregoing results are summarized in Fig. 2, but more can be said if more is known about the frictional torque at the bearings B, B'. If $f(u_\theta) = 0$ for all $u_\theta \in R^1$, then Q is pseudoconservative ($D \equiv 0$) and Corollary 3.1 shows that each claim of "stability" becomes "stable but not asymptotically stable." If, instead, $\mathbf{c}_{11} = f'(0) > 0$, each conclusion of "stability" is strengthened to "asymptotic stability," and all conclusions can be obtained from Corollary 3.1; Corollary 3.2 is not needed.

5 Concluding Remarks

Our stability conclusions for the highly nonlinear example of Section 4 were obtained from Corollaries 3.1–3.2, rather than the more general and complicated Theorems 3.1–3.2. The simplicity of Corollaries 3.1–3.2 may suggest that these corollaries were produced by "linearization," an often dubious approximation technique for stability analysis. The proofs of Corollaries 3.1–3.2 show that linearization has not been employed.

On the other hand, if $(q^e,0)$ is a generalized equilibrium and assumptions (a)–(b) of Corollaries 3.1–3.2 hold, then the approximate linearized motion eqation have the form

$$\mathbf{M}\ddot{x}(t) + (\mathbf{B}^T - \mathbf{B} + \mathbf{C})\dot{x}(t) + \mathbf{K}x(t) = 0 \tag{25}$$

(where $x(t) \approx q(t) - q^e$), and stability conclusions for the equilibrium $(x^e,0) = (0,0)$ of equation (25) are in agreement with those guaranteed by Corollaries 3.1–3.2 for $(q^e,0)$. The reason for this is that we have assumed the generalized force to be pseudodissipative (see Definition 2.1). Pseudodissipative Q seems to be an unstated validating assumption of small oscillation theory.

If U and D meet condition (2) of Definition 2.1, then the motion equations (3)–(4) are valid even if D does *not* satisfy the monotonicity condition (1); so are the equilibrium equations (5)–(6) if $L \equiv T - U$ is time-invariant. Theorems 3.1–3.2 and Corollaries 3.1–3.2 remain valid if Q is merely "locally pseudodissipative at $u = 0$" in the following sense: U is C^1-smooth and affine in u, U and D satisfy condition (2), but condition (1) need hold only for $v = 0$.

Without linearizing the motion equations, we were able to obtain some very simple stability results (Corollaries 3.1–3.2) which require only the ability to determine definiteness of matrices. These results are so simple that the author has found them to be both teachable and worthwhile in a standard course on advanced dynamics. This has also been found to be true of some closely related stability results for reduced equilibria (related to steady motions) of pseudodissipative systems; these results will be presented in a second paper.

References

Lagrange, J. L., 1788, *Mecanique Analytique*, New ed. Mme. Ve. Courcier, Paris, 1811.

LaSalle, J. P., and Lefschetz, S., 1961, *Stability by Liapunov's Direct Method*, Academic Press, New York.

Liapunov, A. M., 1892, "Probleme General de la Stabilite du Mouvement," Annals of Mathematical Studies, No. 17, Princeton University Press, 1949.

Malkin, I. G., 1952, "Theory of Stability of Motion," AEC-tr-3352, Office of Technical Services, Department of Commerce, Washington, DC.

Routh, E. J., 1960, *Advanced Dynamics of a System of Rigid Bodies*, 6th ed., Dover Publications, New York, 1955.

Walker, J. A., 1980, *Dynamical Systems and Evolution Equations*, Plenum Press, New York.

APPENDIX

Proof of Corollary 3.1. Due to condition (b),

$$|G(q,u) - G(q^e,0) - (1/2)[u^T\mathbf{M}u + (q-q^e)^T\mathbf{K}(q-q^e)]| \leq o(\|q-q^e\|^2 + \|u\|^2).$$

If $\mathbf{M}$ and $\mathbf{K}$ are positive definite, it follows that $G(q,u) > G(q^e,0)$ for all $(q,u) \in n_h$ with sufficiently small $h > 0$. As our current conditions (a)–(c) assure the satisfaction of the corresponding conditions of Theorem 3.1, that theorem states that $(q^e,0)$ is stable (but not asymptotically stable for pseudoconservative Q) under conditions (a)–(c).

On the other hand, if $\mathbf{K}$ is not even positive semidefinite, our estimate for G implies that the set Ω_h is non-empty for every $h > 0$.

If the dissipative part $D: R \times O \times R^n \to R^n$ is time-invariant and C^1-smooth, condition (b) implies that

$$\left| \sum_{\ell=1}^{n} u_\ell[D_\ell(t_o,q,u) - D_\ell(t_o,q^e,0) + u^T\tilde{\mathbf{C}}u \right| \leq o(\|u\|^2).$$

for all $(q, u) \in n_h$, some $h > 0$.

If $\tilde{\mathbf{C}}$ is positive definite, it follows that

$$\sum_{\ell=1}^{n} u_\ell[D_\ell(t_o,q,u) - D_\ell(t_o,q^e,0)] < 0$$

for all $(q,u) \in n_h$ such that h is sufficiently small and $\|u\| \neq 0$. We also note that if $\det(\mathbf{K}) \neq 0$, then conditions (a)–(b) and equation (6) imply that $(q^e,0)$ is an isolated generalized equilibrium.

Downloaded 03 May 2010 to 171.66.16.21. Redistribution subject to ASME license or copyright; see http://www.asme.org/terms/Terms_Use.cfm

It now follows that our current conditions (*a*)–(*d*) imply satisfaction of the corresponding conditions (*a*)–(*d*) of Theorem 3.1. Alternatively, under our current conditions (*a*), (*b*), (*d*), and (*e*), our estimates imply that the corresponding conditions of Theorem 3.1 are met.

Proof of Corollary 3.2. Clearly, we need only show that our current conditions (*a*)–(*d*) imply the satisfaction of conditions (*c*)–(*e*) of Theorem 3.2. The estimate made for G in the proof of Corollary 3.1 remains valid. Therefore our current condition (*c*) implies that the set Ω_h of equation (12) is nonempty for every $h>0$, and condition (*c*) of Theorem 3.2 is met.

Employing conditions (*a*)–(*b*) and the equilibrium condition (6), we find that

$$|2R(q,u;\Gamma) - [U^T(\Gamma\mathbf{M}+\mathbf{M}\Gamma^T)u + 2(q-q^e)^T \times (\Gamma\mathbf{B}+\mathbf{B}\Gamma^T-\Gamma\mathbf{C})u - (q-q^e)^T(\Gamma\mathbf{K}+\mathbf{K}\Gamma^T)(q-q^e)]|$$

$$\leq o(\|q-q^e\|^2+\|u\|^2).$$

Nonuniqueness of U allows $\mathbf{B}$ to be replaced by $\mathbf{B}-\mathbf{S}$ in this estimate, where $\mathbf{S}$ is any symmetric real $n\times n$ matrix, if R is replaced by some "equivalent" $\hat{R}$ (see equation (13) with $F(q)\equiv 1/2q^T\mathbf{S}q$). Hence, combining this estimate with those made in the proof of Corollary 3.1, we find that our current condition (*d*) implies

$$\nu[G(q,u)-G(q^e,0)] + R(q,u;\Gamma) - \mu\sum_{\ell=1}^{n} u_\ell[D_\ell(t_o,q,u)-D_\ell(t_o,q^e,0)] > 0$$

for all $(q,u)\in\eta_h$, some $h\geq 0$. Since $\nu\geq 0$ and $G(q,u)<G(q^e,0)$ for all $(q,u)\in\Omega_h$, it follows that conditions (*d*)–(*e*) of Theorem 3.2 are met.

Downloaded 03 May 2010 to 171.66.16.21. Redistribution subject to ASME license or copyright; see http://www.asme.org/terms/Terms_Use.cfm

A Recursive Formulation for the Dynamic Analysis of Open Loop Deformable Multibody Systems

K. Changizi

A. A. Shabana

Department of Mechanical Engineering,
University of Illinois at Chicago,
Chicago, IL 60680

In this paper, a recursive formulation for the spatial kinematic and dynamic analysis of open chain mechanical systems containing interconnected deformable bodies, each of which may undergo large translational and rotational displacements, is developed. While approximation techniques such as the finite element method, Rayleigh-Ritz methods, or experimentally identified modal parameters can be used to introduce the elastic coordinates that describe the deformation of the bodies with respect to selected body references, the large rotational and translational displacements of a set of intermediate joint axes are described using a minimum set of relative translational and rotational coordinates. A set of time-invariant quantities that depend on the assumed displacement field and provide a systematic approach to study the spatial dynamics of open loop mechanical systems are obtained. The method developed is applicable to open loop mechanical systems containing revolute, prismatic and cylindrical joints. Furthermore, the formulation developed is independent of the type of finite element or the modal identification technique used.

1 Introduction

The multibody mechanical systems in general can be classified into two main groups: open and closed chains. The mathematical models of such systems can be formulated using Newton-Euler equations, Lagrange's equation or using variations of Newton-Euler and Lagrange's equations (Vokobratovic and Potkonjak, 1979), (Potkonjak and Vokobratovic, 1979), and (Orin et al., 1979). Chace (1967) proposed a method for the analysis of highly constrained, multi-degree of freedom mechanical systems using the relative coordinates. In his work, the second order derivatives were used to formulate the joint kinematic constraint equations and the kinetic and potential energies of each body in the system were written in terms of the relative coordinates. A set of nonlinear simultaneous differential equations which represent the motion of each body in the system were then obtained using the Lagrangian formulation. It was also pointed out by Chace (1967) that the use of relative coordinates in a highly constrained mechanical system simplified the statement of the constraints and reduced the number of differential equations required to describe the system dynamics. Sherby and Chmielewski (1968), presented general expressions for the kth-order derivative of a relative position and angular velocity vector measured in any moving frame of reference. As a special case of these expressions, a procedure for deriving the vector equations of motion in relative coordinates for a multibody mechanical systems by routine substitution was developed. Kim and Vanderploeg (1986), presented a new formulation for the equations of motion of interconnected rigid bodies. In this formulation, Cartesian coordinates were initially used to define the configuration of the system, the kinematic constraint equations, and general forcing functions. The equations of motion were then written using the Lagrangian formulation in terms of relative joint coordinates using a velocity transformation matrix which relates relative coordinates to Cartesian coordinates. The kinematic relationships for each joint type were formulated and the graph theory was used to identify the system topology. Luh et al. (1980) expressed the equations of motion of each manipulator link exclusively in local coordinate systems. The process involved the successive transformation of velocities and accelerations from the base of the manipulator to the hand, link by link, using the kinematic relationships between the moving coordinate systems presented by Symon (1971). Renaud (1974), derived equations of motion for a system of $n+1$ bodies, forming a branch structure relative to the reference body O. The neighboring bodies were permitted relative rotation and

Contributed by the Applied Mechanics Division for presentation at the Winter Annual Meeting, Chicago, IL, November 28 to December 2, 1988, of THE AMERICAN SOCIETY OF MECHANICAL ENGINEERS.

Discussion on this paper should be addressed to the Editorial Department, ASME United Engineering Center, 345 East 47th Street, New York, N.Y. 10017, and will be accepted until two months after final publication of the paper itself in the JOURNAL OF APPLIED MECHANICS. Manuscript received by ASME Applied Mechanics Division, August 17, 1987; final revision, February 26, 1988.

Copyright © 1988 by ASME

Downloaded 03 May 2010 to 171.66.16.21. Redistribution subject to ASME license or copyright; see http://www.asme.org/terms/Terms_Use.cfm

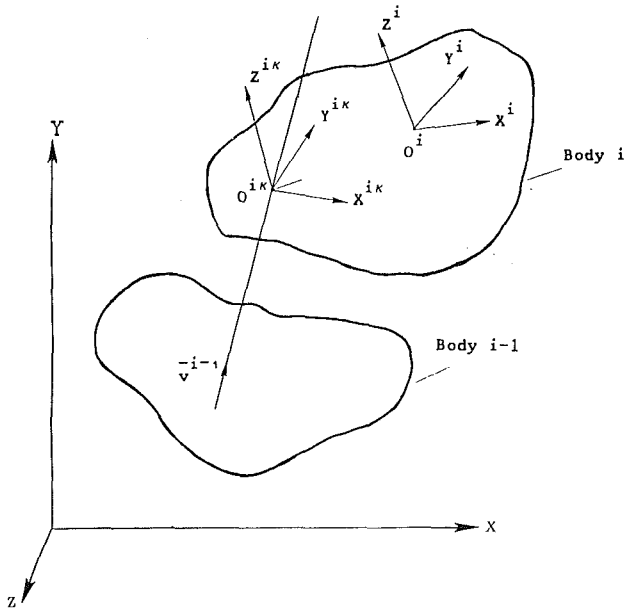


Fig. 1 Intermediate coordinate systems

translation. Huston and Kelly (1982) developed the equations of motion for a single arm robot using Kane's dynamical equations. Kane's equations, which were developed essentially for spatial mechanisms by Kane (1965) and extended to robot arm dynamics (Kane, 1983), have the advantage of eliminating internal constraint forces without differentiation of scalar energy functions. In most of the above mentioned investigations, an assumption is made that the multibody system consists of rigid components. The limitation of the rigid body assumption in the dynamic analysis of manipulators was investigated by Book (1974). Book (1979, 1984) and Book et al. (1975) suggested control schemes for flexible manipulators. Lilov (1985), presented a dynamic formulation of chains of rigid and elastic rods with revolute and prismatic joints based on the principle of virtual power. Finite set of hybrid coordinates is assumed to account for the large relative displacements in the joints and small deformation of the elastic bodies.

In this paper a recursive Lagrangian formulation for the kinematic and dynamic analysis of general open loop mechanical systems is developed. The multibody system under investigation is assumed to consist of a set of interconnected deformable bodies which may undergo large relative translational and rotational displacements. The configuration of each deformable body in the open loop kinematic chain is identified using a coupled set of relative joint variables and elastic coordinates. The elastic coordinates define the displacement field of the deformable body with respect to a body coordinate system selected in a manner consistent with the kinematic constraints. The relative joint variables, however, describe the large translational and rotational displacements between a set of intermediate coordinate systems whose origins are rigidly attached to the joint definition points. These intermediate coordinate systems experience only infinitesimal rotations with respect to their body coordinate systems. A set of recursive kinematic relationships are developed in terms of the coupled sets of relative joints and elastic coordinates. These kinematic equations are then used to develop a set of dynamic differential equations in terms of a set of invariants that depend on the assumed displacement field.

2 Background

The formulation of the kinematic and dynamic equations of open loop flexible multibody systems using the relative coordinates requires the introduction of basic concepts and definitions. In this investigation, multibody systems are assumed to consist of interconnected deformable bodies each of which may experience large relative translational or rotational displacements. We assume that a global, inertial coordinate system exists. This coordinate system is fixed in time and forms a single standard for the entire assembly of bodies. The displacement of deformable components can be described using a finite set of elastic coordinates that can be introduced using the finite element method or a set of experimentally identified parameters (Shabana, 1986). In order to define a unique displacement field in the finite element formulation, a set of reference conditions that are consistent with the kinematic constraints on the boundary of the deformable body have to be imposed (Agrawal and Shabana, 1986). These reference conditions define the nature of the body reference. The origin of this reference, however, does not have to be rigidly attached to a point on the deformable body. In fact a moving frame of reference is suggested for deformable bodies that undergo large rotations (Agrawal and Shabana, 1986). In addition, intermediate reference frames having no mass or inertia, may be introduced at selected nodal points for the convenience of defining various joints between interconnected bodies. The intermediate reference frames are assumed to experience infinitesimal, or no rotations, with respect to the body reference. As shown in Fig. 1, XYZ is the global inertial frame, $X^i\ Y^i\ Z^i$ is the body coordinate system and $X^{ik}\ Y^{ik}\ Z^{ik}$ is an intermediate frame of reference attached to the kth nodal point on body i. O^i and O^{ik} are, respectively, the origins of the coordinate systems $X^i\ Y^i\ Z^i$ and $X^{ik}\ Y^{ik}\ Z^{ik}$. Let θ_1^{ik}, θ_2^{ik} and θ_3^{ik} be, respectively, the infinitesimal rotations associated with node k relative to the body axes $X^i\ Y^i\ Z^i$. Then the orientation of the intermediate frame of reference $X^{ik}\ Y^{ik}\ Z^{ik}$ with respect to the $X^i\ Y^i\ Z^i$ body coordinate system is defined by the orthogonal transformation

$$A_s^{ik} = \mathbf{I} + \tilde{\Omega}^{ik} \tag{1}$$

where $\mathbf{I}$ is a 3×3 identity matrix and $\tilde{\Omega}^i$ is a skew symmetric matrix defined as

$$\tilde{\Omega}^{ik} = \begin{bmatrix} 0 & -\theta_3^{ik} & \theta_2^{ik} \\ \theta_3^{ik} & 0 & -\theta_1^{ik} \\ -\theta_2^{ik} & \theta_1^{ik} & 0 \end{bmatrix} \tag{2}$$

The frame of reference $X^{ik}\ Y^{ik}\ Z^{ik}$ is allowed to translate along and rotate about an axis in the direction of the unit vector $\bar{\mathbf{v}}^{i-1}$ which is rigidly attached to body $i-1$. This large translation and rotation between body i and body $i-1$ can be described by the two relative coordinates $\tau^{i,i-1}$ and $\theta^{i,i-1}$. Similarly, the large relative translation and rotation between body $i-1$ and body $i-2$ can be described by the relative coordinates $\tau^{i-1,i-2}$ and $\theta^{i-1,i-2}$ and continuing in this manner, the relative translation and rotation between body 2 and body 1 (base body) can be described using the relative coordinates $\tau^{2,1}$ and $\theta^{2,1}$.

3 Position Vector in the Intermediate Coordinate Systems

In this section and the following section a general expression for the position vector of an arbitrary point on the deformable body i is derived in terms of the joints relative and elastic coordinates. The open loop multibody system considered in this investigation may consist of any number of bodies connected by revolute, prismatic or/and cylindrical joints. Figure 2 shows a set of interconnected deformable bodies. Let $X_2^1\ Y_2^1\ Z_2^1$ be the inertial frame of reference that is

Downloaded 03 May 2010 to 171.66.16.21. Redistribution subject to ASME license or copyright; see http://www.asme.org/terms/Terms_Use.cfm

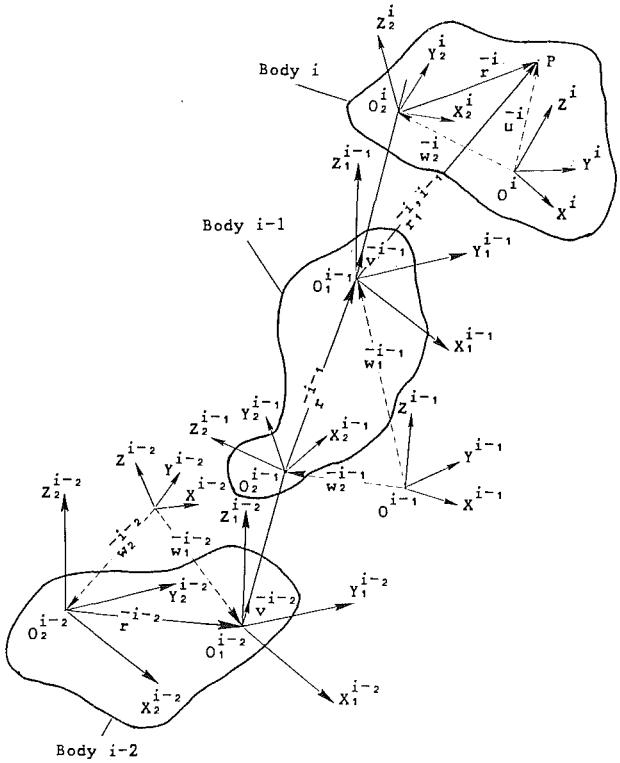


Fig. 2 Relative motion between deformable bodies

fixed in time and represents a unique standard for the entire assembly of bodies. For each deformable body i we assign a body coordinate system $X^i\ Y^i\ Z^i$ in which the body displacement field is defined. This body coordinate system does not have to be rigidly attached to a point on the body. In addition to the body references, two intermediate frames of reference, denoted as $X_1^i\ Y_1^i\ Z_1^i$ and $X_2^i\ Y_2^i\ Z_2^i$ are assigned to the deformable body i as shown in Fig. 2. The origins of these intermediate frame of references are rigidly attached to the joint definition points on the deformable body i. The relative position of point p with respect to the origin of the intermediate axes $X_2^i\ Y_2^i\ Z_2^i$ can be described by the vector $\bar{\mathbf{r}}^{\,i}$ where

$$\bar{\mathbf{r}}^{\,i} = \bar{\mathbf{r}}_0{}^i + \bar{\mathbf{r}}_f{}^i \tag{3}$$

in which

$$\bar{\mathbf{r}}_f^i = \mathbf{S}^i \mathbf{q}_f^i \tag{4}$$

Where $\bar{\mathbf{r}}_0{}^i$ and $\bar{\mathbf{r}}_f{}^i$ are, respectively, the position vector in the undeformed state and the deformation of an arbitrary point p on the deformable body i, defined with respect to the reference frame $X_2^i\ Y_2^i\ Z_2^i$, $\mathbf{q}_f^i$ is the vector of elastic nodal coordinates of body i, and $\mathbf{S}^i$ is a space and time dependent appropriate shape function. The matrix $\mathbf{S}^i$ accounts for the inifinitesimal rotation of the intermediate coordinate system with respect to the body coordinate system. If the nodal rotations are not considered in the analysis, the matrix $\mathbf{S}^i$ is only a space-dependent matrix.

4 Translations and Rotations Between the Intermediate Coordinate Systems

Let $\bar{\mathbf{v}}^{\,i-1}$ be a unit vector along the joint axes that is rigidly attached to the origin of the intermediate frame $X_1^{i-1}\ Y_1^{i-1}\ Z_1^{i-1}$ as shown in Fig. 2. The origin of this frame is rigidly attached to the joint definition point O_1^{i-1} which is assumed to be a nodal point on body $i-1$. The position vector of point p of body i relative to O_1^{i-1} in the $X_1^{i-1}\ Y_1^{i-1}\ Z_1^{i-1}$ coordinate system, can be written as

$$\bar{\mathbf{r}}_1{}^{i,i-1} = \tau^{i,i-1}\bar{\mathbf{v}}^{\,i-1} + \mathbf{A}^{i,i-1}\bar{\mathbf{r}}^{\,i} \tag{5}$$

where $\mathbf{A}^{i,i-1}$ is the transformation matrix that describes the finite rotation between the frames $X_2^i\ Y_2^i\ Z_2^i$ and $X_1^{i-1}\ Y_1^{i-1}\ Z_1^{i-1}$, and $\tau^{i,i-1}$ is the relative translation between these two frames of references. The position of point O_1^{i-1} relative to the O_2^{i-1}, a nodal point on body $i-1$, can be defined in the $X_2^{i-1}\ Y_2^{i-1}\ Z_2^{i-1}$ coordinate system in terms of the elastic coordinates of body $i-1$ by the vector $\bar{\mathbf{r}}^{\,i-1}$ where

$$\bar{\mathbf{r}}^{\,i-1} = \bar{\mathbf{r}}_0{}^{i-1} + \bar{\mathbf{r}}_f{}^{i-1} \tag{6}$$

where $\bar{\mathbf{r}}_0{}^{i-1}$ and $\bar{\mathbf{r}}_f{}^{i-1}$ are, respectively, the position vector in the undeformed state and the deformation vector of the point O_1^{i-1}, defined with respect to the reference frame $X_2^{i-1}\ Y_2^{i-1}\ Z_2^{i-1}$. Since O_1^{i-1} and O_2^{i-1} are assumed to be nodal points, the vector $\bar{\mathbf{r}}_f{}^{i-1}$ in contrast with $\bar{\mathbf{r}}_f{}^i$ is only time dependent and can be written in terms of the elastic nodal coordinates of body $i-1$ as

$$\bar{\mathbf{r}}_f{}^{i-1} = \mathbf{S}^{i-1}\mathbf{q}_f^{i-1} \tag{7}$$

where $\mathbf{S}^{i-1}$ is an appropriate matrix and $\mathbf{q}_f^{i-1}$ is the set of elastic coordinates of body $i-1$. The position of point p on body i with respect to the intermediate system $X_2^{i-1}\ Y_2^{i-1}\ Z_2^{i-1}$ can then be written as

$$\bar{\mathbf{r}}_2{}^{i,i-1} = \bar{\mathbf{r}}^{\,i-1} + \mathbf{A}_s^{i-1}\bar{\mathbf{r}}_1{}^{i,i-1} \tag{8}$$

where $\mathbf{A}_s^{i-1} = \mathbf{I} + \tilde{\mathbf{\Omega}}^{i-1}$ is the infinitesimal rotation matrix between the two coordinate systems $X_1^{i-1}\ Y_1^{i-1}\ Z_1^{i-1}$ and $X_2^{i-1}\ Y_2^{i-1}\ Z_2^{i-1}$, $\mathbf{I}$ is the identity matrix and $\tilde{\mathbf{\Omega}}^{i-1}$ is a skew symmetric matrix whose elements are the infinitesimal relative rotations between the two intermediate coordinates systems $X_1^{i-1}\ Y_1^{i-1}\ Z_1^{i-1}$ and $X_2^{i-1}\ Y_2^{i-1}\ Z_2^{i-1}$. Substituting equation (5) into equation (8), one obtains

$$\bar{\mathbf{r}}_2^{i,i-1} = \bar{\mathbf{r}}^{\,i-1} + \mathbf{A}_s^{i-1}\tau^{i,i-1}\bar{\mathbf{v}}^{\,i-1} + \mathbf{A}_s^{i-1}\mathbf{A}^{i,i-1}\bar{\mathbf{r}}^{\,i} \tag{9}$$

Let

$$\mathbf{T}^\kappa = \mathbf{A}_s^\kappa \mathbf{A}^{\kappa+1,\kappa}, \quad \kappa = 1,2,\ldots,i \tag{10}$$

Where $\mathbf{A}_s^\kappa$ is the infinitesimal rotation matrix between the two intermediate coordinate systems of body k, and $\mathbf{A}^{\kappa+1,\kappa}$ is the transformation matrix that describes the finite rotation between the bodies $k+1$ and k. Since $\mathbf{A}_s^\kappa$ and $\mathbf{A}^{\kappa+1,\kappa}$ are orthogonal transformation matrices, it is an easy matter to verify that $\mathbf{T}^\kappa$ is also an orthogonal matrix, that is

$$\mathbf{T}^{\kappa T}\mathbf{T}^\kappa = \mathbf{I} \tag{11}$$

Where superscript T indicates the transpose of a vector or a matrix. Using the above identity, and proceeding in the same manner as described above, one can write the position of point P on body i relative to the fixed inertial frame $X_2^1\ Y_2^1\ Z_2^1$ of the base body one as follows:

$$\bar{\mathbf{r}}_2{}^{i,1} = \sum_{\kappa=2}^{i} \mathbf{C}^\kappa \mathbf{b}^\kappa \tau^{\kappa,\kappa-1} + \sum_{\kappa=1}^{i} \mathbf{C}^{\kappa+1}\bar{\mathbf{r}}^\kappa \tag{12}$$

where

$$\mathbf{C}^\kappa = \mathbf{T}^1\mathbf{T}^2\ldots\mathbf{T}^{\kappa-2} \quad \text{for } \kappa > 2 \tag{13}$$

$$\mathbf{C}^2 = \mathbf{T}^0 = \mathbf{I}, \quad \mathbf{C}^\kappa = 0 \quad \text{for } \kappa < 2$$

$$\mathbf{b}^k = \mathbf{A}_s^{k-1}\mathbf{v}^{k-1}, \quad k = 2,\ldots,i \tag{14}$$

It is important to emphasize at this point that the only term which is both space and time dependent in equation (12) is $\bar{\mathbf{r}}^{\,i}$, while $\bar{\mathbf{r}}^{\,k}$ for $k<i$ depends only on the elastic coordinates of the respective body and accordingly it is only time dependent.

5 Virtual Changes and Velocity Coefficients

In this section an expression for the virtual change in the global position of the arbitrary point P on the deformable body i is derived in terms of the virtual change of the joint variables and the elastic coordinates. The vector $\bar{\mathbf{r}}_2{}^{i,1}$ of equation (12) can be written as the sum of two vectors as follows

Downloaded 03 May 2010 to 171.66.16.21. Redistribution subject to ASME license or copyright; see http://www.asme.org/terms/Terms_Use.cfm

$$\bar{\mathbf{r}}_2^{\,i,1} = \bar{\mathbf{r}}_\tau^{\,i,1} + \bar{\mathbf{r}}_r^{\,i,1} \tag{15}$$

Where

$$\bar{\mathbf{r}}_\tau^{\,i,1} = \sum_{\kappa=2}^{i} \mathbf{C}^\kappa \mathbf{b}^\kappa \tau^{\kappa,\kappa-1} \quad \text{and} \quad \bar{\mathbf{r}}_r^{\,i,1} = \sum_{\kappa=1}^{i} \mathbf{C}^{\kappa+1} \bar{\mathbf{r}}^{\,\kappa} \tag{16}$$

The variation of vectors $\bar{\mathbf{r}}_\tau^{\,i,1}$ and $\bar{\mathbf{r}}_r^{\,i,1}$ can then be written as

$$\delta\bar{\mathbf{r}}_\tau^{\,i,1} = \sum_{\kappa=2}^{i} [\delta\mathbf{C}^\kappa \mathbf{b}^\kappa \tau^{\kappa,\kappa-1} + \mathbf{C}^\kappa \delta\mathbf{b}^\kappa \tau^{\kappa,\kappa-1} + \mathbf{C}^\kappa \mathbf{b}^\kappa \delta\tau^{\kappa,\kappa-1}] \tag{17}$$

$$\delta\bar{\mathbf{r}}_r^{\,i,1} = \sum_{\kappa=1}^{i} (\delta\mathbf{C}^{\kappa+1} \bar{\mathbf{r}}^{\,\kappa} + \mathbf{C}^{\kappa+1} \delta\bar{\mathbf{r}}^{\,\kappa}) \tag{18}$$

It can be verified that

$$\sum_{\kappa=2}^{i} \delta\mathbf{C}^\kappa \mathbf{b}^\kappa \tau^{\kappa,\kappa-1} = \sum_{\kappa=2}^{i} (\mathbf{e}_3^{\kappa-1} \delta\mathbf{q}_f^{\kappa-1} + \mathbf{e}_4^{\kappa-1} \delta\theta^{\kappa,\kappa-1}) \text{ and}$$

$$\mathbf{e}_3^{i-1} = \mathbf{e}_4^{i-1} = 0 \tag{19}$$

$$\sum_{\kappa=2}^{i} \mathbf{C}^\kappa \delta\mathbf{b}^\kappa \tau^{\kappa,\kappa-1} = \sum_{\kappa=2}^{i} \mathbf{e}_2^{\kappa-1} \delta\mathbf{q}_f^{\kappa-1} \tag{20}$$

$$\sum_{\kappa=2}^{i} \mathbf{C}^\kappa \mathbf{b}^\kappa \delta\tau^{\kappa,\kappa-1} = \sum_{\kappa=2}^{i} e_1^{\kappa-1} \delta\tau^{\kappa,\kappa-1} \tag{21}$$

$$\sum_{\kappa=1}^{i} \delta\mathbf{C}^{\kappa+1} \bar{\mathbf{r}}^{\,\kappa} = \sum_{\kappa=2}^{i} (\mathbf{e}_6^{\kappa-1} \delta\mathbf{q}_f^{\kappa-1} + \mathbf{e}_7^{\kappa-1} \delta\theta^{\kappa,\kappa-1}) \tag{22}$$

$$\sum_{\kappa=1}^{i} \mathbf{C}^{\kappa+1} \delta\bar{\mathbf{r}}^{\,\kappa} = \sum_{\kappa=1}^{i-1} \mathbf{C}^{\kappa+1} \delta\bar{\mathbf{r}}^{\,\kappa} + \mathbf{C}^{i+1} \delta\bar{\mathbf{r}}^{\,i} \tag{23}$$

Where, the coefficients $\mathbf{e}_1$ through $\mathbf{e}_7$ are defined in the Appendix. Equation (23) can be written as

$$\sum_{\kappa=1}^{i} \mathbf{C}^{\kappa+1} \delta\bar{\mathbf{r}}^{\,\kappa} = \sum_{\kappa=1}^{i-1} \mathbf{e}_8^\kappa \, \delta\mathbf{q}_f^\kappa + \mathbf{e}_8^i \, \delta\mathbf{q}_f^i = \sum_{\kappa=2}^{i} \mathbf{e}_8^{\kappa-1} \delta\mathbf{q}_f^{\kappa-1} + \mathbf{e}_8^i \, \delta\mathbf{q}_f^i \tag{24}$$

Where $\mathbf{e}_8^\kappa$ and $\mathbf{e}_8^i$ are the matrices resulting, respectively, from taking the virtual changes in the vector $\bar{\mathbf{r}}^{\,\kappa}$ and $\bar{\mathbf{r}}^{\,i}$. The virtual change of the vector $\bar{\mathbf{r}}_\tau^{\,i,1}$ given by equation (17) can then be written, by combining equations (19)–(21), as follows

$$\begin{aligned} \delta\bar{\mathbf{r}}_\tau^{\,i,1} &= \sum_{\kappa=2}^{i} (\mathbf{e}_1^{\kappa-1} \delta\tau^{\kappa,\kappa-1} + \mathbf{e}_2^{\kappa-1} \delta\mathbf{q}_f^{\kappa-1} \\ &\qquad + \mathbf{e}_3^{\kappa-1} \delta\mathbf{q}_f^{\kappa-1} + \mathbf{e}_4^{\kappa-1} \delta\theta^{\kappa,\kappa-1}) \\ &= \sum_{\kappa=2}^{i} (\mathbf{e}_1^{\kappa-1} \delta\tau^{\kappa,\kappa-1} + \mathbf{e}_4^{\kappa-1} \delta\theta^{\kappa,\kappa-1} + \mathbf{e}_5^{\kappa-1} \delta\mathbf{q}_f^{\kappa-1}) \end{aligned} \tag{25}$$

Where $\mathbf{e}_5^{\kappa-1}$ is defined as

$$\mathbf{e}_5^{\kappa-1} = \mathbf{e}_2^{\kappa-1} + \mathbf{e}_3^{\kappa-1} \tag{26}$$

Similarly, combining equations (22) and (24), one can write the virtual change $\delta\bar{\mathbf{r}}_r^{\,i,1}$, as

$$\delta\bar{\mathbf{r}}_r^{\,i,1} = \sum_{\kappa=2}^{i} (\mathbf{e}_6^{\kappa-1} \delta\mathbf{q}_f^{\kappa-1} + \mathbf{e}_7^{\kappa-1} \delta\theta^{\kappa,\kappa-1} + \mathbf{e}_8^{\kappa-1} \delta\mathbf{q}_f^{\kappa-1}) + \mathbf{e}_8^i \, \delta\mathbf{q}_f^i \tag{27}$$

The virtual change of the vector $\bar{\mathbf{r}}_2^{\,i-1}$ can then be be written as the sum of the terms $\delta\bar{\mathbf{r}}_\tau^{\,i,1}$ and $\delta\bar{\mathbf{r}}_r^{\,i,1}$ as

$$\delta\bar{\mathbf{r}}_2^{\,i,1} = \sum_{\kappa=2}^{i} [\mathbf{e}_1^{\kappa-1} \delta\tau^{\kappa,\kappa-1} + \mathbf{e}_9^{\kappa-1} \delta\theta^{\kappa,\kappa-1} + \mathbf{e}_{10}^{\kappa-1} \delta\mathbf{q}_f^{\kappa-1}] + \mathbf{e}_8^i \, \delta\mathbf{q}_f^i \tag{28}$$

Where

$$\mathbf{e}_9^{\kappa-1} = \mathbf{e}_4^{\kappa-1} + \mathbf{e}_7^{\kappa-1} \quad \kappa = 2, \ldots, i \tag{29}$$

$$\mathbf{e}_{10}^{\kappa-1} = \mathbf{e}_5^{\kappa-1} + \mathbf{e}_6^{\kappa-1} + \mathbf{e}_8^{\kappa-1} \quad \kappa = 2, \ldots, i \tag{30}$$

or in a matrix form as

$$\delta\bar{\mathbf{r}}_2^{\,i,1} = \mathbf{E}_\tau \delta\tau + \mathbf{E}_\theta \delta\theta + \mathbf{E}_f \delta\mathbf{q}_f = [\mathbf{E}_\tau \mathbf{E}_\theta \mathbf{E}_f] \begin{bmatrix} \delta\tau \\ \delta\theta \\ \delta\mathbf{q}_f \end{bmatrix} \tag{31}$$

Where the coefficient matrices that appear in this equation are given by

$$\mathbf{E}_\tau = [\mathbf{e}_1^1 \;\; \mathbf{e}_1^2 \;\; \ldots \;\; \mathbf{e}_1^{i-1}] \tag{32}$$

$$\mathbf{E}_\theta = [\mathbf{e}_9^1 \;\; \mathbf{e}_9^2 \;\; \ldots \;\; \mathbf{e}_9^{i-1}] \tag{33}$$

$$\mathbf{E}_f = [\mathbf{e}_{10}^1 \;\; \mathbf{e}_{10}^2 \;\; \ldots \;\; \mathbf{e}_{10}^{i-1} \mathbf{e}_8^i] \tag{34}$$

and the vectors of generalized coordinates τ, θ, and $\mathbf{q}_f$ are

$$\tau = [\tau^{2,1} \tau^{3,2} \;\; \ldots \;\; \tau^{i,i-1}]^T \tag{35}$$

$$\theta = [\theta^{2,1} \theta^{3,2} \;\; \ldots \;\; \theta^{i,i-1}]^T \tag{36}$$

$$\mathbf{q}_f = [\mathbf{q}_f^{1T} \mathbf{q}_f^{2T} \;\; \ldots \;\; \mathbf{q}_f^{iT}]^T \tag{37}$$

Similarly, the global velocity of an arbitrary point on the deformable body i can be written in terms of the coupled set of relative joint and elastic coordinates and their time derivatives as

$$\dot{\bar{\mathbf{r}}}_2^{\,i,1} = [\mathbf{E}_\tau \;\; \mathbf{E}_\theta \;\; \mathbf{E}_f] \begin{bmatrix} \dot{\tau} \\ \dot{\theta} \\ \dot{\mathbf{q}}_f \end{bmatrix} \tag{38}$$

This equation will be used in next section to formulate the kinetic energy for the deformable body i that undergoes large relative translational and orientational displacements.

6 Kinetic Energy and Invariants of Motion

Having defined the velocity vector of an arbitrary point on body i relative to inertial frame $X_2^1 \; Y_2^1 \; Z_2^1$, the kinetic energy of the deformable body i in the open loop multibody system can be written as

$$\mathbf{T}^i = 1/2 \int_{v^i} \rho^i \dot{\bar{\mathbf{r}}}_2^{\,i,1T} \dot{\bar{\mathbf{r}}}_2^{\,i,1} dv^i \tag{39}$$

Where ρ^i and v^i are, respectively, the mass density and the volume of body i. Let

$$\mathbf{q} = [\tau^T \; \theta^T \; \mathbf{q}_f^T]^T \tag{40}$$

and

$$\dot{\mathbf{q}} = [\dot{\tau}^T \; \dot{\theta}^T \; \dot{\mathbf{q}}_f^T]^T \tag{41}$$

Where τ and θ describe, respectively, the large relative translational and rotational displacements between interconnected bodies and $\mathbf{q}_f$ is the vector of generalized elastic coordinates. Similarly, $\dot{\tau}$ and $\dot{\theta}$ are, respectively, the vector of system relative joint translational and rotational velocities, while $\dot{\mathbf{q}}_f$ is the total vector of system elastic velocities. Substituting equatoin (38) into the kinetic energy expressions of equation (39), one may write the kinetic energy of body i as;

$$\mathbf{T}^i = 1/2 \dot{\mathbf{q}}^T \mathbf{M}^i \dot{\mathbf{q}} \tag{42}$$

Where $\mathbf{M}^i$ is the mass matrix of the deformable body i in the open loop multibody system. The mass matrix $\mathbf{M}^i$ can be written in a partitioned form as

$$\mathbf{M}^i = \int_{v^i} \rho^i \begin{bmatrix} \mathbf{E}_\tau^T \mathbf{E}_\tau & \mathbf{E}_\tau^T E_\theta & \mathbf{E}_\tau^T \mathbf{E}_f \\ & \mathbf{E}_\theta^T \mathbf{E}_\theta & \mathbf{E}_\theta^T \mathbf{E}_f \\ \text{Symmetric} & & \mathbf{E}_f^T \mathbf{E}_f \end{bmatrix} dv^i \tag{43}$$

or

$$\mathbf{M}^i = \begin{bmatrix} \mathbf{M}_{\tau\tau}^i & \mathbf{M}_{\tau\theta}^i & \mathbf{M}_{\tau f}^i \\ & \mathbf{M}_{\theta\theta}^i & \mathbf{M}_{\theta f}^i \\ \text{Symmetric} & & \mathbf{M}_{ff}^i \end{bmatrix} \tag{44}$$

Downloaded 03 May 2010 to 171.66.16.21. Redistribution subject to ASME license or copyright; see http://www.asme.org/terms/Terms_Use.cfm

One may observe that the diagonal block matrices $\mathbf{M}^i_{\tau\tau}$, $\mathbf{M}^i_{\theta\theta}$ and $\mathbf{M}^i_{ff}$ are associated, respectively, with the translational, rotational and elastic coordinates. The submatrix $\mathbf{M}^i_{\tau\theta}$ represents the inertia coupling between the relative translational and rotational coordinates, while $\mathbf{M}^i_{\tau f}$ represents the inertia coupling between the gross translational motion and the elastic deformation. The submatrix $\mathbf{M}^i_{\theta f}$ is the inertia coupling between the finite rotation and the elastic deformation. Even though the mass matrix for the deformable body i is highly nonlinear, the components of this matrix can be written in terms of a set of invariant quantities which depend on the assumed displacement field. In fact one can easily verify that the components of the mass matrix of the deformable body i can be written in terms of the following invariants of motion (Changizi, 1989).

$$\mathbf{I}^i_1 = \int_{v^i} \rho^i \bar{\mathbf{u}}^i_0 \, dv^i = \int_{v^i} \rho^i [\bar{x}^i_1 \; \bar{x}^i_2 \; \bar{x}^i_3]^T dv^i \tag{45a}$$

$$I^i_{\kappa l} = \int_{v^i} \rho^i \, \bar{x}^i_\kappa \, \bar{x}^i_l dv^i \quad \kappa, l = 1,2,3 \tag{45b}$$

$$\bar{\mathbf{I}}^i_{\kappa l} = \int_{v^i} \rho^i \bar{x}^{\;i}_\kappa \bar{\mathbf{S}}^i_l dv^i \quad \kappa, l = 1,2,3 \tag{45c}$$

$$\mathbf{J}^i_1 = \int_{v^i} \rho^i \bar{\mathbf{S}}^i dv^i \tag{45d}$$

$$\mathbf{J}^i_{\kappa l} = \int_{v^i} \rho^i \bar{\mathbf{S}}^{iT}_\kappa \bar{\mathbf{S}}^i_l dv^i \quad \kappa, l = 1,2,3 \tag{45e}$$

Where $\bar{\mathbf{u}}^i_0 = [\bar{x}^i_1 \; \bar{x}^i_2 \; \bar{x}^i_3]^T$ is the position vector of an arbitary point on the deformable body i, defined in the body coordinate system in the undeformed state, $\bar{\mathbf{S}}^{\;i}$ is the shape function of the deformable body i and $\bar{\mathbf{S}}^i_\kappa$ is the kth row in the body shape function. For example, one may write the component $\mathbf{M}^i_{\tau\tau}$ of the mass matrix of equation (44) as

$$\mathbf{M}^i_{\tau\tau} = \int_{v^i} \rho^i \mathbf{E}^T_\tau \mathbf{E}_\tau dv^i = \int_{v^i} \rho^i \begin{bmatrix} \mathbf{e}^{1T}_1 \\ \mathbf{e}^{2T}_1 \\ \vdots \\ \mathbf{e}^{i-1T}_1 \end{bmatrix} [\mathbf{e}^1_1 \; \mathbf{e}^2_1 \; \ldots \; \mathbf{e}^{i-1}_1] dv^i \tag{46}$$

From the definition of the vector $\mathbf{e}^{\kappa-1}_1$ given in the Appendix by equation (A22), it is clear that this vector does not depend on the spatial coordinates and accordingly the time dependent kl^{th} element of the matrix $\mathbf{M}^i_{\tau\tau}$ is given by;

$$(\mathbf{M}^i_{\tau\tau})_{\kappa l} = m^i \mathbf{e}^{\kappa T}_1 \mathbf{e}^l_1 \tag{47}$$

Where m^i is the mass of the deformable body i. The vector $\mathbf{e}^\kappa_1$ defines the global components of a unit vector along the k^{th} axis of rotation. It is therefore apparent that if at any instant of time the k^{th} and l^{th} axes of rotation are perpendicular, the kl^{th} element of the matrix $\mathbf{M}^i_{\tau\tau}$ is identically zero. Similarly, the submatrix $\mathbf{M}^i_{\tau\theta}$ that represents the inertia coupling between the relative translational and relative rotational displacements can be written as

$$\mathbf{M}^i_{\tau\theta} = \int_{v^i} \rho^i \mathbf{E}^T_\tau \mathbf{E}_\theta \, dv^i = \mathbf{E}^T_\tau \int_{v^i} \rho^i \mathbf{E}_\theta \, dv^i, \tag{48}$$

Where $\mathbf{E}^T_\tau$ does not depend on the spatial coordinates and

$$\mathbf{E}_\theta = \mathbf{E}_{\theta 1} + \mathbf{E}_{\theta 2} = [\mathbf{e}^1_4 \; \mathbf{e}^2_4 \; \ldots \; \mathbf{e}^{i-1}_4] + [\mathbf{e}^1_7 \; \mathbf{e}^2_7 \; \ldots \; \mathbf{e}^{i-1}_7] \tag{49}$$

Substituting this expression into the expression for $\mathbf{M}^i_{\tau\theta}$ of equation (48) yields

$$\mathbf{M}^i_{\tau\theta} = \mathbf{E}^T_\tau \int_{v^i} \rho^i (\mathbf{E}_{\theta 1} + \mathbf{E}_{\theta 2}) dv^i = m^i \mathbf{E}^T_\tau \mathbf{E}_{\theta 1} + \mathbf{E}^T_\tau \int_{v^i} \rho^i \mathbf{E}_{\theta 2} dv^i \tag{50}$$

The elements $\mathbf{e}^{\kappa-1}_7$ of the space and time dependent matrix $\mathbf{E}_{\theta 2}$ defined in the Appendix by equation (*A*25) as

$$\mathbf{e}^{\kappa-1}_7 = \mathbf{C}^\kappa \mathbf{A}^{\kappa-1}_s \mathbf{A}^{\kappa,\kappa-1}_\theta \mathbf{R}^{\kappa+1} \quad \kappa = 2, \ldots, i \tag{51}$$

Where $\mathbf{R}^{\kappa+1}$ is the vector defined in the Appendix by equation (*A*26), as

$$\mathbf{R}^{\kappa+1} = \mathbf{C}^{\kappa+1T} \sum_{j=\kappa+1}^{i} \mathbf{C}^j \bar{\mathbf{r}}^{\,j-1} + \mathbf{C}^{\kappa+1T} \mathbf{C}^{i+1} \bar{\mathbf{r}}^{\,i} \tag{52}$$

in which $\bar{\mathbf{r}}^{\,i}$ is the only term that depends on the spatial coordinates of the deformable body i. It is, therefore, clear from the definition of the vector $\bar{\mathbf{r}}^{\,i}$ of equation (3) that the matrix $\mathbf{M}^i_{\tau\theta}$ can be expressed in terms of the invariants of equations (45*a*) and (45*d*). Similar comments apply to the remaining submatrices that appear in the mass matrix of equation (44), (Changizi, 1989).

7 Generalized Forces

Equation (31) defines the virtual change in the global position of an arbitrary point on the deformable body i in the open loop multibody kinematic chain. This equation can be used to derive expressions for the generalized forces associated with the system generalized coordinates. Let $\mathbf{F}^i$ be the vector of forces that are defined in the Cartesian inertial frame of reference. This force vector acts on the deformable body i at the arbitrary point whose position vector is defined by sum of the vectors $\bar{\mathbf{r}}^{\,i,1}_\tau$ and $\bar{\mathbf{r}}^{\,i,1}_r$. The virtual work due to this force vector, can be written as

$$\begin{aligned} \delta W^i &= \mathbf{F}^{iT} \delta \bar{\mathbf{r}}^{\,i,1}_2 \\ &= \mathbf{F}^{iT} [\mathbf{E}_\tau \; \mathbf{E}_\theta \; \mathbf{E}_f] \begin{bmatrix} \delta\tau \\ \delta\theta \\ \delta\mathbf{q}_f \end{bmatrix} \\ &= [\mathbf{Q}^{iT}_\tau \; \mathbf{Q}^{iT}_\theta \; \mathbf{Q}^{iT}_f] \begin{bmatrix} \delta\tau \\ \delta\theta \\ \delta\mathbf{q}_f \end{bmatrix} \end{aligned} \tag{53}$$

Where

$$\mathbf{Q}^{iT}_\tau = \mathbf{F}^{iT} \mathbf{E}_\tau, \quad \mathbf{Q}^{iT}_\theta = \mathbf{F}^{iT} \mathbf{E}_\theta, \quad \mathbf{Q}^{iT}_f = \mathbf{F}^{iT} \mathbf{E}_f \tag{54}$$

are the generalized forces of the force $\mathbf{F}^i$ associated, respectively, with the system relative translational, relative rotational and elastic coordinates. The virtual work of all external forces acting on the system can be written in a matrix form as

$$\delta W = \sum_i \delta W^i = \mathbf{Q}^T \delta\mathbf{q} = [\mathbf{Q}^T_\tau \; \mathbf{Q}^T_\theta \; \mathbf{Q}^T_f] \begin{bmatrix} \delta\tau \\ \delta\theta \\ \delta\mathbf{q}_f \end{bmatrix} \tag{55}$$

Where $\mathbf{Q}$ is the total vector of system generalized forces, $\mathbf{q}$ is the total vector of system coordinates and $\mathbf{Q}_\tau$, $\mathbf{Q}_\theta$, and $\mathbf{Q}_f$ are the vectors of generalized forces associated, respectively, with the system relative translational, relative rotational and elastic coordinates.

8 Differential Equations of Motion

In this section the stiffness characteristics of the deformable body i in the open loop multibody kinematic chain are developed. Since the deformation of the flexible body i is defined in the body coordinate system, the strain displacement relationship can be written as

$$\boldsymbol{\epsilon}^i = \mathbf{D}^i \bar{\mathbf{r}}_f{}^i = \mathbf{D}^i \mathbf{S}^i \mathbf{q}^i_f \tag{56}$$

Where $\boldsymbol{\epsilon}^i$ is the strain vector, $\mathbf{D}^i$ is a differential operator and $\bar{\mathbf{r}}_f{}^i$ is the displacement field. The stress-strain relationship is defined as

$$\boldsymbol{\sigma}^i = \mathbf{E}^i \boldsymbol{\epsilon}^i = \mathbf{E}^i \mathbf{D}^i \bar{\mathbf{r}}_f{}^i = \mathbf{E}^i \mathbf{D}^i \mathbf{S}^i \mathbf{q}^i_f \tag{57}$$

Downloaded 03 May 2010 to 171.66.16.21. Redistribution subject to ASME license or copyright; see http://www.asme.org/terms/Terms_Use.cfm

Where σ^i is the stress vector and $\mathbf{E}^i$ is the matrix of elastic coefficients. Using the stress and strain vectors, the strain energy of the deformable body i can be defined as

$$U^i = 1/2\int_{v^i} \sigma^{iT}\epsilon^i dv^i = 1/2\int_{v^i} \mathbf{q}_f^{iT}(\mathbf{D}^i\mathbf{S}^i)^T\mathbf{E}^i(\mathbf{D}^i\mathbf{S}^i)\mathbf{q}_f^i\, dv^i \quad (58)$$

$$= 1/2\mathbf{q}_f^{iT}\mathbf{K}_{ff}^i\mathbf{q}_f^i$$

Where the symmetric stiffness matrix $\mathbf{K}_{ff}^i$ is given by

$$\mathbf{K}_{ff}^i = \int_{v^i} (\mathbf{D}^i\mathbf{S}^i)^T\mathbf{E}^i(\mathbf{D}^i\mathbf{S}^i)dv^i$$

The strain energy due to the deformation of all bodies in the open loop kinematic chain can be obtained by summing the strain energies of the bodies, that is,

$$U = \sum_i U^i = 1/2\sum_i \mathbf{q}_f^{iT}\mathbf{K}_{ff}^i\mathbf{q}_f^i = 1/2\ \mathbf{q}_f^T\mathbf{K}_{ff}\mathbf{q}_f \quad (59)$$

Where $\mathbf{q}_f$ is the total vector of system elastic coordinates and $\mathbf{K}_{ff}$ is the system stiffness matrix. For convenience, we write equation (59) in the following form

$$U = 1/2\ \mathbf{q}^T\mathbf{K}\ \mathbf{q} \quad (60)$$

Where $\mathbf{q}$ is the total vector of system coordinates and $\mathbf{K}$ is the system stiffness matrix. The vector $\mathbf{q}$ and the stiffness matrix $\mathbf{K}$ can be written as

$$\mathbf{q} = [\tau^T\ \theta^T\ \mathbf{q}_f^T]^T \quad (61)$$

$$\mathbf{K} = \begin{bmatrix} 0 & 0 & 0 \\ & 0 & 0 \\ \text{Symmetric.} & & \mathbf{K}_{ff} \end{bmatrix} \quad (62)$$

In which the matrix $\mathbf{K}_{ff}$ is defined by equation (59). Using Lagrange's equation of motion, one can easily verify that the system differential equations of motion can be written as

$$\mathbf{M}\ddot{\mathbf{q}} + \mathbf{K}\mathbf{q} = \mathbf{Q} + \mathbf{F} \quad (63)$$

Where $\mathbf{M}$ and $\mathbf{K}$ are the system mass and stiffness matrices, $\mathbf{Q}$ is the generalized force vector and $\mathbf{F}$ is a quadratic velocity vector that includes the coriolis and gyroscopic force components resulting from the differentiation of the kinetic energy with respect to time and with respect to the system generalized coordinates.

9 Summary

In this paper a Lagrangian formulation for the kinematic and dynamic analysis of open loop multibody systems is developed. The open loop multibody system under investigation is assumed to consist of interconnected deformable bodies which undergo large relative translational and rotational displacements. The configuration of the deformable bodies in the system is identified using coupled sets of relative joint and elastic coordinates. The elastic coordinates define the body deformation with respect to a selected body coordinate system. These coordinates can be introduced using approximation techniques such as Rayleigh-Ritz methods or the finite element method. The relative joint coordinates describe the large relative translational and rotational displacements between the system components. The large relative motion between bodies are defined as the relative translational and rotational displacements between a set of intermediate coordinate systems whose origins are rigidly attached to the bodies at the joint definition points. The recursive kinematic equations that define the global position and velocity of an arbitrary point on the body relative to the base body are developed in terms of the relative joint and elastic coordinates. These kinematic equations are then used to develop the energy expressions for the deformable bodies. The system differential equations are developed using Lagrange's equations of motion, and the nonlinear inertia coupling between the relative joint coordinates and the elastic coordinates is identified and expressed in terms of a set of invariant quantities that depend on the assumed displacement field.

Acknowledgment

The authors would like to express their appreciation to the U.S. Army Research office for supporting this research project through grant P-25170-EG DAAL03-87-k-0124.

References

Agrawal, O. P., and Shabana, A. A., 1986, "Application of Deformable-Body Mean Axis to Flexible Multibody System Dynamics," *Computer Methods in Applied Mechanics and Engineering*, Vol. 56, pp. 217–245.

Book, W. J., 1974, "Modeling, Design, and Control of Flexible Manipulator Arms," Ph.D. Thesis, Department of Mechanical Engineering, Massachusetts Institute of Technology, Cambridge, MA.

Book, W. J., 1979, "Analysis of Massless Elastic Chains With Servo-Controlled Joints," ASME *Journal of Dynamic Systems, Measurements, and Control*, Vol. 101, No. 3, pp. 187–192.

Book, W. J., 1984, "Recursive Lagrangian Dynamics of Flexible Manipulator Arms," *International Journal of Robotics Research*, Vol. 3, No. 3, pp. 87–101.

Book, W. J., Maizza-Neto, O., and Whitney, D. E., 1975, "Feedback Control of Two Beam, Two Joint Systems With Distributed Flexibility," ASME *Journal of Dymamic Systems, Measurement, and Control*, Vol. 97, pp. 424–431.

Chace, M. A., 1967, "Analysis of The Time Dependence of Multi-Freedom Mechanical Systems in Relative Coordinates," ASME *Journal of Engineering for Industry*, Vol. 89, No. 1, Series B, pp. 119–125.

Changizi, K., Summer 1989, "A Recursive Lagrangian Formulation For Open Loop Deformable Mechanical Systems," Ph.D Thesis, Department of Mechanical Engineering, University of Illinois at Chicago.

Huston, R. L., and Kelly, F. A., 1982, "The Development of Equations of Motion of Single Arm Robots," *IEEE Trans. on Systems, Man, and Cybernetics*, Vol. 12, No. 3, pp. 259–266.

Kane, T. R., 1965, "On Derivation of Equations of Motion," *Society For Industrial and Applied Mathematics*, Vol. 13, pp. 487–492.

Kane, T. R., and Levinson, D. A., 1983, "The Use of Kane's Dynamical Equations in Robotics," *International Journal of Robotic Research*, Vol. 2, No. 3, pp. 3–21.

Kim, S. S., and Vanderploeg, M. J., 1986, "A General and Efficient Method for Dynamic Analysis of Mechanical systems Using Velocity Transformations," ASME *Journal of Mechanisms, Transmissions, and Automation in Design*, Vol. 108, pp. 176–182.

Lilov, L., 1985, "Dynamics of Chains of Rigid Bodies and Elastic Rods With Revolute and Prismatic Joints," *Iutam/Iftomm Symposium Udine, Italy, Dynamic of Multibody Systems*, edited by G. Bianchi, and W. Schiehlen, pp. 141–152.

Luh, J. Y. S., Walker, M. W., and Paul, R. R. C., 1980, "On-Line Computational Scheme For Mechanical Manipulators," ASME *Journal of Dynamic Systems, Measurement, and Control*, Vol. 102, pp. 69–76.

Orin, D. E., McGhee, R. B., Vukobratovic, M., and Hartoch, G., 1979, "Kinematic and Kinetic Analysis of Open-Chain Linkages Utilizing Newton-Euler Methods," *Mathematical Biosciences*, Vol. 43, pp. 107–130.

Potkonjak, V., and Vukobratovic, M., 1979, "Two New Methods for Computer Forming of Dynamic Equations of Active Mechanisms," *Mechanism and Machine Theory*, Vol. 14, pp. 189–200.

Renaud, M., 1974, "Energie Cinetique d'un Bras Mecanique Articule," *Note Interne LAAS*, SMA 74.I.09.

Shabana, A., 1986, "Dynamics of Inertia-Variant Flexible Systems Using Experimentally Identified Parameters," ASME *Journal of Mechanisms, Transmissions, and Automation in Design*, Vol. 108, pp. 358–366.

Sherby, T. A., and Chmielewski, J. F., 1968, "Generalized Vector Derivatives for Systems With Multiple Relative Motion," ASME JOURNAL OF APPLIED MECHANICS, Vol. 35, pp. 20–24.

Symon, K. R., 1971, *Mechanics*, 3rd ed., Addison-Wesley, New York, pp. 271–281.

Vokobratovic, M., and Potkonjak, V., 1979, "Contribution of the Forming of Computer Methods for Automatic Modeling of Spatial Mechanisms Motions," *Mechanism and Machine Theory*, Vol. 14, pp. 179–188.

APPENDIX

In the following, some of the identities that have been used in developing the kinematic relationships in this paper are derived. The matrices $\mathbf{T}^\kappa$ and $\mathbf{C}^\kappa$ given by equations 10 and 13 are reproduced for convenience

$$\mathbf{T}^\kappa = \mathbf{A}_S^\kappa\mathbf{A}^{\kappa+1,\kappa} \quad (A1)$$

$$\mathbf{C}^2 = \mathbf{T}^0 = \mathbf{I}, \quad \mathbf{C}^\kappa = \mathbf{T}^1\mathbf{T}^2\ \ldots\ \mathbf{T}^{\kappa-2} \quad \text{for } \kappa = 2, \ldots, i \quad (A2)$$

in which $\mathbf{A}_S^\kappa$ is the infinitesimal rotation matrix defined in

Downloaded 03 May 2010 to 171.66.16.21. Redistribution subject to ASME license or copyright; see http://www.asme.org/terms/Terms_Use.cfm

equation 1, and $\mathbf{A}^{\kappa+1,\kappa}$ is the rotation matrix that describes the finite rotation between body k and body $k+1$. One can easily verify that $\mathbf{T}^{\kappa}$ and $\mathbf{C}^{\kappa}$ are orthogonal matrices, that is

$$\mathbf{T}^{\kappa T}\mathbf{T}^{\kappa}=\mathbf{I}, \quad \mathbf{C}^{\kappa T}\mathbf{C}^{\kappa}=\mathbf{I} \tag{A3}$$

For a virtual change $\delta\theta^{\kappa+1,\kappa}$ in the joint angle, one has

$$\delta\mathbf{A}^{\kappa+1,\kappa}=\mathbf{A}_{\theta}^{\kappa+1,\kappa}\delta\theta^{\kappa+1,\kappa} \tag{A4}$$

Where $\mathbf{A}_{\theta}^{\kappa+1,\kappa}$ is the partial derivative of the rotation matrix $\mathbf{A}^{\kappa+1,\kappa}$ with respect to the joint variable $\theta^{\kappa+1,\kappa}$. It follows that

$$\delta\mathbf{T}^{\kappa}=\delta\tilde{\Omega}^{\kappa}\mathbf{A}^{\kappa+1,\kappa}+\mathbf{A}_{s}^{\kappa}\mathbf{A}_{\theta}^{\kappa+1,\kappa}\delta\theta^{\kappa+1,\kappa} \tag{A5}$$

Where $\mathbf{A}_{s}^{\kappa}=\mathbf{I}+\tilde{\Omega}^{\kappa}$ and $\tilde{\Omega}^{\kappa}$ is the skew symmetric matrix defined by equation 2. Let $\mathbf{a}_1^j$ be an arbitrary three dimensional vector. Using equation (A5), one gets

$$\begin{aligned}\delta\mathbf{T}^{\kappa}\mathbf{a}_1^j &= \delta\tilde{\Omega}^{\kappa}\mathbf{A}^{\kappa+1,\kappa}\mathbf{a}_1^j+\mathbf{A}_s^{\kappa}\mathbf{A}_{\theta}^{\kappa+1,\kappa}\mathbf{a}_1^j\delta\theta^{\kappa+1,\kappa} \\ &= -\tilde{\mathbf{a}}_2^j\mathbf{S}_r^{\kappa}\delta\mathbf{q}_f^{\kappa}+\mathbf{A}_s^{\kappa}\mathbf{A}_{\theta}^{\kappa+1,\kappa}\mathbf{a}_1^j\delta\theta^{\kappa+1,\kappa}\end{aligned} \tag{A6}$$

Where the following identities are utilized

$$\mathbf{a}_2^j=\mathbf{A}^{\kappa+1,\kappa}\mathbf{a}_1^j, \quad \delta\tilde{\Omega}^{\kappa}\mathbf{a}_2^j=-\tilde{\mathbf{a}}_2^j\mathbf{S}_r^{\kappa}\delta\mathbf{q}_f^{\kappa} \tag{A7}$$

in which $\mathbf{S}_r^{\kappa}$ is an appropriate matrix, $\tilde{\mathbf{a}}_2^j$ is a three dimensional vector and $\tilde{\mathbf{a}}_2^j$ is a skew symmetric matrix. If $\mathbf{d}^{\kappa}$ is an arbitrary three dimensional vector, one may write

$$\sum_{\kappa=1}^{i}\delta\mathbf{C}^{\kappa+1}\mathbf{d}^{\kappa}=\delta\mathbf{C}^{2}\mathbf{d}^{1}+\delta\mathbf{C}^{3}\mathbf{d}^{2}+\ \ldots\ .+\delta\mathbf{C}^{i+1}\mathbf{d}^{i} \tag{A8}$$

Using equation (A2) and utilizing the orthogonality condition given by equation (A3), one can show that equation (A8) can be written as

$$\sum_{\kappa=1}^{i}\delta\mathbf{C}^{\kappa+1}\mathbf{d}^{\kappa}=\sum_{\kappa=2}^{i}\mathbf{C}^{\kappa}\delta\mathbf{T}^{\kappa-1}\mathbf{f}^{\kappa+1} \tag{A9}$$

Where

$$\mathbf{f}^{\kappa}=\mathbf{C}^{\kappa T}\sum_{j=\kappa}^{i+1}\mathbf{C}^{j}\mathbf{d}^{j-1} \quad \kappa=3,\ \ldots\ ,\ i+1 \tag{A10}$$

In the following, equations (19)–(22) that have been used in developing kinematic relationships are derived. Using equation (A9), the first term of equation (17) can be written as

$$\sum_{\kappa=2}^{i}\delta\mathbf{C}^{\kappa}\mathbf{b}^{\kappa}\tau^{\kappa,\kappa-1}=\sum_{\kappa=2}^{i}(\mathbf{e}_3^{\kappa-1}\delta\mathbf{q}_f^{\kappa-1}+\mathbf{e}_4^{\kappa-1}\delta\theta^{\kappa,\kappa-1}) \tag{A11}$$

Where

$$\mathbf{l}^{\kappa-1}=\mathbf{b}^{\kappa}\tau^{\kappa,\kappa-1} \quad \kappa=2,\ \ldots\ ,\ i \tag{A12}$$

$$\mathbf{L}_1^{\kappa}=\mathbf{C}^{\kappa T}\sum_{j=\kappa}^{i}\mathbf{C}^{j}\mathbf{l}^{\,j-1}=\mathbf{C}^{\kappa T}\sum_{j=\kappa}^{i}\mathbf{C}^{j}\mathbf{b}^{j}\tau^{j,j-1} \quad \kappa=3,\ \ldots\ ,\ i \tag{A13}$$

$$\mathbf{L}_2^{\kappa}=\mathbf{A}^{\kappa-1,\kappa-2}\mathbf{L}_1^{\kappa}, \quad \kappa=3,\ \ldots\ ,\ i \tag{A14}$$

$$\mathbf{e}_3^{\kappa-1}=-\mathbf{C}^{\kappa}\tilde{\mathbf{L}}_2^{\kappa+1}\mathbf{S}_r^{\kappa-1} \quad \kappa=2,\ \ldots\ ,\ i \tag{A15}$$

$$\mathbf{e}_4^{\kappa-1}=\mathbf{C}^{\kappa}\mathbf{A}_s^{\kappa-1}\mathbf{A}_{\theta}^{\kappa,\kappa-1}\mathbf{L}_1^{\kappa+1} \quad \kappa=2,\ \ldots\ ,\ i \tag{A16}$$

$$\mathbf{e}_3^{i-1}=\mathbf{e}_4^{i-1}=0 \tag{A17}$$

in which $\mathbf{L}_1^{\kappa}$ is a vector which does not depend on the spatial coordinates, $\tilde{\mathbf{L}}_2^{\kappa}$ is a skew symmetric matrix, $\mathbf{S}_r^{\kappa}$ is an appropriate matrix associated with body k, $\mathbf{q}_f^{\kappa}$ is the vector of elastic coordinates of body k, and $\theta^{\kappa,\kappa-1}$ is the relative rotational coordinate of body k with respect to body $k-1$. Therefore, it is obvious that $\mathbf{e}_3^{\kappa-1}$ and $\mathbf{e}_4^{\kappa-1}$ are not space dependent.

The central term of equation 17 can be written as

$$\begin{aligned}\sum_{\kappa=2}^{i}\mathbf{C}^{\kappa}\delta\mathbf{b}^{\kappa}\tau^{\kappa,\kappa-1} &= \sum_{\kappa=2}^{i}-\mathbf{C}^{\kappa}\tau^{\kappa,\kappa-1}\tilde{\bar{\mathbf{v}}}^{\kappa-1}\mathbf{S}_r^{\kappa-1}\delta\mathbf{q}_f^{\kappa-1} \\ &= \sum_{\kappa=2}^{i}\mathbf{e}_2^{\kappa-1}\delta\mathbf{q}_f^{\kappa-1}\end{aligned} \tag{A18}$$

Where

$$\mathbf{e}_2^{\kappa-1}=-\mathbf{C}^{\kappa}\tau^{\kappa,\kappa-1}\tilde{\bar{\mathbf{v}}}^{\kappa-1}\mathbf{S}_r^{\kappa-1} \quad \kappa=2,\ \ldots\ ,\ i \tag{A19}$$

$$\delta\mathbf{b}^{\kappa}=\delta\tilde{\Omega}^{\kappa-1}\bar{\mathbf{v}}^{\kappa-1}=-\tilde{\bar{\mathbf{v}}}^{\kappa-1}\mathbf{S}_r^{\kappa-1}\delta\mathbf{q}_f^{\kappa-1} \quad \kappa=2,\ \ldots\ ,\ i \tag{A20}$$

in which $\bar{\mathbf{v}}^{\kappa}$ is a unit vector along the kth joint axis, $\tilde{\bar{\mathbf{v}}}^{\kappa}$ is a skew symmetric matrix, $\tilde{\Omega}^{\kappa-1}$ is the skew symmetric matrix whose elements are the infinitesimal nodal rotations, $\tau^{\kappa,\kappa-1}$ is the relative translational coordinate of body k with respect to body $k-1$ and $\mathbf{e}_2^{\kappa-1}$ is a space indpendent matrix. One may write the last term of equation 17 as

$$\sum_{\kappa=2}^{i}\mathbf{C}^{\kappa}\mathbf{b}^{\kappa}\delta\tau^{\kappa,\kappa-1}=\sum_{\kappa=2}^{i}\mathbf{e}_1^{\kappa-1}\delta\tau^{\kappa,\kappa-1} \tag{A21}$$

Where

$$\mathbf{e}_1^{\kappa-1}=\mathbf{C}^{\kappa}\mathbf{b}^{\kappa} \tag{A22}$$

$\mathbf{e}_1^{\kappa-1}$ is a vector that does not depend on the spatial coordinates and defines the components of a unit vector $\bar{\mathbf{v}}^{\kappa-1}$ along the joint axis in the global coordinate system. Finally, using equations (A9) and (A6), one can write

$$\begin{aligned}\sum_{\kappa=1}^{i}\delta\mathbf{C}^{\kappa+1}\bar{\mathbf{r}}^{\kappa} &= \sum_{\kappa=2}^{i}\mathbf{C}^{\kappa}\delta\mathbf{T}^{\kappa-1}\mathbf{R}^{\kappa+1} \\ &= \sum_{\kappa=2}^{i}(\mathbf{e}_6^{\kappa-1}\delta\mathbf{q}_f^{\kappa-1}+\mathbf{e}_7^{\kappa-1}\delta\theta^{\kappa,\kappa-1})\end{aligned} \tag{A23}$$

Where

$$\mathbf{e}_6^{\kappa-1}=-\mathbf{C}^{\kappa}\tilde{\mathbf{R}}_1^{\kappa+1}\mathbf{S}_r^{\kappa-1} \quad \kappa=2,\ \ldots\ ,\ i \tag{A24}$$

$$\mathbf{e}_7^{\kappa-1}=\mathbf{C}^{\kappa}\mathbf{A}_s^{\kappa-1}\mathbf{A}_{\theta}^{\kappa,\kappa-1}\mathbf{R}^{\kappa+1} \quad \kappa=2,\ \ldots\ ,\ i \tag{A25}$$

$$\begin{aligned}\mathbf{R}^{\kappa+1}=\mathbf{C}^{\kappa+1T}\sum_{j=\kappa+1}^{i+1}\mathbf{C}^{j}\bar{\mathbf{r}}^{\,j-1} &= \mathbf{C}^{\kappa+1T}\sum_{j=\kappa+1}^{i}\mathbf{C}^{j}\bar{\mathbf{r}}^{\,j-1} \\ &+\mathbf{C}^{\kappa+1T}\mathbf{C}^{i+1}\bar{\mathbf{r}}^{i}\end{aligned} \tag{A26}$$

$$\mathbf{R}^{i+1}=\bar{\mathbf{r}}^{\,i} \tag{A27}$$

$$\mathbf{R}_1^{\kappa+1}=\mathbf{A}^{\kappa,\kappa-1}\mathbf{R}^{\kappa+1} \tag{A28}$$

Downloaded 03 May 2010 to 171.66.16.21. Redistribution subject to ASME license or copyright; see http://www.asme.org/terms/Terms_Use.cfm

Jian-Qiao Sun
Graduate Student.
Assoc. Mem. ASME

C. S. Hsu
Professor.
Fellow, ASME

Department of Mechanical Engineering,
University of California,
Berkeley, CA 94720

A Statistical Study of Generalized Cell Mapping

In this paper a statistical error analysis of the generalized cell mapping method for both deterministic and stochastic dynamical systems is examined, based upon the statistical analogy of the generalized cell mapping method to the density estimation. The convergence of the mean square error of the one step transition probability matrix of generalized cell mapping for deterministic and stochastic systems is studied. For stochastic systems, a well-known trade-off feature of the density estimation exists in the mean square error of the one step transition probability matrix, which leads to an optimal design of generalized cell mapping for stochastic systems. The conclusions of the study are illustrated with some examples.

1 Introduction

Very early work using cellularly structured state space to study dynamical systems dated back to 1964 (Chandiramani, 1964; Crandall et al., 1966). Using that approach, Crandall, Chandiramani, and Cook (1966) studied certain first-passage problems of single degree-of-freedom systems. In recent years the theory of generalized cell mapping (GCM) has been developed also using the cell state space concept, and it has been applied to a variety of problems. It has been employed to study random vibration problems (Chiu, 1984), and various solution aspects of nonlinear dynamical systems, such as strange attractors, domains of attraction, limit cycles, etc. (Hsu and Kim, 1985a; Polchai and Hsu, 1985; Xu et al., 1985; Chiu and Hsu, 1986; Kim and Hsu, 1986; Ushio and Hsu, 1987; Hsu, 1987). In (Hsu and Chiu, 1986), a compatible cell mapping method and a refinement procedure are proposed. As a result, the efficiency of computing and the precision by which the fine structure of the solutions of nonlinear dynamical systems may be determined by the GCM method have been greatly enhanced. Although the accuracy of the approximations obtained by the GCM method may be checked with either a known exact solution, or a solution which is considered reliable, a systematic error analysis of the GCM method is, nevertheless, highly needed. In this paper, we present a systematic study of certain statistical errors of the GCM method for both deterministic and stochastic systems. The key questions in using the GCM method are (*i*) how the cell size affects the accuracy of the method, (*ii*) how the number size of the samples used in each cell affects the accuracy, and (*iii*) the interplay, if any, between these two factors.

In this paper we first establish a statistical analogy of the GCM method to the density estimation. Then, we study the statistical errors of the one step transition probability matrix of GCM, and the statistical errors of its density estimate for both deterministic and stochastic systems. The results, demonstrated by a few examples, will enable us to better understand GCM and to obtain the optimal approximations with the GCM method.

2 Statistical Analogy of GCM

Consider a deterministic system defined by

$$\ddot{x}+f(\mathbf{x})\dot{x}+g(\mathbf{x})x=F(t) \tag{2.1}$$

where $\mathbf{x}=(x,\dot{x})$, $F(t)=F(t+T)$, and other terms in (2.1) are self explanatory. Let us consider the calculation of a one step transition probability matrix from $t=0$ to $t=T$ of a generalized cell mapping for (2.1) in the cell state space by using the sampling point method. For the basic notions of generalized cell mapping, the reader is referred to (Hsu and Chiu, 1986; Hsu, 1987). Assume that the cells in a certain domain of interest are properly numbered. The transition probability from cell i to cell j in one mapping step, denoted by P_{ji}, is calculated in the following way. Randomly pick n points uniformly distributed in cell i, and assign to each point a weight of probability such that the sum of the probabilities of the n points is one; numerically integrate (2.1) for a mapping time step T, using n sampled points as initial conditions; and locate the end points of n trajectories. The cells in which these end points lie are called the image cells of cell i. Finally, one calculates the transition probability to each image cell based upon the number of points found in that cell and their weights.

The statistical properties of the generalized cell mapping obtained by the sampling point method can be studied in the following manner. Consider the dynamical system (2.1). Let $p_0(\mathbf{x}_0)$ be the probability density function of initial conditions such that

$$p_0(\mathbf{x}_0)=\begin{cases}1/\Delta x\Delta\dot{x} & \text{if } \mathbf{x}_0 \text{ is in cell } i\\ 0 & \text{otherwise}\end{cases} \tag{2.2}$$

where Δx and $\Delta\dot{x}$ are cell dimensions. The probability density function of the system at time T is given by (Soong, 1973)

$$p(\mathbf{x},t)=p_0[\mathbf{h}^{-1}(\mathbf{x},t)]\cdot|J(\mathbf{x};\mathbf{x}_0)|, \tag{2.3}$$

Contributed by the Applied Mechanics Division for publication in the JOURNAL OF APPLIED MECHANICS.

Discussion on this paper should be addressed to the Editorial Department, ASME United Engineering Center, 345 East 47th Street, New York, N.Y. 10017, and will be accepted until two months after final publication of the paper itself in the JOURNAL OF APPLIED MECHANICS. Manuscript received by ASME Applied Mechanics Division, April 24, 1987; final revision March 29, 1988.

Copyright © 1988 by ASME
Downloaded 03 May 2010 to 171.66.16.21. Redistribution subject to ASME license or copyright; see http://www.asme.org/terms/Terms_Use.cfm

where $\mathbf{x}_0 = \mathbf{h}^{-1}(\mathbf{x},t)$ is the inverse of the solution of (2.1), $J(\cdot)$ the Jacobian of the motion given by

$$J(\mathbf{x};\mathbf{x}_0) = \det\left(\frac{\partial \mathbf{x}_0^T}{\partial \mathbf{x}}\right). \tag{2.4}$$

Let $P(j, i) = \int_{C_j} p(\mathbf{x}, T) \times d\mathbf{x}$ where C_j denotes cell j. Apparently $P(j, i)$ is a discrete representation of (2.3) at time T over the cell state space. For a general nonlinear system, $\mathbf{h}^{-1}$ and J are not available in closed form. One way to estimate $p(\mathbf{x}, T)$, and in turn $P(j, i)$, is to use the numerical sampling point method. The sampling point method for computing the transition probability from cell i to its image cells is mathematically equivalent to finding the histogram sampling estimator $\hat{p}(\mathbf{x}, T)$ of the probability density function $p(\mathbf{x}, T)$ of the system (2.1) at time T with the initial condition given by (2.2). $\hat{p}(\mathbf{x}, T)$ is a pointwise defined function, constant within each cell. Let p_{ji} denote the value of $\hat{p}(\mathbf{x}, T)$ in cell j. Then $P_{ji} = \Delta x \Delta \dot{x} p_{ji}$ and p_{ji} can be taken as the density of P_{ji} in cell j. It is then natural to call p_{ji} a density estimator. In statistical language, P_{ji} obtained by the sampling point procedure is called the sampling estimator of probability $P(j, i)$ for the system (2.1) with the initial distribution (2.2). Once this identification is made, many statistical results of the density estimation become available for the improvement of the estimation of $p(\mathbf{x}, T)$.

3 Statistical Errors of P_{ji}

In this paper we assume that the n initial conditions are randomly and uniformly sampled from the initial cell i. Hence, each initial point and its image point at time T carry an equal weight $1/n$. This viewpoint is sufficient for the present work. A general discussion on the advantages and statistical implications of various other sampling techniques is outside the scope of this work.

Let $R(T, i)$ denote the image domain of cell i at time T. For the convenience of subsequent discussions, we assume that $\Delta x = \Delta \dot{x} = h$, and introduce two definitions.

Definition 1. If an image cell is completely covered by $R(T, i)$ it is called an *interior image cell* of cell i.

Definiton 2. If an image cell is on the boundary of $R(T, i)$, and a portion α, $0 < \alpha < 1$, of the area of the cell is covered by $R(T, i)$ it is called an α *boundary image cell* of cell i.

We rewrite (2.3) as

$$p(\mathbf{x},T) = \begin{cases} 1/h^2 \cdot |J(\mathbf{x};\mathbf{x}_0)| & \mathbf{x} \in R(T,i), \mathbf{x}_0 \in C_i \\ 0 & \mathbf{x} \notin R(T,i). \end{cases} \tag{3.1}$$

It is clear that $p(\mathbf{x}, T)$ satisfies a normalization condition

$$\int_{R(T,i)} p(\mathbf{x},T)\,d\mathbf{x} = 1. \tag{3.2}$$

Suppose that cell j is an α boundary image cell of cell i. Let $C_j(\alpha)$ denote the intersection of cell j and $R(T, i)$. Let n_j be the number of image points falling in cell j. It is known (Davenport, 1970) that n_j is a random variable of a binomial distribution, and

$$E[P_{ji}] = E\left[\frac{n_j}{n}\right] = \int_{C_j(\alpha)} p(\mathbf{x},T)\,d\mathbf{x}, \tag{3.3}$$

$$\text{var}[P_{ji}] = \frac{1}{n}\left[1 - \int_{C_j(\alpha)} p(\mathbf{x},T)\,d\mathbf{x}\right] \cdot \int_{C_j(\alpha)} p(\mathbf{x},T)\,d\mathbf{x}. \tag{3.4}$$

When $\alpha \to 1$, cell j is completely inside $R(T, i)$ and $C_j(\alpha) \to C_j$. When $\alpha \to 0$, cell j is outside $R(T, i)$, and is not an image of cell i, hence $C_j(\alpha) \to \varnothing$. (3.3) and (3.4) are valid in both limit cases. In statistics it is a common practice to define the bias of an estimator $\hat{q}$ of q as $E[\hat{q}] - q$. For the present work, it is, however, more appropriate, as is to be seen in Section 4, to define the bias of $\hat{q}$ as the absolute value of $E[\hat{q}] - q$ in order to avoid cancellation. Using this definition, it is seen from (3.3) that P_{ji} is unbiased because

$$\text{bias}[P_{ji}] = |E[P_{ji}] - \int_{C_j(\alpha)} p(\mathbf{x},T)\,d\mathbf{x}| = 0.$$

The mean square error (MSE) of P_{ji} is defined by

$$\text{MSE}[P_{ji}] = [\text{bias}(P_{ji})]^2 + \text{var}[P_{ji}]$$
$$= \frac{1}{n}\left[1 - \int_{C_j(\alpha)} p(\mathbf{x},T)\,d\mathbf{x}\right]\int_{C_j(\alpha)} p(\mathbf{x},T)\,d\mathbf{x}. \tag{3.5}$$

Result 1. If cell i has only one image cell j, then var $[P_{ji}] = 0$.

Proof. If cell i has only one image cell, the $R(T, i)$ must be completely covered by cell j so that $C_j(\alpha) = \text{R(T, } i)$ and

$$\int_{C_j(\alpha)} p(\mathbf{x},T)\,d\mathbf{x} = \int_{R(T,i)} p(\mathbf{x},T)\,d\mathbf{x} = 1.$$

The conclusion follows from (3.4).

Result 2. For a given structure of the cell state space, var $[P_{ji}]$ converges to zero as $n \to \infty$, and P_{ji} converges in probability to the exact value $\int_{C_j(\alpha)} p(\mathbf{x}, T)d\mathbf{x}$ as $n \to \infty$.

Proof. Since $\int_{C_j(\alpha)} p(\mathbf{x}, T)d\mathbf{x}$ does not depend on n, the convergence of var $[P_{ji}]$ follows from (3.4). The convergence of P_{ji} is a direct consequence of the law of large numbers (Feller, 1971).

The convergence of sampling estimation with sample size stated in Result 2 is well known in statistics. The change of var $[P_{ji}]$ with cell size h while n is fixed is more complicated. It depends on $C_j(\alpha)$ and $p(\mathbf{x}, T)$. To find $C_j(\alpha)$ and $p(\mathbf{x}, T)$ is equivalent to obtaining the solution for the original system. Obviously, they cannot be obtained analytically for general nonlinear systems. However, the following result of maximum variance can be readily proved.

Result 3. The variance of P_{ji} is bounded by $(4n)^{-1}$.

Proof. Since $0 \le \int_{C_j(\alpha)} p(\mathbf{x}, T)d\mathbf{x} \le 1$ and it does not depend on n, it is readily shown from (3.4) that when $\int_{C_j(\alpha)} p(\mathbf{x}, T)d\mathbf{x} = 1/2$, the variance var $[P_{ji}]$ achieves its maximum

$$\max[\text{var}(P_{ji})] = (4n)^{-1}. \tag{3.6}$$

Hence, we have var $[P_{ji}] \le (4n)^{-1}$.

4 Statistical Errors of the Density Estimation

In the last section we have studied the statistical properties of P_{ji} which is the total transition probability residing in cell j. In this section we turn our attention to the distributional aspect of the transition probability from cell i to cell j within cell j. The one step transition probability density function is given by $p(\mathbf{x}, T)$, according to (2.3). In the sampling point procedure of the GCM method, this density function is approximated or estimated by $\hat{p}(\mathbf{x}, T)$ which is a piecewise constant function, constant within each image cell. Previously, we have denoted the constant density value of $\hat{p}(\mathbf{x}, T)$ in cell j by p_{ji} which is also equal to $P_{ji}h^{-2}$ ($h^2 = \Delta x \Delta \dot{x}$). It is convenient to call p_{ji} a density estimator of $p(\mathbf{x}, T)$ for cell j. We now proceed to study the statistical properties of this density estimator p_{ji}, and the effect of the estimation errors on the accuracy of the prediction of the system behavior.

The analysis of statistical errors of the density estimation is a well studied topic in statistics (Silverman, 1986; Wertz, 1978). In the statistics literature, the true density function is often assumed to be sufficiently smooth in the domain of definition. In GCM, however, the density function $p(\mathbf{x}, T)$ is piecewise smooth and discontinuous on the boundary of $R(T, i)$. A special treatment of the statistical analysis of the density

Downloaded 03 May 2010 to 171.66.16.21. Redistribution subject to ASME license or copyright; see http://www.asme.org/terms/Terms_Use.cfm

estimator p_{ji} of the sampling point procedure is therefore required.

First, we note that there are two kinds of quantities involved here. Quantities like p_{ji} are cellwise defined, while $\hat{p}(\mathbf{x}, T)$ and $p(\mathbf{x}, T)$ are pointwise defined. It is necessary that we define in a precise manner the statistical properties of the density estimator p_{ji} we are interested in. Consider first the bias of p_{ji}. An appropriate bias of p_{ji} can be introduced through a pointwise consideration. If $p(\mathbf{x}, T)$ is sufficiently smooth in a cell, it is a common practice (see, for example, Silverman, 1986) to define the bias of the density estimator p_{ji} for a cell by using the bias of $\hat{p}(\mathbf{x}, T)$ at the geometrical center of the cell. However, such a convenient definition is not adequate for an α boundary image cell, in which $p(\mathbf{x}, T)$ is discontinuous. Let cell j be an α boundary image cell of the initial cell i. Since $p(\mathbf{x}, T) \neq 0$ if $\mathbf{x} \in C_j(\alpha)$, and $p(\mathbf{x}, T) = 0$ if $\mathbf{x} \in C_j / C_j(\alpha)$, the bias of $\hat{p}(\mathbf{x}, T)$ is given by one of the following two expressions

$$\text{bias}[\hat{p}(\mathbf{x}', T)] = \left| \frac{1}{h^2} \int_{C_j(\alpha)} p(\mathbf{x}, T) d\mathbf{x} - p(\mathbf{x}', T) \right|, \ \mathbf{x}' \in C_j(\alpha)$$

$$\text{bias}[\hat{p}(\mathbf{x}', T)] = \left| \frac{1}{h^2} \int_{C_j(\alpha)} p(\mathbf{x}, T) d\mathbf{x} - 0 \right|, \ \mathbf{x}' \in C_j / C_j(\alpha), \tag{4.1}$$

where $E[p_{ji}] = E[P_{ji}] h^{-2} = h^{-2} \int_{C_j(\alpha)} p(\mathbf{x}, T) d\mathbf{x}$, according to (3.3).

The bias of p_{ji} for an α boundary image cell should be defined in such a way that the bias becomes zero as $\alpha \to 0$ because then cell j is no longer an image cell of cell i, and the bias converges to the bias for an interior image cell of cell i as $\alpha \to 1$. The bias of p_{ji} for an interior image cell should be, of course, consistent with the conventional bias for a sufficiently smooth density function as studied in the statistics literature because $p(\mathbf{x}, T)$ is sufficiently smooth in an interior image cell. There are a number of valid ways to define the bias under consideration. An appropriate and convenient one is to define the bias of p_{ji} for an α boundary image cell as the following weighted average of the two possible biases of $\hat{p}(\mathbf{x}, T)$ given by (4.1):

$$\text{bias}[p_{ji}] = \alpha \left| \frac{1}{h^2} \int_{C_j(\alpha)} p(\mathbf{x}, T) d\mathbf{x} - p(\mathbf{x}_c, T) \right| + (1-\alpha) \left| \frac{1}{h^2} \int_{C_j(\alpha)} p(\mathbf{x}, T) d\mathbf{x} - 0 \right|, \tag{4.2}$$

where $\mathbf{x}_c$ is the geometrical center of $C_j(\alpha)$. The choice of $\mathbf{x}_c$ as the geometrical center of $C_j(\alpha)$ makes the present analysis consistent with the analysis of bias in statistics. Equation (4.2) can be further simplified by using the Taylor expansion of $p(\mathbf{x}, T)$ about $\mathbf{x}_c$:

$$\text{bias}[p_{ji}] = \alpha \left| (1-\alpha) p(\mathbf{x}_c, T) - ch^2 \right| + (1-\alpha) \left| \alpha p(\mathbf{x}_c, T) + ch^2 \right|, \tag{4.3}$$

where the notation $O(h^4)$ representing the neglected higher order terms is dropped for brevity in (4.3) and some of the equations listed below, and

$$c = \frac{1}{2h^4} \int_{C_j(\alpha)} \left\{ \frac{\partial^2 p}{\partial x^2} (x - x_c)^2 + 2 \frac{\partial^2 p}{\partial x \partial \dot{x}} (x - x_c)(\dot{x} - \dot{x}_c) + \frac{\partial^2 p}{\partial \dot{x}^2} (\dot{x} - \dot{x}_c)^2 \right\} d\mathbf{x}. \tag{4.4}$$

It is clear that when $\alpha \to 0$, $C_j(\alpha) \to \varnothing$ and bias $[p_{ji}] \to 0$, and when $\alpha \to 1$, $C_j(\alpha) \to C_j$ and $\mathbf{x}_c \to \mathbf{x}_j$ (4.3) becomes

$$\text{bias}[p_{ji}] = \frac{h^2}{24} \left| \nabla^2 p(\mathbf{x}_j, T) \right|, \tag{4.5}$$

where $\mathbf{x}_j$ is the geometrical center of an interior image cell j.

Next, we consider the variance of p_{ji}, which can be evaluated by using $p_{ji} = P_{ji} h^{-2}$. We obtain $\text{var}[p_{ji}] = \text{var}[P_{ji}] h^{-4}$. Some conclusions follow immediately. According to Result 1, $\text{var}[p_{ji}] = 0$ if cell i has only one image cell j. According to Result 3, var $[p_{ji}]$ is bounded by $(4n)^{-1} h^{-4}$. By using the Taylor expansion of $p(\mathbf{x}, T)$ in (3.4) about $\mathbf{x}_c$, after neglecting higher order terms, the variance of p_{ji} for an α boundary image cell j can be written as

$$\text{var}[p_{ji}] = \frac{\alpha}{nh^2} [1 - \alpha h^2 p(\mathbf{x}_c, T)] p(\mathbf{x}_c, T). \tag{4.6}$$

Here, $\mathbf{x}_c$ is defined as before. The MSE of p_{ji} is given by

$$\text{MSE}[p_{ji}] = [\alpha \left| (1-\alpha) p(\mathbf{x}_c, T) - ch^2 \right| + (1-\alpha) \left| \alpha p(\mathbf{x}_c, T) + ch^2 \right|]^2 + \frac{\alpha p(\mathbf{x}_c, T)}{nh^2} [1 - \alpha h^2 p(\mathbf{x}_c, T)]. \tag{4.7}$$

Since the magnitude of $p(\mathbf{x}, T)$ varies from point to point, it is convenient to examine a normalized MSE of p_{ji} defined by

$$\epsilon^2[p_{ji}] = \frac{\text{MSE}[p_{ji}]}{p^2(\mathbf{x}_c, T)},$$

for $p(\mathbf{x}_c, T) \neq 0$. The normalized MSE of (4.7) is given by

$$\epsilon^2[p_{ji}] = \left[\alpha \left| (1-\alpha) - \frac{c'}{|J|} h^2 \right| + (1-\alpha) \left| \alpha + \frac{c'}{|J|} h^2 \right| \right]^2 + \frac{\alpha}{n|J|} (1 - \alpha |J|), \tag{4.8}$$

where

$$c' = \frac{1}{2h^4} \int_{C_j(\alpha)} \left\{ \frac{\partial^2 |J|}{\partial x^2} (x - x_c)^2 + 2 \frac{\partial^2 |J|}{\partial x \partial \dot{x}} (x - x_c)(\dot{x} - \dot{x}_c) + \frac{\partial^2 |J|}{\partial \dot{x}^2} (\dot{x} - \dot{x}_c)^2 \right\} d\mathbf{x}.$$

In deriving (4.8), (3.1) is used. J and its partial derivatives in (4.8) are evaluated at $\mathbf{x}_c$. The analysis in this section is valid for $0 \leq \alpha \leq 1$. In particular, when $\alpha = 1$, (4.7) and (4.8) are reduced to

$$\text{MSE}[p_{ji}] = \frac{h^4}{576} [\nabla^2 p(\mathbf{x}_j, T)]^2 + \frac{p(\mathbf{x}_j, T)}{nh^2} [1 - h^2 p(\mathbf{x}_j, T)], \tag{4.9}$$

and

$$\epsilon^2[p_{ji}] = \frac{h^4}{576} \left[\frac{\nabla^2 p(\mathbf{x}_j, T)}{p(\mathbf{x}_j, T)} \right]^2 + \frac{1 - h^2 p(\mathbf{x}_j, T)}{nh^2 p(\mathbf{x}_j, T)} = \frac{h^4}{576} \left[\frac{\nabla^2 J}{J} \right]^2 + \frac{1 - |J|}{n|J|}. \tag{4.10}$$

where cell j is now an interior image cell of cell i.

Result 4. For deterministic systems, if cell j is an interior image cell of an initial cell i, the normalized MSE of the density estimator p_{ji} for the one step transition probability from cell i to cell j converges to zero as $h \to 0$ and $n \to \infty$ independently and simultaneously, and is bounded below as $n \to \infty$ while h is fixed, or as $h \to 0$ while n is fixed.

The conclusion stated in Result 4 is observable from (4.10). The proof is thus omitted. It is evident from (4.10) that for interior image cells, the effects of reducing cell size and increasing sample size are independent and different, the former reduces the bias error, while the later reduces the variance error.

For a boundary image cell j, the limit value of $\epsilon^2[p_{ji}]$ depends on α, and therefore on the partition of the state space. If a partition is such that for sufficiently small h,

Downloaded 03 May 2010 to 171.66.16.21. Redistribution subject to ASME license or copyright; see http://www.asme.org/terms/Terms_Use.cfm

$$(1-\alpha)p(\mathbf{x}_c,T) > ch^2 \text{ and } \alpha p(\mathbf{x}_c,T) > -ch^2, \tag{4.11}$$

then (4.7) and (4.8) can be written as

$$\text{MSE}[p_{ji}] = [2\alpha(1-\alpha)p(\mathbf{x}_c,T) + (1-2\alpha)ch^2]^2 + \frac{\alpha p(\mathbf{x}_c,T)}{nh^2}[1-\alpha h^2 p(\mathbf{x}_c,T)], \tag{4.12}$$

and

$$\epsilon^2[p_{ji}] = \left[2\alpha(1-\alpha) + \frac{(1-2\alpha)c'h^2}{|J|}\right]^2 + \frac{\alpha}{n|J|}(1-\alpha|J|). \tag{4.13}$$

It is readily seen from (4.13) that the normalized MSE of the density estimator p_{ji} contains a lower order term $4\alpha^2(1-\alpha)^2$ and is dominated by this term as $n\to\infty$ for sufficiently small h. This result brings out the possible severe error of p_{ji} caused by the "artificial diffusion" in the boundary image cells. The boundary image cells as well as their biases depend on the discretization scheme of the state space, and can be removed in principle by using Markov partitions of the state space, if they exist, associated with the dynamical system under consideration (Cornfeld et al, 1982; Hsu and Kim, 1985b).

5 The GCM for Stochastic Systems

Assume that $F(t)$ in (2.1) is a white noise random process. It is known that the response $\mathbf{x}(t)$ is a two-dimensional stationary Markov process. The transition probability density function of the system satisfies the Fokker-Planck-Kolmogorov (FPK) equation associated with the system (2.1). The transition probability matrix of GCM for the system is a discrete representation of the transition probability density function.

Consider again the computation of the one step transition probability P_{ji} by the sampling point method. Suppose that k points in cell i are uniformly sampled just as before, and out of each sampled point, l different trajectories are generated by using l white noise sample functions simulated by an appropriate Monte Carlo procedure. At time T, there will be $n = k \cdot l$ image points in the image domain $R(T, i)$. Quite different from deterministic systems, $R(T, i)$ of the stochastic system under consideration is equal to $\mathbf{R}^2$ for any $T>0$, and any i, due to the diffusion effect of white noise excitation. We therefore, drop the notation $R(T, i)$ in this section, and use $\mathbf{R}^2$ for the image domain without causing any ambiguity. There are some consequences of this fact. First, there will be no boundary image cells. Second,

$$\int_{C_j} p(\mathbf{x},T)d\mathbf{x} = O(h^2), \tag{5.1}$$

and the magnitude of $p(\mathbf{x},T)$ does not change with h significantly. It is interesting to note that for deterministic systems, $\int_{C_j} p(\mathbf{x},T)d\mathbf{x} = O(1)$, if $|J| = O(1)$ at $t = T$ and if cell j is an interior image cell. The MSE and normalized MSE for P_{ji} can be readily obtained. After neglecting higher order term, they are given by

$$\text{MSE}[P_{ji}] = \frac{h^2}{n} p(\mathbf{x}_j,T), \tag{5.2}$$

and

$$\epsilon^2[P_{ji}] = \frac{1}{nh^2 p(\mathbf{x}_j,T)}. \tag{5.3}$$

The estimation of P_{ji} is nearly as good as that of deterministic systems: it is unbiased, and its variance diminishes at the rate $n^{-1}h^2$ as $n\to\infty$ and $h\to 0$. However, the normalized MSE of P_{ji} converges to zero as $nh^2\to\infty$. This is a special feature of stochastic systems, which is further studied below in terms of the density estimator p_{ji}.

Result 5. For stochastic systems, the MSE or normalized MSE of the density estimator p_{ji} of the one step transition probability from cell i to its image cells converges to zero if $h\to 0$ and $nh^2\to\infty$.

Proof. Since every image cell of cell i is interior, the bias for an image cell j of cell i is the same as the one given by (4.5). The variance for cell j is given by

$$\text{var}[p_{ji}] = \frac{1}{nh^4}\left[1-\int_{C_j} p(\mathbf{x},T)d\mathbf{x}\right]\cdot\int_{C_j} p(\mathbf{x},T)d\mathbf{x} = \frac{1}{nh^4}\int_{C_j} p(\mathbf{x},T)d\mathbf{x} + O(n^{-1}h^0) = \frac{p(\mathbf{x}_j,T)}{nh^2} + O(n^{-1}h^0) \tag{5.4}$$

Hence, we obtain

$$\text{MSE}[p_{ji}] = \frac{h^4}{576}[\nabla^2 p(\mathbf{x}_j,T)]^2 + \frac{p(\mathbf{x}_j,T)}{nh^2} \tag{5.5}$$

$$\epsilon^2[p_{ji}] = \frac{h^4}{576}\left[\frac{\nabla^2 p(\mathbf{x}_j,T)}{p(\mathbf{x}_j,T)}\right]^2 + \frac{1}{nh^2 p(\mathbf{x}_j,T)} \tag{5.6}$$

The proof is thus completed.

Displayed in (5.5) is the well known trade-off feature of the density estimation. It states that for a fixed n, if the bias is to be reduced by taking smaller h, the variance is increased; if the variance is to be reduced by taking larger h, the bias is increased. This feature makes it possible to find an optimal h for a given n in the sense of minimizing the MSE or normalized MSE of p_{ji}. By minimizing the MSE of (5.5) with respect to h, for example, an optimal h is obtained as

$$h_{\text{opt}} = \left[\frac{288p(\mathbf{x}_j,T)}{n[\nabla^2 p(\mathbf{x}_j,T)]^2}\right]^{1/6}. \tag{5.7}$$

It is noted that h_{opt} given by (5.7) depends on the location $\mathbf{x}_j$. Sometimes, it is desirable to define an h_{opt} for the entire image domain of cell i, and furthermore, for all the initial cells i in the whole domain of interest. One way to obtain the optimal cell size for the entire image domain of cell i is to minimize the sum of MSE $[p_{ji}]$ over all image cells j of cell i. This approach can be applied to every initial cell i in the domain of interest. We shall not discuss these tasks further in this introductory paper. In the next section we shall demonstrate the application of the optimal cell size h_{opt} given by (5.7). It is found that in the case of linear and weakly nonlinear systems under white noise excitation, the optimal cell size h_{opt}, for a particular choice of image cell j of an initial cell i, when used as the optimal cell size of GCM for the domain of interest, can obtain sufficiently accurate solutions.

In ending the analysis it is pointed out that all the studies carried out in the previous sections can also be done for one dimensional, and higher dimensional state spaces in the same way, leading to similar conclusions.

6 Examples

To better appreciate the results presented in the foregoing sections, let us study a few examples.

First, we consider the point mapping of the population dynamics model (Hsu et al., 1982) defined by

$$x(n+1) = 4x(n)[1-x(n)]. \tag{6.1}$$

The domain of interest for this system is [0, 1]. Let the domain [0, 1] be divided into 50 cells of size $h = 0.02$. Consider the one step transition probabilities of an initial cell $i = 12$, covering the region [0.22, 0.24), to its image cells. The initial probability density function as defined by (2.2) for this case is given by

$$p_0(x) = \begin{cases} 50 & \text{if } x\in[0.22,\ 0.24) \\ 0 & \text{otherwise} \end{cases} \tag{6.2}$$

Downloaded 03 May 2010 to 171.66.16.21. Redistribution subject to ASME license or copyright; see http://www.asme.org/terms/Terms_Use.cfm

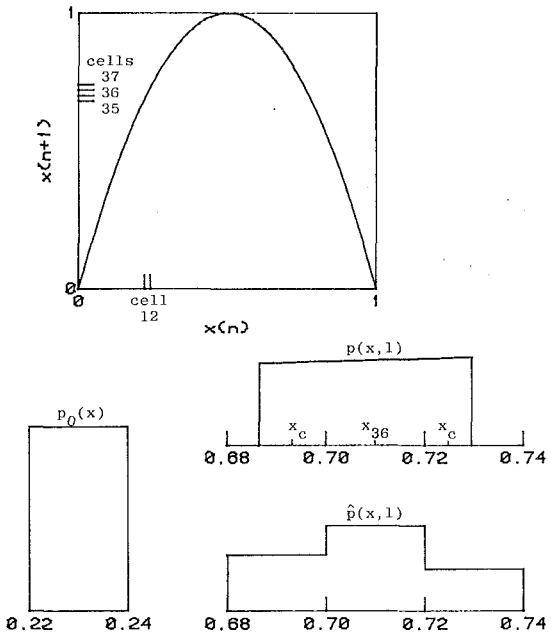


Fig. 1 One step image cells of initial cell 12 of system (6.1) and the one step transition probability density of the initial cell

Table 1

$h = 0.02$ $n = 50$ Initial cell = 12

	Normalized var $[p_{ji}]$		Normalized bias $[p_{ji}]$	
Image	Predicted	Computed	Predicted	Computed
cell 35	0.0209	0.0205	0.4352	0.4320
cell 36	0.0231	0.0223	0.0001	0.0054
cell 37	0.0155	0.0128	0.4992	0.4992

Table 2

$h = 0.01$ $n = 50$ Initial cell = 23

	Normalized var $[p_{ji}]$		Normalized bias $[p_{ji}]$	
Image	Predicted	Computed	Predicted	Computed
cell 69	0.0135	0.0128	0.4608	0.4622
cell 70	0.0242	0.0228	0.0000	0.0056
cell 71	0.0224	0.0192	0.2688	0.2653

Table 3

$h = 0.01$ $n = 500$ Initial cell = 23

	Normalized var $[p_{ji}]$		Normalized bias $[p_{ji}]$	
Image	Predicted	Computed	Predicted	Computed
cell 69	0.0013	0.0013	0.4608	0.4639
cell 70	0.0024	0.0009	0.0000	0.0005
cell 71	0.0022	0.0016	0.2688	0.2763

The probability density function after one mapping step can be obtained exactly as

$$p(x,1) = \begin{cases} \dfrac{12.5}{\sqrt{1-x}} & \text{if } x \in R(1,12) \\ 0 & \text{otherwise} \end{cases} \tag{6.3}$$

where $R(1, 12) = [0.6864, 0.7296)$ is the one step image domain of cell 12. $p_0(x)$ and $p(x, 1)$ are shown in Fig. 1. From Fig. 1, it is seen that cell 12 has three image cells, which are cells $j = 35$, 36, and 37. Cell 35 and cell 37 are α boundary image cells with $\alpha_{35} = 0.68$, and $\alpha_{37} = 0.48$. Cell 36 is an interior image cell. The statistical errors of estimation of the transition probability and the density function can be calculated by using the formulas presented in Sections 3 and 4. With the above α values for the boundary image cells, it can be shown that (4.11) is satisfied for the present case, and (4.12) and (4.13) can be applied to the boundary image cells under consideration. A number of numerical computations are conducted in order to confirm those predicted results. The estimation for the transition probabilities and the density function with n initial points sampled uniformly from cell 12 is repeated 500 times. The statistical errors are then computed. The normalized variance and bias of density estimator p_{ji} of the step transition probability for the case $n = 50$ are listed in Table 1. The normalized variance and bias are defined by var $[p_{ji}] \cdot p^{-2}(x_c, 1)$ and bias $[p_{ji}] \cdot p^{-1}(x_c, 1)$, where x_c is the center of the intersection of the image cell and the image domain. For this case, $x_c = 0.6932$ for the image cell 35, $x_c = x_j = 0.71$ for the image cell 36, and $x_c = 0.7248$ for the image cell 37, as shown in Fig. 1. Also listed in Tables 2 and 3 are the normalized variance and bias of p_{ji} for the cases $n = 50$ and 500, and $h = 0.01$. The initial cell is number 23, and its image cells are 69, 70, and 71, where cell 69 and cell 71 are α boundary image cells with $\alpha_{69} = 0.36$ and $\alpha_{71} = 0.84$, and cell 70 is an interior image cell. It is seen from Tables 1–3 that the bias of the boundary image cell is several orders larger than that of the interior image cell. It can also be shown that the variance of the density estimator is indeed bounded by the maximum variance $(4n)^{-1}h^{-2}$. For example, for the case $h = 0.02$, and the initial cell 12, the predicted and computed variances of the density estimator for the image cells 35, 36 and 37 are (10.6356, 12.4363, 8.8225) and (10.4602, 12.0387, 7.2629), while the maximum variance is given by $(4n)^{-1}h^{-2} = 12.5$.

Next, we examine the effect of the statistical errors of the one step transition probability matrix on the steady state solution, which is often of more concern. It is known that the system has a long-term chaotic motion in the domain [0, 1]. The steady state probability density function of the chaotic motion has been obtained analytically, and is given by

$$p(x) = \frac{1}{\pi\sqrt{x(1-x)}} \tag{6.4}$$

Some results of a series of computations with various cell sizes and sample sizes, and by the uniform sampling point method are plotted in Figs. 2(*a–h*). It can be seen from the figures that, for a fixed number of sample size (see in the order: *a*, *b*, *c*, and *d* of Fig. 2), the error in the limiting probability density of the system, shown up as the band width of the curves in the figures, does not decrease, but rather changes irregularly as cell size reduces. On the other hand, when cell size is fixed (see in the order: *e*, *f*, and *g* of Fig. 2), the band width of the curves in the figures becomes thinner and thinner as n increases, indicating the decrease of the MSE of the transition probability matrix with the increase of sample size. The combined effect of large sample size and small cell size for the case $n = 500$ and $h = 0.00025$ is shown in Fig. 2(*h*).

The above pictorial observations are then quantified by considering the following intergrated square error, denoted by ISE,

$$\text{ISE} = \int_0^1 [p(x) - \hat{p}(x)]^2 dx. \tag{6.5}$$

where $p(x)$ is the limiting probability density function given by (6.4), $\hat{p}(x)$ the estimator of $p(x)$ obtained by the GCM method. The data of a series of computations of the ISE for different values of n and h are listed in Table 4, where h^{-1} is equal to the number of cells used in [0, 1]. The pictorial observations described in the last paragraph are indeed confirmed by the ISE values in Table 4. As can be seen from Table 4, the ISE decreases slowly as n increases for a fixed h before the

Downloaded 03 May 2010 to 171.66.16.21. Redistribution subject to ASME license or copyright; see http://www.asme.org/terms/Terms_Use.cfm

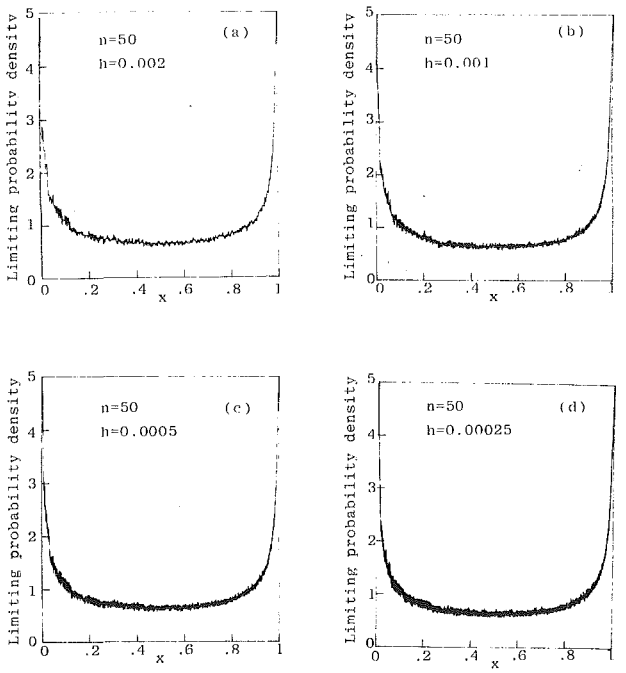


Fig. 2(*a-d*) Limiting probability density function of system (6.1). (*a*) $n=50$, $h=0.002$; (*b*) $n=50$, $h=0.001$; (*c*) $n=50$, $h=0.0005$; (*d*) $n=50$, $h=0.00025$.

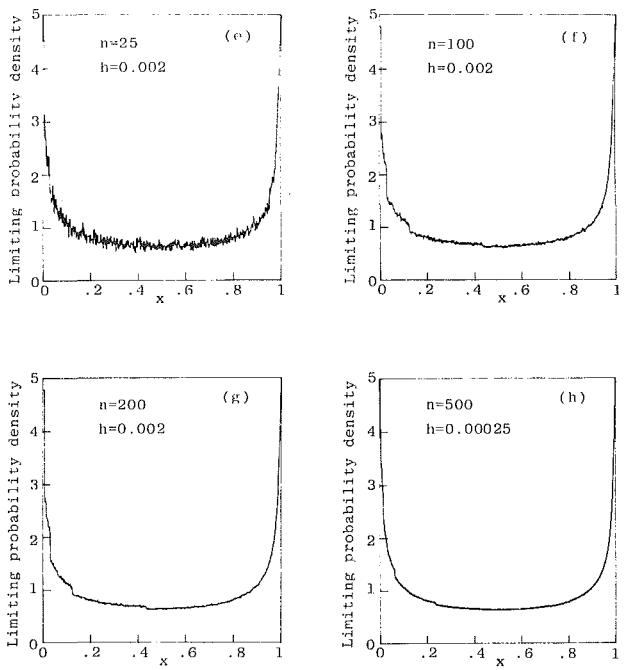


Fig. 2(*e-h*) Limiting probability density function of system (6.1). (*e*) $n=25$, $h=0.002$; (*f*) $n=100$, $h=0.002$; (*g*) $n=200$, $h=0.002$; (*h*) $n=500$, $h=0.00025$.

lower bound due to the finite cell size is reached. On the other hand, for a fixed n, the ISE changes irregularly with h. Although the bias of the interior image cells decreases as h decreases, the bias of the boundary image cells may not decrease. The MSE and hence the ISE depend on the partition of the domain [0, 1] by the cells. If the system and the cell structure are such that the partition is a Markov partition with cell boundaries mapped into cell boundaries, then the boundary image cells are absent and the undesirable large bias due to the boundary image cells is removed. From this observation, one might expect that, in general, the closer the partition is to a Markov partition, the smaller would be the bias of the boundary image cells. A quantitative description and discussion of the closeness of the partition to a Markov partition is yet to be studied.

As the second example, we study a stochastic system defined by

$$\dot{x} = -x + w(t) \tag{6.6}$$

where

$$E[w(t)] = 0,\ E[w(t)w(t+\tau)] = 2\delta(\tau). \tag{6.7}$$

$x(t)$ is known as an Ornstein-Uhlenbeck process. The exact conditional probability density function of $x(t)$ as a solution to the FPK equation associated with the system can be obtained as (Soong, 1973)

$$p(x,t,|x_0,t_0) = \frac{1}{\sqrt{2\pi}\sigma_t} \exp\left[\frac{1}{2\sigma_t^2}(x-\bar{x})^2\right], \tag{6.8}$$

where

$$\bar{x} = x_0 e^{-(t-t_0)},\ \sigma_t^2 = 1 - e^{-2(t-t_0)}. \tag{6.9}$$

When the conditional probability density function of the system is a function of the time increment $\Delta t = t - t_0$, a mapping time step T for GCM of the system can be chosen flexibly at one's own discretion. Here, we take a mapping time step $T=0.2$, and $t_0=0$. The cell size is expressed in terms of the standard deviation of the system at $t=T$ as

$$\Delta x \triangleq h = \beta\sigma_t(t=0.2) = 0.5742\beta. \tag{6.10}$$

Assume that the system starts from a cell centered at $x=0$. We shall present two kinds of results. First, we show the density estimation of one step transition probability from the cell centered at $x=0$ to its image cells. Second, we calculate the steady state mean square value of x, the exact value of which can be obtained from (6.9) as $t\to\infty$. These two results should show the capabilities of GCM in describing the transient and stationary motions of a stochastic system, and it should also give us some feelings about how the accuracy of the solutions obtained by the GCM method is affected by the statistical errors of one step transition probabilities.

For our purposes stated above, it is found sufficient to consider the normalized MSE of the density estimator p_{ji} for the cell centered at $x=0$. It is readily shown that

$$\epsilon^2[p_{ji}] = \frac{1}{nhp(0,T)} + \frac{h^4}{576}\left[\frac{p''(0,T)}{p(0,T)}\right]^2 = \frac{\sqrt{2\pi}}{n\beta} + \frac{\beta^4}{576}. \tag{6.11}$$

By minimizing ϵ^2, we find that

$$\beta_{\text{opt}}^5 = \frac{144\sqrt{2\pi}}{n}. \tag{6.12}$$

The numerical experiments with $n=400$, $k=1$, and $l=400$ are conducted for different β values around β_{opt} given by (6.12) in order to see if the optimality is indeed achieved. The antivariate method (Rubenstein, 1981; Chiu, 1984) is used in this and the next example to ensure the zero ensemble mean of a finite number of sample functions of the white noise process.

The density estimations with different cell sizes at $t=0.2$ by the GCM method are plotted in Figs. 3(*a*)-(*d*) against the exact solution. The trade-off phenomenon is clearly displayed as cell size changes across the optimal cell size predicted by (6.12). The results of the steady state mean square values of x are listed in Table 5. Notice that for $n=400$, $h_{\text{opt}}=0.56$. In Table 5 the error is defined by

$$\frac{|E(x^2)-\hat{E}(x^2)|}{E(x^2)} \times 100.$$

From both Figs. 3(*a*)-(*d*) and Table 5, one can see that there is indeed an optimal cell size for a given n, which gives the best approximations.

Downloaded 03 May 2010 to 171.66.16.21. Redistribution subject to ASME license or copyright; see http://www.asme.org/terms/Terms_Use.cfm

Table 4

n/h^{-1}	125	250	500	1000	2000	4000
25	0.1094	0.1172	0.1071	0.1153	0.1101	0.1193
50	0.1088	0.1109	0.1050	0.1081	0.1049	0.1059
100	0.1029	0.1057	0.1004	0.1017	0.0997	0.1001
200	0.1027	0.1041	0.0998	0.1013	0.0992	0.0991
500	0.1020	0.1038	0.0999	0.1009	0.0990	0.0994
1000	0.1022	0.1040	0.0999	0.1009	0.0990	0.0994

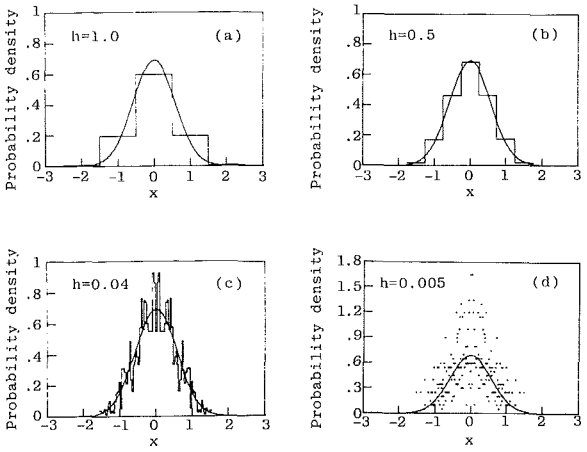


Fig. 3 Probability density function of system (6.6) for the case $t=0.2$, $x_0=0$, and $n=400$. (a) $h=1.0$; (b) $h=0.5$; (c) $h=0.04$; (d) $h=0.005$, random error dominates.

Finally, we consider a Duffing oscillator under white noise excitation

$$\ddot{x}+2\zeta\dot{x}+x+\epsilon x^3=\sqrt{2\zeta}\,w(t), \tag{6.13}$$

where $w(t)$ is the same one as defined by (6.7). The MSE of the density estimator p_{ji} of the system can be derived as

$$\mathrm{MSE}[p_{ji}]=\frac{p(\mathbf{x}_j,t)}{n\Delta x\Delta\dot{x}}+\frac{1}{576}\left[\Delta x^2\frac{\partial^2 p}{\partial x^2}+\Delta\dot{x}^2\frac{\partial^2 p}{\partial\dot{x}^2}\right]^2. \tag{6.14}$$

Since the exact density function of the system for $\epsilon\neq 0$ is not available, we shall use the exact density function for the case $\epsilon=0$ (Wang and Uhlenbeck, 1945) to obtain the optimal cell sizes Δx and $\Delta\dot{x}$ for the image cell centered at $\mathbf{x}_j=(0,0)$, assuming that the system starts from that cell. These should hopefully provide good approximate estimates of the optimal cell sizes for the weakly nonlinear system with $0<\epsilon<<1$. Furthermore, we apply these optimal cell sizes to strongly nonlinear system to see in what way, these approximate estimates become inadequate.

In the computations we choose $n=200$, $k=1$, $l=200$, $\zeta=0.1$, and $T=2\pi/4$. With the exact density function of the linear system, we obtain, by minimizing the MSE of (6.14), the optimal cell sizes as

$$(\Delta x_{\mathrm{opt}})^6=\frac{2.3412}{n},\quad (\Delta\dot{x}_{\mathrm{opt}})^6=\frac{3.0740}{n}. \tag{6.15}$$

For $n=200$, we have

$$\Delta x_{\mathrm{opt}}=0.4765,\ \Delta\dot{x}_{\mathrm{opt}}=0.4986. \tag{6.16}$$

The steady state mean square values of x and $\dot{x}$, calculated by the GCM method with different cell sizes around the optimal ones, and for different ϵ values, are listed in Tables 6-8, together with the errors against the analytical results which are

Table 5

h	1.0	0.8	0.5	0.1	0.08	0.04
$\hat{E}(x^2)$	1.1327	1.0598	0.9978	0.9512	0.9502	0.9494
error	13.27	5.98	0.22	4.88	4.98	5.06

obtained from the exact steady state probability density function of the system (6.13) (Caughey, 1971) as follows

$$\begin{aligned} &E(x^2)=1.0000, \quad E(\dot{x}^2)=1.0, \quad \epsilon=0.0\\ &E(x^2)=0.9974, \quad E(\dot{x}^2)=1.0, \quad \epsilon=0.001\\ &E(x^2)=0.4681, \quad E(\dot{x}^2)=1.0, \quad \epsilon=1.0 \end{aligned} \tag{6.17}$$

In Tables 6-8 the errors are defined by

$$\mathrm{Er}(x)\%=\frac{|E(x^2)-\hat{E}(x^2)|}{E(x^2)}\times 100$$

$$\mathrm{Er}(\dot{x})\%=\frac{|E(\dot{x}^2)-\hat{E}(\dot{x}^2)|}{E(\dot{x}^2)}\times 100$$

$$\text{Error }\%=\mathrm{Er}(x)\%+\mathrm{Er}(\dot{x})\%.$$

From Tables 6-8, it is observed that the overall optimal performance of the GCM method, as measured by the sum of the errors defined above, is achieved at the cell sizes very close to the predicted optimal cell sizes for the linear and weakly nonlinear systems, and at some smaller unknown cell sizes for the strongly nonlinear system. It may thus be concluded that it is a viable approach to apply the optimal cell sizes estimated for a linear system to the associated weakly nonlinear system. For strongly nonlinear systems, however, some other method has to be explored to estimate the optimal cell sizes.

7 Conclusions

By making an analogy of the GCM method to the density estimation, it is possible to carry out a statistical error analysis of GCM so as to help better understand GCM and to improve it from the statistical point of view.

For deterministic systems, and the interior image cells, it has been shown that the normalized MSE of the density estimator of the transition probability vanishes as $n\to\infty$ and $h\to 0$ at the same time because the effects of n and h on the normalized MSE are separate and different. It means that the solutions of probabilistic evolution of the system obtained by the GCM method will be asymptotically improved as n increases and h decreases at the same time. This result is important for studies of strange attractors and fractal boundaries of domains of attraction, for which a probabilistic description of the behavior of the trajectories is pertinent or highly desirable. On the other hand, when the geometrical aspect of the solutions of the system such as periodic solutions, limit cycles, and domains of attraction is sought, and the probabilistic information is not relevant, the GCM method can give very good results with only a limited number of sample points as long as h is reasonably small (Chiu and Hsu, 1986). For the boundary image cells, the normalized MSE may have a dominant lower order term

Downloaded 03 May 2010 to 171.66.16.21. Redistribution subject to ASME license or copyright; see http://www.asme.org/terms/Terms_Use.cfm

Table 6

$\epsilon = 0$

Cell Size	$\hat{E}(x^2)$	$\hat{E}(\dot{x}^2)$	Er(x)%	Er($\dot{x}$)%	Error %
(0.70, 0.70)	1.0533	1.0910	5.33	9.10	14.43
(0.60, 0.60)	0.9983	1.0301	1.17	3.01	3.18
(0.50, 0.50)	0.9802	1.0092	1.98	0.90	2.88
(0.40, 0.40)	0.9660	0.9983	3.4	0.17	3.57
(0.20, 0.50)	0.9528	0.9951	4.72	0.49	5.21

Table 7

$\epsilon = 0.001$

Cell Size	$\hat{E}(x^2)$	$\hat{E}(\dot{x}^2)$	Er(x)%	Er($\dot{x}$)%	Error %
(0.70, 0.70)	1.0527	1.0932	5.54	9.32	14.86
(0.60, 0.60)	0.9964	1.0308	0.1	3.08	3.18
(0.60, 0.50)	1.0162	1.0480	1.88	4.8	6.68
(0.50, 0.50)	0.9770	1.0085	2.05	0.85	2.90
(0.40, 0.40)	0.9637	0.9987	3.38	0.13	3.51

Table 8

$\epsilon = 1.0$

Cell Size	$\hat{E}(x^2)$	$\hat{E}(\dot{x}^2)$	Er(x)%	Er($\dot{x}$)%	Error %
(0.70, 0.70)	0.5694	1.2570	21.64	25.70	47.30
(0.60, 0.60)	0.5086	1.1393	8.65	13.93	22.58
(0.50, 0.50)	0.5038	1.1219	7.63	12.19	19.82
(0.40, 0.40)	0.4781	1.0824	2.14	8.24	10.38
(0.30, 0.30)	0.4636	1.0370	0.96	3.70	4.66

depending on the discretization scheme of the state space. This effect of the boundary image cells can be minimized in principle by using more desirable and nonuniform cell structure.

For stochastic systems under white noise excitation, the GCM method exhibits two interesting features. First, it does not have any boundary image cells so that there is no lower order term of bias for any image cells. Second, the trade-off feature of the density estimation makes it possible to find an optimal cell size for a given sample size, and thus to obtain the optimal approximations by the GCM method. The detailed procedure for finding the optimal relations of cell size and sample size for general nonlinear stochastic systems is yet to be investigated.

Acknowledgment

This material is based upon work supported by the National Science Foundation under grant No. MSM-8519950.

References

Caughey, T. K., 1971, *Nonlinear Theory of Random Vibration, Advances in Applied Mechanics, Vol. 11*, pp. 209–253, Academic Press, New York.

Chandiramani, K. L., 1964, "First-Passage Probabilities of a Linear Oscillator," Doctoral thesis, Department of Mechanical Engineering, M.I.T., Cambridge, Mass.

Chiu, H. M., 1984, "Random Vibration Analysis by Cell Mapping Methods," Ph.D. Thesis, Mechanical Engineering, University of California, Berkeley.

Chiu, H. M., and Hsu, C. S., 1986, "A Cell Mapping Method for Nonlinear Deterministic and Stochastic Systems-Part II: Examples of Application," ASME JOURNAL OF APPLIED MECHANICS, Vol. 53, pp. 702–710.

Cornfeld, I. P., Fomin, S. V., and Sinai, Ya. G., 1982, *Ergodic Theory*, Springer-Verlag, New York.

Crandall, S. H., Chandiramani, K. L., and Cook, R. G., 1966, "Some First-Passage Problems in Random Vibration, ASME JOURNAL OF APPLIED MECHANICS, Vol. 33, pp. 532–538.

Davenport, W. B., Jr., 1970, *Probability and Random Process*, McGraw-Hill, New York.

Feller, William, 1971, *An Introduction to Probability Theory and Its Application*, Vol. 2, John Wiley & Sons, New York.

Hsu, C. S., 1987, *Cell-to-Cell Mapping: A Method of Global Analysis for Nonlinear Systems*, Springer-Verlag, New York.

Hsu, C. S., and Chiu, H. M., 1986, "A Cell Mapping Method for Nonlinear Deterministic and Stochastic Systems-Part I: The Method of Analysis," ASME JOURNAL OF APPLIED MECHANICS, Vol. 53, pp. 695–701.

Hsu, C. S., Guttalu, R. S., and Zhu, W. H., 1982, "A Method of Analyzing Generalized Cell Mapping," ASME JOURNAL OF APPLIED MECHANICS, Vol. 49, pp. 885–894.

Hsu, C. S., and Kim, M. C., 1985a, "Statistics of Strange Attractors by Generalized Cell Mapping," *J. of Statist. Phys.*, Vol. 38, No. 3/4, pp. 735–761.

Hsu, C. S., and Kim, M. C., 1985b, "Construction of Maps with Generating Partitions for Entropy Evaluation,' *Physical Review A*, Vol. 31, pp. 3253–3265.

Kim, M. C., and Hsu, C. S., 1986, "Computation of the Largest Lyapunov Exponent by the Generalized Cell Mapping," *J. of Statist. Phys.*, Vol. 45, No. 1/2, pp. 49–61.

Polchai, A. and Hsu, C. S., 1985, "Domain of Stability of Synchronous Generators by a Cell Mapping Approach," *Int. J. Control*, Vol. 41, No. 5, pp. 1253–1271.

Rubinstein, R. Y., 1981, *Simulation and the Monte Carlo Method*, John Wiley & Sons, New York.

Siverman, B. W., 1986, *Density Estimation for Statistics, and Data Analysis*, Chapman and Hall, London.

Soong, T. T., 1973, *Random Differential Equations in Science and Engineering*, Academic Press, New York.

Ushio, T., and Hsu, C. S., 1987, "Simple Example of Digital Systems With Chaotic Rounding Errors," *Int. J. Control*, Vol. 45, No. 1, pp. 17–31.

Wang, M. C., and Uhlenbeck, G. E., 1945, "On the Theory of Brownian Motion II," *Review of Modern Physics*, Vol. 13, pp. 323–342.

Wertz, W., 1978, *Statistical Density Estimation: A Survey*, Göttingen: Vandenhoeck and Ruprecht.

Xu, J., Guttalu, R. S., and Hsu, C. S., 1985, "Domains of Attraction for Multiple Limit Cycles of Coupled van der Pol Equations by Simple Cell Mapping, *Int. J. Non-Linear Mech.*, Vol. 20, No. 5/6, pp. 507–517.

Downloaded 03 May 2010 to 171.66.16.21. Redistribution subject to ASME license or copyright; see http://www.asme.org/terms/Terms_Use.cfm

Exact Stationary Response Solution for Second Order Nonlinear Systems Under Parametric and External White Noise Excitations: Part II

Y. K. Lin
Professor and Director.

Guoqiang Cai
Research Assistant.

Center for Applied Stochastics Research,
Florida Atlantic University,
Boca Raton, FL 33431

A systematic procedure is developed to obtain the stationary probability density for the response of a nonlinear system under parametric and external excitations of Gaussian white noises. The procedure is devised by separating the circulatory portion of the probability flow from the noncirculatory flow, thus obtaining two sets of equations that must be satisfied by the probability potential. It is shown that these equations are identical to two of the conditions established previously under the assumption of detailed balance; therefore, one remaining condition for detailed balance is superfluous. Three examples are given for illustration, one of which is capable of exhibiting limit cycle and bifurcation behaviors, while another is selected to show that two different systems under two differents sets of excitations may result in the same probability distribution for their responses.

Introduction

The problem of a randomly excited nonlinear system is of common interest to researchers in many technical fields. Some mathematically exact solutions have been obtained when the excitations can be idealized as Gaussian white noises, so that the system response, represented as a vector in a state space, is a Markov vector. In this case, the probability density of the system response, conditional on a given initial state, is governed by a parabolic partial differential equation, called the Fokker-Planck equation, which can be derived from the equations of motion. Still, full exact solutions for the Fokker-Planck equation are known only for very special first order nonlinear systems (Caughey and Dienes, 1961).

For second order nonlinear systems, solutions have been obtained only for limited cases and only for the reduced Fokker-Planck equations, namely, Fokker-Planck equations without the time-derivative term. The unknown in a reduced Fokker-Planck equation is the unconditional probability density of the response vector when it reaches statistical stationarity after the system is exposed to the stationary excitations for a sufficiently long time. When the excitations appear only as inhomogeneous terms on the right hand sides of the equations of motion, called external or additive excitations, the known solutions can be grouped in a general class as shown by Caughey and Ma (1983).

When parametric (or multiplicative) white noise excitations are also present, namely, the excitations also appear in the coefficients of the unknowns in the equations of motion, solution to a reduced Fokker-Planck equation becomes more difficult. This more general case was considered in an earlier paper by Yong and Lin (1987) where a systematic procedure was given to obtain the solution under an assumption called detailed balance (Graham and Haken, 1971; Van Kampen, 1957).

In the present paper, the class of solvable cases will be extended further to what we shall call the class of generalized stationary potential. Comparisons will be made with the class of detailed balance. Its application will be illustrated by examples. As a preliminary, however, we shall introduce first the concept of stationary potential.

Stationary Potential

The concept of stationary potential (Stratonovich, 1963) can be explained more clearly by considering the case of the one-dimensional Markov process, say, $X(t)$, for which the Fokker-Planck equation reads

$$\frac{\partial q}{\partial t}+\frac{\partial G}{\partial x}=0 \tag{1}$$

where q is the probability density of $X(t)$ conditional on an initial value of $X(t)$, G is called the probability flow given by

Contributed by the Applied Mechanics Division for presentation at the Winter Annual Meeting, Chicago, IL, November 28 to December 2, 1988, of THE AMERICAN SOCIETY OF MECHANICAL ENGINEERS.

Discussion on this paper should be addressed to the Editorial Department, ASME, United Engineering Center, 345 East 47th Street, New York, N.Y. 10017, and will be accepted until two months after final publication of the paper itself in the JOURNAL OF APPLIED MECHANICS. Manuscript received by ASME Applied Mechanics Division, March 23, 1987; final revision, March 25, 1988.

Paper No. 88-WA/APM-45.

Copyright © 1988 by ASME
Downloaded 03 May 2010 to 171.66.16.21. Redistribution subject to ASME license or copyright; see http://www.asme.org/terms/Terms_Use.cfm

$$G = Aq - \frac{1}{2}\frac{\partial}{\partial x}(Bq) \tag{2}$$

and A and B are, respectively, the first and second derivate moments defined as

$$A = \lim_{\Delta t \to 0} \frac{1}{\Delta t} E\{X(t+\Delta t) - X(t) \mid X(t) = x\} \tag{3}$$

$$B = \lim_{\Delta t \to 0} \frac{1}{\Delta t} E\{[X(t+\Delta t) - X(t)]^2 \mid X(t) = x\} \tag{4}$$

In equations (3) and (4) $E\{\ \}$ indicates an ensemble average, and a vertical bar precedes a specified condition. We shall restrict our consideration to the case of natural boundaries S, namely,

$$G(x) = 0, \quad \text{for } x \epsilon S \tag{5}$$

If the nature of the dynamic system is such that $X(t)$ eventually attains the stationary state, then at such a state q tends to the unconditional stationary probability $p_s(x)$, independent of t, and it is governed by the reduced Fokker-Planck equation

$$\frac{dG}{dx} = \frac{d}{dx}\left[Ap_s - \frac{1}{2}\frac{d}{dx}(Bp_s)\right] = 0 \tag{6}$$

However, when equation (6) is solved with the boundary condition, equation (5), the solution must, in fact, satisfy

$$G = Ap_s - \frac{1}{2}\frac{d}{dx}(Bp_s) = 0 \tag{7}$$

namely, the probability flow must vanish everywhere, not merely at the boundaries. It is easy to show that this solution may be expressed as

$$p_s = Ce^{-\phi} \tag{8}$$

where C is a normalization constant and

$$\phi = \ell nB - 2\int AB^{-1}dx \tag{9}$$

Function ϕ will be referred to as the stationary potential of the probability density.

The exponential form of the solution, equation (8), imposes no real limitation, and it guarantees that p_s is always nonnegative.

The generalization of equations (1) through (6) for the case of multidimensional Markov vector is straightforward. In particular, the reduced Fokker-Planck equation is now

$$\frac{\partial G_i}{\partial x_i} = \frac{\partial}{\partial x_i}\left[A_i p_s - \frac{1}{2}\frac{\partial}{\partial x_j}(B_{ij}p_s)\right] = 0 \tag{10}$$

with

$$A_i = \lim_{\Delta t \to 0} \frac{1}{\Delta t} E\{X_i(t+\Delta t) - X_i(t) \mid X(t) = \mathbf{x}\} \tag{11}$$

$$B_{ij} = \lim_{\Delta t \to 0} \frac{1}{\Delta t} E\{[X_i(t+\Delta t) - X_i(t)][X_j(t+\Delta t) - X_j(t)] \mid X(t) = \mathbf{x}\} \tag{12}$$

The natural boundary conditions for equation (10) are specified as

$$G_i = 0, \quad \text{for } \mathbf{x} \epsilon S \tag{13}$$

However, satisfaction of these conditions does not guarantee generally that $G_i = 0$ everywhere. Analogous to the situation in fluid mechanics, a steady pattern of probability flow may exist in a multidimensional space, even though it is required to vanish at the boundaries.

In this section, we shall consider the special case where the probability flow does vanish everywhere, referred to also as the case of stationary potential. A more general case will be treated in the following section.

In case of stationary potential, equation (10) can be replaced by

$$A_i p_s - \frac{1}{2}\frac{\partial}{\partial x_j}(B_{ij}p_s) = 0 \tag{14}$$

Substituting $p_s = C\exp(-\phi)$ into (14), we obtain

$$B_{ij}\frac{\partial \phi}{\partial x_j} = \frac{\partial B_{ij}}{\partial x_j} - 2A_i \tag{15}$$

For an n-dimensional Markov vector, we may have as many as n equations of the type of (15) to determine the potential function ϕ. A stationary potential exists if a compatible ϕ funtion can be found which satisfies all these equations.

If matrix $[B_{ij}]$ is non-singular so that its inverse $[D_{ij}]$ exists, than (15) may be simplified to

$$\frac{\partial \phi}{\partial x_\ell} = D_{\ell i}\left(\frac{\partial B_{ij}}{\partial x_j} - 2A_i\right) \tag{16}$$

A consistent ϕ function is obtainable if the following compatibility conditions are satisfied:

$$\frac{\partial}{\partial x_m} D_{\ell i}\left(\frac{\partial B_{ij}}{\partial x_j} - 2A_i\right) = \frac{\partial}{\partial x_\ell} D_{mi}\left(\frac{\partial B_{ik}}{\partial x_k} - 2A_i\right) \tag{17}$$

Specializing further to the case of isotropic diffusion (Stratonovich, 1963) defined as $B_{ij} = K\delta_{ij}$, equations (16) and (17) become, respectively,

$$\frac{\partial \phi}{\partial x_i} = \frac{1}{K}\left(\frac{\partial K}{\partial x_i} - 2A_i\right) \tag{18}$$

and

$$\frac{\partial}{\partial x_m} A_\ell = \frac{\partial}{\partial x_\ell} A_m \tag{19}$$

When (19) is satisfied, the stationary potential obtained from (18) is given by

$$\phi = \ell nK - \frac{2}{K}\int A_i dx_i \tag{20}$$

which has the same form as equation (9).

In passing, we remark that for many practical problems, matrix $[B_{ij}]$ is singular, but it contains mostly zero elements to allow the determination of a possible consistent ϕ function by inspection.

Generalized Stationary Potential

When a consistent ϕ function is not obtainable under the assumption of vanishing probability flow everywhere, a more general procedure is required. We devise such a procedure by splitting up the first derivate moments A_i into two parts:

$$A_i = A_i^I + A_i^R \tag{21}$$

Replace A_i in equation (15) by A_i^I to obtain

$$B_{ij}\frac{\partial \phi}{\partial x_j} = \frac{\partial B_{ij}}{\partial x_j} - 2A_i^I \tag{22}$$

Then, by substituting $p_s = C\exp(-\phi)$, and equations (21) and (22) into the reduced Fokker-Planck equation, we find that function ϕ must also satisfy

$$\frac{\partial A_i^R}{\partial x_i} - A_i^R\frac{\partial \phi}{\partial x_i} = 0 \tag{23}$$

A reduced Fokker-Planck equation is said to possess a solution of the type of generalized stationary potential if a ϕ function can be found which satisfies equations (22) and (23). The implication is that only one part of A_i, namely A_i^R, is associated with the possible "circulatory" probability flow.

It is interesting to note that equations (22) and (23) are exactly the same as equations (15) and (28) in Part I of Yong and Lin (1987) which were derived on the basis of detailed balance. Therefore, A_i^I and A_i^R are, in fact, the same irreversible and

Downloaded 03 May 2010 to 171.66.16.21. Redistribution subject to ASME license or copyright; see http://www.asme.org/terms/Terms_Use.cfm

reversible parts of A_i; they can be obtained systematically as follows in Yong and Lin (1987).

First, we identify two types of state variables, according to the transformation from x_i to $\tilde{x}_i$ upon the time reversal $t \to -t$. The even variables do not change their signs when time is reversed, whereas the odd variables do. Thus, we denote

$$\tilde{x}_i = \epsilon_i x_i, \quad \text{no summation on } i \tag{24}$$

where $\epsilon_i = \pm 1$ corresponding to the even and odd variables, respectively. Then A_i^I and A_i^R are obtained as

$$A_i^I(\mathbf{x}) = \frac{1}{2}[A_i(\mathbf{x}) + \epsilon_i A_i(\tilde{\mathbf{x}})] \tag{25}$$

$$A_i^R(\mathbf{x}) = \frac{1}{2}[A_i(\mathbf{x}) - \epsilon_i A_i(\tilde{\mathbf{x}})] \tag{26}$$

Again, the subscript for each ϵ in equations (25) and (26) does not imply the usual summation convention.

It should be noted that in addition to equations (22) and (23), the state of detailed balance requires the following condition [8]

$$B_{ij}(\mathbf{x}) = \epsilon_i \epsilon_j B_{ij}(\tilde{\mathbf{x}}) \tag{27}$$

Therefore, the class of generalized stationary potential is less restrictive than that of detailed balance, and to the knowledge of the writers, it includes the broadest solvable cases at the present time. The present analysis shows that condition (27) is actually superfluous.

Examples

1 Consider an equation of motion of the following type

$$\ddot{X} + h(X, \dot{X}) = W(t) \tag{1-1}$$

where $(h(.,.)$ is an arbitrary nonlinear function and $W(t)$ is a Gaussian white noise external excitation. In many practical cases, this h function may be approximated by a polynomial in X and $\dot{X}$. For a rather general 4th degree polynomial

$$\begin{aligned} h(X,\dot{X}) = {} & a_{10}X + a_{01}\dot{X} + a_{20}|X|X + a_{11}|X|\dot{X} \\ & + a_{02}|\dot{X}|\dot{X} + a_{30}X^3 + a_{21}X^2\dot{X} + a_{12}X\dot{X}^2 \\ & a_{03}\dot{X}^3 + a_{40}|X^3|X + a_{31}|X^3|\dot{X} + a_{22}X^2|\dot{X}|\dot{X} \\ & + a_{13}|X|\dot{X}^3 + a_{04}|\dot{X}^3|\dot{X} \end{aligned} \tag{1-2}$$

we can determine from equations (22) and (23) the admissible coefficients in order to be in the class of generalized stationary potential. Under the assumption $a_{10} \neq 0$ and $a_{01} \neq 0$ the following two nonlinear systems have been identified:

$$h_1(X,\dot{X}) = 2\zeta\omega_0\dot{X} + \omega_0^2 X(1 + \alpha|X| + \beta X^2 + \gamma X^2|X|) \tag{1-3}$$

$$\begin{aligned} h_2(X,\dot{X}) = {} & 2\zeta\omega_0\dot{X}\left(1 + \delta\dot{X}^2 + \delta\omega_0^2 X^2 + \frac{2}{3}\lambda\delta\omega_0^2|X^3|\right) \\ & + \omega_0^2 X(1 + \lambda|X|) \end{aligned} \tag{1-4}$$

where ω_0, ζ, α, β, γ, δ, and λ are arbitrary constants. The corresponding potential functions are, respectively,

$$\begin{aligned} \phi_1 = {} & \frac{2\zeta\omega_0}{\pi K}\left[\frac{1}{2}\dot{x}^2\right. \\ & \left. + \frac{1}{2}\omega_0^2 x^2\left(1 + \frac{2}{3}\alpha|x| + \frac{1}{2}\beta x^2 + \frac{2}{5}\gamma x^2|x|\right)\right] \end{aligned} \tag{1-5}$$

$$\begin{aligned} \phi_2 = {} & \frac{2\zeta\omega_0}{\pi K}\left[\frac{1}{2}\dot{x}^2\left(1 + \delta\omega_0^2 x^2 + \frac{1}{2}\delta\dot{x}^2 + \frac{2}{3}\lambda\delta\omega_0^2 x^2|x|\right)\right. \\ & + \frac{1}{2}\omega_0^2 x^2\left(1 + \frac{2}{3}\lambda|x| + \frac{1}{2}\delta\omega^2 x^2 + \frac{2}{3}\lambda\delta\omega_0^2 x^2|x|\right. \\ & \left.\left. + \frac{2}{9}\lambda^2\delta\omega_0^2 x^4\right)\right] \end{aligned} \tag{1-6}$$

where K is the spectral density of the external excitation $W(t)$. The h_1 function permits five arbitrary constants, and it represents a system with linear damping and nonlinear restoring force. On the other hand, the h_2 function represents a system with both nonlinear damping and nonlinear restoring force but it allows the flexibility of only four arbitrary constants. Still, there is one general restriction on the combination of these arbitrary constants for either case: They must be such that the potential function ϕ tends to infinity sufficiently fast as x or $\dot{x}$ tends to $\pm\infty$, to ensure the existence of a finite total probability. Additional flexibility can be obtained by including higher polynomial terms in the h function.

2 As the second example, consider a nonlinear system under both parametric and external random excitations as follows

$$\ddot{X} + 2\zeta\omega_0\dot{X}(1 + \alpha X^2) + \omega_0^2[1 + W_1(t)]X + f(X) = W_2(t) \tag{2-1}$$

where $f(\,)$ is an arbitrary nonlinear function. It can be shown that if $\alpha = \omega_0^4 K_1/K_2$ where K_1 and K_2 are spectral densities of $W_1(t)$ and $W_2(t)$, respectively, then the system response has a generalized stationary potential

$$\phi = \frac{2\zeta\omega_0}{\pi K_2}\left[\frac{1}{2}(\dot{x}^2 + \omega_0^2 x^2) + \int_0^x f(u)\,du\right] \tag{2-2}$$

Of course, the arbitrary $f(\,)$ must satisfy the general condition that the probability density of the stationary system response exists.

It is interesting to note the neither α nor K_1 appears in equation (2-2); thus, the same probability density results for the well-known case of nonlinear spring, linear damping ($\alpha = 0$), and without parametric excitation ($K_1 = 0$). This well-known case has been investigated independently by several authors (e.g., Andronov, Pontryagin, and Witt, 1933; Kramers, 1940). The fact that two different systems under two different sets of excitations lead to the same probability distribution for their responses may not be so surprising as we recall an earlier discovery that the response of a nonlinear system under combined Gaussian parametric and external excitations can also be Gaussian (Yong and Lin, 1987).

3 For the last example, we choose an interesting nonlinear oscillator which is capable of exhibiting limit cycle and bifurcation behaviors, and is governed by the equation

$$\ddot{X} + X^2\left[\beta + \frac{4\alpha}{X^2 + \dot{X}^2}\right]\dot{X} + [1 + W(t)]X = 0 \tag{3-1}$$

where $\beta > 0$, and $W(t)$ is a Gaussian white noise parametric excitation with a spectral density K. Without the random excitation, the equation has a nontrivial solution, corresponding to a stable limit-cycle if $\alpha < 0$. If $\alpha > 0$, then the only stable configuration is the trivial $X = 0$.

It can be shown that the system possesses a generalized stationary potential

$$\phi = \frac{\beta}{2\pi K}[x^2 + \dot{x}^2] + (1 - \upsilon)\ell n(x^2 + \dot{x}^2) \tag{3-2}$$

where $\upsilon = 1 - 2\alpha/\pi K$. Equation (3-2) implies that if $\alpha > 0$ then a nontrivial stationary probability density exists only if $K > 2\alpha/\pi$. Thus, $2\alpha/\pi$ represents a critical spectral level for the parametric excitation at which bifurcation occurs, and below which the trivial solution is stable in probability.

When a stationary probability density of the system response exists ($K > 2\alpha/\pi$), its shape depends greatly on whether $\alpha \geq 0$ or $\alpha < 0$. It can be shown that if $\alpha \geq 0$, the potential function ϕ has a minimum at $x = \dot{x} = 0$. Since a minimum for ϕ corresponds to a maximum for the probability density p_s, $x = \dot{x} = 0$ is the most probable value for the response vector. On the other hand, if $\alpha < 0$, then ϕ has a minimum at $x^2 + \dot{x}^2 = 4|\alpha|/\beta$ and it tends to infinity as $x^2 + \dot{x}^2$ approaches to either zero or infinity. This implies that the probability density

Downloaded 03 May 2010 to 171.66.16.21. Redistribution subject to ASME license or copyright; see http://www.asme.org/terms/Terms_Use.cfm

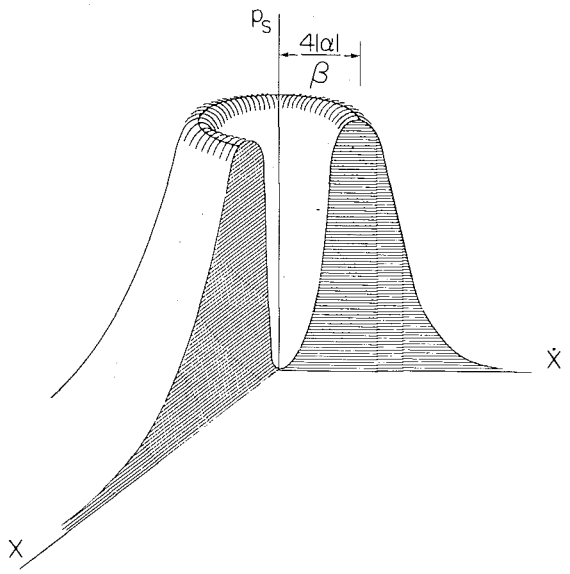


Fig. 1

has a shape shown in Fig. 1, and the most probable values for the response lie on the circle $x^2 + \dot{x}^2 = 4|\alpha|/\beta$, which is the stochastic analogue of the limit cycle.

Concluding Remarks

Compared with the earlier paper, Part I of Yong and Lin (1987) the analytical development herein is more appealing to the engineers, since it is based on a more graphical idea of splitting the probability flow into two parts. The first part corresponds to a stationary potential for which the probability flow must vanish everywhere if natural boundary conditions are imposed. Therefore, the second part is, in fact, the total flow; it corresponds to a fixed circulatory pattern invariant with respect to time.

The three examples selected illustrate three aspects of nonlinear systems under random excitations. The first example is concerned with a very general polynomial type nonlinearity, either in damping or in the restoring force or both, under an external white noise excitation. The object is to identify the restrictions under which an exact solution is presently obtainable. In the second example, we show that identical probability distribution may result for different nonlinear systems under different random excitations. The particular probability distribution selected for illustration is among the most well known in the literature. The third example is a nonlinear system under a parametric random excitation alone, for which a probability distribution exists either when the system is inherently capable of limit cycle behavior, or when the spectral level of the excitation is sufficiently high to cause a bifurcation.

Acknowledgment

Support from the National Science Foundation for Y. K. Lin under Grant ECE-8607183 and from the Pao Zao-long and Pao Yu-kong Scholarship for Guoqiang Cai are gratefully acknowledged. Opinions, findings and conclusions expressed are those of the writers and do not necessarily reflect the views of the sponsors.

References

Andronov, A., Pontryagin, L., and Witt, A., 1933, "On the Statistical Investigation of Dynamic Systems," in Russian, *Zh. Eksperim, i Teor. Fiz.*, Vol. 3, pp. 165–180.

Caughey, T. K., and Dienes, J. K., 1961, "Analysis of a Nonlinear First-Order System with a White Noise Input," *Journal of Applied Physics*, Vol. 23, pp. 2476–2479.

Caughey, T. K., and Ma, F., 1983, "The Exact Steady-State Solution of a Class of Nonlinear Stochastic Systems," *International Journal of Nonlinear Mechanics*, Vol. 17, No. 3, pp. 137–142.

Graham, R., and Haken, H., 1971, "Generalized Thermo-Dynamic Potential for Markoff System in Detailed Balance and Far from Thermal Equilibrium," *Zeitschrift fur Physik*, Vol. 203, pp. 289–302.

Kramers, H. A., 1940, "Brownian Motion in a Field of Force and Diffusion Model of Chemical Reactions," *Physica*, Vol. 7, pp. 284–304.

Stratonovich, R. L., 1963, *Topics in the Theory of Random Noise*, Vol. 1, Gordon and Beach, New York.

Van Kampen, N. G., 1957, "Derivation of the Phenomenological Equations from the Master Equation, II. Even and Odd Variables," *Physica*, Vol. 23, pp. 816–829.

Yong, Y., and Lin, Y. K., 1987, "Exact Stationary-Response Solution for Second-Order Nonlinear Systems Under Parametric and External White-Noise Excitations," ASME JOURNAL OF APPLIED MECHANICS, Vol. 54, pp. 414–418.

Downloaded 03 May 2010 to 171.66.16.21. Redistribution subject to ASME license or copyright; see http://www.asme.org/terms/Terms_Use.cfm

Experimental Observation of Amplitude- and Phase-Modulated Responses of Two Internally Coupled Oscillators to a Harmonic Excitation

A. H. Nayfeh
Department of Engineering Science and Mechanics,
Virginia Polytechnic Institute and State University,
Blacksburg, Virginia 24061

L. D. Zavodney
Department of Engineering Mechanics,
The Ohio State University,
Columbus, Ohio 43210

An experiment is performed on a two degree-of-freedom mechanical system having quadratic nonlinearities and linear natural frequencies ω_1 and ω_2 approximately in the ratio of two-to-one (i.e., $\omega_2 \approx 2\omega_1$). When the lower mode is excited by a harmonic excitation whose frequency Ω is nearly equal to ω_1, amplitude- and phase-modulated responses of the system have been observed for a range of the excitation frequency Ω, in qualitative agreement with the results of a second-order perturbation theory.

1 Introduction

Recently, the nonlinear response of internally coupled oscillators to a harmonic excitation have received considerable attention (Nayfeh and Mook, 1979; Nayfeh, 1988a). They model the nonlinear response of ships, elastic pendulums, robots, shells, arches, bowed structures, and beams and plates under static and dynamic loadings. If u_1 and u_2 are the generalized coordinates of the two linear normal modes, then the governing equations have the form

$$\ddot{u}_1 + \omega_1^2 u_1 + 2\mu_1 \dot{u}_1 + \delta_1 u_1^2 + \delta_2 u_1 u_2 + \delta_3 u_2^2 + \delta_4 \dot{u}_1^2 + \delta_5 \dot{u}_1 \dot{u}_2 + \delta_6 \dot{u}_2^2 + \delta_7 u_1 \ddot{u}_1 + \delta_8 u_2 \ddot{u}_1 + \delta_9 u_1 \ddot{u}_2 + \delta_{10} u_2 \ddot{u}_2 + (h_{11} u_1 + h_{12} u_2)\cos\Omega t = F \cos\Omega t \quad (1)$$

$$\ddot{u}_2 + \omega_2^2 u_2 + 2\mu_2 \dot{u}_2 + \alpha_1 u_1^2 + \alpha_2 u_1 u_2 + \alpha_3 u_2^2 + \alpha_4 \dot{u}_1^2 + \alpha_5 \dot{u}_1 \dot{u}_2 + \alpha_6 \dot{u}_2^2 + \alpha_7 u_1 \ddot{u}_1 + \alpha_8 u_2 \ddot{u}_1 + \alpha_9 u_1 \ddot{u}_2 + \alpha_{10} u_2 \ddot{u}_2 + (h_{12} u_1 + h_{22} u_2)\cos\Omega t = G \cos\Omega t \quad (2)$$

where only linear and quadratic terms have been retained. Here, ω_1 and ω_2 are the linear undamped natural frequencies of the system, Ω is the excitation frequency, the μ_n are the damping coefficients of the two modes, and F, G, Ω, ω_n, δ_n, α_n, and h_{mn} are constants.

In this paper, we consider the case $\omega_2 \approx 2\omega_1$ and $\Omega \approx \omega_1$. Special cases of the present problem were studied using various techniques by Sethna (1965), Nayfeh, Mook, and Marshall (1973), Yamamoto and Yasuda (1977), Sethna and Bajjaj (1978), Nayfeh and Mook (1979), Hatwal, Mallik, and Ghosh (1983), Haddow, Barr, and Mook (1984), Miles (1984), and Nayfeh (1988b). Four first-order ordinary differential equations that describe the modulation of the amplitudes and the phases of the interacting two modes were derived by Sethna (1965) and Miles (1984) using the method of averaging, and Nayfeh, Mook, and Marshall (1973), Haddow, Barr, and Mook (1984), and Nayfeh (1988b) using the method of multiple scales. These equations were used to determine the fixed points and their stability. The stable fixed points correspond to periodic responses. For some range of system and excitation parameters, Hopf bifurcations exist. The fixed points of the averaged equations lose their stability when the real part of a complex conjugate pair of eigenvalues changes sign from negative to positive. In these ranges, steady-state periodic responses do not exist. Instead, the response consists of amplitude- and phase-modulated motion, and for small damping the amplitude and phases may experience period-multiplying bifurcations and chaos. Sethna (1965) used an analog computer to integrate the averaged equations in this interval and found periodic amplitudes and phases. Nayfeh, Mook, and Marshall (1973) integrated a special form of equations (1) and (2) in this range and obtained amplitude- and phase-modulated responses. Later, Yamamoto and Yasuda (1977) observed amplitude- and phase-modulated responses in their analog-computer simulations of a special form of equations (1) and (2). Hatwal, Mallik, and Ghosh (1983) reported numerical results for a special form of equations (1) and (2) showing periodically modulated motions and chaos. Miles (1984) reported numerical calculations of the averaged equations showing chaotic and periodically modulated solutions. In this paper, we present an experimental observation of amplitude- and phase-modulated responses in a simple

Contributed by the Applied Mechanics Division for presentation at the Winter Annual Meeting, Chicago, IL, November 28 to December 2, 1988, of THE AMERICAN SOCIETY OF MECHANICAL ENGINEERS.

Discussion on this paper should be addressed to the Editorial Department, ASME, United Engineering Center, 345 East 47th Street, New York, N.Y. 10017, and will be accepted until two months after final publication of the paper itself in the JOURNAL OF APPLIED MECHANICS. Manuscript received by ASME Applied Mechanics Division, July 31, 1988; final revision, April 5, 1988.

Paper No. 88-WA/APM-52.

Copyright © 1988 by ASME
Downloaded 03 May 2010 to 171.66.16.21. Redistribution subject to ASME license or copyright; see http://www.asme.org/terms/Terms_Use.cfm

mechanical system, and present a second-order perturbation solution of equations (1) and (2).

2 Analysis

We use the method of multiple scales (Nayfeh, 1973, 1981) to determine a second-order uniform expansion of the solution of equations (1) and (2) when $\omega_2 \approx 2\omega_1$ and $\Omega \approx \omega_1$. To this end, we introduce a small dimensionless parameter ϵ as a bookkeeping device and seek a uniform expansion in the form

$$u_1 = \epsilon u_{11}(T_o, T_1) + \epsilon^2 u_{12}(T_o, T_1) + \ldots \quad (3)$$

$$u_2 = \epsilon u_{21}(T_o, T_1) + \epsilon^2 u_{22}(T_o, T_1) + \ldots \quad (4)$$

where $T_o = t$, a fast scale characterizing motions with the frequencies ω_1, ω_2, and Ω, and $T_1 = \epsilon t$, a slow scale characterizing the modulations of the amplitudes and phases with damping and the resonances. Moreover, we order the damping coefficients and the excitation amplitudes F and G so that their influence balances the nonlinearity. Consequently, we replace μ_n by $\epsilon\mu_n$ and F and G by ϵF and ϵG, respectively. Substituting equations (3) and (4) into equations (1) and (2) and equating coefficients of like powers of ϵ on both sides, we obtain

Order ϵ

$$D_o^2 u_{11} + \omega_1^2 u_{11} = 0 \quad (5)$$

$$D_o^2 u_{21} + \omega_2^2 u_{21} = 0 \quad (6)$$

Order ϵ

$$\begin{aligned} D_o^2 u_{12} + \omega_1^2 u_{12} = &-2D_o D_1 u_{11} - 2\mu_1 D_o u_{11} - \delta_1 u_{11}^2 - \delta_2 u_{11} u_{21} \\ &- \delta_3 u_{21}^2 - \delta_4 (D_o u_{11})^2 - \delta_5 D_o u_{11} D_o u_{21} - \delta_6 (D_o u_{21})^2 \\ &- \delta_7 u_{11} D_o^2 u_{11} - \delta_8 u_{21} D_o^2 u_{11} - \delta_9 u_{11} D_o^2 u_{21} - \delta_{10} u_{21} D_o^2 u_{21} \\ &- (h_{11} u_{11} + h_{12} u_{21}) \cos\Omega T_o + F \cos\Omega T_o \end{aligned} \quad (7)$$

$$\begin{aligned} D_o^2 u_{22} + \omega_2^2 u_{22} = &-2D_o D_1 u_{21} - 2\mu_2 D_o u_{21} - \alpha_1 u_{11}^2 - \alpha_2 u_{11} u_{21} \\ &- \alpha_3 u_{21}^2 - \alpha_4 (D_o u_{11})^2 - \alpha_5 D_o u_{11} D_o u_{21} - \alpha_6 (D_o u_{21})^2 \\ &- \alpha_7 u_{11} D_o^2 u_{11} - \alpha_8 u_{21} D_o^2 u_{11} - \alpha_9 u_{11} D_o^2 u_{21} - \alpha_{10} u_{21} D_o^2 u_{21} \\ &- (h_{21} u_{11} h_{22} u_{21}) \cos\Omega T_o + G \cos\Omega T_o \end{aligned} \quad (8)$$

where $D_n = \partial/\partial T_n$.

The general solution of equations (5) and (6) can be expressed as

$$u_{n1} = A_n(T_1)\exp(i\omega_n T_o) + cc \quad (9)$$

where cc stands for the complex conjugate of the preceding terms and the A_n are arbitrary functions of T_1 to this order of approximation; they are determined by imposing the solvability conditions (elimination of secular and small-divisor terms) at the next level of approximation.

To express quantitatively the nearness of the resonances, we introduce the detuning parameters σ_1 and σ_2 defined according to

$$\omega_2 = 2\omega_1 + \epsilon\sigma_1 \quad \text{and} \quad \Omega = \omega_1 + \epsilon\sigma_2 \quad (10)$$

Substituting equation (9) into equations (7) and (8) and using equations (10), we obtain

$$\begin{aligned} D_o^2 u_{12} + \omega_1^2 u_{12} = &-2i\omega_1(A_1' + \mu_1 \bar{A}_1) e^{i\omega_1 T_o} \\ &- 4\omega_1 \Lambda_1 A_2 \bar{A}_1 e^{i(\omega_1 T_o + \sigma_1 T_1)} + \frac{1}{2} F e^{i(\omega_1 T_o + \sigma_2 T_1)} + cc + NST \end{aligned} \quad (11)$$

$$\begin{aligned} D_o^2 u_{22} + \omega_2^2 u_{22} = &-2i\omega_2(A_2' + \mu_1 A_2) e^{i\omega_2 T_o} \\ &- 4\omega_2 \Lambda_2 A_1^2 e^{i(\omega_2 T_o - \sigma_1 T_1)} + cc + NST \end{aligned} \quad (12)$$

where the prime indicates the derivative with respect to T_1, NST stands for terms that do not produce secular terms, and

$$4\omega_1 \Lambda_1 = \delta_2 + \delta_5 \omega_1 \omega_2 - \delta_8 \omega_1^2 - \delta_9 \omega_2^2 \quad (13)$$

$$4\omega_2 \Lambda_2 = \alpha_1 - \alpha_4 \omega_1^2 - \alpha_7 \omega_1^2 \quad (14)$$

For a uniform expansion, the A_n must be chosen so that the terms in equations (11) and (12) that produce secular terms must vanish, thereby yielding the solvability conditions

$$2i\omega_1(A_1' + \mu_1 A_1) + 4\omega_1 \Lambda_1 A_2 \bar{A}_1 e^{i\sigma_1 T_1} - \frac{1}{2} F e^{i\sigma_2 T_1} = 0 \quad (15)$$

$$2i(A_2' + \mu_2 A_2) + 4\Lambda_2 A_1^2 e^{-i\sigma_1 T_1} = 0 \quad (16)$$

To analyze the solutions of equations (15) and (16), we express the A_n in the polar form

$$A_1 = \frac{1}{2} a_1 (\Lambda_1 \Lambda_2)^{-1/2} e^{i\beta_1}$$

and

$$A_2 = \frac{1}{2} a_2 (\Lambda_1)^{-1} e^{i\beta_2} \quad (17)$$

Substituting equations (17) into equations (15) and (16) and separating real and imaginary parts yields

$$a_1' = -\mu_1 a_1 - a_1 a_2 \sin\gamma_1 + f \sin\gamma_2 \quad (18)$$

$$a_2' = -\mu_2 a_2 + a_1^2 \sin\gamma_1 \quad (19)$$

$$a_1 \beta_1' = a_1 a_2 \cos\gamma_1 - f \cos\gamma_2 \quad (20)$$

$$a_2 \beta_2' = a_1^2 \cos\gamma_1 \quad (21)$$

where

$$\gamma_1 = \sigma_1 T_1 + \beta_2 - 2\beta_1, \quad \gamma_2 = \sigma_2 T_1 - \beta_1 \quad (22)$$

$$f = F\sqrt{\Lambda_1 \Lambda_2}/2\omega_1 \quad (23)$$

It turns out that for the physical systems mentioned above, $\Lambda_1 \Lambda_2 > 0$. If $\Lambda\Lambda_2 < 0$ and $\omega_2 \approx 2\omega_1$, the governing equations admit self-sustained oscillations in the absence of any excitation (i.e., $h_{mn} = 0$, $F = 0$, and $\sigma = 0$) in spite of the presence of positive damping. Therefore, to the first approximation, the solution of equations (1) and (2) is

$$u_1 \approx \frac{a_1(t)}{\sqrt{\Lambda_1 \Lambda_2}} \cos[\omega_1 t + \beta_1(t)],$$

$$u_2 \approx \frac{a_2(t)}{\Lambda_1} \cos[\omega_2 t + \beta_2(t)] \quad (24)$$

where the amplitudes a_n and phases β_n are governed by equations (18)–(22).

Equations (18)–(22) are generic and describe the behavior of the responses of all two degree-of-freedom systems with quadratic nonlinearities whose frequencies are in the ratio of two-to-one when the lower mode is excited by a primary excitation.

Periodic solutions of equations (1) and (2) correspond to the fixed points of equations (18)–(22), which in turn correspond to $a_1' = a_2' = 0$ and $\gamma_1' = \gamma_2' = 0$. It follows from equations (22) that

$$\beta_1' = \sigma_2 = \nu_1 \quad \text{and} \quad \beta_2' = 2\sigma_2 - \sigma_1 = \nu_2 \quad (25)$$

Then, the fixed points of equations (18)–(22) are given by

$$a_1^6 + 2(\mu_1\mu_2 - \nu_1\nu_2)a_1^4 + (\mu_1^2 + \nu_1^2)(\mu_2^2 + \nu_2^2)a_1^2 - f^2(\mu_2^2 + \nu_2^2) = 0 \quad (26)$$

and

$$a_2 = a_1^2(\mu_2^2 + \nu_2^2)^{-1/2} \quad (27)$$

The stability of a particular fixed point with respect to a perturbation proportional to $\exp(\lambda T_1)$ is determined by the zeros of

$$\begin{aligned} &\lambda^4 + 2(\mu_1 + \mu_2)\lambda^3 + (\mu_1^2 + \mu_2^2 + 4\mu_1\mu_2 + \nu_1^2 + \nu_2^2 - a_2^2 + 4a_1^2)\lambda^2 \\ &+ [2\mu_1\mu_2^2 + 2\mu_1^2\mu_2 + 2\mu_1\nu_2^2 + 2\mu_2\nu_1^2 - 2\mu_2 a_2^2 + 4(\mu_1 + \mu_2)a_1^2]\lambda \\ &+ \mu_1^2\mu_2^2 + \mu_1^2\nu_2^2 + \mu_2^2\nu_1^2 + \nu_1^2\nu_2^2 - \mu_2^2 a_2^2 - \nu_2^2 a_2^2 + 4\mu_1\mu_2 a_1^2 \\ &- 4\nu_1\nu_2 a_1^2 + 4a_1^4 = 0 \end{aligned} \quad (28)$$

According to the Routh-Hurwitz criterion, at least one root of equation (28) has a positive real part and, hence, a fixed point

Downloaded 03 May 2010 to 171.66.16.21. Redistribution subject to ASME license or copyright; see http://www.asme.org/terms/Terms_Use.cfm

given by equations (26) and (27) is unstable if all of the following conditions are not satisfied:

$$r_1 r_2 - r_3 > 0,\ r_3(r_1 r_2 - r_3) - r_1^2 r_4 > 0,\ r_4 > 0 \qquad (29)$$

where r_1, r_2, r_3, and r_4 are, respectively, the coefficients of λ^3, λ^2, λ^1, and λ^0 in equation (28). The violation of the second condition in (29) would imply the existence of a pair of complex conjugate λ with a positive real part, and hence replacing the inequality by an equality yields the parameters for the Hopf bifurcation.

Representative variations of a_1 and a_2 with σ_2 for given values of σ_1, μ_1, and μ_2 are shown in Fig. 1. The local stability of a fixed point is determined from conditions (29). The unstable parts are shown by the broken lines in Fig. 1. As one varies the control parameter σ_2 and hence Ω, the fixed points lose their stability in one of two ways: Either an eigenvalue crosses the imaginary axis into the right-half plane along the real axis or a pair of complex-conjugate eigenvalues cross the imaginary axis into the right-half plane. The first type of instability corresponds to the jump phenomenon, whereas the second type corresponds to the extensively studied problem of the Hopf bifurcation (Marsden and McCracken, 1976). Based on the Hopf-bifurcation theorem (Hale, 1963), the modulation equations (18)–(22) are expected to exhibit limit-cycle oscillations near the Hopf-bifurcation values Ω_1 and Ω_2. Sethna and Bajjaj (1978) carried out a bifurcation analysis for the latter case and determined the amplitudes of the limit cycles. Hence, the amplitudes a_n and phases β_n of u_1 and u_2 are expected to modulate with time and consequently, u_1 and u_2 are expected to be aperiodic. Sethna (1965) integrated the averaged equations using an analog computer in the interval $\Omega_1 \le \Omega \le \Omega_2$ and found that the a_n and β_n are periodic. A digital solution (Nayfeh, Mook, Marshall, 1973) of a special case of equations (1) and (2) for a value of Ω in the interval $\Omega_1 \le \Omega \le \Omega_2$ is shown in Fig. 2; it represents an amplitude- and phase-modulated motion. Similar results were obtained by Yamamoto and Yasuda (1977) and Nayfeh and Raouf (1987) using analog and digital simulations, respectively. Numerical solutions of equations (18)–(22) show that the limit-cycle solutions may undergo period-doubling bifurcations, leading to chaos (Miles, 1984).

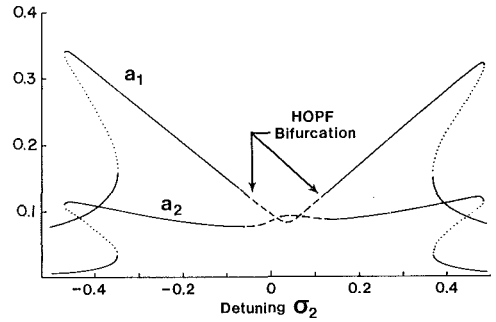


Fig. 1 Theoretically determined frequency-response curves when the excitation frequency is nearly equal to the lower frequency. $\sigma_1 = 0.08$, $\mu_1 = \mu_2 = 0.075$, $f = 0.075$: solid curves, stable; ...., unstable with at least one eigenvalue being positive; — — — —, unstable with the real part of a complex-conjugate pair of eigenvalues being positive.

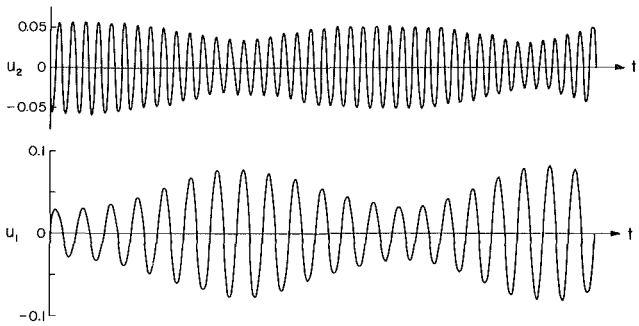


Fig. 2 The long-time behavior of a numerically calculated amplitude- and phase-modulated motion of a special case of equations (1) and (2): all δ_i and α_i are zero except $\delta_2 = -1$, $\alpha_1 = -1$, $\omega_1 = 0.5$, $\omega_2 = 1.0$, $\Omega = 0.5$, $\mu_1 = \mu_2 = 0.85$, $F = 0.001$, $G = 0$, and $h_{mn} = 0$.

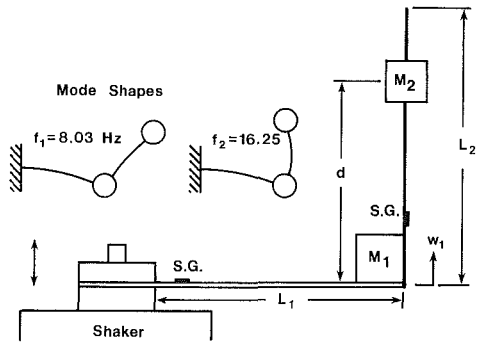


Fig. 3 Two degree-of-freedom model tuned for a 2:1 internal resonance and accompanying linear mode shapes. Beam 1: 1.651 mm x 12.83 mm x 158.7 mm, $\rho_1 = 0.164$ g/mm, $m_1 = 31.1$ g; Beam 2: 0.507 mm x 12.70 mm x 152.4 mm, $\rho_2 = 0.057$ g/mm, $m_2 = 40.0$ g; $d = 89.2$ mm.

3 Experiment

To observe these amplitude- and phase-modulated motions, we conducted an experiment using a mechanical system consisting of two light-weight beams and two concentrated masses as shown in Fig. 3 and described in Appendix A. A similar model was used by Haddow, Barr, and Mook (1984) to investigate some nonlinear phenomena; the parameters of their model are also given in Appendix A. The model was excited by a 250 lb electrodynamic shaker driven by a 2500 watt power amplifier. The shaker was driven by a sinusoidal waveform generated by a waveform synthesizer that has a 0.0001 Hz resolution. The response of the system to a harmonic excitation at the base is governed by a special form of equations (1) and (2). The lengths L_1 and d were adjusted so that the linear natural frequencies of the system were approximately in the ratio of two-to-one (i.e., $f_2 \approx 2f_1$). The linear resonant frequencies were determined by performing a routine modal analysis using random excitations to be $f_1 = 8.03$ Hz and $f_2 = 16.25$ Hz. Since the damping in the structure is very small, these resonant frequecies are very close to the linear natural frequencies. The associated mode shapes obtained from the theoretical analysis are also shown in Fig. 3. Relative displacements of the two masses were measured by strain gages mounted near the bases of the beams. The excitation frequency f was slowly varied (in steps of 0.0001 Hz) up and down between 7.6 Hz and 8.6 Hz while keeping all other parameters constant, including the table acceleration. The acceleration level of the table was kept constant by a digital computer that was used as a closed-loop feedback controller.

The response was analyzed using an FFT analyzer and the steady-state amplitudes a_1^* and a_2^* of the two modes comprising the total displacement w_1 of M_1 for the periodic cases were determined. They are plotted in Fig. 4 as a function of f. The a_i^* are measures that are proportional to the amplitudes a_i of the modes. This happens because in general, the governing partial differential equation is typically separated into spatial and temporal functions, such as

$$v(s, t) = \sum_i r\, \psi_i(s) G_i(t) \qquad (30)$$

where r is a scaling factor, the $\psi_i(s)$ are the spatial functions, typically the linear eigenfunctions, and the $G_i(t)$ are the tem-

Downloaded 03 May 2010 to 171.66.16.21. Redistribution subject to ASME license or copyright; see http://www.asme.org/terms/Terms_Use.cfm

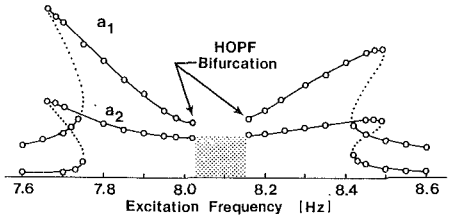


Fig. 4 Experimentally determined frequency-response curves when the excitation frequency f is near the first natural frequency $f_1 = 8.03$ Hz; the shaded region corresponds to aperiodic long-time motions. These amplitudes are proportional to the actual amplitudes of the modes of the structure.

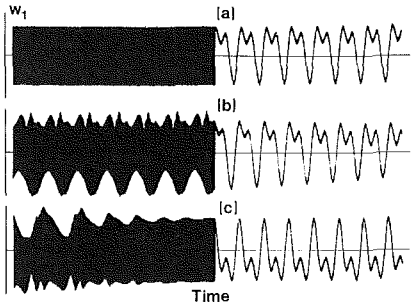


Fig. 5 Time traces of the displacement of mass M_1 before and after the bifurcation from periodic to aperiodic responses. The left portion shows the envelope of modulation by compressing time, and the right portion shows a sample with an expanded time scale; (a) $f = 8.02$ Hz, (b) $f = 8.03$ Hz, and (c) transition from $f = 8.15$ Hz to $f = 8.16$ Hz.

poral modulations, which appear as equations (1) and (2). The displacement of mass M_1 can be related to the surface strain at the base of beam 1 as measured by the strain gage provided the mode shape (eigenfunction) is known. Hence, we are measuring a discrete value of $\psi(s)$ to indicate the value of $\psi(L_1)$ which is dependent upon the mode shape; the magnitudes a_i^* will be proportional to the values of $\psi(s)$ at the gage location and will be scaled by r. The excitation frequencies marking the transition from periodic to aperiodic responses are marked in Fig. 4 as the Hopf-bifurcation points. The experimental results in this figure are qualitatively in agreement with the theoretically determined frequency-response curves in Fig. 1.

Representative time traces of the displacement w_1 of mass M_1 are shown in Fig. 5 before and after the Hopf bifurcation; this displacement is a linear combination of the generalized coordinates u_1 and u_2 of the two modes. The displacements of the individual modes obtained by filtering the signal are shown in Fig. 6. These experimentally-determined time traces are qualitatively in agreement with those obtained numerically and shown in Fig. 2. The constant-amplitude response that occurs before the bifurcation corresponds to a stable fixed point (point attractor) in the projection of the trajectory on the $a_2 - a_1$ plane. These amplitudes were simultaneously monitored on an osilloscope as the system experienced a bifurcation. The constant amplitude periodic motion gave rise to an aperiodic motion whose nature changed as the unstable region was penetrated. As the frequency approached the other "Hopf-bifurcation point," the aperiodic motion gave way to a constant amplitude periodic motion. Fig. 7 shows a projection of the long-time trajectory on the $u_2 - u_1$ plane. Before the bifurcation, the periodic response is stationary and appears as a "figure eight" since the nonlinearity adjusts the frequencies of the two modes so that the response period of one mode is exactly twice that of the other mode. Inside the unstable region the "figure eight" response is observed to evolve because the two modes are constantly exchanging energy.

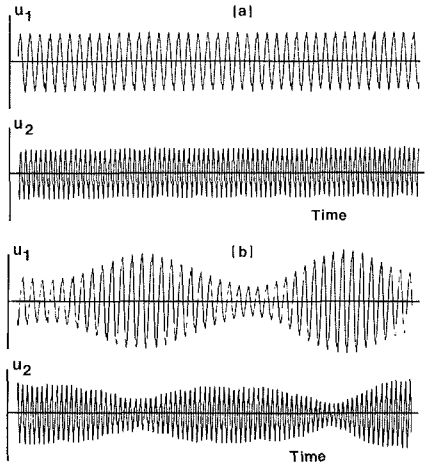


Fig. 6 Modal components of the displacement of mass M_1 as a function of time (a) before the bifurcation ($f = 8.02$ Hz) and (b) after the bifurcation ($f = 8.03$ Hz). These traces were filtered from the data of Fig. 5. The higher harmonics that appear most noticeably in u_2 are a consequence of the sampling frequency of the digital scope and were not present in the analogue waveform.

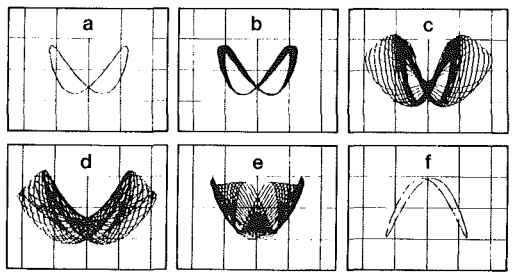


Fig. 7 Variation of the displacement u_2 of the second mode with the displacement u_1 of the first mode: (a) periodic motion before the bifurcation, $f = 8.02$ Hz; (b) aperiodic motion just after the bifurcation, $f = 8.025$ Hz; (c)-(e) aperiodic motion in the unstable region, $8.03 < f < 8.15$; and (f) return to a periodic motion $f = 8.16$ Hz. Only portions of a "complete cycle" are shown for the aperiodic responses because the overlapping of a complete cycle obscures the projection of the amplitude- and phase-modulated motion.

4 Summary

We have presented in this paper observations of amplitude- and phase-modulated responses of a two degree-of-freedom mechanical system with quadratic nonlinearities to a harmonic excitation. The linear natural frequencies of the system were tuned so that they were approximately in the ratio of two-to-one and the excitation frequency was slowly varied up and down around the lower natural frequency. We observed the transition from periodic to aperiodic motions, indicating the occurrence of a Hopt bifurcaton.

Acknowledgment

This work was supported by the Air Force Office of Scientific Research under Grant No. AFOSR-86-0090, and the National Science Foundation under Grant No. MSM-8521748.

References

Haddow, A. G., Barr, A. D. S., and Mook, D. T., 1984, "Theoretical and Experimental Study of Modal Interaction in a Two Degree-of-Freedom Structure," *Journal of Sound and Vibration*, Vol. 97, pp. 451-473.

Hale, J. K., 1963, *Oscillations in Nonlinear Systems*, McGraw-Hill, New York.

Hatwal, H., Mallik, A. K., and Ghosh, A., 1983, "Forced Nonlinear Oscilla-

Downloaded 03 May 2010 to 171.66.16.21. Redistribution subject to ASME license or copyright; see http://www.asme.org/terms/Terms_Use.cfm

tions of an Autoparametric System–Part 2: Chaotic Responses," ASME JOURNAL OF APPLIED MECHANICS, Vol. 50, pp. 663–668.

Marsden, J. E., and McCracken, M., 1976, *Hopf Bifurcation and its Applications*, Springer-Verlag, New York.

Miles, J. W., 1984, "Resonantly Forced Motion of Two Quadratically Coupled Oscillators," *Physica D*, Vol. 13, pp. 247–260.

Nayfeh, A. H., 1973, *Perturbation Methods*, Wiley, New York.

Nayfeh, A. H., 1981, *Introduction of Perturbation Techniques*, Wiley New York.

Nayfeh, A. H., 1988a, "Application of the Method of Multiple Scales to Nonlinearly Coupled Oscillators," Chapter for the Lasers, Molecules, and Methods, a Volume in the *Advances in Chemical Physics* Series, Wiley, New York.

Nayfeh, A. H., 1987b, "On the Undesirable Roll Characteristics of Ships in Regular Seas," *Journal of Ship Research*, Vol. 32, pp. 92–100.

Nayfeh, A. H., and Mook, D. T., 1979, *Nonlinear Oscillations*, Wiley, New York.

Nayfeh, A. H., Mook, D. T., and Marshall, L. R., 1973, "Nonlinear Coupling of Pitch and Roll Modes in Ship Motions," *Journal of Hydronautics*, Vol. 7, pp. 145–152.

Nayfeh, A. H., and Raouf, R. A., 1987, "Nonlinear Oscillation of Circular Cylindrical Shells," *International Journal of Solids and Structures*, Vol. 23, pp. 1625–1638.

Sethna, P. R., 1965, "Vibrations of Dynamical Systems with Quadratic Nonlinearities," ASME JOURNAL OF APPLIED MECHANICS, Vol. 32, pp. 576–582.

Sethna, P. R., and Bajaj, A. K., 1978, "Bifurcations in Dynamical Systems with Internal Resonance," ASME JOURNAL OF APPLIED MECHANICS, Vol. 43, pp. 895–902.

Yamamoto, T., and Yasuda, K., 1977, "On the Internal Resonance in a Nonlinear Two Degree-of-Freedom System (Forced Vibrations New the Lower Resonance Point When the Natural Frequencies are in the Ratio 1:2)," *Bulletin of the Japanese Society of Mechanical Engineering*, Vol. 20, pp. 168–175.

APPENDIX A

Description of the Model

The model was fabricated from mild steel according to the following dimensions (see Fig. 3): $L_1 = 158.7$ mm, $L_2 = 152.4$ mm, and $d = 89.2$ mm. The cross-sectional dimensions of beam 1 are 1.651 mm × 12.83 mm and beam 2 are 0.507 mm × 12.70 mm. The mass density per unit length are $\rho_1 = 0.164$ g/mm and $\rho_2 = 0.057$ g/mm. The cross-sectional dimensions of mass 1 are 19.0 mm × 19.0 mm and mass 2 are 15.9 mm × 12.7 mm. The depths are such that their total mass, including the mounting screws, is $m_1 = 31.1$ g and $m_2 = 40.0$ g. Using these dimensions, the frequency of the third mode (characterized by the out-of-plane motion of beam 2 caused by the torsion of beam 1) is far removed from the frequency of the second mode; hence a two-mode formulation is adequate to describe the response of the model. We have conducted experiments with similar models whose dimensions are more than twice those of this model; all that is required is the two-to-one internal resonance and higher resonances far removed.

The model tested by Haddow, Barr, and Mook (1984) has the following parameters:

Beam 1, 3.2 mm × 25.1 mm × 263 mm, total mass = 204 g, $m_1 = 170$g

Beam 2, 1.6 mm × 25.1 mm × 181 mm, total mass = 57 g, $m_2 = 190$g

$$d = 172 \text{ mm}$$

APPENDIX B

Description of Test Procedure

The test model was excited by a 250 lb electrodynamic shaker driven by a 2500 watt power amplifier. Sinusoidal waveforms used to drive the shaker were generated by a waveform synthesizer that had a 0.0001 Hz resolution. Frequency sweeps were made in small steps of 0.0001 Hz to minimize the transient response. The acceleration level of the table was held constant (as the frequency was swept) by a digital computer used as a closed-loop feedback controller. The amplitude of each mode was monitored on an FFT analyzer. The natural frequencies and mode shapes were obtained by performing a routine modal analysis using a random excitation. The linear natural frequencies were varied by adjusting the lengths L_1 and d. A schematic of the experimental setup is shown in Fig. 8.

Since any one transducer location will detrct one mode more directly than another mode, the amplitudes of the responses shown in Figs. 4, 5, 6, and 7 are to be understood as being proportional to the amplitude of the mode, not a direct measurement of the mode. For this reason, no scale is put on these plots. To determine the direct amplitudes would require a nonlinear parametric identification of the model, which is beyond the scope of this paper. During the large amplitude response shown in Fig. 4, the peak-to-peak amplitude of M_1 was on the order of 5 mm, or approximately 3 percent of L_1.

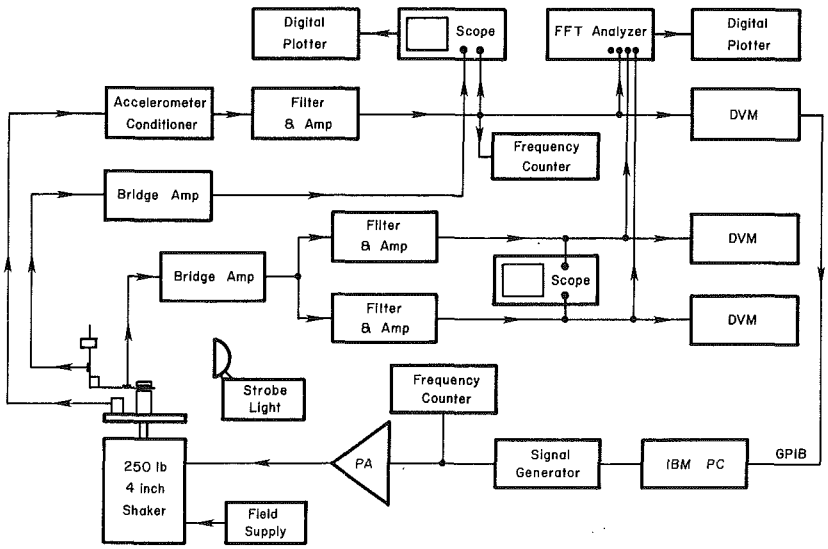


Fig. 8 A schematic of the experimental setup

Downloaded 03 May 2010 to 171.66.16.21. Redistribution subject to ASME license or copyright; see http://www.asme.org/terms/Terms_Use.cfm

T. R. Kane
Professor of Applied Mechanics,
Stanford University,
Stanford, California
Fellow ASME

D. A. Levinson
Research Scientist,
Lockheed Palo Alto Research Laboratory,
Palo Alto, California
Mem. ASME

A Method for Testing Numerical Integrations of Equations of Motion of Mechanical Systems

It is common practice to use conservation principles, such as the principles of conservation of energy or angular momentum, to test results of numerical integrations of differential equations of motion of mechanical systems. This paper deals with a testing method that can be used even when no conservation principle is applicable.

1 Introduction

When one performs a numerical integration of differential equations governing the behavior of a mechanical system, one generally is using this solution method because one is unable to obtain desired information by any other means; that is, the equations cannot be solved in closed form. Now, the results of numerical integrations, like those generated by any other complex computational procedure, cannot be taken at face value: the equations being solved may be incorrect, a mistake having been made in their formulation; the equations may be correct, but coded improperly; or the integration procedure may be flawed. Therefore, it is always advisable to test numerical integration results by all available means.

One familiar method for testing numerical integration results is to make use of known integrals of the differential equations under consideration. For instance, it may be possible to appeal to the principle of conservation of energy to obtain a relationship between the time t, the dependent variables, and the first time-derivatives of the dependent variables. Consider, for example, the motion of a particle P (see Fig. 1) that is constrained to remain on a circular wire W which is made to made to rotate with an angular speed $\Omega(t)$ about a fixed, vertical axis passing through the center O of W and lying in the plane of W. Let m be the mass of P, R the radius of W, q_1 the angle between the vertical and line OP, and u_1 the first time-derivative of q_1; and suppose, first, that Ω is permanently equal to zero, that is, that W is kept at rest, and that W is perfectly smooth, so that P is free to slide on W. Under these circumstances, the equations of motion of P are

$$\dot{q}_1 = u_1 \tag{1}$$

and

$$\dot{u}_1 = -(g/R)\sin q_1 \tag{2}$$

where g is the acceleration of gravity. A numerical integration of these equations can be tested by evaluating at each integration step the quantity E defined as

$$E = -mgR\cos q_1 + \frac{1}{2}m(Ru_1)^2 \tag{3}$$

which, being the total mechanical energy of P, that is, the sum of P's potential and kinetic energy, should remain constant. Similarly, if Ω, rather than being equal to zero, has a constant value, say $\bar{\Omega}$, that is, W is made to rotate with a constant angular speed, then equation (2) gives way to

$$\dot{u}_1 = -(g/R)\sin q_1 + \frac{1}{2}\bar{\Omega}^2 \sin 2q_1 \tag{4}$$

and the Hamiltonian function H, here given by

$$H = -mgR\cos q_1 + \frac{1}{2}m(Ru_1)^2 - \frac{1}{2}m(R\bar{\Omega}\sin q_1)^2 \tag{5}$$

must remain constant.

Frequently, neither the total energy of a system nor the

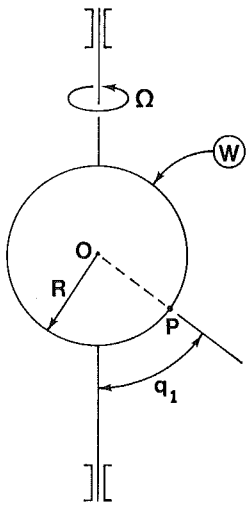


Fig. 1 Particle on a rotating circular wire

Contributed by the Applied Mechanics Division for publication in the JOURNAL OF APPLIED MECHANICS.
Discussion on this paper should be addressed to the Editorial Department, ASME, United Engineering Center, 345 East 47th Street, New York, N.Y. 10017, and will be accepted until two months after final publication of the paper itself in the JOURNAL OF APPLIED MECHANICS. Manuscript received by ASME Applied Mechanics Division, November 24, 1987; final revision, March 1, 1988.

Copyright © 1988 by ASME
Downloaded 03 May 2010 to 171.66.16.21. Redistribution subject to ASME license or copyright; see http://www.asme.org/terms/Terms_Use.cfm

system's Hamiltonian remains constant. For the particle P just considered, this is the case whenever $\dot{\Omega}$ differs from zero, for equation (2) or equation (4) then must be replaced with

$$\dot{u}_1 = -(g/R)\sin q_1 + \frac{1}{2}\Omega^2 \sin 2q_1 \tag{6}$$

and, with E and H given by equations (3) and (5), neither $\dot{E}$ nor $\dot{H}$ then vanishes. It is the purpose of this paper to show how one can test a numerical integration of the equations of motion in such situations.

The sequel is arranged as follows. In section 2, a six step method for testing numerical integrations of equations of motion is set fourth in detail. The rationale underlying the method is explained in section 3, and illustrative examples are discussed in section 4.

2 Method

Given a simple nonholonomic system S possessing generalized coordinates $q_r (r=1, \ldots, n)$ in a Newtonian reference frame N and subject to $n-p$ motion constraints,

(1) let $u_r (r=1, \ldots, n)$ denote generalized speeds defined in such a way that

$$\dot{q}_s \triangleq \sum_{r=1}^{n} W_{sr} u_r + X_s \quad (s=1, \ldots, n) \tag{7}$$

where W_{sr} and X_s are functions of $q_1, \ldots, q_n$, and t, the time; and number the generalized speeds in such a way that the motion constraints can be expressed as

$$u_k = \sum_{r=1}^{p} A_{kr} u_r + B_k \quad (k=p+1, \ldots, n) \tag{8}$$

where A_{kr} and B_k are functions of $q_1, \ldots, q_n$, and t;

(2) find functions $V(q_1, \ldots, q_n, t)$ and $G_r(q_1, \ldots, q_n; u_1, \ldots, u_p; t)$ $(r=1, \ldots, p)$ such that the nonholonomic generalized active forces $\tilde{F}_r$ $(r=1, \ldots, p)$ are given by

$$\tilde{F}_r = -\sum_{s=1}^{n} \frac{\partial V}{\partial q_s}\left(W_{sr} + \sum_{k=p+1}^{n} W_{sk} A_{kr}\right) + G_r \quad (r=1, \ldots, p) \tag{9}$$

while

$$\frac{\partial V}{\partial t} + \sum_{s=1}^{n} \frac{\partial V}{\partial q_s}\left(X_s + \sum_{k=p+1}^{n} W_{sk} B_k\right) = 0 \tag{10}$$

(If S is a *holonomic* system, $\tilde{F}_r$ in equation (9) is replaced with F_r, the holonomic generalized active force associated with u_r, and the second summation is omitted.)

(3) after expressing the kinetic energy K of S in N as a function of $q_1, \ldots, q_n, u_1 \ldots, u_p$, and t, identify functions K_0, K_1, K_2 of $q_1, \ldots, q_n$, $u_1, \ldots, u_p$, and t, with K_i homogeneous and of degree i $(i=0, 1, 2)$ in $u_1, \ldots, u_p$, such that K is given by

$$K = K_0 + K_1 + K_2 \tag{11}$$

(4) let Z denote a function of t that satisfies the differential equation

$$\dot{Z} = -\sum_{r=1}^{p} G_r u_r + \frac{\partial K}{\partial t} + \sum_{s=1}^{n} \frac{\partial K}{\partial q_s}\left(X_s + \sum_{k=p+1}^{n} W_{sk} B_k\right) \tag{12}$$

(5) introduce the *checking function* C as

$$C \triangleq V + Z + K_2 - K_0 \tag{13}$$

(6) integrate equation (12) simultaneously with equations (7) and the p dynamical differential equations governing all motions of S in N. If C fails to remain constant, at least some of the integration results are incorrect. If C remains constant, this does not guarantee the validity of the integration results; but it may be regarded as reassuring.

3 Rationale

Multiplication of both sides of equation (9) with u_r and subsequent summation yields

$$\sum_{r=1}^{p} \tilde{F}_r u_r = -\sum_{r=1}^{p} \left[\sum_{s=1}^{n} \frac{\partial V}{\partial q_s}\left(W_{sr} + \sum_{k=p+1}^{n} W_{sk} A_{kr}\right)\right] u_r + \sum_{r=1}^{p} G_r u_r \tag{14}$$

or, equivalently,

$$-\sum_{r=1}^{p} \tilde{F}_r u_r = \sum_{s=1}^{n} \left[\frac{\partial V}{\partial q_s} \sum_{r=1}^{p} \left(W_{sr} + \sum_{k=p+1}^{n} W_{sk} A_{kr}\right) u_r\right] - \sum_{r=1}^{p} G_r u_r \tag{15}$$

Now,

$$\sum_{r=1}^{p} \left(W_{sr} + \sum_{k=p+1}^{n} W_{sk} A_{kr}\right) u_r = \sum_{r=1}^{p} W_{sr} u_r + \sum_{k=p+1}^{n} W_{sk} \sum_{r=1}^{p} A_{kr} u_r \tag{16}$$

which, in view of equation (8), can be rewritten

$$\sum_{r=1}^{p} \left(W_{sr} + \sum_{k=p+1}^{n} W_{sk} A_{kr}\right) u_r = \sum_{r=1}^{p} W_{sr} u_r + \sum_{k=p+1}^{n} W_{sk} (u_k - B_k) \tag{17}$$

or, equivalently,

$$\sum_{r=1}^{p} \left(W_{sr} + \sum_{k=p+1}^{n} W_{sk} A_{kr}\right) u_r = \sum_{r=1}^{n} W_{sr} u_r - \sum_{k=p+1}^{n} W_{sk} B_k \tag{18}$$

whereupon elimination of the first sum by reference to equation (7) yields

$$\sum_{r=1}^{p} \left(W_{sr} + \sum_{k=p+1}^{n} W_{sk} A_{kr}\right) u_r = \dot{q}_s - \left(X_s + \sum_{k=p+1}^{n} W_{sk} B_k\right) \quad (s=1, \ldots, n) \tag{19}$$

Returning to equation (15), one thus finds that

$$-\sum_{r=1}^{p} \tilde{F}_r u_r = \sum_{s=1}^{n} \frac{\partial V}{\partial q_s}\left[\dot{q}_s - \left(X_s + \sum_{k=p+1}^{n} W_{sk} B_k\right)\right] - \sum_{r=1}^{p} G_r u_r \tag{20}$$

or, equivalently,

$$-\sum_{r=1}^{p} \tilde{F}_r u_r = \dot{V} - \left[\frac{\partial V}{\partial t} + \sum_{s=1}^{n} \frac{\partial V}{\partial q_s}\left(X_s + \sum_{k=p+1}^{n} W_{sk} B_k\right)\right] - \sum_{r=1}^{p} G_r u_r \tag{21}$$

Hence, when equation (10) is satisfied, in which event the expression within the square brackets vanishes, then

$$-\sum_{r=1}^{p} \tilde{F}_r u_r = \dot{V} - \sum_{r=1}^{p} G_r u_r \tag{22}$$

In accordance with equations (5.6.15) and (5.6.25) of Kane

Downloaded 03 May 2010 to 171.66.16.21. Redistribution subject to ASME license or copyright; see http://www.asme.org/terms/Terms_Use.cfm

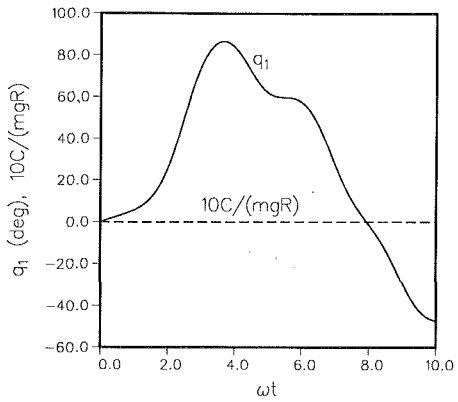


Fig. 2 Correct integration results; correct indication of validity

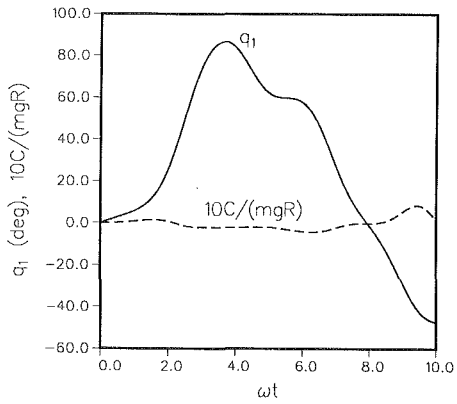


Fig. 4 Correct integration results; false indication of invalidity

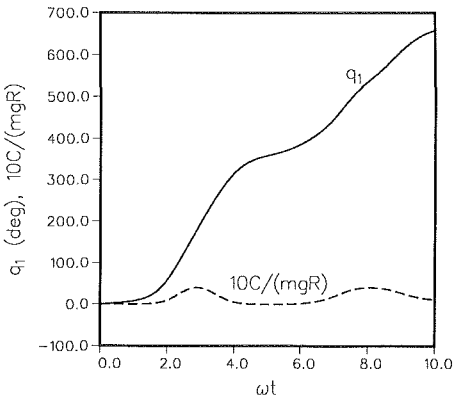


Fig. 3 Incorrect integration results; correct indication of invalidity

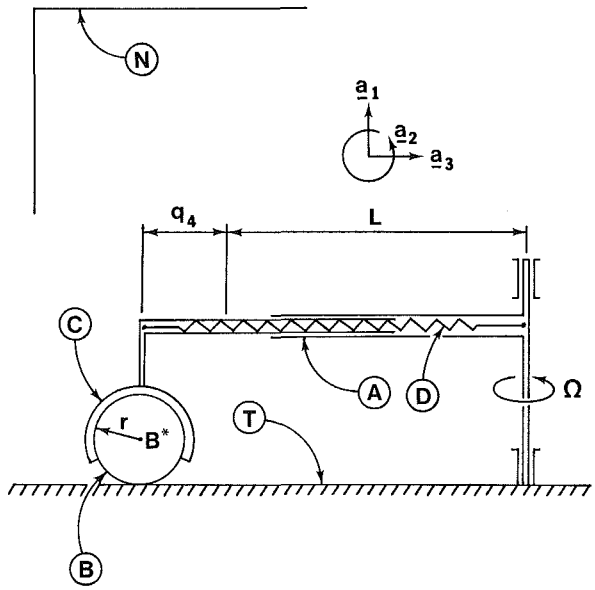


Fig. 5 Nonholonomic, dissipative, two-degree-of-freedom system

and Levinson (1985), the nonholonomic generalized inertia forces $\tilde{F}_r^*$ corresponding to u_r $(r=1, \ldots, p)$ satisfy the equation

$$-\sum_{r=1}^{p} \tilde{F}_r^* u_r = \dot{K}_2 - \dot{K}_0 + \frac{\partial K}{\partial t} + \sum_{s=1}^{n} \frac{\partial K}{\partial q_s}\left(X_s + \sum_{k=p+1}^{n} W_{sk} B_k\right) \tag{23}$$

Addition of this equation to equation (22) leads to

$$-\sum_{r=1}^{n} (\tilde{F}_r + \tilde{F}_r^*) u_r = \dot{V} - \sum_{r=1}^{p} G_r u_r + \dot{K}_2 - \dot{K}_0 + \frac{\partial K}{\partial t} + \sum_{s=1}^{n} \frac{\partial K}{\partial q_s}\left(X_s + \sum_{k=p+1}^{n} W_{sk} B_k\right) \tag{24}$$

or, when $\dot{Z}$ is given by equation (12), to

$$-\sum_{r=1}^{n} (\tilde{F}_r + \tilde{F}_r^*) u_r = \dot{V} + \dot{Z} + \dot{K}_2 - \dot{K}_0 \tag{25}$$

The law of motion $\tilde{F}_r + \tilde{F}_r^* = 0$ $(r=1, \ldots, p)$ [see Kane and Levinson (1985), equation (6.1.1)] guarantees that the left-hand member of equation (25) vanishes for all values of r throughout all motions of S in N; and the right-hand member of this equation is the first time-derivative of C as defined in equation (13). Consequently, $0 = \dot{C}$, which means that C remains constant throughout all motions of S in N.

4 Examples

The particle P considered in section 1 can be regarded as a system S free of motion constraints, so that $n-p=0$, and S possesses a single generalized coordinate, q_1, in a Newtonian reference frame, which means that $n=1$ and, hence, $p=1$. If a generalized speed u_1 is introduced as the first time-derivative of q_1, then equation (1) plays the role of equation (7), and comparison of these two equations shows that

$$W_{11} = 1, \qquad X_1 = 0 \tag{26}$$

The generalized active force F_1 is given by

$$F_1 = -mgR \sin q_1 \tag{27}$$

Hence, if V and G_1 are taken to be

$$V = -mgR\cos q_1, \qquad G_1 = 0 \tag{28}$$

then equations (9) and (10) are satisfied.

The kinetic energy of P can be written

$$K = \frac{1}{2} mR^2 [u_1^2 + (\Omega \sin q_1)^2] \tag{29}$$

which shows that

$$K_0 = \frac{1}{2} m (R\Omega \sin q_1)^2, \quad K_1 = 0, \quad K_2 = \frac{1}{2} m (Ru_1)^2 \tag{30}$$

Equation (12) requires that Z satisfy the differential equation [see equations (26), (28), and (29) for W_{11}, X_1, G_1, and K]

$$\dot{Z} = mR^2 \Omega \dot{\Omega} \sin^2 q_1 \tag{31}$$

Downloaded 03 May 2010 to 171.66.16.21. Redistribution subject to ASME license or copyright; see http://www.asme.org/terms/Terms_Use.cfm

and C, formed in accordance with equation (13), is given by [see equations (28) and (30) for V, K_0 and K_2]

$$C = -mgR\cos q_1 + Z + \frac{1}{2}m(Ru_1)^2 - \frac{1}{2}m(R\Omega\sin q_1)^2 \quad (32)$$

Suppose now that W is being made to perform an oscillatory motion such that

$$\Omega = 2\omega\sin\omega t \quad (33)$$

where ω is defined as $\omega \triangleq \sqrt{g/R}$, and that it is desired to determine the motion that takes place while $0 \le \omega t \le 10$ if, at $t = 0$, q_1 and u_1 are equal to zero and 0.1ω, respectively. To find q_1 as a function of t, we let the initial value of Z be the initial value of $K_0 - K_2 - V$, which guarantees that C is initially equal to zero [see equation (13)]; integrate equations (1), (6), and (31) simultaneously, referring to equation (33) for Ω, and, accordingly, taking $\dot{\Omega} = 2\omega^2\cos\omega t$; use equation (32) to evaluate C; and plot q_1 and the dimensionless quantity $10C/(mgR)$ as functions of ωt, as shown in Fig. 2, which suggests strongly that C remains equal to zero throughout the time interval under consideration. The reason for working with $10C$ rather than C, itself, is that this renders departures of C from zero more clearly visible than they would be otherwise. In the case at hand, however, it does not matter, for the largest value of $|C/(mgR)|$ that is actually encountered in the course of the numerical integration, while differing from zero as a consequence of unavoidable roundoff errors, is smaller than 10^{-8}. Thus, Fig. 2 is representative of situations in which use of the present method strengthens one's confidence in the validity of results of a numerical integration.

Use of an incorrect dynamical differential equation, one that has become so as the result of the intentional introduction of a defect, permits us to illustrate the capability of our method to bring errors to light. To demonstrate this, we replace equation (6) with (note the sign of the leading term)

$$\dot{u}_1 = (g/R)\sin q_1 + \frac{1}{2}\Omega^2\sin 2q_1 \quad (34)$$

and then proceed exactly as before, thus obtaining the plots in Fig. 3. Here it is immediately evident that C fails to remain constant throughout the integration, and the variation in C cannot be attributed to roundoff errors. Hence, the results must be regarded as suspect. But in situations of this kind, one cannot be certain that the motion simulation, per se, is flawed, for it may be an error in the equation governing Z that is the culprit. For instance, using once again equations (1) and (6), that is, correct kinematical and dynamical differential equations, but replacing equation (31) with

$$\dot{Z} = mR^2\Omega\dot{\Omega}\sin q_1 \quad (35)$$

one arrives at the plots in Fig. 4. Here, the q_1 curve is the same as in Fig. 2, that is, correct, despite the fact that the $10C/(mgR)$ curve signals trouble.

The absence of motion constraints, the fact that S possesses but one degree of freedom, and the use of $\dot{q}_1$ as a generalized speed render the example just considered somewhat degenerate. Consequently, this example fails to provide the opportunity to illuminate some of the quantities appearing in equations (7)–(13). Moreover, an issue of particular interest in connection with the method set forth in section 2, namely, the accommodation of energy dissipation mechanisms, has not yet been addressed. Therefore, we now turn to an example that permits us to fill these lacunae.

Figure 5 is a schematic representation of a system S formed by three rigid bodies, A, B, and C, and a linear spring D. Body A is a tube rigidly attached to a vertical shaft whose axis is fixed in a Newtonian reference frame N and that is made to rotate about this axis with a prescribed angular speed $\Omega(t)$; B is a homogeneous sphere of radius r and mass M, in contact

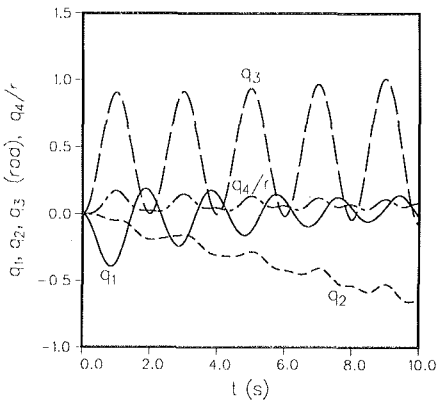


Fig. 6 Response curves for the system shown in Fig. 5

with a rigid, horizontal table T; C, which connects A and B, consists of two parts, namely, a rod coaxial with A, and free to slide in A (but not able to rotate relative to A), and a hemispherical shell that serves as a housing for B; and D, which has a spring constant σ and a natural length L, connects A and C as shown in the figure. The masses of A, C, and D are negligible.

Motion constraints come into play if one focuses attention on motions of S such that B rolls on T without slipping; and one can bring energy dissipation into the picture by assuming that the surfaces of B and the hemispherical portion of C are separated by a thin fluid film such that the set of contact forces exerted by C on B can be regarded as equivalent to a force applied to B at B^*, the center of B, together with a couple whose torque is equal to $-\delta^C\omega^B$, where δ is a constant and ${}^C\omega^B$ is the angular velocity of B in C.

Since the motion of A in N is prescribed, all one needs to do in order to arrive at a complete description of the motion of S in N as a function of time t is to determine the orientation of B in A and the distance from the axis of rotation of A to point B^*. To this end, one can introduce as generalized coordinates q_1, q_2, q_3, the radian measures of three orientation angles, and as a generalized coordinate q_4, a distance, as follows. Let $\mathbf{a}_1$, $\mathbf{a}_2$, $\mathbf{a}_3$ be a dextral set of mutally perpendicular unit vectors fixed in A and oriented as shown in Fig. 5; $\mathbf{b}_1$, $\mathbf{b}_2$, $\mathbf{b}_3$ a similar set fixed in B; and, after aligning $\mathbf{b}_i$ with $\mathbf{a}_i$ ($i = 1, 2, 3$), subject B to successive rotations relative to A, these rotations characterized by the vectors $q_1\mathbf{b}_1$, $q_2\mathbf{b}_2$, $q_3\mathbf{b}_3$; and let q_4 be such that the distance from the axis of rotation of A to point B^* is equal to $L + q_4$. In addition, define generalized speeds u_i ($i = 1, 2, 3$) as

$$u_i \triangleq {}^N\omega^B \cdot \mathbf{a}_i \quad (i = 1,2,3) \quad (36)$$

where ${}^N\omega^B$ is the angular velocity of B in N, and a generalized speed u_4 as

$$u_4 \triangleq \dot{q}_4 \quad (37)$$

Note that, if B is to roll on T without slipping, u_3 and u_4 must satisfy the nonholonomic constraint equations

$$u_3 = \frac{L + q_4}{r}\Omega, \quad u_4 = ru_2 \quad (38)$$

which here play the role of equation (8); that is, $n = 4$, $p = 2$, and

$$A_{31} = 0, \qquad A_{32} = 0, \qquad B_3 = \frac{L + q_4}{r}\Omega \quad (39)$$

while

$$A_{41} = 0, \qquad A_{42} = r, \qquad B_4 = 0 \quad (40)$$

Downloaded 03 May 2010 to 171.66.16.21. Redistribution subject to ASME license or copyright; see http://www.asme.org/terms/Terms_Use.cfm

Next, verify that the time-derivatives of $q_1, \ldots, q_4$ are related to $u_1, \ldots, u_4$ as in equation (7); that is, with s_i and c_i used as abbreviations for sin q_i and cos q_i, respectively, the kinematical differential equations for S are

$$\dot{q}_1 = (c_2 u_1 + s_1 s_2 u_2 - c_1 s_2 u_3)/c_2 - \Omega \tag{41}$$

$$\dot{q}_2 = c_1 u_2 + s_1 u_3 \tag{42}$$

$$\dot{q}_3 = (-s_1 u_2 + c_1 u_3)/c_2 \tag{43}$$

$$\dot{q}_4 = u_4 \tag{44}$$

so that W_{sr} $(s, r = 1, \ldots, 4)$ are given by

$$W_{11} = 1 \quad W_{12} = s_1 s_2/c_2 \quad W_{13} = -c_1 s_2/c_2 \quad W_{14} = 0 \tag{45}$$

$$W_{21} = 0 \quad W_{22} = c_1 \quad W_{23} = s_1 \quad W_{24} = 0 \tag{46}$$

$$W_{31} = 0 \quad W_{32} = -s_1/c_2 \quad W_{33} = c_1/c_2 \quad W_{34} = 0 \tag{47}$$

$$W_{41} = 0 \quad W_{42} = 0 \quad W_{43} = 0 \quad W_{44} = 1 \tag{48}$$

and

$$X_1 = -\Omega, \quad X_2 = 0, \quad X_3 = 0, \quad X_4 = 0 \tag{49}$$

Finally, we use the law of motion $\tilde{F}_r + \tilde{F}_r^* = 0$ with $r = 1,2$ to write the two dynamical differential equations of motion

$$\frac{2}{5} Mr^2 \dot{u}_1 + \delta(u_1 - \Omega) = 0 \tag{50}$$

$$\frac{7}{5} Mr^2 [\dot{u}_2 - (L + q_4)\Omega^2/r] + \sigma r q_4 + \delta u_2 = 0 \tag{51}$$

Given $\Omega(t)$ and the values of $q_1, \ldots, q_4$, u_1, and u_2 at $t = 0$, one can now obtain a complete description of the motion of S for $t > 0$ by numerically integrating equations (41)–(44), (50), and (51) simultaneously. Suppose, for example, that

$$M = 0.2 \text{ kg}, \quad r = 0.3 \text{ m}, \quad L = 0.4 \text{ m} \tag{52}$$

while

$$\sigma = 0.280\,\pi^2 \text{ N/m}, \quad \delta = 0.00252\,\pi \text{ Nms/rad} \tag{53}$$

and, with t in seconds, Ω is given in radians per second by

$$\Omega = \sin \pi t \tag{54}$$

Then, if $q_1, \ldots, q_4, u_1$, and u_2 all vanish at $t = 0$, the plots in Fig. 6 show how q_1, q_2, q_3, and q_4/r behave as functions of t during the first ten seconds of the motion of S.

To test the results reported in Fig. 6, we note, first, that if V, G_1, and G_2 are taken to be

$$V = \frac{1}{2}\sigma q_4^2, \quad G_1 = -\delta(u_1 - \Omega), \quad G_2 = -\delta u_2 \tag{55}$$

then equations (9) and (10) are satisfied. Next, the kinetic energy of S in N can be written

$$K = \frac{1}{2} Mr^2 \left\{ u_2^2 + \left[\frac{\Omega(L + q_4)}{r} \right]^2 \right\} + \frac{1}{5} Mr^2 \left\{ u_1^2 + u_2^2 + \left[\frac{\Omega(L + q_4)}{r} \right]^2 \right\} \tag{56}$$

so that, in accordance with equation (11),

$$K_0 = \frac{7}{10} M[\Omega(L + q_4)]^2, \quad K_1 = 0, \quad K_2 = \frac{1}{10} Mr^2(2u_1^2 + 7u_2^2) \tag{57}$$

while

$$\frac{\partial K}{\partial t} = \frac{7}{5} M(L + q_4)^2 \Omega \dot{\Omega} \tag{58}$$

Consequently, equation (12) leads to

$$\dot{Z} = \delta[(u_1 - \Omega)u_1 + u_2^2] + \frac{7}{5} M\Omega\dot{\Omega}(L + q_4)^2 \tag{59}$$

and, from equation (13), the checking function C is

$$C = \frac{1}{2}\sigma q_4^2 + Z + \frac{1}{10} Mr^2(2u_1^2 + 7u_2^2) - \frac{7}{10} M[\Omega(L + q_4)]^2 \tag{60}$$

When equation (59) is numerically integrated simultaneously with equations (41)–(44), (50), and (51), with Z arbitrarily set equal to zero at $t = 0$, it is found that the absolute value of C as given by equation (60) remains smaller than 10^{-11} throughout the time interval $0 \le t \le 10$ s, which is reassuring as regards the results reported in Fig. 6.

5 Conclusion

As the last example shows, use of the method at hand permits one to deal straightforwardly with systems involving energy dissipation; and the method encompasses nonholonomic systems, as well as systems with moving constraints. Thus, it may be regarded as a generalization of the idea of using an energy integral to test the results of numerical integrations of equations of motion of mechanical systems.

Reference

Kane, T. R., and Levinson, D. A., 1985, *Dynamics: Theory and Applications*, McGraw-Hill Book Co., New York, p. 158.

Downloaded 03 May 2010 to 171.66.16.21. Redistribution subject to ASME license or copyright; see http://www.asme.org/terms/Terms_Use.cfm

Approximate Decoupling of the Equations of Motion of Linear Underdamped Systems

S. M. Shahruz
F. Ma
Mem. ASME

Department of Mechanical Engineering
University of California
Berkeley, CA 94720

One common procedure in the solution of a normalized damped linear system with small off-diagonal damping elements is to replace the normalized damping matrix by a selected diagonal matrix. The extent of approximation introduced by this method of decoupling the system is evaluated, and tight error bounds are derived. Moreover, if the normalized damping matrix is diagonally dominant, it is shown that decoupling the system by neglecting the off-diagonal elements indeed minimizes the error bound.

1 Introduction

The equations of motion of an n-degree-of-freedom linear system under external excitation can be written as

$$\mathbf{M}\ddot{x}+\mathbf{C}\dot{x}+\mathbf{K}x=f(t),x(0)=x_0,\dot{x}(0)=\dot{x}_0,t\geq 0, \quad (1.1)$$

where the mass matrix $\mathbf{M}$, the damping matrix $\mathbf{C}$, and the stiffness matrix $\mathbf{K}$ are of order $n\times n$; the displacement vector $x(t)$ and the external excitation $f(t)$ are n-dimensional vectors. For passive systems, the matrices $\mathbf{M}$, $\mathbf{C}$, and $\mathbf{K}$ are symmetric and positive definite.

Let $\mathbf{U}$ denote the $n\times n$ modal matrix (see, e.g., Meirovitch, 1967; Müller and Schiehlen, 1985) corresponding to the system (1.1). The modal matrix is a nonsingular matrix whose columns are the eigenvectors of the symmetric generalized eigenvalue problem

$$\mathbf{K}u^{(i)}=\omega_i^2\mathbf{M}u^{(i)}, \quad (1.2)$$

where $\omega_i^2>0$ and $u^{(i)}$, $i=1,\ldots,n$, are the eigenvalues and the corresponding eigenvectors, respectively. The modal matrix is usually orthonormalized according to $\mathbf{U}^T\mathbf{M}\mathbf{U}=I_n$, ($\mathbf{U}^T$ denotes the transpose of $\mathbf{U}$, and I_n denotes the $n\times n$ identity matrix) and, hence, satisfies $\mathbf{U}^T\mathbf{K}\mathbf{U}=\text{diag}(\omega_1^2,\ldots,\omega_n^2)=\Omega^2$. It is well known that by the linear change of coordinates $x(t)=\mathbf{U}q(t)$, (1.1), can be written in the normalized form

$$\ddot{q}+\tilde{\mathbf{C}}\dot{q}+\Omega^2 q=g(t),q(0)=\mathbf{U}^T\mathbf{M}x_0,\dot{q}(0)=\mathbf{U}^T\mathbf{M}\dot{x}_0,t\geq 0, \quad (1.3)$$

where $\tilde{\mathbf{C}}=\mathbf{U}^T\mathbf{C}\mathbf{U}$, $g(t)=\mathbf{U}^Tf(t)$, and $q(t)$ are the normalized coordinates. The symmetric matrix $\tilde{\mathbf{C}}$ is called the normalized damping matrix.

The normalized damping matrix $\tilde{\mathbf{C}}$ is not diagonal in general; when $\tilde{\mathbf{C}}$ is not diagonal, the system (1.1) is said to be nonclassically damped. If the damping matrix $\mathbf{C}$ is a linear combination of the mass and the stiffness matrices, then $\tilde{\mathbf{C}}$ is diagonal; this is a sufficient condition under which $\tilde{\mathbf{C}}$ is diagonal, and was originally given by Lord Rayleigh (1945, p. 130). The necessary and sufficient condition under which $\tilde{\mathbf{C}}$ is diagonal has been given by Caughey (1960) and Caughey and O'Kelly (1965). When $\tilde{\mathbf{C}}$ is diagonal, (1.3) is a set of n decoupled second order differential equations, which can be solved for $q(t)$ conveniently. Then, the solution of (1.1) is obtained by $x(t)=\mathbf{U}q(t)$, for all $t\geq 0$.

When $\tilde{\mathbf{C}}$ is not diagonal, (1.1) may be solved for $x(t)$ either by direct numerical integration or by the method proposed by Foss (1958); these methods, although quite accurate, are involved. Several authors have studied nonclassically damped linear systems by approximate techniques. For instance, Cronin (1976) obtained an approximate solution for a nonclassically damped system under harmonic excitation by perturbation technique. Chung and Lee (1986) applied perturbation technique to obtain the eigensolutions of damped systems with weakly nonclassical damping. Prater and Singh (1986), and Nair and Singh (1986) developed several indices to determine quantitatively the extent of nonproportional damping in discrete vibratory systems. Yae and Inman (1987) obtained bounds on the response of nonclassically underdamped systems. Nicholson (1987) gave upper bounds for the response of nonclassically damped systems under impulsive loads and step loads.

An approximate technique to solve (1.3) is to replace $\tilde{\mathbf{C}}$ by a diagonal matrix $\mathbf{C}_d$, and hence decouple the equations in (1.3). The solution of the decoupled equations leads to an approximate solution for (1.1); this solution would be close to the exact solution of (1.1), if a reasonable $\mathbf{C}_d$ is chosen. Several approaches to choosing $\mathbf{C}_d$ are given by Meirovitch (1967), Thomson et al. (1974), and Cronin (1976); most of these approaches are quite involved. The simplest approach to choosing $\mathbf{C}_d$ is to neglect the off-diagonal elements of $\tilde{\mathbf{C}}$, and take the remaining diagonal matrix for $\mathbf{C}_d$. Intuitively, the solution of such an approximately decoupled system is close to the exact solution of (1.3), if the off-diagonal elements of $\tilde{\mathbf{C}}$ are small compared to its diagonal elements. One probable way to decide whether the off-diagonal elements of $\tilde{\mathbf{C}}$ are small com-

Contributed by the Applied Mechanics Division for publication in the JOURNAL OF APPLIED MECHANICS.

Discussion on this paper should be addressed to the Editorial Department, ASME, United Engineering Center, 345 East 47th Street, New York, N.Y. 10017, and will be accepted until two months after final publication of the paper itself in the JOURNAL OF APPLIED MECHANICS. Manuscript received by ASME Applied Mechanics Division, August 7, 1987; final revision, March 11, 1988.

Copyright © 1988 by ASME
Downloaded 03 May 2010 to 171.66.16.21. Redistribution subject to ASME license or copyright; see http://www.asme.org/terms/Terms_Use.cfm

pared to its diagonal elements is to check if the matrix is diagonally dominant. Strict diagonal dominance of $\tilde{\mathbf{C}}$ would be a necessary condition for disregarding the off-diagonal elements of $\tilde{\mathbf{C}}$. Approximate decoupling of a damped linear system is often convenient and practical. An attempt to evaluate the extent of approximation, introduced by replacing $\tilde{\mathbf{C}}$ with a selected $\mathbf{C}_d$, has not been reported in the open literature.

In this paper, we examine the errors introduced by approximate decoupling, when $\tilde{\mathbf{C}}$ is replaced by a selected diagonal matrix $\mathbf{C}_d$; and tight error bounds are obtained by analytical methods. The organization of the paper is as follows. In Section 2, we take $\mathbf{C}_d$ to be the diagonal matrix obtained by omitting the off-diagonal element of $\tilde{\mathbf{C}}$. An expression for the error in the solution of the approximately decoupled system is derived, so that the relation between the error and the elements of $\tilde{\mathbf{C}}$ becomes transparent. The derivation in this section permits clarification of the mathematical methods used throughout the paper. In the process, we furnish a rigorous proof of the fact that, if the off-diagonal elements of $\tilde{\mathbf{C}}$ are *small compared to its diagonal elements, then the approximately decoupled* (1.3) obtained by neglecting the off-diagonal elements of $\tilde{\mathbf{C}}$ has a solution close to the exact solution of (1.3). In Section 3, $\mathbf{C}_d$ is assumed to be any diagonal matrix, and error bounds are again derived. In addition, it is shown that if $\tilde{\mathbf{C}}$ is diagonally dominant, then among all approximating diagonal matrices $\mathbf{C}_d$, the one that minimizes the error bound is simply the diagonal matrix obtained by neglecting the off-diagonal elements of $\tilde{\mathbf{C}}$. An example in Section 4 illustrates the theoretical developments pursued herein. There are two appendices in which we take care of the algebra leading to several expressions.

2 Dereliction of Off-Diagonal Elements

Consider system (1.1) with bounded external excitation $f(t)$. Without loss of generality, we can assume that $x_0 = 0$. The system (1.1) with zero input is asymptotically stable (see, e.g., Shieh et al., 1987). It is trival to show that the system (1.1) is bounded-input-bounded-output stable (see, e.g., Chen 1984) as well. In the following, we shall use the L_∞-norm of vector functions, defined by $\|h\| = \max_{1\le i\le n} \sup_{t\ge 0} |h_i(t)|$, for $h(t) = [h_1(t),\ldots,h_n(t)]^T$. We rewrite (1.3) as

$$\ddot{q} + (\tilde{\mathbf{C}}_d + \tilde{\mathbf{C}}_r)\dot{q} + \Omega^2 q = g(t), q(0) = 0, \dot{q}(0) = \mathbf{U}^T\mathbf{M}\dot{x}_0, t \ge 0, \quad (2.1)$$

where $\tilde{\mathbf{C}}_d + \tilde{\mathbf{C}}_r = \tilde{\mathbf{C}}, \tilde{\mathbf{C}}_d = \text{diag}(2\xi_1\omega_1, \ldots, 2\xi_n\omega_n)$, a matrix composed of the diagonal elements of $\tilde{\mathbf{C}}$, and $\tilde{\mathbf{C}}_r = [\tilde{c}_{ij}]$ is a symmetric $n \times n$ matrix with zero diagonal elements. We assume throughout that $\xi_i < 1$, for all $i = 1, \ldots, n$. Note that by the positive definiteness of $\mathbf{C}$, $\xi_i > 0$ for all $i = 1, \ldots, n$. When $\tilde{\mathbf{C}}_r$ is neglected in (2.1), the modes of resulting decoupled system are underdamped, and this is usually the case of most practical interest. An analysis of the conditions under which the modes of a damped linear system are either all underdamped, critically damped, or overdamped, has been given by Inman and Andry (1980).

We decouple (2.1) by neglecting $\tilde{\mathbf{C}}_r$, and denote the solution of the resulting equation by $q_a(t)$. Thus, we have

$$\ddot{q}_a + \tilde{\mathbf{C}}_d\dot{q}_a + \Omega^2 q_a = g(t), t \ge 0, \quad (2.2)$$

with $q_a(0) = q(0) = 0$, and $\dot{q}_a = \dot{q}(0)$. Subtracting (2.2) from (2.1), and denoting the n-dimensional vector of error $e = q - q_a$, we obtain

$$\ddot{e} + \tilde{\mathbf{C}}_d\dot{e} + \Omega^2 e + \tilde{\mathbf{C}}_r\dot{q} = 0, t \ge 0. \quad (2.3)$$

Applying the Laplace transform to (2.3), and noting that $e(0) = \dot{e}(0) = 0$, and $q(0) = 0$, we have

$$\hat{e}(s) = -s(I_n s^2 + \tilde{\mathbf{C}}_d s + \Omega^2)^{-1}\tilde{\mathbf{C}}_r\hat{q}(s), \quad (2.4)$$

where $\hat{e}(s) = L(e(t))$ is the Laplace transform of $e(t)$. Define the $n \times n$ matrix

$$\hat{H}(s) = -s(I_n s^2 + \tilde{\mathbf{C}}_d s + \Omega^2)^{-1}\tilde{\mathbf{C}}_r. \quad (2.5)$$

The ith row of $\hat{H}(s)$ is

$$\frac{s}{s^2 + 2\xi_i\omega_i s + \omega_i^2}[-\tilde{c}_{i1} \ldots -\tilde{c}_{i,i-1}\, 0 - \tilde{c}_{i,i+1} \ldots -\tilde{c}_{in}], \quad (2.6)$$

where $\tilde{c}_{ij}$ are the elements of $\tilde{\mathbf{C}}_r$. Hence, if (2.4) is written as $\hat{e}(s) = \hat{H}(s)\hat{q}(s)$, the error function $e(t)$ is given by

$$e(t) = (H^* q)(t) = \int_0^t H(t-\tau)q(\tau)d\tau, \quad (2.7)$$

where $H(t) = L^{-1}(\hat{H}(s))$, and H^*q denotes the convolution of the functions $H(t)$ and $q(t)$. The above expression for the approximation error $e(t)$ is exact. Define the linear operator $\bar{H}$ by

$$\bar{H}(q) = H^* q, \quad (2.8)$$

where $\bar{H}(q(t)) = (H^*q)(t)$ for all $t \ge 0$, is given by (2.7). To obtain an upper bound for $\|e\|$ from (2.7) and (2.8), we have

$$\|e\| = \|\bar{H}(q)\| \le \|\bar{H}\|\ \|q\|, \quad (2.9)$$

where $\|\bar{H}\|$ is the L_∞-induced norm of $\bar{H}$. Invoking an identity given by Desoer and Vidyasagar (1975, p. 26),

$$\|\bar{H}\| = \max_{1\le i\le n} \sigma_i \int_0^\infty |h_{ii}(\tau)|\, d\tau, \quad (2.10)$$

where for all $i = 1, \ldots, n$, the quantity σ_i is the row sum of the absolute values of the off-diagonal elements

$$\sigma_i = \sum_{\substack{j=1 \\ j\ne i}}^{n} |\tilde{c}_{ij}|, \quad (2.11)$$

and the function $h_{ii}(t)$ is given by

$$h_{ii}(t) = L^{-1}\left(\frac{s}{s^2 + 2\xi_i\omega_i s + \omega_i^2}\right)$$

$$= \frac{-1}{(1-\xi_i^2)^{1/2}} e^{-\xi_i\omega_i t}\sin(\omega_i(1-\xi_i^2)^{1/2}t - \phi_i), \quad (2.12a)$$

for which

$$\phi_i = \tan^{-1}\frac{(1-\xi_i^2)^{1/2}}{\xi_i}. \quad (2.12b)$$

Note that (2.12) is valid only for $\xi_i < 1$. Substituting $h_{ii}(t)$ into (2.10) and carrying out the integration (see appendix A), we obtain

$$\|\bar{H}\| = \max_{1\le i\le n} \frac{2\sigma_i}{\omega_i} \cdot \frac{\exp(V(\xi_i))}{1 - \exp(W(\xi_i))}, \quad (2.13)$$

where

$$V(\xi_i) = -\frac{\xi_i}{(1-\xi_i^2)^{1/2}} \tan^{-1}\frac{(1-\xi_i^2)^{1/2}}{\xi_i}, \quad (2.14a)$$

$$W(\xi_i) = -\frac{\pi\xi_i}{(1-\xi_i^2)^{1/2}}. \quad (2.14b)$$

Equation (2.9) can now be cast in the form

$$\max_{1\le i\le n} \sup_{t\ge 0} |e_i(t)| = \|e\| \le \left[\max_{1\le i\le n} \frac{2\sigma_i}{\omega_i} \cdot \frac{\exp(V(\xi_i))}{1 - \exp(W(\xi_i))}\right]\|q\|. \quad (2.15)$$

By the definition of operator norm, it is straightforward to see

Downloaded 03 May 2010 to 171.66.16.21. Redistribution subject to ASME license or copyright; see http://www.asme.org/terms/Terms_Use.cfm

that (2.15) gives the tightest bound among all error bounds of the type

$$\|e\| \le m\|q\|. \tag{2.16}$$

That is, $\|\bar{H}\|$ given in (2.13) is the smallest possible value for m. To arrive at an easily manageable bound, we utilize inequality (B.1), established in appendix B, namely,

$$0.3183 = \pi^{-1} \le \frac{\xi_i \exp(V(\xi_i))}{1-\exp(W(\xi_i))} \le e^{-1} = 0.3679, \tag{2.17}$$

for $0 \le \xi_i \le 1$. From (2.13), we have

$$4\pi^{-1} \max_{1\le i\le n} \frac{\sigma_i}{2\xi_i\omega_i} \le \|\bar{H}\| \le 4e^{-1} \max_{1\le i\le n} \frac{\sigma_i}{2\xi_i\omega_i}. \tag{2.18}$$

Now, the relation between $\|\bar{H}\|$ and the sums of the off-diagonal elements σ_i and the diagonal elements $2\xi_i\omega_i$ of $\tilde{\mathbf{C}}$ is transparent. Clearly, $\|\bar{H}\|$ and consequently the error bound are small if and only if, $\sigma_i/2\xi_i\omega_i << 1$ for all $i=1, \ldots, n$, i.e., if and only if the off-diagonal elements of $\tilde{\mathbf{C}}$ on each row are much smaller than the corresponding diagonal element. Intuitively, this conclusion is expected, for which we have furnished a rigorous proof in the process of deriving tight error bounds.

We shall continue with further analysis of the approximation error. Suppose that for all $i=1, \ldots, n, \sigma_i/2\xi_i\omega_i$ is sufficiently small and that the decoupled system (2.2) has been readily solved to obtain $q_a(t)$. It would be of interest to derive a neighborhood of $q_a(t)$ in which the actual solution $q(t)$ lies. Since $q = e + q_a$, by the triangle inequality $\|q\| \le \|e\| + \|q_a\|$; using this inequality in (2.9), we obtain

$$\|e\| \le \frac{\|\bar{H}\|}{1-\|\bar{H}\|}\|q_a\|. \tag{2.19}$$

That is, $q(t)$ lies in the $(\|\bar{H}\|/(1-\|\bar{H}\|))\|q_a\|$ neighborhood of $q_a(t)$. It has been assumed that $1-\|\bar{H}\| > 0$, which is always the case if $\sigma_i/2\xi_i\omega_i$ is small for all $i=1, \ldots, n$. In fact, by invoking inequality (2.18),

$$\frac{\|\bar{H}\|}{1-\|\bar{H}\|} \le \frac{4e^{-1} \max_{1\le i\le n} (\sigma_i/2\xi_i\omega_i)}{1-4e^{-1} \max_{1\le i\le n} (\sigma_i/2\xi_i\omega_i)} = r, \tag{2.20}$$

so that $q(t)$ always lies in a band centered at $q_a(t)$ with $r\|q_a\|$ as the half-width.

3 Replacement by Arbitrary Diagonal Matrices

In this section we consider the system (2.1),

$$\ddot{q} + \tilde{\mathbf{C}}\dot{q} + \Omega^2 q = g(t), q(0) = 0, \dot{q}(0) = \mathbf{U}^T\mathbf{M}\dot{\mathbf{x}}_0, t \ge 0, \tag{3.1}$$

and evaluate the error introduced by replacing $\tilde{\mathbf{C}}$ with an arbitrarily fixed diagonal matrix $\mathbf{C}_d = \text{diag}(2\eta_1\omega_1, \ldots, 2\eta_n\omega_n)$, where for all $i=1, \ldots, n$, $0 < \eta_i < 1$ are parameters to be specified. We denote the solution of the resulting decoupled equations by $p(t)$. Thus we have

$$\ddot{p} + \mathbf{C}_d\dot{p} + \Omega^2 p = g(t), t \ge 0, \tag{3.2}$$

with $p(0) = q(0) = 0$, and $\dot{p}(0) = \dot{q}(0)$. Subtracting (3.2) from (3.1) and denoting $e = q - p$, we obtain

$$\ddot{e} + \mathbf{C}_d\dot{e} + \Omega^2 e + (\tilde{\mathbf{C}} - \mathbf{C}_d)\dot{q} = 0, \; t \ge 0. \tag{3.3}$$

By an approach similar to that in the previous section, we obtain

$$\hat{e}(s) = \hat{G}(s)\hat{q}(s), \tag{3.4}$$

where

$$\hat{G}(s) = -s(I_n s^2 + \mathbf{C}_d s + \Omega^2)^{-1}(\tilde{\mathbf{C}} - \mathbf{C}_d). \tag{3.5}$$

The ith row of $\hat{G}(s)$ is

$$\frac{s}{s^2 + 2\eta_i\omega_i s + \omega_i^2}[-\tilde{c}_{i1} \; \ldots \; -\tilde{c}_{i,i-1} \; -2(\xi_i - \eta_i)\omega_i - \tilde{c}_{i,i+1} \; \ldots \; -\tilde{c}_{in}]. \tag{3.6}$$

Furthermore, we obtain

$$\|e\| \le \|\bar{G}\| \; \|q\|, \tag{3.7}$$

where $\|\bar{G}\|$ is the L_∞ – induced norm of the linear operator $\bar{G}$, defined by

$$\bar{G}(q) = G^* q = e, \tag{3.8}$$

where $\bar{G}(q(t)) = (G^*q)(t) = L^{-1}(\hat{G}(s)\hat{q}(s))$. In this case

$$\|\hat{G}\| = \max_{1\le i\le n} \frac{2}{\omega_i}(\sigma_i + 2\omega_i|\xi_i - \eta_i|)\frac{\exp(V(\eta_i))}{1-\exp(W(\eta_i))}, \tag{3.9}$$

where σ_i, $V(\eta_i)$, and $W(\eta_i)$ are given by (2.11), (2.14a), and (2.14b), respectively. Equation (3.8) is an exact expression for the approximation error. Applying inequality (2.17), we immediately have

$$\|e\| \le 4e^{-1} \max_{1\le i\le n} \frac{\sigma_i + 2\omega_i|\xi_i - \eta_i|}{2\eta_i\omega_i}\|q\|, \tag{3.10}$$

which obviously is an extension of previous results. Likewise, we can easily evaluate the half-width $r\|p\|$ of a band, centered at $p(t)$, in which the actual solution $q(t)$, lies. Denoting

$$s = \max_{1\le i\le n} \frac{\sigma_i + 2\omega_i|\xi_i - \eta_i|}{2\eta_i\omega_i}, \tag{3.11}$$

the half-width is $r\|p\|$, where

$$r = \frac{4e^{-1}s}{1-4e^{-1}s}. \tag{3.12}$$

At this point a different direction of development is followed. Let us assume that the normalized damping matrix $\tilde{\mathbf{C}}$ is diagonally dominant, that is

$$\sigma_i \le 2\xi_i\omega_i, \tag{3.13}$$

for all $i=1, \ldots n$. We shall determine $\mathbf{C}_d$, namely η_i, $i=1, \ldots, n$, in order to have the smallest error bound between the solution of the approximately decoupled (3.1) and the exact solution of (3.1). It will turn out that the smallest error bound is achieved when $\eta_i = \xi_i$, for all $i=1, \ldots, n$; for this reason, neglecting the off-diagonal elements of $\tilde{\mathbf{C}}$ is probably the most appropriate approach to decouple (3.1) when $\tilde{\mathbf{C}}$ is diagonally dominant.

The error bound (3.7) is the smallest when $\|\bar{G}\|$ is minimum. The minimum value of $\|\bar{G}\|$ is achieved if for all $i=1, \ldots, n$, we choose η_i such that

$$\bar{g}_i = \frac{2}{\omega_i}(\sigma_i + 2\omega_i|\xi_i - \eta_i|)\frac{\exp(V(\eta_i))}{1-\exp(W(\eta_i))}, \tag{3.14}$$

is minimum. The function $\bar{g}_i$ is differentiable over (0,1] except at $\eta_i = \xi_i$. Let $\xi_i < \eta_i$, then $|\xi_i - \eta_i| = \eta_i - \xi_i$, and

$$\bar{g}_i'(\eta_i) = \frac{2}{\omega_i} \cdot \frac{\exp(V(\eta_i))}{[1-\exp(W(\eta_i))]^2}\{2\omega_i[(1 + \eta_i V'(\eta_i))(1-\exp(W(\eta_i))) + \eta_i W'(\eta_i)\exp(W(\eta_i))] + (\sigma_i - 2\xi_i\omega_i)[V'(\eta_i)(1-\exp(W(\eta_i))) + W'(\eta_i)\exp(W(\eta_i))]\}. \tag{3.15}$$

Using (3.13) and (B.2), (B.3), (B.4) of Appendix B, we con-

Downloaded 03 May 2010 to 171.66.16.21. Redistribution subject to ASME license or copyright; see http://www.asme.org/terms/Terms_Use.cfm

clude that $\bar{g}_i'(\eta_i)>0$, for $\xi_i<\eta_i\le 1$. Hence, $\bar{g}_i(\eta_i)$ is monotonically increasing over $(\xi_i,1]$ and achieves its infinum at ξ_i. Let $\xi_i>\eta_i$, then $|\xi_i-\eta_i|=\xi_i-\eta_i$, and

$$\bar{g}_i'(\eta_i)=\frac{2}{\omega_i}\cdot\frac{\exp(V(\eta_i))}{[1-\exp(W(\eta_i))]^2}\{-2\omega_i[(1+\eta_i V'(\eta_i))(1-\exp(W(\eta_i)))+\eta_i W'(\eta_i)\exp(W(\eta_i))] + (\sigma_i+2\xi_i\omega_i)[V'(\eta_i)(1-\exp(W(\eta_i)))+W'(\eta_i)\exp(W(\eta_i))]\}. \tag{3.16}$$

Using (B.2), (B.3), and (B.4) of Appendix B, we conclude that $\bar{g}_i'(\eta_i)<0$, for $0\le\eta_i<\xi_i$. Hence, $\bar{g}_i(\eta_i)$ is monotonically decreasing over $[0,\xi_i)$ and achieves its infimum at ξ_i. Therefore, for all $i=1,\ldots,n$, $\bar{g}_i(\eta_i)$ is minimum at $\eta_i=\xi_i$; consequently, when $\eta_i=\xi_i$, the minimum of $\|\bar{G}\|$ is equal to $\|\bar{H}\|$ given in (2.13). This shows that the diagonal matrix which minimizes the error bound is obtained by simply neglecting the off-diagonal elements of the diagonally dominant normalized damping matrix.

4 Example

In this section we give an example to illustrate possible application of the results obtained in the previous sections; for convenience a low order system is used. Consider a system whose normalized equation is

$$\begin{bmatrix}1&0\\0&1\end{bmatrix}\begin{bmatrix}\ddot{q}_1\\\ddot{q}_2\end{bmatrix}+\begin{bmatrix}1.559&-0.2\\-0.2&1.6\end{bmatrix}\begin{bmatrix}\dot{q}_1\\\dot{q}_2\end{bmatrix}+\begin{bmatrix}3.8&0\\0&4\end{bmatrix}\begin{bmatrix}q_1\\q_2\end{bmatrix}=\begin{bmatrix}1\\1\end{bmatrix}\sin 2t \tag{4.1}$$

We have $\omega_1=1.9493$, $\omega_2=2$, $\xi_1=\xi_2=0.4$. An approximate solution of (4.1) is obtained by solving the following decoupled equations

$$\begin{bmatrix}1&0\\0&1\end{bmatrix}\begin{bmatrix}\ddot{q}_{a1}\\\ddot{q}_{a2}\end{bmatrix}+\begin{bmatrix}1.559&0\\0&1.6\end{bmatrix}\begin{bmatrix}\dot{q}_{a1}\\\dot{q}_{a2}\end{bmatrix}+\begin{bmatrix}3.8&0\\0&4\end{bmatrix}\begin{bmatrix}q_{a1}\\q_{a2}\end{bmatrix}=\begin{bmatrix}1\\1\end{bmatrix}\sin 2t. \tag{4.2}$$

The steady-state solution of (4.2) is

$$q_s(t)=\begin{bmatrix}0.32\sin(2t-1.635)\\0.313\sin(2t-1.571)\end{bmatrix}. \tag{4.3}$$

For the system (4.2), $\|q_a\|=\|q_s\|=0.32$. By (2.13) and (2.19), we obtain $\|e\|\le(0.199)\|q_a\|=0.064$, whereas by (2.20), $\|e\|\le(0.233)\|q_a\|=0.075$. The exact solution $q_1(t)$ and the corresponding approximate solution $q_{a1}(t)$, as well as the more accurate error band, are plotted in Fig. 1. Since the exact solution has been calculated, expression (2.15) can be employed to obtain $\|e\|\le(0.166)\|q\|=0.061$. This error bound is the tightest possible in a functional form specified by (2.16), where the coefficient m is independent of the driving force. By using other types of external excitation, there are indeed cases where $q_1(t)$ is quite close to the error bounds. Perhaps it would be worthwhile in the future to study classes of systems for which the errors approach the error bounds.

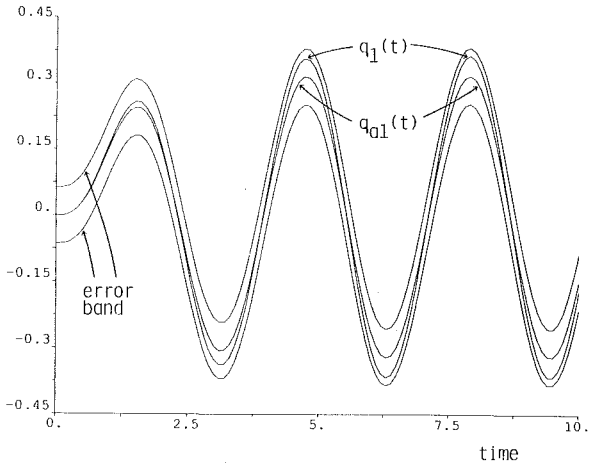


Fig. 1 Exact and approximate solutions and error band

5 Conclusions

A common procedure in the solution of a normalized damped linear system with small off-diagonal damping elements is to replace the normalized damping matrix $\tilde{\mathbf{C}}$ by a selected diagonal matrix $\mathbf{C}_d$. In this paper the errors in solution introduced by this approximate decoupling have been evaluated, and tight error bounds have been derived. The results, summarized in the following, are applicable to linear systems that become underdamped when the off-diagonal elements of the normalized damping matrices are neglected. Extension to cases involving other damping modes, for which $\xi_i\ge 1$ for some i, will be given elsewhere.

1 When $\mathbf{C}_d$ is obtained from $\tilde{\mathbf{C}}_d$ by neglecting the off-diagonal elements, the error in solution is given by (2.7), and the error bound by (2.15).
2 When $\mathbf{C}_d$ is an arbitrarily fixed diagonal matrix, the error in solution is given by (3.8), and the error bound by (3.7) and (3.9).
3 The error bounds derived are the tightest possible in a functional form specified by (2.16).
4 When the approximately decoupled system has been conveniently solved, neighborhoods have been specified in which the exact solution of the original system lies.
5 It has been rigorously proved that if $\mathbf{C}_d$ is obtained from $\tilde{\mathbf{C}}$ by neglecting the off-diagonal elements, then the solution errors are small if the off-diagonal elements of $\tilde{\mathbf{C}}$ are small.
6 If $\tilde{\mathbf{C}}$ is diagonally dominant, then among all approximating diagonal matrices $\mathbf{C}_d$, the one that minimizes the error bound is simply the diagonal matrix obtained by omitting the off-diagonal elements of $\tilde{\mathbf{C}}$.

An example is employed to illustrate the theoretical developments. It is obvious that the results would apply to steady-state errors in the case of periodic external excitation. There are a few places where the results mentioned above can be generalized in a strictly mathematical sense; we have, however, suppressed any temptation to do so.

Acknowledgment

This research has been supported in part by the National Science Foundation under Grant No. MSM-8657619. Opinions, findings, and conclusions expressed in this paper are those of the authors and do not necessarily reflect the views of the National Science Foundation.

References

Caughey, T. K., 1960, "Classical Normal Modes in Damped Linear Dynamic Systems," ASME Journal of Applied Mechanics, Vol. 27, pp. 269–271.

Downloaded 03 May 2010 to 171.66.16.21. Redistribution subject to ASME license or copyright; see http://www.asme.org/terms/Terms_Use.cfm

Caughey, T. K., and O'Kelly, M. E. J., 1965, "Classical Normal Modes in Damped Linear Dynamic Systems," ASME JOURNAL OF APPLIED MECHANICS, Vol. 32, pp. 583–588.

Chen, C. T., 1984, *Linear System Theory and Design*, Holt, Rinehart and Wiston, New York

Chung, K. R., and Lee, C. W., 1986, "Dynamic Reanalysis of Weakly Non-proportionally Damped Systems," *J. Sound and Vib.*, Vol. 111, pp. 37–50.

Cronin, D. L., 1976, "Approximation for Determining Harmonically Excited Response of Nonclassically Damped Systems," *ASME Journal of Engineering for Industry*, Vol. 98, pp. 43–47.

Desoer, C. A., and Vidyasagar, M., 1975, *Feedback Systems: Input-Output Properties*, Academic Press, New York.

Foss, K. A., 1958, "Co-ordinates which Uncouple the Equations of Motion of Damped Linear Dynamic Systems," ASME JOURNAL OF APPLIED MECHANICS, Vol. 25, pp. 361–364.

Inman, D. J., and Andry, A. N., 1980, "Some Results on the Nature of Eigenvalues of Discrete Damped Linear Systems," ASME JOURNAL OF APPLIED MECHANICS, Vol. 47, pp. 927–930.

Meirovitch, L., 1967, *Analytical Methods in Vibrations*, Macmillan, New York.

Müller, P. C., and Schiehlen, W. O., 1985, *Linear Vibrations*, Martinus Nijhoff Publishers, Dordrecht, The Netherlands.

Nair, S. S., and Singh, R., 1986, "Examination of the Validity of Proportional Damping Approximations with Two Further Numerical Indices," *J. Sound and Vibration*, Vol. 104, pp. 348–350.

Nicholson, D. W., 1987, "Response Bounds for Nonclassically Damped Mechanical Systems Under Transient Loads," ASME JOURNAL OF APPLIED MECHANICS, Vol. 54, pp. 430–433.

Prater, Jr., G., and Singh, R., 1986, "Quantification of the Extent of Non-Proportational Viscous Damping in Discrete Vibratory Systems," *J. Sound and Vibration*, Vol. 104, pp. 109–125.

Lord Rayleigh, 1945, *The Theory of Sound*, Vol. 1, Dover, New York.

Shieh, L. S., Mehio, M. M., and Dib, H. M., 1987, "Stability of the Second-order Matrix Polynomial," *IEEE Trans. Automat. Contr.*, Vol. AC-32, pp. 231–233.

Thomson, W. T., Calkin, T., and Caravani, P., 1974, "A Numerical Study of Damping," *Earthquake Eng. Struc. Dyn.*, Vol. 3, pp. 97–103.

Yae, K. H., and Inman, D. J., 1987, "Response Bounds for Linear Underdamped Systems," ASME JOURNAL OF APPLIED MECHANICS, Vol. 54, pp. 419–423.

APPENDIX A

For all $i=1, \ldots, n$, $h_{ii}(t)=1$ at $t=0$, and vanishes at $t_k = \frac{1}{\omega_i(1-\xi_i^2)^{1/2}}(k\pi+\phi_i)$, for $k=0,1,2, \ldots$, where ϕ_i is given by (2.12*b*). We have

$$\int_0^\infty |h_{ii}(\tau)|\,d\tau = \int_0^{t_0} h_{ii}(\tau)d\tau + \sum_{k=0,2,4,\ldots}^{\infty} \left| \int_{t_k}^{t_{k+1}} h_{ii}(\tau)d\tau \right| + \sum_{k=1,3,5,\ldots}^{\infty} \int_{t_k}^{t_{k+1}} h_{ii}(\tau)d\tau$$

$$= \frac{1}{\omega_i}\exp\left(-\frac{\xi_i}{(1-\xi_i^2)^{1/2}}\tan^{-1}\frac{(1-\xi_i^2)^{1/2}}{\xi_i}\right) + \frac{1}{\omega_i}\exp\left(-\frac{\xi_i}{(1-\xi_i^2)^{1/2}}\tan^{-1}\frac{(1-\xi_i^2)^{1/2}}{\xi_i}\right) \times \left[1+2\sum_{k=1}^{\infty}\exp\left(\frac{-\pi\xi_i k}{(1-\xi_i^2)^{1/2}}\right)\right]$$

$$= \frac{2}{\omega_i}\exp\left(-\frac{\xi_i}{(1-\xi_i^2)^{1/2}} \times \tan^{-1}\frac{(1-\xi_i^2)^{1/2}}{\xi_i}\right)\sum_{k=0}^{\infty}\exp\left(\frac{-\pi\xi_i k}{(1-\xi_i^2)^{1/2}}\right). \tag{A.1}$$

Since $\sum_{k=0}^{\infty}\exp\left(\frac{-\pi\xi_i k}{(1-\xi_i^2)^{1/2}}\right) = \frac{1}{1-\exp(-\pi\xi_i/(1-\xi_i^2)^{1/2})}$,

we obtain (2.13).

APPENDIX B

The following inequalities have been drawn upon in Section 2 and Section 3:

$$\pi^{-1} \le y_1(\xi_i) = \frac{\xi_i \exp(V(\xi_i))}{1-\exp(W(\xi_i))} \le e^{-1}, \quad 0 \le \xi_i \le 1; \tag{B.1}$$

$$V'(\eta_i)(1-\exp(W(\eta_i))) + W'(\eta_i)\exp(W(\eta_i)) < 0, \quad 0 \le \eta_i \le 1; \tag{B.2}$$

$$y_2(\eta_i) = \frac{\exp(V(\eta_i))}{[1-\exp(W(\eta_i))]^2} > 0, \quad 0 \le \eta_i \le 1, \tag{B.3}$$

and $y_2(\eta_i) \to +\infty$ as $\eta_i - 0$;

$$(1+\eta_i V'(\eta_i))(1-\exp(W(\eta_i))) + \eta_i W'(\eta_i)\exp(W(\eta_i)) \ge 0, \quad 0 \le \eta_i \le 1, \tag{B.4}$$

where the equality holds only for $\eta_i = 0$.

Proof of (B.1): We have

$$y_1'(\xi_i) = \frac{\exp(V(\xi_i))}{[1-\exp(W(\xi_i))]^2}[(1+\xi_i V'(\xi_i))(1-\exp(W(\xi_i))) + \xi_i W'(\xi_i)\exp(W(\xi_i))]. \tag{B.5}$$

By (B.3) and (B.4), to be proved in the following, $y_1'(\xi_i) > 0$, $0 < \xi_i \le 1$, and $y_1'(0) = 0$. Therefore, $y_1(\xi_i)$ is monotonically increasing over [0,1], and achieves its minimum and maximum at 0 and 1, respectively; we have $y_1(0) = \pi^{-1}$ and $y_1(1) = e^{-1}$.

Proof of (B.2): We have

$$V'(\eta_i) = \frac{\eta_i(1-\eta_i^2)^{1/2} - \tan^{-1}((1-\eta_i^2)^{1/2}/\eta_i)}{(1-\eta_i^2)^{3/2}}. \tag{B.6}$$

We let $\eta_i = \cos\theta$ in (B.6), then

$$V'(\theta) = \frac{\cos\theta\ \sin\theta - \theta}{\sin^3\theta}, \quad 0 \le \theta \le \frac{\pi}{2}. \tag{B.7}$$

By the L'Hopital's rule, $V'(0) = -2/3$. For $0 < \theta \le \pi/2$, we have $\sin\theta < \theta$; using this inequality in (B.7), we obtain $V'(\theta) < (\cos\theta - 1)/\sin^2\theta < 0$, for $0 < \theta \le \pi/2$. Thus, for all $0 \le \eta_i \le 1$,

$$V'(\eta_i) < 0. \tag{B.8}$$

Furthermore, having $W(\eta_i)$ defined by (2.14*b*), for $0 \le \eta_i \le 1$, we have

$$V'(\eta_i)(1-\exp(W(\eta_i))) \le 0, \tag{B.9}$$

where the equality holds only for $\eta_i = 0$. By the L'Hopital's rule $V'(1)(1-\exp(W(1))) = -\pi/2$. We have

$$W'(\eta_i)\exp(W(\eta_i)) = \frac{-\pi}{(1-\eta_i^2)^{3/2}}\exp\left(\frac{\pi\eta_i}{(1-\eta_i^2)^{1/2}}\right), \tag{B.10}$$

for $0 \le \eta_i \le 1$. Clearly, $W'(\eta_i)\exp(W(\eta_i)) < 0$, for $0 \le \eta_i < 1$. By the L'Hopital's rule $W'(1)\exp(W(1)) = 0$. Thus

$$W'(\eta_i)\exp(W(\eta_i)) \le 0, \quad 0 \le \eta_i \le 1, \tag{B.11}$$

where the equality holds only for $\eta_i = 1$. Hence, (B.2) follows.

Proof of (B.3): By (2.14*a*) and (2.14*b*), it is clear that $y_2(\eta_i) > 0$, for $0 < \eta_i < 1$. Furthermore, $y_2 \to +\infty$ as $\eta_i \to 0$, and by the L'Hopital's rule $y_2(1) = e^{-1}$. Hence, (B.3) holds.

Proof of (B.4): proof of (B.4) is straightforward, but laborious; it is therefore omitted.

Downloaded 03 May 2010 to 171.66.16.21. Redistribution subject to ASME license or copyright; see http://www.asme.org/terms/Terms_Use.cfm

Synchronized Periodic Solutions of a Class of Periodically Driven Nonlinear Oscillators

Gamal M. Mahmoud
Department of Mathematics and Computer Science, Clarkson University, Potsdam, NY 13676

Tassos Bountis[1]
Department of Theoretical Mechanics, University of Thessaloniki, Thessaloniki, Greece

We consider a class of parametrically driven nonlinear oscillators: $\ddot{x}+k_1x+k_2f(x,\dot{x})P(\Omega t)=0$, $P(\Omega t+2\pi)=P(\Omega t)$ (*) *which can be used to describe, e.g., a pendulum with vibrating length, or the displacements of colliding particle beams in high energy accelerators. Here we study numerically and analytically the subharmonic periodic solutions of* (*), *with frequency* $1/m\cong\sqrt{k_1}$, $m=1, 2, 3, \ldots$. *In the cases of* $f(x,\dot{x})=x^3$ *and* $f(x,\dot{x})=x^4$, *with* $P(\Omega t)=\cos t$, *all of these so called* synchronized *periodic orbits are obtained numerically, by a new technique, which we refer to here as the* indicatrix method. *The theory of generalized averaging is then applied to derive highly accurate expressions for these orbits, valid to the second order in* k_2. *Finally, these analytical results are used, together with the perturbation methods of multiple time scaling, to obtain second order expressions for regions of instability of synchronized periodic orbits in the* k_1, k_2 *plane, which agree very well with the results of numerical experiments.*

1 Introduction

Ever since the time of Poincaré (1957), periodic solutions have been known to play a very important role in the study of nonlinear dynamical systems (Lieberman and Lichtenberg, 1983; Gruckenheimer and Holmes, 1983). In particular, their stability properties under small perturbations are especially significant in the analysis not only of local bifurcation phenomena, but of certain "global" changes in the dynamics of the system as well (Helleman, 1981; Collet and Eckmann, 1980).

Of particular importance among periodic solutions of two (or higher) dimensional systems, are those for which the "fundamental" frequencies of the problem are rationally related by an expression of the form

$$m\omega-n\Omega=0,\ n, m=1, 2, 3, \ldots, \tag{1.1}$$

in the two-frequency case. These periodic solutions (or orbits) correspond to the lowest order resonances of the system (Bountis et al., 1984; Chirikov, 1979) and have, in most cases, large regions of regular (respectively chaotic) behavior about them, depending on whether they are stable (respectively, unstable), with respect to small disturbances (Helleman and Bountis, 1979; Budinsky and Bountis, 1983).

It is this type of physically interesting periodic orbits that we wish to study analytically, as well as numerically, in the present paper. More specifically, we concentrate on a class of periodically driven oscillators, whose motion is described by

$$\ddot{x}+k_1x+k_2f(x,\dot{x})P(\Omega t)=0, \tag{1.2}$$

where $P(\Omega t)=P(\Omega t+2\pi)$, f becomes a nonlinear function of x, $\dot{x}$, k_1 and k_2 are constant parameters and $\dot{(\ )}\equiv d(\ )/dt$.

Equations of motion of the type (1.2) appear in many problems of mechanics (Sevin, 1961; Hsu, 1963). For example, in the case of a pendulum with vibrating length, the equation of motion

$$\ddot{x}+g\ \sin x/(l_0+\epsilon\cos\Omega t)=0,$$

for a hard spring (i.e., $|\epsilon/l_0|\ll 1$), and small displacement becomes

$$\ddot{x}+\frac{q}{l_0}(1-\epsilon\cos\ \Omega t)\left(x-\frac{x^3}{6}\right)=0,$$

which is clearly of the form (1.2) with $k_1=0$. Parametrically excited one-dimensional models have also been used to study vibrations of mono-symmetric thin-wall beams of open section (Tso and Caughy, 1965). More recently, the equations and methods of this paper have been applied to the problem of stability of colliding particle beams in high energy accelerators (Tennyson, 1982; Bountis and Mahmoud, 1987).

We are interested here in periodic solutions of (1.2), whose frequency ω satisfies the resonance condition (1.1), with $n=1$, $k_1\cong\omega^2$ and k_2 "small". Such periodic orbits are called *synchronized*, and can be studied by our methods, for the general choices of $P(\Omega t)$ and $f(x,\dot{x})$ in (1.2). We will, however, restrict our attention to the specific examples

$$\ddot{x}+k_1x+k_2x^3\cos\ t=0, \tag{1.3a}$$

$$\ddot{x}+k_1x+k_2x^4\cos\ t=0, \tag{1.3b}$$

[1]Permanent address: Department of Mathematics, University of Patras, Patras, Greece.

Contributed by the Applied Mechanics Division for publication in the JOURNAL OF APPLIED MECHANICS.

Discussion on this paper should be addressed to the Editorial Department, ASME, United Engineering Center, 345 East 47th Street, New York, N.Y. 10017, and will be accepted until two months after final publication of the paper itself in the JOURNAL OF APPLIED MECHANICS. Manuscript received by ASME Applied Mechanics Division, May 19, 1986; final revision, November 13, 1987.

Copyright © 1988 by ASME
Downloaded 03 May 2010 to 171.66.16.21. Redistribution subject to ASME license or copyright; see http://www.asme.org/terms/Terms_Use.cfm

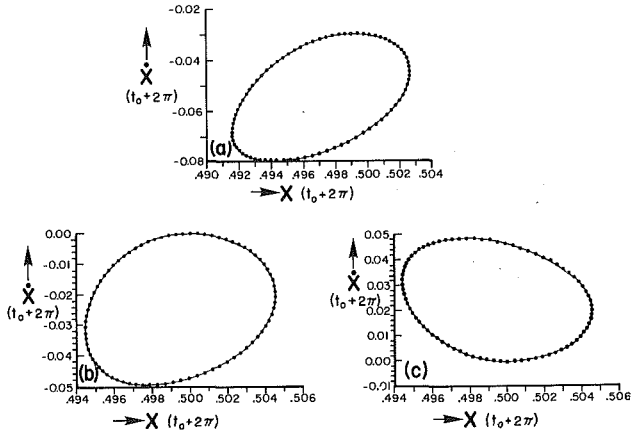


Fig. 1 Indicatrix plots of equation (2.2*b*) for $k_2 = 0.2$ for: (*a*) $k_1 = 1.0345$, $t_0 \in [0, 2\pi]$, (*b*) $k_1 = 1.01565$: (0.5, 0) at $t_0 = \pi$, and (*c*) $k_1 = 0.9844$: (0.5, 0) at $t_0 = 0$

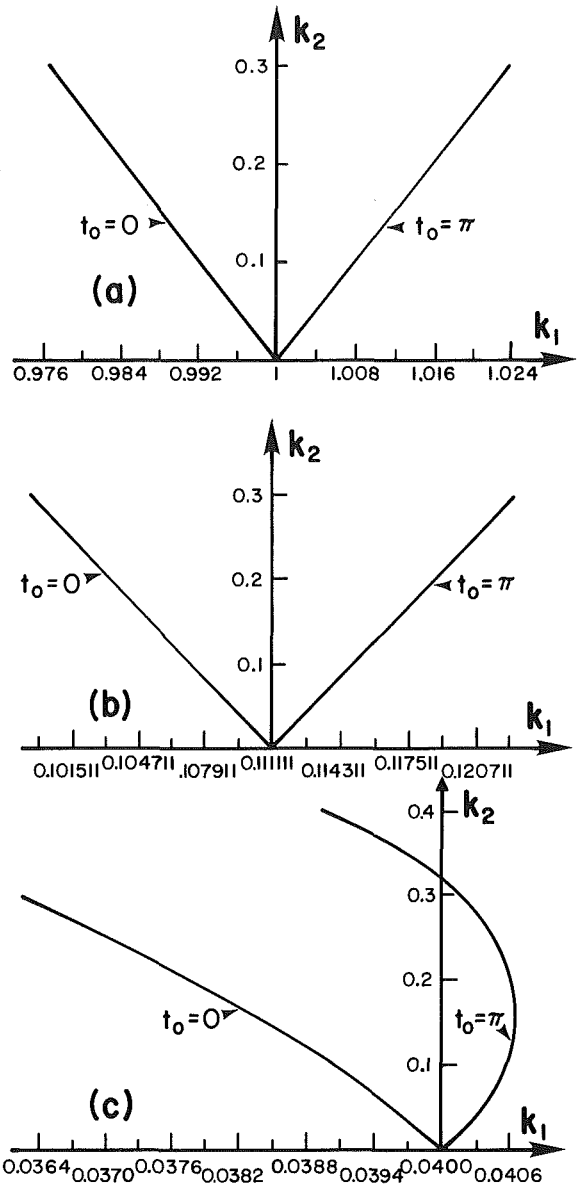


Fig. 2 Periodic orbits of equation (2.2*b*) with period: (*a*) $T = 2\pi$, (*b*) $T = 6\pi$, and (*c*) $T = 10\pi$

and obtain for them explicit results which, at least qualitatively, may be expected to hold in more general cases as well.

We begin, in Section 2, by presenting a systematic numerical scheme for finding synchronized periodic orbits of equation (1.2), which we refer to as the *indicatrix method*. This method is applied to equations (1.3) for $\sqrt{k_1} \cong \omega = 1/m$, $m = 1, 2, 3, \ldots$, (cf. 1.1), and either *two or four* such periodic orbits are found for each k_2: (1.3*a*) has two, with m even, and four with m odd, while (1.3*b*) has two with m odd and four with m even.

In Section 3, these periodic orbits are studied analytically by the methods of generalized averaging (Balbi, 1973). Explicit expressions are derived for them (to second order in k_2, $|k_2| \ll 1$), which turn out to be very accurate, when compared with the numerical results of Section 2, up to $k_2 \lesssim 0.3$.

Finally, in Section 4, we use the analytical formulas of Section 3 to study the stability properties of our synchronized periodic solutions: Linearizing equations (1.3) about them, we derive Hill's type equations (Magnus and Winkler, 1966) to which we apply the standard perturbation techniques of multiple time scales (Nayfeh and Mook, 1979; Cole, 1968; Kevorkian and cole, 1965). Thus, regions of instability are obtained in the k_1, k_2 plane (to second order in k_2), whose predictions are in very good agreement with the results of numerical experiments, on the x, $\dot{x}$ surface of section of the system.

2 A Numerical Method for Finding Synchronized Periodic Orbits

In this section we present a method for numerically finding synchronized periodic orbits of a class of nonlinear oscillators of the form

$$\ddot{x} + k_1 x + k_2 f(x, \dot{x}) P(\Omega t) = 0 \tag{2.1}$$

where $P(\Omega t)$ is a periodic function of frequency Ω and k_2 is a small parameter. In particular, we shall illustrate this method here on the following examples

$$\ddot{x} + k_1 x + k_2 x^3 \cos t = 0 \tag{2.2a}$$

$$\ddot{x} + k_1 x + k_2 x^4 \cos t = 0 \tag{2.2b}$$

where the unperturbed frequency $\sqrt{k_1}$ takes values in the neighborhood of the rationals $1/m$, $m = 1, 2, 3, \ldots$.

Using our so called *indicatrix method* we shall determine the values of the parameters k_1, k_2 at which periodic orbits of (2.2) with frequency $1/m$ ($\cong \sqrt{k_1}$) *pass by a specified initial condition*, e.g., $(x(t_0), \dot{x}(t_0)) = (0.5, 0)$.

Clearly, for $k_2 = 0$, all points $[x(t_0), \dot{x}(t_0)]$ can serve as initial conditions for periodic orbits with frequency $1/m$. However, for $k_2 \neq 0$, the set of points $[x(t_0 + T), \dot{x}(t_0 + T)]$ with $T = 2\pi m$ form a closed curve parameterized by $t_0 \in [0, 2\pi]$ which may or may not pass by our specified initial condition (0.5, 0). This closed curve is called the *indicatrix* and is plotted here in Fig. 1*a* for $k_1 \cong 1$[and equation (2.2*b*)].

By slightly varying k_1 and k_2, we obtain the desired periodic orbits when the indicatrix is observed to pass by our initial condition at some value of t_0. This can happen, of course, for more than one value of $t_0 \in [0, 2\pi]$, see Figs. 1(*b*) and 1(*c*) where $t_0 = \pi$ and 0, respectively.

In the case of the quartic nonlinearity in equation (2.2*b*), we have studied the existence of periodic orbits with period $T = 2m\pi$, $m = 1, 2, 3, \ldots$ corresponding to $k_1 \cong 1/m^2$. For $k_1 \cong 1$, 1/9, and 1/25 for example, we find with our indicatrix method *two* curves in the k_1, k_2 plane corresponding to two periodic orbits for $t_0 = 0$, and π, (see Fig. 2). On the other hand, for $k_1 \cong 1/4$ and $k_1 \cong 1/16$, equation (2.2*b*) appears to have *four* periodic orbits (with period 4π and 8π, respectively) for $t_0 = 0$, π, $(\pi/2) - \tau$, $(3/2)\,\pi + \tau$ where $\tau \in (0, \pi/2)$ (see Fig. 3).

Downloaded 03 May 2010 to 171.66.16.21. Redistribution subject to ASME license or copyright; see http://www.asme.org/terms/Terms_Use.cfm

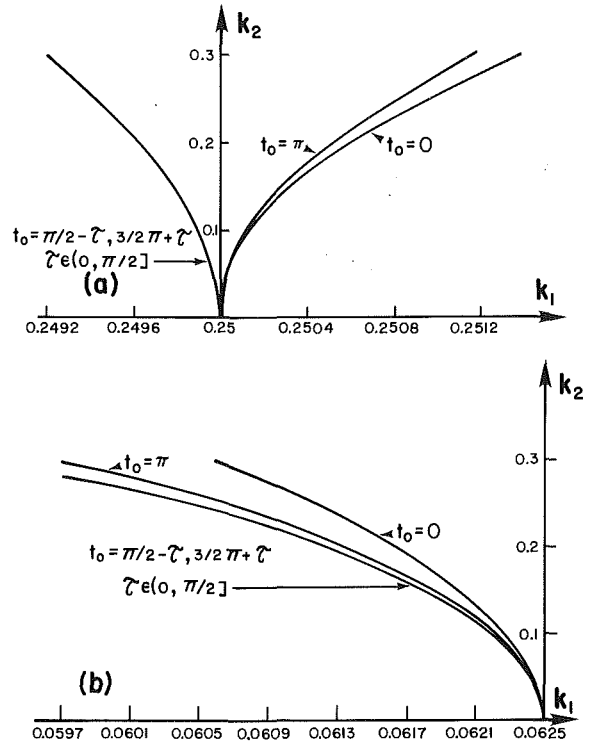


Fig. 3 Periodic orbits of equation (2.2*b*) with period: (*a*) $T = 4\pi$ and (*b*) $T = 8\pi$

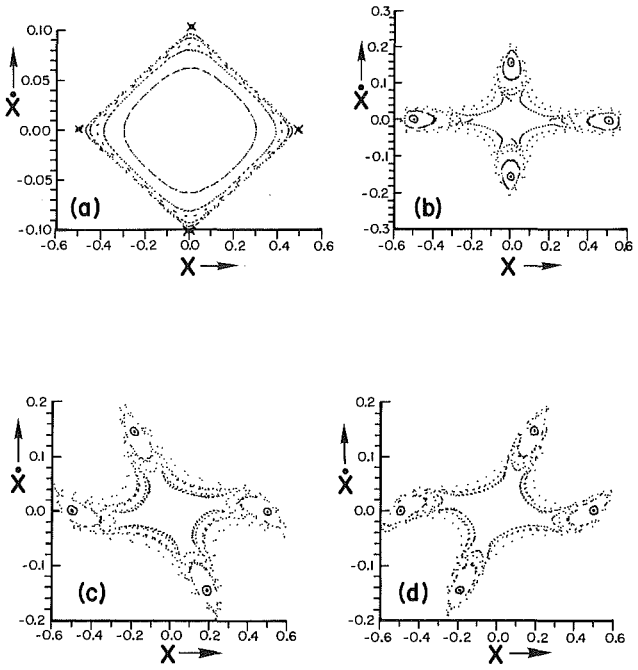


Fig. 4 Surface of sections for equation (2.2*a*) for $k_2 = 0.35$, and: (*a*) $k_1 = 0.0465$, $t_0 = 0$, (*b*) $k_1 = 0.064$, $t_0 = \pi$, (*c*) $k_1 = 0.06425$, $t_0 = 1.8849535$, and (*d*) $k_1 = 0.06425$, $t_0 = 4.3982248$, x denotes the unstable ones and ○ the stable ones

In the case in which the nonlinear term is odd, i.e., equation (2.2*a*), one finds only two periodic orbits for $k_1 \cong 1/m^2$ with $m = 2, 4, \ldots$ and four periodic orbits with $m = 1, 3, \ldots$ (Elnaggar and Elboughy, 1981).

To examine these periodic orbits in more detail, we use the Poincaré map associated with equation (2.2), at the parameter values suggested by the indicatrix method. In fact, using this map we can even determine the *stability properties* of these periodic orbits under small perturbations in the initial conditions. This is illustrated here for the case $k_1 \cong 1/16$, since all other cases can be similarly treated.

Thus, let us consider the Poincaré map, or the $(x, \dot{x})$ surface of section $\Sigma^{t_0} = \{[x(t_n), \dot{x}(t_n)],\ t_n = t_0 + 2n\pi\}$. We know from the Poincaré-Birkhoff fixed point theorem (Helleman, 1981) that for $k_2 \neq 0$ the invariant curves corresponding to periodic orbits of the $k_2 = 0$ case "break up" into an even number of periodic orbits, half of which are *stable* (elliptic) and half *unstable* (hyperbolic).

Integrating equation (2.2*a*) numerically for $k_1 \cong 1/16$ and several initial conditions and plotting the intersections of orbits on the $x, \dot{x}$ surface of section of Fig. 4, we find—as predicted by the indicatrix method—that the system has two different periodic orbits with period 8π: One of them is clearly seen to be unstable ($t_0 = 0$) and the other stable ($t_0 = \pi$), marked by x and ⊙ in Figs. 4(*a*) and (*b*), respectively. In the case (2.2*b*), however, there are four periodic orbits with period 8π: Two of them ($t_0 = 0$, π marked S_1, S_2) are stable and two are unstable (with $t_0 = 1.02101$, 5.26216), marked by U_1, U_2 in Fig. 5.

We remark at this point that the indicatrix method described above does not always pick different periodic orbits for different values of t_0. For example, in the case of equation (2.2*a*), the curve of $t_0 = \pi$ identifies the unstable period 8π orbit for $0 \leq k_2 \leq 0.26$, (see Fig. 6). However, there is an interesting "bifurcation" phenomenon occurring at $k_2 \cong 0.26$, and $k_1 \cong 0.0659$: Near that point, the stable and stable unstable period 8π orbits coalesce at the initial condition (0.5, 0). Thus, for $k_2 \gtrsim 0.26$, the indicatrix method starts to follow the *stable* period 8π orbit and, in fact, does so at three different values of t_0: $t_0 = \pi$ (Fig. 4(*b*)) and $t_0 = \pi - \tau$, $\pi + \tau$, (see Figs. 4(*c*), 4(*d*)). This is evident in Fig. 6, where, as it is now clear from Fig. 4, the two curves "bifurcating" out of the $t_0 = \pi$ curve for $k_2 \gtrsim 0.26$ actually identify one and only one period 8π orbit.

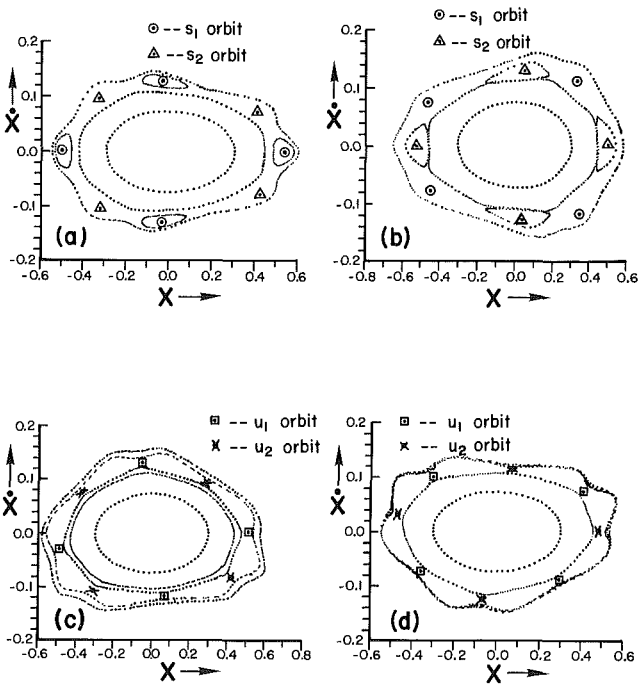


Fig. 5 Surface of sections for equation (2.2*b*) for $k_2 = 0.25$, and: (*a*) $k_1 = 0.061185$, $t_0 = 0$, (*b*) $k_1 = 0.0607$, $t_0 = \pi$, (*c*) $k_1 = 0.060615$, $t_0 = 1.02101$, and (*d*) $k_1 = 0.060615$, $t_0 = 5.26216$

Downloaded 03 May 2010 to 171.66.16.21. Redistribution subject to ASME license or copyright; see http://www.asme.org/terms/Terms_Use.cfm

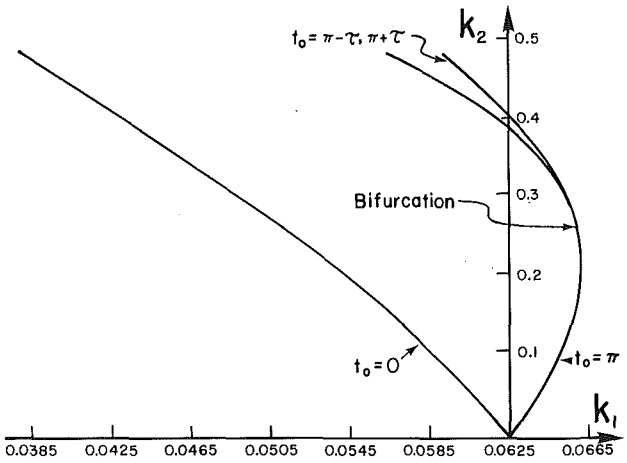


Fig. 6 Periodic orbits with period $T=8\pi$ for equation (2.2a)

3 An Analytical Study of Synchronized Periodic Orbits

In this section, we use the method of *generalized averaging* (Balbi, 1973; Haag, 1962) to derive to first and second order in λ, analytical expressions for the synchronized periodic solutions of

$$\ddot{x}+\omega^2 x+\lambda x^4\cos t=0 \tag{3.1}$$

obtained numerically by the indicatrix method of Section 2.

When $\lambda=0$, the general solution of (3.1) is:

$$x=a\cos(\omega t+\phi),\ \dot{x}=-a\omega\sin(\omega t+\phi),\ a,\ \phi \text{ const.} \tag{3.2}$$

For $\lambda\neq 0$ small enough, let a and ϕ be unknown functions of time t in (3.2). By differentiating the first equation of (3.2) and equating with the second, and differentiating the second equation of (3.2) and substituting in (3.1), we get a system of equations which we solve for $\dot{a}(t)$, $\dot{\phi}(t)$ to obtain:

$$\frac{d}{dt}\begin{bmatrix} a(t) \\ \\ \phi(t) \end{bmatrix}=\frac{\lambda a^3(t)}{32\omega}\begin{bmatrix} a(t)(2\sin\psi_1+2\sin\psi_2+3\sin\psi_3+3\sin\psi_4+\sin\psi_5+\sin\psi_6) \\ \\ (10\cos\psi_1+10\cos\psi_2+5\cos\psi_3+5\cos\psi_4+\cos\psi_5+\cos\psi_6) \end{bmatrix} \tag{3.3}$$

where the $\cos^4(\omega t+\phi)$ term has been expanded in trigonometric terms with arguments:

$$\begin{aligned}&\psi_1=(\omega+1)t+\phi(t),\ \psi_2=(\omega-1)t+\phi(t),\\ &\psi_3=(3\omega+1)t+3\phi(t)\\ &\psi_4=(3\omega-1)t+3\phi(t),\ \psi_5=(5\omega+1)t+5\phi(t),\\ &\psi_6=(5\omega-1)t+5\phi(t)\end{aligned} \tag{3.4}$$

We now attempt to solve system (3.3) with (3.4) by the generalized averaging method, briefly described below (see also Balbi, 1973, for more details):

Starting with the second order differential system

$$\frac{dz}{dt}=\lambda f(z,t),\quad z=\begin{bmatrix} a(t) \\ \\ \phi(t) \end{bmatrix} \tag{3.5a}$$

and writing

$$f(z,t)=\bar{f}(y)+\tilde{f}(y,t),\ y=\begin{bmatrix} a(t_0) \\ \\ \phi(t_0) \end{bmatrix}=\begin{bmatrix} A \\ \\ \Phi \end{bmatrix} \tag{3.5b}$$

where $\bar{f}(y)$ contains the constant terms and terms of smallest frequency and $\tilde{f}(y,t)$ the terms of higher frequency, one associates with (3.5) the following reduced system

$$\frac{dy}{dt}=\lambda\,\bar{F}(y), \tag{3.6a}$$

where

$$z=y+\lambda\tilde{G}(y,t). \tag{3.6b}$$

Expanding $\bar{F}(y)$ and $\tilde{G}(y,t)$ as a series in λ,

$$\bar{F}(y)=\bar{F}_1(y)+\lambda\bar{F}_2(y)+\ \ldots\ +\lambda^{m-1}\bar{F}_m(y)+\ \ldots, \tag{3.7a}$$

$$\tilde{G}(y,t)=\tilde{G}_1(y,t)+\lambda\,\tilde{G}_2(y,t)+\ \ldots\ +\lambda^{m-1}\tilde{G}_m(y,t)+\ \ldots, \tag{3.7b}$$

and substituting (3.6b) into (3.5) and using (3.6a) and (3.7), yields upon equating like powers of λ:

$$\bar{F}_1(y)=\overline{f(y,t)},\qquad \bar{F}_2(y)=\overline{\frac{\partial\tilde{f}}{\partial y}\int\tilde{f}(y,t)dt},\ \ldots,$$

$$\tilde{G}_1(y,t)=\int\tilde{f}(y,t)dt,\ \ldots \tag{3.8}$$

Note that system (3.3) is split in such a way that small frequency components occur at $\omega\cong 1$, 1/3, and 1/5. This means that we can get periodic orbits with periods 2π, 6π, and 10π already by the first approximation. To find periodic orbits with periods 4π, 8π, . . . , we need to go to second or higher order approximations. The approximate formulas for the amplitude and phase are written as follows:

$$a(t)=A+\lambda\tilde{G}_{1a}(y,t)+\lambda^2\tilde{G}_{2a}(y,t)+0(\lambda^3) \tag{3.9a}$$

$$\phi(t)=\Phi+\lambda\,\tilde{G}_{1\phi}(y,t)+\lambda^2\tilde{G}_{2\phi}(y,t)+0(\lambda^3) \tag{3.9b}$$

where

$$\tilde{G}_1(y,t)=\begin{bmatrix} \tilde{G}_{1a}(y,t) \\ \tilde{G}_{1\phi}(y,t) \end{bmatrix},\ \tilde{G}_2(y,t)=\begin{bmatrix} \tilde{G}_{2a}(y,t) \\ \tilde{G}_{2\phi}(y,t) \end{bmatrix}$$

(cf. 3.5), where $\tilde{G}_1(y,t)$, and $\tilde{G}_2(y,t)$ are to be solved as described previously to obtain the synchronized solution of equation (3.2) to order λ, λ^2, etc.

We present here the analytical expressions for such synchronized orbits with period 2π, up to the second order in λ: Note that for $\omega\cong 1$ the terms of smallest frequency are:

$$\bar{F}_1(y)=\overline{f(y,t)}=\begin{bmatrix} \overline{f_1(y,t)} \\ \\ \overline{f_2(y,t)} \end{bmatrix}=\frac{A^3}{16\omega}\begin{bmatrix} A\ \sin((\omega-1)t+\Phi) \\ \\ 5\ \cos((\omega-1)t+\Phi) \end{bmatrix} \tag{3.10a}$$

and those of higher frequency:

$$\tilde{f}(y,t)=\begin{bmatrix} \tilde{f}_1(y,t) \\ \\ \tilde{f}_2(y,t) \end{bmatrix}$$

$$=\frac{A^3}{32\omega}\begin{bmatrix} A(2\sin\psi_1+3\sin\psi_3+3\sin\psi_4+\sin\psi_5+\sin\psi_6) \\ \\ (10\cos\psi_1+5\cos\psi_3+5\cos\psi_4+\cos\psi_5+\cos\psi_6) \end{bmatrix} \tag{3.10b}$$

Downloaded 03 May 2010 to 171.66.16.21. Redistribution subject to ASME license or copyright; see http://www.asme.org/terms/Terms_Use.cfm

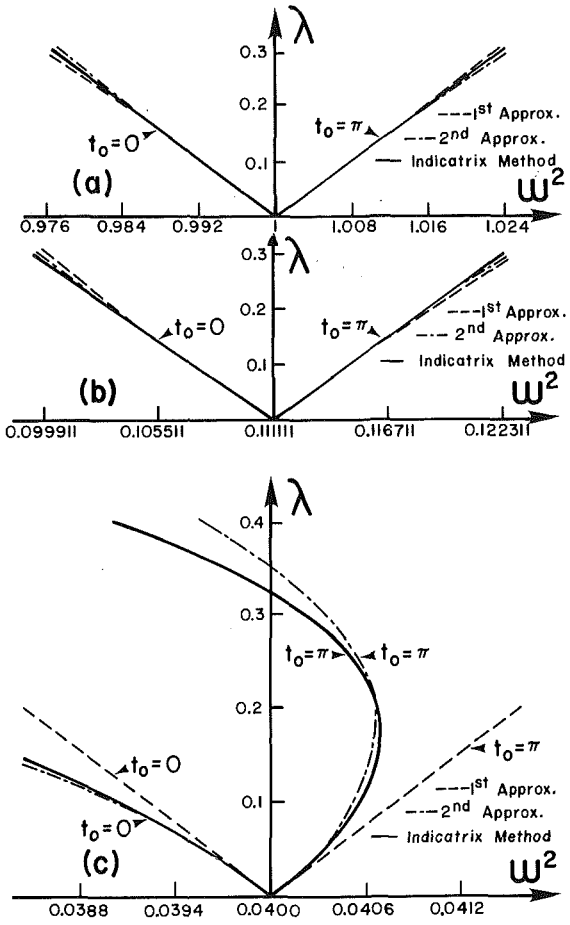


Fig. 7 Comparison between the analytical formulas (3.15-17) and the numerical results of Fig. 2

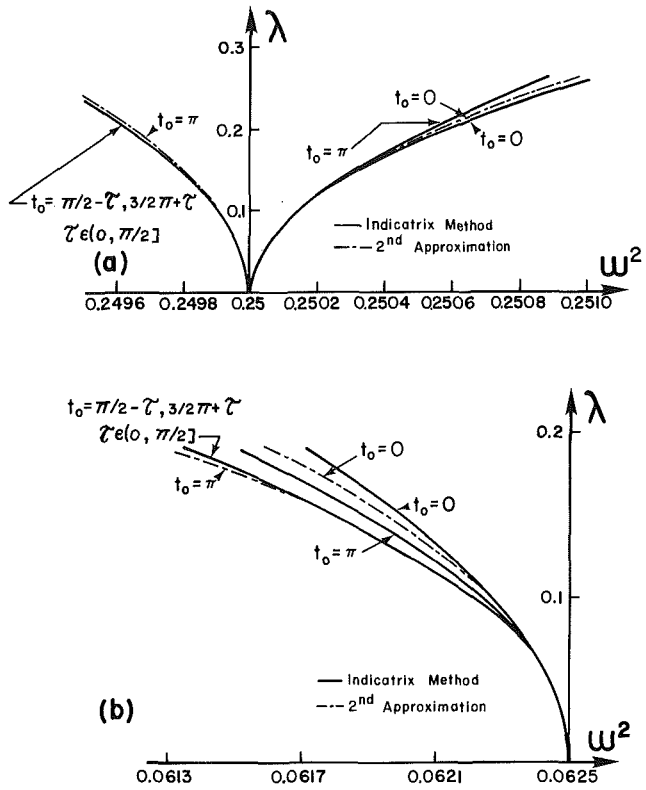


Fig. 8 Comparison between the analytical formulas (3.18 and 3.19) and the numerical results of Fig. 3

where

$$\psi_1=(\omega+1)t+\Phi,\ \psi_3=(3\omega+1)t+3\Phi,\ \psi_4=(3\omega-1)t+3\Phi$$
$$\psi_5=(5\omega+1)t+5\Phi,\ \psi_6=(5\omega-1)t+5\Phi, \tag{3.11}$$

To derive the reduced system (3.6*a*) to second approximation, we also need to calculate the function $\bar{F}_2(y)$ from (3.8), using (3.10*b*), and (3.11). Then, using all of these results, we can write our reduced system (3.6*a*) in the form:

$$\frac{d}{dt}\begin{bmatrix} A \\ \\ \Phi \end{bmatrix}=\lambda\bar{F}_1(y)+\lambda^2\bar{F}_2(y)+0(\lambda^3) \tag{3.12}$$

To satisfy the condition $(dA/dt)=0$, we make the contribution of $\bar{F}_1(y)$ and $\bar{F}_2(y)$ vanish by choosing:

$$(\omega-1)t+\Phi=k\pi\,(k=0,1 \text{ for period } 2\pi \text{ orbits}) \tag{3.13}$$

Now, the second equation of (3.12) [with $\omega=1-d\Phi/dt$, (cf. 3.13)] yields:

$$\omega=1+\frac{\lambda A^3}{16\omega}\left[5(-1)^{k+1}+\frac{\lambda A^3}{128\omega}\left(\frac{340}{\omega+1}+\frac{154}{3\omega+1}+\frac{210}{3\omega-1}+\frac{8}{5\omega+1}+\frac{38}{5\omega-1}\right)\right] \tag{3.14}$$

which provides us with approximate expressions for the curves in the k_1, and k_2 plane discussed in Section 2.

The $t_0=0(k=0)$ curve is:

$$\omega^2=1-\frac{5}{8}\lambda A^3+0.22\,\lambda^2A^6+0(\lambda^3) \tag{3.15a}$$

while the $t_0=\pi\,(k=1)$ curve is:

$$\omega^2=1+\frac{5}{8}\lambda A^3+0.22\,\lambda^2A^6+0(\lambda^3) \tag{3.15b}$$

Expressions (3.15*a*,*b*) are already in very good agreement with the curves computed directly by the indicatrix method (see Figs. 7(*a*) and 2(*a*)).

By a similar analysis we obtained the following expressions for the periodic orbits of period 6π:

$$\omega^2=\frac{1}{9}-\frac{5}{16}\lambda A^3-0.07\,\lambda^2A^6+0(\lambda^3)\quad \text{for } t_0=0 \tag{3.16a}$$

$$\omega^2=\frac{1}{9}+\frac{5}{16}\lambda A^3-0.07\,\lambda^2A^6+0(\lambda^3)\quad \text{for } t_0=\pi \tag{3.16b}$$

while for period 10π we found:

$$\omega^2=\frac{1}{25}-\frac{\lambda A^3}{16}-1.429\,\lambda^2A^6+0(\lambda^3)\quad \text{for } t_0=0 \tag{3.17a}$$

$$\omega^2=\frac{1}{25}+\frac{\lambda A^3}{16}-1.429\,\lambda^2A^6+0(\lambda^3)\quad \text{for } t_0=\pi \tag{3.17b}$$

Comparing (3.16) and (3.17) with the numerically computed curves of Figs. 2(*b*) and 2(*c*), we find, again, very good agreement for a considerable range of parameter values (see Figs. 7(*b*) and 7(*c*)).

Using the same approach, as in the case of 2π-periodic orbits, to obtain analytic expressions for synchronized orbits with period 4π, and 8π, we find for the periodic orbits with period 4π

$$\omega^2=\frac{1}{4}+0.91\,\lambda^2A^6+0(\lambda^3),\quad t_0=0 \tag{3.18a}$$

$$\omega^2=\frac{1}{4}-0.589\,\lambda^2A^6+0(\lambda^3),\quad t_0=\pi \tag{3.18b}$$

Downloaded 03 May 2010 to 171.66.16.21. Redistribution subject to ASME license or copyright; see http://www.asme.org/terms/Terms_Use.cfm

and for the periodic orbits of period 8π

$$\omega^2 = \frac{1}{16} - 1.55\,\lambda^2 A^6 + 0(\lambda^3), \quad t_0 = 0 \tag{3.19a}$$

$$\omega^2 = \frac{1}{16} - 2.05\,\lambda^2 A^6 + 0(\lambda^3), \quad t_0 = \pi \tag{3.19b}$$

Expressions (3.18) and (3.19) are compared with the numerical results of Section 2, and, again, very good agreement is found for λ to be small enough (see Figs. 8(a), 8(b), 3(a), and 3(b)).

4 Instability Regions for Synchronized Periodic Solutions

In this section, we use the results of Section 3 to obtain by second order perturbation methods the boundaries of the instability regions of some synchronized periodic solutions of:

$$\ddot{x} + \omega^2 x + \lambda x^3 \cos t = 0 \tag{4.1a}$$

$$\ddot{x} + \omega^2 x + \lambda x^4 \cos t = 0 \tag{4.1b}$$

in the (λ, ω^2) plane for $0 < \lambda < 1$. We consider solutions of (4.1) which oscillate with unperturbed frequency

$$\omega^2 = n^2 + \lambda a_1 + \lambda^2 a_2 + \ldots, \quad n = 1, \frac{1}{2}, \frac{1}{3}, \frac{1}{4}, \ldots \tag{4.2}$$

We will study here the case $n = 1/4$ (other values of n can be similarly treated) and look for uniformly valid (in t) solutions of (4.1), linearized about a synchronized periodic solution of the problem.

The solutions $\hat{x}(t)$ we shall perturb about, can be obtained by the method of the previous section: Deriving $\tilde{G}_1(y,t)$, from (3.8), substituting in (3.9) and then in (3.2) we find after some calculations (Elnaggar and Elbouhy, 1981):

$$\hat{x}(t) = \frac{1}{2}\cos\frac{t}{4} - \frac{\lambda}{128}\left[\frac{3}{4}\cos\frac{9t}{4} + \frac{31}{12}\cos\frac{7t}{4} + \cos\frac{5t}{4} - 9\cos\frac{3}{4}t - 4\cos\frac{t}{4}\right] \tag{4.3a}$$

at $t_0 = 0$, for equation (4.1a), and

$$\hat{x}(t) = \frac{1}{2}\cos\frac{t}{4} + \frac{\lambda}{16}\left[\frac{2}{63}\cos 2t + \frac{8}{35}\cos\frac{3t}{2} - \frac{38}{15}\cos t + \cos\frac{t}{2} + 3\right] \tag{4.3b}$$

for equation (4.1b), also at $t_0 = 0$. We now set

$$x(t) = \hat{x}(t) + z(t), \quad z(t) \text{ ``small''} \tag{4.4}$$

and linearize equation (4.1a) about (4.3a) to obtain:

$$\ddot{z}(t) + \omega^2 z(t) + 3\lambda \hat{x}^2(t) z(t) \cos t = 0 \tag{4.5}$$

which is a (linear) Hill's equation in $z(t)$ (Magnus and Winkler, 1966).

Using the standard "multiple-scaling" techniques of perturbation theory (Nayfch and Mook, 1979; Cole, 1968) we write the solution of (4.5) as a series expansion in λ:

$$z(t,\lambda) = F_0(t,\tilde{t}) + \lambda F_1(t,\tilde{t}) + \lambda^2 F_2(t,\tilde{t}) + \ldots \tag{4.6}$$

where

$$\tilde{t} \equiv \lambda t \tag{4.7}$$

By substituting from (4.2) and (4.6) in (4.5), using (4.3a) and equating like powers of λ, we obtain the following equations:

$$\frac{\partial^2 F_0}{\partial t^2} + \frac{1}{16} F_0 = 0 \tag{4.8}$$

$$\frac{\partial^2 F_1}{\partial t^2} + \frac{1}{16} F_1 = -2\frac{\partial^2 F_0}{\partial t \partial \tilde{t}} - F_0\left(a_1 + \frac{3}{4}\cos t \cos^2\frac{t}{4}\right) \tag{4.9}$$

$$\frac{\partial^2 F_2}{\partial t^2} + \frac{1}{16} F_2 = -\frac{\partial^2 F_0}{\partial \tilde{t}^2} - 2\frac{\partial^2 F_1}{\partial t \partial \tilde{t}} - a_2 F_0 - a_1 F_1 - \frac{3}{4} F_1 \cos t \cos^2\frac{t}{4} + \frac{3}{128} F_0 \cos t \cos\frac{t}{4}\left(\frac{3}{4}\cos\frac{9}{4}t + \frac{31}{12}\cos\frac{7t}{4} + \cos\frac{5t}{4} - 9\cos\frac{3t}{4} - 4\cos\frac{t}{4}\right), \tag{4.10}$$

etc.

The solution of (4.8) is

$$F_0(t,\tilde{t}) = A_0(\tilde{t})\cos\frac{t}{4} + B_0(\tilde{t})\sin\frac{t}{4} \tag{4.11}$$

where $A_0(\tilde{t})$, $B_0(\tilde{t})$ are two as yet undetermined functions. Substituting (4.11) in (4.9) and requiring—for uniformly valid solutions—that terms proportional to sin $t/4$ and cos $t/4$ on the right-hand side vanish, leads to the following equations for A_0, and B_0:

$$\frac{1}{2}\frac{dA_0}{d\tilde{t}} + \left(\frac{3}{32} - a_1\right)B_0 = 0, \qquad \frac{1}{2}\frac{dB_0}{d\tilde{t}} + \left(a_1 + \frac{3}{32}\right)A_0 = 0 \tag{4.12}$$

It can be easily verified that the solutions of (4.12) grow exponentially if $a_1^2 < (3/32)^2$ and oscillate if $a_1^2 > (3/32)^2$. Therefore, on the boundary of the instability region $a_1 = \pm 3/32$, whence the boundary curves of the instability regions in the (λ,ω^2) plane are given to first order in λ, by

$$\omega_-^2 \cong \frac{1}{16} - \frac{3}{32}\lambda: \quad \text{Left Branch} \tag{4.13a}$$

$$\omega_+^2 \cong \frac{1}{16} + \frac{3}{32}\lambda: \quad \text{Right Branch} \tag{4.13b}$$

Repeating this procedure at second order, we demand that all resonance producing terms on the rhs of (4.10) cancel, and obtain:

$$\frac{1}{2}\frac{dA_1}{d\tilde{t}} + \left(\frac{3}{32} - a_1\right)B_1 = \frac{d^2 B_0}{d\tilde{t}^2} + a_2 B_0 + \frac{187}{4(32)^2} B_0$$
$$\frac{1}{2}\frac{dB_1}{d\tilde{t}} + \left(a_1 + \frac{3}{32}\right) = -\frac{d^2 A_0}{d\tilde{t}^2} - a_2 A_0 - \frac{1181}{4(32)^2} A_0 \tag{4.14}$$

The functions $A_0(\tilde{t})$, $B_0(\tilde{t})$ are readily obtained from (4.12):

$A_0(\tilde{t}) = a_0 e^{\mu\tilde{t}} + a_0^* e^{-\mu\tilde{t}}$, $B_0(\tilde{t}) = b_0 e^{\mu\tilde{t}} + b_0^* e^{-\mu\tilde{t}}$

with

$$\mu = 2\sqrt{\left(\frac{3}{32}\right)^2 - a_1^2} \tag{4.15}$$

and a_0, b_0, and their complex conjugates are specified by the initial conditions. [The solutions of the *homogeneous* equation (4.14) are of the same type as (4.15).]

Looking for *particular* solutions of (4.14) of the form

$$\vec{X}_p(\tilde{t}) = \sum_{i=1}^{2} C_i(\tilde{t})\vec{X}_i(\tilde{t}), \quad [\vec{X} \equiv (A_1, B_1)^t]$$

where $\vec{X}_i(\tilde{t})$, $i = 1, 2$, are a basis set of solutions of the homogeneous equation (4.14), we derive equations for $C_1(\tilde{t})$,

Downloaded 03 May 2010 to 171.66.16.21. Redistribution subject to ASME license or copyright; see http://www.asme.org/terms/Terms_Use.cfm

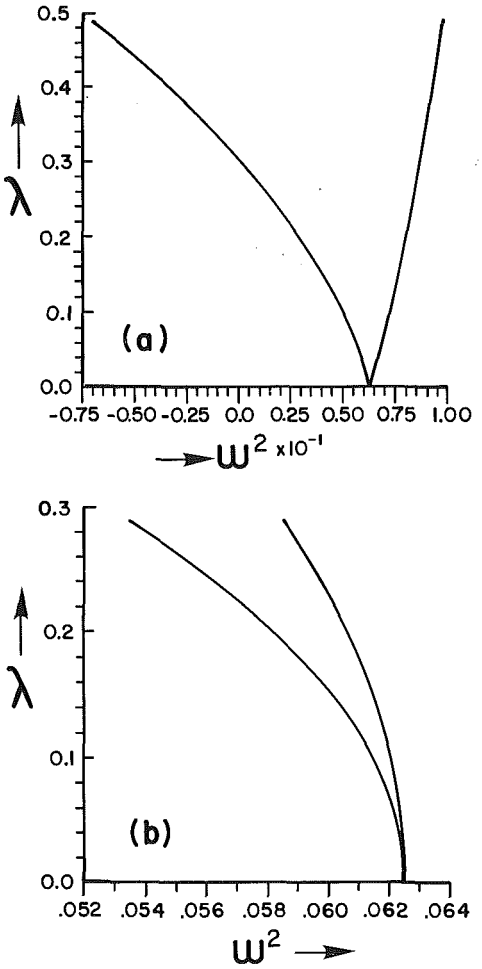


Fig. 9 *(a)* **Instability region (4.16) for equation (4.1*a*)for the 8π-periodic solution at $t_0 = 0$, with $x(0) = 0.5$ and $\dot{x}(0) = 0$. *(b)* Instability region (4.17) for equation (4.1*b*) for the 8π-periodic solution at $t_0 = 0$ and the same initial conditions as in (*a*).

$C_2(\tilde{t})$ which, when evaluated on the boundaries of the instability region, where $a_1 = \pm 3/32$, yield

$$a_2 = -\frac{1181}{4096} : \text{Left Boundary},$$

$$a_2 = -\frac{187}{4096} : \text{Right Boundary}$$

Hence, (4.13) becomes to second order in λ:

$$\omega_-^2 \cong \frac{1}{16} - \frac{3}{32}\lambda - \frac{1181}{4096}\lambda^2 : \text{Left Branch} \qquad (4.16a)$$

$$\omega_+^2 \cong \frac{1}{16} + \frac{3}{32}\lambda - \frac{187}{4096}\lambda^2 : \text{Right Branch} \qquad (4.16b)$$

Expressions (4.16*a* and *b*) are plotted here in Fig. 9(*a*), and are in agreement with the results of Section 2 (see, e.g., Fig. 4(*a*), where the values of $k_1 = 0.465$; $k_2 = 0.35$ *lie inside* the instability region of Fig. 9(*a*)).

By a similar analysis for equation (4.1*b*), we obtained the following expressions:

$$\omega_-^2 \cong \frac{1}{16} - \frac{2161}{20160}\lambda^2 \qquad (4.17a)$$

$$\omega_-^2 \cong \frac{1}{16} - \frac{95}{2016}\lambda^2 \qquad (4.17b)$$

Again, these expressions are plotted here in Fig. 9(*b*), and are in agreement with the results of Section 2 (see, e.g., Fig. 5(*a*), where the values of $k_1 = 0.061185$; $k_2 = 0.25$ *lie outside* the instability regions of Fig. 9(*b*)).

We have checked the predictions of formulas (4.16) and (4.17) displayed graphically in Figs. 9(*a*) and (*b*) against numerical computations, and have found very satisfactory agreement, for several values of k_1, k_2 (or ω^2, λ), beyond the ones mentioned above. Thus, the applicability and usefulness of these perturbation methods have been amply demonstrated in this study of synchronized periodic solutions of driven anharmonic oscillators.

5 Concluding Remarks

In this paper, we have applied analytical methods of perturbation theory to some fundamental, subharmonic solutions of equations of the form

$$\ddot{x} + k_1 x + k_2 f(x,\dot{x}) P(\Omega t) = 0, \quad P(\Omega t + 2\pi) = P(\Omega t), \qquad (5.1)$$

and have verified the validity of our results, by comparing them against numerical experiments, for small values of k_2. In fact, all our methods would apply equally well to an even broader class of models, described by

$$\ddot{x} + k_1 x + k_3 g(x,\dot{x}) + k_2 f(x,\dot{x}) P(\Omega t) = 0, \; P(\Omega t + 2\pi) = P(\Omega t), \qquad (5.2)$$

provided that k_3 was also small enough for our perturbation methods to remain applicable (Mahmoud, 1987).

For quite some time now, parametrically excited nonlinear systems of the type (5.1) or (5.2) have been known to arise in problems of applied mechanics. It is particularly interesting that they are also being used, more recently to study the stability of colliding particle beams, where the particles' horizontal displacement obeys the equation

$$\ddot{x} + Q^2 x + \epsilon\left(\frac{1}{2} + \cos t + \cos 2t + \ldots\right) \times \left(x - \frac{x(x^2+y^2)}{4}\right) = 0,$$

where Q and ϵ are machine parameters and the parametric excitation is caused by the electromagnetic, so-called beam-beam interaction (Tennyson, 1982; Bountis and Mahmoud, 1987).

Synchronized, subharmonic solutions of the kind we have investigated in this paper are certainly very important in such studies; for within the parameter ranges over which they exist, their stability properties determine the global behavior of many other solutions around them.

It is hoped, therefore, that the results of the work presented here not only demonstrate the applicability of perturbation methods to parametrically excited systems, but also underline the importance of synchronized subharmonics in gaining a better understanding of these physically relevant models.

Acknowledgments

One of us (G. M. M.) would like to acknowledge many useful conversations with Professor A. M. Elnaggar of Assiut University, Egypt, on some of the work presented here. Partial support for this research was provided by the D. O. E. grant DE-FG02-84ER40144.

References

Balbi, J. H., 1973, "Generalisation Del La Methode De La Moyenne," *Int. J. Nonlinear Mech.*, Vol. 8, pp. 313-324.

Bountis, T., and Mahmoud, G., 1987, "Synchronized Periodic Orbits in Beam-Beam Interaction Models in One and Two Space Dimensions," *Particles and Accelerators*, Vol. 22, pp. 129-147.

Downloaded 03 May 2010 to 171.66.16.21. Redistribution subject to ASME license or copyright; see http://www.asme.org/terms/Terms_Use.cfm

Bountis, T., Budinsky, N., and Eminhizer, C. R., 1984, "Resonance Criteria for Minimizing Blow-Up Effects in Colliding Proton Beams," *Nucl. Instr. Meth.*, Vol. 227, pp. 205–216.

Budinsky, N., and Bountis, T., 1983, "Stability of Nonlinear Modes and Chaotic Properties of 1D Fermi-Pasta-Ulam Lattices," *Physica D*, Vol. 8, pp. 445–452.

Chirikov, B. V., 1979, "Universal Instability of Many Dimensional Oscillator Systems," Physics Report 52.

Cole, J. D., 1968, *Perturbation Methods in Applied Mathematics*, Blaisdell, Waltham, MA.

Collet, P., and Eckmann, J.-P. 1980, *Iterated Maps on the Interval as Dynamical Systems*, Birkhauser.

Elnaggar, A., and Elbouhy, T., 1981, "Harmonic and Sub-Harmonic Solutions of a Weakly Nonlinear Conservative Differential Equation with a Periodically Varying Coefficient," *Proc. Math. Phys. Soc. Egypt*, No. 52, pp. 11–17.

Guckenheimer, J., and Holmes, P., 1983, *Nonlinear Oscillations, Dynamical Systems and Bifurcations of Vector Fields*, Springer.

Haag, J., 1962, *Oscillatory Motions*, Wadsworth Publ.

Helleman, R. H. G., and Bountis, T., 1979, "Stochastic Behavior in Classical Quantum Systems," *Lect. Notes in Physics*, Vol. 93, pp. 353–375.

Hsu, C. S., 1963, "On the Parametric Excitation of a Dynamic System Having Multiple Degrees of Freedom," ASME JOURNAL OF APPLIED MECHANICS, Vol. 85, pp. 367–372.

Kevorkian, J., and Cole, J. D., 1965, *Nonlinear Differential Equations and Nonlinear Mechanics*, Academic Press, New York.

Lieberman, M., and Lichtenberg, A., 1983, *Regular and Stochastic Motion*, Springer.

Magnus, W., and Winkler, S., 1966, *Hill's Equation*, Interscience.

Mahmoud, G. M., 1987, "Analytical and Numerical Approaches to Periodic Orbits of Nonlinear Dynamical Systems," Ph.D. Thesis, Clarkson University, Potsdam, NY.

Nayfeh, A. H., and Mook, D. T., 1979, *Nonlinear Oscillations*, John Wiley, New York.

Poincaré, H., 1957, *Les Methods Nouvelles De La Mecanique Cèlèste*, Dover.

Sevin, E., 1961, "On the Parametric Excitation of Pendulum-Type Vibration Absorber," ASME JOURNAL OF APPLIED MECHANICS, Vol. 28, pp. 330–334.

Tennyson, J. F., 1982, "Physics of High Energy Accelerators," Carrigan, R. A., Huson, F. R., and Month, M., eds., *A.I.P. Conference Proceedings*, Vol. 87, A.I.P., New York.

Tso, W. K., and Caughey, T. K., 1965, "Parametric Excitation of a Nonlinear System," ASME JOURNAL OF APPLIED MECHANICS, Vol. 32, pp. 899–902.

Downloaded 03 May 2010 to 171.66.16.21. Redistribution subject to ASME license or copyright; see http://www.asme.org/terms/Terms_Use.cfm

A Recursive Householder Transformation for Complex Dynamical Systems With Constraints

F. M. L. Amirouche
Assistant Professor.
Mem. ASME

Tongyi Jia
Graduate Research Assistant.

Sitki K. Ider
Graduate Research Assistant.

Department of Mechanical Engineering
University of Illinois at Chicago
Chicago, Ill. 60680

A new method is presented by which equations of motion of complex dynamical systems are reduced when subjected to some constraints. The method developed is used when the governing equations are derived using Kane's equations with undetermined multipliers. The solution vectors of the constraint equations are determined utilizing the recursive Householder transformation to obtain a Pseudo-Uptriangular matrix. The most general solution in terms of new independent coordinates is then formulated. Methods previously used for handling such systems are discussed and the new method advantages are illustrated. The procedures developed are suitable for computer automation and especially in developing generic programs to study a large class of systems dynamics such as robotics, biosystems, and complex mechanisms.

1 Introduction

The purpose of this paper is to present a new approach to the study of Constrained Multibody System Dynamics. In the past few years there has been a great deal of motivation to improve on the efficiency of the methods used to automatically reduce the governing equations of motion from n degrees of freedom to n-m when the system is subject to m constraints. Kamman and Huston (1984) have illustrated the use of the zero eigenvalue theorem developed by Steeves and Walton (1969) in obtaining the reduced set of equations when the governing equations of motion are derived using Kane's equations. Likins and Singh (1985) demonstrated the use of the singular value decomposition and again for when the equations of motion are obtained through Kane's equations. Wampler, Buffington, and Shu-Hui (1985) used a simple procedure to reduce the equations of motion based on finding the inverse of a matrix whose first m rows constitute the constraint Jacobian matrix and the last n-m rows correspond to the augmented matrix that relates the generalized speeds. There are a number of efforts in this area included other methodologies that utilized Lagrange's and Newton-Eulers dynamical principles [Hemami and Weimer (1987), Kirgetov (1967), Wehage and Haug (1982)]. It is also useful to refer to some previous work on the advantages of Kane's equations when applied to complex dynamical systems [Huston and Passerello (1973), Kane (1961), Kane and Levinson (1980)]. Recently it has been suggested by Huston and Wang (1986) that the extension of Kane's equations to include the undetermined multipliers could have some useful applications in robotics. It should be noted, however, that if the constraint forces are of no interest in the analysis one can proceed directly with Kane's equations without the introduction and subsequent elimination of the undetermined multipliers. This approach is utilized in this paper to apply the Pseudo-Uptriangular Decomposition Method (PUTD) to reduce and, hence, eliminate the generalized constraint forces from the equations of motion. The automatic elimination of the undetermined multipliers makes the analysis of constrained multibody systems more pronounced since the undetermined multipliers do not have to be calculated.

The advantages to the approach presented stems from the use of Kane's equations with the undetermined multipliers and the reduced equations in their developed form. The recursive Householder transformation has an advantage over the previously developed methods which require the computation of the eigenvalue problem of a symmetric matrix, since it employs successive multiplication of the Householder transformations relating two linearly independent vectors.

The procedure is tailored for the automatic computer generation of the governing equations of motion of complex multibody systems subject to constraints.

This paper is divided into five sections. The first section gives an introduction to the background and motivation; in the second section Kane's equations with undetermined multipliers are developed; the third and most important section is devoted to the development of the Pseudo-Uptriangular Decomposition Method; the relation of the method presented to previous methods is presented in section four; and the conclusion forms the last section.

Contributed by the Applied Mechanics Division for publication in the JOURNAL OF APPLIED MECHANICS.

Discussion on this paper should be addressed to the Editorial Department, ASME, United Engineering Center, 345 East 47th Street, New York, N.Y. 10017, and will be accepted until two months after final publication of the paper itself in the JOURNAL OF APPLIED MECHANICS. Manuscript received by ASME Applied Mechanics Division, January 8, 1987; final revision, February 1, 1988.

Copyright © 1988 by ASME
Downloaded 03 May 2010 to 171.66.16.21. Redistribution subject to ASME license or copyright; see http://www.asme.org/terms/Terms_Use.cfm

II Kane's Equations With Undetermined Multipliers

The governing equations of motion of a multibody system could be obtained using Kane's equations (see Kane and Levinson, 1985)

$$f_l + f_l^* = 0 \tag{1}$$

$$(l = 1, 2, \ldots, 6N)$$

where f_l is defined to be the generalized active forces array and is given by

$$f_l = V_{klm} F_{km} + \omega_{klm} T_{km} \tag{2}$$

whereas f_l^* is the generalized inertia force array given by

$$f_l^* = V_{klm} F_{km} + \omega_{klm} T_{km}^* \tag{3}$$

in both equations (2) and (3) V_{klm} and ω_{klm} are the corresponding partial velocity (see Huston and Wang, 1986) associated with the mass center velocity and angular velocity of B_k in a reference frame R. In equation (2) F_{km} and T_{km} are the $\underset{\sim}{n}_{om}$ components of the vectors force $\underset{\sim}{F}_k$ and the torque $\underset{\sim}{T}_k$. (Note that a force acting on a body B_k could be replaced by a force and moment acting at the mass center of B_k.)

In equation (3), however, the F_{km}^* and T_{km}^* are the $\underset{\sim}{n}_{om}$ components of the inertia forces $\underset{\sim}{F}_k^*$ and $\underset{\sim}{T}_k^*$, where

$$\underset{\sim}{F}_k^* = -m_k \underset{\sim}{a}_k \tag{4}$$

and

$$\underset{\sim}{T}_k^* = -\underset{\sim}{I}_k \cdot \underset{\sim}{\alpha}_k - \underset{\sim}{\omega}_k \times (\underset{\sim}{I}_k \cdot \underset{\sim}{\omega}_k) \tag{5}$$

In equation (4) m_k denotes the mass of body B_k, and $\underset{\sim}{a}_k$ is its mass center acceleration, $\underset{\sim}{I}_k$ is the inertia dyadic of B_k relative to its center mass and expressed with respect to the $\underset{\sim}{n}_{om}$ components in R; $\underset{\sim}{\omega}_k$ is the angular velocity of B_k and $\underset{\sim}{\alpha}_k$ it's corresponding angular acceleration. Regarding the notation of the repeated indices in equations (2) and (3) see reference [22].

Constraint Equations. If a multibody system or a complex structure dynamics is subject to some constraints which might result from close loops or prescribed motions then, in addition to the $6N$ equations of motion given by equation (1), we have a set of m constraint equations that must be satisfied. Let the constraint equations be given by

$$\phi_i(X_1, X_2 \ldots, t) = 0$$

$$(i = 1, 2, \ldots m)$$

by differentiation equation (6) could be expressed as

$$B_{il} Y_l = g_i \tag{7}$$

where

$$Y_l = \dot{X}_l \tag{8}$$

Y_i are the generalized speeds as described by Kane [18]. For simple holonomic constraints equation (7) reduces to

$$B_{il} Y_l = 0 \tag{9}$$

It is seen in Kane and Levinson (1985) that from Kane's equations we can obtain Lagrange equations, hence equation (1) could be modified so we can introduce the so-called Lagrange multipliers such that

$$f_l + f_l^* + \lambda_i B_{il} = 0 \tag{10}$$

Equation (10) then becomes the Kane's equations with undetermined multipliers (5), where λ_i denotes the undetermined multipliers. Rewriting equation (10) in a different form leads to

$$f_l + f_l^* + f_l^c = 0 \tag{11}$$

where f_l^c are the generalized constraint forces.

It is obvious that the governing equations of motion for a constrained multibody system are given by equations (10) or (11) together with equation (7).

If a system has $6N$ deg of freedom, (N is the number of bodies in the structure) and m constraint equations, then the system reduces to $6N$-m deg of freedom which are the independent coordinates or generalized coordinates of the system. A method by which the equations of motion given by equation (10) are reduced and therefore automatically eliminate the undetermined multipliers forms the basis for this paper.

III Pseudo Uptriangular Decomposition (PUTD) Theorem

Consider the equation

$$\mathbf{B}\, Y = 0 \tag{12}$$

where $\mathbf{B}$ is a matrix with any number of columns and any number or rows. Let n be the number of columns and m the number of rows.

First, let's introduce the well known Householder transformation which states that for any two given vectors $\underset{\sim}{x}$ and $\underset{\sim}{y}$ ϵR^n, where R^n denotes an n-dimensional real space, $\exists$ a unit vector $\underset{\sim}{u}$ such that

$$H\underset{\sim}{x} = \sigma \underset{\sim}{y} \tag{13}$$

where

$$H = \mathbf{I} - 2\underset{\sim}{u}\underset{\sim}{u}^T \tag{14}$$

and

$$\sigma = \sqrt{\frac{\underset{\sim}{x}^T \underset{\sim}{x}}{\underset{\sim}{y}^T \underset{\sim}{y}}}$$

$\underset{\sim}{x}^T$ and $\underset{\sim}{y}^T$ denotes the transpose of $\underset{\sim}{x}$ and $\underset{\sim}{y}$, respectively, and $\mathbf{I}$ is the identity matrix. The Householder transformation also states that

(a) If $\underset{\sim}{x} \neq \underset{\sim}{o}$ and $\sigma \underset{\sim}{y} \neq x$ then $\underset{\sim}{u}$ is uniquely defined as

$$\underset{\sim}{u} = \frac{\sigma \underset{\sim}{y} - \underset{\sim}{x}}{\sqrt{(\sigma \underset{\sim}{y} - \underset{\sim}{x})^T (\sigma \underset{\sim}{y} - \underset{\sim}{x})}} \tag{15}$$

(b) If $\underset{\sim}{y} \neq o$ and $\sigma \underset{\sim}{y} = \underset{\sim}{x}$, then

$$\underset{\sim}{u} = \underset{\sim}{o} \tag{16}$$

(c) If $\underset{\sim}{x} = \underset{\sim}{o}$ $\underset{\sim}{u}$ can be chosen by any vector which is not necessarily unity. For the case when the vectors are linearly independent such as is the case for the vectors given by the Jacobian matrix $\mathbf{B}$, then we can write the following

$$H\underset{\sim}{x} = \underset{\sim}{W} \tag{17}$$

where $\underset{\sim}{W}$ is given by the right-hand side of equation (13). Equation (15) can then be rewritten such as

$$\underset{\sim}{u} = \frac{\underset{\sim}{W} - \underset{\sim}{x}}{\sqrt{(\underset{\sim}{W} - \underset{\sim}{x})^T (\underset{\sim}{W} - \underset{\sim}{x})}} \tag{18}$$

it can also be shown that

$$H H^T = \mathbf{I} \tag{19}$$

therefore

$$H^{-1} = H^T \tag{20}$$

which implies that the Householder transformation matrix is an orthogonal matrix which gives a full rank transformation.

The constraint Jacobian matrix $\mathbf{B}_{il}^T$ ($i = 1, 2, \ldots, m$) has m linearly independent column vectors. Our objective is to use the Householder transformation technique to formulate an

Downloaded 03 May 2010 to 171.66.16.21. Redistribution subject to ASME license or copyright; see http://www.asme.org/terms/Terms_Use.cfm

upper triangular matrix which consists of m linearly independent vectors, and then find n-m orthonormal vectors in the n dimensional space which are orthogonal to these vectors.

Consider the first column vector of $\mathbf{B}$ where

$$\mathbf{B}_{li}^{\{1\}} = [\underset{\sim}{\mathbf{B}}_1^{\{1\}}, \underset{\sim}{\mathbf{B}}_2^{\{1\}}, \ldots, \underset{\sim}{\mathbf{B}}_m^{\{1\}}] \tag{21}$$

Let

$$\underset{\sim}{x}^{(1)} = \underset{\sim}{\mathbf{B}}_1^{\{1\}} \tag{22}$$

and

$$y^{(1)} = \left\{ \| \mathbf{B}_1^{\{1\}} \|, \underbrace{0, \ldots, 0}_{6N-1} \right\}^T \tag{23}$$

Then

$$\underset{\sim}{W}^{(1)} = \underset{\sim}{y}^{(1)} \tag{24}$$

from Equation (17) we can write

$$H^{(1)} \underset{\sim}{\mathbf{B}}_1^{\{1\}} = \underset{\sim}{W}^{(1)} \tag{25}$$

Using Equations (14) and (18) we can easily obtain $H^{(1)}$.

The Householder transformation matrix is then used to define a new set of linearly independent vectors as

$$\mathbf{B}_{li}^{\{2\}} = H_{lj}^{\{1\}} \quad \mathbf{B}_{ji} = \{ \underset{\sim}{W}^{(1)}, \mathbf{B}_2^{\{2\}}, \mathbf{B}_3^{\{2\}}, \ldots, \mathbf{B}_m^{\{2\}} \} \tag{26}$$

Similarly, consider $\mathbf{B}_2^{\{2\}}$

$$\underset{\sim}{x}^{(2)} = \underset{\sim}{\mathbf{B}}_2^{\{2\}} \tag{27}$$

With

$$\underset{\sim}{W}^{(2)} = \begin{Bmatrix} \mathbf{B}_{12}^{\{2\}} \\ [\| \mathbf{B}_2^{\{2\}} \|^2 - (\mathbf{B}_{12}^{\{2\}})^2]^{1/2} \\ 0 \\ 0 \\ \cdot \\ \cdot \\ 0 \end{Bmatrix} \tag{28}$$

where $\| \mathbf{B}_2^{\{2\}} \| \neq (\mathbf{B}_{12}^{\{2\}})^2$, otherwise $\underset{\sim}{W}^{(1)}$ and $\underset{\sim}{\mathbf{B}}_2^{\{2\}}$ become dependent. Proceeding with the foregoing procedure up to $q-1$ steps, with $2 \leq q \leq m$ we obtain

$$H_{lj}^{q-1} \mathbf{B}_{ji}^{q-1} = \mathbf{B}_{li}^{\{q\}}$$

$$= [\underset{\sim}{W}^{(1)}, \underset{\sim}{W}^{(2)}, \ldots, \underset{\sim}{W}^{(q-1)}, \underset{\sim}{\mathbf{B}}_q^q, \ldots, \underset{\sim}{\mathbf{B}}_m^{(q)}] \tag{29}$$

again, let

$$\underset{\sim}{x}^{(q)} = \underset{\sim}{\mathbf{B}}^{(q)} \tag{30}$$

and

$$\underset{\sim}{W}^{(q)} = \begin{Bmatrix} \mathbf{B}_{1q}^{\{q\}} \\ \mathbf{B}_{2q}^{\{q\}} \\ \cdot \\ \cdot \\ \cdot \\ \cdot \\ \mathbf{B}_{q-1,\,q}^{\{q\}} \\ \| \mathbf{B}_q^{(q)} \|^2 - \sum_{r=1}^{q-1} (\mathbf{B})_{rq}^q \Big)^2 \Big]^{1/2} \\ 0 \\ \cdot \\ \cdot \\ \cdot \\ 0 \end{Bmatrix} \tag{31}$$

Solving for $H^{(q)}$ then $\mathbf{B}_{li}^{(q+1)}$ could be obtained and the procedure continues up to $q=m$. At the final step the following result is obtained

$$H_{lj}^m \mathbf{B}_{ji}^{\{m\}} = [\underset{\sim}{W}^{(1)}, \underset{\sim}{W}^{(2)}, ____, \underset{\sim}{W}^m] \tag{32}$$

it can easily be seen that

$$H_{lj}^m \mathbf{B}_{ji}^{\{m\}} = H_{lj}^{\{m\}} H_{js}^{\{m-1\}} ___ H_{tp}^{(1)} \mathbf{B}_{pi} \tag{33}$$

$$= \mathbf{B}_{li}^{\{m+1\}}$$

$\mathbf{B}_{li}^{\{m+1\}}$ gives an uptriangular matrix of the form

$$\mathbf{B}_{li}^{\{m+1\}} = \begin{bmatrix} * & * & * & \cdot & \cdot & \cdot & * \\ 0 & * & * & \cdot & \cdot & \cdot & * \\ 0 & 0 & * & \cdot & \cdot & \cdot & * \\ \cdot & \cdot & \cdot & & & & \cdot \\ \cdot & \cdot & \cdot & & & & \cdot \\ \cdot & \cdot & \cdot & & & & \cdot \\ 0 & 0 & 0 & \cdot & \cdot & \cdot & * \\ 0 & 0 & 0 & \cdot & \cdot & \cdot & 0 \\ \cdot & \cdot & \cdot & & & & \cdot \\ 0 & 0 & 0 & & & & 0 \end{bmatrix} \tag{34}$$

From equation (33) we define a transformation matrix H such that

$$H \triangleq H^{(m)} H^{(m-1)} \ldots H^{(1)}$$

$$\triangleq \prod_{i=1}^{m} (I - 2u^{(i)} \cdot u^{(i)^T}) \tag{35}$$

Equation (33) shows that the columns of $\mathbf{B}^{m+1}$ are linearly independent and, hence, an orthogonal basis for the column vectors could be obtained through the Gramm-Schmidt process.

Introducing the Gramm-Schmidt process, an orthonormal set of vectors $\underset{\sim}{d}_j$ $(1 = 1,2, \ldots, m)$ can be expressed as

$$\underset{\sim}{d}_1 = \frac{\underset{\sim}{W}^{(1)}}{\| \underset{\sim}{W}^{(1)} \|} \tag{36}$$

and

$$d_2 = \left[\underset{\sim}{W}^{(i)} - \sum_{j=1}^{i-1} (\underset{\sim}{d}_j \cdot \underset{\sim}{W}^{(i)}) d_j \right] \Big/ \Big\| \underset{\sim}{W}^{(i)} - \sum_{j=1}^{i-1} (d_j \cdot \underset{\sim}{W}^{(i)}) \underset{\sim}{d}_j \Big\|$$

$$(i = 2, 3, \ldots, m) \tag{37}$$

From equations (37) and (36) we get

$$\begin{aligned} d_1 &= \{1, 0, 0, \ldots, 0\}^T \\ d_2 &= \{0, 1, 0, \ldots, 0\}^T \\ &\cdot \\ &\cdot \\ d_m &= \{0, 0, 0, \ldots, 1, 0, \ldots, 0\}^T \end{aligned} \tag{38}$$

Thus, we can define an identity matrix such as

$$\mathbf{D}_{(6N \times 6N)} \triangleq [\mathbf{D}^1_{(6N \times m)} | \mathbf{D}^2_{(6N \times (6N-m))}] = [\underset{\sim}{d}_1, \underset{\sim}{d}_2 \ldots d_m | \mathbf{D}_2] \tag{39}$$

$$\triangleq I_{6N \times 6N}$$

where

$$\mathbf{D}_2^T = [d_{m+1}, d_{m+2}, \ldots, d_{6N}] \tag{40}$$

or

$$\mathbf{D}_2^T = \begin{bmatrix} 0 & \cdot & \cdot & \cdot & \cdot & \cdot & 0 & 1 & 0 & \cdot & \cdot & \cdot & 0 \\ 0 & \cdot & \cdot & \cdot & \cdot & \cdot & 0 & 0 & 1 & \cdot & \cdot & \cdot & 0 \\ \cdot & & & & & & & & \cdot & \cdot & & & \\ \cdot & & & & & & & & \cdot & \cdot & & & \\ \cdot & & & & & & & & \cdot & \cdot & & & \\ 0 & \cdot & \cdot & \cdot & \cdot & \cdot & 0 & 0 & 0 & \cdot & \cdot & \cdot & 1 \end{bmatrix} \tag{41}$$

Downloaded 03 May 2010 to 171.66.16.21. Redistribution subject to ASME license or copyright; see http://www.asme.org/terms/Terms_Use.cfm

Since $6N$-m columns of $\mathbf{D}_2$ are orthogonal to the m columns of $\mathbf{B}_{ii}^{(m+1)}$, we have

$$\mathbf{D}_2^T \mathbf{H} \mathbf{B}^T = 0 \tag{42}$$

or

$$\mathbf{B}\mathbf{H}^T \mathbf{D}_2 = 0$$

A linear combination of the $6N$-m solution vectors is also a solution. Therefore, in general

$$\mathbf{B}\mathbf{H}^T \mathbf{D}_2 q = 0 \tag{42.a}$$

where q is an arbitrary column vector of order $6N$-m.

Hence, the following theory has been proved:

Theorem: Consider any set of m independent linear homogeneous equations in n unknowns, where $n > m$,

$$\mathbf{B}Y = 0 \tag{43}$$

There exists an orthogonal matrix $\mathbf{H}^T\mathbf{D}_2$ such that $\mathbf{B}\mathbf{H}^T\mathbf{D}_2 = 0$, where $\mathbf{H}$ is defined by recursive multiplication of Householder's transformation such that $\mathbf{H}\mathbf{B}^T$ is an up-triangular matrix, and $\mathbf{D}_2$ is a matrix whose columns are the last n-m columns of the identity matrix of order n.

Also, the general solution of the equations are

$$Y = \mathbf{H}^T \mathbf{D}_2 q \tag{44}$$

where q is any arbitrary column vector of order n-m.

IV Relation to Previous Methods

Zero-Eigenvalue Theorem: A connection between the method presented in this paper and the ones previously developed by Walton and Steeves (1969) and presented by Kamman and Huston (1984) is as follows:

Let the constraint equations be given by

$$C\dot{q} = 0 \tag{45}$$

and let the symmetric matrix $\mathbf{E}$ be defined by

$$\mathbf{E} = CC^T \tag{46}$$

the most general solution of the equations may be expressed in the form

$$\dot{q} = \mathbf{T}q \tag{47}$$

where $\mathbf{T}$ is a matrix whose columns are the columns of any modal matrix of $\mathbf{E}$ corresponding to eigenvalues of $\mathbf{E}$ which have the value zero, and where q is an arbitrary column matrix comformable with T.

From equations (44), (45), and (47) it is obvious that the matrix $\mathbf{T}$ is equivalent to matrix given by $\mathbf{H}^T\mathbf{D}_2$.

(b) Singular Value Decomposition: In singular value decomposition the orthogonal complement matrix, denoted as $\bar{T}$, could be obtained as follows

$$\bar{T} = \mathbf{I} - \mathbf{B}^+ \mathbf{B} \tag{48}$$

where $\mathbf{I}$ is the identity matrix and $\mathbf{B}^+$ is given by

$$\mathbf{B}^+ = RD^{-1}Q \tag{49}$$

where R is an array of eigenvectors of $\mathbf{B}^T\mathbf{B}$, D is a diagonal array of square roots of eigenvalues of $\mathbf{B}\mathbf{B}^T$ and Q is an array whose columns are eigenvectors of $\mathbf{B}\mathbf{B}^T$.

(c) C−D Decomposition. In the C−D decomposition method presented by Wampler, Buffington, and Shu-Hui (1985), if a mechanical system is subjected to m constraints given as

$$\mathbf{B}u + g = 0$$

then the generalized speeds denoted by u can be expressed as

$$u = \alpha \bar{u} + \beta \tag{51}$$

where $\bar{u}$ is the vector of new generalized speeds, and the $nx(n\text{-}m)$ matrix α and the $n \times l$ matrix β satisfy the relations

$$\mathbf{B}\alpha = 0, \mathbf{B}\beta = -g \tag{52}$$

The new generalized speeds can be defined as

$$\bar{u} = \mathbf{C}u + \mathbf{D} \tag{53}$$

by a proper selection of the $(n\text{-}m)xn$ matrix $\mathbf{C}$ and the $(n\text{-}m)xl$ matrix $\mathbf{D}$. $\mathbf{C}$ and $\mathbf{D}$ are usually chosen such that a subset of u is selected as $\bar{u}$.

The solution to the n equation system obtained by augmenting equations (50) and (53) yields a solution of the form of equation (51) where the orthogonal complement matrix α is obtained as

$$\alpha = \mathbf{E}^{-1}\left[\frac{0}{\mathbf{I}_{n\text{-}m}}\right] \tag{54}$$

where

$$\mathbf{E} = \left[\frac{\mathbf{B}}{\mathbf{C}}\right] \tag{55}$$

and $\mathbf{I}_{n\text{-}m}$ is the identity matrix of order n-m.

(d) Relation Between methods. Since the vector of new generalized speeds, q, is arbitrary in equation (44), the solution could be written in the form

$$Y = \mathbf{H}^T \mathbf{D}_2 \mathbf{G} \bar{q} \tag{56}$$

where $\mathbf{G}$ is any nonsingular square matrix of order $(n\text{-}m)$.

In general, the coordinate transformation matrices in each of the above methods correspond to different generalized speeds. In fact, the new generalized speeds obtained by the transformations of equations (44), (47), and (48) are abstract in character and do not lend themselves to physical interpretations. On the other hand, in the transformation given by (54) the new generalized speeds are selected among the physical generalized speeds. In view of equation (56), the relation between the transformation matrices is

$$\mathbf{H}^T \mathbf{D}_2 \mathbf{G} = P \tag{57}$$

where P is either $\mathbf{T}$, $\bar{\mathbf{T}}$ or α with corresponding nonsingular matrix $\mathbf{G}$. The columns of P are linear combinations of the columns of $\mathbf{H}^T\mathbf{D}_2$. Hence, the columns of each of the matrices $\mathbf{H}^T\mathbf{D}_2$, $\mathbf{T}$, $\bar{\mathbf{T}}$ and α form a different basis for the same n-m dimensional subspace of R^n, which is the space composed of the linear combinations of the solution vectors of equation (43).

In the special case that P is orthogonal, then $\mathbf{G}$ is an orthogonal matrix. This is seen by writing the ith and jth columns of P, $p_i = (\mathbf{H}^T\mathbf{D}_2)g_i$ and $p_j = (\mathbf{H}^T\mathbf{D}_2)g_j$ where g_i is the ith column of $\mathbf{G}$. Then, since $(\mathbf{H}^T\mathbf{D}_2)^T(\mathbf{H}^T\mathbf{D}_2) = \mathbf{I}_{n-m}$, $p_i \cdot p_j = 0$ if and only if $g_i \cdot g_j = 0$ $(i \neq j)$ and $t_i \cdot t_i = 1$ if and only if $g_i \cdot g_i = 1$.

As discussed in reference [11], the selection of $\bar{u}$ among the generalized speeds u, hence, the selection of the matrices $\mathbf{C}$ and $\mathbf{D}$, require physical judgement, since an improper selection may result in having the matrix $\mathbf{E}$ in equation (55) to be singular at the configuration of interest. In this case a different subset for $\bar{u}$ needs to be selected.

At this point it is a matter of computational efficiency to which method is best suitable for the determination of P. In order to obtain a matrix P to automatically eliminate the undetermined multipliers in the equations of motion and hence reduce the governing equations from n to n-m for m given constraints, we have shown an altnernative to the zero eigenvalue theorem, the singular value decomposition, and the

Downloaded 03 May 2010 to 171.66.16.21. Redistribution subject to ASME license or copyright; see http://www.asme.org/terms/Terms_Use.cfm



Fig. 1 Spring-Mass System, cut at the inner masses

C-D decomposition. While all four methods lead to the same answer, their computational procedures differ.

V Reduction of the Equations of Motion

Applying the Pseudo-Uptriangular Decomposition method illustrated in this paper and applying the implications of the Theorem, equation (10) reduces to

$$f_j \mathbf{H}_{jl}^T \mathbf{D}_{2_{lp}} + f_j^* \mathbf{H}_{jl}^T \mathbf{D}_{2_{lp}} = 0 \tag{58}$$

or

$$K_p + K_p^* = 0 \tag{59}$$

where

$$K_p = f_j \mathbf{H}_{jl}^T \mathbf{D}_{2lp}$$

and

$$K_p^* = f_j^* \mathbf{H}_{jl}^T \mathbf{D}_{2_{lp}} \tag{60}$$

The governing dynamical equations of motion of a complex multibody system subject to holonomic and simple nonholonomic constraints are given by equation (59) together with equation (7).

Procedure Verification. The main intent is to illustrate an application of the method. The following example is taken from Huston and Passerello (1973). Consider the following system as shown in Fig. 1 where the inner masses are of one-half-unit-magnitudes of the other masses. The displacement of the masses is measured positive to the right. It is assumed that three equations of constraint are imposed on the coordinates; namely,

$$X_2 = X_3$$

$$X_4 = X_5$$

$$X_6 = X_7 \tag{61}$$

Thus, if the coordinates $X_l (l = 1, 2, \ldots, 8)$ are chosen to describe the generalized coordinates they are not independent. The constraint equations could be put in a form given by equation (12) where the **B** matrix is as follows

$$\mathbf{B} = \begin{bmatrix} 0 & 1 & -1 & 0 & 0 & 0 & 0 & 0 \\ 0 & 0 & 0 & 1 & -1 & 0 & 0 & 0 \\ 0 & 0 & 0 & 0 & 0 & 1 & -1 & 0 \end{bmatrix} \tag{62}$$

The equations of motion for the system shown in Fig. 1 lead to eight second-order differential equations in terms of the coordinates $X_1, X_2, \ldots,$ and X_8. In solving for the system dynamic response those equations, along with the constraint equations given by equation (12), must be solved together. It is obvious that the number of degrees of freedom for the system should be five (8–3). To automatically reduce the equations of motion the method presented in this paper could be employed. Let's find the orthogonal matrix $\mathbf{H}^T\mathbf{D}_2$ which will eliminate the undetermined multipliers and, hence, reduce the equations of motion to a set of five equations.

First Step. Consider the first row of the constraint matrix **B** given by equation (56)

$$\mathbf{B}_1^{(1)} = \{0\ 1\ -1\ 0\ 0\ 0\ 0\ 0\} \tag{63}$$

Let

$$x^{(1)} = \mathbf{B}^{(1)} \tag{64}$$

and

$$W^{(1)} = \{\ |\ |x^{(1)}|\ |\ 0\ 0\ 0\ 0\ 0\ 0\ 0\} \tag{65}$$

Then equation (35) could be used to find $\mathbf{H}^{(1)}$ where it is found to be

$$\mathbf{H}^{(1)} = \begin{bmatrix} 0.0000 & 0.7071 & -0.7071 & 0.0000 & 0.0000 & 0.0000 & 0.0000 & 0.0000 \\ 0.7071 & 0.5000 & 0.5000 & 0.0000 & 0.0000 & 0.0000 & 0.0000 & 0.0000 \\ -0.7071 & 0.5000 & 0.5000 & 0.0000 & 0.0000 & 0.0000 & 0.0000 & 0.0000 \\ 0.0000 & 0.0000 & 0.0000 & 1.0000 & 0.0000 & 0.0000 & 0.0000 & 0.0000 \\ 0.0000 & 0.0000 & 0.0000 & 0.0000 & 1.0000 & 0.0000 & 0.0000 & 0.0000 \\ 0.0000 & 0.0000 & 0.0000 & 0.0000 & 0.0000 & 1.0000 & 0.0000 & 0.0000 \\ 0.0000 & 0.0000 & 0.0000 & 0.0000 & 0.0000 & 0.0000 & 1.0000 & 0.0000 \\ 0.0000 & 0.0000 & 0.0000 & 0.0000 & 0.0000 & 0.0000 & 0.0000 & 1.0000 \end{bmatrix} \tag{66}$$

$\mathbf{H}^{(1)}$ is then used to obtain the vector $\mathbf{x}^{(2)}$ as

$$\mathbf{x}^{(2)} = \mathbf{H}^{(1)}\mathbf{B} \tag{67}$$

From equation (31) we get the corresponding $W^{(2)}$ and the analysis will proceed in that manner.

The reduction of the equations of motion is obtained by multiplying the equations of motion by $\mathbf{H}^T\mathbf{D}_2$ given by

$$\mathbf{H}^T\mathbf{D}_2 = \begin{bmatrix} 0.5000 & -0.5000 & -0.5000 & 0.5000 & 0.0000 \\ 0.3536 & -0.3536 & 0.3536 & -0.3536 & 0.0000 \\ 0.3536 & -0.3536 & 0.3536 & -0.3536 & 0.0000 \\ 0.5000 & 0.5000 & 0.0000 & 0.0000 & 0.0000 \\ 0.5000 & 0.5000 & 0.0000 & 0.0000 & 0.0000 \\ 0.0000 & 0.0000 & 0.5000 & 0.5000 & 0.0000 \\ 0.0000 & 0.0000 & 0.5000 & 0.5000 & 0.0000 \\ 0.0000 & 0.0000 & 0.0000 & 0.0000 & 1.0000 \end{bmatrix} \tag{68}$$

The result obtained by equation (68) could also be achieved through the use of the zero eigenvalue theorem or the singular value decomposition. Walton and Steeves (1969) illustrated the procedure for the zero eigenvalues theorem procedure verification, their result is found to be

$$\mathbf{T} = \begin{bmatrix} 1 & 0 & 0 & 0 & 0 \\ 0 & 1/\sqrt{2} & 0 & 0 & 0 \\ 0 & 1/\sqrt{2} & 0 & 0 & 0 \\ 0 & 0 & 1/\sqrt{2} & 0 & 0 \\ 0 & 0 & 1/\sqrt{2} & 0 & 0 \\ 0 & 0 & 0 & 1/\sqrt{2} & 0 \\ 0 & 0 & 0 & 1/\sqrt{2} & 0 \\ 0 & 0 & 0 & 0 & 1 \end{bmatrix} \tag{69}$$

where **T** is the transformation matrix relating the independent coordinates (which are five in this case) and the displacement used to describe the degrees of freedom of the system given by Fig. 1.

It is readily seen by inspection that the columns of $\mathbf{H}^T\mathbf{D}_2$ are linear combinations of the columns of **T**. In other words the columns of $\mathbf{H}^T\mathbf{D}_2$ constitute another basis of the vector space composed of the linear combinations of the eigenvectors of **E** (in equation 46) corresponding to the zero eigenvalues.

Downloaded 03 May 2010 to 171.66.16.21. Redistribution subject to ASME license or copyright; see http://www.asme.org/terms/Terms_Use.cfm

The relation between the two sets is the orthogonal **G** matrix defined in equation 51, which is calculated to be

$$\mathbf{G} = \begin{bmatrix} 0.5 & 0.5 & 0.707 & 0 & 0 \\ -0.5 & -0.5 & 0.707 & 0 & 0 \\ -0.5 & 0.5 & 0 & 0.707 & 0 \\ 0.5 & -0.5 & 0 & 0.707 & 0 \\ 0 & 0 & 0 & 0 & 1 \end{bmatrix} \tag{70}$$

V Conclusion

The first observation we can make is that the Pseudo-Uptriangular Decomposition method developed in this paper gives an equivalent transformation to those developed through the zero eigenvalue theorem or the singular value decomposition. Thus, the method presented is another approach to computing the eigenvectors corresponding to the zero eigenvalues of the symmetric matrix obtained by the product of the constraint matrix and its transpose. One of the advantages to this approach must be in the computational efficiency and time involved in developing the transformation matrix. We can see that the Pseudo-Uptriangular Decomposition does not involve the computation of inverses, and modal matrices, neither does it require a symmetric matrix to obtain the required transformation matrix. The Pseudo-Uptriangular Decomposition method is achieved by successive multiplications of the Householder base transformations.

In this paper we have presented an efficient method for modifying the governing equations of motion for complex structure dynamics when subjected to holonomic and simple nonholonomic constraints. The Pseudo-Uptriangular Decomposition Method (PUTD) takes advantage of the extended version of Kane's equations where the generalized constraint forces are introduced using the undetermined multipliers. The elimination of the generalized constraint forces from the governing equations of motion gives the reduced set of equations corresponding to the independent generalized coordinates of the system. It should be noted, however, that the procedures developed in this paper also present an automated approach into solving for the generalized constraint forces should they become important in a given problem. A last observation on the method developed herein is that based on the same analysis presented in this paper a Pseudo-Lower Triangular Decomposition transformation could also be obtained. The results are the same.

References

Hemami, H., and Weimer, F. C., 1981, "Modelling of Nonholonomic Dynamic Systems with Applications," ASME JOURNAL OF APPLIED MECHANICS, Vol. 48, p. 177.

Huston, R. L., and Passerello, C. E., 1973, "On Lagrange's Form of d'Alemberts Principle," *The Matrix and Tensor Quarterly*, Vol. 23, pp. 109–112.

Huston, R. L., and Wang, J. T., 1986, "Kane's Equations with Undetermined Multipliers-Application with Constrained Multibody Systems," *ARO Symposium Kinematics and Dynamics of Robot Manipulators*, RPI, NY.

Kamman, J. W., and Huston, R. L., 1984, "Dynamics of Constrained Multibody Systems," ASME JOURNAL OF APPLIED MECHANICS, Vol. 51, pp. 899–903.

Kane, T. R., 1961, "Dynamics of Nonholonomic Systems," ASME JOURNAL OF APPLIED MECHANICS, Vol. 28, pp. 574–578.

Kane, T. R., and Levinson, D. A., 1980, "Formulation of Equations of Motion for Complex Spacecrafts," *Journal of Guidance and Control*, Vol. 3, No. 2, pp. 99–112.

Kane, T. R., and Levinson, D. A., 1985, *Dynamics: Theory and Applications*, McGraw-Hill Book Company, New York.

Kirgetov, V. I., 1967, "The Motion of Controlled Mechanical Systems with Prescribed Constraints (Servo Constraints)," *Prikl. Matem. Mekhan, (PPM)*, Vol. 31, No. 3, pp. 433–446.

Singh, R. P., and Likins, P. W., December 1985, "Singular Value Decomposition for Constrained Dynamical Systems," ASME JOURNAL OF APPLIED MECHANICS, Vol. 52, pp. 943–948.

Walton, W. C., Jr., and Steeves, E. C., 1969, "A New Matrix Theorem and Its Application for Establishing Independent Coordinates for Complex Dynamical Systems with Constraints," NASA Technical Report, TR R-326.

Wampler, C., Buffington, K., and Shu-Hui, J., 1985, "Formulation of Equations of Motion for Systems Subject to Constraints," ASME JOURNAL OF APPLIED MECHANICS, Vol. 52, pp. 465–470.

Wehage, R. A., and Haug, E. J., 1982, "Generalized Coordinate Partitioning for Dimension Reduction in Analysis of Constrained Dynamic Systems, ASME *Journal of Mechanical Design*, Vol. 104, No. 1, pp. 247.

Downloaded 03 May 2010 to 171.66.16.21. Redistribution subject to ASME license or copyright; see http://www.asme.org/terms/Terms_Use.cfm

Journal of Applied Mechanics

Brief Notes

A Brief Note is a short paper that presents a specific solution of technical interest in mechanics but which does not necessarily contain new general methods or results. A Brief Note should not exceed 1500 words *or equivalent* (a typical one-column figure or table is equivalent to 250 words; a one line equation to 30 words). Brief Notes will be subject to the usual review procedures prior to publication. After approval such Notes will be published as soon as possible. The Notes should be submitted to the Technical Editor of the JOURNAL OF APPLIED MECHANICS. Discussions on the Brief Notes should be addressed to the Editorial Department, ASME, United Engineering Center, 345 East 47th Street, New York, N. Y. 10017, or to the Technical Editor of the JOURNAL OF APPLIED MECHANICS. Discussions on Brief Notes appearing in this issue will be accepted until two months after publication. Readers who need more time to prepare a Discussion should request an extension of the deadline from the Editorial Department.

Thin Ellipse in Ground Effect: Lift Without Circulation

A. Plotkin[1]

1 Introduction

Applications in automotive aerodynamics have sparked renewed interest in the problem of ground effect, especially for bodies with non-airfoil shapes. Some recent computational studies include Katz (1985) (vortex lattice and panel method) and Hashiguchi, Ohta, and Kuwahara (1987) (Navier-Stokes equations).

For the idealized problem of steady two-dimensional incompressible irrotational flow, the airfoil in ground effect, including the effect of thickness, was first studied analytically by Havelock (1938) and Green (1947). A combination of thin-airfoil theory and an expansion in chord to wall clearance was used by Plotkin and Kennell (1981) to obtain the lift coefficient for an arbitrary thin airfoil at moderate distance from a ground plane. The explicit dependence on thickness, angle of attack and chord to wall clearance ratio was clearly displayed.

In this paper, the thin ellipse is chosen to provide an example of lift without circulation and the techniques developed in Plotkin and Kennell (1981) are modified to obtain a solution.

2 Problem Formulation and Method of Solution

The problem under consideration is the steady two-dimensional incompressible irrotational flow of a uniform stream of speed U past a thin ellipse of chord $2c$ aligned at an angle of attack α to the stream. The midchord of the ellipse is located a distance hc above a plane wall parallel to the stream. All lengths are normalized by c and speeds by U. The coordinate system is shown in Fig. 1. Distances parallel and normal to the wall are denoted by x and y, respectively, and the origin is located at midchord.

The ellipse is described by the equation

$$y = \pm\epsilon T(x) - \alpha x;\ T = (1-x^2)^{1/2} \tag{1}$$

where ϵ is the thickness ratio. The velocity field is characterized by a velocity potential Φ that is normalized by Uc. For small values of ϵ and α, the velocity potential is expanded in a perturbation series

$$\Phi = x + \phi + \ldots \tag{2}$$

where ϕ is linear in ϵ and α. The mathematical problem for ϕ is

$$\nabla^2\phi = 0 \tag{3}$$

$$\phi_y\,(x,0\pm) = \pm\epsilon\, T'(x) - \alpha \quad -1 \le x \le 1 \tag{4}$$

$$\phi_y\,(x,-h) = 0 \tag{5}$$

$$\nabla\phi \to 0 \text{ as } x^2 + y^2 \to \infty \tag{6}$$

In addition, the circulation associated with Φ is taken to be zero since the ellipse has a round trailing edge.

The disturbance to the stream is modeled by a distribution of sources of strength $\sigma(x)$ per unit length and vortices of strength $\gamma\,(x)$ per unit length, both normalized by U, along the strip $-1 \le x \le 1$, $y = 0$. When the images of these singularities in the wall are added, the only one of equations (3)–(6) that is not satisfied is the body condition (4). The source strength is found to be

$$\sigma(x) = 2\epsilon T'(x) \tag{7}$$

which is the unbounded fluid ($h \to \infty$) result. Equation (4) is then an integral equation to determine $\gamma\,(x)$. For $h >> 1$, an expansion in h^{-1} is used and except for the absence of a Kutta condition, the problem is identical to the corresponding thin-airfoil problem of Plotkin and Kennell (1981) and is solved using the same solution technique.

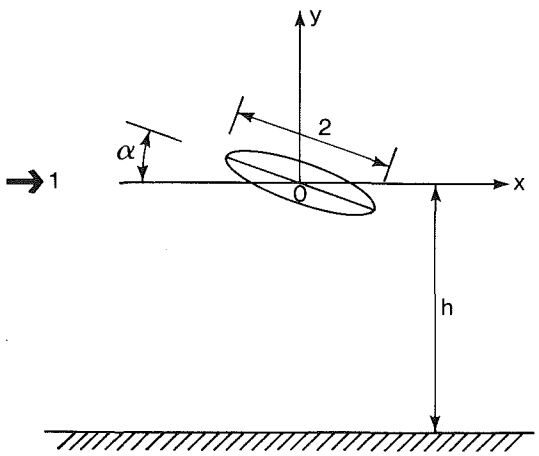


Fig. 1 Coordinate system

[1]Department of Aerospace Engineering and Engineering Mechanics, San Diego State University, San Diego, CA 92182, Mem. ASME.

Manuscript received by ASME Applied Mechanics Division, October 13, 1987; final revision, February 16, 1988.

Copyright © 1988 by ASME
Downloaded 03 May 2010 to 171.66.16.21. Redistribution subject to ASME license or copyright; see http://www.asme.org/terms/Terms_Use.cfm

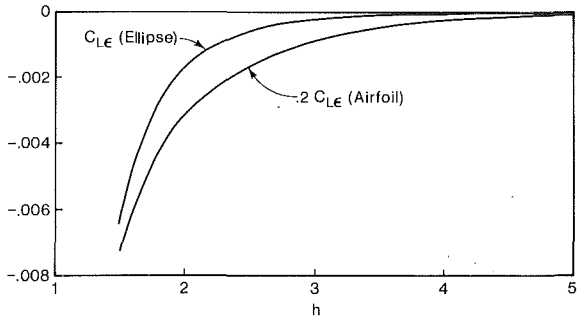


Fig. 2 Slope of lift coefficient versus thickness ratio curve for ellipse and "elliptical airfoil"

3 Results and Discussion

The solution for $\gamma(x)$ has been obtained to terms of $0(h^{-5})$. Additional terms can be obtained in a straightforward manner. The vortex strength is

$$(1-x^2)^{1/2}\gamma(x)=\epsilon\left\{\frac{1}{4}\left(x^2-\frac{1}{2}\right)h^{-3}-\frac{1}{8}\left(x^4+\frac{x^2}{4}-\frac{1}{2}\right)h^{-5}+0(h^{-7})\right\}+\alpha\{-2x-\frac{x}{4}h^{-2}+\left(\frac{x}{64}+\frac{3\pi x}{16}(x^2-\frac{1}{2}\right)h^{-4}+0(h^{-6})\} \quad (8)$$

The lift force on the ellipse cannot be determined by an integration of the surface pressure. Instead, an integral momentum balance is used to determine that the lift force on the ellipse is equal to the negative of the lift force on the ground plane. A lift coefficient C_L is defined in a standard manner and with the use of the linearized Bernoulli equation, the lift coefficient is

$$C_L=-\int_{-\infty}^{\infty}\phi_x(x,-h)\,dx \quad (9)$$

In terms of the singularity distributions equation (9) becomes

$$C_L=\frac{1}{\pi}\int_{-\infty}^{\infty}\int_{-1}^{1}\frac{h\gamma(x_0)-(x-x_0)\sigma(x_0)}{(x-x_0)^2+h^2}\,dx_0\,dx \quad (10)$$

The angle of attack and thickness effects can be treated separately. With the use of the source and vortex strengths in equations (7) and (8), equation (10) can be written

$$C_L=C_{L\alpha}\alpha+C_{L\epsilon}\epsilon \quad (11)$$

Consider first the angle of attack dependence. It can be seen from equation (8) that the vortex strength proportional to α is anti-symmetric with respect to the midchord and therefore does not contribute to C_L (equation (10)). From equation (11),

$$C_{L\alpha}=0 \quad (12)$$

To determine the lift coefficient linear in the thickness ratio, the double integral in equation (10) is integrated numerically using standard techniques. The source term in the integrand is $0(h^2)$ larger than the vortex term and it would appear to provide the major contribution to the lift coefficient. However, the integrated contribution of the source term is found to be zero so that the complete contribution to the lift coefficient for the ellipse comes from the vortex term in equation (8) which is proportional to ϵ.

The lift coefficient as a function of h (wall clearance to semi-chord ratio) is shown in Fig. 2. It is noted that the force is downward toward the wall, decays rapidly with distance from the wall, and is quite small. (It is expected that it would be difficult to calculate this force with a panel method solution).

A purpose of studying the thin ellipse in ground effect is to determine the differences in the nature of the solution for an airfoil with circulation and a comparable thin body without circulation. It is, therefore, of interest to consider the solution for a thin "elliptical airfoil" in ground effect. The "elliptical airfoil" must satisfy a Kutta condition at the trailing edge which determines its circulation. The solution technique of Plotkin and Kennel (1981) is used to obtain

$$C_L=2\pi\alpha\left\{1+\frac{1}{4}h^{-2}-\frac{3}{32}h^{-4}+0(h^{-6})\right\}+\epsilon\left\{-\frac{1}{8}h^{-3}+\frac{1}{32}h^{-5}+0(h^{-7})\right\} \quad (13)$$

The term proportional to angle of attack is the solution for a flat plate airfoil in ground effect. The Kutta condition leads to a vortex distribution which no longer has midchord antisymmetry and the lift is augmented by the presence of the ground plane. The term proportional to the thickness is compared with the ellipse solution in Fig. 2. It also provides a downforce and the airfoil lift is larger in magnitude than the lift for the ellipse. (Note that the elliptical airfoil solution of Green (1947) does not contain a term linear in thickness and independent of angle of attack as in (13) and, therefore, predicts no lift at zero angle of attack.)

Acknowledgments

The author thanks the Computer Science Center of San Diego State University for supplying computer time.

References

Green, A. E., 1947, "The Two-Dimensional Aerofoil in a Bounded Stream," *Quarterly Journal of Mathematics*, Vol. 18, pp. 167–177.

Hashiguchi, M., Ohta, T., and Kuwahara, K., 1987, "Computational Study of Aerodynamic Behavior of a Car Configuration," AIAA 87-1386.

Havelock, T. H., 1938, "The Lift and Moment on a Flat Plate in a Stream of Finite Width," *Proceedings of the Royal Society of London, Series A*, Vol. 166, pp. 178–196.

Katz, J., 1985, "Calculation of the Aerodynamic Forces on Automotive Lifting Surfaces," *Journal of Fluids Engineering*, Vol. 107, pp. 438–443.

Plotkin, A., and Kennell, C., 1981, "Thickness-induced Lift on a Thin Airfoil in Ground Effect," *AIAA Journal*, Vol. 19, pp. 1484–1486.

A Semi-Infinite Crack Penetrating an Inclusion

Chien H. Wu[2]

1 Introduction

The SIF's for the title problem are determined by an approximate method. Both the inclusion and the infinite plane are assumed to be homogeneous and isotropic. The difference between the J-tip and J-infinity integrals is expressed in terms of Eshelby's energy-momentum traction jump along the interface. This jump is then expressed in terms of values of quantities defined on the inclusion side of the interface via continuity conditions. The approximation that the K-tip field dominates the field variables on the inclusion side completes the needed explicit calculation.

The case of a circular inclusion under mode-I condition is used as a benchmark problem, as the numerically exact solution is known (Steif, 1987). Very good agreement is obtained for the case where the inclusion is either softer than or no more than twice as hard as the matrix. A similar expression is also obtained for Mode-II deformation.

[2]Professor, Department of Civil Engineering, Mechanics and Metallurgy, University of Illinois at Chicago, Chicago, IL 60680. Fellow ASME.

Manuscript received by the ASME Applied Mechanics Division, August 21, 1987; final revision, February 16, 1988.

Downloaded 03 May 2010 to 171.66.16.21. Redistribution subject to ASME license or copyright; see http://www.asme.org/terms/Terms_Use.cfm

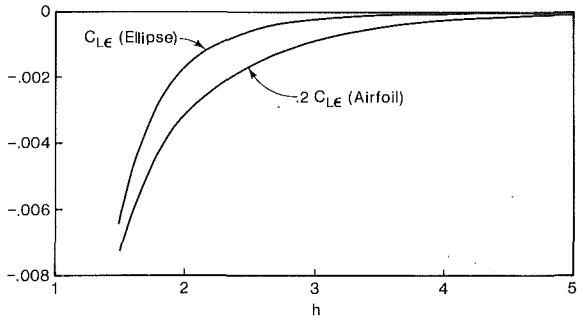


Fig. 2 Slope of lift coefficient versus thickness ratio curve for ellipse and "elliptical airfoil"

3 Results and Discussion

The solution for $\gamma(x)$ has been obtained to terms of $0(h^{-5})$. Additional terms can be obtained in a straightforward manner. The vortex strength is

$$(1-x^2)^{1/2}\gamma(x)=\epsilon\left\{\frac{1}{4}\left(x^2-\frac{1}{2}\right)h^{-3}-\frac{1}{8}\left(x^4+\frac{x^2}{4}-\frac{1}{2}\right)h^{-5}+0(h^{-7})\right\}+\alpha\{-2x-\frac{x}{4}h^{-2}+\left(\frac{x}{64}+\frac{3\pi x}{16}(x^2-\frac{1}{2}\right)h^{-4}+0(h^{-6})\} \quad (8)$$

The lift force on the ellipse cannot be determined by an integration of the surface pressure. Instead, an integral momentum balance is used to determine that the lift force on the ellipse is equal to the negative of the lift force on the ground plane. A lift coefficient C_L is defined in a standard manner and with the use of the linearized Bernoulli equation, the lift coefficient is

$$C_L=-\int_{-\infty}^{\infty}\phi_x(x,-h)\,dx \quad (9)$$

In terms of the singularity distributions equation (9) becomes

$$C_L=\frac{1}{\pi}\int_{-\infty}^{\infty}\int_{-1}^{1}\frac{h\gamma(x_0)-(x-x_0)\sigma(x_0)}{(x-x_0)^2+h^2}\,dx_0\,dx \quad (10)$$

The angle of attack and thickness effects can be treated separately. With the use of the source and vortex strengths in equations (7) and (8), equation (10) can be written

$$C_L=C_{L\alpha}\alpha+C_{L\epsilon}\epsilon \quad (11)$$

Consider first the angle of attack dependence. It can be seen from equation (8) that the vortex strength proportional to α is anti-symmetric with respect to the midchord and therefore does not contribute to C_L (equation (10)). From equation (11),

$$C_{L\alpha}=0 \quad (12)$$

To determine the lift coefficient linear in the thickness ratio, the double integral in equation (10) is integrated numerically using standard techniques. The source term in the integrand is $0(h^2)$ larger than the vortex term and it would appear to provide the major contribution to the lift coefficient. However, the integrated contribution of the source term is found to be zero so that the complete contribution to the lift coefficient for the ellipse comes from the vortex term in equation (8) which is proportional to ϵ.

The lift coefficient as a function of h (wall clearance to semi-chord ratio) is shown in Fig. 2. It is noted that the force is downward toward the wall, decays rapidly with distance from the wall, and is quite small. (It is expected that it would be difficult to calculate this force with a panel method solution).

A purpose of studying the thin ellipse in ground effect is to determine the differences in the nature of the solution for an airfoil with circulation and a comparable thin body without circulation. It is, therefore, of interest to consider the solution for a thin "elliptical airfoil" in ground effect. The "elliptical airfoil" must satisfy a Kutta condition at the trailing edge which determines its circulation. The solution technique of Plotkin and Kennel (1981) is used to obtain

$$C_L=2\pi\alpha\left\{1+\frac{1}{4}h^{-2}-\frac{3}{32}h^{-4}+0(h^{-6})\right\}+\epsilon\left\{-\frac{1}{8}h^{-3}+\frac{1}{32}h^{-5}+0(h^{-7})\right\} \quad (13)$$

The term proportional to angle of attack is the solution for a flat plate airfoil in ground effect. The Kutta condition leads to a vortex distribution which no longer has midchord antisymmetry and the lift is augmented by the presence of the ground plane. The term proportional to the thickness is compared with the ellipse solution in Fig. 2. It also provides a downforce and the airfoil lift is larger in magnitude than the lift for the ellipse. (Note that the elliptical airfoil solution of Green (1947) does not contain a term linear in thickness and independent of angle of attack as in (13) and, therefore, predicts no lift at zero angle of attack.)

Acknowledgments

The author thanks the Computer Science Center of San Diego State University for supplying computer time.

References

Green, A. E., 1947, "The Two-Dimensional Aerofoil in a Bounded Stream," *Quarterly Journal of Mathematics*, Vol. 18, pp. 167–177.

Hashiguchi, M., Ohta, T., and Kuwahara, K., 1987, "Computational Study of Aerodynamic Behavior of a Car Configuration," AIAA 87-1386.

Havelock, T. H., 1938, "The Lift and Moment on a Flat Plate in a Stream of Finite Width," *Proceedings of the Royal Society of London, Series A*, Vol. 166, pp. 178–196.

Katz, J., 1985, "Calculation of the Aerodynamic Forces on Automotive Lifting Surfaces," *Journal of Fluids Engineering*, Vol. 107, pp. 438–443.

Plotkin, A., and Kennell, C., 1981, "Thickness-induced Lift on a Thin Airfoil in Ground Effect," *AIAA Journal*, Vol. 19, pp. 1484–1486.

A Semi-Infinite Crack Penetrating an Inclusion

Chien H. Wu[2]

1 Introduction

The SIF's for the title problem are determined by an approximate method. Both the inclusion and the infinite plane are assumed to be homogeneous and isotropic. The difference between the J-tip and J-infinity integrals is expressed in terms of Eshelby's energy-momentum traction jump along the interface. This jump is then expressed in terms of values of quantities defined on the inclusion side of the interface via continuity conditions. The approximation that the K-tip field dominates the field variables on the inclusion side completes the needed explicit calculation.

The case of a circular inclusion under mode-I condition is used as a benchmark problem, as the numerically exact solution is known (Steif, 1987). Very good agreement is obtained for the case where the inclusion is either softer than or no more than twice as hard as the matrix. A similar expression is also obtained for Mode-II deformation.

[2]Professor, Department of Civil Engineering, Mechanics and Metallurgy, University of Illinois at Chicago, Chicago, IL 60680. Fellow ASME.

Manuscript received by the ASME Applied Mechanics Division, August 21, 1987; final revision, February 16, 1988.

Copyright © 1988 by ASME
Downloaded 03 May 2010 to 171.66.16.21. Redistribution subject to ASME license or copyright; see http://www.asme.org/terms/Terms_Use.cfm

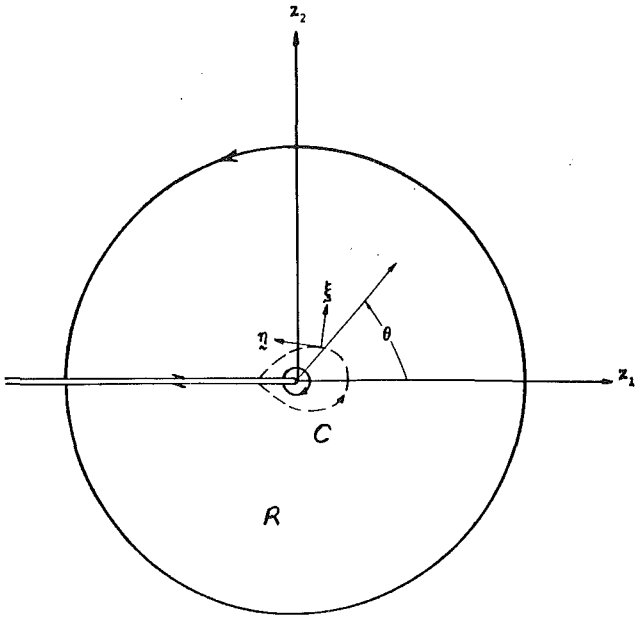


Fig. 1 A semi-infinite crack penetrating an inclusion. *R* is the region bounded by the two circles and the crack faces.

2 Energy-Momentum Traction Discontinuity Along a Two-Phase Boundary

Let a two-phase boundary be denoted by a smooth curve C in R, a two-phase composite region. With respect to a Cartesian preference (z_α, z_3), with unit vectors $(\mathbf{i}_\alpha, \mathbf{i}_3)$, the curve C is defined by

$$C: z_\alpha = x_\alpha(\sigma) \tag{2.1}$$

where σ is the arc length along C. The unit targent and normal to C are t and n, respectively, and $n \times t = i_3$. We shall also use n to denote the distance from C along n. The portions of R on the $^{\pm}n$ sides of C are $R^{\pm}$, respectively. The radius of curvature of C is denoted by $\rho(\sigma)$. Using $t=\sigma$, a set of orthogonal curvilinear coordinates (n,t) may be constructed along C. There are the following strain-displacement relations:

$$\epsilon_{nn} = u_{n,n}, \tag{2.2}$$

$$\epsilon_{tt} = u_n/(\rho+n) + u_{t,t}/\left(1+\frac{n}{\rho}\right), \tag{2.3}$$

$$\epsilon_{nt} = \frac{1}{2}\left[u_{t,n} - u_t/(\rho+n) + u_{n,t}/\left(1+\frac{n}{\rho}\right)\right], \tag{2.4}$$

The two regions $R^{\pm}$ are of different elastic materials characterized by shear moduli $\mu^{\pm}$ and plane-elasticity constants

$$\kappa^{\pm} = \begin{cases} 3-4\upsilon^{\pm} & \text{plane strain} \\ (3-\upsilon^{\pm})/(1+\upsilon^{\pm}) & \text{lane stress} \end{cases} \tag{2.5}$$

where $\upsilon^{\pm}$ are Poisson's ratio. Let $W(u_{\alpha,\beta}, z_\alpha)$ be the strain-energy density so that the stresses $\tau_{\alpha\beta}$ are given by $\partial W/\partial u_{\alpha,\beta}$. The explicit dependence of W on z_α signifies the fact that W actually consists of $W^{\pm}$.

It was shown by Eshelby (1951, 1956, and 1970) that the energy-momentum tensor $\mathbf{p}_{\beta\alpha}$ defined by

$$\mathbf{p}_{\beta\alpha} = W\delta_{\beta\alpha} - \tau_{\beta\lambda}u_{\lambda,\alpha} \tag{2.6}$$

satisfy the field equations

$$\mathbf{p}_{\beta\alpha,\beta} = W_{,\alpha(\text{explicit})}. \tag{2.7}$$

Integrating the above over R, we get

$$\int_{\partial R} p\,d\sigma = \int_R \mathbf{i}_\alpha W_{,\alpha(\text{explicit})}\,da = \int_C q(\sigma)\,d\sigma \tag{2.8}$$

where $p = p_\alpha \mathbf{i}_\alpha = \mathbf{p}_{\beta\alpha} n_\beta \mathbf{i}_\alpha$ is the energy-momentum traction and

$$q(\sigma) = q(\sigma)n = <\mathbf{p}_{\beta\alpha}(0,\sigma)> n_\beta \mathbf{i}_\alpha \tag{2.9}$$

in which $<f(0,\sigma)> = f(n=+0,\ t=\sigma) - f(n=-0,\ t=\sigma)$. The above relation was obtained by Eshelby (1970) in studying martensitic transformation, and (2.8) in just one of the conservation integrals (Knowles and Sternberg, 1972).

We proceed to express $q(\sigma)$ in terms of values of quantities on the R^- side of C. The condition that $\mathbf{u}(0,t)$ is continuous across C implies that $\mathbf{u}_{,t}(0,t)$ has the same property. It follows that

$$<\epsilon_{tt}> = <u_{n,t} - \frac{u_t}{\rho}> = 0. \tag{2.10}$$

Continuity in τ_{nt}, together with (2.4) and the second of the above, yields

$$<u_{t,n}> = -\frac{1}{\mu^-}\left(1-\frac{\mu^-}{\mu^+}\right)\tau_{nt}. \tag{2.11}$$

the first of (2.10), together with stress-strain relations, gives

$$<\tau_{tt}> = \frac{\mu^+}{\mu^-}\left\{-4\left[\left(1-\frac{\mu^-}{\mu^+}\right)(1+\kappa^+)\right]\tau_{nn} + \left[\frac{1+\kappa^-}{1+\kappa^+} - \frac{\mu^-}{\mu^+}\right](\tau_{nn}+\tau_{tt}^-)\right\}. \tag{2.12}$$

Continuity in τ_{nn} yields

$$<\epsilon_{nn}> = -\frac{1}{\mu^-}\left\{\left(1-\frac{\mu^-}{\mu^+}\right)\frac{\kappa^+-1}{\kappa^++1}\tau_{nn} + \frac{1}{2}\left(\frac{\kappa^-+1}{\kappa^++1}-1\right)(\tau_{nn}+\tau_{tt}^-)\right\}. \tag{2.13}$$

Finally, the function $q(\sigma)$ defined by (2.9) is

$$q(\sigma) = \frac{1}{2}<\tau_{tt}><\epsilon_{tt}> - \frac{1}{2}\tau_{nn}<\epsilon_{nn}> - \frac{1}{2}\tau_{nt}<u_{t,n}> \tag{2.14}$$

where (2.4) and (2.10) have been used.

It was shown by Dundurs (1969) that for a two-phase composite body the solution may be expressed in terms of two composite parameters. We use the parameters introduced by Hutchinson (1986):

$$\delta_1 = \frac{4}{\kappa^++1}\left(\frac{\mu^+}{\mu^-}-1\right),\quad \delta_2 = \frac{3-\kappa^+}{1+\kappa^+}\left(\frac{3-\kappa^-}{3-\kappa^+}\frac{\mu^+}{\mu^-}-1\right). \tag{2.15}$$

The explicit result for $q(\sigma)$ now becomes

$$q(\sigma) = \frac{\kappa^-+1}{8\mu^-}\left[\frac{\delta_1-\delta_2+\delta_2}{2(1+\delta_1-\delta_2)}\tau_{nn}^2 + \frac{\delta_1}{1+\delta_1-\delta_2}\tau_{nt}^2 + \frac{1}{2}(\delta_1-\delta_2)\tau_{tt}^2 - \delta_2\tau_{nn}\tau_{tt}\right] \tag{2.16}$$

where all τ's are evaluated on the R^- side of C.

3 The SIF Problem

The conservation integral (2.8) is now applied to the region R depicted in Fig. 1 where the inclusion boundary C is symmetric with respect to z_1:

$$C: \quad r = R(\theta) = R(-\theta)\ (-\pi < \theta < \pi) \tag{3.1}$$

Downloaded 03 May 2010 to 171.66.16.21. Redistribution subject to ASME license or copyright; see http://www.asme.org/terms/Terms_Use.cfm

where (r,θ) is a crack-tip polar coordinate system so that $d\sigma$ along C is

$$d\sigma = (R'^2 + R^2)^{1/2} d\theta. \tag{3.2}$$

It is assumed that the applied loading condition is either symmetric or antisymmetric so that the elastic field approaches either the Mode-I or Mode-II field with SIF K_∞ as $r \to \infty$. As $t \to 0$, the elastic field is dominated by the corresponding near-tip solution characterized by SIF K.

The z_1-component of (2.8) is now considered. The integrals along the infinity large and small circles are just the well-known J_1-integral (Rice, 1968) and the integrals along the crack faces vanish. Thus,

$$\left(\frac{K}{K_\infty}\right)^2 = \frac{\mu^-(1+\kappa^+)}{\mu^+(1+\kappa^-)} - \frac{1}{K_\infty^2}\int_C \frac{8\mu^-}{\kappa^- + 1} q(\sigma) n_1(\sigma) d\sigma \tag{3.3}$$

where the K's are either K_I or K_{II}. Since the stresses on either side of C are not known, the identity (3.3) offers no practical value. To derive an approximate result, we merely substitute the K-field into (2.16) to approximate $q(\sigma)$. An approximate expression for the SIF is then obtained from (3.3).

To test the usefulness of the approximation, the case of a circular inclusion is considered. The associated Mode-I problem was solved by Steif (1987) and his result is numerically exact. Substituting the K_I-field into (2.16) and integrating (3.3), we obtain

$$\frac{K_I}{K_{I\infty}} = \left(1 + \frac{5}{4}\delta_1 - \frac{3}{2}\delta_2 - \frac{1}{2}\delta_1\delta_2 + \frac{1}{2}\delta_2^2 + \frac{15}{128}\delta_1^2\right)^{-1/2} \tag{3.4}$$

which reduces to Hutchinson's (1986) "lowest order formula" as δ_1 and δ_2 tend to zero. Our ad hoc approximation, (3.4), compares favorably with Steif's solution for $\upsilon^- = \upsilon^+ = 3/10$ and $0 < \mu^-/\mu^+ < 2$. For the case of a pure Mode-II problem, the result is

$$\frac{K_{II}}{K_{II\infty}} = \left(1 + \frac{3}{4}\delta_1 - \frac{1}{2}\delta_2 - \frac{1}{2}\delta_2^2 + \frac{9}{128}\delta_1^2\right)^{-1/2} \tag{3.5}$$

which tends to 1 as δ_1 and δ_2 tend to zero and becomes zero as $\mu^-/\mu^+ \to 0$.

References

Dundurs, J., 1969, "Edge-Bonded Dissimilar Orthogonal Elastic Wedges Under Normal and Shear Loading-Discussion," ASME JOURNAL OF APPLIED MECHANICS, Vol. 36, pp. 650-652.

Eshelby, J. D., 1951, "The Force on an Elastic Singularity," *Phil. Trans. R. Soc. Lond. A*, No. 244, pp. 87-112.

Eshelby, J. D., 1956, "The Continuum Theory of Lattice Defects," *Advances in Research and Applications; Solid State Physics*, F. Seitz and D. Trumbull, eds., Academic Press, New York, Vol. III, pp. 79-144.

Eshelby, J. D., 1970, "Energy Relations and the Energy-Momentum Tensor in Continuum Mechanics," *Inelastic Behavior of Solids*, M. F. Kanninen, W. F. Adler, A. R. Rosenfield, and R. I. Jaffee eds., McGraw-Hill, New York, pp. 77-114.

Hutchinson, J. W., 1986, "Crack Tip Shielding by Micro-Cracking in Brittle Solids,' Harvard University, Mech-87.

Knowles, J. K., and Sternberg, E., 1972, "On a Class of Conservation Laws in Linearized and Finite Elastostatics," *Arch. Ration. Mech. Analysis*, Vol. 44, pp. 187-211.

Rice, J. R., 1968, "A Path Independent Integral and the Approximate Analysis of Strain Concentration by Notches and Cracks," ASME JOURNAL OF APPLIED MECHANICS, Vol. 35, pp. 379-386.

Steif, P. S., 1987, "A Semi-infinite Crack Partially Penetrating or Circular Inclusion," ASME JOURNAL OF APPLIED MECHANICS, Vol. 54, pp. 87-92.

Large-Strain Behavior of Unsymmetric Laminates

Larry A. Taber[3]

Introduction

This note examines cylindrical bending of a laminated plate undergoing large elastic strains.[4] Since the publication of the paper by Reissner and Stavsky (1961), it has been known that, for unsymmetrically laminated plates, the *linear* constitutive equations contain a coupling between bending and stretching. More recently, Libai and Simmonds (1981) have shown that a similar type of constitutive coupling occurs in *homogeneous* plates as strains grow large. Here, we study the relative influence of both of these coupling mechanisms during large strain of an unsymmetrically laminated plate.

A first-approximation nonlinear plate theory is used to investigate fundamental behavior. The governing equations, which are developed for general incompressible, hyperelastic materials, allow thickness changes but neglect transverse shear deformation. Results are presented for the special case of a plate composed of two layers of different neo-Hookean materials.

Geometry

Consider a plate of initial length a and thickness t that is composed of N laminae (Fig. 1). To facilitate the analysis, we first define the nondimensional quantities

$$\epsilon = h/a, \quad (z,Z) = h^{-1}(\bar{z},\bar{Z}), \quad k = a\bar{k}, \quad \kappa = t\bar{k}$$
$$W_n = \bar{W}_n/\bar{C}_1, \quad w = \bar{w}/\bar{C}_1 h, \quad C_n = \bar{C}_n/\bar{C}_1 \tag{1}$$
$$T = \bar{T}/\bar{C}_1 t, \quad M = \bar{M}/\bar{C}_1 t^2$$

where $h = t/2$, and bars indicate dimensional variables which will be defined subsequently. The foregoing development, which follows that of Simmonds (1986) for homogeneous shells, is based on expansions in the parameter ϵ, which, for a thin plate, is small compared to unity.

The geometry of deformation follows a relaxed Kirchhoff's hypothesis, which assumes that normals to the reference surface remain normal but can change in length. Thus, a point originally a distance z from the undeformed reference surface S_0 moves to a distance Z from the deformed reference surface S. In addition, the longitudinal gradient of Z is assumed to be small so that transverse shear strains can be neglected.

In the linear theory for *cylindrical bending* of a laminated plate, $S \simeq S_0$ can be chosen as the neutral surface. For a given plate construction, the position of this surface is determined by the condition $\int \sigma dz = 0$, where σ is the bending stress, which varies linearly across the thickness of each lamina. In a theory incorporating material nonlinearity, however, since the distribution of σ is nonlinear and depends on the magnitude of the deformation, the location of the "neutral surface" depends on the constitutive relations for the laminae and can change as the plate deforms. Hence, as in the case of general deformation of an unsymmetrically laminated plate, the choices of S_0 and S are arbitrary, and bending generally will be coupled to stretching. Here, S_0 is taken as the undeformed geometric midsurface, and, following Simmonds (1986), we define the position of S according to the condition

Manuscript received by the ASME Applied Mechanics Division, October 8, 1987; final revision, March 25, 1988.

[3]Department of Mechanical Engineering, University of Rochester, Rochester, NY 14627, Mem. ASME.

[4]Since Simmonds (1985) has shown that, for moderately large bending strains, the first-approximation constitutive relations for a shell are the same as those for a flat plate, the current analysis also applies to cylindrical bending of shells.

Downloaded 03 May 2010 to 171.66.16.21. Redistribution subject to ASME license or copyright; see http://www.asme.org/terms/Terms_Use.cfm

where (r,θ) is a crack-tip polar coordinate system so that $d\sigma$ along C is

$$d\sigma = (R'^2 + R^2)^{1/2} d\theta. \tag{3.2}$$

It is assumed that the applied loading condition is either symmetric or antisymmetric so that the elastic field approaches either the Mode-I or Mode-II field with SIF K_∞ as $r \to \infty$. As $t \to 0$, the elastic field is dominated by the corresponding near-tip solution characterized by SIF K.

The z_1-component of (2.8) is now considered. The integrals along the infinity large and small circles are just the well-known J_1-integral (Rice, 1968) and the integrals along the crack faces vanish. Thus,

$$\left(\frac{K}{K_\infty}\right)^2 = \frac{\mu^-(1+\kappa^+)}{\mu^+(1+\kappa^-)} - \frac{1}{K_\infty^2}\int_C \frac{8\mu^-}{\kappa^- + 1} q(\sigma) n_1(\sigma) d\sigma \tag{3.3}$$

where the K's are either K_I or K_{II}. Since the stresses on either side of C are not known, the identity (3.3) offers no practical value. To derive an approximate result, we merely substitute the K-field into (2.16) to approximate $q(\sigma)$. An approximate expression for the SIF is then obtained from (3.3).

To test the usefulness of the approximation, the case of a circular inclusion is considered. The associated Mode-I problem was solved by Steif (1987) and his result is numerically exact. Substituting the K_I-field into (2.16) and integrating (3.3), we obtain

$$\frac{K_I}{K_{I\infty}} = \left(1 + \frac{5}{4}\delta_1 - \frac{3}{2}\delta_2 - \frac{1}{2}\delta_1\delta_2 + \frac{1}{2}\delta_2^2 + \frac{15}{128}\delta_1^2\right)^{-1/2} \tag{3.4}$$

which reduces to Hutchinson's (1986) "lowest order formula" as δ_1 and δ_2 tend to zero. Our ad hoc approximation, (3.4), compares favorably with Steif's solution for $\upsilon^- = \upsilon^+ = 3/10$ and $0 < \mu^-/\mu^+ < 2$. For the case of a pure Mode-II problem, the result is

$$\frac{K_{II}}{K_{II\infty}} = \left(1 + \frac{3}{4}\delta_1 - \frac{1}{2}\delta_2 - \frac{1}{2}\delta_2^2 + \frac{9}{128}\delta_1^2\right)^{-1/2} \tag{3.5}$$

which tends to 1 as δ_1 and δ_2 tend to zero and becomes zero as $\mu^-/\mu^+ \to 0$.

References

Dundurs, J., 1969, "Edge-Bonded Dissimilar Orthogonal Elastic Wedges Under Normal and Shear Loading-Discussion," ASME JOURNAL OF APPLIED MECHANICS, Vol. 36, pp. 650-652.

Eshelby, J. D., 1951, "The Force on an Elastic Singularity," *Phil. Trans. R. Soc. Lond. A*, No. 244, pp. 87-112.

Eshelby, J. D., 1956, "The Continuum Theory of Lattice Defects," *Advances in Research and Applications; Solid State Physics*, F. Seitz and D. Trumbull, eds., Academic Press, New York, Vol. III, pp. 79-144.

Eshelby, J. D., 1970, "Energy Relations and the Energy-Momentum Tensor in Continuum Mechanics," *Inelastic Behavior of Solids*, M. F. Kanninen, W. F. Adler, A. R. Rosenfield, and R. I. Jaffee eds., McGraw-Hill, New York, pp. 77-114.

Hutchinson, J. W., 1986, "Crack Tip Shielding by Micro-Cracking in Brittle Solids,' Harvard University, Mech-87.

Knowles, J. K., and Sternberg, E., 1972, "On a Class of Conservation Laws in Linearized and Finite Elastostatics," *Arch. Ration. Mech. Analysis*, Vol. 44, pp. 187-211.

Rice, J. R., 1968, "A Path Independent Integral and the Approximate Analysis of Strain Concentration by Notches and Cracks," ASME JOURNAL OF APPLIED MECHANICS, Vol. 35, pp. 379-386.

Steif, P. S., 1987, "A Semi-infinite Crack Partially Penetrating or Circular Inclusion," ASME JOURNAL OF APPLIED MECHANICS, Vol. 54, pp. 87-92.

Large-Strain Behavior of Unsymmetric Laminates

Larry A. Taber[3]

Introduction

This note examines cylindrical bending of a laminated plate undergoing large elastic strains.[4] Since the publication of the paper by Reissner and Stavsky (1961), it has been known that, for unsymmetrically laminated plates, the *linear* constitutive equations contain a coupling between bending and stretching. More recently, Libai and Simmonds (1981) have shown that a similar type of constitutive coupling occurs in *homogeneous* plates as strains grow large. Here, we study the relative influence of both of these coupling mechanisms during large strain of an unsymmetrically laminated plate.

A first-approximation nonlinear plate theory is used to investigate fundamental behavior. The governing equations, which are developed for general incompressible, hyperelastic materials, allow thickness changes but neglect transverse shear deformation. Results are presented for the special case of a plate composed of two layers of different neo-Hookean materials.

Geometry

Consider a plate of initial length a and thickness t that is composed of N laminae (Fig. 1). To facilitate the analysis, we first define the nondimensional quantities

$$\epsilon = h/a, \quad (z,Z) = h^{-1}(\bar{z},\bar{Z}), \quad k = a\bar{k}, \quad \kappa = t\bar{k}$$
$$W_n = \bar{W}_n/\bar{C}_1, \quad w = \bar{w}/\bar{C}_1 h, \quad C_n = \bar{C}_n/\bar{C}_1 \tag{1}$$
$$T = \bar{T}/\bar{C}_1 t, \quad M = \bar{M}/\bar{C}_1 t^2$$

where $h = t/2$, and bars indicate dimensional variables which will be defined subsequently. The foregoing development, which follows that of Simmonds (1986) for homogeneous shells, is based on expansions in the parameter ϵ, which, for a thin plate, is small compared to unity.

The geometry of deformation follows a relaxed Kirchhoff's hypothesis, which assumes that normals to the reference surface remain normal but can change in length. Thus, a point originally a distance z from the undeformed reference surface S_0 moves to a distance Z from the deformed reference surface S. In addition, the longitudinal gradient of Z is assumed to be small so that transverse shear strains can be neglected.

In the linear theory for *cylindrical bending* of a laminated plate, $S \simeq S_0$ can be chosen as the neutral surface. For a given plate construction, the position of this surface is determined by the condition $\int \sigma dz = 0$, where σ is the bending stress, which varies linearly across the thickness of each lamina. In a theory incorporating material nonlinearity, however, since the distribution of σ is nonlinear and depends on the magnitude of the deformation, the location of the "neutral surface" depends on the constitutive relations for the laminae and can change as the plate deforms. Hence, as in the case of general deformation of an unsymmetrically laminated plate, the choices of S_0 and S are arbitrary, and bending generally will be coupled to stretching. Here, S_0 is taken as the undeformed geometric midsurface, and, following Simmonds (1986), we define the position of S according to the condition

Manuscript received by the ASME Applied Mechanics Division, October 8, 1987; final revision, March 25, 1988.

[3]Department of Mechanical Engineering, University of Rochester, Rochester, NY 14627, Mem. ASME.

[4]Since Simmonds (1985) has shown that, for moderately large bending strains, the first-approximation constitutive relations for a shell are the same as those for a flat plate, the current analysis also applies to cylindrical bending of shells.

Copyright © 1988 by ASME
Downloaded 03 May 2010 to 171.66.16.21. Redistribution subject to ASME license or copyright; see http://www.asme.org/terms/Terms_Use.cfm

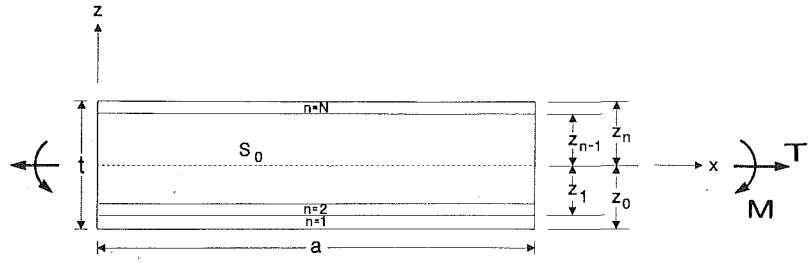


Fig. 1 Undeformed plate geometry

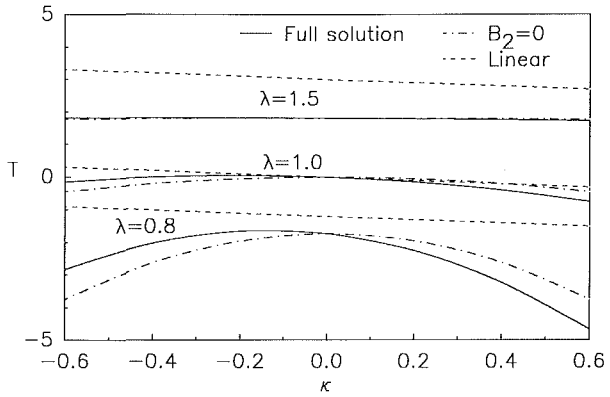


Fig. 2 Effect of curvature on membrane stress resultant

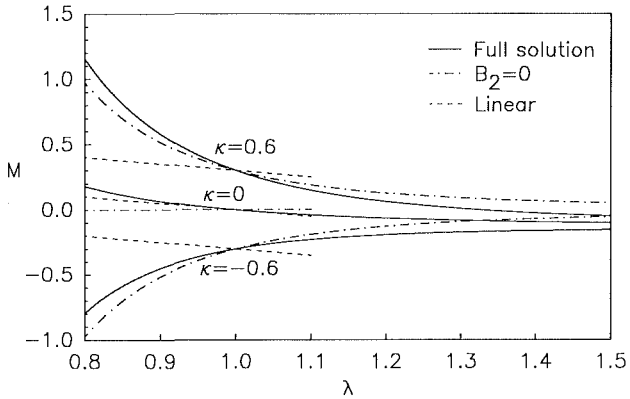


Fig. 3 Effect of stretching on bending moment

$$\int_{-1}^{1} Z dz = 0. \tag{2}$$

Note that, with this definition, S is not necessarily composed of the same material points as S_0.

With $\Lambda_y \equiv 1$, the other (approximate) stretch ratios, i.e., the ratios of deformed to undeformed lengths, are (Taber, 1985)

$$\Lambda_x = \lambda + \epsilon Z k, \quad \Lambda_z = \partial Z/\partial z \tag{3}$$

where λ and k are the respective stretch ratio and curvature measure of S. After substitution of equations (3) and the expansion

$$Z = Z_0 + \epsilon Z_1 + \ldots \tag{4}$$

into the incompressibility condition, $\Lambda_x \Lambda_z = 1$, equating like powers of ϵ and noting equation (2) yield

$$Z_0 = z/\lambda, \quad Z_1 = (1 - 3z^2)k/6\lambda^3. \tag{5}$$

Insertion of equation (4) into (3) now gives

$$\Lambda_x = \lambda + \epsilon Z_0 k + \epsilon^2 Z_1 k + \ldots \equiv \Lambda_0 + \epsilon \Lambda_1 + \epsilon^2 \Lambda_2 + \ldots \tag{6}$$

Strain Energy Density Function

With $\Lambda_y = 1$ and Λ_z determined from incompressibility, $W_n(\Lambda_x)$ is the strain energy density per unit undeformed volume of the nth lamina. Then, the strain energy density per unit undeformed area of the reference surface is

$$w = \sum_{n=1}^{N} \int_{z_{n-1}}^{z_n} W_n dz. \tag{7}$$

A Taylor series expansion about the membrane state gives

$$W_n = \overset{0}{W}_n + \epsilon \frac{\partial \overset{0}{W}_n}{\partial \epsilon} + \frac{\epsilon^2}{2} \frac{\partial^2 \overset{0}{W}_n}{\partial \epsilon^2} + \ldots \tag{8}$$

where $(^0) \equiv (\,)_{\epsilon=0}$, and the chain rule and equation (6) give

$$\frac{\partial \overset{0}{W}_n}{\partial \epsilon} = \Lambda_1 \overset{0}{W}_{n,1}, \quad \frac{\partial^2 \overset{0}{W}_n}{\partial \epsilon^2} = \Lambda_1^2 \overset{0}{W}_{n,2} + 2\Lambda_2 \overset{0}{W}_{n,1} \tag{9}$$

in which

$$W_{n,m} \equiv \frac{\partial^m W_n}{\partial \Lambda_x^m}. \tag{10}$$

Now, after substitution of equations (8) and (9) into (7), integration yields

$$w = A_1 + \epsilon A_2 k/\lambda + \epsilon^2 (A_3 + A_4/3\lambda) k^2/2\lambda^2 \tag{11}$$

where the $A_m(\lambda)$ are

$$A_m = \sum_{n=1}^{N} \overset{0}{W}_{n,(m-1)} \Delta z_n^{(m)}, \quad m = 1, 2, 3$$

$$A_4 = \sum_{n=1}^{N} \overset{0}{W}_{n,1} (\Delta z_n^{(1)} - 3\Delta z_n^{(3)}) \tag{12}$$

with

$$\Delta z_n^{(m)} = (z_n^m - z_{n-1}^m)/m. \tag{13}$$

Given the W_n and the lamination geometry, $w(\lambda, k)$ can be computed in closed form. In equation (11), the A_2-term represents the bending-stretching coupling due to lamination unsymmetric with respect to S_0, the A_3-term contains the coupling due to large-strain effects, and the A_4-term gives a correction for unsymmetric motion of points relative to S_0. For a homogeneous plate, $A_2 = A_4 = 0$, and equation (11) reduces to the form previously derived by Simmonds (1986).

Equation (11) now will be specialized to the case of a laminated neo-Hookean plate with

$$W_n = C_n(\Lambda_x^2 + \Lambda_x^{-2} - 2) \tag{14}$$

where C_n is a nondimensional material constant for the nth layer. Combination of equations (1), (6), (11), (12), and (14) yields

$$w = B_1(\lambda^2 + \lambda^{-2} - 2) + B_2(1 - \lambda^{-4})\kappa + [3B_3(1 + 3\lambda^{-4}) + B_4(1 - \lambda^{-4})]\kappa^2/12\lambda^2 \tag{15}$$

in which

Downloaded 03 May 2010 to 171.66.16.21. Redistribution subject to ASME license or copyright; see http://www.asme.org/terms/Terms_Use.cfm

$$B_m = \sum_{n=1}^{N} C_n \Delta z_n^{(m)}, \quad m = 1, 2, 3$$

$$B_4 = B_1 - 3B_3. \tag{16}$$

Physically, the B_m correspond to the same effects as the A_m. The linear form of w, given by letting $e = \lambda - 1 \to 0$ and retaining terms up to quadratic in the strains in equation (15), is

$$w_{\text{LIN}} = 4(B_1 e^2 + B_2 e\kappa) + B_3 \kappa^2, \tag{17}$$

which contains bending-stretching coupling due only to unsymmetric lamination.

Results

With $w^* = w/2$, the membrane stress resultant and bending moment per unit length of S_0 are given by

$$T = \partial w^*/\partial\lambda, \quad M = \partial w^*/\partial\kappa, \tag{18}$$

which are plotted in Figs. 2 and 3 for a two-layered neo-Hookean plate with $C_1 = 1$ and $C_2 = 0.5$. To illustrate the bending-stretching coupling for this unsymmetrically laminated plate, these plots show three cases:

1 The full solution based on equation (15);
2 A solution based on equation (15) with B_2 set to zero, i.e., coupling due to large-strain effects is included, but that due to unsymmetric lamination is neglected (note that $B_4 = 0$ for a two-layered plate);
3 The linear solution based on equation (17).

First, consider the effect of bending on the stress resultant T (Fig. 2). As shown by the *nonlinear* curves, stretching decreases the influence of κ on T, while compression ($\lambda < 1$) increases this coupling effect. In fact, $\lambda = 1.5$ produces a near-membrane state, with T virtually independent of κ and M very small (Fig. 3). For $B_2 = 0$, the $T - \kappa$ curves are symmetric about $\kappa = 0$, with bending either way inducing a compressive stress resultant (with λ held fixed). Unsymmetric lamination ($B_2 \neq 0$) mainly just tilts these curves. The results in Fig. 2 indicate that the effects on T of both coupling terms are comparable and should be included in a large-strain theory.

The effects of reference surface stretching on the bending moment are depicted in Fig. 3. For $\kappa = 0$, the coupling is given solely by the B_2-term, and the large-strain effects are relatively mild. Strong bending, however, magnifies these effects, with compression increasing and stretching decreasing the magnitude of M. For very large stretching, $M \to B_2/2$ independently of κ, and so a true membrane state is approached only if the lamination is symmetric ($B_2 = 0$). Finally, when κ is large, the coupling contained in the B_3-term (large strain) dominates that in the B_2-term (unsymmetric lamination).

Acknowledgment

This work was supported by the National Science Foundation under Grant No. MSM-8611490.

References

Libai, A., and Simmonds, J. G., 1981, "Large-Strain Constitutive Laws for the Cylindrical Deformation of Shells," *International Journal of Non-Linear Mechanics*, Vol. 16, pp. 91-103.

Reissner, E., and Stavsky, Y., 1961, "Bending and Stretching of Certain Types of Heterogeneous Aelotropic Elastic Plates," ASME JOURNAL OF APPLIED MECHANICS, Vol. 28, pp. 402-408.

Simmonds, J. G., 1985, "The Strain Energy Density of Rubber-like Shells," *International Journal of Solids and Structures*, Vol. 21, pp. 67-77.

Simmonds, J. G., 1986, "The Strain Energy Density of Rubber-like Shells of Revolution Undergoing Torsionless, Axisymmetric Deformation (Axishells)," ASME JOURNAL OF APPLIED MECHANICS, Vol. 53, pp. 593-596.

Taber, L. A., 1985, "On Approximate Large Strain Relations for a Shell of Revolution," *International Journal of Non-Linear Mechanics*, Vol. 20, pp. 27-39.

Response of the Duffing Oscillator to a Non-Gaussian Random Excitation

Ismail I. Orabi[5] and Goodarz Ahmadi[6]

Introduction

Recently, Jahedi and Ahmadi (1983) and Orabi and Ahmadi (1987a,b) developed a new technique for response analysis of nonlinear random systems. This method makes use of the Wiener-Hermite (W-H) functional series representation of a random function. The technique is fully realizable at any order of approximation and is not limited to Gaussian stochastic approximation. Orabi and Ahmadi (1987b) showed that the response statistics of the Duffing oscillator obtained by a three-term W-H expansion were in excellent agreement with the digital simulations results.

The goal of the present study is to show the applicability of the Wiener-Hermite expansion method for response analysis of nonlinear systems subjected to non-Gaussian excitations. The procedure of the method is illustrated by an example of the Duffing oscillator subjected to a non-Gaussian nonstationary random excitation. The first three terms in the Wiener-Hermite series representations of the excitation and the response are considered. The equations governing the evolution of the deterministic kernel functions are derived and the transient mean-square responses of the Duffing oscillator are analyzed. To check the differences between the Gaussian and non-Gaussin excitations, the mean-square reponses are compared with those found by the single- and three-term expansions of the oscillator response to the Gaussian part of the excitation. It is shown that the non-Gaussian statistics increase the mean-square responses of the Duffing oscillator.

Basic Formulation

The governing equation of the Duffing oscillator subjected to a random force $f(t)$ is given by

$$\ddot{x} + 2\xi\omega_o\dot{x} + \omega_o^2(x + \epsilon x^3) = f(t). \tag{1}$$

Here, x is the relative displacement, ω_o is the natural frequency of the corresponding linear system, ξ is the damping coefficient and ϵ is a constant corresponding to the strength of nonlinearity.

To analyze the response of the Duffing oscillator, the random force $f(t)$ and the response $x(t)$ are expanded in terms of the Wiener-Hermite set. These are given by

$$\begin{aligned} f(t) = {} & \int_{-\infty}^{\infty} F^{(1)}(t,t_1) H^{(1)}(t_1)\, dt_1 \\ & + \int_{-\infty}^{\infty}\int_{-\infty}^{\infty} F^{(2)}(t,t_1,t_2) H^{(2)}(t_1,t_2)\, dt_1 dt_2 \\ & + \int_{-\infty}^{\infty}\int_{-\infty}^{\infty}\int_{-\infty}^{\infty} F^{(3)}(t,t_1,t_2,t_3) H^{(3)}(t_1,t_2,t_3)\, dt_1 dt_2 dt_3 \\ & + \cdots\cdots\cdots\cdots \end{aligned} \tag{2}$$

and

$$\begin{aligned} x(t) = {} & \int_{-\infty}^{\infty} X^{(1)}(t,t_1) H^{(1)}(t_1)\, dt_1 \\ & + \int_{-\infty}^{\infty}\int_{-\infty}^{\infty} X^{(2)}(t,t_1,t_2) H^{(2)}(t_1,t_2)\, dt_1 dt_2 \\ & + \int_{-\infty}^{\infty}\int_{-\infty}^{\infty}\int_{-\infty}^{\infty} X^{(3)}(t,t_1,t_2,t_3) H^{(3)}(t_1,t_2,t_3)\, dt_1 dt_2 dt_3 \\ & + \cdots\cdots\cdots \end{aligned} \tag{3}$$

where $F^{(i)}$ and $X^{(i)}$ are deterministic kernel functions.

[5]Department of Mechanical Engineering, University of New Haven, New Haven, CT 06516.

[6]Department of Mechanical and Industrial Engineering, Clarkson University, Potsdam, NY 13676.

Manuscript received by ASME Applied Mechanics Division, January 8, 1987; final revision, December 23, 1987.

Downloaded 03 May 2010 to 171.66.16.21. Redistribution subject to ASME license or copyright; see http://www.asme.org/terms/Terms_Use.cfm

$$B_m = \sum_{n=1}^{N} C_n \Delta z_n^{(m)}, \quad m = 1, 2, 3$$

$$B_4 = B_1 - 3B_3. \tag{16}$$

Physically, the B_m correspond to the same effects as the A_m. The linear form of w, given by letting $e = \lambda - 1 \to 0$ and retaining terms up to quadratic in the strains in equation (15), is

$$w_{\text{LIN}} = 4(B_1 e^2 + B_2 e\kappa) + B_3 \kappa^2, \tag{17}$$

which contains bending-stretching coupling due only to unsymmetric lamination.

Results

With $w^* = w/2$, the membrane stress resultant and bending moment per unit length of S_0 are given by

$$T = \partial w^*/\partial\lambda, \quad M = \partial w^*/\partial\kappa, \tag{18}$$

which are plotted in Figs. 2 and 3 for a two-layered neo-Hookean plate with $C_1 = 1$ and $C_2 = 0.5$. To illustrate the bending-stretching coupling for this unsymmetrically laminated plate, these plots show three cases:

1 The full solution based on equation (15);
2 A solution based on equation (15) with B_2 set to zero, i.e., coupling due to large-strain effects is included, but that due to unsymmetric lamination is neglected (note that $B_4 = 0$ for a two-layered plate);
3 The linear solution based on equation (17).

First, consider the effect of bending on the stress resultant T (Fig. 2). As shown by the *nonlinear* curves, stretching decreases the influence of κ on T, while compression ($\lambda < 1$) increases this coupling effect. In fact, $\lambda = 1.5$ produces a near-membrane state, with T virtually independent of κ and M very small (Fig. 3). For $B_2 = 0$, the $T - \kappa$ curves are symmetric about $\kappa = 0$, with bending either way inducing a compressive stress resultant (with λ held fixed). Unsymmetric lamination ($B_2 \neq 0$) mainly just tilts these curves. The results in Fig. 2 indicate that the effects on T of both coupling terms are comparable and should be included in a large-strain theory.

The effects of reference surface stretching on the bending moment are depicted in Fig. 3. For $\kappa = 0$, the coupling is given solely by the B_2-term, and the large-strain effects are relatively mild. Strong bending, however, magnifies these effects, with compression increasing and stretching decreasing the magnitude of M. For very large stretching, $M \to B_2/2$ independently of κ, and so a true membrane state is approached only if the lamination is symmetric ($B_2 = 0$). Finally, when κ is large, the coupling contained in the B_3-term (large strain) dominates that in the B_2-term (unsymmetric lamination).

Acknowledgment

This work was supported by the National Science Foundation under Grant No. MSM-8611490.

References

Libai, A., and Simmonds, J. G., 1981, "Large-Strain Constitutive Laws for the Cylindrical Deformation of Shells," *International Journal of Non-Linear Mechanics*, Vol. 16, pp. 91-103.

Reissner, E., and Stavsky, Y., 1961, "Bending and Stretching of Certain Types of Heterogeneous Aelotropic Elastic Plates," ASME JOURNAL OF APPLIED MECHANICS, Vol. 28, pp. 402-408.

Simmonds, J. G., 1985, "The Strain Energy Density of Rubber-like Shells," *International Journal of Solids and Structures*, Vol. 21, pp. 67-77.

Simmonds, J. G., 1986, "The Strain Energy Density of Rubber-like Shells of Revolution Undergoing Torsionless, Axisymmetric Deformation (Axishells)," ASME JOURNAL OF APPLIED MECHANICS, Vol. 53, pp. 593-596.

Taber, L. A., 1985, "On Approximate Large Strain Relations for a Shell of Revolution," *International Journal of Non-Linear Mechanics*, Vol. 20, pp. 27-39.

Response of the Duffing Oscillator to a Non-Gaussian Random Excitation

Ismail I. Orabi[5] and Goodarz Ahmadi[6]

Introduction

Recently, Jahedi and Ahmadi (1983) and Orabi and Ahmadi (1987a,b) developed a new technique for response analysis of nonlinear random systems. This method makes use of the Wiener-Hermite (W-H) functional series representation of a random function. The technique is fully realizable at any order of approximation and is not limited to Gaussian stochastic approximation. Orabi and Ahmadi (1987b) showed that the response statistics of the Duffing oscillator obtained by a three-term W-H expansion were in excellent agreement with the digital simulations results.

The goal of the present study is to show the applicability of the Wiener-Hermite expansion method for response analysis of nonlinear systems subjected to non-Gaussian excitations. The procedure of the method is illustrated by an example of the Duffing oscillator subjected to a non-Gaussian nonstationary random excitation. The first three terms in the Wiener-Hermite series representations of the excitation and the response are considered. The equations governing the evolution of the deterministic kernel functions are derived and the transient mean-square responses of the Duffing oscillator are analyzed. To check the differences between the Gaussian and non-Gaussin excitations, the mean-square reponses are compared with those found by the single- and three-term expansions of the oscillator response to the Gaussian part of the excitation. It is shown that the non-Gaussian statistics increase the mean-square responses of the Duffing oscillator.

Basic Formulation

The governing equation of the Duffing oscillator subjected to a random force $f(t)$ is given by

$$\ddot{x} + 2\xi\omega_o\dot{x} + \omega_o^2(x + \epsilon x^3) = f(t). \tag{1}$$

Here, x is the relative displacement, ω_o is the natural frequency of the corresponding linear system, ξ is the damping coefficient and ϵ is a constant corresponding to the strength of nonlinearity.

To analyze the response of the Duffing oscillator, the random force $f(t)$ and the response $x(t)$ are expanded in terms of the Wiener-Hermite set. These are given by

$$\begin{aligned} f(t) = {} & \int_{-\infty}^{\infty} F^{(1)}(t,t_1) H^{(1)}(t_1)\, dt_1 \\ & + \int_{-\infty}^{\infty}\int_{-\infty}^{\infty} F^{(2)}(t,t_1,t_2) H^{(2)}(t_1,t_2)\, dt_1 dt_2 \\ & + \int_{-\infty}^{\infty}\int_{-\infty}^{\infty}\int_{-\infty}^{\infty} F^{(3)}(t,t_1,t_2,t_3) H^{(3)}(t_1,t_2,t_3)\, dt_1 dt_2 dt_3 \\ & + \cdots\cdots\cdots\cdots \end{aligned} \tag{2}$$

and

$$\begin{aligned} x(t) = {} & \int_{-\infty}^{\infty} X^{(1)}(t,t_1) H^{(1)}(t_1)\, dt_1 \\ & + \int_{-\infty}^{\infty}\int_{-\infty}^{\infty} X^{(2)}(t,t_1,t_2) H^{(2)}(t_1,t_2)\, dt_1 dt_2 \\ & + \int_{-\infty}^{\infty}\int_{-\infty}^{\infty}\int_{-\infty}^{\infty} X^{(3)}(t,t_1,t_2,t_3) H^{(3)}(t_1,t_2,t_3)\, dt_1 dt_2 dt_3 \\ & + \cdots\cdots\cdots \end{aligned} \tag{3}$$

where $F^{(i)}$ and $X^{(i)}$ are deterministic kernel functions.

[5]Department of Mechanical Engineering, University of New Haven, New Haven, CT 06516.

[6]Department of Mechanical and Industrial Engineering, Clarkson University, Potsdam, NY 13676.

Manuscript received by ASME Applied Mechanics Division, January 8, 1987; final revision, December 23, 1987.

Copyright © 1988 by ASME
Downloaded 03 May 2010 to 171.66.16.21. Redistribution subject to ASME license or copyright; see http://www.asme.org/terms/Terms_Use.cfm

The elements of the Wiener-Hermite set, $H^{(i)}$, are zero-mean random function (with the exception of $H^{(0)}$) and form a statistically orthogonal complete random basis, i.e.,

$$<H^{(i)}> = 0 \qquad \text{for } i=0. \tag{4}$$

$$<H^{(i)}H^{(j)}> = 0 \qquad \text{for } i=j. \tag{5}$$

The explicit expressions for the first few terms of the W-H basis are given by Orabi and Ahmadi (1987). The zeroth order term in a Wiener-Hermite series corresponds to the mean value. We have assumed that the means of f and x are zero, therefore, the zeroth order terms are omitted from the series expansions in equations (2) and (3). The first order term in the Wiener-Hermite series corresponds to the Gaussian part of the random process. The second and higher order terms corresponds to the non-Gaussian part of the random function.

Once the deterministic kernel functions are found, equation (3) provides an explicit series representation for the random response of the oscillator. From this series and the known properties of the Wiener-Hermite set, various statistics of the response can be generated. For instance, the variance of x is given by

$$\sigma_x^2(t) = <x^2(t)> = \int_{-\infty}^{\infty}[X^{(1)}(t,t_1)]^2dt_1 + 2\int_{-\infty}^{\infty}\int_{-\infty}^{\infty}[X^{(2)}(t,t_1,t_2)]^2dt_1dt_2 + 6\int_{-\infty}^{\infty}\int_{-\infty}^{\infty}\int_{-\infty}^{\infty}[X^{(3)}(t,t_1,t_2,t_3)]^2dt_1dt_2dt_3 + \ldots \tag{6}$$

Other statistical moments of the response could be obtained by algebraic manipulations in a similar fashion.

Response to Non-Gaussian Excitations

When the excitation $f(t)$ is a non-Gaussian process, the expansion of $f(t)$ in terms of the Wiener-Hermite series is given by equation (2). Particular choices of the kernel functions, $F^{(1)}$, $F^{(2)}$, and $F^{(3)}$ lead to various non-Gaussian excitations. Here, we consider, the case when

$$F^{(1)}(t,t_1) = (2\pi S_1)^{1/2}e_1(t)\delta(t-t_1),\ F^{(2)}(t,t_1,t_2) = 0, \tag{7}$$

$$F^{(3)}(t,t_1,t_2,t_3) = S_2e_2(t)e_2(t_1)e_2(t_2)e_2(t_3), \tag{8}$$

where S_1 and S_2 are some constants and e_1 and e_2 are deterministic envelope functions. Using the properties of the Wiener-Hermite basis, it may be shown that

$$f(t) = (2\pi S_1)^{1/2}e_1(t)n(t) + S_2\{[\int_0^t e_2(t_1)n(t_1)dt_1]^3 - 3\int_0^t n(t_2)e_2(t_2)dt_2\int_0^t e_2^2(t_3)dt_3. \tag{9}$$

The excitation given by equation (9) is clearly a non-Gaussian process.

In this section, the response of the Duffing oscillator to the non-Gaussian excitation given by equation (9) is analyzed. It is assumed that $e_1(t)$ is a unit step function, i.e.,

$$e_1(t) = u(t) = \begin{cases} 1 & t>0, \\ 0 & t<0, \end{cases} \tag{10}$$

and $e_2(t)$ is given as

$$e_2(t) = \exp(-\beta t)u(t), \tag{11}$$

in which β is a constant. For a motion which starts from rest the initial conditions are

$$X^{(1)}(0,t_1) = X^{(2)}(0,t_1,t_2) = X^{(3)}(0,t_1,t_2,t_3) = 0, \tag{12}$$

$$\dot{X}^{(1)}(0,t_1) = \dot{X}^{(2)}(0,t_1,t_2) = \dot{X}^{(3)}(0,t_1,t_2,t_3) = 0. \tag{13}$$

For a non-Gaussian excitation with $F^{(2)} = 0$ such as the one given by equation (7) and the initial conditions in equations (12) and (13), it follows that $X^{(2)}$ is identically zero. For $X^{(3)} << X^{(1)}$, the equations governing the kernel functions become (Orabi and Ahmadi, 1987b)

$$\ddot{X}^{(1)}(t,t_1) + 2\xi\omega_0\dot{X}^{(1)}(t,t_1) + \omega_e^2(t)X^{(1)}(t,t_1) = F^{(1)}(t,t_1), \tag{14}$$

and

$$\ddot{X}^{(3)}(t,t_1,t_2,t_3) + 2\xi\omega_o\dot{X}^{(3)}(t,t_1,t_2,t_3) + \omega_e^2(t)X^{(3)}(t,t_1,t_2,t_3) = -\epsilon\omega_o^2\{X^{(1)}(t,t_1)X^{(1)}(t,t_2)X^{(1)}(t,t_3) + 6\int_o^t X^{(1)}(t,t_1)X^{(1)}(t,t_4)X^{(3)}(t,t_2,t_3,t_4)dt_4 + 6\int_0^t X^{(1)}(t,t_2)X^{(1)}(t,t_4)X^{(3)}(t,t_1,t_3,t_4)dt_4 + 6\int_0^t X^{(1)}(t,t_3)X^{(1)}(t,t_4)X^{(3)}(t,t_1,t_2,t_4)dt_4 + F^{(3)}(t,t_1,t_2,t_3). \tag{15}$$

Here, ω_e is the time-dependent equivalent frequency defined as

$$\omega_e^2(t) = \omega_o^2[1+3\epsilon\sigma_1^2(t)]. \tag{16}$$

where

$$\sigma_1^2(t) = \int_0^t[X^{(1)}(t,t_1)]^2dt_1. \tag{17}$$

An iterative procedure for obtaining the kernel functions and the mean-square responses was developed by Orabi and Ahmadi (1987a,b).

Following this procedure, the mean-square response is given by

$$\sigma_x^2(t) = \sigma_1^2(t) + \sigma_3^2(t), \tag{18}$$

where σ_1^2 is given by equation (17) and

$$\sigma_3^2 = 6\epsilon^2\omega_o^4(1+18a^2(t))[\int_0^t d\tau_1\int_0^t d\tau_2 h(t,\tau_1)h(t,\tau_2) R_1^3(\tau_1,\tau_2)] + 6\{S_2^2e_3^3(t)h_2^2(t) - 2\epsilon\omega_o^2S_2(2\pi S_1)^{3/2} h_2(t)(1+18a(t))\int_0^t h(t,\tau)h_3^3(\tau)d\tau\}, \tag{19}$$

where

$$h_2(t) = \int_0^t h(t,\tau)d\tau,\ e_3(t) = \int_0^t e_2(\tau)d\tau, \tag{20}$$

$$h_3(t) = \int_0^t \exp(-\beta t)h(t,\tau)d\tau. \tag{21}$$

The expressions for the approximate impulse response $h(t,\tau)$, the function $a(t)$, and the first order autocorrelation $R_1(t,\tau)$ were given by Orabi and Ahmadi (1987b) and Orabi (1986). Equation (19) is a convenient form for evaluating the contributions of the third term in the Wiener-Hermite series to the mean-square responses of the Duffing oscillator subjected to the non-Gaussian excitation given by equation (9).

Numerical Solution and Results

For $S_1 = S_2 = 1/2\pi$ cm$^2/s^3$, $\omega_o = 1$ rad/s, $\beta = 0.2$ and several values of ϵ and ξ, the transient mean-square (M-S) responses of the Duffing oscillator as given by equation (18) are evaluated and the results are plotted as functions of time in Figs. 1-5. These figures also show the resulting M-S responses when the non-Gaussian parts of the excitation and the response are neglected. The features of the responses of the Duffing oscillator to Gaussian and non-Gaussian excitations may be studied from these figures.

For $\xi = .20$ and several values of ϵ, the mean-square responses of the Duffing oscillator are shown in Figs. 1-3. It is observed that the M-S responses decrease as ϵ increases. These figures also show that the M-S responses of the Duffing oscillator subjected to the Gaussian part of the excitations obtained by the single-term and the three-term W-H series expan-

Downloaded 03 May 2010 to 171.66.16.21. Redistribution subject to ASME license or copyright; see http://www.asme.org/terms/Terms_Use.cfm

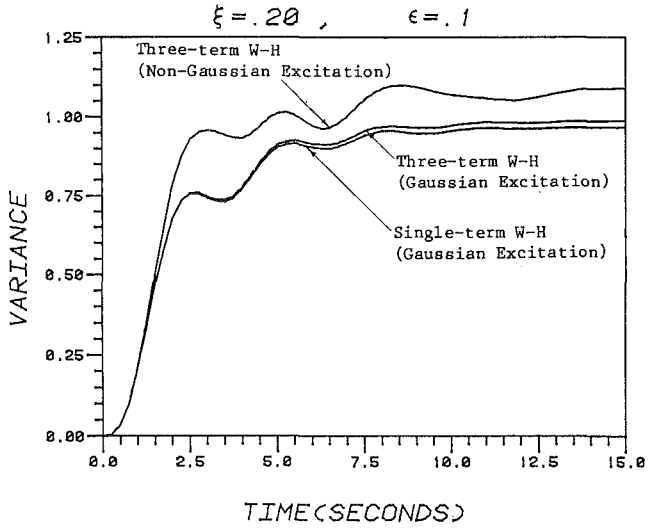


Fig. 1 Mean-square displacement response of the Duffing oscillator subject to a non-Gaussian excitation

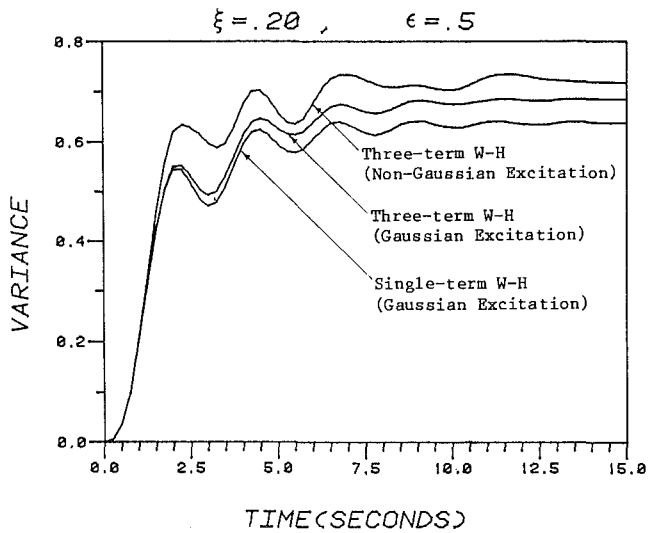


Fig. 2 Mean-square displacement response of the Duffing oscillator subject to a non-Gaussian excitation

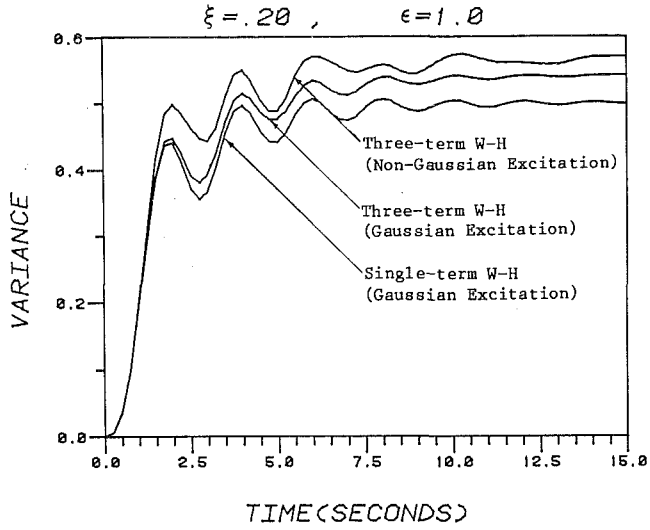


Fig. 3 Mean-square displacement response of the Duffing oscillator subject to a non-Gaussian excitation

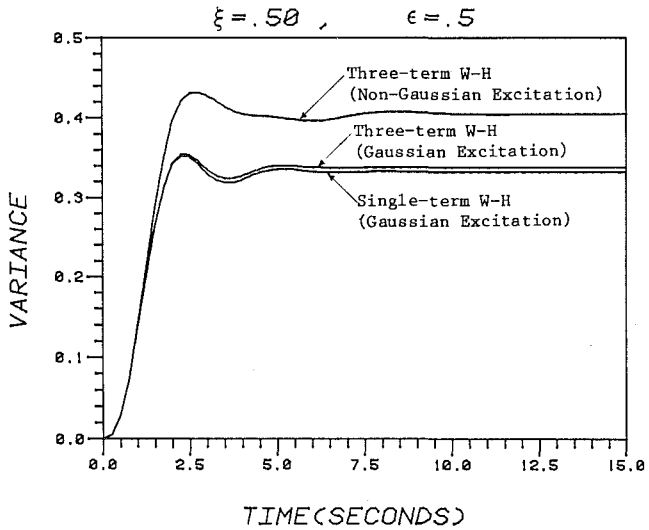


Fig. 4 Mean-square displacement response of the Duffing oscillator subject to a non-Gaussian excitation

sions are always lower than the results found for the same system subjected to the combined Gaussian and non-Gaussian excitation given by equation (9).

Figures 4 and 5 show the effect of damping coefficient and the strength of nonlinearity on the mean-square responses. It is clear from these figures that the M-S responses decrease as ϵ increases. It is also observed that the M-S responses for the Gaussian part of the excitation approach the corresponding stationary limits faster when compared with the response of the system subjected to the combined Gaussian and non-Gaussian excitation.

An examination of Figs. 1–5 reveals that the non-Gaussian part of the response increases the mean-square reponses. For a Gaussian excitation, the nonlinearity produces non-Gaussian statistics for the response. The contribution of the non-Gaussian part of the response increases with the strength of nonlinearity. Non-Gaussian excitation leads to non-Gaussian response both for linear and nonlinear systems which further increases the M-S responses. It is also observed that the Gaussian closure methods always underestimate the mean-square reponses of the Duffing oscillator. Here, by considering the third terms in the W-H series expansions of the excitation and

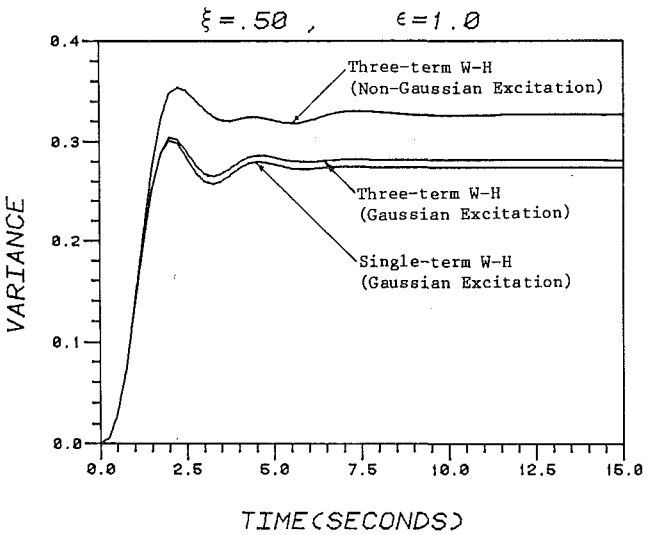


Fig. 5 Mean-square displacement response of the Duffing oscillator subject to a non-Gaussian excitation

Downloaded 03 May 2010 to 171.66.16.21. Redistribution subject to ASME license or copyright; see http://www.asme.org/terms/Terms_Use.cfm

the response, the non-Gaussian statistics of the random reponses are, inpart, captured.

Conclusions

The Wiener-Hermite functional series expansion method is used for response analysis of the Duffing oscillator subjected to a non-Gaussian excitation. The first three terms in the series expansion are used and the nonstationary responses of the Duffing oscillator are analyzed. An iterative procedure for evaluating the kernel functions and the mean-square responses of the Duffing oscillator is used.

For several values of nonlinearity strength and damping coefficient, the nonstationary mean-square responses of the Duffing oscillator are evaluated. The results are compared with those found by the single- and three-term Wiener-Hermite expansions of the response when the oscillator is subjected to the Gaussian part of the excitation. It is shown that the M-S response of the Duffing oscillator subjected to a non-Gaussian excitation is always larger than the M-S responses of the same system subjected to the Gaussian part of the excitation.

Based on the presented results, it is concluded that the W-H functional expansion method provides a systematic tool for response analysis of nonlinear systems subjected to non-Gaussian excitations.

References

Jahedi, A., and Ahmadi, G., 1983, "Application of Wiener-Hermite Expansion to Nonstationary Random Vibration of a Duffing Oscillator," ASME JOURNAL OF APPLIED MECHANICS, Vol. 50, pp. 436–442.

Orabi, I. I., 1986, "A Functional Series Expansion Method for Reponse Analysis of Nonlinear Systems Subjected to Random Excitations," Ph.D. Thesis, Clarkson University.

Orabi, I. I., and Ahmadi, G., 1987a, "A Functional Series Expansion Method for Response Analysis of Nonlinear Systems Subjected to Random Excitations," *Int. J. of Nonlinear Mech.*, Vol. 6, pp. 451–465.

Orabi, I. I., and Ahmadi, G., 1987b, "Nonstationary Response Analysis of a Duffing Oscillator by the Wiener-Hermite Expansion Method," ASME JOURNAL OF APPLIED MECHANICS, Vol. 54, pp. 434–440.

Downloaded 03 May 2010 to 171.66.16.21. Redistribution subject to ASME license or copyright; see http://www.asme.org/terms/Terms_Use.cfm

Journal of Applied Mechanics

Discussion

Closed-Form Analysis for Elastic Deformations of Multilayered Strands[1]

Steven A. Velinsky.[2] The authors have presented closed-form solutions for the elastic deformations of multilay wire strands and have additionally presented a simple design criteria for "nonrotating" cables. However, they have overlooked the content of a body of literature that addresses cable and wire rope analysis. The authors state "Costello's analysis, although based on conventional linear theory of deformations, involves several nonlinear geometric deformation relations." While Costello and associates' original work (1973–1982) did, in fact, involve the solution of nonlinear geometric relations, Velinsky, Anderson, and Costello (1984) linearized the solutions of these equations to allow the analysis of complex wire ropes. Additionally, Velinsky (1985a) has compared the linear theory to the general nonlinear theory for both strands and wire ropes and has advocated the use of the linear theory due to the excellent agreement and computational simplicity. Both Costello and Velinsky have used this linear theory exclusively since then; see, for example, Chien and Costello (1985); Phillips and Costello (1985); Velinsky (1985b). Thus, it is apparent that the authors have merely represented equations that have been derived previously in a slightly different form.

The authors have also presented a plot (Fig. 4) that allows a strand designer to select the helix angle of the third lay of wires, α_3, based on the helix angle of the second lay of wires, α_2, such that the cable is "nonrotating." Beside the fact that this problem has been solved previously in a more general form (see Knapp, 1981), the authors are not clear nor consistent in the manner in which the helix angles are measured. The third lay of wires has to be laid opposite in direction to that of the second lay in order for there to be no net twist when a strand undergoes a pure axial load and thus, the sign of the cosine of α_3 must be opposite the sign of the cosine of α_2. However, the authors show both of these angles to lie between 0 and 90 degrees. Additionally, for each α_2, there is not a unique α_3, but there are two solutions that cause the cable to be "nonrotating" (or "torque balanced") as shown by Knapp (1981).

References

Chien, C., and Costello, G. A., 1985, "Effective Length of a Fractured Wire in Wire Rope," ASCE *Journal of Engineering Mechanics*, Vol. 111, pp. 952–961.

Knapp, R. H., 1981, "Torque and Stress Balanced Design of Helically Armored Cables," ASME *Joural of Engineering for Industry*, Vol. 103, pp. 61–66.

Phillips, J. W., and Costello, G. A., 1985, "Analysis of Wire Ropes with Internal-Wire-Rope Cores," ASME JOURNAL OF APPLIED MECHANICS, Vol. 52, pp. 510–516.

Velinsky, S. A., Anderson, G. L., and Costello, G. A., 1984, "Wire Rope with Complex Cross Sections," ASCE *Journal of Engineering Mechanics*, Vol. 110, pp. 380–391.

Velinsky, S. A., 1985a, "General Nonlinear Theory for Complex Wire Rope," *International Journal of Mechanical Sciences*, Vol. 27, pp. 497–507.

Velinsky, S. A., 1985b, "Analysis of Fiber Core Wire Rope," ASME *Journal of Energy Resources Technology*, Vol. 107, pp. 388–393.

Authors' Closure

The authors appreciate the discussor's interest in our paper. He has pointed out some references which we did not have at the time the first of us conceived the *idea* of obtaining the closed-form solutions presented in our paper. As the rather extensive list of references we cite in the paper indicates, we did search diligently for similar solutions and found none.

It is hardly surprising that more than one investigator had the idea of treating a strand of wire rope as a linear system. Of course, once that idea is in hand, there is more than one way to apply it. In this regard, we wish to emphasize that the use of the "Linear Theory" by many, including Velinsky himself, has been limited. It has been used to relate changes in variables/parameters of helical wires to those of strands as well as the changes in variables/parameters of strands to those of the cable in the loaded configuration. However, we know of no previous attempt to "integrate" explicitly these linearized relations in a concise form.

Although linearization of the equations achieves some economy of computational time, it does not alter the fact that the approach is basically a numerical simulation which requires the simultaneous solution of a set of usually a large number of algebraic equations depending upon the geometry of the cable cross-section. Without extensive parametric variations, such an approach fails to provide any direct design insights as to the influence of the various cable parameters on elastic deformations.

On the other hand, our results are explicitly stated in dimensionless form in equations (6) and (9)—with constants F_ϵ, F_β, M_ϵ and M_β directly available from equations (12)–(15). These equations represent, we believe, a significant step not taken by others. The three examples subsequently considered in our paper clearly demonstrate the ease and effectiveness with which our analytical solutions can be utilized in various studies of static elastic cable deformations. Needless to say, the benefits of the closed-form representation would be even more pronounced in formulations of dynamic models of systems which involve the use of cables as recently proposed for augmentation of structural damping in large space structures.

It may be stressed that the study of "nonrotating" cables is merely one of three examples presented to demonstrate the effectiveness of our closed-form solution. The assertion that

[1] By K. Kumar and J. E. Cochran, Jr., published in the December, 1987 issue of the ASME JOURNAL OF APPLIED MECHANICS, Vol. 54, No. 4, pp. 898–903.

[2] Assistant Professor, Department of Mechanical Engineering, University of Wisconsin-Madison, 1513 University Avenue, Madison, WI 53706.

Copyright © 1988 by ASME
Downloaded 03 May 2010 to 171.66.16.21. Redistribution subject to ASME license or copyright; see http://www.asme.org/terms/Terms_Use.cfm

"this problem has been solved previously in a more general form" by Knapp is not correct. Even if the strong nature of some of the assumptions in Knapp's treatment is overlooked, one cannot lose sight of the fact that his analysis applies only in the two extreme cases of cables with either rigid or perfectly incompressible core; i.e., when $\nu = 0.5$. In contrast, our treatment does not suffer from this limitation and applies to any general linear material having an arbitrary ν.

We concur with the assertion that for each α_2, there are, in general, two solutions for α_3 that cause the cable to be "nonrotating." This characteristic is also evident from Fig. 4 in our paper.

Regarding the convention followed in presenting the helix angles, it has been stated in the first paragraph under the heading—Results and Discussion. Accordingly, ". . . for each of the layers with left lay, its helix angle α_i must be replaced by the corresponding obtuse angle $\pi - \alpha_i$ . . . " This convention has been adhered to throughout the paper. In Fig. 4, from the context of the discussion, it is understood that the two layers have opposite lays (see first paragraph under subheading "Nonrotating Rope"); however, to avoid any possible ambiguities, it might have been better to have the ordinate read as $\pi - \alpha_3$ in place of α_3. With this change, the apparent inconsistencies would disappear.

Chaotic Motion of an Elastic-Plastic Beam[3]

P. S. Symonds[4], G. Borino[5], and U. Perego[6]. The authors looked for evidence of chaotic behavior both under impulsive loading and under periodic excitation, in the pin ended elastic-plastic Shanley model. Their results and conclusions in the impulsive loading ("free vibration") case disagree with ours, in recent studies. The disagreement seems to arise from the different ways of treating damping. Here we demonstrate this briefly. Details are given in a forthcoming paper by Borino et al. (1988).

The authors purport to show in their Figs. 3 and 4 how certain initial conditions lead to final displacements of negative sign—i.e., in the opposite direction to the loading ("anomalous"). In these figures a dot is entered if the prediction is for a negative value, and a blank for a positive outcome. Figure 3 shows a complex pattern. Figure 4 shows a portion of this to expanded scales, and is equally complex. This suggests a fine structure, with possible resemblance to fractal boundaries between attracting basins. They observe that the "slightest change in initial conditions can cause a drastic change in the response, and attempts at obtaining detailed numerical solutions to the problem are meaningless".

Our work on the response due to short pulse loading in the presence of damping (Genna and Symonds (1988); Borino et al. (1988)) leads to the opposite conclusion. For any value of damping ratio ζ, there are regions in the initial condition space such that the final displacement is negative, and outside of which it is positive. For the value $\zeta = 0.1$ used by the authors, there are two bands that are loci of pairs $(a_0, \dot{a}_0)$ leading to negative final displacements. These are shown in Fig. 1 for the region of the authors' Fig. 3 (we use the authors' notation, a_0 and $\dot{a}_0$ being initial displacement and velocity, respectively). Within each band, e.g., holding $\dot{a}_0$ constant, the final displacement is a piecewise continuous function of the initial displacement a_0. It must be found by a numerical integration scheme, but standard schemes of different types readily furnish essentially identical results. The curves separating the (+) and (−) regions do require more care for their determination, but only that normally demanded in problems involving bifurcations.

To explain why our results and conclusions differ from the authors' is not hard. In our calculations we took the system to be damped from the outset. In contrast, the authors started all their calculations with $\zeta = 0$. For each loading they "compute(d) the solution for a certain number of cycles". They then examined the maximum and minimum values of displacement. If they found $a_{max} < 0$, they took the final displacement

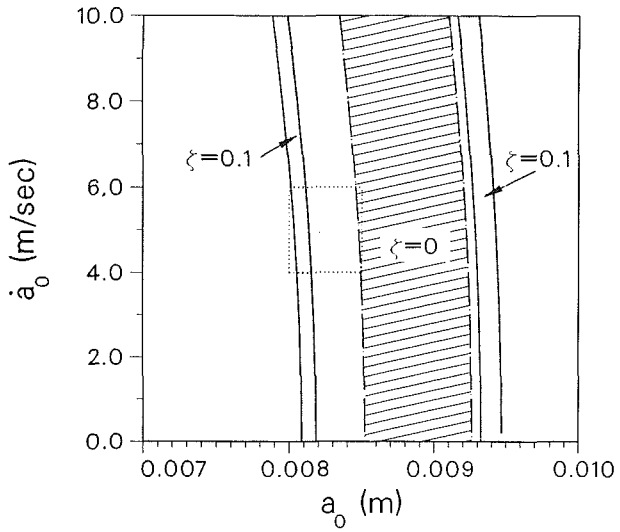


Fig. 1 Regions of initial conditions such that for damping ratio $\zeta = 0.1$ the final displacement is negative (shaded) and positive (unshaded). Cross-hatched region defines initial conditions such that the limit cycle of the *undamped* system is negative. Small rectangle enclosed by dotted lines indicates area shown to enlarged scales in authors' Fig. 4. (Our figure would merely increase in size.)

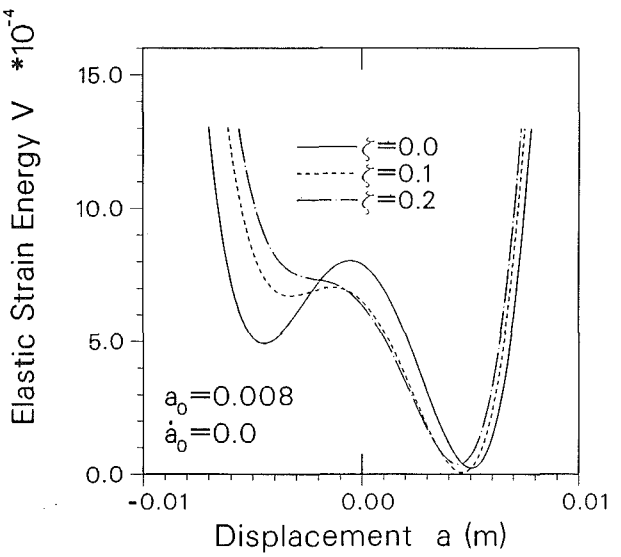


Fig. 2 Curves of elastic strain energy versus displacement for three damping ratios ζ. These curves describe the elastic vibrations; their shapes are determined by the prior plastic flow, and are seen to depend on the magnitude of damping.

[3] By B. Poddar, F. C. Moon, and S. Mukherjee and published in the March, 1988 issue of the ASME JOURNAL OF APPLIED MECHANICS, Vol. 55, No. 1, pp. 185–189.

[4] Professor of Engineering, Research, Brown University, Division of Engineering, Providence, RI 02912. Fellow ASME.

[5] Visiting Research Associate, Brown University, Division of Engineering, Providence, RI 02912. (On leave from Universita di Palermo, Dipartmento di Ingegneria Strutturale e Geotecnica, Viale delle Scienze, 90128 Palermo, Italy.)

[6] Visiting Research Associate, Brown University, Division of Engineering, Providence, RI 02912. (On leave from Politecnico di Milano, Dipartimento di Ingegneria Strutturale, Piazza L. Da Vinci 32, 20133 Milano, Italy.)

Downloaded 03 May 2010 to 171.66.16.21. Redistribution subject to ASME license or copyright; see http://www.asme.org/terms/Terms_Use.cfm

"this problem has been solved previously in a more general form" by Knapp is not correct. Even if the strong nature of some of the assumptions in Knapp's treatment is overlooked, one cannot lose sight of the fact that his analysis applies only in the two extreme cases of cables with either rigid or perfectly incompressible core; i.e., when $\nu = 0.5$. In contrast, our treatment does not suffer from this limitation and applies to any general linear material having an arbitrary ν.

We concur with the assertion that for each α_2, there are, in general, two solutions for α_3 that cause the cable to be "nonrotating." This characteristic is also evident from Fig. 4 in our paper.

Regarding the convention followed in presenting the helix angles, it has been stated in the first paragraph under the heading—Results and Discussion. Accordingly, ". . . for each of the layers with left lay, its helix angle α_i must be replaced by the corresponding obtuse angle $\pi - \alpha_i$ . . . " This convention has been adhered to throughout the paper. In Fig. 4, from the context of the discussion, it is understood that the two layers have opposite lays (see first paragraph under subheading "Nonrotating Rope"); however, to avoid any possible ambiguities, it might have been better to have the ordinate read as $\pi - \alpha_3$ in place of α_3. With this change, the apparent inconsistencies would disappear.

Chaotic Motion of an Elastic-Plastic Beam[3]

P. S. Symonds[4], G. Borino[5], and U. Perego[6]. The authors looked for evidence of chaotic behavior both under impulsive loading and under periodic excitation, in the pin ended elastic-plastic Shanley model. Their results and conclusions in the impulsive loading ("free vibration") case disagree with ours, in recent studies. The disagreement seems to arise from the different ways of treating damping. Here we demonstrate this briefly. Details are given in a forthcoming paper by Borino et al. (1988).

The authors purport to show in their Figs. 3 and 4 how certain initial conditions lead to final displacements of negative sign—i.e., in the opposite direction to the loading ("anomalous"). In these figures a dot is entered if the prediction is for a negative value, and a blank for a positive outcome. Figure 3 shows a complex pattern. Figure 4 shows a portion of this to expanded scales, and is equally complex. This suggests a fine structure, with possible resemblance to fractal boundaries between attracting basins. They observe that the "slightest change in initial conditions can cause a drastic change in the response, and attempts at obtaining detailed numerical solutions to the problem are meaningless".

Our work on the response due to short pulse loading in the presence of damping (Genna and Symonds (1988); Borino et al. (1988)) leads to the opposite conclusion. For any value of damping ratio ζ, there are regions in the initial condition space such that the final displacement is negative, and outside of which it is positive. For the value $\zeta = 0.1$ used by the authors, there are two bands that are loci of pairs $(a_0, \dot{a}_0)$ leading to negative final displacements. These are shown in Fig. 1 for the region of the authors' Fig. 3 (we use the authors' notation, a_0 and $\dot{a}_0$ being initial displacement and velocity, respectively). Within each band, e.g., holding $\dot{a}_0$ constant, the final displacement is a piecewise continuous function of the initial displacement a_0. It must be found by a numerical integration scheme, but standard schemes of different types readily furnish essentially identical results. The curves separating the (+) and (−) regions do require more care for their determination, but only that normally demanded in problems involving bifurcations.

To explain why our results and conclusions differ from the authors' is not hard. In our calculations we took the system to be damped from the outset. In contrast, the authors started all their calculations with $\zeta = 0$. For each loading they "compute(d) the solution for a certain number of cycles". They then examined the maximum and minimum values of displacement. If they found $a_{max} < 0$, they took the final displacement

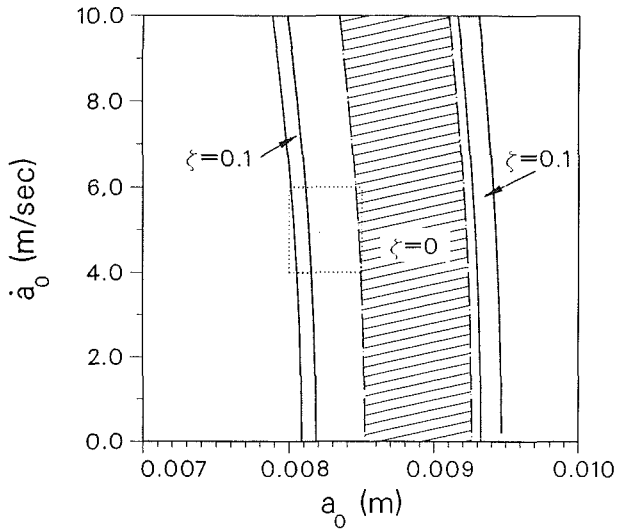


Fig. 1 Regions of initial conditions such that for damping ratio $\zeta = 0.1$ the final displacement is negative (shaded) and positive (unshaded). Cross-hatched region defines initial conditions such that the limit cycle of the *undamped* system is negative. Small rectangle enclosed by dotted lines indicates area shown to enlarged scales in authors' Fig. 4. (Our figure would merely increase in size.)

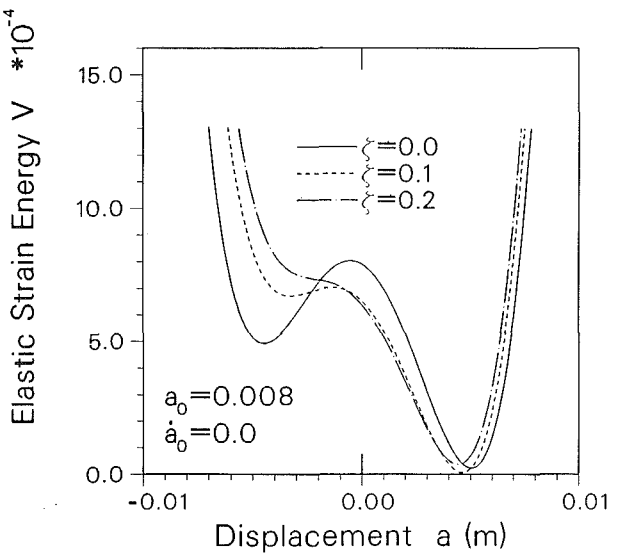


Fig. 2 Curves of elastic strain energy versus displacement for three damping ratios ζ. These curves describe the elastic vibrations; their shapes are determined by the prior plastic flow, and are seen to depend on the magnitude of damping.

[3]By B. Poddar, F. C. Moon, and S. Mukherjee and published in the March, 1988 issue of the ASME JOURNAL OF APPLIED MECHANICS, Vol. 55, No. 1, pp. 185–189.

[4]Professor of Engineering, Research, Brown University, Division of Engineering, Providence, RI 02912. Fellow ASME.

[5]Visiting Research Associate, Brown University, Division of Engineering, Providence, RI 02912. (On leave from Universita di Palermo, Dipartmento di Ingegneria Strutturale e Geotecnica, Viale delle Scienze, 90128 Palermo, Italy.)

[6]Visiting Research Associate, Brown University, Division of Engineering, Providence, RI 02912. (On leave from Politecnico di Milano, Dipartimento di Ingegneria Strutturale, Piazza L. Da Vinci 32, 20133 Milano, Italy.)

Copyright © 1988 by ASME
Downloaded 03 May 2010 to 171.66.16.21. Redistribution subject to ASME license or copyright; see http://www.asme.org/terms/Terms_Use.cfm

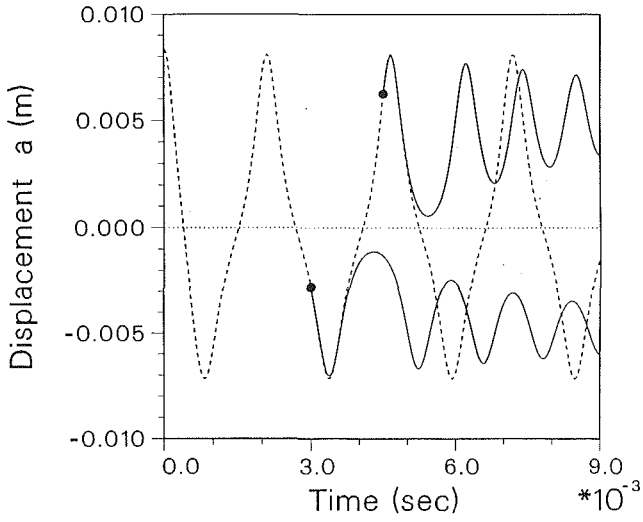


Fig. 3 Dashed curve shows response of undamped system for $a_0 = 0.0083$m, $\dot{a}_0 = 4$m/sec. Solid curves show responses when damping with $\zeta = 0.1$ is inserted at two different times (black circles); the final displacement is positive in one case, negative in the other.

to be negative and entered a dot. If they found $a_{max} > 0$, they then (and only then) set $\zeta = 0.1$ and ran the problem to an equilibrium point a_E. If they found $a_E < 0.1(a_{max} - a_{min})$, they entered a dot. Only by accident does this procedure furnish the sign of the final rest displacement in agreement with that of the structure damped from the outset.

The authors' procedure tacitly involves the assumptions (1) that the plastic deformation are unaffected by damping, and (2) that it is immaterial when damping is inserted. Neither is valid, even approximately, in their calculations. For example, Fig. 2 illustrates the effects of damping on the strain energy function $V(a)$ of the elastic vibration for the initial conditions $a_0 = 0.008$, $\dot{a}_0 = 0.$; the shape of this function is determined, of course, by the prior plastic flow. A negative final state requires there to be a stable equilbrium point at a negative a. There is such a state for $\zeta = 0$ and 0.1, but not for $\zeta = 0.2$. However the authors' method always presumes the curve for $\zeta = 0$. Hence, it can predict anomalous results when none exist. Figure 3 shows that by inserting the damping at different times in the elastic vibration one can obtain either a positive or a negative final state. Exactly how the authors chose the instant to introduce damping is not stated, but their procedure probably accounts for the (spurious) complexity of their Figs. 3 and 4.

In the cases where the authors found $a_{max} < 0$, their procedure furnishes the correct sign of the final state (limit cycle) of the undamped system. Thus, it agrees with early results for this case (Symonds and Yu (1985)). The region in the initial condition space of anomalous outcomes for this case ($\zeta = 0$) is shown in Fig. 1 as the cross-hatched band between dot-dash lines; this agrees with the wide band of dense points in the authors' Fig. 3. However, for the damped system, the loci of points which actually lead to anomalous final displacements are the shaded areas. The authors' procedure predicts no anomalous points correctly in this case, $\zeta = 0.1$. If ζ is quite small (about 0.01 or less—see Genna and Symonds (1988)), the wide band of anomalous outcomes of the damped model approaches that of the undamped system, and the authors' method will predict these points correctly. However, in the cases where $a_{max} > 0$ it will predict the correct sign only by accident, for any ζ.

Contrary to the authors' assertion, the response is in general predictable by standard numerical methods. The exceptional case is that of vanishingly small (nonzero) damping. As ζ is taken smaller, the final state alternates in sign more rapidly, e.g., in a plot against the initial displacement (Genna and Symonds (1988)). Eve tually, as ζ is decreased, the widths of the bands become less than the error of the computation (for a given algorithm and device). The outcome is then unpredictable. Chaotic behavior does not seem to be involved in this kind of unpredictability. However, under *periodic* loading the authors have clearly demonstrated that fractal structures and chaos do occur. We conjecture that their existence *depends on the possibility of anomalous response under impulsive loading*. If so, the bounds discussed by Borino et al. (1988) would be relevant, in an appropriate sense, to the question of bounds on chaotic behavior under periodic loading.

References

Borino, G., Perego, U., and Symonds, P. S., 1988, "An Energy Approach to Anomalous Damped Elastic-Plastic Response to Short Pulse Loading," submitted to ASME JOURNAL OF APPLIED MECHANICS, April.

Genna, F., and Symonds, P. S., 1988, "Dynamic Plastic Instabilities in Response to Short Pulse Excitation—Effects of Slenderness Ratio and Damping," *Proc. Royal Society*, Vol. A417, pp. 31–44.

Symonds, P. S., and Yu, T. X., 1985, "Counter-Intuitive Behavior in a Problem of Elastic-Plastic Beam Dynamics," ASME JOURNAL OF APPLIED MECHANICS, Vol. 52, pp. 517–522.

An Approximate Solution of the Axisymmetric von Karman Equations for a Point-Loaded Circular Plate[7]

C. W. Bert,[8] S. K. Jang,[9] and A. G. Striz[10]. The authors are to be congratulated for their approximate analytical solution of the static, axisymmetric von Karman plate equations. In particular, the provision for the change in deflection shape with increasing load is to be commended.

Recently, several other approximate solutions, which also provide for a change in deflection shape with increasing load, have appeared. A two-term energy solution was obtained for clamped plates by Bert and Martindale (1987) for both point and uniformly distributed loadings. Striz et al. (1987, 1988) used the method of differential quadrature (*DQ*) to solve the problems of both point and uniformly distributed loadings for both clamped and simply supported plates. For cases in which an exact solution was not available, the *DQ* method results were compared with those obtained by the finite element method (FEM). However, the actual CPU time for a solution by the *DQ* method was up to 80 percent less than for a solution of comparable accuracy by the FEM.

Also, the present authors (Bert et al., 1988) obtained excellent results using the *DQ* method for the case of a rectangular plate either clamped or simply supported.

References

Bert, C. W., and Martindale, J. L., 1987, "An Accurate, Simplified Method for Analyzing Thin Plates Undergoing Large Deflections," *Proc., 28th AIAA/ASME/AHS/ASCE Structures, Structural Dynamics and Materials Conference*, Pt. 1, pp. 480–487; also to appear in *AIAA Journal*, 1988.

Bert, C. W., Striz, A. G., and Jang, S. K., 1988, "Nonlinear Deflection of Rectangular Plates by Differential Quadrature," *Computational Mechanics '88. Proc., 2nd International Conference on Computational Engineering Science*, Vol. I, Chap. 23, pp. *iii*.1–*iii*.4.

[7] By A. T. Dolovich, G. W. Brodland, and A. B. Thornton-Trump and published in the March, 1988 issue of the ASME JOURNAL OF APPLIED MECHANICS, Vol. 55, No. 1, pp. 241–243.

[8] Perkinson Chair Professor, School of Aerospace, Mechanical, and Nuclear Engineering, University of Oklahoma, Norman, OK. Fellow ASME.

[9] Visting Assistant Professor, School of Aerospace, Mechanical, and Nuclear Engineering, University of Oklahoma, Norman, OK.

[10] Assistant Professor, School of Aerospace, Mechanical, and Nuclear Engineering, University of Oklahoma, Norman, OK. Member ASME.

Downloaded 03 May 2010 to 171.66.16.21. Redistribution subject to ASME license or copyright; see http://www.asme.org/terms/Terms_Use.cfm

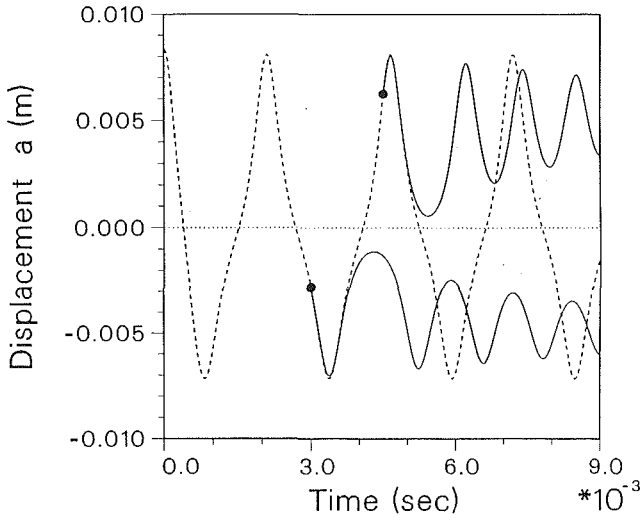


Fig. 3 Dashed curve shows response of undamped system for $a_0 = 0.0083$m, $\dot{a}_0 = 4$m/sec. Solid curves show responses when damping with $\zeta = 0.1$ is inserted at two different times (black circles); the final displacement is positive in one case, negative in the other.

to be negative and entered a dot. If they found $a_{\max} > 0$, they then (and only then) set $\zeta = 0.1$ and ran the problem to an equilibrium point a_E. If they found $a_E < 0.1(a_{\max} - a_{\min})$, they entered a dot. Only by accident does this procedure furnish the sign of the final rest displacement in agreement with that of the structure damped from the outset.

The authors' procedure tacitly involves the assumptions (1) that the plastic deformation are unaffected by damping, and (2) that it is immaterial when damping is inserted. Neither is valid, even approximately, in their calculations. For example, Fig. 2 illustrates the effects of damping on the strain energy function $V(a)$ of the elastic vibration for the initial conditions $a_0 = 0.008$, $\dot{a}_0 = 0.$; the shape of this function is determined, of course, by the prior plastic flow. A negative final state requires there to be a stable equilbrium point at a negative a. There is such a state for $\zeta = 0$ and 0.1, but not for $\zeta = 0.2$. However the authors' method always presumes the curve for $\zeta = 0$. Hence, it can predict anomalous results when none exist. Figure 3 shows that by inserting the damping at different times in the elastic vibration one can obtain either a positive or a negative final state. Exactly how the authors chose the instant to introduce damping is not stated, but their procedure probably accounts for the (spurious) complexity of their Figs. 3 and 4.

In the cases where the authors found $a_{\max} < 0$, their procedure furnishes the correct sign of the final state (limit cycle) of the undamped system. Thus, it agrees with early results for this case (Symonds and Yu (1985)). The region in the initial condition space of anomalous outcomes for this case ($\zeta = 0$) is shown in Fig. 1 as the cross-hatched band between dot-dash lines; this agrees with the wide band of dense points in the authors' Fig. 3. However, for the damped system, the loci of points which actually lead to anomalous final displacements are the shaded areas. The authors' procedure predicts no anomalous points correctly in this case, $\zeta = 0.1$. If ζ is quite small (about 0.01 or less—see Genna and Symonds (1988)), the wide band of anomalous outcomes of the damped model approaches that of the undamped system, and the authors' method will predict these points correctly. However, in the cases where $a_{\max} > 0$ it will predict the correct sign only by accident, for any ζ.

Contrary to the authors' assertion, the response is in general predictable by standard numerical methods. The exceptional case is that of vanishingly small (nonzero) damping. As ζ is taken smaller, the final state alternates in sign more rapidly, e.g., in a plot against the initial displacement (Genna and Symonds (1988)). Eve tually, as ζ is decreased, the widths of the bands become less than the error of the computation (for a given algorithm and device). The outcome is then unpredictable. Chaotic behavior does not seem to be involved in this kind of unpredictability. However, under *periodic* loading the authors have clearly demonstrated that fractal structures and chaos do occur. We conjecture that their existence *depends on the possibility of anomalous response under impulsive loading*. If so, the bounds discussed by Borino et al. (1988) would be relevant, in an appropriate sense, to the question of bounds on chaotic behavior under periodic loading.

References

Borino, G., Perego, U., and Symonds, P. S., 1988, "An Energy Approach to Anomalous Damped Elastic-Plastic Response to Short Pulse Loading," submitted to ASME JOURNAL OF APPLIED MECHANICS, April.

Genna, F., and Symonds, P. S., 1988, "Dynamic Plastic Instabilities in Response to Short Pulse Excitation—Effects of Slenderness Ratio and Damping," *Proc. Royal Society*, Vol. A417, pp. 31–44.

Symonds, P. S., and Yu, T. X., 1985, "Counter-Intuitive Behavior in a Problem of Elastic-Plastic Beam Dynamics," ASME JOURNAL OF APPLIED MECHANICS, Vol. 52, pp. 517–522.

An Approximate Solution of the Axisymmetric von Karman Equations for a Point-Loaded Circular Plate[7]

C. W. Bert,[8] S. K. Jang,[9] and A. G. Striz[10]. The authors are to be congratulated for their approximate analytical solution of the static, axisymmetric von Karman plate equations. In particular, the provision for the change in deflection shape with increasing load is to be commended.

Recently, several other approximate solutions, which also provide for a change in deflection shape with increasing load, have appeared. A two-term energy solution was obtained for clamped plates by Bert and Martindale (1987) for both point and uniformly distributed loadings. Striz et al. (1987, 1988) used the method of differential quadrature (*DQ*) to solve the problems of both point and uniformly distributed loadings for both clamped and simply supported plates. For cases in which an exact solution was not available, the *DQ* method results were compared with those obtained by the finite element method (FEM). However, the actual CPU time for a solution by the *DQ* method was up to 80 percent less than for a solution of comparable accuracy by the FEM.

Also, the present authors (Bert et al., 1988) obtained excellent results using the *DQ* method for the case of a rectangular plate either clamped or simply supported.

References

Bert, C. W., and Martindale, J. L., 1987, "An Accurate, Simplified Method for Analyzing Thin Plates Undergoing Large Deflections," *Proc., 28th AIAA/ASME/AHS/ASCE Structures, Structural Dynamics and Materials Conference*, Pt. 1, pp. 480–487; also to appear in *AIAA Journal*, 1988.

Bert, C. W., Striz, A. G., and Jang, S. K., 1988, "Nonlinear Deflection of Rectangular Plates by Differential Quadrature," *Computational Mechanics '88. Proc., 2nd International Conference on Computational Engineering Science*, Vol. I, Chap. 23, pp. *iii*.1–*iii*.4.

[7] By A. T. Dolovich, G. W. Brodland, and A. B. Thornton-Trump and published in the March, 1988 issue of the ASME JOURNAL OF APPLIED MECHANICS, Vol. 55, No. 1, pp. 241–243.

[8] Perkinson Chair Professor, School of Aerospace, Mechanical, and Nuclear Engineering, University of Oklahoma, Norman, OK. Fellow ASME.

[9] Visting Assistant Professor, School of Aerospace, Mechanical, and Nuclear Engineering, University of Oklahoma, Norman, OK.

[10] Assistant Professor, School of Aerospace, Mechanical, and Nuclear Engineering, University of Oklahoma, Norman, OK. Member ASME.

Copyright © 1988 by ASME
Downloaded 03 May 2010 to 171.66.16.21. Redistribution subject to ASME license or copyright; see http://www.asme.org/terms/Terms_Use.cfm

Striz, A. G., Jang, S. K., and Bert, C. W., 1987, "Analysis by Differential Quadrature of Thin Circular Plates Undergoing Large Deflections," *Developments in Mechanics*, Vol. 14, Purdue University, pp. 900-905.

Striz, A. G., Jang, S. K., and Bert, C. W., 1988, "Nonlinear Bending Analysis of Thin Circular Plates by Differential Quadrature," *Thin-Walled Structures*, Vol. 6, pp. 51-62.

Authors' Closure

The authors would like to thank Professors Bert, Jang, and Striz for their comments. We have noted their work with interest, and are pleased to see that our differing approaches have produced results which appear to be both compatible and complementary. In addition, knowing how difficult it is to spot typographical errors, we are sure that readers will appreciate the list of apparent errata for Chien and Yeh (1954) and Chia (1980) given in Striz et al. (1988).

References

Chia, C. Y., 1980, *Nonlinear Analysis of Plates*, McGraw-Hill, New York.

Chien, W. Z., and Yeh, K. T., 1954, "On the Large Deflection of Circular Plates," *Scientia Sinica*, Vol. 3, pp. 405-436.

Striz, A. G., Jang, S. K., and Bert, C. W., 1988, "Nonlinear Bending Analysis of Thin Circular Plates by Differential Quadrature," *Thin-Walled Structures*, Vol. 6, pp. 51-62.

On the Dynamic Response of a Single-Degree-of-Freedom Structure Attached to the Interior of a Rotating Rigid Ring[11]

David A. Peters[12] and Dewey H. Hodges[13]. The authors provide an interesting mathematical analysis of their nonlinear equation (9)

$$\ddot{u}+\left[\omega^2-\frac{R}{h}\,\Omega^2-\frac{2}{h}\,\Omega\dot{u}\right]u=0 \tag{1}$$

that supposedly represents the nonlinear dynamics of a rotating structure. Unfortunately, the nonlinear term in that equation, $(2/h)\Omega\dot{u}u$, which the authors identify as a "Coriolis effect," is extraneous. It appears in their equation (9) due to an error in the derivation.

The source of this error is in the development of the initial acceleration vector, $\ddot{\mathbf{r}}_p$ of a point mass attached to a flexible structure. Figure 1 of this discussion gives a schematic description of a general single-degree-of-freedom structure attached to the interior of a rotating rigid ring. All inertia is concentrated in a point mass p (of mass m), and all elasticity (i.e., stiffness) is carried in the flexible support. (The support is depicted as a beam, but any massless flexible structure can be considered here.) If we take the position vector of p as measured from the center of rotation, we have

$$\vec{\mathbf{r}}_p=u(t)\hat{\imath}+[-R+h-v(t)]\hat{\jmath} \tag{2}$$

where $v(t)$ is the foreshortening of any particular structure to be analyzed. As a simple example, for a cantilever beam, the foreshortening due to inextensibility depends upon the shape function $w(y)$ (with $w(1)\equiv u$) and can be expressed as

$$v=\frac{1}{2}\int_0^h\left(\frac{dw}{dy}\right)^2 dy\equiv fu^2/h \tag{3}$$

We can define f as the foreshortening factor. For example, if

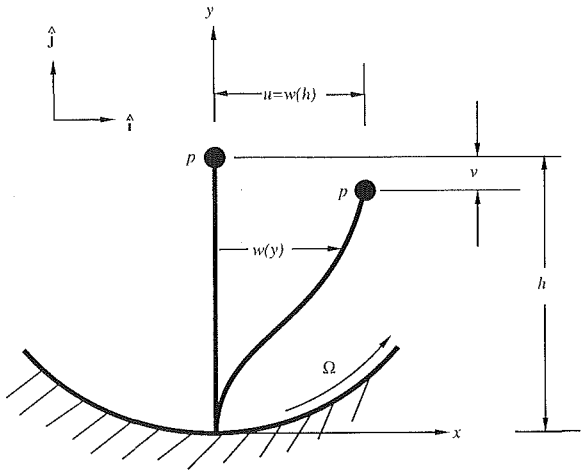


Fig. 1 Schematic of the particle p attached to the interior of rigid ring by a flexible structure

$w=uy/h$, then $f=\frac{1}{2}$; and, if $w=uy^2/h^2$, then $f=\frac{2}{3}$. Although f is always postive for a cantilever beam, for a general structure, f might take on any value, positive, negative, or zero.

It follows that the initial velocity and acceleration of m (for the general case) are

$$\dot{\vec{\mathbf{r}}}_p=[\Omega(r-h+fu^2/h)+\dot{u}]\hat{\imath}+[u\Omega-2fu\dot{u}/h]\,\hat{\jmath} \tag{4}$$

$$\ddot{\vec{\mathbf{r}}}_p=[\ddot{u}-u\Omega^2+4fu\dot{u}\Omega/h]\hat{\imath}+[(R-h+fu^2/h)\Omega^2+2\dot{u}\Omega-2f(\dot{u}^2+u\ddot{u})/h]\,\hat{\jmath} \tag{5}$$

Equations (3)-(5) are taken to second-order in u because we wish the final differential equation to be of second-order. In the paper under discussion, however, the acceleration is *taken only to first-order in* u; see their equation (3). Thus, the term $4fu\dot{u}\Omega/h$ is missing from the $\hat{\imath}$ component of $\ddot{\vec{\mathbf{r}}}_p$ in that paper. This, as we will see, is the source of the error.

We now turn to the development of the force vector, which is correct in the subject paper for the special case $f=\frac{1}{2}$. Here, we give a slightly more general derivation for arbitrary f. The tangential force can be found from virtual work as

$$F_T=-ku+\frac{\partial v}{\partial u}\,F_N=-ku+2fF_Nu/h \tag{6}$$

where ku is the elastic restoring force and F_N is the normal force. Notice that the virtual work principle implies that F_N enters the analysis through the *same* parameter, f, that defines the foreshortening. Since we are taking F_T to second-order in u, we need F_N only to first-order in u (as is correctly done by the authors).

$$F_N=m[(R-h)\Omega^2+2\dot{u}\Omega]+0(u^2) \tag{7}$$

The correct equations of motion follow from setting F_T equal to the $\hat{\imath}$ component of $m\ddot{\vec{r}}_p$.

$$-ku+2fm[(R-h)\Omega^2+2\dot{u}\Omega]u/h=m[\ddot{u}-\Omega^2u+4fu\dot{u}\Omega/h] \tag{8}$$

We notice that the $u\dot{u}$ nonlinearity appears on both sides of the equation. Thus, the term is cancelled, which leads to

$$\ddot{u}-\Omega^2u-2fm(R-h)\Omega^2u/h+ku=0 \tag{9}$$

(The identical equation can be derived from the energy method.) Here we note that, regardless of the foreshortening factor f, the second-degree nonlinearity $u\dot{u}$ is eliminated from the equation. Therefore, the correct equation of motion for

[11] By A. G. Hernried and G. B. Gustafson and published in the March, 1988, issue of the ASME JOURNAL OF APPLIED MECHANICS, Vol. 55, No. 1, pp. 201-205.

[12] Professor, School of Aerospace Engineering, Georgia Institute of Technology, Atlanta, GA 30332-0150. Member ASME.

[13] Professor, School of Aerospace Engineering, Georgia Institute of Technology, Atlanta, GA 30332-0150.

Downloaded 03 May 2010 to 171.66.16.21. Redistribution subject to ASME license or copyright; see http://www.asme.org/terms/Terms_Use.cfm

Striz, A. G., Jang, S. K., and Bert, C. W., 1987, "Analysis by Differential Quadrature of Thin Circular Plates Undergoing Large Deflections," *Developments in Mechanics*, Vol. 14, Purdue University, pp. 900-905.

Striz, A. G., Jang, S. K., and Bert, C. W., 1988, "Nonlinear Bending Analysis of Thin Circular Plates by Differential Quadrature," *Thin-Walled Structures*, Vol. 6, pp. 51-62.

Authors' Closure

The authors would like to thank Professors Bert, Jang, and Striz for their comments. We have noted their work with interest, and are pleased to see that our differing approaches have produced results which appear to be both compatible and complementary. In addition, knowing how difficult it is to spot typographical errors, we are sure that readers will appreciate the list of apparent errata for Chien and Yeh (1954) and Chia (1980) given in Striz et al. (1988).

References

Chia, C. Y., 1980, *Nonlinear Analysis of Plates*, McGraw-Hill, New York.

Chien, W. Z., and Yeh, K. T., 1954, "On the Large Deflection of Circular Plates," *Scientia Sinica*, Vol. 3, pp. 405-436.

Striz, A. G., Jang, S. K., and Bert, C. W., 1988, "Nonlinear Bending Analysis of Thin Circular Plates by Differential Quadrature," *Thin-Walled Structures*, Vol. 6, pp. 51-62.

On the Dynamic Response of a Single-Degree-of-Freedom Structure Attached to the Interior of a Rotating Rigid Ring[11]

David A. Peters[12] and Dewey H. Hodges[13]. The authors provide an interesting mathematical analysis of their nonlinear equation (9)

$$\ddot{u}+\left[\omega^2-\frac{R}{h}\,\Omega^2-\frac{2}{h}\,\Omega\dot{u}\right]u=0 \tag{1}$$

that supposedly represents the nonlinear dynamics of a rotating structure. Unfortunately, the nonlinear term in that equation, $(2/h)\Omega\dot{u}u$, which the authors identify as a "Coriolis effect," is extraneous. It appears in their equation (9) due to an error in the derivation.

The source of this error is in the development of the initial acceleration vector, $\ddot{\mathbf{r}}_p$ of a point mass attached to a flexible structure. Figure 1 of this discussion gives a schematic description of a general single-degree-of-freedom structure attached to the interior of a rotating rigid ring. All inertia is concentrated in a point mass p (of mass m), and all elasticity (i.e., stiffness) is carried in the flexible support. (The support is depicted as a beam, but any massless flexible structure can be considered here.) If we take the position vector of p as measured from the center of rotation, we have

$$\vec{\mathbf{r}}_p=u(t)\hat{\imath}+[-R+h-v(t)]\hat{\jmath} \tag{2}$$

where $v(t)$ is the foreshortening of any particular structure to be analyzed. As a simple example, for a cantilever beam, the foreshortening due to inextensibility depends upon the shape function $w(y)$ (with $w(1)\equiv u$) and can be expressed as

$$v=\frac{1}{2}\int_0^h\left(\frac{dw}{dy}\right)^2 dy\equiv fu^2/h \tag{3}$$

We can define f as the foreshortening factor. For example, if

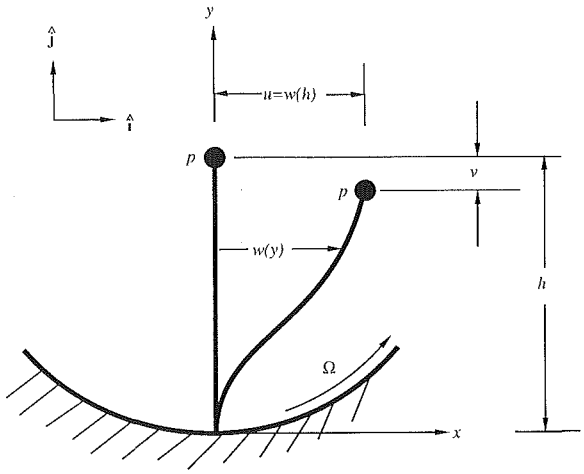


Fig. 1 Schematic of the particle p attached to the interior of rigid ring by a flexible structure

$w=uy/h$, then $f=\frac{1}{2}$; and, if $w=uy^2/h^2$, then $f=\frac{2}{3}$. Although f is always postive for a cantilever beam, for a general structure, f might take on any value, positive, negative, or zero.

It follows that the initial velocity and acceleration of m (for the general case) are

$$\dot{\vec{\mathbf{r}}}_p=[\Omega(r-h+fu^2/h)+\dot{u}]\hat{\imath}+[u\Omega-2fu\dot{u}/h]\,\hat{\jmath} \tag{4}$$

$$\ddot{\vec{\mathbf{r}}}_p=[\ddot{u}-u\Omega^2+4fu\dot{u}\Omega/h]\hat{\imath}+[(R-h+fu^2/h)\Omega^2+2\dot{u}\Omega-2f(\dot{u}^2+u\ddot{u})/h]\,\hat{\jmath} \tag{5}$$

Equations (3)-(5) are taken to second-order in u because we wish the final differential equation to be of second-order. In the paper under discussion, however, the acceleration is *taken only to first-order in* u; see their equation (3). Thus, the term $4fu\dot{u}\Omega/h$ is missing from the $\hat{\imath}$ component of $\ddot{\vec{\mathbf{r}}}_p$ in that paper. This, as we will see, is the source of the error.

We now turn to the development of the force vector, which is correct in the subject paper for the special case $f=\frac{1}{2}$. Here, we give a slightly more general derivation for arbitrary f. The tangential force can be found from virtual work as

$$F_T=-ku+\frac{\partial v}{\partial u}\,F_N=-ku+2fF_Nu/h \tag{6}$$

where ku is the elastic restoring force and F_N is the normal force. Notice that the virtual work principle implies that F_N enters the analysis through the *same* parameter, f, that defines the foreshortening. Since we are taking F_T to second-order in u, we need F_N only to first-order in u (as is correctly done by the authors).

$$F_N=m[(R-h)\Omega^2+2\dot{u}\Omega]+0(u^2) \tag{7}$$

The correct equations of motion follow from setting F_T equal to the $\hat{\imath}$ component of $m\ddot{\vec{r}}_p$.

$$-ku+2fm[(R-h)\Omega^2+2\dot{u}\Omega]u/h=m[\ddot{u}-\Omega^2u+4fu\dot{u}\Omega/h] \tag{8}$$

We notice that the $u\dot{u}$ nonlinearity appears on both sides of the equation. Thus, the term is cancelled, which leads to

$$\ddot{u}-\Omega^2u-2fm(R-h)\Omega^2u/h+ku=0 \tag{9}$$

(The identical equation can be derived from the energy method.) Here we note that, regardless of the foreshortening factor f, the second-degree nonlinearity $u\dot{u}$ is eliminated from the equation. Therefore, the correct equation of motion for

[11] By A. G. Hernried and G. B. Gustafson and published in the March, 1988, issue of the ASME JOURNAL OF APPLIED MECHANICS, Vol. 55, No. 1, pp. 201-205.

[12] Professor, School of Aerospace Engineering, Georgia Institute of Technology, Atlanta, GA 30332-0150. Member ASME.

[13] Professor, School of Aerospace Engineering, Georgia Institute of Technology, Atlanta, GA 30332-0150.

Copyright © 1988 by ASME
Downloaded 03 May 2010 to 171.66.16.21. Redistribution subject to ASME license or copyright; see http://www.asme.org/terms/Terms_Use.cfm

$f=\frac{1}{2}$ is identical to equation (9) of Hernried and Gustafson, but without the extraneous nonlinearity, $u\dot{u}$.

For the class of systems considered in the subject paper, the Lagrangean L does not contain time explicity. It is simple to show that a term proportional to $u\dot{u}$ can never exist for such a single-degree-of-freedom structure. In particular, we can write the Lagrangean of a structure in the form

$$L=A(q_1,q_2\ldots,q_n)+B_i(q_1,q_2,\ldots,q_n)\dot{q}_i + C_{ij}(q_1,q_2,\ldots,q_n)\dot{q}_i\dot{q}_j \tag{10}$$

where here and hereafter, repeated indices are summed over their range from 1 to n, the number of degrees-of-freedom. If the virtual work is given by

$$\delta W=F_i\delta q_i \tag{11}$$

then Lagrange's equation for q_i is

$$(C_{ij}+C_{ji})\ddot{q}_j+\left(\frac{\partial C_{ji}}{\partial q_k}+\frac{\partial C_{ij}}{\partial q_k}-\frac{\partial C_{jk}}{\partial q_i}\right)\dot{q}_j\dot{q}_k + \left(\frac{\partial B_i}{\partial q_j}-\frac{\partial B_j}{\partial q_i}\right)\dot{q}_j-\frac{\partial A}{\partial q_i}=F_i \quad (i=1,2,\ldots,n) \tag{12}$$

The only nonlinear terms that *can* involve products of q's and the $\dot{q}$'s are the B terms. These terms *clearly* vanish for one-degree-of-freedom systems ($n=1$). Only in systems with more than one-degree-of-freedom can these terms occur, and then they produce only antisymmetric coupling which is, of course, nondissipative.

In conclusion, we must emphasize that second-order nonlinearities of the type studied in the subject paper, for systems with one-degree-of-freedom, do not exist. The nonlinear term only appears in that paper because the authors include the foreshortening effect in the virtual work but not in the acceleration. Furthermore, the authors cannot assume zero foreshortening in the acceleration vector without *also* modifying the force expression in their equation (5). These two effects are physically related through f and always eliminate the term in question. Therefore, the erroneous terms cannot be interpreted as an alternative structural model (unless one is proposing an alternative to Newtonian mechanics); it is simply incorrect. There *are* nonlinearities for this type of single-degree-of-freedom structure, but they involve either quadratic powers of $\dot{u}$ or higher-order terms in u alone.

Authors' Closure

Equation (9) of our paper is *not* Lagrange's equation. We have traded traditional energy assumptions for ones that lead to a mathematically simple nonlinear model.

The derivation of (9) parallels the work of Weber (1976) (see references in our paper), specifically, we assume:

$$F_T=-ku+\frac{u}{h}F_N \quad \text{(Clough and Penzien, 1975)} \tag{1}$$

$$\mathbf{r}_P=u(t)\mathbf{i}+(h-R)\mathbf{j} \quad (v=0 \text{ in Fig. 1})$$

In contrast, Peters and Hodges assume:

$$F_T=-ku+\frac{\partial v}{\partial u}F_N \tag{2}$$

$$\mathbf{r}_P=u(t)\mathbf{i}+[h-R-v(t)]\mathbf{j}$$

The issue is whether or not assumption (1) can be made. For if so, then equation (9) of our paper follows just as published.

We happen to think that both modeling assumptions have some virtue, and are delighted to have different models to compare. Our delight is caused in part by the desire to have an inventory of models close to the rotating structure problem. We envision such models as prime candidates for starting a bifurcation analysis, such as suggested in the computational package AUTO by E. Doedel.

Downloaded 03 May 2010 to 171.66.16.21. Redistribution subject to ASME license or copyright; see http://www.asme.org/terms/Terms_Use.cfm

Journal of Applied Mechanics

Book Reviews

Cell-to-Cell Mapping, A Method of Global Analysis for Nonlinear Systems, by C. S. Hsu. Springer-Verlag, New York, 1987. 352 pages.

REVIEWED BY B. H. TONGUE[1]

This very interesting book is devoted almost entirely to the research results of Professor Hsu and his colleagues. The overall thrust of this research has been the determination of all possible solutions to a given system of nonlinear equations, i.e., "global" analyses. Professor Hsu is one of the primary researchers in this area and this book provides a convenient opportunity to see his personal viewpoints and opinions gathered into a single volume.

Chapter 1 gives short overviews of the contents of the following chapters. In Chapter 2, Hsu introduces the concept of point mappings. Point mappings refer to dynamical systems in which individual points in phase space are mapped to image points in a discrete way. The chapter concludes with a discussion of index theory for N-dimensional systems.

One case in which it is possible to extract point mappings that exactly represent the solutions of systems that are governed by differential equations is if the system equations can be broken into both a linear part and a nonlinear parametric excitation term that only acts in an impulsive manner. Such a system leads to a series of initial condition problems in which the initial conditions for each successive time interval are determined from the end conditions of the previous interval and the value of the impuslive loading. Chapter 3 presents a series of such systems.

The essential concept of this book is that of Cell-to-Cell Mapping and the most elementary Cell-to-Cell Map is the Simple Cell Map, the topic of Chapter 4. Simple Cell Mapping can be viewed as a point mapping in which only a finite number of states exist in phase space. Recall that the point mapping concept takes an arbitrary input to some image point. In Simple Cell Mapping, the input as well as the output are restricted to a particular set of values. Thus, $x_{n+1} = 6x_n - x_n^2$, (x_n an integer), is a Simple Cell Mapping.

The following three chapters, 5 through 7, examine the properties of Simple Cell Maps. As seems reasonable, a Simple Cell Mapping will have properties that may or may not have analogues in a system governed by differential equations. These properties can be examined and classified. Chapter 5 is mainly concerned with singularities of the Simple Cell Map (equilibrium points, limit cycles, etc.). Chapter 6 develops an index theory for Simple Cell Maps that parallels the index theory of point mappings introduced in Chapter 2. A specific application of this theory is also discussed, namely a method to locate the zeros of a vector function. Chapter 7 presents a classification of the various types of singular behaviors exhibited by a Simple Cell Map.

Chapter 8 contains algorithms that can be used to implement a Simple Cell Map. Chapter 9 presents some applications of the Simple Cell Method to systems governed by differential equations. This is likely to be one of the most interesting chapters to engineers since it demonstrates how one can approximate the dynamics of a system of differential equations with an iterative mapping. The essential element in this procedure is to perform a discretization of the actual phase space within which the system exists into separate pieces, or cells. Under the Simple Cell Map, each cell of phase space is assumed to map precisely onto another cell after a given interval of time. Thus, the number of possible states for the systems is exactly equal to the total number of cells.

Chapter 10 introduces a more sophisticated technique that is based upon a statistical examination of an additional array of initial points that lie within each of the individual cells. This method, called Generalized Cell Mapping, is far more computationally intensive and leads to a probabilistic description of the system dynamics. The end result of the method is a matrix of transition probabilities for the entire cell array. The long term dynamics of the system are thus represented by a finite Markov chain. The chapter concludes by reviewing some concepts of Markov chain theory. Algorithms for implementing Generalized Cell Mapping are presented in Chapter 11.

Chapter 12 explores the implications of utilizing a hybrid of both Simple and Generalized Cell Mapping to successively approximate the system dynamics through a series of more and more detailed Cell Maps. In Chapter 13, Generalized Cell Mapping is used to define the regions in phase space in which a strange attractor occurs and the technique is used to gain some insight into the statistical properties of these solutions.

One of the major stumbling blocks to research in nonlinear systems is the sheer amount of computation required for many types of analysis. The methodology introduced by Professor Hsu is aimed at alleviating some of this computational burden. For many problems, these techniques can be used effectively to characterize the qualitative and sometimes quantitative nature of the solutions.

Perhaps the most significant difficulty with the text is the use of nomenclature. Although Professor Hsu is very thorough in defining many of the terms used in the book, they are often defined in rapid succession, without motivating background material or simple examples of the meaning behind the definitions. Thus, the reader must refer back to these definitions with some regularity as the text progresses.

In this reviewer's opinion, the development of computational techniques that allow fast and accurate characterizations of nonlinear system responses is an important and timely subject, as is the question of global nonlinear response determinations. Professor Hsu has developed an interesting set of techniques for performing such analyses, techniques that

[1]Assistant Professor, George W. Woodruff School of Mechanical Engineering, Georgia Institute of Technology, Atlanta, GA 30332. Mem. ASME.

Copyright © 1988 by ASME
Downloaded 03 May 2010 to 171.66.16.21. Redistribution subject to ASME license or copyright; see http://www.asme.org/terms/Terms_Use.cfm

nonlinear analysts should certainly be aware of. A large reference list has been included as an aid to those readers unfamiliar with the current state of nonlinear theory.

Turbulence Management and Relaminarisation, edited by H. W. Liepmann and R. Narasimha. Springer-Verlag, New York, 1988. 524 pages. Price: $89.70.

REVIEWED BY C. R. SMITH[2]

Effective methods of turbulence management and control are prizes which have been actively pursued by scientists and engineers for more than seventy years, with the pace quickening over the past two decades. A timely examination of some of the more recent methods and approaches for turbulence management is the general topic of the present book, which is a collection of 35 invited papers presented at a IUTAM Symposium on Turbulence Management and Relaminarisation in 1987. The papers are generally divided (somewhat unevenly) into the topics of wall-bounded flows, transition, relaminarisation, free-shear flows, and separated flows.

The papers on wall-bounded flows cover both flow structure and flow manipulation devices. The three papers on flow structure primarily reinforce the fact that confusion still reigns in establishing a "coherent" structure for a turbulent boundary layer, although the authors are in agreement that streamwise vorticity plays an important, but yet unclear role in turbulent boundary layers. The four papers on outer layer manipulation devices also instill a sense of uncertainty as to how effective (if at all) such devices are in reducing drag; it appears that there is still a high degree of variability in the results from different laboratories. However, the six papers on surface manipulation techniques are pretty well agreed that streamwise surface modifications have a positive effect (possibly as high as a 10 percent drag reduction). This latter group of papers provides a particularly nice cross-section of results and ideas on surface modification techniques, although it is clear that the functional rationale for these type of modifications is still under significant debate; I personally felt this section was one of the better collections in the book.

The sections on transition and relaminarisation contain several interesting papers on dynamics and control. The five papers on transition dynamics are interesting, but I often found myself searching for the relationship of the paper and the physics discussed therein to the topic of control and flow management. The four transition control papers were also quite useful, but left me wondering whether compliant surfaces (the subject of two of the papers) can ever be made truly effective for drag reduction at practical nautical speeds. The section of only four relaminarisation papers, only two of which were of real utility, left me wondering why there were so few papers on a topic which shares center stage in the main book title.

The last two sections on free-shear flows and separated flows were quite good. The seven free-shear papers, with the exception of the first paper, were basically concerned with jets. The topics were fairly split between discussion of the physical mechanisms by which jet growth can be affected, and methods for active/passive control. I particularly liked papers by Hakkinen et al. on turbulence control in jets and shear flows, and the paper by Hussain and Husain on the control of jets through manipulation of coherent structure. The last section on separated flows is rather anemic in quantity, but quite good in quality, with two papers on rather diverse topics: reattaching flow, and unsteady separation on an airfoil.

Taken as a whole, this collection of papers provides a broad overview of the areas of turbulence and preturbulence management. My main criticism is the variability in both length (from 2 to 26 pages) and quality of the papers presented. A second criticism is that the range of topic areas within the original symposium was probably too broad to provide a definitive enough focus on the question of turbulence management. However, these criticisms aside, I would recommend the book as a useful reference to those involved in, or requiring an overview of, the field of turbulence management and control.

Contact Mechanics of Rail/Wheel Systems II, by G. M. L. Gladwell, H. Ghonem, and J. Kalousek. University of Waterloo Press, Waterloo, ON, Canada, 1987. 476 pages. Price: $55.00.

REVIEWED BY BURTON PAUL[3]

How can one effectively review twenty-seven papers within the confines of a single printed page? There probably is no satisfactory answer to that question, but this collection contains so many items of interest to the readers of the journal, that we feel it is desirable to list all of the authors and titles. We shall also single out for individual comment a sampling of those papers which might have been published in this journal, as opposed to those which would more probably have been submitted to journals devoted to metallurgy, wear, or railroad engineering. The average quality in this collection is quite high, and no negative inferences should be drawn about papers not specifically commented on below.

Kalker discusses the many capabilities of his computer program CONTACT, which treats the following problems (among others): normal contact, Mindlin-Cattaneo shift, steady state rolling, transient rolling, subsurface stresses, etc.

Björkman and Klarbring discuss the differences and similarities between frictional and plastic systems, and the corresponding differences in shakedown theorems for the two classes.

Barber reviews the general area of thermal effects in elastic contact. He points out that classical existence and uniqueness theorems cease to apply for an important class of problems in which the temperature and elastic fields are coupled through boundary conditions. This frequently leads to a phenomenon of thermoelastic instability.

Selvadurai finds stress intensity factors for penny-shaped cracks which contain a concentric rigid disk inclusion.

Johnson presents a review of recent progress, at Cambridge University and elsewhere, in problems of plastic flow and shakedown due to rolling contact. He considers both perfectly plastic and strain hardening materials.

McDowell and Moyar also treat the problem of elastic-plastic rolling contact, utilizing a "sophisticated, two-surface cyclic plasticity theory, known to correlate nonproportional cyclic plasticity experiments . . . " They suggest that an accurate representation of work hardening response and kinematic hardening enhances the solution for subsurface plastic shear strain accumulation.

Bower and Johnson discuss the conditions under which the corner of rails (or ideal infinite quarter-spaces) suffer incremental plastic collapse (ratchetting) due to a "traveling Hertz pressure distribution," and compare their analysis to experiments on elastic disks.

[2]Professor, Department of Mechanical Engineering and Mechanics, Lehigh University, Bethlehem, PA 18015.

[3]Asa Whitney Professor of Dynamical Engineering, University of Pennsylvania, Philadelphia, PA. Fellow ASME.

Downloaded 03 May 2010 to 171.66.16.21. Redistribution subject to ASME license or copyright; see http://www.asme.org/terms/Terms_Use.cfm

nonlinear analysts should certainly be aware of. A large reference list has been included as an aid to those readers unfamiliar with the current state of nonlinear theory.

Turbulence Management and Relaminarisation, edited by H. W. Liepmann and R. Narasimha. Springer-Verlag, New York, 1988. 524 pages. Price: $89.70.

REVIEWED BY C. R. SMITH[2]

Effective methods of turbulence management and control are prizes which have been actively pursued by scientists and engineers for more than seventy years, with the pace quickening over the past two decades. A timely examination of some of the more recent methods and approaches for turbulence management is the general topic of the present book, which is a collection of 35 invited papers presented at a IUTAM Symposium on Turbulence Management and Relaminarisation in 1987. The papers are generally divided (somewhat unevenly) into the topics of wall-bounded flows, transition, relaminarisation, free-shear flows, and separated flows.

The papers on wall-bounded flows cover both flow structure and flow manipulation devices. The three papers on flow structure primarily reinforce the fact that confusion still reigns in establishing a "coherent" structure for a turbulent boundary layer, although the authors are in agreement that streamwise vorticity plays an important, but yet unclear role in turbulent boundary layers. The four papers on outer layer manipulation devices also instill a sense of uncertainty as to how effective (if at all) such devices are in reducing drag; it appears that there is still a high degree of variability in the results from different laboratories. However, the six papers on surface manipulation techniques are pretty well agreed that streamwise surface modifications have a positive effect (possibly as high as a 10 percent drag reduction). This latter group of papers provides a particularly nice cross-section of results and ideas on surface modification techniques, although it is clear that the functional rationale for these type of modifications is still under significant debate; I personally felt this section was one of the better collections in the book.

The sections on transition and relaminarisation contain several interesting papers on dynamics and control. The five papers on transition dynamics are interesting, but I often found myself searching for the relationship of the paper and the physics discussed therein to the topic of control and flow management. The four transition control papers were also quite useful, but left me wondering whether compliant surfaces (the subject of two of the papers) can ever be made truly effective for drag reduction at practical nautical speeds. The section of only four relaminarisation papers, only two of which were of real utility, left me wondering why there were so few papers on a topic which shares center stage in the main book title.

The last two sections on free-shear flows and separated flows were quite good. The seven free-shear papers, with the exception of the first paper, were basically concerned with jets. The topics were fairly split between discussion of the physical mechanisms by which jet growth can be affected, and methods for active/passive control. I particularly liked papers by Hakkinen et al. on turbulence control in jets and shear flows, and the paper by Hussain and Husain on the control of jets through manipulation of coherent structure. The last section on separated flows is rather anemic in quantity, but quite good in quality, with two papers on rather diverse topics: reattaching flow, and unsteady separation on an airfoil.

Taken as a whole, this collection of papers provides a broad overview of the areas of turbulence and preturbulence management. My main criticism is the variability in both length (from 2 to 26 pages) and quality of the papers presented. A second criticism is that the range of topic areas within the original symposium was probably too broad to provide a definitive enough focus on the question of turbulence management. However, these criticisms aside, I would recommend the book as a useful reference to those involved in, or requiring an overview of, the field of turbulence management and control.

Contact Mechanics of Rail/Wheel Systems II, by G. M. L. Gladwell, H. Ghonem, and J. Kalousek. University of Waterloo Press, Waterloo, ON, Canada, 1987. 476 pages. Price: $55.00.

REVIEWED BY BURTON PAUL[3]

How can one effectively review twenty-seven papers within the confines of a single printed page? There probably is no satisfactory answer to that question, but this collection contains so many items of interest to the readers of the journal, that we feel it is desirable to list all of the authors and titles. We shall also single out for individual comment a sampling of those papers which might have been published in this journal, as opposed to those which would more probably have been submitted to journals devoted to metallurgy, wear, or railroad engineering. The average quality in this collection is quite high, and no negative inferences should be drawn about papers not specifically commented on below.

Kalker discusses the many capabilities of his computer program CONTACT, which treats the following problems (among others): normal contact, Mindlin-Cattaneo shift, steady state rolling, transient rolling, subsurface stresses, etc.

Björkman and Klarbring discuss the differences and similarities between frictional and plastic systems, and the corresponding differences in shakedown theorems for the two classes.

Barber reviews the general area of thermal effects in elastic contact. He points out that classical existence and uniqueness theorems cease to apply for an important class of problems in which the temperature and elastic fields are coupled through boundary conditions. This frequently leads to a phenomenon of thermoelastic instability.

Selvadurai finds stress intensity factors for penny-shaped cracks which contain a concentric rigid disk inclusion.

Johnson presents a review of recent progress, at Cambridge University and elsewhere, in problems of plastic flow and shakedown due to rolling contact. He considers both perfectly plastic and strain hardening materials.

McDowell and Moyar also treat the problem of elastic-plastic rolling contact, utilizing a "sophisticated, two-surface cyclic plasticity theory, known to correlate nonproportional cyclic plasticity experiments . . . " They suggest that an accurate representation of work hardening response and kinematic hardening enhances the solution for subsurface plastic shear strain accumulation.

Bower and Johnson discuss the conditions under which the corner of rails (or ideal infinite quarter-spaces) suffer incremental plastic collapse (ratchetting) due to a "traveling Hertz pressure distribution," and compare their analysis to experiments on elastic disks.

[2]Professor, Department of Mechanical Engineering and Mechanics, Lehigh University, Bethlehem, PA 18015.

[3]Asa Whitney Professor of Dynamical Engineering, University of Pennsylvania, Philadelphia, PA. Fellow ASME.

Copyright © 1988 by ASME
Downloaded 03 May 2010 to 171.66.16.21. Redistribution subject to ASME license or copyright; see http://www.asme.org/terms/Terms_Use.cfm

In railroad engineering parlance, a "shell" is a plate-like fragment which flakes or "spalls" off the surface of a rail due to a shallow subsurface crack running parallel to the rail surface. When shells turn downward, they can lead to a "transverse defect or detail fracture" on a transverse cross section of the rail. Keer, Farris, and Steele use a two-dimensional linear fracture mechanics model as a "first step towards gaining insight into the shell/detail fracture transition." They draw upon a number of their previous publications dealing with crack path stability and the interaction of surface indenters with discrete dislocations, to determine the Mode I and Mode II stress intensity factors for various positions of a sliding indenter (representing a wheel). In this preliminary report on the complex problem, they highlight numerical results on their studies of crack path deviation.

The literature (forty references) dealing with the mechanics of spalling failures is reviewed by Sheppard and Comninou.

This reviewer regrets that space limitations prevent him from calling specific attention to the many other fine papers in this excellent compendium. Since the problems it deals with are of great interest to engineers working outside the field of rail/wheel contact mechanics, it is likely that readers of this journal will find one or more papers of interest to them in the complete list of papers given below.

Elastic Contact Mechanics

J. J. Kalker, Wheel-rail wear calculations with the program CONTACT.

G. Björkman and Anders Klarbring, Shakedown and residual stresses in frictional systems.

J. R. Barber, Thermal effects on elastic contact.

W. Poole, The measurement of the contact area between opague objects under static and dynamic rolling conditions.

A. P. S. Selvadurai, A contact problem for the penny-shaped crack.

Inelastic Contact Mechanics

K. L. Johnson, Plastic flow, residual stress and shakedown in rolling contact.

D. L. McDowell and G. J. Moyar, A more realistic model of nonlinear material response: Application to elastic-plastic rolling contact.

A. F. Bower, K. L. Johnson, A ratcheting limit for plastic deformation of a quarter-space under rolling contact loads.

V. Bhargava, G. T. Hahn, G. Ham, S. Kuklarni, and C. A. Rubin, Influence of kinematic hardening on rolling contact deformation.

J. Orkisz, A. B. Perlman, A. Harris, and O. Orringer, Recent progress in the development of a rail residual stress calculation method.

Adhesion and Dynamics in Contact Mechanics

S. Kumar, and H. Chung, Some energy and adhesion aspects of wheel-rail contact.

C. O. Frederick, Theory of rail corrugation.

J. Elkins, R. A. Allen, and N. G. Wilson, Effect of wheel/rail contact on train rolling resistance.

D. Taylor, W. H. Elmaraghy, and W. Pak, Hunting of rail vehicles with conformed wheel profiles: Theory and in-service experience.

Wear and Contact Fatigue

H. Krause and H. Lehna, Investigations of tribological characteristics of rolling/sliding friction systems.

I. J. McEwen and R. F. Harvey, Wheel/rail and wear lubrication-laboratory studies and their relevance to field situations.

D. M. Fegredo and J. Kalousek, The effects of mixed microstructures on wear.

M. Dollar, A. W. Thompson, I. M. Bernstein, and D. H. Stone, Deformation and wear in rail steels.

L. M. Keer, T. N., Farris, and R. Steele, On some aspects of fatigue crack growth in rails induced by wheel/rail contact loading.

H. Ghonem and J. Kalousek, Experimental study of surface crack initiation in rolling contact.

P. Clayton and D. N. Hill, Rolling contact fatigue in rail steel.

H.-P. Lieurade, R. Y. Deroche, R. Derboule, and R. Cont, A study of the shelling mechanism of rails.

D. Jeong, O. Orringer, A. B. Perlman, and R. C. Rice, Beam theory prediction of shell nucleation life.

S. Sheppard and M. Comninou, The mechanics of surface fatigue failure.

A. K. Hellier, D. J. H. Corderoy, and M. B. McGirr, A study of subsurface rail/wheel contact stresses with application to modelling rail fatigue.

K. Sugino, H. Kageyama, and M. Sato, Effect on wheel and rail profiles on wear and fatigue behaivour of rail.

M. A. Daeubler, A. W. Thompson, and I. M. Bernstein, Short fatigue cracks in rail steels.

The Mathematics of Surfaces II, by R. R. Martin. Oxford University Press, New York, 1987.

REVIEWED BY J. TINSLEY ODEN[4]

This volume is the proceedings of a second conference on The Mathematics of Surfaces, sponsored by the Institute of Mathematics and Its Applications and held at University College, Cardiff, in September 1986. However, the book is not merely a collection of random papers on the subject; it is a fairly well organized account of the modern theory of surfaces beginning with tutorial lectures and including a number of papers on computational methods for the generation of surfaces. While there are a few American contributors to the work, the majority of papers are from western Europe.

The volume begins with an introductory chapter on "The Intelligence of Curves" by I. R. Porteous of Liverpool. This is a well-written tutorial introduction to the subject containing elementary definitions and examples. This provides a good introduction to the geometry of three-dimensional curves. This is followed by a paper from J. G. Hayes on "Fitting Surfaces to Data," a companion paper by A. A. Ball on "The Parametric Representation of Curves and Surfaces Using Rotational Polynomial Functions," and a chapter on reparametrization of rational surfaces by J. M. Hands. There are a number of interesting papers on rather specialized problems. Among these, we mention the paper by M. Gasca and J. J. Martinez on the computation of multivariant Vandermonde determinants, the use of radial basis functions for approximation of continuous functions by I. R. H. Jackson, a paper on the matching of an initial surface to a worn surface by R. DeLong and M. C. Bramwell, and a paper by S. Heatherington on the generation of surfaces in civil engineering. Also in this category are papers by T. J. Sharrock on bi-arcs in three dimensions and by F. Munchmeyer on surface imperfections. The paper by DeLong and Bramwell is a curious one, with DeLong from a school of dentistry and Bramwell from a school of statistics on computing. The paper focuses on matching and fitting surfaces that arise when attempting to estimate the wear of teeth using laboratory techniques.

There are several papers in the volume which discuss the use of surface patches. T. Varady surveys new results on n-sided patch generations, G. Renner provides a chapter on interpatch continuity, and R. J. Y. McLeod describes an alternate approach to surface patching. There is also a lengthy survey on blends in geometrical modeling by J. R. Woodward, by which is meant the use of "secondary surfaces" to model complex shapes, such as pipe bends. D. Catley, C. Whittle, and P. Thornton describe a general purpose program called GENSURF for generating general surfaces. T. W. Sederberg and J. P. Snively discuss parametrization of cubic algebraic surfaces, and a paper by R. Andesson et al. describes automatic generation of convex surfaces. T. N. T. Goodman and S. L. Lee describe geometrically continuous surfaces defined parametrically from piecewise polynomials, and R. T. Farouki discusses graphical methods for surface differential geometry.

There are several papers which exploit modern computational devices for surface generation. The interesting paper by A. Saia, M. S. Bloor, and A. D. Pennington is the only paper in the volume devoted to solid modeling and discusses sculptured solids in a geometric modeling system. A related paper on tetrahedral triangulation is provided by G. L. Tindle. M. Sabin contributed a short paper on the ideas of duality in the context of numerical geometry entitled "Envelope Curves and Surfaces."

[4]Department of Aerospace Engineering and Engineering Mechanics, The University of Texas at Austin, Austin, TX 78712.

Copyright © 1988 by ASME
Downloaded 03 May 2010 to 171.66.16.21. Redistribution subject to ASME license or copyright; see http://www.asme.org/terms/Terms_Use.cfm

The volume also contains a paper on shape preserving approximations by B. E. J. Dahlberg and B. Johansson, and another paper by I. R. Porteous on ridges and umbilics of surfaces. M. A. Lachance discusses data proliferation in the exchange of surfaces. The volume is concluded by a chapter entitled "Curve and Surface Modeling with Ugly Mathematics" by A. A. Ball. The message in this paper is that many of the constraints imposed on piecewise representations of curves and surfaces are really only formal mathematical constraints which shouldn't stand in the way of a practical use of piecewise representation by the designer. This would mean the use of "ugly mathematics" which he defines as primarily mathematics where the natural structure of curve fitting has been broken down in some way. Ball claims that ugliness is "often only skin deep" and simply reflects the designer's preoccupation with the practical problem and its solution rather than the mathematical theory and its presentation.

My general impression of this book is that it is a good contribution to the field of surface approximation, though it may not represent a broad look at the subject. There are many important areas of current research in geometrical modeling and surface fitting that are not touched upon in this volume, and there is a large number of important contributors to the subject worldwide who did not attend this meeting. Nevertheless, there are a number of very informative and useful papers in this work and it should not be ignored by either the theorist of the practitioner interested in contemporary thinking on surface modeling.

Downloaded 03 May 2010 to 171.66.16.21. Redistribution subject to ASME license or copyright; see http://www.asme.org/terms/Terms_Use.cfm